

The Geology of Colombia book provides an updated background of the geological knowledge of Colombia by integrating the most up-to-date research covering paleontology, biostratigraphy, sedimentary basin analysis, sedimentology, sequence stratigraphy, stratigraphy, geophysics, geochronology, geochemistry, thermochronology, tectonics, structure, volcanology, petrology, environmental science, climate change, and space geodesy.

Each chapter has a complete framework of a major branch of geology providing an invaluable resource for geologists interested in the geological history of Colombia.

The third volume has seventeen chapters that present the best preserved record of Chicxulub impact deposits at the Cretaceous/Paleogene boundary on Gorgonilla Island; geologic evolution of the Tumaco Forearc, Amagá, the San Jacinto fold belt, the Middle and Lower Magdalena and Llanos Basins; uplift and structural styles of the Eastern Cordillera; fluvial-lacustrine and volcanic records of the Morales Formation; Cenozoic marine carbonate systems of Colombia; provenance in modern rivers draining the Eastern and Central Cordilleras, as well as different levels of exhumation across the Bucaramanga Fault in south-western Santander Massif; new information on the Chocó-Panamá Arc and the Isthmian bedrock geology; Miocene tholeiitic and calc-alkaline magmatism from the northern Andes; and Cenozoic geologic evolution of the Sierra Nevada de Santa Marta.

Other volumes in *The Geology of Colombia* book

Volume 1: Proterozoic – Paleozoic

Volume 2: Mesozoic

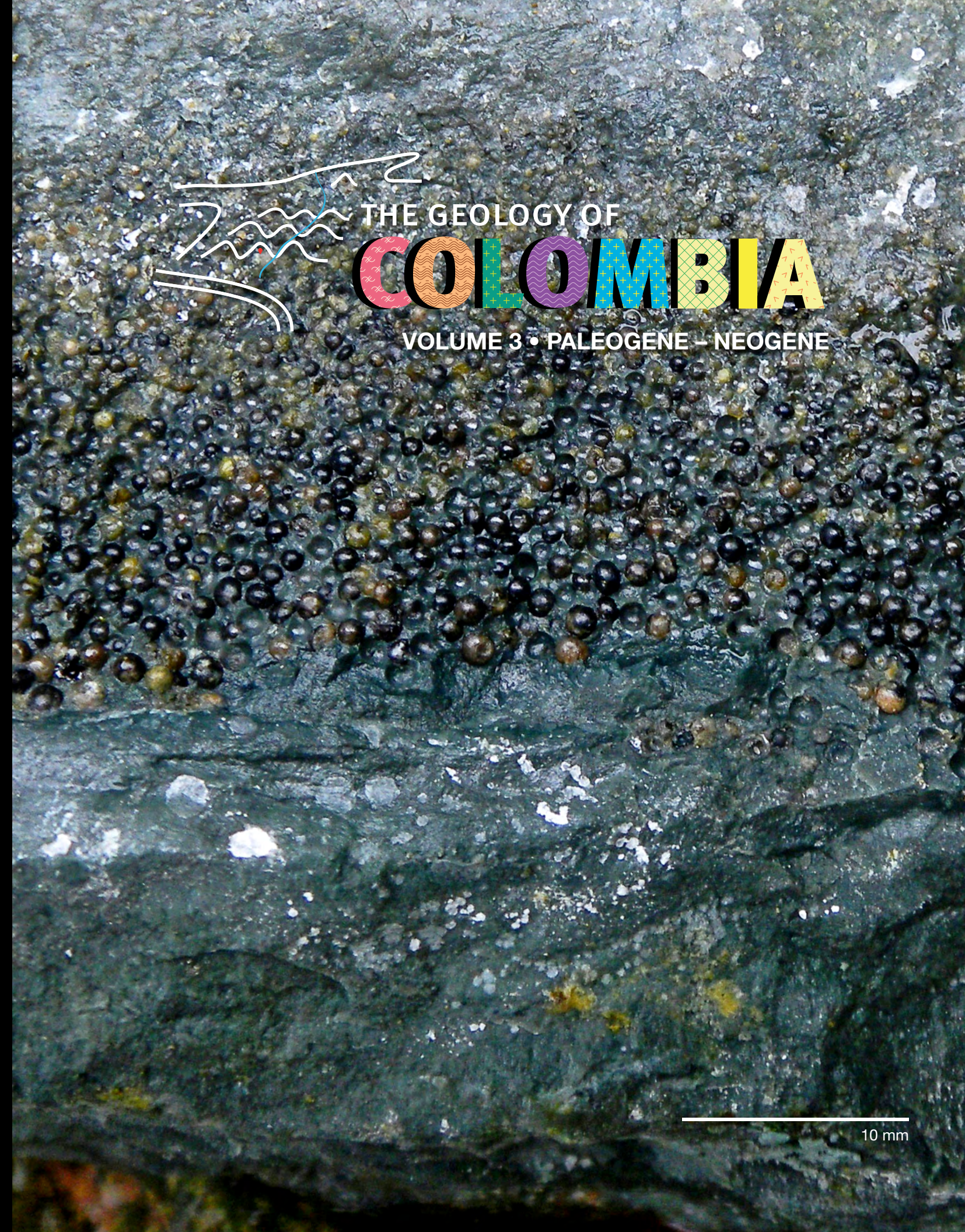
Volume 4: Quaternary



Jorge GÓMEZ TAPIAS
Daniela MATEUS-ZABALA
Editors

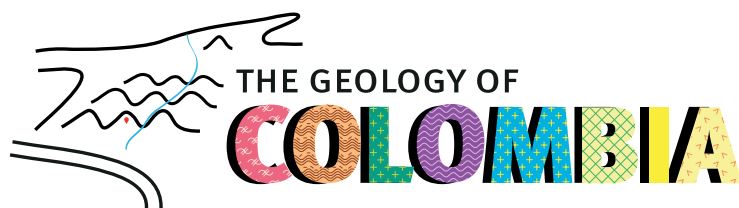
THE GEOLOGY OF COLOMBIA

VOLUME 3 • PALEOGENE – NEOGENE





Publicaciones Geológicas
Especiales



Jorge GÓMEZ TAPIAS and Daniela MATEUS-ZABALA
Servicio Geológico Colombiano
Editors



El futuro
es de todos

Minenergía

República de Colombia

Iván DUQUE MÁRQUEZ
Presidente de la República

Diego MESA PUYO
Ministro de Minas y Energía

Sandra SANDOVAL VALDERRAMA
Viceministra de Minas

Miguel LOTERO ROBLEDO
Viceministro de Energía



Servicio Geológico Colombiano

Consejo Directivo

Diego MESA PUYO
Ministro de Minas y Energía

Jonathan MALAGÓN GONZÁLEZ
Ministro de Vivienda, Ciudad y Territorio

Mabel Gisela TORRES TORRES
Ministra de Ciencia, Tecnología e Innovación

José Armando ZAMORA REYES
Presidente
Agencia Nacional de Hidrocarburos (ANH)

Juan Miguel DURÁN PRIETO
Presidente
Agencia Nacional de Minería (ANM)

Eduardo José GONZÁLEZ ANGULO
Director General
Unidad Nacional para la Gestión del Riesgo
de Desastres (UNGRD)

Contralmirante Juan Francisco HERRERA LEAL
Director General
Representante del Presidente de la República
Dirección General Marítima (Dimar)

© Servicio Geológico Colombiano

ISBN impreso obra completa: 978-958-52959-1-9
ISBN digital obra completa: 978-958-52959-6-4

ISBN impreso Vol. 3: 978-958-52959-4-0
ISBN digital Vol. 3: 978-958-53131-0-1



Esta obra está bajo licencia internacional
Creative Commons Reconocimiento 4.0.

Servicio Geológico Colombiano

Oscar PAREDES ZAPATA
Director General

Jhon Jairo CORREDOR CALDAS
Secretario General

Mario Andrés CUELLAR CÁRDENAS
Director de Geociencias Básicas

Gloria PRIETO RINCÓN
Directora de Recursos Minerales

Marta Lucía CALVACHE VELASCO
Directora de Geoamenazas

Hernán OLAYA DÁVILA
Director de Asuntos Nucleares

Humberto Andrés FUENZALIDA ETCHEVERRY
Director de Hidrocarburos

Hernando Alberto
CAMARGO GARCÍA
Director de Laboratorios

Jaime Alberto GARZÓN
Director (e) de Gestión de Información

Vanessa BARRENECHE SAMUR
Jefe Oficina Asesora Jurídica

María Esperanza PÉREZ PÉREZ
Jefe Oficina de Control Interno

Jorge GÓMEZ TAPIAS
Daniela MATEUS-ZABALA
Ana PINILLA-PACHON
Editores

Miguel Gerardo RAMÍREZ-LEAL
Diseñador

Imprenta Nacional de Colombia
Impresión

Bogotá D. C., Colombia
2020

Cover

Photograph showing spherules-rich bed in Gorgonilla Island which represents the first record of the Cretaceous/Paleogene boundary in Colombia and the best preserved around the world. See chapter 1, *The Cretaceous/Paleogene Boundary Deposits on Gorgonilla Island*, for discussing this finding.

Photograph courtesy of Hermann Darío BERMÚDEZ, geologist, at the Grupo de Investigación Paleoexplorer.

Suggested citation for Volume 3

Gómez, J. & Mateus-Zabala, D., editors. 2020. The Geology of Colombia, Volume 3 Paleogene – Neogene. Servicio Geológico Colombiano, Publicaciones Geológicas Especiales 37, 507 p. Bogotá. <https://doi.org/10.32685/pub.esp.37.2019>

Editorial Team

Jorge GÓMEZ TAPIAS
Editor-in-chief

Daniela MATEUS-ZABALA
Deputy editor

Ana PINILLA-PACHON
Deputy editor

Rubby Melissa LASSO-MUÑOZ
Science outreach coordinator

Alberto NÚÑEZ-TELLO
Thematic copyediting

María Paula MARROQUÍN-GÓMEZ
Thematic copyediting

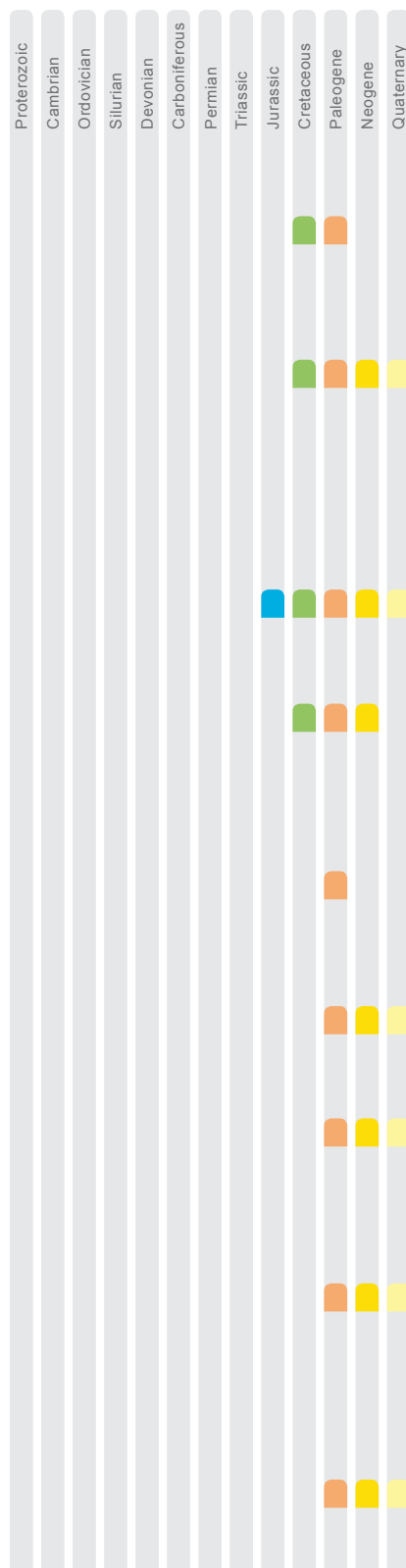
Fernando ALCÁRCEL-GUTIÉRREZ
Graphic arts coordinator

Eliana MARÍN-RINCÓN
Graphic arts

Lisbeth FOG-CORRADINE
Press office















Alejandra CARDONA-MAYORGA
Photography and video

Miguel Gerardo RAMÍREZ-LEAL
Design and layout



Volume 3

Chapter 1	The Cretaceous/Paleogene boundary deposits on Gorgonilla Island Hermann Darío BERMÚDEZ, Ignacio ARENILLAS, José Antonio ARZ, Vivi VAJDA, Paul R. RENNE, Vicente GILABERT, and José Vicente RODRÍGUEZ	1
Chapter 2	Formation and evolution of the Lower Magdalena Valley Basin and San Jacinto fold belt of northwestern Colombia: Insights from Upper Cretaceous to recent tectono-stratigraphy Josué Alejandro MORA-BOHÓRQUEZ, Onno ONCKEN, Eline LE BRETON, Mauricio IBAÑEZ-MEJIA, Gabriel VELOZA, Andrés MORA, Vickye VÉLEZ, and Mario DE FREITAS	21
Chapter 3	Construction of the Eastern Cordillera of Colombia: Insights from the sedimentary record Brian K. HORTON, Mauricio PARRA, and Andrés MORA	67
Chapter 4	Late Cretaceous to Cenozoic uplift of the northern Andes: Paleogeographic implications Andrés MORA, Diego VILLAGÓMEZ, Mauricio PARRA, Víctor M. CABALLERO, Richard SPIKINGS, Brian K. HORTON, Josué Alejandro MORA-BOHÓRQUEZ, Richard A. KETCHAM, and Juan Pablo ARIAS-MARTÍNEZ	89
Chapter 5	The Eastern Foothills of Colombia Andrés MORA, Eliseo TESÓN, Jaime MARTÍNEZ, Mauricio PARRA, Álvaro LASSO, Brian K. HORTON, Richard A. KETCHAM, Antonio VELÁSQUEZ, and Juan Pablo ARIAS-MARTÍNEZ	123
Chapter 6	Structural styles of the Eastern Cordillera of Colombia Andreas KAMMER, Alejandro PIRAQUIVE, Cristhian GÓMEZ, Andrés MORA, and Antonio VELÁSQUEZ	143
Chapter 7	Cenozoic evolution of the Sierra Nevada de Santa Marta, Colombia Mauricio PARRA, Sebastián ECHEVERRI, Ana María PATIÑO, Juan Carlos RAMÍREZ, Andrés MORA, Edward R. SOBEL, Ariel ALMENDRAL, and Andrés PARDO-TRUJILLO	185
Chapter 8	Cenozoic geologic evolution of the southern Tumaco Forearc Basin (SW Colombian Pacific) Andrés PARDO-TRUJILLO, Sebastián ECHEVERRI, Carlos BORRERO, Alejandro ARENAS, Felipe VALLEJO, Raúl TREJOS, Ángel PLATA, José-Abel FLORES, Agustín CARDONA, Sergio RESTREPO, Ángel BARBOSA, Hugo MURCIA, Carlos GIRALDO, Sergio CELIS, and Sergio A. LÓPEZ	215
Chapter 9	Cenozoic marine carbonate systems of Colombia Juan Carlos SILVA-TAMAYO, Daniel RINCÓN-MARTÍNEZ, Lina M. BARRIOS, Juan C. TORRES-LASSO, and Chixel OSORIO-ARANGO	249

Proterozoic	Cambrian	Ordovician	Silurian	Devonian	Carboniferous	Permian	Triassic	Jurassic	Cretaceous	Paleogene	Neogene	Quaternary				
													Chapter 10	From facies analysis, stratigraphic surfaces, and depositional sequences to stratigraphic traps in the Eocene – Oligocene record of the southern Llanos Basin and northern Magdalena Basin	Víctor M. CABALLERO, Guillermo RODRÍGUEZ, Julián F. NARANJO, Andrés MORA, and Felipe DE LA PARRA	283
													Chapter 11	Oligocene – Miocene coal-bearing successions of the Amagá Formation, Antioquia, Colombia: Sedimentary environments, stratigraphy, and tectonic implications	Juan Carlos SILVA–TAMAYO, Mario LARA, and Ana Milena SALAZAR–FRANCO	331
													Chapter 12	The Combia Volcanic Province: Miocene post-collisional magmatism in the northern Andes	Marion WEBER, José Fernando DUQUE, Susana HOYOS, Andrés L. CÁRDENAS–ROZO, Jorge GÓMEZ TAPIAS, and Rob WILSON	355
													Chapter 13	The Morales Formation (new unit): Record of fluvial–lacustrine environments and the beginning of the Miocene explosive volcanism in the Patía Sub–basin (SW Colombia)	Andrés F. GALLEGÓ–RÍOS, Andrés PARDO–TRUJILLO, Guillermo A. LÓPEZ–PLAZAS, and Sebastián ECHEVERRI	395
													Chapter 14	New contributions to the knowledge about the Chocó–Panamá Arc in Colombia, including a new segment south of Colombia	Gilberto ZAPATA–GARCÍA and Gabriel RODRÍGUEZ–GARCÍA	417
													Chapter 15	Isthmian bedrock geology: Tilted, bent, and broken	Camilo MONTES and Natalia HOYOS	451
													Chapter 16	Zircon U–Pb and fission–track dating applied to resolving sediment provenance in modern rivers draining the Eastern and Central Cordilleras, Colombia	Cindy Lizeth URUEÑA–SUÁREZ, Mary Luz PEÑA–URUEÑA, Jimmy Alejandro MUÑOZ–ROCHA, Lorena del Pilar RAYO–ROCHA, Nicolás VILLAMIZAR–ESCALANTE, Sergio AMAYA–FERREIRA, Mauricio IBAÑEZ–MEJIA, and Matthias BERNET	469
													Chapter 17	Different levels of exhumation across the Bucaramanga Fault in the Cepitá area of the southwestern Santander Massif, Colombia: Implications for the tectonic evolution of the northern Andes in northwestern South America	Sergio AMAYA–FERREIRA, Carlos Augusto ZULUAGA, and Matthias BERNET	491

Contributing authors

Ariel ALMENDRAL
Sergio AMAYA-FERREIRA
Alejandro ARENAS
Ignacio ARENILLAS
Juan Pablo ARIAS-MARTÍNEZ
José Antonio ARZ
Ángel BARBOSA
Lina M. BARRIOS
Hermann Darío BERMÚDEZ
Matthias BERNET
Carlos BORRERO
Víctor M. CABALLERO
Andrés L. CÁRDENAS-ROZO
Agustín CARDONA
Sergio CELIS
Mario DE FREITAS
Felipe DE LA PARRA
José Fernando DUQUE
Sebastián ECHEVERRÍ
José-Abel FLORES
Andrés F. GALLEGÓ-RÍOS
Vicente GILABERT
Carlos GIRALDO
Cristhian GÓMEZ
Jorge GÓMEZ TAPIAS
Brian K. HORTON
Natalia HOYOS
Susana HOYOS
Mauricio IBAÑEZ-MEJIA
Andreas KAMMER
Richard A. KETCHAM
Mario LARA
Álvaro LASSO
Eline LE BRETON
Sergio A. LÓPEZ
Guillermo A. LÓPEZ-PLAZAS
Jaime MARTÍNEZ
Camilo MONTES
Andrés MORA

Josué Alejandro MORA-BOHÓRQUEZ
Jimmy Alejandro MUÑOZ-ROCHA
Hugo MURCIA
Julián F. NARANJO
Onno ONCKEN
Chixel OSORIO-ARANGO
Andrés PARDO-TRUJILLO
Mauricio PARRA
Ana María PATIÑO
Mary Luz PEÑA-URUEÑA
Alejandro PIRAQUIVE
Ángelo PLATA
Juan Carlos RAMÍREZ
Lorena del Pilar RAYO-ROCHA
Paul R. RENNE
Sergio RESTREPO
Daniel RINCÓN-MARTÍNEZ
Guillermo RODRÍGUEZ
José Vicente RODRÍGUEZ
Gabriel RODRÍGUEZ-GARCÍA
Ana Milena SALAZAR-FRANCO
Juan Carlos SILVA-TAMAYO
Edward R. SOBEL
Richard SPIKINGS
Eliseo TESÓN
Juan C. TORRES-LASSO
Raúl TREJOS
Cindy Lizeth URUEÑA-SUÁREZ
Vivi VAJDA
Felipe VALLEJO
Antonio VELÁSQUEZ
Vickye VÉLEZ
Gabriel VELOZA
Diego VILLAGÓMEZ
Nicolas VILLAMIZAR-ESCALANTE
Marion WEBER
Rob WILSON
Gilberto ZAPATA-GARCÍA
Carlos Augusto ZULUAGA

Chapter 1



The Cretaceous/Paleogene Boundary Deposits on Gorgonilla Island

<https://doi.org/10.32685/pub.esp.37.2019.01>

Published online 11 October 2019

Hermann Darío BERMÚDEZ^{1*}, Ignacio ARENILLAS², José Antonio ARZ³, Vivi VAJDA⁴, Paul R. RENNE⁵, Vicente GILABERT⁶, and José Vicente RODRÍGUEZ⁷

Abstract A ca. 20 mm thick spherule bed representing Chicxulub impact ejecta deposits and marking the Cretaceous/Paleogene (K/Pg) boundary was recently discovered on Gorgonilla Island (Gorgona National Natural Park, Pacific of Colombia). This discovery represents the first confirmed record of the K/Pg event in Colombia, South America, and the eastern Pacific Ocean. The deposit consists of extraordinarily well-preserved glass spherules (microtektites and microkrystites) reaching 1.1 mm in diameter. Importantly, the Gorgonilla spherule bed is unique relative to other K/Pg boundary sites in that up to 90% of the spherules are intact and not devitrified, and the bed is virtually devoid of lithic fragments and microfossils. The spherules were deposited in a deep marine environment, possibly below the calcite compensation depth. The preservation, normal size-gradation, presence of fine textures within the spherules, and absence of bioturbation or traction transport indicate that the Gorgonilla spherules settled within a water column with minimal disturbance. The spherule bed may represent one of the first parautochthonous primary deposits of the Chicxulub impact known to date. ⁴⁰Ar/³⁹Ar dating and micropaleontological analysis reveal that the Gorgonilla spherule bed resulted from the Chicxulub impact. Intense soft-sediment deformation and bed disruption in Maastrichtian sediments of the Gorgonilla Island K/Pg section provide evidence for seismic activity triggered by the Chicxulub bolide impact, 66 million years ago. It is also notable that the basal deposits of the Danian in the Colombian locality present the first evidence of a recovery vegetation, characterized by ferns from a tropical habitat, shortly following the end-Cretaceous event.

Keywords: K/Pg boundary, Chicxulub, microtektites, seismites, Gorgonilla Island, Colombia.

Resumen Una capa de aproximadamente 20 mm de espesor con depósitos de eyecta del impacto de Chicxulub, que marca el límite Cretácico-Paleógeno (K/Pg), fue recientemente descubierta en la isla Gorgonilla (Parque Nacional Natural Gorgona, Pacífico colombiano). Este es el primer registro confirmado del evento K/Pg en Colombia, Suramérica y el Pacífico oriental. El depósito consiste en una acumulación de esferulitas de vidrio (microtectitas y microcristitas) de hasta 1,1 mm de diámetro extraordinariamente bien preservadas. La capa de esferulitas de Gorgonilla es única entre los depósitos conocidos de eyecta de Chicxulub; hasta un 90 % de las esférulas está aún completamente vitrificadas y la capa está prácticamente desprovista de líticos o microfósiles. Las esferulitas fueron depositadas en un paleoambiente marino de aguas profundas, posiblemente por debajo

- 1 hdbermudez@yahoo.com
Grupo de Investigación Paleoexplorer
4690 W. Eldorado parkway, apt 1016, McKinney,
Texas
75070 USA
- 2 ias@unizar.es
Universidad de Zaragoza
Instituto Universitario de Ciencias
Ambientales de Aragón
Departamento de Ciencias de la Tierra
E-50009 Zaragoza, Spain
- 3 josearz@unizar.es
Universidad de Zaragoza
Instituto Universitario de Ciencias
Ambientales de Aragón
Departamento de Ciencias de la Tierra
E-50009 Zaragoza, Spain
- 4 vivi.vajda@nrm.se
Swedish Museum of Natural History
Department of Palaeobiology
Stockholm, Sweden
- 5 prene@bgc.org
Berkeley Geochronology Center (BGC)
2455 Ridge Road, Berkeley, CA 94709, USA
University of California, Berkeley
Department of Earth and Planetary Science
Berkeley, CA, 94720, USA
- 6 vgilabert@unizar.es
Universidad de Zaragoza
Departamento de Ciencias de la Tierra
E-50009 Zaragoza, Spain
- 7 jovicrodri@yahoo.com
4690 W. Eldorado parkway, apt 1016, McKinney,
TX, 75070

* Corresponding author

Citation: Bermúdez, H.D., Arenillas, I., Arz, J.A., Vajda, V., Renne, P.R., Gilabert, V. & Rodríguez, J.V. 2019. The Cretaceous/Paleogene boundary deposits on Gorgonilla Island. In: Gómez, J. & Mateus-Zabala, D. (editors), *The Geology of Colombia, Volume 3 Paleogene – Neogene*. Servicio Geológico Colombiano, *Publicaciones Geológicas Especiales* 37, p. 1–19. Bogotá. <https://doi.org/10.32685/pub.esp.37.2019.01>

del nivel de compensación de la calcita. La preservación, gradación normal, presencia de estructuras delicadas dentro de las esférulas y ausencia de evidencias de bioturbación o de transporte indican que la capa de esférulas de Gorgonilla se asentó a través de la columna de agua con mínima perturbación subsecuente. Esta capa puede representar uno de los primeros depósitos paraautóctonos primarios del impacto de Chicxulub conocidos hasta el momento. Dataciones $^{40}\text{Ar}/^{39}\text{Ar}$ y resultados de análisis micropaleontológicos muestran que la capa de esférulas de Gorgonilla fue producida por el impacto del asteroide que formó el cráter de Chicxulub. Adicionalmente, la intensa deformación sinsedimentaria y la perturbación de las capas del Maastrichtiano en la sección K/Pg de la isla Gorgonilla proporcionan evidencia de la actividad sísmica producida por el impacto de Chicxulub hace 66 millones de años. Es también notable que las capas basales del Daniano en la localidad colombiana muestran las primeras evidencias de la recuperación de la vegetación, representada por helechos de un hábitat tropical, justo después del evento del fin del Cretácico.

Palabras clave: límite K/Pg, Chicxulub, microtectitas, sismitas, isla Gorgonilla, Colombia.

1. Introduction

The Cretaceous/Paleogene (K/Pg) boundary marks one of the five major mass extinctions in Earth's history and has long been associated with the Chicxulub impact in the Yucatán Peninsula, 66 million years ago (Alvarez et al., 1980; Hildebrand et al., 1991; Pope et al., 1991; Schulte et al., 2010). However, some authors question this vast evidence, suggesting that the Chicxulub impact predated the K/Pg boundary by several hundred thousand years and that it was not responsible for the K/Pg mass extinction (Keller, 2011; Keller et al., 2001, 2003a, 2003b; Stinnesbeck et al., 1997, 2002).

Ejecta deposits containing melt droplets in the form of tiny glass spherules, with a similar chemical composition as the glass from the Yucatán impact breccia, have been documented throughout Central and North America and the Caribbean (Keller et al., 2013; Norris et al., 1999; Ocampo et al., 1996; Olsson et al., 1997; Schulte et al., 2010; Smit et al., 1992; Wigforss–Lange et al., 2007). However, in South America, K/Pg boundary sections are exceedingly rare, and only two sections have been formally associated with the Chicxulub impact event. In the Neuquén Basin, Argentina, Scasso et al. (2005) described a coarse-grained sandstone bed, which occurs in a homogeneous shallow shelf mudstone sequence. The authors suggested that this siliciclastic unit represents a tsunami deposit, triggered by the Chicxulub impact. In a subsequent analysis from the same section, however, Keller et al. (2007) suggested that the deposition of the sandstone occurred 500 ky after the K/Pg hiatus and is unrelated to the Chicxulub impact. At Poty quarry, Pernambuco, Northeast Brazil, Albertão & Martins (1996) described a shallow-marine marl and limestone succession with impact-derived exotic products (microtektite-like microspherules and shock-metamorphosed quartz), associated with a possible impact-generated tsunamite. However, subsequent work by Albertão et al. (2004), Morgan et al. (2006),

and Gertsch et al. (2013) concluded that there is no evidence supporting the impact origin of those spherules. The breccia unit, interpreted as a tsunamite, is composed of intraformational lime- and marlstone clasts but also contains bones, phosphatic lumps, phosphatized foraminifera, glauconite, and small pyrite concretions, which indicate reworking and erosion from near-shore areas (Stinnesbeck & Keller, 1996). Gertsch et al. (2013) suggested that this unit represented a gravity flow formed during the latest Maastrichtian lowstand.

A new pristine K/Pg section has been discovered on Gorgonilla Island, in the Pacific of Colombia (Bermúdez et al., 2016). Although most of the glass spherules formed during the Chicxulub impact are now devitrified and have been altered to secondary clay minerals, such as smectite, the spherules from Gorgonilla Island are virtually unaltered and represent the most pristine K/Pg boundary spherules known to date. This unique boundary section is the first confirmed record of this event in Colombia, South America, and the eastern Pacific Ocean and it has been studied with respect to stratigraphy, sedimentology, mineralogy, chemistry, micropaleontology, palynology, and $^{40}\text{Ar}/^{39}\text{Ar}$ geochronology (Renne et al., 2018). The present paper is a summary of an international interdisciplinary research project, still in progress, and condenses the information available to date.

1.1. Location and Geological Setting

The Gorgonilla Island K/Pg section (2° 56' N, 78° 12' W) is located in Gorgona National Natural Park, south of the Playa del Amor, SW coast of Gorgonilla Island, approximately 35 kilometers off the Colombian Pacific coast (Figure 1a). The island is 0.5 to 1 km in diameter and is located approximately 500 m SW of the larger Gorgona Island. Rock units only crop out along the coast at both islands, and as a result, outcrops are generally only accessible during low tide. Gorgona and Gor-



Figure 1. (a) Map of the Gorgonilla K/Pg section's location, Pacific of Colombia. (b) Global distribution of key K/Pg boundary sections (outcrops and deep sea drill sites). Modified from Schulte et al. (2009, 2010).

gonilla are among the less deformed and last accreted portions of the Caribbean Plateau and expose a mafic and ultramafic magmatic sequence of Late Cretaceous to early Paleocene age, which includes basalts, gabbros, peridotites, basaltic komatiites, microgabbroic intrusions, and pyroclastic sediments (Dietrich *et al.*, 1981; Echeverría & Aitken, 1986; Gansser, 1950; Gansser *et al.*, 1979; Kerr, 2005; Serrano *et al.*, 2011). The sedimentary rock sequence at Gorgona and Gorgonilla Islands consists of Paleogene litharenite, mudstone, tuffaceous shale, radiolarite, limestone, and minor conglomerate, and Neogene mudstone, fossiliferous shale, and sandstone (Gansser, 1950).

Gorgonilla is interpreted to form the southernmost part of the Caribbean Oceanic Plateau or part of Gorgona Plateau that was accreted to northern South America in the middle Eocene (Kennan & Pindell, 2009; Kerr & Tarney, 2005). At the time of the Chicxulub impact, the Gorgonilla site was thus located approximately 2000–3000 km southwest of the impact site in northern Yucatán (Figure 1b).

2. Materials and Methods

Field work was performed during geological campaigns in 2014 and 2015. The exposure hosting the K/Pg boundary deposits was measured and examined for lithological changes, composition, sedimentologic structures, trace fossils, erosion surfaces, and deformation, and documented through drawings and high-resolution photographs. Sediments were sampled at close intervals for microfossils, and petrographic, mineralogical, and geochemical analyses; a total of 140 rock samples were collected. For petrographic and electron microprobe analysis, polished thin sections were generated from cuts normal and parallel to the bedding in the spherule deposit, as well as from Maastrichtian and Danian sediments enclosing the event bed.

To investigate their shapes and surface structures, spherules were hand-picked from gently disintegrated samples at the Paleoexplorer SAS laboratory, Bogotá, Colombia. Polished cut slabs and disaggregated spherules were coated with graphite, under prevacuum conditions (<10–1 torr), in an Emscope TB500 SEM Carbon Coater, at the Departamento de Geociencias of the Universidad Nacional de Colombia, Bogotá. The typical thickness of coating was ± 60 nm. Imaging and microanalysis of the spherules were executed in a scanning electron microscope (FEI QUANTA 200), equipped with an Everhart–Thornley detector (ETD) and a solid-state detector (SSD). Additional imaging, chemical analysis, and mapping of spherules were performed at the Institut für Geowissenschaften of Ruprecht–Karls–Universität, Heidelberg, Germany, with an LEO 440 scanning electron microscope equipped with an Oxford Inca EDX system. Electron microprobe analyses were performed using a CAMECA SX51 instrument equipped with five wavelength-dispersive spectrometers (methods described in Bermúdez *et al.*, 2016).

For the $^{40}\text{Ar}/^{39}\text{Ar}$ geochronology study (Renne *et al.*, 2017, 2018), spherules were irradiated in the Cd-lined CLICIT of the Oregon State University TRIGA reactor, along with the Fish Canyon sanidine (FCs–EK) standard; they were analyzed individually by stepwise degassing in 9–15 steps, with a defocused CO_2 laser, and Ar ion beams were measured using peak hopping with an MAP 215C mass spectrometer, following procedures essentially identical to those of Renne *et al.* (2013). Decay and interference corrections were those of Renne *et al.* (2013). Ages were calculated using the optimization calibration of Renne *et al.* (2011).

For the planktic foraminiferan study, samples were disaggregated using a solution of 80% acetic acid and 20% H_2O_2 or a 2M NaOH solution, and subsequently washed through a 63 μm sieve; all foraminiferan specimens were identified, sorted, and fixed on standard 60-square micropaleontological slides; some of these were examined under the scanning electron microscope (Zeiss MERLIN FE–SEM), at the Electron Microscopy Service of the Universidad de Zaragoza, Spain.

Ten samples spanning the K/Pg boundary succession were processed for palynological analysis at the palynological laboratory at the Department of Paleobiology, in the Swedish Museum of Natural History, following standard methods. Two strewn slides per sample, one kerogen sample (not sieved, nor oxidized), and one where the residue was sieved and oxidized, were analyzed for organic particles, including pollen and spores.

3. Results

The sedimentary record of the Cretaceous – Paleogene transition in Gorgonilla Island (Figure 2) is composed of thin to medium-bedded light olive-gray tuffaceous litharenite (locally conglomeratic), with calcitic cement rhythmically alternating with massive gray-yellow tuffaceous marl, siltstone, and claystone (Figure 2a–d). Sandstone components are lithic and include feldspar, olivine, quartz, pyroxene, and mica, as well as abundant volcanic lithics, and floating clasts of siliciclastic sedimentary rocks. Diverse microfossils are present in the intercalated mudstone, including abundant radiolarians, coccoliths, rare poorly preserved foraminifers, and sponge spicules (Bermúdez *et al.*, 2016).

Slump and other soft-sediment deformation features are abundant at the Gorgonilla K/Pg boundary section in the beds underlying the spherule bed (Figure 2g), leading to uneven surfaces and disrupted bedding. Upsection from the spherule bed, soft sediment deformation is also occasionally present, but markedly rarer and restricted to small-scale slumps and the contortion of individual thin sediment units, while other units appear to be unaffected (Figure 2f). Soft-sediment deformation structures include syndepositional faulting and fault-grading, hydroplastic mixed layers, pillar and flame structures, small and medium-scale slumps with internal folding and associated

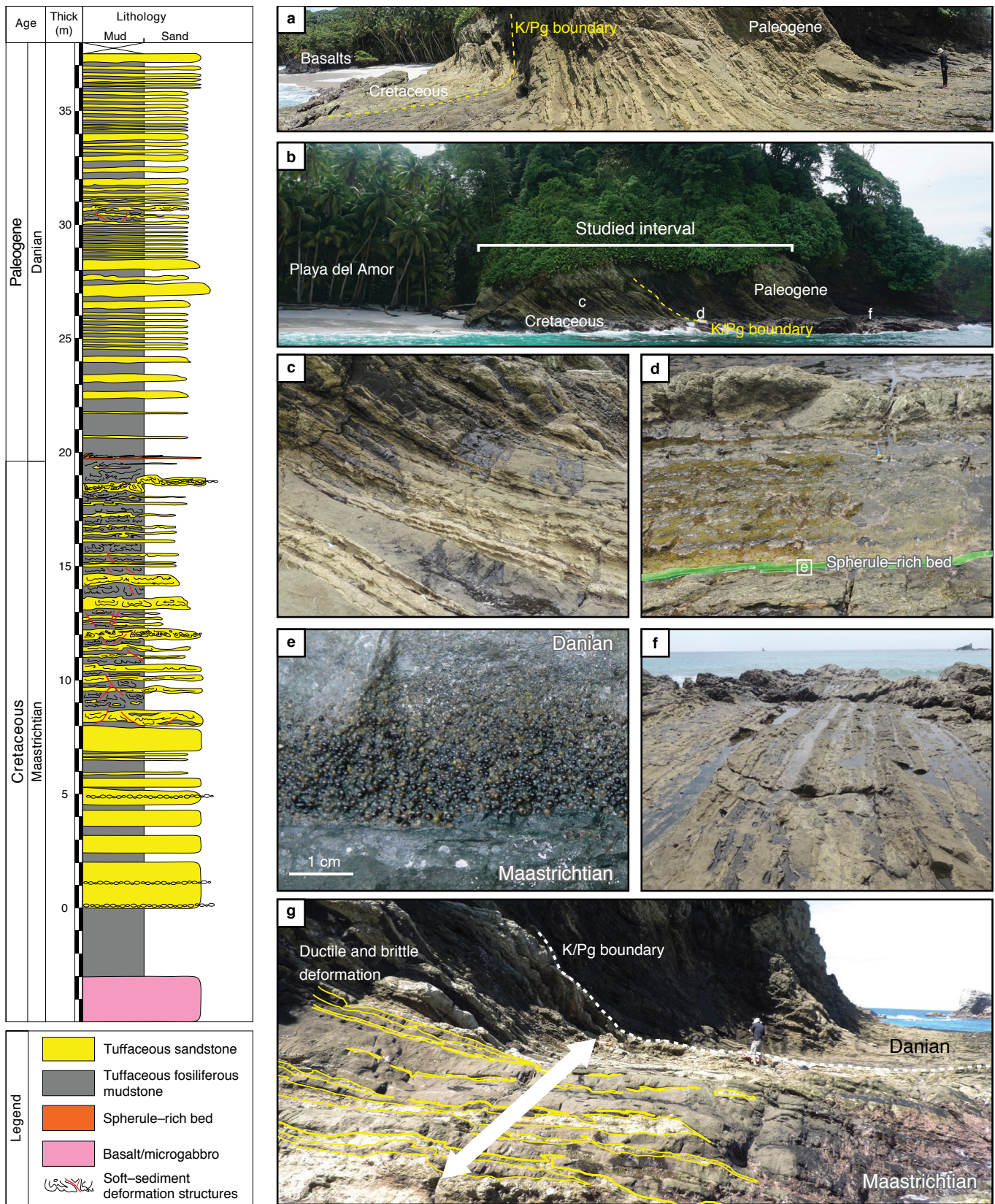


Figure 2. Stratigraphic section at Gorgonilla Island. **(a)** Panoramic view of the studied outcrop during low tide. **(b)** Outcrop overview of the Gorgonilla K/Pg section (c, d, and f indicate location of Figure 2c, 2b, and 2f). **(c)** Maastrichtian rocks below the spherule-rich bed. **(d)** Aspect of the K/Pg boundary showing the interval from the uppermost Maastrichtian to the lowermost Danian. **(e)** Spherule deposit showing the normally graded sequence. **(f)** Danian rocks above the K/Pg boundary. **(g)** Upper Maastrichtian deposits with soft-sediment deformation structures and microfaults.

thrusting, contorted laminae, small-scale convolution, abundant sand injections, and convolute structures (Bermúdez et al., 2015; Renne et al., 2018).

The K/Pg boundary sequence includes a ca. 20 mm thick pristine grayish green to dark green spherule-rich bed (Figure 2e). The deposit is traceable over approximately 20 meters laterally, without significant changes in thickness or lithology; it is normally graded and composed of rounded and compressed 0.1–1.1 mm sized spherules in a matrix composed of calcitic cement, with an absence of clastic grains or microfossils (Figure 3a). The spherule deposit lacks sedimentary structures suggestive of traction or mass flow transport (such as cross bedding, basal or internal scours, reversals, or interruptions in grading).

Spherules are black to olive or translucent-honey colored. The majority are round, but oval, teardrop and dumbbell morphologies are also frequent (Figure 3b), in addition to irregular grape-like clusters of two, three, four, or even more spherules; when broken apart, convex-concave contacts are observed (Bermúdez et al., 2016). Approximately 70% of the spherules are massive glass (microtektites); the other 30% contain single, or more rarely two or more vesicles. Up to 90% of the glass spherules are unaltered or only partly altered. In thin section, the glass is usually colorless; some spherules are faintly green or yellow. Schlieren textures are frequent. Backscattered electron images occasionally reveal the presence of tiny dendritic and/or fibrous crystals of mafic primary microlites, which suggests that some Gorgonilla spherules are microkrystites (Figure 3c–f).

The chemical composition of unaltered or minimally altered glass spherules at Gorgonilla is variable (Figure 4), especially in spherules with schlieren textures. SiO_2 ranges from 48 to 69 wt %, Al_2O_3 from 8 to 15 wt %, FeO from 4.0 to 6.6 wt %, MgO from 1.8 to 4.6 wt %, CaO from 5 to 29 wt %, Na_2O from 0.9 to 5 wt %, and K_2O from 0.1 to 1.9 wt %. In contrast, totals from the microprobe analyses are close to 100 wt %, indicating a rather low volatiles (Bermúdez et al., 2016).

Planktic foraminiferans are absent in the Cretaceous deposits at Gorgonilla, except for scarce specimens identified in G–11.20 and G–15.30 samples (the numbers represent the stratigraphic position in the sequence), which includes the Maastrichtian index-species *Pseudoguembelina palpebra* (Figure 5). No planktic foraminifera were identified in samples from the deformed microtektite bed, nor in washed residues or thin sections, contrary to previous claims by Gerta KELLER in Bermúdez et al. (2016). Foraminiferans are absent in the 50 mm thick stratigraphic interval between the top of the spherule bed and the first sample (G–19.98), with preserved planktic foraminifera, whose assemblages belong to the Zone Pa, in the basal Danian (Renne et al., 2018). These assemblages include index-species such as *Parvularugoglobigerina longiapertura*, *Parvularugoglobigerina eugubina*, and *Eoglobigerina simplicissima*.

All samples, without exception, were poor in organic matter. Green algae are present through the succession, which possibly reflect an influx of fresh-water from tropical wetland environments. Importantly, relatively abundant assemblages of the water fern *Azolla*, represented by microspores and the megaspore *massulae*, appear above the spherule bed together with fern spores, including *Cyathidites minor*, *Gleicheniidites senonicus*, and *Deltoidospora toralis* (Figure 5). These cooccur with sparse fungal spores and clusters of fungal hyphae.

To test whether the Gorgonilla spherules are Chicxulub-derived tektites, Renne et al. (2018) used $^{40}\text{Ar}/^{39}\text{Ar}$ methods to date them. Incremental heating of 25 individual spherules, in 9 to 15 steps, yielded plateau ages for all spherules, with 19/25 yielding 100% concordant plateau and the remainder comprising >85% of the ^{39}Ar released. The weighted mean of all plateau ages is 66.051 ± 0.031 Ma (1 sd, analytical uncertainties only). This age is indistinguishable from the $^{40}\text{Ar}/^{39}\text{Ar}$ ages (66.038 ± 0.025 Ma) of the Haitian tektites, and from the age (66.043 ± 0.010 Ma) of the K/Pg boundary (Renne et al., 2013).

4. Discussion

The external geometry, faint normal grain size gradation and sorting, and micropaleontological assemblages at the Gorgonilla Island K/Pg section suggest that this rhythmic bedding sequence was deposited as turbidites in pelagic bathyal environments. The evidence suggests that the Gorgonilla site was close enough (2000–3000 km) to the impact site to receive 20 mm of ejecta, yet also located far enough away from the shelf edge so as not to be affected by the destabilization and collapse of the continental margin. Its pelagic position in deep water in the tropical western Pacific likely protected the Gorgonilla spherule bed from reworking by impact-induced tsunami waves (Bermúdez et al., 2016). The absence of siliciclastic debris, bioturbation, or microfossils indicates rapid deposition and an absence of reworking. This is also supported by the excellent preservation of delicate details of the texture, such as the convex-concave contacts and agglutination of spherules. This suggests parautochthonous deposition and indicates that Gorgonilla's spherules settled within a water column with minimal disturbance.

The stratigraphic position of the Gorgonilla spherule bed, coupled with preliminary biostratigraphic and geochemical data (Bermúdez et al., 2016), suggests that these spherules are correlative with those found in many circum-Caribbean locations closely associated with the K/Pg boundary and ascribed to impact melt produced by the Chicxulub impact. The range of the main elemental compositions and the oxide variation of the Gorgonilla glasses are compatible with those from Beloc, Haiti and Mimbral, and Mexico. The average chemical compositions are similar to those of yellow and black glasses from

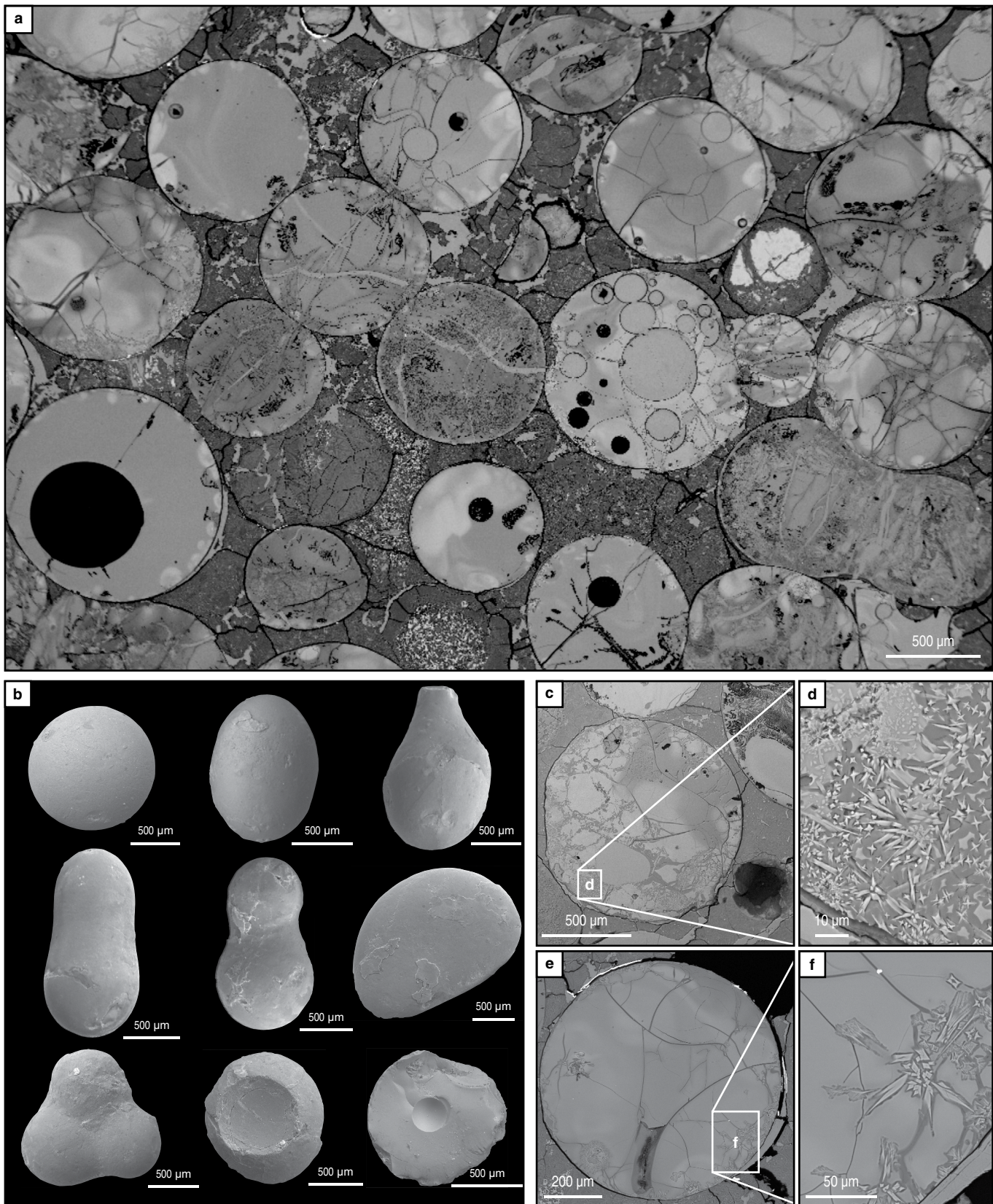


Figure 3. Spherules from the Gorgonilla Island K/Pg section. **(a)** SEM microphotograph of the bottom of the spherule-rich bed, showing a matrix composed by calcitic cement, absence of clastic grains or reworked microfossils, and round, oval, and compressed spherules with concave/convex contacts. **(b)** Backscattered electron microscope images of selected glass spherules illustrating round, oval, tear-drop, and dumbbell morphologies (scale bar = 500 μm). **(c-f)** Backscattered electron microscope images of microkrystites of the Gorgonilla Island. **(d, f)** Details, illustrating primary microlites.

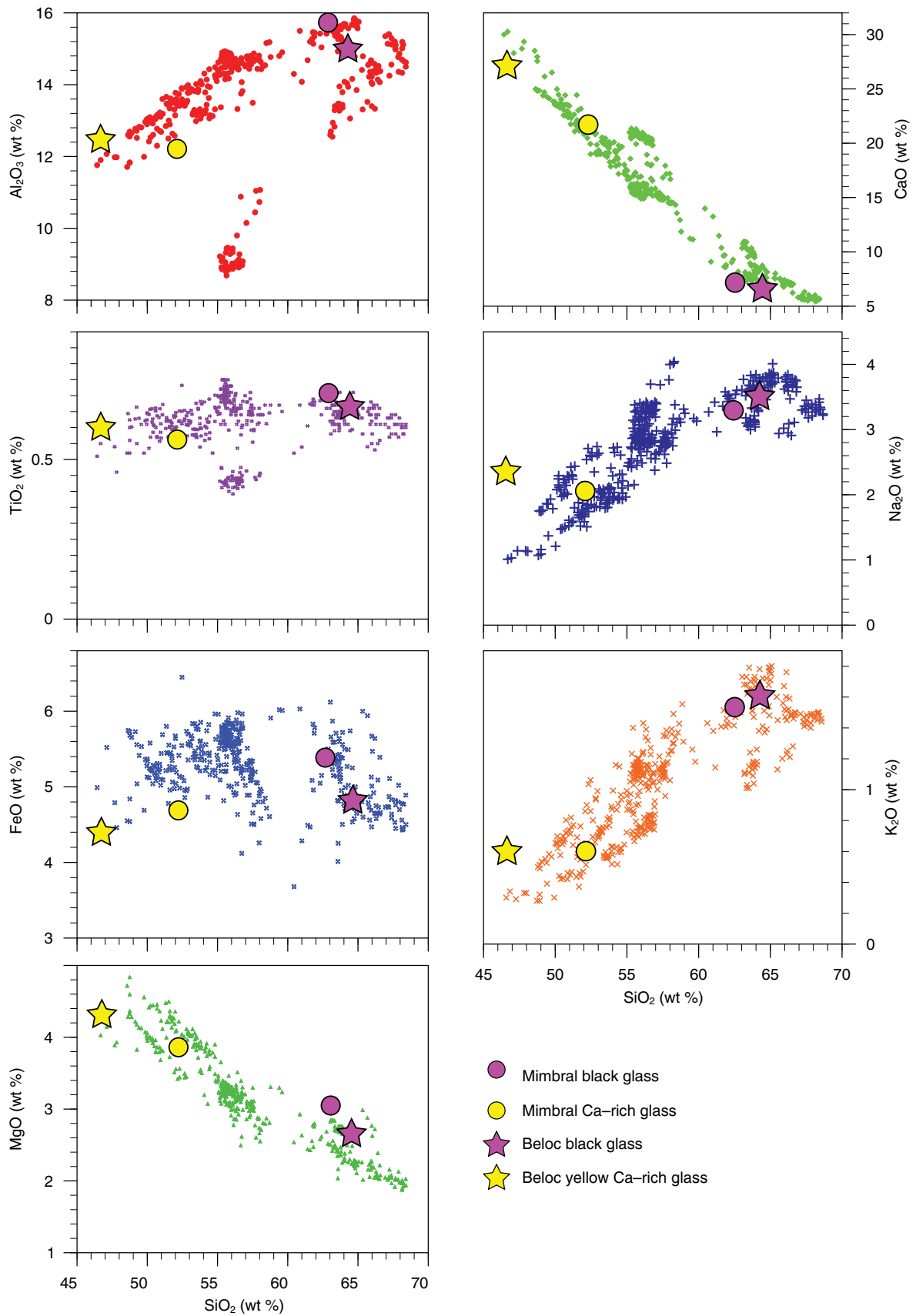


Figure 4. Harker diagrams of selected major and minor elements of the Gorgonilla Island glass spherules. For comparison, average compositions of glasses are shown from the Mimbral (Mexico) and Beloc (Haiti) sites, according to Glass & Simonson (2013). Data from Bermúdez et al. (2016).

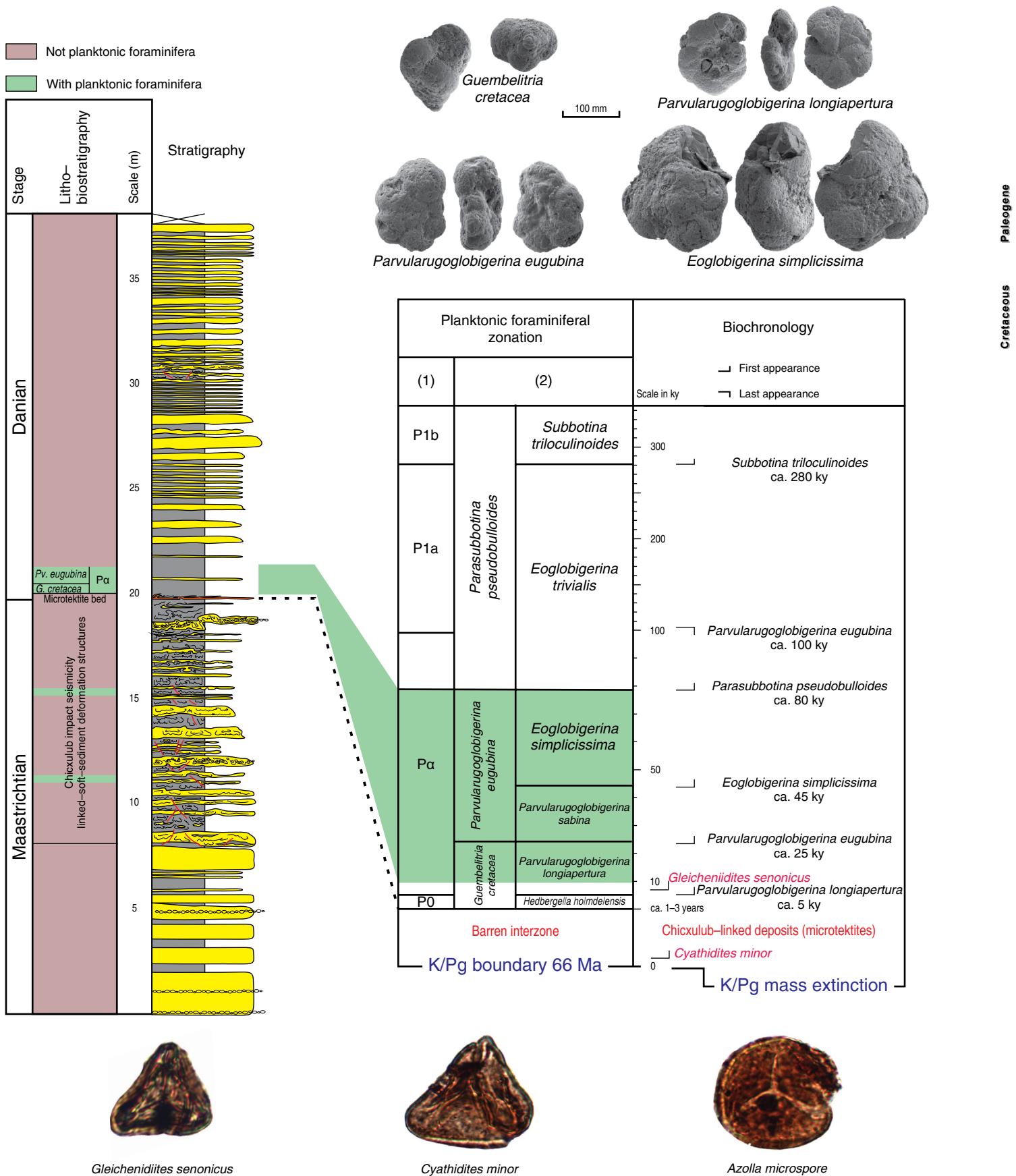


Figure 5. Planktic foraminiferal and palynological record in the Gorgonilla section. The green shading indicates stratigraphic intervals with preserved planktic foraminifera. (1) Zonation of Berggren & Pearson (2005). (2) Zonation of Arenillas et al. (2004).

Beloc (Glass & Simonson, 2013; Izett et al., 1991; Koeberl & Sigurdsson, 1992).

New micropaleontological and geochemical data confirm a K/Pg age for the spherule bed (Renne et al., 2018). The first Danian biozone (Zone P0) within planktic foraminiferan scales has not been recognized in Gorgonilla. If it were absent, we should infer that there is a small hiatus of no more than 10 ka, according to the biochronological scale of Arenillas et al. (2004). However, this short hiatus would not preclude the conclusion that the spherule bed is chronostratigraphically correlatable to the K/Pg boundary. Moreover, this hiatus could be a local taphonomic artifact in the planktic foraminiferal record. The absence of preserved calcareous microfossils (foraminifera) and the abundance of siliceous microfossils (radiolarians) suggest that the substrate was below the carbonate compensation depth (CCD) for much of the time interval recorded in the Gorgonilla section. Foraminiferans are absent in the 50 mm thick stratigraphic interval between the top of the spherule bed and the first sample with preserved planktic foraminifera, suggesting these sediments were still deposited below the CCD. The dissolution of the foraminiferan tests in this thin stratigraphic interval prevents the verification of whether Zone P0 is present or absent in Gorgonilla.

The fern spores, which only occur above the K/Pg boundary at Gorgonilla, are represented by ground fern taxa such as Gleicheniaceae and *Dictyophyllum*, together with the abundant occurrence of the aquatic fern *Azolla* (Renne et al., 2018). Interestingly, these cooccur with fungal spores and hyphae. A posited fungal spike has previously been described from a New Zealand K/Pg boundary clay coincident with the iridium-enriched layer and was interpreted as a response to short-term darkness (Vajda & McLoughlin, 2004; Vajda et al., 2015). The genus *Azolla* consistently characterizes warm-climate lacustrine environments and first appears in the geological record in Lower Cretaceous successions (Vajda, 1999; Vajda & McLoughlin, 2005). The ranges of many *Azolla* species span the K/Pg boundary and the identification of *Azolla* microspores and massulae in Colombia, directly following the K/Pg boundary event, which at the Gorgonilla locality is marked by the spherule bed (Bermúdez et al., 2016), shows their potential to endure altered environmental conditions. Aquatic ferns such as *Azolla* can reproduce asexually through vegetative regeneration in association with nitrogen-fixing cyanobacterial symbionts, which are shown to be abundant in the same samples. These characteristics provided an advantage in the aftermath of the Chicxulub impact and our results show that not only high-latitude settings but also low-latitude tropical environments were indeed affected by cooling and darkness.

The global pattern of recovery in the vegetation following the K/Pg mass extinction event is typified in North America (Schulte et al., 2010), Japan (Saito et al., 1986), and New Zea-

land (Vajda et al., 2001), by a posited fern-spike, an interval of short duration represented by a pioneering succession of ferns (Vajda & Bercovici, 2014). Although end-Cretaceous successions in Europe mainly represent marine depositional settings, the ecological collapse on land following the Chicxulub impact is also traceable in marine strata. In the Netherlands, for example, an anomalous abundance of bryophyte (moss) spores characterize the recovery community preserved within the basal part of the boundary clay (Brinkhuis & Schiøler, 1996; Hergreen et al., 1998). Here, we show the first evidence of post-impact recovery vegetation expressed by a fern-spike from the paleo-tropics.

The $^{40}\text{Ar}/^{39}\text{Ar}$ dating suggests the spherule age is 66.051 ± 0.031 Ma (Renne et al., 2018). This age is indistinguishable from the $^{40}\text{Ar}/^{39}\text{Ar}$ ages (66.038 ± 0.025 Ma) of the Haitian tektites and from the age (66.043 ± 0.010 Ma) of the K/Pg boundary (Renne et al., 2013). Thus, we conclude that the Gorgonilla spherules are tektites produced by the Chicxulub impact at the K/Pg boundary.

The uppermost Maastrichtian and the K/Pg boundary deposits at Gorgonilla were affected by intense soft-sediment deformation and bed disruption, and provide evidence for syn-depositional microfaulting and faulting, injectites, hydroplastic mixed layers, small-scale slumping, fault-graded beds, and pillar and flame structures. These features are found between undisturbed Maastrichtian and Danian sediments, including the spherule-rich bed (Bermúdez et al., 2015, 2017; Renne et al., 2018). They show the development of three different zones (soupy zone, rubble zone, and segmented zone) and make evident gradational contacts between these zones and the bottom, but with a sharp boundary at the top (Figure 6). These features are typical of seismites (Montenat et al., 2007; Obermeier, 1996; Seilacher, 1969).

The evidence indicates that the bed-disruption processes began slightly before but continued during the emplacement of the ejecta deposit. The ubiquitous and obvious deformation of the Maastrichtian sediments cannot be explained by differences in lithology between the Maastrichtian and Paleogene strata, local tectonism, or the paleogeographic setting, but must result from seismic activity produced by the single very-high-energy Chicxulub impact. Large-scale seismicity, including magnitude 10+ earthquakes, are a predicted consequence of this impact (e.g., Boslough et al., 1996; Pierazzo & Artemieva, 2012; Schulte et al., 2010, 2012; Shoemaker et al., 1990). Accordingly, soft-sediment deformation structures, chaotic sediments mixtures and disturbed beds, “shale diapirs”, injection structures, steeply to vertically inclined sedimentary beds, slumps, folds, microfaults and faults, steeply and chaotic seismic reflectors, etc. were reported from a variety of sections in Mexico, USA, the NW Atlantic Ocean, Caribbean, and the Gulf of Mexico (Figure 7); they have been explained as sediment liquefaction, platform collapse, large-scale slope failures, and

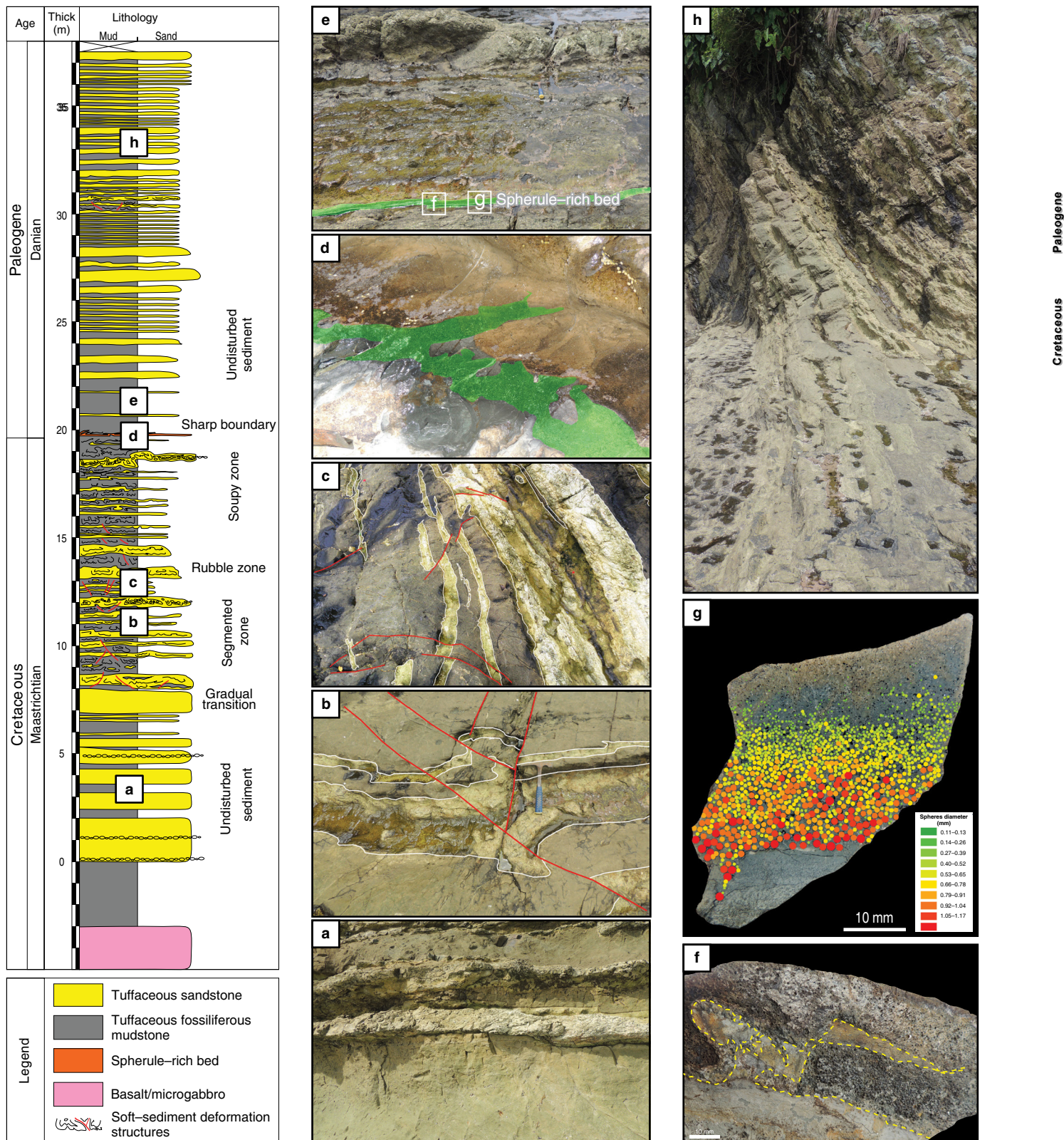


Figure 6. Stratigraphic section, illustrating the position of deformed zones and representative examples. **(a)** Maastrichtian undisturbed sediments, approximately 15 m below the K/Pg boundary. **(b)** Opposite vergent structures in the segmented zone, 10 m below the K/Pg boundary. **(c)** Rubble zone, 8 m below the K/Pg boundary, with predominance of plastic deformation in opposite directions, but with no major lateral transport. **(d)** Plastic deformation at the top of the soupy zone, involving the K/Pg spherule-rich bed. **(e)** Undisturbed sediments of the lowermost Danian, just above the K/Pg boundary. **(f-g)** Detail of the soft-sediment deformation in the K/Pg spherule-rich bed (f and g in Figure 6e). **(h)** Undisturbed sediments of the Danian, 12 m above the K/Pg boundary.

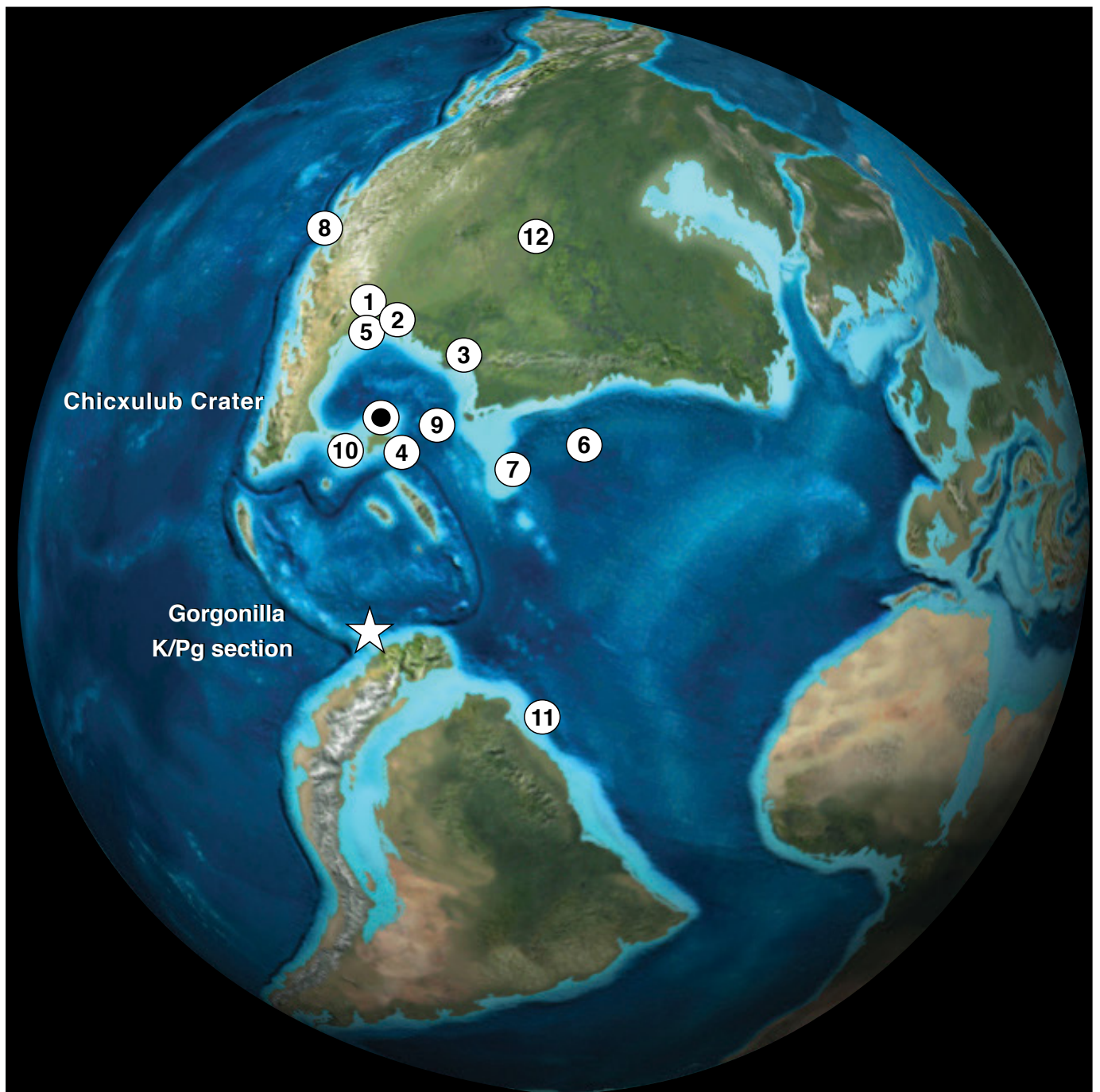


Figure 7. Paleogeographic map of key areas exhibiting evidence of Chicxulub impact-induced seismicity. **(1)** La Popa Basin, NE Mexico. **(2)** Brazos Texas, USA; NE Mexico (La Sierrita, Mimbral, El Toro sections). **(3)** Alabama, USA. **(4)** DSDP Sites 536 & 540, Gulf of Mexico. **(5)** El Tecolote, NE Mexico. **(6)** Bermuda Rise. **(7)** Black Nose. **(8)** Baja California, Mexico. **(9)** Gulf of Mexico. **(10)** SE Mexico. **(11)** Demerara Rise, South Atlantic. **(12)** South Dakota, USA. Source: Bermúdez et al. (2015).

catastrophic sedimentation by bolide impact-related seismic shocking (e.g., Arenillas et al., 2006; Arz et al., 2001, 2004; Bralower et al., 1998; Busby et al., 2002; Denne et al., 2013; Grajales–Nishimura et al., 2000; Klaus et al., 2000; MacLeod et al., 2007; Norris & Firth, 2002; Norris et al., 2000; Schulte et al., 2009, 2010, 2012; Smit et al., 1996; Soria et al., 2001; Stoffer et al., 2001).

Different from the situation in these proximal sections, the seismic energy did not cause erosion, slope failure, and severe reworking of fossils and lithologies of different ages at this study site (frequently known as the K/T (now K/Pg) “impact cocktail”; Bralower et al., 1998). Slope failure debris deposits or evident traction transport of sediments are not seen in the deformed Maastrichtian sequence at Gorgonilla (Bermúdez et

al., 2017). Even though intense ductile and brittle deformation reaches to 12 m below the ejecta bed, these sediments are still placed in their correct stratigraphic order, and the sequence appears structurally intact. The spherule bed, for instance, is continuous over a distance of more than 15 meters and does not show changes in thickness or texture. Soft sediment deformation at this deep ocean site, at approximately 2000–3000 km distance from Chicxulub impact site, thus resulted in in situ liquefaction and microfaulting of soft and semilithified sediments.

The presence of in situ deformed sediments in northern South America strengthens the evidence that seismic shaking generated by the impact, and possible aftershocks, represents a major geological event that affected the uppermost Maastrichtian sediments in a vast region; the seismic energy released was sufficient to affect localities more than 2000 km from the Chicxulub impact site (Renne et al., 2018). The interpretation of the K/Pg boundary deposits in areas proximal to the impact site should be revised with caution, since the effects of seismic deformation would affect the position and distribution of ejecta in the Chicxulub-linked clastic units (e.g., deposits of eventual collapse of continental shelves and/or associated tsunamites).

5. Conclusions

This study confirms the first evidence of Chicxulub ejecta deposits (K/Pg boundary) in Colombia, South America, and the eastern Pacific Ocean.

The Gorgonilla Island spherule bed is approximately 20 mm thick and consists of extraordinarily well-preserved glass spherules (microtektites and microkrystites) up to 1.1 mm in diameter.

The size, morphology, and chemical composition of these spherules are similar to Chicxulub spherule ejecta from North and Central America, and the Caribbean, but differ in their unrivaled excellent preservation (up to 90% of the spherules are still completely vitrified). The Gorgonilla spherule bed thus represents a deposit of the most pristine K/Pg boundary spherules known to date.

The ejecta deposit is normally graded, with no evidence for traction transport, subsequent reworking or bioturbation, and thus, indicates that the Gorgonilla spherules settled within a water column with minimal disturbance.

$^{40}\text{Ar}/^{39}\text{Ar}$ dating, geochemical, and micropaleontological analyses reveal that the Gorgonilla spherule bed resulted from the Chicxulub impact.

The basal deposits of the Danian in Gorgonilla Island demonstrate the first evidence of a recovery vegetation represented by ferns from a tropical habitat closely following the end-Cretaceous event.

The presence of intense soft-sediment deformation and bed disruption in Maastrichtian sediments of the Gorgonilla Island K/Pg section, provide proof for seismic activity triggered by

the Chicxulub bolide impact, and strengthens the evidence that seismic shaking generated by the meteorite collision, and possible aftershocks, represents a major geological event that affected the uppermost Maastrichtian sediments in a vast region.

Acknowledgments

We thank Francisco J. VEGA, and Wolfgang STINNESBECK for corrections and suggestions that significantly improved this manuscript. This research was supported by Grupo de Investigación Paleoexplorer (Paleoexplorer SAS, Colombia). Victoria Elena CORREDOR, Luz Stella BOLÍVAR, and Alejandro NUMPAQUE are acknowledged for their assistance in the 2014 geological campaign. We acknowledge Parques Nacionales Naturales de Colombia, particularly María Ximena ZORRILLA and Luis Fernando PAYÁN, for their support during the fieldwork and for granting access to Gorgona National Natural Park. We thank Liliana BOLÍVAR (CEO Paleoexplorer SAS), Wolfgang STINNESBECK, Mario TRIELOFF, Michael HANEL, Jens HOPP, and Winfried H. SCHWARZ (Heidelberg University), and Francisco J. VEGA (Universidad Nacional Autónoma de México) for their invaluable contribution to the 2016 report. For José ARZ, Ignacio ARENILLAS, and Vicente GILABERT this study is a contribution to project CGL2015–64422–P (MINECO/FEDER–UE) and is also partially supported by the Departamento de Educación y Ciencia of the Aragonian Government, co-financed by the European Social Fund (grant number DGA group E05). Vicente GILABERT acknowledges support from the Spanish Ministerio de Economía, Industria y Competitividad (FPI grant BES–2016–077800). P.R. was supported by the Ann and Gordon Getty Foundation. V.V. was supported by the Swedish Research Council (VR grant 2015–4264, and LUCCI, Lund University Carbon Cycle Centre).

References

- Albertão, G.A. & Martins, P.P. 1996. A possible tsunami deposit at the Cretaceous – Tertiary boundary in Pernambuco, Northeastern Brazil. *Sedimentary Geology*, 104(1–4): 189–201. [https://doi.org/10.1016/0037-0738\(95\)00128-X](https://doi.org/10.1016/0037-0738(95)00128-X)
- Albertão, G.A., De Azevedo-Grassi, A., Marini, F., Martins, P.P. & De Ross, L.F. 2004. The K–T boundary in Brazilian marginal sedimentary basins and related spherules. *Geochemical Journal*, 38(2): 121–128. <https://doi.org/10.2343/geochemj.38.121>
- Alvarez, L.W., Alvarez, W., Asaro, F. & Michel, H.V. 1980. Extraterrestrial cause for the Cretaceous – Tertiary extinction. *Science*, 208(4448): 1095–1108. <https://doi.org/10.1126/science.208.4448.1095>
- Arenillas, I., Arz, J.A. & Molina, E. 2004. A new high-resolution planktic foraminiferal zonation and subzonation for the lower Danian. *Lethaia*, 37(1): 79–95. <https://doi.org/10.1080/00241160310005097>

- Arenillas, I., Arz, J.A., Grajales–Nishimura, J.M., Murillo–Muñetón, G., Alvarez, W., Camargo–Zanoguera, A., Molina, E. & Rosales–Domínguez, C. 2006. Chicxulub impact event is Cretaceous/Paleogene boundary in age: New micropaleontological evidence. *Earth and Planetary Science Letters*, 249(3–4): 241–257. <https://doi.org/10.1016/j.epsl.2006.07.020>
- Arz, J.A., Alegret, L., Arenillas, I., Liesa, C., Molina, E. & Soria, A.R. 2001. Extinción de foraminíferos en el límite Cretácico/terciario en Coxquihui (México) y su relación con las evidencias de impacto. *Revista Española de Micropaleontología*, 33(2): 221–236.
- Arz, J.A., Alegret, L. & Arenillas, I. 2004. Foraminiferal biostratigraphy and paleoenvironmental reconstruction at the Yaxcopoil–1 drill hole, Chicxulub Crater, Yucatán Peninsula. *Meteoritics & Planetary Science*, 39(7): 1099–1111. <https://doi.org/10.1111/j.1945-5100.2004.tb01131.x>
- Berggren, W.A. & Pearson, P.N. 2005. A revised tropical to subtropical Paleogene planktonic foraminiferal zonation. *Journal of Foraminiferal Research*, 35(4): 279–298. <https://doi.org/10.2113/35.4.279>
- Bermúdez, H.D., Stinnesbeck, W., Bolívar, L., Rodríguez, J.V., García, J. & Vega, F.J. 2015. Paleosismos asociadas al límite K/Pg en la isla de Gorgonilla, Pacífico colombiano. XV Congreso Colombiano de Geología. Abstracts CD ROM, p. 1080.
- Bermúdez, H.D., García, J., Stinnesbeck, W., Keller, G., Rodríguez, J.V., Hanel, M., Hopp, J., Schwarz, W., Trieloff, M., Bolívar, L. & Vega, F.J. 2016. The Cretaceous – Paleogene boundary at Gorgonilla Island, Colombia, South America. *Terra Nova*, 28(1): 83–90. <https://doi.org/10.1111/ter.12196>
- Bermúdez, H.D., Arz, J.A., Renne, P.R., Arenillas, I., Gilabert, V., Rodríguez, J.V., Bolívar, L. & Bolívar, L.S. 2017. Evidence for Chicxulub impact seismicity at Gorgonilla Island K/Pg section, Pacific of Colombia. *Geological Society of America Abstracts with Programs*, 49(6). <https://doi.org/10.1130/abs/2017AM-299005>
- Boslough, M.B., Chael, E.P., Trucano, T.G., Crawford, D.A. & Campbell, D.L. 1996. Axial focusing of impact energy in the Earth's interior: A possible link to flood basalts and hotspots. In: Ryder, G., Fastovsky, D. & Gartner, S. (editors), *The Cretaceous – Tertiary event and other catastrophes in Earth history*. Geological Society of America, Special Paper 307, p. 541–550. <https://doi.org/10.1130/0-8137-2307-8.541>
- Bralower, T.J., Paull, C.K. & Leckie, R.M. 1998. The Cretaceous – Tertiary boundary cocktail: Chicxulub impact triggers margin collapse and extensive sediment gravity flows. *Geology*, 26(4): 331–334. [https://doi.org/10.1130/0091-7613\(1998\)026<0331:TCTBCC>2.3.CO;2](https://doi.org/10.1130/0091-7613(1998)026<0331:TCTBCC>2.3.CO;2)
- Brinkhuis, H. & Schiøler, P. 1996. Palynology of the Geulhemmerberg Cretaceous/Tertiary boundary section (Limburg, SE Netherlands). *Geologie en Mijnbouw*, 75(2): 193–213.
- Busby, C.J., Yip, G., Blikra, L. & Renne, P. 2002. Coastal landsliding and catastrophic sedimentation triggered by Cretaceous – Tertiary bolide impact: A Pacific margin example? *Geology*, 30(8): 687–690. [https://doi.org/10.1130/0091-7613\(2002\)030<0687:CLACST>2.0.CO;2](https://doi.org/10.1130/0091-7613(2002)030<0687:CLACST>2.0.CO;2)
- Denne, R.A., Scott, E.D., Eickhoff, D.P., Kaiser, J.S., Hill, R.J. & Spaw, J.M. 2013. Massive Cretaceous – Paleogene boundary deposit, deep–water Gulf of Mexico: New evidence for widespread Chicxulub–induced slope failure. *Geology*, 41(9): 983–986. <https://doi.org/10.1130/G34503.1>
- Dietrich, V.J., Gansser, A., Sommerauer, J. & Cameron, W.E. 1981. Palaeogene komatiites from Gorgona Island, East Pacific—A primary magma for ocean floor basalts? *Geochemical Journal*, 15(3): 141–161. <https://doi.org/10.2343/geochemj.15.141>
- Echeverría, L.M. & Aitken, B.G. 1986. Pyroclastic rocks: Another manifestation of ultramafic volcanism on Gorgona Island, Colombia. *Contributions to Mineralogy and Petrology*, 92(4): 428–436. <https://doi.org/10.1007/BF00374425>
- Gansser, A. 1950. Geological and petrographical notes on Gorgona Island in relation to north–western South America. *Schweizerische Mineralogische und Petrographische Mitteilungen*, 30: 219–237.
- Gansser, A., Dietrich, V.J. & Cameron, W.E. 1979. Palaeogene komatiites from Gorgona Island. *Nature*, 278: 545–546. <https://doi.org/10.1038/278545a0>
- Gertsch, B., Keller, G., Adatte, T. & Berner, Z. 2013. The Cretaceous – Tertiary boundary (KTb) transition in NE Brazil. *Journal of the Geological Society*, 170(2): 249–262. <https://doi.org/10.1144/jgs2012-029>
- Glass, B.P. & Simonson, B.M. 2013. *Distal impact ejecta layers: A record of large impacts in sedimentary deposits*. Springer, 716 p. Berlin. <https://doi.org/10.1007/978-3-540-88262-6>
- Grajales–Nishimura, J.M., Cedillo–Pardo, E., Rosales–Domínguez, M.C., Morán–Zenteno, D.J., Alvarez, W., Claeys, P., Ruiz–Morales, J., García–Hernández, J., Padilla–Avila, P. & Sánchez–Ríos, A. 2000. Chicxulub impact: The origin of reservoir and seal facies in the southeastern Mexico oil fields. *Geology*, 28(4): 307–310. [https://doi.org/10.1130/0091-7613\(2000\)28<307:CITOOOR>2.0.CO;2](https://doi.org/10.1130/0091-7613(2000)28<307:CITOOOR>2.0.CO;2)
- Herngreen, G.F.W., Schuurman, H.A.H.M., Verbeek, J.W., Brinkhuis, H., Burnett, J.A., Felder, W.M. & Kedves, M. 1998. Biostratigraphy of Cretaceous/Tertiary boundary strata in the Curfs quarry, the Netherlands. *Mededelingen Nederlands Instituut voor Toegepaste Geowetenschappen* (61), 58 p. Haarlem, the Netherlands.
- Hildebrand, A.R., Penfield, G.T., Kring, D.A., Pilkington, M., Camargo, A., Jacobsen, S.B. & Boynton, W.V. 1991. Chicxulub Crater: A possible Cretaceous/Tertiary boundary impact crater on the Yucatán Peninsula, Mexico. *Geology*, 19(9): 867–871. [https://doi.org/10.1130/0091-7613\(1991\)019<0867:CCAPCT>2.3.CO;2](https://doi.org/10.1130/0091-7613(1991)019<0867:CCAPCT>2.3.CO;2)
- Izett, G.A., Dalrymple, G.B. & Snee, L.W. 1991. $^{40}\text{Ar}/^{39}\text{Ar}$ age of Cretaceous – Tertiary boundary tektites from Haiti. *Science*, 252(5012): 1539–1542. <https://doi.org/10.1126/science.252.5012.1539>

- Keller, G. 2011. The Cretaceous – Tertiary mass extinction: Theories and controversies. In: Keller, G. & Adatte, T. (editors), *End-Cretaceous mass extinction and the Chicxulub impact in Texas*. Society for Sedimentary Geology, Special Publication 100, p. 7–22. Tulsa, USA. <https://doi.org/10.2110/sepmsp.100.007>
- Keller, G., Adatte, T., Stinnesbeck, W., Stüben, D. & Berner, Z. 2001. Age, chemo- and biostratigraphy of Haiti spherule-rich deposits: A multi-event K–T scenario. *Canadian Journal of Earth Sciences*, 38(2): 197–227. <https://doi.org/10.1139/e00-087>
- Keller, G., Stinnesbeck, W., Adatte, T. & Stüben, D. 2003a. Multiple impacts across the Cretaceous – Tertiary boundary. *Earth-Science Reviews*, 62(3–4): 327–363. [https://doi.org/10.1016/S0012-8252\(02\)00162-9](https://doi.org/10.1016/S0012-8252(02)00162-9)
- Keller, G., Stinnesbeck, W., Adatte, T., Holland, B., Stüben, D., Harting, M., De León, C. & De la Cruz, J. 2003b. Spherule deposits in Cretaceous – Tertiary boundary sediments in Belize and Guatemala. *Journal of the Geological Society*, 160(5): 783–795. <https://doi.org/10.1144/0016-764902-119>
- Keller, G., Adatte, T., Tantawy, A.A., Berner, Z., Stinnesbeck, W., Stüben, D. & Lanza, H.A. 2007. High stress late Maastrichtian – early Danian palaeoenvironment in the Neuquén Basin, Argentina. *Cretaceous Research*, 28(6): 939–960. <https://doi.org/10.1016/j.cretres.2007.01.006>
- Keller, G., Khozyem, H., Adatte, T., Malarkodi, N., Spangenberg, J. & Stinnesbeck, W. 2013. Chicxulub impact spherules in the North Atlantic and Caribbean: Age constraints and Cretaceous – Tertiary boundary hiatus. *Geological Magazine*, 150(5): 885–907. <https://doi.org/10.1017/S0016756812001069>
- Kennan, L. & Pindell, J.L. 2009. Dextral shear, terrane accretion and basin formation in the northern Andes: Best explained by interaction with a Pacific-derived Caribbean Plate? In: James, K.H., Lorente, M.A. & Pindell, J.L. (editors), *The origin and evolution of the Caribbean Plate*. Geological Society of London, Special Publication 328, p. 487–531. <https://doi.org/10.1144/SP328.20>
- Kerr, A.C. 2005. La isla de Gorgona, Colombia: A petrological enigma? *Lithos*, 84(1–2): 77–101. <https://doi.org/10.1016/j.lithos.2005.02.006>
- Kerr, A.C. & Tarney, J. 2005. Tectonic evolution of the Caribbean and northwestern South America: The case for accretion of two Late Cretaceous oceanic plateaus. *Geology*, 33(4): 269–272. <https://doi.org/10.1130/G21109.1>
- Klaus, A., Norris, R.D., Kroon, D. & Smit, J. 2000. Impact-induced mass wasting at the K–T boundary: Blake Nose, western North Atlantic. *Geology*, 28(4): 319–322. [https://doi.org/10.1130/0091-7613\(2000\)28<319:IMWATK>2.0.CO;2](https://doi.org/10.1130/0091-7613(2000)28<319:IMWATK>2.0.CO;2)
- Koeberl, C. & Sigurdsson, H. 1992. Geochemistry of impact glasses from the K/T boundary in Haiti: Relation to smectites and a new types of glass. *Geochimica et Cosmochimica Acta*, 56(5): 2113–2129. [https://doi.org/10.1016/0016-7037\(92\)90333-E](https://doi.org/10.1016/0016-7037(92)90333-E)
- MacLeod, K.G., Whitney, D.L., Huber, B.T. & Koeberl, C. 2007. Impact and extinction in remarkably complete Cretaceous – Tertiary boundary sections from Demerara Rise, tropical western North Atlantic. *Geological Society of America Bulletin*, 119(1–2): 101–115. <https://doi.org/10.1130/B25955.1>
- Montenat, C., Barrier, P., Ott-d’Estevou, P. & Hibsich, C. 2007. Seismites: An attempt at critical analysis and classification. *Sedimentary Geology*, 196(1–4): 5–30. <https://doi.org/10.1016/j.sedgeo.2006.08.004>
- Morgan, J., Lana, C., Kearsley, A., Coles, B., Belcher, C., Montanari, S., Díaz-Martínez, E., Barbosa, A. & Neumann, V. 2006. Analyses of shocked quartz at the global K–P boundary indicate an origin from a single, high-angle, oblique impact at Chicxulub. *Earth and Planetary Science Letters*, 251(3–4): 264–279. <https://doi.org/10.1016/j.epsl.2006.09.009>
- Norris, R.D. & Firth, J.V. 2002. Mass wasting of Atlantic continental margins following the Chicxulub impact event. In: Koeberl, C. & MacLeod, K.G. (editors), *Catastrophic events and mass extinctions: Impacts and beyond*. Geological Society of America, Special Paper 356, p. 79–95. <https://doi.org/10.1130/0-8137-2356-6.79>
- Norris, R.D., Huber, B.T. & Self-Trail, J. 1999. Synchronicity of the K–T oceanic mass extinction and meteorite impact: Blake Nose, western North Atlantic. *Geology*, 27(5): 419–422. [https://doi.org/10.1130/0091-7613\(1999\)027<0419:SOTK-TO>2.3.CO;2](https://doi.org/10.1130/0091-7613(1999)027<0419:SOTK-TO>2.3.CO;2)
- Norris, R.D., Firth, J., Blusztajn, J. & Ravizza, G. 2000. Mass failure of the North Atlantic margin triggered by the Cretaceous – Paleogene bolide impact. *Geology*, 28(12): 1119–1122. [https://doi.org/10.1130/0091-7613\(2000\)28<1119:mfotna>2.0.co;2](https://doi.org/10.1130/0091-7613(2000)28<1119:mfotna>2.0.co;2)
- Obermeier, S.F. 1996. Use of liquefaction-induced features for paleoseismic analysis—An overview of how seismic liquefaction features can be distinguished from other features and how their regional distribution and properties of source sediment can be used to infer the location and strength of Holocene paleo-earthquakes. *Engineering Geology*, 44(1–4): 1–76. [https://doi.org/10.1016/S0013-7952\(96\)00040-3](https://doi.org/10.1016/S0013-7952(96)00040-3)
- Ocampo, A.C., Pope, K.O. & Fischer, A.G. 1996. Ejecta blanket deposits of the Chicxulub Crater from Albion Island, Belize. In: Ryder, G., Fastovsky, D. & Gartner, S. (editors), *The Cretaceous – Tertiary event and other catastrophes in Earth history*. Geological Society of America, Special Paper 307, p. 75–88. Boulder, USA. <https://doi.org/10.1130/0-8137-2307-8.75>
- Olsson, R.K., Miller, K.G., Browning, J.V., Habib, D. & Sugarman, P.J. 1997. Ejecta layer at the Cretaceous – Tertiary boundary, Bass River, New Jersey (Ocean Drilling Program Leg 174AX). *Geology*, 25(8): 759–762. [https://doi.org/10.1130/0091-7613\(1997\)025<0759:ELATCT>2.3.CO;2](https://doi.org/10.1130/0091-7613(1997)025<0759:ELATCT>2.3.CO;2)
- Pierazzo, E. & Artemieva, N. 2012. Local and global environmental effects of impacts on Earth. *Elements*, 8(1): 55–60. <https://doi.org/10.2113/gselements.8.1.55>
- Pope, K.O., Ocampo, A.C. & Duller, C.E. 1991. Mexican site for K/T impact crater? *Nature*, 351: 105. <https://doi.org/10.1038/351105a0>

- Renne, P.R., Balco, G., Ludwig, K.R., Mundil, R. & Min, K. 2011. Response to the comment by W.H. Schwarz et al. on “Joint determination of ^{40}K decay constants and $^{40}\text{Ar}^*/^{40}\text{K}$ for the Fish Canyon sanidine standard, and improved accuracy for $^{40}\text{Ar}/^{39}\text{Ar}$ geochronology” by P.R. Renne et al. (2010). *Geochimica et Cosmochimica Acta*, 75(17): 5097–5100. <https://doi.org/10.1016/j.gca.2011.06.021>
- Renne, P.R., Deino, A.L., Hilgen, F.J., Kuiper, K.F., Mark, D.F., Mitchell, W.S., Morgan, L.E., Mundil, R. & Smit, J. 2013. Time scales of critical events around the Cretaceous – Paleogene boundary. *Science*, 339(6120): 684–687. <https://doi.org/10.1126/science.1230492>
- Renne, P.R., Arenillas, I., Arz, J.A., Gilabert, V. & Bermúdez, H.D. 2017. New $^{40}\text{Ar}/^{39}\text{Ar}$ and planktonic foraminiferal data indicate a KPB age for the Chicxulub-linked spherule bed at Gorgonilla Island, Pacific of Colombia. *Geological Society of America Abstracts with Programs*, 49(6). <https://doi.org/10.1130/abs/2017AM-299581>
- Renne, P.R., Arenillas, I., Arz, J.A., Vajda, V., Gilabert, V. & Bermúdez, H.D. 2018. Multi-proxy record of the Chicxulub impact at the Cretaceous – Paleogene boundary from Gorgonilla Island, Colombia. *Geology*, 46(6): 547–550. <https://doi.org/10.1130/G40224.1>
- Saito, T., Yamanoi, K. & Kaiho, K. 1986. End-Cretaceous devastation of terrestrial flora in the boreal Far East. *Nature*, 323: 253–255. <https://doi.org/10.1038/323253a0>
- Scasso, R.A., Concheyro, A., Kiessling, W., Aberhan, M., Hecht, L., Medina, F.A. & Tagle, R. 2005. A tsunami deposit at the Cretaceous/Paleogene boundary in the Neuquén Basin of Argentina. *Cretaceous Research*, 26(2): 283–297. <https://doi.org/10.1016/j.cretres.2004.12.003>
- Schulte, P., Deutsch, A., Salge, T., Berndt, J., Kontny, A., MacLeod, K.G., Neuser, R.D. & Krumm, S. 2009. A dual-layer Chicxulub ejecta sequence with shocked carbonates from the Cretaceous – Paleogene (K–Pg) boundary, Demerara Rise, western Atlantic. *Geochimica et Cosmochimica Acta*, 73(4): 1180–1204. <https://doi.org/10.1016/j.gca.2008.11.011>
- Schulte, P., Alegret, L., Arenillas, I., Arz, J.A., Barton, P.J., Bown, P.R., Bralower, T.J., Christeson, G.L., Claeys, P., Cockell, C.S., Collins, G.S., Deutsch, A., Goldin, T.J., Goto, K., Grajales-Nishimura, J.M., Grieve, R.A.F., Gulick, S.P.S., Johnson, K.R., Kiessling, W., Koeberl, C., Kring, D.A., MacLeod, K.G., Matsui, T., Melosh, J., Montanari, A., Morgan, J.V., Neal, C.R., Nichols, D.J., Norris, R.D., Pierazzo, E., Ravizza, G., Rebolledo-Vieyra, M., Reimold, W.U., Robin, E., Salge, T., Speijer, R.P., Sweet, A.R., Urrutia-Fucugauchi, J., Vajda, V., Whalen, M.T. & Willumsen, P.S. 2010. The Chicxulub asteroid impact and mass extinction at the Cretaceous – Paleogene boundary. *Science*, 327(5970): 1214–1218. <https://doi.org/10.1126/science.1177265>
- Schulte, P., Smit, J., Deutsch, A., Salge, T., Friese, A. & Beichel, K. 2012. Tsunami backwash deposits with Chicxulub impact ejecta and dinosaur remains from the Cretaceous – Paleogene boundary in the La Popa Basin, Mexico. *Sedimentology*, 59(3): 737–765. <https://doi.org/10.1111/j.1365-3091.2011.01274.x>
- Seilacher, A. 1969. Fault-graded beds interpreted as seismites. *Sedimentology*, 13(1–2): 155–159. <https://doi.org/10.1111/j.1365-3091.1969.tb01125.x>
- Serrano, L., Ferrari, L., López-Martínez, M., Petrone, C.M. & Jaramillo, C. 2011. An integrative geologic, geochronologic and geochemical study of Gorgona Island, Colombia: Implications for the formation of the Caribbean Large Igneous Province. *Earth and Planetary Science Letters*, 309(3–4): 324–336. <https://doi.org/10.1016/j.epsl.2011.07.011>
- Shoemaker, E.M., Wolfe, R.F. & Shoemaker, C.S. 1990. Asteroid and comet flux in the neighborhood of Earth. In: Sharpton, V.L. & Ward, P.D. (editors), *Global catastrophes in Earth history: An interdisciplinary conference on impacts, volcanism, and mass mortality*. Geological Society of America, Special Paper 247, p. 155–170. <https://doi.org/10.1130/SPE247-p155>
- Smit, J., Montanari, A., Swinburne, N.H.M., Alvarez, W., Hildebrand, A., Margolis, S.V., Claeys, P., Lowrie, W. & Asaro, F. 1992. Tektite-bearing, deep-water clastic unit at the Cretaceous – Tertiary boundary in northeastern Mexico. *Geology*, 20(2): 99–103. [https://doi.org/10.1130/0091-7613\(1992\)020<0099:TBDWCU>2.3.CO;2](https://doi.org/10.1130/0091-7613(1992)020<0099:TBDWCU>2.3.CO;2)
- Smit, J., Roep, T.B., Alvarez, W., Montanari, A., Claeys, P., Grajales-Nishimura, J.M. & Bermúdez, J. 1996. Coarse-grained, clastic sandstone complex at the K/T boundary around the Gulf of Mexico: Deposition by tsunami waves induced by the Chicxulub impact? In: Ryder, G., Fastovsky, D. & Gartner, S. (editors), *The Cretaceous – Tertiary event and other catastrophes in Earth history*. Geological Society of America, Special Paper 307, p. 151–182. <https://doi.org/10.1130/0-8137-2307-8.151>
- Soria, A.R., Liesa, C.L., Mata, M.P., Arz, J.A., Alegret, L., Arenillas, I. & Meléndez, A. 2001. Slumping and a sandbar deposit at the Cretaceous – Tertiary boundary in the El Tecolote section (northeastern Mexico): An impact-induced sediment gravity flow. *Geology*, 29(3): 231–234. [https://doi.org/10.1130/0091-7613\(2001\)029<0231:SAASDA>2.0.CO;2](https://doi.org/10.1130/0091-7613(2001)029<0231:SAASDA>2.0.CO;2)
- Stinnesbeck, W. & Keller, G. 1996. K/T boundary coarse-grained siliciclastic deposits in northeastern Mexico and northeastern Brazil: Evidence for mega-tsunami or sea-level changes? In: Ryder, G., Fastovsky, D. & Gartner, S. (editors), *The Cretaceous – Tertiary event and other catastrophes in Earth history*. Geological Society of America, Special Paper 307, p. 197–209. <https://doi.org/10.1130/0-8137-2307-8.197>
- Stinnesbeck, W., Keller, G., De la Cruz, J., De León, C., MacLeod, N. & Whittaker, J.E. 1997. The Cretaceous – Tertiary transition in Guatemala: Limestone breccia deposits from the South Petén Basin. *Geologische Rundschau*, 86(3): 686–709. <https://doi.org/10.1007/s005310050171>

Stinnesbeck, W., Keller, G., Schulte, P., Stüben, D., Berner, Z., Kra-mar, U. & López-Oliva, J.G. 2002. The Cretaceous – Tertiary (K/T) boundary transition at Coxquihui, state of Veracruz, Mexico: Evidence for an early Danian impact event? *Journal of South American Earth Sciences*, 15(5): 497–509. [https://doi.org/10.1016/S0895-9811\(02\)00079-2](https://doi.org/10.1016/S0895-9811(02)00079-2)

Stoffer, P.W., Messina, P., Chamberlain, J.A., Jr. & Terry, D.O., Jr. 2001. The Cretaceous – Tertiary boundary interval in Badlands National Park, South Dakota. U.S. Geological Survey, open–file report 01–56, 49 p. <https://doi.org/10.3133/ofr0156>

Vajda, V. 1999. Miospores from Upper Cretaceous – Paleocene strata in northwestern Bolivia. *Palynology*, 23(1): 181–196. <https://doi.org/10.1080/01916122.1999.9989527>

Vajda, V. & Bercovici, A. 2014. The global vegetation pattern across the Cretaceous – Paleogene mass extinction interval: A template for other extinction events. *Global and Planetary Change*, 122: 29–49. <https://doi.org/10.1016/j.gloplacha.2014.07.014>

Vajda, V. & McLoughlin, S. 2004. Fungal proliferation at the Cretaceous – Tertiary boundary. *Science*, 303(5663): 1489. <https://doi.org/10.1126/science.1093807>

Vajda, V. & McLoughlin, S. 2005. A new Maastrichtian – Paleocene *Azolla* species from of Bolivia, with a comparison of the global record of coeval *Azolla* microfossils. *Alcheringa: An Australasian Journal of Palaeontology*, 29(2): 305–329. <https://doi.org/10.1080/03115510508619308>

Vajda, V., Raine, J.I. & Hollis, C. 2001. Indication of global deforestation at the Cretaceous – Tertiary boundary by New Zealand fern spike. *Science*, 294(5547): 1700–1702. <https://doi.org/10.1126/science.1064706>

Vajda, V., Ocampo, A., Ferrow, E. & Bender–Koch, C. 2015. Nano particles as the primary cause for long–term sunlight suppression at high southern latitudes following the Chicxulub impact—Evidence from ejecta deposits in Belize and Mexico. *Gondwana Research*, 27(3): 1079–1088. <https://doi.org/10.1016/j.gr.2014.05.009>

Wigforss–Lange, J., Vajda, V. & Ocampo, A. 2007. Trace element concentrations in the Mexico–Belize ejecta layer: A link between the Chicxulub impact and the global Cretaceous – Paleogene boundary. *Meteoritics & Planetary Science*, 42(11): 1871–1882. <https://doi.org/10.1111/j.1945-5100.2007.tb00546.x>

Explanation of Acronyms, Abbreviations, and Symbols:

CCD	Carbonate compensation depth	SEM	Scanning electron microscope
K/Pg	Cretaceous/Paleogene		

Authors' Biographical Notes



Hermann Darío BERMÚDEZ is a senior Colombian geologist and director of Grupo de Investigación Paleoeexplorer. Although he is currently living in the United States, he continues to develop research projects focused on the geology of Colombia. He studied geology at the Universidad Nacional de Colombia (1995) and currently is working in his doctoral dissertation. For more than 25

years, he has studied the stratigraphy and paleontology of Colombia, especially the sedimentary sequences of the cordillera Oriental, Llanos, Magdalena Valley, Perijá, Sinú–San Jacinto, and Tumaco Basin. He serves as member of the Scientific Committee of Gorgona National Park, international editor of *Paleontología Mexicana*, and referee for the *Journal of South American Earth Sciences*. Currently his main research is focused on the study of the Gorgonilla Island K/Pg boundary section and the paleontology of crustaceans and mollusks of Colombia.



José Antonio ARZ is the vice dean for Quality and Teaching Innovation of the Faculty of Sciences and assistant professor in paleontology of the Department of Earth Sciences, Universidad de Zaragoza, Spain. He studied geology at the Universidad de Zaragoza, where he obtained his PhD degree in 1996, working on detailed studies on Upper Cretaceous biochronology and paleoenvironmental reconstruction with planktonic foraminifera. Since then, his main research has been focused on high-resolution micropaleontological analyses and their applications in biostratigraphy, paleoecology, paleoceanography, and paleoclimatology. He is particularly concerned with the study of geological and paleobiological events, such as the Chicxulub meteorite impact at the Cretaceous/Paleogene boundary and the Deccan Traps eruptions and oceanic anoxic events during the Late Cretaceous. For more than 20 years, he has studied the K/Pg boundary mass extinction event in sections around the world (Europe, North Africa, Gulf of Mexico–Caribbean, Argentina, and recently in Colombia). He has published more than 100 scientific articles, some of them in high-impact journals such as *Science*, *Nature Communications*, and *Geology*. He is coauthor of 4 new genera and 11 new species of Foraminifera. As a current member of the working groups of the International Subcommission on Cretaceous Stratigraphy, he has been involved in the definition of chronostratigraphic boundaries (GSSPs) of the Santonian and Maastrichtian. He has also been involved in projects such as the Chicxulub Scientific Drilling Project (IODP) and in others on Upper Cretaceous to Paleogene biochronology, paleoceanography, paleoclimatology, and mass extinction events.

about the history of the earth, life, ocean, and climate, his main research is focused on high-resolution studies in biostratigraphy, paleoecology, paleoceanography, and paleoclimatology. He is particularly concerned with the study of geological and paleobiological events, such as the Chicxulub meteorite impact and mass extinction of the Cretaceous/Paleogene boundary, as well as global warming (hyperthermal) events of the Paleocene and early Eocene. He has published more than 100 scientific articles (some in journals such as *Science*) and is coauthor of 5 new genera and 12 new species of Foraminifera. He served as editor of the journal *Geogaceta* and assistant editor of the *Revista Española de la Sociedad Geológica de España*. Additionally, he has participated in and led projects on micropaleontology of the Upper Cretaceous and Paleogene. Arenillas has also participated in working groups such as those of the Chicxulub Scientific Drilling Project (IODP), specifically regarding the multidisciplinary study of the Chicxulub meteorite impact at Cretaceous/Paleogene boundary, and those of the International Subcommission on Paleogene Stratigraphy for the definition of chronostratigraphic boundaries (GSSPs) such as the Paleocene/Eocene, Danian/Selandian, Selandian/Thanetian, and Bartonian/Priabonian boundaries.



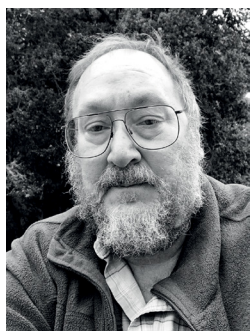
Ignacio ARENILLAS is assistant professor of micropaleontology in the Department of Earth Sciences, Universidad de Zaragoza, Spain. He studied geology at the Universidad de Zaragoza, where he obtained his PhD degree in 1996, specializing in Paleocene and Lower Eocene biochronology and paleoenvironmental reconstruction with planktonic foraminifera. Passionate

about the history of the earth, life, ocean, and climate, his main research is focused on high-resolution studies in biostratigraphy, paleoecology, paleoceanography, and paleoclimatology. He is particularly concerned with the study of geological and paleobiological events, such as the Chicxulub meteorite impact and mass extinction of the Cretaceous/Paleogene boundary, as well as global warming (hyperthermal) events of the Paleocene and early Eocene. He has published more than 100 scientific articles (some in journals such as *Science*) and is coauthor of 5 new genera and 12 new species of Foraminifera. He served as editor of the journal *Geogaceta* and assistant editor of the *Revista Española de la Sociedad Geológica de España*. Additionally, he has participated in and led projects on micropaleontology of the Upper Cretaceous and Paleogene. Arenillas has also participated in working groups such as those of the Chicxulub Scientific Drilling Project (IODP), specifically regarding the multidisciplinary study of the Chicxulub meteorite impact at Cretaceous/Paleogene boundary, and those of the International Subcommission on Paleogene Stratigraphy for the definition of chronostratigraphic boundaries (GSSPs) such as the Paleocene/Eocene, Danian/Selandian, Selandian/Thanetian, and Bartonian/Priabonian boundaries.



Vivi VAJDA is a Swedish paleontologist, professor, and head of the Paleobiology Department at the Swedish Museum of Natural History in Stockholm. She specializes in microscopic fossils, mostly pollen, spores, algae, and fungi from Earth's early history, with aims to resolve questions concerning the extinction and evolution of ecosystems related to major mass extinctions. By comparing the mag-

nitude of the extinctions, the timing of recovery and radiation traced in the fossil vegetation, her research answers several major questions concerning Earth's history. The results from her research on New Zealand K/Pg boundary localities have, for example, been instrumental in resolving the global consequences of the Chicxulub impact. She coordinates several research projects and is active in the geo-community. In 2010, she received the national "Geologist of the Year" award, has served as chair of the Geological Society of Sweden, as Swedish delegate of the European Federation of Geologists, and is presently the chair of the Swedish National Committee for Geology.



Paul R. RENNE was born in 1957 in San Antonio, Texas. He received his AB with highest honors in geology from the University of California, Berkeley, in 1982. He received his PhD in Geology from the University of California at Berkeley in 1987. After a postdoctoral fellowship at Princeton University, he returned to Berkeley in 1990 as a research associate at the Institute of

Human Origins and became director of Geochronology in 1991. He was the founding director of the Berkeley Geochronology Center in 1994 and has served in that role (and as board president) since then, with a hiatus from 2000 to 2003. In 1995, Renne was appointed adjunct professor in the Earth and Planetary Science Department at U.C. Berkeley, where he teaches courses in petrology, geochronology, and field geology and serves as formal research advisor to graduate and postdoctoral students. Renne specializes in $^{40}\text{Ar}/^{39}\text{Ar}$, geochronology and paleomagnetism applied to broad topics in the evolution of Earth's biosphere and lithosphere and to the relationships between these and extraterrestrial processes such as meteoroid impacts in the inner solar system. He is also heavily engaged in the refinement of the methodologies for these techniques. Renne's contributions are recognized by his election as a Fellow of the Geological Society of America, the American Geophysical Union, and the American Association for the Advancement of Science.



Vicente GILABERT is a PhD student of micropaleontology in the Department of Earth Sciences, Universidad de Zaragoza, Spain. His doctoral thesis and research pertain to the Cretaceous/Paleogene mass extinction event, using the planktonic foraminifera as proxies. His work is focused on the planktonic foraminifera assemblage turnovers and extinctions across the Cretaceous/

Paleogene boundary, as well as their possible relationship with both the Chicxulub meteorite impact and the Deccan Traps eruptions. GILABERT obtained his degree in geology from the Universidad de Zaragoza in 2013 and a MS in geology in 2015. His master's thesis focused on biostratigraphy with planktonic foraminifera of the Upper Cretaceous of Zumaia (Basque Country, Spain), which served as the starting point of his current research career. In 2016, he obtained a predoctoral contract from the Ministry of Economy, Industry, and Competitiveness of Spain, and he also joined the micropaleontology research group of the Universidad de Zaragoza. Although he is an early-stage researcher, GILABERT has already published several scientific articles, participated in national and international conferences, and is coauthor of 3 new species of Foraminifera.



José Vicente RODRÍGUEZ received a BSc in geology and a MEng in materials from the Universidad Nacional de Colombia. He has vast first-hand knowledge of Colombian geology, which stems from extensive fieldwork experience including geological mapping, stratigraphy, and sampling in Colombia. He also has lab expertise on sedimentological core studies of Colombian Cretaceous rocks and on magnetic fabric studies of igneous rocks. His most relevant and recent work is related to participation in the discovery of a section within the Cretaceous/Paleogene boundary (K/Pg) at Gorgonilla Island.

ceous rocks and on magnetic fabric studies of igneous rocks. His most relevant and recent work is related to participation in the discovery of a section within the Cretaceous/Paleogene boundary (K/Pg) at Gorgonilla Island.

Chapter 2



Formation and Evolution of the Lower Magdalena Valley Basin and San Jacinto Fold Belt of Northwestern Colombia: Insights from Upper Cretaceous to Recent Tectono–Stratigraphy

Josué Alejandro MORA-BOHÓRQUEZ^{1*}, Onno ONCKEN²,
Eline LE BRETON³, Mauricio IBAÑEZ-MEJIA⁴, Gabriel VELOZA⁵,
Andrés MORA⁶, Vickye VÉLEZ⁷, and Mario DE FREITAS⁸

Abstract Using a regional geological and geophysical dataset, we reconstructed the stratigraphic evolution of the Lower Magdalena Valley Basin and San Jacinto fold belt of northwestern Colombia. Detailed interpretations of reflection seismic data and new geochronology analyses reveal that the basement of the Lower Magdalena Basin is the northward continuation of the basement terranes of the northern Central Cordillera and consists of Permian – Triassic metasedimentary rocks intruded by Upper Cretaceous granitoids. Structural analyses suggest that the NE–SW strike of faults in basement rocks underlying the northeastern Lower Magdalena is inherited from a Jurassic rifting event, while the ESE–WNW striking faults in the western part originated from a Late Cretaceous to Eocene strike–slip and extensional episode. The Upper Cretaceous to lower Eocene sedimentary rocks preserved in the present-day San Jacinto fold belt were deposited in a submarine, forearc basin formed during the coeval oblique convergence between the Caribbean and South American Plates. A lower to middle Eocene angular unconformity at the top of the upper Paleocene to lower Eocene San Cayetano Sequence, the termination of the activity of the Romeral Fault System, and the cessation of arc magmatism are all interpreted to indicate the onset of low-angle orthogonal subduction of the Caribbean Plateau beneath South America between 56 and 43 Ma. Flat subduction of the plateau has continued to the present and would be the main cause of amagmatic post–Eocene deposition and formation of the Lower Magdalena Valley forearc basin. Extensional reactivation of inherited, pre–Oligocene basement faults was crucial for the tectonic segmentation of the basin and the formation of its two depocenters (Plato and San Jorge). Late Oligocene to early Miocene fault-controlled subsidence allowed initial infill of the Lower Magdalena, while uplift of Andean terranes made possible the connection of the Lower and Middle Magdalena Valleys, and the formation of the largest Colombian drainage system (Magdalena River system). This drainage system started delivering enormous amounts of sediments in middle Miocene times, as fault-controlled subsidence was gradually replaced by sedimentary

<https://doi.org/10.32685/pub.esp.37.2019.02>
Published online 26 November 2020

- 1 alejandro.mora@hocol.com.co
Hocol S.A.
Vicepresidencia de Exploración
Carrera 7 n.º 113–46, piso 16
Bogotá, Colombia
 - 2 onno.oncken@gfz-potsdam.de
Deutsches GeoForschungsZentrum GFZ
Telegrafenberg 14473
Potsdam, Germany
 - 3 eline.lebreton@fu-berlin.de
Freie Universität Berlin
Institute of Geological Sciences
Malteserstraße 74–100, D-12249
Berlin, Germany
 - 4 ibanezm@arizona.edu
Department of Geosciences
University of Arizona
Tucson, Arizona, 85721, USA
 - 5 gabriel.veloza@hocol.com.co
Hocol S.A.
Vicepresidencia de Exploración
Carrera 7 n.º 113–46, piso 16
Bogotá, Colombia
 - 6 andres.mora@ecopetrol.com.co
Ecopetrol S.A.
Vicepresidencia de Exploración
Bogotá, Colombia
 - 7 vickyvelez@hocol.com.co
Hocol S.A.
Vicepresidencia de Exploración
Carrera 7 n.º 113–46, piso 16
Bogotá, Colombia
 - 8 defreitas.mario@gmail.com
Caravela Energy
Bogotá, Colombia
- * Corresponding author

Supplementary Information:

S: <https://www2.sgc.gov.co/LibroGeologiaColombia/tgc/sgcpubesp37201902s.pdf>

Citation: Mora–Bohórquez, J.A., Oncken, O., Le Breton, E., Ibañez–Mejía, M., Veloza, G., Mora, A., Vélez, V. & De Freitas, M. 2020. Formation and evolution of the Lower Magdalena Valley Basin and San Jacinto fold belt of northwestern Colombia: Insights from Upper Cretaceous to recent tectono–stratigraphy. In: Gómez, J. & Mateus–Zabala, D. (editors), *The Geology of Colombia, Volume 3 Paleogene – Neogene*. Servicio Geológico Colombiano, Publicaciones Geológicas Especiales 37, p. 21–66. Bogotá. <https://doi.org/10.32685/pub.esp.37.2019.02>

loading. Such dramatic increase in sedimentation and the huge volume of sediment being delivered to the trench caused the formation of forearc highs in San Jacinto and of an accretionary prism farther to the west. Our results highlight the fundamental role of plate kinematics, inherited basement structure, and sediment flux on the evolution of forearc basins such as the Lower Magdalena and San Jacinto.

Keywords: *forearc basin, basement, flat-slab subduction, tectono-stratigraphy, Lower Magdalena, San Jacinto fold belt, Caribbean, subsidence, sedimentation.*

Resumen Utilizando una base de datos regional de geología y geofísica reconstruimos la evolución estratigráfica de la Cuenca del Valle Inferior del Magdalena y del cinturón plegado de San Jacinto al noroeste de Colombia. Interpretaciones detalladas de sísmica de reflexión y nuevos análisis geocronológicos revelan que el basamento de la Cuenca del Magdalena Inferior es la continuación hacia el norte de terrenos de basamento del norte de la cordillera Central y consiste en rocas metasedimentarias del Pérmico–Triásico intruidas por granitoides del Cretácico Superior. Análisis estructurales sugieren que el patrón NE–SW de fallas de basamento en el noreste del Magdalena Inferior es heredado de un evento de *rifting* jurásico, mientras que el patrón ESE–WNW de la parte oeste es heredado de un episodio Cretácico Tardío a Eoceno caracterizado por deformación de rumbo y extensión. Los sedimentos del Cretácico Superior a Eoceno inferior que se encuentran preservados en el actual cinturón de San Jacinto fueron depositados en una cuenca marina de antearco formada durante la convergencia oblicua entre las placas del Caribe y de Suramérica. Una discordancia angular del Eoceno inferior a medio al tope de la secuencia San Cayetano del Paleoceno–Eoceno inferior, la terminación de la actividad del Sistema de Fallas de Romeral y el cese del magmatismo de arco se interpretan como indicativos del comienzo de la subducción ortogonal y de bajo ángulo del *Plateau* del Caribe bajo Suramérica entre 56 y 43 Ma. La subducción plana del *plateau* ha continuado hasta el presente y sería la causa del depósito pos–Eoceno y la formación del Valle Inferior del Magdalena con ausencia de magmatismo. La reactivación extensional de fallas heredadas de basamento preoligocenas fue crucial para la segmentación tectónica de la cuenca y la formación de sus dos depocentros (Plato y San Jorge). La subsidencia controlada por fallas entre el Oligoceno Tardío y el Mioceno temprano permitió el llenado inicial del Magdalena Inferior, mientras que pulsos de levantamiento coetáneos en terrenos andinos posibilitaron la conexión de los valles Inferior y Medio del Magdalena, y la formación del sistema de drenaje más grande de Colombia (sistema del río Magdalena). Este sistema de drenaje comenzó a aportar grandes cantidades de sedimento en el Mioceno medio, a medida que la subsidencia controlada por fallas fue reemplazada por subsidencia debido a la carga sedimentaria incremental. Este dramático incremento en sedimentación y los grandes volúmenes de sedimento a la fosa causaron la formación de altos de antearco en San Jacinto y de un prisma de acreción más al oeste. Nuestros resultados resaltan el papel fundamental de la cinemática de placas, de la estructura heredada del basamento y del aporte de sedimentos en la evolución de cuencas de antearco como el Magdalena Inferior y San Jacinto.

Palabras clave: *cuenca de antearco, basamento, subducción plana, tectonoestratigrafía, Magdalena Inferior, cinturón de San Jacinto, Caribe, subsidencia, sedimentación.*

1. Introduction

The formation and evolution of the Lower Magdalena Valley Basin (LMV) and San Jacinto fold belt (SJFB) of northwestern Colombia (Figure 1) have not only been influenced by the interaction between the Caribbean and South American Plates

and the Chocó–Panamá Block, but also by the uplift of different provinces within the northern Andes and the evolution of related drainage systems. Though these provinces have been the focus of several previous, important research studies (Duque–Caro, 1979, 1984, 1991; Reyes–Harker et al., 2000; Cerón et al., 2007; Mantilla–Pimiento, 2007; Mantilla–Pimiento et al.,

2009; Bernal–Olaya et al., 2015a, 2015b, 2015c), there continues to be an active debate in certain fundamental aspects, such as the origin and classification of the basins (Cerón et al., 2007; Bernal–Olaya et al., 2015c). Hydrocarbon exploration, reflection–seismic, borehole drilling, and earthquake seismology and tomography in the LMV has led to a better understanding of its formation and evolution, whereas the San Jacinto fold belt has remained less understood due to intense deformation and scarcity of data. Several litho–tectonic provinces and terranes have been proposed in northern Colombia based on outcrop studies (Etayo–Serna et al., 1983; Toussaint & Restrepo, 1994; Cediel et al., 2003), but their extension and geometry beneath sedimentary basins such as the LMV and SJFB has remained speculative. Concerning the sedimentary succession, previous studies have described in some detail the stratigraphy and paleogeography of San Jacinto (e.g., Duque–Caro, 1979, 1991; Guzmán, 2007; Guzmán et al., 2004) and the LMV (e.g., Reyes–Harker et al., 2000; Bernal–Olaya et al., 2015c), and though they discuss their possible origin, they do not link their stratigraphic and paleo–geographic models with plate tectonic kinematics and Andean uplift events in NW South America.

The main goal of this contribution is to characterize the LMV and San Jacinto Basins in terms of their mechanisms of formation, evolution, and present configuration, through the integration of a regional geological and geophysical database provided by Hocol S.A. (Figure 2). The basement underneath the LMV was characterized, based on the integration of a regional subsurface database, which included geochronologic analyses of borehole samples in combination with outcrop data from the literature (Figure 3; Mora et al., 2017a). Then, the tectono–stratigraphy of Upper Cretaceous to Eocene sequences in the forearc basin that today corresponds to the SJFB was studied, linking them with the plate tectonic kinematics (Mora et al., 2017b). Finally, the Oligocene to recent tectono–stratigraphic sequences in the LMV were studied, and the subsidence, extension, sedimentation, and paleo–geographic history of the basin was reconstructed, proposing possible mechanisms controlling its evolution (Mora et al., 2018). It will be shown here that while Late Cretaceous to Eocene kinematics of the Caribbean and South American Plates controlled the evolution of the San Jacinto Forearc Basin and left a clear imprint on its stratigraphy, Oligocene to recent stratigraphy and evolution of the Lower Magdalena forearc were apparently more influenced by changes in the hinterland, such as the uplift of the Andes and the formation of the proto–Magdalena and Cauca River systems. The influence of inherited basement faults, sediment flux, flat subduction, and underplating processes in forearc basin evolution will be discussed.

2. Geological Framework

The LMV and SJFB of northwestern Colombia are located in an area in which the Caribbean oceanic plate, including the Chocó–

Panamá Block, and the South American continental plate have been interacting throughout the Cenozoic (Figure 1). Though there has been some debate about the occurrence of flat–subduction of the Caribbean Plate under South America, beneath the LMV and SJFB (e.g., Rosello & Cossey, 2012), GPS data have shown (e.g., Müller et al., 1999; Trenkamp et al., 2002; Boschman et al., 2014; Matthews et al., 2016) that NW South America and the Caribbean are converging in a nearly orthogonal fashion (Symithe et al., 2015). Furthermore, seismicity data indicates the existence of a Benioff zone in the eastern LMV (Bernal–Olaya et al., 2015a; Syracuse et al., 2016; Mora et al., 2017a, 2017b), while geophysical studies including tomography data (Mantilla–Pimiento, 2007; Mantilla–Pimiento et al., 2009; Bernal–Olaya et al., 2015a), have provided new and more robust evidence supporting a flat–subduction geometry. Hence, there is agreement between the results and interpretations of this study and previous proposals (e.g., Mantilla–Pimiento et al., 2009), which consider the LMV as a forearc basin within a convergent margin where flat–slab subduction is operational (Bernal–Olaya et al., 2015a, 2015b, 2015c).

The present–day SJFB is a NNE–SSW–trending and WNW–verging fold and thrust belt located between the LMV to the E and the Sinú accretionary prism to the W. The SJFB covers an area of 17 500 km², it is ca. 370 km long, 40 to 57 km wide, and it is limited by the Romeral Fault System (RFS) to the E and by the Sinú Fault to the W. The LMV is a lozenge–shaped basin, covering an area of 42 000 km², located between two major basement terranes, the northern Central Cordillera (CC) in the S and SE and the Sierra Nevada de Santa Marta (SNSM) in the NE (Figures 1–3). The Santa Marta left–lateral, strike–slip fault is separating the northeastern part of the basin from the SNSM, while the northern extension of the Romeral Fault System (RFS) is separating the Lower Magdalena from the SJFB to the west. Pre–Oligocene sedimentary units are exposed in the SJFB, which has been considered the northward extension of the Western Cordillera of Colombia (Barrero et al., 1969; Duque–Caro, 1979, 1984; Cediel et al., 2003) and has been related to an oceanic to transitional–type basement. The RFS, which is also considered to continue from the south to form the western boundary of the LMV, separates the oceanic to transitional basement under the belt from the felsic continental basement of the South American crust, which floors the LMV in the east (Duque–Caro, 1979, 1984; Flinch, 2003; Mora et al., 2017a). In the SJFB, located west of the RFS, there are Upper Cretaceous to Eocene sedimentary units that are not preserved in the LMV to the east (Duque–Caro, 1979, 1984; Mora et al., 2017b). By contrast, Oligocene to recent units have been mostly eroded in the SJFB and are well preserved in the LMV (Figures 4 and 5).

3. Materials and Methods

This chapter summarizes the main results of previous work presented in recent publications (Mora et al., 2017a, 2017b, 2018).

Figure 1. (a) Tectonic map of northwestern South America with topography and bathymetry, showing the location of the Lower Magdalena Valley Basin (LMV) and the Sinú–San Jacinto fold belt (SSJFB). Present-day tectonic plate motions are shown in yellow (after Trenkamp *et al.*, 2002). **(b)** Geological map of the Lower Magdalena Valley Basin and San Jacinto fold belt (Gómez *et al.*, 2015), showing major structural and morphologic features. (OF) Oca Fault; (SNSM) Sierra Nevada de Santa Marta; (SMF) Santa Marta Fault; (BoF) Boconó Fault; (PFS) Palestina Fault System; (WC) Western Cordillera; (CC) Central Cordillera; (MMV) Middle Magdalena Valley; (BF) Bucaramanga Fault; (EC) Eastern Cordillera; (RFS) Romeral Fault System; (CF) Cuisa Fault; (SiF) Sinú Fault; (UF) Uramita Fault.

Hocol S.A. provided the regional database that was used in this study, with reflection–seismic and drillhole data, for the interpretation of the structure of the basement in the LMV and for the construction of the tectono–stratigraphic framework of the SJFB and LMV (Figures 2–5). Regional data of potential methods (Bouguer gravity and magnetics; Figure 6) was also used to constrain the basement depth and configuration, as well as publicly available seismicity data from the Red Sismológica Nacional (RSNC) of the Servicio Geológico Colombiano (<https://www.datos.gov.co/Minas-y-Energ-a/Estaciones-Red-Sismol-gica-Nacional-de-Colombia-Se/sefu-3xqc/data>), to study the lithospheric configuration of NW Colombia. More than 30 000 km of 2D and more than 2000 km² of 3D–reflection–seismic data were interpreted in two–way–time (TWT), all of which were tied to most of the ca. 400 wells that have been drilled in the basin. New zircon U–Pb geochronology and Hf isotope geochemistry results from basement and sedimentary borehole samples were integrated and analyzed. We have based our interpretations in the biostratigraphic data and charts that Duque–Caro (1979, 1984, 1991, 2000, 2001, 2010, 2014) has constructed for the LMV and SJFB (Figures 4 and 5), based on previous planktonic foraminiferal zonations (Blow, 1969; Petters & Sarmiento, 1956).

Interpretation in TWT of the top of the acoustic basement, the main unconformities, and the tops of the main sequences in the LMV and SJFB, was done using Schlumberger’s Petrel seismic interpretation package, provided by Hocol S.A. After performing well–seismic ties, these horizons were mapped in TWT and depth–converted. In order to reconstruct the basin paleo–geography, seismic–stratigraphic analyses were carried out to define stratal stacking patterns, terminations, and contacts (Catuneanu *et al.*, 2009), and integrate the well data (electrical logs, cores, and reports). Paleo–tectonic reconstructions from Late Cretaceous to recent were done using the open access software package GPlates (version 2.0.0, www.gplates.org; Boyden *et al.*, 2011) and two paleo–tectonic models available for this area (Boschman *et al.*, 2014; Matthews *et al.*, 2016 from the GPlates database). Based on such reconstructions, convergence velocities and obliquities were calculated at different time windows, in order to correlate them with plate kinematics, subsidence patterns, sedimentation rates, and the main regional Andean tectonic events.

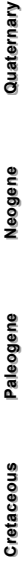
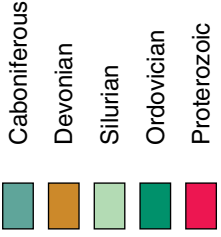
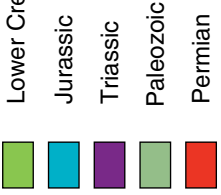
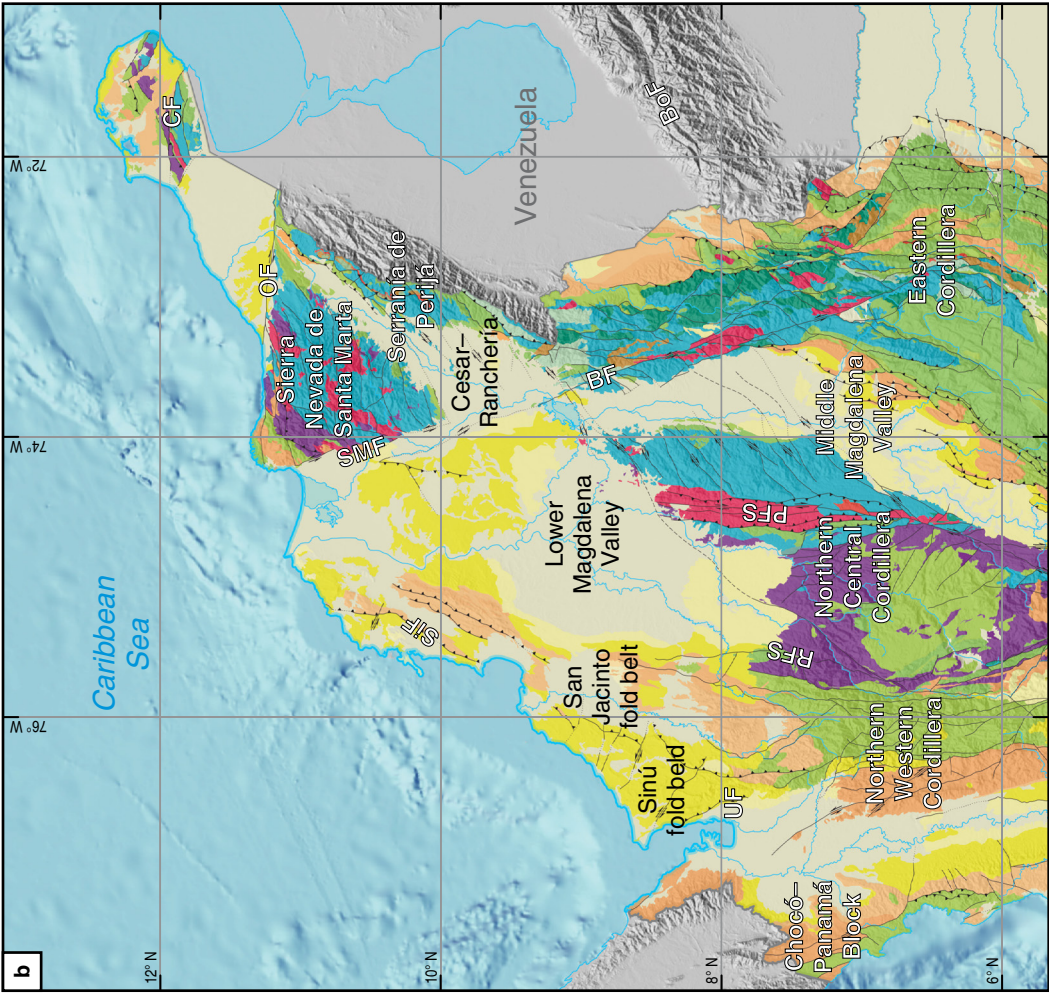
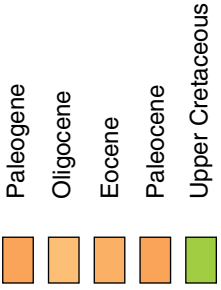
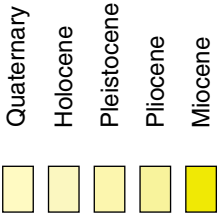
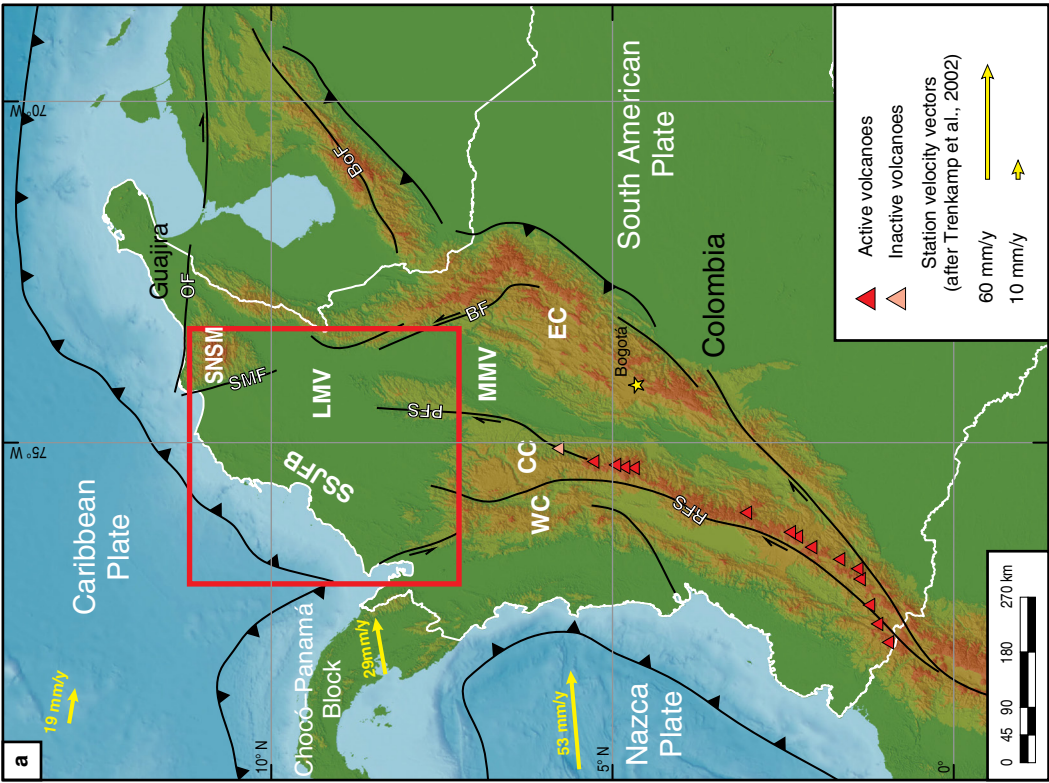
In the LMV, 1D geohistory and subsidence analyses (Allen & Allen, 2005; Steckler & Watts, 1978; Watts & Ryan, 1976) were carried out with data from 32 representative wells in dif-

ferent parts of the basin, including the San Jacinto fold belt, and from 12 wells drilled in the Sinú onshore and offshore accretionary prism (Mora *et al.*, 2018). Three different approaches were followed in order to obtain well–supported extension estimates for the crust beneath the LMV (Mora *et al.*, 2018). The first approach was to do a simple line–length calculation using a NNE–SSW–trending, depth–converted structural cross–section, which we built in the Move software of Midland Valley. The second approach was a backstripping technique assuming an Airy isostasy model and using sediment thickness data from the drill holes, in order to construct the total versus tectonic subsidence curves and to obtain the stretching factor (β factor, McKenzie, 1978). The third approach was to compile crustal thickness and Moho depth data from NW Colombia (e.g., Bernal–Olaya *et al.*, 2015a; Poveda *et al.*, 2015) and use our basin floor (basement) depth map to obtain the crustal thickness beneath the LMV, after removing the sedimentary infill. Of the three approaches, the third one implies less error, while the line–length balancing method considerably underestimates the amounts of extension. The calculation of the amount of stretching (β factor, McKenzie, 1978) is used in basins with a fast initial fault–related “synrift” subsidence, followed by a slower thermal “post–rift” subsidence. Therefore, the application of this methodology to basins that show different subsidence curves, such as the LMV as will be discussed farther on, can lead to an overestimation of the amount of stretching.

4. Results

4.1. Potential Methods and Reflection Seismic

Initial analyses of the LMV and SJFB basement configuration involved potential methods and the comparison with the depth–converted basement map obtained from regional reflection seismic data (Figures 2 and 3; Mora *et al.*, 2017a). In the Total Bouguer gravity anomaly map (Figure 6a), the most notorious basement lows are marked by negative gravity anomalies, while the most prominent positive gravity anomaly occurs in the SNSM, a very high (>5000 m) basement massif that is not in isostatic equilibrium (Case & MacDonald, 1973). While the gravity data provided a much broader image of the basement morphology, the data from the total magnetic intensity reduced to the pole (TMIRP; Figure 6b) shows more localized concentrations of highly–magnetic rocks which correspond to



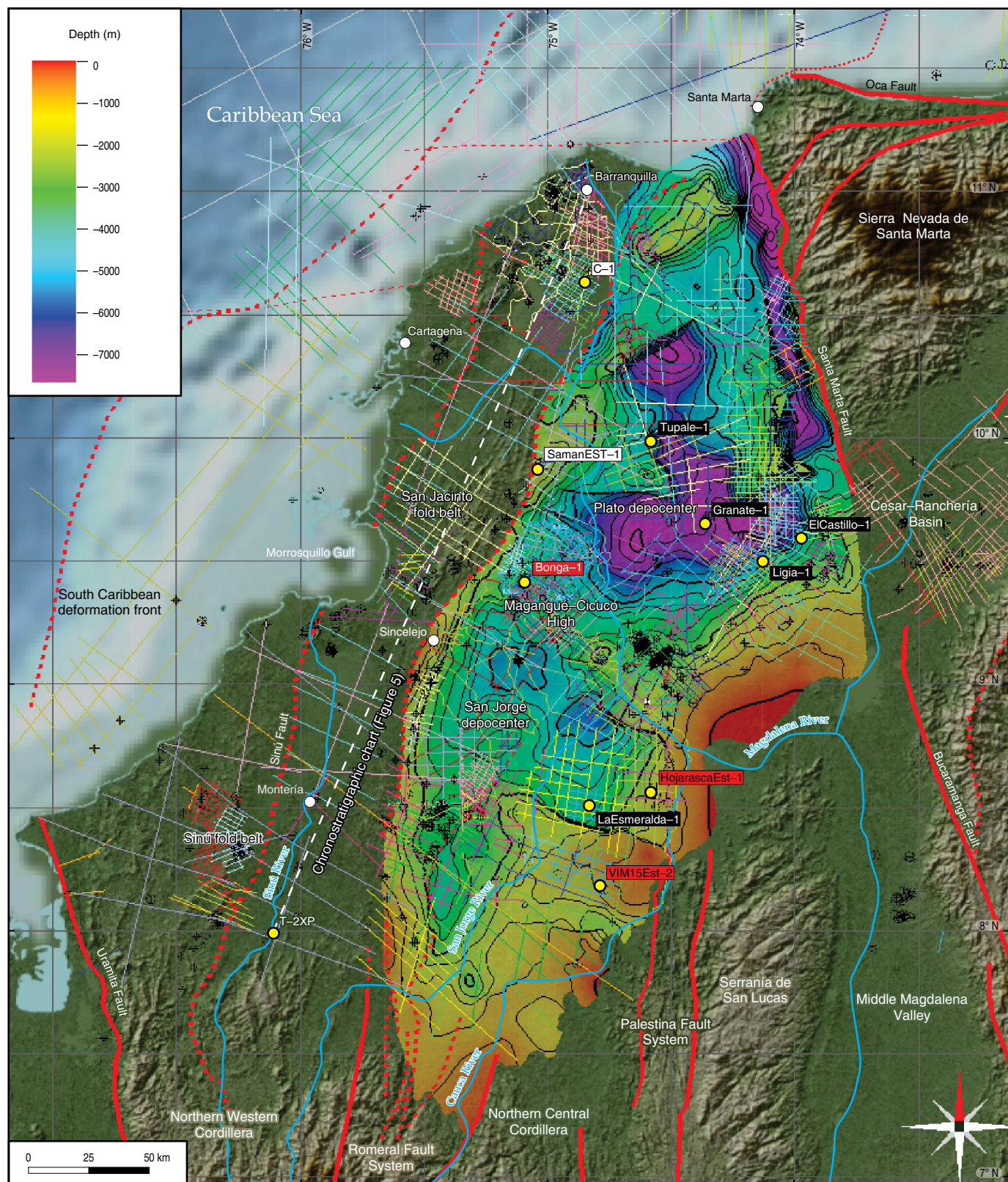


Figure 2. Reflection seismic and well database used for this study and provided by Hocol S.A. All wells are shown as small black crosses or circles with crosses, and relevant wells are highlighted: wells with red labels have basement U-Pb geochronological analyses, the two wells with white labels have detrital zircon U-Pb geochronological analyses, and wells with black labels have subsidence analyses (note Bonga-1 well has basement geochronology and subsidence analysis). Colors of seismic lines represent different seismic surveys. Topography and main drainages are also shown, as well as the structural map in depth of the basement under the LMV, after Mora et al. (2017a).

basement highs or to elongated features related to major fault zones. When comparing the Bouguer anomaly map with the depth-converted top basement map of the LMV (Figure 6a), a very good match can be seen in terms of basement configuration. The southeastern boundaries of the LMV are the Palestina Fault System (PFS) and the basement outcrops of the northernmost CC, while the boundaries in the northeast are the Santa Marta Fault (SMF) and the SNSM. The western limit of the LMV has been considered the northward extension of the RFS (Duque-Caro, 1979, 1984), which would be separating the basin from the San Jacinto deformed belt to the west. However, based on reflection seismic data, an east-verging fault splay was interpreted in the southwestern LMV (Mora et al., 2017a), which correlates at surface with the San Jerónimo Fault (SJF; Figures 3 and 6) and appears to correspond to the southwestern limit of the continental affinity basement of the LMV. The main morphological features of the basement underneath the LMV are the Plato depocenter in the north, with depths in excess of 7 km (23 000 feet), the Magangué-Cicuco High (MCH) in the center, and the San Jorge depocenter in the south, with depths of more than 5 km (17 000 feet).

4.2. Basement Fault Families

Detailed seismic mapping of the basement underneath the LMV showed that the fault pattern is much more complex than previously considered (Figure 7; Mora et al., 2017a). The basement faults were divided into four fault families according mainly to their trend and to their age, and found that these families define two structural regions in the LMV: a western region with a dominant ESE–WNW–trending fault family and a northeastern region with a dominant NE–SW–trending family (Figure 7). The oldest fault family (family 1, green traces in Figure 7) comprises normal faults trending NE–SW (40–60°) and includes the southern El Difícil Fault, the Pivijay Fault, and the fault that limits the Remolino-Ciénaga High to the south. The second fault family (family 2, red traces in Figure 7) comprises extensional faults which exhibit subtle strike-slip and inversion deformation affecting the sedimentary infill and which have an WNW–ESE–trend (265–320°). The third fault family (orange traces in Figure 7) trends NNW–SSE (330–360°) and corresponds to the Algarrobo Fault, a trans-tensional strike-slip fault, and to the northern Apure Fault. The fourth family in the LMV (blue traces in Figure 7) comprises normal faults with subtle inversion and a NNE–SSW–orientation (0–30°), hence implying an ESE–WNW–oriented extensional component. Neogene to recent, E–W and SE–NW contraction has obscured the original Cretaceous to Paleogene structural fabric in most of the San Jacinto fold belt, except for the northernmost area, where NW–SE–trending Eocene extensional features that influenced sedimentation have been recently interpreted (Figure 7; Mora et al., 2013a).

4.3. Basement Zircon U–Pb Geochronology and Hf Isotope Geochemistry

Mora et al. (2017a) selected eight samples from deep exploratory and stratigraphic wells that drilled through the basement to be processed for zircon U–Pb geochronology and Hf isotope geochemistry. Three core samples were analyzed from the metamorphic basement drilled in the VIM15Est–2 stratigraphic well in the southeastern part of the basin (Figures 2 and 3). Five ditch cutting samples were analyzed from the basement in the HojarascaEst–1 stratigraphic well in the eastern part of the San Jorge depocenter, and from the Bonga–1 exploratory well, located in the western MCH. Detrital zircon U–Pb dates from low-grade metasedimentary rocks indicated a Middle to Late Triassic maximum depositional age for their sedimentary protoliths, estimated to 234 ± 5 Ma ($n = 4$, MSWD = 0.7) for Hojarasca and 233 ± 4 Ma for VIM15 ($n = 4$, MSWD = 0.7) based on the youngest group of at least three zircons that define an equivalent population within 2σ uncertainties (e.g., Dickinson & Gehrels, 2009). The age spectra retrieved for both localities was dominated by zircons with early Permian to Middle Triassic crystallization ages, with subdued older populations in the early Paleozoic (Cambrian – Ordovician) and the Meso- and Neoproterozoic. A comparison with the known age distributions of pre-Jurassic basement domains in NW South America revealed that these DZ age populations are most similar to the igneous and detrital zircon U–Pb ages found in the basement of the CC and the SNSM (Mora et al., 2017a), thus suggesting a close paleo-geographic connection.

In the Bonga–1 well, located in the western part of the MCH (Figures 2 and 3), samples of a granitic basement were recovered, yielding zircon U–Pb ages in the range of 76 to 89 Ma (Coniacian – Campanian). The results from the Bonga–1 well clearly indicated that magmatism in this portion of the LMV basement was ongoing for this time interval in the Late Cretaceous, as has been observed in other parts of the basin; for instance, a granite sample from the Cicuco Field in the MCH was dated as Santonian (Aleman, 1983 in Reyes-Harker et al., 2000), while a recent study by Silva-Arias et al. (2016), provided a similar age (84.5 Ma, U–Pb in zircon) for the granodioritic basement in the Cicuco–22 well in the eastern MCH. Another Late Cretaceous age was reported in the Coral–9 well (74.5 Ma, Silva-Arias et al., 2016). In addition to the new U–Pb results for the Bonga–1 well, the Hf isotopic compositions of the dated zircons also indicated a rather juvenile affinity for this portion of the LMV basement (Mora et al., 2017a). Several analyses conducted in two of the Bonga samples yielded $\epsilon\text{Hf}(t)$ values in excess of +10 and up to +15, exceeding the values typical for arc-related crust (Dhuime et al., 2011) and overlapping with a depleted mantle-like composition (Vervoort & Blichert-Toft, 1999). In contrast, samples from the VIM15 and Hojarasca wells discussed above yielded much lower

Figure 3. Geological map of the NW Colombia (modified after Gómez et al., 2007), highlighting basement terranes and pre-Tertiary sedimentary units, and integrating a subsurface basement map in depth (meters) of the LMV. Colored circles are wells that drilled into the basement and have basic rock descriptions; previous and new geochronological data from the basement is depicted. (OF) Oca Fault; (RFS) Romeral Fault System; (SL) Sevilla Lineament; (LMV) Lower Magdalena Valley; (CRB) Cesar–Ranchería Basin; (SP) serranía de Perijá; (MCH) Magangué–Cicuco High; (SJF) San Jerónimo Fault; (SM) Santander Massif; (CAF) Cauca–Almaguer Fault; (ESF) Espíritu Santo Fault; (PFS) Palestina Fault System; (CC) Central Cordillera; (WC) Western Cordillera; (MMV) Middle Magdalena Valley; (EC) Eastern Cordillera. Modified from Mora et al. (2017a).

$\epsilon\text{Hf}(t)$ values, mostly ranging between +4 and –8, thus indicating a much older crustal source for the preceding magmas from which these detrital zircons crystalized.

4.4. Detrital Zircon U–Pb Geochronology and Hf Isotope Geochemistry of Pre–Oligocene Units

Samples (cuttings) for petrography and detrital zircon U–Pb and Hf isotope analyses were recovered from two wells located in the northern half of the SJFB (Figure 2; Mora et al., 2017b). Six samples from upper Paleocene to upper Eocene units (San Cayetano and Chengue) were collected in the C–1 well, located in the northern San Jacinto fold belt, while two more samples from an upper Eocene to lower Oligocene unit (San Jacinto) were collected in the SamanEST–1 well, located farther south, close to the boundary between the SJFB and the LMV (Figure 2). U–Pb dates of detrital zircon from samples of upper Paleocene to Eocene strata (Sequences 2 to 4) showed three clear provenance peaks, namely a main Late Cretaceous (70–88 Ma, Coniacian – Maastrichtian) peak, a secondary peak of Permian – Triassic age (230–250 Ma) which is less evident in the SamanEST–1 well, and a minor Albian – Cenomanian peak (ca. 100 Ma; Mora et al., 2017b). However, the Paleocene to middle Eocene samples also evidenced both early Paleozoic and Proterozoic provenance. Therefore, detrital zircon U–Pb geochronology indicated that the upper Paleocene to lower Oligocene sediments of Sequences 2 to 4 were mostly sourced from Upper Cretaceous and Permian – Triassic basement blocks.

Hf isotopic data showed that the three dated detrital zircon populations (Coniacian – Maastrichtian, Albian – Cenomanian, and Permian – Triassic) are related to different magmatic sources. While the Coniacian – Maastrichtian zircons would be related to a juvenile mantle source (i.e., positive ϵHf), the older Albian – Cenomanian and Permian – Triassic zircons have much lower $\epsilon\text{Hf}(t)$ values, indicating a much older crustal source. Furthermore, in the SamanEST–1 well there were two sub-populations within the Late Cretaceous Coniacian – Maastrichtian population, and both overlapped quite well with the compositions of the Bonga Pluton (Mora et al., 2017a), located 50 km to the south (Figures 2 and 3). The Permian – Triassic Hf isotopic compositions from the C–1 well also showed a good match with the Hf compositions of the Permian – Triassic basement in the HojarascaEST–1 and VIM15Est–2 wells (Mora et

al., 2017a) and with data from previous studies (Cardona et al., 2012; Cochrane et al., 2014).

4.5. Upper Cretaceous to Eocene Tectono–Stratigraphy in the SJFB

Though this tectono–stratigraphic framework is mostly based on previous research, it was built after incorporating a great deal of recent regional drill hole, seismic, and outcrop data and interpretations (Figures 4 and 5). The same sequence definition and numbering proposed by Mora et al. (2017b) is used here. Upper Cretaceous to Eocene deposits are better preserved and exposed in the SJFB, while they are only locally preserved in the western portion of the LMV. The general characteristics of the identified and studied Upper Cretaceous to Eocene tectono–stratigraphic sequences are presented in Table 1 of the Supplementary Information.

The oldest, 2nd–order sequence is of Coniacian to Maastrichtian age (Mora et al., 2017b) and comprises the bituminous shales, cherts, and limestones of the Canzona unit (Sequence 1 in Figures 4 and 5). Biostratigraphic data compiled by Duque–Caro (2000, 2001) and Guzmán (2007) showed an absence of lower Paleocene planktonic foraminiferal zones (P.0 to P.2) in the SJFB, indicating the existence of a regional unconformity which marks the upper limit of this sequence. Sequence 2, called San Cayetano, is also a 2nd–order sequence which has been dated as late Paleocene to early Eocene (planktonic foraminiferal zones P.3 to P.9). The late Paleocene was characterized by a high global sea level (eustatic curves in Figure 4; Haq et al., 1987), which could have influenced the onset and extension of San Cayetano sedimentation. Biostratigraphic data showed that there is a big hiatus in the center of the SJFB, where the lower Eocene is missing, while to the north the section is more complete and the contact with the overlying sequence appears to be a disconformity (Figures 4 and 5; Table 1 of the Supplementary Information). A middle to upper Eocene, 2nd–order sequence (Sequence 3) corresponds to the Chengue Group, defined by the P.10 to P.14 planktonic foraminiferal zones of middle to late Eocene age. Biostratigraphy indicated that the unconformity between Sequences 2 (San Cayetano) and 3 (Chengue) corresponds to the P.9 to P.10 foraminiferal zones, implying a time interval of 46 to 51 Ma which includes the limit between the early and middle Eocene. This syn–tectonic sequence has



Figure 4. WNW–ESE–trending chronostratigraphic chart of the Sinú, San Jacinto, and Lower Magdalena areas, based on different sources (Guzmán, 2007; Hocol S.A., 1993; Instituto Colombiano del Petróleo, 2000) and adjusted with our recent analyses of well and outcrop samples. Biostratigraphy is based on numerous papers and industry reports by Duque–Caro (1979, 1984, 1991, 2000, 2001, 2010, 2014), tectonic events are after Villagómez *et al.* (2011), Parra *et al.* (2012), Saylor *et al.* (2012), Mora *et al.* (2013b), Caballero *et al.* (2013), Mora *et al.* (2015), De la Parra *et al.* (2015), while the eustatic curves are from Haq *et al.* (1987) and the climatic events from Zachos *et al.* (2001). Modified from Mora *et al.* (2017b).

been eroded in the southern part of the SJFB and is more preserved in the northern part (Figure 5). Sequence 4 is a locally preserved 2nd–order sequence comprising the siliciclastic San Jacinto unit and the calcareous Toluviejo unit (Figures 4 and 5), which according to biostratigraphic studies (Duque–Caro, 1979; Guzmán, 2007; Guzmán *et al.*, 2004) are defined by the P.15 to P.20 planktonic foraminiferal zones of late Eocene to early Oligocene age.

4.6. Upper Oligocene to Recent Tectono–Stratigraphy and Paleo–Geography in the LMV and SJFB

Due to Pliocene to recent uplift and erosion in the SJFB, Oligocene to recent deposits are more preserved in the LMV. The general characteristics of the identified sequences are summarized in Table 2 of the Supplementary Information and in Mora *et al.* (2018). Since there is seismic and well data in the LMV, it was possible to reconstruct the Oligocene to recent paleo–geography of the LMV, which is depicted in Figures 8 to 10 for selected time windows. The detrital zircon U–Pb geochronology of Montes *et al.* (2015) was also integrated, to better constrain the sediment provenance.

The Oligocene to lower Miocene deposits are interpreted as a transgressive, 2nd–order sequence (Sequence 5), which filled from NW to SE the lowest paleo–topographic areas formed by the basement of the LMV (Figure 8a; Mora *et al.*, 2018). This sequence, called “Lower Ciénaga de Oro”, was associated to the planktonic zones P.20 to N.6 (M.3), equivalent to an early Oligocene to early Miocene age (Figure 4; Table 2 of the Supplementary Information). Seismic data shows that the Oligocene to lower Miocene shallow marine deposits gradually filled the proto–San Jorge and Plato depocenters from the W and NW and that the main structural basement features, such as the Sucre, Mojana, and Pivijay Faults, were actively extending (Figure 8a).

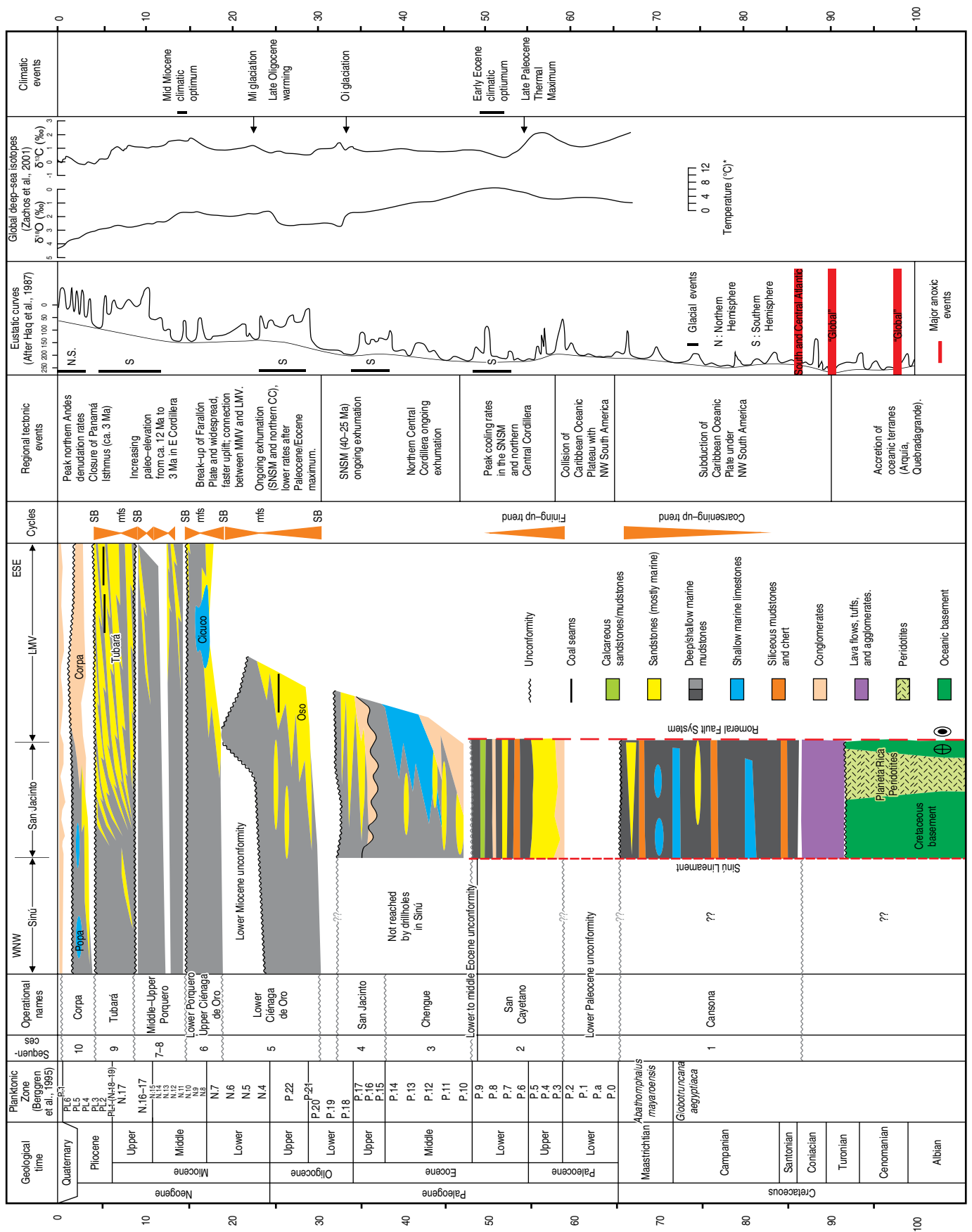
Sequence 6, deposited after a regional early Miocene tectonic event, records a major change in sedimentation in the basin. Biostratigraphic analyses indicate that it is a 3rd–order sequence of early to middle Miocene age (Burdigalian to Serravallian, zones N.7/M.4 to N.11/M.8) (Figure 4; Table 2 of the Supplementary Information; Mora *et al.*, 2018). Deposition of this sequence, called “Upper Ciénaga de Oro” and “Lower

Porquero”, extends farther to the E and SE and begins with retrogradational, shallow marine, clastic sedimentation in low areas and carbonate deposition in high areas, which then changed to progradational deltaic sedimentation (Figures 8b and 9a).

Although Sequences 7 and 8 of middle to late Miocene age were partially eroded, they also continue to display a progradational pattern to the NW. These sequences represent 3rd–order cycles of middle to late Miocene age (Serravallian – Tortonian) and they are also limited by regional unconformities (Figure 4; Duque–Caro, 1979; Duque–Caro *et al.*, 1996; Guzmán, 2007; Hocol S.A., 1993; Reyes–Harker *et al.*, 2000). The sequences, called “Middle and Upper Porquero”, exhibit mainly fine–grained facies with progradational stacking patterns, which are best preserved in the depocenters where erosion was less intense.

Sequence 9 is a 3rd–order sequence of late Miocene to early Pliocene age (zones N.17/M.14 to PL2 zones, Tortonian to Zanclean; Figure 4; Table 2 of the Supplementary Information). Reflection–seismic data shows that this sequence, which is better preserved in the Plato depocenter, is composed of low–angle (0.3–0.6°) and wide (100–200 km) sigmoidal clinoforms which advanced from SSE to NNW, representing the gradual advance of the proto–Magdalena River (Figure 9b).

Sequence 10 has been very poorly studied and comprises several higher order sequences, representing renewed subsidence in the southern LMV, focused in the San Jorge Graben where the thickest deposits occur (Figure 10). It is well preserved in the southern LMV, south of the Magangué–Cicuco High, where it is called “Corpa”, while in the north it was mostly eroded. Taking into account the unconformities above the upper Miocene to lower Pliocene Tubará Sequence (9), and below the upper Pleistocene to recent deposits, we infer here a late Pliocene to early Pleistocene age for this sequence, spanning from 3 to 1.3 Ma (3rd–order cycle; Figure 4; Table 2 of the Supplementary Information). The expression of the Corpa Sequence in reflection–seismic data consists of low–angle clinoforms broadly prograding from south to north, which appear to represent the deposits of the paleo–Cauca drainage system, including fluvial channels, lakes, and swamps (Figure 10). The internal seismic–stratigraphic architecture of the Corpa Sequence reveals the time when the SJFB started to be uplifted (Mora *et al.*, 2018), which appears to be close to the boundary between the Pliocene and Pleistocene.



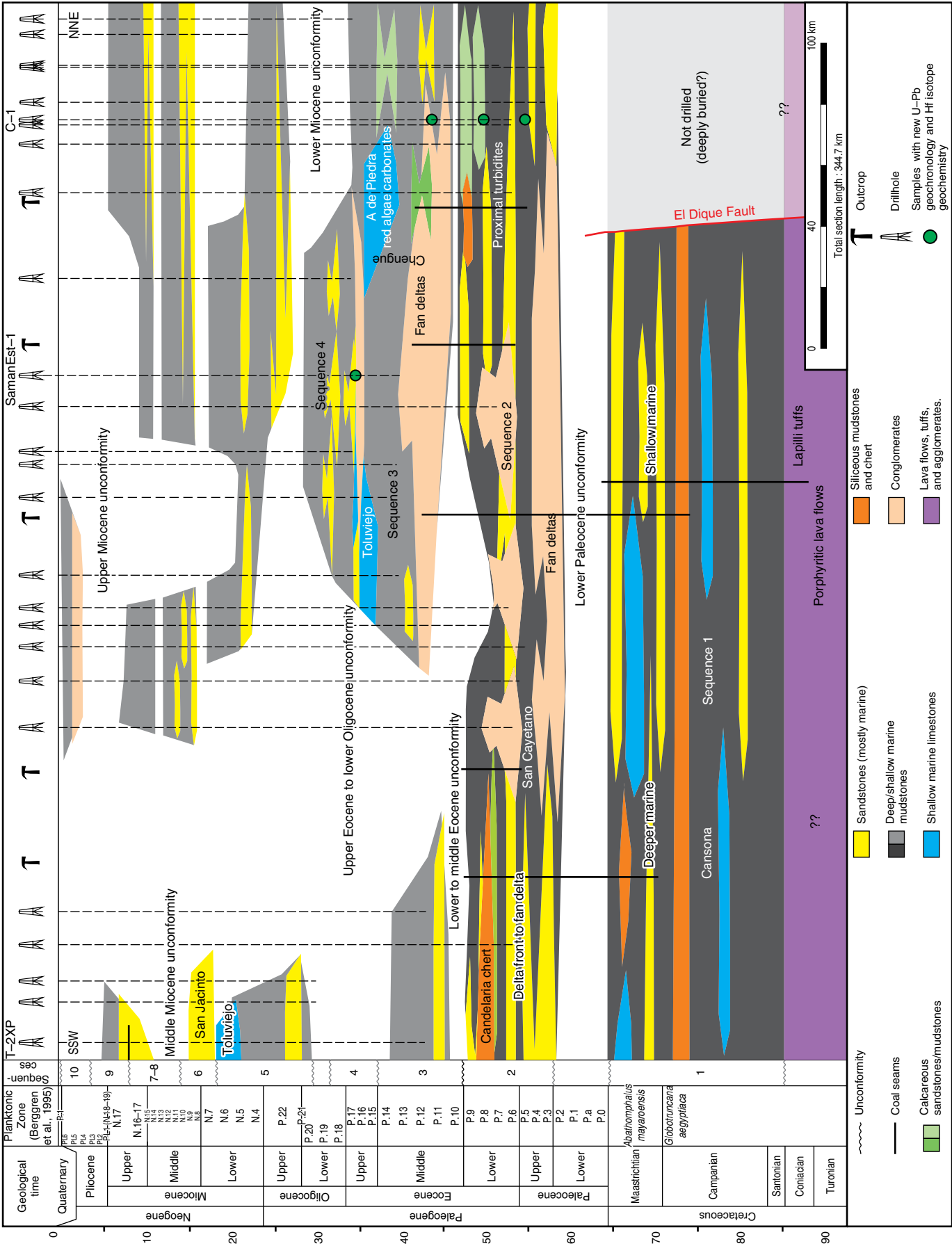




Figure 5. SSW–NNE–trending chronostratigraphic chart with wells and outcrops compiled along–strike (NE–SW) from the San Jacinto fold belt. Wells with new detrital zircon geochronological analyses are highlighted (green circles show approximate location of samples). Modified from Mora et al. (2017b).

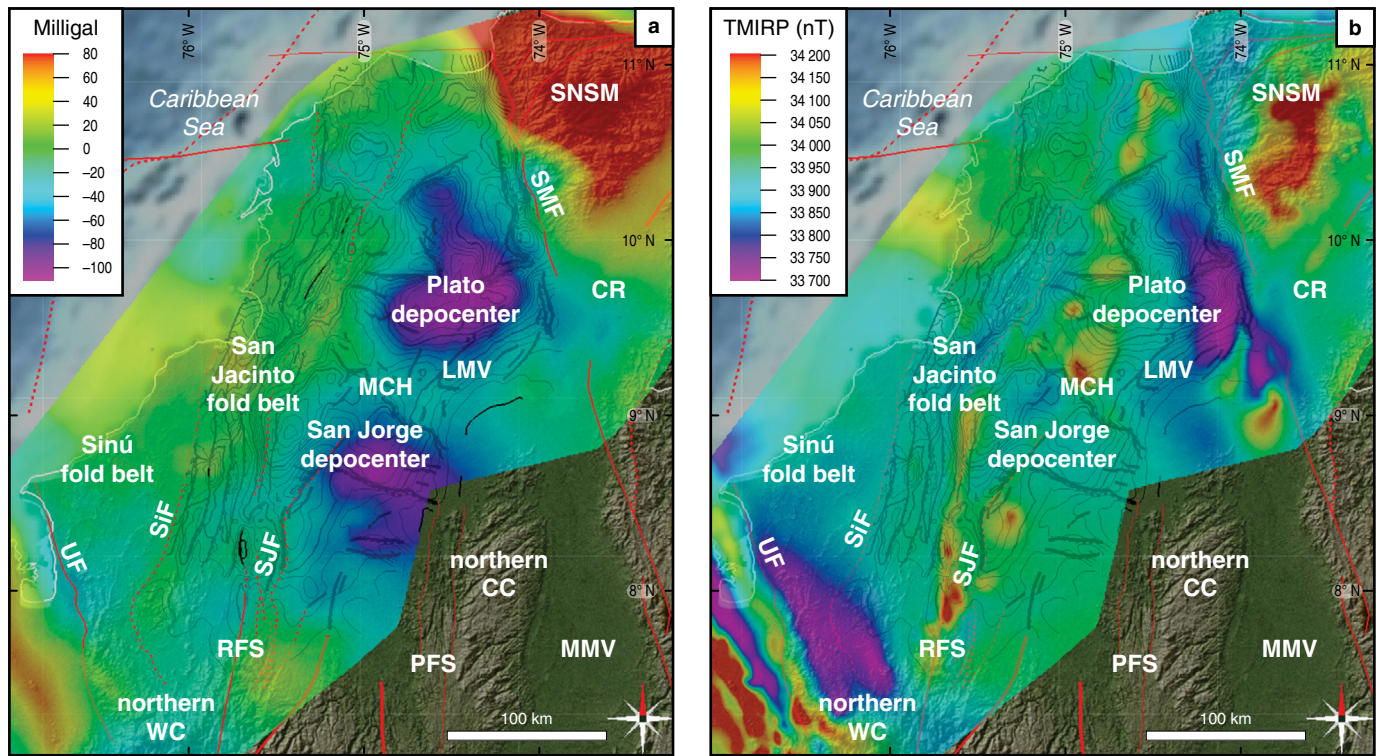


Figure 6. Airborne gravity and magnetic data from northern Colombia, acquired by Lithosfera Ltda. (2010) for Hocol S.A. and the Agencia Nacional de Hidrocarburos (ANH). **(a)** Total Bouguer anomaly, scale from -80 to 80 mGal. **(b)** Total magnetic intensity reduced to the pole (TMIRP) with scale from 33700 to 34200 nT. In the background we included the contours of the near top basement structural map in depth, after Mora et al. (2017a). (SNSM) Sierra Nevada de Santa Marta; (SMF) Santa Marta Fault; (CR) Cesar–Ranchería Basin; (MCH) Magangué–Cicuco High; (LMV) Lower Magdalena Valley Basin; (UF) Uramita Fault; (SiF) Sinú Fault; (SJF) San Jerónimo Fault; (CC) Central Cordillera; (RFS) Romeral Fault System; (PFS) Palestina Fault System; (MMV) Middle Magdalena Valley Basin; (WC) Western Cordillera. Modified after Mora et al. (2017a).

4.7. Seismicity Data and Present–Day Lithospheric Configuration of Northwestern Colombia

Using the publicly available seismicity data and data from previous research (e.g., Bezada et al., 2010b), the present–day geometry and configuration of the subduction zone of NW Colombia was studied by Mora et al. (2017a, 2017b). A depth map of the top of the subducted oceanic slab beneath South America and a cross–section depicting its geometry and the configuration of the subduction zone of NW Colombia were constructed (Figure 11). The study area is characterized by a low seismicity, with very few scattered, shallow (<70 km), and low magnitude (<4 Mw) events (Mora et al., 2017a), and there are no available focal mechanism solutions in the area of the San Jacinto fold belt.

According to Mora et al. (2017b), the Caribbean Plate subducted beneath NW South America appears to be formed by three different slab segments, separated by kinks or bends (Figure 11): a northwestern shallow and very flat slab segment, a central intermediate–depth and flat–slab segment (the “Caribbean” flat–slab of Syracuse et al., 2016), and a southeastern deep and very steep slab segment imaged by Bezada et al. (2010b). However, such segmented slab geometry of the subducted Caribbean Plate does not seem to continue to the north of the Oca–El Pilar–San Sebastian Fault System (OEPFS) and seismicity changes abruptly from the southern to the northern block of the OEPFS (see Figure S1 in Mora et al., 2017b).

Based on the steep descent of the Caribbean Plate under Maracaibo and the Mérida Andes, previous researchers have proposed that there should be a tear in the Caribbean Plate (Bezada et al., 2010b; Masy et al., 2011; Levander et al., 2015), which

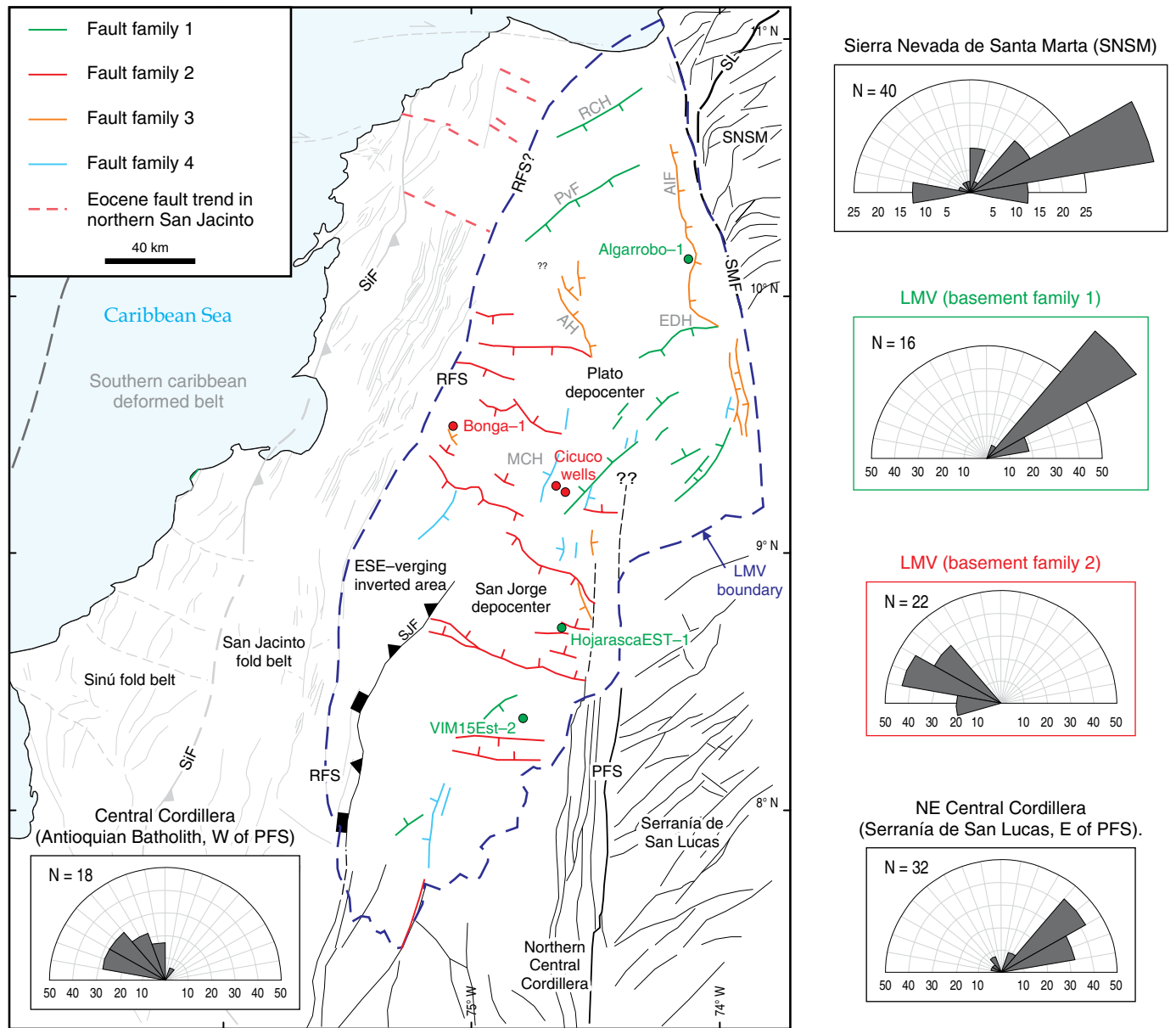
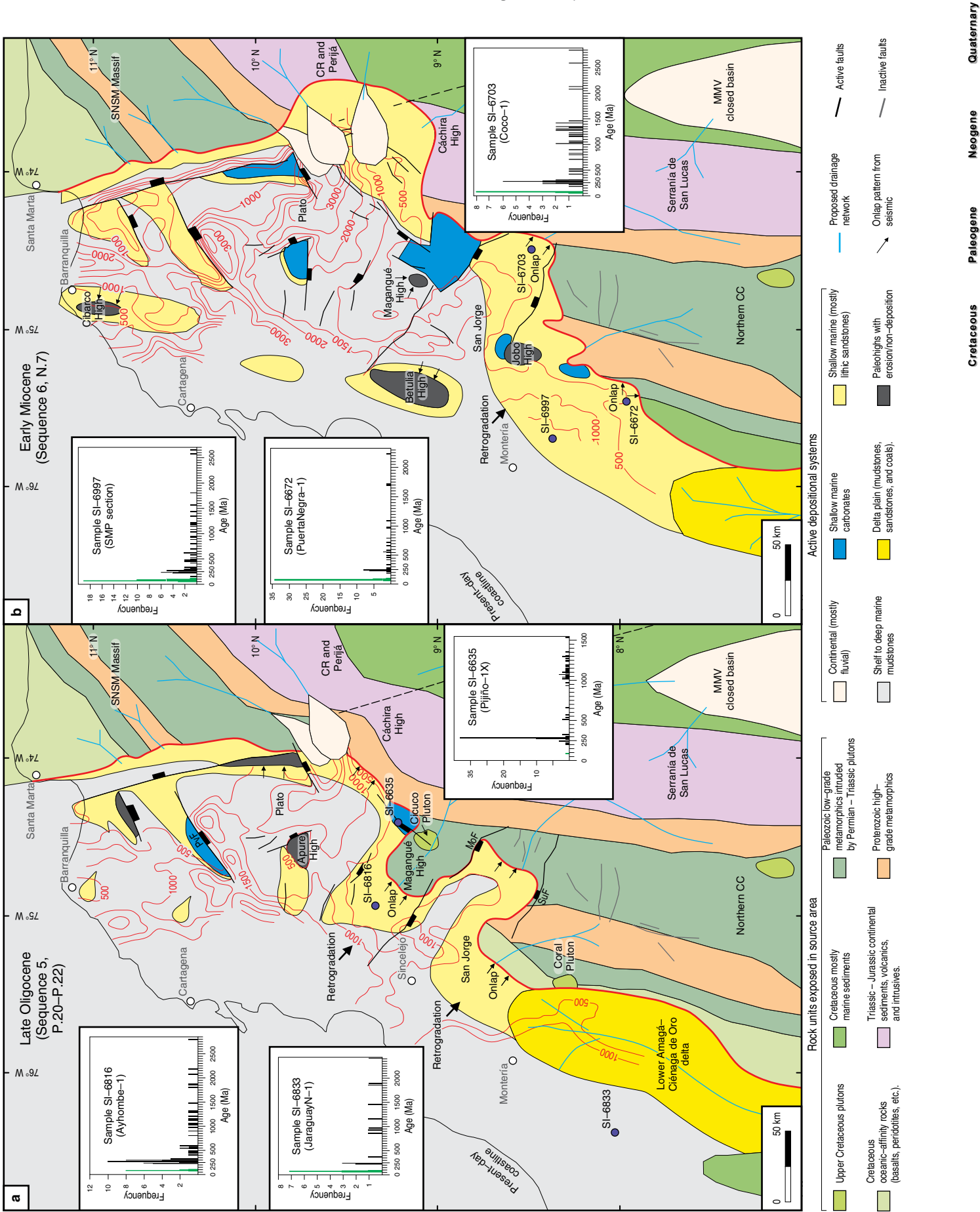


Figure 7. Fault families and structural fabric of the basement terranes in northwestern Colombia (northern CC, western SNSM, and LMV). Surface faults and lineaments were drawn from the Geological Map of Colombia (Gómez et al., 2007) and subsurface fault families were interpreted and drawn from our basement depth-models. In all rose diagrams, the bin size was set to 20 degrees. Light gray features drawn in the Sinú and San Jacinto fold belts are Neogene to recent structures. (SL) Sevilla Lineament; (RCH) Remolino-Ciénaga High; (RFS) Romeral Fault System; (SNSM) Sierra Nevada de Santa Marta; (SiF) Sinú Fault; (PvF) Pivijay Fault; (AIF) Algarrobo Fault; (SMF) Santa Marta Fault; (AH) Apure High; (EDH) El Dificil High; (MCH) Magangué-Cicuco High; (SJF) San Jerónimo Fault; (LMV) Lower Magdalena Valley; (PFS) Palestina Fault System. Modified from Mora et al. (2017a).

Figure 8. Interpreted late Oligocene (a) and early Miocene (b) paleogeography, based on seismic interpretation and well data, showing interpreted source areas (based on Mora et al., 2017a and others), active sedimentation areas, and proposed paleo-drainages in blue; thin red contours are thicknesses in meters of each sequence and the thick red contour represents the interpreted limit of deposition of each sequence. Detrital zircon U-Pb geochronology from Montes et al. (2015) is also plotted (purple circles with their respective histograms), and it shows a greater influence in the SE of Permian – Triassic and older basement sources (black bars in histograms), while Cretaceous sources in the Western and Central Cordilleras are more important in the NW (green bars in histograms). The development of local paleo-highs (e.g., Betulia and Cibarco) in the present-day SJFB, as interpreted from seismic data, is also shown. (SNSM) Sierra Nevada de Santa Marta; (PvF) Pivijay Fault; (CR) Cesar Ranchería; (MoF) Mojana Fault; (SuF) Sucre Fault; (CC) Central Cordillera; (MMV) Middle Magdalena Valley Basin.



would be separating the steeper dipping Caribbean slabs, located to the south of the OEPFS, from the shallow Caribbean Plate that has been imaged north of the same fault system. Using data from previous research and our new depth map of the shallow subducted Caribbean oceanic segment under the San Jacinto fold belt, Lower Magdalena Valley Basin, and the serranía de Perijá (inset in Figure 11), Mora *et al.* (2017b) proposed a new interpretation of the three-dimensional plate tectonic configuration of northern Colombia and western Venezuela (Figure 12). This interpretation implies that the boundary between northern South America and the Caribbean Plate consists of two tears or subduction–transform edge propagator (STEP, Govers & Wortel, 2005) faults instead of only one. The Oca–San Sebastián–El Pilar dextral fault system would then be the surface expression of the tear fault that limits the Caribbean and South American/Atlantic Plates at deeper crustal and mantle levels.

4.8. Cretaceous to Recent Paleo–Tectonic Reconstructions

Late Cretaceous to recent paleo–tectonic reconstructions were performed, using the free software package GPlates (Boyden *et al.*, 2011) and two paleo–tectonic models available for this area (Boschman *et al.*, 2014; Matthews *et al.*, 2016, from the GPlates database) (Figure 13; Figures 1 and 2 of the Supplementary Information; Mora *et al.*, 2017b, 2018). The reconstructions show the motion of the Caribbean Plate relative to a fixed South American Plate, but it is important to highlight that plate tectonic processes between the Caribbean and the Americas were driven by relatively fast, westward motion of North and South America, while the Caribbean Plate has remained nearly stationary since the Eocene (Müller *et al.*, 1999). The constructed models were used to study the kinematic evolution of the tectonic plates, in order to relate them to the Upper Cretaceous to recent tectono–stratigraphy in the LMV and SJFB (Mora *et al.*, 2017b, 2018).

Using average plate convergence velocities of the Caribbean Plate relative to South America over the last 45 Ma, Mora *et al.* (2017b) calculated for both models the geological time when each of the three subducted slab segments of the Caribbean Plate imaged along cross-section A–A' (Figure 11) entered the trench (Table 1). The age of entrance in the trench of the

whole Caribbean slab (total length of 1065 ± 15 km) ranges from early Eocene (ca. 56 ± 2 Ma) to middle Eocene (ca. 43 ± 2 Ma) depending on the model used (Boschman *et al.*, 2014 or Matthews *et al.*, 2016, respectively). Kroehler *et al.* (2011) estimated the age of the initiation of subduction of the Venezuelan Basin at the southern Caribbean deformed belt based on the wedge-shaped asymmetrical thickness of the sediments in the trench adjacent to the thrust zones. The beginning of tectonic wedging appears in a middle Eocene megasequence in the west and is younger towards the east (Kroehler *et al.*, 2011).

Equivalence of the obtained age of entrance in the trench of the Caribbean slab with the identified unconformities in the stratigraphic succession in the SJFB, and with the convergence velocities and obliquities, as shown in Figure 14, will be discussed in forthcoming sections.

4.9. Cross-Section Structure of the SJFB and LMV

The present-day SJFB is a west-verging and NNE–SSW-trending, fold and thrust belt that has been formed by Pliocene to recent contraction and inversion (Figure 15), but that experienced a complex pre-Oligocene tectonic history. Its structure has been influenced by the strike-slip activity of the Romeral Fault System (RFS), and by the contraction along the west-verging Sinú Fault (SiF), which appears to be related to the Sinú accretionary prism (Mora *et al.*, 2017a, 2017b). Such complex deformation obscured the original Cretaceous to Eocene structural fabric, making seismic imaging very poor. However, Mora *et al.* (2017b) documented several areas in which pre-Oligocene sequences have preserved their original extensional structural fabric, exhibiting extensional rotated fault blocks which are forming two sets of extensional faults, one with a SSW–NNE orientation and the second one with a WNW–ESE orientation (Mora *et al.*, 2013a). Sequences 1 and 2 are mostly restricted to the western side of the RFS (Figure 15), and would be limited to the east by the San Jerónimo Fault (SJF), while Sequences 3 and 4 extend farther to the east, into the western LMV. Interpreted seismic cross-sections also showed that the activity of the RFS considerably decreases from the south, close to the outcrops between the Central and Western Cordilleras, to the north. In fact, the RFS has been sealed by the lower to mid-

Figure 9. Interpreted middle Miocene (a) and late Miocene to early Pliocene (b) paleogeography, based on seismic interpretation and well data, showing interpreted source areas, active sedimentation areas, and interpreted paleo-drainages in blue. Thin red contours are thicknesses in meters of each sequence and the thick red contour represents the interpreted limit of deposition of each sequence. Detrital zircon U–Pb geochronology from Montes *et al.* (2015) is also plotted (purple circles with their respective histograms) in the left panel, showing a greater influence in the SE and north (Plato and Magangué–Cicuco High) of Permian – Triassic and older basement sources (black bars in histograms); Cretaceous (green bars) and Eocene to middle Miocene (yellow–orange bars) sources are more important in the SW, suggesting a much greater influence of the Western and Central Cordilleras as source areas in middle Miocene times. The development of paleo-highs, as interpreted from seismic data, is also shown. (SNSM) Sierra Nevada de Santa Marta; (CR) Cesar Ranchería; (LMV) Lower Magdalena Valley; (MMV) Middle Magdalena Valley; (CC) Central Cordillera.



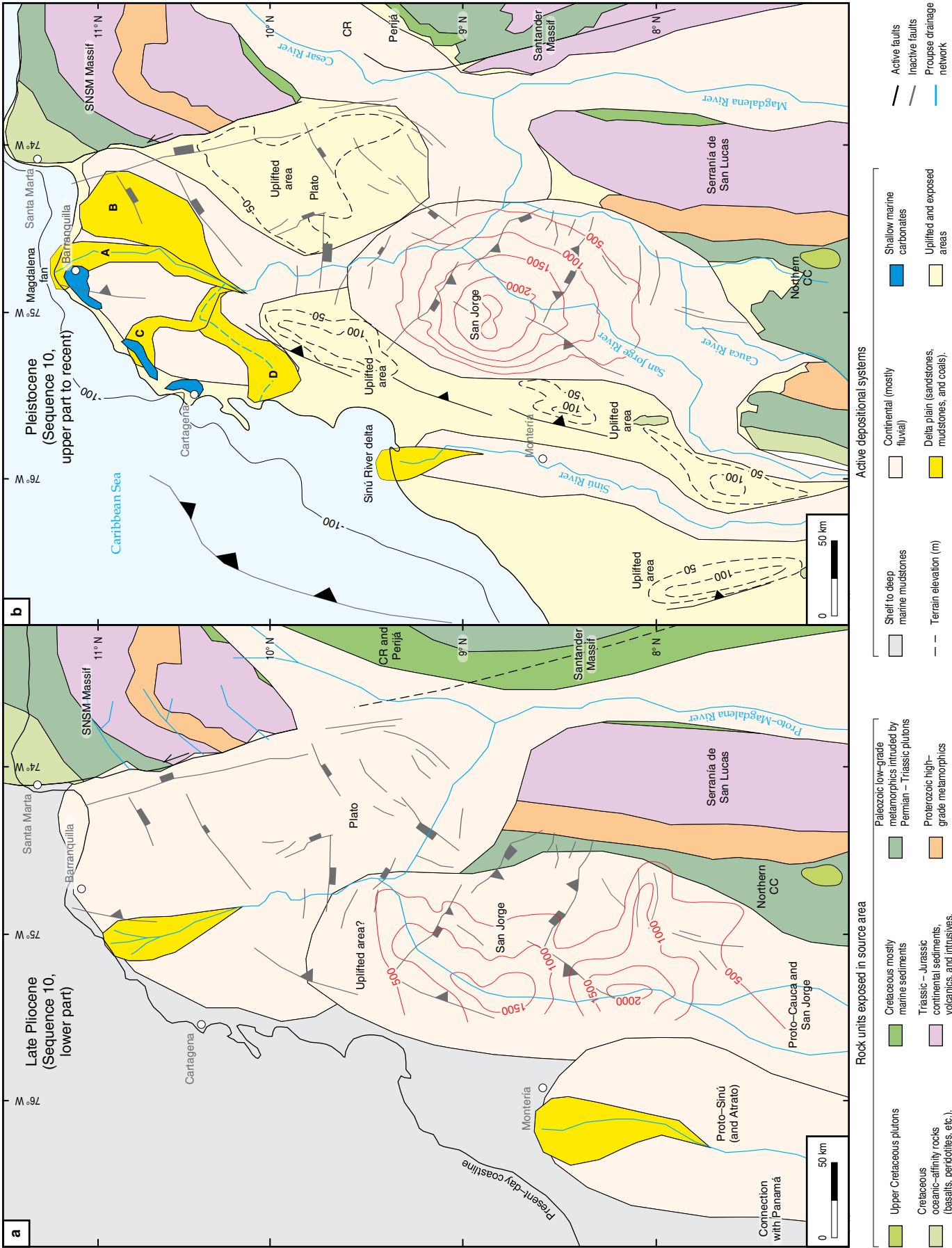


Figure 10. Interpreted late Pliocene (a) and Pleistocene (b) paleogeography, based on seismic interpretation and well data, showing interpreted source areas (based in Mora et al., 2017a and others), active sedimentation areas, and interpreted paleo-drainages in blue; thin red contours are thicknesses in meters of each sequence. In late Pliocene times, when the Magdalena River system reached the present-day coastline, the Plato depocenter was already overfilled, whereas sedimentation continued in the western San Jorge depocenter, which continued subsiding. In the Pleistocene, while the Magdalena River delta shifted its position, uplift of the San Jacinto fold belt and of the Plato depocenter created a round depocenter, which continues to subside today. Letters A to D represent positions of the Magdalena deltas (from Romero-Otero et al., 2015), with A representing the current position. (SNSM) Sierra Nevada de Santa Marta; (CR) Cesar Ranchería; (CC) Central Cordillera.

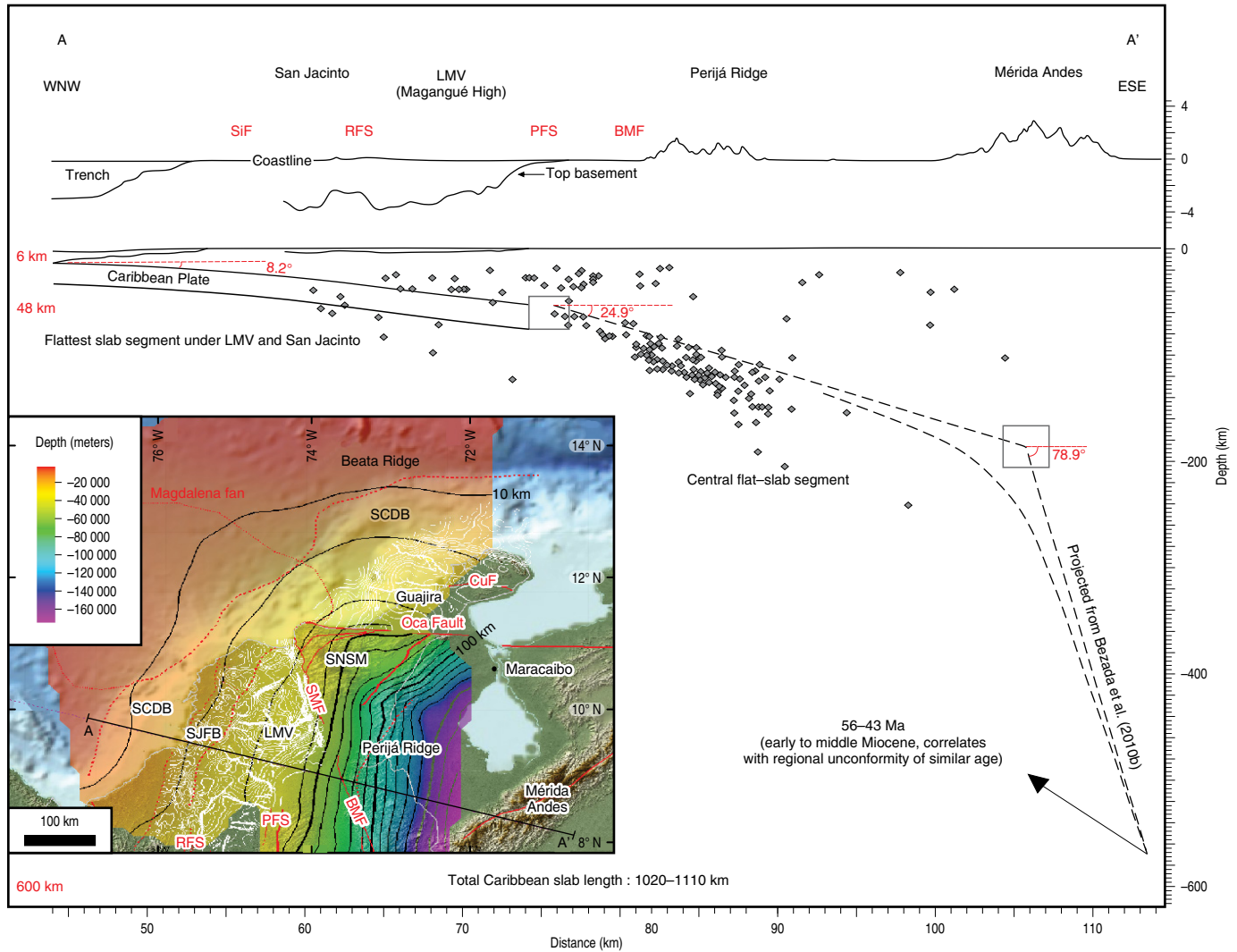


Figure 11. Regional WNW-ESE-trending cross-section showing the lithospheric configuration of the convergent margin of NW Colombia, as interpreted from reflection–seismic mapping for the shallowest part, intermediate–depth seismicity for the central, “Caribbean flat-slab” segment, and from published tomography data (Bezada et al., 2010b) for the deepest part of the cross-section. The top of the basement under the LMV from reflection–seismic mapping and the topography are also displayed. Gray squares represent the uncertainty in the horizontal and vertical measurements. Inset: Integrated depth map in meters of the top of the oceanic Caribbean Plate (in colors), which has been subducted under NW South America since middle Eocene times. Note the change in dip of the slab in the location of the Palestina Fault System (PFS) and how it changes its strike as it approaches the Oca Fault. The white contours are the depth structure of the basement below the LMV, SJFB, and Guajira Basins. (SiF) Sinú Fault; (RFS) Romeral Fault System; (LMV) Lower Magdalena Valley; (PFS) Palestina Fault System; (BMF) Bucaramanga Fault; (SCDB) South Caribbean deformed belt; (CuF) Cuisa Fault; (SNSM) Sierra Nevada de Santa Marta; (SMF) Santa Marta Fault; (SJFB) San Jacinto fold belt. Modified from Mora et al. (2017b).

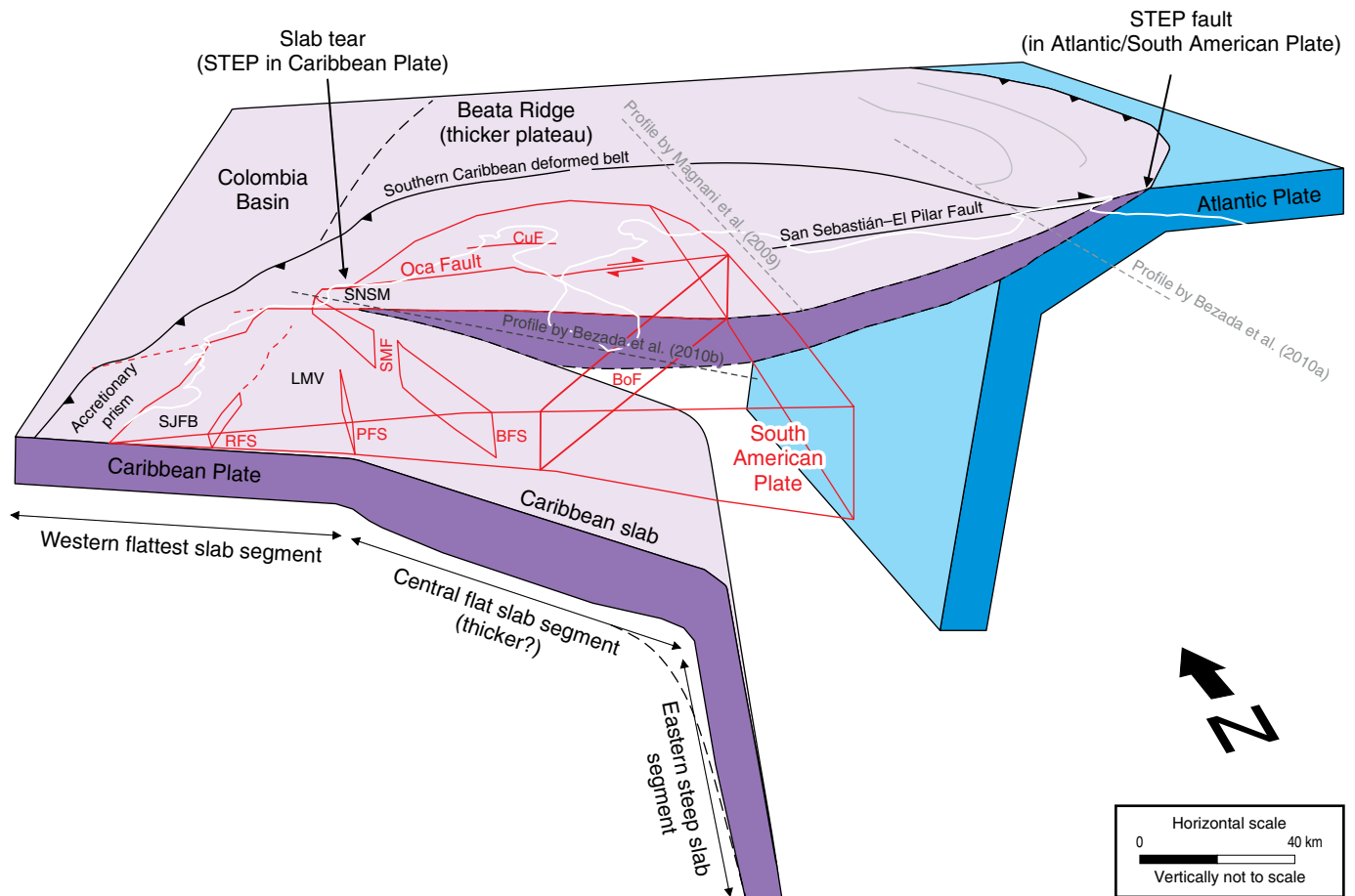


Figure 12. Proposed three-dimensional lithospheric configuration of NW South America, as interpreted from shallow reflection–seismic mapping, intermediate–depth seismicity, and deep tomographic imaging from previous studies (e.g., Bezada et al., 2010b); according to our interpretation, there would be a slab tear or STEP fault (subduction transform edge-propagator, Govers & Wortel, 2005) in the Caribbean Plate, probably represented in the upper crust by the western tip of the Oca–El Pilar–San Sebastián dextral fault system. (CuF) Cuisa Fault; (SNSM) Sierra Nevada de Santa Marta; (SJFB) San Jacinto fold belt; (RFS) Romeral Fault System; (LMV) Lower Magdalena Valley; (PFS) Palestina Fault System; (SMF) Santa Marta Fault; (BFS) Bucaramanga Fault System; (BoF) Boconó Fault. Modified from Mora et al. (2017b).

dle Eocene unconformity, except for local, later reactivations. The eastward tilting of the whole SJFB has been caused by a deeper and younger major fault that probably extends to the deformation front of the accretionary prism, located in offshore areas farther to the west.

The two main basement fault families defined by Mora et al. (2017a), trending ESE–WNW and ENE–WSW, are responsible for most of the extension in the LMV, and consist of nearly vertical extensional faults, which exhibit small heaves. Seismic–stratigraphic analyses show that deposition of the upper Oligocene to lower Miocene sequences (Ciénaga de Oro and Lower Porquero) had fault control, and that after the early Miocene, deposition was mainly due to sagging or non-fault related subsidence, giving rise to the classic Steer’s Head model of basin geometry (Miall, 2000). This is evident in the regional cross-section in depth along the LMV (Figure 16), where the majority of the extensional faults are displacing the upper Oligocene to middle Miocene sequences, with related thickness

changes across the major faults (Mora et al., 2018). By contrast, the upper Miocene to Pleistocene sequences filled broader depocenters in a uniform way, with only minor and localized fault displacements. The latest subsidence episode, which appears to continue active, is related to non-fault related subsidence of the San Jorge Graben that allowed the deposition of the very thick Pliocene to Pleistocene Sequence 10 (Corpa).

4.10. Sedimentation Rates and Subsidence in the LMV and San Jacinto Fold Belt

Thicknesses and ages from 32 wells drilled in the LMV and SJFB were compiled to calculate sedimentation rates and to carry out subsidence analyses of those provinces. Our analyses in the LMV indicate that after the lower Miocene unconformity there was an important increase in sedimentation and subsidence rates (Figure 17a, 17b). Though sedimentation rates were not corrected for compaction, the rates calculated for Sequence

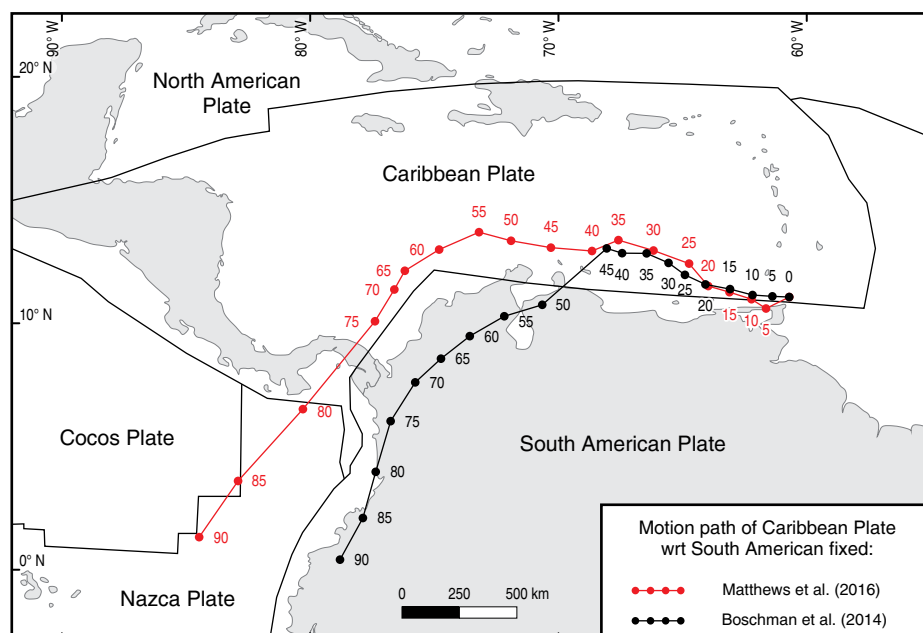


Figure 13. Displacement vectors of the Caribbean Plate relative to South America from the Cretaceous (90 Ma) to present day, shown in red according to the model of Matthews et al. (2016, GPlates database) and in black according to Boschman et al. (2014). Major changes in convergence velocity and obliquity are highlighted. Matthews et al. 's (2016) model shows a decrease in obliquity at 55 Ma (from 78 to 34° in average) and in velocity at 75 Ma (from 8.3 to 2.8 cm/y in average) and Boschman et al. 's (2014) model shows a decrease in obliquity (from 74 to 30° in average) and in velocity (from 4.3 to 1.9 cm/y in average) both at 45 Ma. Modified from Mora et al. (2017b).

Table 1. Compilation of the slab segment lengths, convergence velocities, and ages of entrance in the trench of each slab segment shown in Figure 11 (from Mora et al., 2017b).

	Slab segment length (km) (±15 km error)	Calculated age of slab entrance in the trench using mean plate velocities over the last 45 Ma	
		Boschman et al. (2014)	Matthews et al. (2016)
		19 mm/y	25 mm/y
Western flat slab segment under SJFB and LMV	278–308	14.6–16.2 Ma	11.1–12.3 Ma
Central intermediate–depth flat slab segment	341–371	18–19.5 Ma	13.6–14.8 Ma
Eastern deepest and steepest slab segment	401–431	21.1–22.7 Ma	16–17.2 Ma
Western plus central flat slab segments	619–679	32.6–35.7 Ma	24.8–27.2 Ma
All three slab segments	1020–1110	53.7–58.4 Ma (56 ± 2 Ma)	40.8–44.4 Ma (43 ± 2 Ma)
Slab length by van Benthem et al. (2013)*	900	47.4 Ma	36 Ma

Note: We calculated average velocities over the last 45 Ma according to each of the two available models (Boschman et al., 2014; Matthews et al., 2016). Using such velocities and the measured lengths of each slab segment, we could calculate the time at which each segment entered the trench. From these calculations, we found that the ca. 1000 km long Caribbean slab entered the trench in early to middle Eocene times, coinciding with regional unconformities identified in the San Jacinto fold belt.

* They interpret three slab segments, each one 300 km long.

6 (lower to middle Miocene) are generally above 60 m/my and locally exceed 300 m/my. In spite of being locally eroded, middle Miocene to Pliocene sequences (7 to 9) exhibit values close to 150 m/my, while Sequence 10 (Corpa, Pliocene to Pleistocene) displays high sedimentation rates, with an average of 530 m/my (Mora et al., 2018). A major increase in sedimentation rates after middle Miocene times is also seen in the Sinú fold

belt and other offshore areas (Figure 18), where rates in excess of 2000 m/my were calculated.

Estimates of corrected total and tectonic subsidence show important variations depending on the geographic location (Figure 19a; Mora et al., 2018). The highest subsidence estimates were obtained in the southern Plato depocenter where 4.8 km of total subsidence and 2.1 km of tectonic subsidence were calcu-

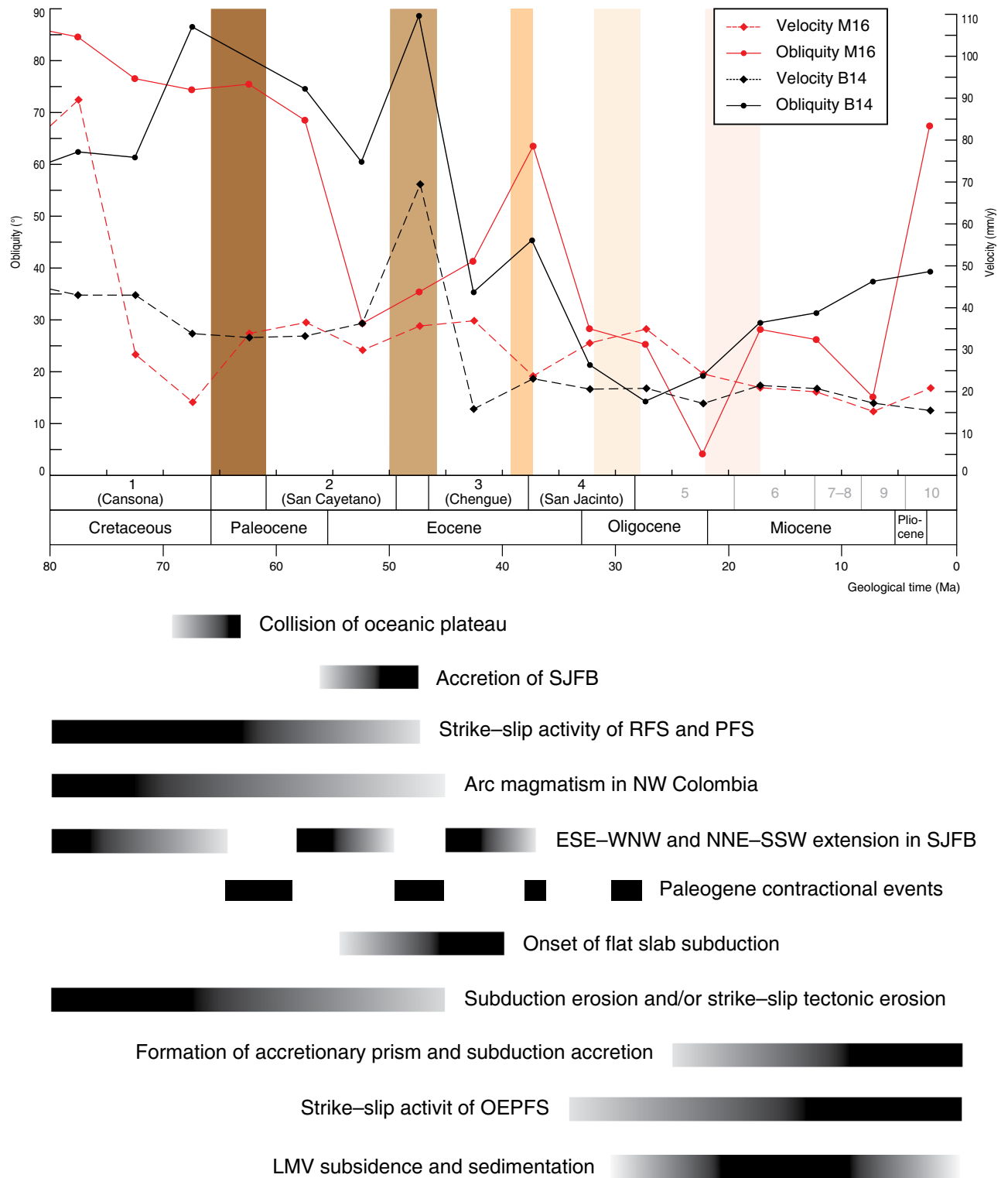


Figure 14. Evolution of Late Cretaceous to present-day tectonic plate convergence velocity and obliquity compared with major tectonic events and tectono-stratigraphic unconformities. The upper panel shows the changes in plate convergence velocity and obliquity with time for both models, compared with the pre-Oligocene tectono-stratigraphic sequences and unconformities (vertical bars of brown shades) and major tectonic events (black horizontal bars in the lower panel). We calculated velocities and obliquities in time-steps of 5 Ma, hence the points in the graph represent the middle of each time interval. The identified Paleogene unconformities correlate with major tectonic events such as the Late Cretaceous to early Paleocene collision of the Caribbean Plateau and the Eocene onset of Caribbean flat-slab subduction. Modified from Mora *et al.* (2017b). However, the best correlation is seen between the early to middle Eocene unconformity and the tectonic events listed in the lower part. (SJFB) San Jacinto fold belt; (RFS) Romeral Fault System; (PFS) Palestina Fault System; (OEPFS) Oca-El Pilar Fault System; (LMV) Lower Magdalena Valley.

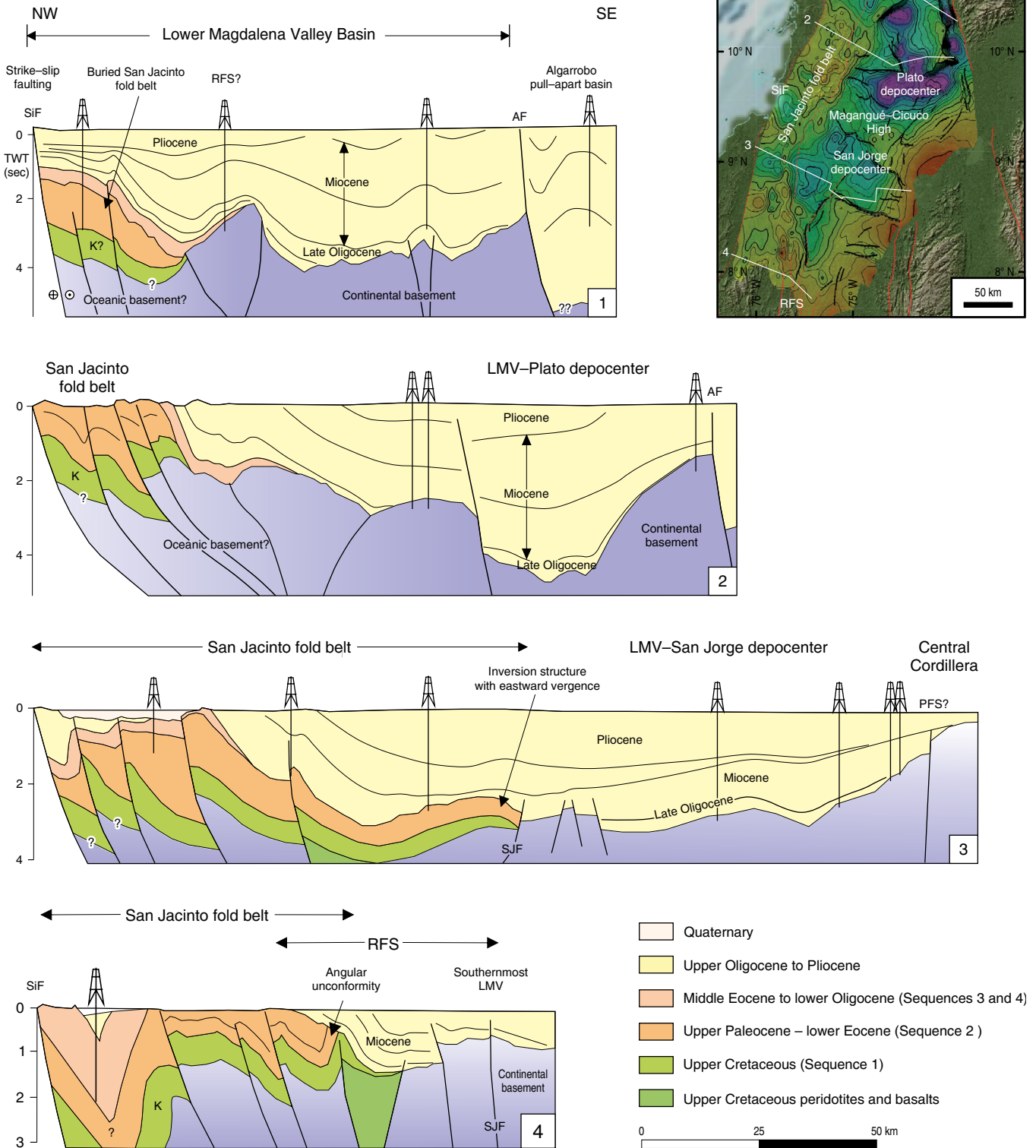


Figure 15. NW-SE-trending, interpreted, seismic cross-sections in two-way-time (TWT), showing the along strike variation in structure of the SJFB, LMV, and RFS, and highlighting tectono-stratigraphic relationships among the studied sequences (modified from Mora et al., 2017b). (SiF) Sinú Fault; (RFS) Romeral Fault System; (AF) Algarrobo Fault; (LMV) Lower Magdalena Valley; (PFS) Palestina Fault System; (SJF) San Jerónimo Fault System.

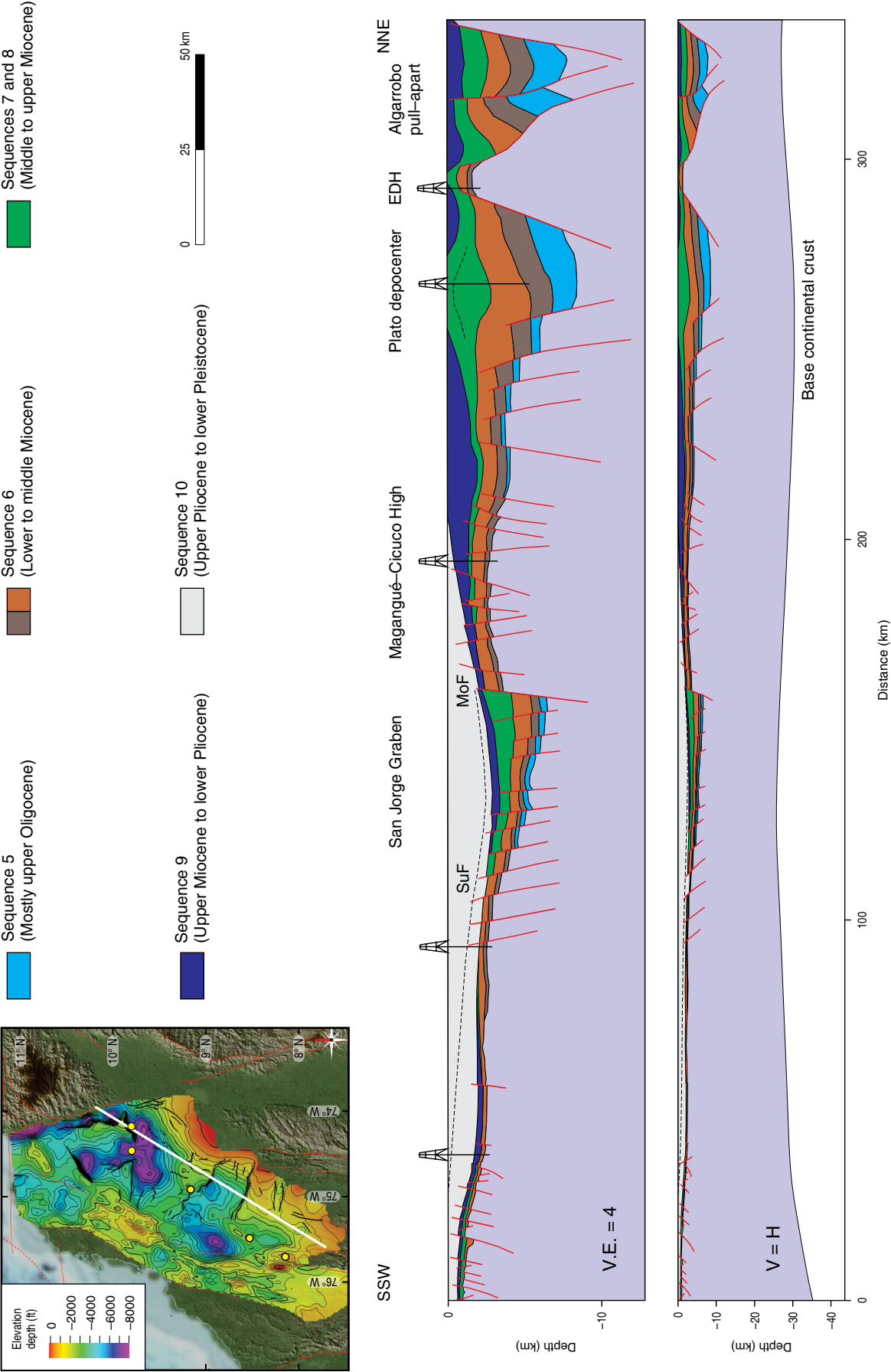


Figure 16. Regional structural cross-section in depth (meters), in two different scales to show the stratigraphic relationships, thicknesses and preservation of the studied Oligocene to Quaternary sequences. The lower section (scale 1:1), also shows the base of the continental crust, based on data by Poveda et al. (2015) and Bernal-Olaya et al. 2015a. Dashed line in Sequence 10 represents clinoform progradation to the north white dashed line in green unit (Sequences 7–8) represents thickening due to internal deformation. (SuF) Sucre Fault; (MoF) Mojana Fault; (EDH) El Dificil High.

lated. In the San Jorge Graben, 3.7 km of total subsidence and 1.8 km of tectonic subsidence were calculated. An increase in tectonic subsidence after 18 Ma is followed by a general decrease after 13 Ma, except for the wells located in the SW (La Esmeralda and Bonga), where there's an increase in tectonic and total subsidence after 3 Ma.

4.11. Extension in the LMV

The simple line-length calculation along the SSW–NNE transect (Figure 16) showed that the basement of the LMV has been extended 40.7 km, which represents 12.1% of extension or a stretching factor of 1.13 (Mora et al., 2018). However, the Algarrobo pull-apart would be accounting for 7% of the total extension in the LMV. According to the tectonic subsidence curves, β values oscillate between 1.1 and 2 in most of the LMV, while in deep parts of the Plato depocenter, β values range from 2 to 4, which are clearly overestimated. Compilation of the crustal thickness and Moho depth data from Poveda et al. (2015) and Bernal–Olaya et al. (2015a) showed that they range from 24 km in the northern LMV, to 50 km in the southeastern boundary of the basin against the northern Central Cordillera (Figure 19b–d). The basement beneath the LMV reaches depths of 8 km in the Plato depocenter and 6 to 7 km in the San Jorge Graben (Mora et al., 2017a). Removal of the sedimentary fill suggests that the crust is thinnest in the northwestern part of the basin and in the western San Jorge depocenter (ca. 20 km; Figure 19d).

Crustal thickness calculations in northern Colombia (Poveda et al., 2012) suggest that the continental crustal thickness in relatively undeformed areas such as the Middle Magdalena Valley Basin ranges from 40 to 45 km. Chulick et al. (2013) obtained a weighted average thickness of the continental South American of 38.17 km, while Assumpção et al. (2013) measured an average thickness of the crust in stable continental areas of Brasil of 39 ± 5 km and 35 km in sub-Andean foredeeps. Therefore, assuming an initial crustal thickness in the LMV area of 40 km and using the present-day crustal thickness map, crustal thinning would be >50% ($\beta=2$) in the Plato depocenter in the north, and around 50% in the Montería–San Jorge graben area, while in the rest of the basin there is much less crustal thinning (32–25 km, 20–38 % thinning). This means that the LMV experienced high extension in the two depocenters (Plato and San Jorge) and low extension in the rest of the basin. Table 2 summarizes our extension estimates using the three different approaches previously described and the previous extension calculations by Montes et al. (2010).

4.12. Oligocene to Recent Paleo–Geography and Kinematics of the LMV

In this section, we present the results of the integration and analysis of all our seismic, well and outcrop data, which are

the basis for proposing an Oligocene to recent kinematic and paleogeographic evolution of the LMV. Such evolution is illustrated both in map view (Figures 8–10) and in cross-section view (Figures 20 and 21).

Seismic and well data shows that the LMV basin was initially filled by Oligocene, shallow-marine deposits of Sequence 5, which filled the paleo-topographic lows, as the sea transgressed from NW to SE (Figures 8a, 20, and 21). Fault-controlled subsidence observed in the seismic indicates that there was an extensional, NE–SW and SE–NE-trending reactivation of pre-existing basement faults. After a lower Miocene unconformity, basal deposits of Sequence 6 covered wider areas to the E, and correspond to shallow-marine clastic deposits in low areas and calcareous deposits in high areas (Figure 8b). Fault controlled subsidence continued, indicating similar extensional regime and trends as in the Oligocene. At least two important forearc highs (Betulia and Cibarco) are documented towards the western LMV, based on seismic onlap patterns. The upper part of the sequence starts displaying progradational patterns, which together with the occurrence of Cretaceous and Grenvillian detrital zircons in the eastern San Jorge depocenter, suggest the onset of drainages from the S or SE.

In middle Miocene times (Figures 9a, 20, and 21), seismic and well data show that deposition became strongly progradational to the NW and N. Though the upper part of Sequence 6 and Sequence 7 exhibit progradational patterns to the WNW (Figure 8), deep marine deposits prevail and the basin reached its maximum flooding at ca. 14 Ma, in agreement with a global sea-level rise (Figure 4). After such maximum flooding episode and in spite of continued basin subsidence and creation of accommodation space, progradational packages of Sequences 8 and 9 advance to the NW (Figure 9). We interpret the fact that progradation was able to overcome increasing subsidence and creation of accommodation space in middle to late Miocene times, as a clear indication of an increase in sediment supply from the SE.

Connection between the LMV and Middle Magdalena Valley (MMV) is probable, and correlates well with thick progradational packages filling the San Jorge depocenter in the south, and turbiditic and gravity-driven deposits filling the deep part of the Plato depocenter in the north. The main evidence for proposing a connection between the eastern LMV and the northern MMV comes from the seismic, well data, and facies models, all of which show that at middle Miocene times, there was progradation of marine stratigraphic packages from the northern MMV towards the NW. Furthermore, while the geochronology data of Montes et al. (2015) shows a Mesoproterozoic (Grenvillian) population of detrital zircons in samples from the eastern LMV, Gómez et al. (2005) and Caballero et al. (2013) proposed that a connection between the northern MMV and the north-eastern LMV was established in earliest middle Miocene times, when the Colorado Formation covered the Cáchira Arch.

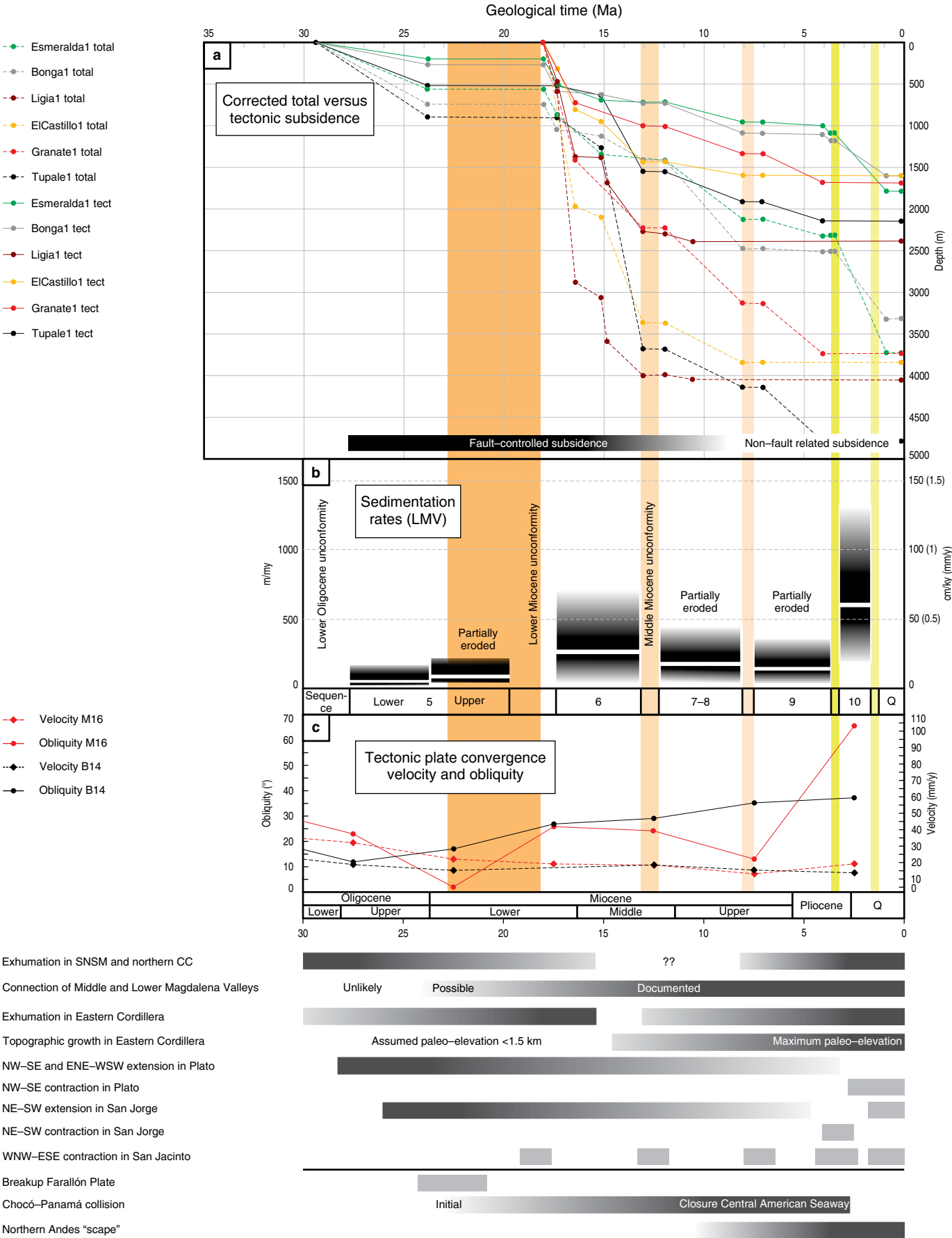


Figure 17. Integration of the subsidence (total vs. tectonic), sedimentation rate and Oligocene to present day, tectonic plate convergence velocity and obliquity, compared with major tectonic events and tectono-stratigraphic unconformities. Tectonic (continuous lines) and total (dashed lines) subsidence plots of representative wells in the LMV and San Jacinto are displayed in (a), and sedimentation rates in (b). (c) From top to bottom exhibits the changes in plate convergence velocity and obliquity with time, for two different paleo-tectonic models (Boschman et al., 2014 in black, B14; Matthews et al., 2016 in red, M16), compared with the Oligocene to Quaternary (Q) tectono-stratigraphic sequences and unconformities (vertical bars with diagonal lines) and major tectonic events (black to grey horizontal bars in the lower panel). We calculated velocities and obliquities in time-steps of 5 Ma, hence the points in the convergence velocity and obliquity graph represent the middle of each time interval. (LMV) Lower Magdalena Valley; (SNSM) Sierra Nevada de Santa Marta; (CC) Central Cordillera.

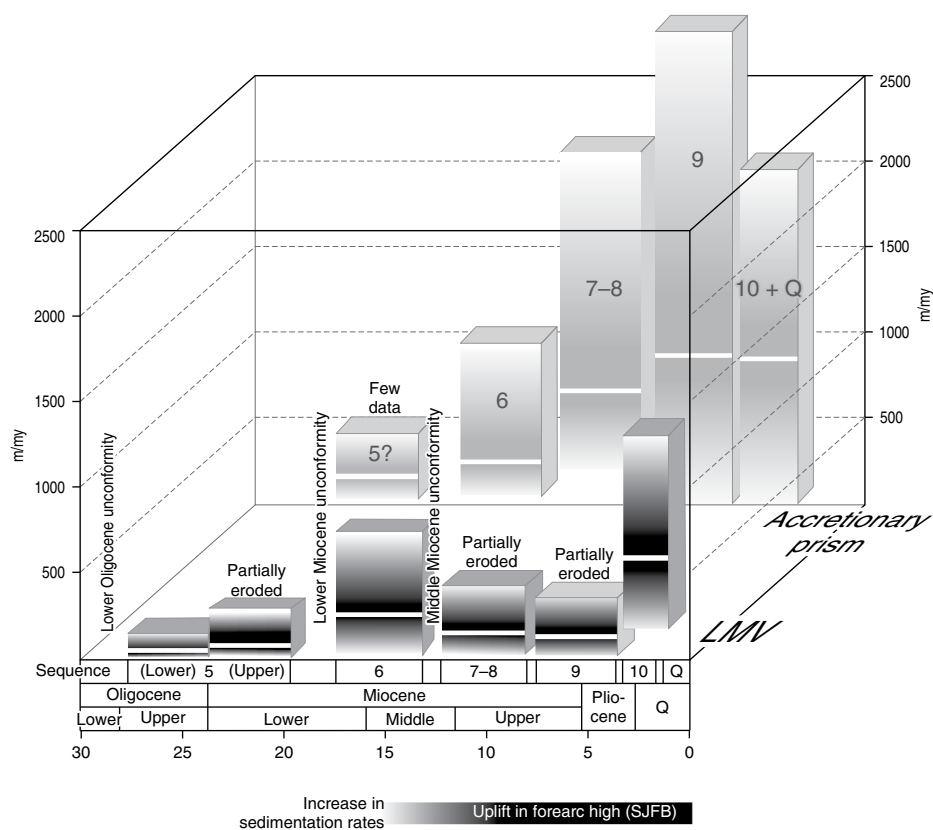
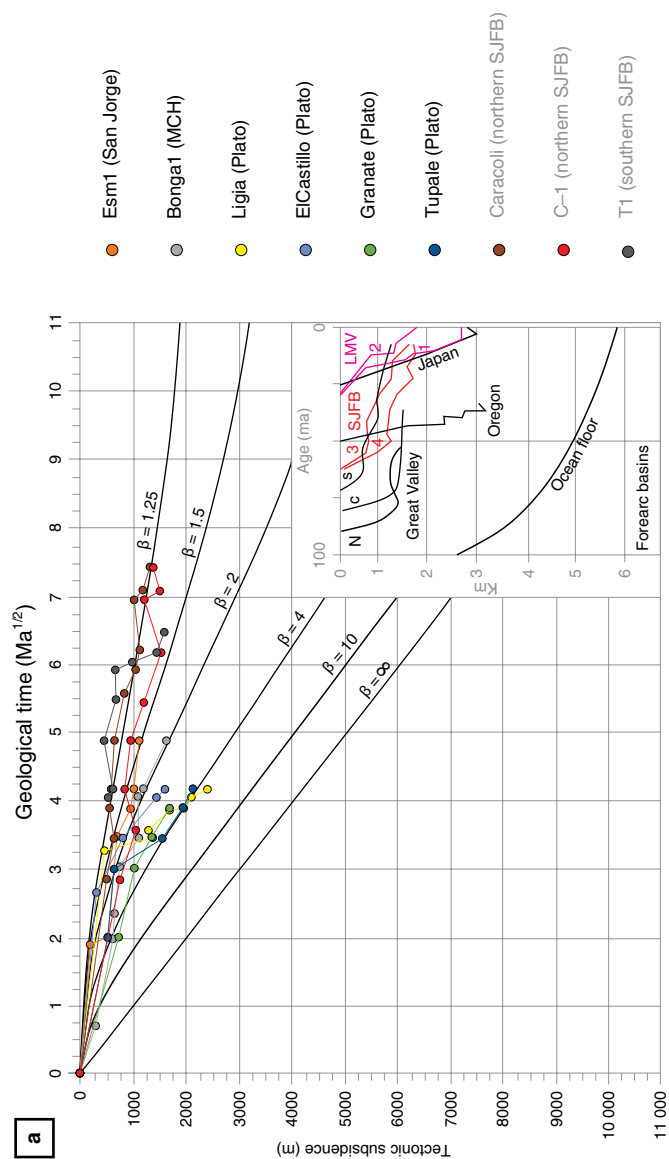


Figure 18. Comparison of Oligocene to recent, compacted sedimentation rates in the LMV and the accretionary prism (Sinú onshore and offshore) from well and seismic data. While there was partial erosion of middle and upper Miocene sequences in the LMV, very high sedimentation rates were measured in the accretionary prism for those sequences. The graph shows the proposed link between high sediment supply, sediment underplating, and uplift in San Jacinto with the formation of forearc highs. (LMV) Lower Magdalena Valley; (SJFB) San Jacinto fold belt.

In late Miocene to early Pliocene times (Sequence 9), the proto-Magdalena shelf clinoforms rapidly prograde to the NW and fill the Plato depocenter until they reach the current coastline, while the proto-Cauca and proto-San Jorge deposits also fill the southern LMV (Figures 9b, 20, and 21). Fault control ceased in the Plato depocenter, while the San Jorge Graben and the forearc highs experienced Pliocene, NE-SW and SE-NW-trending contraction, which was probably not coeval. Upper Pliocene deposits of Sequence 10 are poorly preserved in Plato, while they are well preserved in the San Jorge area, which is actively subsiding (Figure 10a). In the Pleistocene, the Plato area and the forearc highs

are uplifted, while the San Jorge area continues to subside and accumulates thick fluvio-deltaic deposits in a round basin (Figures 10b and 20). Digital elevation models from the study area show that today, the northern LMV (Plato) and the San Jacinto fold belt are positive relief areas, while the southern LMV (San Jorge) continues subsiding. These patterns suggest that SE-NW-trending contraction and NE-SW-trending extension have been active since late Pliocene times, in agreement with the displacement vector of the Caribbean Plate relative to fixed South America.

Thickness analyses of each sequence allowed us to study the development and migration of depocenters since late Oli-



- Esm1 (San Jorge)
- Bongat1 (MCH)
- Ligia (Plato)
- ElCastillo (Plato)
- Granate (Plato)
- Tupale (Plato)
- Caracoli (northern SJFB)
- C-1 (northern SJFB)
- T1 (southern SJFB)

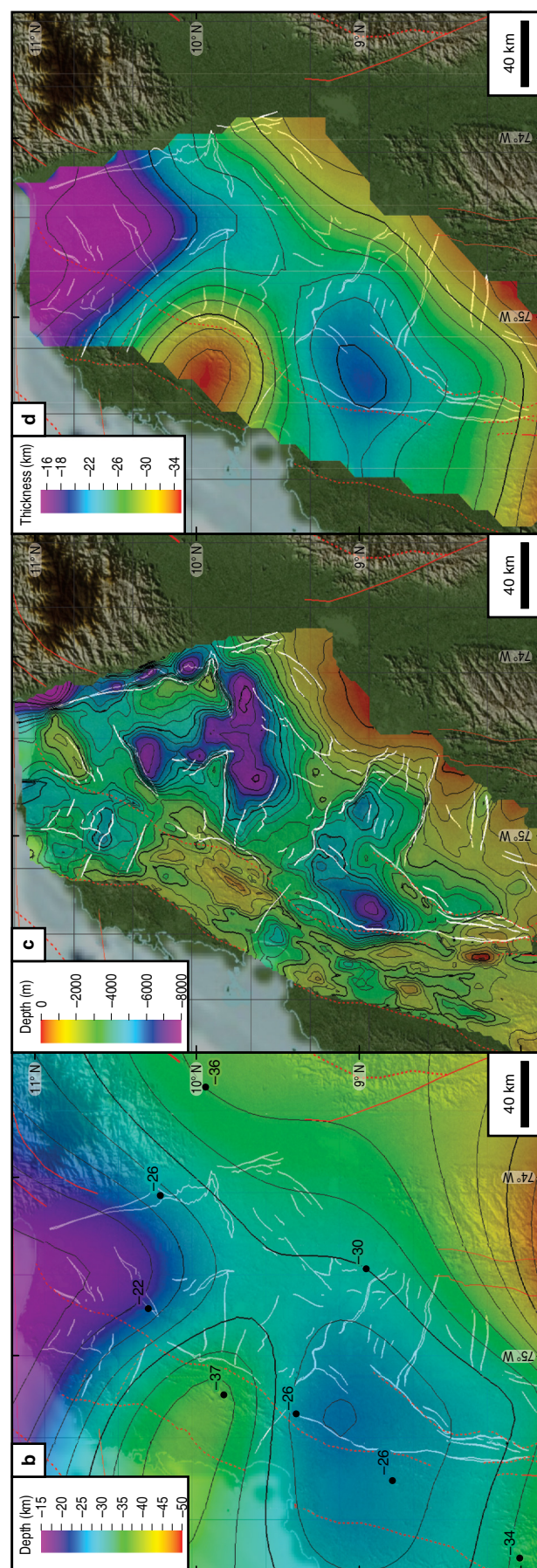




Figure 19. (a) Tectonic subsidence data plotted against the square root of the geological time (time since end of extension), in order to estimate stretching in the LMV (β -factor; McKenzie, 1978). Inset shows a comparison of our tectonic subsidence curves for the LMV and SJFB with data from other forearc basins compiled by Angevine et al. (1990), showing a good correlation with some basins. 1–Northern LMV (Plato); 2–Southern LMV (San Jorge); 3–Southern San Jacinto; 4–Northern San Jacinto. (b–d) Maps used to calculate extension in the LMV and SJFB. **(b)** Depth map of the Moho discontinuity, representing the crustal thickness, based on Poveda et al. (2015) and Bernal–Olaya et al. (2015a), showing that the crust thickness ranges from 22 km in the northern LMV to >30 km in the central and SW San Jacinto. Stations with measured values are depicted in black (values obtained from Bernal–Olaya et al. (2015a) were extrapolated as points from their regional gravity sections). **(c)** Basement map in depth (km) of the LMV, based on Mora et al. (2017a). **(d)** Crustal thickness map without sedimentary infill, obtained by subtracting the basement map in (c) from the crustal map in (b). It must be noted that the thinner crust (<20 km) in the NW of the LMV, where no thickness data is available, resulted from mapping extrapolation. (MCH) Magangué–Cicuco High; (SJFB) San Jacinto fold belt; (LMV) Lower Magdalena Valley.

Table 2. Compilation of extension calculations in previous (e.g., Montes et al., 2010) and this study, according to the different methods that were used. Further explanation in the text.

	Stretch factor	Extension in LMV	Comments
Line–length in cross–section	1.13	40.7 km (12.1%)	only the Algarrobo Fault System has been extended 26.7 km
Tectonic subsidence curves	$\beta = 1.1$ to 4		β values very high in depocenters (overestimated)
Crustal thickness measurements	$\beta \leq 2$		maximum 50% in depocenters; 20–38 % elsewhere*
Montes et al. (2010)	$\beta = 1.1$ to >4	86 to 115 km	both extension calculations are overestimated

*Assuming initial crustal thickness of 40km.

gocene times. The detailed depocenter evolution and the possible reasons for depocenter migration are discussed in the following section.

5. Discussion

5.1. Structure and Age of the LMV Basement

5.1.1. Correlations with Outcropping Basement Terranes

The integration of potential methods, reflection seismic, and detrital zircon U–Pb geochronology and Hf isotope geochemistry allowed Mora et al. (2017a) to propose more robust correlations between the basement terranes in the surrounding massifs and the basement terranes identified in the LMV basement. These authors confirmed the extension of the Tahamí–Panzenú Terrane to the north into the LMV and proposed that an oceanic terrane, which could correspond to the Quebradagrande Complex or to a younger Late Cretaceous, allochthonous intra–oceanic arc, also extends in the western LMV, while the San Lucas (Chibcha) Terrane terminates against the northeastern LMV (Figure 22a; Mora et al., 2017a).

The data obtained from the Cicuco–22 well (Silva–Arias et al., 2016) and the new Coniacian – Campanian crystallization ages from the Bonga–1 granitoid confirmed the continuity to the north of the Late Cretaceous magmatic arc in the northern

CC, which includes important plutons like the Antioquian Batholith (88–83 Ma, Ibañez–Mejía et al., 2007 and 93–87 Ma, Villagómez et al., 2011). Geochemical analyses of the Upper Cretaceous Cicuco intrusive suggested that this granitoid is related to a subduction environment and corresponds to calc–alkaline magmas, interpreted to be emplaced in a continental Andean–type crust (Silva–Arias et al., 2016). However, the new Bonga Hf isotopic data indicate a clear juvenile component, with limited evidence for significant contamination with older continental crust. Furthermore, the highly positive Bonga ϵ_{Hf} values obtained are in contrast with the less radiogenic values obtained for the Upper Cretaceous granitoids of the northern CC such as the Antioquian Batholith (Restrepo et al., 2007). Considering these observations, and taking into account the proximity of the Bonga granitoid to the Romeral Fault System, Mora et al. (2017a) considered that the Bonga Pluton intruded a previously accreted oceanic terrane possibly located within the Romeral System, which may correspond to the northern continuation of the Quebradagrande Complex (Nivia et al., 2006). The Quebradagrande Terrane was accreted to South America along the San Jerónimo Fault in Albian times (115 to 105 Ma, Villagómez & Spikings, 2013).

An alternative possibility contemplates that the Bonga Pluton formed within an allochthonous intra–oceanic arc, which collided against the Permian – Triassic continental margin in latest Cretaceous to early Paleocene times (Bayona et al., 2011; Cardona et al., 2012). According to this interpretation, this pluton would correspond to the Great Arc of the Caribbean (Al-

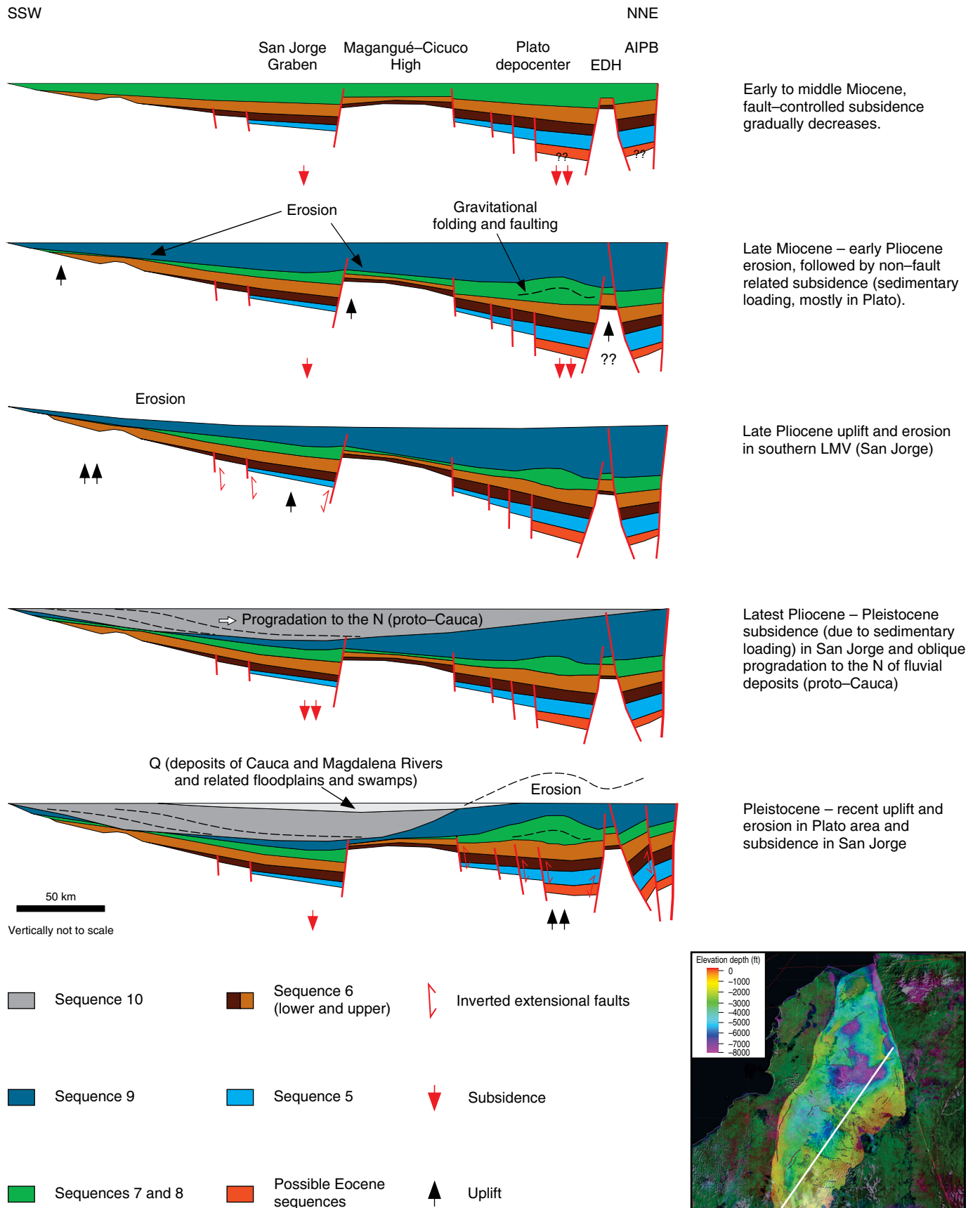




Figure 20. Simplified Oligocene to recent evolution of the LMV, shown in a NNE–SSW–trending regional section. Oligocene to middle Miocene fault-controlled subsidence, which affected Sequences 5 to 7, was replaced by non-fault related subsidence (sagging) during deposition of Sequences 8 to 10. After the middle Miocene, the two depocenters (Plato and San Jorge) started to experience different subsidence and uplift phases. Figure vertically not to scale. (EDH) El Dificil High; (AIPB) Algarrobo pull-apart basin.

tamira & Burke, 2015; Burke, 1988; Escalona & Mann, 2011; Kroehler et al., 2011; Villagómez & Spikings, 2013), a regional arc that appears to extend from Ecuador to the Lesser Antilles.

5.1.2. Formation of LMV Basement Fabric and Late Cretaceous Geodynamic Setting

The basement architecture of northwestern Colombia was built from Cretaceous to middle Eocene times and resulted in the formation of two major suture zones, the Romeral and the Palestina Fault Systems (Cediel et al., 2003; Restrepo & Toussaint, 1988). Based on previous studies and recent data and interpretations, Mora et al. (2017a) proposed that the basement fabric in the LMV and San Jacinto fold belt was formed by two main, regional tectonic processes (Figure 22b): (i) Jurassic rifting and (ii) Late Cretaceous to middle Eocene oblique convergence of the Caribbean and South American Plates, producing large-scale, dextral strike-slip displacement, arc-parallel extension due to displacement partitioning, and clockwise block rotation. The inherited pre-Oligocene basement fabric was later reactivated during the late Oligocene and early Miocene, allowing the formation and infill of the LMV. The new results allowed the reconstruction of the Late Cretaceous geodynamic setting of the LMV and San Jacinto, consisting of an east-dipping subduction of the “normal” thickness oceanic plate beneath South America, generating intracontinental arc magmatism of the Bonga and Cicuco Plutons. The current proximity of the Bonga Pluton to the trench suggests that significant erosion of the older forearc occurred by subduction erosion (Clift & Vannucchi, 2004) and/or by dextral strike-slip. However, there is also the possibility of formation of the Bonga Pluton in an intraoceanic arc, such as the Great Arc of the Caribbean (Altamira & Burke, 2015; Burke, 1988), which collided with northwestern South America in Late Cretaceous times (ca. 70 Ma, Luzieux et al., 2006).

5.2. San Jacinto: An Late Cretaceous to Early Eocene Marine Forearc Basin Formed in an Oblique Convergence Tectonic Setting

5.2.1. San Jacinto Late Cretaceous to Early Eocene Forearc Evolution

From the available information, it appears that during Late Cretaceous (Coniacian to Campanian) times, a forearc basin existed SW of the study area, with an intra-continental, magmatic arc

to the east, formed by the east-dipping subduction of a “normal” thickness, Caribbean oceanic plate under South America (Mora et al., 2017a). Magmatism affected both continental and accreted oceanic crust (the Quebradagrande Terrane or a younger, allochthonous intra-oceanic arc) and supplied abundant mafic and felsic, volcanoclastic material to the proximal parts of the basin. Abundant outcrop and the very few available well data show that sedimentation in the area of the present-day SJFB occurred in a marine shelf in which proximal marine environments occurred in the central area (San Jacinto) while deeper marine environments occurred in the south.

The absence of lower Paleocene deposits in northwestern Colombia (planktonic zones P.0 to P.2., 65 to 61 Ma) and the unconformity that has been reported in outcrops between Sequence 1 (Cansona) and Sequence 2 (San Cayetano) are the expression of a regional shortening event which took place in latest Cretaceous to early Paleocene times, and which would be related to a collision episode of the Caribbean Plateau. The abrupt decrease in convergence velocity between 75 and 70 Ma, according to Matthews et al. (2016) could be related to this collision event (Figure 14). After the early Paleocene shortening episode, forearc extension, subsidence, and marine sedimentation resumed. New U–Pb geochronology and Hf isotope geochemistry results (Mora et al., 2017b) suggest that the upper Paleocene – lower Eocene sedimentites of Sequence 2 were mainly sourced from Upper Cretaceous plutons of both oceanic (e.g., Bonga, Mora et al., 2017a) and continental affinity (Mangué Arc, Silva–Arias et al., 2016; Antioquian Batholith), and from the Permian – Triassic igneous–metamorphic terranes in the LMV and northern CC (Cochrane et al., 2014; Mora et al., 2017a). Paleo-tectonic reconstructions (Mora et al., 2017b) show that after a considerable (ca. 1077 km) northwestward displacement of the Caribbean oceanic terranes in Late Cretaceous times, such terranes including San Jacinto, had almost reached their current position, thus supporting the previously mentioned provenance considerations. These data also support a forearc basin setting in which both the oceanic and continental affinity, Late Cretaceous to Paleocene magmatic arcs were being eroded and providing sediment for the marine basin to the northwest.

5.2.2. The Lower to Middle Eocene Unconformity and the Onset of Flat Subduction

The prominent lower to middle Eocene angular unconformity that marks the top of Sequence 2 (San Cayetano) is the most im-

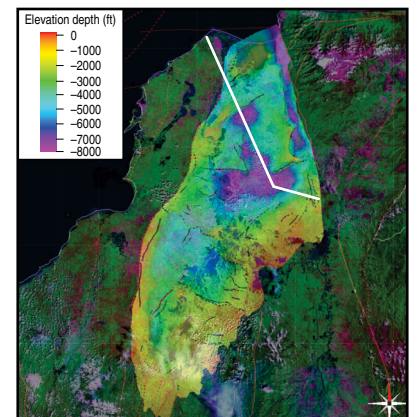
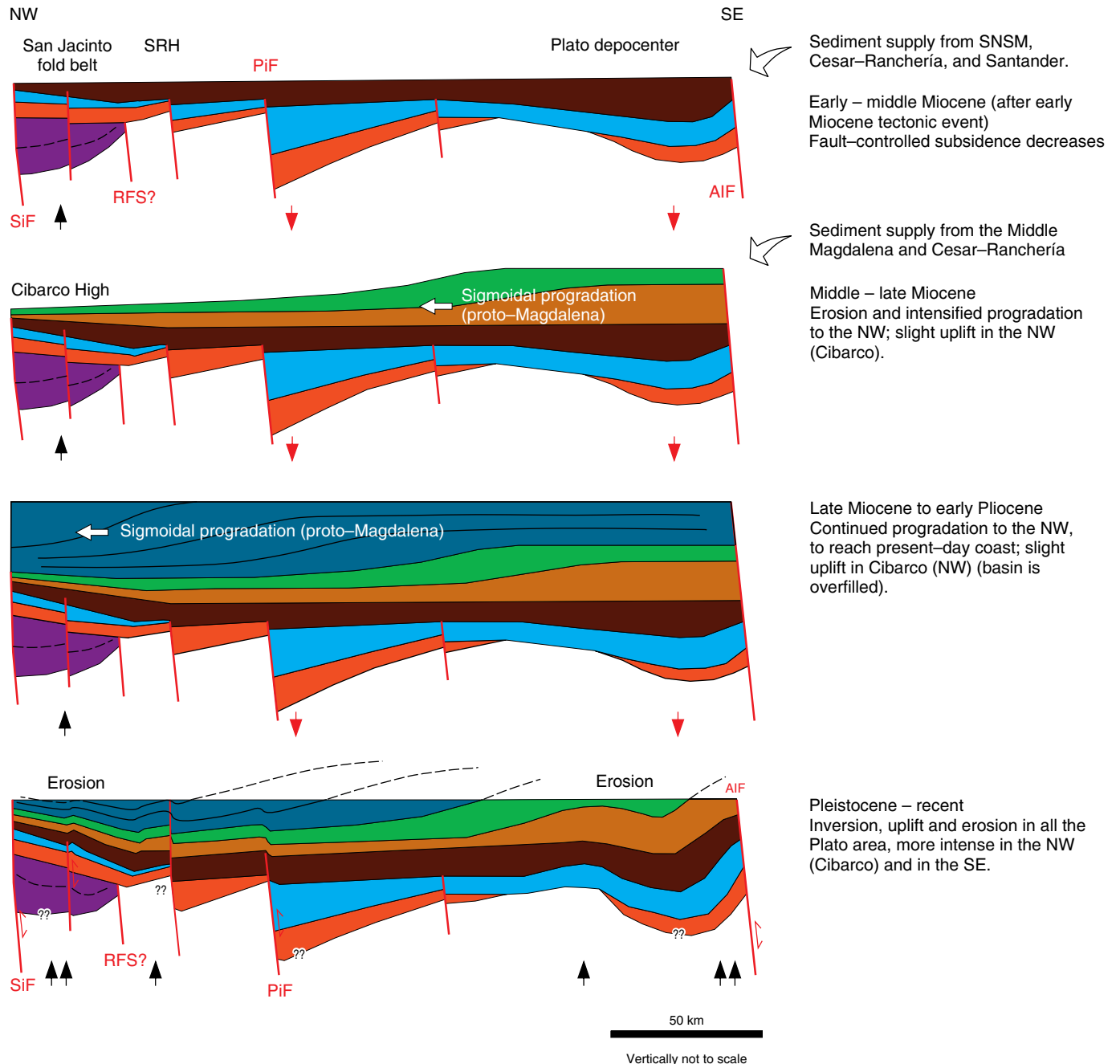


Figure 21. Simplified Oligocene to recent evolution of the LMV, shown in a SE–NW–trending regional section. After Eocene to middle Miocene, fault-controlled extension, connection with the Middle Magdalena caused sigmoidal progradation to the NW of Sequences 7 to 9 in the Plato depocenter, until it became overfilled. Pleistocene to recent shortening was responsible for the inversion of previous extensional faults and intense erosion towards the area of the Algarrobo Fault (AF). Figure vertically not to scale. (SiF) Sinú Fault; (RFS) Romeral Fault System; (SRH) Santa Rita High; (PiF) Pivijay Fault; (AlF) Algarrobo (Arjona) Fault; (SNSM) Sierra Nevada de Santa Marta; (AF) Algarrobo Fault.

portant evidence of the final episode of activity of the Romeral Fault System and of a major shortening event in northern Colombia. Seismic data shows that this event also marks the end and fossilization of the San Jacinto Forearc Basin and the birth of a new basin of middle Eocene to recent age (Lower Magdalena, Mora et al., 2017b). Taking into account the present-day lithospheric and mantle geometry, as interpreted in Figure 11, the onset of subduction of the Caribbean Plate occurred in early to middle Eocene times, 56 to 43 Ma ago (Table 1; Mora et al., 2017b). Interestingly, this calculated time of onset of subduction of the Caribbean Plateau coincides with the time of plate tectonic readjustment between the Caribbean and the Americas (Figure 14), with the estimated age of the lower to middle Eocene unconformity in the San Jacinto fold belt (planktonic foraminiferal zones P.9 to P.10, 50.4 to 45.8 Ma) and with the time of cessation of magmatism in northern Colombia (50–45 Ma; Bayona et al., 2012). Therefore, it appears that a major early to middle Eocene plate–tectonic readjustment, consisting of an abrupt decrease in both convergence velocity and obliquity in early to middle Eocene times, seems to be the most likely cause of: (i) the onset of flat–slab subduction in northwestern Colombia, (ii) the cessation of magmatism in northern Colombia in the middle Eocene, (iii) a major shortening event with the exhumation and partial erosion of the Late Cretaceous to early Eocene San Jacinto Forearc Basin, (iv) the end of the tectonic activity of major Cretaceous fault systems such as Romeral and Palestina, and (v) the later onset of right–lateral strike–slip displacement along the newly formed Oca–El Pilar Fault System (Boschman et al., 2014; Müller et al., 1999; Pindell & Kennan, 2009).

The imprint of such tectonic readjustment in the stratigraphic record of the San Jacinto fold belt is the lower to middle Eocene unconformity, though the upper Eocene unconformity could also be related. These unconformities could also be the result of the early to middle Eocene, collision episode of the Great Arc of the Caribbean with South America, which caused a subduction polarity reversal (Escalona & Mann, 2011; Kroehler et al., 2011), as seen in other areas of active, arc–continent collision. According to this interpretation, the previously described events would be collisional effects.

After the early to middle Eocene plate tectonic readjustment (or collision with polarity reversal, according to Kroehler et al., 2011) and the onset of flat subduction, the San Jacinto area experienced renewed forearc extension, subsidence, and sedimentation which comprised coarse–grained

clastics and shallow marine carbonates of Sequences 3 and 4 (Chengue and San Jacinto). U–Pb geochronology and Hf isotope geochemistry results (Mora et al., 2017b) show the same Late Cretaceous and Permian – Triassic peaks as seen in samples from the sequence below (San Cayetano), hence sediment supply was mostly coming from the northern CC and SNSM in the SE and NE respectively. Figure 17c clearly shows that the Caribbean–NW South America convergent margin became relatively stable since Oligocene times, exhibiting low convergence velocities and obliquities. The margin probably evolved from a highly oblique convergent margin, possibly exhibiting subduction erosion (Clift & Vannucchi, 2004) in Late Cretaceous to Eocene times, to a more orthogonal convergent margin, exhibiting subduction accretion since early Miocene times, when the accretionary prism probably started forming.

5.3. Lower Magdalena Valley: A Middle Eocene to Recent Amagmatic Forearc Basin, Formed in a Nearly–Orthogonal, Flat Subduction Tectonic Setting

5.3.1. Formation of the LMV

We consider that the formation of the LMV is related to the cooling of the Cretaceous to early Eocene, intra–continental magmatic arc of NW Colombia, and to the fault–controlled subsidence at the initial subduction stages (Figure 23). Cooling caused the extensional reactivation of the main pre–Oligocene basement features such as the Mojana and Sucre Faults that limit the San Jorge Graben, and the Pivijay, Apure, Pijiño, and other faults of the Plato depocenter. Extensional reactivation of the main pre–Oligocene basement structures was crucial for the tectonic segmentation of the basin and for the formation of its two depocenters (Plato and San Jorge). However, it is also possible that initial subsidence could have been caused by crustal thinning due to possible Cretaceous to Eocene subduction erosion (Clift & Vannucchi, 2004), as suggested by Mora et al. (2017a, 2017b). Tectonic clockwise block rotation caused by Paleogene oblique convergence, and older than previously proposed block rotations (e.g., Montes et al., 2010; Reyes–Harker et al.), could have also influenced the formation of the LMV. Bernal–Olaya et al. (2015c) proposed that the extension in the

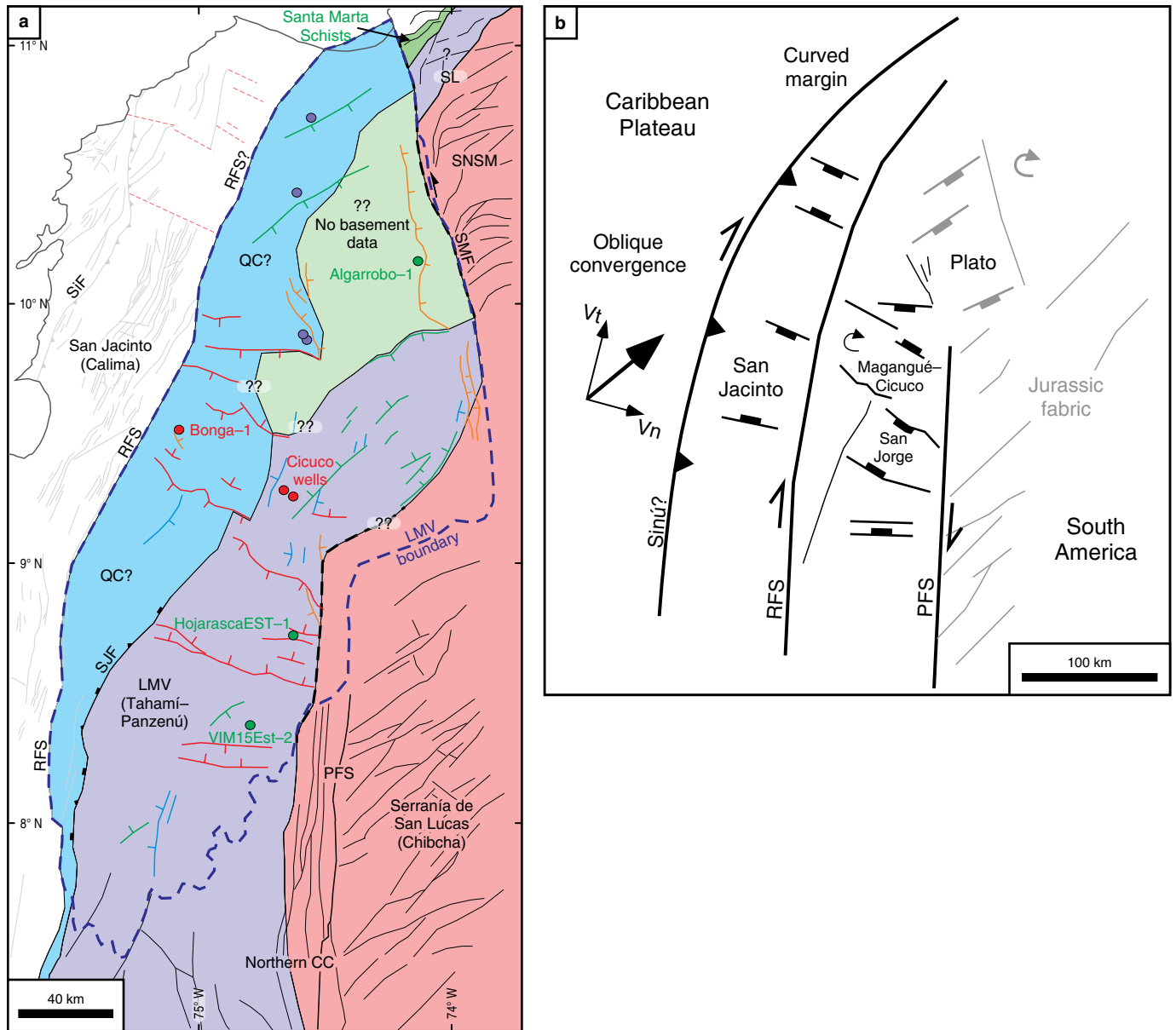
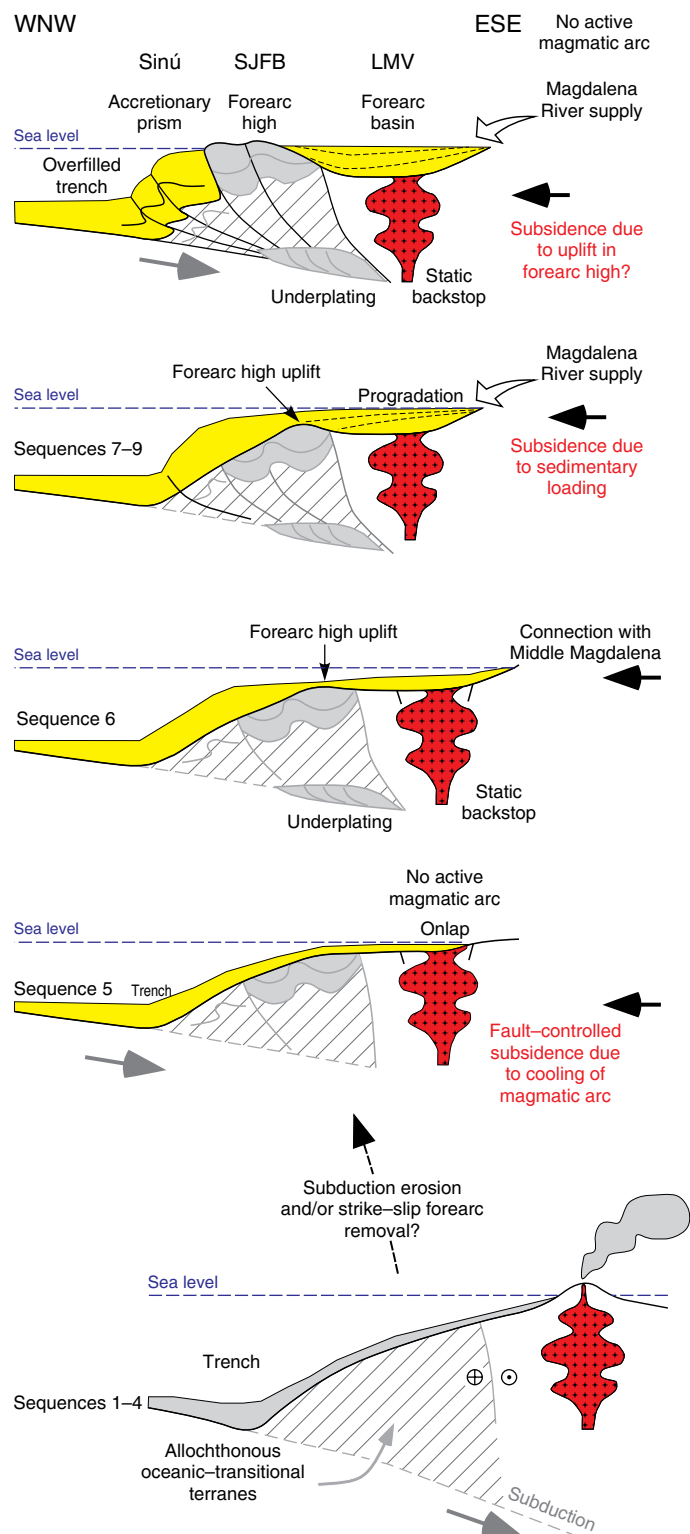


Figure 22. (a) Interpreted basement terranes in the LMV and surrounding massifs (after Mora et al., 2017a). Chibcha Terrane is in pink, Tahamí–Panzenú in lavender, Quebradagrande Complex (QC) in blue, and Calima is white. Upper Cretaceous, low-grade metamorphic terranes in LMV (El Dificil and Algarrobo) and in the northwestern SNSM are colored in green. Correlation of the Tahamí–Panzenú Terrane towards the N (SNSM) is being revised to include new data from Piráquive (2017). Modified from Mora et al. (2017a). **(b)** Sketch illustrating the proposed mechanisms of formation of the basement architecture in the LMV and San Jacinto areas of northwestern Colombia, which acted during Late Cretaceous to middle Eocene times. Modified from Mora et al. (2017a). (SL) Sevilla Lineament; (RFS) Romeral Fault System; (SNSM) Sierra Nevada de Santa Marta; (SiF) Sinú Fault; (SMF) Santa Marta Fault; (LMV) Lower Magdalena Valley; (SJF) San Jerónimo Fault; (PFS) Palestina Fault System; (CC) Central Cordillera; (V_t) displacement vector component parallel to the margin; (V_n) displacement vector component normal to the plate margin.

LMV and formation of the two depocenters was related to the curvature of the margin. This could also be valid considering the oblique convergence model presented in Figure 22b, displaying a curved margin.

Recent estimates of extension in the LMV (Table 2; Mora et al., 2018) show that the basin has been moderately extended (stretching factor from 1.1 to 1.5), except for local areas where

the crust has been considerably thinned (western San Jorge depocenter and northern LMV). The LMV thus appears to have a relatively thin crust, with thicknesses varying from 18 to 28 km, whereas a thicker crust would occur in the central SJFB (30–34 km; Figure 19d). A relatively thin crust could be related to the location of the LMV close to the plate margin, and/or to the proposed pre-Oligocene subduction erosion (Mora et al.,



Pleistocene to recent:
LMV overfilled, benching, continental forearc basin; amagmatic, flat-slab subduction; compressional accretionary forearc basin (sensu Noda, 2016).

Middle Miocene to Pliocene:
LMV overfilled, terraced to shelved, deep marine to marine deltaic, to transitional forearc basin.

Early to middle Miocene:
LMV underfilled, sloped to ridge, shallow to deep marine forearc basin; increase in sediment supply and onset of underplating.

Late Oligocene:
Magmatic-arc collapsed and LMV underfilled, mostly sloped, shallow marine forearc basin; low-angle, amagmatic subduction.

Late Cretaceous to early Eocene:
San Jacinto underfilled (?), deep-marine, sloped forearc basin; subduction with active magmatic arc.

Figure 23. Interpreted cross section evolution of the morphology of the Lower Magdalena Valley (LMV) and San Jacinto fold belt (SJFB), from an Upper Cretaceous to Eocene underfilled, sloped forearc basin (sensu Dickinson, 1995) with an active magmatic arc, to the current amagmatic and overfilled, benching continental forearc basin. Increased Miocene sediment flux, the inherited basement structure, and flat-slab subduction were the main controls on Oligocene to recent forearc basin evolution.

2017b). Such thinned crust would have made easier an extensional reactivation of pre-existing features.

5.3.2. Oligocene to Recent Forearc Evolution

Eocene deposits are mostly preserved in the SJFB, though they could also be preserved at great depths in the footwall of extensional faults in the LMV. According to paleo-tectonic reconstructions (Boschman *et al.*, 2014; Müller *et al.*, 1999; Pindell & Kennan, 2009) and to reconstructions using the GPlates software (Figure 13; Figures 1 and 2 of the Supplementary Information), the last 30 Ma were characterized by low convergence obliquities and relatively low velocities, which do not appear to show abrupt changes in their trend (Figure 17c), making difficult clear correlations with reported tectonic events such as subsidence or uplift pulses. In spite of the relative stability of the Oligocene to recent convergence between the Caribbean Plate and NW South America, the analyses carried out by Mora *et al.* (2018) indicate that after the early Miocene tectonic event, there was an increase in subsidence and sedimentation in the LMV, possibly related to the formation of the Magdalena fluvial system, when the eastern LMV was connected to the Middle Magdalena Valley (Anderson *et al.*, 2016; Hoorn *et al.*, 2010; Reyes-Harker *et al.*, 2015).

Second-order processes such as flat-slab subduction of a buoyant oceanic plateau substantially modify the tectonic configuration of the upper plate and produce modified forearc basins (Ridgway *et al.*, 2012). This could be the case of the LMV, which according to Mora *et al.* (2017b), was formed during low-angle subduction of the Caribbean oceanic plateau beneath South America. Fault-controlled subsidence took place in the LMV from Oligocene to middle Miocene times (29–13 Ma), spanning for 16 my, and then it was replaced by non-fault related subsidence (Mora *et al.*, 2018). However, in the SW (San Jorge depocenter, Bonga and Esmeralda wells), there is an increase in tectonic subsidence after 3 Ma, related to the deposition of Sequence 10.

A dramatic increase in sedimentation at ca. 17 Ma, after an lower Miocene regional unconformity, would have influenced the change of fault-controlled subsidence to non-fault related subsidence, implying that sedimentary loading became the main subsidence mechanism since late Miocene times. A relatively thin and not very strong crust in the LMV would have made easier for sedimentary loading to become the main subsidence mechanism since middle Miocene times. The increased sediment supply also strongly influenced the plate interface, by lubricating the subduction channel, thus affecting the transmission of stresses to the upper plate and producing underplating. Crustal thickening by tectonic underplating of subducted materials has been proposed as a cause of uplift in forearc coastal terranes such as the Chile Forearc (e.g., Clift & Hartley, 2007; Glodny *et al.*, 2005), the Aleutians (Moore *et al.*, 1991), the

Hikurangi margin (Scherwath *et al.*, 2010), and the Cascadia subduction zone (Calvert *et al.*, 2011). In the Aleutians (Moore *et al.*, 1991), layered reflectors beneath the Kodiak accretionary complex were interpreted as the result of underplating and may represent an antiformal stack of thrust sheets, such as those interpreted by Mora *et al.* (2017a, their Figure S1), based on deep seismic imaging. Therefore, uplift in the forearc high in the SJFB as seen in the western LMV and current San Jacinto fold belt, may be related to tectonic underplating. The occurrence of a deformed outer high to the W (San Jacinto fold belt) and an undeformed forearc basin behind it, to the E (LMV), is explained if the continental basement beneath the LMV acted as a static backstop, with geologically reasonable contrasts in mechanical properties compared to the sediments just trenchward of it (Byrne *et al.*, 1993; Mantilla-Pimiento *et al.*, 2009).

5.3.3. A Comment about the Connection of Panamá with the LMV

Based on a few U–Pb detrital zircon geochronology analyses in localized wells in the LMV, Montes *et al.* (2015) proposed a mixed provenance for middle Miocene strata including material derived from the old northwestern South American orogens and from the Panamá Arc. For such proposal they suggest the existence of fluvial channels flowing from the Panamá Arc in the SW to the NE, along more than 300 km, to reach areas such as the Apure High in the Plato depocenter (BH3 in Montes *et al.*, 2015). Our regional study, which includes thousands of kilometers of reflection–seismic data, hundreds of boreholes and outcrop data, does not support such interpretation: while seismic data allowed the mapping of the stratigraphic features (e.g., clinoforms) clearly prograding to the WNW in early Miocene to Pliocene times (Mora *et al.*, 2018), data from hundreds of wells indicate that middle to upper Miocene units (Sequences 6 to 8) consist of fine-grained, distal deltaic, shelf and even turbiditic deposits and that unambiguous fluvial facies only appear in Sequences 9 and 10, after 7 Ma (late Miocene to Pliocene). Furthermore, the middle Miocene to recent forearc highs in the area of the present-day SJFB, proposed by Bernal-Olaya *et al.* (2015c) and Mora *et al.* (2018), would have acted as a barrier, making very difficult a sedimentary connection with the distant Panamá Arc in the SW. Such results show that the northern LMV was clearly not sourced from the Panamá Arc in Miocene times. We thus consider that geochronological analyses must be taken with extreme caution; they must be integrated with other types of methods and all the data together must be interpreted within a robust regional tectono-stratigraphic framework. In addition, researchers dealing with mixed provenance results should always propose several possible interpretations instead of assuming a single, unique interpretation.

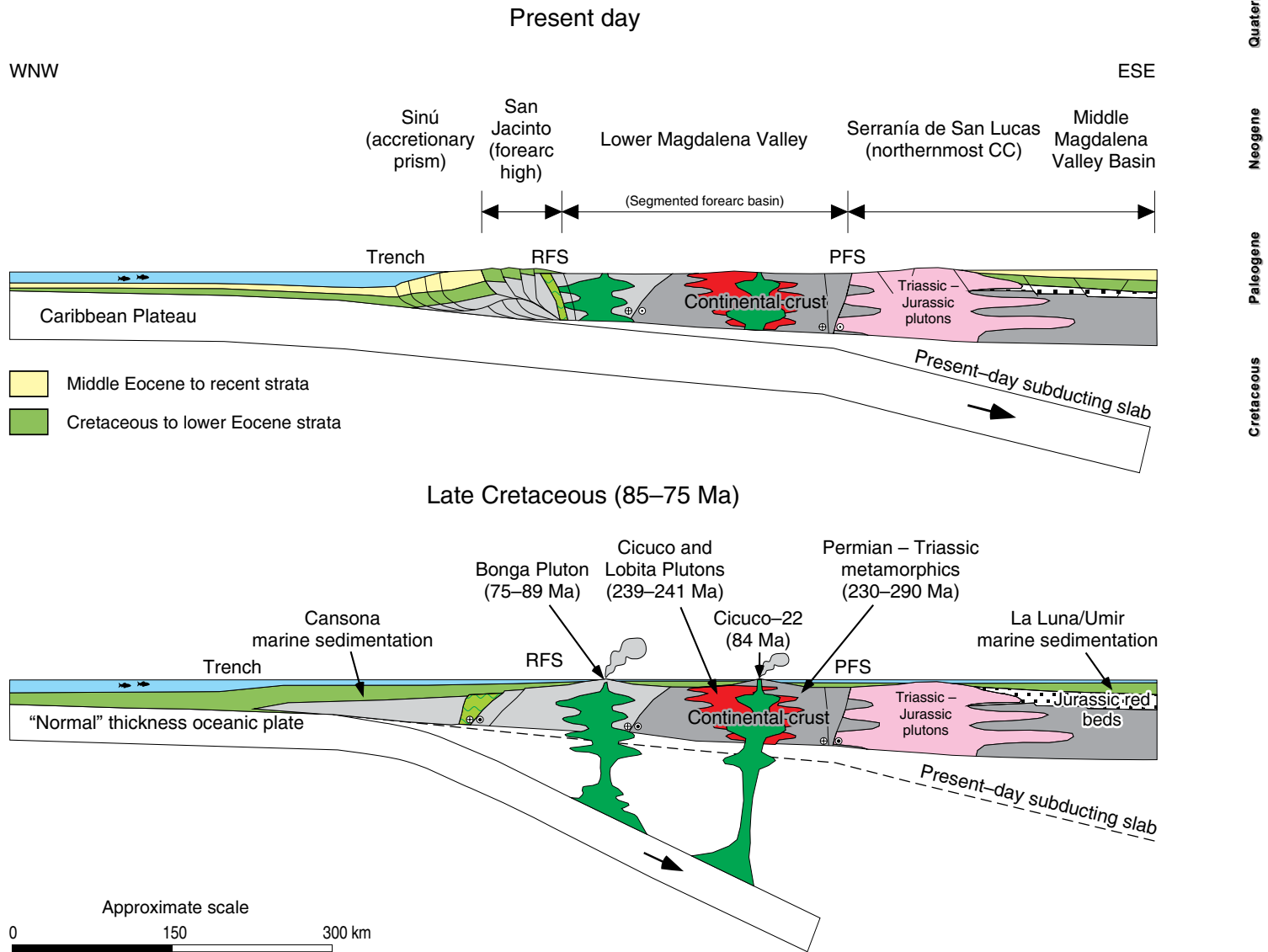


Figure 24. In the lower part we show a hypothetical cross section with the interpreted geodynamic setting at the Magangué–Cicuco High, in Late Cretaceous times (modified from Mora et al., 2017a). In the upper part, the interpreted present-day geodynamic and basin configuration of the Lower Magdalena Valley (LMV) and San Jacinto fold belt (SJFB). Though the present-day trench shown in the figure appears to be located farther to the east than the Cretaceous trench, it should really be located farther to the west in a mantle reference frame, considering that plate tectonic processes between the Caribbean and the Americas have been driven by relatively fast, westward motion of North and South America (Müller et al., 1999). In Late Cretaceous times, subduction was probably of a “normal” thickness plate while today, an oceanic plateau is being subducted. (RFS) Romeral Fault System; (PFS) Palestina Fault System; (CC) Central Cordillera.

5.3.4. Tectonic Segmentation and Depocenter Evolution in the LMV

Based on the measured thicknesses of the tectono-stratigraphic sequences, the Oligocene to recent depocenter evolution in the LMV was studied, and it was found that there was a depocenter landward migration and shifting from north to south. Landward migration of depocenters is a distinctive feature of compressional accretionary forearc basins (*sensu* Noda, 2016), whereas the depocenter shifting from north to south indicates tectonic segmentation into differentially subsiding

zones. Forearc basin segmentation has also been related to continental forearc basins formed in flat-slab subduction settings (Ridgway et al., 2012), where marked along-strike changes in basin configuration were related to insertion of wide fragments of thick crust. However, our results suggest that the pre-Oligocene basement fabric in the LMV, which is different beneath each depocenter (Figure 7), was the main cause of the tectonic segmentation of the basin, especially after 10 Ma, due to the differential response of each fault family to the stress regime. Uplift pulses in the forearc high could have also influenced depocenter migration.

5.3.5. LMV Subsidence History and Trends

Global studies of basin subsidence history (Xie & Heller, 2009) concluded that subsidence curves from forearc basins, as a group, have a diverse range of shapes, indicating that a variety of factors may contribute to basin subsidence. According to Dickinson (1995), there are four subsidence mechanisms in forearc basins: negative buoyancy of the descending slab, loading by the subduction (accretionary) complex, sediment or volcanic loading, and thermal subsidence of the arc massif. Results obtained by Mora *et al.* (2018) suggest that in the LMV, fault-controlled subsidence probably due to cooling of a pre-Oligocene arc was more important initially (late Oligocene to middle Miocene), and then it was replaced by sedimentary loading as the main subsidence mechanism in the basin during the late Miocene. An exception would be an increase in tectonic subsidence in the SW at 3 Ma (Figure 17a), probably related to uplift in forearc highs to the west.

Comparison with subsidence curves from other forearc basins in the world shows a fair match (Angevine *et al.*, 1990, inset in Figure 19a). However, as previously noted, the LMV curves show the opposite pattern compared to the passive rift basins considered in the stretching model of McKenzie (1978); therefore, they show that LMV is not suitable for applying the uniform stretching methodology by McKenzie (1978) and that extension using this methodology is overestimated in this basin, as previously shown by Montes *et al.* (2010) (Table 2). Data from the few wells in the northern SJFB show that the area experienced lower but constant subsidence rates compared to the LMV, and the SJFB curves show a similar trend to other forearc basins in the world. The high sedimentation rates in the LMV, especially in the Miocene, suggest that there was an important influence of sediment load in the total basin subsidence. Tectonic segmentation of both the LMV and the SJFB is also evident from the subsidence curves (inset in Figure 19a).

5.3.6. Proposed Mechanisms that Controlled LMV Evolution

Among all the mechanisms that control the evolution of forearc basins, Mora *et al.* (2018) suggest that three mechanisms strongly controlled the evolution of the LMV. Such mechanisms are: sediment flux due to uplift and drainage evolution in hinterland areas, pre-existing basement fabric, and configuration of the subducting plate. The reconstruction of the extension, subsidence, sedimentation, and paleogeographic history suggests that sediment flux in the LMV was the most important mechanism in controlling basin evolution because, (i) it supplied sediment to the trench and as a consequence, triggered underplating and uplift in forearc high areas, (ii) it rapidly filled the basin, providing sedimentary loads which kept the depocenters subsid-

ing, as previous subsidence mechanisms became less effective, and (iii) it defined the type and geometry of the basin. Due to the sediment flux, the LMV evolved from an underfilled, sloped, marine forearc basin to an overfilled, benched, terrestrial forearc basin (*sensu* Dickinson, 1995, Figure 23). Considering the classification by Noda (2016), the whole margin evolved from an Oligocene extensional non-accretionary type to the present-day compressional accretionary type forearc basin, and such evolution was strongly controlled by changes in sediment flux.

The pre-existing basement fabric underneath the LMV was fundamental for the evolution of this basin and its tectonic segmentation, because the different fault families identified under the two depocenters (Mora *et al.*, 2017a), were probably reactivated in different ways, according to the regional stress fields. Basement fabric and tectonic segmentation also controlled the distribution of sedimentary environments and facies.

Concerning the configuration of the subducting plate, the LMV evolution has also been controlled by the low-angle subduction of an irregular Caribbean oceanic plateau, which would have influenced the along-strike tectonic segmentation and stratigraphic variations observed in the LMV, as observed in other similar basins (Ridgway *et al.*, 2012). The variations in geometry of the subducted Caribbean Plateau under the LMV, described by Mora *et al.* (2017b) could represent irregularities, such as the Beata Ridge which separates the Colombian Basin from the Venezuelan Basin, at the top of the plateau (Duque-Caro, 1979). Flat-slab subduction would also be responsible for the lack of a magmatic arc in the LMV, a condition that would otherwise have formed a completely different forearc basin.

The results of the studies by Mora *et al.* (2017a, 2017b, 2018) allow the comparison of the geometry and configuration of the convergent margin of NW Colombia in Late Cretaceous times with the present-day geometry (Figure 24). The LMV basement and the SJFB were formed in a Late Cretaceous “normal” subduction margin, due to oblique convergence of the Caribbean relative to South America, with active dextral strike-slip displacement and possible subduction erosion. The onset of more orthogonal, low-angle subduction of the oceanic Caribbean Plateau after Eocene times resulted in a major change in the convergent margin, causing the cessation of magmatism and the formation of an accretionary, tectonically segmented forearc basin in the LMV, and forearc highs in the SJFB (Figures 23 and 24). However, it is also possible that if the lower to middle Eocene unconformity is related to the collision of the Caribbean Arc, causing a subduction polarity reversal as proposed by Kroehler *et al.* (2011). Nevertheless, this is only one of the many issues that remains to be solved and that make necessary that we continue doing research in these basins of NW South America.

6. Conclusions

Using a regional geological and geophysical dataset, the formation and evolution of the Lower Magdalena Valley Basin (LMV) and San Jacinto fold belt (SJFB) of NW Colombia has been illustrated. Detailed interpretations of reflection seismic data and new geochronological analyses revealed that the basement of the LMV is the northward continuation of the basement terranes of the northern Central Cordillera, and that it consists of Permian – Triassic metasedimentary rocks, which were subsequently intruded by Upper Cretaceous granitoids. Structural analyses suggest that the NE–SW trend of basement faults in the northeastern LMV is inherited from a Jurassic rifting event, while the ESE–WNW trend in the western LMV is inherited from a Late Cretaceous to Eocene strike–slip and extension episode. The Upper Cretaceous to lower Eocene sedimentites preserved in the present–day SJFB were deposited in a forearc marine basin formed by the oblique convergence between the Caribbean Plateau and the South American Plate, with a related intracontinental magmatic arc. A lower to middle Eocene angular unconformity at the top of the San Cayetano Sequence, the termination of the activity of the Romeral Fault System and the cessation of arc magmatism are interpreted to indicate the onset of low–angle orthogonal subduction of the Caribbean Plateau beneath South America, which occurred between 56 and 43 Ma. Flat subduction of the plateau has continued to the present and would be the main cause of amagmatic post–Eocene deposition and formation of the LMV. After the collapse of a pre–Oligocene magmatic arc, late Oligocene to early Miocene fault–controlled subsidence allowed initial infill of the LMV. Extensional reactivation of inherited, pre–Oligocene basement faults allowed tectonic segmentation and the formation of the two basin depocenters (Plato and San Jorge). Oligocene to early Miocene uplift of Andean terranes made possible the connection of the Lower and Middle Magdalena Valleys, and the formation of the most important Colombian drainage system (Magdalena River system). The proto–Magdalena River in the north and the proto–Cauca River in the south both started delivering enormous amounts of sediment in middle Miocene times, as fault controlled subsidence was gradually replaced by non–fault related subsidence, due to increased sedimentary load. Such dramatic increase in sedimentation delivered huge amounts of sediments to the trench, causing the formation of an accretionary prism farther west of San Jacinto. This probably weakened the plate interface and caused underplating, with the development of forearc highs in the San Jacinto area. A stronger backstop under the Lower Magdalena would explain shortening in the forearc high and accretionary wedge areas to the W, while the Lower Magdalena remained essentially unaffected. Our results highlight the fundamental role of plate kinematics, inherited basement structure, and sediment flux on the evolution of forearc basins such as San Jacinto and the Lower Magdalena.

Acknowledgments

This work is part of the PhD thesis by Josué Alejandro MORA–BOHÓRQUEZ at the Freie Universität Berlin and at the German Research Centre for Geosciences (GFZ) in Potsdam, Germany. This research was entirely supported by Hocol S.A. Josué Alejandro MORA–BOHÓRQUEZ thanks Hocol S.A. for permission to publish this study and all the exploration staff for fruitful discussions and suggestions. Elsa JAIMES, Exploration Vicepresident of Hocol S.A., is acknowledged for permission to present this research, for supporting this project, and for providing the time to prepare it. We also thank Jorge GÓMEZ TAPIAS and the Servicio Geológico Colombiano for inviting us to participate in this important project and for all their help during the manuscript preparation. We are also grateful to Hernán CARVAJAL and Jaime LÓPEZ (Hocol S.A.) for their help in preparing most of the figures. We thank reviewers Mauricio PARRA and Paul MANN whose comments greatly improved the quality of this manuscript.

References

- Allen, P.A. & Allen, J.R. 2005. Basin analysis: Principles and applications, 2nd edition. Blackwell Publishing Ltd., 549 p. Singapore.
- Altamira, A. & Burke, K. 2015. The Ribbon continent of South America in Ecuador, Colombia, and Venezuela. In: Bartolini, C. & Mann, P. (editors), Petroleum geology and potential of the Colombian Caribbean margin. American Association of Petroleum Geologists, Memoir 108, p. 39–84. <https://doi.org/10.1306/13531931M108846>
- Anderson, V.J., Horton, B.K., Saylor, J.E., Mora, A., Tesón, E., Breecker, D.O. & Ketcham, R.A. 2016. Andean topographic growth and basement uplift in southern Colombia: Implications for the evolution of the Magdalena, Orinoco, and Amazon River systems. *Geosphere*, 12(4): 1235–1256. <https://doi.org/10.1130/GES01294.1>
- Angevine, C.L., Heller, P.L. & Paola, C. 1990. Quantitative sedimentary basin modeling. American Association of Petroleum Geologists Continuing Education Course, Note Series 32, 133 p.
- Assumpção, M., Bianchi, M., Julia, J., Dias, F., Sand Franca, G., Nascimento, R., Drouet, S., Garcia Pavão, C., Farrapo, D. & Lopes, A. 2013. Crustal Thickness map of Brazil: Data compilation and main features. *Journal of South American Earth Sciences*, 43: 74–85. <http://dx.doi.org/10.1016/j.jsames.2012.12.009>
- Barrero, D., Álvarez, J. & Kassem, T. 1969. Actividad ígnea y tectónica en la cordillera Central durante el Meso–Cenozoico. *Boletín Geológico*, 17(1–3): 145–173.
- Bayona, G., Montes, C., Cardona, A., Jaramillo, C.A., Ojeda, G., Valencia, V. & Ayala–Calvo, C. 2011. Intraplate subsidence and basin filling adjacent to an oceanic arc–continent collision: A case from the southern Caribbean–South America plate mar-

- gin. *Basin Research*, 23(4): 403–422. <https://doi.org/10.1111/j.1365-2117.2010.00495.x>
- Bayona, G., Cardona, A., Jaramillo, C., Mora, A., Montes, C., Valencia, V., Ayala, C., Montenegro, O. & Ibañez-Mejía, M. 2012. Early Paleogene magmatism in the northern Andes: Insights on the effects of oceanic plateau–continent convergence. *Earth and Planetary Science Letters*, 331–332: 97–111. <https://doi.org/10.1016/j.epsl.2012.03.015>
- Berggren, W.A., Kent, D.V., Swisher III, C.C. & Aubry, M.P. 1995. A revised Cenozoic geochronology and chronostratigraphy. In: Berggren, W.A., Kent, D.V., Swisher III, C.C., Aubry, M.P. & Hardenbol, J. (editors), *Geochronology, Time Scales and Global Stratigraphic Correlation*. Society of Economic Paleontologists and Mineralogists, Special Publication 54, p. 129–212. <https://doi.org/10.2110/pec.95.04.0129>
- Bernal-Olaya, R., Mann, P. & Vargas, C.A. 2015a. Earthquake, tomographic, seismic reflection, and gravity evidence for a shallowly dipping subduction zone beneath the Caribbean margin of northwestern Colombia. In: Bartolini, C. & Mann, P. (editors), *Petroleum geology and potential of the Colombian Caribbean margin*. American Association of Petroleum Geologists, Memoir 108, p. 247–269. <https://doi.org/10.1306/13531939M1083642>
- Bernal-Olaya, R., Sánchez, J., Mann, P. & Murphy, M. 2015b. Along-strike crustal thickness variations of the subducting Caribbean Plate produces two distinctive styles of thrusting in the offshore South Caribbean deformed belt, Colombia. In: Bartolini, C. & Mann, P. (editors), *Petroleum geology and potential of the Colombian Caribbean margin*. American Association of Petroleum Geologists, Memoir 108, p. 295–322. <https://doi.org/10.1306/13531941M1083645>
- Bernal-Olaya, R., Mann, P. & Escalona, A. 2015c. Cenozoic tectonostratigraphic evolution of the Lower Magdalena Basin, Colombia: An example of an under- to overfilled forearc basin. In: Bartolini, C. & Mann, P. (editors), *Petroleum geology and potential of the Colombian Caribbean margin*. American Association of Petroleum Geologists, Memoir 108, p. 345–397. <https://doi.org/10.1306/13531943M1083645>
- Bezada, M., Magnani, M., Zelt, C., Schmitz, M. & Levander, A. 2010a. The Caribbean–South American plate boundary at 65°W: Results from wide-angle seismic data. *Journal of Geophysical Research: Solid Earth*, 115(B08): 1–17.
- Bezada, M.J., Levander, A. & Schmandt, B. 2010b. Subduction in the southern Caribbean: Images from finite-frequency P wave tomography. *Journal of Geophysical Research: Solid Earth*, 115(B12): 1–19. <https://doi.org/10.1029/2010JB007682>
- Blow, W.H. 1969. Late middle Eocene to recent planktonic foraminiferal biostratigraphy. In: Bronnimann, P. & Renz, H.H. (editors), *Proceedings of the First International Conference on Planktonic Microfossils*, 1, p. 199–422. Geneva, Switzerland.
- Boschman, L.M., van Hinsbergen, D.J.J., Torsvik, T.H., Spakman, W. & Pindell, J.L. 2014. Kinematic reconstruction of the Caribbean region since the Early Jurassic. *Earth–Science Reviews*, 138: 102–136. <https://doi.org/10.1016/j.earscirev.2014.08.007>
- Boyden, J.A., Müller, R.D., Gurnis, M., Torsvik, T.H., Clark, J.A., Turner, M., Ivey–Law, H., Watson, R.J. & Cannon, J.S. 2011. Next-generation plate–tectonic reconstructions using GPlates. In: Keller, R. & Baru, C. (editors), *Geoinformatics: Cyberinfrastructure for the solid earth sciences*. Cambridge University Press, p. 95–114. <https://doi.org/10.1017/CBO9780511976308.008>
- Burke, K. 1988. Tectonic evolution of the Caribbean. *Annual Review of Earth and Planetary Sciences*, 16: 201–230. <https://doi.org/10.1146/annurev.ea.16.050188.001221>
- Byrne, D.E., Wang, W.H. & Davis, D.M. 1993. Mechanical role of backstops in the growth of forearcs. *Tectonics*, 12(1): 123–144. <https://doi.org/10.1029/92TC00618>
- Caballero, V., Mora, A., Quintero, I., Blanco, V., Parra, M., Rojas, L.E., López, C., Sánchez, N., Horton, B.K., Stockli, D. & Duddy, I. 2013. Tectonic controls on sedimentation in an intermontane hinterland basin adjacent to inversion structures: The Nuevo Mundo Syncline, Middle Magdalena Valley, Colombia. In: Nemčok, M., Mora, A. & Cosgrove, J.W. (editors), *Thick-skin-dominated orogens: From initial inversion to full accretion*. Geological Society of London, Special Publication 377, p. 315–342. <https://doi.org/10.1144/SP377.12>
- Calvert, A.J., Preston, L.A. & Farahbod, A.M. 2011. Sedimentary underplating at the Cascadia mantle–wedge corner revealed by seismic imaging. *Nature Geoscience*, 4: 545–548. <https://doi.org/10.1038/ngeo1195>
- Cardona, A., Montes, C., Ayala, C., Bustamante, C., Hoyos, N., Montenegro, O., Ojeda, C., Niño, H., Ramírez, V., Valencia, V., Rincón, D., Vervoort, J. & Zapata, S. 2012. From arc–continent collision to continuous convergence, clues from Paleogene conglomerates along the southern Caribbean–South America plate boundary. *Tectonophysics*, 580: 58–87. <https://doi.org/10.1016/j.tecto.2012.08.039>
- Case, J.E. & MacDonald, W.D. 1973. Regional gravity anomalies and crustal structure in northern Colombia. *Geological Society of America Bulletin*, 84(9): 2905–2916. [https://doi.org/10.1130/0016-7606\(1973\)84<2905:RGAACS>2.0.CO;2](https://doi.org/10.1130/0016-7606(1973)84<2905:RGAACS>2.0.CO;2)
- Catuneanu, O., Abreu, V., Bhattacharya, J.P., Blum, M.D., Dalrymple, R.W., Eriksson, P.G., Fielding, C.R., Fisher, W.L., Galloway, W.E., Gibling, M.R., Giles, K.A., Holbrook, J.M., Jordan, R., Kendall, C.G.St.C., Macurda, B., Martinsen, O.J., Miall, A.D., Neal, J.E., Nummedal, D., Pomar, L., Posamentier, H.W., Pratt, B.R., Sarg, J.F., Shanley, K.W., Steel, R.J., Strasser, A., Tucker, M.E. & Winker, C. 2009. Towards the standardization of sequence stratigraphy. *Earth–Science Reviews*, 92(1–2): 1–33. <https://doi.org/10.1016/j.earscirev.2008.10.003>
- Cediel, F., Shaw, R.P. & Cáceres, C. 2003. Tectonic assembly of the northern Andean block. In: Bartolini, C., Buffler, R.T. & Blickwede, J. (editors), *The circum–Gulf of Mexico and the Caribbean: Hydrocarbon habitats, basin formation, and plate*

- tectonics. American Association of Petroleum Geologists, Memoir 79, p. 815–848. Tulsa, USA.
- Cerón, J.F., Kellogg, J.N. & Ojeda, G.Y. 2007. Basement configuration of the northwestern South America–Caribbean margin from recent geophysical data. *Ciencia, Tecnología y Futuro*, 3(3): 25–49.
- Chulick, G., Detweiler, Sh. & Mooney, W. 2013. Seismic structure of the crust and uppermost mantle of South America and surrounding oceanic basins. *Journal of South American Earth Sciences*, 42: 260–276. <http://dx.doi.org/10.1016/j.jsames.2012.06.002>
- Clift, P.D. & Hartley, A.J. 2007. Slow rates of subduction erosion and coastal underplating along the Andean margin of Chile and Perú. *Geology*, 35(6): 503–506. <https://doi.org/10.1130/G23584A.1>
- Clift, P. & Vannucchi, P. 2004. Controls on tectonic accretion versus erosion in subduction zones: Implications for the origin and recycling of the continental crust. *Reviews of Geophysics*, 42(2), p. 1–31. <https://doi.org/10.1029/2003RG000127>
- Cochrane, R., Spikings, R., Gerdes, A., Ulianov, A., Mora, A., Villagómez, D., Putlitz, B. & Chiaradia, M. 2014. Permo–Triassic anatexis, continental rifting and the disassembly of western Pangaea. *Lithos*, 190–191: 383–402. <https://doi.org/10.1016/j.lithos.2013.12.020>
- De la Parra, F., Mora, A., Rueda, M. & Quintero, I. 2015. Temporal and spatial distribution of tectonic events as deduced from reworked palynomorphs in the eastern northern Andes. *American Association of Petroleum Geologists Bulletin*, 99(8): 1455–1472. <https://doi.org/10.1306/02241511153>
- Dhuime, B., Hawkesworth, C. & Cawood, P. 2011. When continents formed. *Science*, 331(6014): 154–155. <https://doi.org/10.1126/science.1201245>
- Dickinson, W. 1995. Forearc basins. In: Busby, C.J. & Ingersoll, R.V. (editors), *Tectonics of sedimentary basins*. Blackwell Science, p. 221–261. Cambridge, USA.
- Dickinson, W.R. & Gehrels, G.E. 2009. Use of U–Pb ages of detrital zircons to infer maximum depositional ages of strata: A test against a Colorado Plateau Mesozoic database. *Earth and Planetary Science Letters*, 288(1–2): 115–125. <https://doi.org/10.1016/j.epsl.2009.09.013>
- Duque–Caro, H. 1979. Major structural elements and evolution of northwestern Colombia. In: Watkins, J.S., Montadert, L. & Wood–Dickerson, P. (editors), *Geological and geophysical investigations of continental margins*. American Association of Petroleum Geologists, Memoir 29, p. 329–351. Tulsa, USA.
- Duque–Caro, H. 1984. Structural style, diapirism, and accretionary episodes of the Sinú–San Jacinto Terrane, southwestern Caribbean borderland. In: Bonini, W.E., Hargraves, R.B. & Shagam, R. (editors), *The Caribbean–South American plate boundary and regional tectonics*. Geological Society of America, Memoir 162, p. 303–316. <https://doi.org/10.1130/MEM162-p303>
- Duque–Caro, H. 1991. Contributions to the geology of the Pacific and the Caribbean coastal areas of northwestern Colombia and South America. Doctoral thesis, Princeton University, 132 p. Princeton, USA.
- Duque–Caro, H. 2000. Análisis bioestratigráficos de 400 muestras de 34 pozos y 16 muestras de superficie de las cuencas de San Jorge, Sinú, Plato y Barranquilla en el Valle Inferior del Magdalena. Ecopetrol, unpublished report, 403 p. Bogotá.
- Duque–Caro, H. 2001. Análisis bioestratigráficos de 250 muestras de 5 pozos de las cuencas de San Jorge, Sinú, Plato y Barranquilla en el Valle Inferior del Magdalena. Ecopetrol, unpublished report, 293 p. Bogotá.
- Duque–Caro, H. 2010. Análisis microestratigráficos de 36 muestras del pozo Saman Norte–1. Hocol, unpublished report, 4 p. Bogotá.
- Duque–Caro, H. 2014. Microstratigraphic analyses of 39 samples from the Well Calipso–1, Barranquilla Province. Hocol, unpublished report, 47 p. Bogotá.
- Duque–Caro, H., Guzmán–Ospitia, G. & Hernández, R. 1996. Memoria explicativa: Mapa geológico de la plancha 38 Carmen de Bolívar. Scale 1:100 000. Ingeominas, 83 p. Bogotá.
- Escalona, A. & Mann, P. 2011. Tectonics, basin subsidence mechanisms, and paleogeography of the Caribbean–South American plate boundary zone. *Marine and Petroleum Geology*, 28(1): 8–39. <https://doi.org/10.1016/j.marpetgeo.2010.01.016>
- Etayo–Serna, F., Barrero, D., Lozano, H., Espinosa, A., González, H., Orrego, A., Ballesteros, I., Forero, H., Ramírez, C., Zambraño–Ortiz, F., Duque–Caro, H., Vargas, R., Núñez, A., Álvarez, J., Ropaín, C., Cardozo, E., Galvis, N., Sarmiento, L., Alberts, J.P., Case, J.E., Singer, D.A., Bowen, R.W., Berger, B.R., Cox, D.P. & Hodges, C.A. 1983. Mapa de terrenos geológicos de Colombia. Publicaciones Geológicas Especiales del Ingeominas, 14 (I), 235 p. Bogotá.
- Flinch, J.F. 2003. Structural evolution of the Sinu–Lower Magdalena area (northern Colombia). In: Bartolini, C., Buffler, R.T. & Blickwede, J. (editors), *The circum–Gulf of Mexico and the Caribbean: Hydrocarbon habitats, basin formation, and plate tectonics*. American Association of Petroleum Geologists, Memoir 79, p. 776–796.
- Glodny, J., Lohrmann, J., Echter, H., Gräfe, K., Seifert, W., Collao, S. & Figueroa, O. 2005. Internal dynamics of a paleoaccretionary wedge: Insights from combined isotope tectonochronology and sandbox modelling of the South–Central Chilean forearc. *Earth and Planetary Science Letters*, 231(1–2): 23–39. <https://doi.org/10.1016/j.epsl.2004.12.014>
- Gómez, E., Jordan, T.E., Allmendinger, R.W., Hegarty, K. & Kelley, S. 2005. Syntectonic Cenozoic sedimentation in the northern Middle Magdalena Valley Basin of Colombia and implications for exhumation of the northern Andes. *Geological Society of America Bulletin*, 117(5–6): 547–569. <https://doi.org/10.1130/B25454.1>
- Gómez, J., Nivia, Á., Montes, N.E., Tejada, M.L., Jiménez, D.M., Sepúlveda, M.J., Osorio, J.A., Gaona, T., Diederix, H., Uribe,

- H. & Mora, M., compilers. 2007. Geological Map of Colombia 2007. Scale 1:1 000 000. Ingeominas, 2 sheets. Bogotá.
- Gómez, J., Montes, N.E., Nivia, Á. & Diederix, H., compilers. 2015. Geological Map of Colombia 2015. Scale 1:1 000 000. Servicio Geológico Colombiano, 2 sheets. Bogotá. <https://doi.org/10.32685/10.143.2015.936>
- Govers, R. & Wortel, M.J.R. 2005. Lithosphere tearing at STEP faults: Response to edges of subduction zones. *Earth and Planetary Science Letters*, 236(1–2): 505–523. <https://doi.org/10.1016/j.epsl.2005.03.022>
- Guzmán, G. 2007. Stratigraphy and sedimentary environment and implications in the Plato Basin and the San Jacinto Belt north-western Colombia. Doctoral thesis, Université de Liège, 275 p. Liège, Belgium.
- Guzmán, G., Gómez-Londoño, E. & Serrano-Suárez, B.E. 2004. Geología de los cinturones del Sinú, San Jacinto y borde occidental del Valle Inferior del Magdalena, Caribe Colombiano. Ingeominas, unpublished report, 134 p. Bogotá.
- Haq, B.U., Hardenbol, J. & Vail, P.R. 1987. Chronology of fluctuating sea levels since the Triassic. *Science*, 235: 1156–1167.
- Hocot S.A. 1993. Lower Magdalena Valley technical evaluation agreement. Phase I. Unpublished report, 200 p. Cartagena.
- Hoorn, C., Wesselingh, F.P., ter Steege, H., Bermúdez, M.A., Mora, A., Sevink, J., Sanmartin, I., Sánchez-Meseguer, A., Anderson, C.L., Figueiredo, J.P., Jaramillo, C., Riff, D., Negri, F.R., Hooghiemstra, H., Lundberg, J., Stadler, T., Särkinen, T. & Antonelli, A. 2010. Amazonia through time: Andean uplift, climate change, landscape evolution, and biodiversity. *Science*, 330(6006): 927–931. <https://doi.org/10.1126/science.1194585>
- Ibañez-Mejía, M., Tassinari, C.C.G. & Jaramillo-Mejía, J.M. 2007. U–Pb zircon ages of the “Antioquian Batholith”: Geochronological constraints of late Cretaceous magmatism in the central Andes of Colombia. XI Congreso Colombiano de Geología. *Memoirs*. 11p. Bucaramanga.
- Instituto Colombiano del Petróleo. 2000. Evaluación regional integrada cuenca Valle Inferior del Magdalena. Unpublished report, 360 p. Piedecuesta, Colombia.
- Kroehler, M.E., Mann, P., Escalona, A. & Christeson, G.L. 2011. Late Cretaceous – Miocene diachronous onset of back thrusting along the South Caribbean deformed belt and its importance for understanding processes of arc collision and crustal growth. *Tectonics*, 30(6): 31 p. <https://doi.org/10.1029/2011TC002918>
- Levander, A., Bezada, M.J., Niu, F. & Schmitz, M. 2015. The two subduction zones of the southern Caribbean: Lithosphere tearing and continental margin recycling in the east, flat slab subduction and Laramide-style uplifts in the west. *American Geophysical Union, Fall Meeting. Abstracts*, 1 p. San Francisco, USA.
- Lithosphaera Ltda. 2010. Interpretación gravimétrica cuantitativa, región Sinú–San Jacinto y Valle Inferior del Magdalena. Unpublished report, 21 p. Bogotá.
- Luzieux, L.D.A., Heller, F., Spikings, R., Vallejo, C.F. & Winkler, W. 2006. Origin and Cretaceous tectonic history of the coastal Ecuadorian forearc between 1° N and 3° S: Paleomagnetic, radiometric and fossil evidence. *Earth and Planetary Science Letters*, 249(3–4): 400–414. <https://doi.org/10.1016/j.epsl.2006.07.008>
- Magnani, M.B., Zelt, C.A., Levander, A. & Schmitz, M. 2009. Crustal structure of the South American–Caribbean plate boundary at 67°W from controlled source seismic data. *Journal of Geophysics Research*, 114: B02312.
- Mantilla–Pimiento, A.M. 2007. Crustal structure of the southwestern Colombian Caribbean margin: Geological interpretation of geophysical data. Doctoral thesis, Friedrich–Schiller–Universität Jena, 98 p. Jena, Germany.
- Mantilla–Pimiento, A.M., Jentszsch, G., Kley, J. & Alfonso–Pava, C. 2009. Configuration of the Colombian Caribbean margin: Constraints from 2D seismic reflection data and potential fields interpretation. In: Lallemand, S. & Funiciello, F. (editors), *Subduction zone geodynamics. Frontiers in Earth Sciences*. Springer, p. 247–272. Berlin, Heidelberg. https://doi.org/10.1007/978-3-540-87974-9_13
- Masy, J., Niu, F., Levander, A. & Schmitz, M. 2011. Mantle flow beneath northwestern Venezuela: Seismic evidence for a deep origin of the Mérida Andes. *Earth and Planetary Science Letters*, 305(3–4): 396–404. <https://doi.org/10.1016/j.epsl.2011.03.024>
- Matthews, K.J., Maloney, K.T., Zahirovic, S., Williams, S.E., Seton, M. & Muller, D. 2016. Global plate boundary evolution and kinematics since the late Paleozoic. *Global and Planetary Change*, 146: 226–250. <https://doi.org/10.1016/j.gloplacha.2016.10.002>
- McKenzie, D. 1978. Some remarks on the development of sedimentary basins. *Earth and Planetary Science Letters*, 40(1): 25–32. [https://doi.org/10.1016/0012-821X\(78\)90071-7](https://doi.org/10.1016/0012-821X(78)90071-7)
- Miall, A.D. 2000. *Principles of sedimentary basin analysis*, 3rd edition. Springer–Verlag, 616 p. Berlin–Heidelberg. <https://doi.org/10.1007/978-3-662-03999-1>
- Montes, C., Guzmán, G., Bayona, G., Cardona, A., Valencia, V. & Jaramillo, C. 2010. Clockwise rotation of the Santa Marta Massif and simultaneous Paleogene to Neogene deformation of the Plato–San Jorge and Cesar–Ranchería Basins. *Journal of South American Earth Sciences*, 29(4): 832–848. <https://doi.org/10.1016/j.jsames.2009.07.010>
- Montes, C., Cardona, A., Jaramillo, C., Pardo, A., Silva, J.C., Valencia, V., Ayala, C., Pérez–Ángel, L.C., Rodríguez–Parra, L.A., Ramírez, V. & Niño, H. 2015. Middle Miocene closure of the Central American Seaway. *Science*, 348(6231): 226–229. <https://doi.org/10.1126/science.aaa2815>
- Moore, J.C., Diebold, J., Fisher, M.A., Sample, J., Brocher, T., Talwani, M., Ewing, J., von Huene, R., Rowe, C., Stone, D., Stevens, C. & Sawyer, D. 1991. EDGE deep seismic reflection transect of the eastern Aleutian arc–trench layered lower crust reveals underplating and continental growth. *Geology*, 19(5): 420–424. [https://doi.org/10.1130/0091-7613\(1991\)019<0420:EDSRTO>2.3.CO;2](https://doi.org/10.1130/0091-7613(1991)019<0420:EDSRTO>2.3.CO;2)
- Mora, A., De Freitas, M. & Vélez, V. 2013a. Cenozoic tectonostratigraphy of the northern San Jacinto fold belt, northwestern

- Colombia. American Association of Petroleum Geologists International Convention and Exhibition. Poster. Cartagena.
- Mora, A., Reyes–Harker, A., Rodríguez, G., Tesón, E., Ramírez–Arias, J.C., Parra, M., Caballero, V., Mora, J.P., Quintero, I., Valencia, V., Ibañez–Mejía, M., Horton, B.K. & Stockli, D.F. 2013b. Inversion tectonics under increasing rates of shortening and sedimentation: Cenozoic example from the Eastern Cordillera of Colombia. In: Nemčok, M., Mora, A. & Cosgrove, J.W. (editors), *Thick–skin–dominated orogens: From initial inversion to full accretion*. Geological Society of London, Special Publication 377, p. 411–442. <https://doi.org/10.1144/SP377.6>
- Mora, A., Parra, M., Rodríguez–Forero, G., Blanco, V., Moreno, N., Caballero, V., Stockli, D., Duddy, I. & Ghorbal, B. 2015. What drives orogenic asymmetry in the northern Andes?: A case study from the apex of the northern Andean orocline. In: Bartolini, C. & Mann, P. (editors), *Petroleum geology and potential of the Colombian Caribbean margin*. American Association of Petroleum Geologists, Memoir 108, p. 547–586. <https://doi.org/10.1306/13531949M1083652>
- Mora, J.A., Ibañez–Mejía, M., Oncken, O., De Freitas, M., Vélez, V., Mesa, A. & Serna, L. 2017a. Structure and age of the Lower Magdalena Valley Basin basement, northern Colombia: New reflection–seismic and U–Pb–Hf insights into the termination of the central Andes against the Caribbean Basin. *Journal of South American Earth Sciences*, 74: 1–26. <https://doi.org/10.1016/j.jsames.2017.01.001>
- Mora, J.A., Oncken, O., Le Breton, E., Ibañez–Mejía, M., Faccenna, C., Veloza, G., Vélez, V., De Freitas, M. & Mesa, A. 2017b. Linking Late Cretaceous to Eocene tectono–stratigraphy of the San Jacinto fold belt of NW Colombia with Caribbean plateau collision and flat subduction. *Tectonics*, 36(11): 2599–2629. <https://doi.org/10.1002/2017TC004612>
- Mora, J.A., Oncken, O., Le Breton, E., Mora, A., Veloza, G., Vélez, V. & De Freitas, M. 2018. Controls on forearc basin formation and evolution: Insights from Oligocene to recent tectono–stratigraphy of the Lower Magdalena Valley basin of northwest Colombia. *Marine and Petroleum Geology*, 97: 288–310. <https://doi.org/10.1016/j.marpetgeo.2018.06.032>
- Müller, R.D., Royer, J.Y., Cande, S.C., Roest, W.R. & Maschenkov, S. 1999. New constraints on the Late Cretaceous/Tertiary plate tectonic evolution of the Caribbean. *Sedimentary Basins of the World*, 4: 33–59. [https://doi.org/10.1016/S1874-5997\(99\)80036-7](https://doi.org/10.1016/S1874-5997(99)80036-7)
- Nivia, A., Marriner, G.F., Kerr, A.C. & Tarney, J. 2006. The Quebradagrande Complex: A Lower Cretaceous ensialic marginal basin in the Central Cordillera of the Colombian Andes. *Journal of South American Earth Sciences*, 21(4): 423–436. <https://doi.org/10.1016/j.jsames.2006.07.002>
- Noda, A. 2016. Forearc basins: Types, geometries, and relationships to subduction zone dynamics. *Geological Society of America Bulletin*, 128(5–6): 879–895. <https://doi.org/10.1130/B31345.1>
- Parra, M., Mora, A., López, C., Rojas, L.E. & Horton, B.K. 2012. Detecting earliest shortening and deformation advance in thrust belt hinterlands: Example from the Colombian Andes. *Geology*, 40(2): 175–178. <https://doi.org/10.1130/G32519.1>
- Petters, V. & Sarmiento, R. 1956. Oligocene and lower Miocene biostratigraphy of the Carmen–Zambrana area, Colombia. *Micropaleontology*, 2(1): 7–35. <https://doi.org/10.2307/1484490>
- Pindell, J.L. & Kennan, L. 2009. Tectonic evolution of the Gulf of Mexico, Caribbean and northern South America in the mantle reference frame: An update. In: James, K.H., Lorente, M.A. & Pindell, J.L. (editors), *The origin and evolution of the Caribbean Plate*. Geological Society of London, Special Publication 328, p. 1–55. <https://doi.org/10.1144/SP328.1>
- Piraique, A. 2017. Structural framework, deformation and exhumation of the Santa Marta Schists: Accretion and deformational history of the Caribbean Terrane at the north of the Sierra Nevada de Santa Marta. Doctoral thesis, Université Grenoble Alpes, 237 p. Grenoble, France.
- Poveda, E., Monsalve, G. & Vargas, C.A. 2012. Crustal thickness estimation beneath the northern Andes (Colombia) from teleseismic receiver functions. American Geophysical Union, Fall Meeting. Poster. San Francisco, USA.
- Poveda, E., Monsalve, G. & Vargas, C.A. 2015. Receiver functions and crustal structure of the northwestern Andean region, Colombia. *Journal of Geophysical Research: Solid Earth*, 120(4): 2408–2425. <https://doi.org/10.1002/2014JB011304>
- Restrepo, J.J. & Toussaint, J.F. 1988. Terranes and continental accretion in the Colombian Andes. *Episodes*, 11(3): 189–193. <https://doi.org/10.18814/epiugs/1988/v11i3/006>
- Restrepo, S., Foster, D.A. & Kamenov, G.D. 2007. Formation age and magma sources for the Antioqueño Batholith derived from LA–ICP–MS uranium–lead dating and hafnium–isotope analysis of zircon grains. Geological Society of America Annual Meeting, Abstracts, p. 181. Denver, USA.
- Reyes–Harker, A., Montenegro–Buitrago, G. & Gómez–Gutiérrez, P.D. 2000. Evolución tectonoestratigráfica del Valle Inferior del Magdalena, Colombia. VIII Simposio Bolivariano–Exploración Petrolera en las Cuencas Subandinas. Memoir, p. 293–309. Caracas.
- Reyes–Harker, A., Ruiz–Valdivieso, C.F., Mora, A., Ramírez–Arias, J.C., Rodríguez, G., De la Parra, F., Caballero, V., Parra, M., Moreno, N., Horton, B.K., Saylor, J.E., Silva, A., Valencia, V., Stockli, D. & Blanco, V. 2015. Cenozoic paleogeography of the Andean foreland and retroarc hinterland of Colombia. *American Association of Petroleum Geologists Bulletin*, 99(8): 1407–1453. <https://doi.org/10.1306/06181411110>
- Ridgway, K.D., Trop, J.M. & Finzel, E.S. 2012. Modification of continental forearc basins by flat–slab subduction processes: A case study from southern Alaska. In: Busby, C. & Azor, A. (editors), *Tectonics of sedimentary basins: Recent advances*, first edition, P. 327–346. Blackwell Publishing Ltd. <https://doi.org/10.1002/9781444347166.ch16>

- Romero–Otero, G.A., Slatt, R.M. & Pirmez, C. 2015. Evolution of the Magdalena deepwater fan in a tectonically active setting, offshore Colombia. In: Bartolini, C. & Mann, P. (editors), Petroleum geology and potential of the Colombian Caribbean margin. American Association of Petroleum Geologists, Memoir 108, p. 675–708. <https://doi.org/10.1306/M1081307>
- Rosello, E. & Cossey, S. 2012. What is the evidence for subduction in the Caribbean margin of Colombia? XI Simposio Bolivariano: Petroleum Exploration in Subandean Basins, Memoirs, p. 1–7. Cartagena de Indias, Colombia.
- Saylor, J.E., Horton, B.K., Stockli, D.F., Mora, A. & Corredor, J. 2012. Structural and thermochronological evidence for Paleogene basement-involved shortening in the axial Eastern Cordillera, Colombia. *Journal of South American Earth Sciences*, 39: 202–215. <https://doi.org/10.1016/j.jsames.2012.04.009>
- Scherwath, M., Kopp, H., Flueh, E.R., Henrys, S.A., Sutherland, R., Stagpoole, V.M., Barker, H.N., Reyners, M.E., Bassett, D.G., Planert, L. & Dannowski, P.A. 2010. Fore-arc deformation and underplating at the northern Hikurangi margin, New Zealand. *Journal of Geophysical Research*, 115(B6): 23 P. <https://doi.org/10.1029/2009JB006645>
- Silva–Arias, A., Páez–Acuña, L.A., Rincón–Martínez, D., Tamara–Guevara, J.A., Gómez–Gutiérrez, P.D., López–Ramos, E., Restrepo–Acevedo, S.M., Mantilla–Figueroa, L.C. & Valencia, V. 2016. Basement characteristics in the Lower Magdalena Valley and the Sinú and San Jacinto fold belts: Evidence of a Late Cretaceous magmatic arc at the South of the Colombian Caribbean. *Ciencia, Tecnología y Futuro*, 6(4): 5–36.
- Steckler, M.S. & Watts, A.B. 1978. Subsidence of the Atlantic-type continental margin off New York. *Earth and Planetary Science Letters*, 41(1): 1–13. [https://doi.org/10.1016/0012-821X\(78\)90036-5](https://doi.org/10.1016/0012-821X(78)90036-5)
- Symithe, S., Calais, E., De Chabaliér, J.B., Robertson, R. & Higgins, M. 2015. Current block motions and strain accumulation on active faults in the Caribbean. *Journal of Geophysical Research: Solid Earth*, 120(5): 3748–3774. <https://doi.org/10.1002/2014JB011779>
- Syracuse, E.M., Maceira, M., Prieto, G.A., Zhang, H. & Ammon, C.J. 2016. Multiple plates subducting beneath Colombia, as illuminated by seismicity and velocity from the joint inversion of seismic and gravity data. *Earth and Planetary Science Letters*, 444: 139–149. <https://doi.org/10.1016/j.epsl.2016.03.050>
- Toussaint, J.F. & Restrepo, J.J. 1994. The Colombian Andes during Cretaceous times. In: Salfity, J.A. (editor), *Cretaceous tectonics of the Andes*. Earth Evolution Series. Vieweg and Teubner Verlag, Wiesbaden, p. 61–100. https://doi.org/10.1007/978-3-322-85472-8_2
- Trenkamp, R., Kellogg, J.N., Freymueller, J.T. & Mora, H. 2002. Wide plate margin deformation, southern Central America and northwestern South America, CASA GPS observations. *Journal of South American Earth Sciences*, 15(2): 157–171. [https://doi.org/10.1016/S0895-9811\(02\)00018-4](https://doi.org/10.1016/S0895-9811(02)00018-4)
- van Benthem, S., Govers, R., Spakman, W. & Wortel, R. 2013. Tectonic evolution and mantle structure of the Caribbean. *Journal of Geophysical Research*, 118: 3019–3036.
- Vervoort, J.D. & Blichert–Toft, J. 1999. Evolution of the depleted mantle: Hf isotope evidence from juvenile rocks through time. *Geochimica et Cosmochimica Acta*, 63(3–4): 533–556. [https://doi.org/10.1016/S0016-7037\(98\)00274-9](https://doi.org/10.1016/S0016-7037(98)00274-9)
- Villagómez, D. & Spikings, R. 2013. Thermochronology and tectonics of the Central and Western Cordilleras of Colombia: Early Cretaceous – Tertiary evolution of the northern Andes. *Lithos*, 160–161: 228–249. <https://doi.org/10.1016/j.lithos.2012.12.008>
- Villagómez, D., Spikings, R., Magna, T., Kammer, A., Winkler, W. & Beltrán, A. 2011. Geochronology, geochemistry and tectonic evolution of the Western and Central Cordilleras of Colombia. *Lithos*, 125(3–4): 875–896. <https://doi.org/10.1016/j.lithos.2011.05.003>
- Watts, A.B. & Ryan, W.B.F. 1976. Flexure of the lithosphere and continental margin basins. *Tectonophysics*, 36(1–3): 25–44. [https://doi.org/10.1016/0040-1951\(76\)90004-4](https://doi.org/10.1016/0040-1951(76)90004-4)
- Xie, X. & Heller, P.L. 2009. Plate tectonics and basin subsidence history. *Geological Society of America Bulletin*, 121(1–2): 55–64. <https://doi.org/10.1130/B26398.1>
- Zachos, J.C., Pagani, M., Sloan, L., Thomas, E. & Billups, K. 2001. Trends, rhythms, and aberrations in global climate 65 Ma to present. *Science*, 292(5517): 686–693. <https://doi.org/10.1126/science.1059412>

Explanation of Acronyms, Abbreviations, and Symbols:

CC	Central Cordillera	SiF	Sinú Fault
LMV	Lower Magdalena Valley Basin	SJF	San Jerónimo Fault
MCH	Magangué–Cicuco High	SJFB	San Jacinto fold belt
MMV	Middle Magdalena Valley	SMF	Santa Marta Fault
OEPFS	Oca–El Pilar–San Sebastian Fault System	SNSM	Sierra Nevada de Santa Marta
PFS	Palestina Fault System	STEP	Subduction–transform edge propagator
RFS	Romeral Fault System	TWT	Two–way–time

Authors' Biographical Notes



Josué Alejandro MORA-BOHÓRQUEZ graduated as a geologist from the Universidad Nacional de Colombia, Bogotá, in 1998, then obtained a MS degree in basin evolution and dynamics at Royal Holloway, University of London, United Kingdom, in 2001 and a PhD degree at the Freie Universität Berlin/GFZ Potsdam, Germany in 2018 (magna cum laude). He works as senior

exploration geologist for Hocol S.A. since 2006. Prior to working for Hocol S.A., he was an exploration geologist at Petrobras Colombia doing regional studies of the Upper and Middle Magdalena Valley Basins from 2002 to 2004, and then he worked in coalbed methane and conventional hydrocarbon exploration for Drummond Ltd. Colombia, from 2004 to 2006. His research interests are tectonics and sedimentation, basin analysis, petroleum exploration, and hydrocarbon systems.



Onno ONCKEN is a full professor at the Department of Earth Sciences of the Freie Universität Berlin and is the head of Department 4—"Geomaterials" and of section 4.1—"Lithosphere Dynamics" of the German Research Centre for Geosciences (GFZ) at Potsdam, Germany. He has published widely and received several awards such as Leibniz Price in 1998. His research interests are

tectonics of plate margins and orogens, deformation analysis, and analogue modelling.



Eline LE BRETON obtained her Masters and PhD degrees in geology from the University of Rennes 1, France. Since 2012, she is postdoctoral research associate and lecturer at the Department of Earth Sciences of the Freie Universität Berlin. She has several publications and her research interests are plate tectonics and kinematic reconstructions, geodynamics, and structural geology.



Mauricio IBAÑEZ-MEJIA graduated as a geologist from the Universidad Nacional de Colombia, Bogotá, in 2007. He obtained MS (2010) and PhD (2014) degrees in petrology and geochemistry from the University of Arizona, USA, followed by two years as a W.O. Crosby postdoctoral fellow in the Massachusetts Institute of Technology in Cambridge, USA, and four years as an assistant

professor in the Department of Earth and Environmental Sciences at University of Rochester, USA. He is currently an assistant professor in the Department of Geosciences at the University of Arizona, USA. His main research interests are in the fields of isotope geochemistry, geochronology, petrology, and crustal evolution.



Gabriel VELOZA obtained his Bachelor degree in geology in 2005 from the Universidad Nacional de Colombia, Bogotá and after working for the oil industry with Hocol S.A., Emerald Energy and Maurel et Prom, he moved to the University of Kansas, USA, where he obtained his Masters degree in 2012. While at the U.S., he also worked as a development geologist with the California Resources Corporation and in 2015, he returned to Colombia and

joined Hocol S.A., where he is currently working as a senior exploration geologist. He is also pursuing a PhD at the University of Kansas. His research interests are tectonics and sedimentation, hydrocarbon exploration, and reservoir characterization.



Andrés MORA is the technical leader of onshore Colombia and foothills exploration at Ecopetrol. He received his BS in geology from the Universidad Nacional de Colombia and PhD from the Institut für Geowissenschaften, Universität Potsdam. His research interests include structural geology, petroleum exploration, and petroleum geology.



Vickye VÉLEZ obtained her bachelor's degree in geology from the Universidad Nacional de Colombia in 1990 and her Master of Science degree focused on structural geology from the University of Texas at Austin, U.S.A. in 2000. She worked for 14 years as senior exploration geologist and technical leader in the Llanos Foothills and Middle Magdalena Valley for Ecopetrol and then joined

Hocol S.A. in 2006. She is currently exploration manager of the northern Colombia team of Hocol S.A. Her research interests are structural geology and hydrocarbon exploration.



Mario DE FREITAS obtained his bachelor's degree in earth sciences from the Universidade de São Paulo, Brasil in 1983. He joined Petrobras International in 1985 and worked primarily in projects in Brasil, UK, Norway, and Colombia. In 2002 he joined Hocol S.A. as senior geophysicist, then as exploration vice president from 2006 to 2015. He was responsible for a large diversification of

Hocol's portfolio, including incursions into the Llanos, where several oil discoveries were made, the Lower Magdalena Valley Basin and San Jacinto fold belt of NW Colombia, where the company also made gas discoveries. His research interests are structural geology, hydrocarbon exploration, and regional basin studies.

Chapter 3



Construction of the Eastern Cordillera of Colombia: Insights from the Sedimentary Record

<https://doi.org/10.32685/pub.esp.37.2019.03>

Published online 7 May 2020

Brian K. HORTON^{1*}, Mauricio PARRA², and Andrés MORA³

Abstract A continuous, long-lived sedimentary record contains important evidence bearing on the geologic evolution of the Eastern Cordillera in the northern Andes of Colombia. Today, this largely isolated NNE-trending mountain range forms a ca. 1–3 km high topographic barrier separating the Magdalena Valley hinterland basin from the Llanos foreland basin. A Mesozoic – Cenozoic history of marine and nonmarine sedimentation affected the Eastern Cordillera and flanking Magdalena and Llanos provinces during contrasting tectonic regimes. (i) Jurassic to earliest Cretaceous extension led to the development and linkage of extensional sub-basins (commonly half graben features governed by normal faults) in selected regions. (ii) A subsequent phase of postextensional thermal subsidence generated a thermal sag basin across a broader region. (iii) In latest Cretaceous to Paleocene time, initial crustal shortening in the Central Cordillera created a regional flexural basin that was successively broken by the Paleocene – Oligocene emergence of thrust/reverse-fault related uplifts within the Eastern Cordillera partitioning the original regional basin into the Magdalena hinterland basin and Llanos foreland basin. (iv) Major Neogene uplift and establishment of an effective topographic barrier occurred as continued shortening became focused along the bivergent eastern and western flanks of the fold-thrust belt comprising the Eastern Cordillera. Shortening commonly involved contractional reactivation of preexisting normal faults and inversion of pre-foreland basin elements. This geologic history is largely expressed in the clastic sedimentary archives of the Eastern Cordillera, Magdalena Valley Basin, and Llanos Basin. Growth strata and cross-cutting relationships among fold-thrust structures and basin fill provide essential timing constraints for individual structures, particularly when integrated with thermochronological data. Regional stratigraphic correlations and sediment accumulation histories help identify shared and divergent stratigraphic histories during progressive basin compartmentalization. Substantial shifts in sediment provenance, identified through U–Pb geochronology, demonstrate the changes in sediment source regions and paleodrainage patterns during several changes in tectonic conditions.

Keywords: Eastern Cordillera, fold-thrust belt, foreland basin, provenance, U–Pb geochronology.

Resumen Un registro sedimentario continuo y prolongado en los Andes del norte alberga evidencia importante sobre la evolución geológica de la cordillera Oriental de Colombia. Actualmente, esta cadena montañosa, en gran medida aislada y de orientación N–NE, forma una barrera topográfica de 1–3 km de altura que separa la cuen-

- 1 horton@jsg.utexas.edu
University of Texas at Austin
Department of Geological Sciences and
Institute for Geophysics, Jackson School
of Geosciences
Austin, Texas 78712, USA
- 2 mparra@iee.usp.br
Universidade de São Paulo
Instituto de Energia e Ambiente
Av. Professor Luciano Gualberto 1289,
Cidade Universitária, 05508–010
São Paulo, Brasil
- 3 andres.mora@ecopetrol.com.co
Ecopetrol S.A
Vicepresidencia de Exploración
Bogotá, Colombia

* Corresponding author

Citation: Horton, B.K., Parra, M. & Mora, A. 2020. Construction of the Eastern Cordillera of Colombia: Insights from the sedimentary record. In: Gómez, J. & Mateus-Zabala, D. (editors), *The Geology of Colombia, Volume 3 Paleogene – Neogene*. Servicio Geológico Colombiano, Publicaciones Geológicas Especiales 37, p. 67–88. Bogotá. <https://doi.org/10.32685/pub.esp.37.2019.03>

ca intramontana del valle del Magdalena de la cuenca de antepaís de los Llanos. La sedimentación marina y continental mesozoica–cenozoica tuvo lugar en la cordillera Oriental y las provincias adyacentes Magdalena y Llanos durante regímenes tectónicos contrastantes. (i) Extensión durante el Jurásico al Cretácico más temprano tuvo como resultado el desarrollo e interconexión de subcuencas extensionales (comúnmente en forma de semigrábenes controlados por fallas normales) en áreas localizadas. (ii) Una fase subsecuente de subsidencia termal posextensional generó una cuenca de subsidencia térmica en una región más amplia. (iii) Durante el Cretácico más tardío al Paleoceno, el inicio del acortamiento cortical en la cordillera Central generó una cuenca flexural regional que fue posteriormente fragmentada en el Paleoceno–Oligoceno tras la emergencia de altos de basamento relacionada con fallas inversas en la cordillera Oriental, subdividiendo la cuenca regional inicial en la cuenca intramontana del Magdalena y la cuenca de antepaís de los Llanos. (iv) Levantamiento neógeno considerable y el establecimiento de una barrera topográfica efectiva ocurrieron en la medida en que el acortamiento persistente fue acomodado de forma bivergente en el cinturón de pliegues y cabalgamientos marginales de los flancos oriental y occidental de la cordillera Oriental. Este acortamiento involucró la reactivación contraccional de antiguas fallas normales y la inversión de segmentos de cuencas de antepaís preexistentes. Esta historia geológica está registrada en gran medida en los archivos sedimentarios de la cordillera Oriental y las cuencas del valle del Magdalena y de los Llanos. Estratos de crecimiento y relaciones de corte entre estructuras de pliegues y cabalgamientos y el relleno sedimentario proporcionan la información esencial para restringir la temporalidad de deformación en estructuras particulares, especialmente cuando se integran con la evidencia termocronológica. Correlaciones estratigráficas e historias regionales de acumulación de sedimentos permiten discriminar entre fases de desarrollo coincidentes y divergentes durante la historia progresiva de fragmentación de la cuenca. Cambios marcados en la procedencia sedimentaria, identificados mediante geocronología U–Pb, demuestran variaciones en las áreas fuente de sedimentos y en los patrones de drenajes ancestrales asociados a cambios en las condiciones tectónicas.

Palabras clave: *cordillera Oriental, cinturón de pliegues y cabalgamientos, cuenca de antepaís, proveniencia, geocronología U–Pb.*

1. Introduction

The Eastern Cordillera of Colombia (Figure 1) forms a major topographic barrier in the northern Andes that profoundly influences climate, erosion, and the delivery of clastic sediment to major rivers and continental–margin deltas, including the Magdalena, Orinoco, and Amazon drainage systems (Hoorn et al., 2010, 2017; Mora et al., 2010a; Anderson et al., 2016). Construction of the Eastern Cordillera also guided the evolution of major sedimentary basins across the northern Andes, including the Magdalena Valley and Llanos Basins, sources of considerable hydrocarbon resources (Morales, 1958; Van Houten & Travis, 1968; Van Houten, 1976; Dengo & Covey, 1993; Cazier et al., 1995; Cooper et al., 1995; Gómez et al., 2003, 2005a, 2005b; Parra et al., 2009a, 2009b; Mora et al., 2010b; Londono et al., 2012).

For several reasons, the Eastern Cordillera is particularly well suited to addressing tectonic issues using the sedimentary

record. First, there is a long–duration sediment accumulation history spanning from the Late Jurassic – earliest Cretaceous through Neogene. Second, the associated stratigraphic archives are widely distributed and well preserved over a large segment of the Eastern Cordillera and flanking Magdalena Valley and Llanos provinces (Figure 2). Third, the depositional history in these three sectors involved sedimentation prior to, during, and after upper–crustal deformation.

The extensive temporal and spatial coverage offered by the stratigraphic record affords multiple opportunities to identify whether accumulation of specific stratigraphic intervals in different localities involved pre–, syn–, or post–deformational sedimentation (e.g., Bayona et al., 2008, 2013; Moreno et al., 2011; Parra et al., 2010; 2012; Horton, 2012; Mora et al., 2015). Another key part of the tectonic history involves the issue of when and how the multiple segments of a formerly integrated basin were compartmentalized by upper–crustal structures—specifically, the Magdalena Valley (including the Upper, Middle, and

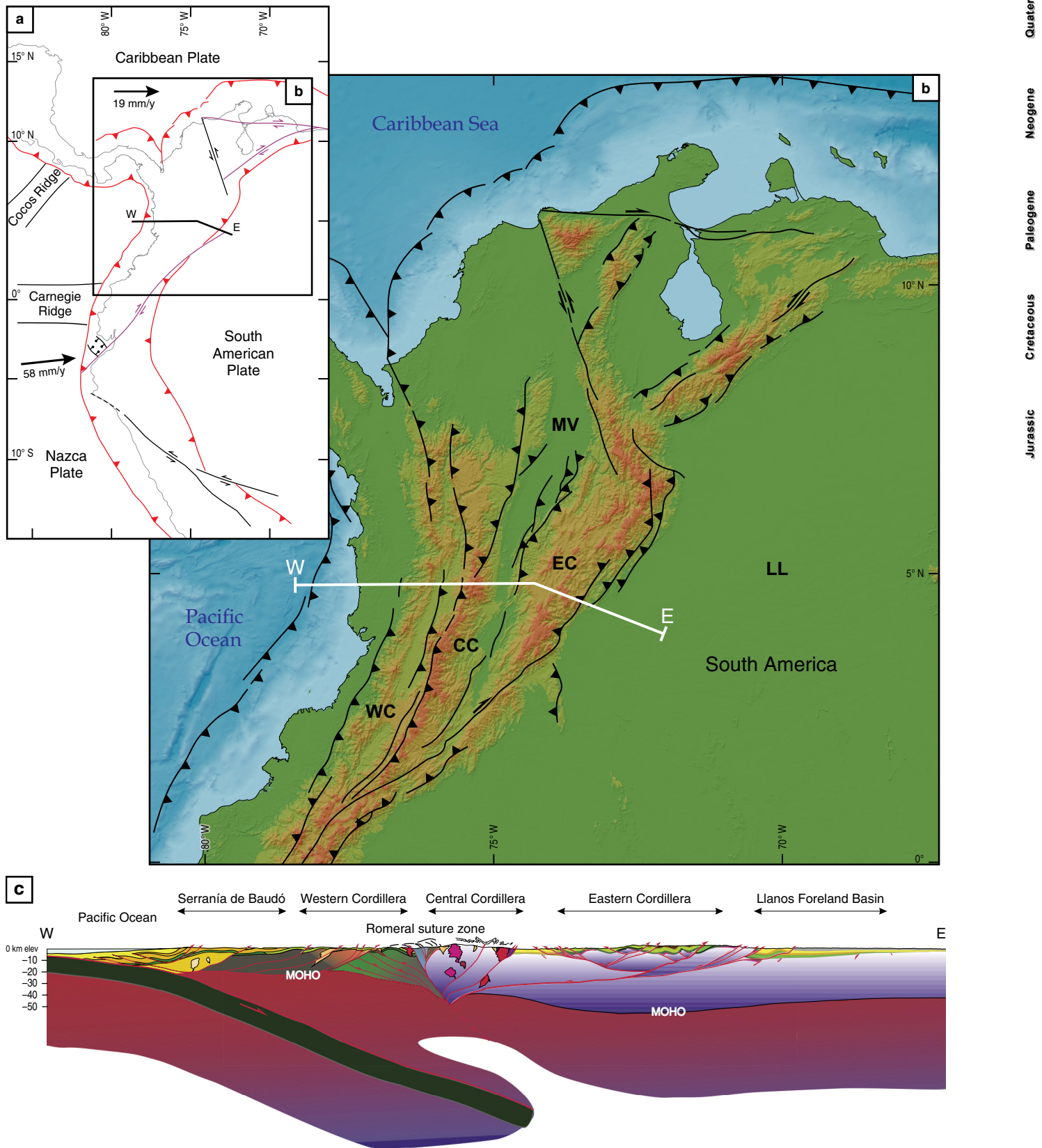


Figure 1. (a) Tectonic map of northwestern South America (from Velloza et al., 2012) showing major structures, plate boundaries, and plate velocities relative to a stable South American Plate (MORVEL-2010 plate model of DeMets et al., 2010). (b) Shaded relief map (after Mora et al., 2006) and (c) cross section (after Restrepo-Pace et al., 2004) of the northern Andes of Colombia, showing the subduction zone, and various tectonomorphic provinces: (WC) Western Cordillera; (CC) Central Cordillera; (MV) Magdalena Valley; (EC) Eastern Cordillera; (LL) Llanos foreland basin.

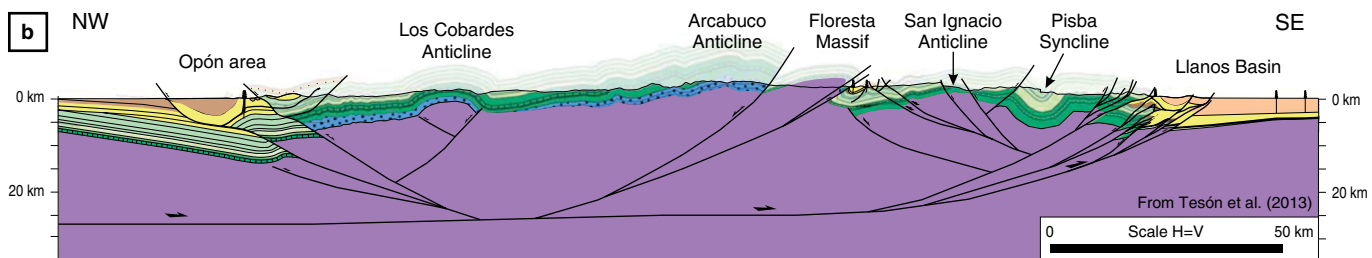
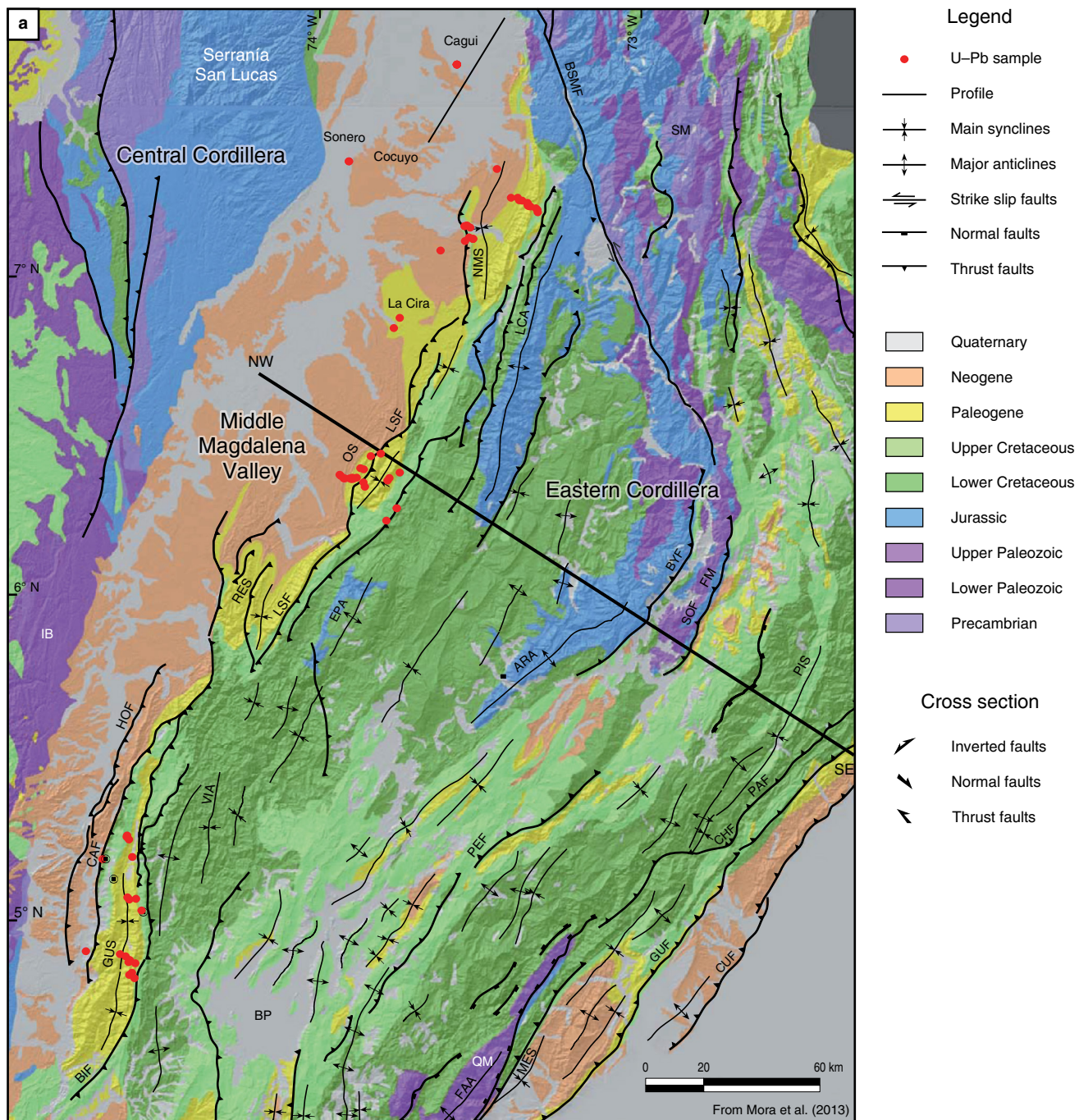


Figure 2. (a) Regional geologic map (Mora et al., 2015) and (b) cross section (Caballero et al., 2013b; Tesón et al., 2013) of the Central Cordillera, Magdalena Valley, Eastern Cordillera, and Llanos Basin. (BSMF) Bucaramanga–Santa Marta Fault; (SM) Santander Massif; (NMS) Nuevo Mundo Syncline; (LCA) Los Cobardes Anticline; (OS) Opón Syncline; (LSF) La Salina Fault; (IB) Ibagué Batholith; (RES) Ermitaño Syncline; (EPA) El Peñon Anticline; (ARA) Arcabuco Anticline; (BYF) Boyacá Fault; (SOF) Soapaga Fault; (FM) Floresta Massif; (HOF) Honda Fault; (PIS) Pisba Syncline; (CAF) Cambao Fault; (VIA) Villeta Anticlinorium; (PEF) Pesca Fault; (CHF) Chámeza Fault; (PAF) Pajarito Fault; (GUS) Guaduas Syncline; (BIF) Bituima Fault; (BP) Bogotá Plateau; (GUF) Guaicáramo Fault; (CUF) Cusiana Fault; (FAA) Farallones Anticline; (QM) Quetame Massif; (MES) Medina Syncline.

Lower Magdalena Valley basins), axial Eastern Cordillera (including the Floresta Basin), and the Eastern Cordillera foothills and Llanos Basin.

The utility of sediment provenance studies in tectonic and paleogeographic reconstructions has been demonstrated clearly in the consideration of the Mesozoic – Cenozoic evolution of the Eastern Cordillera (e.g., Bayona et al., 2008; Horton et al., 2010a, 2010b, 2015; Nie et al., 2010, 2012; Saylor et al., 2011, 2013; Bande et al., 2012; Ramírez–Arias et al., 2012; Caballero et al., 2013a, 2013b; Silva et al., 2013; Reyes–Harker et al., 2015). The application of techniques such as detrital zircon U–Pb geochronology is enabled by distinctive detrital signatures, owing to considerable contrasts in the geologic column for the Eastern Cordillera relative to the Central Cordillera and distal eastern craton (Guiana Shield). From the Cretaceous – Cenozoic stratigraphic successions of the Eastern Cordillera and flanking Magdalena Valley and Llanos provinces, one can extract not only the erosional history but also the broader consequences of uplift and exhumation.

The motivation here is to highlight the stratigraphic framework and sediment provenance records from the Eastern Cordillera, flanking Magdalena Valley, and Llanos Basins in an attempt to discern the generalized pattern of deformation, exhumation, and sediment delivery associated with construction of the Eastern Cordillera. We further emphasize that the stratigraphic record is but one component of a complete regional tectonic analysis. A critical complementary method involves low–temperature thermochronology, which offers the ability to understand the time–temperature history of rock materials, which reflects exhumational processes in relationship to tectonic and climatic mechanisms. In the case of the Eastern Cordillera, the combination of extensive sedimentary cover and selected crystalline basement massifs offers excellent opportunities to illuminate the evolution of crustal structures and sedimentary basins, including tectonic inversion of precursor structural and stratigraphic heterogeneities during Andean mountain building.

2. Materials and Methods

This chapter draws upon published work that informs the understanding of the geologic history of the Eastern Cordillera and its margins, with emphasis on the sedimentary record. Structural geologic relationships, stratigraphic nomenclature,

and basic geochronologic constraints largely derive from long efforts of the Servicio Geológico Colombiano (Gómez et al., 2015a, 2015b, 2015c, 2017, and references therein). Further advances have been motivated by the research efforts of Ecopetrol and the Instituto Colombiano del Petróleo (Mora, 2015 and references therein), which emphasized integrated structural, stratigraphic, and thermochronometric approaches to understanding the evolution of petroleum systems.

Many studies have explored detrital zircon U–Pb geochronology, and low–temperature (fission–track and (U–Th)/He) geochronology in Colombia, with several comprehensive approaches for selected regions (e.g., Horton et al., 2010a, 2015; Mora et al., 2010b, 2015; Parra et al., 2010, 2012; Bayona et al., 2012, 2013; Ramírez–Arias et al., 2012; Caballero et al., 2013a, 2013b; Silva et al., 2013; Reyes–Harker et al., 2015). Rather than an exhaustive synthesis of all published results bearing on the sedimentary and tectonic evolution of the Eastern Cordillera, we highlight key observations from selected representative zones that contain the type sections of several important stratigraphic units.

3. Results

3.1. Geologic Background

The Eastern Cordillera is the manifestation of Cenozoic retroarc shortening and transpressional deformation in the northernmost Andes of northwestern South America (Figure 1). This distinctive, nearly isolated mountain range is composed of series of fold–thrust structures and transpressional strike–slip faults. The NNE–trending Eastern Cordillera and its immediate margins have accommodated 50–150 km of horizontal shortening and up to 50 km of right–lateral strike–slip displacement (Colletta et al., 1990; Dengo & Covey, 1993; Cooper et al., 1995; Roeder & Chamberlain, 1995; Toro et al., 2004; Mora et al., 2006, 2008, 2013; Acosta et al., 2007; Tesón et al., 2013). This deformation of principally Cenozoic age has been accomplished during east–dipping subduction beneath northwestern South America of an oceanic slab defined by the modern Nazca Plate and precursor Farallon Plate (Pennington, 1981; van der Hilst & Mann, 1994; Lonsdale, 2005; Wagner et al., 2017). Consideration of the structural relief between the Eastern Cordillera and the flanking Magdalena Valley to the west and the Llanos Basin to the east indicates that Cretaceous units have been elevated

up to ca. 8 km above regional levels. Associated surface uplift in the Eastern Cordillera has generated a ca. 100–250 km wide by ca. 500 km long range of ca. 1.5–3 km average elevation.

The structural architecture of the Eastern Cordillera is one of a bivergent fold–thrust belt defined by sharp eastern and western mountain fronts against flanking sedimentary basins (Figure 2). This contractional range contains a relatively uniform distribution of NNE–striking thrust/reverse faults, with a prominent west–directed fault system along the western front (Magdalena Valley) and east–directed fault system along the eastern front (Llanos Basin) (Casero *et al.*, 1997; Corredor, 2003; Restrepo–Pace *et al.*, 2004; Mora *et al.*, 2006, 2010b; Sánchez *et al.*, 2012; Wolaver *et al.*, 2015). Individual structures accommodate several kilometers of dip–slip reverse displacement, with locally important dextral strike–slip offset. Although most structures have a thin–skinned ramp–flat geometry above regional décollements within the Cretaceous stratigraphic succession, there are several thrust/reverse faults involving crystalline basement rocks. The spatial association of such basement–involved structures with Jurassic – lowermost Cretaceous synextensional sub–basins suggests a common pattern of normal fault reactivation and basin inversion during later contraction (e.g., Cooper *et al.*, 1995; Branquet *et al.*, 2002; Cortés *et al.*, 2006; Kammer & Sánchez, 2006; Mora *et al.*, 2006, 2009).

The Eastern Cordillera is dominated by exposures of Mesozoic – Cenozoic sedimentary rocks with localized basement massifs (Bürgli, 1967; Julivert, 1970; Gómez *et al.*, 2015a, 2015b). The relative proportions of the various geologic units exposed across the ca. 100 000 km² surface area are as follows (in order of decreasing abundance): Upper Cretaceous (50%), Lower Cretaceous (30%), Cenozoic (10%), Jurassic (10%), basement (10%). Jurassic to Neogene sedimentary rocks of mixed marine and nonmarine origin are comprised of mostly clastic facies with limited carbonate (estimated 60% mudrock, 30% sandstone, 10% conglomerate).

The Mesozoic – Cenozoic record reflects a combination of regionally extensive and locally restricted stratigraphic units. The three major basin elements include (from west to east): (i) the Magdalena Valley, a NNE–trending longitudinal basin situated between the Central and Eastern Cordilleras and commonly divided into the Upper, Middle, and Lower Magdalena Valleys; (ii) basin fill now exposed in the axial Eastern Cordillera notably the Floresta Basin (and Bogotá/Altiplano Basin); and (iii) the Llanos Basin, on the eastern cratonic flank of the Eastern Cordillera.

A complex but discernible evolution is preserved within the stratigraphic record, in which these three sectors were either joined together as a single integrated basin or structurally partitioned by upper–crustal structures. The broad sedimentary history involves three principal phases: (i) Middle or Late Jurassic to early Early Cretaceous extension with the growth and coalescence of extensional sub–basins across the Eastern

Cordillera; (ii) Late Early Cretaceous to Late Cretaceous development of a single regionally integrated postextensional sag basin spanning the Eastern Cordillera, Magdalena Valley, and Llanos regions; and (iii) Latest Cretaceous – Cenozoic evolution of shortening–related basins in foreland, hinterland, and intermontane settings associated with the progressive growth of the Andean fold–thrust belt.

Multiple tectonic provinces may have acted as sources of clastic sediment to the Eastern Cordillera and its neighboring regions. Potential source areas include: (i) eastern cratonic zones of crystalline basement in the distal Llanos Basin and Guiana Shield; (ii) western zones of the Andean magmatic arc and its substrate; and (iii) the retroarc fold–thrust belt forming the Eastern Cordillera, including its pre–Devonian basement substrate. These morphostructural zones exhibit distinctive geologic units that lend themselves to discrimination through various geochronological and geochemical techniques (Cardona *et al.*, 2010; Horton *et al.*, 2010b, 2015; Nie *et al.*, 2012; Saylor *et al.*, 2013).

3.2. Stratigraphic Framework

The stratigraphic framework for the Eastern Cordillera must be considered along with that of the flanking hinterland and foreland provinces. It is instructive to emphasize the geologic records of three basin sectors—the Magdalena Valley, axial Eastern Cordillera, and Llanos Basin—and the shared versus divergent components of their stratigraphic histories (Figure 3). Here we review the principal stratigraphic units and briefly outline regional stratigraphic correlations and growth strata relationships.

The Magdalena, Eastern Cordillera, and Llanos regions share a similar crystalline basement that is regarded as the westernmost segments of South American continent crust, of Mesoproterozoic to early Paleozoic age, with accreted oceanic materials of late Mesozoic to Cenozoic age defining regions farther west (Aspden & McCourt, 1986; Forero, 1990; Taboada *et al.*, 2000; Cedié *et al.*, 2003; Restrepo–Pace *et al.*, 2004; Cordani *et al.*, 2005; Ordóñez–Carmona *et al.*, 2006; Ibañez–Mejía *et al.*, 2011; Montes *et al.*, 2012; Saylor *et al.*, 2012a).

Paleozoic sedimentary rocks of marine origin are locally preserved, but generally absent from most sectors of the Eastern Cordillera and its peripheral regions, which are dominated by Mesozoic – Cenozoic clastic basin fill. In several localized regions, crystalline basement is capped by coarse–grained nonmarine deposits, commonly sandstone and conglomerate and associated volcanoclastic components, of Middle/Late Jurassic to Early Cretaceous age (Girón Group). These extensional sub–basins are overlain by a more regionally extensive Lower Cretaceous marine succession of clastic and subordinate carbonate facies that directly rests upon isolated Jurassic deposits or crystalline basement. Upsection, an Upper Cretaceous to Cenozoic clastic succession chronicles the transition from marine to nonmarine deposition and rapid accumula-

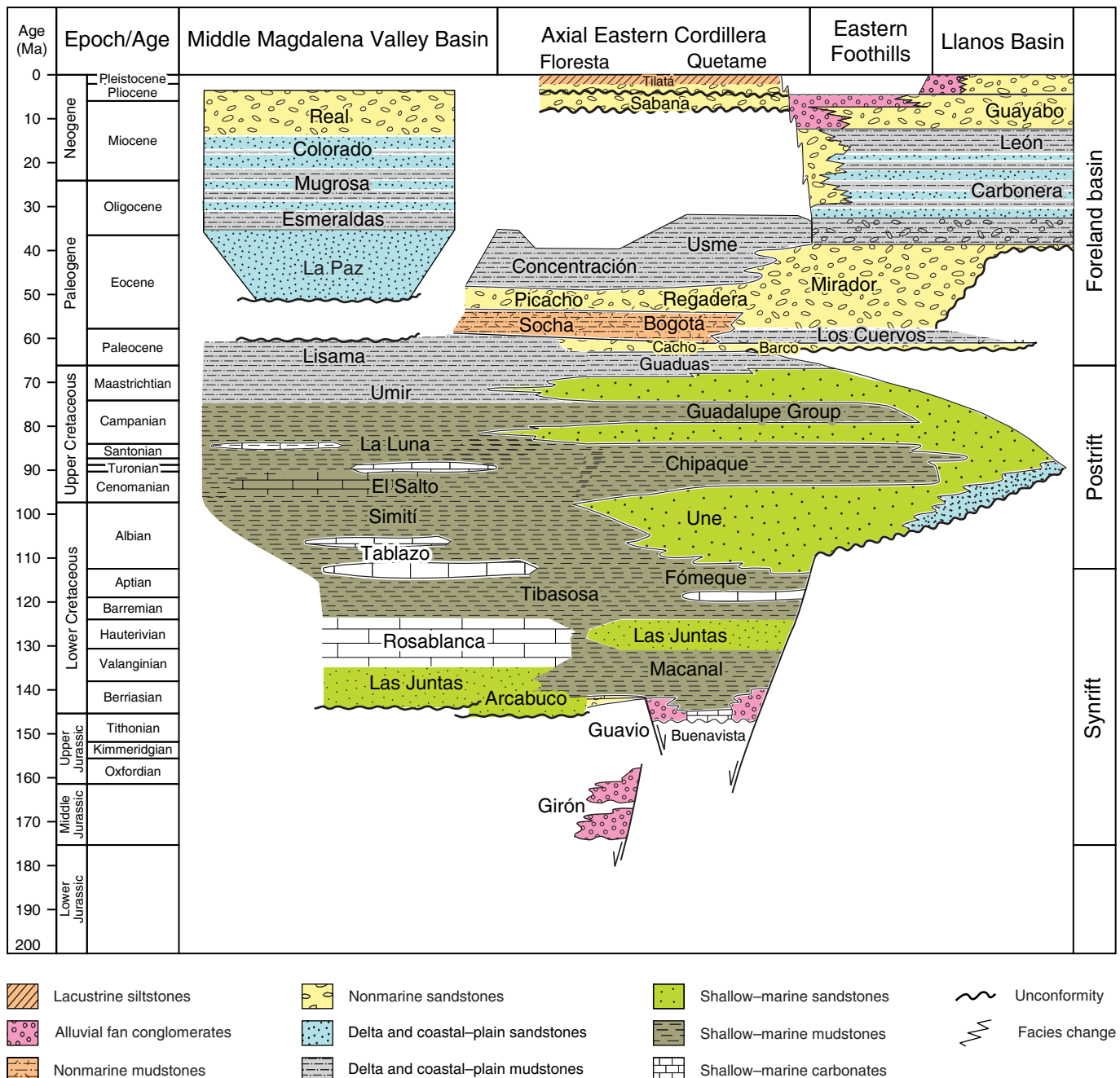


Figure 3. Cross-strike (west-east) geologic column for the Eastern Cordillera and flanking Magdalena Valley and Llanos Basins (after Mora et al., 2006; Parra et al., 2009a, 2009b).

tion during Andean shortening and flexural subsidence. Age control is provided by Cretaceous marine invertebrate fossils (Etayo-Serna et al., 1983; Etayo-Serna & Laverde-Montaño, 1985) and ubiquitous preservation of fossil pollen (palynomorph) assemblages that provide age resolution within several million years for Cenozoic basin fill across Colombia (e.g., Jaramillo et al., 2009, 2011). Further age control is provided by isotopic ages for selected volcanic horizons and syndepositional volcanogenic zircons (e.g., Gómez et al., 2003, 2005a,

2005b; Bayona et al., 2012; Saylor et al., 2012b; Gómez et al., 2015c; Anderson et al., 2016).

The Upper Cretaceous – Cenozoic stratigraphic intervals within the Magdalena Valley Basin, axial Eastern Cordillera, and Llanos Basin define broad upward coarsening packages (Figure 4) with some internal variability that makes lithostratigraphic correlations difficult. The sediment provenance characteristics (discussed in a following section) provide additional constraints on potential correlations, and prove instrumental in

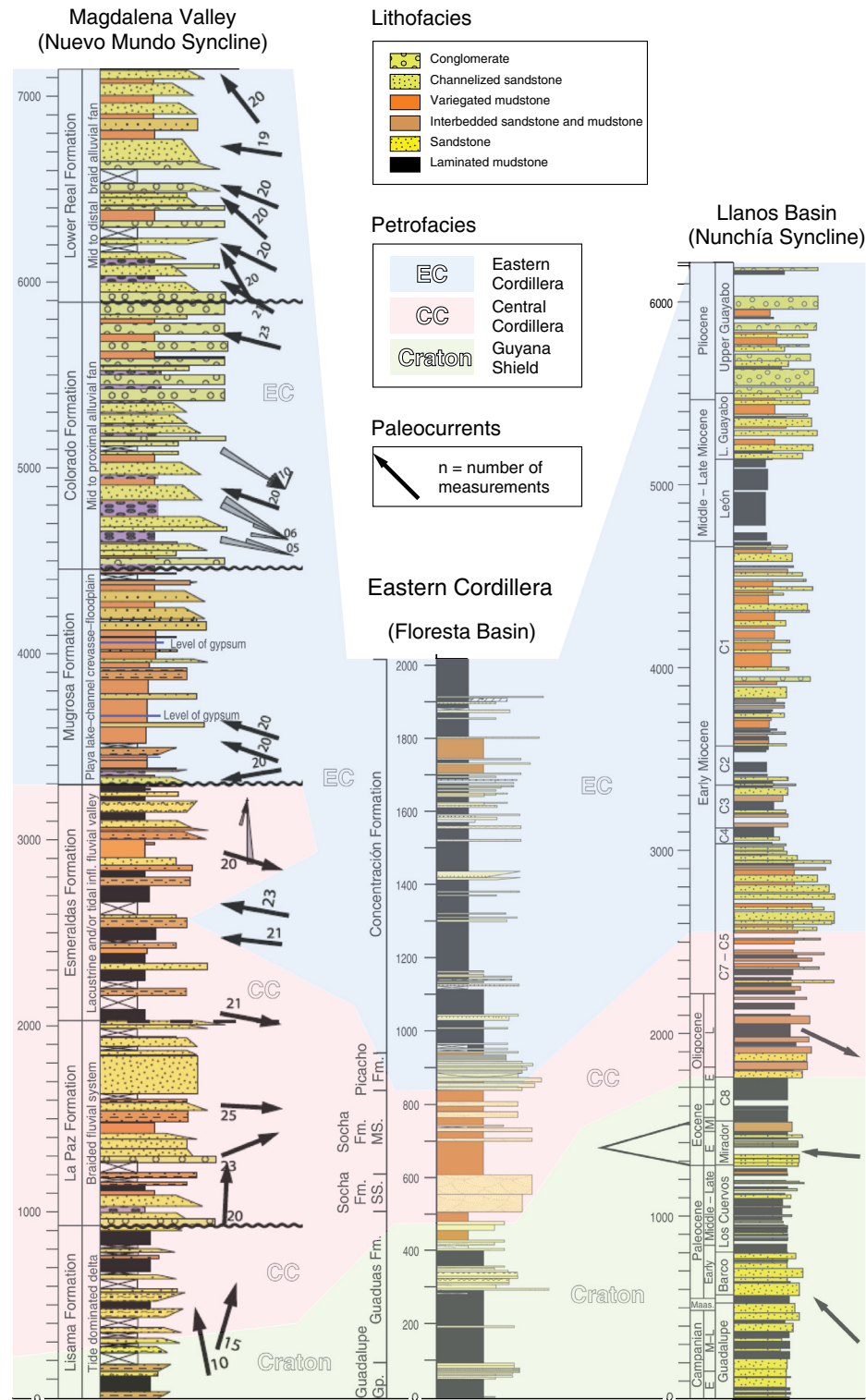


Figure 4. Measured stratigraphic sections and approximate chronostratigraphic correlations for the Middle Magdalena Valley (Caballero et al., 2013a), axial Eastern Cordillera (Saylor et al., 2011), and Llanos basins (Parra et al., 2010).

assessing sediment source regions and overall “petrofacies” of different levels of the Cretaceous – Cenozoic successions.

Widespread sandstone facies of Campanian, Maastrichtian, and early Paleocene age (including the Guadalupe Group, Gua-

duas Formation, Barco Formation, and Lisama Formation) are distributed across the Eastern Cordillera and its margins. These deposits are routinely correlated across broad regions, show a general axial northward transport, and appear to be principal-

ly derived from cratonic sources, with limited input from the emerging Eastern Cordillera (Bayona et al., 2008, 2012; Saylor et al., 2011; Silva et al., 2013; Vallejo et al., 2017). In contrast, the overlying mid–Paleocene through Quaternary panels show significant variability among the three basin systems, which are considered individually.

In the Magdalena Valley, the ca. 7000 m thick Cenozoic succession consists of alternating distal fluvial, proximal fluvial, alluvial fan, and limited lacustrine facies organized into an alternating upward coarsening and fining packages (Morales, 1958; Van Houten, 1976; Gómez et al., 2003, 2005b; Caballero et al., 2010, 2013a; Horton et al., 2010b, 2015; Nie et al., 2010, 2012; Moreno et al., 2011). At the base, the Maastrichtian – lower Paleocene Umir and Lisama Formations contain the transition from marine to nonmarine sedimentation. These organic-rich shale and sandstone are overlain by the upper Paleocene to middle Eocene La Paz Formation, which represents a major clastic wedge of sandstone and conglomerate derived from early Andean sources to the west. This panel is abruptly capped by a fine-grained late Eocene – lowermost Oligocene interval (Esmeralda Formation) representative of mud-dominated overbank fluvial and lacustrine deposition. This is capped, in turn, by a thick upward coarsening panel of sandstone and conglomerate in alternating channel-belt fluvial and alluvial fan deposits of Oligocene to Quaternary age (Mugrosa, Colorado, and Real Formations).

In the axial Eastern Cordillera, the Floresta Basin and smaller satellite sub-basins contain a partial stratigraphic record (ca. 2000 m total thickness) that spans from the Upper Cretaceous through Oligocene (Bayona et al., 2010; Saylor et al., 2011; Ochoa et al., 2012; Silva et al., 2013). The Maastrichtian – lower Paleocene Guadalupe Group and Guaduas Formation (ca. 500 m thick) are part of a regionally extensive sandy interval that contains the final marine to nonmarine transition in the region, similar to the Magdalena Valley Basin. This diagnostic part of the section is commonly defined by resistant, well-exposed sandstones that can be correlated across the Eastern Cordillera, albeit with variable stratigraphic names (Cacho and Barco Formations). In the axial Eastern Cordillera, including the Floresta Basin (and Bogotá/Altiplano Basin), these sandstones are capped by a mixed collection of fluvial and lacustrine sandstone, mudstone, and subordinate conglomerate, comprising the Paleocene Socha (Bogotá) Formation, lower – middle Eocene Picacho (Regadera) Formation, and upper Eocene – Oligocene Concentración (Usme) Formation. These units are broadly organized into a generally upward fining panel ca. 1500 m in thickness. The lack of Miocene and younger deposits is considered to reflect a history of nondeposition during Andean uplift, rather than deposition and subsequent erosional removal.

On the eastern flank of the Eastern Cordillera, exposed stratigraphic panels in the proximal (western) segments of the Llanos Basin attain ca. 6000 m in total thickness and provide access to Cretaceous – Cenozoic depositional histories (Parra

et al., 2009a, 2009b, 2010; Bande et al., 2012). The regionally extensive Upper Cretaceous – lower Paleocene section (Guadalupe Group, and Barco and Los Cuervos Formations) represents protracted pre–Andean marine accumulation (up to 1500 m) during post–extensional thermal subsidence. Progressively diminished accommodation resulted in a relatively thin (100–200 m) but diagnostic middle – upper Eocene unit, the fluvial to coastal marine Mirador Formation (Jaramillo et al., 2009, 2011). Capping the Mirador Formation is a ca. 4500 m thick Oligocene – Quaternary upward coarsening succession representative of a classic distal to proximal evolution of a foreland basin. This interval is best exposed along the deformation front, including the Nazareth Syncline (Medina Basin) and Nunchía Syncline adjacent to the Guaicáramo and Yopal thrust faults, respectively (Parra et al., 2009a, 2010; Bande et al., 2012). In many ways, the Oligocene – Quaternary deposits of the proximal Llanos foreland can be considered as a mirror image of the western flank of the Eastern Cordillera and the comparable and contemporaneous upward coarsening succession of the Magdalena Valley Basin.

Evaluation of potential regional lithostratigraphic correlations for Mesozoic – Cenozoic units reveals contrasting situations, in which Cretaceous – Paleocene units show clear laterally continuous facies, yet Eocene and younger units show greater variability. Multiple stratigraphic levels of the largely marine Cretaceous succession have been correlated across the Eastern Cordillera and flanking Magdalena and Llanos basins, on the basis of comparable lithology, lithofacies assemblages, depositional conditions, and marine fossil assemblages (Morales, 1958; Bürgli, 1961; Etayo–Serna & Laverde–Montaño, 1985; Cooper et al., 1995; Mora et al., 2010c; Gómez et al., 2015a, 2015b). The upper levels of this interval uniformly show regional-scale upward coarsening and a shift to nonmarine conditions. These Maastrichtian – Paleocene stratigraphic units are correlated regionally across the Eastern Cordillera and adjacent basin sectors, and represent large fluvial systems characterized by generally northward longitudinal transport within a broad early Andean foreland basin system (Villamil, 1999; Gómez et al., 2005a, 2005b; Caballero et al., 2013b; Silva et al., 2013). This stratigraphic continuity contrasts sharply with the Eocene depositional record, for which regional correlation proves challenging. A significant hiatus, the Middle Magdalena Valley unconformity, can be linked to structural activity along a series of local fault-related uplifts (Gómez et al., 2003, 2005b; Moreno et al., 2011; Parra et al., 2012). Although many earlier studies inferred a long (ca. 20 my) early – middle Eocene hiatus across the Eastern Cordillera, (e.g., Dengo & Covey, 1993; Cooper et al., 1995; Villamil, 1999), recent, higher-resolution palynological studies demonstrate continuous sedimentation, albeit at a reduced rate (e.g., Jaramillo et al., 2009, 2011). Stratigraphic contrasts in lithofacies, deposystems, and thicknesses suggest that structural partitioning of the early Andean foreland basin

was underway during the Eocene. Nevertheless, the common occurrence of relatively fine-grained uppermost Eocene – lower Oligocene successions (Figure 4) (Parra *et al.*, 2010; Saylor *et al.*, 2011; Ochoa *et al.*, 2012) may suggest a regional-scale reduction in exhumation and flexural accommodation, conceivably related to a transient reduction in the pace of orogenesis in the northern Andes (Gómez *et al.*, 2003; Londono *et al.*, 2012; Mora *et al.*, 2013; Horton, 2018a), similar to large segments of the southern Andes (e.g., Horton & Fuentes, 2016; Horton, 2018b). Importantly, the lack of regionally correlative stratigraphic units points to a late Eocene to Quaternary evolution of compartmentalized basins across the Magdalena, Eastern Cordillera, and Llanos Basin sectors, with strongly contrasting depositional conditions, sediment dispersal, and accumulation.

Stratigraphic correlations are further supported by a series of localities reported to contain growth strata. In contractional systems, growth strata are characterized by an upsection reduction in stratal dip, thinning of individual beds or bed packages toward the structure, and common internal angular unconformities (e.g., Riba, 1976; Perez & Horton, 2014). In Colombia, the recognition of growth strata in surface and subsurface datasets is critical to assessing basin evolution in relationship with upper-crustal structures (e.g., Julivert, 1963; Corredor, 2003; Gómez *et al.*, 2003, 2005a; Restrepo–Pace *et al.*, 2004; Cortés *et al.*, 2006; Parra *et al.*, 2010, 2012; Mora *et al.*, 2013). These features are unambiguous indicators of fault activity, and with sufficient stratigraphic age control, provide a direct means of dating deformation. Although growth strata are commonly elusive within the fold–thrust belt interiors, as reported for most of Eastern Cordillera (Mora *et al.*, 2015), key examples in Colombia include: (i) upper Paleocene – Eocene growth strata in the Magdalena Valley and along the Magdalena–Eastern Cordillera transition zone (Gómez *et al.*, 2003; Restrepo–Pace *et al.*, 2004; Parra *et al.*, 2012; Sánchez *et al.*, 2012); (ii) isolated Paleogene examples within the Eastern Cordillera (Julivert, 1963; Gómez *et al.*, 2005a; Bayona *et al.*, 2010); and (iii) Oligocene – Pliocene growth strata along the eastern Andean deformation front and proximal zone of the Llanos foreland basin (Corredor, 2003; Cortés *et al.*, 2006; Bayona *et al.*, 2008; Parra *et al.*, 2010; Mora *et al.*, 2013).

3.3. Sediment Accumulation

The history of basin development along the flanks and interior of the Eastern Cordillera is contained in the lithofacies patterns, accumulation histories, and shifts in sediment provenance. Sediment accumulation histories for the Magdalena Valley and Llanos foreland register periods of rapid, thrust-induced subsidence and possible spatial variations in a cross-strike (east–west) direction (Gómez *et al.*, 2005b; Bayona *et al.*, 2008; Parra *et al.*, 2009a; Saeid *et al.*, 2017; Horton, 2018a). Sufficient age control from basin fill in the Middle Magdalena Valley (Gua-

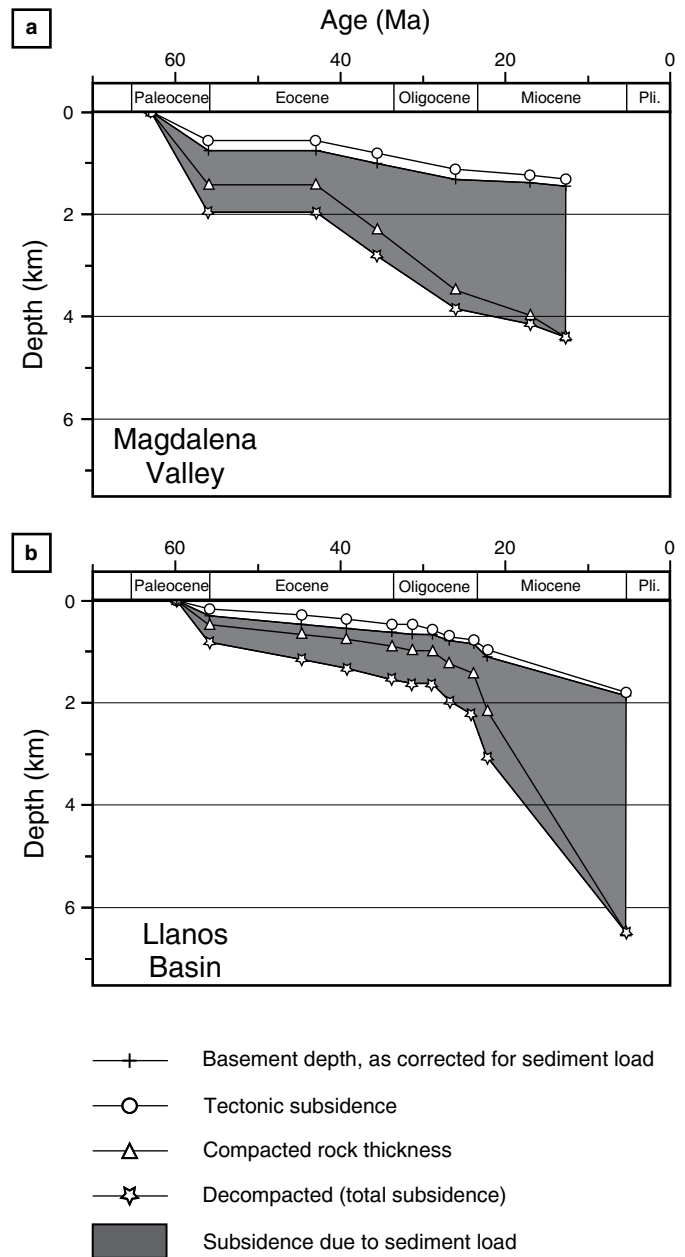


Figure 5. Sediment accumulation plots for (a) the Middle Magdalena Valley Basin and (b) Llanos Basin (Parra *et al.*, 2010).

duas Syncline; Gómez *et al.*, 2005a) and western Llanos Basin (Medina Basin; Parra *et al.*, 2010) enables a geohistory analysis that accounts for incremental sediment compaction. This analysis yields the Cenozoic history of subsidence, depicted in time–depth plots (Figure 5), and allows for discrimination of tectonic subsidence and subsidence due to sediment loading.

Although both the Magdalena Valley Basin and Llanos foreland basin show sustained rapid subsidence, they experienced relatively abrupt increases in accommodation at different moments in their Cenozoic histories. In the Magdalena Valley, a

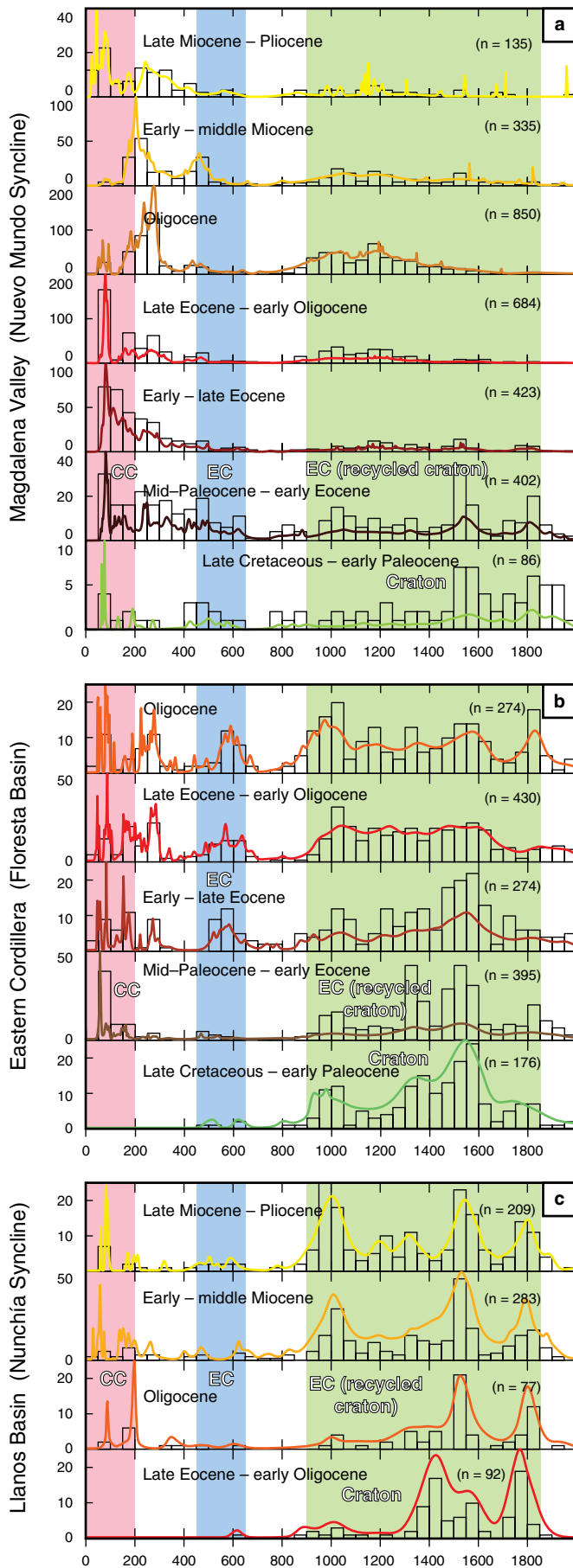


Figure 6. Comparative plots of detrital zircon U–Pb age distributions for latest Cretaceous – Cenozoic basin fill of the **(a)** Middle Magdalena Valley Basin (Nuevo Mundo Syncline; Horton et al., 2015), **(b)** axial Eastern Cordillera (Floresta Basin; Saylor et al., 2011), and **(c)** Llanos Basin (Yopal/Nunchía Syncline; Bande et al., 2012). Bold white text labels identify the initial craton provenance followed by the first appearance of detritus from the Central Cordillera (CC), Eastern Cordillera (EC), and recycled cratonic detritus from the Eastern Cordillera.

multi-phase history involves rapid Paleocene accumulation followed by sharply diminished accommodation, then a renewed rapid period of accumulation commencing at about 45–40 Ma. The early record probably reflects initial flexural subsidence due to Paleocene shortening and crustal thickening in the Central Cordillera followed by limited early Eocene accumulation above growing basement-involved structures in the Magdalena Valley. It is important to note that other local zones on the flanks of these basement highs in the Magdalena Valley likely underwent rapid subsidence during the early Eocene, suggesting significant spatial variability in accommodation. Subsequent to this record, an inflection point at 45–40 Ma in the sediment accumulation curve suggests that considerable flexural accommodation was underway by middle to late Eocene time. This subsidence, however, was likely generated by shortening within the Eastern Cordillera, suggesting that the Magdalena Valley had transformed from a proximal foreland basin into an intermontane hinterland basin.

In the Llanos Basin, a more straightforward sediment accumulation history is revealed in which continuous Paleocene – Eocene accommodation is replaced by rapid accommodation in Oligocene time, as shown by a ca. 30 Ma inflection point. The ca. 10–15 my difference in the onset of rapid subsidence between the Magdalena Valley and Llanos Basin is attributed to patterns of fold–thrust deformation across the Eastern Cordillera. The timing constraints are consistent with an overall eastward advance of upper–crustal shortening, which is compatible with low–temperature thermochronological records (mentioned below) in suggesting early Andean exhumational cooling in western sectors followed by late Andean exhumation near the eastern deformation front (Mora et al., 2008, 2010a, 2015; Parra et al., 2009b, 2010; Saylor et al., 2012b).

3.4. Sediment Provenance

U–Pb geochronological data are fundamental to assessing the sediment sources and paleodrainage patterns in Colombia. Several major shifts in sediment provenance can be linked to the tectonic evolution of the Eastern Cordillera and its peripheral regions. During the Mesozoic, sediment was overwhelmingly derived from eastern sources of the Guiana Shield, including

possible minor sources that are now buried beneath Cenozoic fill of the Llanos Basin. The ages of these cratonic crystalline basement rocks span the late Paleoproterozoic to early Neoproterozoic (Teixeira *et al.*, 1989; Horton *et al.*, 2010b; Cardona *et al.*, 2010, and references therein). Detrital zircon U–Pb geochronological results for Upper Cretaceous deposits show comparable age populations, concentrated at 900–2000 Ma (Figure 6). The lack of significant Phanerozoic grains indicates very limited erosional input from the present-day Central or Eastern Cordilleras. These results confirm a pre-Andean extensional to post-extensional landscape involving west-directed sediment dispersal from cratonic sources uniformly across all three basin sectors—the Llanos Basin, Eastern Cordillera, and Magdalena Valley—as interpreted by many previous studies on the basis of lateral facies changes, thickness trends, and paleocurrents (Toussaint & Restrepo, 1994; Cazier *et al.*, 1995; Cooper *et al.*, 1995; Villamil, 1999; Sarmiento-Rojas *et al.*, 2006).

A major reversal in sedimentary polarity archived by sediment provenance signatures within Upper Cretaceous – Cenozoic basin fill points to the initial effects of Andean orogenesis. The initial delivery of detritus from the Central Cordillera is evidenced by the first appearance of Mesozoic – Cenozoic age populations that must originate in the Andean magmatic arc. Paleogene deposits across the region record the arrival of a significant population of 50–200 Ma grains emblematic of Andean igneous materials from the Central Cordillera (McCourt *et al.*, 1984; Aspden *et al.*, 1987; Villagómez *et al.*, 2011; Villagómez & Spikings, 2013). Although this first appearance of Andean detritus can be identified in all three basin sectors, it occurred at different moments in their respective sedimentary histories. Whereas the reversal in sediment dispersal occurred in the Paleocene in the Magdalena Valley and axial Eastern Cordillera (Lisama, La Paz, Socha Formations; Figure 6a, 6b), it was delayed until the Oligocene for the Llanos Basin (Carbonera Formation; Figure 6c). This delay is consistent with the pattern of flexural loading inferred from the sediment accumulation histories (Figure 5), in which the Magdalena Valley experienced rapid flexural accommodation prior to the Llanos Basin.

Following the initial delivery of Andean sediment, diverse provenance patterns characterize the three basin sectors during their independent evolution from Eocene to present (Figure 6). (i) In the west, the Magdalena Valley underwent a complex alternating history of Eastern Cordillera versus Western Cordillera detrital input (Nie *et al.*, 2010, 2012; Caballero *et al.*, 2013b; Silva *et al.*, 2013), prior to establishment of a throughgoing Magdalena River in late Miocene time (Horton *et al.*, 2015). This pattern (Figure 6a) is revealed by Eocene to Pliocene alternations between Andean arc (<200 Ma) signals from the Central Cordillera and two signals from the Eastern Cordillera: a late Neoproterozoic – early Paleozoic (650–450 Ma) population from local basement and a recycled cratonic (900–1800 Ma) population derived from ubiquitous Cretaceous Eastern Cordil-

lera strata originally derived from cratonic sources (Horton *et al.*, 2010a, 2010b, 2015). (ii) In contrast, the axial Eastern Cordillera was fed mostly by local sources within the fold–thrust belt, with limited input of Andean arc detritus (Bayona *et al.*, 2010, 2012; Saylor *et al.*, 2011; Silva *et al.*, 2013). This pattern (Figure 6b) is reflected in Eocene – Oligocene strata by the dominance of Eastern Cordillera signatures. Although a minor signal from the Central Cordillera arc (<200 Ma) persists, the dominant populations are diagnostic of the Eastern Cordillera (the aforementioned 650–450 Ma and recycled 900–1800 Ma populations). (iii) In the east, the Llanos Basin was dominated by erosional input from the Eastern Cordillera, with very limited delivery of arc detritus (Horton *et al.*, 2010a, 2010b; Bande *et al.*, 2012). This pattern (Figure 6c) is attributed to exhumation within the Eastern Cordillera of not only Cretaceous strata, which provided recycled cratonic populations (900–1800 Ma), but also Cenozoic basin fill, which provided the restricted amounts of Andean arc (<200 Ma) material.

The power of provenance applications in Colombia is enabled by the distinctive morphostructural zones of the northern Andes, which have diagnostic geochronological signatures that can be identified in the stratigraphic record (Cardona *et al.*, 2010; Horton *et al.*, 2010b, 2015; Nie *et al.*, 2010, 2012; Saylor *et al.*, 2011, 2013). When integrated with considerations of regional stratigraphic continuity and the timing of basin compartmentalization, the provenance record provides a robust understanding of the spatial and temporal evolution of the Eastern Cordillera. These first-order constraints from the stratigraphic record can be augmented by higher resolution studies that seek to assess changes in climate and absolute elevation (Guerrero, 1997; Mora *et al.*, 2008; Anderson *et al.*, 2015) and the exhumational history of individual structures from thermochronological data (Mora *et al.*, 2008, 2013, 2015; Parra *et al.*, 2009b, 2010, 2012; Saylor *et al.*, 2012b; Almendral *et al.*, 2015).

3.5. Low-Temperature Thermochronometry

Thrust-induced rock uplift histories in the Eastern Colombia have been diagnosed through multi-method fission track and (U–Th)/He thermochronometry assisted by vitrinite reflectance data (see Mora *et al.*, 2015 and references therein). Analytical results from multiple samples provide the basis for 1–D time–temperature histories extracted through thermal modeling (e.g., HeFTy software; Ketcham, 2005). Mineral cooling ages and thermal modeling of thermally reset Mesozoic to Paleogene strata and their underlying basement rocks along a cross-strike transect from the Magdalena Valley to the Llanos Basin reveal a diachronous inception of fold–thrust belt development (Figure 7).

First, Paleocene – early Eocene onset of thrusting along the western margin of the Eastern Cordillera and in basement highs beneath the Magdalena Valley reveal the extent of a relict Paleocene thrust–belt associated with arc collision and early

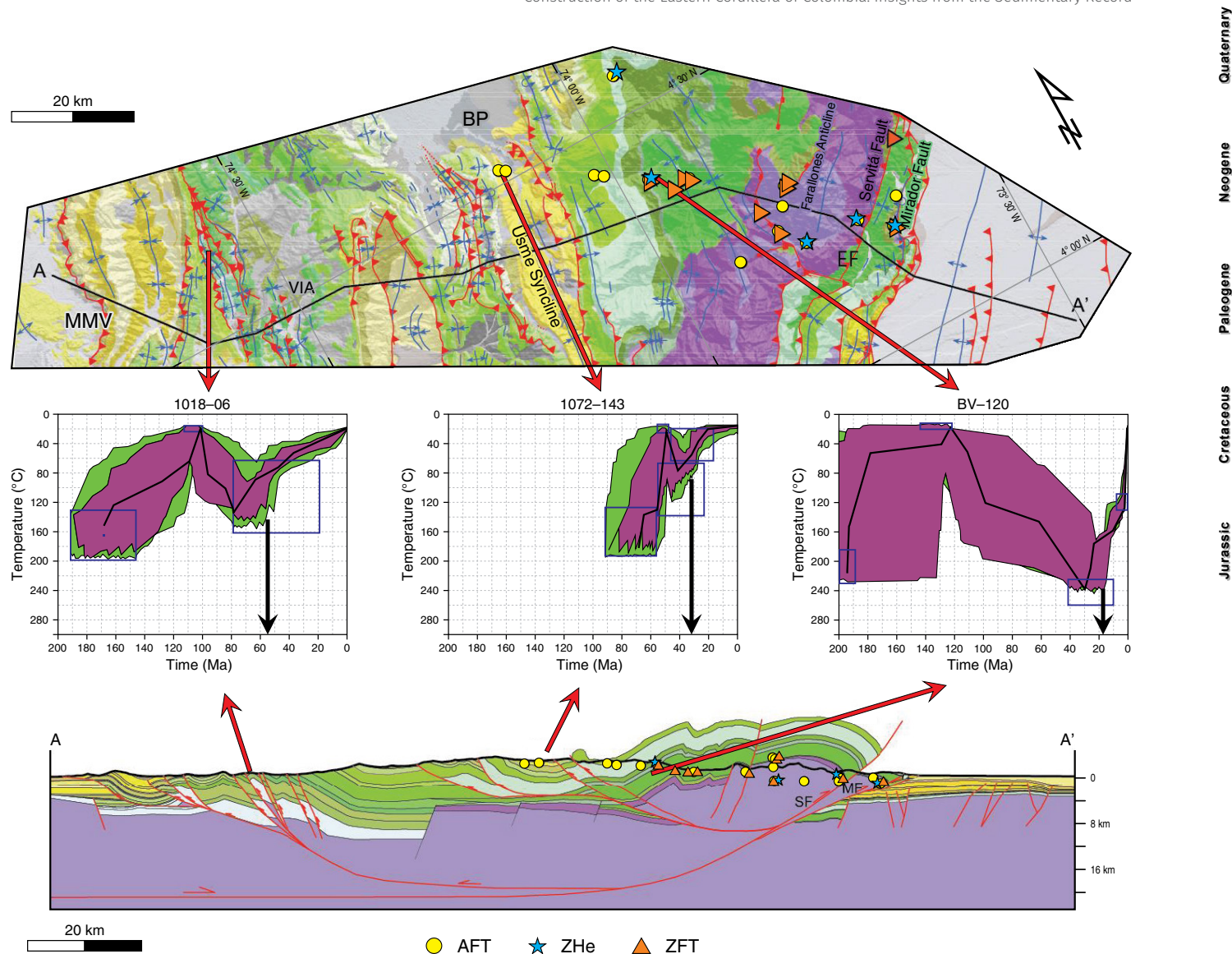


Figure 7. Geologic map (above) and structural cross section (below) at the latitude of Bogotá (4° N, after Mora et al., 2015) showing geologic context for three representative 1D thermal models constructed using multiple thermochronometers with HeFTy software (Ketcham, 2005). The time-temperature (t-T) paths show good (purple) and acceptable (green) thermal histories that fit the observed data. (MMV) Middle Magdalena Basin; (VIA) Villeta Anticlinorium; (BP) Bogotá Plateau; (EF) Eastern Foothills.

shortening in the Western and Central Cordilleras (Parra et al., 2012; Caballero et al., 2013b). An eastward advance of thrusting induced cooling and rock exhumation at 40–35 Ma in the axial Eastern Cordillera (Parra et al., 2009b; Mora et al., 2010b; Ramírez-Arias et al., 2012; Saylor et al., 2012b) and ca. 10 my later, at 30–25 Ma along the eastern margin of the Eastern Cordillera (Parra et al., 2009b; Horton et al., 2010a; Mora et al., 2010b; Bande et al., 2012; Ramírez-Arias et al., 2012; Mora et al., 2015). Remarkably, in all three of these regions, cooling associated with rock exhumation was associated with contractional reactivation of major ancestral normal faults (active during Mesozoic extension) and coincide with major shifts in sediment delivery and accommodation revealed by provenance and facies distributions.

3.6. Discussion

The preceding synthesis of sedimentary datasets and representative thermochronometric data provides a foundation for a generalized reconstruction of the Mesozoic – Cenozoic history of the Eastern Cordillera and adjacent regions in the Magdalena Valley and Llanos Basin of Colombia. A multi-step two-dimensional cross-sectional reconstruction shows an east-west profile of evolving basin configurations from Late Jurassic to present. We consider and incorporate elements from many similar regional reconstructions depicted by previous authors (e.g., Restrepo-Pace et al., 2004; Bayona et al., 2008, 2013; Horton et al., 2010b, 2015; Mora et al., 2010b, 2013, 2015; Bande et al., 2012; Caballero et al., 2013a, 2013b; Wolaver et

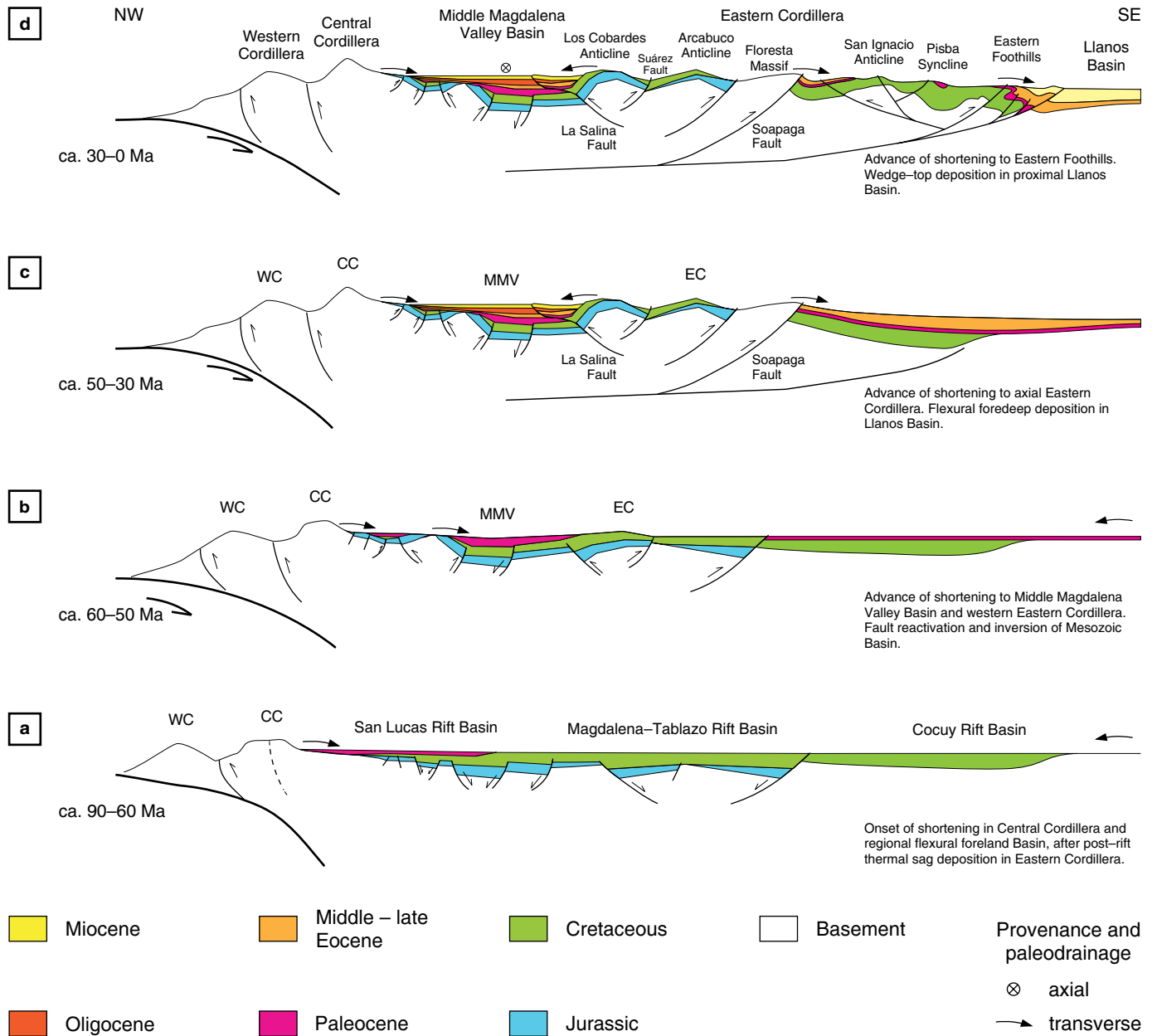


Figure 8. Highly schematic reconstruction of Cretaceous – Cenozoic basin evolution, with emphasis on the structural and topographic development of the Eastern Cordillera (after Horton *et al.*, 2010b and Caballero *et al.*, 2013b). **(a)** Late Cretaceous, **(b)** Maastrichtian – Paleocene, **(c)** Eocene – Oligocene, **(d)** Miocene – Quaternary. (WC) Western Cordillera; (CC) Central Cordillera; (MMV) Middle Magdalena Basin; (EC) Eastern Cordillera.

et al., 2015). In drafting these reconstructions, we relied heavily on the three datasets summarized above: (i) the regional stratigraphic framework; stratigraphic correlations, and depositional conditions; (ii) sediment accumulation histories; and (iii) sediment provenance constraints principally from detrital zircon U–Pb geochronology.

During the Late Jurassic – earliest Cretaceous, a series of newly formed normal faults guided the generation of individual extensional sub-basins with half-graben geometries. Progressive east–west extension in backarc regions was accommodated by the linkage of normal faults and the coalescence of sub-ba-

sins into larger extensional basins. Basin evolution was largely governed by two major extensional basins, the Tablazo–Magdalena and Cocuy basins, occupying the Magdalena Valley and Eastern Cordillera provinces, respectively (Cooper *et al.*, 1995; Sarmiento–Rojas *et al.*, 2006). Sedimentation during upper-crustal extension consisted of initial, locally source nonmarine facies (Girón Group) followed by regional accommodation with widespread marine conditions.

The Late Cretaceous history (Figure 8a) involved a shift to a neutral tectonic regime in which basin subsidence was no longer controlled by individual faults, but was governed by re-

gional postextensional cooling of lithosphere and associated thermal subsidence. The dominant sediment source regions throughout Jurassic – Cretaceous basin evolution were situated to the east, in the Guiana Shield. Clastic detritus derived from cratonic crystalline basement (900–1800 Ma) was transported westward to principally marine deposystems.

The Maastrichtian – Paleocene (Figure 8b) marked the initial topographic emergence of the Colombian Andes and a fundamental reorganization of paleodrainage systems in northwestern South America (Horton, 2018a). The abrupt reversal in sedimentary polarity from west-directed to east-directed drainage coincided with the appearance of detritus from the Andean magmatic arc (<200 Ma zircons from the Central Cordillera; Figure 6), accelerated accumulation rates in the Magdalena Valley (Figure 5), and a regional shift from marine to nonmarine conditions (Figure 4). This episode marks the first major Andean shortening, crustal loading, and flexural subsidence in Colombia, with reverse/thrust faulting limited to the Central Cordillera, and locally, to the Magdalena Valley, as suggested by Paleocene – early Eocene cooling. The reversal in sedimentary polarity appears to have been time transgressive, with a Maastrichtian – early Paleocene age in the Magdalena Valley and Eastern Cordillera, ca. 30 my prior to the reversal in the Llanos region. This dynamic pattern, as reflected in three sedimentary “petrofacies” indicative of direct input from either the Central Cordillera, Eastern Cordillera, or craton (Figure 4) requires the eastward advance of an effective drainage axis separating western (Andean) from eastern (cratonic) contributors of sediment (Silva et al., 2013; Reyes-Harker et al., 2015).

During Eocene – Oligocene time (Figure 8c), the regionally contiguous foreland basin system that spanned from the Magdalena to Llanos provinces was partitioned by a series of fault-related uplifts within the Eastern Cordillera. These structures commonly include former normal faults reactivated during Andean shortening, inducing basin inversion and severing the topographic and depositional continuity among the Magdalena, Eastern Cordillera, and Llanos basins. Evidence for this phase of basin compartmentalization comes from the progressively greater contributions of detritus from the Eastern Cordillera, in the form of Eastern Cordillera basement (450–650 Ma) and recycled cratonic (900–1800 Ma) grains from the thick widespread cover succession spanning the Eastern Cordillera (Figure 6). Although this period marks the initiation of the Magdalena Valley as a hinterland basin, the axial Eastern Cordillera persisted as a low subsiding region, with an intermontane basin system (Floresta Basin) with potential minor depositional links with the Llanos foreland basin farther east.

The final Miocene to Quaternary phase (Figure 8d) reflects the final establishment of the Eastern Cordillera in the form observed today. By the end of the Paleogene, substantial shortening had ceased in the Central Cordillera, yet the range persisted as an intermittent sedimentary source to the Magdalena Valley.

Full emergence of the Eastern Cordillera led to the termination of subsidence in its axial zone (Floresta Basin) and the establishment of elevated topography that served as an orographic barrier and dominated sediment delivery to the Llanos Basin. This stage in the evolution of the northern Andes also coincides with accelerated accumulation rates in the Llanos Basin (Figure 5), attributable to shortening and crustal loading within the Eastern Cordillera.

The proposed reconstruction (Figure 8) focuses on the construction of the Eastern Cordillera of Colombia, from the perspective of the sedimentary record and supportive thermochronometric data, and their utility as an archive of tectonic processes associated with contractional mountain building. However, important along-strike variations are expressed in the northern Andes, such that the Ecuadorian Andes to the south experienced substantially lower degrees of shortening, thrust-front advance, and basin compartmentalization (Aleman & Ramos, 2000; Ruiz, 2002; Baby et al., 2004; Vallejo, 2007; Horton, 2018a). Within a broader, continental-scale framework, the issues discussed here have further implications for the evolution of major paleodrainage systems in South America, including the Magdalena, Orinoco, and Amazon river systems (Hoorn et al., 2010, 2017; Mora et al., 2010a; Horton et al., 2015; Anderson et al., 2016).

4. Conclusions

The tectonic history of the Eastern Cordillera in the northern Andes of Colombia is largely contained in the clastic sedimentary record preserved in three principal regions (from west to east): the Magdalena Valley Basin, the Eastern Cordillera (notably axial basins such as the Floresta Basin), and the Llanos Basin. We find several critical elements in the long-lived stratigraphic record of Colombia. These include: (i) stratigraphic correlations and deposystems, (ii) sediment accumulation histories, and (iii) sediment provenance. These three elements are represented by observational and laboratory-generated data that are similarly retrievable from many sedimentary basins in tectonically active regions.

A Mesozoic – Cenozoic history of marine and nonmarine sedimentation affected the Eastern Cordillera and flanking Magdalena Valley Basin and Llanos Basin during contrasting tectonic regimes. (i) Jurassic to earliest Cretaceous extension led to the development and linkage of extensional sub-basins (commonly half graben features governed by normal faults) in selected regions. (ii) A subsequent phase of postextensional thermal subsidence generated a thermal sag basin across a broader region. (iii) In latest Cretaceous to Paleocene time, initial crustal shortening in the Central Cordillera created a regional flexural basin that was successively broken by the Paleocene – Oligocene emergence of thrust/reverse-fault related uplifts within the Eastern Cordillera and the partitioning of the

original regional basin into the Magdalena hinterland basin and Llanos foreland basin. (iv) Major Neogene uplift and establishment of an effective topographic barrier occurred as continued shortening (commonly involved contractional reactivation of preexisting normal faults) became focused along the bivergent eastern and western flanks of the fold–thrust belt comprising the Eastern Cordillera. Fundamentally, (i) regional stratigraphic correlations, (ii) sediment accumulation histories, (iii) sediment provenance data, and (iv) supporting thermochronometric data help identify shared and divergent stratigraphic histories during progressive basin compartmentalization, changes in sediment source regions, and the evolution of paleodrainage patterns during changing tectonic regimes.

Acknowledgments

This research was supported by a collaborative research agreement between Ecopetrol's, Instituto Colombiano del Petróleo (ICP), and the University of Texas at Austin, within the framework of ICP project “Cronología de la deformación en las cuencas subandinas”. Additional support was provided by U.S. National Science Foundation grants EAR–1019857 and EAR–1338694, and FAPESP (São Paulo Research Foundation) grant 2013/03265–5. We thank Cristian VALLEJO and the editorial board for helpful comments that improved the presentation.

References

- Acosta, J., Velandia, F., Osorio, J., Lonergan, L. & Mora, H. 2007. Strike–slip deformation within the Colombian Andes. In: Ries, A.C., Butler, R.W.H. & Graham, R.H. (editors), *Deformation of the continental crust: The legacy of Mike Coward*. Geological Society of London, Special Publication 272, p. 303–319. <https://doi.org/10.1144/GSL.SP.2007.272.01.16>
- Aleman, A. & Ramos, V.A. 2000. Northern Andes. In: Cordani, U.G., Milani, E.J., Thomaz–Filho, A. & Campos, D.A. (editors), *Tectonic evolution of South America*. 31st International Geological Congress. Proceedings, p. 453–480. Rio de Janeiro, Brazil.
- Almendral, A., Robles, W., Parra, M., Mora, A., Ketcham, R.A. & Raghib, M. 2015. FetKin: Coupling kinematic restorations and temperature to predict thrusting, exhumation histories, and thermochronometric ages. *American Association of Petroleum Geologists Bulletin*, 99(8): 1557–1573. <https://doi.org/10.1306/07071411112>
- Anderson, V.J., Saylor, J.E., Shanahan, T.M. & Horton, B.K. 2015. Paleoelevation records from lipid biomarkers: Application to the tropical Andes. *Geological Society of America Bulletin*, 127(11–12): 1604–1616. <https://doi.org/10.1130/B31105.1>
- Anderson, V.J., Horton, B.K., Saylor, J.E., Mora, A., Tesón, E., Breecker, D.O. & Ketcham, R.A. 2016. Andean topographic growth and basement uplift in southern Colombia: Implications for the evolution of the Magdalena, Orinoco, and Amazon River systems. *Geosphere*, 12(4): 1235–1256. <https://doi.org/10.1130/GES01294.1>
- Aspden, J.A. & McCourt, W.J. 1986. Mesozoic oceanic terrane in the central Andes of Colombia. *Geology*, 14(5): 415–418. [https://doi.org/10.1130/0091-7613\(1986\)14<415:MOTITC>2.0.CO;2](https://doi.org/10.1130/0091-7613(1986)14<415:MOTITC>2.0.CO;2)
- Aspden, J.A., McCourt, W.J. & Brook, M. 1987. Geometrical control of subduction–related magmatism: The Mesozoic and Cenozoic plutonic history of western Colombia. *Journal of the Geological Society*, 144(6): 893–905. <https://doi.org/10.1144/gsjgs.144.6.0893>
- Baby, P., Rivadeneira, M. & Barragán, R. (editors). 2004. *La cuenca oriente: Geología y petróleo*. Travaux de le Institut Français d'Études Andines, 144, 295 p. <https://doi.org/10.4000/books.ifea.2971>
- Bande, A., Horton, B.K., Ramírez, J.C., Mora, A., Parra, M. & Stockli, D.F. 2012. Clastic deposition, provenance, and sequence of Andean thrusting in the frontal Eastern Cordillera and Llanos foreland basin of Colombia. *Geological Society of America Bulletin*, 124(1–2): 59–76. <https://doi.org/10.1130/B30412.1>
- Bayona, G., Cortés, M., Jaramillo, C., Ojeda, G., Aristizábal, J.J. & Reyes–Harker, A. 2008. An integrated analysis of an orogen–sedimentary basin pair: Latest Cretaceous – Cenozoic evolution of the linked Eastern Cordillera Orogen and the Llanos foreland basin of Colombia. *Geological Society of America Bulletin*, 120(9–10): 1171–1197. <https://doi.org/10.1130/B26187.1>
- Bayona, G., Montenegro–Castillo, O.C., Cardona–Molina, A., Jaramillo, C., Lamus, F., Morón, S.E., Quiroz, L., Ruiz, M.C., Valencia, V., Parra, M. & Stockli, D.F. 2010. Estratigrafía, procedencia, subsidencia y exhumación de las unidades paleógenas en el Sinclinal de Usme, sur de la zona axial de la cordillera Oriental. *Geología Colombiana*, 35: 5–35.
- Bayona, G., Cardona, A., Jaramillo, C., Mora, A., Montes, C., Valencia, V., Ayala, C., Montenegro, O. & Ibañez–Mejía, M. 2012. Early Paleogene magmatism in the northern Andes: Insights on the effects of oceanic plateau–continent convergence. *Earth and Planetary Science Letters*, 331–332: 97–111. <https://doi.org/10.1016/j.epsl.2012.03.015>
- Bayona, G., Cardona, A., Jaramillo, C., Mora, A., Montes, C., Caballero, V., Mahecha, H., Lamus, F., Montenegro, O., Jiménez, G., Mesa, A. & Valencia, V. 2013. Onset of fault reactivation in the Eastern Cordillera of Colombia and proximal Llanos Basin; Response to Caribbean–South American convergence in early Palaeogene time. In: Nemčok, M., Mora, A. & Cosgrove, J.W. (editors), *Thick–skin–dominated orogens: From initial inversion to full accretion*. Geological Society of London, Special Publication 377, p. 285–314. <https://doi.org/10.1144/SP377.5>
- Branquet, Y., Cheilletz, A., Cobbold, P.R., Baby, P., Laumonier, B. & Giuliani, G. 2002. Andean deformation and rift inversion, eastern edge of cordillera Oriental (Guateque–Medina area), Colombia. *Journal of South American Earth Sciences*, 15(4): 391–407. [https://doi.org/10.1016/S0895-9811\(02\)00063-9](https://doi.org/10.1016/S0895-9811(02)00063-9)

- Bürgl, H. 1961. Sedimentación cíclica en el geosinclinal cretáceo de la cordillera Oriental de Colombia. Servicio Geológico Nacional, Internal report 1347, 60 p. Bogotá.
- Bürgl, H. 1967. The orogenesis in the Andean system of Colombia. *Tectonophysics*, 4(4–6): 429–443. [https://doi.org/10.1016/0040-1951\(67\)90009-1](https://doi.org/10.1016/0040-1951(67)90009-1)
- Caballero, V., Parra, M. & Mora–Hohórquez, A.R. 2010. Levantamiento de la cordillera Oriental de Colombia durante el Eoceno tardío–Oligoceno temprano: Proveniencia sedimentaria en el Sinclinal de Nuevo Mundo, Cuenca Valle Medio del Magdalena. *Boletín de Geología*, 32(1): 45–77.
- Caballero, V., Mora, A., Quintero, I., Blanco, V., Parra, M., Rojas, L.E., López, C., Sánchez, N., Horton, B.K., Stockli, D. & Duddy, I. 2013a. Tectonic controls on sedimentation in an intermontane hinterland basin adjacent to inversion structures: The Nuevo Mundo Syncline, Middle Magdalena Valley, Colombia. In: Nemčok, M., Mora, A. & Cosgrove, J.W. (editors), *Thick-skin-dominated orogens: From initial inversion to full accretion*. Geological Society of London, Special Publication 377, p. 315–342. <https://doi.org/10.1144/SP377.12>
- Caballero, V., Parra, M., Mora, A., López, C., Rojas, L.E. & Quintero, I. 2013b. Factors controlling selective abandonment and reactivation in thick-skin orogens: A case study in the Magdalena Valley, Colombia. In: Nemčok, M., Mora, A. & Cosgrove, J.W. (editors), *Thick-skin-dominated orogens: From initial inversion to full accretion*. Geological Society of London, Special Publication 377, p. 343–367. <https://doi.org/10.1144/SP377.4>
- Cardona, A., Chew, D., Valencia, V.A., Bayona, G., Mišković, A. & Ibañez–Mejía, M. 2010. Grenvillian remnants in the northern Andes: Rodinian and Phanerozoic paleogeographic perspectives. *Journal of South American Earth Sciences*, 29(1): 92–104. <https://doi.org/10.1016/j.jsames.2009.07.011>
- Casero, P., Salel, J.F. & Rossato, A. 1997. Multidisciplinary correlative evidences for polyphase geological evolution of the foot-hills of the cordillera Oriental (Colombia). VI Simposio Bolivariano Exploración Petrolera en las Cuencas Subandinas. *Memorias*, 1: 100–118. Cartagena.
- Cazier, E.C., Hayward, A.B., Espinosa, G., Velandia, J., Mugniot, J.F. & Leel Jr., W.G. 1995. Petroleum geology of the Cusiana Field, Llanos Basin Foothills, Colombia. *American Association of Petroleum Geologists Bulletin*, 79(10): 1444–1462. <https://doi.org/10.1306/7834D9FE-1721-11D7-8645000102C1865D>
- Cediel, F., Shaw, R.P. & Cáceres, C. 2003. Tectonic assembly of the northern Andean Block. In: Bartolini, C., Buffler, R.T. & Blickwede, J. (editors), *The circum-Gulf of Mexico and the Caribbean: Hydrocarbon habitats, basin formation, and plate tectonics*. American Association of Petroleum Geologists, Memoir 79, p. 815–848. Tulsa, USA.
- Colletta, B., Hebrard, F., Letouzey, J., Werner, P. & Rudkiewicz, J.L. 1990. Tectonic style and crustal structure of the Eastern Cordillera (Colombia), from a balanced cross section. In: Letouzey, J. (editor), *Petroleum and tectonics in mobile belts*. Editions Technip, p. 81–100. Paris.
- Cooper, M.A., Addison, F.T., Álvarez, R., Coral, M., Graham, R.H., Hayward, A.B., Howe, S., Martínez, J., Naar, J., Peñas, R., Pulham, A.J. & Taborda, A. 1995. Basin development and tectonic history of the Llanos Basin, Eastern Cordillera, and Middle Magdalena Valley, Colombia. *American Association of Petroleum Geologists Bulletin*, 79(10): 1421–1442.
- Cordani, U.G., Cardona, A., Jiménez, D.M., Liu, D. & Nutman, A.P. 2005. Geochronology of Proterozoic basement inliers in the Colombian Andes: Tectonic history of remnants of a fragmented Grenville belt. In: Vaughan, A.P.M., Leat, P.T. & Pankhurst, R.J. (editors), *Terrane processes at the margins of Gondwana*. Geological Society of London, Special Publication 246, p. 329–346. London. <https://doi.org/10.1144/GSL.SP.2005.246.01.13>
- Corredor, F. 2003. Eastward extent of the late Eocene – early Oligocene onset of deformation across the northern Andes: Constraints from the northern portion of the Eastern Cordillera fold belt, Colombia. *Journal of South American Earth Sciences*, 16(6): 445–457. <https://doi.org/10.1016/j.jsames.2003.06.002>
- Cortés, M., Colletta, B. & Angelier, J. 2006. Structure and tectonics of the central segment of the Eastern Cordillera of Colombia. *Journal of South American Earth Sciences*, 21(4): 437–465. <https://doi.org/10.1016/j.jsames.2006.07.004>
- DeMets, C., Gordon, R.G. & Argus, D.F. 2010. Geologically current plate motions. *Geophysical Journal International*, 181(1): 1–80. <https://doi.org/10.1111/j.1365-246X.2009.04491.x>
- Dengo, C. & Covey, M. 1993. Structure of the Eastern Cordillera of Colombia: Implications for trap styles and regional tectonics. *American Association of Petroleum Geologists Bulletin*, 77(8): 1315–1337. <https://doi.org/10.1306/BDFF8E7A-1718-11D7-8645000102C1865D>
- Etayo–Serna, F. & Laverde–Montaño, F., editors. 1985. *Proyecto Cretácico: Contribuciones. Publicaciones Geológicas Especiales del Ingeominas 16, I-1–XXX-1*. Bogotá.
- Etayo–Serna, F., Barrero, D., Lozano, H., Espinosa, A., González, H., Orrego, A., Ballesteros, I., Forero, H., Ramírez, C., Zambrano–Ortiz, F., Duque–Caro, H., Vargas, R., Núñez, A., Álvarez, J., Ropaín, C., Cardozo, E., Galvis, N., Sarmiento, L., Alberts, J.P., Case, J.E., Singer, D.A., Bowen, R.W., Berger, B.R., Cox, D.P. & Hodges, C.A. 1983. *Mapa de terrenos geológicos de Colombia*. Publicaciones Geológicas Especiales del Ingeominas, 14(I), 235 p. Bogotá.
- Forero, A. 1990. The basement of the Eastern Cordillera, Colombia: An allochthonous terrane in northwestern South America. *Journal of South American Earth Sciences*, 3(2–3): 141–151. [https://doi.org/10.1016/0895-9811\(90\)90026-W](https://doi.org/10.1016/0895-9811(90)90026-W)
- Gómez, E., Jordan, T.E., Allmendinger, R.W., Hegarty, K., Kelly, S. & Heizler, M. 2003. Controls on architecture of the Late Cretaceous to Cenozoic southern Middle Magdalena Valley Basin, Colombia. *Geological Society of America Bulletin*, 115(2): 203–214.

- 131–147. [https://doi.org/10.1130/0016-7606\(2003\)115<0131:COAOTL>2.0.CO;2](https://doi.org/10.1130/0016-7606(2003)115<0131:COAOTL>2.0.CO;2)
- Gómez, E., Jordan, T.E., Allmendinger, R.W. & Cardozo, N. 2005a. Development of the Colombian foreland–basin system as a consequence of diachronous exhumation of the northern Andes. *Geological Society of America Bulletin*, 117(9–10): 1272–1292. <https://doi.org/10.1130/B25456.1>
- Gómez, E., Jordan, T.E., Allmendinger, R.W., Hegarty, K. & Kelley, S. 2005b. Syntectonic Cenozoic sedimentation in the northern Middle Magdalena Valley Basin of Colombia and implications for exhumation of the northern Andes. *Geological Society of America Bulletin*, 117(5–6): 547–569. <https://doi.org/10.1130/B25454.1>
- Gómez, J., Montes, N.E., Nivia, Á. & Diederix, H., compilers. 2015. Geological Map of Colombia 2015. Scale 1:1 000 000. Servicio Geológico Colombiano, 2 sheets. Bogotá. <https://doi.org/10.32685/10.143.2015.936>
- Gómez, J., Nivia, Á., Montes, N.E., Diederix, H., Almanza, M.F., Alcárcel, F.A. & Madrid, C.A. 2015b. Explanatory notes: Geological Map of Colombia. In: Gómez, J. & Almanza, M.F. (editors), *Compilando la geología de Colombia: Una visión a 2015*. Servicio Geológico Colombiano, Publicaciones Geológicas Especiales 33, p. 35–60. Bogotá.
- Gómez, J., Montes, N.E., Alcárcel, F.A. & Ceballos, J.A. 2015c. Catálogo de dataciones radiométricas de Colombia en ArcGIS y Google Earth. In: Gómez, J. & Almanza, M.F. (editors), *Compilando la geología de Colombia: Una visión a 2015*. Servicio Geológico Colombiano, Publicaciones Geológicas Especiales 33, p. 63–419. Bogotá.
- Gómez, J., Montes–Ramírez, N.E., Almanza–Meléndez, M.F., Alcárcel–Gutiérrez, F.A., Madrid–Montoya, C.A. & Diederix, H. 2017. Geological Map of Colombia 2015. Episodes, 40(3): 201–212. <https://doi.org/10.18814/epiiugs/2017/v40i3/017023>
- Guerrero, J. 1997. Stratigraphy, sedimentary environments, and the Miocene uplift of the Colombian Andes. In: Kay, R.F., Madden, R.H., Cifelli, R.L. & Flynn, J.J. (editors), *Vertebrate paleontology in the Neotropics: The Miocene fauna of La Venta, Colombia*. Smithsonian Institution Press, p. 15–43. Washington, D.C.
- Hoorn, C., Wesselingh, F.P., ter Steege, H., Bermúdez, M.A., Mora, A., Sevink, J., Sanmartín, I., Sánchez–Meseguer, A., Anderson, C.L., Figueiredo, J.P., Jaramillo, C., Riff, D., Negri, F.R., Hooghiemstra, H., Lundberg, J., Stadler, T., Sarkinen, T. & Antonelli, A. 2010. Amazonia through time: Andean uplift, climate change, landscape evolution, and biodiversity. *Science*, 330(6006): 927–931. <https://doi.org/10.1126/science.1194585>
- Hoorn, C., Bogotá–A, G.R., Romero–Baez, M., Lammertsma, E., Flantua, S.G.A., Dantas, E.L., Dino, R., do Carmo, D.A. & Chemale, F. 2017. The Amazon at sea: Onset and stages of the Amazon River from a marine record, with special reference to Neogene plant turnover in the drainage basin. *Global and Planetary Change*, 153: 51–65. <https://doi.org/10.1016/j.gloplacha.2017.02.005>
- Horton, B.K. 2012. Cenozoic evolution of hinterland basins in the Andes and Tibet. In: Busby, C. & Azor, A. (editors), *Tectonics of sedimentary basins: Recent advances*. Wiley–Blackwell, p. 427–444. Oxford, UK.
- Horton, B.K. 2018a. Sedimentary record of Andean mountain building. *Earth–Science Reviews*, 178: 279–309. <https://doi.org/10.1016/j.earscirev.2017.11.025>
- Horton, B.K. 2018b. Tectonic regimes of the central and southern Andes: Responses to variations in plate coupling during subduction. *Tectonics*, 37(2): 402–429. <https://doi.org/10.1002/2017TC004624>
- Horton, B.K. & Fuentes, F. 2016. Sedimentary record of plate coupling and decoupling during growth of the Andes. *Geology*, 44(8): 647–650. <https://doi.org/10.1130/G37918.1>
- Horton, B.K., Parra, M., Saylor, J.E., Nie, J., Mora, A., Torres, V., Stockli, D.F. & Strecker, M.R. 2010a. Resolving uplift of the northern Andes using detrital zircon age signatures. *GSA Today*, 20(7): 4–10. <https://doi.org/10.1130/GSATG76A.1>
- Horton, B.K., Saylor, J.E., Nie, J., Mora, A., Parra, M., Reyes–Harker, A. & Stockli, D.F. 2010b. Linking sedimentation in the northern Andes to basement configuration, Mesozoic extension, and Cenozoic shortening: Evidence from detrital zircon U–Pb ages, Eastern Cordillera, Colombia. *Geological Society of America Bulletin*, 122(9–10): 1423–1442. <https://doi.org/10.1130/B30118.1>
- Horton, B.K., Anderson, V.J., Caballero, V., Saylor, J.E., Nie, J., Parra, M. & Mora, A. 2015. Application of detrital zircon U–Pb geochronology to surface and subsurface correlations of provenance, paleodrainage, and tectonics of the Middle Magdalena Valley Basin of Colombia. *Geosphere*, 11(6): 1790–1811. <https://doi.org/10.1130/GES01251.1>
- Ibañez–Mejía, M., Ruiz, J., Valencia, V.A., Cardona, A., Gehrels, G.E. & Mora, A. 2011. The Putumayo Orogen of Amazonia and its implications for Rodinia reconstructions: New U–Pb geochronological insights into the Proterozoic tectonic evolution of northwestern South America. *Precambrian Research*, 191(1–2): 58–77. <https://doi.org/10.1016/j.precamres.2011.09.005>
- Jaramillo, C., Rueda, M., Bayona, G., Santos, C., Flórez, P. & Parra, F. 2009. Biostratigraphy breaking paradigms: Dating the Mirador Formation in the Llanos Basin of Colombia. In: Demchuk, T.D. & Gary, A.C. (editors), *Geologic problem solving with microfossils: A volume in honor of Garry D. Jones*. Society for Sedimentary Geology, Special Publication 93, p. 29–40. <https://doi.org/10.2110/sepmsp.093.029>
- Jaramillo, C., Rueda, M. & Torres, V. 2011. A palynological zonation for the Cenozoic of the Llanos and Llanos Foothills of Colombia. *Palynology*, 35(1): 46–84. <https://doi.org/10.1080/01916122.2010.515069>
- Julivert, M. 1963. Los rasgos tectónicos de la región de la Sabana de Bogotá y los mecanismos de formación de las estructuras. *Boletín de Geología*, (13–14): 5–102.

- Julivert, M. 1970. Cover and basement tectonics in the cordillera Oriental of Colombia, South America, and a comparison with some other folded chains. *Geological Society of America Bulletin*, 81(12): 3623–3646. [https://doi.org/10.1130/0016-7606\(1970\)81\[3623:CABTIT\]2.0.CO;2](https://doi.org/10.1130/0016-7606(1970)81[3623:CABTIT]2.0.CO;2)
- Kammer, A. & Sánchez, J. 2006. Early Jurassic rift structures associated with the Soapaga and Boyacá Faults of the Eastern Cordillera, Colombia: Sedimentological inferences and regional implications. *Journal of South American Earth Sciences*, 21(4): 412–422. <https://doi.org/10.1016/j.jsames.2006.07.006>
- Ketcham, R.A. 2005. Forward and inverse modeling of low-temperature thermochronometry data. *Reviews in Mineralogy and Geochemistry*, 58(1): 275–314. <https://doi.org/10.2138/rmg.2005.58.11>
- Londono, J., Lorenzo, J.M. & Ramírez, V. 2012. Lithospheric flexure and related base-level stratigraphic cycles in continental foreland basins: An example from the Putumayo Basin, northern Andes. In: Gao, D. (editor), *Tectonics and sedimentation: Implications for petroleum systems*. American Association of Petroleum Geologists, Memoir 100, p. 357–375. <https://doi.org/10.1306/13351561M100357>
- Lonsdale, P. 2005. Creation of the Cocos and Nazca Plates by fission of the Farallon Plate. *Tectonophysics*, 404(3–4): 237–264. <https://doi.org/10.1016/j.tecto.2005.05.011>
- McCourt, W.J., Aspdén, J.A. & Brook, M. 1984. New geological and geochronological data from the Colombian Andes: Continental growth by multiple accretion. *Journal of the Geological Society*, 141(5): 831–845. <https://doi.org/10.1144/gsjgs.141.5.0831>
- Montes, C., Bayona, G., Cardona, A., Buchs, D.M., Silva, C.A., Morón, S., Hoyos, N., Ramírez, D.A., Jaramillo, C. & Valencia, V. 2012. Arc-continent collision and orocline formation: Closing of the Central American Seaway. *Journal of Geophysical Research: Solid Earth*, 117(B4), 25 p. <https://doi.org/10.1029/2011JB008959>
- Mora, A. 2015. Petroleum systems of the Eastern Cordillera, foothill basins, and associated Llanos Basin: Impacts on the prediction of large scale foreland and foothill petroleum accumulations. *American Association of Petroleum Geologists Bulletin*, 99(8): 1401–1406. <https://doi.org/10.1306/blmintro032615>
- Mora, A., Parra, M., Strecker, M.R., Kammer, A., Dimaté, C. & Rodríguez, F. 2006. Cenozoic contractional reactivation of Mesozoic extensional structures in the Eastern Cordillera of Colombia. *Tectonics*, 25(2): 19 p. <https://doi.org/10.1029/2005TC001854>
- Mora, A., Parra, M., Strecker, M.R., Sobel, E.R., Hooghiemstra, H., Torres, V. & Vallejo-Jaramillo, J. 2008. Climatic forcing of asymmetric orogenic evolution in the Eastern Cordillera of Colombia. *Geological Society of America Bulletin*, 120(7–8): 930–949. <https://doi.org/10.1130/B26186.1>
- Mora, A., Gaona, T., Kley, J., Montoya, D., Parra, M., Quiroz, L.I., Reyes, G. & Strecker, M.R. 2009. The role of inherited extensional fault segmentation and linkage in contractional orogenesis: A reconstruction of Lower Cretaceous inverted rift basins in the Eastern Cordillera of Colombia. *Basin Research*, 21(1): 111–137. <https://doi.org/10.1111/j.1365-2117.2008.00367.x>
- Mora, A., Baby, P., Roddaz, M., Parra, M., Brusset, S., Hermoza, W. & Espurt, N. 2010a. Tectonic history of the Andes and sub-Andean zones: Implications for the development of the Amazon drainage basin. In: Hoorn, C. & Wesselingh, F.P. (editors), *Amazonia: Landscape and species evolution: A look into the past*. Wiley-Blackwell, John Wiley & Sons Ltd., Publication, p. 38–60. Chichester, UK. <https://doi.org/10.1002/9781444306408.ch4>
- Mora, A., Horton, B.K., Mesa, A., Rubiano, J., Ketcham, R.A., Parra, M., Blanco, V., García, D. & Stockli, D.F. 2010b. Migration of Cenozoic deformation in the Eastern Cordillera of Colombia interpreted from fission track results and structural relationships: Implications for petroleum systems. *American Association of Petroleum Geologists Bulletin*, 94(10): 1543–1580. <https://doi.org/10.1306/01051009111>
- Mora, J.A., Mantilla, M. & de Freitas, M. 2010c. Cretaceous paleogeography and sedimentation in the Upper Magdalena and Putumayo Basins, southwestern Colombia. *American Association of Petroleum Geologists, International Conference and Exhibition*. Abstract, 11 p. Rio de Janeiro, Brazil.
- Mora, A., Reyes-Harker, A., Rodríguez, G., Tesón, E., Ramírez-Arias, J.C., Parra, M., Caballero, V., Mora, J.P., Quintero, I., Valencia, V., Ibañez-Mejía, M., Horton, B.K. & Stockli, D.F. 2013. Inversion tectonics under increasing rates of shortening and sedimentation: Cenozoic example from the Eastern Cordillera of Colombia. In: Nemčok, M., Mora, A. & Cosgrove, J.W. (editors), *Thick-skin-dominated orogens: From initial inversion to full accretion*. Geological Society of London, Special Publication 377, p. 411–442. London. <https://doi.org/10.1144/SP377.6>
- Mora, A., Casallas, W., Ketcham, R.A., Gómez, D., Parra, M., Namson, J., Stockli, D.F., Almendral, A., Robles, W. & Ghorbal, B. 2015. Kinematic restoration of contractional basement structures using thermokinematic models: A key tool for petroleum system modeling. *American Association of Petroleum Geologists Bulletin*, 99(8): 1575–1598. <https://doi.org/10.1306/04281411108>
- Morales, L.G. 1958. General geology and oil occurrences of Middle Magdalena Valley, Colombia. In: Weeks, L.G. (editor), *Habitat of oil*. American Association of Petroleum Geologists, Special Publications SP18, p. 641–695. Tulsa, USA.
- Moreno, C.J., Horton, B.K., Caballero, V., Mora, A., Parra, M. & Sierra, J. 2011. Depositional and provenance record of the Paleogene transition from foreland to hinterland basin evolution during Andean Orogenesis, northern Middle Magdalena Valley Basin, Colombia. *Journal of South American Earth Sciences*, 32(3): 246–263. <https://doi.org/10.1016/j.jsames.2011.03.018>
- Nie, J., Horton, B.K., Mora, A., Saylor, J.E., Housh, T.B., Rubiano, J. & Naranjo, J. 2010. Tracking exhumation of Andean rang-

- es bounding the Middle Magdalena Valley Basin, Colombia. *Geology*, 38(5): 451–454. <https://doi.org/10.1130/G30775.1>
- Nie, J., Horton, B.K., Saylor, J.E., Mora, A., Mange, M., Garziona, C.N., Basu, A., Moreno, C.J., Caballero, V. & Parra, M. 2012. Integrated provenance analysis of a convergent retroarc foreland system: U–Pb ages, heavy minerals, Nd isotopes, and sandstone compositions of the Middle Magdalena Valley Basin, northern Andes, Colombia. *Earth–Science Reviews*, 110(1–4): 111–126. <https://doi.org/10.1016/j.earscirev.2011.11.002>
- Ochoa, D., Hoorn, C., Jaramillo, C., Bayona, G., Parra, M. & De la Parra, F. 2012. The final phase of tropical lowland conditions in the axial zone of the Eastern Cordillera of Colombia: Evidence from three palynological records. *Journal of South American Earth Sciences*, 39: 157–169. <https://doi.org/10.1016/j.jsames.2012.04.010>
- Ordóñez–Carmona, O., Restrepo, J.J. & Pimentel, M.M. 2006. Geochronological and isotopic review of pre–Devonian crustal basement of the Colombian Andes. *Journal of South American Earth Sciences*, 21(4): 372–382. <https://doi.org/10.1016/j.jsames.2006.07.005>
- Parra, M., Mora, A., Jaramillo, C., Strecker, M.R., Sobel, E.R., Quiroz, L., Rueda, M. & Torres, V. 2009a. Orogenic wedge advance in the northern Andes: Evidence from the Oligocene – Miocene sedimentary record of the Medina Basin, Eastern Cordillera, Colombia. *Geological Society of America Bulletin*, 121(5–6): 780–800. <https://doi.org/10.1130/B26257.1>
- Parra, M., Mora, A., Sobel, E.R., Strecker, M.R. & González, R. 2009b. Episodic orogenic front migration in the northern Andes: Constraints from low–temperature thermochronology in the Eastern Cordillera, Colombia. *Tectonics*, 28(4), 27 p. <https://doi.org/10.1029/2008TC002423>
- Parra, M., Mora, A., Jaramillo, C., Torres, V., Zeilinger, G. & Strecker, M.R. 2010. Tectonic controls on Cenozoic foreland basin development in the north–eastern Andes, Colombia. *Basin Research*, 22(6): 874–903. <https://doi.org/10.1111/j.1365-2117.2009.00459.x>
- Parra, M., Mora, A., López, C., Rojas, L.E. & Horton, B.K. 2012. Detecting earliest shortening and deformation advance in thrust belt hinterlands: Example from the Colombian Andes. *Geology*, 40(2): 175–178. <https://doi.org/10.1130/G32519.1>
- Pennington, W.D. 1981. Subduction of the eastern Panama Basin and seismotectonics of northwestern South America. *Journal of Geophysical Research: Solid Earth*, 86(B11): 10753–10770. <https://doi.org/10.1029/JB086iB11p10753>
- Perez, N.D. & Horton, B.K. 2014. Oligocene – Miocene deformational and depositional history of the Andean hinterland basin in the northern Altiplano Plateau, southern Peru. *Tectonics*, 33(9): 1819–1847. <https://doi.org/10.1002/2014TC003647>
- Ramírez–Arias, J.C., Mora, A., Rubiano, J., Duddy, I., Parra, M., Moreno, N., Stockli, D.F. & Casallas, W. 2012. The asymmetric evolution of the Colombian Eastern Cordillera. Tectonic inheritance or climatic forcing? New evidence from thermochronology and sedimentology. *Journal of South American Earth Sciences*, 39: 112–137. <https://doi.org/10.1016/j.jsames.2012.04.008>
- Restrepo–Pace, P.A., Colmenares, F., Higuera, C. & Mayorga, M. 2004. A fold–and–thrust belt along the western flank of the Eastern Cordillera of Colombia–Style, kinematics, and timing constraints derived from seismic data and detailed surface mapping. In: McClay, K.R. (editor), *Thrust tectonics and hydrocarbon systems*. American Association of Petroleum Geologists, Memoir 82, p. 598–613. <https://doi.org/10.1306/M82813C31>
- Reyes–Harker, A., Ruiz–Valdivieso, C.F., Mora, A., Ramírez–Arias, J.C., Rodríguez, G., de la Parra, F., Caballero, V., Parra, M., Moreno, N., Horton, B.K., Saylor, J.E., Silva, A., Valencia, V., Stockli, D. & Blanco, V. 2015. Cenozoic paleogeography of the Andean foreland and retroarc hinterland of Colombia. *American Association of Petroleum Geologists Bulletin*, 99(8): 1407–1453. <https://doi.org/10.1306/06181411110>
- Riba, O. 1976. Syntectonic unconformities of the Alto Cardener, Spanish Pyrenees: A genetic interpretation. *Sedimentary Geology*, 15(3): 213–233. [https://doi.org/10.1016/0037-0738\(76\)90017-8](https://doi.org/10.1016/0037-0738(76)90017-8)
- Roeder, D. & Chamberlain, R.L. 1995. Eastern Cordillera of Colombia: Jurassic – Neogene crustal evolution. In: Tankard, A.J., Suárez–Soruco, R. & Welsink, H.J. (editors), *Petroleum basins of South America*. American Association of Petroleum Geologists, Memoir 62, p. 633–645. Tulsa, USA.
- Ruiz, G.M.H. 2002. Exhumation of the northern sub–Andean zone of Ecuador and its source region: A combined thermochronological and heavy mineral approach. Doctoral thesis, Swiss Federal Institute of Technology Zürich, 260 p. Zürich, Switzerland. <https://doi.org/10.3929/ethz-a-004489528>
- Saeid, E., Bakioglu, K.B., Kellogg, J., Leier, A., Martínez, J.A. & Guerrero, E. 2017. Garzón Massif basement tectonics: Structural control on evolution of petroleum systems in Upper Magdalena and Putumayo Basins, Colombia. *Marine and Petroleum Geology*, 88: 381–401. <https://doi.org/10.1016/j.marpetgeo.2017.08.035>
- Sánchez, J., Horton, B.K., Tesón, E., Mora, A., Ketcham, R.A. & Stockli, D.F. 2012. Kinematic evolution of Andean fold–thrust structures along the boundary between the Eastern Cordillera and Middle Magdalena Valley Basin, Colombia. *Tectonics*, 31(3): 24 p. <https://doi.org/10.1029/2011TC003089>
- Sarmiento–Rojas, L.F., van Wess, J.D. & Cloetingh, S. 2006. Mesozoic transtensional basin history of the Eastern Cordillera, Colombian Andes: Inferences from tectonic models. *Journal of South American Earth Sciences*, 21(4): 383–411. <https://doi.org/10.1016/j.jsames.2006.07.003>
- Saylor, J.E., Horton, B.K., Nie, J., Corredor, J. & Mora, A. 2011. Evaluating foreland basin partitioning in the northern Andes using Cenozoic fill of the Floresta Basin, Eastern Cordillera, Colombia. *Basin Research*, 23(4): 377–402. <https://doi.org/10.1111/j.1365-2117.2010.00493.x>

- Saylor, J.E., Horton, B.K., Stockli, D.F., Mora, A. & Corredor, J. 2012a. Structural and thermochronological evidence for Paleogene basement-involved shortening in the axial Eastern Cordillera, Colombia. *Journal of South American Earth Sciences*, 39: 202–215. <https://doi.org/10.1016/j.jsames.2012.04.009>
- Saylor, J.E., Stockli, D.F., Horton, B.K., Nie, J. & Mora, A. 2012b. Discriminating rapid exhumation from syndepositional volcanism using detrital zircon double dating: Implications for the tectonic history of the Eastern Cordillera, Colombia. *Geological Society of America Bulletin*, 124(5–6): 762–779. <https://doi.org/10.1130/B30534.1>
- Saylor, J.E., Knowles, J.N., Horton, B.K., Nie, J. & Mora, A. 2013. Mixing of source populations recorded in detrital zircon U–Pb age spectra of modern river sands. *The Journal of Geology*, 121(1): 17–33. <https://doi.org/10.1086/668683>
- Silva, A., Mora, A., Caballero, V., Rodríguez, G., Ruiz, C., Moreno, N., Parra, M., Ramírez–Arias, J.C., Ibañez–Mejía, M. & Quintero, I. 2013. Basin compartmentalization and drainage evolution during rift inversion: Evidence from the Eastern Cordillera of Colombia. In: Nemčok, M., Mora, A. & Cosgrove, J.W. (editors), *Thick–skin–dominated orogens: From initial inversion to full accretion*. Geological Society of London, Special Publication 377, p. 369–409. <https://doi.org/10.1144/SP377.15>
- Taboada, A., Rivera, L.A., Fuenzalida, A., Cisternas, A., Philip, H., Bijwaard, H., Olaya, J. & Rivera, C. 2000. Geodynamics of the northern Andes: Subductions and intracontinental deformation (Colombia). *Tectonics*, 19(5): 787–813. <https://doi.org/10.1029/2000TC900004>
- Teixeira, W., Tassinari, C.C.G., Cordani, U.G. & Kawashita, K. 1989. A review of the geochronology of the Amazonian Craton: Tectonic implications. *Precambrian Research*, 42(3–4): 213–227. [https://doi.org/10.1016/0301-9268\(89\)90012-0](https://doi.org/10.1016/0301-9268(89)90012-0)
- Tesón, E., Mora, A., Silva, A., Namson, J., Teixell, A., Castellanos, J., Casallas, W., Julivert, M., Taylor, M., Ibañez–Mejía, M. & Valencia, V. 2013. Relationship of Mesozoic graben development, stress, shortening magnitude, and structural style in the Eastern Cordillera of the Colombian Andes. In: Nemčok, M., Mora, A. & Cosgrove, J.W. (editors), *Thick–skin–dominated orogens: From initial inversion to full accretion*. Geological Society of London, Special Publication 377, p. 257–283. London. <https://doi.org/10.1144/SP377.10>
- Toro J., Roure, F., Bordas–Le Floch, N., Le Cornec–Lance, S. & Sassi, W. 2004. Thermal and kinematic evolution of the Eastern Cordillera fold and thrust belt, Colombia. In: Swennen, R., Roure, F. & Granath, J.W. (editors), *Deformation, fluid flow, and reservoir appraisal in foreland fold and thrust belts*. American Association of Petroleum Geologists, Hedberg Series 1, p. 79–115
- Toussaint, J.F. & Restrepo, J.J. 1994. The Colombian Andes during Cretaceous times. In: Salfity, J.A. (editor), *Cretaceous tectonics of the Andes*. Earth Evolution Sciences. Vieweg + Teubner Verlag, p. 61–100. https://doi.org/10.1007/978-3-322-85472-8_2
- Vallejo, C. 2007. Evolution of the Western Cordillera in the Andes of Ecuador (Late Cretaceous – Paleogene). Doctoral thesis, Swiss Federal Institute of Technology Zürich, 208 p. Zürich, Switzerland.
- Vallejo, C., Tapia, D., Gaibor, J., Steel, R., Cárdenas, M., Winkler, W., Valdéz, A., Esteban, J., Figuera, M., Leal, J. & Cuenca, D. 2017. Geology of the Campanian M1 sandstone oil reservoir of eastern Ecuador: A delta system sourced from the Amazon Craton. *Marine and Petroleum Geology*, 86: 1207–1223. <https://doi.org/10.1016/j.marpetgeo.2017.07.022>
- van der Hilst, R. & Mann, P. 1994. Tectonic implications of tomographic images of subducted lithosphere beneath northwestern South America. *Geology*, 22(5): 451–454. [https://doi.org/10.1130/0091-7613\(1994\)022<0451:TIOTIO>2.3.CO;2](https://doi.org/10.1130/0091-7613(1994)022<0451:TIOTIO>2.3.CO;2)
- Van Houten, F.B. 1976. Late Cenozoic volcanoclastic deposits, Andean foredeep, Colombia. *Geological Society of America Bulletin*, 87(4): 481–495. [https://doi.org/10.1130/0016-7606\(1976\)87<481:LCVDAF>2.0.CO;2](https://doi.org/10.1130/0016-7606(1976)87<481:LCVDAF>2.0.CO;2)
- Van Houten, F.B. & Travis, R.B. 1968. Cenozoic deposits, Upper Magdalena Valley, Colombia. *American Association of Petroleum Geologists Bulletin*, 52(4): 675–702. <https://doi.org/10.1306/5D25C455-16C1-11D7-8645000102C1865D>
- Veloza, G., Styron, R., Taylor, M. & Mora, A. 2012. Open–source archive of active faults for northwest South America. *GSA Today*, 22(10): 4–10. <https://doi.org/10.1130/GSAT-G156A.1>
- Villagómez, D. & Spikings, R. 2013. Thermochronology and tectonics of the Central and Western Cordilleras of Colombia: Early Cretaceous – Tertiary evolution of the northern Andes. *Lithos*, 160–161: 228–249. <https://doi.org/10.1016/j.lithos.2012.12.008>
- Villagómez, D., Spikings, R., Magna, T., Kammer, A., Winkler, W. & Beltrán, A. 2011. Geochronology, geochemistry and tectonic evolution of the Western and Central Cordilleras of Colombia. *Lithos*, 125(3–4): 875–896. <https://doi.org/10.1016/j.lithos.2011.05.003>
- Villamil, T. 1999. Campanian – Miocene tectonostratigraphy, depocenter evolution and basin development of Colombia and western Venezuela. *Palaeogeography, Palaeoclimatology, Palaeoecology*, 153(1–4): 239–275. [https://doi.org/10.1016/S0031-0182\(99\)00075-9](https://doi.org/10.1016/S0031-0182(99)00075-9)
- Wagner, L.S., Jaramillo, J.S., Ramírez–Hoyos, L.F., Monsalve, G., Cardona, A. & Becker, T.W. 2017. Transient slab flattening beneath Colombia. *Geophysical Research Letters*, 44(13): 6616–6623. <https://doi.org/10.1002/2017GL073981>
- Wolaver, B.D., Coogan, J.C., Horton, B.K., Suarez–Bermúdez, L., Sun, A.Y., Wawrzyniec, T.F., Zhang, T., Shanahan, T.M., Dunlap, D.B., Costley, R.A. & de la Rocha, L. 2015. Structural and hydrogeologic evolution of the Putumayo Basin and adjacent fold–thrust belt, Colombia. *American Association of Petroleum Geologists Bulletin*, 99(10): 1893–1927. <https://doi.org/10.1306/05121514186>

Authors' Biographical Notes



Brian K. HORTON is the Alexander Deussen Professor of Energy Resources at The University of Texas at Austin and has a joint appointment with the Department of Geological Sciences and Institute for Geophysics in the Jackson School of Geosciences. He received his BS from the University of New Mexico, MS from Montana State University, and PhD from the University of Arizona. His

research addresses the tectonics of sedimentary basins and the evolution of orogenic systems.











Andrés MORA is the technical leader of onshore Colombia and foothills exploration at Ecopetrol. He received his BS in geology from the Universidad Nacional de Colombia and PhD from the Institut für Geowissenschaften, Universität Potsdam. His research interests include structural geology, petroleum exploration, and petroleum geology.



Mauricio PARRA is an Assistant Professor at the Instituto de Energia e Ambiente of the Universidade de São Paulo, where he leads the Low-Thermochronology Laboratory. He received his BS in geology from the Universidad Nacional de Colombia and his PhD from the Institut für Geowissenschaften, Universität Potsdam. His research focuses on the tectonic evolution of mountain belts using thermochronometry and sedimentary basin analysis.

Late Cretaceous to Cenozoic Uplift of the Northern Andes: Paleogeographic Implications

Andrés MORA¹ , Diego VILLAGÓMEZ² , Mauricio PARRA³ ,
Víctor M. CABALLERO⁴ , Richard SPIKINGS⁵ , Brian K. HORTON⁶ ,
Josué Alejandro MORA-BOHÓRQUEZ⁷ , Richard A. KETCHAM⁸ ,
and Juan Pablo ARIAS-MARTÍNEZ⁹

Abstract In this chapter, we summarize recent work on the geologic evolution of the northern Andes. Our intention is to present current information so that scientists from other disciplines can differentiate data from interpretations. In this effort, we focus on thermochronological data that provide precise places, dates, and rates. Thermochronological data provide cooling histories for rocks of the upper crust, whereas provenance data offer insights on rocks that have been eroded away. In reviewing published data, we provide a critical overview of recent paleogeographic interpretations. Specifically, we discuss hypotheses such as (i) Eocene proto-Magdalena River draining toward the Maracaibo Basin, (ii) the presence of a closed proto-Magdalena basin from the late Eocene to middle Miocene, (iii) the Miocene closure of the Isthmus of Panamá, (iv) the late Cenozoic surface uplift of the Eastern Cordillera, and (v) the Cenozoic eastward advance of the Orinoco River. We conclude that in most cases, favored ideas remain as intriguing hypotheses, but there remains room for alternative interpretations. The present summary is intended to provide a cautionary note on the use of limited datasets to make paleogeographic interpretations of the northern Andes.

Keywords: paleogeography, thermochronology, U–Pb geochronology, sedimentary provenance, rock uplift, surface uplift, paleoelevation, paleodrainages.

Resumen En este capítulo se resumen trabajos recientes relacionados con la evolución geológica de los Andes del norte. La principal intención es presentar información actual para que los científicos de otras disciplinas puedan diferenciar entre datos e interpretaciones. Este trabajo se enfoca en datos termocronológicos que brindan localizaciones, edades y tasas precisas. Los datos termocronológicos proporcionan historias de enfriamiento para las rocas de la corteza superior, mientras que los de procedencia sedimentaria contribuyen con información sobre las rocas que se han erosionado. A partir de la revisión de datos públicos se da una visión crítica de las interpretaciones paleogeográficas publicadas recientemente. Específicamente,

- 1 andresro.mora@ecopetrol.com.br
Ecopetrol, Brasil
Bogotá, Colombia
- 2 diego.villagomez@gmail.com
University of Geneva
Department of Earth Science
Rue des Maraichers 13, CH-1205
Geneva, Switzerland
- 3 mparra@iee.usp.br
Universidade de São Paulo
Instituto de Energia e Ambiente
Av. Professor Luciano Gualberto 1289, Cidade
Universitária, 05508-010
São Paulo, Brasil
- 4 victor.caballero@ecopetrol.com.co
Ecopetrol S.A.
Instituto Colombiano del Petróleo
Centro de Innovación y Tecnología
Km7 vía Bucaramanga–Piedecuesta
Piedecuesta–Santander, Colombia
- 5 richard.spikings@unige.ch
University of Geneva
Department of Earth Sciences and the
Environment
Rue des Maraichers 13, Geneva 1205
Switzerland
- 6 horton@jsg.utexas.edu
University of Texas at Austin
Department of Geological Sciences and
Institute for Geophysics, Jackson School of
Geosciences
Austin, Texas 78712, USA
- 7 alejandro.mora@hocol.com.co
Hocol S.A.
Vicepresidencia de Exploración
Carrera 7 n.º 113-46, piso 16
Bogotá, Colombia
- 8 ketcham@jsg.utexas.edu
The University of Texas at Austin
Jackson School of Geosciences
Austin, Texas 78759
- 9 juanpabloarma@gmail.com
Ecopetrol S.A.
Vicepresidencia de Exploración
Bogotá, Colombia

Citation: Mora, A., Villagómez, D., Parra, M., Caballero, V.M., Spikings, R., Horton, B.K., Mora-Bohórquez, J.A., Ketcham, R.A. & Arias-Martínez, J.P. 2020. Late Cretaceous to Cenozoic uplift of the northern Andes: Paleogeographic implications. In: Gómez, J. & Mateus-Zabala, D. (editors), *The Geology of Colombia, Volume 3 Paleogene – Neogene*. Servicio Geológico Colombiano, Publicaciones Geológicas Especiales 37, p. 89–121. Bogotá. <https://doi.org/10.32685/pub.esp.37.2019.04>

se discuten las siguientes hipótesis: (i) el proto río Magdalena del Eoceno drenando hacia la Cuenca de Maracaibo, (ii) la presencia de una proto cuenca cerrada del Magdalena entre el Eoceno tardío y el Mioceno medio, (iii) el cierre del Istmo de Panamá durante el Mioceno, (iv) el crecimiento topográfico de la cordillera Oriental en el Cenozoico tardío y (v) el avance hacia el este del trazo del río Orinoco durante el Cenozoico. Se concluye que, en la mayoría de los casos, las ideas más sustentadas permanecen como hipótesis interesantes, pero queda espacio para otras interpretaciones. Este trabajo intenta advertir sobre el uso de una cantidad limitada de datos para hacer interpretaciones paleogeográficas de los Andes del norte.

Palabras clave: paleogeografía, termocronología, geocronología U–Pb, procedencia sedimentaria, levantamiento de roca, levantamiento de superficie, paleoelevación, paleodrenajes.

1. Introduction

The northern Andes, which are positioned north of the Huanabamba Deflection at 6° S (Gansser, 1973), differ from other segments of the Andes because of the presence of accreted oceanic material and a transpressional deformation regime during Cenozoic mountain building (Figure 1; Aleman & Ramos, 2000; Mégard, 1989; Taboada et al., 2000; Trenkamp et al., 2002). The evolution of the northern Andes is of interest not only for geologists and tectonicists, but also for other disciplines. For example, biologists rely on the evolution of topography interpreted by geologists to infer linkages between landscape evolution and the distribution of species deduced from phylogenetics (e.g., Bacon et al., 2012). However, hypotheses proposed by geologists are often imprecise because of the poor preservation of stratigraphic and structural records and a lack of high resolution 3D constraints. With the dawn of the XXI century, techniques such as geochronology and low-temperature thermochronology have become more precise and modeling approaches have become more sophisticated, providing higher resolution timing constraints on tectonic events and episodes of exhumational cooling in the upper crust. In recent years, pioneering studies (Figures 2, 3) have highlighted the role of low temperature thermochronology (Mora, 2015; Mora et al 2010a, 2013a, 2013b, 2015a, 2015b; Parra et al., 2009a, 2009b, 2010, 2012; Saylor et al., 2012a; Spikings et al., 2000, 2001; Villagómez et al., 2011a, 2011b) and detrital geochronology (Caballero et al., 2013a, 2013b; Horton et al., 2010a, 2010b, 2015; Nie et al., 2010, 2012; Saylor et al., 2011, 2012b, 2013; Silva et al., 2013) in the Cretaceous to Cenozoic evolution of the northern Andes. Paleoelevation techniques have also become more sophisticated, but their use has been limited in the tropical northern Andes (Anderson et al., 2015) relative to their use in the arid central Andes (Garzzone et al., 2017; Saylor & Horton, 2014).

These developments have prompted a revolution in our understanding of interrelated processes pertaining to *rock uplift*, *surface uplift*, and *exhumation* as defined by England &

Molnar (1990; Figure 3). Unfortunately, in the northern Andes and elsewhere, these terms have been commonly and incorrectly grouped under a broad and vague definition of “uplift”. For example, some classic interpretations of the Eastern Cordillera of Colombia suggest that molasse deposition, deformational cross-cutting relationships, and topographic growth (e.g., Hooghiemstra et al., 2006; van der Hammen et al., 1973) were all manifestations of a single Miocene event that could be grouped under the broad term of “uplift” (Cooper et al., 1995; Dengo & Covey, 1993).

An appreciation of the role of surface processes only arrived well after many studies of orogenesis in the northern Andes were conducted. Whereas studies in the central Andes recognized the interplay of tectonics, erosion, and climate (Horton, 1999; Masek et al., 1994; Montgomery et al., 2001; Sobel et al., 2003; Strecker et al., 2007, 2009), their role in the northern Andes was only recognized when palynological and thermochronological techniques were combined with structural and geomorphic analysis (e.g., Mora et al., 2008).

Understanding and differentiating *rock uplift* from *surface uplift* and *exhumation*, with their attendant implications for landscape evolution and mountain building, was so new to the northern Andes that, in the words of Henry HOOGHIEMSTRA, it gave a “new eye” to numerous scientists from diverse disciplines. These expanded perspectives have positively impacted new generations of geologists, so it is not uncommon for current studies of the northern Andes to integrate paleoelevation studies with exhumation and structural analyses (Cuervo-Gomez et al., 2015).

Although many pioneering studies have applied state-of-the-art techniques, their results have not been compiled or integrated in a critical way. In this review, we provide an updated summary of recent studies with the intention to filter, present, and discuss the evidence of crustal deformation, surface uplift, and exhumation in the northern Andes and their diverse impacts on Cenozoic surface processes. This manuscript is organized in chronological order with each time interval considered from west to east across the northern Andes.

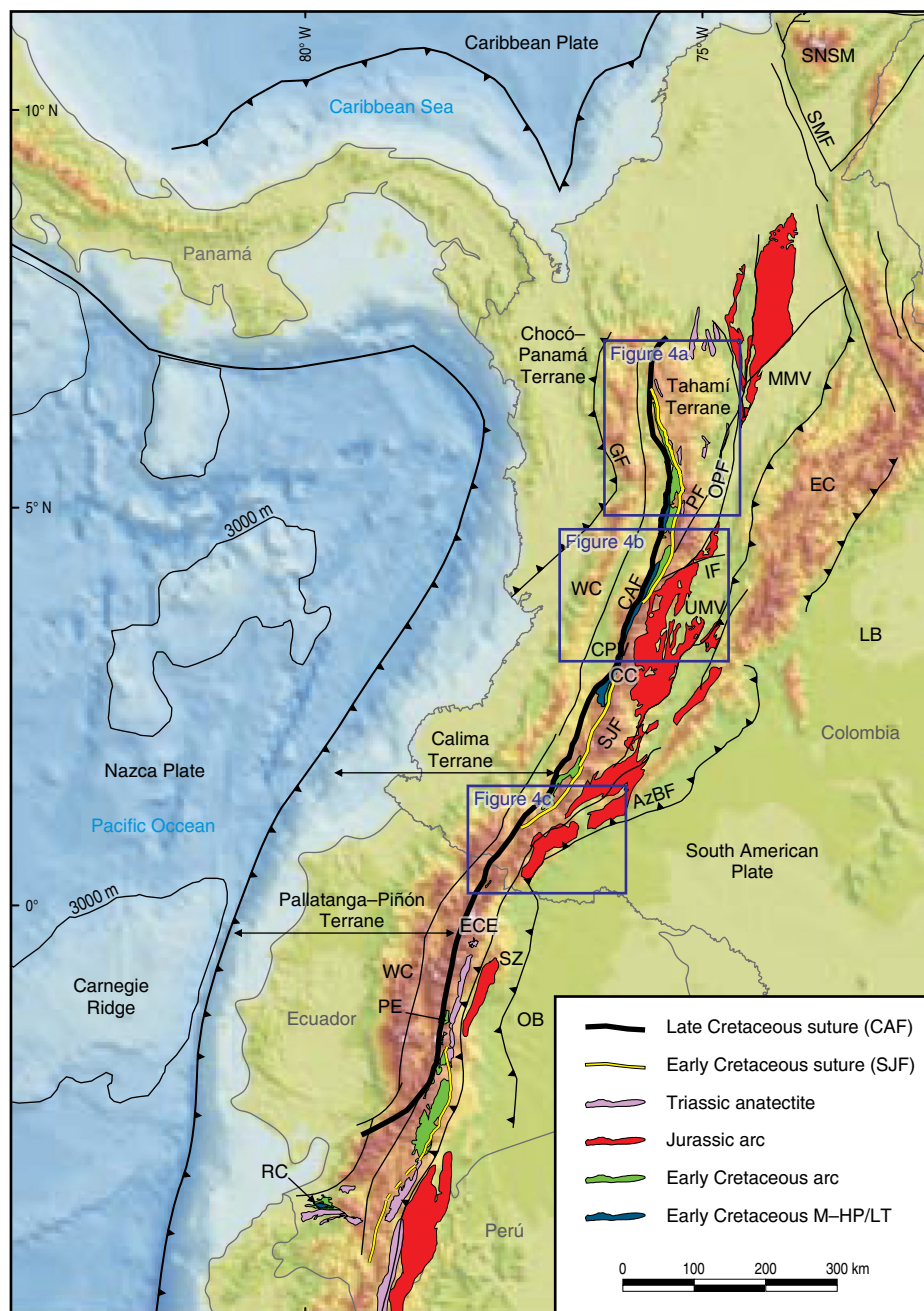


Figure 1. Shaded relief image of northwestern South America and surrounding tectonic plates showing the main cordilleras, faults, and the subducting Carnegie Ridge (background model from Gómez et al., 2007). Cretaceous sutures are shown as thick black and yellow lines, and the three sample regions (a, b, c) by Villagómez & Spikings (2013) in Figure 4 are highlighted. Major rock sequences of the Central Cordillera (Colombia) and Eastern Cordillera (Ecuador) are shown. (SNSM) Sierra Nevada de Santa Marta; (SMF) Santa Marta-Bucaramanga Fault; (GF) Garrapatas Fault; (MMV) Middle Magdalena Valley Basin; (PF) Palestina Fault; (OPF) Otú-Pericos Fault; (WC) Western Cordillera; (CPV) Cauca-Patía valley; (CAF) Cauca-Almaguer Fault; (IF) Ibagué Fault; (UMV) Upper Magdalena Valley Basin; (EC) Eastern Cordillera; (CC) Central Cordillera; (LB) Llanos Basin; (SJF) San-Jeronimo Fault; (AzBF) Amazon Border Fault; (ECE) Eastern Cordillera Ecuador; (WC) Western Cordillera; (SZ) Sub-Andean Zone (Ecuador); (PE) Peltetec Unit; (OB) Oriente Basin; (RC) Raspas Complex. After Villagómez & Spikings (2013).

2. Geological Setting

The northern Andes are the result of complex interactions between the Nazca, Caribbean, and South American Plates. The

northern Andes of Ecuador and Colombia comprise an orogenic system with three N- to NNE-trending mountain chains—the Western, Central, and Eastern Cordilleras, which are separated by prominent topographic depressions (Figures 1, 2). The Cen-

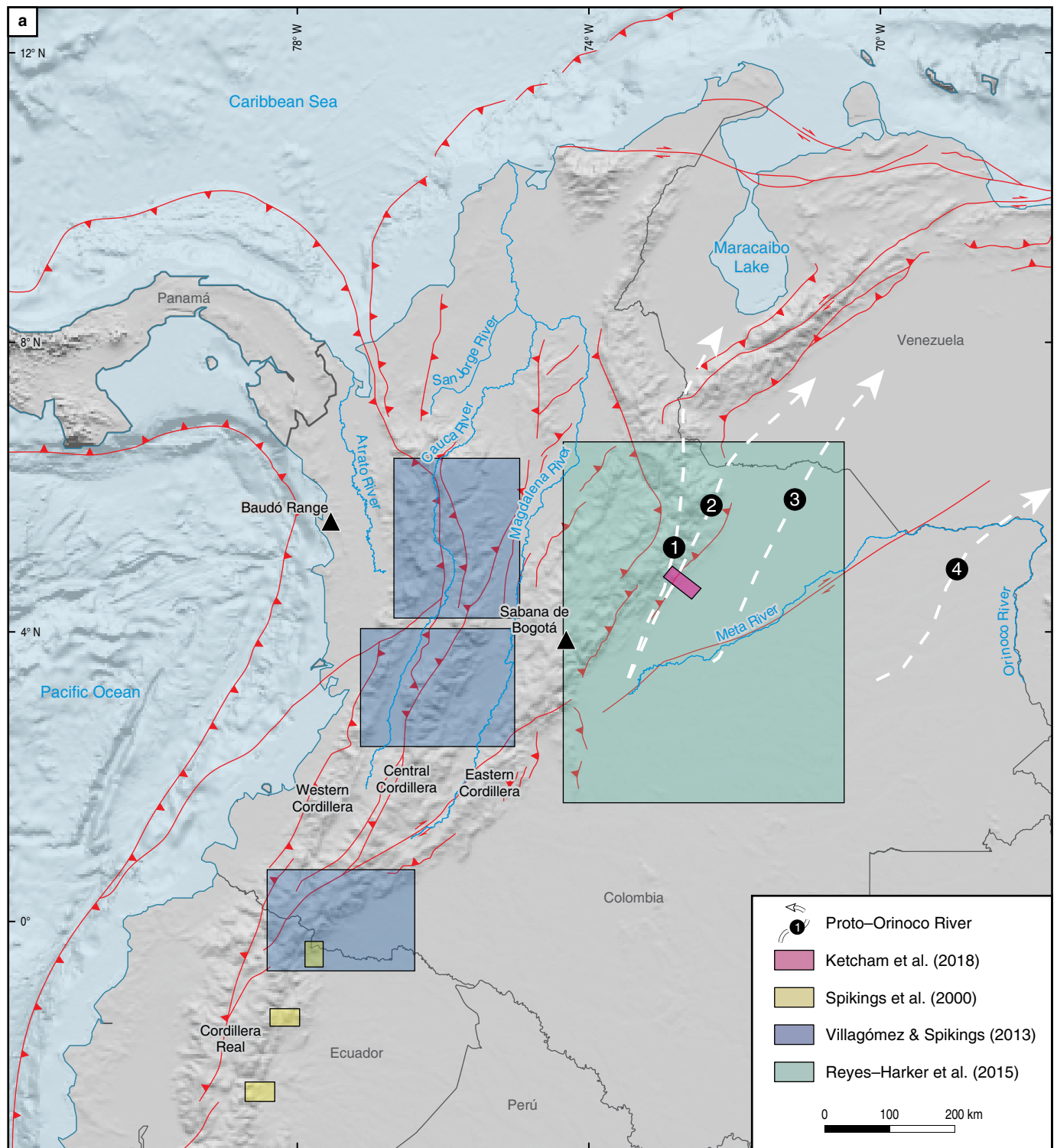


Figure 2. Shaded relief image with the main geographic features (mostly rivers and mountain ranges) discussed in the text as well as the main studies cited. Panels a, b, and c are based on different studies and study areas. White dashed lines with arrows show the inferred locations of the proto-Orinoco River (after Reyes-Harker et al., 2015) at the following times: 1—Paleocene (ca. 60 Ma); 2—middle Eocene (ca. 44 Ma); 3—middle Miocene (ca. 14 Ma); 4—close to recent times.

tral Cordillera of Colombia is referred to as Cordillera Real (or Eastern Cordillera) in Ecuador, whereas the Eastern Cordillera of Colombia has no topographic expression in Ecuador (Figure 2).

The main orogenic phases of the northern Andes have been attributed to Cenozoic changes in plate convergence, the accretion of oceanic terranes (plateaus and island arcs), and the

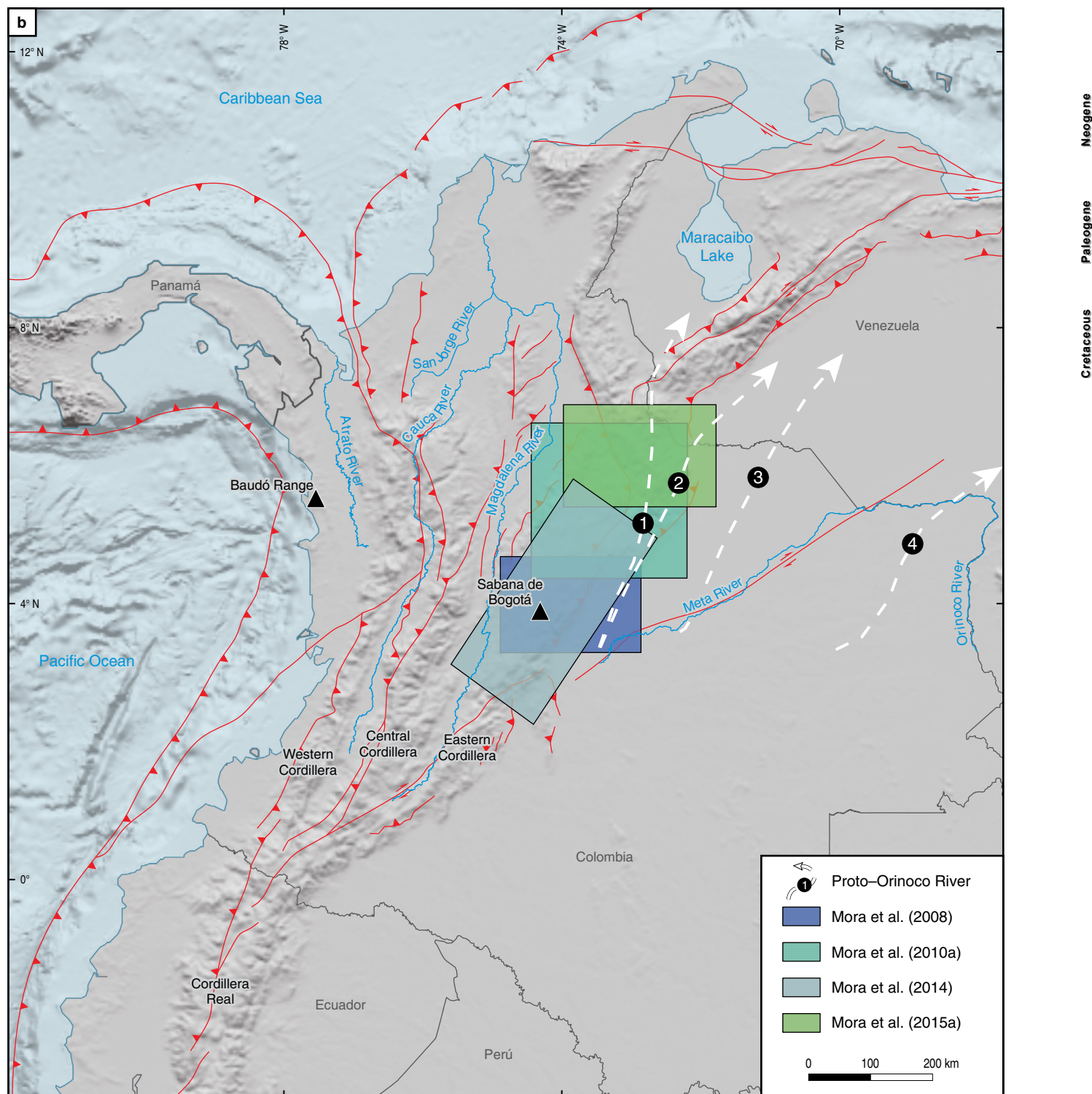


Figure 2. Shaded relief image with the main geographic features (mostly rivers and mountain ranges) discussed in the text as well as the main studies cited. Panels a, b, and c are based on different studies and study areas. White dashed lines with arrows show the inferred locations of the proto-Orinoco River (after Reyes-Harker et al., 2015) at the following times: 1—Paleocene (ca. 60 Ma); 2—middle Eocene (ca. 44 Ma); 3—middle Miocene (ca. 14 Ma); 4—close to recent times (*continued*).

subduction and collision of aseismic ridges. In Colombia, allochthonous oceanic terranes are exposed in the Western Cordillera and forearc region (serranía de Baudó) and have been juxtaposed

against South America along the diffuse, regional-scale Romeral Fault System and its southern continuation toward Ecuador (the Cauca–Almaguer Fault; Figure 1). These allochthonous oceanic

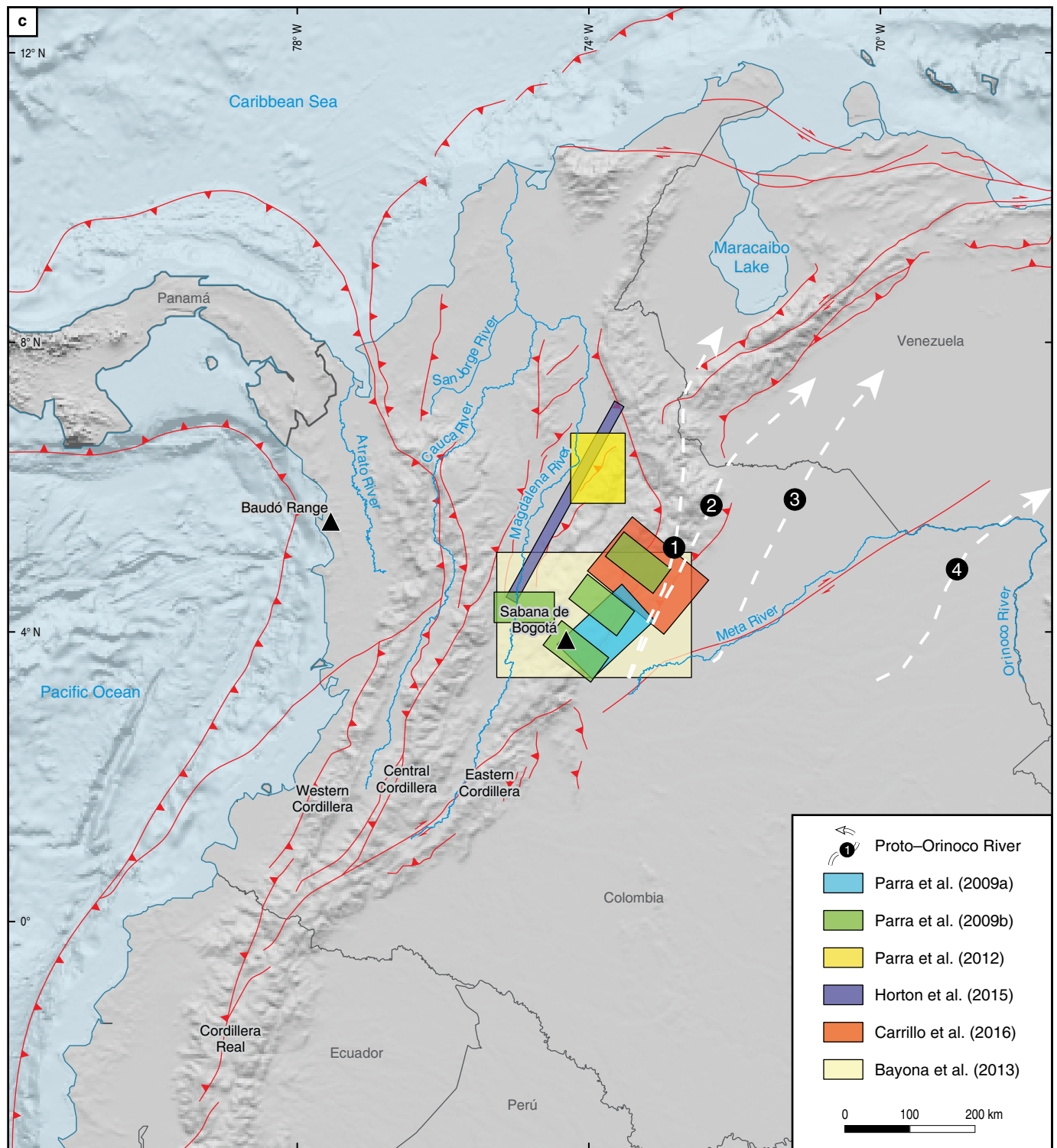


Figure 2. Shaded relief image with the main geographic features (mostly rivers and mountain ranges) discussed in the text as well as the main studies cited. Panels a, b, and c are based on different studies and study areas. White dashed lines with arrows show the inferred locations of the proto-Orinoco River (after Reyes-Harker et al., 2015) at the following times: 1—Paleocene (ca. 60 Ma); 2—middle Eocene (ca. 44 Ma); 3—middle Miocene (ca. 14 Ma); 4—close to recent times (*continued*).

rocks, which are termed the Panamá–Chocó and Calima Terranes, include areas west of the Garrapatas Fault (Figures 1, 2). The terranes correspond to relict slivers of the Caribbean Large

Igneous Province (100–88 Ma; Kerr et al., 1997; Sinton et al., 1998; Villagómez et al., 2011a) accreted to northwestern South America between the latest Cretaceous and middle Miocene.

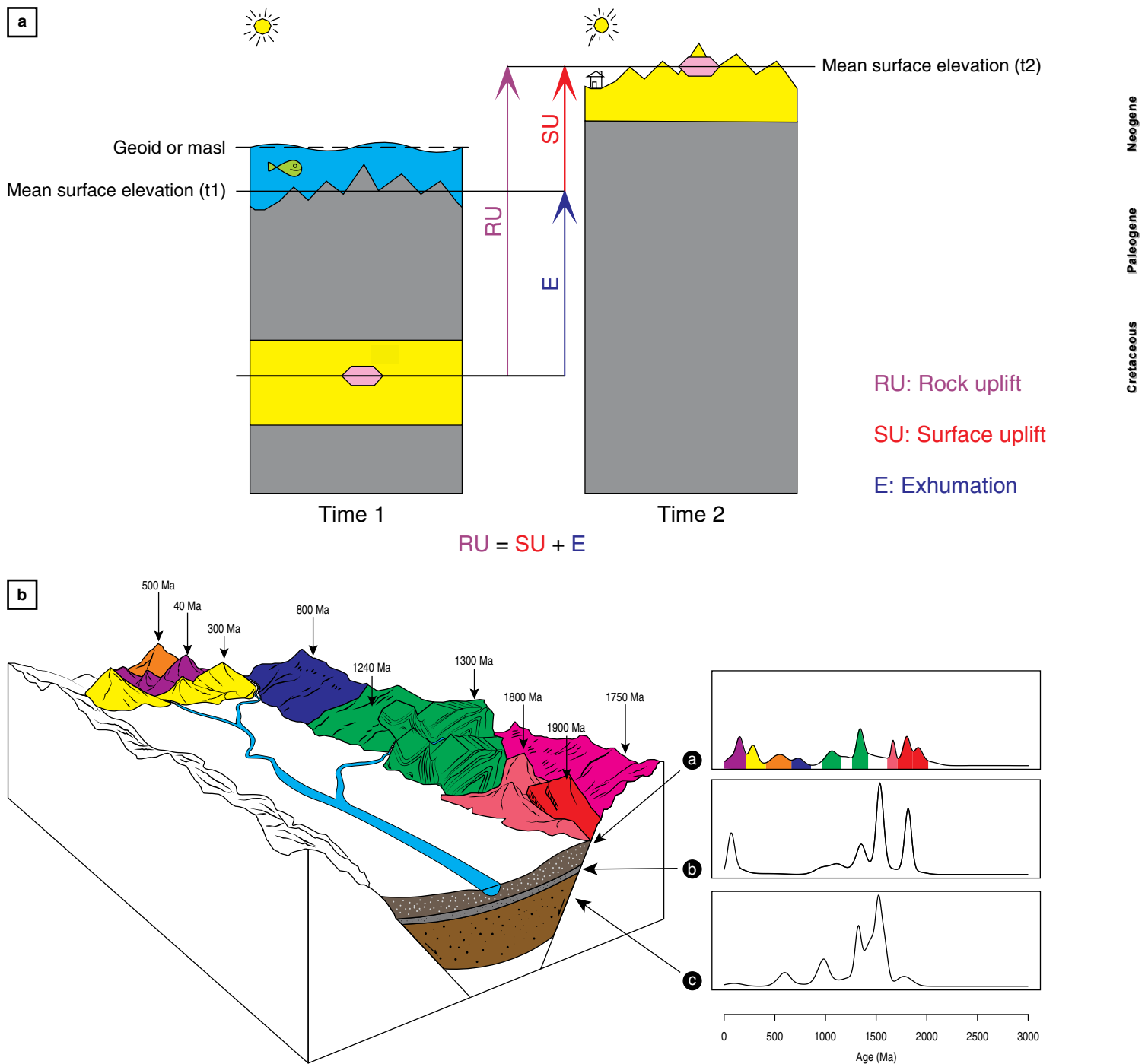


Figure 3. (a) Diagram summarizing definitions of rock uplift, surface uplift, and exhumation. Surface uplift is the displacement of the earth's surface relative to the geoid. Rock uplift is the displacement of rock relative to the geoid and exhumation is the displacement of rock relative to the surface. Rock uplift equals the sum of exhumation plus surface uplift. The diagram shows as an example a two-phase model of progressive cooling in the upper crust that considers the exhumation of an apatite crystal from several kilometers depth to the surface. The process also involved some rock uplift and surface uplift. **(b)** Simplified diagram showing a typical context in which detrital geochronology is applied. In this case, there is a river from which tributaries drain from basement terrains (mountain areas) of different but typical geochronological ages. All age signals are then collected by the main river trunk. When detrital geochronology analyses (e.g., U–Pb) are carried out on active sediments drained by the river, data are typically presented as age versus probability histograms that document different age populations. Different horizons (a, b, and c) can also be sampled in the sedimentary record and show to what extent different basement terrains contributed sediments to the river in geological history. If those basement terrains occupied thousands to even hundreds of thousands of square kilometers in the past and only crop out in specific areas today, one of the challenges is to infer the configuration or headwaters of past drainages. In most cases, geologists do not have enough information to accurately perform such reconstructions.

The Romeral Fault System and Cauca–Almaguer Fault border the Central Cordillera in Colombia (Figure 1) and mark the western limit of the continental lithosphere. The continental basement is traditionally considered to include the Tahamí and Chibcha Terranes (Toussaint & Restrepo, 1989). The Tahamí Terrane forms the core of the Central Cordillera, whereas the Chibcha Terrane forms the basement of the easternmost Central Cordillera, Eastern Cordillera, Santander Massif, and Sierra Nevada de Santa Marta (Figure 1; Martens et al., 2014). This broad continental domain is a complex assemblage of poorly mapped lower Paleozoic ortho- and para-gneisses, which were reheated during Triassic magmatism (e.g., Cochrane et al., 2014; Litherland et al., 1994; Restrepo–Pace et al., 1997). Pre–Jurassic rocks were subsequently intruded by elongated Jurassic granitoids and localized Upper Cretaceous batholiths.

3. Methods Discussed in This Review

In this review we summarize previous research on the northern Andes focused on bedrock low temperature thermochronology and subordinate detrital geochronology. Low temperature thermochronology (Figure 3a) seeks to determine the time at which rocks at depth reached a particular temperature in the upper crust. Apatite fission track (AFT) and zircon fission track (ZFT) techniques (e.g., Ketcham et al., 1999; Wagner & van den Haute, 1992; Reiners et al., 2004) use different mineral species to date the timing when rocks at depth were at temperatures of ca. 140 °C to ca. 50 °C (AFT) and ca. 250 °C (ZFT). Other thermochronological techniques include the use of apatite (U–Th)/He (AHe) and zircon (U–Th)/He (ZHe) for temperatures of ca. 40 °C to ca. 90 °C (AHe) and ca. 100 °C to 190 °C (ZHe) and the use of $^{40}\text{Ar}/^{39}\text{Ar}$ techniques for temperatures of >300 °C.

As an example (Figure 3), a two-phase model of progressive cooling in the upper crust considers the exhumation of an apatite crystal from several kilometers depth to the surface. Because the age when the apatite reached those temperatures can be determined via low temperature thermochronology, the amount of cooling over geological time can be evaluated. Moreover, when assuming a uniform, time-invariant temperature gradient with depth, the original rock overburden and amount of erosional exhumation can be assessed.

While thermochronological data can be simply represented in ages, it is desirable to generate thermal models from those ages that provide cooling histories in the form of time–temperature (T–t) paths that define rock locations through time relative to isotherms (lines of the same temperature in the upper crust). Models and ages obtained through thermochronology can be confidently linked to the exhumation of the precise areas and locations from which samples are taken.

Detrital geochronology is another technique used to evaluate exhumation and the evolution of landscapes and river drain-

ages. It relies on the fact that resilient minerals such as zircons crystallize at very high temperatures (>700 °C) and persist as hard, dense, chemically stable, and often diagnostic signatures of different geological terranes and crustal provinces (e.g., Ibañez–Mejia et al., 2015 and references therein) forming at different temperatures (e.g., Figure 3b). Various basement and sedimentary rocks have diagnostic populations of zircons that can be discriminated on the basis of their contrasting crystallization ages (Figure 3b). For example, the predominantly igneous rock units of the Central and Western Cordilleras (Figure 2) are younger than ca. 250 Ma while most basement rocks of the Eastern Cordillera and South American Craton are older than ca. 250 Ma (Aspden et al., 1987; Cordani et al., 2005; Horton et al., 2010a, 2010b; McCourt et al., 1984; Restrepo–Pace et al., 1997; Silva et al., 2013).

Detrital zircon U–Pb ages (e.g., Ibañez–Mejia et al. 2015 and references therein) have the technical advantage of efficiently dating hundreds of zircon crystals from sedimentary rocks (Figure 3b). In identifying major zircon age populations in the northern Andes, multiple studies have been able to more precisely suggest when particular sediment sources in the northern Andes shed sediments to adjacent basins (e.g., Bande et al., 2012; Caballero et al., 2013a, 2013b; Horton, 2018a; Horton et al., 2010a, 2010b, 2015, 2020; Nie et al., 2010, 2012; Silva et al., 2013;). In addressing the timing of terrane accretion, other works have applied this technique to reveal that basement rocks of the Panamá–Chocó Terrane have a dominant Eocene age signature (ca. 59 to ca. 42 Ma) that contrasts with that of older basement rocks to the east (e.g., Montes et al., 2015).

One issue of detrital geochronology pertains to the fact that contributions of different source areas are often mixed in large drainage systems and may be recycled from older sedimentary rocks. Therefore, the method relies on the presence or absence of diagnostic age populations diagnostic of particular source areas. In practice, interpretations of the northern Andes focus on whether sediment was derived from particular regions (for example, the Eastern Cordillera, Central Cordillera, or Panamá–Chocó Terrane). As a result, geologists have developed hypothesis regarding regions of elevated topography that may have once acted as sources of sediments. Because these source materials have been largely eroded away, there remains considerable ambiguity regarding the precise locations of former regions of positive relief. This problem can be addressed in regions that have not been eroded away, by using low temperature thermochronology results in areas where cooling has occurred in situ in the upper ca. 3–6 km of crustal blocks. In those provinces ages can still be measured today. In this paper, we review several key data sets and discuss interpretations that impact our understanding of the paleogeographic evolution and uplift of the northern Andes.

4. Latest Cretaceous to Early Eocene Accretionary and Deformational Events

4.1. Western and Central Colombia and Ecuador

To decipher the timing and consequences of the accretion of Cretaceous oceanic terranes, several authors have obtained thermochronological data from accreted oceanic rocks and adjacent continental rocks (Figures 1, 2a, 4, 5; e.g., Restrepo–Moreno et al., 2009; Spikings et al., 2000, 2001; Villagómez & Spikings, 2013).

Villagómez & Spikings (2013) concluded that the collision of the Caribbean Large Igneous Province in Colombia started in the Campanian and triggered shortening in the continental interior. The collision is interpreted to have driven uplift and erosional exhumation (at rates of 1 km/my) that persisted until ca. 65 Ma based on modeled AFT and ZFT time–temperature histories for the oceanic and continental blocks (Figures 4–7). Villagómez & Spikings (2013) provide AFT and ZFT data for the Bolívar Batholith in the Western Cordillera that show rapid Late Cretaceous to Paleocene exhumation (Figure 6) similar to that observed in the Central Cordillera (Figure 7 after Villagómez & Spikings, 2013). In northern Colombia, more moderate exhumation rates probably lasted until ca. 55 Ma in the east consistent with progressively more recent cooling east of the Romeral Fault System. Syn- and post-accretionary sedimentary rocks within the accreted terranes and adjacent continental margin confirm the onset of this accretionary event (Villagómez & Spikings, 2013). Similarly, Spikings et al. (2001, 2010) constrained rapid exhumation (>1 km/my) in Ecuador between 73 and 55 Ma and attributed this exhumation to the collision and accretion of the Caribbean Large Igneous Province (Figure 8). A similar Late Cretaceous – Paleocene onset of Andean orogenesis is recorded along the length of the Andes, including the central and southern Andes where oceanic materials were not accreted (Horton, 2018a, 2018b; Ramos, 2009; Ramos & Aleman, 2000).

4.2. Exhumation and Deformation in the Middle Magdalena Basin

By Late Cretaceous time, the Middle Magdalena Valley formed part of an active foreland basin of the proto-Andean orogen. In this area, a widespread unconformity marks a pre-Eocene contractional event in which inverted Jurassic grabens and shortened Cretaceous rocks are documented in surface and subsurface datasets (Figure 2c for location; e.g., Gómez et al., 2003, 2005; Parra et al., 2012). The age of this contractional event was originally attributed to the middle Eocene (Villamil, 1999) or late Paleocene – late Eocene (Restrepo–Pace et al., 2004). However, using thermochronology combined with

vitritinite reflectance data, Parra et al. (2012) demonstrated that deformation predating the widespread unconformity mostly occurred in latest Cretaceous – Paleocene time (Figure 9). Rodríguez–Forero et al. (2012) dated the oldest deposits above the unconformity, the La Paz Formation, and found that they were actually deposited by the earliest Eocene. In addition, Caballero et al. (2010, 2013a, 2013b) documented a folded Paleocene Lisama Formation beneath the unconformity in northern areas of the Middle Magdalena Valley.

Along the western margin of the Eastern Cordillera close to the Arcabuco Anticline, late Paleocene shortening and exhumation are consistent with structural relationships (Restrepo–Pace et al., 2004) and ZHe ages from rocks in which vitritinite reflectance data suggest temperatures sufficient to fully reset the ZHe thermochronometer (Caballero et al., 2013a; Reyes–Harker et al., 2015). Bayona et al. (2013; Figure 2c) further documented thickness changes in Paleocene strata within the axial zone of the Eastern Cordillera, and Mora et al. (2013a) documented minor cooling in the Llanos Basin.

To the south, the Amazon Foreland Basin shows evidence of the initial uplift of the Eastern Cordillera in Ecuador (southern continuation of the Central Cordillera) as recorded by initial input of Andean material within nonmarine sandstones and shales of the Tena Formation (Horton, 2018a; Martín–Gombaj & Winkler, 2008; Spikings et al., 2010).

From the above-mentioned evidence, we suggest that deformation during the collision of the Caribbean Large Igneous Province persisted from the latest Cretaceous through Paleocene time and influenced the growth of the early Andean Foreland Basin. This early shortening prompted strong exhumation in the Central Cordillera and localized basement uplifts in the Middle Magdalena Valley with deformation possibly persisting into the early Eocene (Mora et al., 2013a).

5. Middle Eocene to Early Oligocene Evolution of the Northern Andes (48–28 Ma)

5.1. Middle Eocene to Early Oligocene in Western and Central Colombia and Ecuador: Increased Exhumation and Convergence

Spikings et al. (2001) suggested that in Ecuador <1 km/my exhumation occurred along the Western and Eastern Cordilleras from ca. 43 to 30 Ma (Figure 8). Spikings et al. (2001, 2010) proposed that this exhumation was the product of an abrupt increase in Farallon–South America convergence rather than accretion of an Eocene island arc. This increased exhumation was accompanied by foreland deposition of the coarse-grained Upper Tiyuyacu Formation (Baby et al., 2013). Similarly, the Central Cordillera of Colombia experienced moderate exhu-

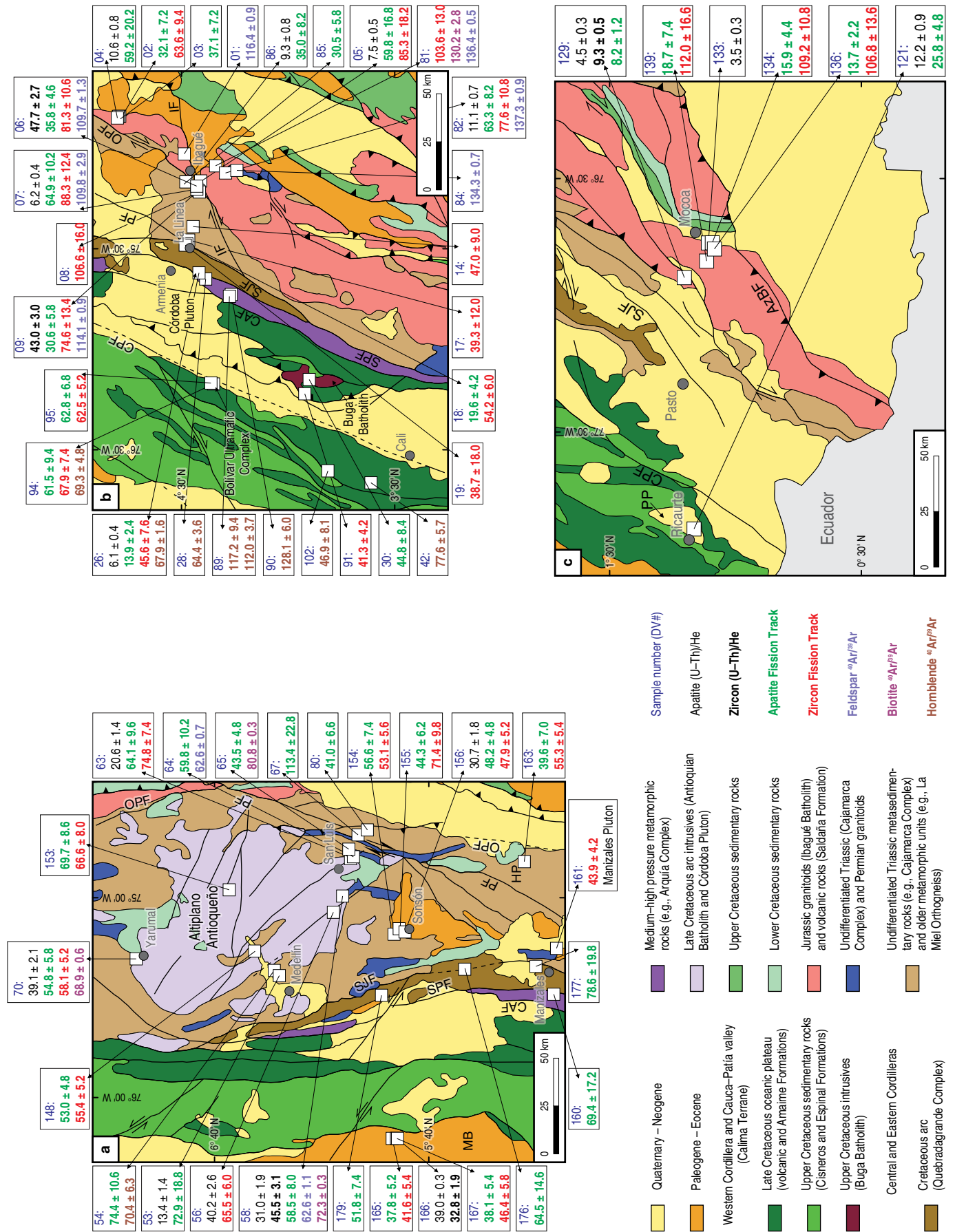




Figure 4. Geological maps of the study regions of Villagómez & Spikings (2013) (see Figures 1, 2a) within the Central and Western Cordilleras and the Cauca–Patía valley of Colombia (after Gómez et al., 2007) showing sample locations and the thermochronological ages acquired in this study. **(a)** Northern Colombia; **(b)** Central Colombia; **(c)** Southern Colombia. All ages are given in Ma with an uncertainty of $\pm 2\sigma$, and sample codes are shown in blue (DV#). (OPF) Otú–Pericos Fault; (PF) Palestina Fault; (SJF) San–Jeronimo Fault; (MB) Mande Batholith; (CAF) Cauca–Almaguer Fault; (SPF) Silvia–Pijao Fault; (HP) Hatillo Pluton; (CPF) Cali–Patía Fault; (IF) Ibagué Fault; (PP) Piedranza Pluton; (AzBF) Amazonian Border Fault.

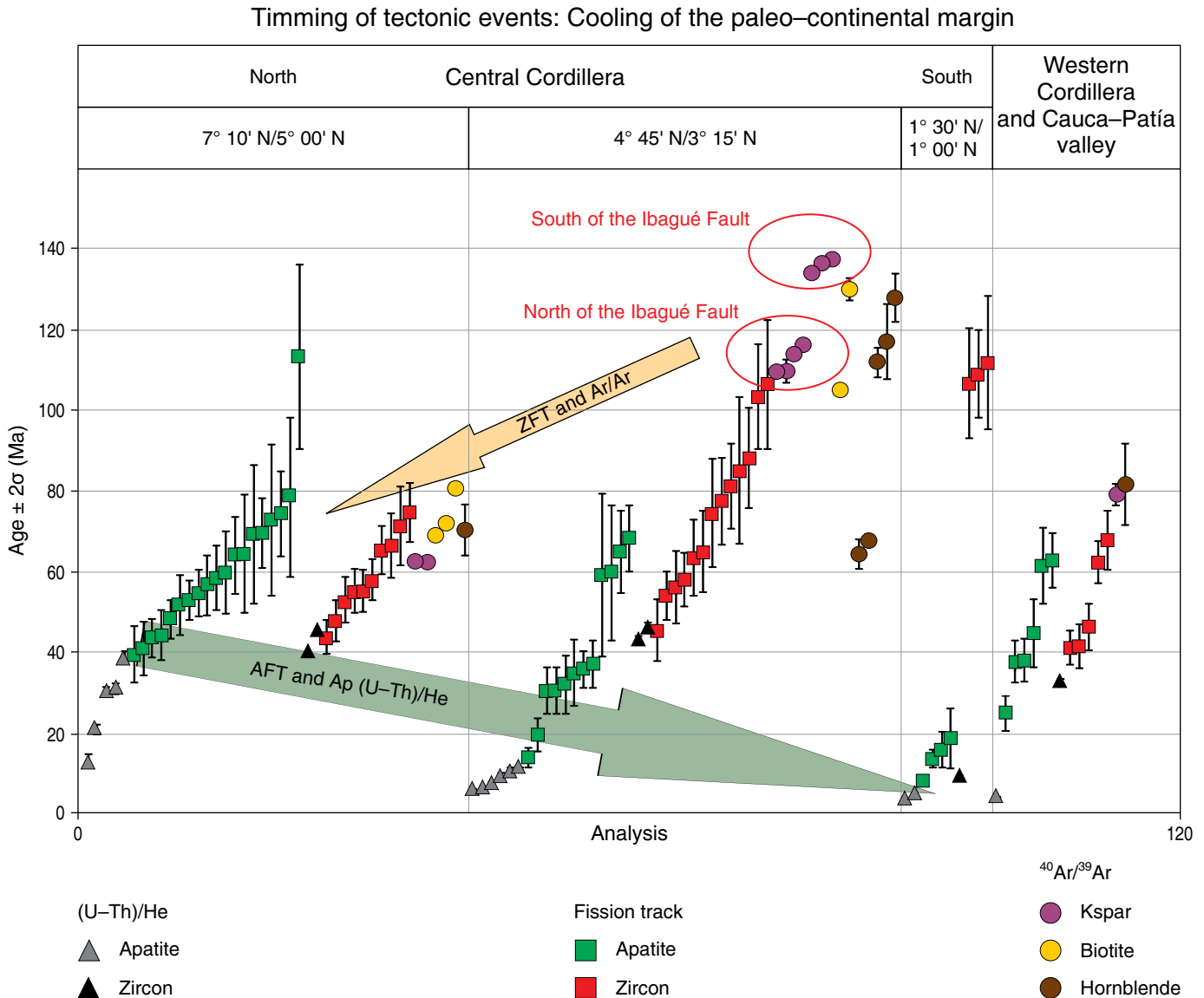


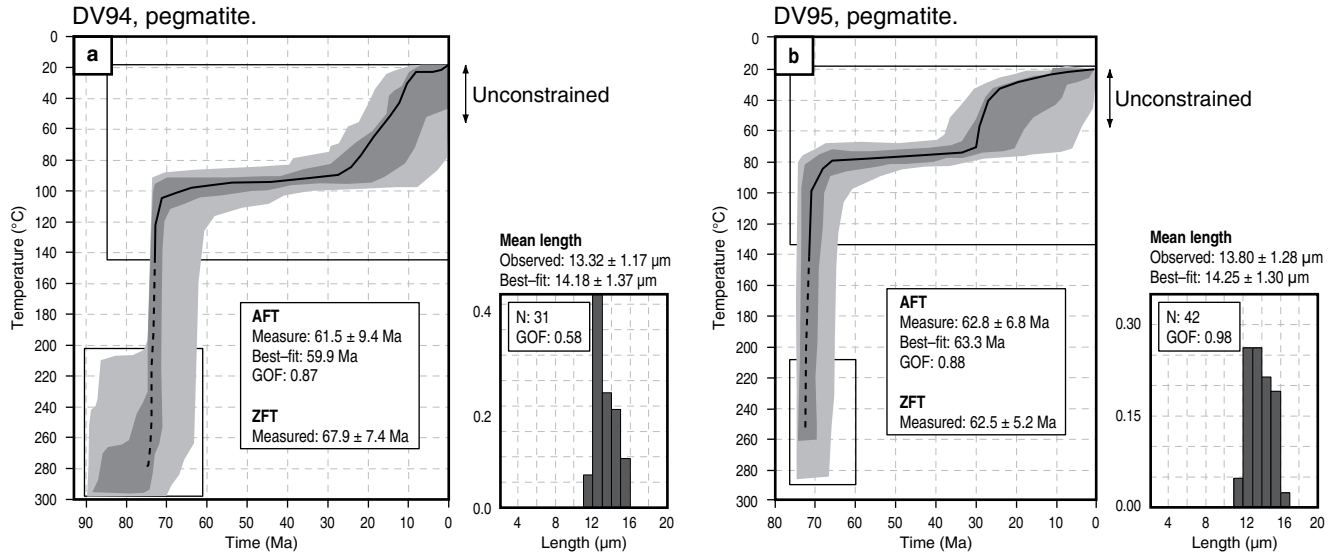
Figure 5. Compilation of thermochronological ages ($\pm 2\sigma$) of the Central and Western Cordilleras and of the Cauca–Patía valley in Colombia (after Villagómez & Spikings, 2013). Apatite FT and (U–Th)/He ages decrease toward the south of the Central Cordillera.

mation (<0.3 km/my) at 40–30 Ma near major faults such as the Palestina, Ibagué, and Otú–Pericos Faults (Figure 10; e.g., Villagómez & Spikings, 2013). A modest ca. 45 to 40 Ma episode of exhumation (<0.2 km/my) has also been identified in the northern Central Cordillera and ascribed to a shift in Farallon–South America convergence (Restrepo–Moreno et al., 2009).

5.2. Middle Eocene in Eastern Colombia: Tectonic Quiescence (48–38 Ma)

Mora et al. (2013a) suggest that the middle Eocene was a time of tectonic quiescence in the Magdalena Basin and Eastern Cordillera on the basis of: (a) Low accumulation rates in the middle Eocene Upper Mirador and Lower Esmeraldas Formations of

Bolívar Ultramafic Complex



Mandé Batholith

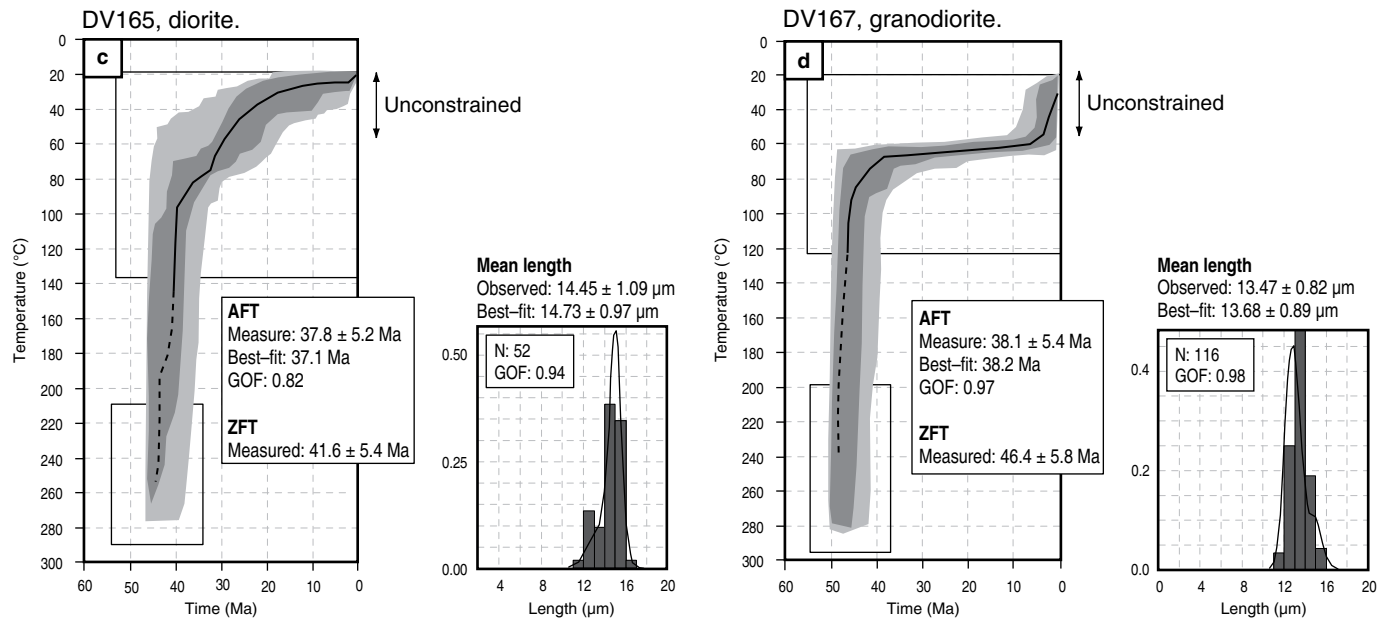


Figure 6. Time-temperature solutions for allochthonous rocks of Colombia's Western Cordillera obtained by (i) the inverse modeling of apatite FT age and length data, (ii) weighted mean (U-Th)/He dates and grain size data (calculated from the weighted mean of diffusion lengths). The modeling referred to Reiners et al. (2004) kinetic relationship for the diffusion of He in zircon, Flowers et al. (2009) for the diffusion of He in apatite and Ketcham et al. (2007) for FT annealing in apatite. A controlled random search procedure was used to search for best-fit data. Dark gray regions are envelopes of "good fit" and light gray areas denote "acceptable fit." The thick black line shows the statistically best fitting solution. Measured and predicted data for the best fit model are shown. Solutions are considered to show good fit when track length histograms and model ages pass Kuiper's statistic test with values of >0.5 and are considered acceptable for values of >0.05 . The models are extrapolated to temperatures for the partial retention of argon when (i) the $^{40}\text{Ar}/^{39}\text{Ar}$ ages of ferromagnesian phases overlap with the timing of cooling obtained by inverting the FT and (U-Th)/He data or when (ii) there are interpretable alkali feldspar $^{40}\text{Ar}/^{39}\text{Ar}$ ages. Dashed lines show paths manually interpolated from the $^{40}\text{Ar}/^{39}\text{Ar}$ data. (GOF) Goodness-of-fit. After Villagómez & Spikings, 2013.

the Eastern Foothills and Middle Magdalena Valley, respectively (Mora et al., 2013a) and (b) U-Pb data suggestive of drainage divide advance toward the deformation front (Silva et al., 2013).

Elevated exhumation rates in Ecuador during the middle Eocene are difficult to reconcile with regional quiescence in Colombia. We speculate that this could be related to along-

strike variations in Pacific margin architecture and Farallon–South America convergence.

5.3. Late Eocene to Early Oligocene in Central and Eastern Colombia: Renewed Deformation

Saylor et al. (2012b) used lag time analyses of detrital zircon low-temperature thermochronological data (Figure 11) to propose late Eocene to early Miocene deformation in the Eastern Cordillera. These findings were interpreted by Mora et al. (2013a) and Reyes–Harker et al. (2015) to represent renewed tectonic activity along the western half of the Eastern Cordillera. In this context, the Soápagua and Machetá Faults would represent the active deformation front of the northern Andes during late Eocene to early Oligocene time with the rapid subsidence of the developing Llanos Foreland Basin to the east. This facilitated a deposition of fine-grained marine units corresponding to the shaly C8 Member of the Carbonera Formation.

6. Middle to Late Oligocene Evolution (28 to 23 Ma)

6.1. Western and Central Colombia and Ecuador

Spikings et al. (2010) linked the fragmentation of the Farallon Plate and associated changes in convergence at 23 Ma (Lonsdale, 2005) to cooling and moderate exhumation (<0.5 km/my) in the Eastern Cordillera of Ecuador. Spikings et al. (2010) suggested that this Oligocene deformation was limited in the Western Cordillera and only affected fault blocks with a favorable orientation.

No evidence of significant Oligocene exhumation has been detected in the Western and Central Cordilleras of Colombia from available, albeit limited, thermochronological data (Villagómez & Spikings, 2013). This could be a consequence of strain partitioning through which the preferential reactivation of the Amazonian Border Fault System and Santa Marta–Bucaramanga Fault deformed and exhumed the Eastern Cordillera of Colombia (Mora et al., 2010a; Parra et al., 2012; Saylor et al., 2012a) and uplifted the Sierra Nevada de Santa Marta (Villagómez et al., 2011b; Piraquive et al., 2018), thus isolating the Central and Western Cordilleras.

6.2. Eastern Cordillera of Colombia

Different studies suggest that the eastern flank of the Eastern Cordillera (Figure 2c) was actively exhuming (Figure 12; Parra et al., 2009b) and shedding sediments (Figure 13; Horton et al., 2010a, 2010b; Parra et al., 2010) to the Llanos Foreland Basin by the Oligocene. Mora et al. (2010a, 2013a; Figure 2b) further employed thermochronological analyses to demonstrate

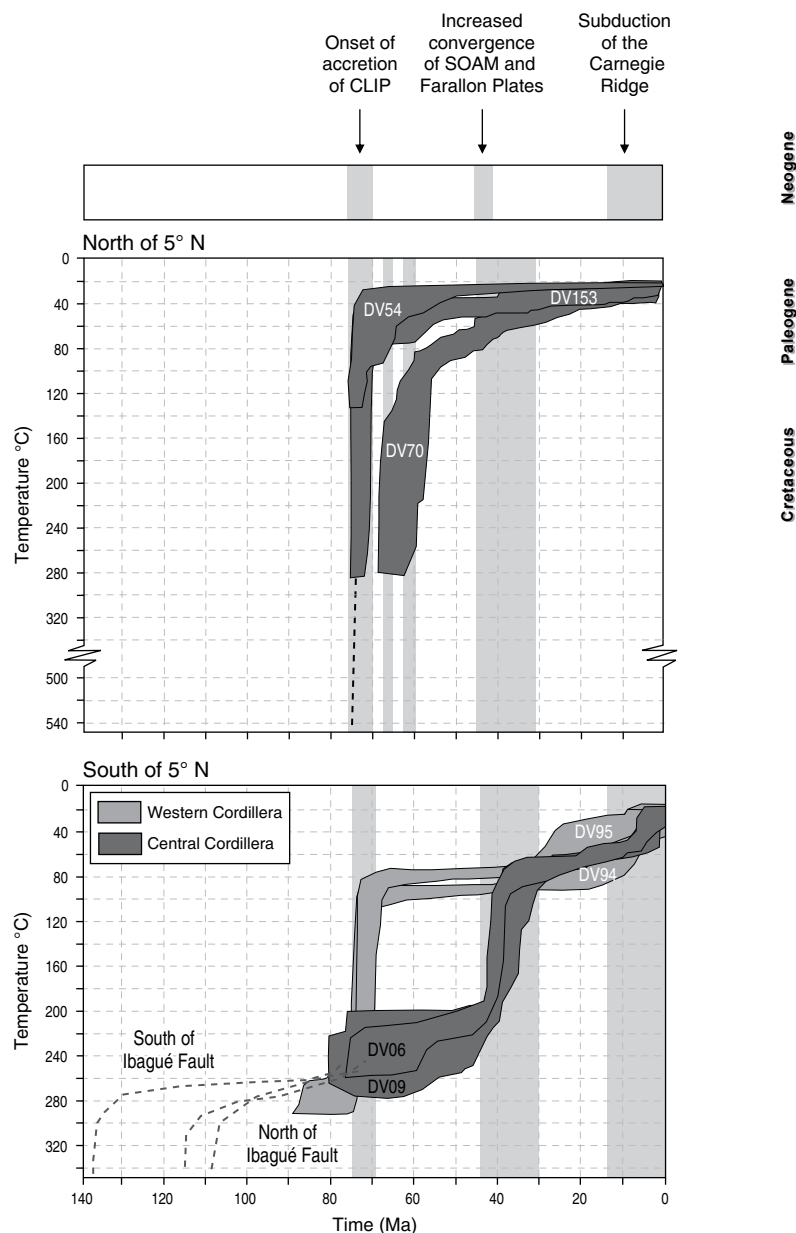


Figure 7. Summary of good-fit thermal history solutions for a representative selection of samples of the Central Cordillera (Late Cretaceous continental margin; dark gray) and Western Cordillera (Late Cretaceous indenter; light gray) after Villagómez & Spikings, (2013). Figure 6 explains their calculation and constraining data. The solutions highlight the main periods of exhumation of the Central and Western Cordilleras. Vertical bands highlight the timing of rapid cooling and exhumation in Colombia, and labels denote sample numbers. (CLIP) Caribbean Large Igneous Province. (SOAM) South America.

that this behavior can be related to the inversion of the entire Neocomian graben of the Eastern Cordillera. In addition, Mora et al. (2013b) use fracture patterns, fluid inclusions, and thermochronology to document several locations with Oligocene low-amplitude folding in the Eastern Cordillera and in coeval growth strata (Figure 14; Mora et al., 2013a). The study covers

Late Cretaceous continental margin, northern Andes.

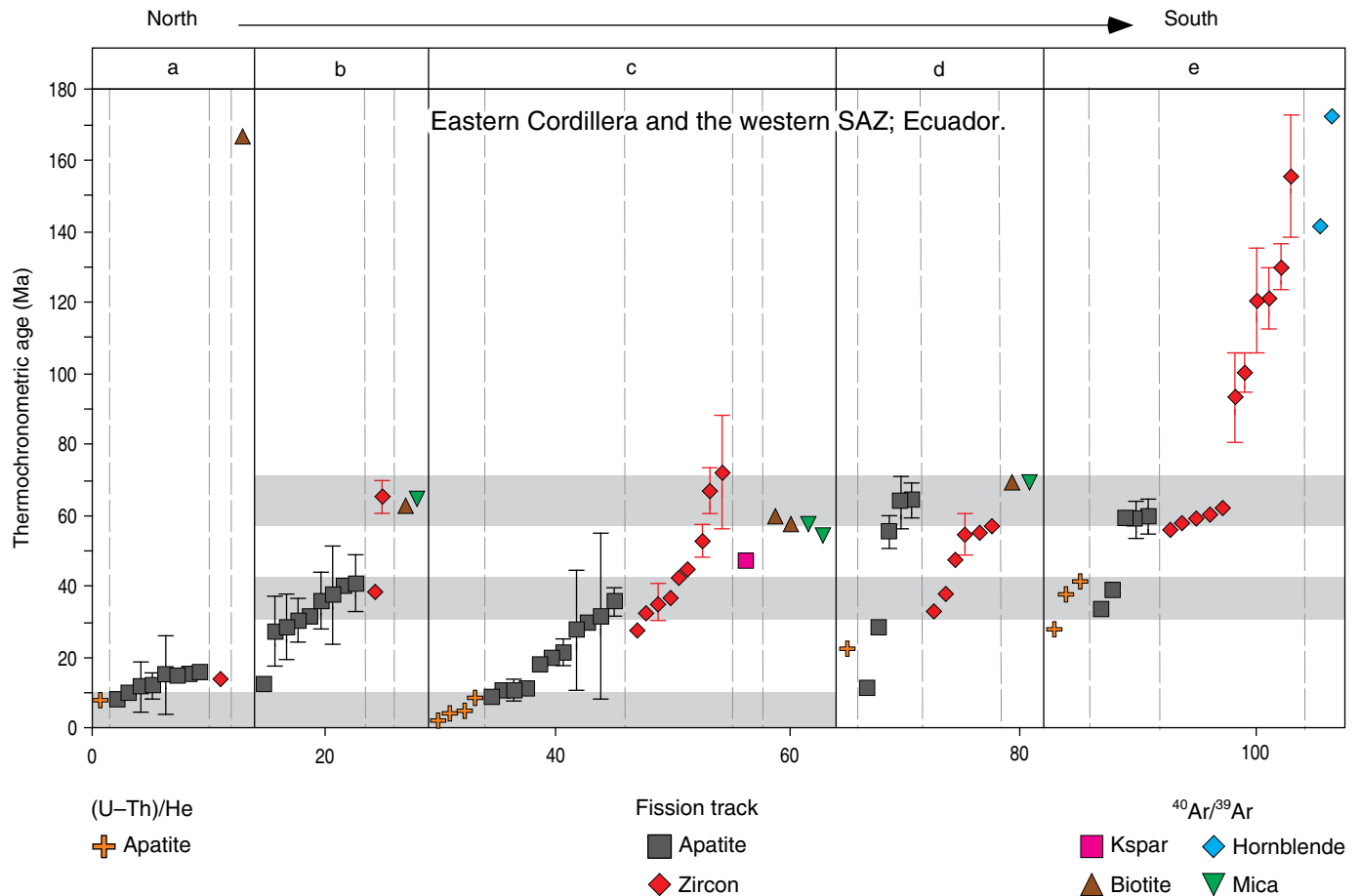


Figure 8. A compilation of white mica and biotite $^{40}\text{Ar}/^{39}\text{Ar}$ and ZFT and AFT ages obtained from traverses across the Cordillera Real of Ecuador. Shaded horizontal bars denote time periods in which regional scale exhumation was occurring at its highest rate (modified after Spikings et al., 2000, see Figure 2a for the location). (SAZ) Sub-Andean Zone (Ecuador).

western and eastern sectors of the Eastern Cordillera, in the Magdalena and Llanos Foothills, respectively.

7. Latest Oligocene to Early Miocene in Northern Colombia (25–16 Ma)

In studying the northernmost Central Cordillera (Figure 1), Restrepo–Moreno et al. (2009) used apatite (U–Th)/He data to constrain modest exhumation in discrete fault blocks during the latest Oligocene – early Miocene (ca. 25–20 Ma). Exhumation rates reached roughly ca. 0.2 km/my and are attributed to increased Nazca–South America convergence (Restrepo–Moreno et al., 2009). Farris et al. (2011) suggest that the early Miocene involved the most interactions of the Panamá–Chocó Terrane with northern Colombia. This exhumation might have been a response to initial Panamá accretion, which ultimately led to the closure of the Central American Seaway (Duque–Caro, 1990; Montes et al., 2015).

For the Eastern Cordillera, Parra et al. (2009a, 2009b; Figure 2c) document continued tectonic activity and exhumation. However, there is no direct evidence of elevations of above 1 km; in fact, pollen records (Figure 15; Hooghiemstra et al., 2006) show that areas of above 2 km elevation today are inferred to be at temperatures equivalent to those of low elevation tropical areas. New paleoelevation records based on geochemistry (lipid biomarkers) support this interpretation (Anderson et al., 2015).

8. Middle Miocene to the Present (16 to 0 Ma)

8.1. Western and Central Colombia and Ecuador

In Ecuador, Spikings et al. (2001) identified a northward–younging, along–strike progression of exhumation during the middle to late Miocene. Spikings et al. (2001, 2010) suggested

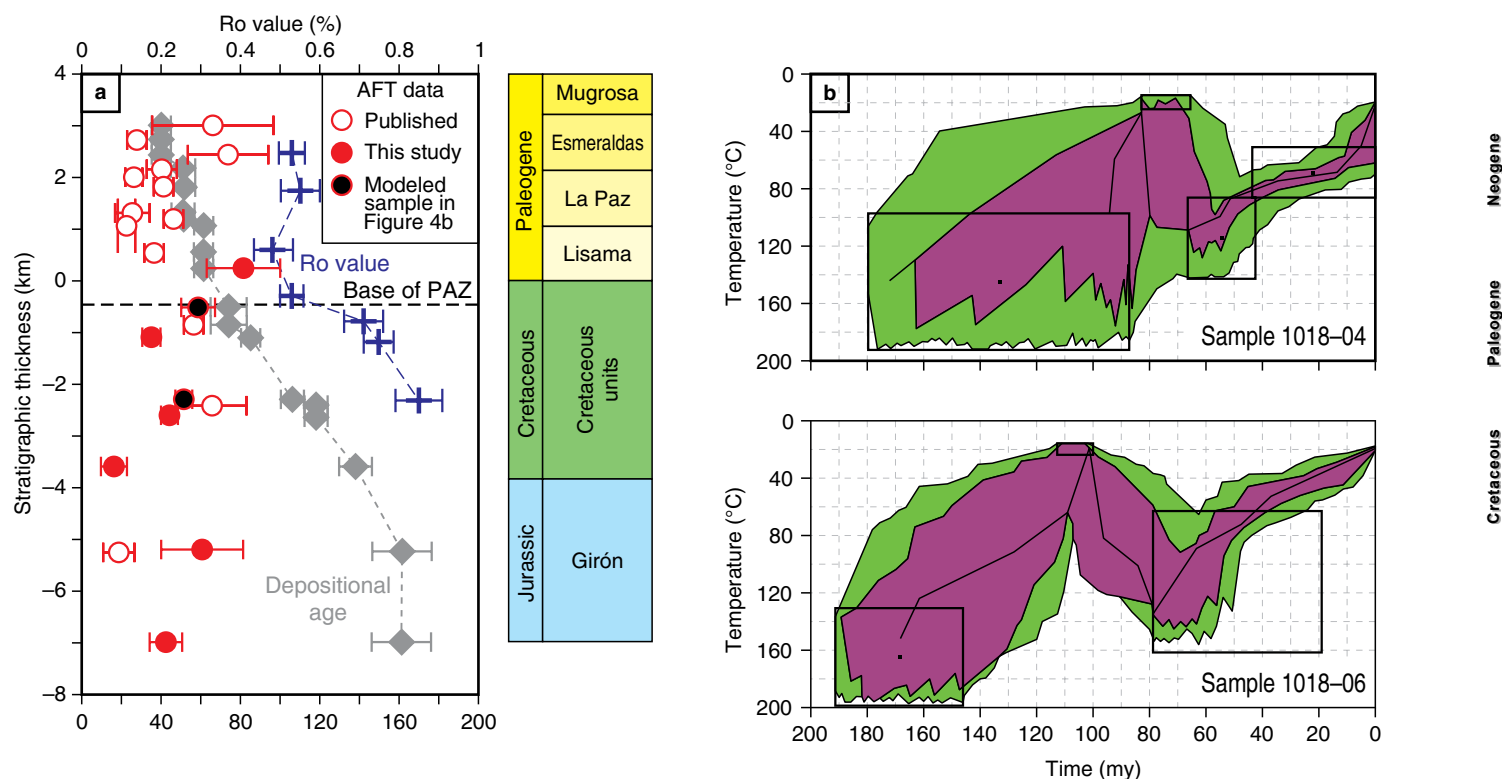


Figure 9. (a) Plot showing apatite fission-track (AFT) ages (red), vitrinite reflectance (Ro) values (blue), and stratigraphic ages (gray). Zero represents the base of the Cenozoic section. (PAZ) Partial annealing zone. (b) Thermal modeling results depicting time-temperature histories of two reset Cretaceous sandstones. Black boxes define time-temperature constraints for provenance, deposition, and burial-exhumation. Purple and green fields represent good and acceptable model fits, respectively. Figure after Parra et al. (2012). See Figure 2c for the location.

that the Eastern Cordillera of northern Ecuador (Central Cordillera of Colombia) was positioned at depths of roughly 3.5 km at ca. 15 Ma while southern latitudes were positioned at depths ≤ 1.3 km. This variation is attributed to rock uplift and exhumation driven by the collision of the Carnegie Ridge with South America. Villagómez & Spikings (2013) similarly constrained amplified exhumation rates at which rocks were exhumed from depths of ≥ 3 km since ca. 15 Ma in the southern Central Cordillera of Colombia (Figure 5).

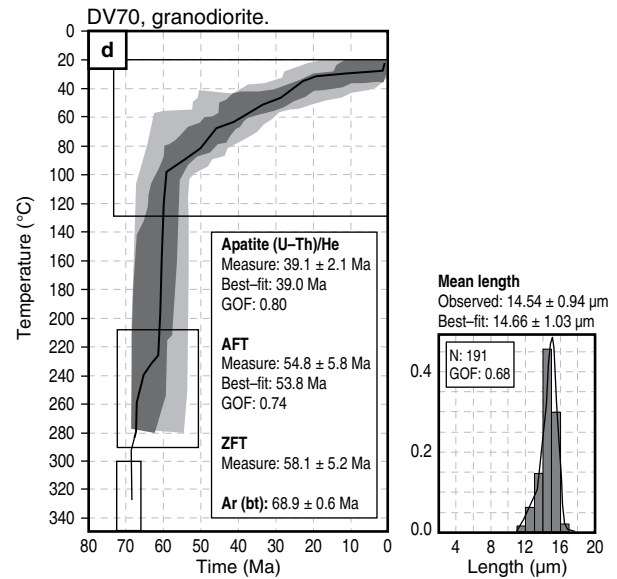
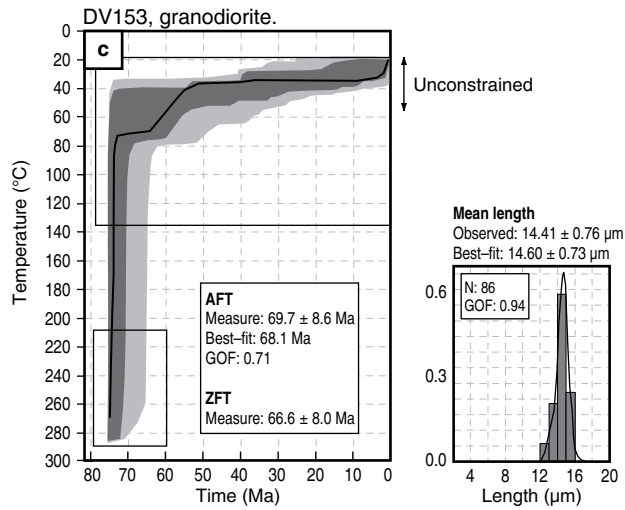
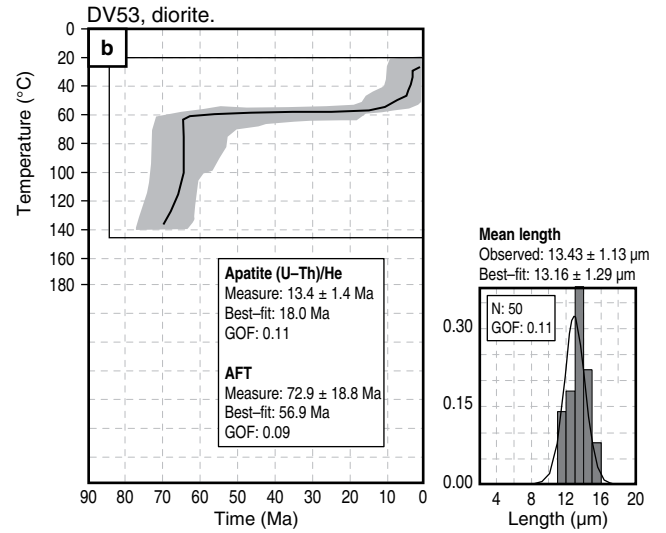
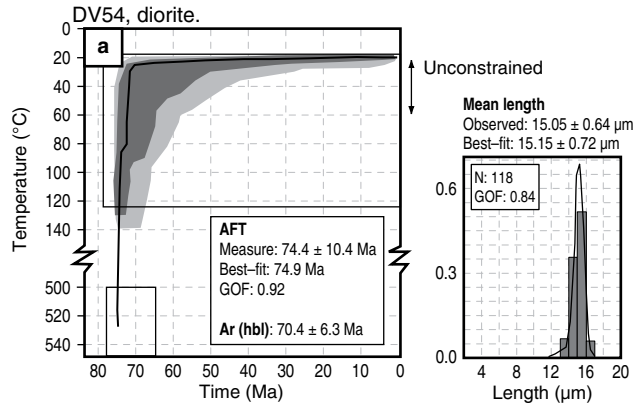
On the other hand, the northernmost continuation of the northwestern Andes and of southern Central America experienced increased tectonic deformation and uplift in the Miocene potentially related to the main collision of the Panamá-Chocó Terrane (Duque-Caro, 1990; Farris et al., 2011; Montes et al., 2015). After the middle Miocene accretion of the Panamá-Chocó Terrane, renewed coupling and the increased convergence of the Nazca Plate beneath South America led to intense magmatism in Colombia and Ecuador south of ca. 5.5° N. Farther north, arc volcanism started to vanish from 9 to 4 Ma due to slab flattening. In around 4 Ma, slab rollback and renewed magmatism occurred as a result of slab failure along the Caldas Tear (Wagner et al., 2017), possibly renewing sedimentation in the Cauca and Magdalena intermontane basins.

8.2. Eastern Cordillera of Colombia

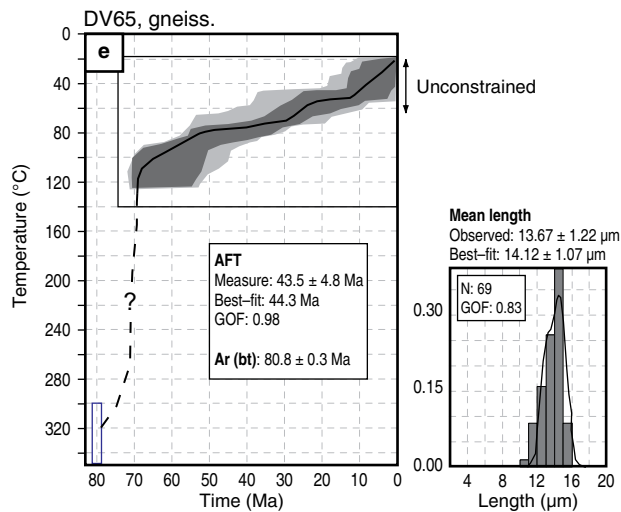
In the Eastern Cordillera of Colombia (Figure 2b), a recent acceleration of exhumation is recorded in the Quetame Massif and Cocuy Range (Figure 16; Mora et al., 2008, 2015a). In these areas, young AFT ages (< 3 Ma) indicate accelerated cooling, and cross-cutting relationships show that most shortening occurred from the late Miocene onward (e.g., Mora et al., 2013a). Finally, paleoelevation data from palynology (Wijninga, 1996) and lipid biomarkers (Anderson et al., 2015) support an interpretation of topographic growth starting by the middle Miocene and finalized by 3 Ma.

Other geomorphic features in Colombia such as deep canyons in the northern Cauca River valley between the Western and Central Cordilleras may suggest youthful rock uplift and river incision. Another outstanding feature is the Sierra Nevada de Santa Marta (Figure 1), whose prominent relief adjacent to the Caribbean Sea suggests renewed tectonic activity consistent with thermochronometric data (Villagómez et al., 2011b). These geomorphic features appear to suggest that recent topographic growth is a ubiquitous phenomenon in the northern Andes. Such rock uplift has been instrumental in renewing coarse-grained sedimentation and basin compartmentalization

Antioquian Batholith



Cajamarca Formation



Sonsón Batholith

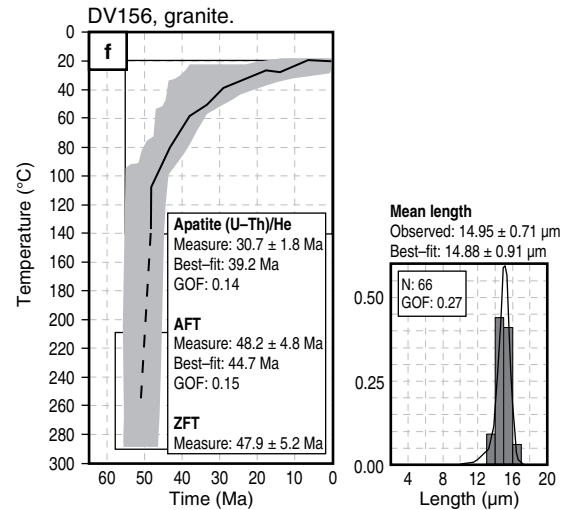




Figure 10. Time–temperature solutions for autochthonous rocks of Colombia’s northern (ca. 6° N) Central Cordillera obtained by the inverse modeling of AFT age and length data, and weighted mean (U–Th)/He dates and grain size data (calculated using the weighted mean of the diffusion lengths) obtained from Reiners et al. (2004) kinetic relationship for the diffusion of He in zircon, Flowers et al. (2009) for the diffusion of He in apatite and Ketcham et al. (2007) for FT annealing in apatite. A controlled random search procedure was used to search for best-fit data. Dark gray regions denote envelopes of “good fit” and light gray denote “acceptable fit.” The thick black line denotes the statistically best fitting solution. Measured and predicted data for the best fit model are shown. Solutions were considered to show good fit when track length histograms and model ages passed Kuiper’s statistic test with values of >0.5 and were considered to be acceptable with values of >0.05 . The models are extrapolated to temperatures for the partial retention of argon when (i) the $^{40}\text{Ar}/^{39}\text{Ar}$ ages of ferromagnesian phases overlap with the timing of cooling obtained by inverting the FT and (U–Th)/He data or when (ii) there are interpretable alkali feldspar $^{40}\text{Ar}/^{39}\text{Ar}$ ages. Dashed lines denote paths manually interpolated from the $^{40}\text{Ar}/^{39}\text{Ar}$ data. (GOF) Goodness-of-fit. (After Villagómez & Spikings, 2013).

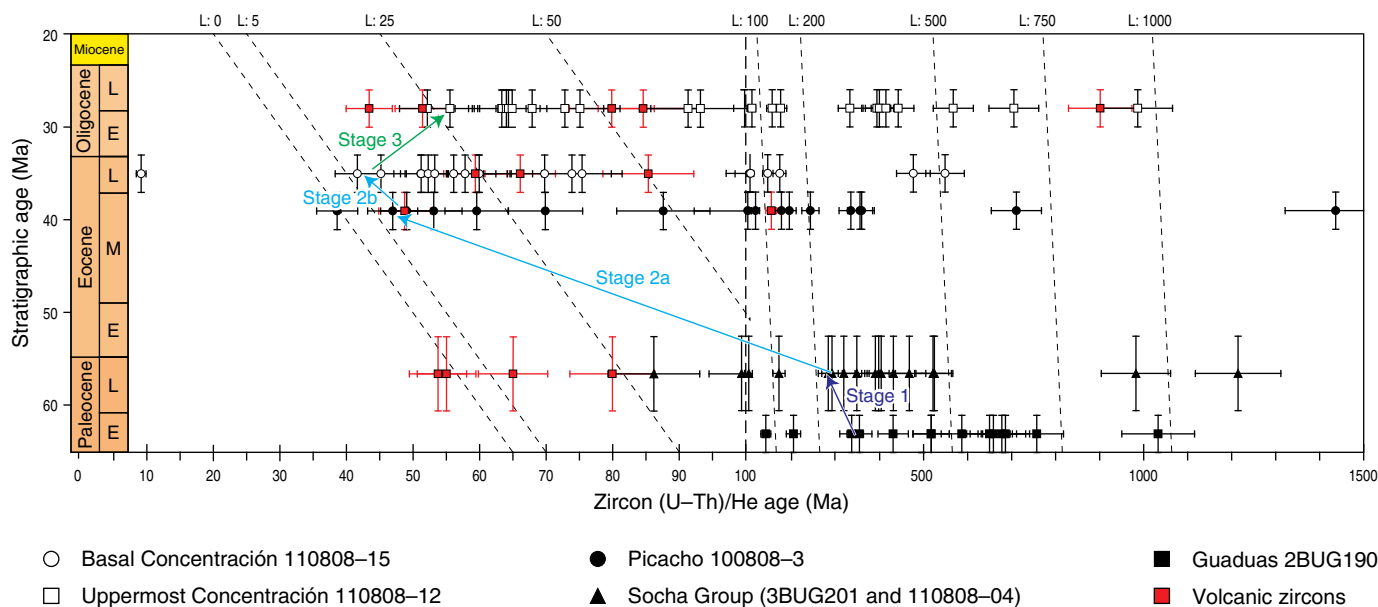


Figure 11. Double-dated ZHe ages plotted by stratigraphic age and lag time (dashed diagonal lines). Zircons are identified as of volcanic origin when their ZHe and Zircon U–Pb ages overlap within their 2σ uncertainty. Volcanic zircons (red) are excluded from the lag time analysis. The three stages are interpreted as episodes of rapid exhumation (Stages 1 and 2) and of the introduction of new supra-partial retention zone sedimentary sources (Stage 3). Lag time values (L) are given in my. Note that the Socha Group includes data from both the Upper Socha and Lower Socha Formations. After Saylor et al. (2012b).

within the Amazonas Foreland and Upper Magdalena Basin. For example, continued fault activity in southern Colombia accommodated the uplift and exhumation of the Garzón Massif (Anderson et al., 2016) between the Late Miocene and Pliocene. This uplift is of paramount importance to large river systems draining northern South America, topographically isolating the Magdalena, Orinoco, and Amazon watersheds (Anderson et al., 2016; Mora et al., 2010b).

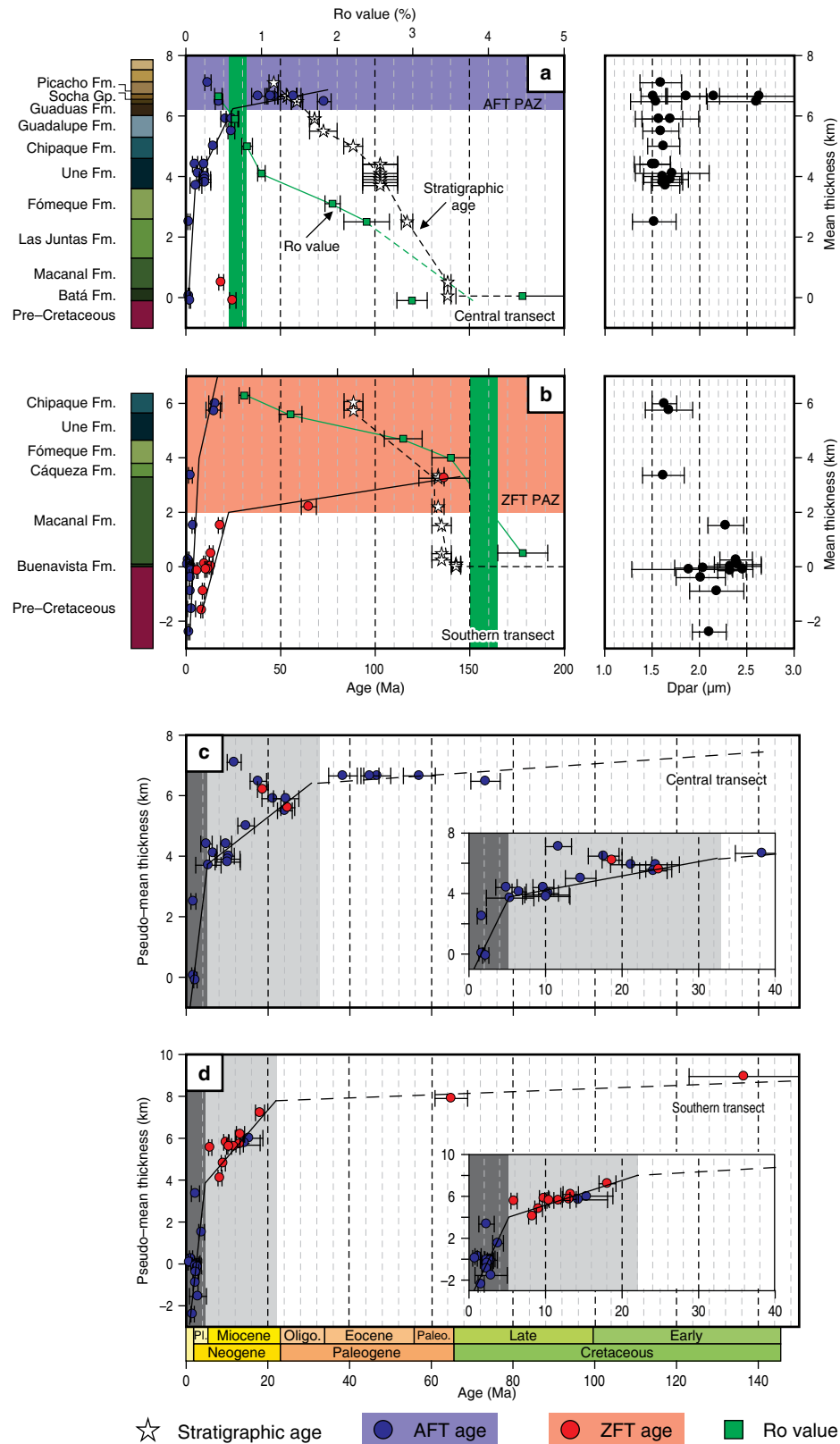
In contrast, neotectonic studies have dated Late Pleistocene to Holocene deformation in the Eastern Foothills (Ketcham et al., 2018; Mora et al., 2010c; Veloza et al., 2015). Relative to late Miocene to Pliocene topographic growth, where vertical uplift appears to dominate, the neotectonic deformation of the Eastern Foothills suggests the occurrence of mostly horizontal shortening perpendicular to frontal ranges (Mora et al., 2006, 2009, 2010c, 2014; Veloza et al., 2012).

Recent thermochronometric and kinematic analyses (Carrillo et al., 2016; Mora et al., 2015b) summarize different deformational styles in a single geometric reconstruction. Carrillo et al. (2016) suggested that the Eastern Cordillera reconstructions require late Miocene to Plio–Pleistocene topographic growth unrelated to fault-related folding with subsequent Pleistocene to Holocene horizontal shortening in the Eastern Foothills. It is intriguing that vertical topographic growth and horizontal shortening in the foothills appear to be non-synchronous phenomena.

9. Discussion

9.1. Discussion of Paleogeographic Implications

Regional geological reconstructions are important for several disciplines and help address recent appreciation of the interac-



tions between genetics and geology (e.g., Baker et al., 2014). This diversification of scientific interest has been particularly impressive in studies of the northern Andes. In the preceding synthesis, we summarize evidence for the timing of different

geological processes from thermochronological records. In this section, we emphasize key interpretations while recognizing that geological reconstructions of past configurations are limited and must be used with caution to review major processes



Figure 12. Fission track data and vitrinite reflectance (R_o) values for samples from the (a) central and (b) southern transects of the Colombian Eastern Cordillera at roughly 4.5° N. The data are plotted against the stratigraphic position of the base of Cretaceous rift-related units (see Figure 1 for the location). Stratigraphic thicknesses and ages are compiled from Ulloa & Rodríguez (1979) and Mora et al. (2008). Vertical green bars represent the range of R_o values corresponding to the temperature delimiting the base of the AFT (central transect) and ZFT (southern transect) partial annealing zones (blue and pink shaded areas, respectively). Stacked pseudovertical profiles are obtained for the (c) central and (d) southern transects. AFT data are plotted at their original stratigraphic positions as in Figure 9a and 9b, but ZFT data are offset upward by an amount proportional to the depth difference between the ZFT and AFT isotherms estimated at 5.7 km. The first break in slope denoted by the vertical light gray band at ca. 40–25 Ma (central profile) and 20 Ma (southern profile) marks the onset of thrust-induced cooling through the AFT and ZFT total annealing isotherms, respectively.

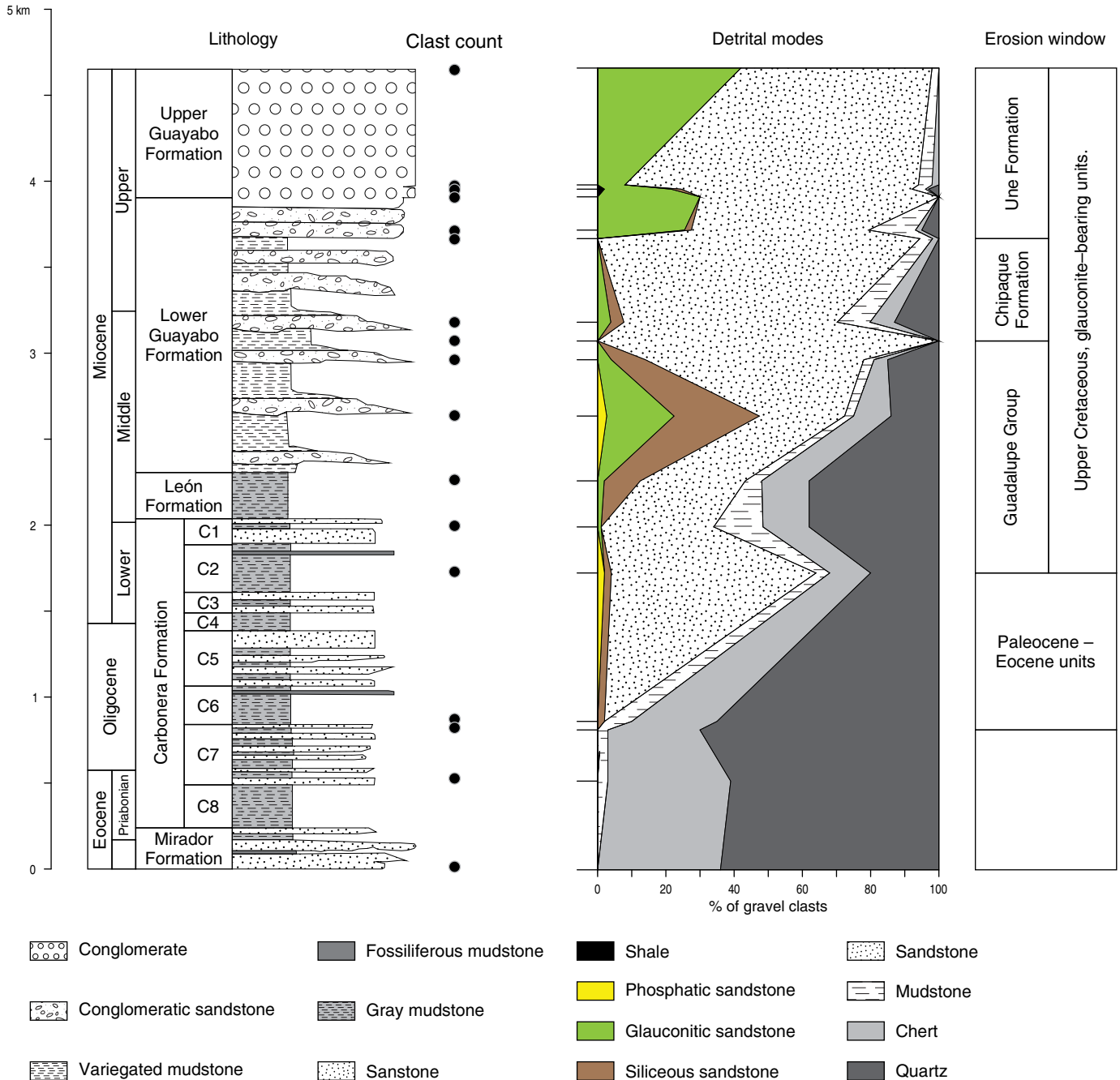


Figure 13. Compositional trends in Eocene to upper Miocene conglomerates of the Medina Basin. Black circles denote the stratigraphic positions of conglomeratic samples. Clasts of Upper Cretaceous glauconitic sandstone, phosphatic sandstone, and siliceous siltstone occur in Miocene strata of the Carbonera Formation and Guayabo Formation, documenting the progressive unroofing of the Eastern Cordillera (right panel). Figure after Parra et al. (2010).

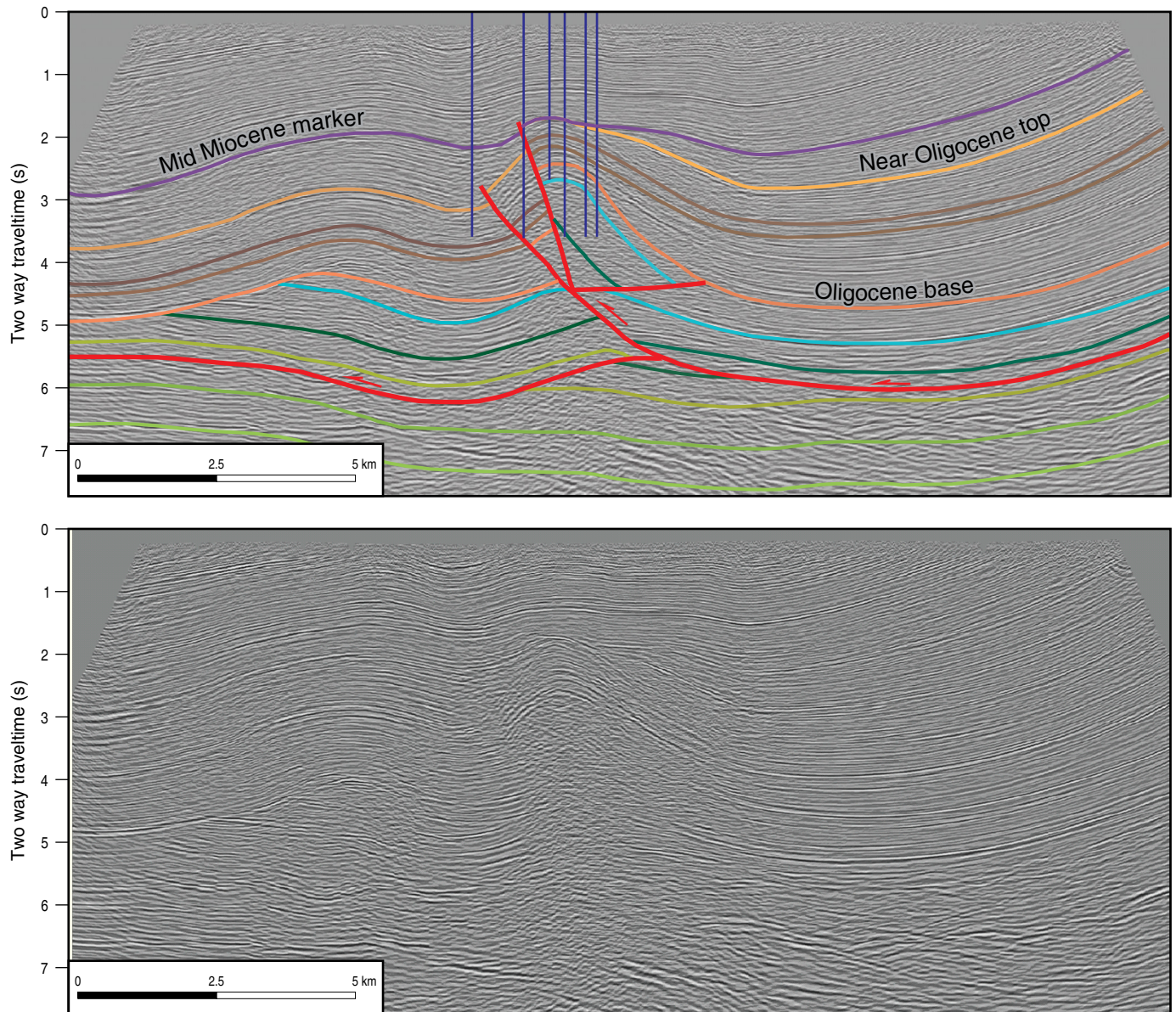


Figure 14. Oligocene growth strata in the Provincia Oil Field of the Middle Magdalena Basin.

and paleogeographic conditions of the Cenozoic evolution of the northern Andes.

Thin- and thick-skinned fold-thrust deformation has prevailed in Colombia throughout the Cenozoic. By the early Cenozoic, the basement of the present-day Western Cordillera was already juxtaposed to the continental margin. The accretion of a buoyant oceanic plateau coincided with the growth of a proto Western and Central Cordillera and the delivery of west-derived sediment to the proto-Magdalena Basin. However, the early Cenozoic accretion of the Western Cordillera did not require complete land emergence or ubiquitous mountain building.

The northern Central Cordillera and Cordillera Real of Ecuador record renewed exhumation during the Eocene based on very limited thermochronological data. A paucity of data on

western Colombia has hampered paleogeographic reconstructions and hindered the identification of Eocene tectonic events. Systematic sampling for thermochronology, paleoelevation, and provenance investigation is required. Fortunately, sedimentary records of the Eastern Cordillera and Magdalena Basin provide valuable information for Eocene and younger reconstructions.

9.1.1. Eocene Proto-Magdalena River Draining to the Maracaibo Basin

Evidence for Eocene mountain building in the Central Cordillera and western Eastern Cordillera allowed Caballero et al. (2013a, 2013b) and Silva et al. (2013) to interpret a proto-Magdalena River draining toward the Maracaibo Basin rather than its present outlet in the Caribbean (Figure 2). Using detrital

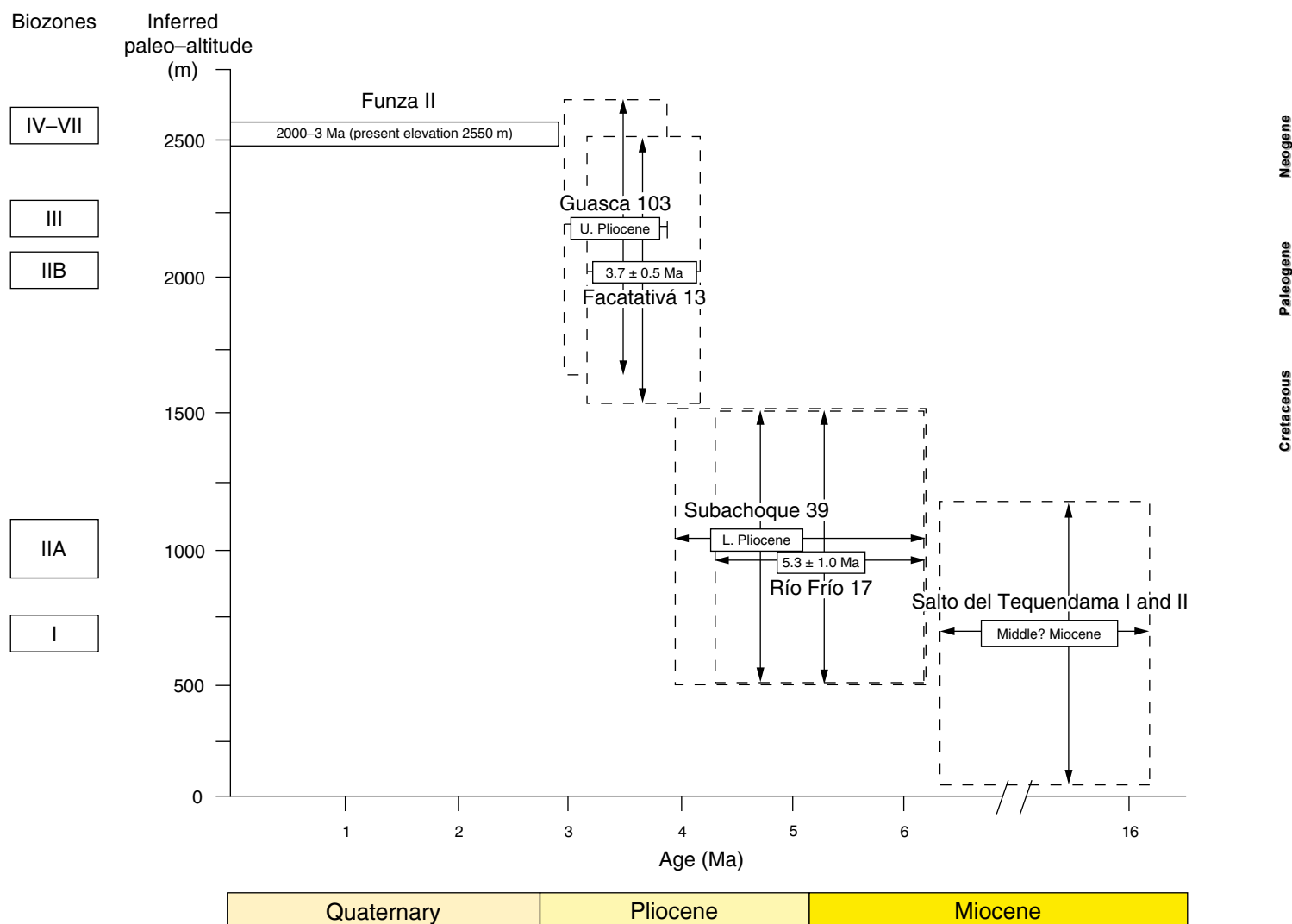


Figure 15. Inferred paleoelevation from reconstructed altitudinal vegetation belts based on characteristic pollen and paleobotanical associations found in sections Salto del Tequendama I and II, Río Frío 17, Subachoque 39, Facatativá 13, and Guasca 103 and in sedimentite core Funza-2. Sections are located in the outer parts of the Bogotá Basin. Uncertainties in age control and inferred paleoaltitude are shown as arrows. Biozones I to VII refer to stages of the uplift history and paleobiogeography of main (arboreal) taxa of the Eastern Cordillera (after van der Hammen et al., 1973; Wijninga, 1996).

zircon U–Pb age signatures, Horton et al. (2015) suggest that local small drainages were not fully integrated into a continuous proto–Magdalena River. Therefore, the main question is not whether Eocene rivers drained toward the Maracaibo region (e.g., Reyes–Harker et al., 2015) but whether a proto–Magdalena River existed. Although there was likely positive relief adjacent to the modern Magdalena valley, current ideas regarding the associated paleodrainage remain speculative.

9.1.2. Late Eocene to Middle Miocene Closed Middle Magdalena Valley

A significant element of Paleogene paleogeography concerns the hypothesis of Caballero et al. (2013a, 2013b) that the Middle Magdalena Valley (Figure 2) was an internally drained basin

with no outlet toward the modern delta or Maracaibo Basin, an idea supported by others (e.g., Horton et al., 2015; Mora et al., 2018; Reyes–Harker et al., 2015). It seems clear that the Central and Eastern Cordilleras were topographically positive areas in the Paleogene. Because thermochronological data cannot address past drainage geometries, we await clear provenance data to provide support for this closed–drainage hypothesis or for possible alternative hypotheses.

9.1.3. Oligocene Proto–Sabana de Bogotá

Mora et al. (2013a) suggested that the axial Eastern Cordillera (Figure 2; i.e., the proto–Sabana de Bogotá) may have been an internally drained basin analogous to closed basins in the Bolivian Altiplano (Strecker et al., 2007, 2009). This idea is based

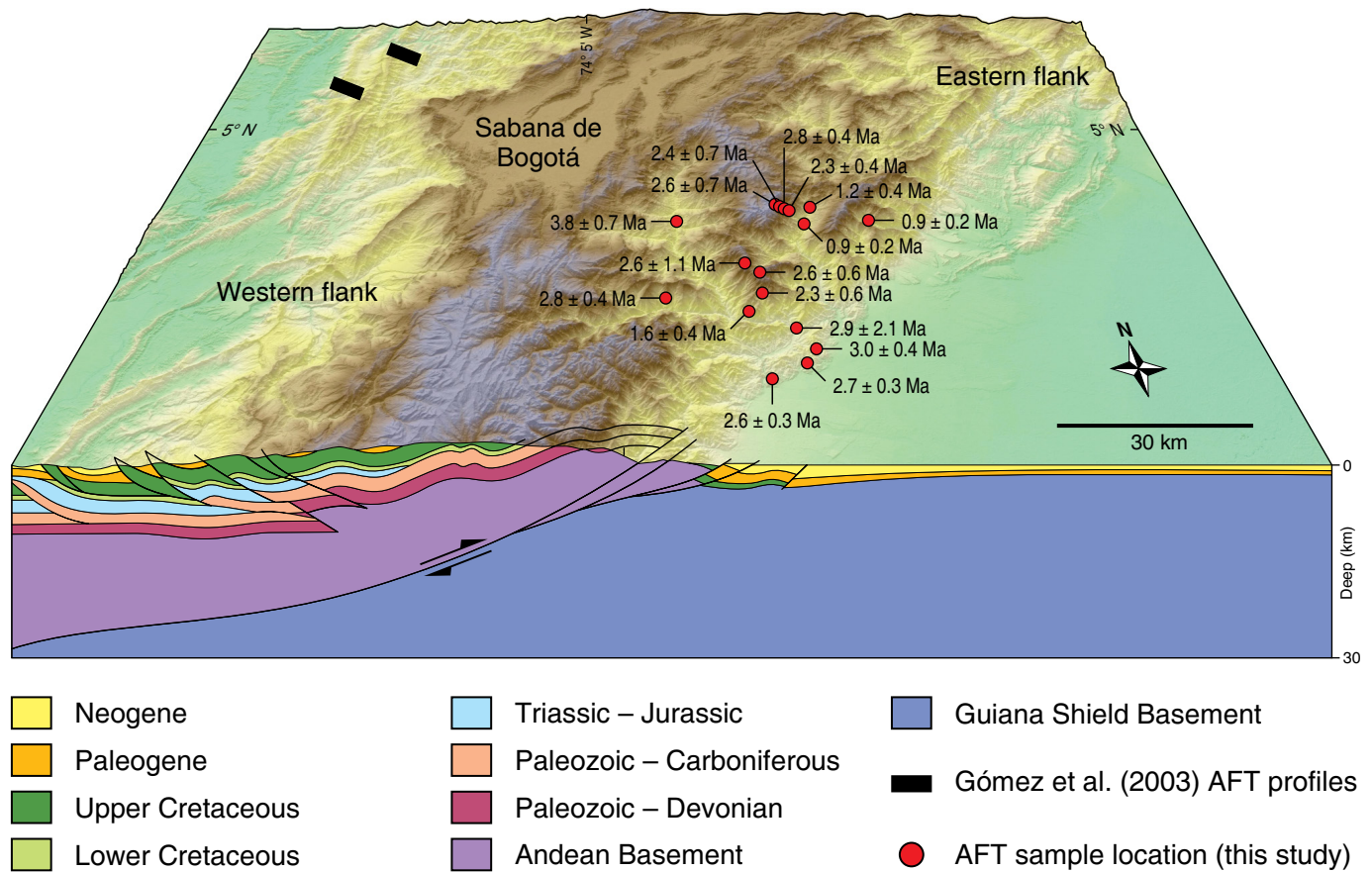


Figure 16. Digital elevation model of the Eastern Cordillera including the deeply dissected Eastern flank, the central flat-lying Sabana de Bogotá Basin, and the topographically lower western flank.

on evidence showing active exhumation on both flanks of the Eastern Cordillera (Figures 1, 2) while Oligocene deposition occurred in the axial zone. An alternative interpretation is that a proto-Sabana de Bogotá was externally drained to the Maracaibo region. More data are required, and therefore, it remains prudent to consider multiple hypotheses.

9.1.4. Middle Miocene Onset of the Magdalena River

Neogene provenance data suggest ongoing contributions from two different sources: The Central Cordillera to the west and the Santander Massif to the east (Caballero et al., 2013a; Horton et al., 2015; Reyes-Harker et al., 2015). The data suggest that the Magdalena Valley Basin (Figure 2) was no longer an internally drained basin based on seismic evidence for middle Miocene sedimentation above former barriers, although the seismic coverage is not robust enough to fully understand the 3D scenario.

Horton et al. (2015) suggest that the appearance of 100–0 Ma zircon grains and a regional switch to broad, multimodal age distributions reflect the late Miocene integration of

the longitudinal proto-Magdalena River, linking the Middle Magdalena Valley Basin to southern headwaters of the Upper Magdalena Valley. The presence of fully integrated Magdalena River draining toward its delta should be detected in contemporaneous deposits. Mora et al. (2018) suggest that delta plain sandstones, mudstones, and coals indicate the presence of a proto-Magdalena delta in the Lower Magdalena Valley by middle Miocene time. However, no data yet link these deposits to potential source areas of the Magdalena valley. Near the modern delta, sedimentary units of the proto-Magdalena River delta and Magdalena submarine fan yield a late Miocene to Pliocene age (Cadena & Slatt, 2013). It could be that a middle Miocene delta feeding the Lower Magdalena Valley was replaced with a larger late Miocene delta in its present location, which was fed by an expanded drainage network comparable to the modern Magdalena watershed.

In summary, present data cannot determine whether the onset of the Magdalena River delta occurred by middle or late Miocene times. Fortunately, Miocene sedimentary records for the Magdalena headwaters to the modern delta have been preserved, providing opportunities for further investigations to distinguish among the competing hypotheses.

9.2. Panamá Accretion and the Central America Seaway

The accretion of the Panamá–Chocó Terrane (Figure 1) to continental Colombia probably commenced in the early Miocene (Farris et al., 2011) with the complete accretion and closure of the Central American Seaway occurring by the middle to late Miocene (Duque–Caro, 1990; Montes et al., 2015) and later (e.g., O’Dea et al., 2016).

Recent studies show that the emergence of Panamá involved a long and complex process starting in the Oligocene (Farris et al., 2011; Sepulchre et al., 2014). Montes et al. (2015) proposed that the Miocene appearance of significant populations of Eocene age zircons (ca. 59 to ca. 42 Ma) near the San Jorge River (e.g., Figure 2a) suggests derivation from Panamá. These studies make a key argument for a middle Miocene closure of the seaway. However, Montes et al. (2015) proposal involves an irregular drainage geometry with sediment coming from a slightly emergent Panamá in the northwest and making a U–turn toward the Lower Magdalena Valley in contrast to the roughly rectilinear fluvial drainage network in the south (Chocó) with the same Panamanian signature. On the basis of such difficulties and of additional geological challenges (e.g., Babault et al., 2013; Silva et al., 2013), paleogeographic reconstructions of emerged land masses do not yet provide an unambiguous answer regarding the timing of the closure of the Central American Seaway. Therefore, it is important to consider alternative hypotheses and to acquire new data regarding the emergence of land masses and the closure of the Central American Seaway.

9.2.1. Cauca and San Jorge Rivers

Geologic data for the region near the Cauca and San Jorge Rivers (Figure 2) provide evidence of Miocene deformation and suggest that positive topography in the westernmost Andes served as source areas for these rivers (Montes et al., 2015; Villagómez & Spikings, 2013). However, it is virtually impossible to know the elevation and continuity of these emergent areas and whether precursors to the modern Cauca and San Jorge Rivers were already in place at the time. Regarding this point, Mora et al. (2018) propose a connection of the Lower Magdalena Valley to the Cauca valley as supported by middle Miocene provenance signatures and delta–plan facies for the Upper Member of the Amagá Formation (Montes et al., 2015; Piedrahita et al., 2017). The interpretation of ancestral rivers reaching the proto–Caribbean is speculative, but Mora et al. (2018) also suggest the presence of a Lower Amagá–Ciénaga de Oro delta by the late Oligocene – early Miocene based on provenance data (Montes et al., 2015), detrital zircon fission track thermochronology, and borehole facies analyses.

Mora et al. (2018) suggest that the first clear appearance of fluvial sedimentites in the Lower Magdalena Valley, Urabá, and

southern Sinú Basins was delayed until the Pliocene deposition of the Corpa Formation. The presence of uplifted regions to the south near the modern Cauca and San Jorge River valleys (Villagómez & Spikings, 2013; Piedrahita et al., 2017) may suggest an advancing pair of prograding river deltas by late Oligocene to middle Miocene time in the Lower Magdalena Valley with the appearance of proximal fluvial sedimentites by the Pliocene. This hypothesis provides an alternative explanation according to which Late Paleogene to Neogene rivers originated in the south rather than from an emergent Isthmus of Panamá. More evidence is needed to discriminate between a proto–Cauca and proto–San Jorge Rivers provenance from the south and U–shaped river drainage from Panamá.

9.3. Key Neogene Tectonic Events

The Neogene subduction of the Carnegie Ridge (Figure 1) in northern Ecuador and southern Colombia had important consequences for the geometry of the subducting slab and the post–middle Miocene uplift and exhumation of the northern Andes. Miocene tectonic events are largely responsible for the present–day topography of Colombia (described in section 7).

9.3.1. Late Cenozoic Surface Uplift in the Eastern Cordillera

The Eastern Cordillera of Colombia (Figure 2) is one of the few areas of the northern Andes with paleoelevation constraints. In one of the oldest studies on this topic, van der Hammen et al. (1973) argued, as later reinforced by others (e.g., Andriessen et al., 1993; Helmens & van der Hammen, 1994; Hooghiemstra, 1984; Hooghiemstra & van der Hammen, 1998; Hooghiemstra et al., 2006; Kroonenberg et al., 1990; Wijninga, 1996; Wijninga & Kuhry, 1990), that late Miocene vegetation records collected at high elevations in the Eastern Cordillera resemble modern tropical lowland regions adjacent to the Eastern Cordillera.

Based on ZFT age control for sedimentary host units (Andriessen et al., 1993), it has been suggested that topographic growth from elevations <1000 m to present >2500 m elevations took place between 6 and 3 Ma (Mora et al., 2008). A refined magnetostratigraphic chronology suggests roughly 1 km of elevation increase between 7.6 and 3 Ma (Anderson et al., 2016). Mora–Páez et al. (2016) further suggested that confining topographic growth to 6–3 Ma is too rapid when compared to extrapolated Global Position System (GPS) rates of shortening. Ultimately, the original proposal made by van der Hammen et al. (1973) of late Miocene topographic growth has been generally confirmed by subsequent studies (Anderson et al. (2016; Mora et al., 2008).

Despite these paleoelevation estimates, many studies suggest that deformation has been active and that thrust–induced denudation was in place in all areas of the current Eastern

Cordillera since roughly 25 Ma (Horton *et al.*, 2010a, 2010b; Mora *et al.*, 2010d, 2013a, 2013b; Nie *et al.*, 2010, 2012; Parra *et al.*, 2009b; Saylor *et al.*, 2011, 2012a, 2012b). This means that there was positive topography in the Eastern Cordillera, but the height of the mountains remains unclear. In other words, paleoelevation studies indicate that late Miocene topographic growth was finalized by 3 Ma (e.g., Wijninga, 1996; Anderson *et al.*, 2016), but given the Paleogene onset of shortening, we do not yet know when topographic growth commenced.

For the cases mentioned above, it is important to realize that the geological record is incomplete. For example, a lack of early to middle Miocene sedimentary records for the Eastern Cordillera (e.g., Ochoa *et al.*, 2012) precludes an assessment of paleoelevations for that time. Once again, such incomplete records suggest the need to consider multiple hypotheses.

9.4. Eastward Advance of the Orinoco River

Based on a detrital (U–Pb) zircon analysis, Escalona & Mann (2011) suggest an eastward advance of a proto–Orinoco River during the Cenozoic evolution of the northern Andes (Figure 2). This assessment was further refined by Reyes–Harker *et al.* (2015) and Mora *et al.* (2019) by correlating abundant new provenance data with exhumation in the Eastern Cordillera of Colombia. The main basis for this hypothesis is the presence of U–Pb ages inferred to originate from the orogen on the western side of the Llanos–Barinas Foreland Basin rather than from cratonic provenance. Although a provenance divide has been proposed by Reyes–Harker *et al.* (2015) and Mora *et al.* (2019) as the trace of a proto–Orinoco channel belt, further data are needed to reach a definitive conclusion.

9.5. Tectonic and Climatic Interactions

Mora *et al.* (2008) reported one of the youngest apatite fission track data sets of the Andes so far (Figures 2, 16). This set of Plio–Pleistocene ages postdates most topographic growth in the Eastern Cordillera of Colombia (e.g., Hooghiemstra *et al.*, 2006; Anderson *et al.*, 2016), yet coincides with faster deformation rates.

Mora *et al.* (2008) suggested that faster denudation rates may have promoted faster shortening rates during the latest Cenozoic. However, other studies have later demonstrated that rapid shortening occurred in zones of focused transpressional deformation, possibly independent of enhanced denudation (e.g., Bermúdez *et al.*, 2013; Graham *et al.*, 2018; Mora *et al.*, 2015a; Ramírez–Arias *et al.*, 2012). Although focused denudation helps, it is unlikely to be the single main factor in enhancing shortening rates. From this discussion, it appears that climate, precipitation, and associated denudation are important but not the principal factors that induce rapid motion along major faults, at least in the northern Andes.

10. Conclusions

In conclusion, although biologists and other scientists understandably desire high resolution data and finalized debates regarding various aspects of the paleogeography, none of the cases we have discussed in the northern Andes and Panamá be considered “solved,” and the current data are consistent with multiple hypotheses. In our view, the geological record has two main problems: (i) In many areas, erosion and general preservation factors render the record incomplete and spatially fragmented, and (ii) in those areas where it is complete, we do not have enough information.

Ideal new information would be 3D seismic data in marine areas, where the quality of the seismic images is high. In contrast, seismic exploration in the northern Andes has its own problems: (i) its quality is poor due to the problems caused by the presence of mountains and deformation interfering with acquisition of proper images; and (ii) seismic coverage is far from being dense. One of the few areas where geological data provide a very good picture of complete geological evolution with the resolution sought by biologists and other scientists is the North Sea in northern Europe (e.g., IHS, 2018).

While some data sets like thermochronology can provide precise information on the places being exhumed and eroded, provenance tools (U/Pb or to an even greater extent petrography) always allow for multiple interpretations regarding drainage directions and timing for fluvial networks. The Orinoco, Magdalena, and Cauca Rivers histories and the Panamá Isthmus history serve as clear examples of this ambiguity. Other studies linked to the Amazon are even more difficult.

Definitive statements regarding the growth of topography are made even more complex by the fact that topography is always destroyed, and thus far we have not considered or been able to detect paleo–elevations of the northern Andes for times preceding the Oligocene (ca. 33 Ma). While undocumented pre–Oligocene high mountains of the northern Andes are possible, it is also possible that Neogene relief features have been destroyed and rebuilt such that river trajectories and connections that we have never imagined may have existed. For example, we assume that the Garzón Massif was already a positive topographic area by the middle Miocene, separating the Orinoco and Amazonas Basins from the Magdalena River Basin. However, Perez–Consuegra *et al.* (2018) have found paleontological signals of Orinoco and Amazonas Rivers connections by the late Miocene in the San Jacinto belt.

In general, we can conclude that thermochronological techniques are the most precise of the three tools discussed here in achieving location–specific rates while provenance techniques are very ambiguous when geologists try to suggest the location of ancestral drainages. In the meantime, paleo–elevation studies of the northern Andes are still very experimental. With the data available, we can identify general patterns of the Eastern

Cordillera, but data on rates and ages can still be improved. To create robust reconstructions, it is necessary to combine bed rock exhumation data with provenance and paleo–elevation studies. Few studies have combined both or all three since the pioneering studies by Mora et al. (2008) and Parra et al (2009a).

In sum, while a number of aspects of Colombia's Cenozoic tectonic evolution remain unclear, our lack of paleogeographic knowledge is more severe. Furthermore, our understanding of Central and Western Cordilleras responses to different regional events is even more limited. Therefore, more detailed and systematic thermochronological data and provenance and paleo–elevation studies will be instrumental to geologists providing more precise answers and support for other disciplines. In the meantime, working with multiple hypotheses and never with rigid assumptions is the most convenient and robust approach.

References

- Aleman, A. & Ramos, V.A. 2000. Northern Andes. In: Cordani, U.G., Milani, E.J., Thomaz-Filho, A. & Campos, D.A. (editors), Tectonic evolution of South America. 31st International Geological Congress. Proceedings, p. 453–480. Rio de Janeiro, Brazil.
- Anderson, V.J., Saylor, J.E., Shanahan, T.M. & Horton, B.K. 2015. Paleoelevation records from lipid biomarkers: Application to the tropical Andes. *Geological Society of America Bulletin*, 127(11–12): 1604–1616. <https://doi.org/10.1130/B31105.1>
- Anderson, V.J., Horton, B.K., Saylor, J.E., Mora, A., Tesón, E., Breecker, D.O. & Ketcham, R.A. 2016. Andean topographic growth and basement uplift in southern Colombia: Implications for the evolution of the Magdalena, Orinoco, and Amazon River systems. *Geosphere*, 12(4): 1235–1256. <https://doi.org/10.1130/GES01294.1>
- Andriessen, P.A.M., Helmens, K.F., Hooghiemstra, H., Riezebos, P.A. & van der Hammen, T. 1993. Absolute chronology of the Pliocene – Quaternary sediment sequence of the Bogota area, Colombia. *Quaternary Science Reviews*, 12(7): 483–501. [https://doi.org/10.1016/0277-3791\(93\)90066-U](https://doi.org/10.1016/0277-3791(93)90066-U)
- Aspden, J.A., McCourt, W.J. & Brook, M. 1987. Geometrical control of subduction-related magmatism: The Mesozoic and Cenozoic plutonic history of western Colombia. *Journal of the Geological Society*, 144(6): 893–905. <https://doi.org/10.1144/gsjgs.144.6.0893>
- Babault, J., van den Driessche, J. & Teixell, A. 2013. Longitudinal to transverse drainage network evolution in the High Atlas (Morocco): The role of tectonics. *Tectonics*, 31(4): 1–15. <https://doi.org/10.1029/2011TC003015>
- Baby, P., Rivadeneira, M., Barragan, R. & Christophoul, F. 2013. Thick-skinned tectonics in the Oriente Foreland Basin of Ecuador. In: Nemčok, M., Mora, A. & Cosgrove, J.W. (editors), Thick-skinned-dominated orogens: From initial inversion to full accretion. Geological Society of London, Special Publication 377, p. 59–76. <https://doi.org/10.1144/SP377.1>
- Bacon, C.D., Mora, A., Wagner, W.L. & Jaramillo, C.A. 2012. Testing geological models of evolution of the Isthmus of Panama in a phylogenetic framework. *Botanical Journal of the Linnean Society*, 171(1): 287–300. <https://doi.org/10.1111/j.1095-8339.2012.01281.x>
- Baker, P.A., Fritz, S.C., Dick, C.W., Eckert, A.J., Horton, B.K., Manzoni, S., Ribas, C.C., Garzone, C.N. & Battisti, D.S. 2014. The emerging field of geogenomics: Constraining geological problems with genetic data. *Earth-Science Reviews*, 135: 38–47. <https://doi.org/10.1016/j.earscirev.2014.04.001>
- Bande, A., Horton, B.K., Ramírez, J.C., Mora, A., Parra, M. & Stockli, D.F. 2012. Clastic deposition, provenance, and sequence of Andean thrusting in the frontal Eastern Cordillera and Llanos Foreland Basin of Colombia. *Geological Society of America Bulletin*, 124(1–2): 59–76. <https://doi.org/10.1130/B30412.1>
- Bayona, G., Cardona, A., Jaramillo, C., Mora, A., Montes, C., Caballero, V., Mahecha, H., Lamus, F., Montenegro, O., Jiménez, G., Mesa, A. & Valencia, V. 2013. Onset of fault reactivation in the Eastern Cordillera of Colombia and proximal Llanos Basin; Response to Caribbean–South American convergence in early Palaeogene time. In: Nemčok, M., Mora, A. & Cosgrove, J.W. (editors), Thick-skin-dominated orogens: From initial inversion to full accretion. Geological Society of London, Special Publication 377, p. 285–314. London. <https://doi.org/10.1144/SP377.5>
- Bermúdez, M.A., van der Beek, P. & Bernet, M. 2013. Strong tectonic and weak climatic control on exhumation rates in the Venezuelan Andes. *Lithosphere*, 5(1): 3–16. <https://doi.org/10.1130/L212.1>
- Caballero, V., Parra, M. & Mora-Hohórquez, A.R. 2010. Levantamiento de la cordillera Oriental de Colombia durante el Eoceno tardío–Oligoceno temprano: Proveniencia sedimentaria en el Sinclinal de Nuevo Mundo, Cuenca Valle Medio del Magdalena. *Boletín de Geología*, 32(1): 45–77.
- Caballero, V., Mora, A., Quintero, I., Blanco, V., Parra, M., Rojas, L.E., López, C., Sánchez, N., Horton, B.K., Stockli, D. & Duddy, I. 2013a. Tectonic controls on sedimentation in an intermontane hinterland basin adjacent to inversion structures: The Nuevo Mundo Syncline, Middle Magdalena Valley, Colombia. In: Nemčok, M., Mora, A. & Cosgrove, J.W. (editors), Thick-skin-dominated orogens: From initial inversion to full accretion. Geological Society of London, Special Publication 377, p. 315–342. London. <https://doi.org/10.1144/SP377.12>
- Caballero, V., Parra, M., Mora, A., López, C., Rojas, L.E. & Quintero, I. 2013b. Factors controlling selective abandonment and reactivation in thick-skin orogens: A case study in the Magdalena valley, Colombia. In: Nemčok, M., Mora, A. & Cosgrove, J.W. (editors), Thick-skin-dominated orogens: From initial inversion to full accretion. Geological Society of London, Special Publication 377, p. 343–367. London. <https://doi.org/10.1144/SP377.4>

- Cadena, A.F. & Slatt, R.M. 2013. Seismic and sequence stratigraphic interpretation of the area of influence of the Magdalena submarine fan, offshore northern Colombia. *Interpretation*, 1(1): SA53–SA74. <https://doi.org/10.1190/INT-2013-0028.1>
- Carrillo, E., Mora, A., Ketcham, R.A., Amoroch, R., Parra, M., Constantino, D., Robles, W., Avellaneda, W., Carvajal, J.S., Corcione, M.F., Bello, W., Figueroa, J.D., Gómez, J.F., González, J.L., Quandt, D., Reyes, M., Rangel, A.M., Román, I., Pelayo, Y. & Porras, J. 2016. Movement vectors and deformation mechanisms in kinematic restorations: A case study from the Colombian Eastern Cordillera. *Interpretation*, 4(1): T31–T48. <https://doi.org/10.1190/INT-2015-0049.1>
- Cochrane, R., Spikings, R., Gerdes, A., Ulianov, A., Mora, A., Villagómez, D., Putlitz, B. & Chiaradia, M. 2014. Permo–Triassic anatexis, continental rifting and the disassembly of western Pangaea. *Lithos*, 190–191: 383–402. <https://doi.org/10.1016/j.lithos.2013.12.020>
- Cooper, M.A., Addison, F.T., Álvarez, R., Coral, M., Graham, R.H., Hayward, A.B., Howe, S., Martínez, J., Naar, J., Peñas, R., Pulham, A.J. & Taborda, A. 1995. Basin development and tectonic history of the Llanos Basin, Eastern Cordillera, and Middle Magdalena Valley, Colombia. *American Association of Petroleum Geologists Bulletin*, 79(10): 1421–1443.
- Cordani, U.G., Cardona, A., Jiménez, D.M., Liu, D. & Nutman, A.P. 2005. Geochronology of Proterozoic basement inliers in the Colombian Andes: Tectonic history of remnants of a fragmented Grenville belt. In: Vaughan, A.P.M., Leat, P.T. & Pankhurst, R.J. (editors), *Terrane processes at the margins of Gondwana*. Geological Society of London, Special Publication 246, p. 329–346. London. <https://doi.org/10.1144/GSL.SP.2005.246.01.13>
- Cuervo–Gómez, A., Pérez–Consuegra, N. & Lamus–Ochoa, F. 2015. Levantamiento de la cordillera Oriental de los Andes colombianos. *Hipótesis*, Apuntes Científicos Uniandinos, 19: 68–73.
- Dengo, C. & Covey, M. 1993. Structure of the Eastern Cordillera of Colombia: Implications for trap styles and regional tectonics. *American Association of Petroleum Geologists Bulletin*, 77(8): 1315–1337. <https://doi.org/10.1306/BDF8E7A-1718-11D7-8645000102C1865D>
- Duque–Caro, H. 1990. The Choco Block in the northwestern corner of South America: Structural, tectonostratigraphic, and paleogeographic implications. *Journal of South American Earth Sciences*, 3(1): 71–84. [https://doi.org/10.1016/0895-9811\(90\)90019-W](https://doi.org/10.1016/0895-9811(90)90019-W)
- England, P. & Molnar, P. 1990. Surface uplift, uplift of rocks, and exhumation of rocks. *Geology*, 18(12): 1173–1177. [https://doi.org/10.1130/0091-7613\(1990\)018<1173:SUUORA>2.3.CO;2](https://doi.org/10.1130/0091-7613(1990)018<1173:SUUORA>2.3.CO;2)
- Escalona, A. & Mann, P. 2011. Tectonics, basin subsidence mechanisms, and paleogeography of the Caribbean–South American Plate boundary zone. *Marine and Petroleum Geology*, 28(1): 8–39. <https://doi.org/10.1016/j.marpetgeo.2010.01.016>
- Farris, D.W., Jaramillo, C., Bayona, G., Restrepo–Moreno, S.A., Montes, C., Cardona, A., Mora, A., Speakman, R.J., Glascock, M.D. & Valencia, V. 2011. Fracturing of the Panamanian Isthmus during initial collision with South America. *Geology*, 39(11): 1007–1010. <https://doi.org/10.1130/G32237.1>
- Flowers, R.M., Ketcham, R.A., Shuster, D.L. & Farley, K.A. 2009. Apatite (U–Th)/He thermochronometry using a radiation damage accumulation and annealing model. *Geochimica et Cosmochimica Acta*, 73(8): 2347–2365. <https://doi.org/10.1016/j.gca.2009.01.015>
- Gansser, A. 1973. Facts and theories on the Andes. *Journal of the Geological Society of London*, 129(2): 93–131. <https://doi.org/10.1144/gsjgs.129.2.0093>
- Garzone, C.N., McQuarrie, N., Perez, N.D., Ehlers, T.A., Beck, S.L., Kar, N., Eichelberger, N., Chapman, A.D., Ward, K.M., Ducea, M.N., Lease, R.O., Poulsen, C.J., Wagner, L.S., Saylor, J.E., Zandt, G. & Horton, B.K. 2017. Tectonic evolution of the Central Andean Plateau and implications for the growth of plateaus. *Annual Review of Earth and Planetary Sciences*, 45(1): 529–559. <https://doi.org/10.1146/annurev-earth-063016-020612>
- Gómez, E., Jordan, T., Allmendinger, R., Hegarty, K., Kelly, S. & Heizler, M. 2003. Controls on architecture of the Late Cretaceous to Cenozoic southern Middle Magdalena Valley Basin, Colombia. *Geological Society of America Bulletin*, 115(2): 131–147. [https://doi.org/10.1130/0016-7606\(2003\)115<0131:COAOTL>2.0.CO;2](https://doi.org/10.1130/0016-7606(2003)115<0131:COAOTL>2.0.CO;2)
- Gómez, E., Jordan, T.E., Allmendinger, R.W., Hegarty, K. & Kelley, S. 2005. Syntectonic Cenozoic sedimentation in the northern Middle Magdalena Valley Basin of Colombia and implications for exhumation of the northern Andes. *Geological Society of America Bulletin*, 117(5–6): 547–569. <https://doi.org/10.1130/B25454.1>
- Gómez, J., Nivia, Á., Montes, N.E., Jiménez, D.M., Tejada, M.L., Sepúlveda, M.J., Osorio, J.A., Gaona, T., Diederix, H., Uribe, H. & Mora, M., compilers. 2007. Geological map of Colombia 2007. Scale 1:1 000 000. Ingeominas, 2 sheets. Bogotá.
- Graham, C.H., Parra, M., Mora, A. & Higuera, C. 2018. The interplay between geological history and ecology in mountains. In: Hoorn, C., Perrigo, A. & Antonelli, A. (editors), *Mountains, climate and biodiversity*. John Wiley & Sons Ltd, p. 231–244. Oxford, UK.
- Helmens, K.F. & van der Hammen, T. 1994. The Pliocene and Quaternary of the High Plain of Bogotá, Colombia: A history of tectonic uplift, basin development and climatic change. *Quaternary International*, 21: 41–61. [https://doi.org/10.1016/1040-6182\(94\)90020-5](https://doi.org/10.1016/1040-6182(94)90020-5)
- Hooghiemstra, H. 1984. Vegetational and climatic history of the High Plain of Bogotá, Colombia. Doctoral thesis, University of Amsterdam, 368 p. Amsterdam, the Netherlands.
- Hooghiemstra, H. & van der Hammen, T. 1998. Neogene and Quaternary development of the Neotropical rain forest: The forest

- refugia hypothesis, and a literature overview. *Earth–Science Reviews*, 44(3–4): 147–183. [https://doi.org/10.1016/S0012-8252\(98\)00027-0](https://doi.org/10.1016/S0012-8252(98)00027-0)
- Hooghiemstra, H., Wijninga, V.M. & Cleef, A.M. 2006. The paleobotanical record of Colombia: Implications for biogeography and biodiversity. *Annals of the Missouri Botanical Garden*, 93(2): 297–325. [https://doi.org/10.3417/0026-6493\(2006\)93\[297:T-PROCI\]2.0.CO;2](https://doi.org/10.3417/0026-6493(2006)93[297:T-PROCI]2.0.CO;2)
- Horton, B.K. 1999. Erosional control on the geometry and kinematics of thrust belt development in the central Andes. *Tectonics*, 18(6): 1292–1304. <https://doi.org/10.1029/1999TC900051>
- Horton, B.K. 2018a. Sedimentary record of Andean mountain building. *Earth–Science Reviews*, 178: 279–309. <https://doi.org/10.1016/j.earscirev.2017.11.025>
- Horton, B.K. 2018b. Tectonic regimes of the central and southern Andes: Responses to variations in plate coupling during subduction. *Tectonics*, 37(2): 402–429. <https://doi.org/10.1002/2017TC004624>
- Horton, B.K., Parra, M., Saylor, J.E., Nie, J., Mora, A., Torres, V., Stockli, D.F. & Strecker, M.R. 2010a. Resolving uplift of the northern Andes using detrital zircon age signatures. *GSA Today*, 20(7): 4–10. <https://doi.org/10.1130/GSATG76A.1>
- Horton, B.K., Saylor, J.E., Nie, J., Mora, A., Parra, M., Reyes–Harker, A. & Stockli, D.F. 2010b. Linking sedimentation in the northern Andes to basement configuration, Mesozoic extension, and Cenozoic shortening: Evidence from detrital zircon U–Pb ages, Eastern Cordillera, Colombia. *Geological Society of America Bulletin*, 122(9–10): 1423–1442. <https://doi.org/10.1130/B30118.1>
- Horton, B.K., Pérez, N.D., Fitch, J.D. & Saylor, J.E. 2015. Punctuated shortening and subsidence in the Altiplano Plateau of southern Peru: Implications for early Andean mountain building. *Lithosphere*, 7(2): 117–137. <https://doi.org/10.1130/L397.1>
- Horton, B.K., Parra, M. & Mora, A. 2020. Construction of the Eastern Cordillera of Colombia: Insights from the sedimentary record. In: Gómez, J. & Mateus–Zabala, D. (editors), *The Geology of Colombia, Volume 3 Paleogene – Neogene*. Servicio Geológico Colombiano, Publicaciones Geológicas Especiales 37, p. 67–88. Bogotá. <https://doi.org/10.32685/pub.esp.37.2019.03>
- Ibañez–Mejía, M., Pullen, A., Arenstein, J., Gehrels, G., Valley, J., Ducea, M., Mora, A., Pecha, M. & Ruiz, J. 2015. Unraveling crustal growth and reworking processes in complex zircons from orogenic lower–crust: The Proterozoic Putumayo Orogen of Amazonia. *Precambrian Research*, 267: 285–310. <https://doi.org/10.1016/j.precamres.2015.06.014>
- IHS. 2018. IHS Markit. <https://ihsmarkit.com/products/oil-gas-reference-materials.html>. (consulted in August 2018).
- Kerr, A.C., Marriner, G.F., Tarney, J., Nivia, Á., Saunders, A.D., Thirlwall, M.F. & Sinton, C.W. 1997. Cretaceous basaltic terranes in western Colombia: Elemental, chronological and Sr–Nd isotopic constraints on petrogenesis. *Journal of Petrology*, 38(6): 677–702. <https://doi.org/10.1093/petrology/38.6.677>
- Ketcham, R.A., Donelick, R.A. & Carlson, W.D. 1999. Variability of apatite fission–track annealing kinetics: III. Extrapolation to geological time scales. *American Mineralogist*, 84(9): 1235–1255. <https://doi.org/10.2138/am-1999-0903>
- Ketcham, R.A., Carter, A., Donelick, R.A., Barbarand, J. & Hurford, A.J. 2007. Improved modeling of fission–track annealing in apatite. *American Mineralogist*, 92(5–6): 799–810. <https://doi.org/10.2138/am.2007.2281>
- Ketcham, R.A., Mora, A. & Parra, M. 2018. Deciphering exhumation and burial history with multi–sample down–well thermochronometric inverse modelling. *Basin Research*, 30(S1): 48–64. <https://doi.org/10.1111/bre.12207>
- Kroonenberg, S.B., Bakker, J.G.M. & van der Wiel, A.M. 1990. Late Cenozoic uplift and paleogeography of the Colombian Andes: Constraints on the development of high–Andean biota. *Geologie en Mijnbouw*, 69(3): 279–290.
- Litherland, M., Aspden, J.A. & Jemielita, R.A. 1994. The metamorphic belts of Ecuador. Overseas Memoir of the British Geological Survey 11, 147 p. Nottingham, England.
- Lonsdale, P. 2005. Creation of the Cocos and Nazca Plates by fission of the Farallon Plate. *Tectonophysics*, 404(3–4): 237–264. <https://doi.org/10.1016/j.tecto.2005.05.011>
- Martens, U., Restrepo, J.J., Ordóñez–Carmona, O. & Correa–Martínez, A.M. 2014. The Tahamí and Anaconda Terranes of the Colombian Andes: Missing links between the South American and Mexican Gondwana margins. *The Journal of Geology*, 122(5): 507–530. <https://doi.org/10.1086/677177>
- Martin–Gombojav, N. & Winkler, W. 2008. Recycling of Proterozoic crust in the Andean Amazon Foreland of Ecuador: Implications for orogenic development of the northern Andes. *Terra Nova*, 20(1): 22–31. <https://doi.org/10.1111/j.1365-3121.2007.00782.x>
- Masek, J.G., Isacks, B.L., Gubbels, T.L. & Fielding, E.J. 1994. Erosion and tectonics at the margins of continental plateaus. *Journal of Geophysical Research; Solid Earth*, 99(B7): 13941–13956. <https://doi.org/10.1029/94JB00461>
- McCourt, W.J., Aspden, J.A. & Brook, M. 1984. New geological and geochronological data from the Colombian Andes: Continental growth by multiple accretion. *Journal of the Geological Society*, 141(5): 831–845. <https://doi.org/10.1144/gsjgs.141.5.0831>
- Mégard, F. 1989. The evolution of the Pacific Ocean margin in South America north of Arica elbow (18° S). In: Ben–Avraham, Z. (editor), *The evolution of the Pacific Ocean margins*. Oxford Monographs on Geology and Geophysics. Oxford University Press, p. 208–230. New York.
- Montes, C., Cardona, A., Jaramillo, C., Pardo, A., Silva, J.C., Valencia, V., Ayala, C., Pérez–Ángel, L.C., Rodríguez–Parra, L.A., Ramírez, V. & Niño, H. 2015. Middle Miocene closure of the Central American Seaway. *Science*, 348(6231): 226–229. <https://doi.org/10.1126/science.aaa2815>
- Montgomery, D.R., Balco, G. & Willet, S.D. 2001. Climate, tectonics and the morphology of the Andes. *Geology*, 29(7): 579–582.

- [https://doi.org/10.1130/0091-7613\(2001\)029<0579:CTAT-MO>2.0.CO;2](https://doi.org/10.1130/0091-7613(2001)029<0579:CTAT-MO>2.0.CO;2)
- Mora, A. 2015. Petroleum systems of the Eastern Cordillera, foothill basins, and associated Llanos Basin: Impacts on the prediction of large scale foreland and foothill petroleum accumulations. *American Association of Petroleum Geologists Bulletin*, 99(8): 1401–1406. <https://doi.org/10.1306/bltnintro032615>
- Mora, A., Parra, M., Strecker, M.R., Kammer, A., Dimaté, C. & Rodríguez, F. 2006. Cenozoic contractional reactivation of Mesozoic extensional structures in the Eastern Cordillera of Colombia. *Tectonics*, 25(2): 19 p. <https://doi.org/10.1029/2005TC001854>
- Mora, A., Parra, M., Strecker, M.R., Sobel, E.R., Hooghiemstra, H., Torres, V. & Vallejo-Jaramillo, J. 2008. Climatic forcing of asymmetric orogenic evolution in the Eastern Cordillera of Colombia. *Geological Society of America Bulletin*, 120(7–8): 930–949. <https://doi.org/10.1130/B26186.1>
- Mora, A., Gaona, T., Kley, J., Montoya, D., Parra, M., Quiroz, L.I., Reyes, G. & Strecker, M. 2009. The role of inherited extensional fault segmentation and linkage in contractional orogenesis: A reconstruction of Lower Cretaceous inverted rift basins in the Eastern Cordillera of Colombia. *Basin Research*, 21(1): 111–137. <https://doi.org/10.1111/j.1365-2117.2008.00367.x>
- Mora, A., Horton, B.K., Mesa, A., Rubiano, J., Ketcham, R.A., Parra, M., Blanco, V., Garcia, D. & Stockli, D.F. 2010a. Migration of Cenozoic deformation in the Eastern Cordillera of Colombia interpreted from fission track results and structural relationships: Implications for petroleum systems. *American Association of Petroleum Geologists Bulletin*, 94(10): 1543–1580. <https://doi.org/10.1306/01051009111>
- Mora, A., Baby, P., Roddaz, M., Parra, M., Brusset, S., Hermoza, W. & Espurt, N. 2010b. Tectonic history of the Andes and sub-Andean zones: Implications for the development of the Amazon drainage basin. In: Hoorn, C. & Wesselingh, F.P. (editors), *Amazonia: Landscape and species evolution: A look into the past*. Wiley–Blackwell, John Wiley & Sons Ltd., Publication, p. 38–60. Chichester, UK. <https://doi.org/10.1002/9781444306408.ch4>
- Mora, A., Parra, M., Strecker, M.R., Sobel, E.R., Zeilinger, G., Jaramillo, C., Ferreira Da Silva, S. & Blanco, M. 2010c. The Eastern Foothills of the Eastern Cordillera of Colombia: An example of multiple factors controlling structural styles and active tectonics. *Geological Society of America Bulletin*, 122(11–12): 1846–1864. <https://doi.org/10.1130/B30033.1>
- Mora, J.A., Mantilla, M. & de Freitas, M. 2010d. Cretaceous paleogeography and sedimentation in the Upper Magdalena and Putumayo Basins, southwestern Colombia. *American Association of Petroleum Geologists, International Conference and Exhibition*. Abstract, 11 p. *American Association of Petroleum Geologists, Search and Discovery Article #50246*. Rio de Janeiro, Brazil.
- Mora, A., Reyes–Harker, A., Rodríguez, G., Tesón, E., Ramírez–Arias, J.C., Parra, M., Caballero, V., Mora, J.P., Quintero, I., Valencia, V., Ibañez–Mejía, M., Horton, B.K. & Stockli, D.F. 2013a. Inversion tectonics under increasing rates of shortening and sedimentation: Cenozoic example from the Eastern Cordillera of Colombia. In: Nemčok, M., Mora, A. & Cosgrove, J.W. (editors), *Thick-skin-dominated orogens: From initial inversion to full accretion*. Geological Society of London, Special Publication 377, p. 411–442. London. <https://doi.org/10.1144/SP377.6>
- Mora, A., Blanco, V., Naranjo, J., Sanchez, N., Ketcham, R.A., Rubiano, J., Stockli, D.F., Quintero, I., Nemčok, M., Horton, B.K. & Davila, H. 2013b. On the lag time between internal strain and basement involved thrust induced exhumation: The case of the Colombian Eastern Cordillera. *Journal of Structural Geology*, 52: 96–118. <https://doi.org/10.1016/j.jsg.2013.04.001>
- Mora, A., Ketcham, R.A., Higuera–Díaz, I.C., Bookhagen, B., Jimenez, L. & Rubiano, J. 2014. Formation of passive–roof duplexes in the Colombian subandes and Perú. *Lithosphere*, 6(6): 456–472. <https://doi.org/10.1130/L340.1>
- Mora, A., Parra, M., Rodríguez–Forero, G., Blanco, V., Moreno, N., Caballero, V., Stockli, D.F., Duddy, I. & Ghorbal, B. 2015a. What drives orogenic asymmetry in the northern Andes? A case study from the apex of the northern Andean orocline. In: Bartolini, C. & Mann, P. (editors), *Petroleum geology and potential of the Colombian Caribbean margin*. American Association of Petroleum Geologists, Memoir 108, p. 547–586. <https://doi.org/10.1306/13531949M1083652>
- Mora, A., Casallas, W., Ketcham, R.A., Gómez, D., Parra, M., Namson, J., Stockli, D., Almendral, A., Robles, W. & Ghorbal, B. 2015b. Kinematic restoration of contractional basement structures using thermokinematic models: A key tool for petroleum system modeling. *American Association of Petroleum Geologists Bulletin*, 99(8): 1575–1598. <https://doi.org/10.1306/04281411108>
- Mora, J.A., Oncken, O., Le Breton, E., Mora, A., Veloza, G., Vélez, V. & de Freitas, M. 2018. Controls on forearc basin formation and evolution: Insights from Oligocene to recent tectono–stratigraphy of the Lower Magdalena Valley Basin of northwest Colombia. *Marine and Petroleum Geology*, 97: 288–310. <https://doi.org/10.1016/j.marpetgeo.2018.06.032>
- Mora, A., García–Bautista, D.F., Reyes–Harker, A., Parra, M., Blanco, V., Sánchez, N., De la Parra, F., Caballero, V., Rodríguez, G., Ruiz, C., Naranjo, J., Tesón, E., Niño, F., Quintero, I., Moreno, N., Cardozo, E., Gamba, N., Horton, B.K. & Arias–Martínez, J.P. 2019. Tectonic evolution of petroleum systems within the onshore Llanos Basin: Insights on the presence of Orinoco heavy oil analogues in Colombia and a comparison with other heavy oil provinces worldwide. *American Association of Petroleum Geologists Bulletin*, 103(5): 1178–1224. <https://doi.org/10.1306/1003181611417236>
- Mora–Páez, H., Mencin, D.J., Molnar, P., Diederix, H., Cardona–Piedrahita, L., Peláez–Gaviria, J.R. & Corchuelo–Cuervo, Y. 2016. GPS velocities and the construction of the Eastern Cor-

- dillera of the Colombian Andes. *Geophysical Research Letters*, 43(16): 8407–8416. <https://doi.org/10.1002/2016GL069795>
- Nie, J., Horton, B.K., Mora, A., Saylor, J.E., Housh, T.B., Rubiano, J. & Naranjo, J. 2010. Tracking exhumation of Andean ranges bounding the Middle Magdalena Valley Basin, Colombia. *Geology*, 38(5): 451–454. <https://doi.org/10.1130/G30775.1>
- Nie, J., Horton, B.K., Saylor, J.E., Mora, A., Mange, M., Garziona, C.N., Basu, A., Moreno, C.J., Caballero, V. & Parra, M. 2012. Integrated provenance analysis of a convergent retroarc foreland system: U–Pb ages, heavy minerals, Nd isotopes, and sandstone compositions of the Middle Magdalena Valley Basin, northern Andes, Colombia. *Earth–Science Reviews*, 110(1–4): 111–126. <https://doi.org/10.1016/j.earscirev.2011.11.002>
- Ochoa, D., Hoorn, C., Jaramillo, C., Bayona, G., Parra, M. & De la Parra, F. 2012. The final phase of tropical lowland conditions in the axial zone of the Eastern Cordillera of Colombia: Evidence from three palynological records. *Journal of South American Earth Sciences*, 39: 157–169. <https://doi.org/10.1016/j.jsames.2012.04.010>
- O’Dea, A., Lessios, H.A., Coates, A.G., Eytan, R.I., Restrepo–Moreno, S., Cione, A.L., Collins, L.S., de Queiroz, A., Farris, D.W., Norris, R.D., Stallard, R.F., Woodburne, M.O., Aguilera, O., Aubry, M.–P., Berggren, W.A., Budd, A.F., Cozzuol, M.A., Coppard, S.E., Duque–Caro, H., Finnegan, S., Gasparini, G.M., Grossman, E.L., Johnson, K.G., Keigwin, L.D., Knowlton, N., Leigh, E.G., Leonard–Pingel, J.S., Marko, P.B., Pyenson, N.D., Rachello–Dolmen, P.G., Soibelzon, E., Soibelzon, L., Todd, J.A., Vermeij, G.J. & Jackson, J.B.C. 2016. Formation of Isthmus of Panama. *Science Advances*, 2(8): 1–11. <https://doi.org/10.1126/sciadv.1600883>
- Parra, M., Mora, A., Jaramillo, C., Strecker, M.R., Sobel, E.R., Quiroz, L., Rueda, M. & Torres, V. 2009a. Orogenic wedge advance in the northern Andes: Evidence from the Oligocene – Miocene sedimentary record of the Medina Basin, Eastern Cordillera, Colombia. *Geological Society of America Bulletin*, 121(5–6): 780–800. <https://doi.org/10.1130/B26257.1>
- Parra, M., Mora, A., Sobel, E.R., Strecker, M.R. & González, R. 2009b. Episodic orogenic front migration in the northern Andes: Constraints from low–temperature thermochronology in the Eastern Cordillera, Colombia. *Tectonics*, 28(4), 27 p. <https://doi.org/10.1029/2008TC002423>
- Parra, M., Mora, A., Jaramillo, C., Torres, V., Zeilinger, G. & Strecker, M.R. 2010. Tectonic controls on Cenozoic foreland basin development in the north–eastern Andes, Colombia. *Basin Research*, 22(6): 874–903. <https://doi.org/10.1111/j.1365-2117.2009.00459.x>
- Parra, M., Mora, A., López, C., Rojas, L.E. & Horton, B.K. 2012. Detecting earliest shortening and deformation advance in thrust belt hinterlands: Example from the Colombian Andes. *Geology*, 40(2): 175–178. <https://doi.org/10.1130/G32519.1>
- Pérez–Consuegra, N., Parra, M., Jaramillo, C., Silvestro, D., Echeverri, S., Montes, C., Jaramillo, J.M. & Escobar, J. 2018. Provenance analysis of the Pliocene Ware Formation in the Guajira Peninsula, northern Colombia: Paleodrainage implications. *Journal of South American Earth Sciences*, 81: 66–77. <https://doi.org/10.1016/j.jsames.2017.11.002>
- Piedrahita, V.A., Bernet, M., Chadima, M., Sierra, G.M., Marín–Cerón, M.I. & Toro, G.E. 2017. Detrital zircon fission–track thermochronology and magnetic fabric of the Amagá Formation (Colombia): Intracontinental deformation and exhumation events in the northwestern Andes. *Sedimentary Geology*, 356: 26–42. <https://doi.org/10.1016/j.sedgeo.2017.05.003>
- Pirave, A., Pinzón, E., Kammer, A., Bernet, M. & von Quadt, A. 2018. Early Neogene unroofing of the Sierra Nevada de Santa Marta, as determined from detrital geothermochronology and the petrology of clastic basin sediments. *Geological Society of America Bulletin*, 130(3–4): 355–380. <https://doi.org/10.1130/B31676.1>
- Ramírez–Arias, J.C., Mora, A., Rubiano, J., Duddy, I., Parra, M., Moreno, N., Stockli, D. & Casallas, W. 2012. The asymmetric evolution of the Colombian Eastern Cordillera. Tectonic inheritance or climatic forcing? New evidence from thermochronology and sedimentology. *Journal of South American Earth Sciences*, 39: 112–137. <https://doi.org/10.1016/j.jsames.2012.04.008>
- Ramos, V.A. 2009. Anatomy and global context of the Andes: Main geologic features and the Andean orogenic cycle. In: Kay, S.M., Ramos, V.A. & Dickinson, W.R. (editors), *Backbone of the Americas: Shallow subduction, plateau uplift, and ridge and terrane collision*. Geological Society of America, Memoirs 204, p. 31–65. [https://doi.org/10.1130/2009.1204\(02\)](https://doi.org/10.1130/2009.1204(02))
- Ramos, V.A. & Aleman, A. 2000. Tectonic evolution of the Andes. In: Cordani, U.G., Milani, E.J., Thomaz–Filha, A. & Campos, D.A. (editors), *Tectonic evolution of South America*. 31st International Geological Congress. Proceedings, p. 635–685. Rio de Janeiro, Brazil.
- Reiners, P.W., Spell, T.L., Nicolescu, S. & Zanetti, K.A. 2004. Zircon (U–Th)/He thermochronometry: He diffusion and comparisons with ⁴⁰Ar/³⁹Ar dating. *Geochimica et Cosmochimica Acta*, 68(8): 1857–1887. <https://doi.org/10.1016/j.gca.2003.10.021>
- Restrepo–Moreno, S.A., Foster, D.A., Stockli, D.F. & Parra–Sánchez, L.N. 2009. Long–term erosion and exhumation of the “Altiplano Antioqueño”, northern Andes, Colombia, from apatite (U–Th)/He thermochronology. *Earth and Planetary Science Letters*, 278(1–2): 1–12. <https://doi.org/10.1016/j.epsl.2008.09.037>
- Restrepo–Pace, P.A., Ruiz, J., Gehrels, G. & Cosca, M. 1997. Geochronology and Nd isotopic data of Grenville–age rocks in the Colombian Andes: New constraints for late Proterozoic – early Paleozoic paleocontinental reconstructions of the Americas. *Earth and Planetary Science Letters*, 150(3–4): 427–441. [https://doi.org/10.1016/S0012-821X\(97\)00091-5](https://doi.org/10.1016/S0012-821X(97)00091-5)
- Restrepo–Pace, P.A., Colmenares, F., Higuera, C. & Mayorga, M. 2004. A fold–and–thrust belt along the western flank of the Eastern

- Cordillera of Colombia—Style, kinematics, and timing constraints derived from seismic data and detailed surface mapping. In: McClay, K.R. (editor), Thrust tectonics and hydrocarbon systems. American Association of Petroleum Geologists, Memoir 82, p. 598–613. <https://doi.org/10.1306/M82813C31>
- Reyes–Harker, A., Ruiz–Valdivieso, C.F., Mora, A., Ramírez–Arias, J.C., Rodríguez, G., de la Parra, F., Caballero, V., Parra, M., Moreno, N., Horton, B.K., Saylor, J.E., Silva, A., Valencia, V., Stockli, D. & Blanco, V. 2015. Cenozoic paleogeography of the Andean Foreland and retroarc hinterland of Colombia. American Association of Petroleum Geologists Bulletin, 99(8): 1407–1453. <https://doi.org/10.1306/06181411110>
- Rodríguez–Forero, G., Oboh–Ikuenobe, F.E., Jaramillo–Munoz, C., Rueda–Serrano, M.J. & Cadena–Rueda, E. 2012. Palynology of the Eocene Esmeraldas Formation, Middle Magdalena Valley Basin, Colombia. Palynology, 36(Supplement 1): 96–111. <https://doi.org/10.1080/01916122.2012.650548>
- Saylor, J.E. & Horton, B.K. 2014. Nonuniform surface uplift of the Andean Plateau revealed by deuterium isotopes in Miocene volcanic glass from southern Peru. Earth and Planetary Science Letters, 387: 120–131. <http://dx.doi.org/10.1016/j.epsl.2013.11.015>
- Saylor, J.E., Horton, B.K., Nie, J., Corredor, J. & Mora, A. 2011. Evaluating foreland basin partitioning in the northern Andes using Cenozoic fill of the Floresta Basin, Eastern Cordillera, Colombia. Basin Research, 23(4): 377–402. <https://doi.org/10.1111/j.1365-2117.2010.00493.x>
- Saylor, J.E., Horton, B.K., Stockli, D.F., Mora, A. & Corredor, J. 2012a. Structural and thermochronological evidence for Paleogene basement-involved shortening in the axial Eastern Cordillera, Colombia. Journal of South American Earth Sciences, 39: 202–215. <https://doi.org/10.1016/j.jsames.2012.04.009>
- Saylor, J.E., Stockli, D.F., Horton, B.K., Nie, J. & Mora, A. 2012b. Discriminating rapid exhumation from syndepositional volcanism using detrital zircon double dating: Implications for the tectonic history of the Eastern Cordillera, Colombia. Geological Society of America Bulletin, 124(5–6): 762–779. <https://doi.org/10.1130/B30534.1>
- Saylor, J.E., Knowles, J.N., Horton, B.K., Nie, J. & Mora, A. 2013. Mixing of source populations recorded in detrital zircon U–Pb age spectra of modern river sands. The Journal of Geology, 121(1): 17–33. <https://doi.org/10.1086/668683>
- Sepulchre, P., Arsouze, T., Donnadieu, Y., Dutay, J.C., Jaramillo, C., Le Bras, J., Martin, E., Montes, C. & Waite, A.J. 2014. Consequences of shoaling of the Central American Seaway determined from modeling Nd isotopes. Paleoceanography and Paleoclimatology, 29(3): 176–189. <https://doi.org/10.1002/2013PA002501>
- Silva, A., Mora, A., Caballero, V., Rodríguez, G., Ruiz, C., Moreno, N., Parra, M., Ramírez–Arias, J.C., Ibañez–Mejía, M. & Quintero, I. 2013. Basin compartmentalization and drainage evolution during rift inversion: Evidence from the Eastern Cordillera of Colombia. In: Nemčok, M., Mora, A. & Cosgrove, J.W. (editors), Thick-skin-dominated orogens: From initial inversion to full accretion. Geological Society of London, Special Publication 377, p. 369–409. London. <https://doi.org/10.1144/SP377.15>
- Sinton, C.W., Duncan, R.A., Storey, M., Lewis, J. & Estrada, J.J. 1998. An oceanic flood basalt province within the Caribbean Plate. Earth and Planetary Science Letters, 155(3–4): 221–235. [https://doi.org/10.1016/S0012-821X\(97\)00214-8](https://doi.org/10.1016/S0012-821X(97)00214-8)
- Sobel, E.R., Hilley, G.E. & Strecker, M.R. 2003. Formation of internally drained contractional basins by aridity-limited bedrock incision. Journal of Geophysical Research: Solid Earth, 108(B7): 1–23. <https://doi.org/10.1029/2002JB001883>
- Spikings, R., Seward, D., Winkler, W. & Ruiz, G.M. 2000. Low-temperature thermochronology of the northern Cordillera Real, Ecuador: Tectonic insights from zircon and apatite fission track analysis. Tectonics, 19(4): 649–668. <https://doi.org/10.1029/2000TC900010>
- Spikings, R., Winkler, W., Seward, D. & Handler, R. 2001. Along-strike variations in the thermal and tectonic response of the continental Ecuadorian Andes to the collision with heterogeneous oceanic crust. Earth and Planetary Science Letters, 186(1): 57–73. [https://doi.org/10.1016/S0012-821X\(01\)00225-4](https://doi.org/10.1016/S0012-821X(01)00225-4)
- Spikings, R., Crowhurst, P.V., Winkler, W. & Villagómez, D. 2010. Syn- and post-accretionary cooling history of the Ecuadorian Andes constrained by their in-situ and detrital thermochronometric record. Journal of South American Earth Sciences, 30(3–4): 121–133. <https://doi.org/10.1016/j.jsames.2010.04.002>
- Strecker, M.R., Alonso, R.N., Bookhagen, B., Carrapa, B., Hilley, G.E., Sobel, E.R. & Trauth, M.H. 2007. Tectonics and climate of the southern central Andes. Annual Review of Earth and Planetary Sciences, 35: 747–787. <https://doi.org/10.1146/annurev.earth.35.031306.140158>
- Strecker, M.R., Alonso, R.N., Bookhagen, B., Carrapa, B., Coutand, I., Hain, M.P., Hilley, G.E., Mortimer, E., Schoenbohm, L. & Sobel, E.R. 2009. Does the topographic distribution of the central Andean Puna Plateau result from climatic or geodynamic processes? Geological Society of America 37(7): 643–646. <https://doi.org/10.1130/G25545A.1>
- Taboada, A., Rivera, L.A., Fuenzalida, A., Cisternas, A., Philip, H., Bijwaard, H., Olaya, J. & Rivera, C. 2000. Geodynamics of the northern Andes: Subductions and intracontinental deformation (Colombia). Tectonics, 19(5): 787–813. <https://doi.org/10.1029/2000TC900004>
- Toussaint, J.F. & Restrepo, J.J. 1989. Acreciones sucesivas en Colombia: Un nuevo modelo de evolución geológica. V Congreso Colombiano de Geología. Memoirs, I, p. 127–146. Bucaramanga.
- Trenkamp, R., Kellogg, J.N., Freymueller, J.T. & Mora, H. 2002. Wide plate margin deformation, southern Central America and northwestern South America, CASA GPS observations.

- Journal of South American Earth Sciences, 15(2): 157–171. [https://doi.org/10.1016/S0895-9811\(02\)00018-4](https://doi.org/10.1016/S0895-9811(02)00018-4)
- Ulloa, C. & Rodríguez, E. 1979. Geología del cuadrángulo K12 Guatemala. *Boletín Geológico*, 22(1): 3–55.
- van der Hammen, T., Werner, J.H. & van Dommelen, H. 1973. Palynological record of the upheaval of the northern Andes: A study of the Pliocene and lower Quaternary of the Colombian Eastern Cordillera and the early evolution of its high-Andean biota. *Review of Palaeobotany and Palynology*, 16(1–2): 1–122. [https://doi.org/10.1016/0034-6667\(73\)90031-6](https://doi.org/10.1016/0034-6667(73)90031-6)
- Veloza, G., Styron, R., Taylor, M. & Mora, A. 2012. Open-source archive of active faults for northwest South America. *GSA Today*, 22(10): 4–10. <https://doi.org/10.1130/GSAT-G156A.1>
- Veloza, G., Taylor, M., Mora, A. & Gosse, J. 2015. Active mountain building along the eastern Colombian subandes: A folding history from deformed terraces across the Tame Anticline, Llanos Basin. *GSA Bulletin*, 127(9–10): 1155–1173. <https://doi.org/10.1130/B31168.1>
- Villagómez, D. & Spikings, R. 2013. Thermochronology and tectonics of the Central and Western Cordilleras of Colombia: Early Cretaceous – Tertiary evolution of the northern Andes. *Lithos*, 160–161: 228–249. <https://doi.org/10.1016/j.lithos.2012.12.008>
- Villagómez, D., Spikings, R., Magna, T., Kammer, A., Winkler, W. & Beltrán, A. 2011a. Geochronology, geochemistry and tectonic evolution of the Western and Central Cordilleras of Colombia. *Lithos*, 125(3–4): 875–896. <https://doi.org/10.1016/j.lithos.2011.05.003>
- Villagómez, D., Spikings, R., Mora, A., Guzmán, G., Ojeda, G., Cortés, E. & van der Lelij, R. 2011b. Vertical tectonics at a continental crust–oceanic plateau plate boundary zone: Fission track thermochronology of the Sierra Nevada de Santa Marta, Colombia. *Tectonics*, 30(4): 1–18. <https://doi.org/10.1029/2010TC002835>
- Villamil, T. 1999. Campanian – Miocene tectonostratigraphy, depocenter evolution and basin development of Colombia and western Venezuela. *Palaeogeography, Palaeoclimatology, Palaeoecology*, 153(1–4): 239–275. [https://doi.org/10.1016/S0031-0182\(99\)00075-9](https://doi.org/10.1016/S0031-0182(99)00075-9)
- Wagner, G.A. & van den Haute, P. 1992. *Fission track dating*. Kulwer Academic Publishers, 285 p. Dordrecht, the Netherlands.
- Wagner, L.S., Jaramillo, J.S., Ramírez-Hoyos, L.F., Monsalve, G., Cardona, A. & Becker, T.W. 2017. Transient slab flattening beneath Colombia. *Geophysical Research Letters*, 44(13): 6616–6623. <https://doi.org/10.1002/2017GL073981>
- Wijninga, V.M. 1996. Paleobotany and palynology of Neogene sediments from the High Plain of Bogota (Colombia). Evolution of the Andean flora from a paleoecological perspective. Doctoral thesis, University of Amsterdam, 370 p. Amsterdam, the Netherlands.
- Wijninga, V.M. & Kuhry, P. 1990. A Pliocene flora from the Suba-choque valley (cordillera Oriental, Colombia). *Review of Palaeobotany and Palynology*, 62(3–4): 249–290. [https://doi.org/10.1016/0034-6667\(90\)90091-V](https://doi.org/10.1016/0034-6667(90)90091-V)

Explanation of Acronyms, Abbreviations, and Symbols:

AFT	Apatite fission track	T–t	Time–temperature
AHe	Apatite (U–Th)/He	ZFT	Zircon fission track
GPS	Global Position System	ZHe	Zircon (U–Th)/He

Authors' Biographical Notes



Andrés MORA is the chief geologist of Onshore Exploration at Ecopetrol. He received his BS in geology from the Universidad Nacional de Colombia and PhD from the Institut für Geowissenschaften, Universität Potsdam. His research interests include structural geology, petroleum exploration, and petroleum geology.



Diego VILLAGÓMEZ is a binational Swiss–Ecuadorian geologist. He has hands-on experience in the E&P of natural resources in Africa, Mexico, the Caribbean, and northern South America. Diego is particularly interested in the thermal fingerprint of processes that occur in the middle and upper parts of the crust, which is fundamental to understanding the “source to sink” relationship between erosional areas and basinal deposition.



Mauricio PARRA is an assistant professor at the Instituto de Energia e Ambiente of the Universidade de São Paulo, where he leads the Low–Thermochronology Laboratory. He received his BS in geology from the Universidad Nacional de Colombia and his PhD from the Institut für Geowissenschaften, Universität Potsdam. His research focuses on the tectonic evolution of mountain belts using thermochronometry and sedimentary basin analysis.



Víctor M. CABALLERO is a senior geologist and researcher of sedimentology and depositional systems at Ecopetrol–ICP. He received his BS and MS degrees in geology from the Universidad Industrial de Santander at Bucaramanga Colombia. His research interests include sedimentology, sequence stratigraphy, thermochronology, geochronology, and basin analysis.



Richard SPIKINGS graduated in geochemistry at the University of St. Andrews in 1993. His research in thermochronology earned a PhD in geology in 1998 from La Trobe University, Melbourne. Since 1998, he has worked as a postdoctoral fellow at the ETH–Zurich, and as tenured research staff at the University of Geneva where he currently manages the $^{40}\text{Ar}/^{39}\text{Ar}$ laboratory. His research has focussed on thermochronology and geochronology of the Andean cordilleras in Ecuador, Colombia, Venezuela, Perú, and Chile. More recently, Richard has focussed his research efforts on bulk and in-situ U–Pb thermochronology of accessory phases.



Brian K. HORTON is the Alexander Deussen professor of Energy Resources at The University of Texas at Austin and has a joint appointment with the Department of Geological Sciences and Institute for Geophysics in the Jackson School of Geosciences. He received his BS from the University of New Mexico, MS from Montana State University, and PhD from the University of Arizona. His research addresses the tectonics of sedimentary basins and the evolution of orogenic systems.



Josué Alejandro MORA-BOHÓRQUEZ graduated as a geologist from the Universidad Nacional de Colombia, Bogotá, in 1998, then obtained a MS degree in basin evolution and dynamics at Royal Holloway, University of London, United Kingdom, in 2001 and he is currently pursuing a PhD degree at the Free University of Berlin/GFZ Potsdam, Germany. He works as senior exploration geologist for Hocol S.A. since 2006. Prior to working for Hocol S.A., he was an exploration geologist at Petrobras Colombia doing regional studies of the Upper and Middle Magdalena Valley Basins from 2002 to 2004, and then he worked in coalbed methane and conventional hydrocarbon exploration for Drummond Ltd. Colombia, from 2004 to 2006. His research interests are tectonics and sedimentation, basin analysis, petroleum exploration, and hydrocarbon systems.



Richard A. KETCHAM is an associate professor with the Jackson School of Geosciences at the University of Texas at Austin. He received his BS in geology and computer science from Williams College in 1987 and his PhD in geological sciences from the University of Texas at Austin in 1995. His active research interests include thermochronology and geological applications of high-resolution X-ray computed tomography.



Juan Pablo ARIAS-MARTÍNEZ holds a BS degree in geology from the Universidad de Caldas, Colombia. He is currently an exploration geologist at Ecopetrol. His research interests include structural geology, sedimentology, and petroleum geology.

Neogene

Paleogene

Cretaceous


Chapter 5



The Eastern Foothills of Colombia

<https://doi.org/10.32685/pub.esp.37.2019.05>

Published online 26 November 2020

Andrés MORA^{1*} , Eliseo TESÓN² , Jaime MARTÍNEZ³, Mauricio PARRA⁴ ,
Álvaro LASSO⁵, Brian K. HORTON⁶ , Richard A. KETCHAM⁷ ,
Antonio VELÁSQUEZ⁸, and Juan Pablo ARIAS-MARTÍNEZ⁹

Abstract In this chapter, we summarize for the first time the structural geometry and evolution of the Eastern Foothills of Colombia based on new and previously published cross-sections. We compare shortening records of the Caguán–Putumayo and Llanos Foothills as two different end-members for thick- and thin-skinned foothill deformation along the Andean deformation front. The Caguán–Putumayo area involves thick-skinned deformation and broad basement uplifts, such as the Garzón Massif, with a simple frontal monoclinical structure expressed in folded and faulted basement rocks, similar to broad thrust-related uplifts in the eastern Rocky Mountains of North America. In contrast, the Llanos Foothills have a more complex array of structural styles, from tightly folded frontal basement structures to thin-skinned antiforms of faulted detachment folds. The main factor controlling the style of basement deformation appears to be basement composition, which is igneous/metamorphic crystalline in the Caguán–Putumayo area and low-grade metasedimentary in the Llanos Foothills, prompting tighter basement folds. The main factors in determining thin- versus thick-skinned deformation appear to be the thickness of the Mesozoic – Cenozoic stratigraphic units and the presence or absence of detachment horizons. The Andean Foothills of Colombia record a geometric evolution that started in the Oligocene, with similar structural styles across all segments at that time. However, the deformation styles diverged rapidly during the Miocene to recent shortening, where rapid deposition of thick fluvial sedimentary units drove source rocks into the oil window and helped form efficient detachment horizons for thin-skinned deformation in deeper sectors of the basin.

Keywords: *thin-skinned, thick skinned, basement, detachments.*

Resumen En este capítulo se sintetiza por primera vez la geometría estructural y evolución del piedemonte oriental de Colombia a partir de secciones estructurales nuevas y otras ya publicadas. Se compara la evolución del acortamiento de los piedemontes del Caguán–Putumayo y Llanos como dos miembros extremos de deformación de piedemonte con y sin basamento implicado a lo largo del frente de deformación andino. El área del Caguán–Putumayo involucra deformación con basamento involucrado y amplios antifórmas de basamento, como el Macizo de Garzón, con una estructura monoclinical frontal simple expresada en un basamento plegado y fallado, similar a los *thrust-uplifts* en las Montañas Rocosas de Norteamérica. En contraste, el piedemonte llanero presenta un arreglo más complejo de estilos estructurales, desde estructuras

1 andresro.mora@ecopetrol.com.br
Ecopetrol, Brasil
Bogotá, Colombia

2 eteson@gmail.com
Ecopetrol S.A.
Vicepresidencia de Exploración
Bogotá, Colombia

3 jaime.martinezhe@ecopetrol.com.co
Ecopetrol S.A.
Vicepresidencia de Exploración
Bogotá, Colombia

4 mparra@iee.usp.br
Universidade de São Paulo
Instituto de Energia e Ambiente
Av. Professor Luciano Gualberto 1289, Cidade
Universitária, 05508-010
São Paulo, Brasil

5 alvaro.lasso@ecopetrol.com.co
Ecopetrol S.A.
Vicepresidencia de Exploración
Bogotá, Colombia

6 horton@jsg.utexas.edu
University of Texas at Austin
Department of Geological Sciences and
Institute for Geophysics, Jackson School of
Geosciences
Austin, Texas 78712, USA

7 ketcham@jsg.utexas.edu
University of Texas at Austin
Jackson School of Geosciences
Austin, Texas 78712, USA

8 antonio.velasquez@ecopetrol.com.co
Ecopetrol S.A.
Vicepresidencia de Exploración
Bogotá, Colombia

9 juan.arias@ecopetrol.com.co
Ecopetrol S.A.
Vicepresidencia de Exploración
Bogotá, Colombia

* Corresponding author

Citation: Mora, A., Tesón, E., Martínez, J., Parra, M., Lasso, Á., Horton, B.K., Ketcham, R.A., Velásquez, A. & Arias-Martínez, J.P. 2020. The Eastern Foothills of Colombia. In: Gómez, J. & Mateus-Zabala, D. (editors), *The Geology of Colombia, Volume 3 Paleogene – Neogene*. Servicio Geológico Colombiano, *Publicaciones Geológicas Especiales* 37, p. 123–142. Bogotá. <https://doi.org/10.32685/pub.esp.37.2019.05>

de basamento frontales con plegamientos apretados hasta estructuras despegadas de basamento en apilamientos antiformes con pliegues de despegue fallados. El principal control en el estilo de deformación del basamento parece ser su composición, la cual es cristalina ígnea/metamórfica en la región del Caguán–Putumayo y metasedimentaria en el piedemonte llanero propiciando así la presencia de pliegues de basamento más apretados. Los principales factores que determinan la presencia de deformación despegada del basamento o deformación con basamento involucrado parecen ser el espesor de las unidades estratigráficas mesozoicas y cenozoicas y la presencia o ausencia de horizontes de despegue. Los piedemontes andinos de Colombia registran una evolución geométrica que empezó en el Oligoceno, con estilos estructurales similares a lo largo de todos los segmentos de ese tiempo. Sin embargo, los estilos de deformación divergieron rápidamente durante el acortamiento mioceno al reciente, en el cual un rápido depósito de unidades sedimentarias fluviales espesas hizo que las rocas generadoras del piedemonte entraran en la ventana de generación de petróleo y ayudó a la formación de horizontes de despegue eficientes para la deformación sin basamento implicado en los sectores más profundos de la cuenca.

Palabras clave: *deformación sin basamento involucrado, deformación con basamento involucrado, basamento, despegues.*

1. Introduction

Foothill belts in contractional orogens normally represent the youngest deformation front, which usually accommodates active shortening in modern mountain belts (Banks & Warburton, 1986; Cooper, 1996; Morley, 1986). The structural geometries and evolution of foothill belts are related to several mechanical factors, including tectonic inheritance, thickness of the stratigraphic succession, and the presence or absence of suitable detachment horizons. Some studies have further suggested that erosion could be a factor controlling the geometry and evolution of foothills (e.g., Horton, 1999; Malavieille, 2010; Mora et al., 2008). Understanding the geometry and evolution of active foothill systems is fundamental for the exploration of hydrocarbon resources (e.g., Cooper et al., 1995; Dengo & Covey, 1993), active tectonics (Veloza et al., 2012), and the general evolution of mountain belts. Regarding mountain building and orogenic evolution, foothill structural systems provide an essential record in understanding deformation patterns within fold–thrust belts and in extrapolating structural geometries and styles from well-known areas to less studied ones, in both surface and subsurface settings (Nemčok et al., 2013).

There are several recent studies related to fold and thrust belts in Colombia (e.g., Anderson et al., 2014; Caballero et al., 2010, 2013a, 2013b; Saylor et al., 2012; Teixell et al., 2015). However, the Eastern Foothills of Colombia have been studied in even greater detail due to a significant effort primarily from the oil industry (e.g., Carrillo et al., 2016; Jimenez et al., 2013; Martinez, 2006; Mora et al., 2010a; Támara et al., 2015). In this contribution, we summarize previous studies and expand upon them by investigating the lesser known Caguán–Putumayo Foothills. Here, we present various observations that help us

reach conclusions regarding the evolution of foothill belts in other Andean provinces and worldwide.

The Eastern Cordillera of Colombia contains several important basement boundaries (e.g., Algeciras Fault; Figure 1; Velandia et al., 2005). We interpret these boundaries as the potential margins of a Precambrian – early Paleozoic mobile belt against the Precambrian Guiana Shield. The fundamental boundaries considered in this contribution include the Algeciras, Tesalia–Servitá, and Pajarito Faults. For example, the Algeciras Fault defines the boundary of known outcrops of lower Paleozoic sedimentary rocks in the Eastern Cordillera south of 4° N (Figure 1). Such Paleozoic rocks are absent east of the Algeciras Fault, where pre–Cretaceous rocks correspond to the Neoproterozoic basement of the Garzón Massif. This configuration also characterizes the pre–Cretaceous substrate farther east in the Caguán Basin (Ibañez–Mejía et al., 2011). Boundaries such as the Algeciras Fault later served as an important boundary for extensional domains characterized by syn–rift Cretaceous and potentially lower Paleozoic rocks (Figure 2). In contrast, in the north, the Tesalia–Servitá and Pajarito Faults are not well documented basement boundaries (i.e., boundaries of different pre–Mesozoic units that also uplift and expose the basement rocks) but rather graben–bounding Cretaceous master faults (Mora et al., 2013a; Tesón et al., 2013). However, and as we document in this contribution, the Algeciras, Servitá, and Pajarito Faults are fundamental pre–existing structural elements that largely controlled the Neogene evolution and geometry of the foothill belts in Colombia.

The foothills of the Caguán and Putumayo Basin display surface exposures of basement (i.e., crystalline igneous or metamorphic rocks), including either Precambrian crystalline or Jurassic igneous (volcanic or intrusive) rocks. In the subsurface,

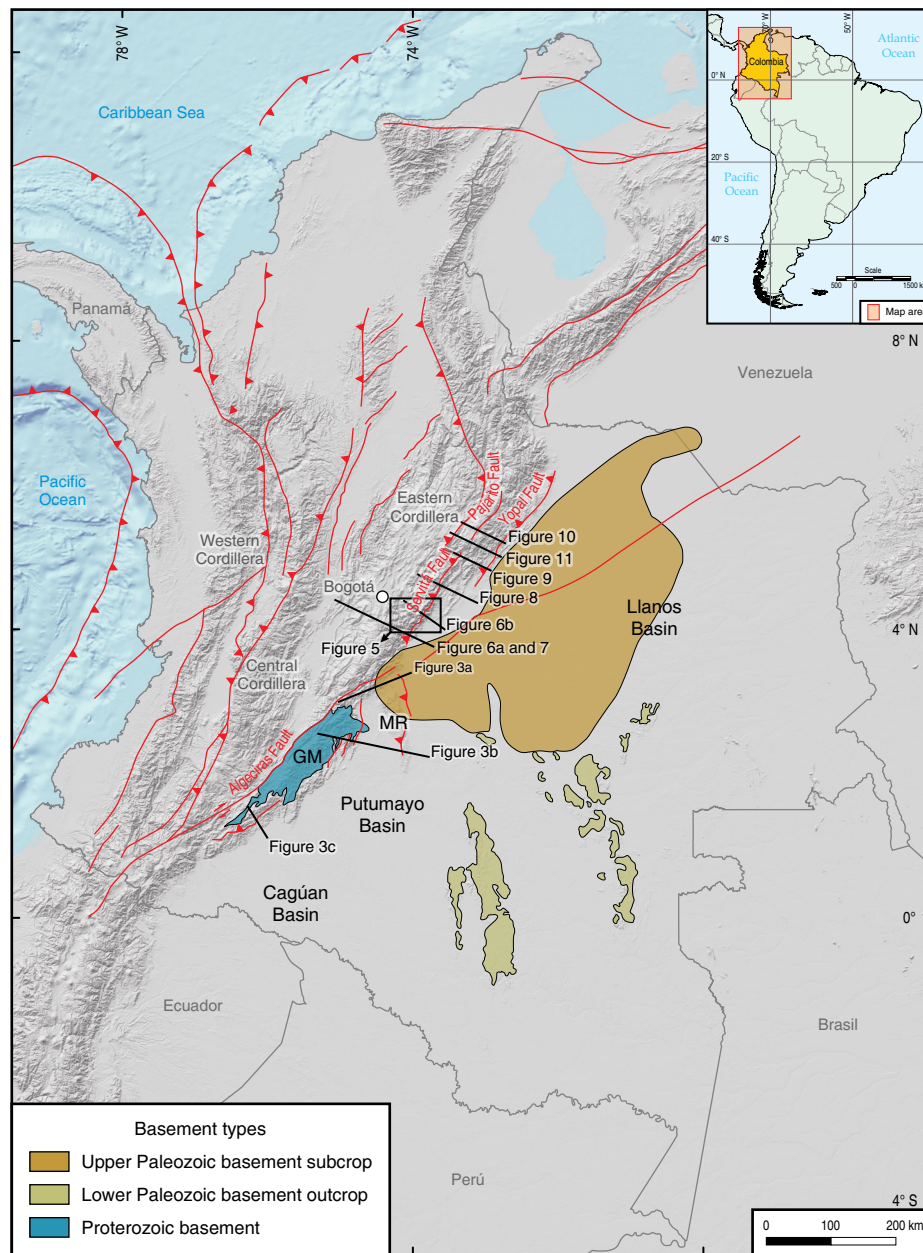


Figure 1. Shaded relief image of Colombia with the location of the figures and cross-sections discussed in the text. The different subcropping and outcropping basement types are also shown. The location of the Guaicáramo Fault (which is a fault shown in Figures 10 and 11) can be inferred in this figure because it is the unnamed fault located between the Yopal and the Pajarito Faults. (GM) Garzón Massif, (MR) Macarena Range.

the foreland basin also consists of basement rocks with local occurrences of Paleozoic sedimentary rocks (Figure 1). This configuration contrasts sharply with that of the Llanos Foothills and Llanos Basin. In the Eastern Foothills of the Llanos province, the exposed rocks include Cenozoic, Cretaceous, or subordinate Paleozoic sedimentary rocks, with local metasedimentary rocks. In the Llanos Basin east of the foothills, the absence of documented crystalline basement rocks is significant, and pre-Cretaceous rocks mostly consist of Paleozoic sedimentary rocks (Delgado et al., 2012; Moreno-Lopez & Escalona, 2015;

Reyes-Harker et al., 2015). Whereas Paleozoic rocks have been documented in different wells in the subsurface of the Llanos Basin, they are absent in western portions of the Caguan Basin (Ibañez-Mejia et al., 2011).

The basement arch of the Caguan Basin, called the Vaupés swell (Mora et al., 2010b), is a significant crystalline basement feature where the entire Phanerozoic sedimentary section is either condensed or absent (Figure 1). This contrast is particularly relevant in comparison to the Llanos Basin, which forms a deeper basin with a thicker sedimentary fill.

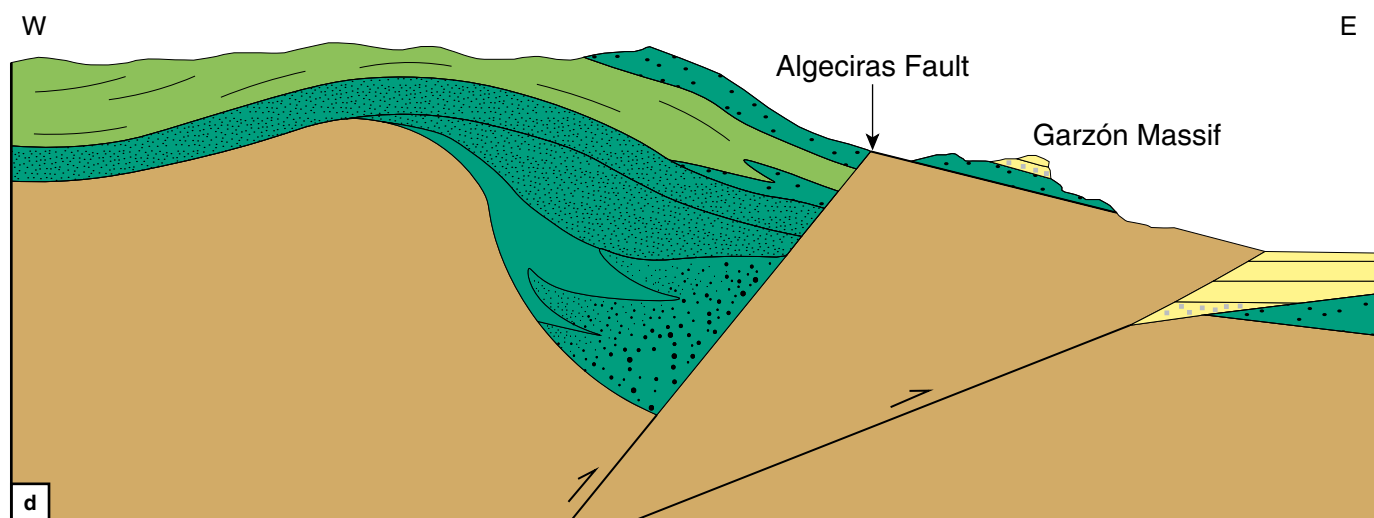
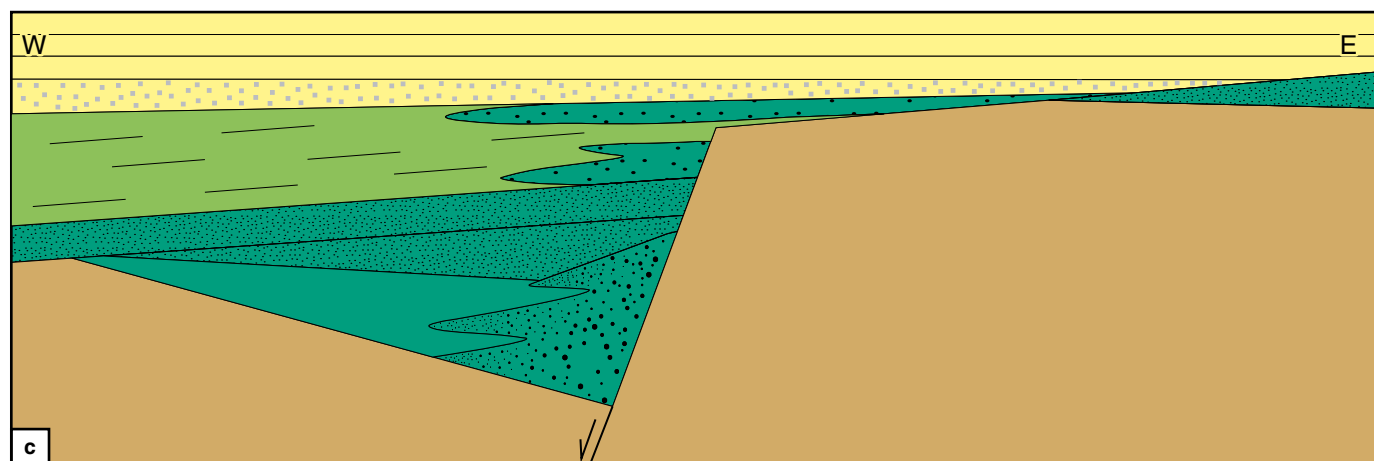
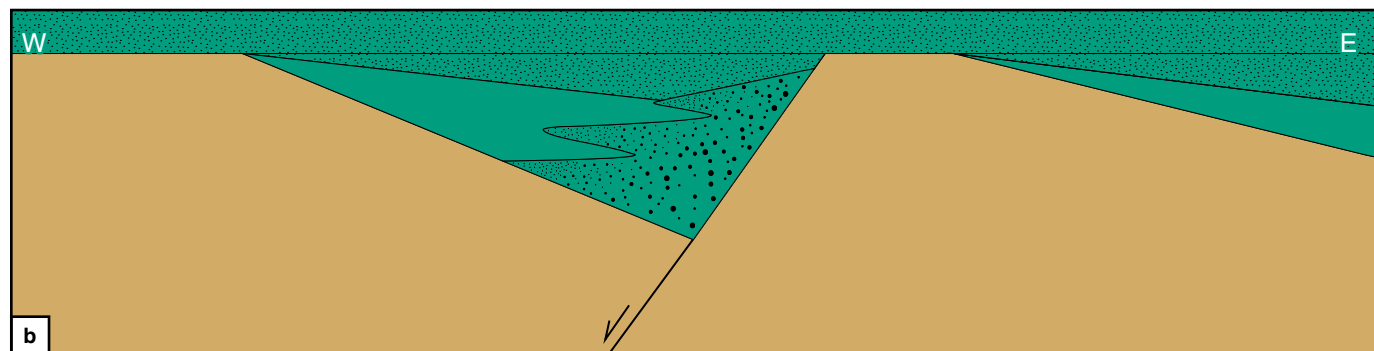
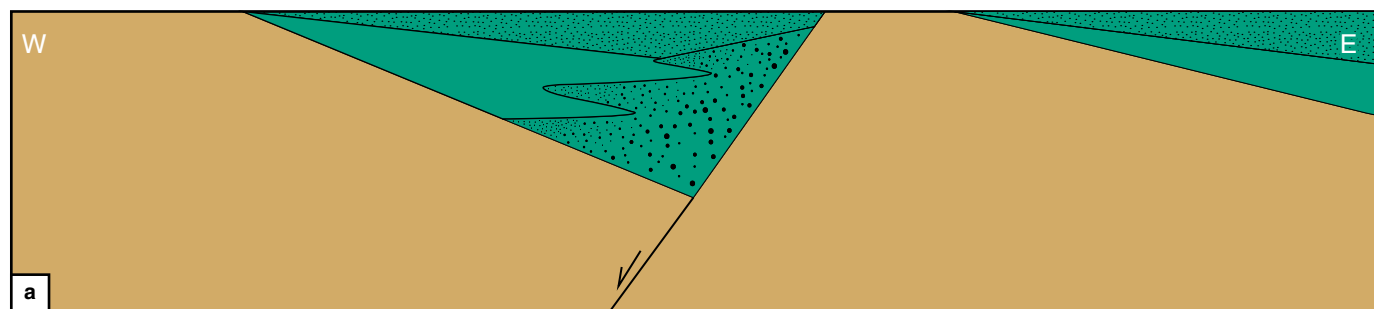


Figure 2. Generalized illustration showing the proposed evolution of the Algeciras Fault as a crustal boundary with lower Paleozoic rocks to the west and Neoproterozoic basement to the east. In this context the uplifted Neoproterozoic basement blocks of the Garzón Massif correspond to footwall shortcuts (Huyghe & Mugnier, 1995) branched from the Algeciras inverted normal fault. The evolutionary steps are not related to precise geological times, they only intend to summarize the geometric evolution of the different crustal domains.

2. Methods

In this chapter, we review the structural styles and evolution of the Eastern Foothills of Colombia, from the Putumayo Basin to the Llanos Basin, using previously published (e.g., Jimenez et al., 2013; Martinez, 2006; Mora et al., 2010a) and new structural cross-sections. Our new cross-sections are mostly from the Caguán–Putumayo Basin and were constructed based on available surface geological maps as well as subsurface information. From these datasets, we discuss folding mechanisms and controlling factors, and we then compare them with brief observations from other foothills segments of comparable fold and thrust belts.

3. Results

3.1. Caguán Foothills

Recent work and our new cross-sections confirm that the southern ends of the Andean deformation front in the Caguán Basin and in the Putumayo Basin (Figure 3) are simple basement uplifts in which the frontal segments are folded and locally disrupted by reverse faults with minor displacement. Wolaver et al. (2015) suggest that this could resemble basement-involved contractional wedges (e.g., Mount et al., 2011), which include a backthrust dipping to the east. However, in our southernmost cross-section in the Caguán Basin (Figure 3), we observed a simple east-dipping monoclinical panel, lacking well documented backthrusts, whose dip never exceeds 45°. This style resembles more that of classical foreland basement-involved structures (Mitra & Mount, 1998; Narr & Suppe, 1994). Recent work (e.g., Saeid et al., 2017) shows that this structural style continues along strike southward into the Putumayo Basin, where local, steeply dipping forelimbs exceed 60°. This structural style has also been interpreted in northern Ecuador in the Napo Uplift area (e.g., Baby et al., 2013). In these domains, the foreland regions east of this deformation zone are consistently undeformed and flat lying.

In the northernmost Caguán Basin (see Figure 3), although shortening is limited, the basement is faulted with one or multiple basement faults delimiting the Andean deformation front. In general, folding in the hanging wall of the basement faults is minor except in the case of the Macarena foreland basement uplift (Figure 3), where both the hanging wall and footwall display east-dipping folded panels.

Comparable geometries have been described by Berg (1962) as thrust-related uplifts, where the rocks were first deformed by basement-involved folds that are potentially linked to deeper-level, foreland-directed contractional faults. In a subsequent evolutionary step, the main faults emerge and partition the east-dipping forelimb panel, stranding part of the former forelimb in the footwall and the remainder in the hanging wall (Figure 4a–c).

3.2. The Ariari–Guatiquía Region and Significant Features that Can Be Extrapolated

The structural style of the Ariari–Guatiquía region has recently been described by Mora & Parra (2008) using maps, cross-sections, and thermochronology data. The data described in Mora & Parra (2008) as well as in Mora et al. (2006) show that the hanging wall of the Servitá Fault has preserved a thick sequence (ca. 3 km) of Neocomian syn-rift sedimentary units that are absent or condensed in the fault blocks to the east. Data also show that the hanging wall has preserved a >4 km thickness of pre-rift upper Paleozoic units (e.g., Mora & Kammer, 1999), which are absent in the adjacent faulted block, where lower Paleozoic metasedimentary units underlie the condensed thickness of Cretaceous syn-rift rocks in those regions where they were deposited. Mora & Parra (2008) and Mora et al. (2006) also show that the Servitá Fault is an inverted rift-boundary master fault that bounds the principal topographic relief at this latitude along the Eastern Foothills (Figure 5a, 5b).

These features allowed Mora & Parra (2008) and Mora et al. (2006) to interpret the Servitá Fault as the main basin boundary fault inverted during the Cenozoic, but they also make it possible to interpret faults to the east, like the Mirador Fault, as footwall shortcuts.

The cross-section in Figure 6a shows the frontal shortcut faults having similar structural styles as those in the Caguán area. However, some deformation in the foreland domain is also visible. This is mostly related to splays departing from the most important shortcuts and to inverted normal faults. In a cross-section close to where the Anaconda well was drilled (Figure 6b; Mora et al., 2015a), the data from the well can be interpreted in terms of a highly deformed and folded hanging wall block of the Mirador Fault when compared to the regions we have shown to be present to the south. The projection of the fault surface trace and the same fault in the Anaconda well allows us to interpret the Mirador Fault plane as a shallowly dipping fault plane (ca. 20°). This behavior and the intense fold-

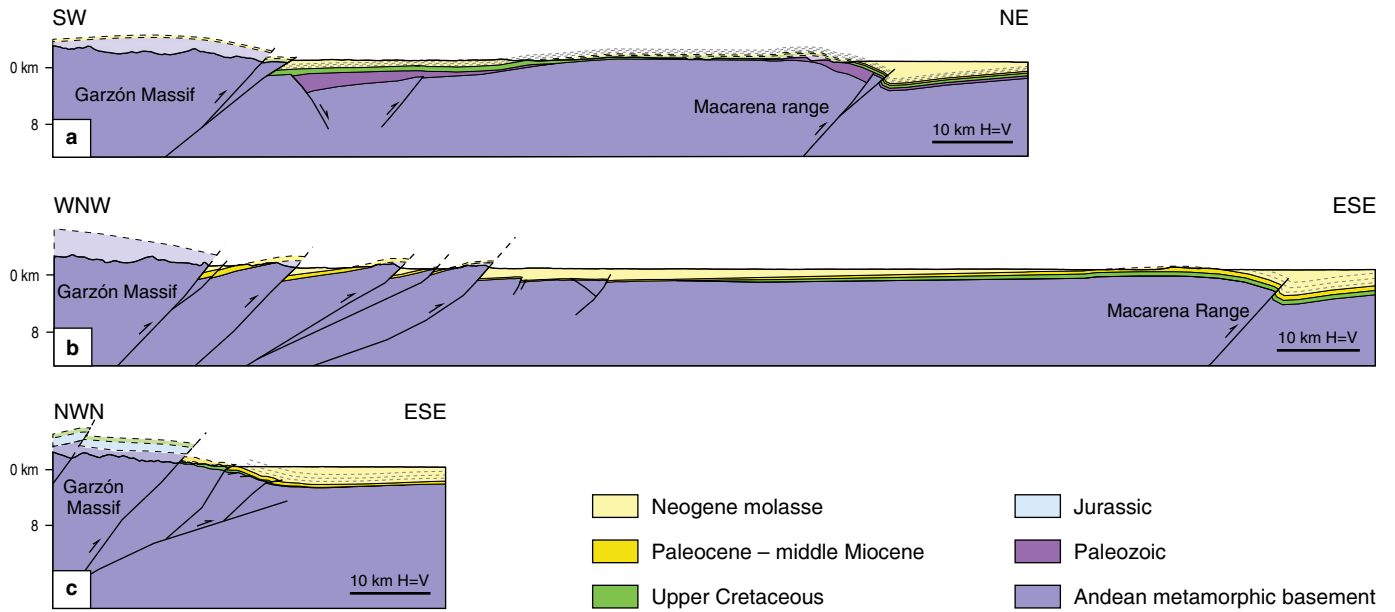
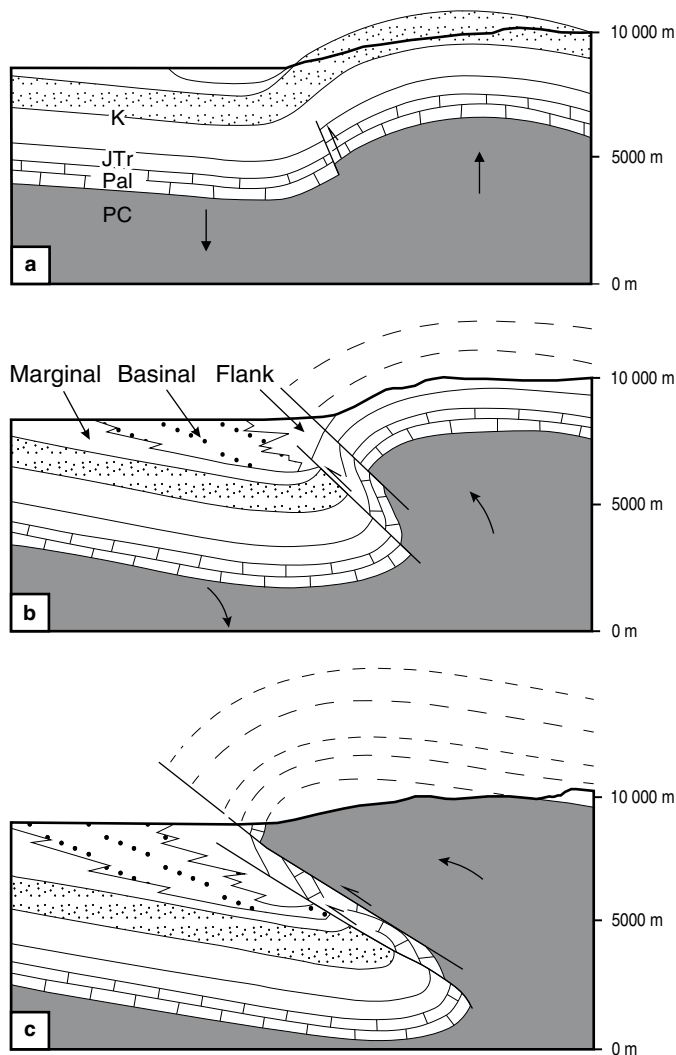


Figure 3. Cross-sections depicting the structural styles of the Caguán–Putumayo basement uplifts between the Garzón Massif and the Macarena range. See Figure 1 for location.



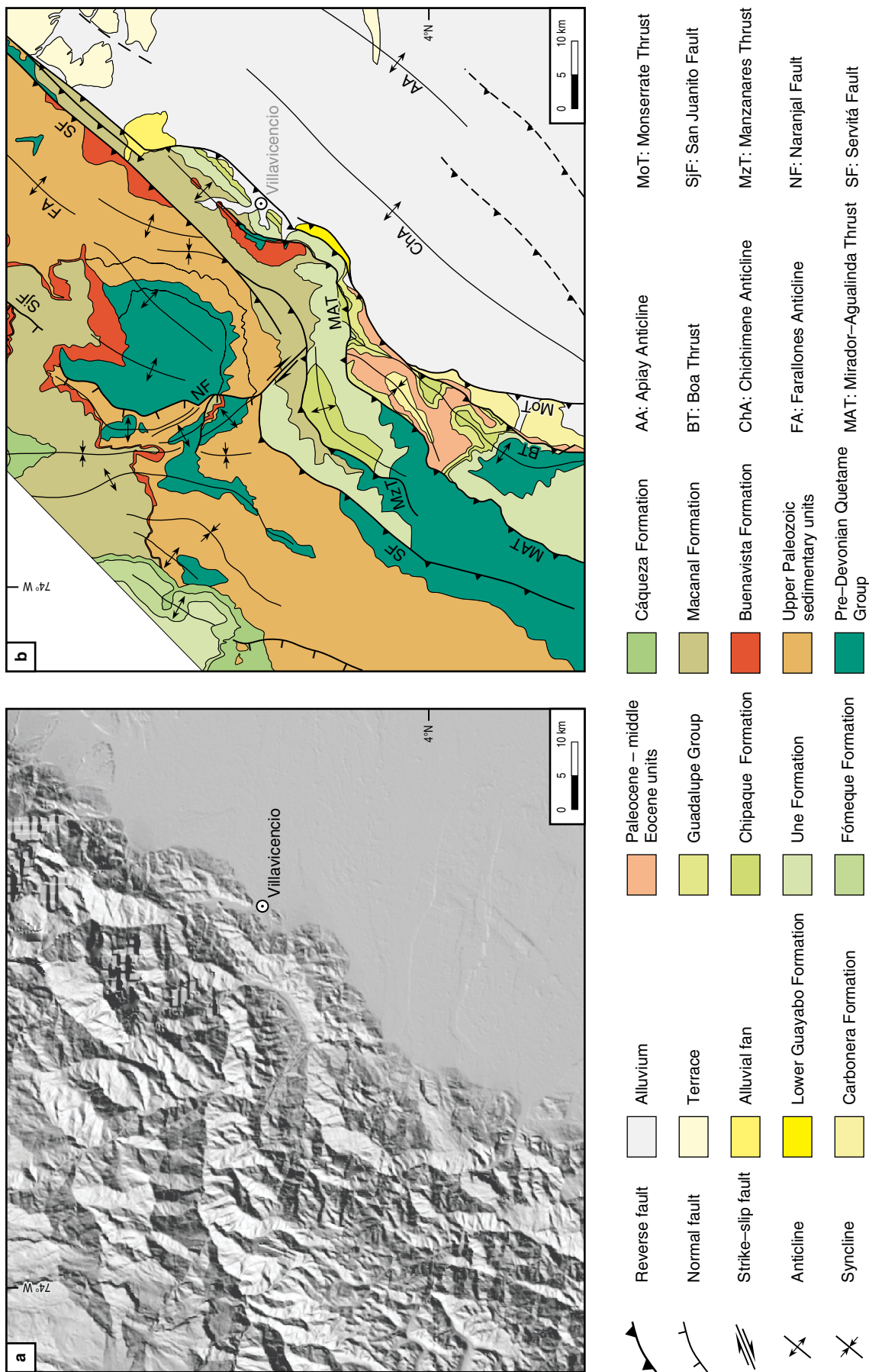
ing in the hanging wall block represent a significantly different structural style than is found in the foothills to the south. It is also worth noting the absence of Paleozoic sedimentary rocks in the faulted blocks of the Garzón Massif to the south (Figure 3) versus the faulted blocks to the north (Figures 6, 7). Moreover, the basement in cross-sections in Figures 6, 7 is not formed of crystalline basement rocks but instead of metasedimentary units, while the deformed basement rock units in the Garzón Massif in cross-sections in Figure 3 are actual crystalline Proterozoic rock units. These are important differences between the Ariari–Guatiquía (Figures 6, 7) and the Caguán (Figure 3) segments of the Colombian foothills.

3.3. The Guavio and Tierranegra Segments

The Guavio segment displays a structural style that has steeply dipping beds in the hanging wall of the Servitá Fault (Tesalia) and an enormous frontal anticline. This frontal anticline, the Guavio Anticline, is in the hanging wall of the Guaicáramo Fault (Figure 8). Shortening associated with the Tesalia Fault (Figure 8) could be related to a thrust uplift style (Figure 4; Berg, 1962), as there is basement folding laterally evolving to a faulted monocline. However, the degree of folding compared to folding at the areas to the south is significantly larger.

In the Tierranegra segment farther north, the Servitá Fault is relayed by the Pajarito Fault as the main graben boundary

Figure 4. Geometric evolutionary model of thrust-uplifts after Berg (1962).



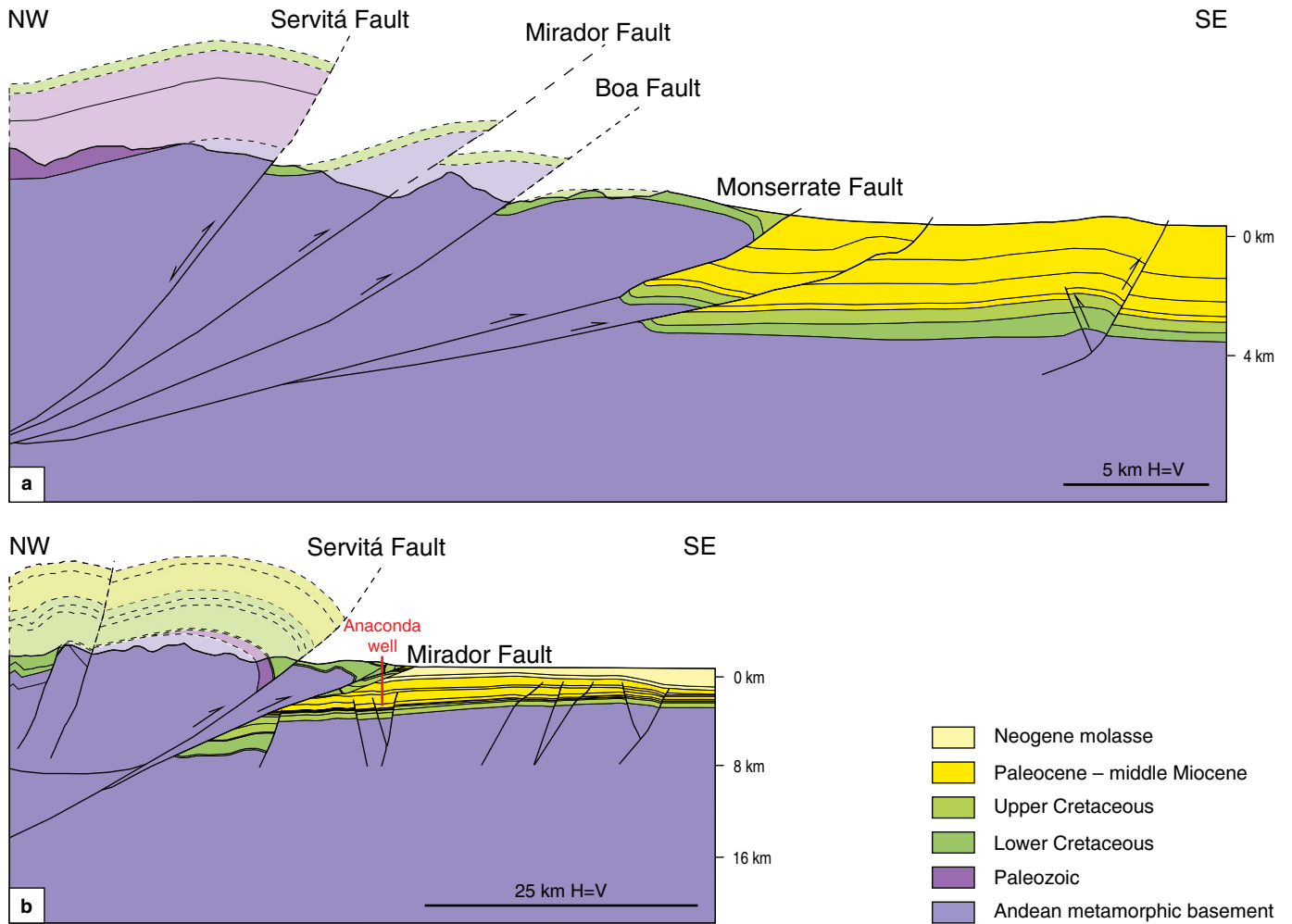


Figure 6. Representative cross-sections of the deformation front of the Ariari-Guatiqúia segment. See Figure 1 for location.

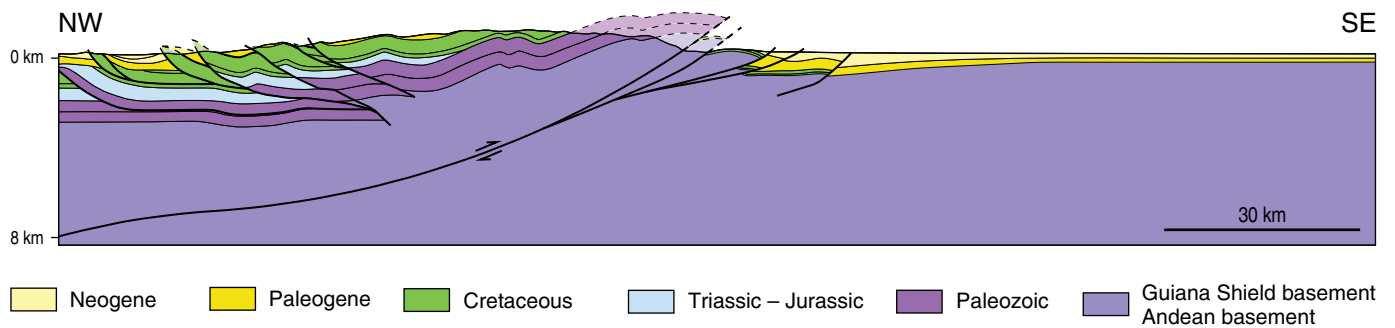


Figure 7. Regional cross-section of the Eastern Cordillera at the latitude of the Ariari-Guatiqúia segment. See Figure 1 for location.

fault. Tight folding has also been documented in the frontal shortcut structures of the Guaicáramo Fault, together with subthrust anticlines (Figure 9). In this region, the Yopal and Cusiana Faults represent the most frontal foothill structures. The Yopal Fault is a low-angle thin-skinned fault with a detachment in the Cenozoic shales.

3.4. The Piedemonte Segment

The piedemonte segment is characterized by a stack of thrust sheets folded into tight anticlines (Figure 10), with trailing structures presumably detaching in Lower Cretaceous units and leading structures detaching in shaley units of the Upper

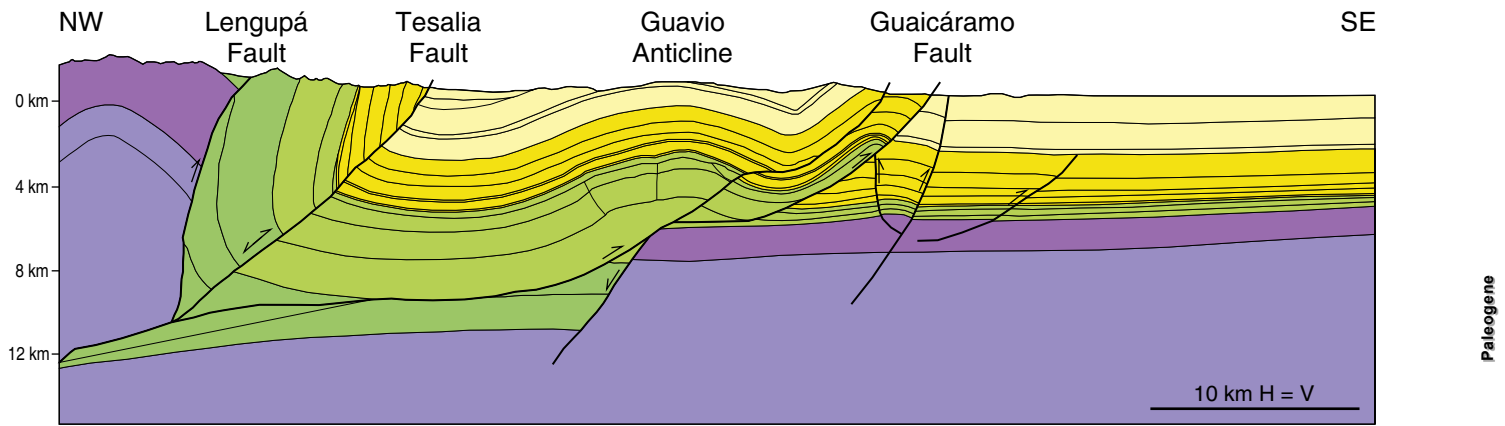


Figure 8. Representative cross-sections of the deformation front of the Guavio segment. See Figure 1 for location.

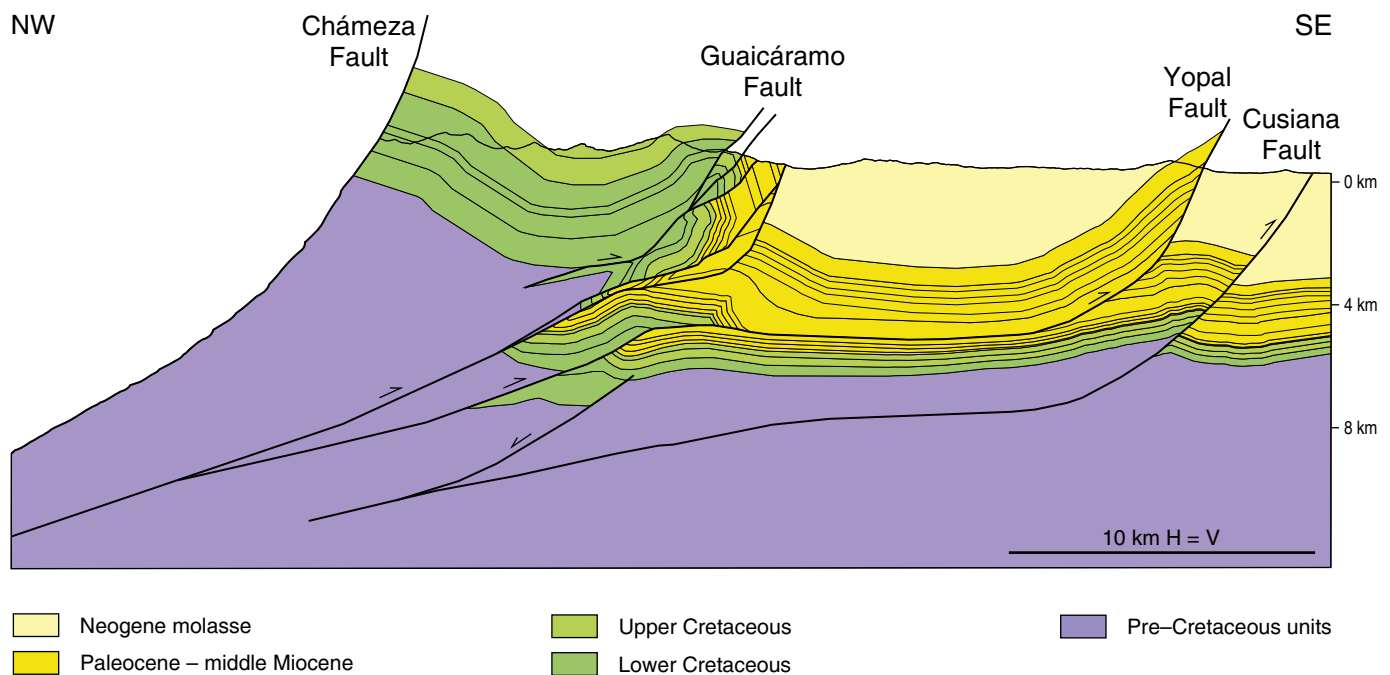


Figure 9. Representative cross-sections of the deformation front of the Tierranegra segment. See Figure 1 for location.

Cretaceous Chipaque Formation (Martínez, 2006). In addition, a rapid thinning of sedimentary units in the stacked anticlines has been documented in several wells, while Lower Cretaceous units are absent in the adjacent foreland. An analogous situation has been described by Castillo et al. (2016) and Gelvez et al. (2016) in the Ariari-Guatiquía area, where syn-rift sedimentary units have been exhumed. In the piedemonte segment, the Pajarito Fault to the west bounds the highest relief area in the foothills (Figure 1), with Lower Cretaceous gabbroic rocks along its fault plane (Vásquez & Altenberger, 2005) and over mature thick syn-rift Cretaceous sequences (Mora & Parra, 2008). This fault could be interpreted as an Early Cretaceous master rift boundary fault, while the structures at the front and

to the east could be part of the uplifted foreland rock formations that lack Cretaceous syn-rift units. The difference then in the piedemonte region is that the exhumation associated with the main foothill structures is much less than in the Ariari-Guatiquía segment.

4. Evolution

Recent studies have helped elucidate the evolution of foothill structures during the Cenozoic (e.g., Ramírez-Arias et al., 2012). Martínez (2006) showed that the presence of tight antiformal thrust structures below the relatively simple shape of the Nunchía Syncline (Figure 11a) proved that there was a late

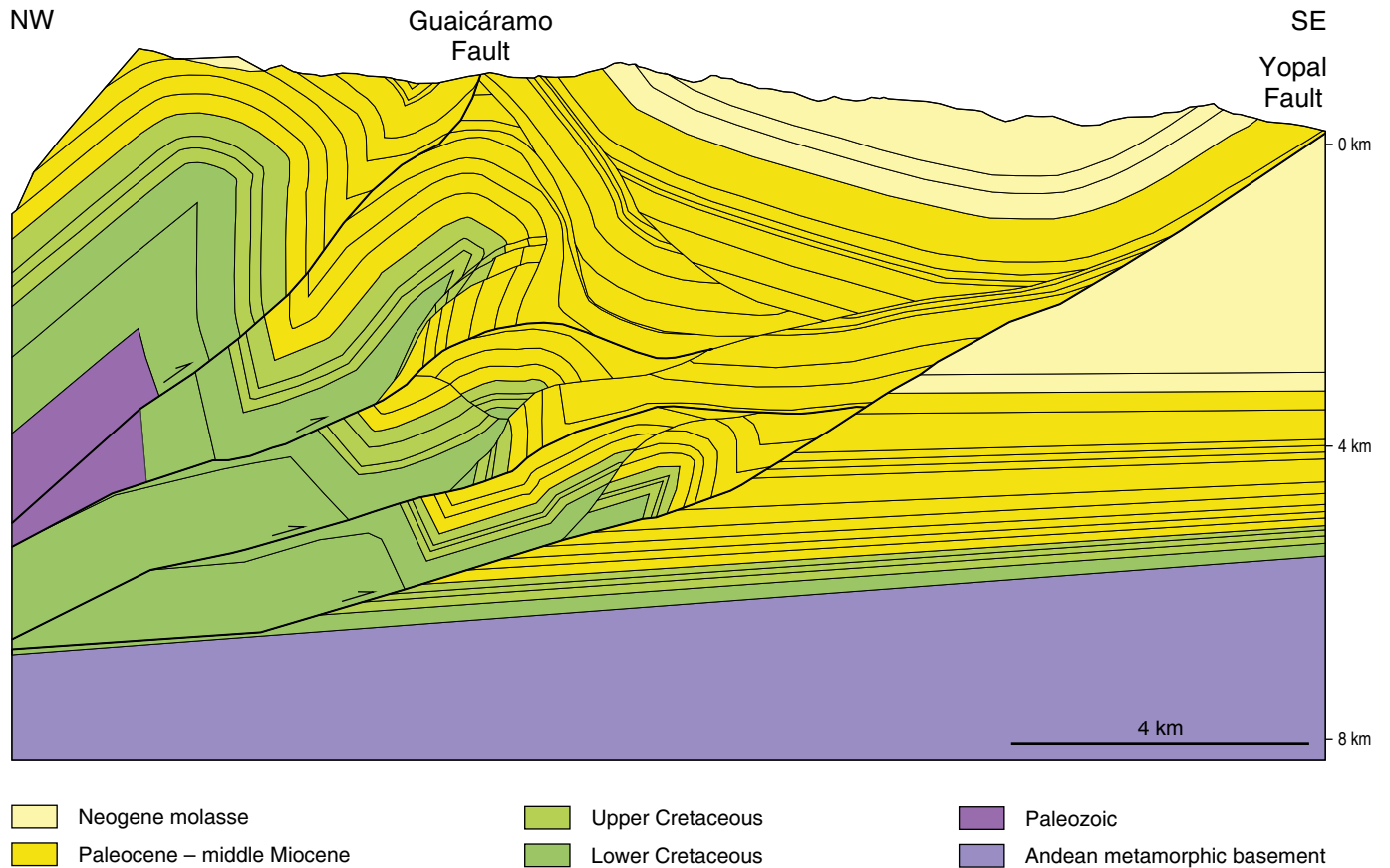


Figure 10. Representative cross-sections of the deformation front of the piedemonte segment. See Figure 1 for location.

Oligocene – early Miocene phase of detachment folding, with the detachment folds forming adjacent to one another. On top of those anticlines, there is the deposition of the Neogene sedimentary units. Thrust stacking of anticlines and a rather passive uplift of the Nunchía Syncline was a deformation event that occurred from the Miocene to Quaternary (Martínez, 2006).

Mora et al. (2010c) detected two cooling events in the same region using AFT (apatite fission tracks) data for samples from the crests of the uppermost anticlines located in the piedemonte antiform described by Martínez (2006) (Figure 11b). The documentation of such early deformation is based on the presence of two age populations (middle Miocene and younger in low-chlorine apatite grains and Oligocene to early Miocene in high-chlorine grains; Mora et al., 2010c). Subsequent thermochronology studies, fracture analysis, and microtectonic studies document a late Oligocene folding event in multiple folds in the Eastern Cordillera (e.g., Mora et al., 2013b). Late Oligocene growth strata in the Eastern Foothills, Magdalena Foothills, and Upper Magdalena Valley indicate that deformation of that age appears to be ubiquitous across the Eastern Cordillera (Mora et al., 2013a). Ramón & Rosero (2006) show evidence of important unconformities and growth strata of the same age in the Upper Magdalena Valley.

Southwards in the Ariari–Guatiquía area, several researchers have described the style of exhumation (e.g., Mora & Parra, 2008; Parra et al., 2009a, 2009b, 2010). It appears that graben–boundary master faults, like the Servitá Fault, started exhuming by the Oligocene while adjacent shortcuts possibly display minor exhumation or folding. Analogous behavior has been shown for the piedemonte segment (Bande et al., 2012).

Finally, Ketcham et al. (2016) provide detailed documentation of the exhumation history of the piedemonte antiform via thermochronology studies, in which the stacked thrust sheets were folded and potentially exhumed by the late Oligocene (Figure 11). A final out-of-sequence deformation event would then have been reactivated, faulting and stacking all the structures of the piedemonte antiform (e.g., Martínez, 2006). As indicated in Mora et al. (2015a), the final out-of-sequence deformation in the foothills was possibly more rapid, as deduced by thermokinematic modeling. Regarding the Garzón Massif, which is the geological province involved in the thick-skinned deformation of the Caguán–Putumayo Foothills, Anderson et al. (2016) suggest ongoing exhumation by the mid-Miocene, while Oligocene exhumation has not been documented so far in that area.

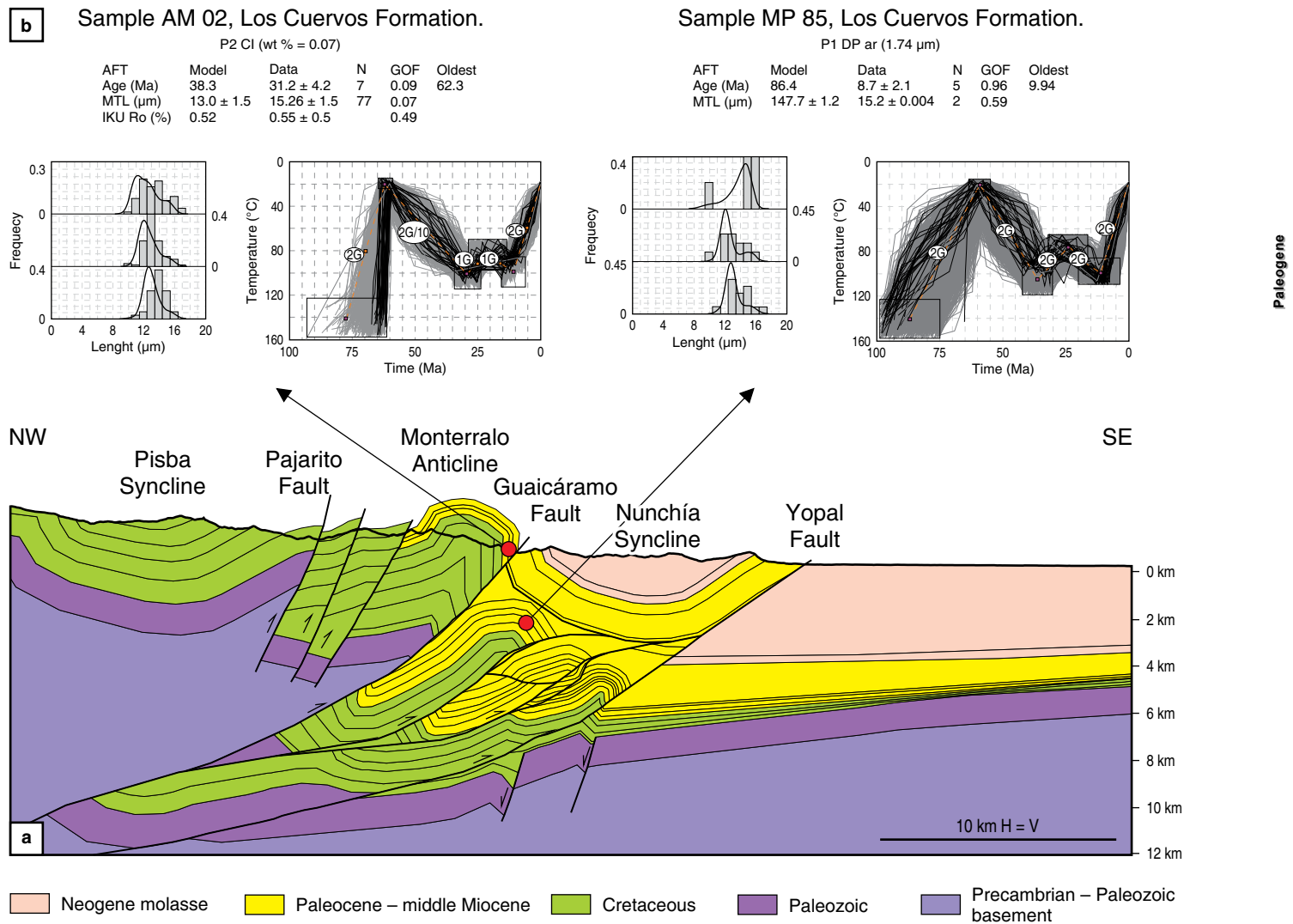


Figure 11. (a) Cross-section for the piedemonte segment and **(b)** high-resolution thermal solutions for anticlines in the same structure (after Mora et al., 2014). See Figure 1 for location.

5. Discussion

Thick-skin deformation has been documented in the southern Llanos Foothills as well as in the Caguán–Putumayo Foothills. Moreover, basement deformation at the frontal Eastern Foothills of Colombia appears to follow the pattern of thrust uplifts suggested by Berg (1962). However, there is a big difference that relates to the degree of folding of the basement rocks. The trishear mechanism of folding (Erslev, 1991; Hardy & Allmendinger, 2011; Hardy & Ford, 1997) can be used to effectively describe this change. Applying this trishear idea, the southern Llanos foothills along the Ariari–Guatiquía segment would be related to a higher propagation versus slip ratio, while the Caguán–Putumayo Foothills would be related to a lower propagation versus slip ratio. Further north in the Guavio and Tierranegra segments, intensely folded pre-Cretaceous rocks have been documented. Here we suggest that this major differ-

ence is related to the type of basement involved in the deformation. To the south, the Caguán–Putumayo Foothills are more related to the deformed crystalline basement rocks (Figure 1). To the north, basement-involved contractile deformation is related to the upper Paleozoic sedimentary units or the lower Paleozoic metasedimentary units, as documented by the Anaconda well. Tightly folded lower Paleozoic metasedimentary rocks of the Quetame Group are involved in an overturned fold, suggesting that the stratified anisotropies of the Paleozoic rocks may promote this behavior. A similar behavior has been suggested by Kammer et al. (2020). Alternative interpretations suggest the influence of salt tectonics in the structural style of this area (e.g., Parravano et al., 2015). Parravano et al. (2015) interpreted an overturned panel of Cretaceous rocks encountered during drilling of the Anaconda well as having been formed under the influence of salt tectonics on the basis of the salt occurrences of the Upin salt mine. However, the occurrence of lower Cre-

taceous salt is not ubiquitous and cannot be generalized for the Eastern Foothills. Moreover, other areas along strike with similar structural styles have documented the absence of salt layers (e.g., Kammer *et al.*, 2020). Therefore, salt could be locally intensifying the degree of folding in overturned panels deforming lower Cretaceous rocks (Parravano *et al.*, 2015); however, the available evidence shows that it is not the most decisive or ubiquitous factor influencing structural styles for the folded Paleozoic rocks in this segment.

An additional consideration is the fact that there is no documented precursor rift system along most of the Caguán Foothills, whereas inverted master faults have been well documented in the Llanos Foothills. We hypothesize that the presence of these faults would act as a buttress or as a strain riser as documented in the same region by Mora *et al.* (2006) or in the Alps (Coward *et al.*, 1991; de Graciansky *et al.*, 1989; Gillcrist *et al.*, 1987; Huyghe & Mugnier, 1995).

North of the Ariari–Guatiquía region, there is another major change in structural style, with thin-skinned deformation becoming very important. However, we draw important distinctions between the two situations, in which a broad thin-skinned anticline such as the Guavio Anticline (Figure 8) contrasts with the narrow antiform containing at least three main thrust stacks in the piedemonte region (Figure 10). It has been suggested that the Guavio Anticline overlies a major basement high, which could be related to a Neocomian normal fault (Figure 12; e.g., Mora *et al.*, 2006; Velasquez, 2002). If this is the case, the Guavio Anticline may reflect a thin-skinned fault–bend fold on top of a basement step (Casero *et al.*, 1997; Jimenez *et al.*, 2013; Mora *et al.*, 2006, 2010b; Rowan & Linares, 2000; Teixell *et al.*, 2015). In contrast, the piedemonte antiform has been attributed to closely spaced faulted detachment folds (e.g., Jimenez *et al.*, 2013; Martinez, 2006). We synthesize these observations as follows. Both the Ariari–Guatiquía and Guavio segments have well-documented Paleozoic rocks below Mesozoic – Cenozoic cover units, which contrasts sharply with the Caguán Foothills. However, the thick-skin structural style in the Ariari–Guatiquía segment is more similar to that documented here for the Caguán Foothills. Therefore, we hypothesize that the spatial onset of thin-skinned deformation in the Guavio segment is closely related to the presence of a thicker Mesozoic – Cenozoic stratigraphic succession in comparison to the southern Ariari–Guatiquía segment.

One critical geometric contradiction—that the Guavio segment has broader thin-skin structures while the piedemonte segment has anticlines stacked atop each other—could be influenced by the spacing of pre-Andean syn-rift features (normal faults) in a foreland position east of the main master syn-rift boundary faults. Such features could be absent, have less displacement, or be closer together in the piedemonte segment, since gravity data reveal no such basement high beneath the piedemonte antiform (see Figures 8, 11 where the frontal

thrust sheets are interpreted as being controlled by underlying Cretaceous normal faults, which are more broadly spaced and have more throw in the Guavio segment [Figure 8] than in the piedemonte antiform [Figure 11]).

Mora *et al.* (2014) suggested several possible reasons for thrust stacking in the piedemonte segment of the Colombian foothills: The presence of minor-displacement syn-rift normal faults; stratigraphic pinch-out or changing properties (becoming thinner or coarser) of the basal Chipaque detachment; and thickness of sedimentary Cenozoic units which act as a backstop for a forelandward propagation of thin-skinned deformation. In areas like the Bolivian Andes, even climate has been suggested as a potential controlling factor for thin-skinned foothill-style deformation (Horton, 1999; Montgomery *et al.*, 2001). However, in both the Bolivian and Colombian cases, the coincidence between the presence and thickness of detachment horizons and the overall width of the thin-skinned deformation front is well expressed. Further, as Mora *et al.* (2015b) documented, the potential role of climate in the evolution of the Colombian foothills could also be suggested as a mechanism in regions of enhanced tectonism such as along contractional horsetails (syntaxes) close to the termination of major basement faults like the Algeciras Fault (e.g., Rosello *et al.*, 2004). This scenario, however, is not applicable to the context of multiple thrust stacks in the piedemonte segment. Instead, in the partially analogous Magdalena Valley Foothills belt, Moreno *et al.* (2013) document so-called bypass structures, which are fold-thrust structures above ancient normal faults. This and the Guavio case could be templates for the piedemonte foothills, where stacking and structural styles are also partially controlled by underlying normal faults (see Figures 8 and 11 where the frontal thrust sheets are interpreted to be controlled by underlying Cretaceous normal faults). Finally, the spatial coincidence between stacked anticlines and the thickest Cenozoic sedimentary record (Mora *et al.*, 2014), suggests a potential causal relationship, as has been shown experimentally (Banks & Warburton, 1986; Bonini, 2001, 2007).

To summarize the evolution of this region, we suggest two situations with similar starting points that later diverged because of the sedimentary sequence thickness (Figure 13a, 13b). Both of them show a prestrained region with a master normal fault to the left (west) and more frontal normal faults with less displacement. For example, this could be the situation during the Early Cretaceous for the Eastern Llanos Foothills in the Ariari–Guatiquía segment and also in the piedemonte segment. The onset of inversion with significant exhumation could have occurred by the Oligocene along the master normal faults, with additional minor inversion in the more frontal normal faults with less displacement. However, deposition from the Oligocene to Neogene is much thicker in areas like the piedemonte segment, leading to more buttressing and intense folding than has occurred in the Ariari–Guatiquía

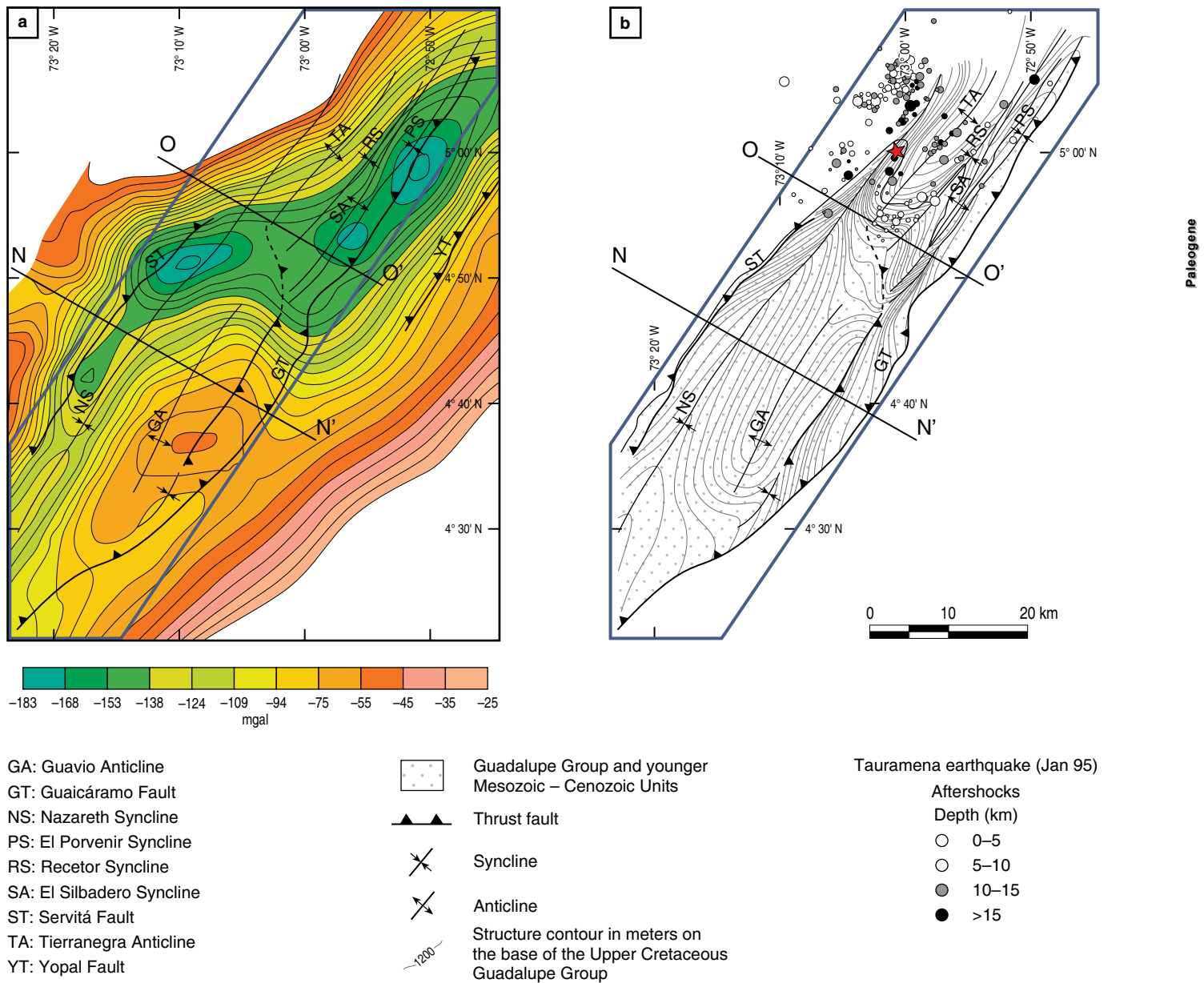


Figure 12. (a) Compilation of the main structural features and gravimetry showing the segmentation of the Eastern Foothills front and the location of the inferred inherited anisotropies. The map depicts variations in Bouguer anomaly in mGal (after Velasquez, 2002). Gravimetric lows are in green colors; orange and red colors show gravimetrical highs. **(b)** Structure contour map to the top of the Cretaceous and aftershocks of the Tauramena earthquake (the star shows the location of the main shock) showing the different structural styles in two different segments of the Guaicáramo thrust. Note the tight folding and periclinal terminations in the northern segment and the presence of seismicity just north of these periclinal terminations (see text for further discussion). Cross-section N–N' shows the location of Figure 8. Cross-section O–O' shows the location of Figure 9. Notice that Figures 8 and 9 are located in Figure 1, therefore with that spatial reference Figure 12 can also be located in Figure 1. Figure after Mora et al. (2006).

segment, which underwent a more classical inversion. In the piedemonte segment, apart from the minor inversion of the smaller Neocomian faults they may prompt the typical case of possible effects of pre-existing basement topography on thrust fault ramping described by Schedl & Wiltshko (1987). The overall differences in styles between the Ariari–Guatiquía segment and the piedemonte segment would therefore have been caused by the thicker sedimentites.

Recent studies (Mora et al., 2019a, 2019b) suggest that the Upper Cretaceous source rocks in the foothills would have been mature and in the oil window by the late Miocene to recent period. Given that this is also the timing of the most important shortening and antiformal stacking in these structures (Ketcham et al., 2016), we suggest, as initially proposed by Mora et al. (2010b) for the thin-skinned sub-Andean basins of South America in general, that the presence of source rocks in the oil

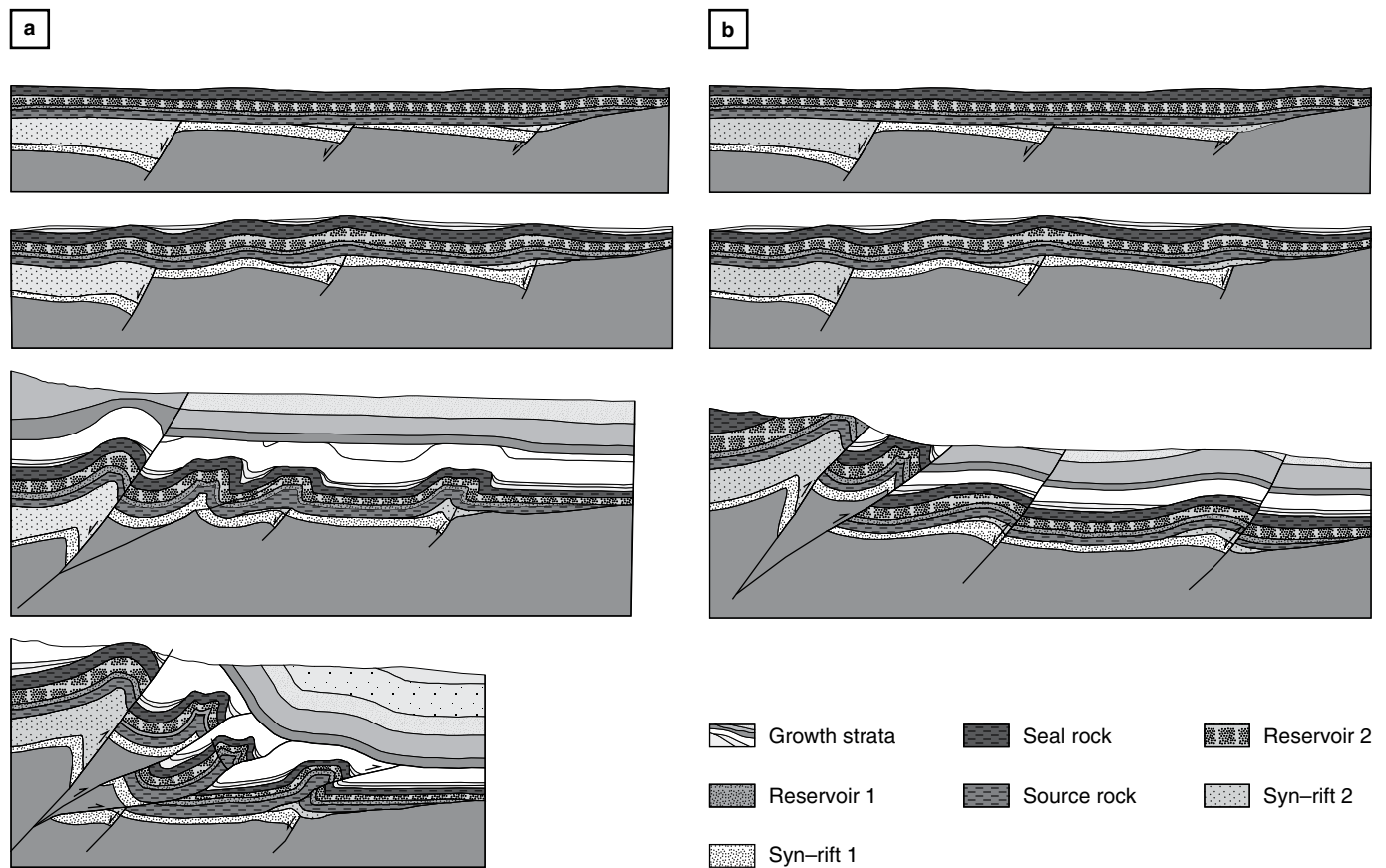


Figure 13. Summary evolutionary sketch of two end members of the Eastern Foothills. **(a)** Thin-skinned end member with thick sedimentary cover. **(b)** Thick-skinned end member with thin sedimentary cover.

window favored the role of those horizons as efficient detachments during the Pliocene – Pleistocene. One important line of evidence to reinforce that idea is the fact that other shaley horizons in the Eastern Foothills, like the Miocene C2 Member of the Carbonera Formation (Gomez et al., 2009), has never been documented as a detachment horizon for shallow foothill structures. Moreover, to the south in the Ariari–Guatiquía segment, poor and immature source rocks and less burial would not favor thin-skinned deformation.

We suggest that this sequence of evolutionary events and deformation geometries potentially can be found in other areas, such as the Sierras Pampeanas (Jordan & Allmendinger, 1986; Ramos et al., 2002) for the thick-skinned end members or the Peruvian sub-Andean ranges for thin-skinned behavior (e.g., Mora et al., 2014).

There is a final aspect that has not been mentioned in this review. This is the role of oblique stresses reactivating pre-existing normal faults in transpressional or contractional terrains. Without this factor, reactivation of normal faults in contraction would be extremely difficult. Our review is based on 2D cross-sections and makes minor mention of this factor. Previous studies (e.g., Branquet et al., 2002; Rosello et al., 2004) have considered that oblique stresses and wrench tectonics are instrumental for the

origin and structural styles in the Eastern Cordillera and associated foothills. We agree that stresses impinging obliquely on the pre-existing anisotropies are instrumental for their reactivation in the foothills (e.g., Mora et al., 2006, 2010a). However, it is significant that well documented strike-slip faults like the Algeciras Fault, display minor strike-slip movements and are localized structures, with narrow deformation zones, mainly south of 4° N latitude. Therefore, we believe that stresses are not purely orthogonal to the structures but also strike-slip tectonics are not dominant in the Eastern Foothills of Colombia. Previous studies support this (e.g., Tesón et al., 2013).

6. Conclusions

In this chapter we propose that the main differences between the Caguán–Putumayo and Llanos Foothills belts of Colombia are related to the type of basement involved in the deformation front, the thickness of the sedimentary units, the presence or absence of detachments, and the spacing and throw inferred in buried inherited Mesozoic normal faults. The presence of a crystalline basement and thin sedimentary cover in Caguán promotes the development of broad basement uplifts with little folding, while thick sedimentary cover and a more metasedi-

mentary basement facilitates the development of thin-skinned structures and duplexes in the Llanos Foothills. Moreover, buried normal faults are more easily reactivated wherever the applied stresses are oblique with respect to the inherited anisotropies. The initial evolution of both foothill belts was similar and progressive, but since the mid-Miocene, their structural styles showed significant departures due to the above-mentioned features. The time (ca. 30 Ma) required to progressively develop the Eastern Foothills of Colombia and the factors involved in such development represent important templates for other folded belts worldwide.

References

- Anderson, V.J., Shanahan, T.M., Saylor, J.E., Horton, B.K. & Mora, A. 2014. Sources of local and regional variability in the MBT'/CBT paleotemperature proxy: Insights from a modern elevation transect across the Eastern Cordillera of Colombia. *Organic geochemistry*, 69: 42–51. <https://doi.org/10.1016/j.orggeochem.2014.01.022>
- Anderson, V.J., Horton, B.K., Saylor, J.E., Mora, A., Tesón, E., Breecker, D.O. & Ketcham, R.A. 2016. Andean topographic growth and basement uplift in southern Colombia: Implications for the evolution of the Magdalena, Orinoco, and Amazon River systems. *Geosphere*, 12(4): 1235–1256. <https://doi.org/10.1130/GES01294.1>
- Baby, P., Rivadeneira, M., Barragan, R. & Christophoul, F. 2013. Thick-skinned tectonics in the Oriente Foreland Basin of Ecuador. In: Nemčok, M., Mora, A. & Cosgrove, J.W. (editors), *Thick-skinned-dominated orogens: From initial inversion to full accretion*. Geological Society of London, Special Publication 377, p. 59–76. <https://doi.org/10.1144/SP377.1>
- Bande, A., Horton, B.K., Ramírez, J.C., Mora, A., Parra, M. & Stockli, D.F. 2012. Clastic deposition, provenance, and sequence of Andean thrusting in the frontal Eastern Cordillera and Llanos Foreland Basin of Colombia. *Geological Society of America Bulletin*, 124(1–2): 59–76. <https://doi.org/10.1130/B30412.1>
- Banks, C.J. & Warburton, J. 1986. 'Passive-roof' duplex geometry in the frontal structures of the Kirthar and Sulaiman mountain belts, Pakistan. *Journal of Structural Geology*, 8(3–4): 229–237. [https://doi.org/10.1016/0191-8141\(86\)90045-3](https://doi.org/10.1016/0191-8141(86)90045-3)
- Berg, R.R. 1962. Mountain flank thrusting in Rocky Mountain Foreland, Wyoming and Colorado. *American Association of Petroleum Geologist Bulletin*, 46(11): 2019–2032.
- Bonini, M. 2001. Passive roof thrusting and forelandward fold propagation in scaled brittle-ductile physical models of thrust wedges. *Journal of Geophysical Research. Solid Earth*, 106(B2): 2291–2311. <https://doi.org/10.1029/2000JB900310>
- Bonini, M. 2007. Deformation patterns and structural vergence in brittle-ductile thrust wedges: An additional analogue modelling perspective. *Journal of Structural Geology*, 29(1): 141–158. <https://doi.org/10.1016/j.jsg.2006.06.012>
- Branquet, Y., Cheilletz, A., Cobbold, P.R., Baby, P., Laumonier, B. & Giuliani, G. 2002. Andean deformation and rift inversion, eastern edge of cordillera Oriental (Guatèque–Medina area), Colombia. *Journal of South American Earth Sciences*, 15(4): 391–407. [https://doi.org/10.1016/S0895-9811\(02\)00063-9](https://doi.org/10.1016/S0895-9811(02)00063-9)
- Caballero, V., Parra, M. & Mora, A. 2010. Levantamiento de la cordillera Oriental de Colombia durante el Eoceno tardío – Oligoceno temprano: Proveniencia sedimentaria en el Sinclinal de Nuevo Mundo, cuenca Valle Medio del Magdalena. *Boletín de Geología*, 32(1): 45–77.
- Caballero, V., Parra, M., Mora, A., López, C., Rojas, L.E. & Quintero, I. 2013a. Factors controlling selective abandonment and reactivation in thick-skin orogens: A case study in the Magdalena Valley, Colombia. In: Nemčok, M., Mora, A. & Cosgrove, J.W. (editors), *Thick-skin-dominated orogens: From initial inversion to full accretion*. Geological Society of London, Special Publication 377, p. 343–367. London. <https://doi.org/10.1144/SP377.4>
- Caballero, V., Mora, A., Quintero, I., Blanco, V., Parra, M., Rojas, L.E., López, C., Sánchez, N., Horton, B.K., Stockli, D. & Duddy, I. 2013b. Tectonic controls on sedimentation in an intermontane hinterland basin adjacent to inversion structures: The Nuevo Mundo Syncline, Middle Magdalena Valley, Colombia. In: Nemčok, M., Mora, A. & Cosgrove, J.W. (editors), *Thick-skin-dominated orogens: From initial inversion to full accretion*. Geological Society of London, Special Publication 377, p. 315–342. London. <https://doi.org/10.1144/SP377.12>
- Carrillo, E., Mora, A., Ketcham, R.A., Amoroch, R., Parra, M., Costantino, D., Robles, W., Avellaneda, W., Carvajal, J.S., Corcione, M.F., Bello, W., Figueroa, J.D., Gómez, J.F., González, J.L., Quandt, D., Reyes, M., Rangel, A.M., Román, I., Pelayo, Y. & Porras, J. 2016. Movement vectors and deformation mechanisms in kinematic restorations: A case study from the Colombian Eastern Cordillera. *Interpretation*, 4(1): T31–T48. <https://doi.org/10.1190/INT-2015-0049.1>
- Casero, P., Salel, J. F. & Rossato, A. 1997. Multidisciplinary correlative evidence for polyphase geological evolution of the foothills of the cordillera Oriental (Colombia). VI Simposio Bolivariano de Exploración Petrolera en la Cuenca Subandinas. *Proceedings* 1, 19 p. Cartagena.
- Castillo, J., Peñas, R., Cardozo, E., Villamizar, C.A., Gelvez, J., Ortiz, J., Velásquez, A.J., Mora, A.R., Caballero, V., De la Parra, F. & Blanco, V. 2016. New exploration ideas leading to discoveries and unlocking new potential in a mature oil province: The T2 unit, Llanos Basin, Colombia. AAPG/SEG International Conference & Exhibition. Abstracts, 1 p. Cancun, Mexico.
- Cooper, M.A. 1996. Passive-roof duplexes and pseudo-passive-roof duplexes at mountain fronts: A review. *Bulletin of Canadian Petroleum Geology*, 44(2): 410–421.
- Cooper, M.A., Addison, F.T., Álvarez, R., Coral, M., Graham, R.H., Hayward, A.B., Howe, S., Martínez, J., Naar, J., Peñas, R., Pulham, A.J. & Taborda, A. 1995. Basin development and tectonic history of the Llanos Basin, Eastern Cordillera, and

- Middle Magdalena Valley, Colombia. *American Association of Petroleum Geologists Bulletin*, 79(10): 1421–1443.
- Coward, M.P., Gillcrust, R. & Trudgill, B. 1991. Extensional structures and their tectonic inversion in the western Alps. In: Roberts, A.M., Yielding, G. & Freeman, B. (editors), *The geometry of normal faults*. Geological Society of London, Special Publication 56, p. 93–112. <https://doi.org/10.1144/GSL.SP.1991.056.01.07>
- de Graciansky, P.C., Dardeau, G., Lemoine, M. & Tricart, P. 1989. The inverted margin in the French Alps and foreland basin inversion. In: Cooper, M.A. & Williams, G.D. (editors), *Inversion Tectonics*. Geological Society of London, Special Publication 44, p. 87–104. <https://doi.org/10.1144/GSL.SP.1989.044.01.06>
- Delgado, A., Mora, A. & Reyes–Harker, A. 2012. Deformation partitioning in the Llanos Foreland Basin during the Cenozoic and its correlation with building in the hinterland. *Journal of South American Earth Sciences*, 39: 228–244. <https://doi.org/10.1016/j.jsames.2012.04.011>
- Dengo, C. & Covey, M. 1993. Structure of the Eastern Cordillera of Colombia: Implications for trap styles and regional tectonics. *American Association of Petroleum Geologists Bulletin*, 77(8): 1315–1337. <https://doi.org/10.1306/BDF8E7A-1718-11D7-8645000102C1865D>
- Erslev, E.A. 1991. Trishear fault–propagation folding. *Geology*, 19(6): 617–620. [https://doi.org/10.1130/0091-7613\(1991\)019<0617:T-FPF>2.3.CO;2](https://doi.org/10.1130/0091-7613(1991)019<0617:T-FPF>2.3.CO;2)
- Gelvez, J., Villamizar, C.A., Mora, A.R., Caballero, V., de la Parra, F., Ortiz, J., Cardozo, E. & Velasquez, A.J. 2016. Re–thinking reservoirs: The case of the T2 sands in the southern Llanos Basin of Colombia. *AAPG/SEG International Conference & Exhibition*, 20 p. Cancún, Mexico.
- Gillcrust, R., Coward, M. & Mugnier, J.L. 1987. Structural inversion and its controls: Examples from the Alpine foreland and the French Alps. *Geodinamica Acta*, 1(1): 5–34. <https://doi.org/10.1080/09853111.1987.11105122>
- Gomez, A., Jaramillo, C., Parra, M. & Mora, A. 2009. Huesser Horizon: A lake and marine incursion in northwestern South America during the early Miocene. *Palaos*, 24(4): 136–147. <https://doi.org/10.2110/palo.2007.p07-074r>
- Hardy, S. & Allmendinger, R.W. 2011. Trishear: A review of kinematics, mechanics, and applications. In: McClay, K., Shaw, J. & Suppe, J. (editors), *Thrust fault–related folding*. American Association of Petroleum Geologists, *Memoirs* 94, p. 95–119. <https://doi.org/10.1306/13251334M943429>
- Hardy, S. & Ford, M. 1997. Numerical modeling of trishear fault propagation folding. *Tectonics*, 16(5): 841–854. <https://doi.org/10.1029/97TC01171>
- Horton, B.K. 1999. Erosional control on the geometry and kinematics of thrust belt development in the central Andes. *Tectonics*, 18(6): 1292–1304. <https://doi.org/10.1029/1999TC900051>
- Huyghe, P. & Mugnier, J.L. 1995. A comparison of inverted basins of the southern North Sea and inverted structures of the external Alps. In: Buchanan, J.G. & Buchanan, P.G. (editors), *Basin inversion*. Geological Society of London, Special Publication 88, p. 339–353. <https://doi.org/10.1144/GSL.SP.1995.088.01.19>
- Ibañez–Mejía, M., Ruiz, J., Valencia, V.A., Cardona, A., Gehrels, G.E. & Mora, A.R. 2011. The Putumayo Orogen of Amazonia and its implications for Rodinia reconstructions: New U–Pb geochronological insights into the Proterozoic tectonic evolution of northwestern South America. *Precambrian Research*, 191(1–2): 58–77. <https://doi.org/10.1016/j.precamres.2011.09.005>
- Jiménez, L., Mora, A., Casallas, W., Silva, A., Tesón, E., Támara, J., Namson, J., Higuera–Díaz, I.C., Lasso, A. & Stockli, D. 2013. Segmentation and growth of foothill thrust–belts adjacent to inverted grabens: The case of the Colombian Llanos Foothills. In: Nemčok, M., Mora, A.R. & Cosgrove, J.W. (editors), *Thick–skin–dominated orogens: From initial inversion to full accretion*. Geological Society of London, Special Publication 377, p. 189–220. <https://doi.org/10.1144/SP377.11>
- Jordan, T.E. & Allmendinger, R.W. 1986. The Sierras Pampeanas of Argentina: A modern analogue of Rocky Mountain foreland deformation. *American Journal of Science*, 286: 737–764. <https://doi.org/10.2475/ajs.286.10.737>
- Kammer, A., Piraquive, A., Gómez, C., Mora, A. & Velásquez, A. 2020. Structural styles of the Eastern Cordillera of Colombia. In: Gómez, J. & Mateus–Zabala, D. (editors), *The Geology of Colombia, Volume 3 Paleogene – Neogene*. Servicio Geológico Colombiano, *Publicaciones Geológicas Especiales* 37, p. 143–183. Bogotá. <https://doi.org/10.32685/pub.esp.37.2019.06>
- Ketcham, R.A., Mora, A., & Parra, M. 2016. Deciphering exhumation and burial history with multi–sample down–well thermochronometric inverse modeling. *Basin Research*, 30(S1): 48–64. <https://doi.org/10.1111/bre.12207>
- Malavieille, J. 2010. Impact of erosion, sedimentation, and structural heritage on the structure and kinematics of orogenic wedges: Analog models and case studies. *GSA Today*, 20(1): 4–10. <https://doi.org/10.1130/GSATG48A.1>
- Martínez, J.A. 2006. Structural evolution of the Llanos Foothills, Eastern Cordillera, Colombia. *Journal of South American Earth Sciences*, 21(4): 510–520. <https://doi.org/10.1016/j.jsames.2006.07.010>
- Mitra, S. & Mount, V.S. 1998. Foreland basement–involved structures. *American Association of Petroleum Geologist Bulletin*, 82(1): 70–109. <https://doi.org/10.1306/1D9BC39F-172D-11D7-8645000102C1865D>
- Montgomery, D.R., Balco, G. & Willett, S.D. 2001. Climate, tectonics, and the morphology of the Andes. *Geology*, 29(7): 579–582. [https://doi.org/10.1130/0091-7613\(2001\)029<0579:CTAT-MO>2.0.CO;2](https://doi.org/10.1130/0091-7613(2001)029<0579:CTAT-MO>2.0.CO;2)
- Mora, A. & Kammer, A. 1999. Comparación de los estilos estructurales en la sección entre Bogotá y los Farallones de Medina, cordillera Oriental de Colombia. *Geología Colombiana*, (24): 55–82.
- Mora, A. & Parra, M. 2008. The structural style of footwall shortcuts along the Eastern Foothills of the Colombian Eastern Cordille-

- ra: Differences with other inversion related structures. *Ciencia, Tecnología y Futuro*, 3(4): 7–21.
- Mora, A., Parra, M., Strecker, M.R., Kammer, A., Dimaté, C. & Rodríguez, F. 2006. Cenozoic contractional reactivation of Mesozoic extensional structures in the Eastern Cordillera of Colombia. *Tectonics*, 25(2): 19 p. <https://doi.org/10.1029/2005TC001854>
- Mora, A., Parra, M., Strecker, M.R., Sobel, E.R., Hooghiemstra, H., Torres, V. & Vallejo–Jaramillo, J. 2008. Climatic forcing of asymmetric orogenic evolution in the Eastern Cordillera of Colombia. *Geological Society of America Bulletin*, 120(7–8): 930–949. <https://doi.org/10.1130/B26186.1>
- Mora, A., Parra, M., Strecker, M.R., Sobel, E.R., Zeilinger, G., Jaramillo, C., Ferreira Da Silva, S. & Blanco, M. 2010a. The Eastern Foothills of the Eastern Cordillera of Colombia: An example of multiple factors controlling structural styles and active tectonics. *Geological Society of America Bulletin*, 122(11–12): 1846–1864. <https://doi.org/10.1130/B30033.1>
- Mora, A., Horton, B.K., Mesa, A., Rubiano, J., Ketcham, R.A., Parra, M., Blanco, V., Garcia, D. & Stockli, D.F. 2010b. Migration of Cenozoic deformation in the Eastern Cordillera of Colombia interpreted from fission track results and structural relationships: Implications for petroleum systems. *American Association of Petroleum Geologists Bulletin*, v. 94 (10): 1543–1580. <https://doi.org/10.1306/01051009111>
- Mora, A., Baby, P., Roddaz, M., Parra, M., Brusset, S., Hermoza, W. & Espurt, N. 2010c. Tectonic history of the Andes and sub-Andean zones: Implications for the development of the Amazon drainage basin. In: Hoorn, C. & Wesselingh, F.P. (editors), *Amazonia: Landscape and species evolution: A look into the past*. Wiley–Blackwell, p. 38–60. Oxford, UK. <https://doi.org/10.1002/9781444306408.ch4>
- Mora, A., Reyes–Harker, A., Rodríguez, G., Tesón, E., Ramírez–Arias, J.C., Parra, M., Caballero, V., Mora, J.P., Quintero, I., Valencia, V., Ibañez–Mejía, M., Horton, B.K. & Stockli, D.F. 2013a. Inversion tectonics under increasing rates of shortening and sedimentation: Cenozoic example from the Eastern Cordillera of Colombia. In: Nemčok, M., Mora, A. & Cosgrove, J.W. (editors), *Thick–skin–dominated orogens: From initial inversion to full accretion*. Geological Society of London, Special Publication 377, p. 411–442. London. <https://doi.org/10.1144/SP377.6>
- Mora, A., Blanco, V., Naranjo, J., Sanchez, N., Ketcham, R.A., Rubiano, J., Stockli, D.F., Quintero, I., Nemčok, M., Horton, B.K. & Davila, H. 2013b. On the lag time between internal strain and basement involved thrust induced exhumation: The case of the Colombian Eastern Cordillera. *Journal of Structural Geology*, 52: 96–118. <https://doi.org/10.1016/j.jsg.2013.04.001>
- Mora, A., Ketcham, R.A., Higuera–Díaz, I.C., Bookhagen, B., Jimenez, L. & Rubiano, J. 2014. Formation of passive–roof duplexes in the Colombian Subandes and Perú. *Lithosphere* 6(6): 456–472. <https://doi.org/10.1130/L340.1>
- Mora, A., Casallas, W., Ketcham, R.A., Gómez, D., Parra, M., Namson, J., Stockli, D., Almendral, A., Robles, W. & Ghorbal, B. 2015a. Kinematic restoration of contractional basement structures using thermokinematic models: A key tool for petroleum system modeling. *American Association of Petroleum Geologists Bulletin*, 99(8): 1575–1598. <https://doi.org/10.1306/04281411108>
- Mora, A., Parra, M., Rodríguez–Forero, G., Blanco, V., Moreno, N., Caballero, V., Stockli, D.F., Duddy, I. & Ghorbal, B. 2015b. What drives orogenic asymmetry in the northern Andes? A case study from the apex of the northern Andean orocline. In: Bartolini, C. & Mann, P. (editors), *Petroleum geology and potential of the Colombian Caribbean margin*. American Association of Petroleum Geologists, Memoir 108, p. 547–586. <https://doi.org/10.1306/13531949M1083652>
- Mora, A., Gomez, R.A., Diaz, C., Caballero, V., Parra, M., Villamizar, C., Lasso, A., Ketcham, R.A., Gonzalez–Penagos, F., Rico, J. & Arias–Martinez, J.P. 2019a. Water flow, oil biodegradation, and hydrodynamic traps in the Llanos Basin. Colombia. *American Association of Petroleum Geologists Bulletin*, 103(5): 1225–1264. <https://doi.org/10.1306/1003181611317237>
- Mora, A., García–Bautista, D.F., Reyes–Harker, A., Parra, M., Blanco, V., Sanchez, N., De la Parra, F., Caballero, V., Rodriguez, G., Ruiz, C., Naranjo, J., Teson, E., Niño, F., Quintero, I., Moreno, N., Cardozo, E., Gamba, N., Horton, B. K. & Arias–Martinez, J. P. 2019b. Tectonic evolution of petroleum systems within the onshore Llanos Basin: Insights on the presence of Orinoco heavy oil analogs in Colombia and a comparison with other heavy oil provinces worldwide. *American Association of Petroleum Geologists Bulletin*, 103(5): 1179–1224. <https://doi.org/10.1306/1003181611417236>
- Moreno, N., Silva, A., Mora, A., Tesón, E., Quintero, I., Rojas, L.E., López, C., Blanco, V., Castellanos, J., Sánchez, J., Osorio, L., Namson, J., Stockli, D. & Casallas, W. 2013. Interaction between thin– and thick–skinned tectonics in the foothill areas of an inverted graben: The Middle Magdalena Foothill belt. In: Nemčok, M., Mora, A.R. & Cosgrove, J.W. (editors), *Thick–skin–dominated orogens: From initial inversion to full accretion*. Geological Society of London, Special Publication 377, p. 221–255. London. <https://doi.org/10.1144/SP377.18>
- Moreno–Lopez, M.C. & Escalona, A. 2015. Precambrian – Pleistocene tectono–stratigraphic evolution of the southern Llanos Basin, Colombia: American Association of Petroleum Geologists Bulletin, 99(8): 1473–1501. <https://doi.org/10.1306/11111413138>
- Morley, C.K. 1986. A classification of thrust fronts. *American Association of Petroleum Geologists Bulletin*, 70(1): 12–25.
- Mount, V.S., Martindale, K.W., Griffith, T.W. & Byrd, J.O.D. 2011. Basement–involved contractional wedge structural styles: Examples from the Hanna Basin, Wyoming. In: McClay, K., Shaw, J. & Suppe, J. (editors), *Thrust fault–related folding*. American Association of Petroleum Geologists, Memoir 94, p. 271–281.
- Narr, W. & Suppe, J. 1994. Kinematics of basement involved compressive structures. *American Journal of Science*, 294(7): 802–860. <https://doi.org/10.2475/ajs.294.7.802>

- Nemčok, M., Mora, A. & Cosgrove, J.W. 2013. Thick-skin-dominated orogens; from initial inversion to full accretion: An introduction. In: Nemčok, M., Mora, A. & Cosgrove, J.W. (editors), *Thick-skin-dominated orogens: From initial inversion to full accretion*. Geological Society of London, Special Publication 377, p. 1–17. <https://doi.org/10.1144/SP377.17>
- Parra, M., Mora, A., Sobel, E.R., Strecker, M.R. & González, R. 2009a. Episodic orogenic front migration in the northern Andes: Constraints from low-temperature thermochronology in the Eastern Cordillera, Colombia. *Tectonics*, 28(4), 27 p. <https://doi.org/10.1029/2008TC002423>
- Parra, M., Mora, A., Jaramillo, C., Strecker, M.R., Sobel, E.R., Quiroz, L., Rueda, M. & Torres, V. 2009b. Orogenic wedge advance in the northern Andes: Evidence from the Oligocene – Miocene sedimentary record of the Medina Basin, Eastern Cordillera, Colombia. *Geological Society of America Bulletin*, 121(5–6): 780–800. <https://doi.org/10.1130/B26257.1>
- Parra, M., Mora, A., Jaramillo, C., Torres, V., Zeilinger, G. & Strecker, M.R. 2010. Tectonic controls on Cenozoic foreland basin development in the north-eastern Andes, Colombia. *Basin Research*, 22(6): 874–903. <https://doi.org/10.1111/j.1365-2117.2009.00459.x>
- Parravano, V., Teixell, A. & Mora, A. 2015. Influence of salt in the tectonic development of the frontal thrust belt of the Eastern Cordillera, Guatiquía area, Colombian Andes. *Interpretation*, 3(4): SAA17–SAA27. <https://doi.org/10.1190/INT-2015-0011.1>
- Ramírez-Arias, J.C., Mora, A., Rubiano, J., Duddy, I., Parra, M., Moreno, N., Stockli, D. & Casallas, W. 2012. The asymmetric evolution of the Colombian Eastern Cordillera. Tectonic inheritance or climatic forcing? New evidence from thermochronology and sedimentology. *Journal of South American Earth Sciences*, 39: 112–137. <https://doi.org/10.1016/j.jsames.2012.04.008>
- Ramón, J. C. & Rosero, A. 2006. Multiphase structural evolution of the western margin of the Girardot Sub-basin, Upper Magdalena Valley, Colombia. *Journal of South American Earth Sciences*, 21(4): 493–509. <https://doi.org/10.1016/j.jsames.2006.07.012>
- Ramos, V.A., Cristallini, E.O. & Pérez, D.J. 2002. The Pampean flat-slab of the Central Andes. *Journal of South American Earth Sciences*, 15(1): 59–78. [https://doi.org/10.1016/S0895-9811\(02\)00006-8](https://doi.org/10.1016/S0895-9811(02)00006-8)
- Reyes-Harker, A., Ruiz-Valdivieso, C.F., Mora, A., Ramírez-Arias, J.C., Rodríguez, G., de la Parra, F., Caballero, V., Parra, M., Moreno, N., Horton, B.K., Saylor, J.E., Silva, A., Valencia, V., Stockli, D. & Blanco, V. 2015. Cenozoic paleogeography of the Andean foreland and retroarc hinterland of Colombia. *American Association of Petroleum Geologists Bulletin*, 99(8): 1407–1453. <https://doi.org/10.1306/061814111110>
- Rossello, E.A., Nevistic, V.A., Araque, L., Bettini, F., Bordampé, C., Castro, E., Colo, C., Córscico, S., Covellone, G., Haring, C., Pina, L., Pinilla, C., Ruiz, J.C. & Salvay, R.O. 2004. La sintaxis tectónica neógena de las cordilleras Oriental y Santander: Aportes de modelos analógicos y controles regionales sobre los sistemas petroleros. 3^{ra} Convención de la Asociación Colombiana de Geólogos y Geofísicos del Petróleo. *Memoirs in CD ROM* 16, 3 p. Bogotá.
- Rowan, M.G. & Linares, R. 2000. Fold-evolution matrices and axial-surface analysis of fault-bend folds: Application to the Medina Anticline, Eastern Cordillera, Colombia. *American Association of Petroleum Geologists Bulletin*, 84(6): 741–764. <https://doi.org/10.1306/A96733E2-1738-11D7-8645000102C1865D>
- Saeid, E., Bakioglu, K.B., Kellogg, J., Leier, A., Martínez, J.A. & Guerrero, E. 2017. Garzón Massif basement tectonics: Structural control on evolution of petroleum systems in Upper Magdalena and Putumayo Basins, Colombia. *Marine and Petroleum Geology*, 88: 381–401. <https://doi.org/10.1016/j.marpetgeo.2017.08.035>
- Saylor, J.E., Horton, B.K., Stockli, D.F., Mora, A. & Corredor, J. 2012. Structural and thermochronological evidence for Paleogene basement-involved shortening in the axial Eastern Cordillera, Colombia. *Journal of South American Earth Sciences*, 39: 202–215. <https://doi.org/10.1016/j.jsames.2012.04.009>
- Schedl, A. & Wiltshko, D. 1987. Possible effects of pre-existing basement topography on thrust fault ramping. *Journal of Structural Geology*, 9(8): 1029–1037. [https://doi.org/10.1016/0191-8141\(87\)90011-3](https://doi.org/10.1016/0191-8141(87)90011-3)
- Támara, J., Mora, A., Robles, W., Kammer, A., Ortiz, A., Sánchez-Villar, N., Piraquive, A., Rueda, L.H., Casallas, W., Castellanos, J., Montaña, J., Parra, L.G., Corredor, J., Ramirez, Á. & Zambrano, E. 2015. Fractured reservoirs in the Eastern Foothills, Colombia, and their relationship with fold kinematics. *American Association of Petroleum Geologists Bulletin*, 99(8): 1599–1633. <https://doi.org/10.1306/09291411109>
- Teixell, A., Ruiz, J.C., Teson, E. & Mora, A. 2015. The structure of an inverted back-arc rift: Insights from a transect across the Eastern Cordillera of Colombia near Bogotá. In: Bartolini, C. & Mann, P. (editors), *Petroleum geology and potential of the Colombian Caribbean margin*. American Association of Petroleum Geologists, Memoir 108, p. 499–516. <https://doi.org/10.1306/M1081307>
- Teson, E., Mora, A., Silva, A., Namson, J., Teixell, A., Castellanos, J., Casallas, W., Julivert, M., Taylor, M., Ibañez-Mejía, M. & Valencia, V. 2013. Relationship of Mesozoic graben development, stress, shortening magnitude, and structural style in the Eastern Cordillera of the Colombian Andes. In: Nemčok, M., Mora, A. & Cosgrove, J.W. (editors), *Thick-skin-dominated orogens: From initial inversion to full accretion*. Geological Society of London, Special Publication 377, p. 257–283. London. <https://doi.org/10.1144/SP377.10>
- Vásquez, M. & Altenberger, U. 2005. Mid-Cretaceous extension-related magmatism in the eastern Colombian Andes. *Journal of South American Earth Sciences*, 20(3): 193–210. <https://doi.org/10.1016/j.jsames.2005.05.010>
- Velandia, F., Acosta, J., Terraza, R. & Villegas, H. 2005. The current tectonic motion of the northern Andes along the Algeciras

- Fault System in SW Colombia. *Tectonophysics*, 399(1–4): 313–329. <https://doi.org/10.1016/j.tecto.2004.12.028>
- Velásquez, A.J. 2002. Modelamiento geofísico cortical por medio de métodos de campos potenciales con base en un modelo estructural del piedemonte llanero, Colombia. Bachelor thesis, Universidad Nacional de Colombia, 115 p. Bogotá.
- Veloza, G., Styron, R., Taylor, M. & Mora, A. 2012. Open-source archive of active faults for northwest South America. *GSA Today*, 22(10): 4–10. <https://doi.org/10.1130/GSAT-G156A.1>
- Wolaver, B.D., Coogan, J.C., Horton, B.K., Suarez-Bermúdez, L., Sun, A.Y., Wawrzyniec, T.F., Zhang, T., Shanahan, T.M., Dunlap, D.B., Costley, R.A. & de la Rocha, L. 2015. Structural and hydrogeologic evolution of the Putumayo Basin and adjacent fold-thrust belt, Colombia. *American Association of Petroleum Geologists Bulletin*, 99(10): 1893–1927. <https://doi.org/10.1306/05121514186>

Authors' Biographical Notes



Andrés MORA is the chief geologist of Onshore Exploration at Ecopetrol. He received his BS in geology from the Universidad Nacional de Colombia and PhD from the Institut für Geowissenschaften, Universität Potsdam. His research interests include structural geology, petroleum exploration, and petroleum geology.



Mauricio PARRA is an Assistant Professor at the Instituto de Energia e Ambiente of the Universidade de São Paulo, where he leads the Low-Thermochronology Laboratory. He received his BS in geology from the Universidad Nacional de Colombia and his PhD from the Institut für Geowissenschaften, Universität Potsdam. His research focuses on the tectonic evolution of mountain belts using thermochronometry and sedimentary basin analysis.



Eliseo TESÓN is a senior structural geologist at the Vicepresidencia de Exploración of Ecopetrol. He holds a PhD in structural geology from the Universidad Autónoma de Barcelona and has experience as a structural geologist in several basins worldwide, in countries like Perú, India, Colombia, and Morocco.



Álvaro LASSO is a senior exploration geologist at Ecopetrol with more than 35 years of experience in different basins in Colombia and in other countries like Libya, Syria, Irak, and Bolivia. He has a MS in petroleum geology and has worked for companies like Lasmo Oil and Chevron Petroleum. His broad experience includes play-based regional-scale exploration, prospect generation, geological operations, and development geology.



Jaime MARTÍNEZ is the Llanos and piedemonte onshore exploration manager at the Vicepresidencia de Exploración of Ecopetrol. He has over 25 years of experience in the oil industry, in companies like BP and Equion Energia. He is an expert in foothill exploration and during the last 2 years he has been part of Ecopetrol.



Brian K. HORTON is the Alexander Deussen Professor of Energy Resources at The University of Texas at Austin and has a joint appointment with the Department of Geological Sciences and Institute for Geophysics in the Jackson School of Geosciences. He received his BS from the University of New Mexico, MS from Montana State University, and PhD from the University of Arizona. His research addresses the tectonics of sedimentary basins and the evolution of orogenic systems.



Richard A. KETCHAM is an associate professor with the Jackson School of Geosciences at the University of Texas at Austin. He received his BS in geology and computer science from Williams College in 1987 and his PhD in geological sciences from the University of Texas at Austin in 1995. His active research interests include thermochronology and geological applications of high-resolution X-ray computed tomography.



Antonio VELÁSQUEZ received his Bachelor of Science and Master of Science degrees in geology from the Universidad Nacional de Colombia, evaluating the structural evolution of the Llanos foothills and modeling their gravitational expression by means of crustal-scale anomalies.



Juan Pablo ARIAS-MARTÍNEZ holds a BS degree in geology from the Universidad de Caldas, Colombia. He is currently an exploration geologist at Ecopetrol. His research interests include structural geology, sedimentology, and petroleum geology.

Chapter 6



Structural Styles of the Eastern Cordillera of Colombia

<https://doi.org/10.32685/pub.esp.37.2019.06>

Published online 29 May 2020

Andreas KAMMER^{1*}, Alejandro PIRAQUIVE² , Cristhian GÓMEZ³,
Andrés MORA⁴, and Antonio VELÁSQUEZ⁵

Abstract The Eastern Cordillera of Colombia is bracketed between the moderately west-dipping flank of the Central Cordillera on its western side and the little disturbed to gently bent Guiana Shield on its eastern side. Unlike other Andean foreland-oriented belts, it is completely disconnected from the main Andean trunk system. Transverse shortening of 4 mm/y records a considerable displacement transfer to the upper plate; this is twice the long-term rate of 2.2 mm/y, which is the average for a shortening of 65 km over a period of 30 Ma and suggests an increased recent shortening phase. We differentiate three structural domains. The southern domain records significant shortening by penetrative strain at lower structural levels and folding at higher structural levels, which supports the idea of partitioning into pure-shear deformation within the pre-Cretaceous basement and into buckling in the Upper Cretaceous to Paleogene units. Similar constellations of a relatively weak crustal welt enclosed between domains with backstop characteristics have been examined in analogue and numerical experiments (“vise model”). A northern intermediate domain is characterized by large-scale, basement-cored antiforms, whose formation may be ascribed to the partial reactivation of Late Triassic normal faults. The northernmost domain comprises the Cocuy Syntaxis, which constitutes an antiformal lobe with significant topographic relief. It is affected by secondary folds with a down-slope vergence. These changes in structural style record increased support by the subducting slab, according to the spatial coincidence of the outer slab hinge and the highest topographic relief within this northern Andean flat slab segment.

To examine a possible cause for a rheological break between deformable cordilleran crust sandwiched between relatively rigid and strong surrounding basement blocks, we review the Cretaceous back-arc setting. Tectonic subsidence and sedimentation patterns suggest its division into a forebulge and flanking basins that may be ascribed to the framework of an impinging mantle plume. Temporal constraints further suggest that forebulge evolution may have been triggered by an initial foundering of the slab at the onset of a Cretaceous subduction cycle. In such a small-scale convection system, downwelling mantle flow between the back-arc region and the stable shield may maintain a relatively well-defined rheological limit over long periods. This situation complies with the model of an edge-driven convective flow.

Rheological contrasts between the back-arc basin and the shield persisted into the Cenozoic and contributed to a protracted evolution of the Andean cordilleran mountain fronts. The eastern mountain front accumulated structural relief of more than

- 1 akammer@unal.edu.co
Universidad Nacional de Colombia
Departamento de Geociencias
Carrera 30 n.º 45-03
Bogotá, Colombia
- 2 apiraquive@sgc.gov.co
Servicio Geológico Colombiano
Dirección de Asuntos Nucleares
Carrera 50 n.º 26-20
Bogotá, Colombia
- 3 cngomezp@unal.edu.co
Universidad Nacional de Colombia
Departamento de Geociencias
Carrera 30 n.º 45-03
Bogotá, Colombia
- 4 andres.mora@ecopetrol.com.co
Ecopetrol S.A.
Vicepresidencia de Exploración
Bogotá, Colombia
- 5 antonio.velasquez@ecopetrol.com.co
Ecopetrol S.A.
Vicepresidencia de Exploración
Bogotá, Colombia

* Corresponding author

Citation: Kammer, A., Piraquive, A., Gómez, C., Mora, A., & Velásquez, A. 2020. Structural styles of the Eastern Cordillera of Colombia. In: Gómez, J. & Mateus-Zabala, D. (editors), *The Geology of Colombia, Volume 3 Paleogene – Neogene*. Servicio Geológico Colombiano, *Publicaciones Geológicas Especiales* 37, p. 143–183. Bogotá. <https://doi.org/10.32685/pub.esp.37.2019.06>

10 000 m during an initial Oligocene to late Miocene shortening phase. Fold growth incited by the buttressing of the strong foreland block of the shield can be tested by the tri-shear model, in which propagation of faulting is halted, and displacement is consumed by fold amplification. During a Pliocene stress reorganization, this Miocene mountain front was breached by a shallowly dipping thrust, which gave rise to a more foreland-oriented deformation front. During this outward-stepped faulting, proximal foreland sequences became involved in a wedge-top position and were exhumed at the thrust tip along emergent ramps. These second-cycle erosion products were widely dispersed into the Llanos Basin and were incorporated into modern fluvial terraces.

Keywords: *back-arc basin, fault reactivation, gravitational collapse, Eastern Cordillera of Colombia.*

Resumen La cordillera Oriental de Colombia está encajada entre el flanco inclinado ligeramente al oeste de la cordillera Central, al costado occidental, y el Escudo de Guayana levemente flexionado, al costado oriental. A diferencia de otros cinturones andinos de antepaís, esta cadena montañosa está completamente desconectada del sistema principal andino. El acortamiento transversal de 4 mm/año registra una transferencia considerable de desplazamiento a la placa superior; este es el doble de una tasa de 2,2 mm/año, que es el promedio para un acortamiento de 65 km durante un intervalo de tiempo de 30 Ma y sugiere una acelerada fase de acortamiento reciente. En este trabajo diferenciamos tres dominios estructurales. El dominio meridional registra un acortamiento significativo por deformación penetrativa a niveles estructurales inferiores y plegamiento a niveles estructurales superiores, lo que respalda la idea de diferenciar entre deformación por cizalla pura en el basamento precretácico y entre un plegamiento por acortamiento horizontal en las unidades del Cretácico Superior al Paleógeno. Constelaciones similares de un entorno cortical relativamente débil contenido entre dominios con características de contrafuerte han sido examinadas en experimentos análogos y numéricos (*vise model*). Un dominio intermedio más septentrional se caracteriza por antiformentes a gran escala, que involucran el basamento en su núcleo y cuya formación está predispuesta por la reactivación parcial de fallas normales del Triásico Tardío. El dominio más septentrional comprende la Sintaxis de Cocuy, un lóbulo antiformal de un mayor relieve topográfico. Esta se ve afectada por pliegues secundarios con una vergencia en dirección de la pendiente. Estos cambios en estilo estructural registran un aumento en el soporte de la losa subducida, como puede concluirse a partir de la coincidencia espacial entre bisagra externa de la losa en subducción y el relieve topográfico descomunal en este segmento de losa plana del norte andino.

Con el fin de examinar una posible causa para la existencia de un cinturón altamente deformable y encajado entre bloques circundantes de basamento relativamente rígidos y fuertes, examinamos la configuración de la cuenca de retroarco del Cretácico. Los patrones de subsidencia tectónica y sedimentación sugieren la existencia de una región axial dominada por un abombamiento amplio o *forebulge*, que se delimita por cuencas marginales y cuyo origen se atribuye al impacto de una pluma mantélica. Las limitaciones temporales sugieren, además, que la evolución del abombamiento puede haber sido desencadenada por un hundimiento inicial de la losa al inicio de un ciclo de subducción cretácico. En un sistema de convección a tan pequeña escala, el flujo del manto descendente entre la región de retroarco y el escudo estable puede mantener un límite reológico relativamente bien definido durante largos períodos de tiempo. Esta situación cumple con el modelo de un flujo convectivo de tipo *edge-driven*.

Contrastes reológicos entre la cuenca de retroarco y el escudo perduraron hasta el Cenozoico y contribuyeron a una evolución prolongada de los frentes cordilleranos andinos. Un antiforme del frente montañoso oriental acumuló un relieve estructural de más de 10 000 m durante una fase de acortamiento inicial entre el Oligoceno y el Mioceno tardío. El crecimiento de este pliegue fue inducido por el efecto de contrafuerte del bloque de antepaís del escudo. Este proceso puede ser probado por el modelo *tri-shear*, en el cual se detiene la propagación de falla y se consume el desplazamiento por la amplificación de este frente montañoso. Durante una reorganización del campo de esfuerzos en el Plioceno, este frente montañoso fue afectado por una falla fuera de secuencia con un buzamiento moderado, que dio lugar a un frente de deformación orientado más hacia el antepaís. En este fallamiento, las secuencias proximales de antepaís se involucraron en una posición de tipo supracuña o *wedge-top* y se exhumaron a lo largo de una falla emergente, que forma la base de un manto corrido. Estos productos de erosión de segundo ciclo se dispersaron ampliamente en la Cuenca de los Llanos, incorporándose a las terrazas fluviales modernas.

Palabras clave: *cuenca de retroarco, reactivación de falla, colapso gravitacional, cordillera Oriental de Colombia.*

1. Introduction

Within the North Andean Terrane, the Eastern Cordillera of Colombia (EC) is completely detached from the main Andean trunk system and forms a distinct morphotectonic feature, before the Andean system reassembles into the morphologically little differentiated mountain belts at the southern Caribbean Plate margin (Figure 1). Its width of >200 km in its central part is comparable to the combined transverse dimensions of the Central and Western Cordilleras further to the west (Figure 1). These three mountain belts are separated from each other by the interandean Cauca and Magdalena Valleys, of which the latter has subdued topography (<500 m) and contains several tectonic elements that are highlighted by an array of intra-basinal basement highs, which were first outlined by Morales (1958, Figure 1). As it approaches the Maracaibo Block, the Eastern Cordillera connects with the northwest-trending leg of the Santander Massif (Figure 1), which is composed of a narrow basement high and is bordered at its western margin by the left-lateral strike-slip Bucaramanga Fault. At their junction, the Bucaramanga Fault splays into an array of curved secondary faults, which are considered to form a horsetail structure at the southern termination of the Bucaramanga Fault (Acosta et al., 2007; Velandia & Bermúdez, 2018). At this same cordilleran relay, the Mérida Andes take off from the EC and constitute an independent chain in its northeasterly continuation, but separated by a sinistral step. Near this relay, the EC reaches its highest elevation at the syntaxial bend of the Cocuy Massif (Figure 1). Together with the peaks of the Sierra Nevada de Santa Marta, this massif contains the only North Andean non-volcanic summits that exceed the present snow line at 5000 m.

This intricate morphotectonic pattern suggests the control of Andean folding by inherited crustal or lithospheric features, as evidenced by Late Triassic – Early Jurassic precursor faults and associated graben structures that straddle the Bucaramanga Fault (Kammer & Sánchez, 2006). Moreover, a back-arc setting involves a long-standing Cretaceous Basin evolution (Guerre-ro, 2002 and references therein) and the inversion of this basin likely attests to a weakened crust that preferentially consumed shortening during Neogene folding, as observed in other back-arc settings (e.g., the Canadian Cordillera; Hyndman & Currie, 2011). A further regional consideration is related to the bend between the Andean and the Caribbean active margin and a consequent relaxation in lateral constraints between the converging mantle flows. This situation promoted lateral mantle flow in the upper plate and the margin-parallel translation of crustal blocks (Beck et al., 1993; Gephart, 1994; Russo & Silver, 1994), as presently occurs with the northward escape of the North Andean Terrane (Egbue & Kellogg, 2010).

In this contribution, we disentangle some of the relationships between the inherited crustal structures of the North Andean basement and the Neogene folding. We restrict ourselves to the middle segment of the EC, which contains the High Plain of Bogotá to the south, extends to the structural bend laid out by the NNW-striking Bucaramanga Fault, and is outlined further by the syntaxial bend of the Cocuy Massif (Figure 1). Since the pioneering works of Campbell & Bürgli (1965), Bürgli (1967), and Julivert (1970), the EC has been considered to have emerged from a Cretaceous rift structure, and its origin by the inversion of a back-arc basin has been further acclaimed in recent studies (Mora et al., 2006, 2009, 2013; Teixell et al., 2015; Tesón et al., 2013). In this account, we re-examine the link between the Cretaceous back-arc tectonics and Andean folding

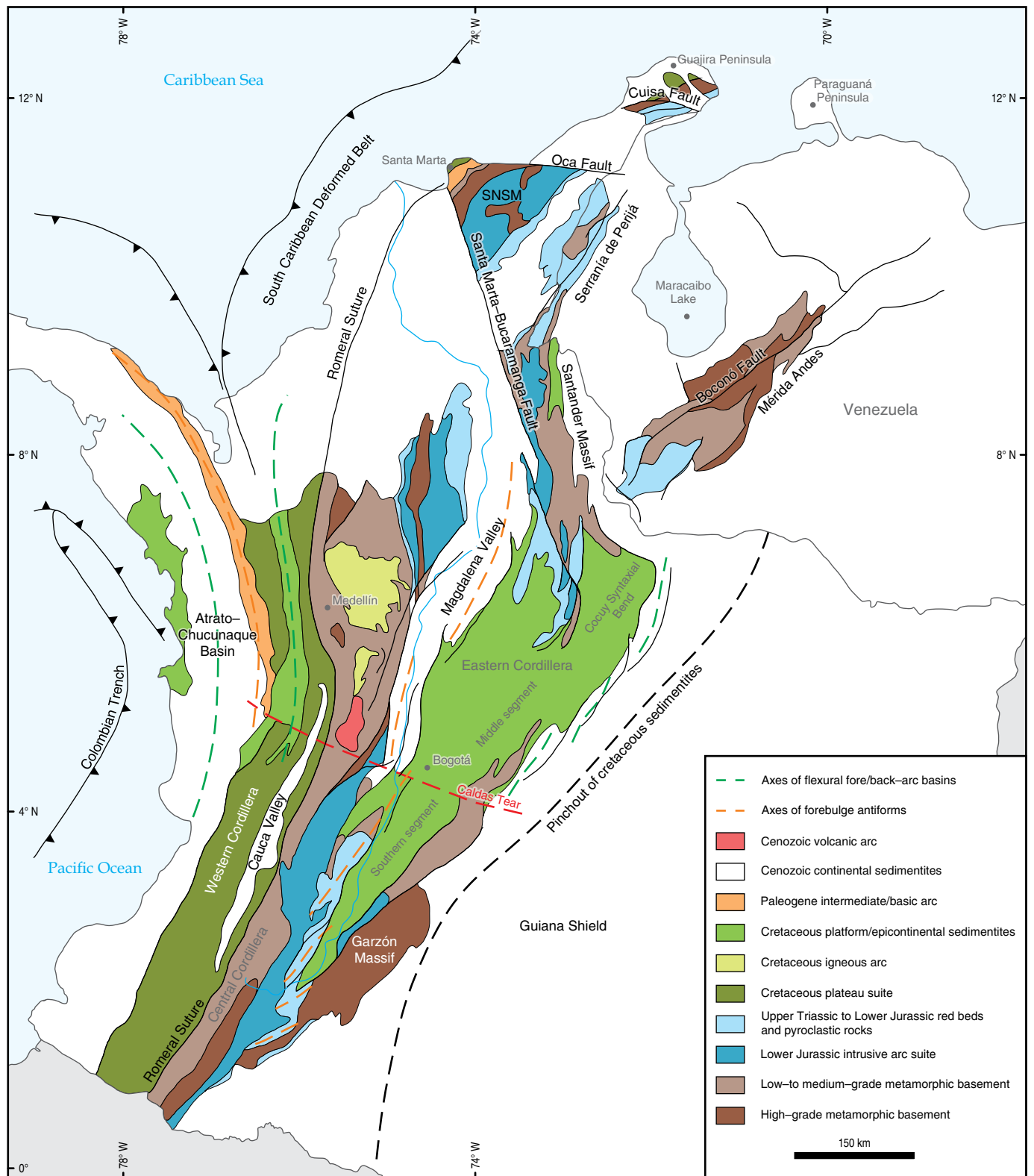


Figure 1. Sketch map of the three Andean mountain chains and the northwestern Maracaibo Block, which form the North Andean Terrane. The map depicts the pre-Cenozoic cordilleran basement units. It highlights the successive branching of the eastern mountain belts from the main Andean trunk system, as documented by the appearance of the interandean Magdalena Valley and the splaying of the EC into the Santander Massif and the Mérida Andes.

and attempt to gain an understanding of its geodynamic implications. We address three questions related to the Cretaceous rift event: (1) how is Cretaceous fault activity linked to the evolution of the marginal basins?, (2) are the Cretaceous border faults of this back-arc domain comparable to breakaway faults in extensional provinces?, and (3) are the extensional processes of the back-arc region related to the subduction dynamics of the Cretaceous active margin?

Much of the discussion of Cenozoic fault reactivation and cordilleran folding has focused on the relative importance of and temporal relationship between basement-involved and thin-skinned deformational styles (see the reviews in Cortés et al., 2006; Tesón et al., 2013). In our approach, we address the following questions: (1) did the overall shortening form a crustal root or result in crustal-scale buckling, which was eventually supported by the oceanic slab?, (2) considering the bivergent structure of the EC, were the deformation phases equally distributed across this orogenic pop-up, or do they record progressively east- (or west-) advancing deformation fronts?, and (3) is the small-scale folding of the High Plain of Bogotá a superficial expression of homogeneous basement shortening, or is it related to detachment folds conditioned by the existence of a basal Cretaceous evaporitic horizon, as contended by Cortés et al. (2006) and Teixell et al. (2015)?

2. Regional Framework

With respect to the modern plate tectonic framework, the EC and its northern extension, the Santander Massif, trend obliquely with respect to the present E–W oriented convergence between the Nazca Plate and South America (Trenkamp et al., 2002). Based on an average convergence rate of 60 mm/y (Trenkamp et al., 2002) and a shortening rate of 4 mm/y across the EC, as derived from GPS measurements (Mora-Páez et al., 2016), approximately 7% of the convergence is presently transferred to the eastern limit of the North Andean Terrane and converted into deformation. More important than this strike-perpendicular shortening is, however, a strike-parallel, apparently widely distributed slip component of 8 mm/y (Mora-Páez et al., 2016). Within the Mérida Andes (northwestern continuation of the EC), much of this slip is converted into dextral displacement along the Boconó Fault (Figure 1), which trends parallel to the axial zone of this mountain chain and has accommodated 7–10 mm/y of dextral displacement for the past 15 000 y (Audemard et al., 2008). This finding points to a recent kinematic plate reorganization, in which the convergence changed from margin-perpendicular to the present margin-oblique E–W direction.

The topographic aspects of the present-day plate interactions between the Nazca, Caribbean, and South American Plates are shown in Figure 2, which combines regional tectonomorphic features of the present-day plate setting with the projections of the hypocentral solutions of >30 000 earthquakes that were

extracted from the catalog of the Colombian National Seismological Network (Chiarabba et al., 2015; Vargas & Mann, 2013). These events are projected onto 8 transverse sections with topographically highly exaggerated elevations, to provide a reference for the different mountain belts. The earthquakes are strongly clustered and highlight the slab contours. This map shows the now well-known relay of a southern, moderately east-dipping slab segment and a northern, flat-dipping slab segment (Chiarabba et al., 2015; Pennington, 1981; Taboada et al., 2000; Vargas & Mann, 2013), which correlates with the onset of a volcanic gap north of 5° N. The seismic response to these slab segments is well-defined and has been referred to as the Caldas Tear (Vargas & Mann, 2013; Figures 1, 2). Surface structures image these different slab configurations in detail and document a doubling of the width of the EC within the flat slab realm, largely brought about by the inception of the frontal thrust sheets on either side of the EC (Figures 1, 3a).

Transverse sections 4 and 5 (Figure 2) document the surface response of the EC above the flat slab segment by its broadening and increased topographic relief. Within the basal Cretaceous sedimentites, paleothermometric index values based on vitrine reflectance, that were obtained from Lower Cretaceous sequences, are anomalously high near the tear zone ($R_o > 6$) with respect to regional background values ($3 < R_o < 4.5$; Parra et al., 2009a, 2009b; Mora et al., 2013) and point to the probable existence of a thermal window, which is further suggested by an elevated geothermal gradient of 44°/km for pre-Campanian sedimentites (Mora et al., 2008). Affirming the existence of a long-standing thermal anomaly, a pronounced ductile deformation style is expected to have persisted close to the relay zone, as may be deduced independently from the fold style at the eastern deformation front, which includes tight fault-related folds (Mora et al., 2006; Kammer et al., 2007). To inquire more about changes in structural style related to this slab-related framework, we investigate the three transverse sections of Figure 4, the locations of which are shown in Figure 3a.

3. Cordilleran Cross-Sections

The southern transverse section (see composite sections 1, 2, 3 in Figure 4) exposes the structural framework just north of the relay between the southern normally dipping and the northern shallowly dipping slab segments (indicated in Figure 2 by the shift of the outer slab bends between transverse sections 7 and 5). Here, the High Plain of Bogotá occupies a depressed axial zone in which the pre-Cretaceous basement is slightly more elevated than the basement of the foreland areas. Its condensed syn- to post-kinematic Neogene sequences mark a starved basin since at least the Pliocene (Torres et al., 2005; van der Hammen et al., 1973). Upper Cretaceous to Paleogene sedimentites are involved in open folds of relatively short and uniform wavelengths, ranging from 5 to 10 km in width.

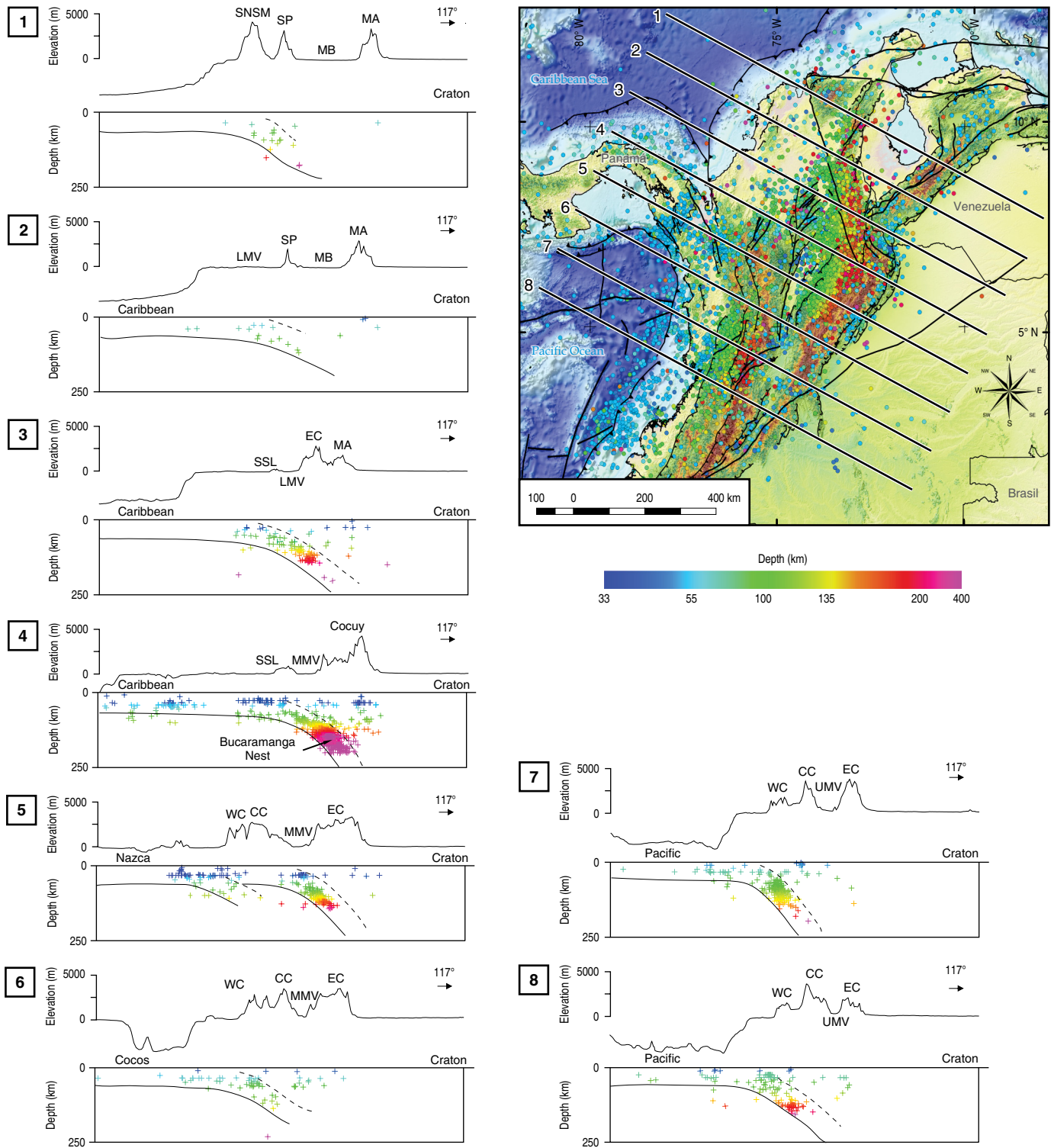


Figure 2. Tectono-morphologic map of northwestern South America with the distribution of the hypocentral solutions of >30 000 earthquakes extracted from the catalog of the Colombian National Seismological Network. The earthquake hypocenters are projected into 8 transverse sections to show the slab geometries. The highly exaggerated topography demarcates the Andean chains. Data compiled by Vargas & Mann (2013) and Chiarabba *et al.* (2015). (SNSM) Sierra Nevada de Santa Marta; (SP) Serranía de Perijá; (MB) Maracaibo Basin; (MA) Mérida Andes; (LMV) Lower Magdalena Valley; (MMV) Middle Magdalena Valley; (UMV) Upper Magdalena Valley; (SSL) Serranía de San Lucas; (EC) Eastern Cordillera; (CC) Central Cordillera; (WC) Western Cordillera.

The bounding marginal highs (the Villeta Anticlinorium to the west and the Montecristo Anticline to the east; Figure 4) expose Lower Cretaceous to upper Paleozoic sequences. Active modern (Pliocene or younger) deformation fronts are represented by the thrusts of the Guaicáramo and Cambao Faults (Figure 4), whose thrust sheets form minor frontal ranges at their leading edge.

The time frame for the formation of the eastern marginal high is given by a thick Oligocene to Pliocene clastic foreland sequence of a relict foreland trough, which is now folded and carried piggyback toward the foreland (see sections 2, 3 in Figure 4). Its clastic input records the exhumation of the Montecristo Anticline in detail, spanning an erosion window from Lower to Upper Cretaceous sedimentites. The final unroofing and deposition of Paleozoic marker clasts, however, was delayed until the deposition of the modern terraces in front of the Guaicáramo Thrust (Figure 4). They highlight a distinct foreland evolution without the formation of a depositional foredeep. This two-stage evolution involved the long-lasting build-up (Oligocene to late Miocene) of a mountain front with a structural relief of >10 km and its collapse as the frontal thrust stepped forward. The final exhumation of the Montecristo Anticline and the inception of the frontal Guaicáramo Thrust are thus closely linked, which is documented by the Pliocene/Pleistocene unroofing of the Paleozoic basement and an accelerated exhumation rate of >1 to 2 mm/y during the past 3 Ma for the Quetame Massif (location in Figure 3b; Mora et al., 2008, 2010a). The sequential processes of crustal thickening and foreland-directed expansion support the scenario of orogenic collapse (Rey et al., 2001).

A similar evolutionary sequence of a relatively stagnant mountain front and the Pliocene/Pleistocene breakdown by the activation of low-angle faults is thought to also apply to the western mountain front (Cortés et al., 2006). In section 1 (Figure 4), Oligocene to Miocene foredeep sedimentites are overthrust by the western flank of the Guaduas Syncline along the Cambao Fault. This thrusting entailed a westward shift of the Pliocene/Pleistocene accumulation space of the volcanoclastic Mesa Formation (Gómez et al., 2003).

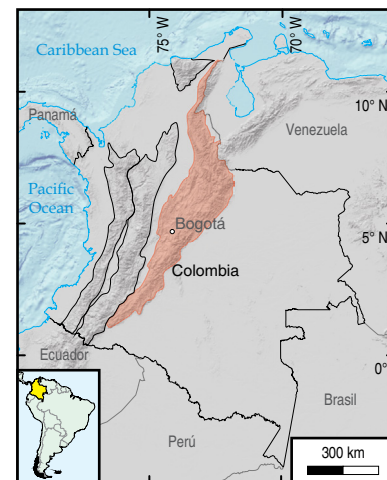
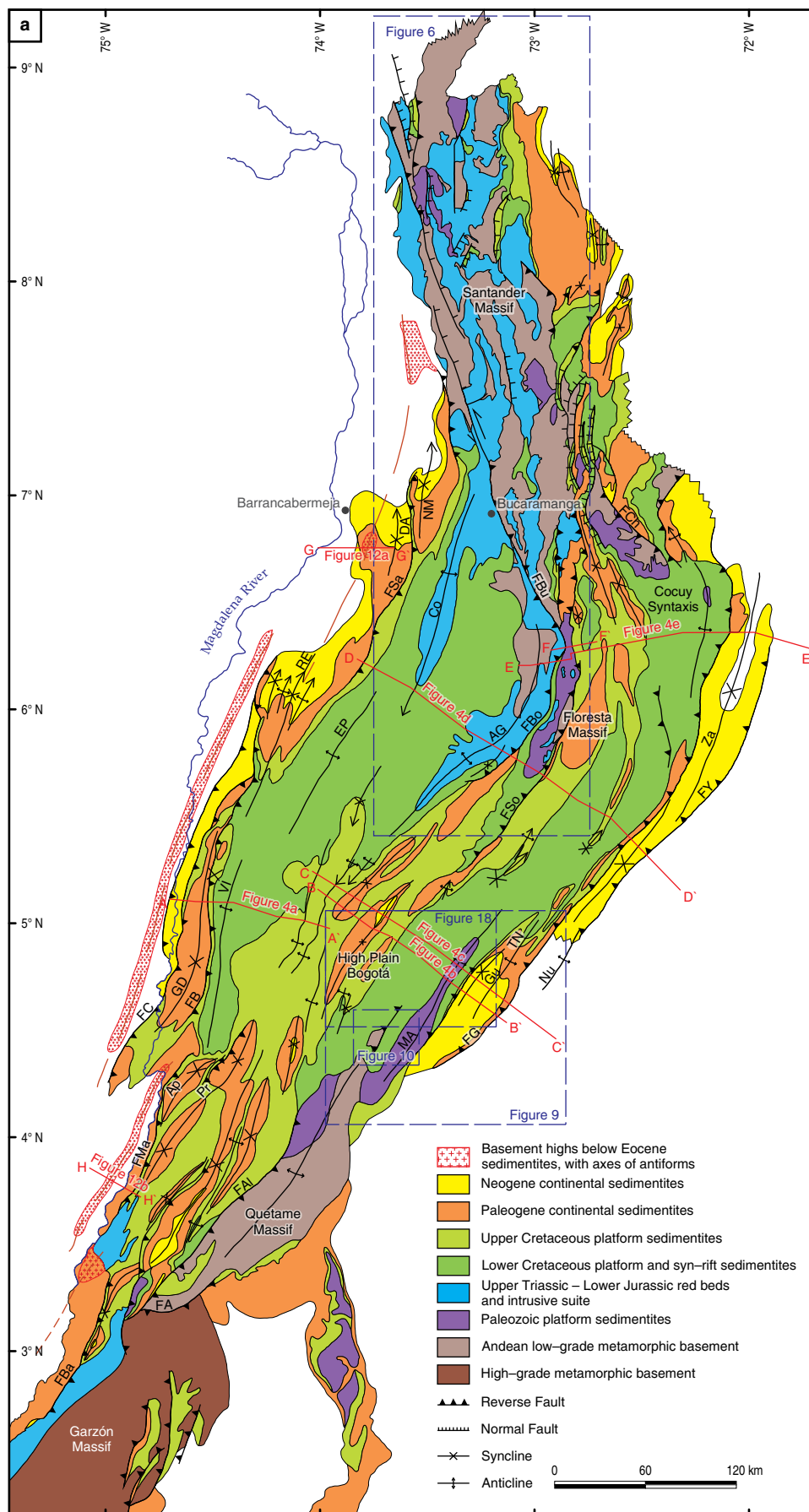
The Cretaceous to Paleogene sequences of the High Plain of Bogotá are affected by upright folds of relatively short wavelengths that, upon reaching the gently inclined flanks of this axial depression, assume a vergence toward the marginal highs (see sections 2, 3 in Figure 4). Within these flanks, deformation partitioning by buckling at higher structural levels and homogeneous shortening by cleavage formation at lower structural levels is observed (Kammer & Mora, 1999). These relations are documented in Figure 3b by the compilation of bed-parallel 2D-strain markers, such as deformed ammonites and brachiopods. Whereas the folded beds of the Paleogene and Upper Cretaceous units are virtually free of strain, strain markers at lower levels (Fómeque and stratigraphically lower formations;

Figure 5) record axial ratios of strain ellipses (R_s) of $1.2 < R_s < 1.6$ within both cordilleran flanks. Muddy lithologies display an axial plane cleavage at strains as low as $R_s = 1.2$. An important transitional zone combines flexural slip folding with axial plane cleavage, suggesting a deformation mode that combines folding and homogeneous shortening (Kammer, 1997).

The structural style of the central region north of the High Plain of Bogotá is explored by means of section 4 (Figure 4), which again pertains to lithospheric transverse section 5 (Figure 2). Uplift is centered on the composite axial highs of the Arcabuco Anticline and the Floresta Massif, both of which are bounded by reactivated faults in their eastern flanks. These faults may be assigned to the extensional horsetail structure at the termination of a Late Triassic precursor of the Bucaramanga Fault, which accommodated dextral displacement within an overall NW–SE extensional regime (Figure 6). The NE–SW-trending splay faults accumulated normal displacement, as documented by Late Triassic graben fills that contain thick alluvial fan sequences near the fault traces (Figure 6). The Lower Jurassic intrusive suite (Santander Plutonic Group with Early Jurassic crystallization ages; van der Lelij et al., 2016) is represented by sheet-like bodies emplaced along formerly tilted basement blocks (Figure 6b), which document a close relationship between faulting, block tilting, and intrusive activity. The syntectonic emplacement of this Lower Jurassic intrusive suite is further demonstrated at a right-stepping relay between two overlapping fault strands, which converged through a fault linkage by curved terminations. The eastern hook-shaped fault of this relay is intruded by the Río Negro Batholith, which is also part of the Santander Plutonic Group (Figure 6b).

The Cenozoic reactivation of these faults dates back to the late Eocene – early Oligocene, as documented by a Paleogene sedimentary fill of a small foreland basin (Concentración Formation; Figure 5) and thermochronological data (Bayona et al., 2013; Mora et al., 2010a, 2015; Parra et al., 2009b; Saylor et al., 2012). Fault reactivation resulted in the formation of asymmetric, fault-related folds with a distinct east-directed vergence or emergent faults displaying rim synclines in their hanging wall (Kammer, 1996).

These basement-cored antiforms form first-order structures, whereas second-order folds of minor widths (<8 km) are located on gently dipping domains on the western (west of the Los Cobardes Anticline; section 4 in Figure 4) and eastern flanks (e.g., Kammer, 1997). The eastern foreland structures involve an imbricated stack of folded slices, the geometry of which was unraveled in detail by exploration campaigns of the oil industry (Jiménez et al., 2013; Martínez, 2006). Their gradual, foreland-directed decrease in fold amplitudes, and fold widths compares to analog experiments, where a decay in fold shape was produced by a push from the rear (Price, 1975). The juxtaposition between the intensely sliced deformation front and the undeformed Llanos Block highlights the contrasting



Eastern Cordillera of Colombia

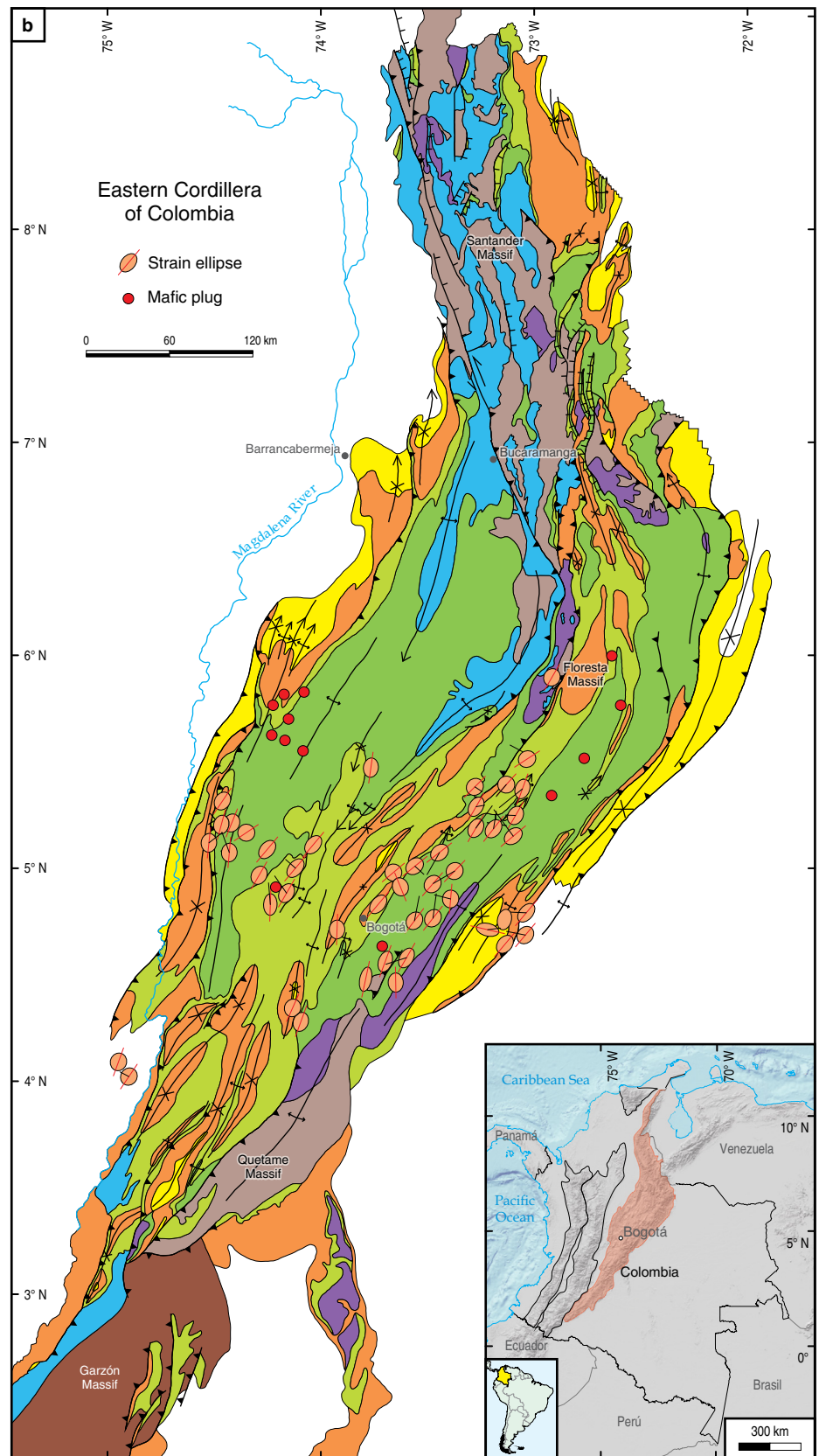
Faults

- FB: Bituima Fault
- FBo: Boyacá Fault
- FBu: Bucaramanga Fault
- FC: Cambao Fault
- FCh: Labateca Fault
- FG: Guaicáramo Fault
- FMa: Magdalena Fault
- FSa: La Salina Fault
- FSo: Soapaga Fault
- FY: Yopal Fault
- FBa: Baraya Fault
- FA: Algeciras Fault
- FAI: Altamira Fault

Folds

- AG: Arcabuco–Guantiva Anticline
- Ap: Carmen de Apicalá Syncline
- VI: Villeta Anticlinorium
- RE: Rio Ermitaño Syncline
- Co: Los Cobardes Anticline
- EP: El Peñon Anticline
- Ma: Montecristo Anticline
- Gd: Guaduas Syncline
- Gu: Guavio Anticline
- NM: Nuevo Mundo Syncline
- DA: De Armas Syncline
- Pr: Prado Syncline
- TN: Tierranegra Anticline
- Za: Zamaricote Syncline
- Nu: Nunchía Syncline

Figure 3. (a) Geological map of the Eastern Cordillera. Lines A–A' to E–E' indicate the locations of the partial and composite transverse sections shown in Figure 4. The dashed blue squares depict the location of the geological maps in Figures 6, 9, and 18. **(b)** Map of strain ellipses and mafic dikes and plugs. The ellipses are derived from deformed fossils and record bedding-parallel strains. Mafic plugs and dikes are restricted to Lower Cretaceous host units and occur in the western and eastern flanks of the EC, respectively.



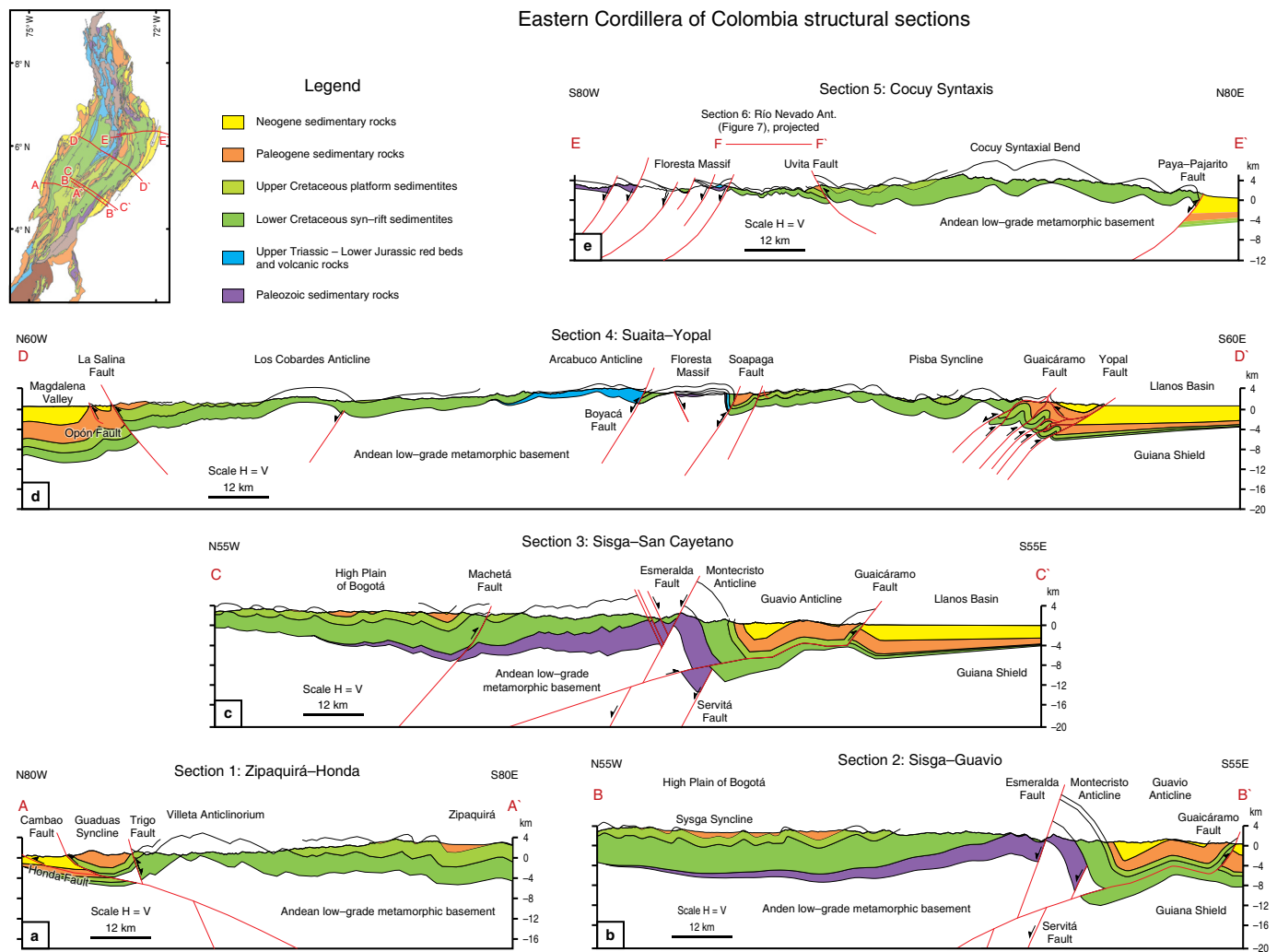


Figure 4. Composite and total transverse sections of the middle segment of the Eastern Cordillera. Locations are given in Figure 3a.

rheology between the cordilleran basement and the shield, which suggests that the latter behaved as a rigid backstop.

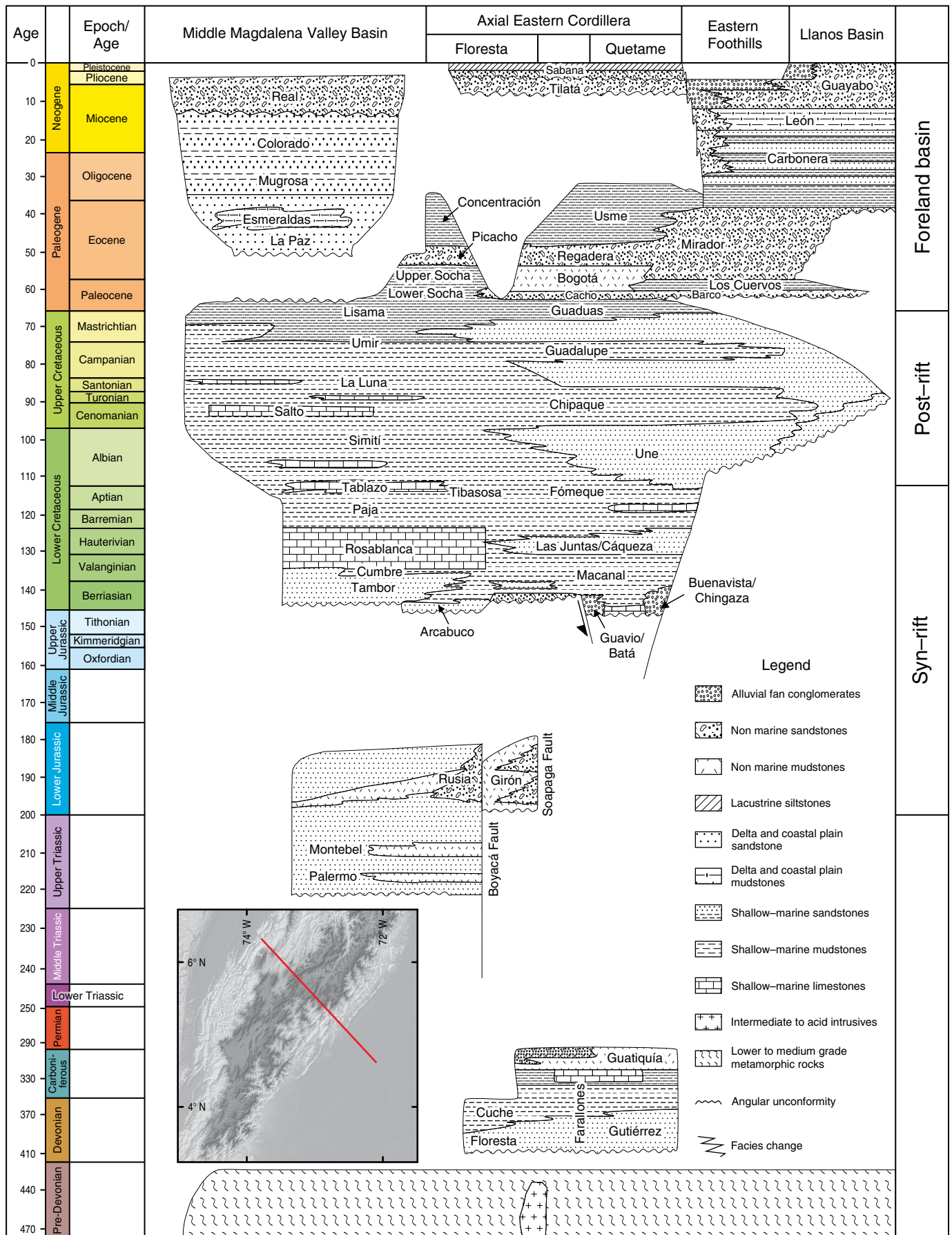
Internal rock deformations deduced from strain markers are mild along the anticlines, that form the backbone of the axial region ($R_s < 1.2$; Figure 3b). The domains affected by second-order folds on the western and eastern flanks display an axial-plane cleavage suggesting strain ratios of $R_s > 1.2$.

Several aspects of the structural style at the junction between the middle segment of the EC and the Santander Massif are shown in cross-section 5 (Figure 4). According to the exceptional topographic relief at the Cocuy Syntaxis, the outer bend of the subducting slab reaches its eastern-most position in this area, as documented by lithospheric transverse section 4 (Figure 2). This section is divided into three parts: a western part that exposes Jurassic batholiths and upper Paleozoic cover in the continuation of the Floresta Massif; an intermediate, intensely folded structural depression, that preserves a

condensed sequence of the Lower Cretaceous succession (Tibasosa to Une Formations, which are <1100 m thick; refer to the stratigraphic chart in Figure 5); and the eastern up-domed syntaxial bend, in which the thickness of this same Lower Cretaceous succession reaches 4700 m.

The salient structural features are closely related to the exhumation ages. The Floresta Massif and the northern Mogotes High expose pre-Cretaceous basement units at a structural level comparable to that of the Cocuy Syntaxis, though denudation reached a more advanced stage in the former areas. Accordingly, exhumation started in the western part in the late Eocene/early Oligocene and was followed by a second early Miocene pulse (Mora *et al.*, 2015). The basement units are compartmentalized by extensional block tectonics with normal faults linked to the Late Triassic dextral precursor of the Bucaramanga Fault. These faults do not record Neogene reactivation, which implies an uplift mechanism by wholesale lithospheric buckling.

Figure 5. Stratigraphic chart of the southern and middle parts of the Eastern Cordillera, including the Llanos Foothills and the Middle Magdalena Valley. Modified from Mora *et al.* (2010b).



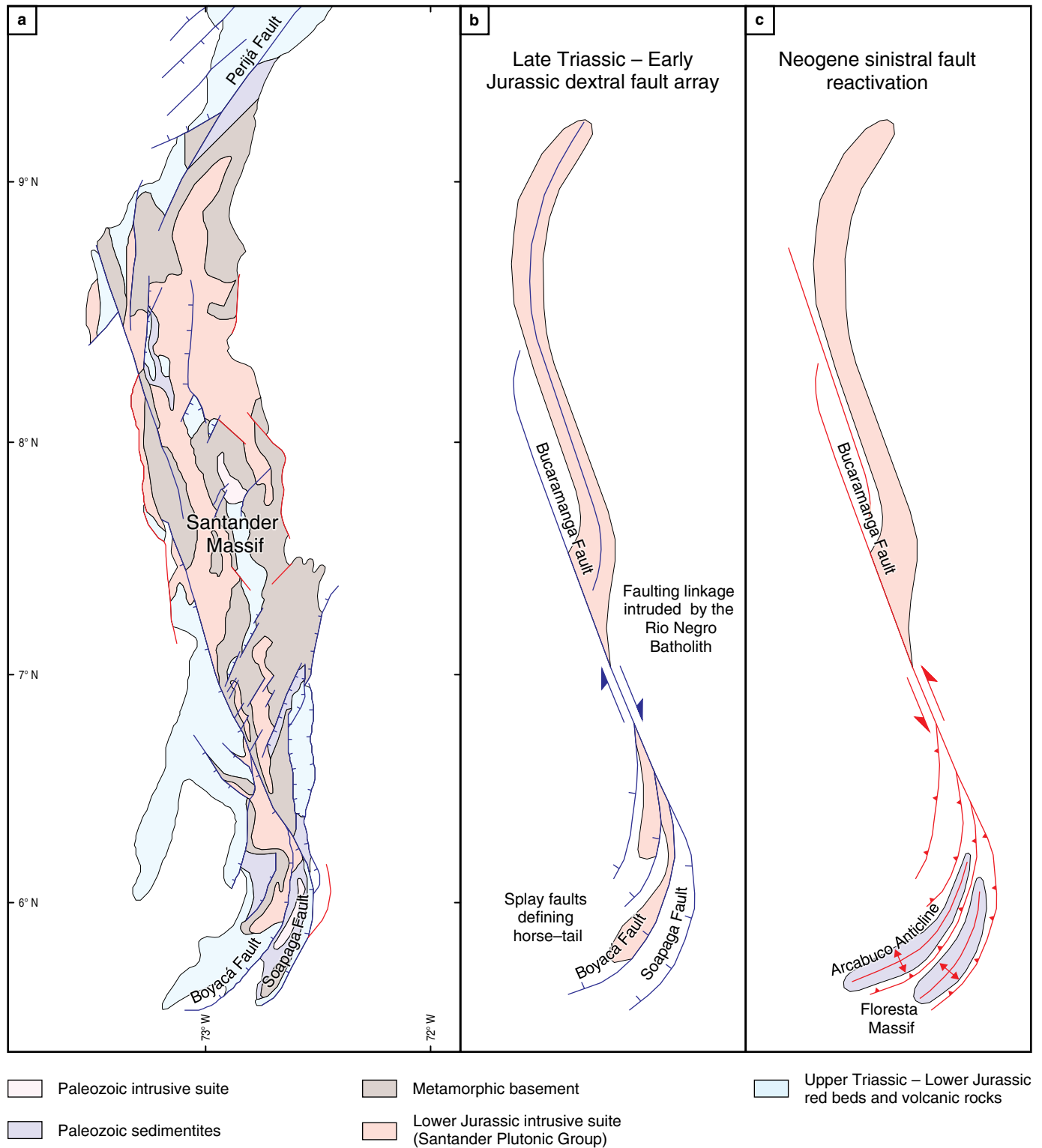


Figure 6. (a) Geological map of the Santander Massif and its southern connection to the middle segment of the Eastern Cordillera. Late Triassic – Early Jurassic faults are highlighted in blue and record a NW–SE extensional setting. The red faults are attributed to the Neogene uplift of this massif. Sketch **(b)** depicts some of the structural relations between the Santander Plutonic Group and the continental red beds with respect to a dextral ancestor Bucaramanga Fault and subsidiary splay faults. Sketch **(c)** illustrates the consequences of dextral fault reactivation under a Cenozoic NW–SE contractional deformation regime.

The Cocuy Syntaxis comprises slightly-deformed sequences, which is concluded from the absence of an axial plane cleavage in the Lower Cretaceous sequences. Its western monoclinial flank contains upright folds within the Lower Cretaceous units. Further up-section, their axial planes turn into a sub-horizontal attitude and folds show, inclusively, a down-dip vergence (the scale of section 5 does not allow for the documentation of these details), which suggests that the folding was partially driven by gravity. In the lower part of this flank, the sedimentary sequence is offset by backthrusts (shown in section 5 in Figure 4 by the Uvita Fault). Thermochronological data from the Lower Cretaceous units indicate a late Oligocene/early Miocene onset of exhumation (Mora et al., 2015).

The strongly folded, intermediate part records complex deformation patterns that are best unraveled with respect to a central, tightly folded syncline, which is referred to as Chicamocha Syncline in section 6 (Figure 7). Within the Lower Cretaceous succession, the fold vergence converges from both the Floresta Massif to the west and the monoclinial western flank of the Cocuy Syntaxis. The minor Chicamocha Anticlinorium of the latter flank contains west-verging folds and displays an incipient, steeply inclined axial plane cleavage within the upper Paleozoic basement units with brachiopods affected by bed-parallel strains of $R_s = 1.2$. In the Upper Cretaceous units, the axial planes fan into a flat attitude, and the folds become increasingly angular. Chevron folds on the opposite (western) flank of the Chicamocha Syncline display a similar down-dip vergence (Figure 7). With regard to this composite fold pattern, the Chicamocha Syncline can be compared to a central syncline (analogous to a pinched “keel” of a Proterozoic structural setting) encased between two vertically rising anticlines, in which the vertical stretching of a core gradually flattens and merges with the axial planes of the enclosing cascading folds. Similar deformation styles typify fold patterns around diapirs, as experimentally shown by Dixon (1975).

The structural change from a plateau-like axial depression in the south to fault-controlled basement-involved and large antiformal lobes further north as well as the concomitant topographic increase may be compared with recently determined Moho depths, which have the greatest values approaching 60 km beneath the High Plain of Bogotá and smaller values of 45–55 km approaching the northern part of the study region (Poveda et al., 2015). By relating these depths to the degree of isostatic compensation, we conclude that isostatic compensation decreases as the topographic relief becomes more significant. This situation may indicate increased slab support in the northern sections.

Table 1 shows the shortening values for each section, which were deduced from a combination of line-length balancing and the de-straining of layers according to R_s values extrapolated from strain markers. Our strain analysis is still a preliminary

approximation and should be refined by textural 3D measurements. Even though, when the strain data are incorporated in the line-length balancing, our shortening estimate of approximately 65 km defines a lower bound with respect to other published shortening values of 70 to 80 km (Cortés et al., 2006; Mora et al., 2008; Teixell et al., 2015; Tesón et al., 2013). These disparities can be attributed to different assumed dips of the marginal faults and the preferred deformation style (shortening by thrusting vs. shortening by folding).

By considering a horizontal shortening of 65 km and averaging it over a time interval of 30 Ma, we obtain a mean shortening rate of 2.2 mm/y. This value is substantially lower than the present rate of 4 mm/y derived from GPS measurements (Mora-Páez et al., 2016). This discrepancy may be resolved by the assumption of an increased neotectonic displacement transfer to the hinterland.

4. Cretaceous Back-Arc Evolution

Knowledge of the geometry of the Cretaceous back-arc basin and its Neogene inversion is crucial for any attempt to restore the folded and faulted strata of the cordillera. The relative importance of rift basin inversion (equivalent to basement-involved shortening) and shortening by the stacking of decoupled supracrustal slices (Colletta et al., 1990; Cooper et al., 1995; Dengo & Covey, 1993; Roeder & Chamberlain, 1995) can only be evaluated by obtaining insight into the geodynamic significance of the inherited faults. For these reasons, we review the latest Jurassic to Early Cretaceous (Tithonian to Valanginian) rifting event.

Two scenarios provide possible tectonic frameworks for the inception of rifting: (1) Crustal stretching related to passive margin evolution that may have prevailed during the Early Cretaceous, before the initiation of a Cretaceous subduction cycle (Pindell & Kennan, 2009). Thinning would have been guided by tensional plate-parallel stresses, and regional breakaway faults would be expected to separate stretched crustal domains from undisturbed regions (Wernicke & Axen, 1988). (2) Rifting associated with an ascending thermal plume with the consequent thinning of the lithosphere mantle by upward displacement of its thermal boundary. This second alternative complies with an active margin setting (Faccenna et al., 2010; Hardebol et al., 2012).

To evaluate these hypotheses, we first re-examine the thermal subsidence curves developed by Sarmiento-Rojas (2001) and Sarmiento-Rojas et al. (2006). We consider a time interval from the Tithonian (i.e., the onset of a rift-related subsidence) to the Aptian (150 Ma to 115 Ma), epoch after which fairly uniform depositional conditions became established across the back-arc basin, as indicated by the near-shore depositional environments of the Une Formation, which prograded from the present Llanos Foothills toward the present axial part of the EC (Figure 5).

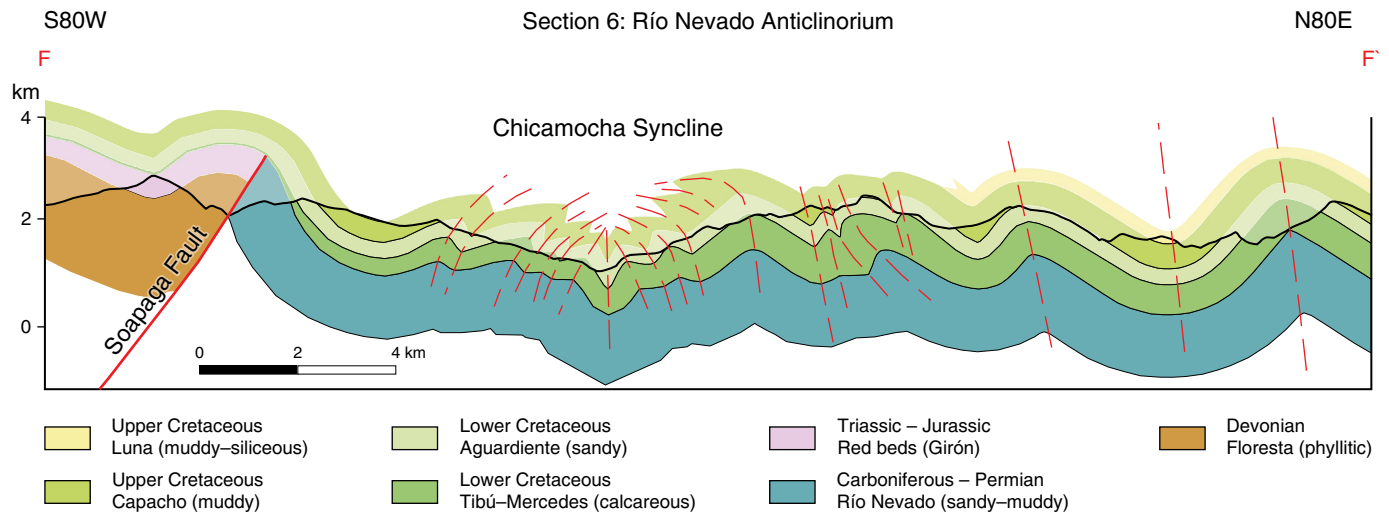


Figure 7. Folds of the Río Nevado section in the central part of the transverse section (Figure 4). The Chicamocha Syncline separates fold trains of different vergences. The axial plains deflect from a sub-vertical attitude at lower structural levels to a sub-horizontal attitude at higher structural levels on either side of the syncline. The Soapaga Fault acted as a graben-bounding fault for the Upper Triassic/Lower Jurassic red beds, and it was not reactivated during folding.

Table 1. Shortening values of the sections shown in Figure 4.

Section	Original length (km)*	Deformed length (km)	Shortening distance (km)	Extension (%)
1. Sisga-Guavio (section A-A')	160.728	128.575	32.153	-20.0
2. Zipaquirá-Honda (section B-B')	127.127	96.358	30.769	-24.2
3. Sisga-San Cayetano (section C-C')	170.406	135.504	34.902	-20.5
4. Suaita-Yopal (section D-D')	295.748	233.714	62.034	-21.0
5. Cocuy (section E-E')	123.143	97.305	25.838	-21.0

*The original lengths have been corrected by the strain values estimated from bed-parallel shortening assuming plain strain conditions.

An architectural framework for this back-arc basin is provided by two marginal troughs, which are referred to as the Magdalena-Tablazo and Cocuy Sub-basins (Fabre, 1983; Sarmiento-Rojas, 2001) and whose depocenters are located close to the Miocene mountain fronts of the present EC. An intervening depositional high coincides with the present Floresta Massif and its southern continuation (Figure 8). Typically, subsidence curves constructed for these sub-basins have a knickpoint between fast (>50 m/Ma) and slow (5 to 15 m/Ma) subsidence rates. These knickpoints lie within the Hauterivian and Barremian, as shown by shaded bars in Figure 8. The peak rates along the marginal troughs approach 100 m/Ma for the Neocomian and may indicate an active rift stage (Figure 5). For the southern Cocuy Sub-basin, however, we find evidence that fault activity was restricted to the Tithonian and Berriasian, as discussed below. In close agreement to elevated subsidence rates, marginal troughs record deeper depositional environments until the Barremian (Polanía & Rodríguez, 1978), suggesting some independence between fault activity and subsidence. The facies associations related to elevated subsidence rates comprise mass

flow and turbidite deposits with paleocurrent indicators oriented parallel to the marginal troughs (Dorado-Galindo, 1992; Pimpirev et al., 1992; Moreno-Murillo, 1991; Sarmiento-Rojas, 2001).

Important clues for the Cretaceous back-arc evolution are provided by mafic sills and minor stocks that were emplaced within Aptian to Albian successions on the western flank and Berriasian host units on the eastern flank, where they form a linear trend (Figure 3b; Fabre & Delaloye, 1983; Moreno-Murillo & Concha-Perdomo, 1993; Vásquez et al., 2010). $^{40}\text{Ar}/^{39}\text{Ar}$ plateau ages obtained from primary plagioclase and hornblende yielded a large range of ages from 136 to 74 Ma (Vásquez et al., 2010). This temporal range exceeds the previously defined periods of elevated subsidence (or “active” rift stage). The mafic intrusions are compositionally heterogeneous and define two different series: a trend similar to alkaline ocean island basalts and a tholeiitic trend with characteristics of mid-ocean ridge basalts. The trace-element patterns are enriched in light rare earth elements (LREE) and display high Ba/Nb and Sr/P ratios, which comply with a possible supra-subduction setting (Vásquez et al., 2010).

Subsidence curves for Eastern Cordillera

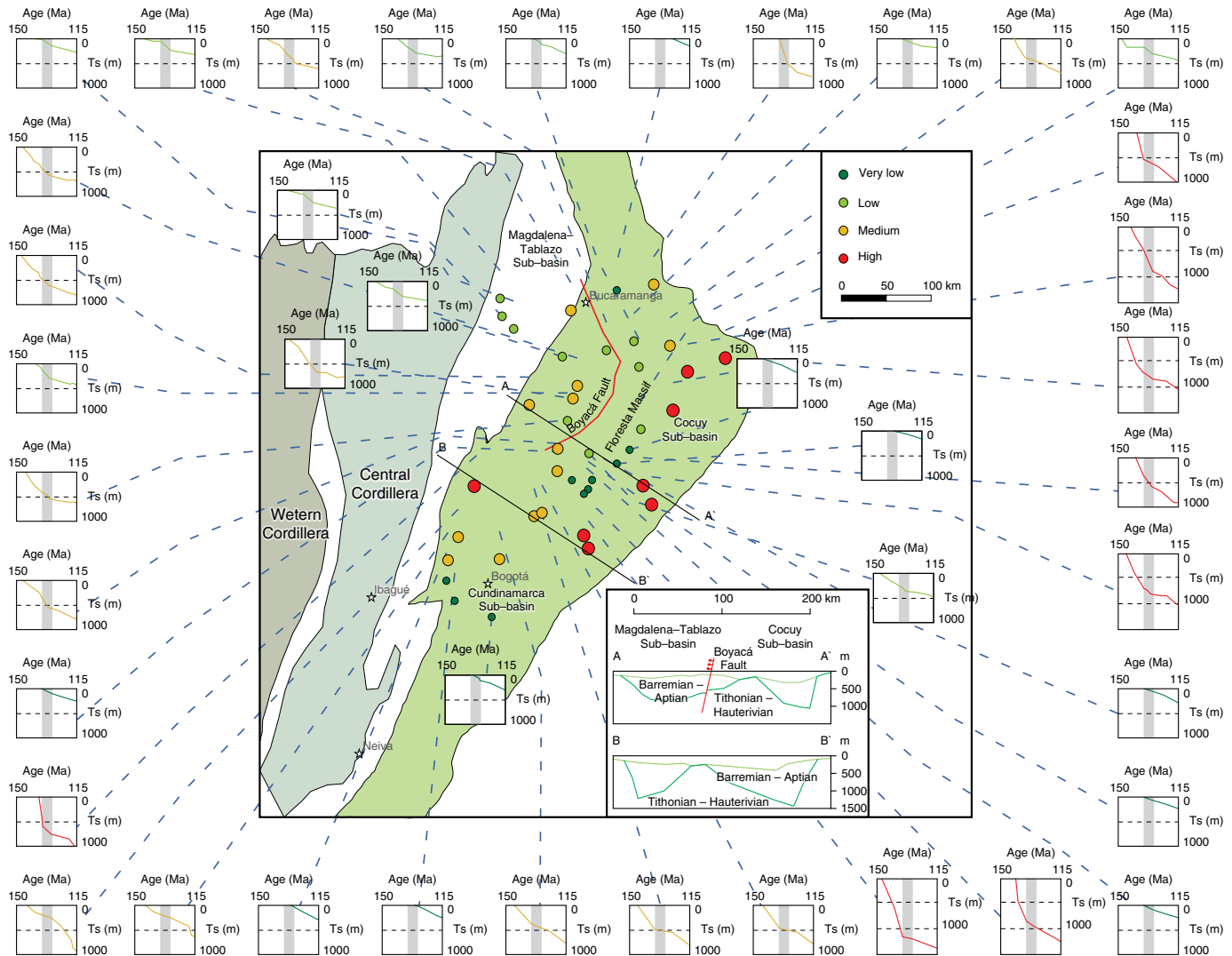


Figure 8. Site map of the Eastern Cordillera showing the locations of the stratigraphic columns for which tectonic subsidence curves were derived (modified from Sarmiento-Rojas, 2001). The tectonic subsidence (Ts) is plotted in small insets for representative stratigraphic profiles and covers an age range from 150 to 115 Ma (Tithonian to Aptian). Lines A-A' and B-B' indicate transverse sections of tectonic subsidence, as plotted in the large inset, in which we differentiate between a Tithonian-Hauterivian “syn-rift” and a Barremian-Aptian “post-rift” subsidence stage.

5. Structural and Sedimentological Evidence for Rift Events at the Eastern Mountain Front

The southern part of the eastern Miocene mountain front exposes upper Paleozoic sequences of an inverted marginal rift basin and the previously discussed Early Cretaceous basin fill of the Cocuy Sub-basin. We present arguments for a Neocomian fault-related subsidence cycle linked to a basal sequence of the Lower Cretaceous syn-rift successions.

5.1. The Late Paleozoic Servitá Fault

The Servitá Fault forms a rheological boundary between the folded Andean-type basement and the nearly undeformed Guiana basement. Its age and normal nature are readily deduced from a Late Devonian to an early Carboniferous rift fill, which is referred to as the Farallones Group (Figure 5; Bürgli, 1960; Stibane, 1967). With regard to its length (>150 km), this fault is comparable to the similarly NNE-trending Palestina Fault of the Central Cordillera (Feininger et al., 1972). Its graben fill

exceeds 3000 m in the proximal region near the fault trace but tapers significantly further west (see sections 2, 3 in Figure 4). The shield area only records an early Paleozoic rift event (Feo–Codecido *et al.*, 1984), and the reported thicknesses of the upper Paleozoic sequences do not exceed 200 m (Dueñas & Césari, 2005). This late Paleozoic extensional setting might be linked to the Late Triassic extensional attenuation of the Andean margin (Riel *et al.*, 2018; Spikings *et al.*, 2015).

The fault plane is mostly concealed by the folded Cretaceous cover along the eastern flanks of the marginal highs (see sections 2, 3 in Figure 4). Evidence for the existence of an important crustal discontinuity is provided by the juxtaposition of cordilleran marginal highs that preserve the Farallones Group in their hinge areas and the more foreland-oriented basement-cored anticlines, where Paleozoic sedimentites are absent (as shown by anticlines immediately west of Villavicencio and further to the southwest; Figure 9).

5.2. Early Cretaceous Extensional Tectonics of the Guavio Region

Of the two marginal troughs of the Cretaceous forebulge, the eastern one deserves special attention because of its well-exposed graben structure in the Guavio area. To the east, this basin is bounded by two master faults, which currently displace the Toquiza and Montecristo Antiforms (Toquiza and Esmeralda Faults; Figure 9). These faults are discontinuous and define a left-stepping array (Figure 10b). Their western hanging-wall blocks are compartmentalized by secondary antithetic faults that curve into an N–S trend to the west of the relay zone (Figure 10b). Next, we re-examine the rift fills of these sub-basins and highlight their paleogeographic setting based on the work of Terraza *et al.* (2008), Mora *et al.* (2009), and proper observations.

Biostratigraphic determinations of ammonites indicate a Tithonian to Berriasian depositional interval for the graben fills (Haas, 1960; Terraza *et al.*, 2008), which indicates a relatively short-lived transgressive–regressive cycle. This fault-related sequence is termed collectively as the Guavio Formation (Figure 10c; a more differentiated nomenclature is used by Terraza *et al.*, 2008). The crests of the footwall blocks of the Toquiza and Esmeralda Faults separated this faulted sub-basin from a possibly unfaulted eastern sub-basin, where the coeval Batá Formation was deposited (Figure 10b, 10c). The sedimentites of these basal sequences are overlain by the Valanginian shaley Macanal Formation via inundation surface (Figure 10c). In the Guavio area, the basal strata of this latter unit comprise small-scale fining-upward depositional cycles with ripple laminations, which indicate a turbiditic depositional regime. The high subsidence rates of this marginal forebulge area thus outlasted the fault-related rift stage, according to our previous subsidence analysis.

The asymmetric nature of the composite rift fills west of the Toquiza–Esmeralda Faults is highlighted by a 50 m isochore

and a pinch-out line (Figure 10b). The block geometry of the minor sub-basins closely correlates with the thickness and facies variations of the measured columns (Figure 10a). A cursory inspection of the facies distribution (Figure 10c) reveals that (1) calcareous and evaporitic lithologies (facies associations G3 and G5; Table 2) increase in importance toward the western margin, and (2) evaporitic associations are ubiquitous in the basal transgressive layers and also predominate in the uppermost unit (facies association G3).

More specifically, facies association G1 (Table 2) comprises a basal mono- to polymict breccia composed of reworked dolostones of facies association G3 as well as quartz fragments and strongly altered sandstone blocks of the Farallones Group. Where it was deposited on foundered blocks along major faults, this basal breccia is several tens of meters thick. Association G2 contains pebble-cobble conglomerates, which are composed of sandstone and limestone fragments embedded in a sandy to muddy groundmass. The beds display trough and inclined stratification, in which conglomeratic sands alternate with sandy muds (“inclined heterolithic” stratification; Thomas *et al.*, 1987). Facies association G3 comprises dolomitic mudstones and laminated dolostones with slightly contorted and variably brecciated laminae of microbial origin (algal mats). This sequence displays isolated to coalesced nodules that, where associated with a strongly contorted lamination, define enterolithic layering (Mora *et al.*, 2009). G4 is a thinly layered, heterolithic mud-sand sequence with linsen and flaser structures that include layers of bivalve shells. G5 comprises mudstones and wackestones with bivalve shell fragments. Below the contact with the Macanal Formation, these sequences are overlain by dolostones of a recurrent G3 association.

The basal breccias and ensuing conglomerates (G1 and G2) are interpreted to represent a transgressive conglomerate above a Paleozoic ravinement surface on down-dropped fault blocks. Considering the remnants of reworked evaporates (G3), we may conclude about a restricted freshwater supply in this likely estuarine environment. This transgressive depositional cycle culminated with the deposition of tidally influenced mudstones (G4) but reverted to a regressive environment with the deposition of limestones and dolostones of salt marsh deposits (uppermost G3). Fault activity ceased at the onset of the ensuing transgressive cycle of the Macanal shales, which buried and sealed the faulted blocks and faults.

The Batá Formation forms a synchronous (Etayo–Serna *et al.*, 2003) but compositionally independent lithic unit with respect to the Guavio Formation. It begins with a basal breccia made up of clast-supported cobble-sized sandstone and bright limestone fragments (<1%). Red sandstone fragments derive from variegated sandstone units and bright limestone pebbles derive from caliche concretions of the adjacent Farallones Group, which likely had undergone erosion at the crests of the fault blocks (Figure 10c).



clude from irregular contours and necking. The grain size variations of the conglomeratic beds reveal reverse grading or a combination of reverse and normal grading. We associate these beds with concentrated, non-cohesive flow units that may have settled in a delta complex (Haughton et al., 2009; Talling et al., 2012).

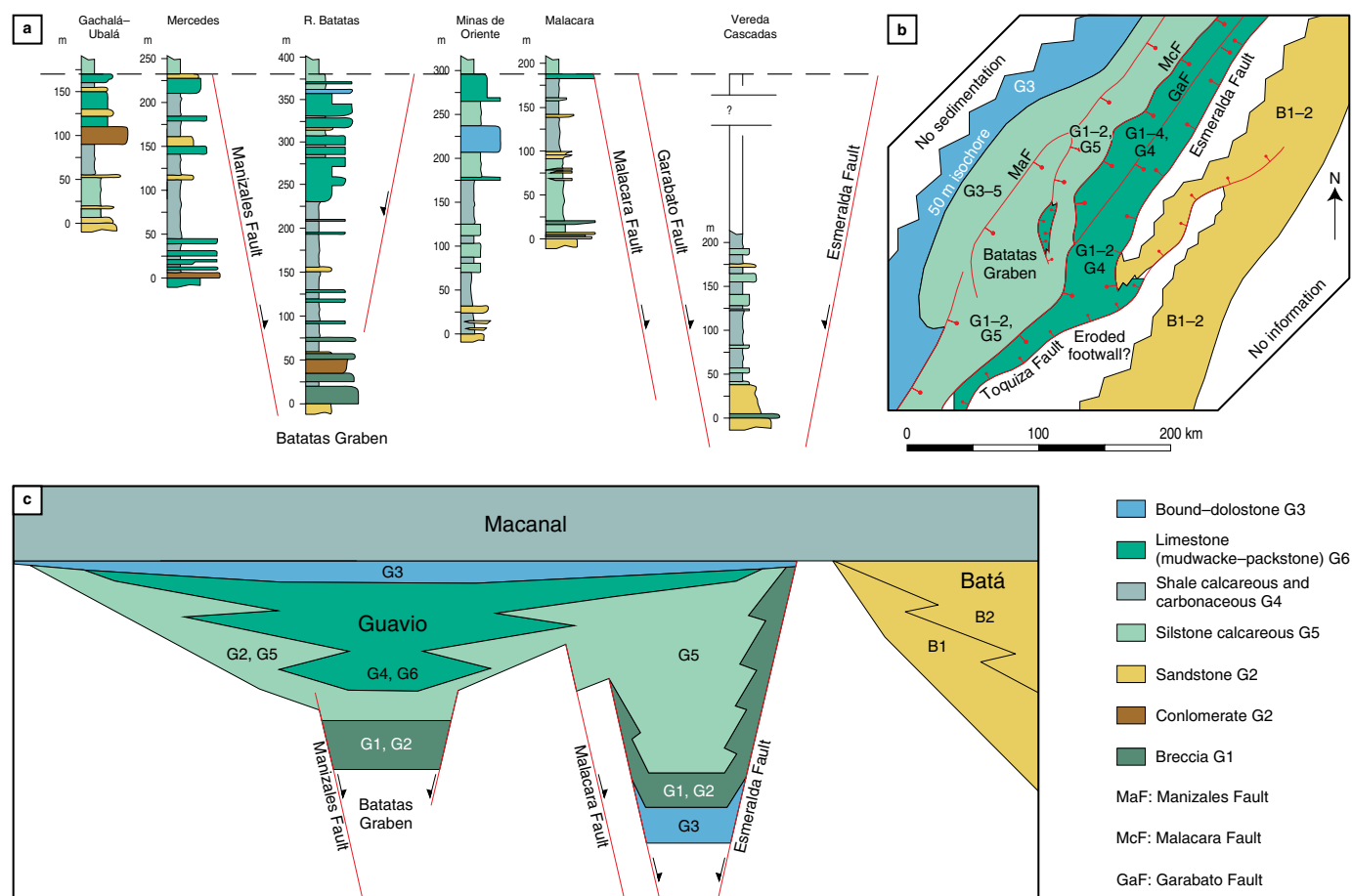


Figure 10. Palinspastic map of the Guavio area with stratigraphic columns in different structural settings. **(a)** Stratigraphic columns. **(b)** Palinspastic map. **(c)** Facial architecture projected into an E-W section.

Table 2. Facies associations and environmental interpretations of the Guavio Formation and the basal conglomeratic unit of the Batá Formation.

FA	Lithologies and principal structures	Interpretation
G1	Poorly sorted, clast-supported breccia with quartzose and lithic fragments.	Transgression lag on a Paleozoic ravinement surface.
G2	(1) Cobble-pebble conglomerate with sandy groundmass and sandstones; trough cross-stratified, scoured bases; or (2) inclined (heterolithic) stratification.	Fluvial to estuarine deposits of a drowned valley, variably influenced by tidal action.
G3	Calcareous or dolomitic shale, laminated or variably brecciated, with pseudomorphs of gypsum crystals and intercalated nodular layers (discrete and coalesced nodules), locally contorted into enterolithic folds; desiccation cracks.	Supratidal algal flats and salt marshes; inter- to supratidal dolostone/limestone beds with gypsum crystals.
G4	Carbonaceous shale with disseminated plant remains and bivalves, the latter including disarticulated shell layers; thinly bedded alternations of sandstone, siltstone, and mudstone layers with linsen-flaser laminations; bioturbation.	Upper and lower reaches of tidal flats and lagoonal deposits; intercalated tempestite beds.
G5	Wackestones and bivalve packstones with well-sorted shell fragments.	Shelf sediments above the base level of storm influence.
B1	Polymict breccia with clast-supported sandstone, quartz, limestone and pedogenetic fragments; variegated muddy groundmass.	Debris flows with few abraded components that derive from sub-aerial erosion of the Paleozoic substratum.
B2	Cobble-pebble conglomerate with a sandy groundmass in tabular to lenticular, medium-sized beds, alternating with sand- and sandy mudstones. The components of the conglomerates are unsorted and may display reverse or combined reverse-normal grading. The conglomeratic beds are affected by fluidization.	Gravity flows in slightly confined channels of a delta complex.

FA—Facies association.

In conclusion, the activity of the Toquiza–Esmeralda Fault System was relatively short-lived and did not exceed 10 my in time (accumulated period of the Tithonian and Berriasian). The composite footwall block separated an eastern marginal area from an intensely faulted western domain. In the western domain, a marine incursion was channeled into structural depressions, giving way to an estuarine depositional environment (Dalrymple & Choi, 2007). The abundance of supratidal evaporitic deposits (facies association G3) argues for a limited fluvial freshwater supply and temporarily suppressed connections to a major seaway, which led to significant brine concentration (Einsele, 1992). As the fault activity ceased, these marginal seaways retreated. Subsidence of the Valanginian successor basin was likewise high, although fault activity came to a standstill, and gave rise to the contrasting subsidence pattern between the marginal troughs and the forebulge high.

6. Time Frame of the Cenozoic Folding

Knowledge of the onset of the Neogene folding phases is closely related to the question of whether the cordillera was formed by migrating (or sequentially eastward-progressing) deformation phases, which implies a diachronous evolution of the mountain fronts and flexural foreland troughs, as envisioned by Villamil (1999), Gómez et al. (2005a) and Parra et al. (2009b), or whether it has acquired its bilateral architecture since the early Neogene. The latter scenario would be supported by concurrent or equally distributed deformation phases. Combining these scenarios, the first orogenic stage could have involved an eastward progression of deformation that was followed by wholesale shortening (Mora et al., 2015).

Thermochronological modeling provides evidence for an initial Paleogene cooling (comprising an interval of 50–30 Ma) within the Guaduas Syncline and the Floresta Massif (for locations see Figure 3a and sections 1 and 4 in Figure 4; Parra et al., 2009b). Clues for deciphering first Paleogene crustal perturbations are provided by the foredeep sediments of relatively narrow basins, as exemplified by the foreland basins straddling the eastern mountain front (Parra et al., 2009a), the Floresta Massif (Saylor et al., 2011) and some intrabasinal depocenters of the High Plain of Bogotá (Bayona et al., 2013).

Among the latter there is evidence for an Eocene folding, as reported from the western flank of the Usme Syncline to the south of the High Plain of Bogotá (Julivert, 1963; locality cited further by Gómez et al., 2005b and Teixell et al., 2015). Here, mid-Eocene estuarine strata of the Usme Formation (Figure 11; Bayona et al., 2010; Ochoa et al., 2012) cap an angular unconformity carved into vertical to overturned Upper Cretaceous strata and mid-Eocene sandstones of the Regadera Formation. The overturned mid-Eocene sandstones display growth unconformities, which indicate thickening toward a depocenter located further west, i.e., within the syncline's present axis. These

outcrop relations suggest a fold-related shortening aided by the diapiric rise of shales of the Chipaque Formation (>800 m thick; Figure 5) within the core of an adjacent, eastern anticline. In conclusion, the deformation appears to have initiated along pre-disposed positive areas that sub-divided the sub-basins of the present High Plain of Bogotá. Notably, the post-folding sediments overlying the overturned flank are paralic and exclude, therefore, a topographic relief that was significantly higher than sea level.

These widely dispersed back-arc basins (presently involved into an intra-cordilleran setting), are exceeded in both the thickness of the sedimentary fill (>2500 m) and the longitudinal dimension (>150 km) by a narrow depositional trough that prefigured the Neogene Guaduas Syncline (Figure 3a). This sedimentary fill is made up of the conglomeratic San Juan de Río Seco Formation (Figure 11), which originated from a stacked pattern of fluvial channel deposits, displaying intras-tratal growth unconformities and northward-directed paleocurrent directions (Gómez et al., 2003). This sedimentation pattern attests to a period of increased subsidence, during which the creation of accommodation space outpaced the accumulation rate. Toward higher stratigraphic levels monocrystalline quartz increases at the expense of polycrystalline quartz and metamorphic fragments (Gómez et al., 2003), suggesting a sourcing from a uniform rock unit, such as the igneous suite of the Jurassic Ibagué Batholith. This batholith constitutes the basement of the footwall block of the Cambao Fault (Figure 3a) and forms the base of an amply exposed pediment that constitutes the eastern flank of the Central Cordillera, some 10 km west of the Guaduas Syncline (refer also to section 1 in Figure 4).

More concise information about similar depositional settings is provided from eastern more sub-basins of the Magdalena Valley (Figure 3a), which have not been affected by the Cenozoic denudation of the Central Cordillera. These depositional systems typically consist of a deeply eroded antiformal high and two flanking synclines, which acted as depositional sinks during the denudational event, accumulating alluvial fan deposits and fluvial sediments during the middle to late Eocene (Figure 12). Their generally tripartite architecture (lower and upper coarse-grained units separated by a fine-grained unit) and conglomeratic nature of the coarse-grained successions compare to the sedimentary fill of the San Juan de Río Seco Formation (De Porta, 1974; van Houten & Travis, 1968).

The spatial association of eroded highs and adjacent marginal sinks suggests a clast supply produced by an unroofing of the antiforms. A gradual thickening of the conglomeratic units away from the antiformal crest has been documented for the Upper Magdalena Valley (see section 8 in Figure 12; Ramón & Rosero, 2006). Variations in clast composition may be explained by erosional windows which successively shifted toward the pre-Cretaceous basement (Anderson, 1972; van Houten & Travis, 1968). Similar relations may be deduced for the Middle Magdalena Valley to the north

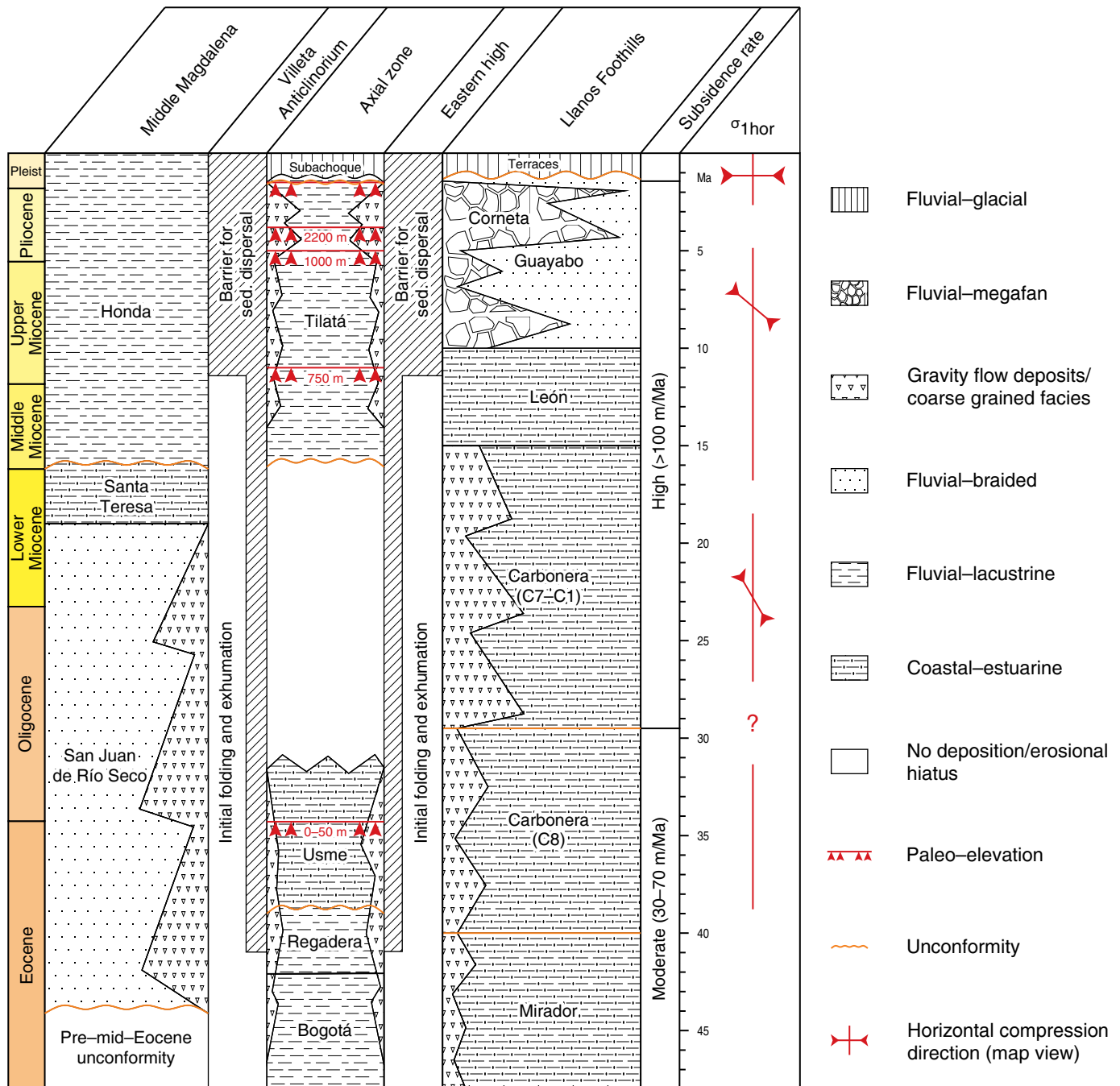
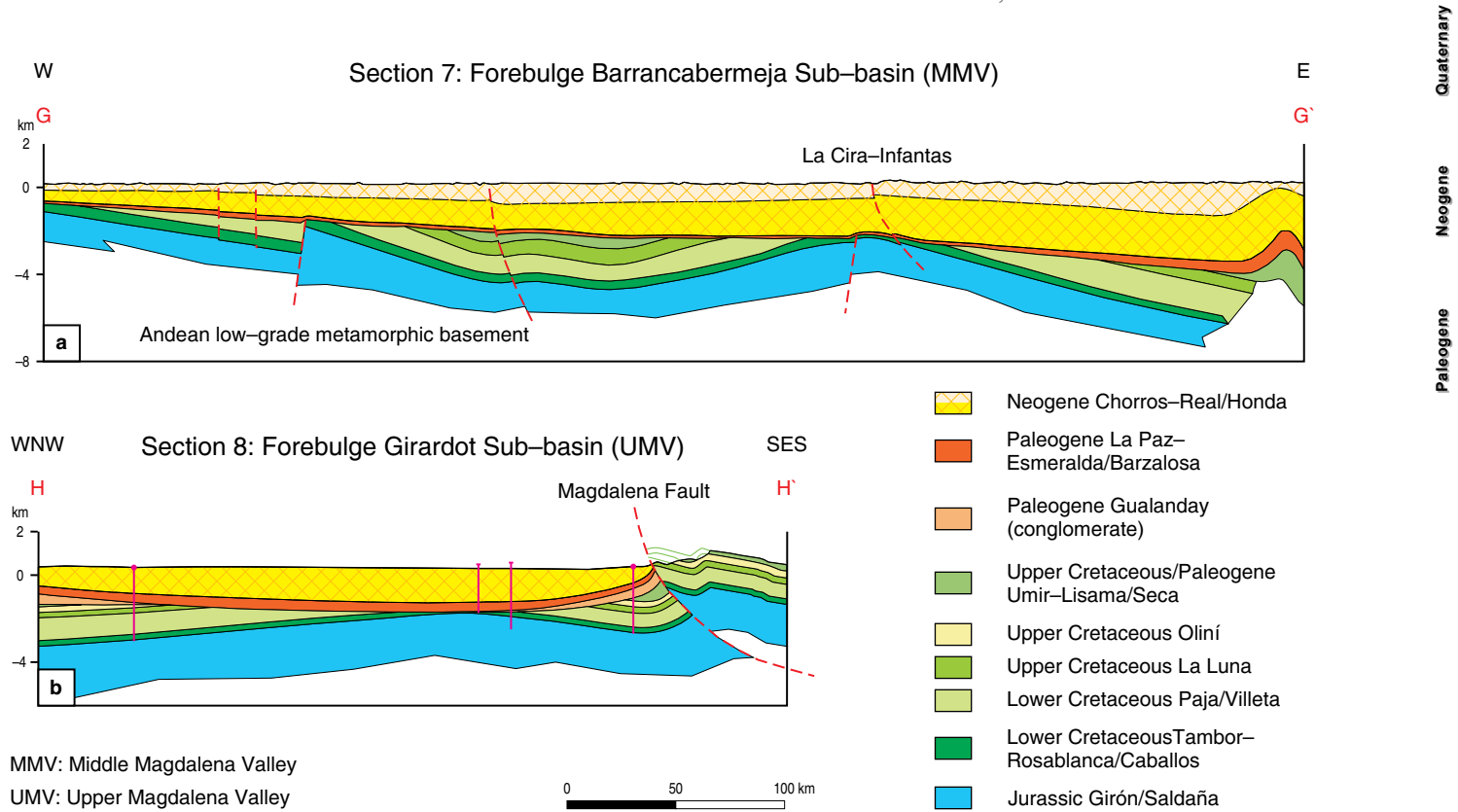


Figure 11. Stratigraphic event chart for the syntectonic basin fills and elevation estimates for the uplift of the axial zone (High Plain of Bogotá). Subsidence estimates for the Llanos Basin are shown on the right-hand side, as well as the regional horizontal stress directions derived from joint sets and sand dikes (horizontal σ_1 is projected in map view). The uplift estimates are taken from Hooghiemstra et al. (2006), and the subsidence estimates are taken from Parra et al. (2009a).

of the Guaduas Syncline, where the La Cira–Infantas Antiform (see section 7 in Figure 12) is bordered by fringing basins preserved within the Nuevo Mundo Syncline to the east (Figure 3a) and within the footwall block of the Cantagallo Fault to the west. Within the latter basin alluvial fan deposits have been identified (Suárez, 1996).

Subsequent to their unroofing, these central antiforms changed to depositional depressions, whose eroded hinge areas

may occupy a position below the Miocene to present drainage axis, as observed in the Upper Magdalena Valley (see section 8 in Figure 12) and as may be inferred for the basement high to the west of the Guaduas Syncline. Along the La Cira–Infantas Antiform, regional tilting of the foreland basin became a predominant factor in the basin evolution and obscured this subsidence pattern (see section 7 in Figure 12). This source-to-sink inversion of antiforms capped by the mid-Eocene unconformity



MMV: Middle Magdalena Valley
UMV: Upper Magdalena Valley

Figure 12. Two sections showing the Paleogene forebulge structures of the Magdalena Valley to the west of the Eastern Cordillera. Section 7 is from the Middle Magdalena Valley (redrawn from Morales, 1958), and section 8 is from the Upper Magdalena Valley (modified from Kammer & Piraquive-Bermúdez, 2013). For the locations, refer to Figure 3a. The forebulge structures of both sections are capped by a middle Eocene unconformity.

demonstrates a limited lifespan for the uplift of these highs, in accordance with the mid-Eocene to Oligocene sedimentary fills of their flanking synclines. Such a transient behavior is best explained by temporary vertical loads and may be compared to surface deflections driven by convective flows. The lateral dimensions (or wavelengths) of these depositional systems do not exceed some 10 km and preclude, by their short wavelengths, the existence of sub-lithospheric convective instabilities (Flament et al., 2013), though time spans of individual convective pulses (comprising 10 to 15 Ma) show a similar magnitude with respect to the denudational mid-Eocene event (Moucha et al., 2008). A crustal origin for these topographic instabilities may be inferred from the present structural setting of the North Andean Terrane, which shows a predominant seismic anisotropy according to the splitting of local shear waves, with fast directions being oriented preferentially parallel to the structural grain of the Andean back-arc realm (Idárraga-García et al., 2016). Accordingly, we may view this crustal corrugation as an expression of a lateral lithospheric flow, which may have been coupled to or largely independent of a lithospheric late Paleogene buckling. The transient nature and structural expression of this folding differs in two important aspects from a classical asymmetric foreland basin evolution associated to a mobile mountain front: (1) Antiformal highs and basins associated to flanking rim

synclines maintained a fixed position within the back-arc realm and (2) rim synclines cannot be related to flexural basins of a mountain front. In contrast to previous proposals (Gómez et al., 2005a; Parra et al., 2009b; Villamil, 1999), we disassociate this late Paleogene back-arc evolution from an early phase of mountain building at the western margin of the back-arc realm. Although not yet fully explainable, we believe that this event is crucial for an understanding as to why the back-arc realm became divided into two orogenic domains during the subsequent Oligocene to Neogene Andean evolution.

Within the region of the nascent EC thermochronological data indicate the onset of moderate exhumation (<1 mm/y) in the late Oligocene/early Miocene, which was followed by accelerated exhumation (>1 mm/y) since the Pliocene; these phases have been identified within both the eastern and western mountain fronts (Mora et al., 2008, 2010a, 2015; Parra et al., 2009b; Sánchez et al., 2012). Thermochronological data of this two-stage evolution support a synchronized tectonic activity at the two mountain fronts.

Information about the early Oligocene/Miocene contractional history of the cordillera may be extracted from its foreland basins. Within the Nuevo Mundo Syncline of the northern Middle Magdalena Valley (for location see Figure 3a), the Oligocene to Miocene Mugrosa and Colorado Formations (Figure

5) record higher sedimentation rates than the earlier Eocene deposits and are increasingly sourced from the EC (Caballero *et al.*, 2013). Their tilting has been associated to a flexural load of the nascent EC (tilted upper Eocene to Miocene sequences are shown in section 7 in Figure 12; Gómez *et al.*, 2005a). This evolution is matched by a coeval increase in the subsidence rate in the foreland basin evolution of the Llanos Foothills (Figure 11; Parra *et al.*, 2009a).

An accelerated mid- to late Miocene buildup of the eastern mountain front was preceded by a mid-Miocene flooding event that gave rise to estuarine deposits of the León Formation (Figure 11). The succeeding alluvial plane and fan deposits of the Guayabo Formation initiated molasse-type sedimentation that is >4000 m thick. Finally, tightly stacked flows of blocky conglomerates of an alluvial “mega-fan” (Corneta Formation; Figure 11) underscore the proximity of a mountain front. The mountain front itself maintained a stagnant position until the Pliocene/Pleistocene, when its foredeep became involved in the Guavio thrust sheet (as discussed in the next section).

The surface uplift of the High Plain of Bogotá has been tracked by pollen spectra (Figure 12; van der Hammen *et al.*, 1973; Hooghiemstra *et al.*, 2006). The vegetation belts evolved from middle Miocene tropical lowlands to pre-montane elevations, until reaching montane elevations in the Pliocene.

7. The Two-Phase Evolution of the Eastern Deformation Front

The major right-stepping thrust faults contributed to the conspicuous segmentation of the eastern foreland structures of the EC (Figure 3a). The southern Guavio segment exemplifies these foreland structures particularly well by the inception of the Guaicáramo Thrust within undeformed Cenozoic deposits to the south and their involvement within the Guavio thrust sheet further north (Figure 9). In its northern part, this segment exposes folded Cretaceous sequences. In this chapter, we return to the topic of the two-phase evolution of this deformation front and address two particular questions: (1) Is it possible to relate the Pliocene (or more recent) shortening absorbed by the southern thrust sheet to the folding of the northern Guavio segment?, and (2) is it kinematically feasible to relate the collapse of the Miocene mountain front with this late-stage thrusting?

7.1. Pliocene Fold-and-Thrust Tectonics

As previously disclosed, the Guavio segment comprises a southern detached domain of the Guavio thrust sheet and a tightly folded northern domain, which are separated by a relay zone (Figure 9). From its southern tip to the structural relay, the slip on the Guaicáramo Fault increases from a few 100 m to 6 km, which may be deduced from mapped and constructed cut-off lines between formation boundaries and the fault

plane (for different structural interpretations, refer to Rowan & Linares, 2000; Branquet *et al.*, 2002; Mora *et al.*, 2010b). As the slip increases, the fault soles into successively lower stratigraphic levels. In cross-section 9 (Figure 13), the Une Formation forms the basal competent sandstone unit of the thrust sheet, with its top marking a cut-off line on the up-ramping fault plane at the surface. This fault extends along its slightly folded flat into the eastern flank of the Montecristo Anticline, where it intersects the steeply inclined Servitá and Esmeralda Faults. From a purely kinematic point of view, the fault caused the translation of a triangular wedge, leaving a void behind it. This void was filled by the gradual collapse of the hanging wall, which may be inferred from the normal reactivation of minor faults that originated as antithetic satellite faults of the Early Cretaceous Esmeralda Fault. Normal faulting is also ubiquitous at a small scale within the Pliocene fluvial deposits of the High Plain of Bogotá (Tilatá Formation; Kammer, 2003) and attests to the distributed extension of the eastern cordilleran flank that might have contributed to the displacement of this out-of-sequence fault.

The relay zone marks a discontinuity between the folds affecting both the southern and northern domains. Exceptions are the marginal Nazareth and Río Amarillo Synclines, which border the Montecristo Anticline and the up-ramping thrust sheet of the Guaicáramo Fault (Figure 9). The folds in the northern domain display increasingly significant foreland-directed vergence toward the Guaicáramo Fault (see section 10 in Figure 13). Active fault planes have been imaged by the aftershocks of the 1995 Tauramena earthquake ($M_w = 6.5$), which occurred near the relay zone (Dimaté *et al.*, 2003). In section 10 (Figure 13; this section coincides with section K–K' of Dimaté *et al.*, 2003), the projected aftershocks cluster around linear arrays along the possible continuation of the Guaicáramo Fault and conjugate fracture planes. In the southern domain, the current slip on the Guaicáramo Fault is aseismic, as evidenced by a seismic gap in this part of the foothill region (Durán *et al.*, 2002).

The retrodeformation of sections 9 and 10 (Figure 13) yields shortening values of 4.5 km. These equivalent amounts of shortening within a similar structural setting are taken as an evidence for the Pliocene/Pleistocene folding of the northern domain. In the following considerations, we attempt to understand the deformation modes of the two domains and the interacting relay zone and sketch, for that purpose, two snapshots of a southward-propagating Guaicáramo Fault. The pre-faulting situation (Figure 14a) depicts the formation of the mountain front at the site of the future Guaicáramo Fault in the northern domain and, to the west, the Miocene mountain front pinned to the Servitá Fault in the southern domain. Assuming a common upper crustal detachment, the relay zone would have accommodated a dextral displacement transfer. In the second snapshot (Figure 14b), the Guaicáramo Fault propagates into the southern domain and may have transitioned to a flat attitude as it accumulated the

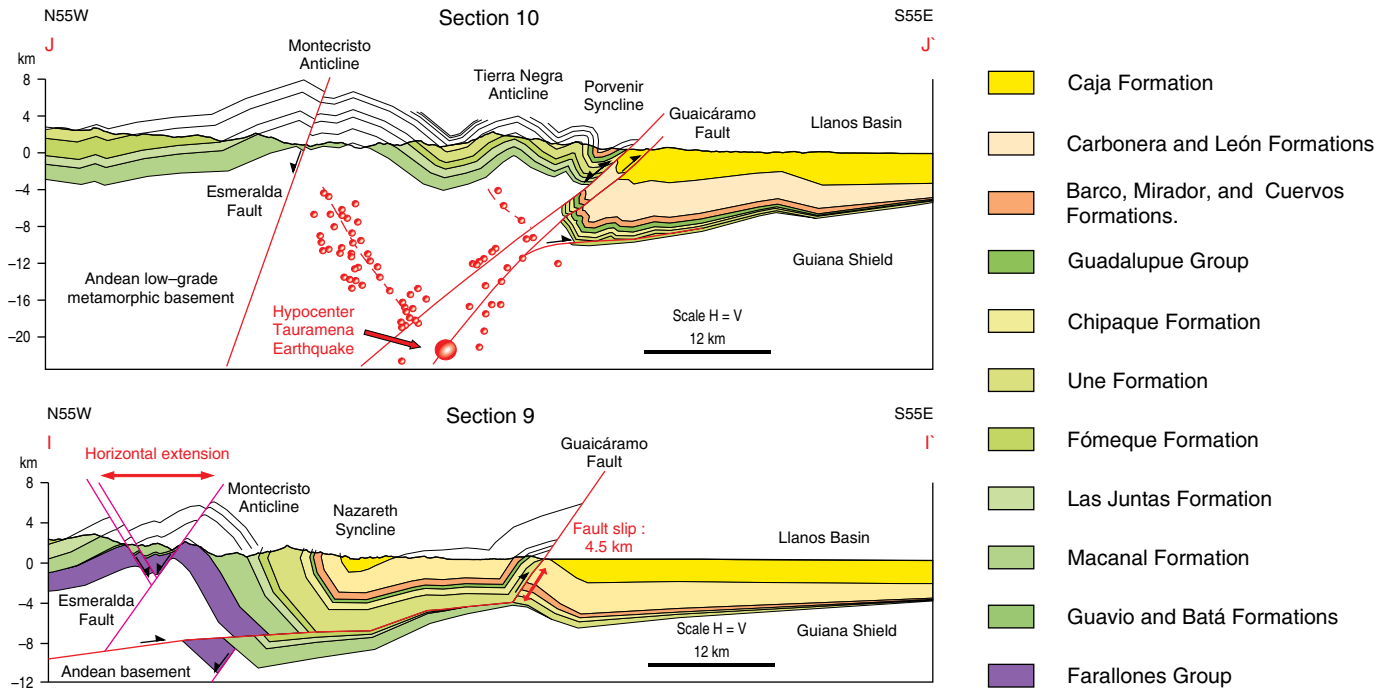


Figure 13. Two structural sections of the eastern deformation fronts, Guavio segment. For the locations, refer to Figure 9. In section 9, the frontal Guaicáramo Fault soles into the basal Cretaceous sequences and is assumed to break the Miocene mountain front of the Montecristo Anticline. In section 10, the same fault involves the pre-Cretaceous basement. Section 10 shows relocated aftershocks and the main shock (small and large red circles, respectively) of the Tauramena earthquake (19 January 1995) projected from a 5-km-wide corridor (Dimaté et al., 2003).

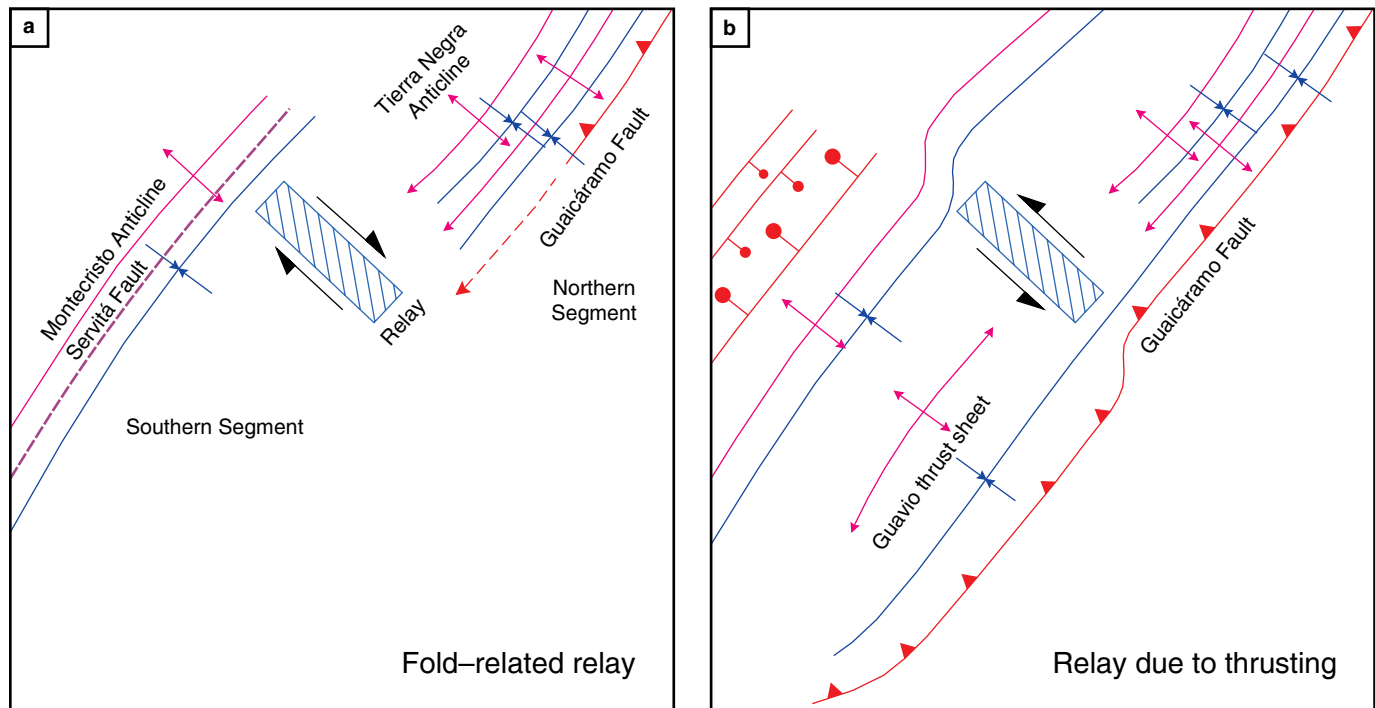


Figure 14. Snapshots of the kinematic evolution of a southward-propagating Guaicáramo Fault across a folded northern domain (a) and the breakdown of the Miocene mountain front in the southern domain (b) of the Guavio segment. **(a)** The right-stepping array between the Miocene mountain front pinned to the Servitá Fault in the southern domain and incipient folds in the northern domain implies dextral displacement transfer on the separating relay zone. **(b)** The activation of the Guavio thrust sheet implies sinistral displacement transfer on this same relay zone.

displacement of the extending Miocene mountain front. Collapse of this latter structure might have been triggered by a drop in lateral support during the initial fault propagation. At this stage, movement of the thrust sheet required the relay zone to accommodate a sinistral displacement transfer.

The juxtaposition between thin- and thick-skinned deformational styles requires further clarification. The relay zone did not behave as an impassable barrier during the southward propagating buckling stage. Limited transmission of the thick-skinned shortening from the northern domain to the southern domain is documented by the open folding of the Guavio Anticline, which affected also the overlying thrust sheet (see section 9 in Figure 13).

7.2. Miocene Mountain Front

The spatial link between the tip line of the Servitá Fault and the eastern flank of the Montecristo and Toquiza Antiforms suggests a fault–fold relationship. The tri–shear method, which was developed by Allmendinger (1998) and re–formulated by Zehnder & Allmendinger (2000), provides a kinematic approximation for testing such a structural framework. The model parameters are adjusted to obtain a satisfactory fold shape (Allmendinger *et al.*, 2004), while neglecting the effects of regional buckling. For the case of a blind fault, the approximate location of the fault tip can be estimated. A comparison between the strains required for the model fold to form and those observed in the field can provide valuable feedback. We base our analysis on the mountain front shown in section 3 (Figures 4, 15a). The restored late Miocene state was obtained by removing the displacements on the Guacáramo and Esmeralda Faults (Figure 15b). Two different solutions for the combined inverse/forward modeling of similar fold shapes are given in Figure 15c. They differ in the apex angles of the tri–shear zone and their internal velocity distributions. By applying a linear velocity gradient, we obtain a relatively open fold affected by moderate strains (though the axial ratios of the finite ellipses reach $R_s > 3$). However, the required fault tip propagation extends for a considerable distance, likely through the entire crust. An alternative case is based on a velocity distribution concentrated in the center of the tri–shear apex (in this case, applying a sine function for the velocity distribution). Under these conditions, the required trajectory of the fault tip is restricted to the upper crust, but the model requires higher strains ($R_s > 4$).

In our case, the strain compatibility between the simulated and the observed structures is a further criterion that helps to assess the relevance of the kinematic modeling. The Paleozoic basement is affected by a transverse cleavage that is concordant to a shape–preferred orientation of pebbles within conglomeratic layers. Measured strain values reflect axial ratios of $1.3 < R_s < 1.5$ (Figure 16). These values support the scenario of widely distributed deformation; however, this implies fault tip propagation over a considerable distance (as predicted by the model of a homogeneous velocity distribution in Figure 15c).

The discrepancy between the model strains and the observed deformations suggests that the tri–shear mechanism was not exclusive, but was combined with buckling.

In conclusion, the deformation style related to the eastern deformation front responded to both deep–seated processes guided by the crustal discontinuity of the Servitá Fault and to supra–crustal dynamics. The long–lasting (>25 Ma) building of the Miocene mountain front ended its life cycle as its stability was surpassed. The ensuing supracrustal processes redistributed the crustal load of the eastern cordilleran flank, decreasing its structural relief and broadening the foreland belt, according to basic mechanical principles, which favor a reduction in the potential energy of a mountain chain (Lyon–Caen & Molnar, 1985). This two–phase evolution is well discernible by the juxtaposition of highly deformed tight internal folds and broad foreland structures, as evidenced in the southern part of the Guavio segment. Further north, this distinction is less clear and deformation may have affected progressively more foreland–oriented regions.

8. Folding and Faulting in the High Plain of Bogotá

As can be seen from the cross–sections, the first–order structure of the High Plain of Bogotá consists of a wide structural depression delimited by the Miocene structural highs on either side (composite sections 1 and 2 in Figure 4). In its axial area, folded strata are mostly composed of sandy Upper Cretaceous to Paleogene rock units, while in its gently inclined flanks Middle to Lower Cretaceous sequences of alternating shaley and sandy units, each from 500 m to 1200 m thick, become exposed. The Río Blanco Anticline is a prominent fold on the eastern margin of the high plain (see section 11 in Figure 17) and borders the central Sisga Syncline. Its eastern flank is segmented longitudinally by isolated faults with lengths of 3 to 10 km, which can be mapped based on the presence of hanging–wall synclines (see section 12 in Figure 17). Otherwise, these sections do not contain faults. All of the sequences are involved in secondary folds with wavelengths ranging between 5 to 10 km. Enveloping surfaces constructed on their trough points outline the regional dips of the cordilleran flanks, which are approximately 5° for the western flank and 12° for the eastern flank. The fold vergence generally points toward the marginal highs (see sections 11, 12 in Figure 17).

Within the eastern flank, the fold trains plunge slightly northeast, as shown by their map pattern (Figure 9) and measured planar and linear fabrics cluster around axes plunging 5° northeast. This regional plunge is not observed within the axial depression, where the fold plunges become highly variable (Figure 18). The fold pattern became established in the late Miocene, as shown by the architecture of the alluvial deposits of the Tilatá Formation (Figure 11). Within the major synclines, conglomeratic channel deposits define stacked patterns, which

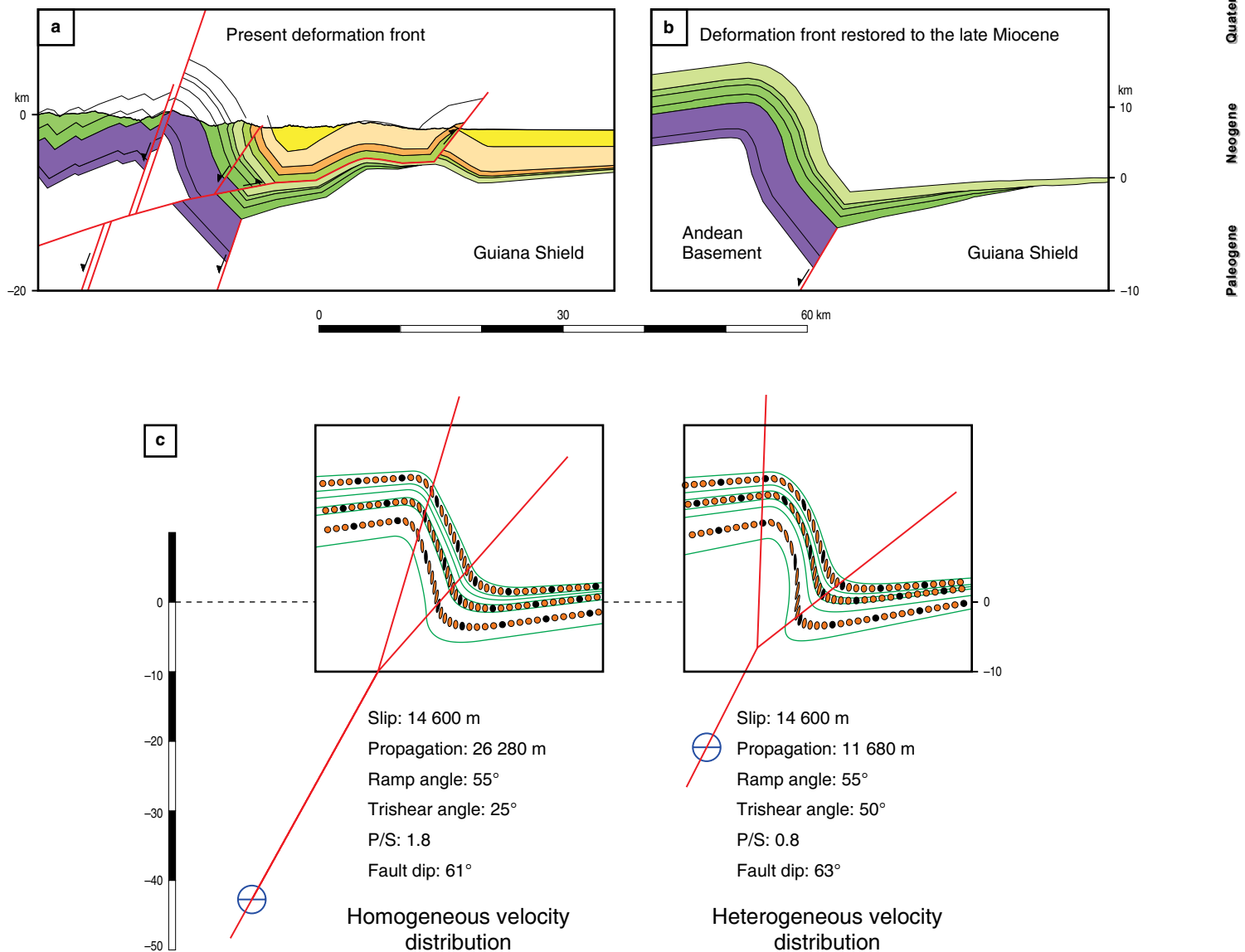


Figure 15. Kinematic model of the late Miocene deformation front of the Guavio segment. **(a)** Present structural section. **(b)** Restored late Miocene deformation front. **(c)** Tri-shear solutions for homogeneous and heterogeneous velocity fields. The model parameters are indicated. The nucleation point of the fault and the trajectory of its tip propagation (presently anchored at the apex point of the tri-shear zone) are plotted with reference to a vertical scale.

indicate that the fold axes have remained fixed since their syn-kinematic deposition during the Miocene (Kammer, 2003).

Adjacent to the Toquiza and Montecristo Antiforms, the fold trends are uniform and strike 45° NE. Toward the axial depression, the fold pattern is composite, as north-south oriented folds interfere with the folds of the regional cordilleran trend. Figure 18 highlights two particular patterns of this superposition: (1) the folds of the cordilleran trend sway into an N-S direction (sites F2(b) and (c); Figure 18), and (2) the gently dipping flanks of the synclines, that parallel the regional trend, are refolded by N-S or NNE-SSW-trending anticline-syncline pairs (sites F2(a) and F2(d); Figure 18). Based on these observations, we conclude that the deformational regime had a shortening

direction that rotated from strike-perpendicular to E-W. However, evidence for these changes in fold orientation are absent in the foothill area, which suggests that the cordilleran topographic load might have suppressed these regional changes in the shortening direction. Support for two different active stress regimes comes from the horizontal principal stress orientations (σ_{1-hor}) derived from borehole breakouts (Tesón et al., 2013; see their Figure 8). All available data define two domains separated by a boundary that coincides with the southern termination of the Guaicáramo Fault. South of this boundary, σ_{1-hor} directions are E-W-oriented, whereas further north σ_{1-hor} directions are strike-perpendicular, illustrating the increased importance of the topographic load in the northern domain, where the eastern

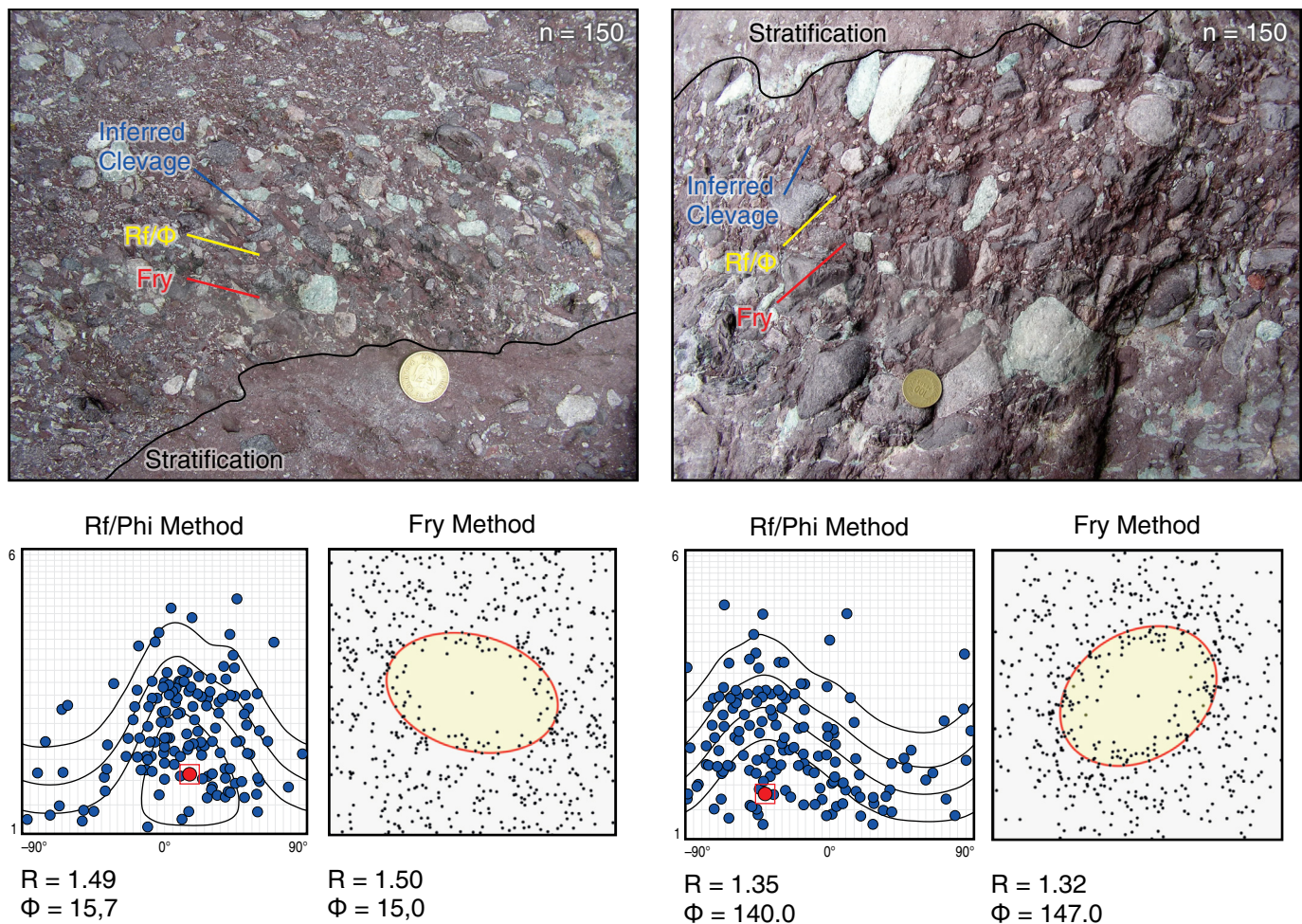


Figure 16. Deformed conglomeratic unit of the upper Paleozoic Farallones Group, eastern flank of the Montecristo Antiform, and strain diagrams. The outcrop faces contain the principal elongation and shortening directions of the pebbles. The strain values are determined by a shape and orientation analysis of the pebbles (Rf/Φ method) and visualized by the normalized distances between the central points of the pebbles (Fry method). For the strain evaluation, we used the program EllipseFit, which was written by Vollmer (2015). Textural inheritance of the sedimentary structures may account for the deviation between the calculated long elongation axis and the observed cleavage direction.

cordilleran flank attains its full width. A detailed fracture analysis is needed to demonstrate the existence of two competing recent stress directions and will be presented elsewhere.

The fold style in the western part of the axial depression is strongly influenced by transverse relay structures, which have been described in detail by Ujueta (1992). These relays may be identified by both sinistral and dextral local bends in the regional fold trend. For example, both right- and left-stepping bends of fold axes may be recognized along lineament R(d) (Figure 18). Left-stepping bends are most conspicuous where the western flank becomes more inclined, as evidenced by curved fold axes along the northwestern segments of lineaments R(b) and R(c) (Figure 18). They cannot be associated with post-fold wrenching because the panels bounded by these lineaments display independent folds. For example, the folds located between lineaments R(b) and R(c), as well as those between R(c) and R(d), differ in number and vergence.

In the eastern, more axial region, the fold axes are not bent but rather abut against these relays or form distinct necks. The particular fold style of each panel advocates for a pre-folding origin of the lineaments.

Linear arrays of minor salt stocks and thermal springs (Ujueta, 1992) provide clues about the origin of the lineaments. Lineament R(b) (Figure 18) hosts the Zipaquirá salt dome, which is a composite diapir with two lobes that are separated by a central saddle (McLaughlin, 1972). Internal structures, such as sheath folds and a foliation caused by intense mixing of recrystallized salt and broken shale fragments, attest to an intrusive emplacement (Warsitzka *et al.*, 2013). The entrained shale fragments contain Berriasian fossils (López *et al.*, 1991).

The salt occurrences are thus strictly limited to fold relays and their associated structures. Rather than associating these restricted occurrences to a regional basal detachment horizon,

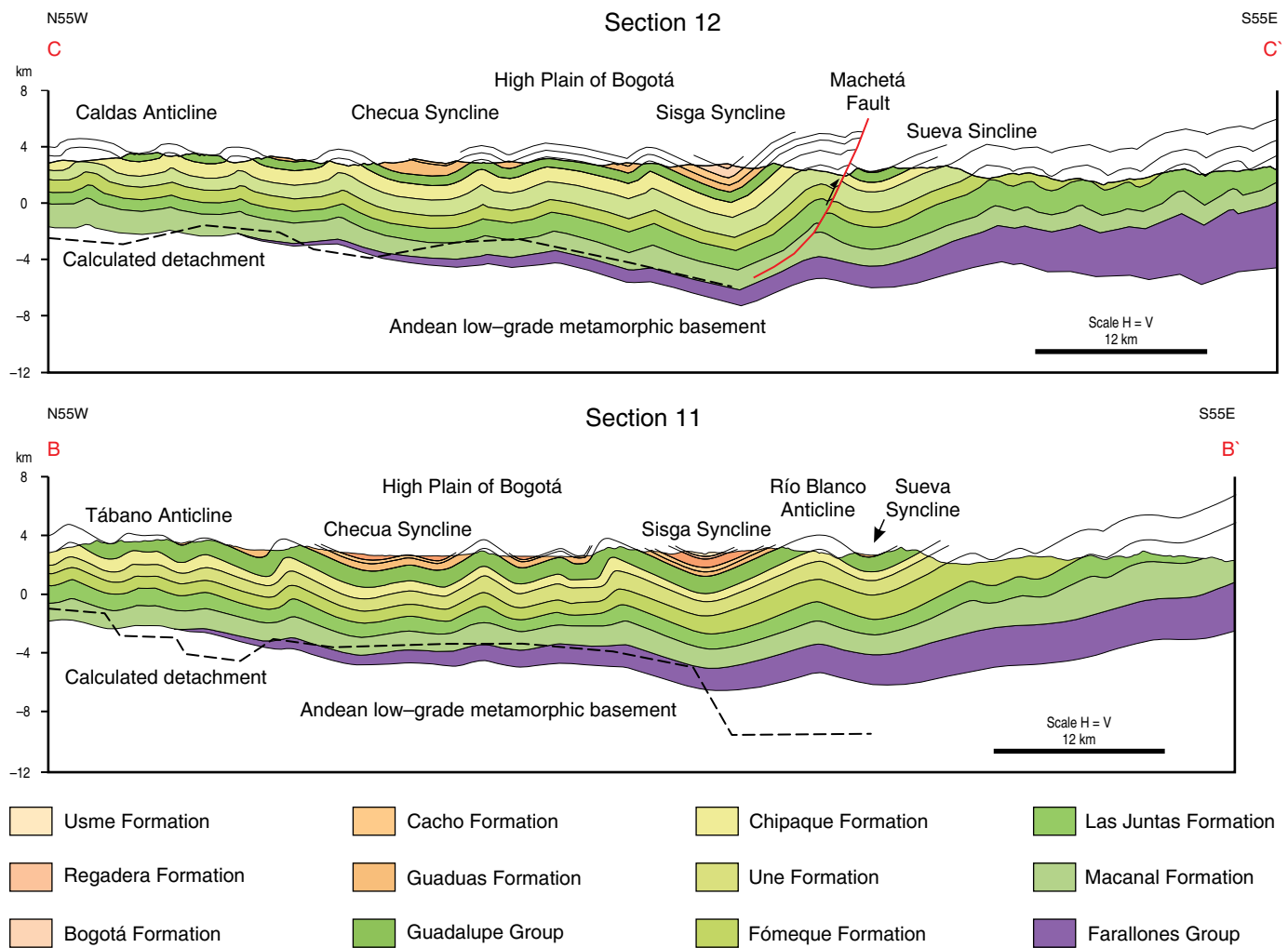


Figure 17. Detailed sections of the axial zone of the High Plain of Bogotá. These sections correspond to the enlarged central portions of sections 2 and 3 in Figure 4. The locations are shown in Figure 18.

as proposed by Cortés et al. (2006) and Teixell et al. (2015), we stress their importance in dividing the axial zone into structural domains. The presence of salt along transverse faults or relay zones might have contributed to their mobility, which is supported by the conspicuous left-lateral bends to the west of the axial zone (northeastern terminations of relay zones R(b) and R(c); Figure 18). This local wrenching may have occurred as a result of a “transpressional” E–W–oriented shortening, as set out above by means of the young folding phase detected in the eastern cordilleran flank. These relay zones are limited to the axial domain of the High Plain of Bogotá. On the western flank, they terminate against a continuous anticline in the Neusa area (northwestern corner of Figure 18); on the eastern flank, they are limited against the Río Blanco Anticline. Their restricted occurrence suggests a Berriasian paleogeographic framework, in which transverse faulting channeled local marine incursions with the subsequent formation of evaporitic deposits.

8.1. Fold Mechanisms

Dismissing the existence of a continuous salt layer that would have facilitated the detachment of the Cretaceous cover, we can investigate alternative fold mechanisms. Periodic wavelengths and systematic changes in the fold vergence across the central Sisga Syncline suggest buckling under uniform contraction. In contrast, the pre-Cretaceous basement underwent shortening by plane strain, as indicated by a ubiquitous axial plane cleavage at this structural level. A mixed deformation mode comprises a wide transitional zone encompassing the Fómeque to Macanal Formations (Figure 5) and combines flexural slip folding and homogeneous shortening by cleavage formation (Kammer, 1997). We address this structurally complex situation in a simple kinematic model that is used to construct cross-sections and a simple mechanical model that applies to buckle folds. Both approximations apply to the situation of detachment folds, in

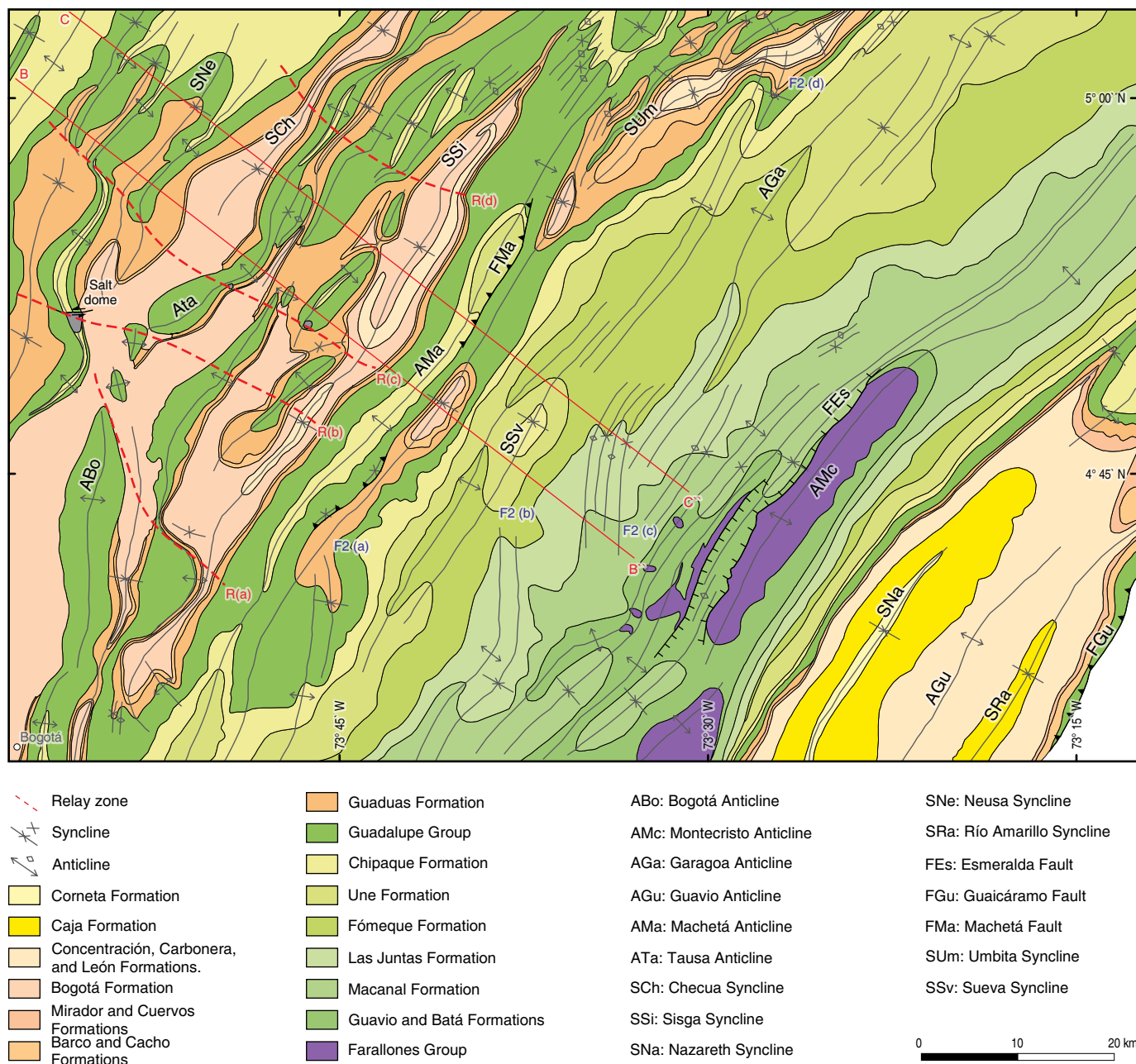


Figure 18. Geological map of the High Plain of Bogotá and its adjacent eastern flank. The Red lines indicate the structural sections in Figure 17. The Red stippled lines, labeled as R(a), R(b), R(c), and R(d), indicate structural relay zones, which are highlighted by fold bends, fold terminations, and aligned salt domes. Second-generation folds are recognized by N-S trending fold terminations, as observed at sites F2(b) and F2(c), and their superposition on folds of the SW-NE striking Cordilleran trend, as exemplified at sites F2(a) and F2(d). Location of relay zones: R(a) Zipaquirá-Río Teusaca, R(b) Zipaquirá-Guatavita, R(c) Neusa, R(d) Tausa-Choconta.

so far as we consider the folding of a layered sequence above an unfolded basement, whose depth is determined by the mitigation of fold amplitudes and whose interface mimics the regional dip of the cordilleran flanks and is, thus, comparable to a detachment.

Of the existing kinematic models, we chose that one developed by Epard & Groshong (1995), which assumes folding above a stratigraphically fixed horizon by a combination of

limb rotation and changes in bed length. We select the contact between the Lower Cretaceous shale unit of the Macanal Formation (Figure 5) and the underlying Paleozoic to Proterozoic sandstones and phyllites (Farallones and Quetame Groups) as the reference horizon for the mitigation of fold amplitudes. Where these pre-Cretaceous units consist of sandstones, they may have acted as a mechanical boundary. The deformation mode considered by Epard & Groshong (1995) allows for the

thickening of beds within anticlinal hinges but excludes material transfer through adjacent synclinal axial planes; stated differently, the fully developed fold shapes, that are observed at the surface, may be projected to the basement–cover interface, assuming a linear decrease in amplitude. This scenario clearly requires observational support. The argument in favor of thickened shaley units in the anticlinal hinges is based on the still poorly investigated diapiric phenomena, which caused the overlying sandstone units to break into overturned flanks or “flaps” (Harrison & Falcon, 1934), where erosion disrupted their continuity (Julivert, 1962, 1963).

The problem of locating the depth of the unfolded basement was overcome in three ways: (1) by extrapolation, we determined the depth of formational units within the cordilleran eastern flank; (2) based on the shortening values and excess areas determined at superficial folds, we estimated the “mitigation” depths for individual folds, according to the calculation of detachment depths (Chamberlin, 1910); this method assumes the beds to be undeformed at the surface, a requirement that is likely met within the Upper Cretaceous and Paleogene sandstone units of the High Plain of Bogotá; and (3) variation diagrams between excess areas and structural levels, as proposed by Epard & Groshong (1993), allow to determine the depth of the basement–cover interface by pinning it to the level where excess areas disappear. The latter method is based on the assumption of area conservation and does not depend on bed-length changes. It was used to check the internal consistency of the constructed sections.

The “mitigation” depths of folding calculated and checked by the two latter methods are plotted for individual anticlines in sections 11 and 12 (Figure 17). The results point to a uniformly east-dipping basement–cover interface within the axial depression and the cordilleran western flank and presume a gradual westward tapering of the Cretaceous units, which is confirmed by the mapped outcrop limits of equivalent units of the Une Formation in the western cordilleran flank. Given the large amplitude of the Río Blanco Anticline, its “mitigation depth” considerably exceeds these calculated depths below the High Plain of Bogotá; therefore, folding should involve the pre-Cretaceous basement units.

The regular spacing of folds within the High Plain of Bogotá suggests that the wavelength is related to the rheological properties of the folded rock units. We approximate this problem by considering the buckling of a competent Upper Cretaceous unit above a predominantly shaley lower sequence, as postulated for single-layer detachment folds (Poblet & McClay, 1996). Theoretical considerations postulate that for the initial buckling, a characteristic dominant wavelength λ_{dom} emerges from the preferential amplification of folds that form along randomly distributed perturbations. The dominant wavelength of detachment folds may be related to the viscosities and thicknesses of the layers involved, considering a viscous power law

rheology for the strong layer and a linear viscosity for the weak layer (Schmalholz et al., 2002):

$$\lambda_{\text{dom}} = 1.2\pi \left(\frac{\mu_{\text{eff}}}{3n\mu_m} \right)^{\frac{1}{6}} \sqrt{\frac{H_m}{H}} H$$

where H and H_m refer to the thicknesses of the strong layer and the weak substrate, respectively, the strong layer has an effective viscosity μ_{eff} and behaves according to a power law with an exponent n , and the viscous matrix has a linear viscosity μ_m .

This relationship ignores the multi-layered stratigraphy of the EC but emphasizes the importance of viscosity (or lithologic) contrasts and layer thicknesses. It predicts an increase in the dominant wavelength as the thickness of the strong layer and the viscosity contrasts increase. In our cross-sections, the matrix thickness decreases eastwards from 5800 m to 4100 m (resulting in a thickness reduction of 30%) and becomes weaker, as the distal facies of the Lower Cretaceous sandy units become muddier. The thickness of the folded Upper Cretaceous Guadalupe Group decreases eastwards to a lesser degree (10%) and keeps its lithological strength. Considering only the thickness variations, the dominant wavelength should decrease toward the east.

To identify regional variations in the wavelength of the High Plain of Bogotá and its adjacent flanks, we sampled fold trains in several sections and measured the fold widths between the mapped synclinal or anticlinal axes. We differentiate three domains (Figure 19). For the eastern cordilleran flank (or eastern domain), we exclude wavelengths that pertain to second-generation N–S oriented folds and folds located near marginal highs. The latter folds represent drape folds related to antithetic faults of the Esmeralda and Toquiza Faults and did not form by buckling. We sampled 4 transverse sections on the eastern flank and the high plain, including sections 2 and 3 (Figure 4). Within the western flank, we sampled section 1 (Figure 4) and 4 sections further north.

In the compilation (Figure 19) the longest wavelengths were recorded on the eastern flank (8 to 12 km) and slightly shorter wavelengths on the High Plain of Bogotá (5 to 10 km). The wavelengths measured on the western flank are bi-modal with a minor population attaining widths of the High Plain of Bogotá, in addition to very short wavelengths, which derive from the tightly folded Villeta Anticlinorium (see section 1 in Figure 4) and represent second-order folds of this marginal high. A comparison of the unimodal results points to a reduction of the wavelengths toward the east, according to the marked decrease in thickness of the Lower Cretaceous units. Further studies should be designed to examine the influence of lithological contrasts which, at present (and ignoring lateral lithological variations), may be approximated by a viscosity ratio of about 20. Assuming that the concept of a dominant wavelength may be applied to the scale of our cross-sections, these preliminary

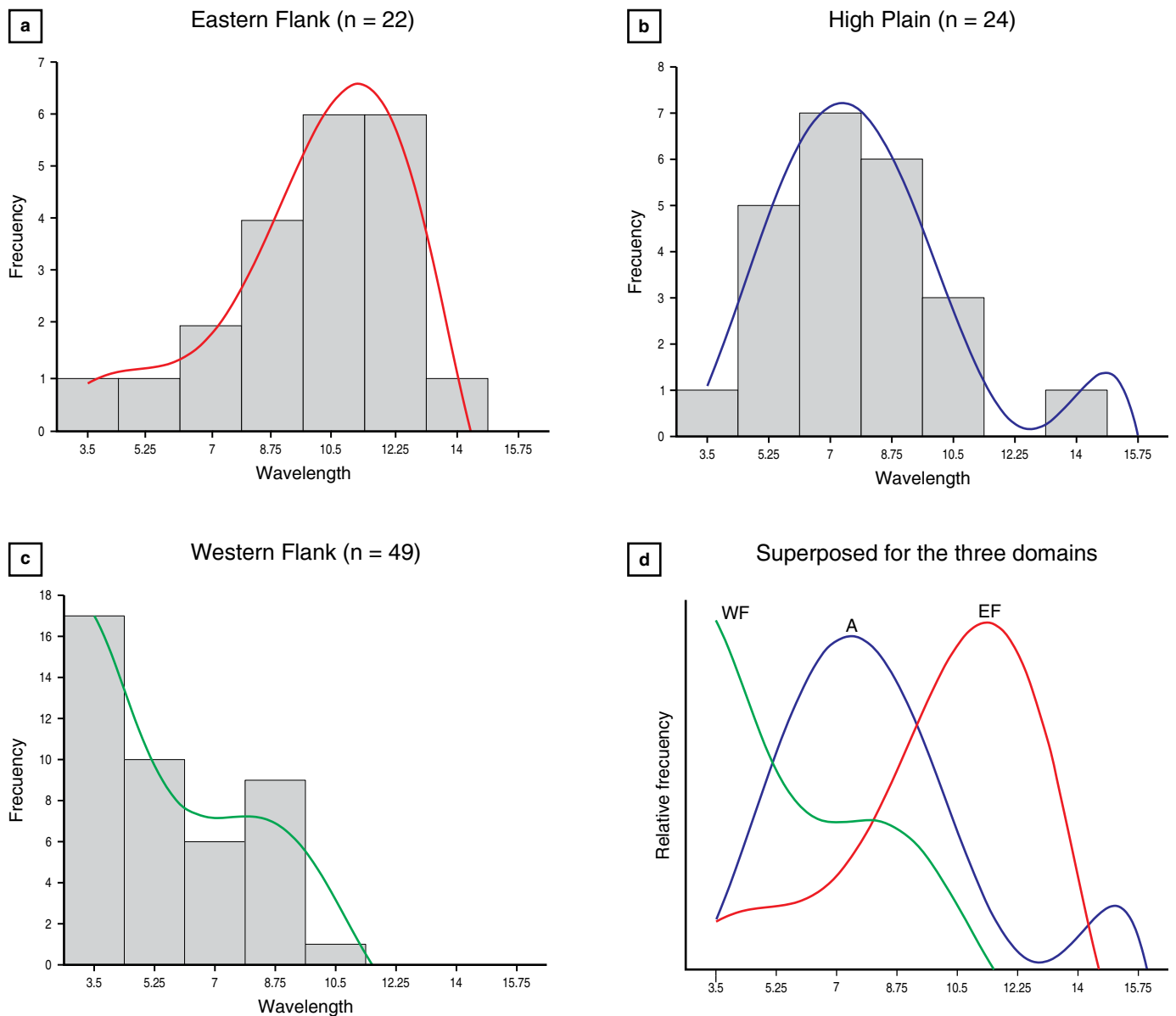


Figure 19. Distribution of fold widths in the structural domains of **(a)** the eastern flank, **(b)** the axial zone and **(c)**, the western flank. Subfigure **(d)** displays the domains superposed. The fold widths of each anticline were determined as the distances between adjacent mapped synclinal axes.

results reinforce our hypothesis that buckling was the principal deformation mechanism at higher structural levels.

9. Discussion

The Cenozoic evolution of the EC is closely tied to the reactivation of inherited Late Triassic/Early Jurassic (splay faults at the southern termination of the Bucaramanga Fault) and Early Cretaceous faults (border faults of the Cretaceous back–arc basin). The reactivation modes include both inversion and further increase in normal displacement (Esmeralda and Toquiza Faults). Notably, some inherited faults lack any evidence of reactivation, even where associated with major folds or moun-

tain fronts. These relationships indicate a complex interplay of crustal rheology, dynamic equilibria, and kinematic conditions, which go beyond a simple mechanical analysis. Next, we discuss the salient features of the Early Cretaceous back–arc configuration and the Neogene folding.

9.1. Cretaceous Back–Arc Evolution

The scenario of a Cretaceous forebulge evolution provides explanations about the Lower Cretaceous paleogeographic division into an axial high and flanking marginal basins. The geodynamic framework should be based on the following considerations:

1. *Marginal basins may, but need not be, fault-bounded.* – Fault inheritance and reactivation has been surmised for many Neogene faults without clear evidence. The case of the Esmeralda Fault is unique because it allows for the identification of a Tithonian to Berriasian depositional cycle related to fault-bounded sag basins. However, elevated subsidence persisted beyond this syn-rift stage to the Hauterivian/Barremian and documents the poorly deciphered dynamics of increased forebulge activity. An enhanced Early Cretaceous subsidence has also been noted along the western margin of the EC (Moreno-Murillo, 1991; Sarmiento-Rojas, 2001), but the existence of conjugate border faults on this flank remains unconfirmed.
2. *Compared to intracontinental rift systems, the Cretaceous back-arc basin is exceptionally wide but is comparable to the dimensions of a cordilleran back-arc domain.* – Intracontinental rift arms, as exemplified by the East African graben systems, vary in width between 60 and 100 km (Corti et al., 2007; Ebinger, 1989). The Cretaceous back-arc realm of the EC, in contrast, displays a restored width of >250 km, which compares to the dimensions of a cordilleran back-arc region (Hyndman, 2010). These relations support the concept of a forebulge-related origin.
3. *Forebulge activity was conterminous with a Cretaceous subduction event.* – Chronologically, the forebulge evolution may be bracketed by the Tithonian rift initiation within the eastern marginal basin and the emplacement of the latest basic intrusive plug at 74 Ma (Vásquez et al., 2010). Within the back-arc realm, the creation of accommodation space along the marginal basins ceased during the Maastriichtian and Paleocene, as may be deduced from reduced subsidence rates and uniformly distributed shallow marine to subaerial depositional environments (Figure 5; Bayona et al., 2013; Cooper et al., 1995; Villamil, 1999). Looking for constraints of its inception, the Cretaceous subduction must have been active since the Aptian, as may be concluded from the supra-subduction signature of the basic effusive to sub-volcanic Quebradagrande suite that was emplaced along the continental margin (Nivia et al., 2006). Accordingly, $^{40}\text{Ar}/^{39}\text{Ar}$ plateau mica and hornblende ages of 120.7 ± 0.6 and 112.0 ± 3.7 Ma (Bustamante et al., 2012; Villagómez et al., 2011) obtained from high-pressure rocks in the suture zone record Aptian exhumation. The suture became locked by the Campanian, as demonstrated by siliciclastic sedimentary sequences that cap the Cretaceous subduction complex and a U–Pb age of 79.7 Ma obtained from a post-kinematic stock emplaced within a major fault zone (Stock of Córdoba; Villagómez et al., 2011). However, the precise onset of subduction (assuming that there was a pause in subduction since the Middle Jurassic) remains conjectural. Numerical modeling suggests that subduction-related plumes might date the initiation of slab foundering

and are most active during the first stage of slab descent (Faccenna et al., 2010).

This spatio-temporal framework for forebulge evolution may be reconciled with the formation of a small-scale upper mantle plume with long-term stability. An associated thermal anomaly could have thinned the lithospheric back-arc region, thereby contributing to a convectively sustained, positive dynamic topography (Flament et al., 2013). Numerical models suggest that the erosive effects of a collateral downwelling asthenospheric mantle flow can lead to highly unstable conditions (or “diffuse” limits; King & Anderson, 1998) unless a high viscosity is assigned to the cratonic lithosphere (Hardebol et al., 2012). Under these conditions, and excluding a thermal shield effect of the craton that could incite sub-lithospheric flow toward the back-arc region (King & Anderson, 1998), the back-arc plume may connect toward the craton side to a relatively narrow zone of a descending “edge-driven” flow at the leading edge of the craton (Figure 20; King & Ritsema, 2000). On the side of the active margin, a subduction-driven corner flow may form a complementary upper mantle circuit (Figure 20; Currie et al., 2004). Such combined convection cells have been postulated for the Canadian back-arc region (Hyndman, 2010) and, considering the similar scale, may be adapted to the Cretaceous back-arc basin of the EC (Figure 20). In these models, a sharp transition between the hot back-arc region and the adjacent cold craton may persist for tens of millions of years (Hardebol et al., 2012), providing thus an analogous setting for the lifetime of the proposed Cretaceous forebulge.

9.2. Cenozoic Faulting and Folding

With respect to the Cenozoic basin inversion, we ask if the proposed impingement of a Cretaceous back-arc plume and the consequent lithospheric thinning influenced the rheological properties of the Cenozoic back-arc region or if the lithospheric properties were restored subsequent to the end of plume activity. A weakened lithospheric block would explain a widely distributed “plain-strain” deformation mode since the onset of Cenozoic shortening. In this scenario of wholesale shortening, the EC is comparable to a “hot” orogenic belt, as conceived by the numerical vise model of Ellis et al. (1998) (see also Cruden et al., 2006). Such a crustal-scale stationary deformation mode stands in contrast to foreland tectonics resulting from migrating deformation fronts and the dynamics of orogenic wedges (as conceptualized, e.g., by DeCelles & DeCelles, 2001).

Support for a widely distributed deformation mode comes from the fold-related diapirism, which we associate with the mobilization of overpressured shales. The pre-late Eocene inversion of the western anticlinal flank at Usme reveals an early inversion of a fold flank, with a resulting structure comparable to the overturned flanks of the Neogene folds in the High Plain of Bogotá (Figure 11; Julivert, 1962, 1963). Evidence of widely

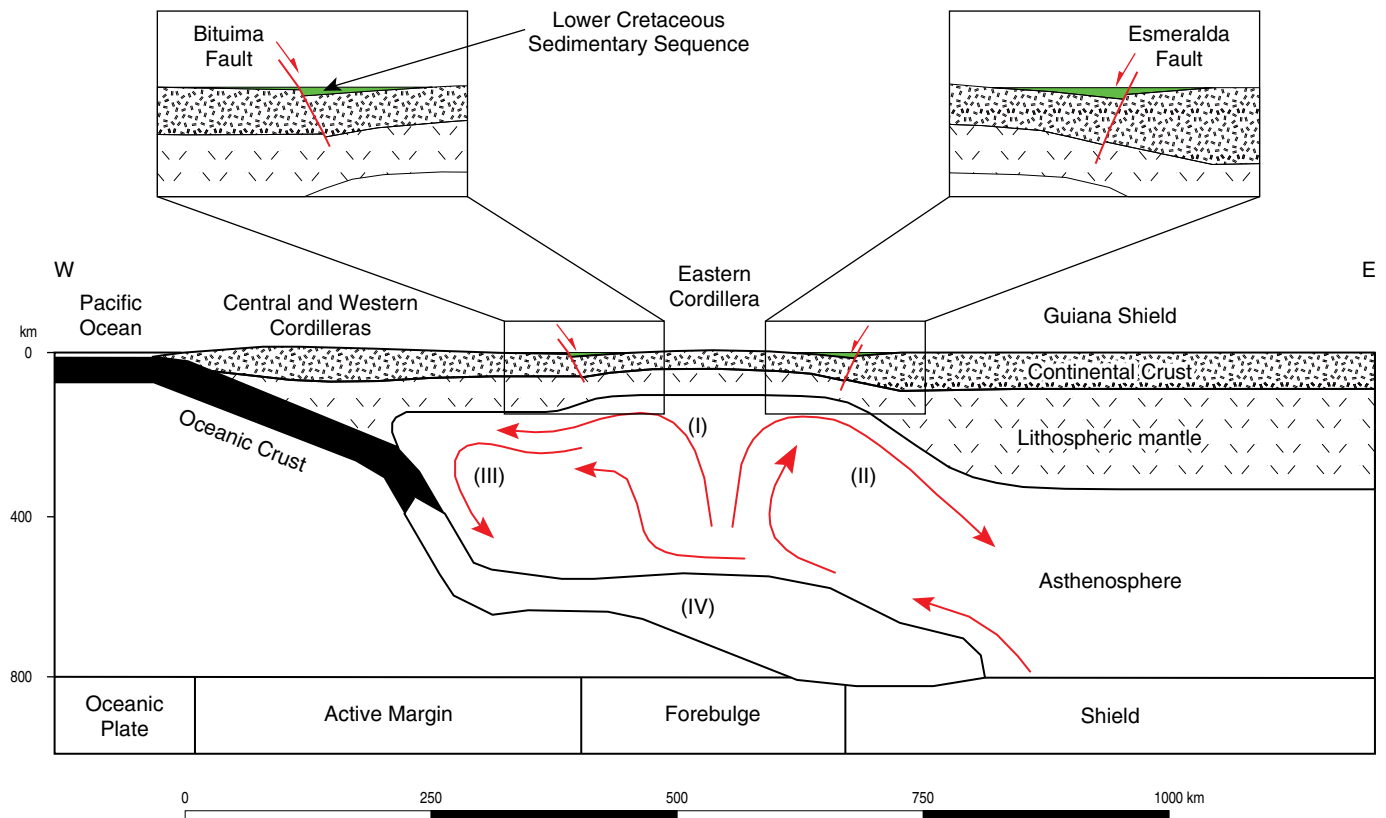


Figure 20. Scenario for the possible mantle dynamics of a cordilleran back-arc basin, as adapted from Hardebol *et al.* (2012). This model integrates the lithospheric structure, heat flow data, and seismic tomography of the Canadian Cordillera, the dimensions of which are comparable to those of the Cretaceous North Andean back-arc region. A mantle plume, possibly triggered by the initiation of subduction, accounts for lithospheric thinning below the back-arc region (I) and feeds two convection cells. The external western cell corresponds to a subduction-driven corner flow (III), whereas the internal eastern cell involves descending “edge-driven” mantle flow at the contact with the eastern shield area (II). The model depicts a major stage in the evolution of the subducting slab (IV) as it becomes docked at the 660 km discontinuity.

distributed shortening during Neogene folding may be deduced from the fold style in the High Plain of Bogotá, where the fold vergence systematically changes across the axial depression, with buckling involving shear toward the marginal highs. This shear acts up-slope (i.e., against gravity) and is viewed to be the result of incipient lateral escape toward the free cordilleran margins since the inception of folding. Fold-assisted diapirism is most pronounced in the axial depression of the High Plain of Bogotá, which attests to increased compression acting sideways from the elevated flanks.

The characteristic features of the formation of an axial depression (see sections 1–3 in Figure 4) have been simulated for both migrating and relatively stationary deformation fronts. A sandbox experiment of the formation of two deformation fronts was performed by Philip Prince of Virginia Tech, and its advanced stage is sketched in Figure 21a. In this experiment, a non-deforming ramp attached to a moving wall acts as a rigid foreland block. In the first deformation stage, the velocity discontinuity at its tip incites backthrusting of the sand layers toward the rear of the box and their thickening by secondary

forward-breaking thrusts. The wedge dynamics then become focused on a second deformation front by major forward-breaking thrusts and the consequent formation of a pop-up structure. Growth of this composite wedge occurs by a migrating deformation front from the backstop into the foreland (model setup) or from the foreland to the hinterland (EC) and results in the decoupling of the mobile sand layers from the base of the sandbox and the moving wedge. The geometric configuration of this scenario corresponds to that of a crustal flake detached above a ductilely deformed substratum of the lower crust or upper mantle. This scenario of mobile deformation fronts compares to crustal-scale setups of many published cross-sections (refer to the compilations of Cortés *et al.*, 2006, and Tesón *et al.*, 2013).

A contrasting analogue experiment involves a layered model lithosphere with scaled strength profiles that floats on a highly fluid asthenosphere (Figure 21b; Sokoutis & Willingshofer, 2011). During compression, a weak intermediate lithospheric block is squeezed between two rigid foreland blocks. A sand layer, which simulates a rigid upper crustal section, detaches from its base and overrides the converging foreland blocks.

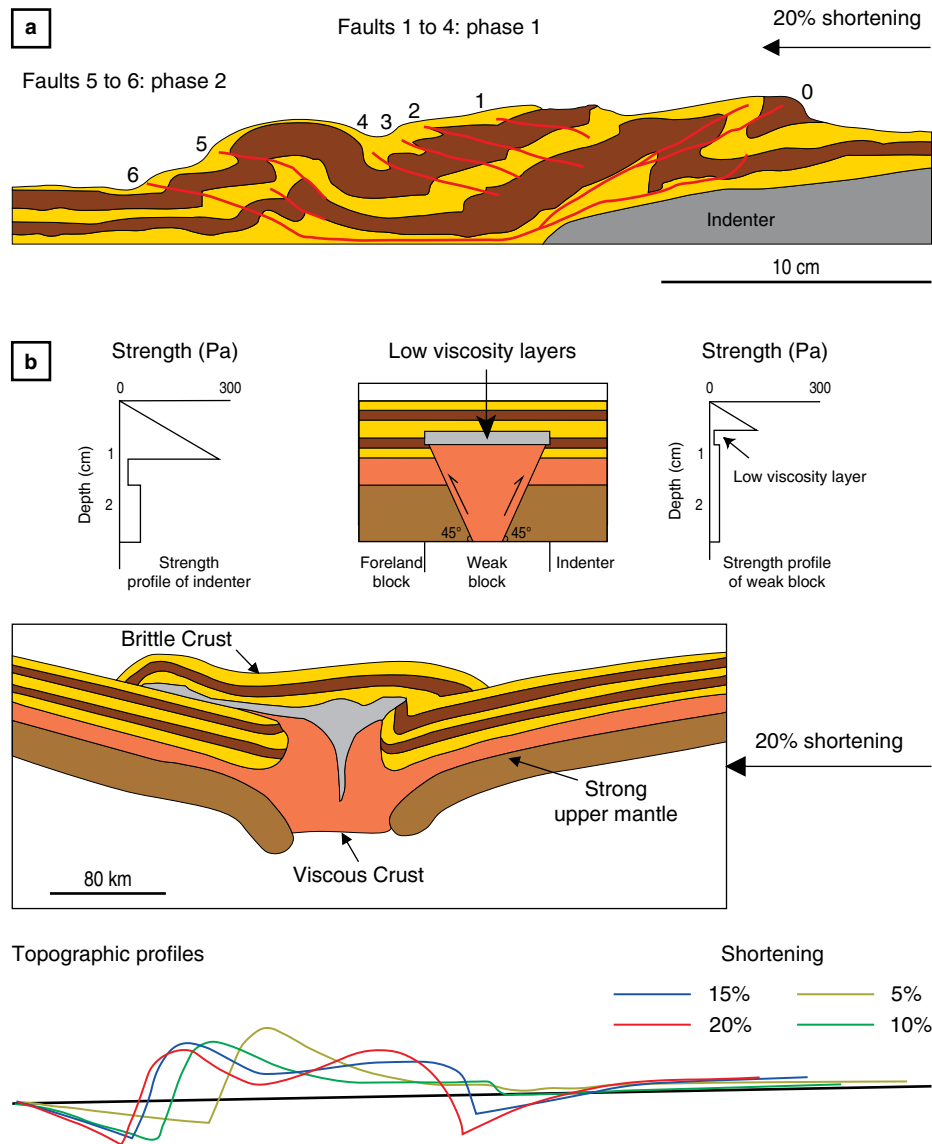


Figure 21. Contrasting experimental models that account for the formation of a plateau-shaped central depression. The sandbox experiment in **(a)** is a snapshot from a run performed by Prince (2015) and refers to the shortening of alternating sand and microbead layers. The layered nature of this granular material allows for some folding. A rigid wedge is attached to the moving wall (right-hand side). During the first stage, the advancing wedge causes the sand package to slip toward the rear (fault 0) and to thicken by the formation of faults 1 to 4. During the second stage, faults propagate from the leading edge of the moving wedge into the foreland block (faults 5 to 6), and associated backthrusts generate a distal pop-up. The resulting double wedge forms a central depression. The experiment in **(b)** is taken from Sokoutis & Willingshofer (2011) and involves the shortening of three layers representing the upper brittle crust (dry quartz sand) and the lower viscous crust (silicone mix I), which rest on a highly viscous upper mantle (silicone mix II). This package floats on a low-viscosity asthenosphere. During shortening, an intermediate downward-tapering weak block preferentially absorbs the convergence. A thin upper crustal layer detaches and overrides the adjacent indenting blocks, forming a central depression. This plateau becomes established in the early deformation stages, as shown by the topographic profiles.

This partial decoupling and lateral thrusting is aided by a low-viscosity layer, which represents a discontinuity between the upper and lower crust. The combination of a weak intermediate block and the partial detachment of an upper crustal lid overlying this same block produces a plateau-like axial depression.

The latter experiment fails to simulate a mountain front pinned to a rheological boundary, as occurred at the Servitá Fault

from the Oligocene to the Miocene. The decoupling of an upper crustal layer characterizes, however, the late Pliocene deformation phase in the Guavio area. In contrast to the continuously forward-breaking thrusts related to wedge dynamics in the first experiment, the setup involving a weak intermediate block allows for equally distributed deformation over the entire orogenic belt (Figure 21b). In this scenario of wholesale lithospheric shorten-

ing, the EC is comparable to a “hot” orogenic belt, as conceptualized by the numerical visé model of Ellis et al. (1998).

These considerations are valid for the High Plain of Bogotá (see sections 1–3 in Figure 4), where the conditions of isostatic equilibrium most likely prevailed, and slab tear may have contributed to an elevated thermal gradient. The long-lasting accumulation of shortening at the crustal discontinuity of the Servitá Fault may be explained by rheological contrasts between the orogenic and the foreland block, which were possibly inherited from the Cretaceous back–arc setting. The short wavelengths of the folds in the superficial Cretaceous units suggest buckling with a degree of decoupling with respect to the uniformly strained basement. Further north, inherited faults dictate the style of the basement-involved folding, but the faults became only partially reactivated (see section 4 in Figure 4). In the antiformal lobes of the Cocuy Syntaxis, the faults were not reactivated, and fault-controlled folding was limited to the weak zone associated with the Chicamocha Syncline (Figure 7). In this section, the concept of rheological contrasts between a weak orogenic block bracketed between rigid foreland blocks is not applicable.

10. Conclusions

We examined in detail the Cretaceous back–arc evolution and its constraints on Cenozoic basin inversion. We highlight the following points:

- The widely accepted scenario of an extensional back–arc province delimited by breakaway faults can be integrated into the evolutionary model of a forebulge flanked by marginal basins.
- Marginal basins need not be fault-bounded, even during their “syn-rift” stage of increased subsidence. In the Guavio area, a fault-related subsidence cycle is constrained to the initial break-up of the back–arc realm.
- The forebulge dynamics temporally coincide with a Cretaceous subduction cycle, and may have been driven by a minor plume within the then-established back–arc realm.

The Cenozoic deformation style of the middle segment of the EC closely relates to the tectonic framework of the North Andean flat-slab segment and the slab tear at its southern termination. We conclude the following:

- Of the three differentiated structural domains, the southern domain, which is typified by the High Plain of Bogotá in its axial depression, is affected by penetrative deformation and therefore behaved like a weak block. Shortening was consumed by small-scale buckling at high structural levels and homogeneous deformation within the pre-Cretaceous basement, with a wide transition zone that combines the two deformation modes.
- In the northern domain, buckling became wider, as it involved the basement and was controlled by inherited Early

Jurassic faults. Although these faults were only partially reactivated, they controlled the folding of their hanging wall blocks and represented, thus, rheological boundaries.

- Fault reactivation is absent within the antiformal lobes of the northernmost transverse section of the Cocuy Syntaxis. The exceptional topographic relief and a fold style that combines buckling and gravity-induced down-slope shear attest to increased surface uplift. The cordilleran eastern front extends to the outer hinge of the subducting slab, which suggests support from the shallowly dipping oceanic slab.

Acknowledgments

The senior authors thank the numerous graduate students and now colleagues who helped us explore the geology of the Llanos Foothills, when access to this area was still restricted. We are indebted to Carlos A. VARGAS, Pasquale DE GORI, and Claudio CHIARABBA for sharing their processed database of earthquake events. Camilo BETANCUR evaluated and compiled the deformation of the conglomerates presented in Figure 16. The tri-shear modeling was performed with the *FaultFold* program written by Rick ALLMENDINGER. We thank Rick for his generous contributions throughout the years. Data processing of earthquakes and cross-section restoration (not included in this chapter) was performed using Move™ (Midland Valley Exploration) through a software grant to the Universidad Nacional de Colombia. We thank Frederick VOLLMER for sharing his strain analysis software *ellipsefit* and Philip PRINCE for the divulgation of his ingenious sandbox experiments. We are indebted to the critical reviews and stimulating observations of Cees PASSCHIER and Eduardo ROSELLO. We especially thank the editorial team of *The Geology of Colombia* for their effort, generous support and patience.

References

- Acosta, J., Velandia, F., Osorio, J., Lonergan, L. & Mora, H. 2007. Strike-slip deformation within the Colombian Andes. In: Ries, A.C., Butler, R.W.H. & Graham, R.H. (editors), *Deformation of the continental crust: The legacy of Mike Coward*. Geological Society of London, Special Publication 272, p. 303–319. London. <https://doi.org/10.1144/GSL.SP.2007.272.01.16>
- Allmendinger, R.W. 1998. Inverse and forward numerical modeling of trishear fault-propagation folds. *Tectonics*, 17(4): 640–656. <https://doi.org/10.1029/98TC01907>
- Allmendinger, R.W., Zapata, T.R., Manceda, R. & Dzelalija, F. 2004. Trishear kinematic modeling of structures, with examples from the Neuquén Basin, Argentina. In: McClay, K.R. (editor), *Thrust tectonics and hydrocarbon systems*. American Association of Petroleum Geologists, Memoir 82, p. 356–371.
- Anderson, T.A. 1972. Paleogene nonmarine Gualanday Group, Neiva Basin, Colombia, and regional development of the Colombian

- Andes. American Association of Petroleum Geologists Bulletin, 83(8): 2423–2438. [https://doi.org/10.1130/0016-7606\(1972\)83\[2423:PNGGNB\]2.0.CO;2](https://doi.org/10.1130/0016-7606(1972)83[2423:PNGGNB]2.0.CO;2)
- Audemard, F.A., Ollarves, R., Bechtold, M., Diaz, G., Beck, C., Carrillo, E., Pantosti, D. & Diederix, H. 2008. Trench investigation on the main strand of the Boconó Fault in its central section, at Mesa del Caballo, Mérida Andes, Venezuela. *Tectonophysics*, 459(1–4): 38–53. <https://doi.org/10.1016/j.tecto.2007.08.020>
- Bayona, G., Montenegro, O.C., Cardona, A., Jaramillo, C., Lamus, F., Morón, S.E., Quiroz, L., Ruiz, M.C., Valencia, V., Parra, M. & Stockli, D.F. 2010. Estratigrafía, procedencia, subsidencia y exhumación de las unidades paleógenas en el Sinclinal de Usme, sur de la zona axial de la cordilla Oriental. *Geología Colombiana*, (35): 5–35.
- Bayona, G., Cardona, A., Jaramillo, C., Mora, A., Montes, C., Caballero, V., Mahecha, H., Lamus, F., Montenegro, O., Jiménez, G., Mesa, A. & Valencia, V. 2013. Onset of fault reactivation in the Eastern Cordillera of Colombia and proximal Llanos Basin: Response to Caribbean–South American convergence in early Paleogene time. In: Nemčok, M., Mora, A. & Cosgrove, J.W. (editors), *Thick-skin-dominated orogens: From initial inversion to full accretion*. Geological Society of London, Special Publication 377, p. 285–314. <https://doi.org/10.1144/SP377.5>
- Beck, M.E., Rojas, C. & Cembrano, J. 1993. On the nature of buttressing in margin-parallel strike-slip fault systems. *Geology*, 21(8): 755–758. [https://doi.org/10.1130/0091-7613\(1993\)021<0755:OTNOBI>2.3.CO;2](https://doi.org/10.1130/0091-7613(1993)021<0755:OTNOBI>2.3.CO;2)
- Branquet, Y., Cheilletz, A., Cobbold, P.R., Baby, P., Laumonier, B. & Giuliani, G. 2002. Andean deformation and rift inversion, eastern edge of Cordillera Oriental (Guateque–Medina area), Colombia. *Journal of South American Earth Sciences*, 15(4): 391–407. [https://doi.org/10.1016/S0895-9811\(02\)00063-9](https://doi.org/10.1016/S0895-9811(02)00063-9)
- Bürgl, H. 1960. El Jurásico e infracretáceo del río Batá, Boyacá. *Boletín Geológico*, 6(1–3): 169–211.
- Bürgl, H. 1967. The orogenesis in the Andean system of Colombia. *Tectonophysics*, 4(4–6): 429–443. [https://doi.org/10.1016/0040-1951\(67\)90009-1](https://doi.org/10.1016/0040-1951(67)90009-1)
- Bustamante, A., Juliani, C., Essene, E.J., Hall, C.M. & Hyppolito, T. 2012. Geochemical constraints on blueschist- and amphibolite facies rocks of the Central Cordillera of Colombia: The Andean Barragán region. *International Geology Review*, 54(9): 1013–1030. <https://doi.org/10.1080/00206814.2011.594226>
- Caballero, V., Mora, A., Quintero, I., Blanco, V., Parra, M., Rojas, L.E., Lopez, C., Sánchez, N., Horton, B.K., Stockli, D. & Duddy, I. 2013. Tectonic controls on sedimentation in an intermontane hinterland basin adjacent to inversion structures: The Nuevo Mundo Syncline, Middle Magdalena Valley, Colombia. In: Nemčok, M., Mora, A. & Cosgrove, J.W. (editors), *Thick-skin-dominated orogens: From initial inversion to full accretion*. Geological Society of London, Special Publication 377, p. 315–342. <https://doi.org/10.1144/SP377.12>
- Campbell, C.J. & Bürgl, H. 1965. Section through the Eastern Cordillera of Colombia, South America. *Geological Society of America Bulletin*, 76(5): 567–590. [https://doi.org/10.1130/0016-7606\(1965\)76\[567:STTECO\]2.0.CO;2](https://doi.org/10.1130/0016-7606(1965)76[567:STTECO]2.0.CO;2)
- Chamberlin, R.T. 1910. The Appalachian folds of central Pennsylvania. *The Journal of Geology*, 18(3): 228–251. <https://doi.org/10.1086/621722>
- Chiarabba, C., De Gori, P., Faccenna, C., Speranza, F., Seccia, D., Dionicio, V. & Prieto, G.A. 2015. Subduction system and flat slab beneath the Eastern Cordillera of Colombia. *Geochemistry, Geophysics, Geosystems*, 17(1): 16–27. <https://doi.org/10.1002/2015GC006048>
- Colletta, B., Hebrard, F., Letouzey, J., Werner, P. & Rudkiewicz, J.L. 1990. Tectonic style and crustal structure of the Eastern Cordillera, Colombia from a balanced cross section. In: Letouzey, J. (editor), *Petroleum and tectonics in mobile belts*. Editions Technip, p. 81–100. Paris.
- Cooper, M.A., Addison, F.T., Alvarez, R., Coral, M., Graham, R.H., Hayward, A.B., Howe, S., Martinez, J., Naar, J., Peñas, R., Pulham, A.J. & Taborda, A. 1995. Basin development and tectonic history of the Llanos Basin, Eastern Cordillera, and Middle Magdalena Valley, Colombia. *American Association of Petroleum Geologists Bulletin*, 79(10): 1421–1443.
- Cortés, M., Colletta, B. & Angelier, J. 2006. Structure and tectonics of the central segment of the Eastern Cordillera of Colombia. *Journal of South American Earth Sciences*, 21(4): 437–465. <https://doi.org/10.1016/j.jsames.2006.07.004>
- Corti, G., van Wijk, J., Cloetingh, S. & Morley, C.K. 2007. Tectonic inheritance and continental rift architecture: Numerical and analogue models of the East African Rift system. *Tectonics*, 26(6): 1–13. <https://doi.org/10.1029/2006TC002086>
- Cruden, A.R., Nasser, M.H.B. & Pysklywec, R. 2006. Surface topography and internal strain variation in wide hot orogens from three-dimensional analogue and two-dimensional numerical vice models. In: Buiter, S.J.H. & Schreurs, G. (editors), *Analogue and numerical modelling of crustal-scale processes*. Geological Society of London, Special Publication 253, p. 79–104. <http://dx.doi.org/10.1144/GSL.SP.2006.253.01.04>
- Currie, C.A., Wang, K., Hyndman, R.D. & He, J. 2004. The thermal effects of steady-state slab-driven mantle flow above a subducting plate: The Cascadia subduction zone and backarc. *Earth and Planetary Science Letters*, 223(1–2): 35–48. <https://doi.org/10.1016/j.epsl.2004.04.020>
- Dalrymple, R.W. & Choi, K. 2007. Morphologic and facies trends through the fluvial-marine transition in tide-dominated depositional systems: A schematic framework for environmental and sequence-stratigraphic interpretation. *Earth Science Reviews*, 81(3–4): 135–174. <https://doi.org/10.1016/j.earsci-rev.2006.10.002>
- DeCelles, P.G. & DeCelles, P.C. 2001. Rates of shortening, propagation, underthrusting, and flexural wave migration in continen-

- tal orogenic systems. *Geology*, 29(2): 135–138. [https://doi.org/10.1130/0091-7613\(2001\)029<0135:ROSPUA>2.0.CO;2](https://doi.org/10.1130/0091-7613(2001)029<0135:ROSPUA>2.0.CO;2)
- Dengo, C.A. & Covey, M.C. 1993. Structure of the Eastern Cordillera of Colombia: Implications for trap styles and regional tectonics. *American Association of Petroleum Geologists Bulletin*, 77(8): 1315–1337. <https://doi.org/10.1306/BDF8E7A-1718-11D7-8645000102C1865D>
- De Porta, J. 1974. *Léxique Stratigraphique International. Amérique Latine, Colombie: (deuxième partie) Tertiaire et Quaternaire*. Centre National de la Recherche Scientifique 5, fascicule 4 b, 626 p. Paris.
- Dimaté, C., Rivera, L.A., Taboada, A., Delouis, B., Osorio, A., Jiménez, E., Fuenzalida, A., Cisternas, A. & Gómez, I. 2003. The 19 January 1995 Tauramena (Colombia) earthquake: Geometry and stress regime. *Tectonophysics*, 363(3–4): 159–180. [https://doi.org/10.1016/S0040-1951\(02\)00670-4](https://doi.org/10.1016/S0040-1951(02)00670-4)
- Dixon, J.M., 1975. Finite strain and progressive deformation in models of diapiric structures. *Tectonophysics*, 28 (1–2): 89–124. [https://doi.org/10.1016/0040-1951\(75\)90060-8](https://doi.org/10.1016/0040-1951(75)90060-8)
- Dorado-Galindo, J. 1992. Contribución al conocimiento de la estratigrafía de la Formación Brechas de Buenavista (límite Jurásico–Cretácico). Región noroeste de Villavicencio, Meta. *Geología Colombiana*, (17): 7–39.
- Dueñas, H. & Césari, S.N. 2005. Systematic study of Early Carboniferous palynological assemblages from the Llanos Orientales Basin, Colombia. *Revista del Museo Argentino de Ciencias Naturales*, 7(2): 139–152. <https://doi.org/10.22179/REVMACN.7.331>
- Durán, J.P., Vargas, C.A. & Briceño, L.A. 2002. Análisis espacial y temporal de Q–Coda en el piedemonte llanero (Colombia). *Earth Sciences Research Journal*, (6): 33–39.
- Ebinger, C.J. 1989. Tectonic development of the western branch of the East African Rift system. *Geological Society of America Bulletin*, 101(7): 885–903. [https://doi.org/10.1130/0016-7606\(1989\)101<0885:TDOTWB>2.3.CO;2](https://doi.org/10.1130/0016-7606(1989)101<0885:TDOTWB>2.3.CO;2)
- Egbue, O. & Kellogg, J. 2010. Pleistocene to present north Andean “escape”. *Tectonophysics*, 489(1–4): 248–257. <https://doi.org/10.1016/j.tecto.2010.04.021>
- Einsele, G. 1992. *Sedimentary basins: Evolution, facies and sediment budget*. Springer-Verlag, 628 p. Berlin. <https://doi.org/10.1007/978-3-662-04029-4>
- Ellis, S., Beaumont, C., Jamieson, R.A. & Quinlan, G. 1998. Continental collision including a weak zone: The vise model and its application to the Newfoundland Appalachians. *Canadian Journal of Earth Sciences*, 35(11): 1323–1346. <https://doi.org/10.1139/e97-100>
- Epard, J.L. & Groshong, R.H. 1993. Excess area and depth to detachment. *American Association of Petroleum Geologists Bulletin*, 77(8): 1291–1302.
- Epard, J.L. & Groshong Jr., R.H. 1995. Kinematic model of detachment folding including limb rotation, fixed hinges and layer-parallel strain. *Tectonophysics*, 247(1–4): 85–103. [https://doi.org/10.1016/0040-1951\(94\)00266-C](https://doi.org/10.1016/0040-1951(94)00266-C)
- Etayo-Serna, F., De Porta, N.S., De Porta, J. & Gaona, T. 2003. The Batá Formation of Colombia is truly Cretaceous, not Jurassic. *Journal of South American Earth Sciences*, 16(3): 113–117. [https://doi.org/10.1016/S0895-9811\(03\)00048-8](https://doi.org/10.1016/S0895-9811(03)00048-8)
- Fabre, A. 1983. La subsidencia de la cuenca del Cocuy (cordillera Oriental de Colombia) durante el Cretáceo y el terciario. Primera parte: Estudio cuantitativo de la subsidencia. *Geología Norandina*, (8): 22–27.
- Fabre, A. & Delaloye, M. 1983. Intrusiones básicas cretácicas en las sedimentitas de la parte central de la cordillera Oriental. *Geología Norandina*, (6): 19–28.
- Faccenna, C., Becker, T.W., Lallemand, S., Lagabriele, Y., Funicello, F. & Piromallo, C. 2010. Subduction-triggered magmatic pulses: A new class of plumes? *Earth and Planetary Science Letters*, 299(1–2): 54–68. <https://doi.org/10.1016/j.epsl.2010.08.012>
- Flament, N., Gurnis, M. & Müller, R.D., 2013. A review of observations and models of dynamic topography. *Lithosphere* 5(2): 189–210. <https://dx.doi.org/10.1130/L245.1>
- Feininger, T., Barrero, D. & Castro, N. 1972. Geología de parte de los departamentos de Antioquia y Caldas–subzona II–B. *Boletín Geológico*, 20(2): 1–173.
- Feo-Codécido, G., Smith, F.D., Aboud, N. & de Di Giacomo, E. 1984. Basement and Paleozoic rocks of the Venezuelan Llanos basins. In: Bonini, W.E., Hargraves, R.B. & Shagam, R. (editors), *The Caribbean–South American Plate boundary and regional tectonics*. Geological Society of America, Memoir 162, p. 175–187. <https://doi.org/10.1130/MEM162-p175>
- Gephart, J.W. 1994. Topography and subduction geometry in the central Andes: Clues to the mechanics of a noncollisional orogeny. *Journal of Geophysical Research: Solid Earth*, 99(B6): 12279–12288. <https://doi.org/10.1029/94JB00129>
- Gómez, E., Jordan, T., Allmendinger, R.W., Hegarty, K., Kelly, S. & Heizler, M. 2003. Controls on architecture of the Late Cretaceous to Cenozoic southern Middle Magdalena Valley Basin, Colombia. *Geological Society of America Bulletin*, 115(2): 131–147. [https://doi.org/10.1130/0016-7606\(2003\)115<0131:COAOTL>2.0.CO;2](https://doi.org/10.1130/0016-7606(2003)115<0131:COAOTL>2.0.CO;2)
- Gómez, E., Jordan, T.E., Allmendinger, R.W., Hegarty, K. & Kelley, S. 2005a. Syntectonic Cenozoic sedimentation in the northern Middle Magdalena Valley Basin of Colombia and implications for exhumation of the northern Andes. *Geological Society of America Bulletin*, 117(5–6): 547–569. <https://doi.org/10.1130/B25454.1>
- Gómez, E., Jordan, T.E., Allmendinger, R.W. & Cardozo, N. 2005b. Development of the Colombian Foreland–Basin system as a consequence of diachronous exhumation of the northern Andes. *Geological Society of America Bulletin*, 117(9–10): 1272–1292. <https://doi.org/10.1130/B25456.1>

- Guerrero, J. 2002. A proposal on the classification of systems tracts: Application to the allostratigraphy and sequence stratigraphy of the Cretaceous Colombian Basin. Part 2: Barremian to Maastrichtian. *Geología Colombiana*, (27): 27–49.
- Haas, O. 1960. Lower Cretaceous ammonites from Colombia, South America. *American Museum Novitates*, (2005), 62 p. New York.
- Hardebol, N.J., Pysklywec, R.N. & Stephenson, R. 2012. Small-scale convection at a continental back-arc to craton transition: Application to the southern Canadian Cordillera. *Journal of Geophysical Research: Solid Earth*, 117(B1): 1–18. <https://doi.org/10.1029/2011JB008431>
- Harrison, J.V. & Falcon, N.L. 1934. Collapse structures. *Geological Magazine*, 71(12): 529–539. <https://doi.org/10.1017/S0016756800095005>
- Haughton, P., Davis, C., McCaffrey, W. & Barker, S. 2009. Hybrid sediment gravity flow deposits—classification, origin and significance. *Marine and Petroleum Geology*, 26(10): 1900–1918. <https://doi.org/10.1016/j.marpetgeo.2009.02.012>
- Hooghiemstra, H., Wijninga, V.M. & Cleef, A.M. 2006. The paleobotanical record of Colombia: Implications for biogeography and biodiversity. *Annals of the Missouri Botanical Garden*, 93(2): 297–325. [https://doi.org/10.3417/0026-6493\(2006\)93\[297:T-PROCI\]2.0.CO;2](https://doi.org/10.3417/0026-6493(2006)93[297:T-PROCI]2.0.CO;2)
- Hyndman, R.D. 2010. The consequences of Canadian Cordillera thermal regime in recent tectonics and elevation: A review. *Canadian Journal of Earth Sciences*, 47(5): 621–632. <https://doi.org/10.1139/E10-016>
- Hyndman, R.D. & Currie, C.A. 2011. Why is the North America Cordillera high? Hot backarcs, thermal isostasy, and mountain belts. *Geology*, 39(8): 783–786. <https://doi.org/10.1130/G31998.1>
- Idárraga-García, J., Kendall, J.M. & Vargas, C.A. 2016. Shear wave anisotropy in northwestern South America and its link to the Caribbean and Nazca subduction geodynamics. *Geochemistry, Geophysics, Geosystems*, 17(9): 3655–3673. <https://doi.org/10.1002/2016GC006323>
- Jiménez, L., Mora, A., Casallas, W., Silva, A., Tesón, E., Támara, J., Namson, J., Higuera-Díaz, I.C., Lasso, A. & Stockli, D. 2013. Segmentation and growth of foothill thrust-belts adjacent to inverted grabens: The case of the Colombian Llanos Foothills. In: Nemčok, M., Mora, A.R. & Cosgrove, J.W. (editors), *Thick-skin-dominated orogens: From initial inversion to full accretion*. Geological Society of London, Special Publication 377, p. 189–220. <https://doi.org/10.1144/SP377.11>
- Julivert, M. 1962. La estratigrafía de la Formación Guadalupe y las estructuras por gravedad en la serranía de Chía (Sabana de Bogotá). *Boletín de Geología*, (11): 5–21.
- Julivert, M. 1963. Los rasgos tectónicos de la región de la Sabana de Bogotá y los mecanismos de formación de las estructuras. *Boletín de Geología*, (13–14): 5–104.
- Julivert, M. 1970. Cover and basement tectonics in the cordillera Oriental of Colombia, South America, and a comparison with some other folded chains. *Geological Society of America Bulletin*, 81(12): 3623–3646. [https://doi.org/10.1130/0016-7606\(1970\)81\[3623:CABTIT\]2.0.CO;2](https://doi.org/10.1130/0016-7606(1970)81[3623:CABTIT]2.0.CO;2)
- Kammer, A. 1996. Estructuras y deformaciones del borde oriental del Macizo de Floresta. *Geología Colombiana*, (21): 65–80.
- Kammer, A. 1997. Los pliegues del Sinclinal de Tunja: Análisis estructural y modelamiento geométrico. *Geología Colombiana*, (22): 3–25.
- Kammer, A. 2003. La Formación Tilatá en los alrededores de Chontá: Marco tectónico y ambientes deposicionales. In: van der Hammen, T. (editor), *Neógeno y Cuaternario del altiplano de Bogotá y alrededores II, zona norte y aspectos generales*. Instituto Geográfico Agustín Codazzi, Análisis Geográficos 26, p. 69–100. Bogotá.
- Kammer, A. & Mora, A. 1999. Structural style and amount of shortening of the folded Bogota segment, Eastern Cordillera of Colombia. *Zentralblatt für Geologie und Paläontologie, Teil I*(7–8), p. 823–838. Bayreuth, Germany.
- Kammer, A. & Piraquive-Bermúdez, A. 2013. Evidencias sedimentológicas y estructurales para un origen paleógeno de la Falla de Chusma, Valle Superior del Magdalena, borde occidental de la sub-cuenca de Neiva. *Geología Colombiana*, (38): 43–64.
- Kammer, A. & Sánchez, J. 2006. Early Jurassic rift structures associated with the Soapaga and Boyacá Faults of the Eastern Cordillera, Colombia: Sedimentological inferences and regional implications. *Journal of South American Earth Sciences*, 21(4): 412–422. <https://doi.org/10.1016/j.jsames.2006.07.006>
- Kammer, A., Tamara, J., Beltrán, A. & Robles, W. 2007. Pliegues sobrepuestos en el Anticlinal de Buenavista, piedemonte llanero. *Boletín de Geología*, 29(2): 85–93.
- King, S.D. & Anderson, D.L. 1998. Edge-driven convection. *Earth and Planetary Science Letters*, 160(3–4): 289–296. [https://doi.org/10.1016/S0012-821X\(98\)00089-2](https://doi.org/10.1016/S0012-821X(98)00089-2)
- King, S.D. & Ritsema, J. 2000. African hot spot volcanism: Small-scale convection in the upper mantle beneath cratons. *Science*, 290(5494): 1137–1140. <https://doi.org/10.1126/science.290.5494.1137>
- López, C., Briceño, A. & Buitrago, J. 1991. Edad y origen de los diapiros de sal de la Sabana de Bogotá. IV Simposio Bolivariano Exploración Petrolera en las Cuencas Subandinas. Trabajo 19, 40 p. Bogotá.
- Lyon-Caen, H. & Molnar, P. 1985. Gravity anomalies, flexure of the Indian Plate, and the structure, support and evolution of the Himalaya and Ganga Basin. *Tectonics*, 4(6): 513–538. <https://doi.org/10.1029/TC004i006p00513>
- Martínez, J.A. 2006. Structural evolution of the Llanos Foothills, Eastern Cordillera, Colombia. *Journal of South American*

- Earth Sciences, 21(4): 510–520. <https://doi.org/10.1016/j.jsames.2006.07.010>
- McLaughlin Jr., D.H. 1972. Evaporite deposits of Bogotá area, Cordillera Oriental, Colombia. *American Association of Petroleum Geologists Bulletin*, 56(11): 2240–2259.
- Mora, A., Parra, M., Strecker, M.R., Kammer, A., Dimaté, C. & Rodríguez, F. 2006. Cenozoic contractional reactivation of Mesozoic extensional structures in the Eastern Cordillera of Colombia. *Tectonics*, 25(2): 1–19. <https://doi.org/10.1029/2005TC001854>
- Mora, A., Parra, M., Strecker, M.R., Sobel, E.R., Hooghiemstra, H., Torres, V. & Vallejo-Jaramillo, J. 2008. Climatic forcing of asymmetric orogenic evolution in the Eastern Cordillera of Colombia. *Geological Society of America Bulletin*, 120(7–8): 930–949. <https://doi.org/10.1130/B26186.1>
- Mora, A., Gaona, T., Kley, J., Montoya, D., Parra, M., Quiroz, L.I., Reyes, G. & Strecker, M. 2009. The role of inherited extensional fault segmentation and linkage in contractional orogenesis: A reconstruction of Lower Cretaceous inverted rift basins in the Eastern Cordillera of Colombia. *Basin Research*, 21(1): 111–137. <https://doi.org/10.1111/j.1365-2117.2008.00367.x>
- Mora, A., Horton, B.K., Mesa, A., Rubiano, J., Ketcham, R.A., Parra, M., Blanco, V., Garcia, D. & Stockli, D.F. 2010a. Migration of Cenozoic deformation in the Eastern Cordillera of Colombia interpreted from fission track results and structural relationships: Implications for petroleum systems. *American Association of Petroleum Geologists Bulletin*, 94(10): 1543–1580. <https://doi.org/10.1306/01051009111>
- Mora, A., Parra, M., Strecker, M.R., Sobel, E.R., Zeilinger, G., Jaramillo, C., Ferreira Da Silva, S. & Blanco, M. 2010b. The eastern foothills of the Eastern Cordillera of Colombia: An example of multiple factors controlling structural styles and active tectonics. *Geological Society of America Bulletin*, 122(11–12): 1846–1864. <https://doi.org/10.1130/B30033.1>
- Mora, A., Reyes-Harker, A., Rodríguez, G., Tesón, E., Ramírez-Arias, J.C., Parra, M., Caballero, V., Mora, J.P., Quintero, I., Valencia, V., Ibañez-Mejía, M., Horton, B.K. & Stockli, D.F. 2013. Inversion tectonics under increasing rates of shortening and sedimentation: Cenozoic example from the Eastern Cordillera of Colombia. In: Nemčok, M., Mora, A. & Cosgrove, J.W. (editors), *Thick-skin-dominated orogens: From initial inversion to full accretion*. Geological Society of London, Special Publication 377, p. 411–442. <https://doi.org/10.1144/SP377.6>
- Mora, A., Parra, M., Rodríguez-Forero, G., Blanco, V., Moreno, N., Caballero, V., Stockli, D.F., Duddy, I. & Ghorbal, B. 2015. What drives orogenic asymmetry in the northern Andes? A case study from the apex of the northern Andean orocline. In: Bartolini, C. & Mann, P. (editors), *Petroleum geology and potential of the Colombian Caribbean margin*. American Association of Petroleum Geologists, Memoir 108, p. 547–586. <https://doi.org/10.1306/13531949M1083652>
- Morales, L.G. 1958. General geology and oil occurrences of Middle Magdalena Valley, Colombia, South America. In: Weeks, L.G. (editor), *Habitat of oil*. American Association of Petroleum Geologists, Special Publications SP18, p. 641–695. Tulsa, USA.
- Mora-Páez, H., Mencin, D.J., Molnar, P., Diederix, H., Cardona-Piedrahita, L., Peláez-Gaviria, J.R. & Corchuelo-Cuervo, Y. 2016. GPS velocities and the construction of the Eastern Cordillera of the Colombian Andes. *Geophysical Research Letters*, 43(16): 8407–8416. <https://doi.org/10.1002/2016GL069795>
- Moreno-Murillo, J.M. 1991. Provenance of the Lower Cretaceous sedimentary sequences, central part, Eastern Cordillera, Colombia. *Revista de la Academia Colombiana de Ciencias Exactas, Físicas y Naturales*, 18(69): 159–173.
- Moreno-Murillo, J.M. & Concha-Perdomo, A.E. 1993. Nuevas manifestaciones ígneas básicas en el flanco occidental de la cordillera Oriental, Colombia. *Geología Colombiana*, (18): 143–150.
- Moucha, R., Forte, A.M., Mitrovica, J.X., Rowley, D.B., Quéré, S., Simmons, N.A. & Grand, S.P. 2008. Dynamic topography and long-term sea-level variations: There is no such thing as a stable continental platform. *Earth and Planetary Science Letters*, 271(1–4): 101–108. <https://doi.org/10.1016/j.epsl.2008.03.056>
- Nivia, Á., Marriner, G.F., Kerr, A.C. & Tarney, J. 2006. The Quebradagrande Complex: A Lower Cretaceous ensialic marginal basin in the Central Cordillera of the Colombian Andes. *Journal of South American Earth Sciences*, 21(4): 423–436. <https://doi.org/10.1016/j.jsames.2006.07.002>
- Ochoa, D., Hoorn, C., Jaramillo, C., Bayona, G., Parra, M. & De la Parra, F. 2012. The final phase of tropical lowland conditions in the axial zone of the Eastern Cordillera of Colombia: Evidence from three palynological records. *Journal of South American Earth Sciences*, 39: 157–169. <https://doi.org/10.1016/j.jsames.2012.04.010>
- Parra, M., Mora, A., Jaramillo, C., Strecker, M.R., Sobel, E.R., Quiroz, L., Rueda, M. & Torres, V. 2009a. Orogenic wedge advance in the northern Andes: Evidence from the Oligocene – Miocene sedimentary record of the Medina Basin, Eastern Cordillera, Colombia. *Geological Society of America Bulletin*, 121(5–6): 780–800. <https://doi.org/10.1130/B26257.1>
- Parra, M., Mora, A., Sobel, E.R., Strecker, M.R. & González, R. 2009b. Episodic orogenic-front migration in the northern Andes: Constraints from low-temperature thermochronology in the Eastern Cordillera, Colombia. *Tectonics*, 28(4): 27 p. <https://doi.org/10.1029/2008TC002423>
- Pennington, W.D. 1981. Subduction of the eastern Panama Basin and seismotectonics of northwestern South America. *Journal of Geophysical Research: Solid Earth*, 86(B11): 10753–10770. <https://doi.org/10.1029/JB086iB11p10753>
- Pimpirev, C.T., Patarroyo, P. & Sarmiento, G. 1992. Stratigraphy and facies analysis of the Caqueza Group: A sequence of Lower Cretaceous turbidites in the cordillera Oriental of the Colombian Andes. *Journal of South American Earth Sciences*, 5(3–4): 297–308. [https://doi.org/10.1016/0895-9811\(92\)90027-V](https://doi.org/10.1016/0895-9811(92)90027-V)
- Pindell, J.L. & Kennan, L. 2009. Tectonic evolution of the Gulf of Mexico, Caribbean and northern South America in the mantle

- reference frame: An update. In: James, K.H., Lorente, M.A. & Pindell, J.L. (editors), *The origin and evolution of the Caribbean Plate*. Geological Society of London, Special Publication 328, p. 1–55. <https://doi.org/10.1144/SP328.1>
- Poblet, J. & McClay, K. 1996. Geometry and kinematics of single-layer detachment folds. *American Association of Petroleum Geologists Bulletin*, 80(7): 1085–1109. <https://doi.org/10.1306/64ED8CA0-1724-11D7-8645000102C1865D>
- Polanía, H. & Rodríguez, G. 1978. Posibles turbiditas del Cretáceo Inferior (Miembro Socotá) en el área de Anapoima (Cundinamarca). *Geología Colombiana*, (10): 87–113.
- Poveda, E., Monsalve, G. & Vargas, C.A. 2015. Receiver functions and crustal structure of the northwestern Andean region, Colombia. *Journal of Geophysical Research: Solid Earth*, 120(4): 2408–2425. <https://doi.org/10.1002/2014JB011304>
- Price, N.J. 1975. Rates of deformation. *Journal of the Geological Society*, 131(6): 553–575. <https://doi.org/10.1144/gsjgs.131.6.0553>
- Prince, P. 2015. Eastern Cordillera, Colombia, northern Andes. TheGeoModels. Active tectonics and geomorphology lab, department of geosciences, Virginia Tech. Virginia, USA. <https://www.youtube.com/watch?v=ruaej-br2c> (consulted in September 2015).
- Ramón, J. C., & Rosero, A. 2006. Multiphase structural evolution of the western margin of the Girardot subbasin, Upper Magdalena Valley, Colombia. *Journal of South American Earth Sciences*, 21(4): 493–509. <https://doi.org/10.1016/j.jsames.2006.07.012>
- Rey, P., Vanderhaeghe, O. & Teyssier, C. 2001. Gravitational collapse of the continental crust: Definition, regimes and modes. *Tectonophysics*, 342(3–4): 435–449. [https://doi.org/10.1016/S0040-1951\(01\)00174-3](https://doi.org/10.1016/S0040-1951(01)00174-3)
- Riel, N., Jaillard, E., Martelat, J.E., Guillot, S. & Braun, J. 2018. Permian – Triassic Tethyan realm reorganization: Implications for the outward Pangea margin. *Journal of South American Earth Sciences*, 81: 78–86. <https://doi.org/10.1016/j.jsames.2017.11.007>
- Roeder, D. & Chamberlain, R.L. 1995. Eastern Cordillera of Colombia: Jurassic–Neogene crustal evolution. In: Tankard, A.J., Suárez–Soruco, R. & Welsink, H.J. (editors), *Petroleum basins of South America*. American Association of Petroleum Geologists, Memoir 62, p. 633–645. Tulsa, USA.
- Rowan, M.G. & Linares, R. 2000. Fold–evolution matrices and axial–surface analysis of fault–bend folds: Application to the Medina Anticline, Eastern Cordillera, Colombia. *American Association of Petroleum Geologists Bulletin*, 84(6): 741–764. <https://doi.org/10.1306/A96733E2-1738-11D7-8645000102C1865D>
- Russo, R.M. & Silver, P.G. 1994. Trench–parallel flow beneath the Nazca Plate from seismic anisotropy. *Science*, 263(5150): 1105–1111. <https://doi.org/10.1126/science.263.5150.1105>
- Sánchez, J., Horton, B.K., Tesón, E., Mora, A., Ketcham, R.A. & Stockli, D.F. 2012. Kinematic evolution of Andean fold–thrust structures along the boundary between the Eastern Cordillera and Middle Magdalena Valley Basin, Colombia. *Tectonics*, 31(3): 1–24. <https://doi.org/10.1029/2011TC003089>
- Sarmiento–Rojas, L.F. 2001. Mesozoic rifting and Cenozoic basin inversion history of the Eastern Cordillera, Colombian Andes: Inferences from tectonic models. Doctoral thesis, Vrije Universiteit, 295 p. Amsterdam, the Netherlands.
- Sarmiento–Rojas, L.F., van Wess, J.D. & Cloetingh, S. 2006. Mesozoic transtensional basin history of the Eastern Cordillera, Colombian Andes: Inferences from tectonic models. *Journal of South American Earth Sciences*, 21(4): 383–411. <https://doi.org/10.1016/j.jsames.2006.07.003>
- Saylor, J.E., Horton, B.K., Nie, J., Corredor, J. & Mora, A. 2011. Evaluating foreland basin partitioning in the northern Andes using Cenozoic fill of the Floresta Basin, Eastern Cordillera, Colombia. *Basin Research*, 23(4): 377–402. <https://doi.org/10.1111/j.1365-2117.2010.00493.x>
- Saylor, J.E., Horton, B., Stockli, D.F., Mora, A. & Corredor, J. 2012. Structural and thermochronological evidence for Paleogene basement–involved shortening in the axial Eastern Cordillera, Colombia. *Journal of South American Earth Sciences*, 39: 202–215. <https://doi.org/10.1016/j.jsames.2012.04.009>
- Schmalholz, S.M., Podladchikov, Y.Y. & Burg, J.P. 2002. Control of folding by gravity and matrix thickness: Implications for large–scale folding. *Journal of Geophysical Research: Solid Earth*, 107(B1): ETG 1–1–ETG 1–16. <https://doi.org/10.1029/2001JB000355>
- Sokoutis, D. & Willingshofer, E. 2011. Decoupling during continental collision and intra–plate deformation. *Earth and Planetary Science Letters*, 305(3–4): 435–444. <https://doi.org/10.1016/j.epsl.2011.03.028>
- Spikings, R., Cochrane, R., Villagómez, D., van der Lelij, R., Vallejo, C., Winkler, W. & Beate, B. 2015. The geological history of northwestern South America: From Pangaea to the early collision of the Caribbean Large Igneous Province (290–75 Ma). *Gondwana Research*, 27(1): 95–139. <https://doi.org/10.1016/j.gr.2014.06.004>
- Stibane, F.R. 1967. Paläogeographie und Tektogenese der kolumbianischen Anden. *Geologische Rundschau*, 56(1): 629–642. <https://doi.org/10.1007/BF01848746>
- Suárez, M. A., 1996. Facies analysis of the Upper Eocene La Paz Formation, and regional evaluation of post–middle Eocene stratigraphy, northern Middle Magdalena Valley Basin, Colombia. Master thesis, University of Colorado, 88 p. Boulder, USA.
- Taboada, A., Rivera, L.A., Fuenzalida, A., Cisternas, A., Philip, H., Bijwaard, H., Olaya, J. & Rivera, C. 2000. Geodynamics of the northern Andes: Subductions and intracontinental deformation (Colombia). *Tectonics*, 19(5): 787–813. <https://doi.org/10.1029/2000TC900004>
- Talling, P.J., Masson, D.G., Sumner, E.J. & Malgesini, G. 2012. Subaqueous sediment density flows: Depositional processes and

- deposit types. *Sedimentology*, 59(7): 1937–2003. <https://doi.org/10.1111/j.1365-3091.2012.01353.x>
- Teixell, A., Ruiz, J.C., Teson, E. & Mora, A. 2015. The structure of an inverted back–arc rift: Insights from a transect across the Eastern Cordillera of Colombia near Bogota. In: Bartolini, C. & Mann, P. (editors), *Petroleum geology and potential of the Colombian Caribbean margin*. American Association of Petroleum Geologists, Memoir 108, p. 499–515. <https://doi.org/10.1306/13531947M1083650>
- Terraza, R., Montoya, D., Reyes, G., Moreno, G. & Fúquen, J. 2008. Geología del cinturón esmeraldífero oriental, planchas 210, 228 y 229. Ingeominas, Internal report 2877, 129 p. Bogotá.
- Teson, E., Mora, A., Silva, A., Namson, J., Teixell, A., Castellanos, J., Casallas, W., Julivert, M., Taylor, M., Ibañez–Mejia, M. & Valencia, V. 2013. Relationship of Mesozoic graben development, stress, shortening magnitude, and structural style in the Eastern Cordillera of the Colombian Andes. In: Nemčok, M., Mora, A. & Cosgrove, J.W. (editors), *Thick–skin–dominated orogens: From initial inversion to full accretion*. Geological Society of London, Special Publication 377, p. 257–283. London. <https://doi.org/10.1144/SP377.10>
- Thomas, R.G., Smith, D.G., Wood, J.M., Visser, J., Calverley–Range, E.A. & Koster, E.H. 1987. Inclined heterolithic stratification–terminology, description, interpretation and significance. *Sedimentary Geology*, 53(1–2): 123–179. [https://doi.org/10.1016/S0037-0738\(87\)80006-4](https://doi.org/10.1016/S0037-0738(87)80006-4)
- Torres, V., Vandenberghe, J. & Hooghiemstra, H. 2005. An environmental reconstruction of the sediment infill of the Bogotá Basin (Colombia) during the last 3 million years from abiotic and biotic proxies. *Palaeogeography, Palaeoclimatology, Palaeoecology*, 226(1–2): 127–148. <https://doi.org/10.1016/j.palaeo.2005.05.005>
- Trenkamp, R., Kellogg, J.N., Freymueller, J.T. & Mora, H. 2002. Wide plate margin deformation, southern Central America and northwestern South America, CASA GPS observations. *Journal of South American Earth Sciences*, 15(2): 157–171. [https://doi.org/10.1016/S0895-9811\(02\)00018-4](https://doi.org/10.1016/S0895-9811(02)00018-4)
- Ujueta, G. 1992. Lineamientos río Ariari, Bogotá y Gachalá en los departamentos de Cundinamarca y Meta, Colombia. *Revista Academia Colombiana de Ciencias Exactas, Físicas y Naturales*, 18(70): 345–358.
- van der Hammen, T., Werner, J.H. & van Dommelen, H. 1973. Palynological record of the upheaval of the northern Andes: A study of the Pliocene and lower Quaternary of the Colombian Eastern Cordillera and the early evolution of its high–Andean biota. *Review of Palaeobotany and Palynology*, 16(1–2): 1–122. [https://doi.org/10.1016/0034-6667\(73\)90031-6](https://doi.org/10.1016/0034-6667(73)90031-6)
- van der Lelij, R., Spikings, R., Ulianov, A., Chiaradia, M. & Mora, A. 2016. Palaeozoic to Early Jurassic history of the northwestern corner of Gondwana, and implications for the evolution of the Iapetus, Rheic and Pacific Oceans. *Gondwana Research*, 31: 271–294. <https://doi.org/10.1016/j.gr.2015.01.011>
- van Houten, F.B. & Travis, R.B. 1968. Cenozoic deposits, Upper Magdalena Valley, Colombia. *American Association of Petroleum Geologists Bulletin*, 52(4): 675–702.
- Vargas, C.A. & Mann, P. 2013. Tearing and breaking off of subducted slabs as the result of collision of the Panama arc–indenter with northwestern South America. *Bulletin of the Seismological Society of America*, 103(3): 2025–2046. <https://doi.org/10.1785/0120120328>
- Vásquez, M., Altenberger, U., Romer, R.L., Sudo, M. & Moreno–Murillo, J.M. 2010. Magmatic evolution of the Andean Eastern Cordillera of Colombia during the Cretaceous: Influence of previous tectonic processes. *Journal of South American Earth Sciences*, 29(2): 171–186. <https://doi.org/10.1016/j.jsames.2009.02.003>
- Velandia, F. & Bermúdez, M.A. 2018. The transpressive southern termination of the Bucaramanga Fault (Colombia): Insights from geological mapping, stress tensors, and fractal analysis. *Journal of Structural Geology*, 115: 190–207. <https://doi.org/10.1016/j.jsg.2018.07.020>
- Villagómez, D., Spikings, R., Magna, T., Kammer, A., Winkler, W. & Beltrán, A. 2011. Geochronology, geochemistry and tectonic evolution of the Western and Central cordilleras of Colombia. *Lithos*, 125(3–4): 875–896. <https://doi.org/10.1016/j.lithos.2011.05.003>
- Villamil, T. 1999. Campanian – Miocene tectonostratigraphy, depocenter evolution and basin development of Colombia and western Venezuela. *Palaeogeography, Palaeoclimatology, Palaeoecology*, 153(1–4): 239–275. [https://doi.org/10.1016/S0031-0182\(99\)00075-9](https://doi.org/10.1016/S0031-0182(99)00075-9)
- Vollmer, F.W. 2015. EllipseFit 3.2.1. Strain Analysis Software. <http://www.frederickvollmer.com/ellipsefit/> (consulted in December 2017).
- Warsitzka, M., Kley, J. & Kukowski, N. 2013. Salt diapirism driven by differential loading–Some insights from analogue modeling. *Tectonophysics*, 591: 83–97. <https://doi.org/10.1016/j.tecto.2011.11.018>
- Wernicke, B. & Axen, G.J. 1988. On the role of isostasy in the evolution of normal fault systems. *Geology*, 16(9): 848–851. [https://doi.org/10.1130/0091-7613\(1988\)016<0848:OTROII>2.3.CO;2](https://doi.org/10.1130/0091-7613(1988)016<0848:OTROII>2.3.CO;2)
- Zehnder, A.T. & Allmendinger, R.W. 2000. Velocity field for the trihear model. *Journal of Structural Geology*, 22(8): 1009–1014. [https://doi.org/10.1016/S0191-8141\(00\)00037-7](https://doi.org/10.1016/S0191-8141(00)00037-7)

Explanation of Acronyms, Abbreviations, and Symbols:

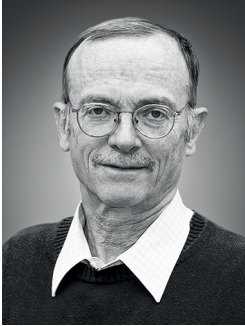
EC

Eastern Cordillera

LREE

Light rare earth element

Authors' Biographical Notes



Andreas KAMMER has been a structural geology professor at the Universidad Nacional de Colombia since 1991. He completed his PhD in 1985 at Neuchâtel, working on the tectonic evolution of the Aar Massif, Central Alps. His work has been focused on the structure, tectonics, and sedimentary evolution of the Colombian Andes since 1985. Together with the senior authors of this

paper, he has initiated research projects on the Eastern foothills of the Eastern Cordillera since 1991.



Alejandro PIRAQUIVE received his Bachelor of Science and Master of Science degrees in geology from the Universidad Nacional de Colombia working on the Eastern foothills of the Eastern Cordillera. For his PhD thesis, he unraveled the tectonic evolution of the Sierra Nevada de Santa Marta, applying geo- and thermochronological methods sponsored by a cotutelle program between the

Université Grenoble—Alpes and the Universidad Nacional de Colombia. He presently holds a research position at the Servicio Geológico Colombiano, which is funded by the postdoc program of Colciencias.



Cristhian GÓMEZ received his Bachelor of Science and Master of Science degrees in geology from the Universidad Nacional de Colombia working on the Triassic rift tectonics of the southern flank of the Sierra Nevada de Santa Marta. His research interests include tectonic sedimentology and thermochronology.



Andrés MORA is the technical leader of onshore Colombia and foothills exploration at Ecopetrol. He received his BS in geology from the Universidad Nacional de Colombia and PhD from the Institut für Geowissenschaften, Universität Potsdam. His research interests include structural geology, petroleum exploration, and petroleum geology.



Antonio VELÁSQUEZ received his Bachelor of Science and Master of Science degrees in geology from the Universidad Nacional de Colombia, evaluating the structural evolution of the Llanos foothills and modeling their gravitational expression by means of crustal-scale anomalies.






Chapter 7



Cenozoic Evolution of the Sierra Nevada de Santa Marta, Colombia

<https://doi.org/10.32685/pub.esp.37.2019.07>

Published online 26 November 2020

Mauricio PARRA^{1*} , Sebastián ECHEVERRI² , Ana María PATIÑO³ ,
Juan Carlos RAMÍREZ⁴ , Andrés MORA⁵, Edward R. SOBEL⁶,
Ariel ALMENDRAL⁷, and Andrés PARDO-TRUJILLO⁸ 

Abstract The highest coastal relief on Earth occurs in the Sierra Nevada de Santa Marta in northern Colombia. With an average elevation of ca. 4 km and peaks up to ca. 5.8 km, this small mountain range lies only 85 km to the south of an abyssal plain ca. 3.5 km deep in the Caribbean Sea. A compilation of sparse bedrock and detrital low-temperature thermochronometric data, new detrital apatite fission-track and apatite (U–Th)/He data from modern river sediments, and stratigraphic patterns of adjacent Miocene – Pliocene basins document episodic tectonic development of the Sierra Nevada de Santa Marta. A Paleocene collision of oceanic crust with western Colombia triggered initial exhumation and westward monoclinical tilting of the formerly contiguous Central Cordillera and Santa Marta Massif. Subsequent late Eocene (ca. 35 Ma) dismembering of both ranges occurred associated with right-lateral translation of the Caribbean Plate against the northwestern continental margin of Colombia. This episode marked the onset of contrasting exhumation histories, characterized by low denudation and pediment formation in the Central Cordillera and rapid, episodic exhumation of the Santa Marta Massif, associated with normal faulting and opening of extensional basins along its southwestern margin. Multiple approaches to extracting exhumation rates from thermochronometry, including 1D and 3D reconstructions, reveal that following rapid late Eocene – early Miocene rock uplift, asymmetric exhumation characterized the Sierra Nevada. On the southwestern margin, moderate to rapid exhumation favored progradation of alluvial fan deposits on top of shallow marine and fan delta facies. In contrast, diminished exhumation prompted a reciprocal stratigraphy in the northern margin, where facies retrograde, leading to the accumulation of shallow marine facies on fan delta and alluvial fan deposits. Thermochronometric ages of outcropping units retrieved from modern river sands imply a very recent (<2 Ma) pulse of exhumation, possibly triggered by removal of lower crust, whose precise magnitude and time constraints remain unknown.

Keywords: *Sierra Nevada de Santa Marta, Caribbean Plate, thermochronology, sediment provenance.*

Resumen El mayor relieve topográfico costero de la Tierra ocurre en la Sierra Nevada de Santa Marta en el norte de Colombia. Con una elevación promedio de ca. 4 km y picos de hasta ca. 5,8 km, esta pequeña cordillera yace tan solo 85 km al sur de una

- 1 mparra@iee.usp.br
Universidade de São Paulo
Instituto de Energia e Ambiente
Av. Professor Luciano Gualberto 1289, Cidade Universitária
São Paulo, Brasil
 - 2 juansebasecheverri@gmail.com
Universidade de São Paulo
Instituto de Geociências
Rua do Lago 562, Cidade Universitária
São Paulo, Brasil
 - 3 anamariapta@gmail.com
Universidade de São Paulo
Instituto de Geociências
Rua do Lago 562, Cidade Universitária
São Paulo, Brasil
 - 4 ramirezjuanc11@yahoo.com
Universidade de São Paulo
Instituto de Geociências
Rua do Lago 562, Cidade Universitária
São Paulo, Brasil
 - 5 andres.mora@ecopetrol.com.co
Ecopetrol S.A.
Vicepresidencia de Exploración
Bogotá, Colombia
 - 6 ed@geo.uni-potsdam.de
Institut fuer Erd- und Umweltwissenschaften
Karl Liebknecht Str 25, 14476
Potsdam, Germany
 - 7 arielalmendral.vazquez@nr.no
Norwegian Computing Center
P.O. Box 114 Blindern
NO-0314 Oslo, Norway
 - 8 andres.pardo@ucaldas.edu.co
Universidad de Caldas
Instituto de Investigaciones en Estratigrafía
Manizales, Colombia
- * Corresponding author

Supplementary Information:

S1: <https://www2.sgc.gov.co/LibroGeologiaColombia/tgc/sgcpubesp37201907s1.pdf>

S2: <https://www2.sgc.gov.co/LibroGeologiaColombia/tgc/sgcpubesp37201907s2.pdf>

Citation: Parra, M., Echeverri, S., Patiño, A.M., Ramírez, J.C., Mora, A., Sobel, E.R., Almendral, A. & Pardo-Trujillo, A. 2020. Cenozoic evolution of the Sierra Nevada de Santa Marta, Colombia. In: Gómez, J. & Mateus-Zabala, D. (editors), *The Geology of Colombia, Volume 3 Paleogene – Neogene*. Servicio Geológico Colombiano, Publicaciones Geológicas Especiales 37, p. 185–213. Bogotá. <https://doi.org/10.32685/pub.esp.37.2019.07>

llanura abisal de ca. 3,5 km de profundidad en el mar Caribe. La compilación de los pocos datos existentes de termocronología de baja temperatura, tanto de roca del basamento como detríticos; nuevos datos detríticos de trazas de fisión y (U-Th)/He en apatitos en sedimentos activos y el estudio estratigráfico de cuencas marginales miocenas–pliocenas adyacentes documentan una evolución tectónica episódica de la Sierra Nevada de Santa Marta. La colisión paleocena de corteza oceánica contra el margen occidental de Colombia desencadenó el levantamiento inicial y el basculamiento monoclinial hacia el oeste de un cinturón contiguo formado por la cordillera Central y el Macizo de Santa Marta. El posterior desmembramiento de estas dos cordilleras en el Eoceno tardío (ca. 35 Ma) ocurrió asociado a la translación dextral lateral de la Placa del Caribe a lo largo del margen continental noroccidental de Colombia. Este episodio marcó el inicio de historias contrastantes de desarrollo orogénico, caracterizadas por bajas tasas de denudación y desarrollo de pedimento en la cordillera Central y exhumación rápida y episódica en la Sierra Nevada de Santa Marta, asociada a fallamiento normal y apertura de cuencas extensionales en su margen suroccidental. Múltiples métodos para calcular tasas de exhumación a partir de termocronología, incluyendo modelado 1D y 3D, sugieren que tras un episodio de levantamiento rápido en el Eoceno tardío–Mioceno temprano se presentó exhumación asimétrica en la Sierra Nevada. En el margen suroccidental, la exhumación moderada a rápida favoreció la progradación de abanicos aluviales sobre depósitos marinos someros y facies de deltas en abanico. Por el contrario, una disminución en las tasas de levantamiento generó un patrón de apilamiento estratigráfico opuesto en el margen norte, en donde las facies retrogradaron, lo que causó la acumulación de facies marinas someras sobre depósitos de abanicos aluviales y deltas en abanico. Las edades termocronométricas de las rocas aflorantes obtenidas en sedimentos activos de barras fluviales revelan un pulso muy reciente (<2 Ma) de exhumación, posiblemente asociado a la remoción de corteza inferior, y cuya magnitud y temporalidad precisas aún están por descubrir.

Palabras clave: Sierra Nevada de Santa Marta, Placa del Caribe, termocronología, procedencia sedimentaria.

1. Introduction

Oblique convergence and dextral shearing along the northwestern South American margin since the Late Cretaceous have shaped one of the areas with highest topographic relief on Earth in the Sierra Nevada de Santa Marta (SNSM) (Figure 1). Although recent investigations have revealed key episodes concerning the kinematics of early orogenic stages along this margin, the timing and associated driving mechanisms for Cenozoic uplift of the SNSM remain elusive. Sparse but relatively old (>15 Ma) low-temperature mineral cooling ages (Cardona et al., 2011a; Villagómez et al., 2011) and a positive gravity anomaly in the SNSM (Figure 1a) have been used to suggest that the range is in a stage of denudational immaturity, that is, recent crustal stacking and rock uplift exceed the magnitude of exhumation (Parra et al., 2016; Villagómez et al., 2011), portraying a case of non-steady state topography likely due to a young pulse of orogenesis.

Here, we summarize the uplift record and Cenozoic tectonic evolution of the SNSM based on geochronologic, thermochronologic, and stratigraphic data. We present and update

published data as well as summarize new results that portray a two-stage uplift history and an E–W asymmetry and pose new hypotheses regarding the mechanisms driving episodic rock uplift and exhumation during the Cenozoic.

2. Geological Setting

The Cenozoic tectonic evolution of the northwestern margin of South America has been controlled by the interactions of the Caribbean and Pacific Oceanic Plates with the continental margin and the attendant stages of ocean terrane accretion, magmatic growth, tectonic deformation, and sedimentary basin formation (Bayona et al., 2012; Duque-Caro, 1984; Gorney et al., 2007; Kellogg, 1984; Mann et al., 2006; McMahon, 2000; Montes et al., 2015; Pindell et al., 1998).

In the northernmost Andes of Colombia, the along-strike continuity of the Andean chain is replaced by a series of discontinuous uplifted massifs surrounded by Cenozoic basins. Such fragmentation has been associated with the eastward migration of the Caribbean Plate since the Eocene. One such massif is the SNSM, a triangular pyramidal, fault-bounded, basement block

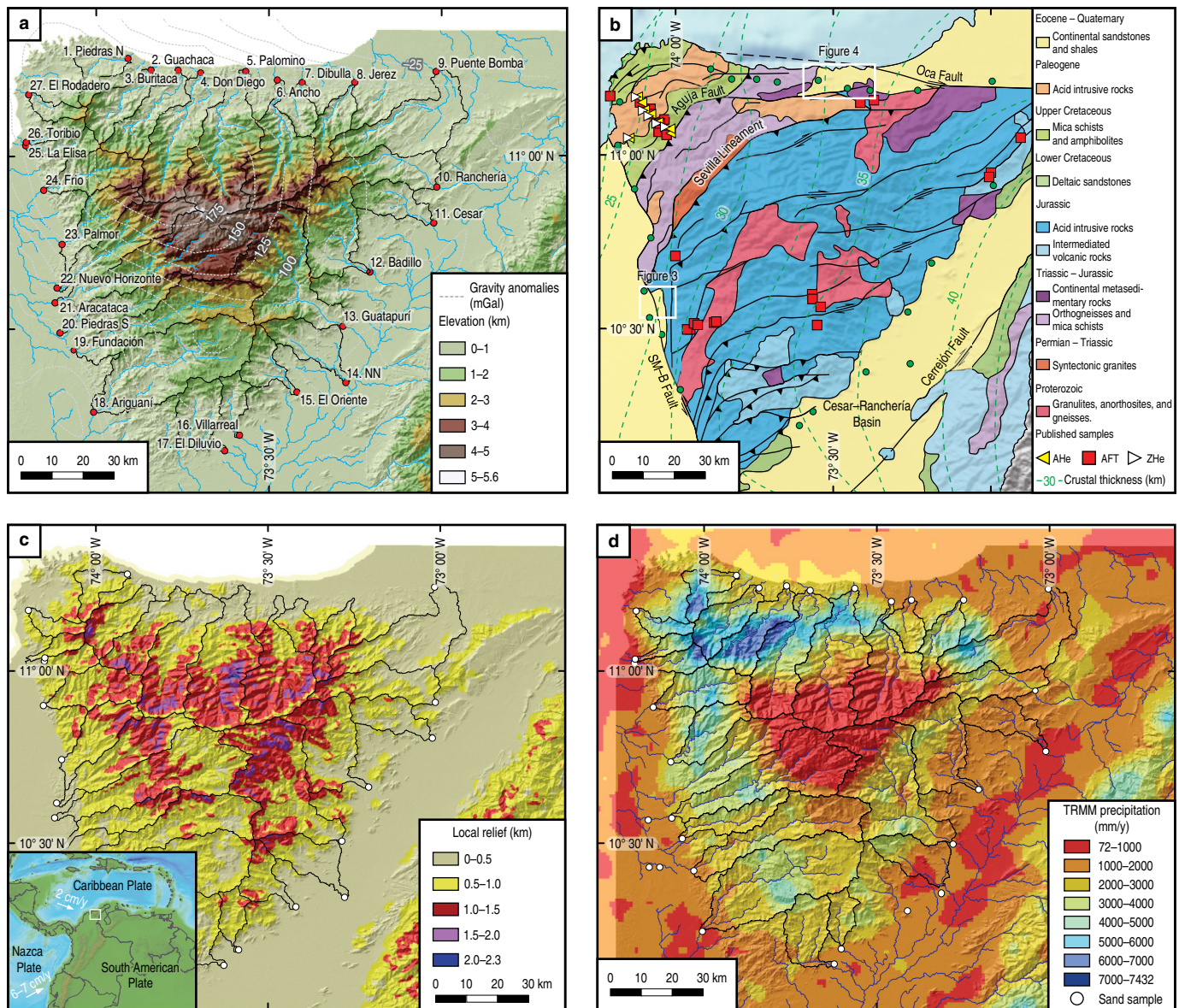


Figure 1. Morphotectonic configuration of the SNSM. **(a)** SRTM 90 topography, Bouguer gravity anomalies (white lines) and location of new detrital thermochronometric samples collected in active river bars and their drainage areas. **(b)** Simplified geologic map (after Tschanz et al., 1969) showing the location of published bedrock thermochronometric samples and values of crustal thickness (after Yarce et al., 2014). White squares denote the areas shown in Figures 3, 4. (SM-B Fault) Santa Marta-Bucaramanga Fault **(c)** Local relief in a 3 km-diameter circular window. Inset map shows the bottom topographic and plate velocities (after Trenkamp et al., 2002). **(d)** Tropical Rainfall Measuring Mission (TRMM) precipitation data (Mulligan, 2006).

isolated between Cenozoic basins in the humid, northwestern corner of the Maracaibo Microplate (Figure 1a, 1d; Burke et al., 1984; Cedié et al., 2003). The range's structural boundaries are the right-lateral Oca Fault in the north and the left-lateral Santa Marta-Bucaramanga Fault in the west, which in addition to a neotectonic strike-slip character (Idárraga-García & Romero, 2010) has an important vertical displacement that has generated the range's structural relief (Figure 1c) and controlled the sedimentation in adjacent basins since the Oligocene. To the east, the serranía de Perijá thrusts along El Cerrejón Fault onto the SNSM basement buried beneath ca. 2.5 km of clastic strata in

the Cesar-Ranchería Basin (Kellogg & Bonini, 1982; Montes et al., 2010).

The SNSM Massif exposes igneous and metamorphic basement rocks of Proterozoic, Permian – Triassic, Triassic – Jurassic, Cretaceous, and Paleocene – Eocene ages (Cardona et al., 2006, 2010a, 2010b, 2011b; Cordani et al., 2005; Duque, 2010; Restrepo-Pace et al., 1997; Tschanz et al., 1969). These rocks are grouped into three geological provinces bounded by SW-NE-striking, subparallel reverse fault systems with NW vergence (Figure 1b; Tschanz et al., 1974): (1) To the southeast, the Sierra Nevada province occupies

more than two-thirds of the SNSM area and consists of an ensialic basement made up of high-grade metamorphic rocks of Grenvillian age (1.0–1.2 Ga; Cardona et al., 2010a; Case & MacDonald, 1973; Tschanz et al., 1974), intruded by undeformed Jurassic – Lower Cretaceous acid plutonic rocks and covered by felsic volcanic rocks of Jurassic age (Cardona et al., 2006); (2) Underthrust beneath the Sierra Nevada province along the Sevilla Fault lies the Sevilla province, made up of an ensialic basement of medium- and low-grade metamorphic rocks (amphibolites and micaceous schists) of Paleozoic age (Cardona et al., 2006; Tschanz et al., 1974; Weber et al., 2009), intruded by Permian – Triassic syntectonic granitoids (Cardona et al., 2010b); (3) Farther to the northwest, the Sevilla province overthrusts an imbricate series of Late Cretaceous – Paleocene allochthonous terranes of Caribbean affinity along the Aguja Fault. They comprise the Santa Marta province, metamorphosed to greenschist to amphibolite facies during an accretionary event along the continental margin in the Late Cretaceous – Paleocene, and made up of a series of low- to middle-grade metavolcanic–sedimentary rocks and orthogneisses arranged in SW–NE-oriented belts. Paleocene to Eocene granitoids (e.g., the Buritaca, Latal, and Toribio Plutons) intruded into both the Santa Marta and Sevilla provinces (Cardona et al., 2011b; Duque, 2010; Salazar et al., 2016; Tschanz et al., 1974) constrain the age of collision between late Maastrichtian and early Paleocene (Cardona et al., 2010c).

Basement correlations from the SNSM (Cardona et al., 2010b) across the Plato–San Jorge and the Lower Magdalena Basins (Ceron et al., 2007; Montes et al., 2010; Mora–Bohórquez et al., 2017) to the Central Cordillera (Ordóñez–Carmona & Pimentel, 2002; Restrepo et al., 2011; Vinasco et al., 2006) support the view of a contiguous Late Cretaceous – Paleocene belt including the Central Cordillera and the SNSM. Tectonic isolation of this ancestral range is thought to have resulted from post–Eocene escape tectonics associated with dextral migration of the Caribbean Plate (e.g., Pindell & Kennan, 2009), generating ca. 30° vertical-axis clockwise rotation (Montes et al., 2010) or a mixture between rotation and translation (Reyes et al., 2004). Such dextral movement led to simultaneous extension in the Ariguaní, Plato, and San Jorge Sub-basins along the southwestern segment (Lower Magdalena Basin) and contraction in the Cesar–Ranchería Basin to the east (Bayona et al., 2010; Montes et al., 2010).

Due to the preservation of strata as young as Miocene in the basins surrounding the SNSM, most of the vertical displacement associated with the Santa Marta–Bucaramanga and Oca Faults is thought to be late Cenozoic in age (Case & MacDonald, 1973). However, older exhumation is supported by late Paleocene and Eocene apatite fission-track ages along the southeastern margin of the range (Villagómez et al., 2011; see section 5.1), as well as by provenance data for Paleogene

strata in the Cesar–Ranchería Basin suggesting an active source area in the Central Cordillera–SNSM (Ayala et al., 2009, 2012; Bayona et al., 2007). Eocene to recent exhumation patterns in the SNSM based on geobarometry and fission-track and (U–Th)/He thermochronology (Cardona et al., 2011a) document peak magnitudes of basement exhumation of ca. 15–19 km in the northwestern range’s corner and decreasing magnitudes toward the SE, so that cooling ages become older (and therefore average exhumation rates lower; see section 5.2). This southward decrease in the magnitude of exhumation has been explained as the result of large-scale clockwise monoclinical tilting that finally results in net basement burial beneath up to ca. 2.2 km of clastic strata in the Cesar–Ranchería Basin (Montes et al., 2010; Sánchez & Mann, 2015).

A positive total Bouguer gravity anomaly of ca. 200 mGal exists in the SNSM (Figure 1a; e.g., Agencia Nacional de Hidrocarburos, 2010) and has been interpreted to reflect (1) the absence of a crustal root due to lack of isostatic compensation (e.g., Case & MacDonald, 1973; Kellogg & Bonini, 1982) or (2) underplating of an abnormally thick oceanic slab that resists subduction (Ceron, 2008).

3. Stratigraphy

The sedimentary archives hosting the SNSM’s ancient denudation are preserved in isolated Cenozoic basins associated with normal and left–lateral movement of the Bucaramanga Fault and right–lateral movement of the Oca Fault on the SW and N sides of the range, respectively (Figure 1b). Tschanz et al. (1969) coined the names Guajira Trough and Riohacha for the northern basins and Ariguaní Trough for the western basin and provided a generalized description of their sedimentary fill. These pioneering works and other stratigraphic studies and geologic mapping at scales of 1:100 000 and 1:25 000 for the western and northern foothills of the SNSM (e.g., Colmenares et al., 2007; Hernández et al., 2003; Piraquive et al., 2017; Tschanz et al., 1969) have produced a series of maps and stratigraphic profiles using different stratigraphic nomenclatures. However, the absence of robust chronostratigraphic control generates problems of synonymy, definition, and stratigraphic correlations (e.g., Hernández et al., 2003; Piraquive et al., 2017). A summary of chronostratigraphic correlations is presented in Figure 2 and associated references.

3.1. Ariguaní Trough

Toward the eastern border of the Lower Magdalena Basin (LMB), the transcurrent movements of the Santa Marta–Bucaramanga and Algarrobo Faults generated a pull-apart basin with up to 7–8 km of sediment thickness preserved, as documented by seismic, gravimetric, and magnetometric data (Bernal–Olaya et al., 2015; Mora et al., 2018; Reyes et al.,

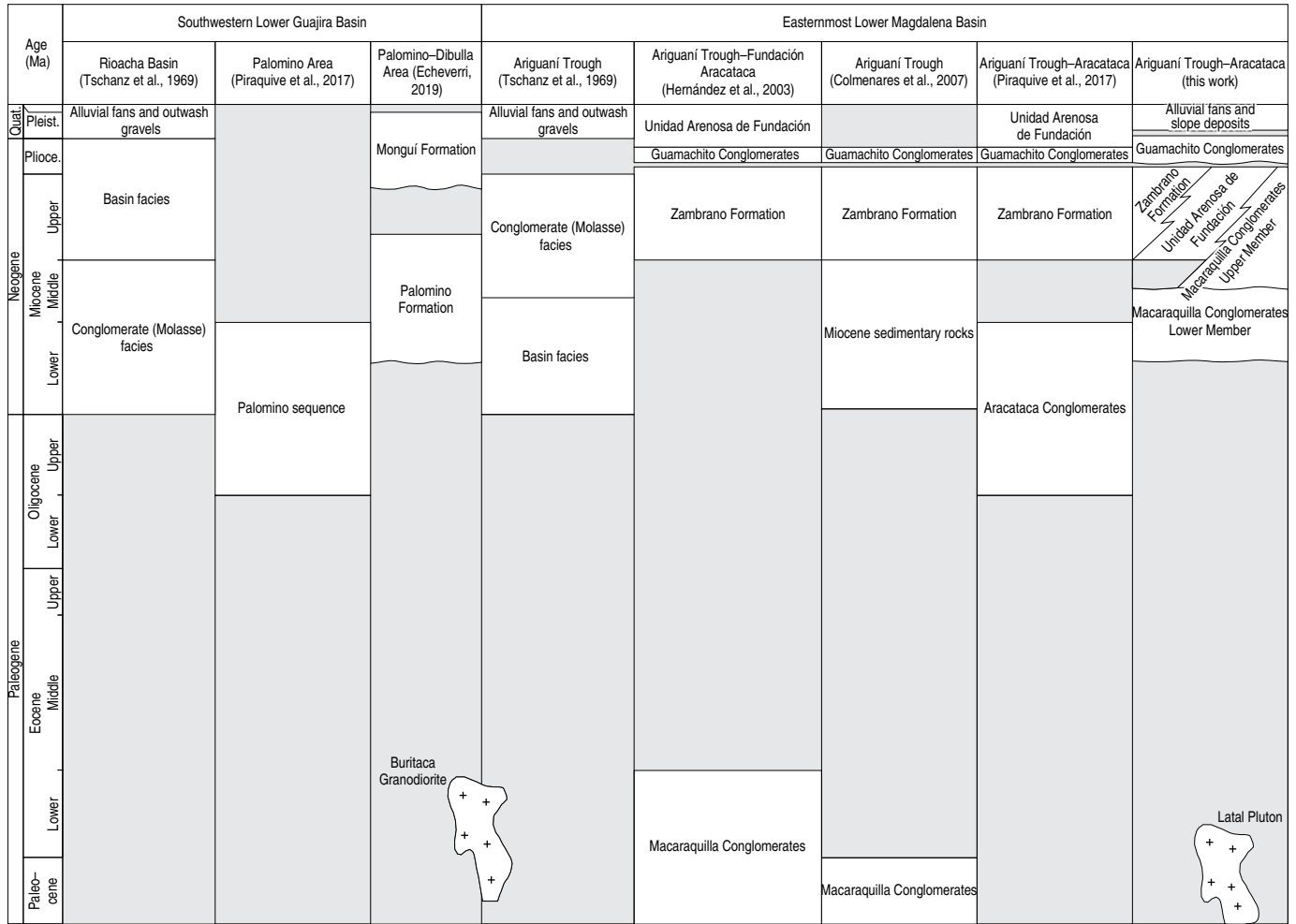


Figure 2. Chronostratigraphic chart of the Lower Guajira and Ariguani Basins.

2004). The fault activity probably began in the early Oligocene, as suggested by correlations with the basal sedimentary strata of the Plato Sub-basin (Rincón et al., 2007), but the age of the oldest sedimentites in the depocenter of the Ariguani Trough remains unknown. Stratigraphic correlations with the lowermost strata found in a structural high to the west in the Alagorrobó-1 well (Rincón et al., 2007) suggest a minimum age of late Oligocene.

The basal strata of this succession are exposed in the western foothills of the SNSM and are limited to the west by the Río Piedras reverse fault (Figure 3; Colmenares et al., 2007). They consist of a west-dipping, dominantly conglomeratic unit (Macaraquilla Conglomerates; Hernández et al., 2003), ca. 1250 m thick (Pinzón-Rodríguez, 2014) and consisting of two members that nonconformably overlie either Jurassic intermediate to acid granitoids or the Precambrian Los Mangos Granulite. Sediment accumulation has been interpreted to have occurred in fan deltas sourced by the SNSM (Piraquive

et al., 2017) and has been assigned, without any chronostratigraphic foundation, to either the Paleocene – Eocene (Hernández et al., 2003) or the Oligocene – early Miocene (Piraquive et al., 2017). However, previous accounts based on inconclusive macrofossils tentatively suggest a Miocene age (Tschanz et al., 1969). West of the Río Piedras Fault, Hernández et al. (2003) identify two lithostratigraphic units exposed along the limbs of the Fundación Anticline: (1) The Zambrano Formation, as described in areas west of the city of Fundación, consists of at least 500–800 m of interbedded sandstones (some of them bioclastic), marls, and mudstones, and accumulated in shallow marine and lagoonal environments in the late Miocene – early Pliocene, according to palynologic data (Hernández et al., 2003); (2) At least 500 m of dominantly coarse- and medium-grained sandstones, variegated mudstones, and thin pebble conglomerates of interpreted estuarine origin have been informally named the “Unidad Arenosa de Fundación”. Based on a faulted contact against the Macaraquilla Conglom-

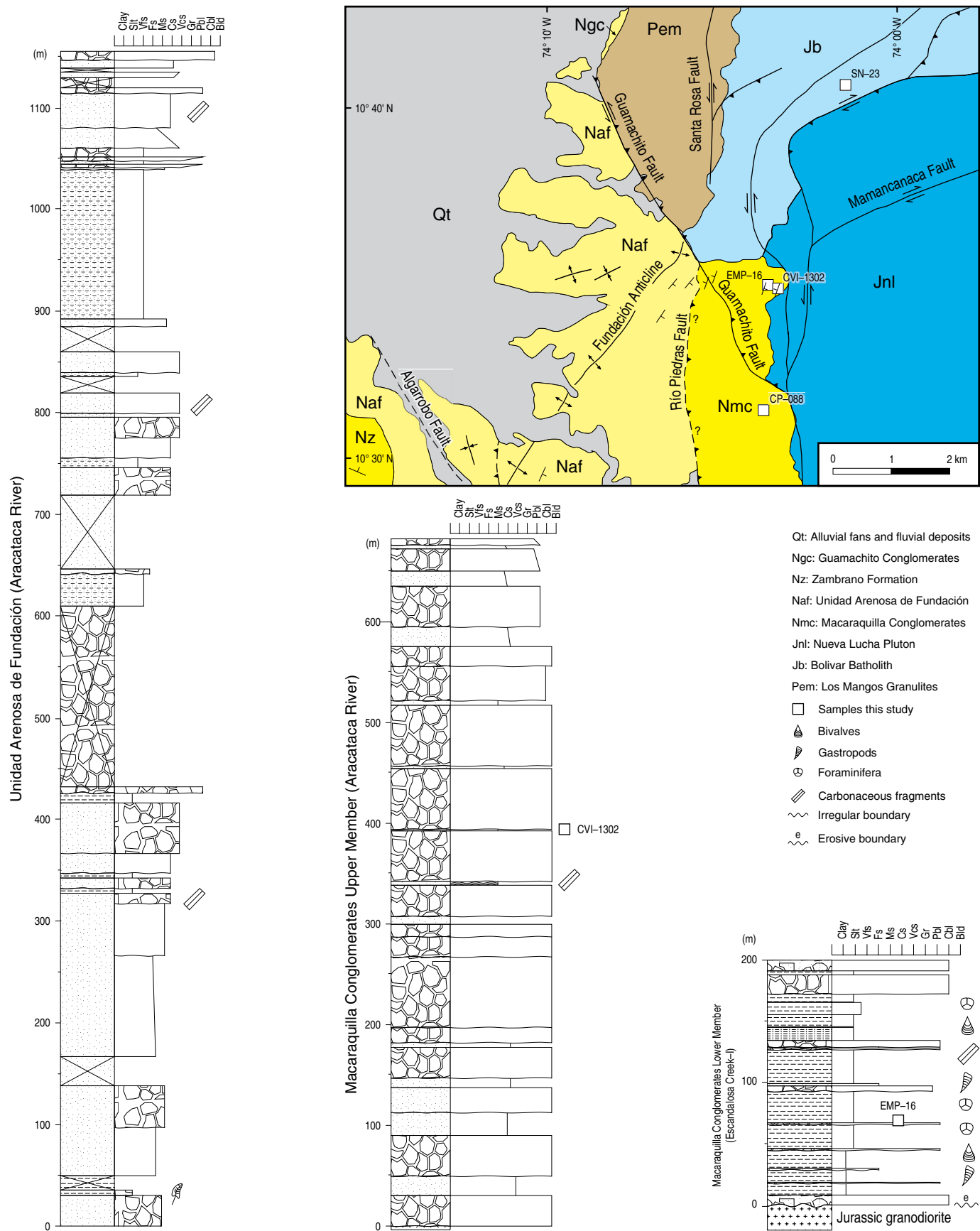




Figure 3. Geologic map (modified after Colmenares et al., 2007) and composite stratigraphic section of the Ariguaní Basin in the western margin of the SNSM.

erates and on the age of the Zambrano Formation, Hernández et al. (2003) assigned a Pliocene age. As shown below (section 5.1), and indicated in Figures 2 and 3, we reinterpret the stratigraphic succession based on our new lithostratigraphic and biostratigraphic observations and group the strata cropping out in the western sector of the Río Piedras Fault's footwall into the Unidad Arenosa de Fundación. The Guamachito Conglomerates constitute the uppermost unit preserved in the Aracataca Trough. It consists of coarse-grained clastic facies made up of matrix-supported polymictic pebble and cobble conglomerates with plutonic clasts up to 1 m in diameter, medium- to coarse-grained lithic micaceous sandstones, and mudstones containing plant remains, and its provenance was assigned by Tschanz et al. (1969), without further details, to the SNSM. The lower contact is erosive and unconformable with the Zambrano Formation, which has led Hernández et al. (2003) to assign a stratigraphic age of Pliocene – Pleistocene to the Guamachito Conglomerates.

3.2. Lower Guajira Basin

North of the SNSM, the Guajira Trough Basin is part of the southwestern extent of the Lower Guajira Basin (Figure 4) and is structurally limited by major basement uplifts brought to the surface along major faults configuring a flat topography where surface outcrops are limited. It hosts north-dipping siliciclastic sedimentary fill consisting of two main facies: (1) To the south of the Oca Fault, the so-called Palomino sequence (Piraquive et al., 2017) is a succession of cobble conglomerates, conglomeratic sandstones, and lithic sandstones with minor sandy variegated mudstones with uncertain thickness, ranging from measured 500 m (Piraquive et al., 2017) to inferred 2400 m (Tschanz et al., 1969). The unit nonconformably overlies Jurassic and Eocene granitoids or is in faulted contact against these granitoids or older Precambrian metamorphic units (Colmenares et al., 2007) and has been interpreted as a nearshore deposit, possibly estuarine. No age constraints have been provided for this unit, but a Miocene age has been inferred due to the stratigraphic position (Piraquive et al., 2017). (2) North of the Oca Fault, the Mongui Formation is a mudstone-dominated succession made up of variegated claystones, some of which are fossiliferous, and fine- to medium-grained sandstones, most likely several thousand meters thick (Tschanz et al., 1969). No age constraints are available onshore, but a stratigraphic correlation based on the projection to the south of biostratigraphically dated subsurface strata from seismic lines in Cadena & Slatt (2013) supports a Pliocene age.

4. Materials and Methods

Here, we present a tectonic evolution history of the SNSM based on published and new thermochronometric data, both bedrock and detrital, and new stratigraphic and provenance data from surrounding basins. Low-temperature thermochronometry is the study of the thermal history of rocks as they cool below ca. 250 °C, based on the study of isotopic systems that involve the accumulation of radiogenic decay products, either fission-tracks (e.g., Gallagher et al., 1998; Tagami & O'Sullivan, 2005) or helium nuclei (Farley, 2002; Harrison & Zeitler, 2005) due to spontaneous decay of U and Th isotopes. These radiogenic products are effectively accumulated in a mineral crystal lattice only at low temperatures. Above a threshold temperature, solid-state diffusion and track annealing occur faster than the rates of daughter production associated with radioactive decay, precluding their accumulation. Rather than at a specific temperature, the thermal loss of radiogenic daughter products occurs in a temperature range that has been called the partial retention zone (e.g., Reiners & Brandon, 2006). The concept of closure temperature is a mathematical approximation of a temperature within this range that usefully describes the thermal sensitivity of thermochronometric systems considering monotonic cooling only (Dodson, 1973). For the (U–Th)/He system in apatite (AHe), this closure temperature is ca. 70 °C for nondamaged crystals (Farley, 2002) but can be as high as ca. 120 °C for heavily radiation-damaged apatites (Flowers et al., 2009; Gautheron et al., 2009). For the apatite fission-track (AFT) system, this temperature varies between 100 and 140 °C, depending mainly on apatite composition and solubility (e.g., Donelick et al., 2005; Gallagher et al., 1998).

We present a new dataset consisting of (1) six bedrock AFT ages and (2) detrital data from AFT and AHe collected in sand bars of 3 modern rivers. Analytical details for these new analyses are presented in the Supplementary Information 1. We further present published fission-track and (U–Th)/He data in apatite and zircon (AFT, AHe, ZFT, and ZHe, respectively) from igneous and metamorphic rocks collected across the SNSM, most of them from an elevation profile in the range's northwestern corner, others from an elevation profile in the western slope, and few additional data from the northern and eastern slopes. In addition, we include a new analysis of existing detrital data collected in Miocene strata in the northern and western margins (Piraquive et al., 2017).

Based on these combined data, which constitute all available low thermochronometric data from the SNSM, we first extract

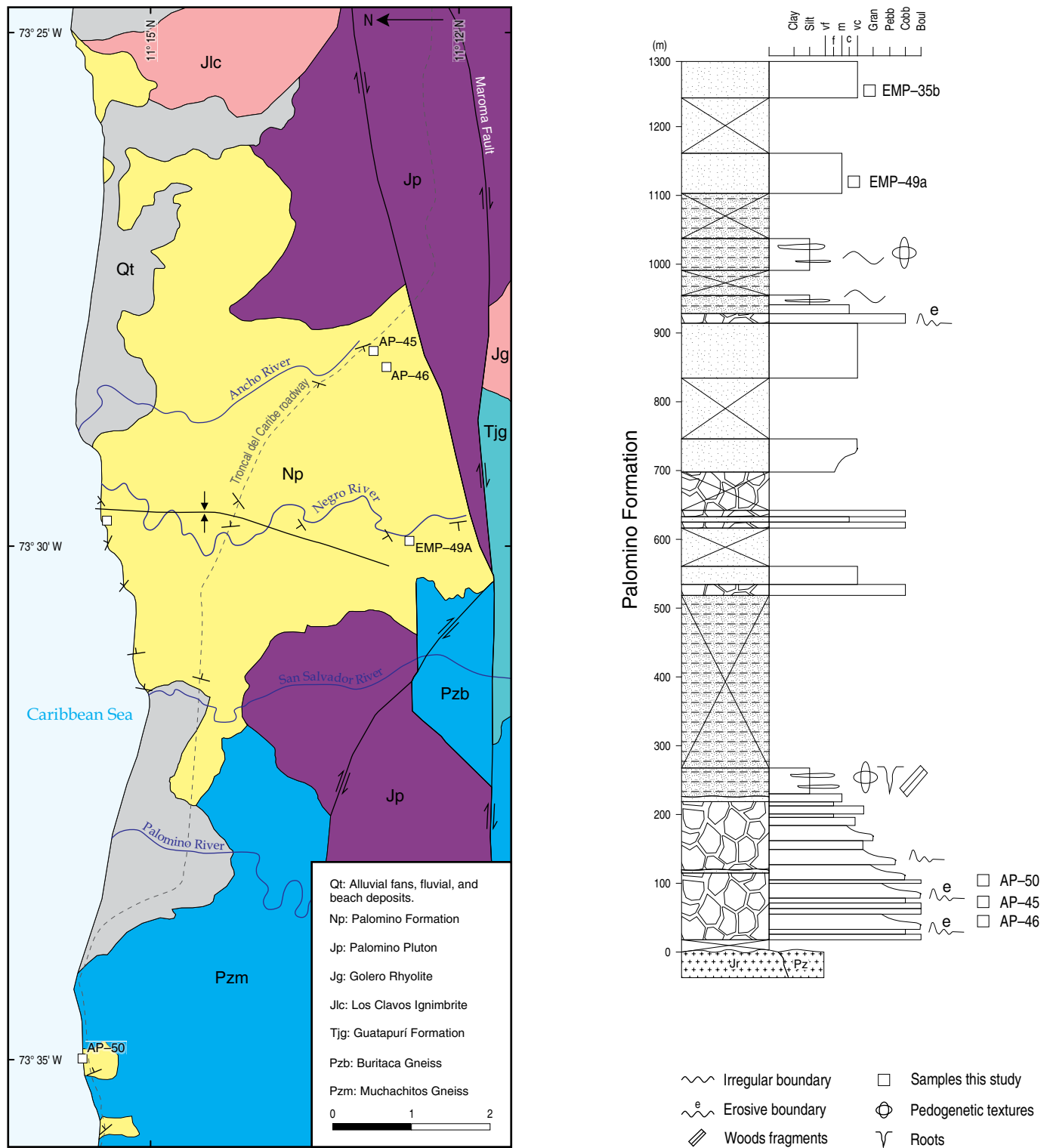


Figure 4. Geologic map (modified after Colmenares et al., 2007) and composite stratigraphic section of the Lower Guajira Basin in the northern margin of the SNSM.

long-term exhumation rates based on a simplified 1D approach that consists of using the youngest cooling age peaks for each particular thermochronometric system as the approximate age for the passage of rocks across the isotherms of 70 °C, 120 °C, and 250 °C, corresponding to average closure temperatures for

the AHe, AFT, and ZFT systems, respectively, and calculate the associated magnitude of exhumation using geothermal gradients of 20–25 °C/km, an acceptable range for retroarc foreland basins (e.g., Allen & Allen, 2005), and a surface temperature of 20 °C. Exhumation rates are thus calculated by dividing the

magnitude of exhumation by the time span between intervening isotherms. We further explore plausible thermotectonic histories that are consistent with bedrock and detrital data through 3D thermokinematic modeling of these combined data using the software Pecube (Braun, 2003; Braun et al., 2012) in order to extract long-term exhumation rates.

Finally, we present new structural and stratigraphic cross-cutting relationships, new biostratigraphic data based on palynomorphs (see Supplementary Information 1), and summarize recent stratigraphic observations that reveal hints about the ages and mechanisms of concurrent basement exhumation and basin formation.

5. Results

5.1. Stratigraphy

Our stratigraphic surveying in the eastern limb of the Fundación Anticline reveals that the Macaraquilla Conglomerates disconformably overlies granitoids with paleo-regolith fabrics (Figure 5a, 5b) of an assigned Jurassic age (Colmenares et al., 2007). The basal sequence exhibits contrasting lithofacies across a NW-dipping fault: to the SE, in the footwall block, the basal facies consists of a ca. 1 m-thick layer of lithic arkosic sandstones overlain by massive grayish sandy mudstones, whereas to the west, they consist of matrix-supported conglomerates containing cobbles and boulders of the Jurassic substratum (Figure 5b). These field relationships document that sediment accumulation occurred concomitant with normal faulting. In a stratigraphic section measured in the footwall block, the Macaraquilla Conglomerates comprises two members. The Lower Member consists of ca. 220 m of fossiliferous siltstones and interlayered marls, limestones, scarce lithic arkosic sandstones, and oligomictic and polymictic conglomerates. Marls and fossiliferous siltstones contain abundant bivalves, gastropods, and wood fragments (Figure 5c). The Upper Member of the Macaraquilla Conglomerates is constituted by a monotonous succession of ca. 900 m-thick, polymictic conglomeratic beds with a few interlayers of coarse-grained, lithic arkosic sandstones (Figure 5c). Heterolithic facies of siltstones and bioturbated sandstones with carbonaceous sheets occur sporadically. Sandstones include heavy minerals such as garnet, clinopyroxene, and hornblende. Southwesterly paleocurrents based on imbricated clast measurements and other provenance data based on sandstone and conglomerate petrography unequivocally document provenance from the SNSM (Echeverri et al., 2017; Piraquive et al., 2017).

We report here the occurrence of spores of *Nijssenosporites fossulatus* (Figure 5c) in samples SNT-93A and SNT-88 from the Lower and Upper Members, respectively, and of pollen *Zonocostites ramonae*, which allow assigning a maximum age of early Miocene, based on the zonation of Jaramillo et al. (2011).

Our observations and published data (Piraquive et al., 2017) suggest that this stratigraphic succession records sediment progradation through a change in sedimentary environments from marine–transitional to deltaic and alluvial environments (Echeverri et al., 2017; Piraquive et al., 2017).

Toward the western segment of the Aracataca River, in the eastern limb of the Fundación Anticline, the Upper Member of the Macaraquilla Conglomerates exhibits an interdigitated to transitional contact with the distal Unidad Arenosa de Fundación (sensu Hernández et al., 2003). The upper limit is defined by either the actual erosive surface or by unconformably overlying Quaternary alluvial fans and slope deposits in the Aracataca River area (Figure 3). The Unidad Arenosa de Fundación thus represents a sandstone-dominated unit laterally equivalent to the Upper Member of the Macaraquilla Conglomerates. This unit has a stratigraphic thickness of ca. 1450 m and consists of medium- to very coarse-grained lithic arkosic sandstones alternating with sporadic intercalations of siltstones and conglomerates. Sandstones display thick and very thick layers with tabular, wavy, and lenticular geometry and massive, gradational, or laminated internal structures. Conglomerates appear as medium and thick layers, sporadically very thick, with lenticular and tabular geometry and massive internal structure, in some segments with imbricated clasts. Carbonized woody remnants and dicotyledonous cuticles are frequent in this unit. This interval records southwesterly paleocurrents and indicates provenance from the SNSM (Echeverri et al., 2017), registering a progradation of sedimentary environments from the platform–prodelta to fluvial and deltaic sedimentation (Echeverri et al., 2017; Hernández et al., 2003; Tschanz et al., 1969).

5.2. Bedrock Thermochronometry

Published bedrock thermochronometry from the SNSM (Figure 6) includes a total of 27 apatite fission-track (AFT) data, mainly collected along two elevation profiles, one in the Sierra Nevada province at the range's western margin (Figure 6b; Fundación profile, 10 samples; Villagómez et al., 2011) and one in the northwestern corner of the Santa Marta province (Figure 6c, 6d; Kennedy profile, 11 samples). AFT ages (2-sigma error) range from 23.3 ± 4.4 Ma to 53.8 ± 8.2 Ma in the Fundación profile and from 16.0 ± 2.5 Ma to 41.0 ± 9.6 Ma in the Kennedy profile, in both cases with relatively good age–elevation correlations. An additional few AFT ages come from a Jurassic granitoid in between the two profiles (26.7 ± 3.6 Ma), from granitoids at the range's northern margin (2 samples, 22.3 ± 3.1 Ma and 27.6 ± 4.6 Ma, from Paleocene and undetermined age, respectively), and from Jurassic granitoids and felsic volcanic rocks at its northeastern margin (3 samples, 40.4 ± 5.7 Ma to 59.6 ± 10.4 Ma) (Figure 6a). In addition, 15 apatite and 14 zircon (U–Th)/He (AHe and ZHe, respectively) single grain ages were obtained from 8 samples along the Kennedy profile, with

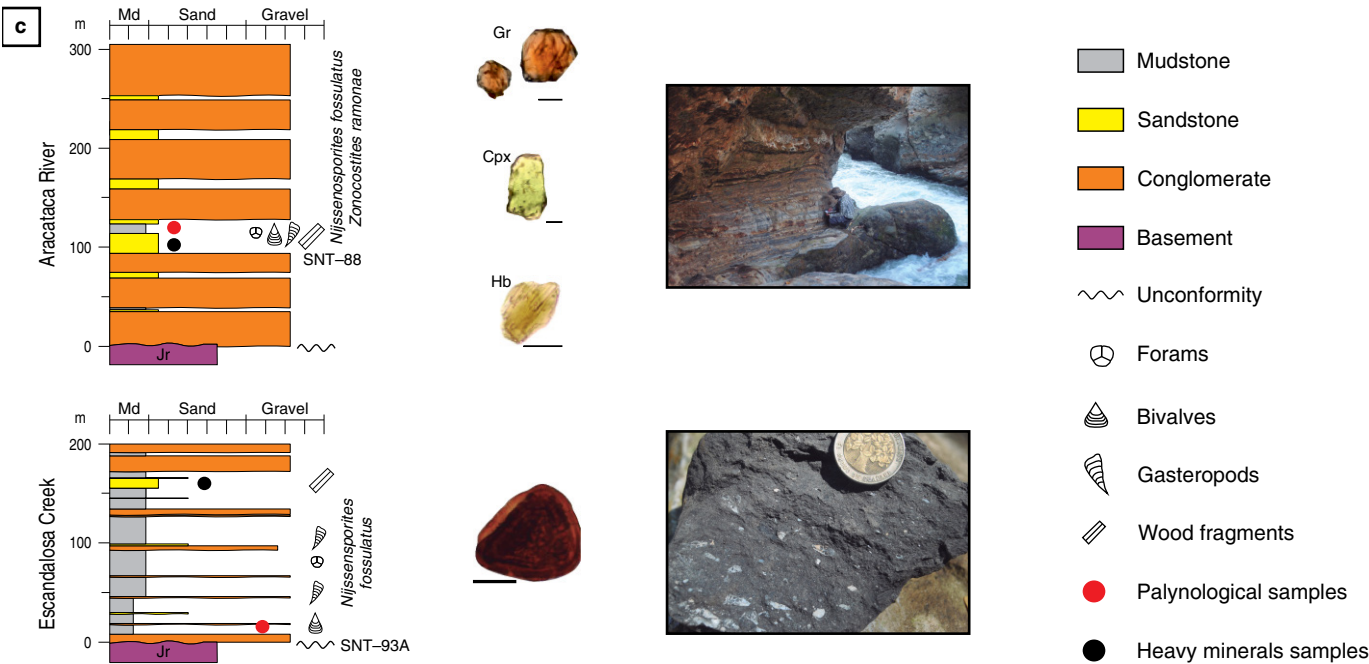
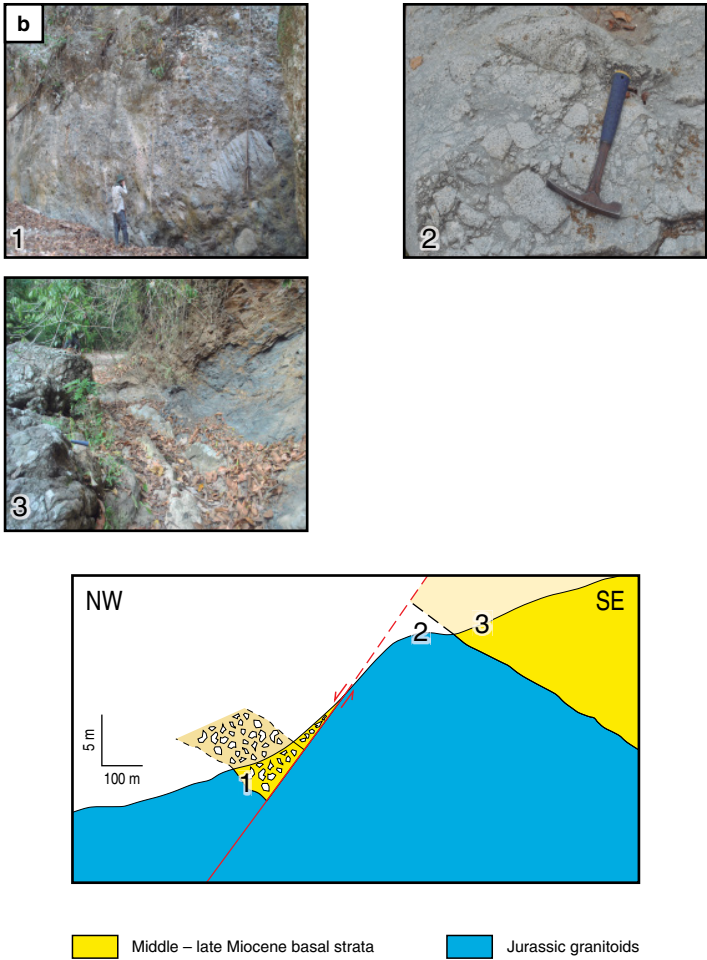
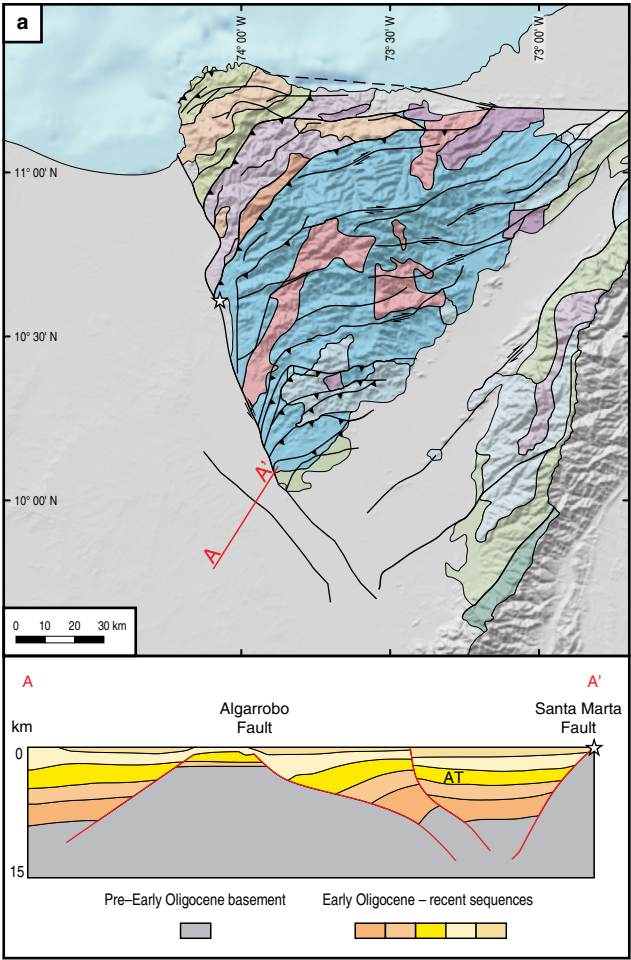




Figure 5. Stratigraphic relationships associated with Miocene synextensional sediment accumulation in the Ariguaní Trough. **(a)** Simplified map of the SNSM and localization of the seismic section A–A' in the northeastern LMB, showing the Ariguaní Trough (AT) and other depocenters associated with post-Oligocene extension (redrawn after Mora et al., 2018). **(b)** Sketch of geologic section along Escandalosa Creek (location marked by white stars on map and its projection on section A–A') showing a normal fault separating two domains with contrasting basal Cenozoic facies overlying Jurassic granitoids with paleo-regolith fabrics (Picture 2); to the west, in the hanging wall block, boulder conglomerates composed of the underlying substrata (Picture 1) contrast with sandstones and mudstones (Picture 3) in the footwall block to the SE. **(c)** Summarized stratigraphic sections from the Escandalosa Creek and the Aracataca River (see location in Figure 3), showing the characteristic palynomorphs and heavy minerals, identified with mollusk-rich marls (lower picture) and cobble conglomerates (upper picture). (Hb) hornblende; (Cpx) clinopyroxene; (Gr) garnet.

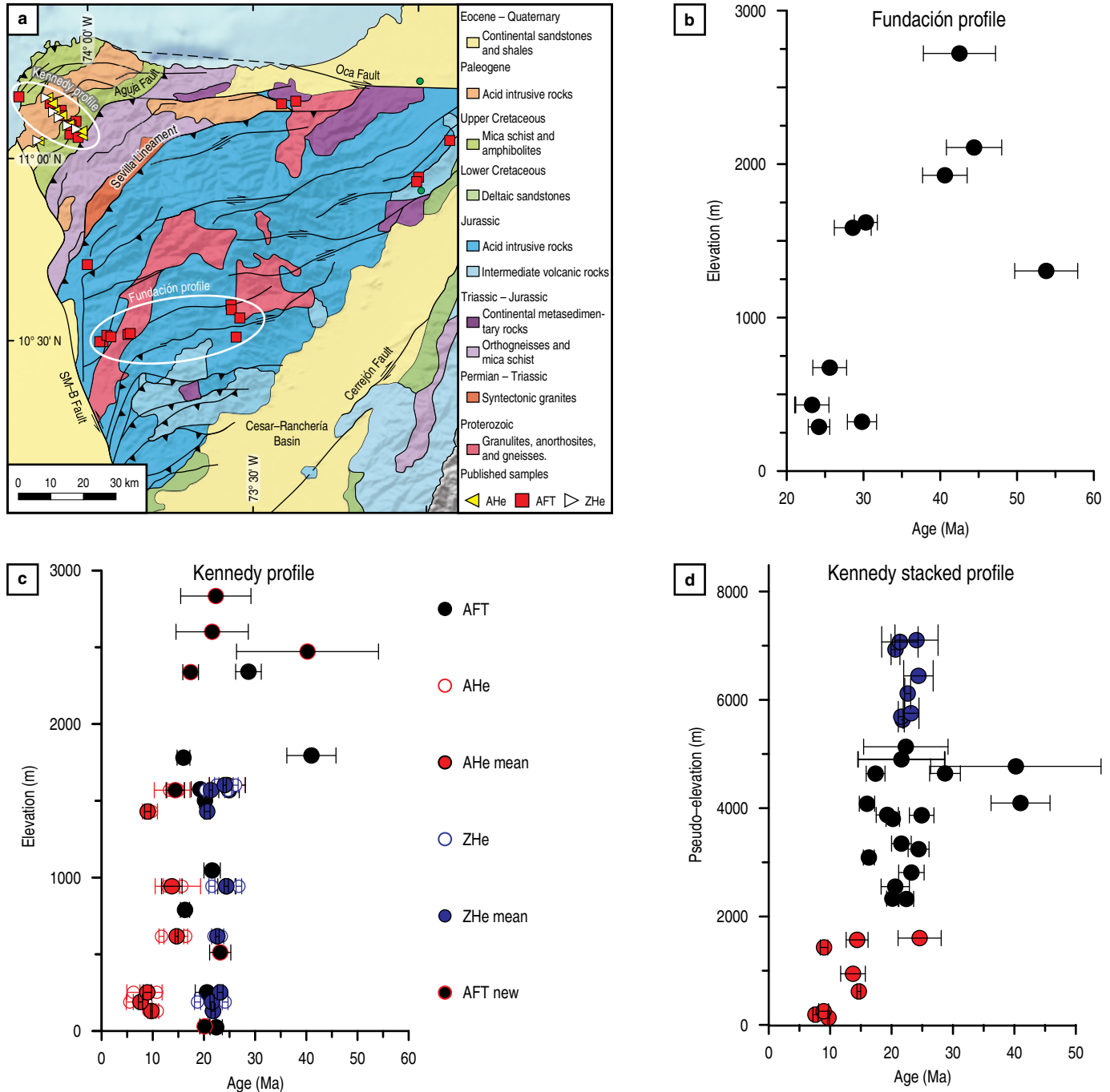


Figure 6. Bedrock thermochronometry. **(a)** Geologic map showing the locations of published thermochronometric samples (Cardona et al., 2011a; Villagómez et al., 2011). **(b), (c)** Age–elevation relationships along the Fundación and Kennedy profiles. **(d)** Age vs. pseudoelevation (stacked profile) in the Kennedy profile.

good within-sample reproducibility and a fair to good age–elevation relationship (Figure 6d; Cardona *et al.*, 2011a). The weighted averaged AHe ages range from 7.6 ± 0.8 Ma to 24.5 ± 7.0 Ma and ZHe ages from 20.6 ± 0.6 Ma to 24.3 ± 0.5 Ma.

Here, we present new AFT results from 6 additional granitoid, amphibole gneiss, and mica schist samples from the uppermost and lowermost reaches along the Kennedy profile (Figure 6c), as well as from 2 samples of granitoids collected at lower elevations. Despite the few grains available for dating in the two samples at highest elevations (three to six grains, samples SNT-14 and SNT-16), ages over an elevation difference of ca. 250 m are indistinguishable within uncertainty (2σ up to 60%), varying between ca. 21 and 23 Ma (Figure 6d; Table 1). Sample SNT-18 yields an older age with a large uncertainty (40.2 Ma), which we ascribe to very low U contents in the apatites. The two lowermost samples yield less uncertain ages between 20.1 ± 1.9 Ma and 23.2 ± 4.1 Ma, which fit with the trend of data from similar elevations analyzed by Villagómez *et al.* (2011) (Figure 6c).

Collectively, all published and new ages reveal a pattern of younging ages in a northwestward direction, suggesting gradually increasing exhumation rates toward the northwest. In addition, the patterns of ages versus elevation and pseudoelevation (stacked profiles and closure depths estimated as in Reiners & Brandon, 2006) for both elevation profiles document an episode of rapid exhumation between ca. 35 and 15 Ma (Figure 6d). Extracting exhumation rates with this 1D approach is an oversimplification, as it involves assumptions that are violated in nature, such as that isotherms are horizontal and time invariant. However, using 2σ error-weighted linear regressions, we calculate a rate of 0.25 ± 0.09 km/my (between ca. 30 and 15 Ma) for the Kennedy stacked profile and of 0.13 ± 0.08 km/my for the Fundación profile (from 30–20 Ma), which represent minimum values for actual rates (for further explanation, see Braun, 2002).

5.3. Detrital Thermochronometry

Published detrital AFT and ZFT data are available for Cenozoic strata from the northern (Lower Guajira) and western (Ariguaní) margins of the range (Piraquive *et al.*, 2017), assigned to the middle Miocene – Pliocene and early – middle Miocene, respectively, based on regional stratigraphic correlations and the new biostratigraphic data presented here. In the north, AFT data collected in one sample from middle Miocene – Pliocene rocks reveal two AFT age populations of ca. 27 Ma and ca. 53 Ma (Figure 7; see Table 1 of the Supplementary Information 2), implying lag times (i.e., the difference between the thermochronometric age and the stratigraphic age [10 ± 5 Ma, in this case], which represents the time of exhumation from the closure depth; Ruiz *et al.*, 2004) of ca. 11–22 Ma and 38–48 Ma. ZFT detrital ages in 5 samples from the same strata collected along

two stratigraphic sections yield age populations of 33–41 Ma, ca. 55 Ma, 74–90 Ma, 108–132 Ma, 156–170 Ma, and 254 Ma (Figure 8; see Table 1 of the Supplementary Information 2). From these data, we interpret that only the two youngest populations may reflect reset ages related to the Cenozoic Andean cycle of exhumation. Despite the large uncertainties derived from both poorly constrained stratigraphic ages and large errors in cooling age populations, the youngest AFT and ZFT detrital populations help furnish rough estimates of long-term denudation rates. For the following calculations (Table 2), we use mean closure temperatures of 120 °C and 250 °C for the AFT and ZFT systems, respectively, geothermal gradients of 20–25 °C/km, and a time-invariant surface temperature of 20 °C, chosen to represent an average temperature above sea level. The AFT lag-time of ca. 12–22 Ma reveals a maximum Miocene exhumation rate of ca. 0.2–0.4 km/my (4–5 km of exhumation between 27 and 15–5 Ma), preceded by slightly faster rates of 0.4–1.1 km/my (Figure 9; Table 2; 65–6.5 km of exhumation between 41–33 and 27 Ma). In the western margin (Aracataca), a similar analysis derived from strata that we document here as early – middle Miocene in age (see section 5.1) is based on 2 AFT samples with age peaks of 19–22 Ma, 30 Ma, and 42–60 Ma and 3 ZFT samples with age peaks of 29 Ma, 48–52 Ma, 74 Ma, 104–108 Ma, and 167 Ma (Table 2; see Table 1 of the Supplementary Information 2). The youngest cooling ages imply a shorter AFT lag time of 3–11 Ma, corresponding to a fast early – middle Miocene exhumation rate (up to 0.4–1.8 km/my) from ca. 22 to 19–11 Ma, preceded by rates of up to 0.2–0.7 km/my for the underlying 5–6.5 km of crust during the Oligocene – early Miocene (47–29 to 22 Ma; Figure 9).

We present new AFT and AHe data from modern sands collected in longitudinal bars from three rivers draining the northern (Cañas River), southwestern (Fundación River), and southeastern (Guatapurí River) slopes of the SNSM (Figure 10a; see Table 3 for summary results, and Tables 2–6 of the Supplementary Information 2 for single-grain ages and track-length data). For each individual sample, we conducted analyses on 89–101 individual grains for AFT and 23–30 aliquots for AHe. We present the results as box plots (Figure 10b) and kernel density plots (Figure 10c) with calculated age populations for each sample and thermochronometric system using the automatic unmixing model available in DensityPlotter (Vermeesch, 2012).

AFT data from the three catchments show similar age spectra, dominantly with ages younger than 50 Ma and a few older ages (Figure 10b; Table 3). The age distributions are narrow for the northern and western catchments and slightly broader in the easternmost catchment (Figure 10c). The age spectra display one (Guatapurí) or two (Cañas, Fundación) populations in the fraction younger than 50 Ma, which we interpret as exhumation ages associated with Cenozoic orogenesis, and an additional population of older grains (ca. 69 Ma, ca. 63 Ma, and 85 Ma,

Table 1. New bedrock apatite fission-track data.

Sample	Latitude N	Longitude W	Elevation (m)	Lithology	#Gr ^a	U (ppm)	Rho-S (NS) ^b	Rho-I (NI) ^b	Rho-D (ND) ^c	P(c2) (%) ^d	Age (Ma) ^e	±2 σ error	Dpar (mm)	±1 s
SNT-14	11.112	74.035	2834	Amphibolite	3	9.2	1.024 (11)	28.58 (307)	35.80 (5899)	71%	22.3	13.7	1.68	0.23
SNT-16-1	11.108	74.048	2601	Schist	6	9.0	0.969 (11)	5.815 (66)	7.448 (2670)	64%	21.6	14.1	1.62	0.20
SNT-18	11.104	74.061	2472	Gneiss	6	3.0	0.612 (9)	9.454 (139)	35.76 (5899)	49%	40.2	27.7	1.45	0.21
SNT-19-2	11.107	74.061	2338	Gneiss	28	17.5	1.521 (163)	10.66 (1143)	7.011 (2670)	32%	17.4	3.1	2.11	0.46
SNT-27	11.152	74.126	512	Granodiorite	30	6.7	0.767 (162)	4.586 (965)	7.934 (2798)	30%	23.2	4.1	2.22	2.07
SNT-30	11.226	74.161	30	Granodiorite	28	47.0	4.727 (844)	31.83 (5684)	7.791 (2798)	9%	20.1	1.9	2.73	0.37

^a Number of grains analyzed.^b Rho-S and Rho-I are the spontaneous and induced tracks density measured, respectively ($\times 105$ tracks/cm²). NS and NI are the number of spontaneous and induced tracks counted for estimating Rho-S and Rho-S, respectively.^c Rho-D is the induced track density measured in the external mica detector attached to CN2 dosimetry glass ($\times 105$ tracks/cm²). ND is the number of induced tracks counted in the mica for estimating Rho-D.^d P(χ^2) (%) is the chi-square probability (Galbraith, 1981; Green, 1981). Values greater than 5% are considered to pass this test and represent a single population of ages.^e Pooled (central) age reported for ages that pass (fail) the χ^2 test.

respectively) that we assume represent ancient exhumation events but partially reset. Among the exhumation ages (i.e., those younger than 50 Ma), the youngest age peak occurs in the western catchment (Fundación River, 16.5 ± 1.2 Ma), whereas the oldest appears in the northern region (Cañas River, 22.5 ± 1.6 Ma). AHe ages exhibit a similar pattern, with catchments in the north and west that display only ages younger than ca. 30 Ma, the western catchment (Fundación) with the youngest ages and an eastern catchment including few outliers of unreset ages as old as ca. 85 Ma. A comparison of eU vs. age (i.e., Flowers et al., 2009) reveals no correlation and thus no evidence of radiation damage controlling the age pattern (Figure 10d). Remarkably, AHe and AFT age signatures, as revealed by box plots and the central tendency (Figure 10b; i.e., second quartile or median of the data set of obtained ages) are very similar to the east (Guatapurí River, 27 and 21 Ma, respectively), whereas they are up to ca. 14 my apart for the northern (Cañas, 27 and 18 Ma, respectively) and western (Fundación, 31 and 17 Ma, respectively) catchments. Using closure temperatures of 70 °C and 120 °C for the AHe and AFT systems, respectively, and geothermal gradients of 20–25 °C/km, the youngest AFT age populations render similar long-term exhumation rates since the early Miocene of 0.2–0.3 km/my for the northern, western, and eastern catchments (Figure 9). Unlike AFT-derived rates, AHe data document long-term asymmetric removal of the up-

permost 2–2.5 km of crust, which has been faster (0.3–0.4 km/my) in the north and west during the last ca. 7 my and much slower (0.10–0.15 km/my) in the eastern margin but integrated since ca. 18 Ma (Figure 9).

Together, detrital thermochronometric data from Miocene strata reveal higher exhumation rates for the northern (Palomino) than for the western (Aracataca) catchments in the Oligocene (and earliest Miocene for the western margin), followed by an opposite pattern of acceleration in exhumation in the west in the early – middle Miocene and a middle – late Miocene deceleration in the north. The comparison of Miocene and modern AFT lag times (Figure 7) shows a subtle increase to values of 15 ± 5 Ma to ca. 20 Ma in the northern face and a marked increase of 4–10 Ma to ca. 17 Ma in the western margin. These data illustrate that following the period of Miocene asymmetric exhumation, rates have decreased ever since across the entire range, yet exhumation continues to be fastest in the western slope, fast in the north, and slower in the eastern margin (Figure 9).

5.4. Thermokinematic Modeling

To obtain a more regionally unified account of exhumation rates across the entire range, we forward modeled 3D topographic and kinematic histories that account for the observed

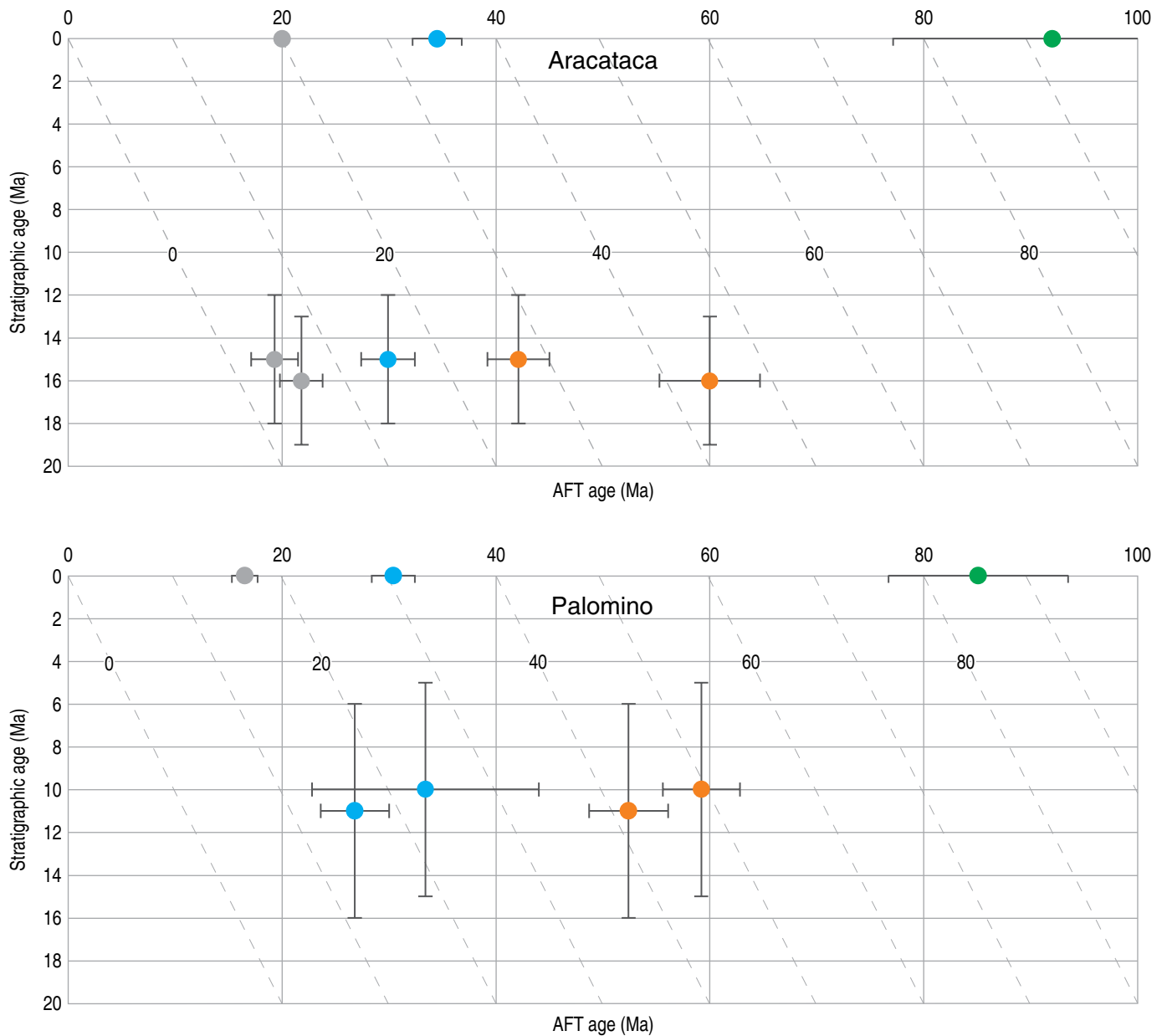


Figure 7. Stratigraphic vs. cooling age plots (lag time plots) for Cenozoic strata in the Aracataca (Ariguaní Trough) and Palomino (Lower Guajira Basin) sections. The inclined lines represent isolines of lag time (i.e., approximate time elapsed between thermochronometric system closure and surface exposure). The figure shows lag time plots for AFT data, representing the approximate time for denudation of the uppermost 4–5 km of rock (between the 120 and 20 °C isotherms). Colored dots represent different populations of detrital ages.

bedrock and detrital thermochronometric data, as well as the structural geometry and asymmetric exhumation, using the software Pecube (Braun, 2003; Braun et al., 2012). Pecube is a numerical model that solves the heat-transfer equation in three dimensions in a crustal block with topographic and fault kinematic evolutions prescribed independently, but in which heat advection is considered to occur only vertically. With such assumptions, this type of thermokinematic

Figure 8. Stratigraphic vs. cooling age plots (lag time plots) for Cenozoic strata in the Aracataca (Ariguaní Trough) and Palomino (Lower Guajira Basin) sections. The inclined lines represent isolines of lag time (i.e., approximate time elapsed between thermochronometric system closure and surface exposure). The figure shows lag time plots for ZFT data, representing the approximate time for erosion of the uppermost 9–11.5 km of rock (between the 250 and 20 °C isotherms). Colored dots represent different populations of detrital ages.

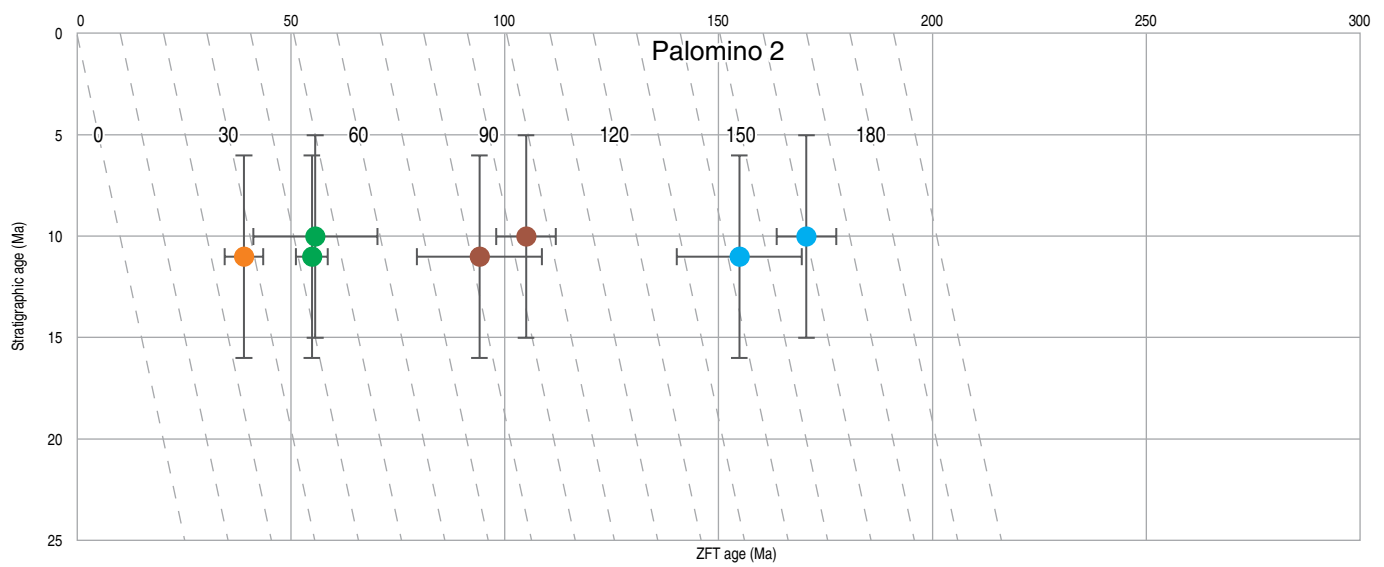
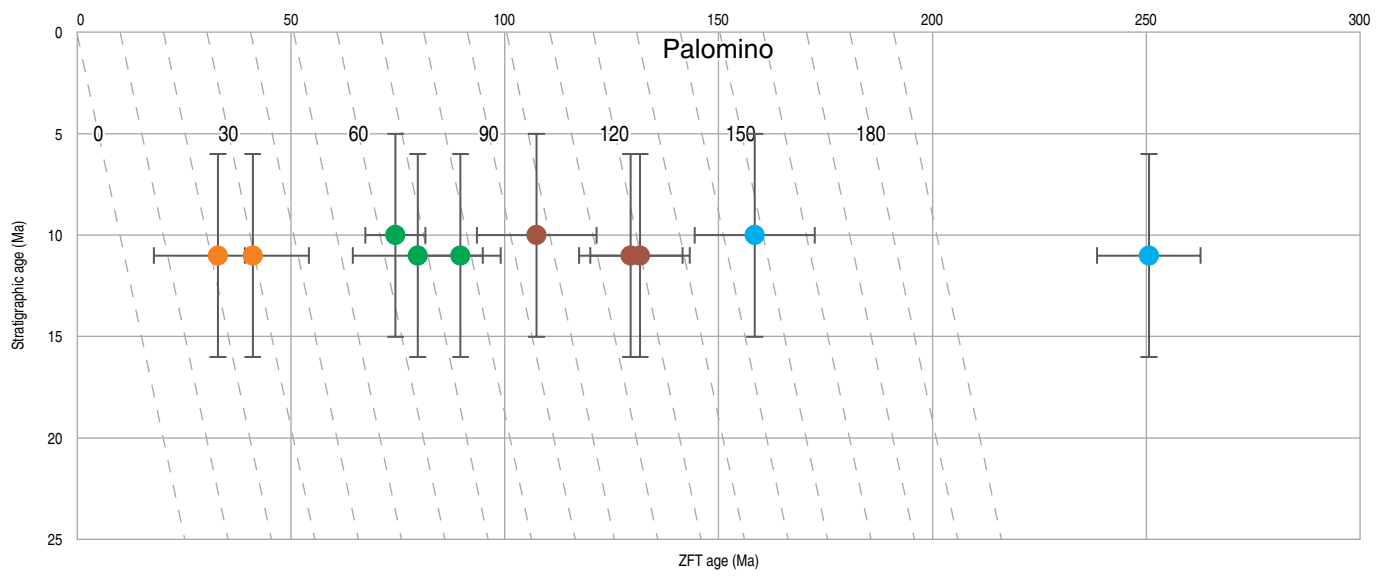
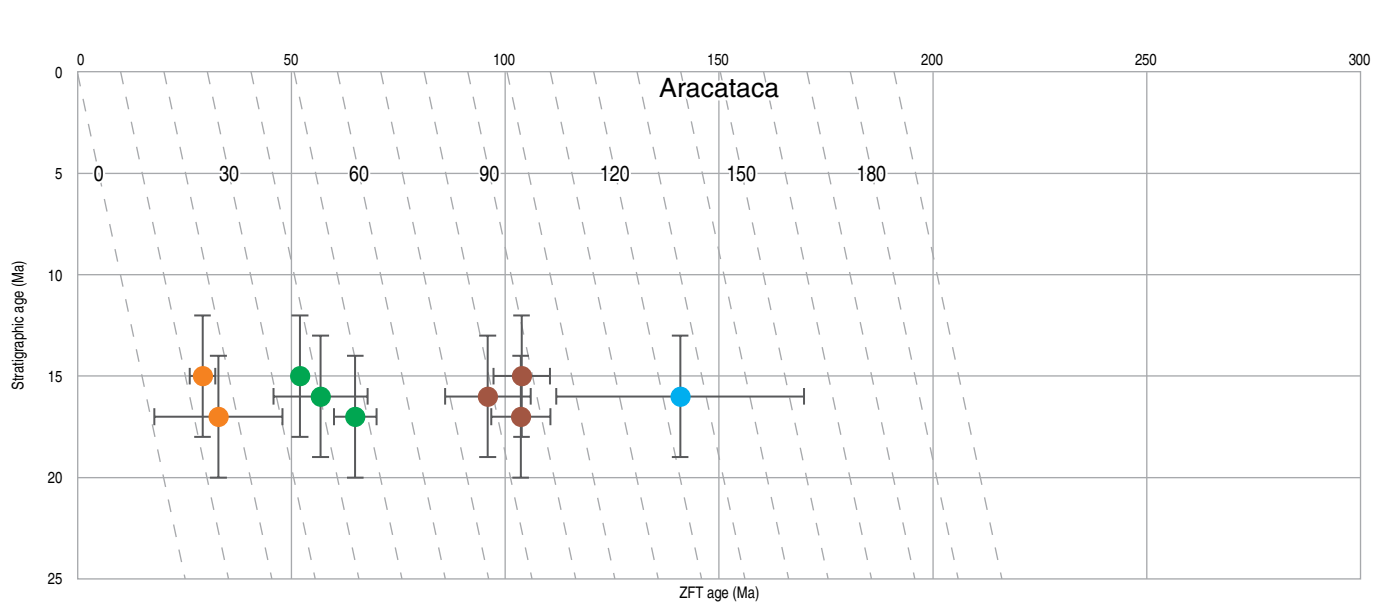


Table 2. Youngest detrital AFT and ZFT age populations in Cenozoic strata in the Palomino and Aracataca sections (data from Piraquive et al., 2017) and calculated exhumation rates.

1. AFT peaks and exhumation rates from the 120 °C isotherm to the surface (20 °C).									
Section	Sample	Youngest AFT peak (Ma)	Stratigraphic age (Ma) ^a	Lag-time (my)		Exhumation rates (km/my)			
						20 °C/km		25 °C/km	
				min	max	min	max	min	max
Aracataca (W)	CVI-1302	19.3	15 ± 4	0.3	8.3	16.7	0.6	13.3	0.5
	EMP-16	21.8	15 ± 4	2.8	10.8	1.8	0.5	1.4	0.4
Palomino (N)	AP-045	26.8	10 ± 5	11.8	21.8	0.4	0.2	0.3	0.2

2. ZFT peaks and exhumation rates between the 250 °C and 120 °C isotherms.									
Section	Sample	Youngest ZFT peak (Ma)	Youngest AFT peak (Ma)	Lag-time AFT–ZFT (my)	Exhumation rates (km/my)				
					20 °C/km		25 °C/km		
Aracataca (W)	CVI-1302	29.2	19.3	9.9	0.7		0.5		
	CP-088	47.4	19.3	28.1	0.2		0.2		
Palomino (N)	AP-046	32.9	26.8	6.1	1.1		0.9		
	AP-045	41	26.8	14.2	0.5		0.4		

^a Stratigraphic ages for Aracataca based in our new biostratigraphic data and for Palomino based on stratigraphic position (see discussion in text).

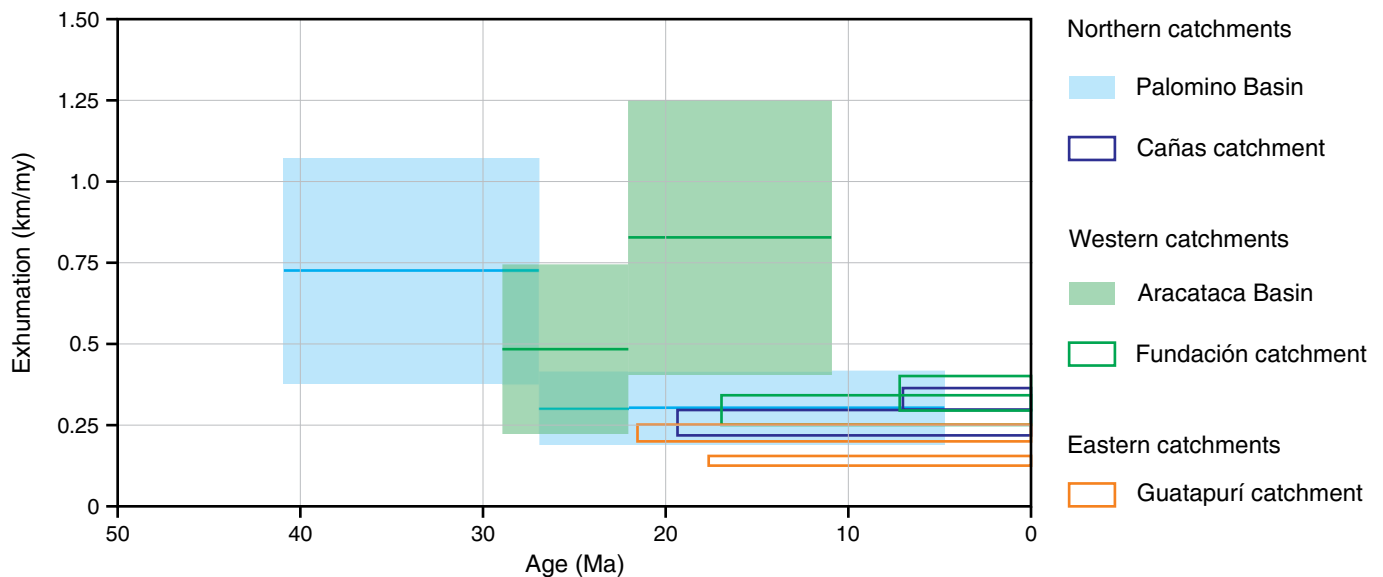


Figure 9. Evolution of Cenozoic exhumation rates estimated with one-dimensional calculations using detrital thermochronometric data from Cenozoic strata and modern sediments. The magnitude of exhumation was estimated using a surface temperature of 20 °C and average closure temperatures of 70 °C, 120 °C, and 250 °C for the AHe, AFT, and ZFT systems, respectively, and a range of geothermal gradients from 20–25 °C/km. The timespan corresponding to the transit of rocks between adjacent isotherms was calculated by subtracting the ages of the corresponding thermochronometric youngest peaks. See the text for further explanation.

modeling is capable of translating a forward modeled kinematic history into a thermal history and, finally, into modeled thermochronometric ages using available kinetic models (i.e., fission-track annealing or He/Ar diffusion in minerals), thereby enabling the comparison of thermochronometric modeled ages

with measured ages and hence allowing the validation of plausible topographic and kinematic scenarios.

In our approach, rather than intending to reliably resolve the kinematics of faulting in the SNSM, we aim at revealing plausible Cenozoic exhumation rates across the range. To ac-

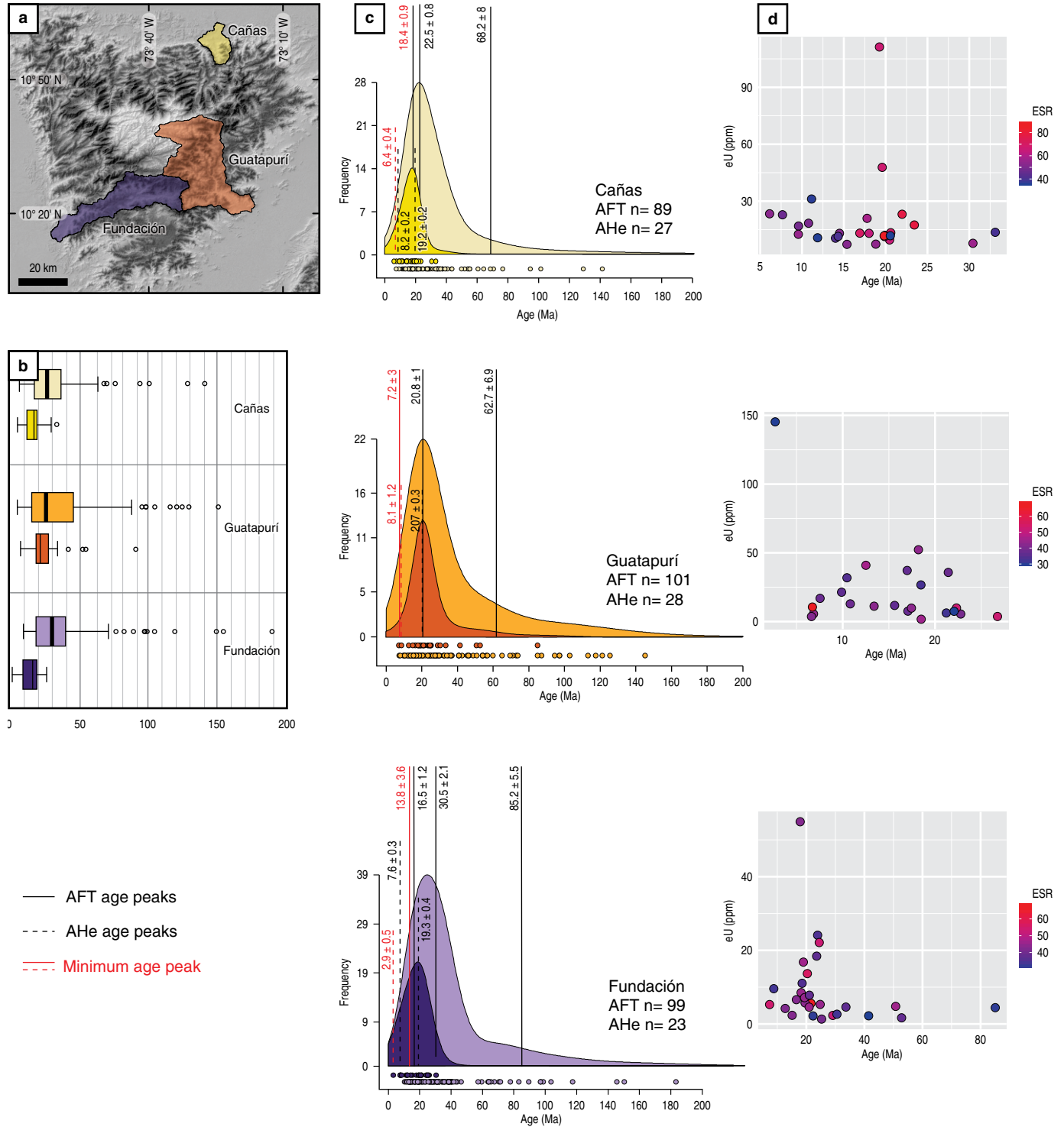


Figure 10. Detrital thermochronometry in selected catchments from the northern (Cañas), western (Fundación), and eastern (Guatapuri) slopes of the SNSM. **(a)** Locations of river catchments. **(b)** Box plots and central tendencies (thick dark lines) for AFT (pale colors) and AHe (dark colors) ages. **(c)** Kernel density plots for AFT (pale colors) and AHe (dark colors). Dots represent individual ages. Thick (dashed) lines and numbers in the upper (lower) part of each plot represent AFT (AHe) age peaks. Red lines and numbers represent the youngest peaks used to calculate integrated maximum exhumation rates. **(d)** Age vs. effective uranium content (eU = $U + 0.235Th$). Each dot represents an individual aliquot and is color-coded based on the aliquot's grain size, reported as the equivalent-sphere radius (ESR).

Table 3. Summary of detrital apatite fission-track and (U–Th)/He data from modern sand samples.

Sample	Latitude N	Longitude W	Elevation (m)	AFT												AHe					
				#Gr ^a	P1 ^b			P2			P3			#Gr ^a	P1			P2			
					Age	2σ	%	Age	2σ	%	Age	2σ	%		Age	2σ	%	Age	2σ	%	
Cañas	11.211	73.402	29	90	22.5	1.6	81.6	68.2	16.0	18.4				28	8.2	0.2	26.2	19.2	0.3	73.8	
Guatapurí	10.506	73.283	237	101	20.8	2.0	73.6	62.7	13.8	26.4				30	20.7	0.3	100.0				
Fundación	10.427	74.031	128	99	16.5	2.4	30.3	30.5	4.2	52.7	85.2	11	17.0	23	7.6	0.3	43.0	19.3	0.8	57.0	

^a Number of grains analyzed.^b P1 to P3 are age populations extracted using the automatic unmixing model implemented in DensityPlotter (Vermeesch, 2012).

count for the observed southeastward monoclinical tilting and the northwestward younging in thermochronometric ages, we chose two kinematic scenarios that simulate a gradient in vertical exhumation rates (Figure 11): (1) a series of NE–striking vertical faults with eastward decreasing velocities and (2) one or multiple southeastward–dipping reverse faults with either ramp–flat or listric geometries and velocities decreasing eastward. For each group of simulations, we departed from a base model with a series of fixed thermal and elastic parameters, as described in Table 4, and systematically modified the geometric, topographic, and kinematic parameters. We ran more than 300 forward Pecube models and for each of them evaluated the misfit between modeled and observed ages, the latter including bedrock AFT and AHe data and detrital data from river sand samples, through the log–likelihood function (LLH). This function describes the plausibility of the model parameters given specific observed data, and its calculation attempts to find an estimate of parameters that maximizes its value (see Supplementary Information 1 for a more detailed description). In short, the LLH calculation yields negative values, so the highest value is the one closest to zero.

5.4.1. Models of Group 1: Southeast–dipping Faults

A first set of models was designed to test the effect of different fault geometries on the vertical exhumation rates. We prescribed a model with one main fault located at the western end of the range, striking parallel to the Aguja and Sevilla Faults, ca. N45°E, and two geometries, listric and a ramp geometry (Figure 11a), and ran simulations using similar topographic evolutions but with different fault velocities since 65 Ma. The better models (i.e., those with higher LLH values, closer to 0) show that the fault slip rates that more suitably reproduce both the AFT and AHe thermochronometric data are 0.20–0.35 km/my (Figure 12a). The results show that either listric geometry reliably reproduces the data, as this geometry is the one that involves a gradient in vertical displacement that is faster in the

western sector of the range. A ramp geometry, which involves uniform vertical displacement along the whole hanging wall, does not adequately reproduce the data. The best model is one with a listric fault with a velocity of 0.32 km/my since 65 Ma. These velocities represent the integrated fault velocities over a period between 65 Ma and the present time. However, AFT data, representing the uppermost 4–5 km of exhumation, are better reproduced with lower velocities, with a range of 0.10–0.20 km/y (Figure 12c), whereas AHe data, representing the erosion of the uppermost 2.0–2.5 km of crust, require faster vertical displacements, of 0.20–0.40 km/my (Figure 12b). Altogether, the modeling results support fault acceleration anytime since the Miocene.

5.4.2. Models of Group 2: Vertical Faults

A second group of models was run imposing a kinematic scenario of vertical displacement only. We chose to reproduce the SW tilting by modeling exhumation with a series of vertical reverse faults also striking N45°E and with fault velocities decreasing eastward, all starting to operate at 65 Ma. We arbitrarily chose 4 faults in order to generate the velocity gradient. The location of the westernmost fault (A) was chosen at the same location as the fault used in the first group of models, and the remaining 3 faults, B, C, and D, were located 25, 30, and 45 km southeastward (Figure 11b). Based on the results of the models with southeast–dipping faults, in which best models with 0.2–0.35 km/my along listric or circular faults set up the maximum vertical velocity, we tested models in which we assumed an initial set of velocities for faults A, B, C, and D and then systematically varied the velocity of each fault, starting with fault A, until the best model was achieved. We departed from initial values of 0.20, 0.12, 0.09, and 0.04 km/my for faults A, B, C, and D and ran a set of 65 models, initially varying only fault A and then each of the remaining faults. The best model required velocities of 0.26, 0.18, 0.15, and 0.10 km/my and implied exhumation rates of 0.05 to 0.26 km/my (Figure 13).

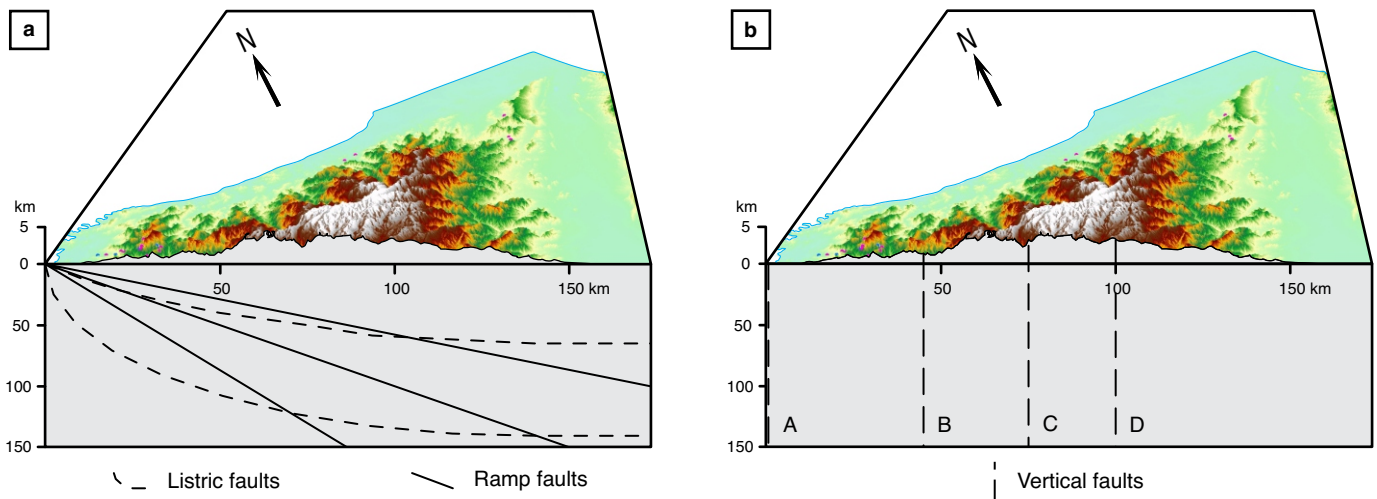


Figure 11. Kinematic scenarios used for Pecube modeling showing the present-day topography and the geometry of faults used for simulations. **(a)** Models of Group 1, showing SE-dipping faults with listric and ramp-only geometries. **(b)** Models of Group 2, showing four vertical faults (A, B, C, D).

Table 4. Typical thermokinematic and elastic parameters used in Pecube.

Parameter (units)	Value
Crustal density (kg/m ³)	2700
Sublithospheric mantle density (kg/m ³)	3200
Equivalent elastic thickness (km)	25
Young modulus (Pa)	1×10^{11}
Poisson's ratio	0.25
Model thickness (km)	40
Thermal diffusivity (km ² /my)	25
Basal model temperature (°C)	750
Sea-level temperature (°C)	25
Atmospheric lapse rate (°C/km)	6
Crustal heat production (°/my)	0
Dpar for AFT calculations (mm)	1.5

5.4.3. Comparison of Model Groups

The best model from each of the two model groups is used for comparison of observed vs. modeled ages along a NW–SE profile (Figure 14a). First, both groups of models reproduce fairly well the pattern of eastward increasing AFT cooling ages as well as the AHe ages (Figure 14b), the latter restricted to the range's NW corner (Figure 14c). We deliberately aimed to obtain plausible exhumation rates coupled to a kinematic model that simulates the observed exhumation gradient rather than attempting to accurately reproduce the range kinematics. However, the modeling results show that a coherent movement

as a single block, as assumed by the SE-dipping fault models (yellow dots in Figure 14), overestimates the AFT ages of the range's eastern end and thus that the compartmentalized model, here approximated with vertical faults, is more likely to represent the actual kinematics (Figure 14d). We note that the spread of observed ages is much larger than that of modeled ages, which we interpret as likely representing observed kinetic variations in particular thermochronometers (chlorine content, grain solubility in AFT, or radiation damage in AHe) that are not captured in this set of models, run with a single kinetic parameter. In summary, we document spatially variable plausible long-term exhumation rates to be lower than 0.25 km/my.

6. Discussion and conclusions

6.1. Episodic Exhumation

We construct a multimethod approach for unravelling exhumation rates in the SNSM by combining 1D calculations derived from bedrock ages and detrital age peaks from multiple thermochronometers, a compilation of age–elevation relationships, and 3D thermokinematic modeling. Together, the combined data unequivocally document episodic exhumation with at least four Cenozoic pulses.

First, triggered by the collision of oceanic terranes along northwestern South America, rapid Paleocene to Eocene (ca. 65–45 Ma) exhumation has been widely recognized in the Central Cordillera (Villagómez & Spikings, 2013) and its northwestern termination at the serranía de San Lucas (Caballero et al., 2013a). A greater magnitude of exhumation farther to the north in the western SNSM precludes the preservation of such

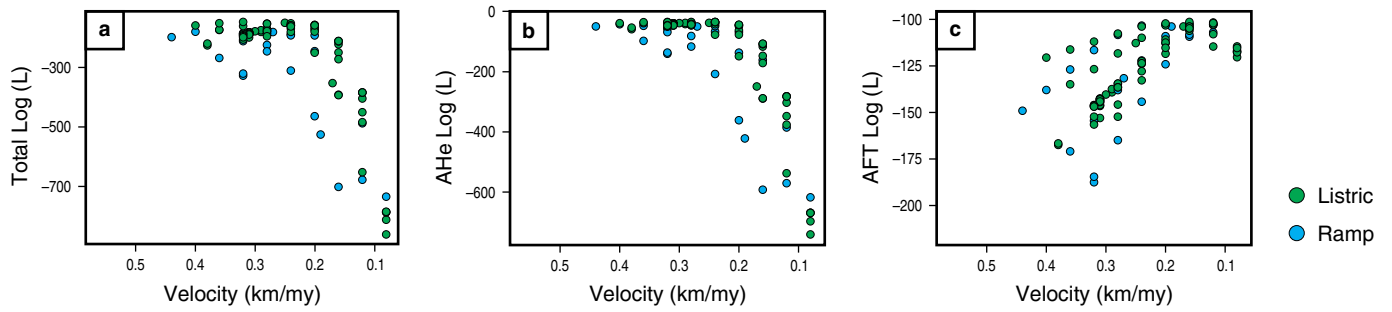


Figure 12. Relation between fault velocity and misfit (evaluated with the log-likelihood, LLH) for ramp and listric fault geometries (Models of Group 1). The highest LLH (i.e., the least negative value) in the upper part of each graph represents the best model. **(a)** Total LLH using both AFT and AHe data. **(b)** LLH using AHe data only. **(c)** LLH using AFT data only.

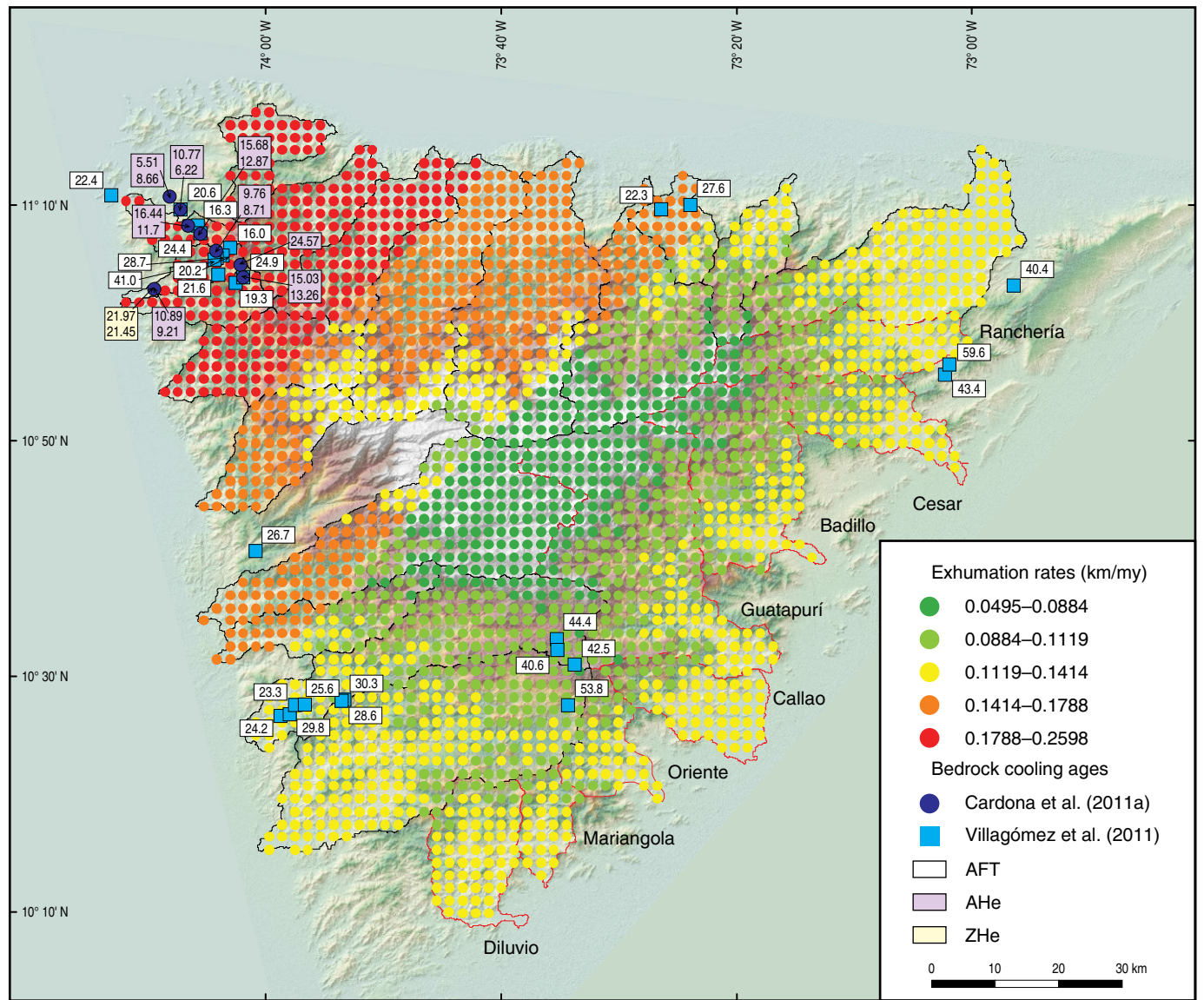
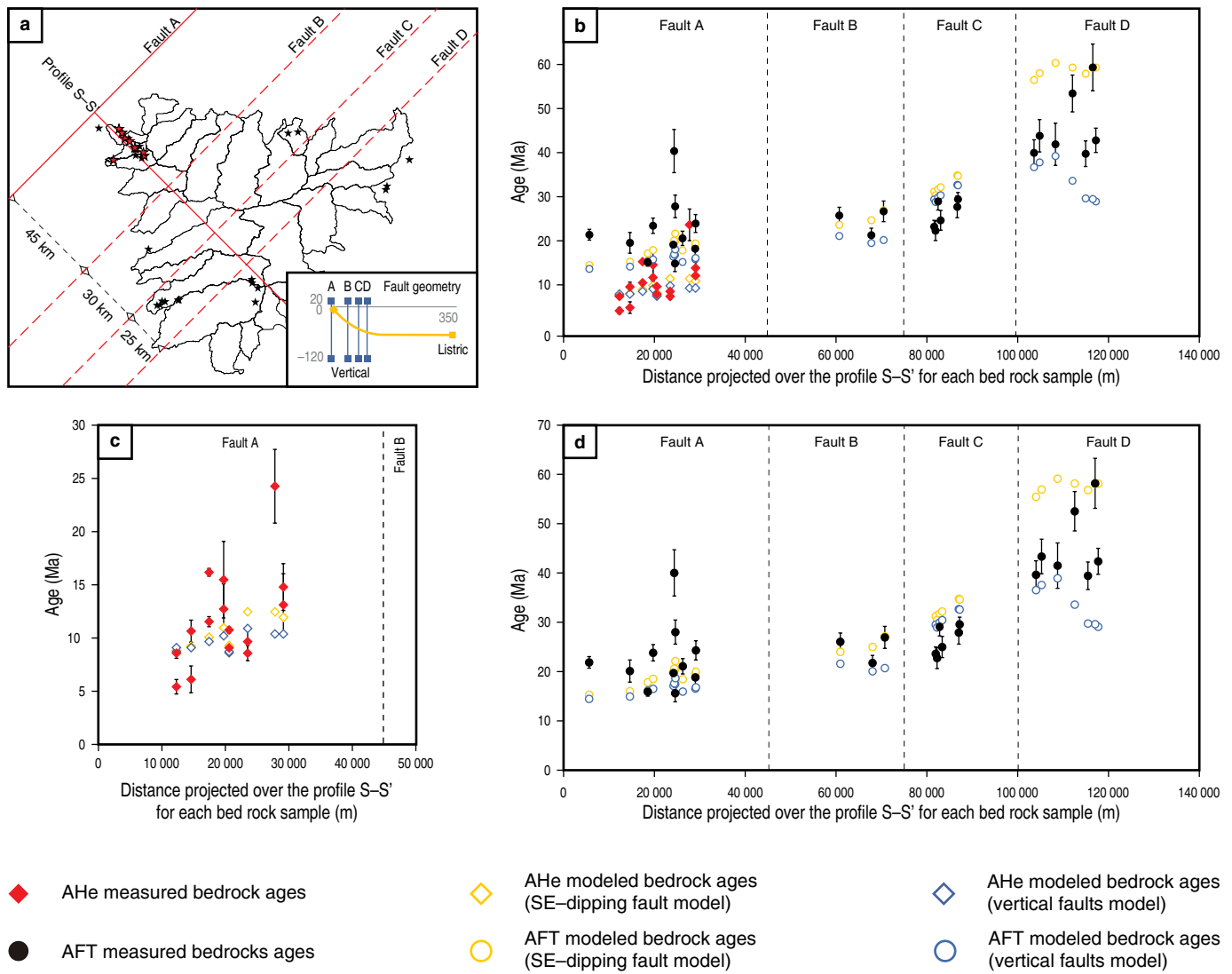


Figure 13. Spatial distributions of exhumation rates for the best solution (i.e., the model with the highest LLH) for Models of Group 2 (vertical faults), showing higher exhumation rates toward the NW.



a signature; however, it has been recognized in the bedrock (Villagómez et al., 2011) and, recently, in the detrital thermochronological (Patiño, 2018) signature of the eastern SNSM.

A second pulse of moderate to rapid exhumation at 35–20 Ma is evident in (1) age–elevation profiles in the NW and SW sectors of the range (Figure 6), (2) 1D estimates based on available detrital ZFT and AFT ages and assumed closure depths from the western margin (Figure 9, Aracataca), and (3) ubiquitous 30–20 Ma AFT and AHe age peaks across the range.

Third, deceleration of exhumation seems to characterize the post-middle Miocene history of the range, as suggested by

our 1D estimates (Figure 9) and age–elevation profiles (Figure 6). In addition, geobarometry data by Cardona et al. (2011a) suggest that Eocene (56–50 Ma) granitoids cropping out in the range's NW corner were emplaced at pressures between ca. 4.9 and 6.4 kbar, corresponding to depths of 14.7–19.2 km. These estimates imply Eocene to recent exhumation rates of 0.26 to 0.38 km/my in this sector of the range. Our exhumation rates derived from 3D modeling in this area typify lower values, up to 0.26 km/my (Figure 13) for the uppermost ca. 6.5 km of the crust, which is the approximate structural depth sensitive to apatite fission-track data, since the late Oligocene (ca. 25 Ma).

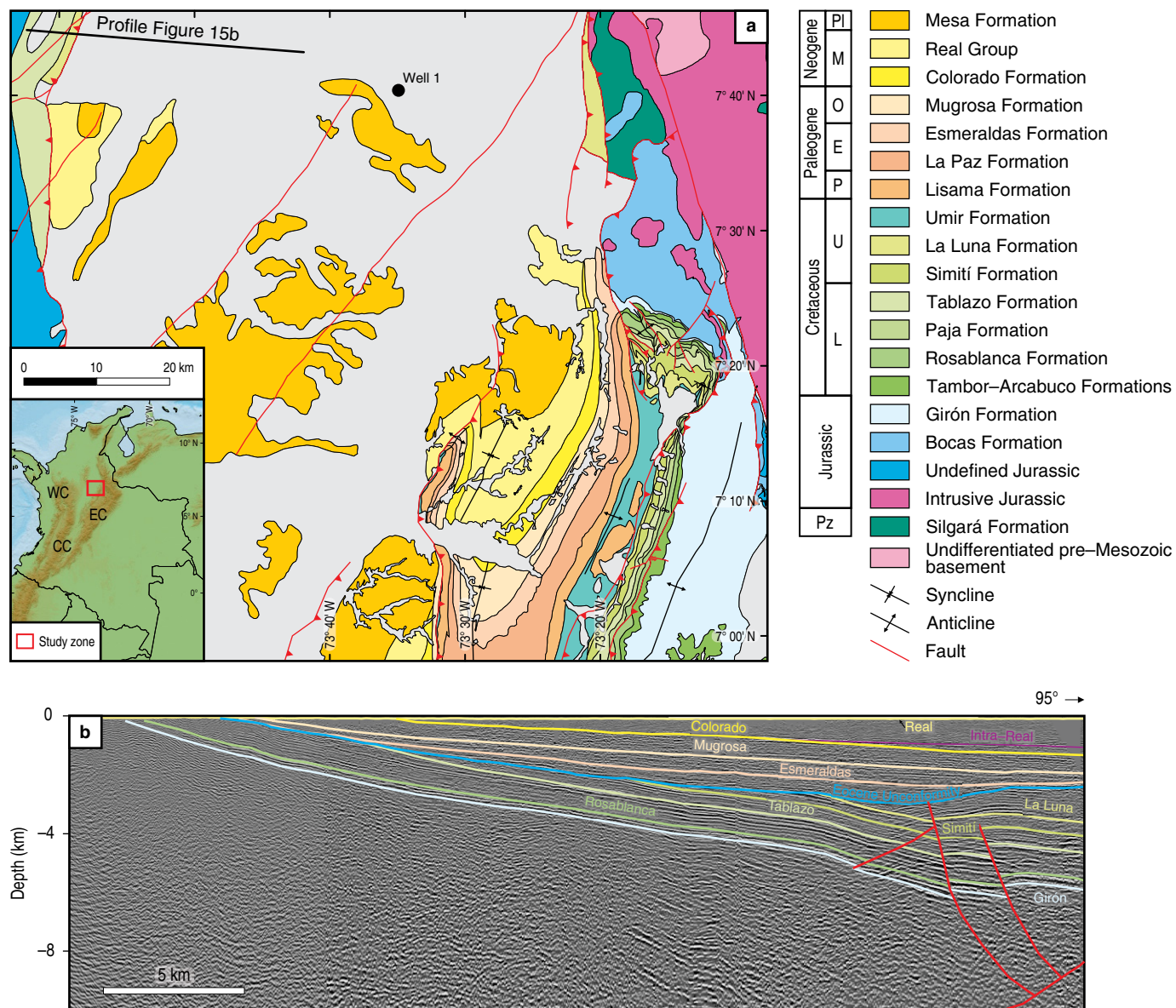


Figure 15. (a) Geologic map of the northern Middle Magdalena Basin and the western foothills of the Eastern Cordillera at ca. 7° N latitude showing the main structures and the location of the seismic line presented in Figure 15b. **(b)** Interpreted seismic line showing onlap of Cenozoic units onto the Central Cordillera's basement, illustrating progressive southward monoclinal tilting of the range. After Parra et al. (2012).

Combined, these independently derived rates suggest that Eocene to late Oligocene rates must have been much faster than post-Oligocene rates.

Finally, both 1D estimations of exhumation rates based on AFT and AHe detrital data from modern sediment (Figure 9) and our 3D modeling results for AFT and AHe data (Figure 13) suggest that the uppermost 2–2.5 km of crust, as documented by AHe data, was exhumed faster than the underlying 2–3 km, as illustrated by AFT data, portraying an acceleration in exhumation at any time since the Miocene. Ongoing work with cosmogenic ^{10}Be -derived rates in river catchments will help place time constraints on this acceleration.

6.2. Continuity with the Central Cordillera

The structural geometry of the SNSM is that of a southeast-tilted monocline, where extreme exhumation of up to 15–19 km since the Eocene at the NW corner gradually diminishes toward the Cesar-Ranchería Basin, located 100 km to the southeast, where up to 3 km of subsidence occurred in a similar time frame. Such geometry is reminiscent of that of the Central Cordillera, where map patterns (e.g., Gómez et al., 2003) and seismic reflection data (Caballero et al., 2013b; Parra et al., 2012) document progressive onlap of Cenozoic units from the Middle Magdalena Basin onto the Central Cordillera basement (Figure 15a, 15b). As

noted by Gómez et al. (2003), such onlap and the concurrent formation of a westward-expanding pediment surface in the Central Cordillera is the result of the eastward migration of active deformation and related exhumation from the Central to the Eastern Cordillera. Similar structural geometries in the Central Cordillera and the SNSM and basement correlations between both areas across the Sinú–San Jacinto from subsurface data (Montes et al., 2010; Mora–Bohórquez et al., 2017) confirm the hypothesis of former structural continuity of the two ranges.

Exhumation patterns in the Central Cordillera support very rapid initial exhumation in the Late Cretaceous to Paleocene and negligible exhumation (less than 2 km) in the last 40 my (Caballero et al., 2013b; Restrepo–Moreno et al., 2009; Villagómez et al., 2011). Our integrated analyses in Santa Marta also suggest such a decrease in exhumation rates during the initial range development, providing further support for the idea of structural continuity with the Central Cordillera. However, unlike in the latter, where only up to ca. 2 km of exhumation has occurred in the last ca. 40 my, a distinctive pulse of late Eocene – early Miocene rapid exhumation characterizes the entire SNSM and is especially marked at its northwestern corner. We suggest that this pulse beginning at 35 Ma marks the time of tectonic exhumation and dismembering of both ranges through deformation that was accommodated in the form of normal faulting, possibly associated with clockwise rotation (Montes et al., 2010) and the opening of extensional basins in the LMB (Bernal–Olaya et al., 2015; Mora et al., 2018). The oldest known sedimentary fill at 4–5 km depth is Oligocene in age (Montes et al., 2010; Mora et al., 2018; Rincón et al., 2007).

A period of contrasting tectonism and opening of sedimentary basins in the range's northern and western margins followed. Post–Miocene tectonic quiescence led to diminished exhumation rates in the northern slope (Figure 9), which favored sediment retrogradation of the Palomino sequence (Figure 4; Piraquive et al., 2017). In contrast, the western slope continued to be exhumed at faster rates until at least 10 Ma (Figure 9), enhancing the range's structural asymmetry and favoring a reciprocal stratigraphy (Cataneanu et al., 1997), characterized by sediment progradation of the Macaraquilla Conglomerates' Lower Member onto its Upper Member (Figure 3).

Finally, the comparison of AFT and AHe ages presently exposed in the range, retrieved in detrital data from catchments in all three margins, support recent (i.e., post–Miocene) acceleration in exhumation, enhanced in the western margin (Figure 10c). Such a pattern, in the context of steep topography (Figure 1a, 1c) and a humid climate (Figure 1d), supports the concept of a very recent exhumation pulse in line with the hypothesis of denudational immaturity, whereby recent crustal stacking and rock uplift would exceed the magnitude of exhumation, generating a non–steady–state (i.e., rising) topography. Diminished

crustal thickness in the range's NW corner (25–35 km, Figure 1b) and a positive gravity anomaly (Figure 1a) allow us to postulate a likely removal of the lower crust as the trigger of such a recent episode. Ongoing work on recent denudation rates with cosmogenic radionuclides will help place more detailed time constraints on this rapid recent exhumation.

Acknowledgments

This research was funded by the São Paulo Research Foundation (FAPESP) Youth Researcher Grant 2013/03265–5 to Mauricio PARRA. The contributions by Sebastián ECHEVERRI and Ana María PATIÑO constitute part of their PhD and MS theses, respectively, at the Universidade de São Paulo, funded by the CAPES Foundation. Juan Carlos RAMÍREZ acknowledges the funding provided by the FAPESP Grant 2016/10094–0 for his PhD thesis, part of which is included in this work. We thank Frederico GENEZINI from IPEN–USP for diligently facilitating neutron irradiation for fission–track dating. Alexandre ALVES and Ana Beatriz de BARROS at IEE–USP and Thays MINELLI at IGC–USP graciously assisted with thermochronology sample preparation. We appreciate the kind collaboration of the TODARO family (Aracataca) and Juan Carlos and Florencia (Palomino) during fieldwork.

References

- Agencia Nacional de Hidrocarburos. 2010. Mapa de Anomalía de Bouguer Total de la República de Colombia. Scale 1: 2 500 000. Bogotá. https://www.anh.gov.co/Informacion-Geologica-y-Geofisica/Pais/Documents/ANOMALIA_DE_BOUGUER_TOTAL_DE_LA_REPUBLICA_DE_COLOMBIA%202010.pdf (consulted in June 2017).
- Allen, P.A. & Allen, J.R. 2005. Basin Analysis: Principles and Applications. Blackwell Publishing company, 549 p. Oxford.
- Ayala, R.C., Bayona, G., Ojeda, C., Cardona, A., Valencia, V., Padron, C., Yoris, F., Mesa, J. & Garcia, A. 2009. Estratigrafía y procedencia de las unidades comprendidas entre el Campaniano y el Paleógeno en la Subcuenca de Cesar: Aportes a la evolución tectónica del área. *Geología Colombiana*, (34): 3–33.
- Ayala, R.C., Bayona, G., Cardona, A., Ojeda, C., Montenegro, O.C., Montes, C., Valencia, V. & Jaramillo, C. 2012. The Paleogene synorogenic succession in the northwestern Maracaibo Block: Tracking intraplate uplifts and changes in sediment delivery systems. *Journal of South American Earth Sciences*, 39: 93–111. <https://doi.org/10.1016/j.jsames.2012.04.005>
- Bayona, G., Lamus–Ochoa, F., Cardona, A., Jaramillo, C., Montes, C. & Tchegliakova, N. 2007. Procesos orogénicos del Paleógeno para la Cuenca de Ranchería (Guajira, Colombia) y áreas adyacentes definidos por análisis de procedencia. *Geología Colombiana*, (32): 21–46.

- Bayona, G., Jiménez, G., Silva, C., Cardona, A., Montes, C., Roncancio, J. & Cordani, U. 2010. Paleomagnetic data and K–Ar ages from Mesozoic units of the Santa Marta Massif: A preliminary interpretation for block rotation and translations. *Journal of South American Earth Sciences*, 29(4): 817–831. <https://doi.org/10.1016/j.jsames.2009.10.005>
- Bayona, G., Cardona, A., Jaramillo, C., Mora, A., Montes, C., Valencia, V., Ayala, C., Montenegro, O. & Ibañez–Mejia, M. 2012. Early Paleogene magmatism in the northern Andes: Insights on the effects of oceanic plateau–continent convergence. *Earth and Planetary Science Letters*, 331–332: 97–111. <https://doi.org/10.1016/j.epsl.2012.03.015>
- Bernal–Olaya, R., Mann, P. & Escalona, A. 2015. Cenozoic tectonostratigraphic evolution of the Lower Magdalena Basin, Colombia: An Example of an under–to overfilled forearc basin. In: Bartolini, C. & Mann, P. (editors), *Petroleum geology and potential of the Colombian Caribbean margin*. American Association of Petroleum Geologists, Memoir 108, p. 345–398. <https://doi.org/10.1306/13531943M1083645>
- Braun, J. 2002. Quantifying the effect of recent relief changes on age–elevation relationships. *Earth and Planetary Science Letters*, 200(3–4): 331–343. [https://doi.org/10.1016/S0012-821X\(02\)00638-6](https://doi.org/10.1016/S0012-821X(02)00638-6)
- Braun, J. 2003. Pecube: A new finite–element code to solve the 3D heat transport equation including the effects of a time–varying, finite amplitude surface topography. *Computers & Geosciences*, 29(6): 787–794. [https://doi.org/10.1016/S0098-3004\(03\)00052-9](https://doi.org/10.1016/S0098-3004(03)00052-9)
- Braun, J., van der Beek, P., Valla, P., Robert, X., Herman, F., Glotzbach, C., Pedersen, V., Perry, C., Simon–Labric, T. & Prigent, C. 2012. Quantifying rates of landscape evolution and tectonic processes by thermochronology and numerical modeling of crustal heat transport using PECUBE. *Tectonophysics*, 524–525: 1–28. <https://doi.org/10.1016/j.tecto.2011.12.035>
- Burke, K., Cooper, C., Dewey, J.F., Mann, P. & Pindell, J.L. 1984. Caribbean tectonics and relative plate motions. In: Bonini, W.E., Hargraves, R.B. & Shagam, R. (editors), *The Caribbean–South American plate boundary and regional tectonics*. Geological Society of America, Memoir 162, p. 31–63. <https://doi.org/10.1130/MEM162-p31>
- Caballero, V., Parra, M., Mora, A., López, C., Rojas, L.E. & Quintero, I. 2013a. Factors controlling selective abandonment and reactivation in thick–skin orogens: A case study in the Magdalena Valley, Colombia. In: Nemčok, M., Mora, A. & Cosgrove, J.W. (editors), *Thick–skin–dominated orogens: From initial inversion to full accretion*. Geological Society of London, Special Publication 377, p. 343–367. London. <https://doi.org/10.1144/SP377.4>
- Caballero, V., Mora, A., Quintero, I., Blanco, V., Parra, M., Rojas, L.E., López, C., Sánchez, N., Horton, B.K., Stockli, D. & Duddy, I. 2013b. Tectonic controls on sedimentation in an intermontane hinterland basin adjacent to inversion structures: The Nuevo Mundo Syncline, Middle Magdalena Valley, Colombia. In: Nemčok, M., Mora, A. & Cosgrove, J.W. (editors), *Thick–skin–dominated orogens: From initial inversion to full accretion*. Geological Society of London, Special Publication 377, p. 315–342. London. <https://doi.org/10.1144/SP377.12>
- Cadena, A.F., & Slatt, R.M. 2013. Seismic and sequence stratigraphic interpretation of the area of influence of the Magdalena submarine fan, offshore northern Colombia. *Interpretation*, 1(1): SA53–SA74. <https://doi.org/10.1190/INT-2013-0028.1>
- Cardona, A., Cordani, U.G. & MacDonald, W.D. 2006. Tectonic correlations of pre–Mesozoic crust from the northern termination of the Colombian Andes, Caribbean region. *Journal of South American Earth Sciences*, 21(4): 337–354. <https://doi.org/10.1016/j.jsames.2006.07.009>
- Cardona, A., Chew, D., Valencia, V.A., Bayona, G., Mišković, A. & Ibañez–Mejia, M. 2010a. Grenvillian remnants in the northern Andes: Rodinian and Phanerozoic paleogeographic perspectives. *Journal of South American Earth Sciences*, 29(1): 92–104. <https://doi.org/10.1016/j.jsames.2009.07.011>
- Cardona, A., Valencia, V., Garzón, A., Montes, C., Ojeda, G., Ruiz, J. & Weber, M. 2010b. Permian to Triassic I to S–type magmatic switch in the northeast Sierra Nevada de Santa Marta and adjacent regions, Colombian Caribbean: Tectonic setting and implications within Pangea paleogeography. *Journal of South American Earth Sciences*, 29(4): 772–783. <https://doi.org/10.1016/j.jsames.2009.12.005>
- Cardona, A., Valencia, V., Bustamante, C., García–Casco, A., Ojeda, G., Ruiz, J., Saldarriaga, M. & Weber, M. 2010c. Tectonomagmatic setting and provenance of the Santa Marta Schists, northern Colombia: Insights on the growth and approach of Cretaceous Caribbean oceanic terranes to the South American continent. *Journal of South American Earth Sciences*, 29(4): 784–804. <https://doi.org/10.1016/j.jsames.2009.08.012>
- Cardona, A., Valencia, V., Weber, M., Duque, J., Montes, C., Ojeda, G.Y., Reiners, P., Domanik, K., Nicolescu, S. & Villagómez, D. 2011a. Transient Cenozoic tectonic stages in the southern margin of the Caribbean plate: U–Th/He thermochronological constraints from Eocene plutonic rocks in the Santa Marta Massif and serranía de Jarar, northern Colombia. *Geologica Acta*, 9(3): 445–466. <https://doi.org/10.1344/105.000001739>
- Cardona, A., Valencia, V., Bayona, G., Duque, J., Ducea, M., Gehrels, G., Jaramillo, C., Montes, C., Ojeda, G. & Ruiz, J. 2011b. Early–subduction–related orogeny in the northern Andes: Turonian to Eocene magmatic and provenance record in the Santa Marta Massif and Ranchería Basin, northern Colombia. *Terra Nova*, 23(1): 26–34. <https://doi.org/10.1111/j.1365-3121.2010.00979.x>
- Case, J.E., & MacDonald, W.D. 1973. Regional gravity anomalies and crustal structure in northern Colombia. *Geological Society of America Bulletin*, 84(9): 2905–2916. [https://doi.org/10.1130/0016-7606\(1973\)84<2905:RGAACS>2.0.CO;2](https://doi.org/10.1130/0016-7606(1973)84<2905:RGAACS>2.0.CO;2)
- Cataneanu, O., Beaumont, C. & Waschbusch, P. 1997. Interplay of static loads and subduction dynamics in foreland basins: Re-

- ciprocal stratigraphies and the “missing” peripheral bulge. *Geology*, 25(12): 1087–1090. [https://doi.org/10.1130/0091-7613\(1997\)025<1087:IOSLAS>2.3.CO;2](https://doi.org/10.1130/0091-7613(1997)025<1087:IOSLAS>2.3.CO;2)
- Cediel, F., Shaw, R.P. & Cáceres, C. 2003. Tectonic assembly of the northern Andean Block. In: Bartolini, C., Buffler, R.T. & Blickwede, J. (editors), *The circum-Gulf of Mexico and the Caribbean: Hydrocarbon habitats, basin formation, and plate tectonics*. American Association of Petroleum Geologists, Memoir 79, p. 815–848. Tulsa, USA.
- Ceron, J.F. 2008. Crustal structure of the Colombian Caribbean Basin and margins. Doctoral thesis, University of South Carolina, 181 p. Columbia.
- Ceron, J.F., Kellogg, J.N. & Ojeda, G.Y. 2007. Basement configuration of the northwestern South America–Caribbean margin from recent geophysical data. *Ciencia, Tecnología y Futuro*, 3(3): 25–49.
- Colmenares, F.H., Mesa, A.M., Roncancio, J.H., Arciniegas, E.G., Pedraza, P.E., Cardona, A., Romero, A.J., Silva, C.A., Alvarado, S.I., Romero, O.A. & Vargas, A.F. 2007. Geología de las planchas 11, 12, 13, 14, 18, 19, 20, 21, 25, 26, 27, 33, 34 y 40. Proyecto: Evolución geohistórica de la Sierra Nevada de Santa Marta. Invenmar–Ingeominas–ICP–Ecopetrol–Geosearch Ltda., 401 p. Bogotá.
- Cordani, U.G., Cardona, A., Jiménez, D.M., Liu, D. & Nutman, A.P. 2005. Geochronology of Proterozoic basement inliers in the Colombian Andes: Tectonic history of remnants of a fragmented Grenville belt. In: Vaughan, A.P.M., Leat, P.T. & Pankhurst, R.J. (editors), *Terrane processes at the margins of Gondwana*. Geological Society of London, Special Publication 246, p. 329–346. London. <https://doi.org/10.1144/GSL.SP.2005.246.01.13>
- Dodson, M.H. 1973. Closure temperature in cooling geochronological and petrological systems. *Contributions to Mineralogy and Petrology*, 40(3): 259–274. <https://doi.org/10.1007/BF00373790>
- Donelick, R.A., O’Sullivan, P.B. & Ketcham, R.A. 2005. Apatite fission-track analysis. *Reviews in Mineralogy and Geochemistry*, 58(1): 49–94. <https://doi.org/10.2138/rmg.2005.58.3>
- Duque–Caro, H. 1984. Structural style, diapirism, and accretionary episodes of the Sinú–San Jacinto terrane, southwestern Caribbean bordeland. In: Bonini, W.E., Hargraves, R.B. & Shagam, R. (editors), *The Caribbean–South American plate boundary and regional tectonics*. Geological Society of America, Memoir 162, p. 303–316. <https://doi.org/10.1130/MEM162-p303>
- Duque, J.F. 2010. Geocronología (U/Pb y $^{40}\text{Ar}/^{39}\text{Ar}$) y geoquímica de los intrusivos paleógenos de la Sierra Nevada de Santa Marta y sus relaciones con la tectónica del Caribe y el arco magmático circum-caribeño. Master thesis, Universidad Nacional Autónoma de México, 189 p. México D. F.
- Echeverri, S. 2019. Cenozoic tectonic evolution of the Sierra Nevada of Santa Marta, northern Colombia: A record of strike–slip tectonics along the southern Caribbean Plate. Doctoral Thesis, Universidade de São Paulo, 350 p. Brasil.
- Echeverri, S., Parra, M., Sobel, E., Pardo, A., Trejos, R., Vallejo, F. & Patiño, A.M. 2017. Registro de exhumación cenozoica de la Sierra Nevada de Santa Marta, Colombia: Entendiendo la interacción entre tectónica y sedimentación a partir de datos de proveniencia y termocronología de baja temperatura. XVI Congreso Colombiano de Geología. Memoirs, p. 1495–1500. Santa Marta.
- Farley, K.A. 2002. (U–Th)/He Dating: Techniques, calibrations, and applications. *Reviews in Mineralogy and Geochemistry*, 47(1): 819–844. <https://doi.org/10.2138/rmg.2002.47.18>
- Flowers, R.M., Ketcham, R.A., Shuster, D.L. & Farley, K.A. 2009. Apatite (U–Th)/He thermochronometry using a radiation damage accumulation and annealing model. *Geochimica et Cosmochimica Acta*, 73(8): 2347–2365. <https://doi.org/10.1016/j.gca.2009.01.015>
- Galbraith, R.F. 1981. On statistical models for fission track counts. *Journal of the International Association for Mathematical Geology*, 13(6): 471–478
- Gallagher, K., Brown, R. & Johnson, C. 1998. Fission track analysis and its applications to geological problems. *Annual Review of Earth and Planetary Sciences*, 26(1): 519–572. <https://doi.org/10.1146/annurev.earth.26.1.519>
- Gautheron, C., Tassan-Got, L., Barbarand, J. & Pagel, M. 2009. Effect of alpha–damage annealing on apatite (U–Th)/He thermochronology. *Chemical Geology*, 266(3–4): 157–170. <https://doi.org/10.1016/j.chemgeo.2009.06.001>
- Gómez, E., Jordan, T., Allmendinger, R., Hegarty, K., Kelley, S. & Heizler, M. 2003. Controls on architecture of the Late Cretaceous to Cenozoic southern Middle Magdalena Valley Basin, Colombia. *Geological Society of America Bulletin*, 115(2): 131–147. [https://doi.org/10.1130/0016-7606\(2003\)115<0131:COAOTL>2.0.CO;2](https://doi.org/10.1130/0016-7606(2003)115<0131:COAOTL>2.0.CO;2)
- Gorney, D., Escalona, A., Mann, P., Magnani, M.B., Levander, A., Christeson, G., Mann, P., Zelt, C.A., Magnani, M.B., Schmitz, M., Clark, S., Guedez, M.C., Bezada, M., Arogunmati, Y., Gorney, D., Aitken, T. & Beardsley, A. 2007. Chronology of Cenozoic tectonic events in western Venezuela and the Leeward Antilles based on integration of offshore seismic reflection data and on–land geology. *American Association of Petroleum Geology Bulletin*, 91(5): 653–684. <https://doi.org/10.1306/11280606002>
- Green, P.F. 1981. A new look at statistics in fission–track dating. *Nuclear Tracks*, 5(1–2): 77–86. [https://doi.org/10.1016/0191-278X\(81\)90029-9](https://doi.org/10.1016/0191-278X(81)90029-9)
- Harrison, T.M. & Zeitler, P.K. 2005. Fundamentals of noble gas thermochronology. In: Reiners, P.W. & Ehlers, T.A. (editors), *Low temperature thermochronology: Techniques, interpretations, and applications*. Mineralogical Society of America, *Reviews in Mineralogy and Geochemistry* 58, p. 123–149. Washington D.C.
- Hernández, M., Maldonado, I., González, J., Martínez, H., Clavijo, J. & Reyes, G. 2003. Memoria explicativa: Geología de las

- planchas 25 Fundación, 32 Monterrubio y 39 El Difícil. Scale 1:100 000. Ingeominas, 74 p. Bogotá.
- Idárraga–García, J. & Romero, J. 2010. Neotectonic study of the Santa Marta Fault System, western foothills of the Sierra Nevada de Santa Marta, Colombia. *Journal of South American Earth Sciences*, 29(4): 849–860. <https://doi.org/10.1016/j.jsames.2009.11.004>
- Jaramillo, C., Rueda, M. & Torres, V. 2011. A palynological zonation for the Cenozoic of the Llanos and Llanos Foothills of Colombia. *Palynology*, 35(1): 46–84. <https://doi.org/10.1080/01916122.2010.515069>
- Kellogg, J.N. 1984. Cenozoic tectonic history of the sierra de Perijá, Venezuela–Colombia, and adjacent basins. In: Bonini, W.E., Hargraves, R.B. & Shagam, R. (editors), *The Caribbean–South American Plate boundary and regional tectonics*. Geological Society of America, Memoir 162, p. 239–261. <https://doi.org/10.1130/MEM162-p239>
- Kellogg, J.N. & Bonini, W.E. 1982. Subduction of the Caribbean Plate and basement uplifts in the overriding South American Plate. *Tectonics*, 1(3): 251–276. <https://doi.org/10.1130/MEM162-p239>
- Mann, P., Escalona, A. & Castillo, M.V. 2006. Regional geologic and tectonic setting of the Maracaibo supergiant Basin, western Venezuela. *American Association of Petroleum Geologists Bulletin*, 90(4): 445–477. <https://doi.org/10.1306/10110505031>
- McMahon, C. 2000. Evaluation of the effects of oblique collision between the Caribbean and South American Plates using geochemistry from igneous and metamorphic bodies of northern Venezuela. Doctoral Thesis, University of Notre Dame, 277 p. Paris.
- Montes, C., Guzmán, G., Bayona, G., Cardona, A., Valencia, V. & Jaramillo, C. 2010. Clockwise rotation of the Santa Marta Massif and simultaneous Paleogene to Neogene deformation of the Plato–San Jorge and Cesar–Ranchería Basins. *Journal of South American Earth Sciences*, 29(4): 832–848. <https://doi.org/10.1016/j.jsames.2009.07.010>
- Montes, C., Cardona, A., Jaramillo, C., Pardo, A., Silva, J.C., Valencia, V., Ayala, C., Pérez–Ángel, L.C., Rodríguez–Parra, L.A., Ramírez, V. & Niño, H. 2015. Middle Miocene closure of the Central American Seaway. *Science*, 348(6231): 226–229. <https://doi.org/10.1126/science.aaa2815>
- Mora–Bohórquez, J.A., Ibañez–Mejía, M., Oncken, O., de Freitas, M., Vélez, V., Mesa, A. & Serna, L. 2017. Structure and age of the Lower Magdalena Valley Basin basement, northern Colombia: New reflection–seismic and U–Pb–Hf insights into the termination of the central Andes against the Caribbean Basin. *Journal of South American Earth Sciences*, 74: 1–26. <https://doi.org/10.1016/j.jsames.2017.01.001>
- Mora, J.A., Oncken, O., Le Breton, E., Mora, A., Veloza, G., Vélez, V. & de Freitas, M. 2018. Controls on forearc basin formation and evolution: Insights from Oligocene to recent tectono–stratigraphy of the Lower Magdalena Valley basin of northwest Colombia. *Marine and Petroleum Geology*, 97: 288–310. [https://doi.org/10.1016/S0895-9811\(02\)00017-2](https://doi.org/10.1016/S0895-9811(02)00017-2)
- Mulligan, M. 2006. Global gridded 1km TRMM rainfall climatology and derivatives, version 1.0 Database: <http://www.ambiotek.com/1kmrainfall> (consulted in November 2017).
- Ordóñez–Carmona, O. & Pimentel, M.M. 2002. Rb–Sr and Sm–Nd isotopic study of the Puquí Complex, Colombian Andes. *Journal of South American Earth Sciences*, 15(2): 173–182. [https://doi.org/10.1016/S0895-9811\(02\)00017-2](https://doi.org/10.1016/S0895-9811(02)00017-2)
- Parra, M., Mora, A., López, C., Rojas, L.E. & Horton, B.K. 2012. Detecting earliest shortening and deformation advance in thrust belt hinterlands: Example from the Colombian Andes. *Geology*, 40(2): 175–178. <https://doi.org/10.1130/G32519.1>
- Parra, M., Echeverri, J.S., Perez–Consuegra, N. & Senatore, C.A. 2016. Episodic uplift patterns of the Sierra Nevada de Santa Marta in northern Colombia. 10th South American Symposium on Isotope Geology. Program and Abstracts, 1, p. 72. Puerto Vallarta, México.
- Patiño, A.M. 2018. Cenozoic exhumation patterns in the eastern Sierra Nevada de Santa Marta, northern Colombia: A detrital thermochronometry study. Master thesis, Universidade de São Paulo, 115 p. São Paulo. <https://doi.org/10.11606/D.44.2018.tde-17072018-144314>
- Pindell, J.L., Higgs, R. & Dewey, J.F. 1998. Cenozoic palinspastic reconstruction, paleogeographic evolution and hydrocarbon setting of the northern margin of South America. In: Pindell, J.L. & Drake, C. (editors), *Paleogeographic evolution and non–glacial eustasy, northern South America*. Society for Sedimentary Geology, Special Publication 58, p. 45–85. <https://doi.org/10.2110/pec.98.58.0045>
- Pindell, J.L. & Kennan, L. 2009. Tectonic evolution of the Gulf of Mexico, Caribbean and northern South America in the mantle reference frame: An update. In: James, K.H., Lorente, M.A. & Pindell, J.L. (editors), *The origin and evolution of the Caribbean Plate*. Geological Society of London, Special Publication 328, p. 1–55. <https://doi.org/10.1144/SP328.1>
- Pinzón–Rodríguez, E.M. 2014. Caracterización litológica y sedimentológica de una unidad conglomerática en cercanías de Aracataca y su significado para el levantamiento de la Sierra Nevada de Santa Marta (SNSM). Bachelor thesis, Universidad Nacional de Colombia, 21 p. Bogotá.
- Piraquive, A., Pinzón, E., Kammer, A., Bernet, M. & von Quadt, A. 2017. Early Neogene unroofing of the Sierra Nevada de Santa Marta, as determined from detrital geothermochronology and the petrology of clastic basin sediments. *Geological Society of America Bulletin*, 130(3–4): 355–380. <https://doi.org/10.1130/B31676.1>
- Reiners, P.W., & Brandon, M.T. 2006. Using thermochronology to understand orogenic erosion. *Annual Review Earth Plane-*

- tary Sciences, 34: 419–466. <https://doi.org/10.1146/annurev.earth.34.031405.125202>
- Restrepo–Moreno, S.A., Foster, D.A., Stockli, D.F. & Parra–Sánchez, L.N. 2009. Long-term erosion and exhumation of the “Altiplano Antioqueño,” northern Andes (Colombia) from apatite (U–Th)/He thermochronology. *Earth and Planetary Science Letters*, 278(1–2): 1–12. <https://doi.org/10.1016/j.epsl.2008.09.037>
- Restrepo–Pace, P.A., Ruiz, J., Gehrels, G. & Cosca, M. 1997. Geochronology and Nd isotopic data of Grenville–age rocks in the Colombian Andes: New constraints for late Proterozoic – early Paleozoic paleocontinental reconstructions of the Americas. *Earth and Planetary Science Letters*, 150(3–4): 427–441. [https://doi.org/10.1016/S0012-821X\(97\)00091-5](https://doi.org/10.1016/S0012-821X(97)00091-5)
- Restrepo, J.J., Ordóñez–Carmona, O., Armstrong, R. & Pimentel, M.M. 2011. Triassic metamorphism in the northern part of the Tahamí Terrane of the Central Cordillera of Colombia. *Journal of South American Earth Sciences*, 32(4): 497–507. <https://doi.org/10.1016/j.jsames.2011.04.009>
- Reyes, H.A., Montenegro, B.M. & Gómez, P.D. 2004. Tectonoestratigrafía y evolución del Valle Inferior del Magdalena. *Boletín de Geología*, 26(42): 19–38.
- Rincón, D.A., Arenas, J.E., Cuartas, C.H., Cárdenas, A.L., Molineros, C.E., Caicedo, C. & Jaramillo, C. 2007. Eocene–Pliocene planktonic foraminifera biostratigraphy from the continental margin of the southwest Caribbean. *Stratigraphy*, 4(4): 261–311.
- Ruiz, G.M.H., Seward, D. & Winkler, W. 2004. Detrital thermochronology – a new perspective on hinterland tectonics, an example from the Andean Amazon Basin, Ecuador. *Basin Research*, 16(3): 413–430. <https://doi.org/10.1111/j.1365-2117.2004.00239.x>
- Salazar, C.A., Bustamante, C. & Archanzo, C.J. 2016. Magnetic fabric (AMS, AAR) of the Santa Marta Batholith (northern Colombia) and the shear deformation along the Caribbean Plate margin. *Journal of South American Earth Sciences*, 70: 55–68. <https://doi.org/10.1016/j.jsames.2016.04.011>
- Sánchez, J. & Mann, P. 2015. Integrated structural and basinal analysis of the Cesar–Ranchería Basin, Colombia: Implications for its tectonic history and petroleum systems. In: Bartolini, C. & Mann, P. (editors), *Petroleum geology and potential of the Colombian Caribbean Margin*. American Association of Petroleum Geologists, Memoirs 108, p. 431–470. <https://doi.org/10.1306/13531945M1083648>
- Tagami, T. & O’Sullivan, P.B. 2005. Fundamentals of fission-track thermochronology. In: Reiners, P.W. & Ehlers, T.A. (editors), *Low temperature thermochronology: Techniques, interpretations, and applications*. Mineralogical Society of America, Reviews in Mineralogy and Geochemistry 58, p. 19–47. Washington.
- Trenkamp, R., Kellogg, J.N., Freymueller, J.T. & Mora, H. 2002. Wide plate margin deformation, southern Central America and northwestern South America, CASA GPS observations. *Journal of South American Earth Sciences*, 15(2): 157–171. [https://doi.org/10.1016/S0895-9811\(02\)00018-4](https://doi.org/10.1016/S0895-9811(02)00018-4)
- Tschanz, C.M., Jimeno, A. & Cruz, J. 1969. Geology of the Sierra Nevada de Santa Marta area (Colombia): Preliminary report. Ingeominas, 288 p. Bogotá.
- Tschanz, C.M., Marvin, R.F., Cruz, J., Mehnert, H.H. & Cebula, G.T. 1974. Geologic evolution of the Sierra Nevada de Santa Marta, northeastern Colombia. *Geological Society of America Bulletin*, 85(2): 273–284. [https://doi.org/10.1130/0016-7606\(1974\)85<273:GEOTSN>2.0.CO;2](https://doi.org/10.1130/0016-7606(1974)85<273:GEOTSN>2.0.CO;2)
- Vermeesch, P. 2012. On the visualization of detrital age distributions. *Chemical Geology*, 312–313: 190–194. <https://doi.org/10.1016/j.chemgeo.2012.04.021>
- Villagómez, D. & Spikings, R. 2013. Thermochronology and tectonics of the Central and Western Cordilleras of Colombia: Early Cretaceous – Tertiary evolution of the northern Andes. *Lithos*, 160–161: 228–249. <https://doi.org/10.1016/j.lithos.2012.12.008>
- Villagómez, D., Spikings, R., Mora, A., Guzmán, G., Ojeda, G., Cortés, E. & van der Lelij, R. 2011. Vertical tectonics at a continental crust–oceanic plateau plate boundary zone: Fission track thermochronology of the Sierra Nevada de Santa Marta, Colombia. *Tectonics*, 30(4): 1–18. <https://doi.org/10.1029/2010TC002835>
- Vinasco, C.J., Cordani, U.G., González, H., Weber, M. & Peláez, C. 2006. Geochronological, isotopic, and geochemical data from Permo – Triassic granitic gneisses and granitoids of the Colombian central Andes. *Journal of South American Earth Sciences*, 21(4): 355–371. <https://doi.org/10.1016/j.jsames.2006.07.007>
- Weber, M., Cardona, A., Paniagua, F., Cordani, U., Sepúlveda, L. & Wilson, R. 2009. The Cabo de la Vela mafic–ultramafic complex, northeastern Colombian Caribbean region: A record of multistage evolution of a Late Cretaceous intra–oceanic arc. In: James, K.H., Lorente, M.A. & Pindell, J.L. (editors), *The origin and evolution of the Caribbean Plate*. Geological Society of London, Special Publication 328, p. 549–568. <https://doi.org/10.1144/SP328.22>
- Yarce, J., Monsalve, G., Becker, T.W., Cardona, A., Poveda, E., Alvira, D. & Ordóñez–Carmona, O. 2014. Seismological observations in northwestern South America: Evidence for two subduction segments, contrasting crustal thicknesses and upper mantle flow. *Tectonophysics*, 637: 57–67. <https://doi.org/10.1016/j.tecto.2014.09.006>

Explanation of Acronyms, Abbreviations, and Symbols:

AFT	Apatite fission-track	ND	Number of induced tracks counted in the mica for estimating Rho-D
AHe	(U-Th)/He in apatites	NI	Number of induced tracks counted for estimating Rho-I
CAPES	Coordination for the Improvement of Higher Education Personnel	NS	Number of spontaneous tracks counted for estimating Rho-S
ESR	Equivalent-sphere radius	Rho-D	Induced track density
eU	Effective uranium content	Rho-I	Induced tracks density measured
IEE-USP	Institute of Energy and Environment, Universidade de São Paulo	Rho-S	Spontaneous tracks density measured
IGc-USP	Institute of Geosciences, Universidade de São Paulo	SNSM	Sierra Nevada de Santa Marta
IPEN-USP	Institute of Energy and Nuclear Research, Universidade de São Paulo	SRTM 90	Shuttle Radar Topography Mission – Resolution 90 meters
LLH	Log-likelihood function	TRMM	Tropical Rainfall Measuring Mission
LMB	Lower Magdalena Basin	ZFT	Zircon fission-track
		ZHe	(U-Th)/He in zircons

Authors' Biographical Notes



Mauricio PARRA is an Assistant Professor at the Instituto de Energia e Ambiente of the Universidade de São Paulo, where he leads the Low-Termochronology Laboratory. He received his BS in geology from the Universidad Nacional de Colombia and his PhD from the Institut für Geowissenschaften, Universität Potsdam. His research focuses on the tectonic evolution of mountain belts

using thermochronometry and sedimentary basin analysis.



Ana María PATIÑO is graduated from the Universidad Nacional de Colombia Sede Medellín. She received a master's degree in Earth sciences at the Universidade de São Paulo, Brasil. She has worked with regional geology issues employing techniques such as geochronology and low-temperature thermochronology. Her research interests include tectonic geology, orogenetic processes, and landscape evolution.



Sebastián ECHEVERRI is a geologist from the Universidad de Caldas, with an MS in Earth sciences from the same university and PhD in science and geotectonics from the Universidade de São Paulo, Brasil. Sebastián works as a researcher in the Grupo de Investigación en Estratigrafía y Vulcanología (GIEV) Cumanday-Instituto de Investigaciones en Estratigrafía (IIES) at the Universidad

de Caldas and is part of the EGEO research group at the Universidad Nacional Sede Medellín. His main research area is the regional geology and tectonostratigraphic evolution of convergent margins.



Juan Carlos RAMÍREZ is a doctoral candidate at the Universidade de São Paulo working on thermal modeling of the Eastern Cordillera of Colombia and adjacent basins. He received his BS and MS degrees in geology from the Universidad Industrial de Santander. He has worked as a consulting geologist for the oil industry in Colombia, including research topics such as stratigraphy, structural geology, basin analysis, and thermochronology.



Andrés MORA is the technical leader of onshore Colombia and foothills exploration at Ecopetrol. He received his BS in geology from the Universidad Nacional de Colombia and PhD from the Institut für Geowissenschaften, Universität Potsdam. His research interests include structural geology, petroleum exploration, and petroleum geology.



Edward R. SOBEL is the thermochronology professor at the Universität Potsdam. He is responsible for running the thermochronology laboratories, including the fission-track lab and the helium extraction line for (U–Th)/He thermochronology. His research interests focus on constraining deformation and exhumation histories by using multiple thermochronometers combined

with geologic, topographic, and climatic data with the aim of understanding the underlying tectonic history and the interactions between tectonic and surface processes. In a larger sense, his research has focused on basin analysis, sedimentology, thermochronology, regional tectonics, and near-surface processes, primarily in the Central Andes and Central Asia.



Ariel ALMENDRAL is a senior research scientist working at the Norwegian Computing Center in Oslo, Norway. His main areas of expertise include stochastic fault/subsurface modeling, history matching, and facies modeling. He holds a PhD from the Universitet i Oslo in the field of numerical mathematics applied to financial derivatives. He also worked in thermokinematic basin modeling in an earlier position as a consultant for the Instituto Colombiano del Petróleo.



Andrés PARDO-TRUJILLO is a geologist in the Departamento de Ciencias Geológicas at the Universidad de Caldas (Manizales, 1998). Andrés obtained his MS in vegetal micropaleontology in 1997 and his PhD in Science from Liège University (Belgium, 2004). He has worked since 1989 as a professor in the Departamento de Ciencias Geológicas at Universidad de Caldas, Colombia, in

sedimentology, regional geology, palynology, and field geology. From 2006–2009, he worked as an advisor at the Agencia Nacional de Hidrocarburos (ANH), where he participated in the geological study of several Colombian sedimentary basins. Andrés is currently the director of the Instituto de Investigaciones en Estratigrafía (IIES) and of the Grupo de Investigación en Estratigrafía y Vulcanología (GIEV) at the Universidad de Caldas. His main interest is the study of the geological and biological evolution of the NW corner of South America during the Cretaceous – Cenozoic.

Chapter 8



Cenozoic Geologic Evolution of the Southern Tumaco Forearc Basin (SW Colombian Pacific)

<https://doi.org/10.32685/pub.esp.37.2019.08>

Published online 26 November 2020

Andrés PARDO-TRUJILLO^{1*} , Sebastián ECHEVERRI² , Carlos BORRERO³ , Alejandro ARENAS⁴ , Felipe VALLEJO⁵ , Raúl TREJOS⁶ , Ángel PLATA⁷ , José-Abel FLORES⁸ , Agustín CARDONA⁹, Sergio RESTREPO¹⁰ , Ángel BARBOSA¹¹ , Hugo MURCIA¹² , Carlos GIRALDO¹³ , Sergio CELIS¹⁴ , and Sergio A. LÓPEZ¹⁵

Abstract Tumaco is a forearc basin that contains insights into the Cenozoic geologic evolution of SW Colombia. In this region, the subduction of the Farallon and Nazca Plates beneath the South American Plate have controlled subsidence and magmatic activity during the Oligocene to recent times. A synthesis of seismic, stratigraphic, petrographic, geochronologic, and biostratigraphic data from outcrops and wells is presented. The Tumaco onshore basin has a trough-shaped symmetric geometry limited to the east by the Western Cordillera and to the west by the Remolino Grande-Gorgona Structural High. ca. 8000 m of sediments were accumulated in its depocenter during the Cenozoic. The sedimentites are composed of mudrocks, sandstones, and conglomerates, which vary in their proportions over time, and were mainly accumulated in open marine and deltaic environments. Calcareous nannofossils, foraminifera, and palynomorphs allowed assignment of the depositional time of the sedimentary units; however, the low abundance, preservation, and reworking of microfossils in some intervals require the use of multi-tools to determine the age of the deposits.

Sandstones are mainly litharenites and feldspathic litharenites, are texturally immature, and are composed of cherts fragments, basic to intermediate volcanic fragments, and crystals such as feldspars (Na and K), pyroxene, amphibole, and biotite, which can be associated with basic-intermediate volcanic, plutonic, and sedimentary rocks of the current basement of Western Cordillera. Sediment provenance analysis (detrital zircon and heavy minerals) suggests continuous volcanism from late Oligocene to Pleistocene times, the activity of which has increased since the middle Miocene. The presence of low percentages of pre-Cenozoic zircons and metamorphic rock fragments in the Miocene units are related to reworking of ancient sedimentary units or to a partial connection with the Central Cordillera basement. The study of Miocene – Pliocene outcrops and well cores allows the interpretation of a shallowing of the basin during the Messinian – Zanclean times. Volcanoclastic fans, as well as fluvial and coastal sediments, associated with the current Patía and Mira Rivers are partially covering the Miocene – Pliocene deposits.

Keywords: Tumaco Basin, sedimentary provenance, biostratigraphy, Colombian Pacific, Cenozoic.

Citation: Pardo-Trujillo, A., Echeverri, S., Borrero, C., Arenas, A., Vallejo, F., Trejos, R., Plata, Á., Flores, J.A., Cardona, A., Restrepo, S., Barbosa, Á., Murcia, H., Giraldo, C., Celis, S., & López, S.A. 2020. Cenozoic geologic evolution of the southern Tumaco Forearc Basin (SW Colombian Pacific). In: Gómez, J. & Mateus-Zabala, D. (editors), *The Geology of Colombia, Volume 3 Paleogene – Neogene. Servicio Geológico Colombiano, Publicaciones Geológicas Especiales 37*, p. 215–247. Bogotá. <https://doi.org/10.32685/pub.esp.37.2019.08>

- 1 andres.pardo@ucaldas.edu.co
Universidad de Caldas
Departamento de Ciencias Geológicas
Instituto de Investigaciones en Estratigrafía-IIES
Grupo de Investigación en Estratigrafía y Vulcanología-GIEV
Calle 65 n.º 26-10
Manizales, Colombia
- 2 sebastian.echeverri@usp.br
Universidad de Caldas
Instituto de Investigaciones en Estratigrafía-IIES
Grupo de Investigación en Estratigrafía y Vulcanología-GIEV
Calle 65 n.º 26-10
Manizales, Colombia
- 3 borrero_c@yahoo.com
Universidad de Caldas
Departamento de Ciencias Geológicas
Instituto de Investigaciones en Estratigrafía-IIES
Grupo de Investigación en Estratigrafía y Vulcanología-GIEV
Calle 65 n.º 26-10
Manizales, Colombia
- 4 alejandro.arenas@ucaldas.edu.co
Universidad de Caldas
Instituto de Investigaciones en Estratigrafía-IIES
Grupo de Investigación en Estratigrafía y Vulcanología-GIEV
Calle 65 n.º 26-10
Manizales, Colombia
- 5 diego.vallejo@ucaldas.edu.co
Universidad de Caldas
Instituto de Investigaciones en Estratigrafía-IIES
Grupo de Investigación en Estratigrafía y Vulcanología-GIEV
Calle 65 n.º 26-10
Manizales, Colombia
- 6 raul.trejos@ucaldas.edu.co
Universidad de Caldas
Instituto de Investigaciones en Estratigrafía-IIES
Grupo de Investigación en Estratigrafía y Vulcanología-GIEV
Calle 65 n.º 26-10
Manizales, Colombia
- 7 angeloplat@icloud.com
Universidad de Caldas
Instituto de Investigaciones en Estratigrafía-IIES
Grupo de Investigación en Estratigrafía y Vulcanología-GIEV
Calle 65 n.º 26-10
Manizales, Colombia
- 8 flores@usal.es
Universidad de Salamanca
Grupo de Geociencias Oceánicas

- 9 agcardonamo@unal.edu.co
Universidad Nacional de Colombia
Sede Medellín
Facultad de Minas
Medellín, Colombia
- 10 sarestrepom@unal.edu.co
Universidad Nacional de Colombia
Medellín, Colombia
- 11 dunito8@hotmail.com
Universidad de Caldas
Instituto de Investigaciones en Estratigrafía-IIES
Grupo de Investigación en Estratigrafía y Vulcanología-GIEV
Calle 65 n.º 26-10
Manizales, Colombia
University of Florida
Gainesville, USA
- 12 hugo.murcia@ucaldas.edu.co
Universidad de Caldas
Departamento de Ciencias Geológicas
Instituto de Investigaciones en Estratigrafía-IIES
Grupo de Investigación en Estratigrafía y Vulcanología-GIEV
Calle 65 n.º 26-10
Manizales, Colombia
- 13 klichegiraldo@gmail.com
Universidad de Caldas
Instituto de Investigaciones en Estratigrafía-IIES
Grupo de Investigación en Estratigrafía y Vulcanología-GIEV
Calle 65 n.º 26-10
Manizales, Colombia
- 14 sergio.celis@ucaldas.edu.co
Universidad de Caldas
Instituto de Investigaciones en Estratigrafía-IIES
Grupo de Investigación en Estratigrafía y Vulcanología-GIEV
Calle 65 n.º 26-10
Manizales, Colombia
- 15 seadlois@gmail.com
Agencia Nacional de Hidrocarburos
- * Corresponding author

Resumen Tumaco es una cuenca de frente de arco que guarda información sobre la evolución geológica cenozoica del SW de Colombia. En esta región, la subducción de las placas de Farallón y de Nazca bajo la Placa de Suramérica ha controlado la subsidencia y actividad magmática durante el Oligoceno al reciente. Se presenta una síntesis de datos sísmicos, estratigráficos, petrográficos, geocronológicos y bioestratigráficos obtenidos a partir de afloramientos y pozos. La Cuenca Tumaco costa adentro tiene una geometría de artesa simétrica limitada al este por la cordillera Occidental y al oeste por el Alto Estructural Remolino Grande–Gorgona. Alrededor de 8000 m de sedimentos fueron acumulados en su depocentro durante el Cenozoico. Las sedimentitas corresponden a lodolitas, arenitas y conglomerados, que varían en su proporción a través del tiempo, y fueron principalmente acumuladas en ambientes marinos abiertos y deltaicos. Los nanofósiles calcáreos, foraminíferos y palinomorfs permitieron controlar la edad de acumulación de las unidades sedimentarias; sin embargo, debido a su baja abundancia y preservación y al retrabajamiento de microfósiles en algunos intervalos, se requiere el uso de herramientas múltiples para determinar la edad de los depósitos.

Las arenitas son principalmente litoarenitas y litoarenitas feldespáticas, texturalmente inmaduras y compuestas por fragmentos de chert, fragmentos volcánicos básicos a intermedios y cristales, tales como feldespato (Na y K), piroxeno, anfíbol y biotita, los cuales pueden asociarse con las rocas volcánicas básicas–intermedias, plutónicas y sedimentarias del actual basamento de la cordillera Occidental. El análisis de procedencia (circones detríticos y minerales densos) sugiere vulcanismo continuo desde el Oligoceno tardío al Pleistoceno, con incremento en la actividad desde el Mioceno medio. La presencia de bajos porcentajes de circones precenozoicos y fragmentos de rocas metamórficas en las unidades del Mioceno puede estar relacionada con el retrabajamiento de unidades sedimentarias antiguas o con una conexión parcial con el basamento de la cordillera Central. El estudio de afloramientos del Mioceno–Plioceno y núcleos de pozo permite interpretar una somerización de la cuenca durante el Mesiniano–Zancliano. Abanicos volcanoclásticos, así como sedimentos fluviales y costeros, asociados a los ríos Patía y Mira se encuentran cubriendo parcialmente los depósitos miocenos–pliocenos.

Palabras clave: Cuenca Tumaco, procedencia sedimentaria, bioestratigrafía, Pacífico colombiano, Cenozoico.

1. Introduction

The Tumaco Basin is part of a series of forearc basins located in the Pacific margin of the northern Andes (SW Colombia), where the Nazca and South American Plates have interacted at least since the Miocene (Aleman & Ramos, 2000; Barrero et al., 2007; Borrero et al., 2012; Hall & Wood, 1985; López–Ramos, 2009; Ramos, 1999). The basin axis has an ~N30°E orientation, which is parallel to the current arc system and the Colombian Pacific subduction zone (Figure 1). Tumaco Basin is divided by the Remolino Grande–Gorgona Structural High into onshore and offshore basins (Figure 1), also called the Manglares Basin by some authors (e.g., López–Ramos, 2009; Marcaillou & Collot, 2008). This region is characterized by a low relief and dense rain forest that has prevented the performance of systematic geological studies; thus, its geological history has remained poorly understood. The available geological maps are mainly based on geomorphology and scarce field and chronologic control (e.g., Nivia et al., 2003). In addition, most of the sedimen-

tary deposits of the basin are below the surface. Therefore, the spatial and temporal relationships of the stratigraphic units are not well known. The presence of hydrocarbon shows within wells and outcrops indicates the existence of an active petroleum system (Barrero et al., 2007). Thus, oil exploration studies are the major source of information for the geology of the basin (e.g., López–Ramos, 2009; Suárez, 1990, 2007). Nevertheless, much of this information remains private and unpublished.

The basement of the Tumaco Basin is composed of Cretaceous basic igneous and sedimentary rocks, formed in the eastern Pacific and accreted to the continental margin of South America during the Late Cretaceous – Paleogene (Echeverri et al., 2015a; Spikings & Simpson, 2014; Villagómez et al., 2011). It is uncomfortably covered by siliciclastic and volcanoclastic rocks deposited from Eocene to Pliocene times (Barrero et al., 2007; Borrero et al., 2012; Echeverri, 2012; López–Ramos, 2009; Marín–Cerón & Sierra, 2011; Suárez, 1990, 2007). These Cenozoic rocks can reach more than 8000 m in the depocenter of the basin (Agencia Nacional de Hidrocarburos & Universi-

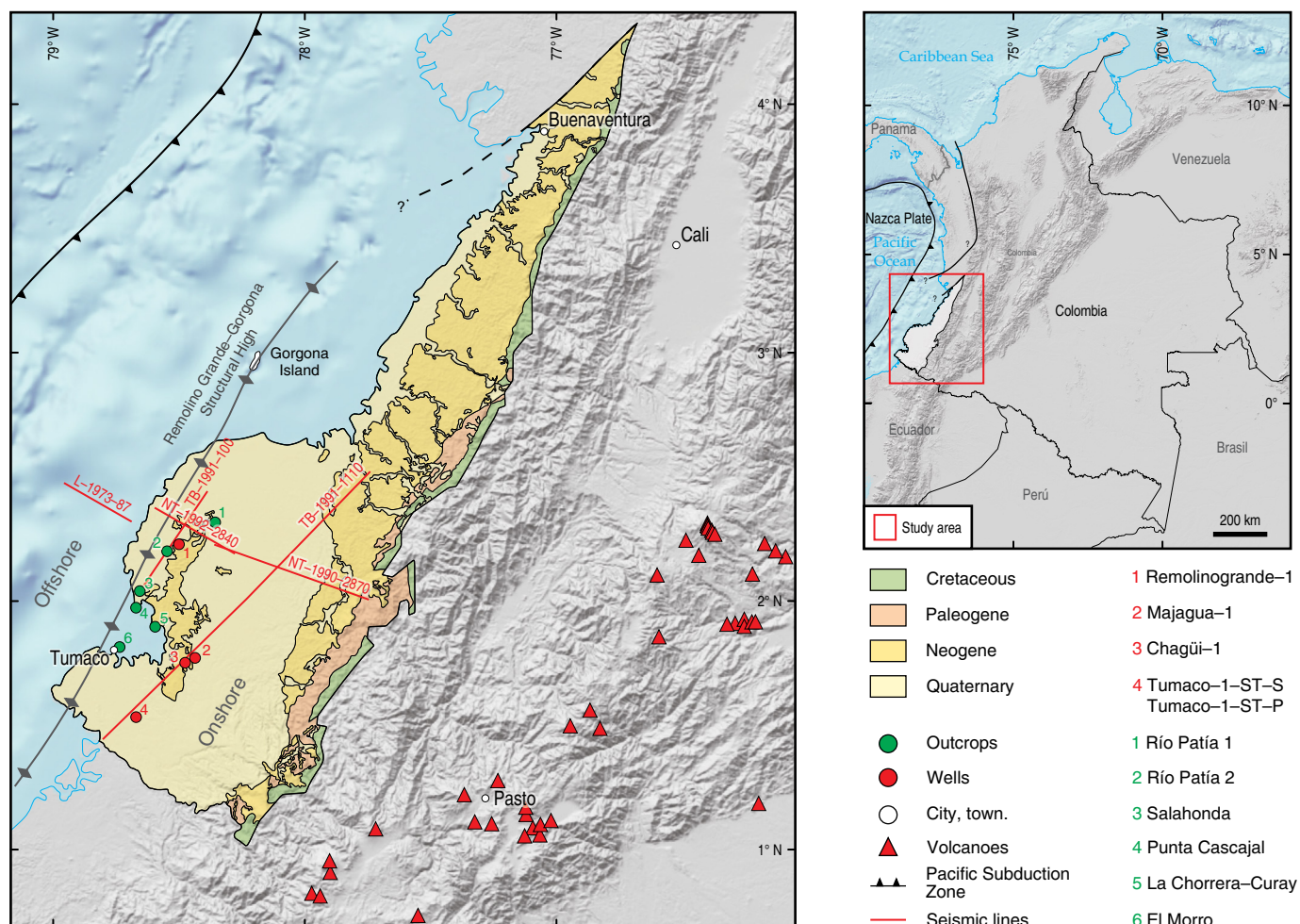


Figure 1. Location of the Tumaco Basin (yellow color) and studied localities mentioned in the text.

dad de Caldas, 2011a; Suárez, 1990, 2007). Neogene units are characterized by thick fluvial and deltaic siliciclastic deposits, which have been particularly considered for hydrocarbon explorations (Agencia Nacional de Hidrocarburos & Antek, 2013; Cediel et al., 2009; Echeverri, 2012; García, 2012; López-Ramos, 2009; Suárez, 1990, 2007).

Due to scarce information from the Pacific basins, in 2008, the Agencia Nacional de Hidrocarburos (ANH) initiated a campaign to drill wells in different sectors of these basins (e.g., ANH-Tumaco 1-ST-S and 1-ST-P wells and Buenaventura 1-ST-P) to investigate their petroleum systems. New geological information from wells and outcrops collected in recent multi-disciplinary studies carried out by the Universidad de Caldas and the ANH (Agencia Nacional de Hidrocarburos & Universidad de Caldas, 2011a, 2011b) shed light on the geological history of the basin. A total of 1544 analyses were performed, including biostratigraphy (palynology, foraminifera, and calcareous nanofossils), petrography, and geochronology (U/Pb, Ar/Ar, and K/Ar methods). The integration of these results along with unpublished reports and published data (Bedoya et al., 2013; Borrero et al., 2012; Echeverri et al., 2015a, 2015b, 2016) allowed an

age model to be established and the provenance and paleoenvironment for the sedimentary rocks of the basin to be illustrated.

2. Stratigraphy of the Tumaco Basin

Different stratigraphic nomenclatures have been proposed for the sedimentary rocks of the Tumaco Basin (Figure 2). Regional studies of the Servicio Geológico Colombiano (Arango & Ponce, 1980) used the stratigraphic model established by van der Hammen (1958), which was based on previous descriptions made by Oppenheim (1949). van der Hammen (1958) reported that the Guapi Formation (Pliocene) uncomfortably overlays the Miocene Naya Formation (Figure 2). Later, using mainly seismic and well information, Suárez (1990) proposed four lithostratigraphic units that have served as references for recent studies (e.g., Agencia Nacional de Hidrocarburos & Universidad de Caldas, 2011a; Borrero et al., 2012; Escovar et al., 1992). This author compared the sedimentary record of the Tumaco Basin to the neighboring Borbón Basin in Ecuador, defining several units from base to top: (i) 1 Sur Unit Formation (Oligocene); (ii) Cayapas, Viche, and Angostura Formations (lower

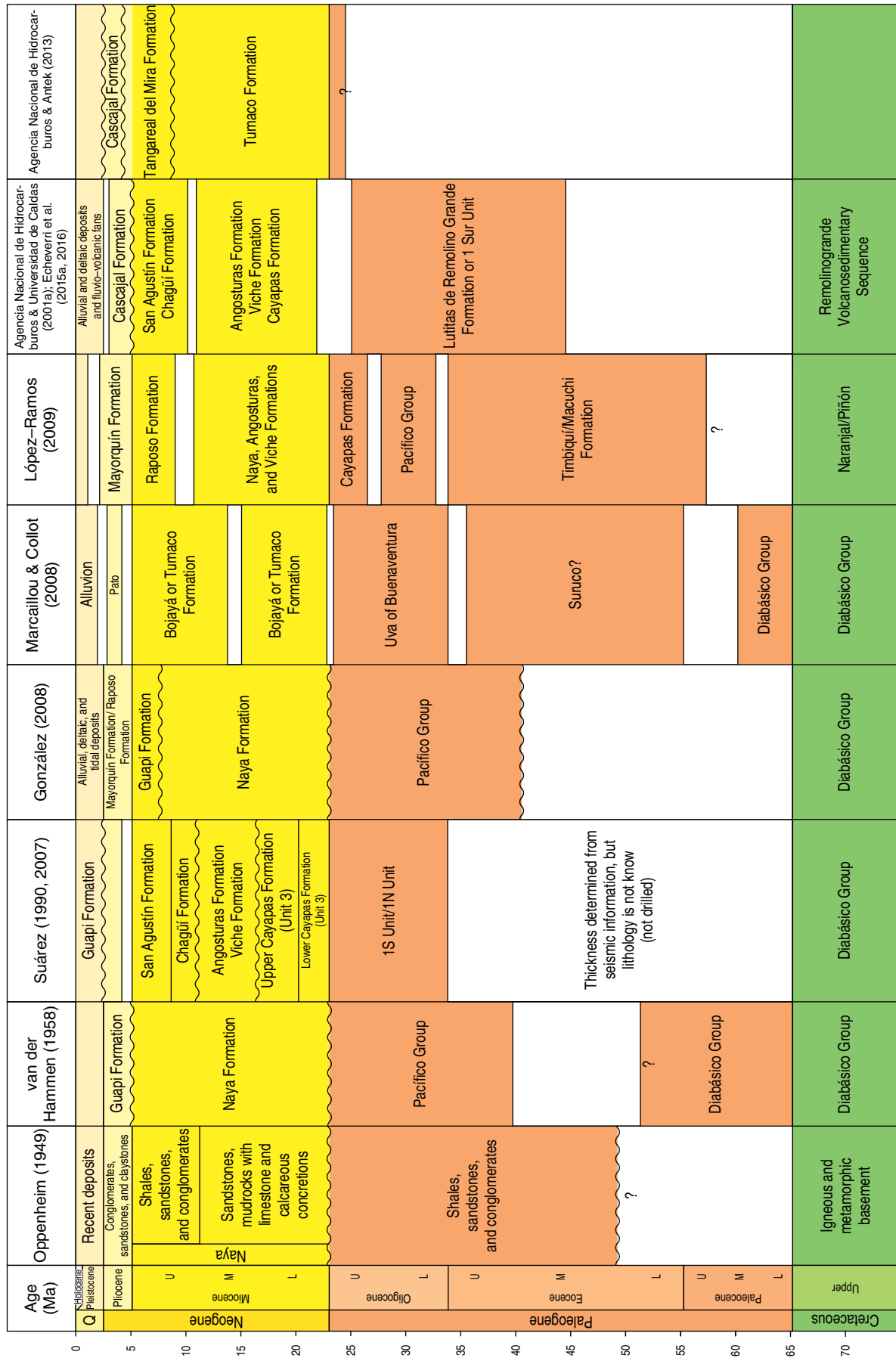


Figure 2. Chronostratigraphic chart showing the different stratigraphic nomenclatures employed for the Tumaco Basin.

– middle Miocene); (iii) Chagüí and San Agustín Formations (middle/upper Miocene – lower Pliocene); and (iv) Guapi Formation (Pliocene). Subsequently, Nivia et al. (2003) separated the youngest alluvial and deltaic deposits from the Guapi Formation, defining as Cascajal and Curay Members those underlying Pliocene and Miocene sedimentary deposits in the Nariño Department. Echeverri et al. (2016) proposed the term Cascajal Formation for the volcanoclastic rocks of the Messinian – Zanclean age reported by Nivia et al. (2003) (Figure 2). In contrast, in the northern part of the Tumaco Basin, Aspden (1984) and Aspden & Nivia (1985) proposed to divide the Neogene sedimentary cover into two formations: (i) Mayorquín Formation, composed mainly of mudrocks, and (ii) Raposo Formation, with conglomerates and sandstones. The stratigraphic and chronostratigraphic relationships of these units are unclear due to the low–biostratigraphic resolution and the absence of continuous outcrops. This has caused difficulties in performing regional correlations between southern and northern units (González, 2008; Instituto Colombiano de Geología y Minería & Instituto Geográfico Agustín Codazzi, 2005; López–Ramos, 2009; Nivia et al., 2003). Although Borrero et al. (2012) followed the stratigraphic nomenclature proposed by Suárez (1990), they grouped the sedimentary record into two megasequences, the Oligocene – middle Miocene sedimentary megasequence and the late Miocene – Holocene volcanoclastic megasequence. Finally, Agencia Nacional de Hidrocarburos & Antek (2013) informally proposed the names Tumaco and Tangareal del Mira Formations for upper Oligocene and Neogene deltaic deposits associated with the paleo–Patía and Mira Rivers (Figure 2). In this chapter, we will use the nomenclature of Borrero et al. (2012), Echeverri et al. (2011), and Echeverri et al. (2016).

3. Materials and Methods

3.1. Stratigraphy and Seismic Data

The stratigraphic information was obtained from electrical logs, ditch cutting, and core samples from the Remolino Grande–1 (total depth (TD) 9080'–2767 m), Majagua–1 (TD 14 280'–4352 m), and Tumaco 1–ST–S (TD 1899.6'–579 m) wells. This information was also integrated with data from outcrops located in the Tumaco Bay (e.g., Echeverri et al., 2016), with previous results reported by Suárez (1990) and López–Ramos (2009) and data from the ANH Tumaco 1–ST–P well (Agencia Nacional de Hidrocarburos & Antek, 2013). The well cores and cuttings are stored at the national core repository of Colombia (Litoteca Nacional, Piedecuesta, Santander).

Two regional seismic profiles were analyzed (Figure 3): (i) Perpendicular to the basin (dip lines) and composed of three seismic lines and (ii) more or less parallel to the strike of the basin (strike lines) and composed of two seismic lines (Figures 1, 3). These data were processed with GeoGraphix, where

the main seismic reflectors and structures were identified (e.g., faults, folds, onlaps, toplaps, progradations). These reflectors were tied with the stratigraphic information of the Remolino Grande–1, Majagua–1, and Tumaco 1–ST–P wells. Additionally, as far as possible, the reflectors were tied with the surface geology map of Gómez et al. (2015). Subsequently, five horizons that represent chronostratigraphic boundaries were identified: (i) Cretaceous/Paleogene, (ii) Paleogene/lower Miocene, (iii) lower/middle Miocene, (iv) middle/upper Miocene, and (v) upper Miocene – Pliocene. Lower Miocene includes the Aquitanian and Burdigalian Stages; the middle Miocene, the Langian – Serravalian; and the upper Miocene, the Tortonian – Messinian.

3.2. Biostratigraphy

Biostratigraphic interpretations are based on distribution patterns and semiquantitative analyses of calcareous nannofossils and planktonic foraminifera reported for Majagua–1, Remolino Grande–1, Tumaco 1–ST–S, and Tumaco 1–ST–P wells (Agencia Nacional de Hidrocarburos & Antek, 2013; Agencia Nacional de Hidrocarburos & Universidad de Caldas, 2011a; Robertson Research inc. & Empresa Colombiana de Petróleos, 1981a, 1981b). The quality of the microfossil record was evaluated, and a composite section was built in which assemblages and age–indicative taxa were indicated. Biostratigraphic models were constructed using the standard biozones proposed by Blow (1969) and Berggren et al. (1995) for planktonic foraminifera and by Martini (1971) and Okada & Bukry (1980) for calcareous nannofossils. The biochronology of calcareous microfossil events follows the integrated scales of Agnini et al. (2014), Backman et al. (2012), Lourens et al. (2004), Raffi et al. (2006), and Wade et al. (2011). Taxonomical and biostratigraphic information described by Aubry (2014, 2015), Kennett & Srinivasan (1983), and Perch–Nielsen (1985) were also considered in the biostratigraphic interpretations. Biochronology of calcareous microfossil events follows the integrated scales of Agnini et al. (2014), Backman et al. (2012), Lourens et al. (2004), Raffi et al. (2006), and Wade et al. (2011). Taxonomical and biostratigraphic information described by Aubry (2014, 2015), Kennett & Srinivasan (1983), and Perch–Nielsen (1985) were also considered in the biostratigraphic models.

Most micropaleontological results were obtained from cutting samples, which in some cases (e.g., Remolino Grande–1) were collected at very large spacing, making its biostratigraphic interpretation difficult. Nevertheless, by integrating both calcareous nannofossils and planktonic foraminifera, it was possible to constrain the age from most of the wells. To achieve a more accurate age model, some considerations were taken in account. (i) Since the examined wells are composed of cuttings and cores that showed very abundant reworked microfossils, biostratigraphic analyses did not include specimens whose oc-

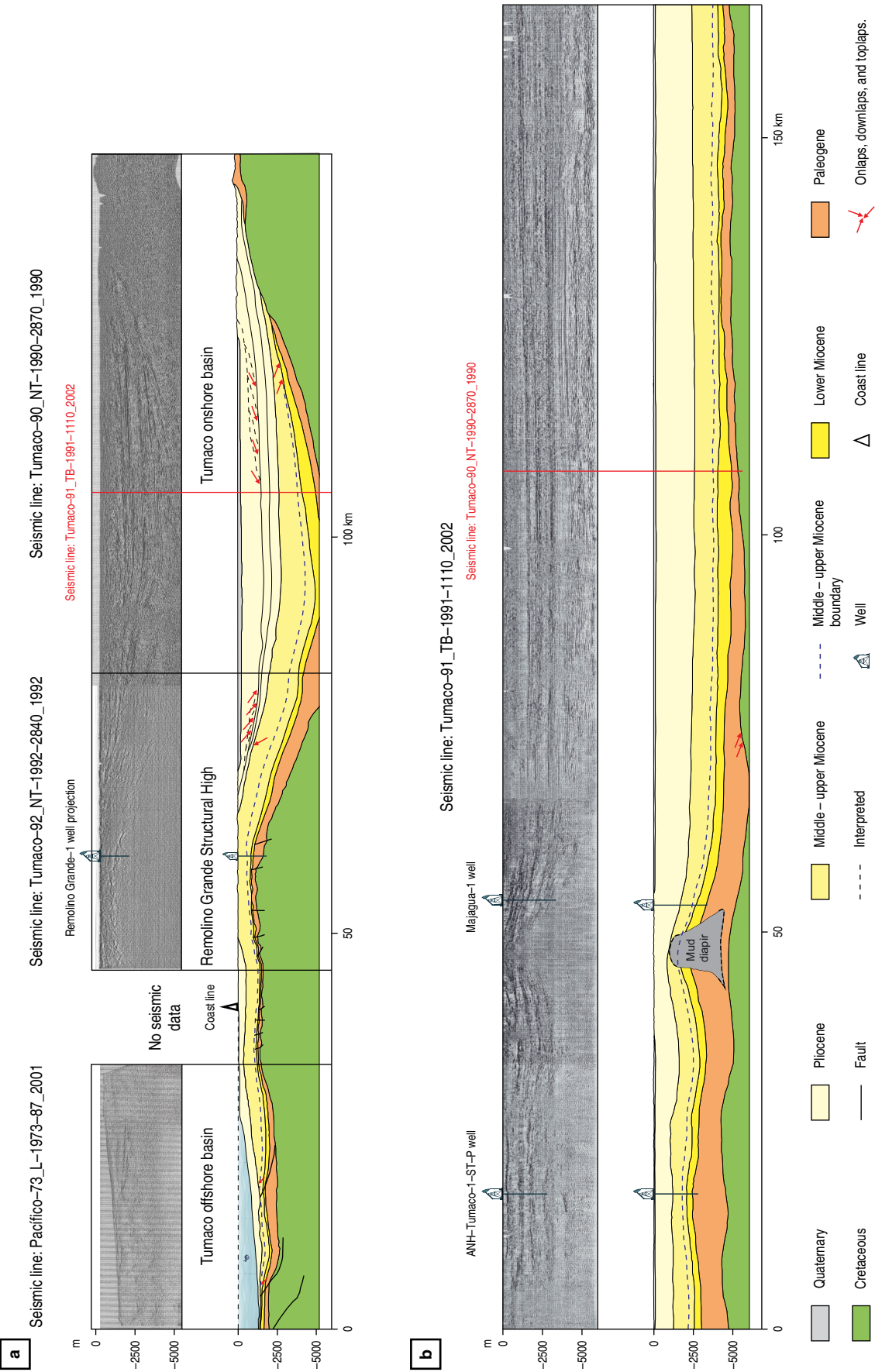


Figure 3. Geological cross-section of Tumaco, Western Cordillera, and Patia Basins based on seismic lines geologic mapping and well data. **(a)** Dip line. **(b)** Strike line. See Figure 1 for locations.

currence was very discontinuous or was observed in only one sample. (ii) Acmes or paracmes, which are regularly used as bioevents in studies of deep-sea sections, were not considered in our results. The fine-grained matrix regularly recorded in the material provokes a dilution, preventing the quantitative signal (Bedoya et al., 2013). (iii) Those stratigraphic intervals lacking biostratigraphic markers but bracketed by confirmed biozones were illustrated as intervals of indeterminate age because there was no micropaleontological support.

3.3. Sediment Provenance Analyses

A total of 30 grams of dried well cuttings was collected for petrographic analyses. This represents a 10-foot interval (3048 m) for the Majagua-1 well and intervals of 10', 20', and 30' for the Remolino Grande-1 well. Wet cutting samples were washed to remove contamination from the drilling process. Subsequently, a selection of very-fine sand to coarse-sand particles from cuttings was collected and mounted on glass slides and cover slips using balsam of Canada for petrographic analyses. A total of 82 thin sections were studied for petrography using ditch cutting samples: 26 from the well Remolino Grande-1, 38 from the well Majagua-1, and 18 from the well Chagüí-1. On average, 250 and 300 grains per slide were identified and counted. These data are represented in bar diagrams showing the relative percentages of the main components. Subsequently, the sandstones with a framework higher than 50% were selected to count their individual particles and to quantify the composition and are represented in Qt-F-L and Qm-F-Lt triangles of Folk (1974).

For heavy minerals and U/Pb geochronologic analyses, samples of ca. 1000 gr of dried cuttings were collected along tens to hundreds of feet and integrated in a single sample. The fraction $> 63 < 250 \mu\text{m}$ was concentrated with sodium polytungstate (density of 2.89 g/cm^3) for heavy mineral analyses. In each sample, a thin section was made using a resin with a refraction index similar to balsam of Canada (1.539). A count of ca. 400 grains per slide was performed following the Ribbon-Counting method (Mange & Maurer, 1992). Mineralogical identification was based on Mange & Maurer (1992). The data obtained are represented in bar and triangular diagrams.

U/Pb geochronology was performed using the laser ablation inductively coupled plasma mass spectrometry (LA-ICPMS) method at a Washington State University Lab (USA). The samples were crushed and sieved (ca. $400\text{-}\mu\text{m}$ mesh). Zircon concentration was initially made following the gravitational methods on a Wifley table, passed through a Frantz magnetic separator and finally separated using methylene iodide. Approximately 100 grains per sample were analyzed in agreement with Gehrels et al. (2006). Separated zircons were mounted on an epoxy resin, manually polished and randomly studied. The maximum depositional U/Pb ages in detrital zircons were performed using the method described by Dickinson & Gehrels

(2009). This age was acquired from the average of at least three grains of zircons with concordant ages (Kochek et al., 2011). These results were plotted in relative probability diagrams using Isoplot 3.00 (Ludwing, 2003). $^{206}\text{Pb}/^{238}\text{U}$ ages were used for grains less than 1000 Ma, and $^{206}\text{Pb}/^{207}\text{Pb}$ ages were used for grains greater than 1000 Ma. Grains with more than 10% of discordance were not considered in the statistical analysis.

4. Results

The seismic lines show that the Tumaco onshore basin has a symmetric through shape limited to the E by the Western Cordillera and to the W by the Remolino Grande-Gorgona Structural High. Subhorizontal seismic reflectors indicate little deformation of the sedimentary sequence. However, in the southern sector of the basin, there is a structure at least 10 km wide that truncates the Paleogene and Neogene strata that has been interpreted as a mud diapir (Figure 3b; Cediel et al., 2009). In the depocenter, a thickness of 6805' (2074 m) is estimated for the Paleogene beds; 5713' (2546 m), for the lower - middle Miocene; and 11986 (3653.3 m), for the upper Miocene - Pliocene (Figure 3a, 3b). Calcareous microfossils are moderately to poorly preserved. Even though the sedimentary record was highly discontinuous, Majagua-1, Remolino Grande-1, and Tumaco 1-ST-P wells covered the largest stratigraphic record (Figures 4, 5). Calcareous microfossils suggest ages spanning from Bartonian (middle Eocene) in the Remolino Grande-1 well up to Pleistocene in the Tumaco 1-ST-P samples (Figures 4, 5). Miocene is the most common interval drilled by the wells, allowing the definition and correlation of different biostratigraphic intervals along the basin (Figures 4, 5). According to the biostratigraphic data in wells and seismic lines, the Tumaco Basin was divided into six chronostratigraphic sequences (Figure 3): (i) Upper Cretaceous, (ii) Paleogene (including Eocene and Oligocene beds), (iii) lower Miocene, (iv) middle Miocene, (v) upper Miocene - Pliocene, and (vi) Pliocene - Quaternary.

4.1. Upper Cretaceous

This series includes the volcano-sedimentary succession of Remolino Grande (Turonian - Campanian) (5630-9080'; 1716-2767 m) (Figure 3). This succession may be divided into two segments: (i) the lower segment, composed of mudrocks and fine sandstones interbedded with basalts and microgabbros, and (ii) the upper segment, formed by layers of basalts and microgabbros. Robertson Research inc. & Empresa Colombiana de Petróleos (1981b) provided a radiometric age in the interval 7250-7260' (2209-2212 m) of $82.2 \pm 8.1 \text{ Ma}$ (K/Ar in total rock). New Ar/Ar geochronological data (Agencia Nacional de Hidrocarburos & Universidad de Caldas, 2011a; Echeverri et al., 2015a) yield ages of $82.9 \pm 4.8 \text{ Ma}$ (6540-6550' or 1993-1996 m) and $76.2 \pm 1.4 \text{ Ma}$ (5680-5690', or 1731-1734 m) (Figure 4). These ages

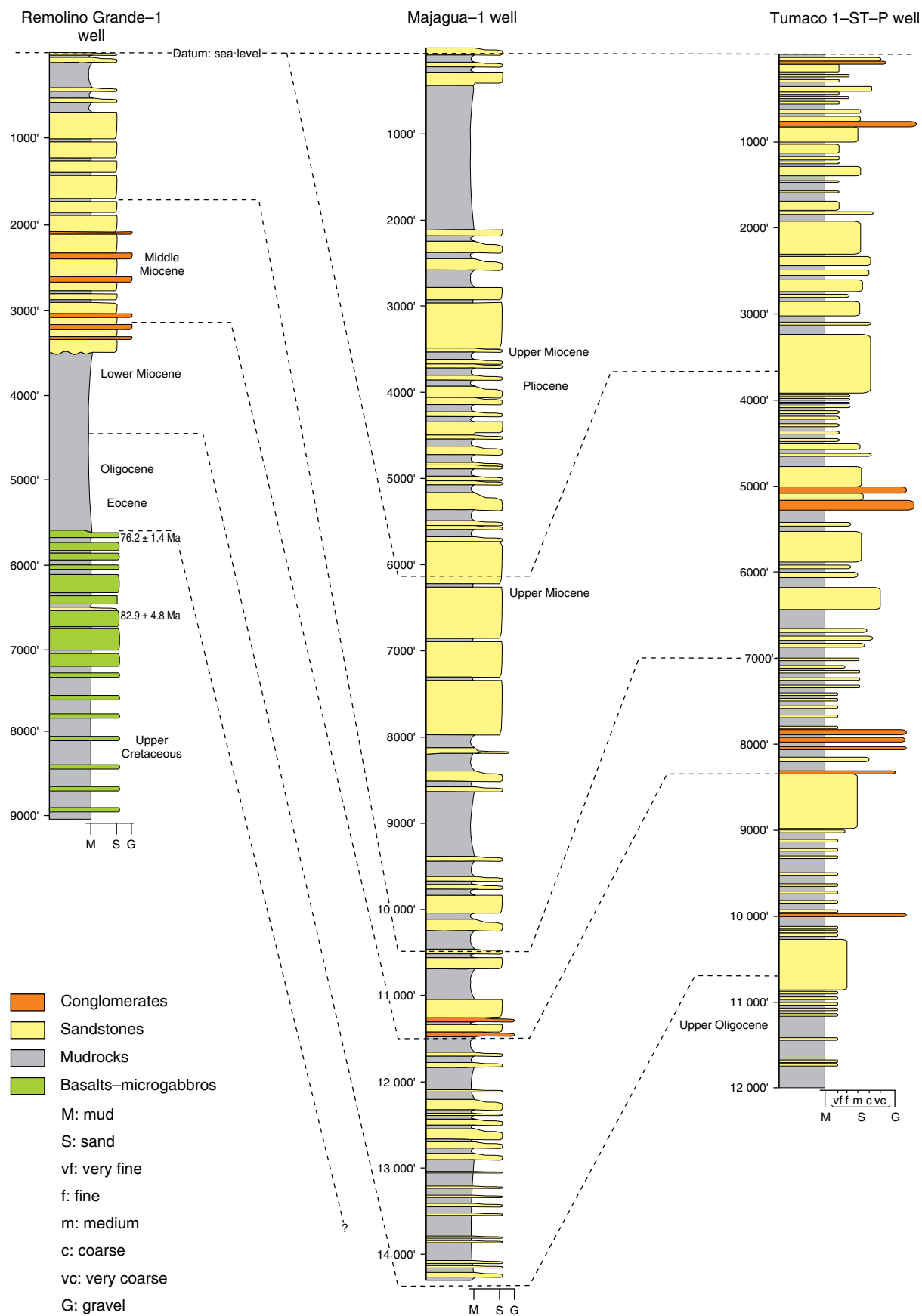
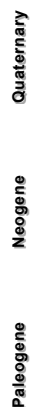


Figure 4. Chronostratigraphic correlation among the Remolino Grande-1, Majagua-1, and Tumaco 1-ST-P wells. Based on Agencia Nacional de Hidrocarburos & Universidad de Caldas (2011a) and Agencia Nacional de Hidrocarburos & Antek (2013).



Paleogene **Neogene** **Quaternary**

can be correlated with the 98–60 Ma ages obtained from Gorgona Island by Serrano et al. (2011) and from the north of Ecuador by Vallejo et al. (2009). These rocks have been correlated by other authors with the Diabásico Group (sensu Nelson, 1962), the Volcánica Formation (sensu Aspdén, 1984), and the Dagua/Piñón Formation (López-Ramos, 2009), located in the Western Cordillera of Colombia and Ecuador (Figure 2).

4.2. Paleogene

4.2.1. Seismic Lines

The Paleogene deposits were accumulated over a relatively smooth surface of the igneous Cretaceous basement. They onlap onto this basement to the east (Figure 3a). Paleogene deposits outcrop on the western border of the Western Cordillera (Figure 3a; Gómez et al., 2015). To the west, Paleogene reflectors can be identified over the Remolino Grande–Gorgona Structural High, where they become thinner and affected by normal faults. In the Tumaco offshore basin, Paleogene reflectors increase in thickness and are affected by thrust faults (Figure 3a). Paleogene deposits become thickened to the south of the basin, and their reflectors locally downlap the Cretaceous basement (Figure 3b).

4.2.2. Lithology

In the Remolino Grande–1 well, the Paleogene is mainly constituted by mudrocks and sandy siltstones interbedded with some sandstone beds (Figure 4). This unit can be correlated with the Lutitas de Remolino Grande Formation or 1 Sur Unit (Echeverri et al., 2015a; Suárez 1990, 2007), as well as the lower part of the Tumaco Formation of Agencia Nacional de Hidrocarburos & Antek (2013) (Figure 2). The Tumaco 1–ST–P well reached mudrocks, sublitharenites, and litharenites, interpreted as late Oligocene (Chattian) shelf–prodelta to delta front deposits. Benthic foraminifera such as *Osangularia* sp., *Gyroidinoides broeckhiana*, *Discorbinella* sp., *Anomalinoides cicatricose*, and *Anomalinoides semicribata* suggest sedimentation in the upper–middle part of the continental slope (Agencia Nacional de Hidrocarburos & Antek, 2013).

4.2.3. Biostratigraphy

The lowest sample with calcareous microfossil recovery in Remolino Grande–1 well yielded *Reticulofenestra bisecta*, *Reticulofenestra reticulata*, and Paleocene and Eocene reworked species (*Sphenolithus anarrhopus* and *Sphenolithus primus*, *Nannotetrina* spp.). The young assemblage suggests the biozones NP16 and NP19 (Bartonian – Priabonian; Agnini et al., 2014; Perch–Nielsen, 1985). For the Oligocene, diagnostic species of planktonic foraminifera were not identified; however, calcareous

nannofossils such as *Cyclicargolithus abisectus*, *Sphenolithus ciperoensis*, and *Sphenolithus distentus* were recorded in some samples. Oligocene/Miocene boundary markers were not found at the Remolino Grande–1 well (Figure 5). Nevertheless, planktonic foraminifera bioevents such as the last occurrence of the *Paragloborotalia opima* at 27.30 Ma in the biozone O6 and the first occurrence of *Paragloborotalia kugleri* at 23.73 Ma in the biozone M1a according to Wade et al. (2011) support the Paleogene/Neogene boundary near 10 740' at the Tumaco 1–ST–P well (Figure 5). This interpretation indicates that Paleogene calcareous nannofossils reported in shallower levels correspond to reworked species. Due to the lack of diagnostic microfossils, this boundary was unclear in the Remolino Grande–1 well; therefore, it was placed at 4500' after seismic correlation with the Tumaco 1–ST–P well (Figures 3, 4, 5). Even though Paleocene deposits were not found in the Remolino Grande–1 well, lower Paleocene deposits have been recently reported in outcrops of the Gorgona Island 85 km to the NE (Bermúdez et al., 2016). In Figure 5, the correlation of the lower part of the Remolino Grande–1 and Tumaco 1–ST–P wells with the calcareous nannofossils and planktonic foraminifera standard zones is shown. This interval ranges between NP19–NP25 and P16–P22, respectively.

4.2.4. Petrography

In the Remolino Grande–1 well, two ditch cutting samples were used for petrographic analyses. They have abundant grains of sedimentary rocks (27–80 %, siltstones, sandy siltstones, and chert; Figure 6). Plagioclase, mono- and polycrystalline quartz, pyroxene, biotite, hornblende, glauconite, and opaque minerals are present in lower proportions. Some algae and foraminifera are observed. Sandstone grains were selected to know their framework composition. They were classified as poorly sorted subarkoses, with fine to coarse angular to subrounded grains. They are composed of monocrystalline (32–44 %) and polycrystalline (21–30 %) quartz, plagioclase (10–23 %), intermediate volcanic rocks (5–6 %), chert (4–15 %), biotite (1–2 %), muscovite (1%), and chlorite (3%). Mud matrix and calcareous cement are common.

4.2.5. Heavy Minerals

The analyzed samples present higher abundances of unstable compared to stable phases. Stable phases include zircon (2–7 %) and tourmaline (1%). Unstable phases correspond to apatite (4–25 %), clinopyroxene (10–52 %), orthopyroxene (1–12 %), hornblende (1–13 %), and minerals of the epidote group (25–40 %). Olivine, oxyhornblende, and biotite are present at 1% each. In the Tumaco 1–ST–P well, the samples contain mainly unstable phases with abundant amphibole, pyroxene and, in lower proportions, epidote, apatite, clinopyroxene, and orthopyroxene. In this interval, detrital zircons were not obtained.

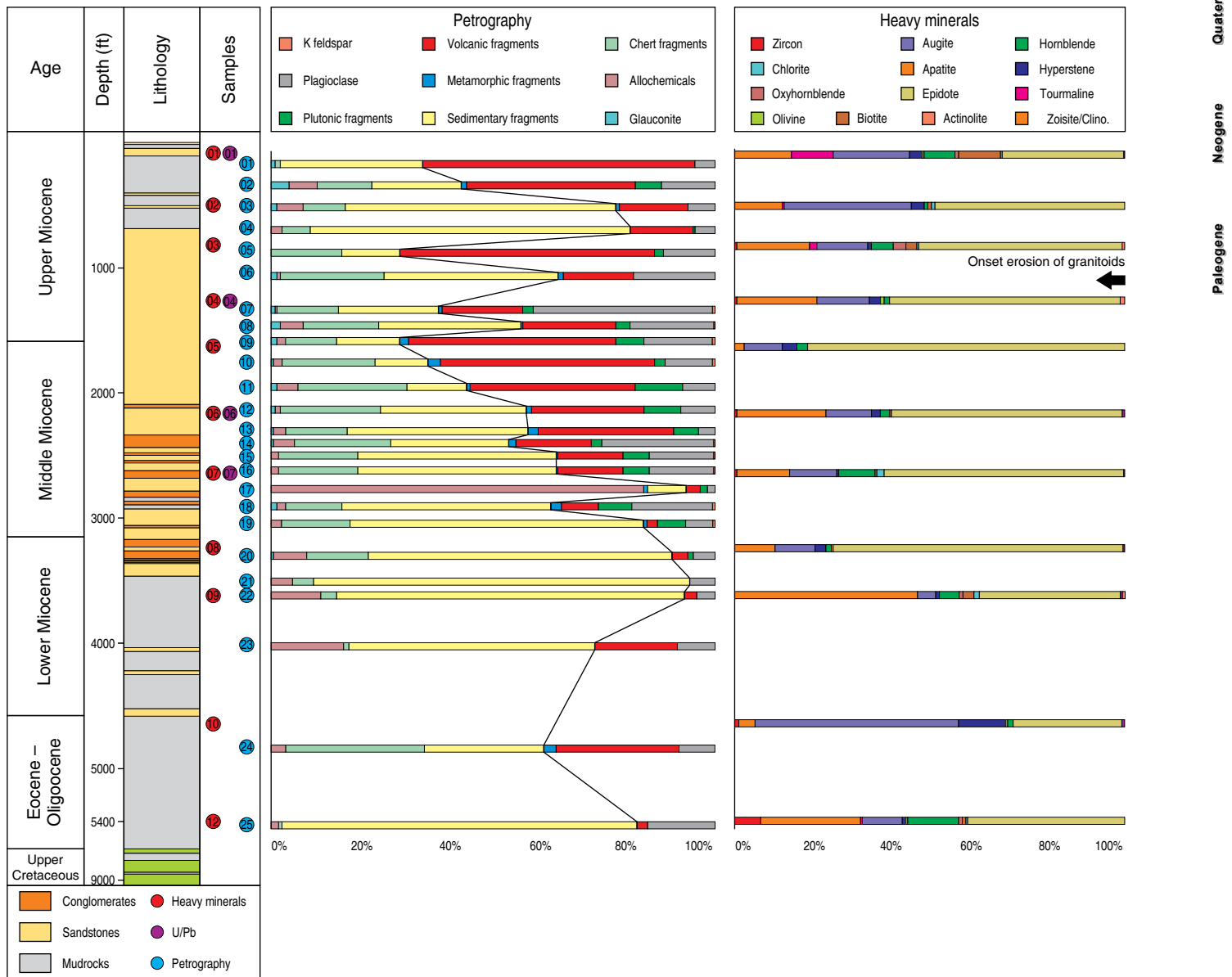


Figure 6. Stratigraphic log of the Remolino Grande-1 well, and bar diagrams representing the composition of the ditch cuttings and heavy minerals. Allochemicals include calcareous fossil remains (mainly foraminifera, bivalves, and gastropods).

4.3. Lower Miocene (Aquitania - Burdigalian)

This interval has been identified in the Remolino Grande-1 (3200–4500'), Majagua-1 (14280–11220), and Tumaco 1-ST-P (8480–10740') wells.

4.3.1. Seismic Lines

The lower Miocene reflectors onlap onto the Paleogene deposits towards the E of the basin (Figure 3a). Westward, they become thinner and pinch-out in the Remolino Grande-Gorgona Structural High. In the offshore Tumaco Basin, the lower Miocene reflectors are concordant with Paleogene and middle Miocene

reflectors and seem to be in toplap against the Pliocene reflectors in the westernmost part of the seismic line (Figure 3a). In the Remolino Grande-Gorgona Structural High, the lower Miocene beds seem to fill some valleys dissected in the Paleogene deposits. In the strike line, the lower Miocene reflectors become thinner to the north, but they are concordant with the Paleogene and middle Miocene sequences.

4.3.2. Lithology

In the Remolino Grande-1 well, there is a dominance of claystones and sandy siltstones interbedded with some sandstone beds, which change abruptly to conglomerates and sandstones

in the upper part of the succession (Figure 4). This interval has abundant fossils of bivalves, gastropods, foraminifera, and carbonized organic matter. In the Majagua-1 well, lower Miocene deposits are composed of mudrocks interbedded with fine-medium sandstones and sandy mudstones. Foraminifera and mollusk shells are abundant. In the Tumaco 1-ST-P, the rocks of this period are characterized by an alternation of highly bioturbated mudrocks, massive and laminated sublitharenites, feldspathic litharenites, litharenites, and some beds of polymictic conglomerates. Paleontological content includes shark teeth (Agencia Nacional de Hidrocarburos & Antek, 2013).

4.3.3. Biostratigraphy

Calcareous nannofossil events are the most efficient biostratigraphic indicator at the Tumaco 1-ST-P and Majagua-1 wells in the lower Miocene deposits. The appearances of *Discoaster druggi*, *Heliscolaphaera ampliaperta*, and *Sphenolithus heteromorphus* and the extinction of *Triquetrorhabdulus carinatus* in these wells mark the beginning of the Miocene (Aubry, 2014, 2015; Backman et al., 2012; Perch-Nielsen, 1985). This is in agreement with the recovery of the short-lived *Sphenolithus belemnoides* in the Majagua-1 well. For this interval, the Remolino Grande-1 well is characterized by the last occurrence of *H. ampliaperta* and *S. heteromorphus* and the occurrence of *Globigerinoides diminutus*, whose biostratigraphic range is described for the late Burdigalian – Langhian (Aubry, 2014; Backman et al., 2012; Kennett & Srinivasan, 1983). This indicates that Remolino Grande-1 encompasses a long-lasting gap (ca. 5 Ma), which includes the Aquitanian and the lower-middle part of the Burdigalian. In Figure 5, the stratigraphic equivalence of the Remolino Grande-1, Majagua-1, and Tumaco 1-ST-P wells with the calcareous nannofossils and planktonic foraminifera standard zones is represented. This portion represents an interval between NN2 to NN6 and N4 to N12, respectively.

4.3.4. Petrography

The ditch cutting samples from the Majagua-1 and Remolino Grande-1 wells are composed mainly of sedimentary rocks (56–90 %; mudrocks, cherts, calcite, sandy shales, sandstones) and, in lower proportions, plagioclase, volcanic and plutonic lithics. Fragments of quartz (mono- and polycrystalline), biotite, hornblende, pyroxene, glauconite, and bioclasts (foraminifera, algae, echinoderms) occur in lower proportions.

The sandstone grains of the Majagua-1 (Figure 7) and Remolino Grande-1 wells were selected to study the composition of their framework. They are classified as feldspathic litharenites and arkoses (Figures 8, 9). The sandstones are poorly sorted, fine to medium size, with rounded to subangular grains. They have a high content of plagioclase (34–68 %), with lower proportions of quartz (3–32 % monocrystalline and 2–21

% polycrystalline) and lithic fragments (1–39 %). Lithic fragments are mainly volcanic of intermediate composition (6–39 %), chert (2–15 %), and low proportions of plutonic rocks, sandstones, micaceous and graphitic schists ($\leq 1\%$) (Figures 7, 9). The accessory minerals are composed of hornblende (5%), epidote (2–3 %), glauconite (1%), biotite (1–3 %), chlorite (2–6 %), and muscovite ($< 1\%$). In the Tumaco 1-ST-P well, the sandstones include litharenites and lithic greywackes, with angular fragments of sedimentary, volcanic, and metamorphic rocks (Agencia Nacional de Hidrocarburos & Antek, 2013).

4.3.5. Heavy Minerals

Two samples from the Remolino Grande-1 well and four from the Majagua-1 well were analyzed (Figures 6, 7, 10). In the Remolino Grande-1 well, stable phases are almost absent, with only 1% zircon. Unstable phases include apatite (47%), clinopyroxene (4–10 %), hornblende (2–5 %), and minerals of the epidote group (36–74 %). Oxyhornblende, actinolite, and chlorite are present in low proportions ($\leq 1\%$). A higher proportion of unstable with respect to the ultrastable phases was found in the Majagua-1 well (Figures 7, 10). Ultrastable phases include zircon (4–26 %) and traces of tourmaline ($\leq 1\%$). Unstable phases include apatite (51–75 %), minerals of the epidote group (1–12 %), biotite (2–4 %), clinopyroxene (2–10 %), orthopyroxene ($\leq 1\%$), chlorite ($\leq 2\%$), hornblende ($\leq 2\%$), and traces of oxyhornblende and glauconite (Figures 7, 10). In the Tumaco 1-ST-P well, a greater proportion of unstable minerals compared to stable ones was also observed (Agencia Nacional de Hidrocarburos & Antek, 2013). Ultrastable phases include zircon and tourmaline ($\leq 1\%$). Unstable phases include hornblende (31–56 %), minerals of the epidote group (1–41 %), apatite ($< 1\%$), clinopyroxene (6–28 %), biotite ($\leq 3\%$), chlorite (1–2 %), sphene ($\leq 1\%$), and garnet ($< 1\%$).

4.3.6. Detrital Geochronology

In the Majagua-1 well, the sample M1MP-014 (depth 11660–11900') was analyzed (Figure 11). A maximum depositional age of 16.1 Ma (Burdigalian) was found. This sample shows four main zircon populations: (i) 18.9 Ma, (ii) 45.0 Ma, (iii) 51.3 Ma, and (iv) 20.7 Ma. Oligocene (28.6 Ma), Late Cretaceous (68.6 Ma, 74.4 Ma, 74.9 Ma, 74.9 Ma, 76.9 Ma, and 83.2 Ma), and Precambrian (556.7 Ma, 557.4 Ma, 844.4 Ma, and 1657.0 Ma) zircons are present, but they are not abundant enough to form a population.

4.4. Middle Miocene (Langhian – Serravallian)

Rocks of this period were identified in the Remolino Grande-1 (1450–3200'), Majagua-1 (10500–11400'), and Tumaco 1-ST-P (7000–8480') wells.

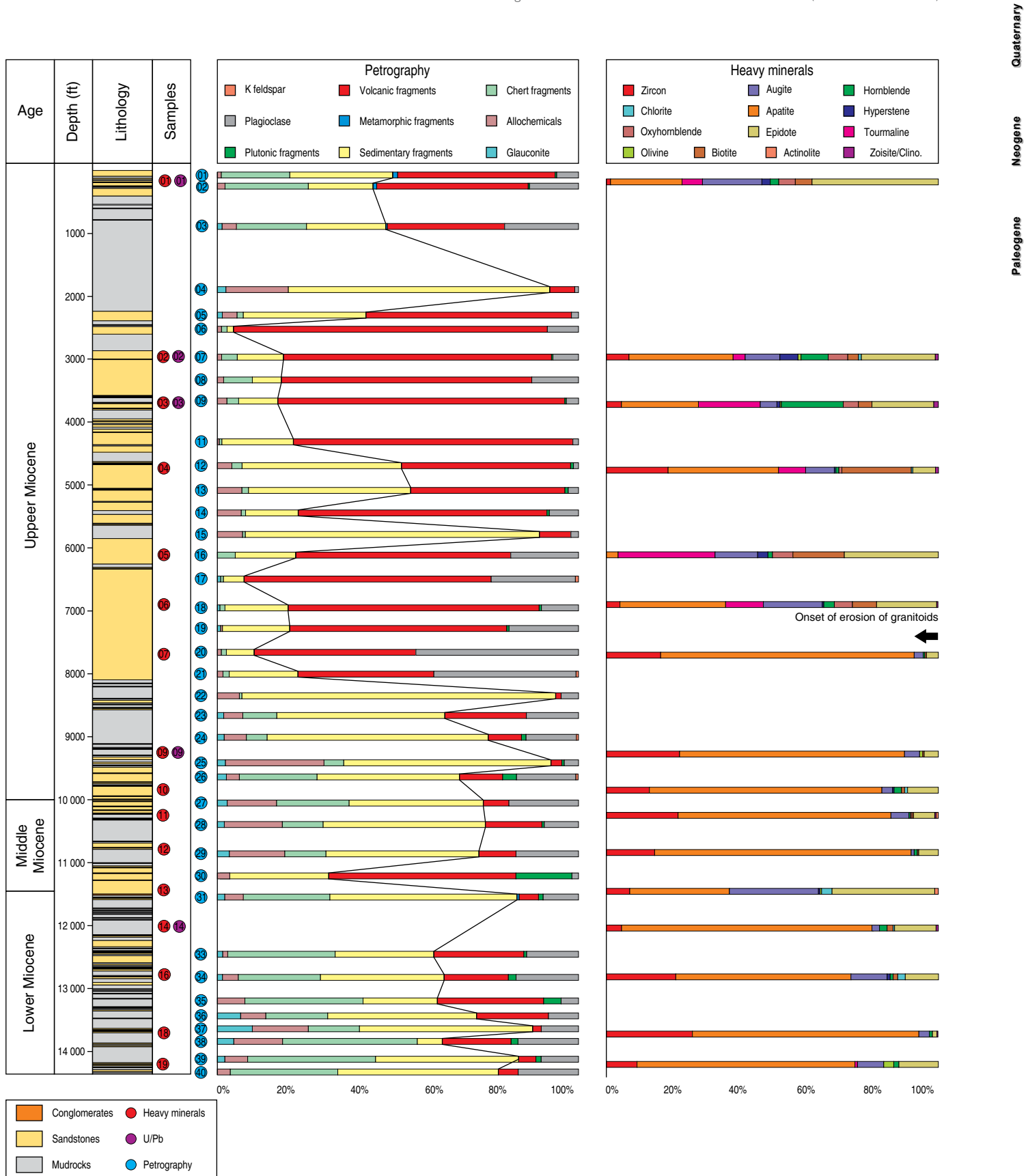


Figure 7. Stratigraphic log of the Majagua-1 well, and bar diagrams representing the composition of the dish cuttings and heavy minerals. Allochemicals include calcareous fossil remains (mainly foraminifera, bivalves, and gastropods).

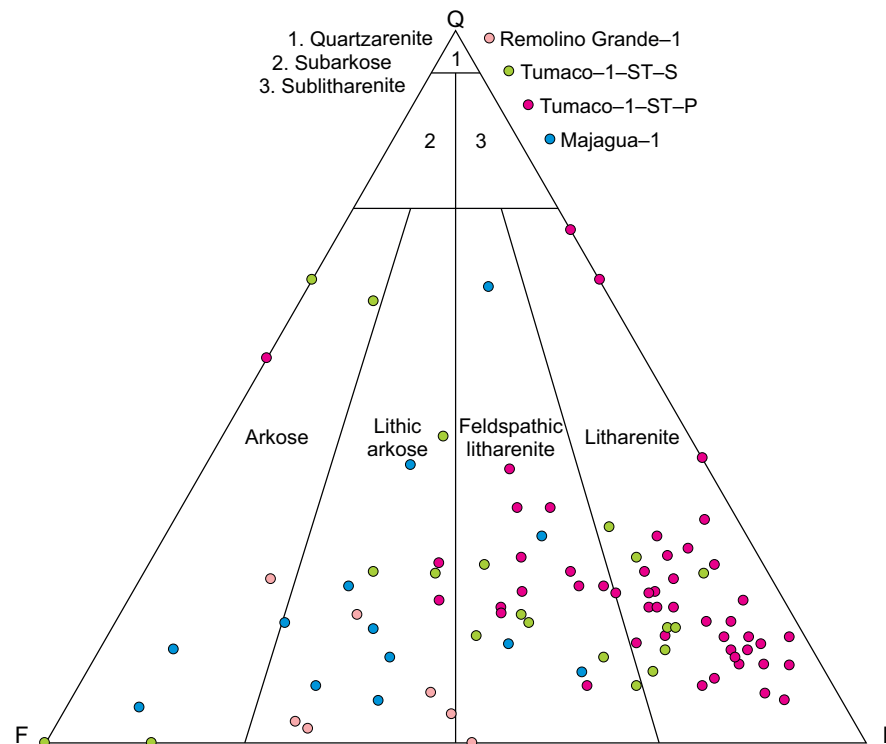


Figure 8. Classification of sandstones (Folk, 1974) in cores from the Tumaco 1-ST-S and Tumaco 1-ST-P wells, and sandstone fragments of the ditch cuttings from the Majagua-1, Remolino Grande-1, and Tumaco 1-ST-P wells. Based on Cortés et al. (2019), and Agencia Nacional de Hidrocarburos & Universidad de Caldas (2011a, 2011b).

4.4.1. Seismic Lines

The middle Miocene reflectors onlap onto the lower Miocene deposits towards the E of the basin (Figure 3a). They became thinner in the Remolino Grande–Gorgona Structural High to the west. In the Tumaco offshore basin, the middle Miocene reflectors are in toplap against Pliocene reflectors (Figure 3a). In the strike seismic line, they are conformable with the lower and upper Miocene reflectors (Figure 3b). It is not clear that the middle Miocene reflectors were affected by the mud diapir; therefore, they are marked with a dotted line.

4.4.2. Lithology

In the Remolino Grande-1 well, the middle Miocene deposits consist of amalgamated sandstones interbedded with conglomerates; in lower proportions, sandy siltstones and calcareous sandstones are present. In the Majagua-1 well, they mainly consist of sandstones and conglomerates interbedded with mudrocks (Figure 4), with abundant foraminifera and mollusk shells. These rocks are interpreted as delta front deposits probably related to a relative shallowing of the depositional environment (Agencia Nacional de Hidrocarburos & Universidad de Caldas, 2011a). In the Tumaco 1-ST-P well, middle Miocene rocks are composed of mudrocks, sublitharenites, feldspathic

litharenites, litharenites, and conglomerates. Fossils of scaphopods, pelecypods, ambulacres, gastropods, and echinoderms are present in this interval. This succession is interpreted as accumulated in different environments of a deltaic system (prodelta, estuarine bars, river mouth bars, and lagoons; Agencia Nacional de Hidrocarburos & Antek, 2013).

4.4.3. Biostratigraphy

The Remolino Grande-1 well contains useful biostratigraphic events such as the last occurrences of *Globorotalia peripheroronda*, *H. ampliaperta*, and *S. heteromorphus*, which were found together with sporadic abundances of *Fohsella fohsi*, *Globigerinoides sicanius*, and *Orbulina universa*. Microfossils of this well do not support an age younger than the nanoplankton biozone NN6 (late Serravallian at 1990', Figure 5). Nevertheless, this information linked to the 11.5 Ma maximum depositional age of detrital zircon at ca. 1450' allows the location of the middle – upper Miocene limit between ca. 1450–1990' (Figures 4, 5). Biostratigraphic records of Tumaco 1-ST-P and Majagua-1 wells have discontinuous abundance patterns of microfossils and very abundant reworked assemblages (Figure 5). In the case of the Tumaco 1-ST-P well, reworked species of *Cyclicargolithus floridanus* and *S. heteromorphus* were reported within younger microfossils of *Discoaster kugleri*. Figure 5

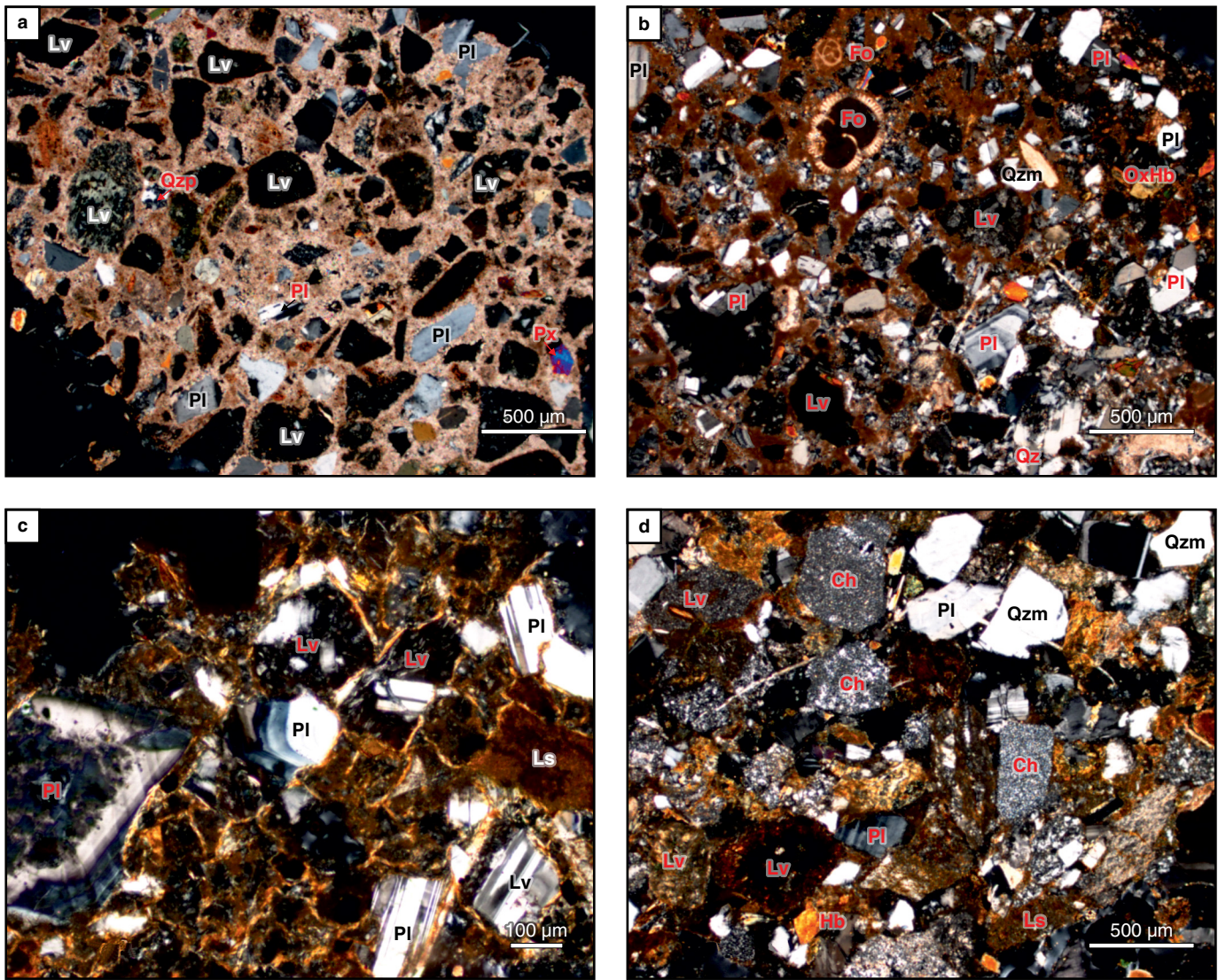


Figure 9. Microphotographs of the Majagua-1 well. **(a)** Sample MIPP-01: Feldspathic litharenite with plagioclase, volcanic lithic, pyroxene, and calcareous cement. Crossed nicols. **(b)** MIPP-13: Feldspathic litharenite with volcanic fragments, plagioclase (zoned and twinned), quartz, oxyhornblende, and foraminifera. Crossed nicols. **(c)** MIPP-18: Feldspathic litharenite with plagioclase, volcanic and sedimentary lithics. Crossed nicols. **(d)** MIPP-28: Feldspathic litharenites with volcanic fragments, plagioclase, quartz, chert, and calcareous cement. Crossed nicols. Abbreviations: (Lv) volcanic lithic; (Ls) sedimentary lithic; (Ch) chert; (Pl) plagioclase; (Qz) quartz; (Qzp) polycrystalline quartz; (Qzm) monocrystalline quartz; (Hb) hornblende; (OxHb) oxyhornblende; (Px) pyroxene; (Fo) foraminifera.

shows the stratigraphic equivalence of the Remolino Grande-1, Majagua-1, and Tumaco 1-ST-P wells, with the calcareous nannofossils and planktonic foraminifera standard biozones. This range covers the interval between zones NN4 to NN6 and N8 to N12, respectively.

4.4.4. Petrography

Ditch cutting samples from the Majagua-1 and Remolino Grande-1 wells are composed mainly by siltstones, sandy siltstones, sandstones, volcanic rocks, chert, and plagioclase (Figures 7, 8), with lower proportions of quartz grains (mono- and polycrystalline), plutonic rocks, potassium feldspar, lime-

stones, amphibole, biotite, chlorite, pyroxene, glauconite, opaque, and bioclasts (foraminifera). The sandstone grains of the Majagua-1 and Remolino Grande-1 wells are classified as lithic arkoses, arkoses, and lower proportions of feldspathic litharenites (Figures 7, 8) and are composed of fine to coarse, angular to rounded grains, with a high content of plagioclase (23–68 %), rock fragments (8–47 %), and a minor proportion of quartz (2–23 %). The lithic fragments are mainly volcanic of intermediate composition (8–39 %), sandstones (2–3 %), shales (1%), chert (3–8 %), and graphite schists (1–2 %) (Figure 7). Accessory minerals as oxyhornblende and hornblende (1–5 %), epidote (1–3 %), muscovite (< 1%), biotite (1–3 %), and chlorite (1–2 %) are present. In the Tumaco 1-ST-P

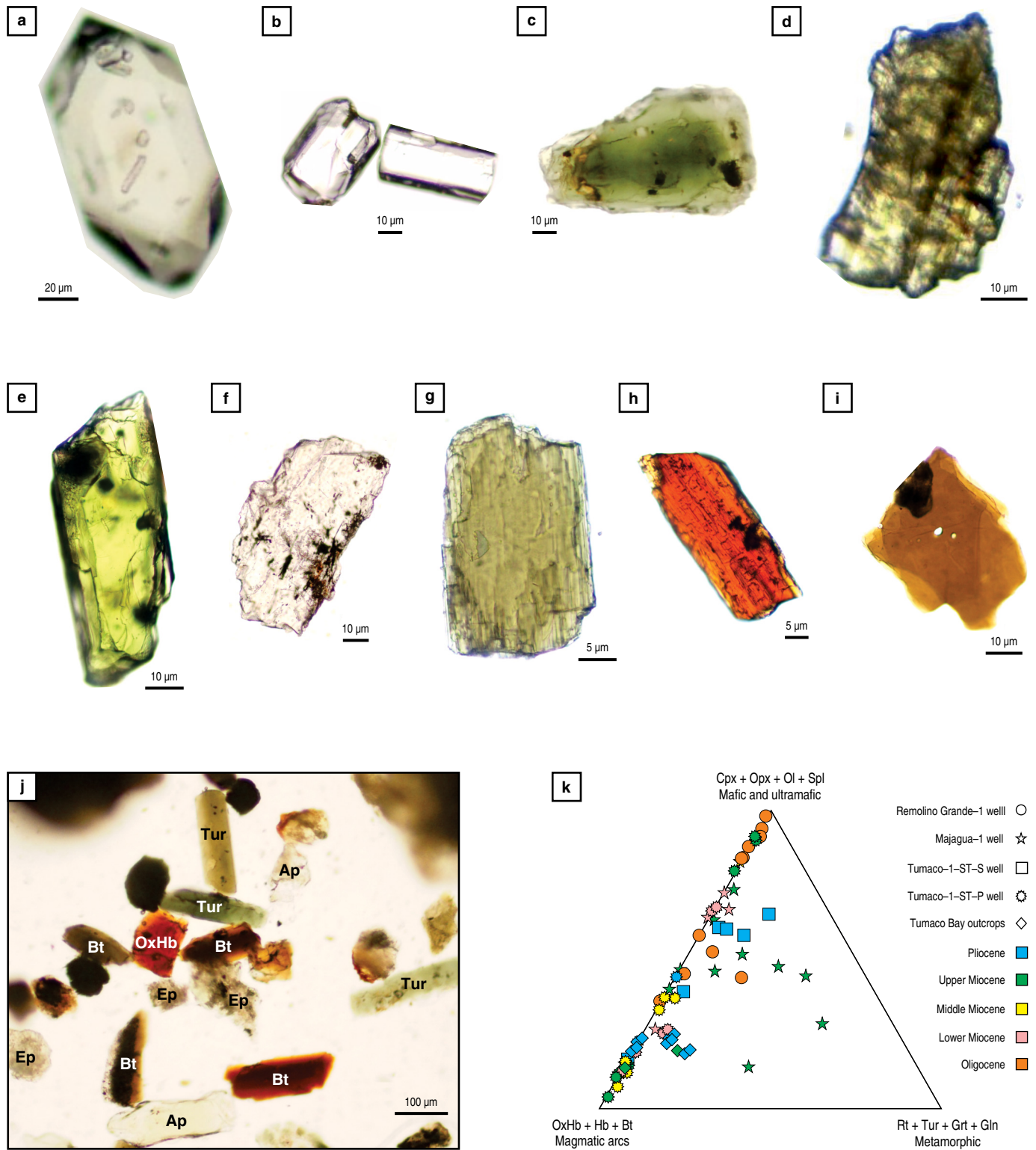


Figure 10. Some heavy minerals found in the sandstones of the Tumaco Basin. **(a)** Zircon. **(b)** Apatite. **(c)** Green tourmaline. **(d)** Epidote. **(e)** Augite. **(f)** Hypersthene. **(g)** Hornblende. **(h)** Oxyhornblende. **(i)** Biotite. **(j)** Association of ultrastable and unstable phases: (Tur) Tourmaline + (Ap) Apatite + (Bt) Biotite + (Ep) epidote + (OxHb) Oxyhornblende. **(k)** Triangular diagram with groups of heavy minerals and their source rocks.

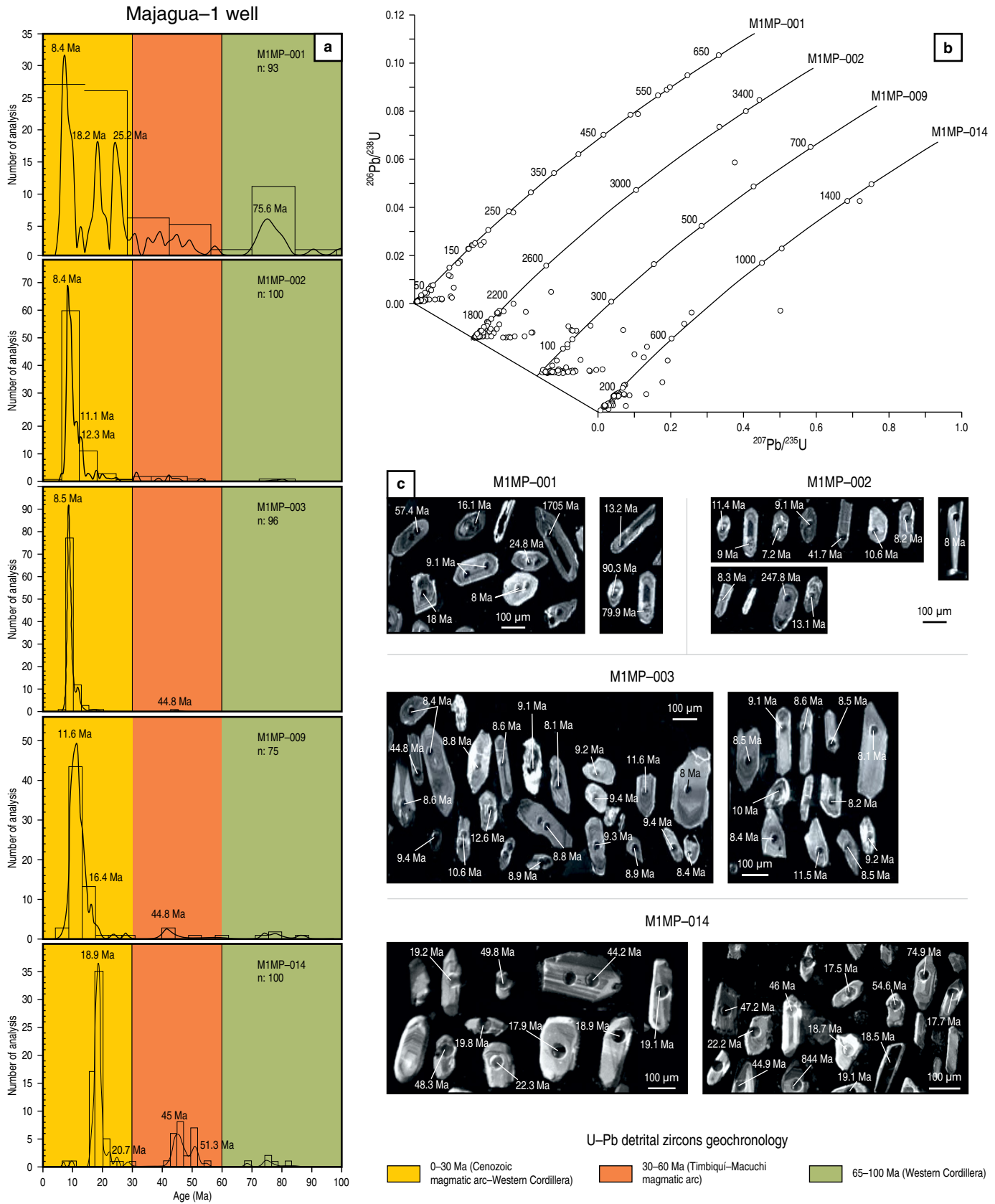


Figure 11. (a) Relative probability diagrams of U/Pb ages of detrital zircons from the Majagua-1 well. (b) Concordia diagrams of the samples (Tera-Wasserburg diagrams, Ludwig, 2003). (c) Cathodoluminescence of some zircon crystals. The presence of zircons with volcanic morphology (euhedral grains with length/width ratios >3) and U/Pb ages between 12 and 8 Ma is noteworthy (from Echeverri et al., 2015b).

well, sandstones are mainly litharenites and lithic greywackes. Rock fragments are mainly sedimentary, metamorphic, volcanic and plutonic mafic and felsic (Agencia Nacional de Hidrocarburos & Antek, 2013).

4.4.5. Heavy Minerals

Two samples from the Remolino Grande–1 well and three from the Majagua–1 well were analyzed (Figures 6, 7). In the Remolino Grande–1, stable phases are almost absent, with only 1% zircon. The unstable phases include apatite (13–23 %), clinopyroxene (12 %), orthopyroxene (1–2 %), hornblende (2–9 %), and minerals of the epidote group (59–61 %). Oxyhornblende, biotite, chlorite, and olivine are present in low proportions ($\leq 2\%$). In the Majagua–1 well, a higher proportion of unstable with respect to the ultrastable phases was found (Figure 7). The ultrastable phases include zircon (7–21 %) and traces of tourmaline ($< 1\%$). The unstable phases include apatite (29–75 %), minerals of the epidote group (6–29 %), biotite (2–5 %), clinopyroxene (1–25 %), chlorite (1–3 %), hornblende ($\leq 1\%$), actinolite ($\leq 1\%$), and traces of oxyhornblende and orthopyroxene. The unstable phases such as apatite, pyroxene, and epidote are dominating and increase with respect to the Oligocene beds in the Tumaco 1–ST–P well (Agencia Nacional de Hidrocarburos & Antek, 2013). In the Tumaco 1–ST–P well, a greater proportion of unstable phases compared to stable was also observed. The ultrastable phases include zircon (1%) and traces of tourmaline ($< 1\%$). The unstable phases include hornblende (48–68 %), minerals of the epidote group (6–26 %), apatite ($< 1\text{--}4\%$), clinopyroxene (2–28 %), orthopyroxene ($< 1\text{--}18\%$), chlorite (1–3 %), and garnet ($< 1\text{--}2\%$).

4.4.6. Detrital Geochronology

Two samples from the Remolino Grande–1 well were analyzed (RG–MP–007: depth 2640–2760'; RG–MP–006: depth 2140–2380'). These samples have maximum depositional ages of 13.3 Ma and 13.1 Ma (Serravallian), respectively. They show similar patterns of zircon distributions: the most abundant population is 12–14 Ma, followed by 22–24 Ma and 45 Ma. Very low percentages of Late Cretaceous, Triassic, early Paleozoic, and Precambrian zircons were recognized (Figure 12).

4.5. Upper Miocene – Pliocene

This time interval has been partially identified in the Remolino Grande–1 (0–1990'), Majagua–1 (0?–10500'), Tumaco 1–ST–P (32–7000'), Tumaco 1–ST–S (0?–1899.6'), and Tumaco Bay outcrops.

4.5.1. Seismic Lines

To the east of the basin, the upper Miocene reflectors onlap over the lower – middle Miocene and the basement rocks (Figure 3a). Towards the west of the basin, some reflectors come to the surface in the Remolino Grande–Gorgona Structural High, forming gentle hills, which are currently subject to erosion. In the offshore basin, the upper Miocene reflectors top lap against the Pliocene (Figure 3a). On the strike line, both the upper Miocene and the Pliocene reflectors become thinner towards the south of the studied area (Figure 3b).

Pliocene reflectors can be divided into three sets. (i) The lower set rests on the Cretaceous basement to the east, and onlap onto the Paleogene (Figure 3a). Towards the west, it decreases in thickness, and is truncated by the reflectors of the middle set. (ii) The middle set shows a clear progradation of the eastern and western reflectors towards the depocenter of the basin showing downlap over the set 1 (red arrows in Figure 3a) and a decrease in their thickness in the same direction. (iii) The upper set truncates the reflectors of the middle set and pinches out towards the E and W borders of the basin (Figure 3a). In the Tumaco offshore basin, Pliocene beds are covering the middle and upper deposits, forming an erosional truncation (toplap) (Figure 3a). In the Remolino Grande–1 well, there is no Pliocene record, probably related to erosion or no deposition during the Remolino Grande–Gorgona Structural High uplift.

4.5.2. Lithology

In the Remolino Grande–1 well, upper Miocene beds are composed by thick beds of sandstones and sandy siltstones interlayered with thin beds of mudrocks. Above 760', mudrocks with thin sandstone beds are dominant (Figure 4). In the Majagua–1 well, the lower part of the beds is composed of sandstones interbedded with sandy mudstones, mudrocks and, in lower proportions, conglomerates. In the upper part (above ca. 8000'), there is a sudden increase in thick sandstone beds (Chagüí Formation; Figures 2, 4). The sandstones in some cases can be calcareous. Remnants of mollusks and carbonized organic matter are locally abundant. The thickness and frequency of sandstones vs. fine grained sedimentites change through the time; for this reason, several units have been proposed (e.g., Angostura, Chagüí, and San Agustín Formations; Agencia Nacional de Hidrocarburos & Universidad de Caldas, 2011a; Suárez, 1990). These deposits can be associated with deltaic systems. Good exposures of these rocks can be studied in the coastal cliffs of the Tumaco Bay (Figure 13). Normal faults, slumped beds, and clastic dykes are common in these units (Figure 13). In the Tumaco 1–ST–P well, mudrocks, calcareous mudrocks, laminated sandstones, and matrix-supported conglomerates can be observed; they are generally bioturbated. An increase upward in volcanic materi-

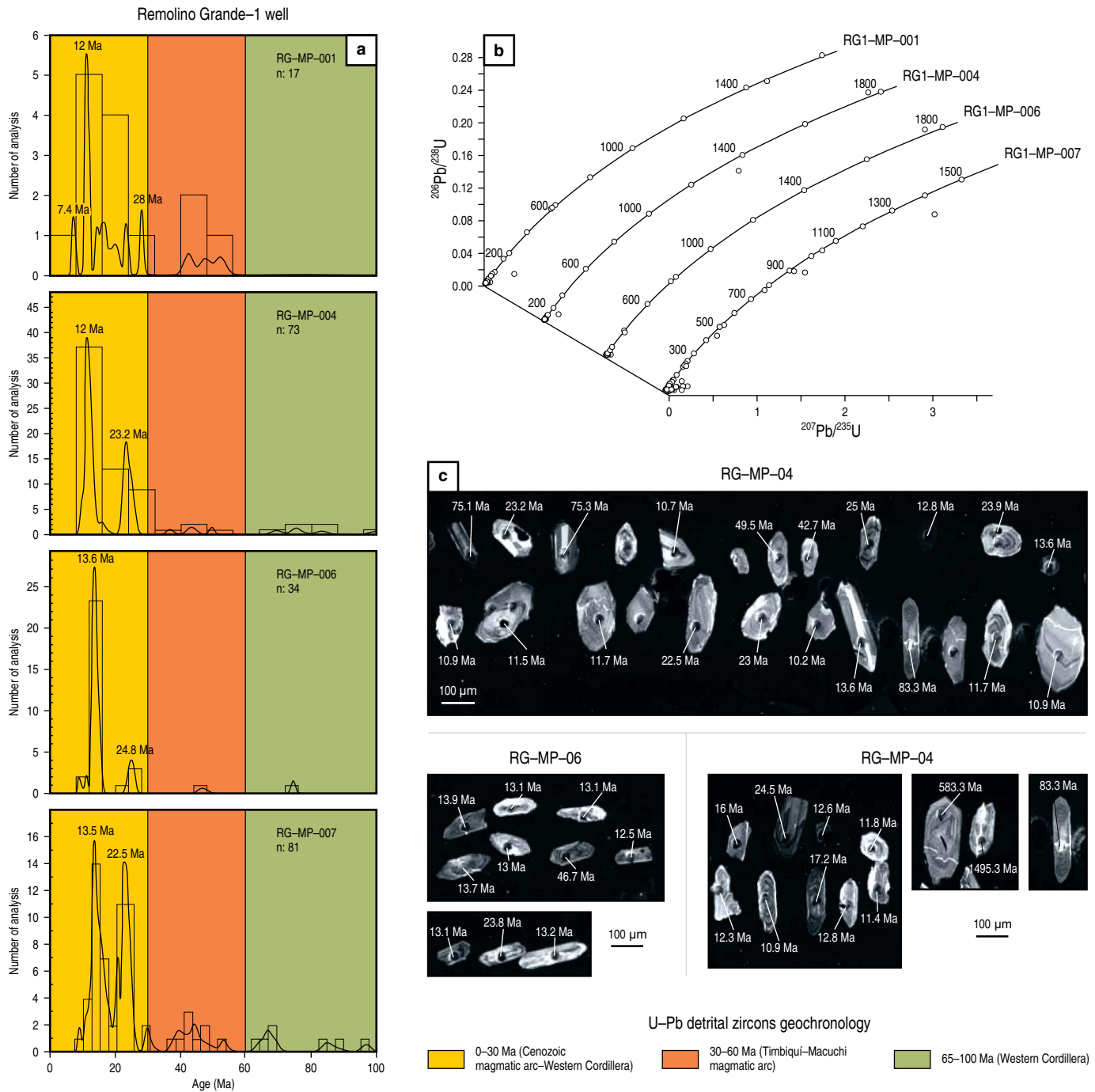


Figure 12. (a) Relative probability diagrams of U/Pb ages of detrital zircons from the Remolino Grande-1 well. (b) Concordia diagrams of the samples. (c) Cathodoluminescence of some zircon crystals (from Echeverri et al., 2015b).

als is notorious. They were interpreted as fluvial and deltaic deposits (Agencia Nacional de Hidrocarburos & Antek, 2013).

During the latest Miocene – Pliocene (Messinian – Zanclean), in the southern part of Tumaco Basin, more than 1300' (400 m) of thick lenticular layers of sandstones and conglomerates, with an important volcanic input (Cascajal Formation of Echeverri et al., 2016), were accumulated and interlayered with some mudrocks and muddy sandstone beds. Locally, bivalves, gastropods, for-

minifera, echinoderms, crustaceans, and well-preserved plant remains were found. The unit was accumulated in a deltaic system influenced by volcanism (Echeverri et al., 2016).

4.5.3. Biostratigraphy

Tumaco 1-ST-P and Majagua-1 are the only wells from which middle Miocene microfossils were recovered. However, our in-

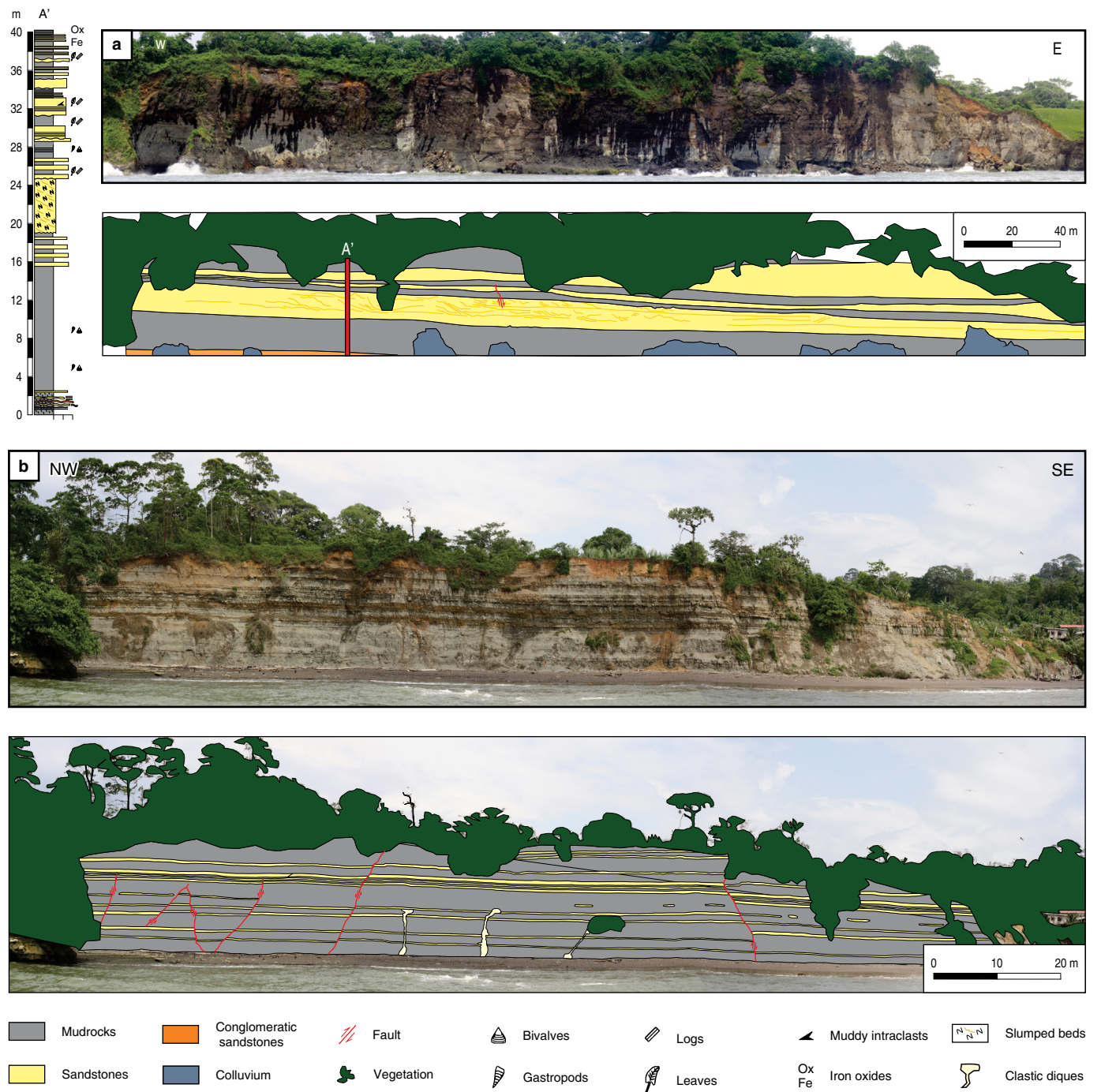


Figure 13. Panoramic pictures of Tumaco Basin outcrops (San Agustín Formation, Tortonian – Messinian). **(a)** Curay. **(b)** La Chorrera. The facies are mainly mudrocks interbedded with sandstone beds. Notice the presence of slumped beds and clastic dykes (see Figure 1 for location).

interpretation suggests that these wells record Tortonian sedimentation. This is supported by the occurrence of *Catinaster coalitus*, *Discoaster bellus*, and *D. hamatus* in both sites. Detailed studies conducted on the Tumaco 1–ST–P well have demonstrated that this assemblage is very abundant and highly resistant to dissolution, making them useful in biostratigraphy. The Serravallian/Tortonian (middle/upper Miocene) boundary was placed at 7000'

in the Tumaco 1–ST–P well according to the last occurrence of *E. kugleri* (Figure 5). After this, we observed several bioevents of the calcareous nannofossils *C. coalitus*, *D. hamatus*, and planktonic foraminifera *Neoglobobadrina acostaensis* and *Paraglobobadrina mayeri*, as well as sporadic nannofossils *D. bellus*, *D. bollii*, *D. brouweri*, and *S. abies*. An increase of the accumulation rate is inferred during the Tortonian at Tumaco 1–ST–P well, as

these taxa are characterized by a short life span and they were found successively in the well. Alternatively, the last consistent biostratigraphic marker in the Majagua-1 well was the last occurrence of *C. coalitus* at 8820'.

As shown in Figure 5, in the Majagua-1 and Tumaco 1-ST-P wells, the equivalence with the calcareous nannofossils and planktonic foraminifera standard zones represents an interval from NN7 to NN10 and N14 to N16, respectively.

Diagnostic species such as *D. neohamatus*, *D. berggrenii*, *D. quinqueramus*, *D. asymmetricus*, and *Globorotalia tumida* were identified in the upper part of the Tumaco 1-ST-P and Majagua-1 wells, occasionally associated with abundant reworked microfossils (mainly Cretaceous and Paleogene). Although it is difficult to identify a succession of standard zonations, the microfossil assemblages allow the designation of a Messinian – Piacenzian age. Palynological data in the Tumaco 1-ST-P well show the first occurrence of *Cyatheacidites annulatus* at 3950' (ditch cutting sample) (Figure 5), considered a late Miocene biostratigraphic marker in the Llanos Basin (first occurrence datum at 7.1 Ma) (Jaramillo et al., 2011).

4.5.4. Petrography

Upper Miocene ditch cutting samples from the Majagua-1 and Remolino Grande-1 wells (upper Viche and Angostura Formations) are mainly composed of mudrocks, volcanic rocks, and plagioclase. Chert, quartz (mono and polycrystalline), potassium feldspar, amphibole, biotite, pyroxene, chlorite, glauconite, and bioclasts (foraminifera, algae, bivalves) are present in a lower proportion. In the middle part (Chagüí Formation), the samples have mainly volcanic fragments and plagioclase, as well as sedimentary rocks (shales, sandstones, and cherts) (Figure 7). In some levels, pyroxene, amphibole, and biotite are frequent. In addition, plutonic grains, potassium feldspar, quartz (mono and polycrystalline), tourmaline, apatite, calcite, chlorite, epidote, glauconite, and foraminifera are present in lower proportions. In the top of the Majagua-1 well, the samples mainly have volcanic grains, plagioclase, and sedimentary rock fragments (chert, shale, limestone, and bioclasts). In lower proportions, schists, intermediate plutonics, potassic feldspars, quartz (mono- and polycrystalline), pyroxenes, amphibole, tourmaline, chlorite, epidote, glauconite, and bioclasts (foraminifera) were identified.

Sandstone grains of the Majagua-1 well are classified as lithic arkoses and feldspathic litharenites (Figure 8). They are fine-grained, poorly sorted, and with angular to rounded grains (Figures 7, 8), composed mainly by plagioclase (12–54 %), quartz (1–25 %), and intermediate volcanic rock fragments (4–54 %). Sedimentary lithics are composed by sandstones (1–8 %), mudrocks (1–14 %), and cherts (1–5 %) (Figure 7). Among accessory minerals were identified oxyhornblende and hornblende (1–16 %), pyroxene (1–5 %),

glauconite (1–2 %), biotite (1–6 %), chlorite (1–4 %), and epidote (1–6 %). In the Tumaco 1-ST-P well, sandstones are litharenites, feldspathic litharenites, and lower proportions of lithic arkose. Constituents are mostly volcanic. Lithics are mainly mudrocks, andesites, and diorites (Agencia Nacional de Hidrocarburos & Antek, 2013).

4.5.5. Heavy Minerals

Five samples from the Remolino Grande-1 well and ten from the Majagua-1 well were analyzed (Figures 6, 7). In the Remolino Grande-1, stable phases are scarce with tourmaline (2–10 %) and zircon (1%). The unstable phases are dominant and include apatite (3–20 %), clinopyroxene (9–33 %), orthopyroxene (1–4 %), hornblende (1–9 %), oxyhornblende (1–3 %), biotite (1–10 %), and minerals of the epidote group (31–81 %). Chlorite, olivine, and actinolite are present in low proportions ($\leq 1\%$). In the Majagua-1 well, a higher proportion of unstable with respect to the ultrastable phases was found (Figure 7). The ultrastable phases include zircon (1–23 %) and tourmaline (1–33 %). The unstable phases include apatite (4–69 %), minerals of the epidote group (4–38 %), biotite (2–6 %), muscovite (1 %), clinopyroxene (2–19 %), orthopyroxene ($< 1\text{--}5\%$), olivine (1%), chlorite (1–3 %), oxyhornblende ($< 1\text{--}7\%$), and hornblende (1–19 %). In the Tumaco 1-ST-P well, a greater proportion of unstable phases compared to stable phases was also observed (Agencia Nacional de Hidrocarburos & Antek, 2013). The ultrastable phases only include zircon (1%), while unstable phases are dominant and include hornblende (9–72 %), minerals of the epidote group ($< 1\text{--}19\%$), apatite ($< 1\text{--}3\%$), clinopyroxene (4–36 %), orthopyroxene (4–63 %), biotite (1–3 %), chlorite ($\leq 1\%$), and garnet (1%).

4.5.6. Detrital Geochronology

Two samples for the Remolino Grande-1 well (RG-MP-004; depth 1210–1450' and RG-MP-001; depth 84–300') were analyzed. They have 10.4 Ma and 11.5 Ma of maximum depositional ages, respectively. These data allow the lower – middle Miocene boundary to be constrained between ca. 1450–1990' depth based on geochronologic and biostratigraphic data (Figure 5). They show similar patterns of zircon distributions: The most abundant population is 12–14 Ma, followed by 22–24 Ma and 45 Ma. Very low percentages of Late Cretaceous, Triassic, early Paleozoic, and Precambrian zircons were recognized (Figure 12).

In the Majagua-1 well, four samples (M1MP-009, depth 9100–9320'; M1MP-003, depth 3430–3950'; M1MP-002, depth 2830–3210'; and M1MP-001, depth 110–800') were analyzed. They have 9.3 Ma, 7.6 Ma, 7.5 Ma, and 6.6 Ma maximum depositional ages, respectively. Three main populations of zircons are recognized: 7–12 Ma, 16–25 Ma (especially to

the top of the well), and 45–50 Ma (Figure 11). In lower proportions are late Oligocene – Miocene, Paleocene, and Late Cretaceous and Jurassic zircons, which are not abundant enough to constitute a population.

Two samples from the Tumaco 1–ST–S well, two from outcrops of the Tumaco Bay, three in the Pleistocene fans and one in recent sedimentites were also analyzed. In the Pliocene beds, similar populations of detrital zircons ages are observed: the most abundant is 4.1–7.6 Ma, followed by 6.5–7.6 Ma, 9.0–13.0 Ma, and 19.0–23.0 Ma. Very low percentages of Late Cretaceous, Triassic, early Paleozoic, and Precambrian zircons were recognized. The maximum depositional ages in two samples of the Tumaco 1–ST–S well were 6.5 Ma (1257') and 4.1 Ma (400') (Figure 5).

4.6. Pliocene – Holocene

Pliocene – Holocene volcanoclastic fans were identified in the eastern border of the basin (Figure 14). The volcanic source probably came from an old Cumbal Volcano and from the Azufral volcanic activity in the Western Cordillera. Three alluvial fans can be differentiated, which prograde in the basin through time (Figure 14): (i) The oldest fan (Pliocene?), 1560 km², is strongly dissected and controlled by the Junín Sambianí Fault, and it is formed by lahar and debris flow deposits mainly composed of dacitic and andesitic rock fragments. (ii) A younger fan, 160 km², formed by lahar and debris flow deposits, is mainly composed of andesitic rock fragments. (iii) The youngest fan covers 2030 km². It is formed by lahar, debris flow, and stream flow deposits and is mainly composed of dacitic pumice fragments. This deposit partially overlays the Cascajal Formation in unconformity, and they are interlayered with recent littoral sediments along the Pacific coast.

The youngest volcanoclastic fan has 2.04 Ma as its maximum depositional age (Figure 14). In the Pleistocene fans and the recent sediments, detrital zircon populations of 26–20 Ma, 14–11 Ma, 9–6 Ma, and 4–3 Ma were identified. These detrital populations are in concordance with those present in the underlying stratigraphic sequence. However, there is a significant presence of zircons between 3–1.5 Ma, which records the most recent activity of the magmatic arc (Figure 14). In the Tumaco Bay outcrops, five samples were analyzed in the Pliocene – Pleistocene deposits (Figure 1). In general, stable phases occur in minor proportions compared with unstable ones. The stable phases are constituted by zircon (10–21 %), tourmaline (5–9 %), and rutile (2%). The unstable phases are dominant and include apatite (3–7 %), pyroxene (10–16 %), hornblende (24–33 %), biotite (24–29 %), and olivine (3–5 %). Chlorite and minerals of the epidote group are present in very low proportions ($\leq 1\%$).

Holocene deposits are mainly composed by coastal and fluvial sediments from the Patía and Mira Rivers. To the upper part of the Tumaco 1–ST–S well, an unconsolidated sedimentary

sequence of (ca. 32'; 9.8 m) sands and muds was identified. There were two ¹⁴C AMS ages in organic sediments, 4360 \pm 30 BP and 4150 \pm 30 BP (Holocene). These sediments belong to the deltaic plain of the Mira River (López *et al.*, 2012).

5. Interpretation

5.1. Cretaceous – Paleogene

The Upper Cretaceous volcano–sedimentary succession of Remolino Grande probably originated in an oceanic arc during the Late Cretaceous (Echeverri *et al.*, 2015a). This unit and its basement collided obliquely against the western margin of Ecuador and Colombia during the Late Cretaceous – Paleogene, which generated thrusting, folding, and clastic sedimentation (Barrero *et al.*, 2006; Moreno–Sánchez & Pardo–Trujillo, 2003; Pindell & Kennan, 2009; Villagómez *et al.*, 2011). The sedimentary record of the Remolino Grande–1 well shows a Upper Cretaceous (Maastrichtian) – Eocene (ca. 20 Ma) unconformity, which could be associated with this tectonic event. In northern Ecuador, the accretion of the Piñon–Naranjal Terrane occurred at ca. 58 Ma (Paleocene) (Jaillard *et al.*, 2009). The presence of Eocene plutonic and volcanic rocks in the Western Cordillera (Agencia Nacional de Hidrocarburos & Geología Regional y Prospección, 2011; Barbosa–Espitia *et al.*, 2016) suggests that an Eocene volcanic arc was developed after the collision of the Tumaco Basin basement with the continental margin (Arco de Ricaute of Spadea & Espinosa, 1996). Over these rocks, upper Eocene – lower Miocene fine-grained clastic sedimentary successions were discordantly accumulated in shelf and prodelta environments (Lutitas de Remolino Grande Formation or 1 Sur Unit; Figure 2).

5.2. Early – Middle Miocene

The facies recorded in the wells suggest sedimentation in shelf, prodelta, and deltaic environments (Angostura, Viche, and Cayapas Formations; Figure 2; Agencia Nacional de Hidrocarburos & Universidad de Caldas, 2011a; Agencia Nacional de Hidrocarburos & Antek, 2013). The common presence of muddy matrix and the angularity and poor sorting of grains in sandstones and conglomerates suggest first-cycle sedimentation and rapid burial. During the early Miocene, an ca. 5 Ma unconformity was identified in the Remolino Grande–1 well (Figure 5). This unconformity could be related to an exhumation pulse of the Western Cordillera and the Remolino Grande–Gorgona Structural High, linked to an increase in the orthogonal convergence rates of the Nazca–South American Plates (cf. Pardo–Casas & Molnar, 1987; Somoza & Ghidella, 2012). Based on thermochronologic analyses of the Gorgona Island, the Tumaco Basin, and the southern part of the Western Cordillera, Barbosa–Espitia *et al.* (2013a) interpreted a progressive and generalized exuma-

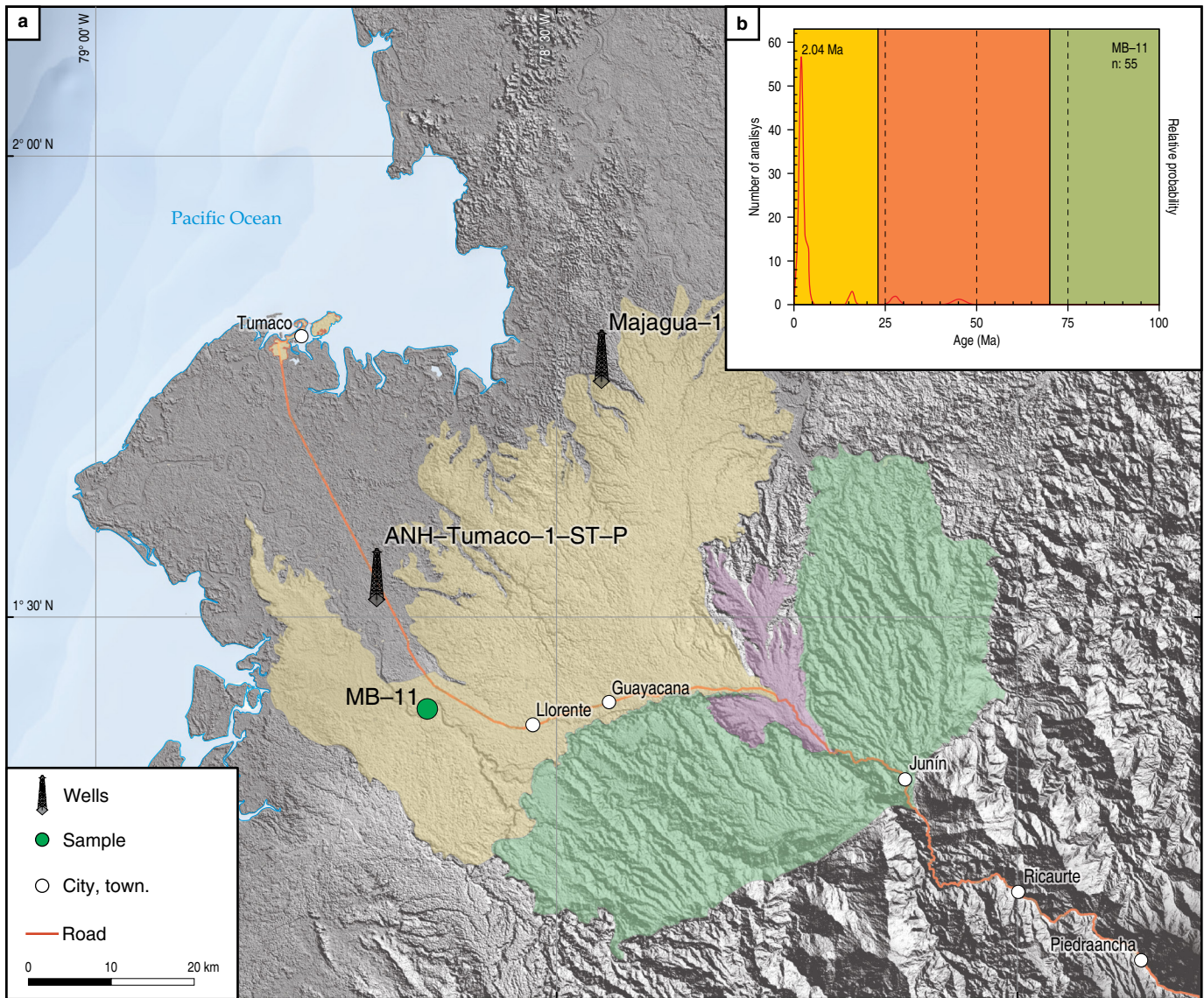


Figure 14. (a) Distribution of Pliocene – Pleistocene volcanoclastic fans in the southern Tumaco Basin. In green: the oldest fan; purple: the younger fan; brown: the youngest fan (see explanation in the text). (b) Relative probability diagrams of U/Pb ages of detrital zircons from the MB-11 sample (color conventions as in Figure 11).

tion cooling in the area between 24–22 and 20–16 Ma. Thermochronologic analyses of the Western and Eastern Cordilleras of Ecuador also recorded an exhumation event between 25–22 Ma, which suggests a regional event linked to plate-scale kinematic changes (Spikings & Crowhurst, 2004; Spikings et al., 2005). In Ecuador, a middle Miocene cooling event has been attributed to the increase in compressive stress during the collision of the Carnegie Ridge with the South American margin, which started at ca. 15 Ma (Spikings et al., 2010). According to López-Ramos (2009) the division of the Tumaco Borbón and Manglares (Tumaco offshore) Basins occurred in the middle Miocene time and was related to the subduction of the young and hot Nazca Plate and the decrease in the convergence rate.

Three compositional associations in lower – middle Miocene sandstones are indicative of sediment sources: (i) Abundance of plagioclase and intermediate volcanic fragments can be associated with volcanic igneous rock sources. (ii) Olivine and pyroxenes (mainly augite) are related to mafic–ultramafic igneous rocks (Figure 10). (iii) Potassium feldspar, quartz, amphibole, and occasionally biotite are related to acid and/or intermediate plutonic rocks. This can be compared to the present-day basement of the Western Cordillera, where upper Eocene and Oligocene granitoids intrude the Cretaceous oceanic sedimentary and basic igneous rocks (Figure 15; Barbosa-Espitia et al., 2016; Gómez et al., 2015). In the Majagua-1 well, there is more than 50% sedimentary lithics with respect to igneous fragments and feldspars. In contrast, the Remolino Grande-1 well

shows an increasing tendency in the content of volcanic, plutonic fragments, and feldspars in the middle Miocene (Figures 6, 7). The analysis of heavy minerals in the Remolino Grande-1 well shows a domain of unstable phases (mainly epidote, augite, and hornblende), and the Majagua-1 well presents a domain of ultrastable phases (mainly zircon and apatite). These compositional contrasts are probably related to different source areas or disconnection in the paleo-drainage systems or may also be influenced by the formation of topographic highs that controlled the drainages and acted as sedimentation barriers.

The 24–18 Ma and 12–14 Ma most frequent populations of detrital zircons indicate a magmatic activity during these periods in the vicinity of the basin, which can be associated with Western Cordillera plutonic bodies that intrude the Cretaceous oceanic sedimentary and basic igneous rocks of the Western Cordillera (Agencia Nacional de Hidrocarburos & Geología Regional y Prospección, 2011; Barbosa-Espitia *et al.*, 2016; Echeverri *et al.*, 2015b). Magmatic activity close to the source is also consistent with the preservation of feldspars and volcanic fragments and is associated with the erosion of middle–upper crustal levels in orogenic zones with magmatic activity. The occurrence of chert and other sedimentary lithics in the sandstones, as well as Mesozoic, Paleozoic, and Precambrian detrital zircons, suggests reworking of pre-Miocene sedimentary sequences of the Western Cordillera or, alternatively, a connection with the Central Cordillera basement. This connection could explain the presence of metamorphic fragments in very low percentages. Additionally, marine fossils (mollusks and foraminifera) have been reported in the rocks of the Cauca–Patía Basin for the Oligocene – Miocene interval (León *et al.*, 1973). This basin is located to the east of the Tumaco Basin between the Central and Western Cordilleras, which could indicate that the Tumaco and Cauca–Patía Basins were connected and that some sediments came directly from erosion of the Central Cordillera basement.

5.3. Late Miocene – Pliocene

In general, the presence of sandstones and conglomerates in the Majagua-1 and Remolino Grande-1 wells, as well as the abundance of mollusks and carbonized organic matter, suggest deposition in the delta plain and nearshore environments (San Agustín and Chagüí Formations; Figure 2). Fine-grained intervals with abundant mollusks and foraminifera could be associated with the lower delta front–prodelta transition. Agencia Nacional de Hidrocarburos & Antek (2013) proposed sedimentary environments varying from fluvial channels, estuarine and mouth bars, delta front and prodelta environments in the Tumaco 1–ST–P well. During this period, an increase in the sedimentation rate is notorious (Figures 5, 15).

The late Miocene increase in the sedimentation rate may be related to high subsidence in the basin (Echeverri, 2012;

López-Ramos, 2009) and to the increase in the volcanic activity of the magmatic arc. López-Ramos (2009) suggests that the considerable sediment accumulation in the Tumaco Basin would have resulted from crustal buckling due to horizontal stress transfer into the overriding plate and the erosion of the Western Cordillera. He also indicates that the Remolino Grande Gorgona High was uplifted and allowed sediments to dam in the Tumaco onshore basin. Late Miocene – Pliocene uplift pulses (ca. 14–10 and ca. 6–4 Ma) recognized in southwestern Colombia (Barbosa-Espitia *et al.*, 2013b) could be related to the following: (i) Subduction of the young oceanic crust with change in the subduction angle between Nazca and the South American Plate (Echeverri *et al.*, 2015b), (ii) orthogonal convergence of the Nazca Plate (Pardo-Casas & Molnar, 1987; Somoza, 1998), or (iii) the collision of a buoyant slab segment, derived from the Nazca Plate, such as a small ridge or seamount, similar to, or being part of, the Carnegie Ridge, and (iv) the collision of the Panamá–Chocó Block (Barbosa-Espitia *et al.*, 2013a).

López-Ramos (2009) indicated a upper Miocene (Tortonian) unconformity (called U2) based on seismic reflectors in the Tumaco Basin. It can be associated with a facies change in the Majagua-1 (8000'; base of the Chagüí Formation) and the Tumaco 1–ST–P wells (ca. 5400'; base of the Tangareal del Mira Formation of Agencia Nacional de Hidrocarburos & Antek, 2013) (Figure 5). This unconformity can be related with an eustatic sea level drop (10.5 Ma; Haq *et al.*, 1987; López-Ramos, 2009). Based on thermochronological constraints, Barbosa-Espitia *et al.* (2013b) proposed that the Remolino Grande–Gorgona Structural High was uplifted between 14–10 Ma. This is also supported by the common presence of early Miocene reworked microfossils (Figure 15).

During the late Miocene, the upward increase in the proportion of unstable minerals such as plagioclase, pyroxene, oxyhornblende, hornblende, and volcanic fragments indicates an intensification of magmatic activity (Figure 7). This is in agreement with a dominant 12–8 Ma zircon population. The presence of microcline and biotite, as well as the occurrence of the 25–18 Ma and 50–30 Ma zircon populations, suggest the onset of the erosion of granitoids (Figures 6, 7), which could be associated with the Western Cordillera basement (e.g., Piedrancha Granodiotrite, Nulpi Gabronorite, and ca. 44 Ma dikes intruding the Timbiquí Formation; Figure 15; Agencia Nacional de Hidrocarburos & Geología Regional y Prospección, 2011a; Agencia Nacional de Hidrocarburos & Universidad de Caldas, 2011a; Barbosa-Espitia *et al.*, 2016; Echeverri *et al.*, 2015b). The presence of chert, sandstone, and shale fragments, as well as Mesozoic, Paleozoic, and Precambrian zircons, suggests reworking of the pre-Miocene sedimentary cover or partial connection with the Central Cordillera basement. The good preservation of plagioclase and volcanic lithics suggests short transport, rapid burial, and negligible diagenesis effects.

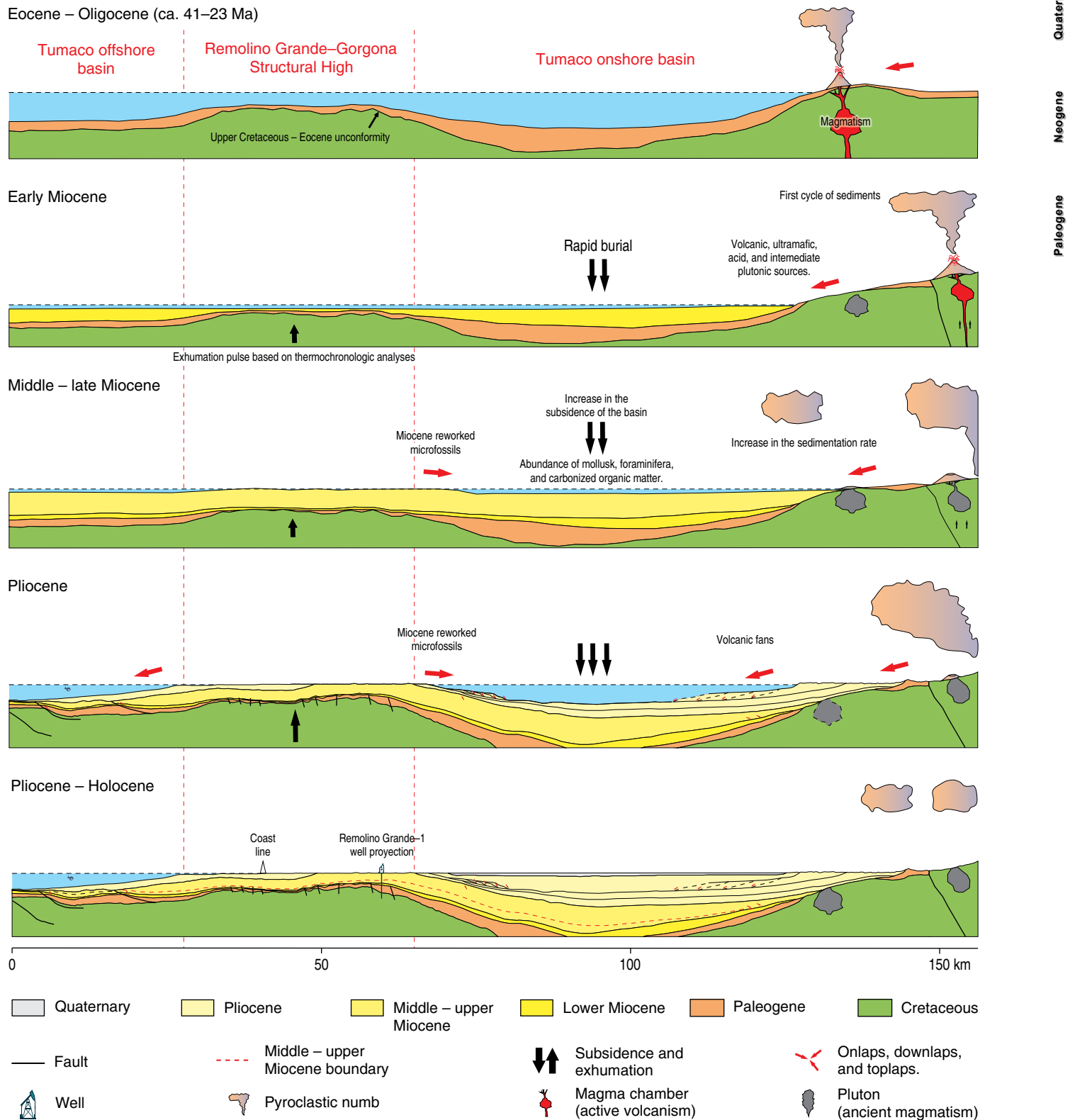


Figure 15. Eocene to Holocene geologic evolution of the southern Tumaco Basin. Not palinsparitically restored. The thick red arrows indicate the direction of sediment transport. See the explanation in the text.

The Miocene – Pliocene boundary is difficult to locate with the available information. Based on paleontological data, Agencia Nacional de Hidrocarburos & Antek (2013) indicated the First Appearance Datum (FAD) of *Cyatheacidites annulatus* in the Tumaco 1–ST–P well at 3950' (ditch cutting sample). The FAD of this species is located approximately at the Tortonian – Messinian boundary (7.1 Ma, Jaramillo et al., 2011). The correlation of seismic reflectors with the Maja-gua-1 well (Figure 3b) allowed the establishment of a depth of ca. 6000' for this boundary. A 4.1 Ma (Zanclean) minimal age of detrital zircons from the Tumaco 1–ST–S at 400' indicates that the Miocene – Pliocene boundary is between 3950–400' (Figure 5). These difficulties show the importance of using multi-tools for chronostratigraphic interpretation, as well as the need to acquire more geological information in other places of the basin.

5.4. Pliocene – Pleistocene

During the Pliocene – Pleistocene, volcanoclastic fans were identified at the SE border of the basin (Figure 14). A progradation of seismic reflectors to the west (Figure 3a) can probably be associated with the increase in the erosion rates and/or the volcanic activity. Seismic information (e.g., onlap surfaces and eastward prograding reflectors in the western border of the onshore basin) also shows an influence of the Remolino Grande–Gorgona Structural High in the sedimentation (Figures 3a, 15).

López-Ramos (2009) identified an important Pliocene (Zanclean) unconformity (U3) marked by a deep erosional surface and an abrupt facies change (sandstones and conglomerates of the Cascajal Formation; Echeverri et al., 2016) and probably related to a regional Andean orogenic event (e.g., van der Hammen et al., 1973). Thermochronological data obtained for the Western Cordillera (Piedrancha Pluton) and in the sedimentary fill of the Tumaco Basin recorded an ca. 4 Ma exhumation event (Barbosa-Espitia et al., 2013a). This time period also coincides with a marine eustatic drop (Haq et al., 1987).

6. Conclusions

The Tumaco Basin has a through symmetric shape with ca. 26 000' (ca. 8000 m) of sediments in its depocenter. These deposits accumulated as a response to the subduction of the Farallon and Nazca Plates beneath the South American Plate, controlling subsidence, magmatic activity, and sedimentation rates.

The sedimentary fill is mainly composed of mudrocks, sandstones, and conglomerates that varied in proportion through time and accumulated in open marine to deltaic environments. The integration of biostratigraphic data obtained by the analysis of calcareous nannofossils, planktonic foraminifera, palynology, and detrital zircons allows us to produce an

age model of the sedimentary deposits. The sequence starts in the Paleogene (NP19 and P16), and the upper part of the record is consistent with a Messinian – Piacenzian age. The information to establish the age of the upper Miocene – Pliocene deposits is still limited.

The Neogene sandstones of the Tumaco Basin are mainly related to nearby intermediate to mafic magmatic sources similar to the present-day Western Cordillera basement. Eocene and Cretaceous zircon populations can be related to the erosion of the Western Cordillera plutonic and volcanic rocks. The presence of Jurassic and older sources would be linked to the reworking coming from units of the Western Cordillera, although it is possible that in some areas, a direct connection with the Central Cordillera basement existed. Differences in petrography and heavy mineral associations for sediments accumulated at the same time could be related to different source areas or disconnection in the paleo-drainage systems related to topographic highs.

Detrital zircons and petrographic data indicate that sedimentation was contemporary with magmatic activity, which started at ca. 26 Ma (late Oligocene) until today, and recorded an increasing activity since the middle Miocene.

The seismic, biostratigraphic, and geochronological data enabled the identification and quantification of the duration of some unconformities in the Tumaco Basin (e.g., Late Cretaceous – Eocene, early Miocene), which seem to be related to regional and global tectonic processes, such as changes in the direction and convergence rates of tectonic plates, subduction of seamounts, and eustasy.

Acknowledgements

We thank the Agencia Nacional de Hidrocarburos and the Vicerrectoría de Investigaciones y Posgrados (Universidad de Caldas) for their financial support (contract 092 of 2009, Universidad de Caldas–Agencia Nacional de Hidrocarburos). Special thanks are due to the Instituto de Investigaciones en Estratigrafía (IIES) staff for their logistic support. People of the communities of Tumaco, Salahonda, Cascajal, and La Chorrera are greatly acknowledged for their hospitality and help during the field work. We give special thanks to many people that participate in the 092 contract: Clemencia GÓMEZ, Jairo Alonso OSORIO, Elvira C. RUÍZ, Gustavo HINCAPIÉ, Sebastián ROSERO, Marcelo JARAMILLO, Juan Carlos PATIÑO, Alejandro PINILLA, César MADRID, Rosa Ester NAVARRETE, Francisco SIERRA, Alejandra MEJÍA, Erika BEDOYA, Diana OCHOA, Silane Da SILVA, Fatima LEITE, Millerlandy ROMERO, Jenny GARCÍA, and José María JARAMILLO, among others. We also thank Jorge GÓMEZ TAPIAS (Servicio Geológico Colombiano) for his help and patience during the editing of this paper. Fundación Carolina supported AP–T with a postdoctoral stay in Salamanca (Spain) for the finalization of

this document. The critical revision of the manuscript by Etienne JAILLARD and Mario SUÁREZ is greatly appreciated. We thank Daniela MATEUS ZABALA and the editorial board of the Servicio Geológico Colombiano for helpful comments that improved the chapter presentation.

References

- Agencia Nacional de Hidrocarburos & Antek. 2013. Estudio integrado de los núcleos obtenidos de los pozos perforados por la ANH y de las muestras de pozo (núcleos y rípios) disponibles en la Litoteca Nacional, localizados en zonas de interés para la ANH. Pozo Tumaco-1-ST-P. Agencia Nacional de Hidrocarburos, unpublished report.
- Agencia Nacional de Hidrocarburos & Geología Regional y Prospección. 2011. Cartografía geológica a escala 1:100 000 de las planchas 340, 362, 385 y 409 localizadas en la Cuenca Tumaco, así como el inherente levantamiento de columnas estratigráficas y muestreo litológico para los análisis petrográficos, bioestratigráficos, geoquímicos, petrofísicos y radiométricos. Contrato 084 de 2010, unpublished report. 207 p.
- Agencia Nacional de Hidrocarburos & Universidad de Caldas. 2011a. Estudio geológico integrado en la Cuenca Tumaco onshore. Síntesis cartográfica, sísmica y análisis bioestratigráfico, petrográfico, geocronológico, termocronológico y geoquímico de testigos de perforación y muestras de superficie. Contrato 092 de 2009. Unpublished report, 191 p. Manizales, Colombia.
- Agencia Nacional de Hidrocarburos & Universidad de Caldas. 2011b. Estudio integrado de los núcleos y registros obtenidos de los pozos someros (slim holes) perforados por la Agencia Nacional de Hidrocarburos. Informe Final Contrato 093 de 2009. unpublished report.
- Agnini, C., Fornaciari, E., Raffi, I., Catanzariti, R., Pálíke, H., Backman, J. & Rio, D. 2014. Biozonation and biochronology of Paleogene calcareous nannofossils from low and middle latitudes. *Newsletters on Stratigraphy*, 47(2): 131–181. <https://doi.org/10.1127/0078-0421/2014/0042>
- Aleman, A. & Ramos, V.A. 2000. Northern Andes. In: Cordani, U.G., Milani, E.J., Thomaz-Filho, A. & Campos, D.A. (editors), *Tectonic evolution of South America*. 31st International Geological Congress. Proceedings, p. 453–480. Rio de Janeiro, Brazil.
- Arango, J.L. & Ponce, A. 1980. Memoria explicativa: Reseña explicativa del mapa geológico del departamento de Nariño. Scale 1:400 000. Ingeominas, 40 p. Bogotá.
- Aspden, J. 1984. The geology of the Western Cordillera and Pacific coastal plain in the Department of Valle del Cauca (sheets 261, 278, 279, 280 and 299). Ingeominas-Misión Británica, Internal report 1959, 61 p. Cali.
- Aspden, J. & Nivia, A. 1985. Memoria explicativa: Reseña explicativa del mapa geológico preliminar de la plancha 278 bahía de Buenaventura. Scale 1:100 000. Ingeominas, 13 p. Bogotá.
- Aubry, M.P. 2014. Cenozoic coccolithophores: Discoasterales (CC-B). Atlas of micropaleontology series, part 1 of 4. The Micropaleontology Press Foundation, 104 p. New York.
- Aubry, M. 2015. Cenozoic coccolithophores: Discoasterales (CC-D). Atlas of micropaleontology series. The Micropaleontology Press Foundation, 433 p. New York.
- Backman, J., Raffi, I., Rio, D., Fornaciari, E. & Pálíke, H. 2012. Biozonation and biochronology of Miocene through Pleistocene calcareous nannofossils from low and middle latitudes. *Newsletters on Stratigraphy*, 45(3): 221–244. <https://doi.org/10.1127/0078-0421/2012/0022>
- Barbosa-Espitia, A.A., Restrepo-Moreno, S.A., Pardo-Trujillo, A., Osorio, J.A. & Ochoa, D. 2013a. Uplift and exhumation of the southernmost segment of the Western Cordillera, Colombia, and development of the neighboring Tumaco Basin. *GSA Annual Meeting 125th Anniversary of GSA. Proceedings* 45(7): p. 548. Denver, USA.
- Barbosa-Espitia, A.A., Restrepo-Moreno, S., Pardo-Trujillo, A., Ochoa, D.I. & Osorio, J.A. 2013b. Uplift and exhumation of the southernmost segment of the Western Cordillera and development of the Tumaco Basin. XIV Congreso Colombiano de Geología. Abstract, p. 387. Medellín.
- Barbosa-Espitia, A.A., Foster, D.A., Restrepo-Moreno, S.A., Pardo-Trujillo, A. & Kamenov, G. 2016. Geochemistry and geochronology of plutonic rocks from the Colombian Western Cordillera: New insights into the Cenozoic tectonics of the NW South American plate margin. *GSA Annual Meeting. Abstracts with Programs*, 48(7): Paper No. 347–27. <https://doi.org/10.1130/abs/2016AM-279826>
- Barrero, D., Laverde, F., Ruiz, C.C. & Alfonso, C.A. 2006. Oblique collision and basin formation in western Colombia: The origin, evolution and petroleum potential of Cauca-Patía Basin. IX Simposio Bolivariano de Exploración en Cuencas Subandinas. Abstracts CD ROM. Cartagena, Colombia.
- Barrero, D., Pardo, A., Vargas, C.A. & Martínez, J.F. 2007. Colombian sedimentary basins: Nomenclature, boundaries and petroleum geology, a new proposal. *Agencia Nacional de Hidrocarburos*, 92 p. Bogotá.
- Bedoya, E.L., Flores, J.A. & Pardo, A. 2013. Nanofósiles calcáreos y bioestratigrafía del Mioceno tardío del SW de la Cuenca Tumaco onshore, Pacífico colombiano. *Boletín de Geología*, 35(1): 55–66.
- Berggren, W.A., Kent, D.V., Swisher III, C.C. & Aubry, M.P. 1995. A revised Cenozoic geochronology and chronostratigraphy. In: Berggren, W.A., Kent, D.V., Aubry, M.P. & Hardenbol, J. (editors), *Geochronology, time scales and global stratigraphic correlation*. SEPM Special Publications 54: p. 129–212. <https://doi.org/10.2110/pec.95.04.0129>
- Bermúdez, H.D., García, J., Stinnesbeck, W., Keller, G., Rodríguez, J.V., Hanel, M., Hopp, J., Schwarz, W., Trieloff, M., Bolívar, L. & Vega, F.J. 2016. The Cretaceous – Paleogene boundary

- at Gorgonilla Island, Colombia, South America. *Terra Nova*, 28(1): 83–90. <https://doi.org/10.1111/ter.12196>
- Blow, W.H. 1969. Late middle Eocene to recent planktonic foraminiferal biostratigraphy. In: Bronnimann, P. & Renz, H.H. (editors), *Proceedings of the First International Conference on Planktonic Microfossils*, 1, p. 199–422. Geneva, Switzerland.
- Borrero, C., Pardo, A., Jaramillo, C.M., Osorio, J.A., Cardona, A., Flores, A., Echeverri, S., Rosero, S., García, J. & Castillo, H. 2012. Tectonostratigraphy of the Cenozoic Tumaco Forearc Basin, Colombian Pacific, and its relationship with the northern Andes orogenic build up. *Journal of South American Earth Sciences*, 39: 75–92. <https://doi.org/10.1016/j.jsames.2012.04.004>
- Cediel, F., Restrepo, I., Marín-Cerón, M.I., Duque-Caro, H., Cuartas, C., Mora, C., Montenegro, G., García, E., Tovar, D. & Muñoz, G. 2009. Geology and hydrocarbon potential, Atrato and San Juan Basins, Chocó (Panamá) Arc. Tumaco Basin (Pacific realm), Colombia. *Agencia Nacional de Hidrocarburos and Fondo Editorial Universidad EAFIT*, 172 p. Medellín, Colombia.
- Cohen, K.M., Finney, S.C., Gibbard, P.L. & Fan, J.X. 2013 (updated 2017/02). The ICS International Chronostratigraphic Chart. *Episodes*, 36(3): 199–204.
- Cortés, J.E., Mejía-Molina, A., Morton, A., Vargas, C.A. & Cortés, S.I. 2019. Provenance, tectonic setting, and weathering of sediments in Tumaco-1 ST-P well, Tumaco Forearc Basin, Colombia: Insights from petrography, heavy minerals, X-ray diffraction, and whole-rock chemostratigraphy. *Journal of South American Earth Sciences*, 96: 102219. <https://doi.org/10.1016/j.jsames.2019.102219>
- Dickinson, W.R. & Gehrels, G.E. 2009. Use of U–Pb ages of detrital zircons to infer maximum depositional ages of strata: A test against a Colorado Plateau Mesozoic database. *Earth and Planetary Science Letters*, 288(1–2): 115–125. <https://doi.org/10.1016/j.epsl.2009.09.013>
- Echeverri, S. 2012. Estratigrafía y análisis de procedencia del intervalo Eoceno – Plioceno de la cuenca de forearc de Tumaco “onshore” (SW de Colombia) y su relación con la tectónica de la margen pacífica del NW de Suramérica. Master thesis, Universidad de Caldas, 127 p. Manizales.
- Echeverri, S., Borrero, C., Moreno, M., Pardo-Trujillo, A. & Castillo, H. 2011. Nomenclatura estratigráfica para la sucesión neógena expuesta en la bahía de Tumaco, Cuenca Tumaco costa adentro, SW de Colombia: Redefinición y formalización. XIV Congreso Latinoamericano de Geología y XIII Congreso Colombiano de Geología. Abstracts, p. 364. Medellín, Colombia.
- Echeverri, S., Cardona, A., Pardo-Trujillo, A., Borrero, C., Rosero, S. & López, S. 2015a. Correlación y geocronología Ar–Ar del basamento cretácico y el relleno sedimentario Eoceno superior – Mioceno (Aquitaniense inferior) de la cuenca de antearco de Tumaco, SW de Colombia. *Revista Mexicana de Ciencias Geológicas*, 32(2): 179–189.
- Echeverri, S., Cardona, A., Pardo, A., Mosalve, G., Valencia, V.A., Borrero, C., Rosero, S. & López, S. 2015b. Regional provenance from southwestern Colombia fore-arc and intra-arc basins: Implications for middle to late Miocene orogeny in the northern Andes. *Terra Nova*, 27(5): 356–363. <https://doi.org/10.1111/ter.12167>
- Echeverri, S., Pardo-Trujillo, A., Borrero, C., Cardona, A., Rosero, S., Celis, S.A. & López, S.A. 2016. Estratigrafía del Neógeno superior al sur de la Cuenca Tumaco (Pacífico colombiano): La Formación Cascajal, propuesta de redefinición litoestratigráfica. *Boletín de Geología*, 38(4): 43–60. <http://dx.doi.org/10.18273/revbol.v38n4-2016003>
- Escovar, R., Gómez, L.A. & Ramírez, J.R. 1992. Interpretación de la sísmica Tumaco 90 y evaluación preliminar del área: Bogotá. *Empresa Colombiana de Petróleos*, unpublished report, 74 p. Bogotá.
- Folk, R. 1974. *Petrology of sedimentary rocks*. Hemphill Publishing Company, 182 p. Austin, USA.
- García, J. 2012. Procedencia de los sedimentos neógenos de Tumaco onshore y Gorgona: Una contribución a la tectónica de antearco del Pacífico sur de Colombia. Master thesis, Universidad de Caldas, 82 p. Manizales, Colombia.
- Gehrels, G.E., Valencia, V. & Pullen, A. 2006. Detrital zircon geochronology by laser-ablation multicollector ICPMS at the Arizona LaserChron Center. In: Loszewski, T. & Huff, W. (editors), *Geochronology: Emerging opportunities*. Paleontology Society Short Course: Paleontology Society Papers, 11, 10 p.
- Giraldo-Villegas, C.A., Celis, S.A., Rodríguez-Tovar, F.J., Pardo-Trujillo, A., Vallejo-Hincapié, D.F. & Trejos-Tamayo, R.A. 2016. Ichnological analysis of the upper Miocene in the ANH-Tumaco-1-ST-P well: Assessing paleoenvironmental conditions at the Tumaco Basin, in the Colombian Pacific. *Journal of South American Earth Sciences*, 71: 41–53. <https://doi.org/10.1016/j.jsames.2016.06.008>
- Gómez, J., Montes, N.E., Nivia, Á. & Diederix, H., compilers. 2015. *Geological Map of Colombia 2015*. Scale 1:1 000 000. Servicio Geológico Colombiano, 2 sheets. Bogotá. <https://doi.org/10.32685/10.143.2015.936>
- González, H., compiler. 2008. *Investigación integral del Andén Pacífico colombiano*. Tomo 1: Geología; Cuenca de Tumaco. Igac-Ingeominas. p. 85–86. Bogotá.
- Hall, M.L. & Wood, C.A. 1985. Volcano-tectonic segmentation of the northern Andes. *Geology*, 13(3): 203–207. [https://doi.org/10.1130/0091-7613\(1985\)13<203:VSOTNA>2.0.CO;2](https://doi.org/10.1130/0091-7613(1985)13<203:VSOTNA>2.0.CO;2)
- Haq, B.U., Hardenbol, J. & Vail, P.R. 1987. Chronology of fluctuating sea levels since the Triassic. *Science*, 235: 1156–1167.
- Instituto Colombiano de Geología y Minería & Instituto Geográfico Agustín Codazzi. 2005. *Mapa geológico de las planchas 361 Bis, 383 Tumaco, 384 La Chorrera, 407 Cabo Manglares y 408 Barbacoas*. Scale 1:100 000. Bogotá.
- Jaillard, E., Lapierre, H., Ordoñez, M., Toro-Álava, J., Amórtegui, A. & Vanmelle, J. 2009. Accreted oceanic terranes in Ecuador: Southern edge of the Caribbean Plate? *Geological Society of*

- London, Special Publications 328, p. 469–485. <https://doi.org/10.1144/SP328.19>
- Jaramillo, C., Rueda, M. & Torres, V. 2011. A palynological zonation for the Cenozoic of the Llanos and Llanos Foothills of Colombia. *Palynology*, 35(1): 46–84. <https://doi.org/10.1080/01916122.2010.515069>
- Kennett, J.P. & Srinivasan, M.S. 1983. Neogene planktonic foraminifera: A phylogenetic atlas. Hutchinson Ross Publishing Company. 265 p.
- Kochelek, E.J., Amato, J.M., Pavlis, T.L. & Clift, P.D. 2011. Flysch deposition and preservation of coherent bedding in an accretionary complex: Detrital zircon 111 ages from the Upper Cretaceous Valdez Group, Chugach Terrane, Alaska. *Lithosphere*, 3(4): 265–274.
- León, L.A., Padilla, L.E. & Marulanda, N. 1973. Geología, recursos minerales y geoquímica de la parte NE del cuadrángulo 0–5 El Bordo, departamento del Cauca. Ingeominas, Internal report 1652, 235 p. Popayán.
- López, P.A., Pardo, A., Ochoa, D. & Rosero, S. 2012. Palinología de los sedimentos recientes del río Mira, Pacífico colombiano. *Geología Colombiana*, 37(1): 21–22.
- López-Ramos, E. 2009. Evolution tectono-stratigraphique du double basin avant-arc de la marge convergente Sud Colombienne–Nord Equatorienne pendant le Cénozoïque. Doctorate thesis, Université de Nice Sophia Antipolis, 349 p. Nice, France.
- Lourens, L.J., Hilgen, F.J., Shackleton, N.J., Laskar, J. & Wilson, D. 2004. The Neogene Period. In: Gradstein, F.M., Ogg, J.G. & Smith, A.G. (editors), *Geological time scale 2004*, Cambridge University Press, pp. 409–440. Cambridge, UK.
- Ludwig, K.R. 2003. User's manual for Isoplot 3.00: A geochronological toolkit for Microsoft Excel. Berkeley Geochronology Center, Special Publication (4), 70 p.
- Mange, M.A. & Maurer, H.F.W. 1992. Heavy minerals in colour. Chapman & Hall, 147 p. London, UK.
- Marcaillou, B. & Collot, J.Y. 2008. Chronostratigraphy and tectonic deformation of the north Ecuadorian–South Colombian offshore Manglares Forearc Basin. *Marine Geology*, 255(1–2): 30–44. <https://doi.org/10.1016/j.margeo.2008.07.003>
- Marín-Cerón, M.I. & Sierra, G. 2011. Tumaco Basin. In: Cedié, F. (editor), *Petroleum geology of Colombia: Geology and hydrocarbon potential*, 13. Agencia Nacional de Hidrocarburos and Universidad EAFIT, 77 p. Medellín.
- Martini, E. 1971. Standard Tertiary and Quaternary calcareous nannoplankton zonation. *Proceedings 2nd Planktonic Conference*, 739–785. Roma, Italy.
- Moreno-Sánchez, M. & Pardo-Trujillo, A. 2003. Stratigraphical and sedimentological constraints on western Colombia: Implications on the evolution of the Caribbean Plate. In: Bartolini, C., Buffler, R.T. & Blickwede, J. (editors), *The circum-Gulf of Mexico and the Caribbean: Hydrocarbon habitats, basin formation, and plate tectonics*. American Association of Petroleum Geologists Memoir 79, p. 891–924. Tulsa, USA.
- Nelson, H.W. 1962. Contribución al conocimiento de la cordillera Occidental: Sección carretera Cali–Buenaventura. *Boletín Geológico*, 10(1–3): 81–108.
- Nivia, A., Pérez, C. & Sepúlveda, J. 2003. Memoria explicativa: Geomorfología y geología de la plancha 383 Tumaco. Scale: 1:100 000. Ingeominas, 39 p. Cali, Colombia.
- Okada, H. & Bukry, D. 1980. Supplementary modification and introduction of code numbers to the low-latitude coccolith biostratigraphic zonation (Bukry, 1973; 1975). *Marine Micropaleontology*, 5: 321–325. [https://doi.org/10.1016/0377-8398\(80\)90016-X](https://doi.org/10.1016/0377-8398(80)90016-X)
- Oppenheim, V. 1949. Geología de la costa sur del Pacífico de Colombia. *Boletín Instituto Geofísico de los Andes Colombianos*, (1), Serie C: 4–23.
- Pardo-Casas, F. & Molnar, P. 1987. Relative motion of the Nazca (Farallon) and South American Plates since Late Cretaceous time. *Tectonics*, 6(3): 233–248. <https://doi.org/10.1029/TC006i003p00233>
- Perch-Nielsen, K. 1985. Mesozoic calcareous nannofossils. In: Bolli, H., Saunders, J.B. & Perch-Nielsen, K. (editors), *Plankton stratigraphy*. Cambridge University Press, p. 329–426.
- Pindell, J.L. & Kennan, L. 2009. Tectonic evolution of the Gulf of Mexico, Caribbean and northern South America in the mantle reference frame: An update. In: James, K.H., Lorente, M.A. & Pindell, J.L. (editors), *The origin and evolution of the Caribbean Plate*. Geological Society of London, Special Publication 328, p. 1–55. <https://doi.org/10.1144/SP328.1>
- Raffi, I., Backman, J., Fornaciari, E., Pälike, H., Rio, D., Lourens, L. & Hilgen, F. 2006. A review of calcareous nannofossil astro-biochronology encompassing the past 25 million years. *Quaternary Science Reviews*, 25(23–24): 3113–3137. <https://doi.org/10.1016/j.quascirev.2006.07.007>
- Ramos, V.A. 1999. Plate tectonic setting of the Andean Cordillera. *Episodes*, 22(3): 183–190.
- Robertson Research inc. & Empresa Colombiana de Petróleos. 1981a. Geochemical and biostratigraphic analysis of Wainoco No.1, Majagua, Colombia. Internal report 413, 61 p. Houston, USA.
- Robertson Research inc. & Empresa Colombiana de Petróleos. 1981b. Biostratigraphic, geochemical and petrological analysis of samples from Arco well Remolino Grande–1, Colombia. Internal report 318, 75 p. Houston, USA.
- Serrano, L., Ferrari, L., López-Martínez, M., Petrone, C.M. & Jaramillo, C. 2011. An integrative geologic, geochronologic and geochemical study of Gorgona Island, Colombia: Implications for the formation of the Caribbean Large Igneous Province. *Earth and Planetary Science Letters*, 309(3–4): 324–336. <https://doi.org/10.1016/j.epsl.2011.07.011>
- Somoza, R. 1998. Updated Nazca (Farallon)–South America relative motions during the last 40 My: Implications for mountain building in the central Andean region. *Journal of South American Earth Sciences*, 11(3): 211–215. [https://doi.org/10.1016/S0895-9811\(98\)00012-1](https://doi.org/10.1016/S0895-9811(98)00012-1)

- Somoza, R. & Ghidella, M.E. 2012. Late Cretaceous to recent plate motions in western South America revisited. *Earth and Planetary Science Letters*, 331–332: 152–163. <https://doi.org/10.1016/j.epsl.2012.03.003>
- Spadea, P. & Espinosa, A. 1996. Petrology and chemistry of Late Cretaceous volcanic rocks from the southernmost segment of the Western Cordillera of Colombia (South America). *Journal of South American Earth Sciences*, 9(1–2): 79–90. [https://doi.org/10.1016/0895-9811\(96\)00029-6](https://doi.org/10.1016/0895-9811(96)00029-6)
- Spikings, R. & Crowhurst, P. 2004. (U–Th)/He thermochronometric constraints on the late Miocene – Pliocene tectonic development of the northern Cordillera Real and the Interandean Depression, Ecuador. *Journal of South American Earth Sciences*, 17: 239–251.
- Spikings, R.A. & Simpson, G. 2014. Rock uplift and exhumation of continental margins by the collision, accretion, and subduction of buoyant and topographically prominent oceanic crust. *Tectonics*, 33(5): 635–655. <https://doi.org/10.1002/2013TC003425>
- Spikings, R.A., Winkler, W., Hughes, R.A. & Handler, R. 2005. Thermochronology of allochthonous terranes in Ecuador: Unravelling the accretionary and post-accretionary history of the northern Andes. *Tectonophysics*, 399(1–4): 195–220.
- Spikings, R., Crowhurst, P.V., Winkler, W. & Villagómez, D. 2010. Syn- and post-accretionary cooling history of the Ecuadorian Andes constrained by their in-situ and detrital thermochronometric record. *Journal of South American Earth Sciences*, 30(3–4): 121–133. <https://doi.org/10.1016/j.jsames.2010.04.002>
- Suárez, M.A. 1990. Estudio geológico regional e interpretación sísmica estratigráfica en la provincia sedimentaria de la costa Pacífica. Ecopetrol, unpublished report, 119 p. Bogotá.
- Suárez, M.A. 2007. Geological framework of the Pacific coast sedimentary basins. *Geología Colombiana*, 32: 47–62.
- Vallejo, C., Winkler, W., Spikings, R.A., Luzieux, L., Heller, F. & Bussy, F. 2009. Mode and timing of terrane accretion in the forearc of the Andes in Ecuador. In: Kay, S.M., Ramos, V.A. & Dickinson, W.R. (editors), *Backbone of the Americas: Shallow subduction, plateau uplift, and ridge and terrane collision*. Geological Society of America, Memoirs 204, p. 197–216. [https://doi.org/10.1130/2009.1204\(09\)](https://doi.org/10.1130/2009.1204(09))
- van der Hammen, T. 1958. Estratigrafía del Terciario y Maastrichtiano continentales y tectogénesis de los Andes colombianos. *Boletín Geológico*, 6(1–3): 67–128.
- van der Hammen, T., Werner, J.H. & van Dommelen, H. 1973. Palynological record of the upheaval of the northern Andes: A study of the Pliocene and lower Quaternary of the Colombian Eastern Cordillera and the early evolution of its high-Andean biota. *Review of Palaeobotany and Palynology*, 16(1–2): 1–122. [https://doi.org/10.1016/0034-6667\(73\)90031-6](https://doi.org/10.1016/0034-6667(73)90031-6)
- Villagómez, D., Spikings, R., Magna, T., Kammer, A., Winkler, W. & Beltrán, A. 2011. Geochronology, geochemistry and tectonic evolution of the Western and Central Cordilleras of Colombia. *Lithos*, 125(3–4): 875–896. <https://doi.org/10.1016/j.lithos.2011.05.003>
- Wade, B.S., Pearson, P.N., Berggren, W.A. & Pälike, H. 2011. Review and revision of Cenozoic tropical planktonic foraminiferal biostratigraphy and calibration to the geomagnetic polarity and astronomical time scale. *Earth-Science Reviews*, 104(1–3): 111–142. <https://doi.org/10.1016/j.earsci-rev.2010.09.003>

Explanation of Acronyms, Abbreviations, and Symbols:

ANH	Agencia Nacional de Hidrocarburos	LA-ICPMS	Laser ablation inductively coupled plasma mass spectrometry
AP-T	Andrés Pardo-Trujillo	TD	Total depth
FAD	First Appearance Datum		

Authors' Biographical Notes



Andrés PARDO-TRUJILLO is a geologist in the Departamento de Ciencias Geológicas at the Universidad de Caldas (Manizales, 1998). Andres obtained his MS in vegetal micropaleontology in 1997 and his PhD in Science from Liège University (Belgium, 2004). He has worked since 1989 as a professor in the Departamento de Ciencias Geológicas at Universidad de Caldas,

Colombia, in sedimentology, regional geology, palynology, and field geology. From 2006–2009, he worked as an advisor at the Agencia Nacional de Hidrocarburos (ANH), where he participated in the geological study of several Colombian sedimentary basins. Andres is currently the director of the Instituto de Investigaciones en Estratigrafía (IIES) and of the Grupo de Investigación en Estratigrafía y Vulcanología (GIEV) at the Universidad de Caldas. His main interest is the study of the geological and biological evolution of the NW corner of South America during the Cretaceous – Cenozoic.



Sebastián ECHEVERRI is a geologist from the Universidad de Caldas (Colombia), with an MS in earth sciences from the same university and a PhD in science–geotectonics from the Universidade de São Paulo (Brasil). Sebastián works as a researcher in the Grupo de Investigación en Estratigrafía y Vulcanología (GIEV) Cumanday – Instituto de Investigaciones en Estratigrafía

(IIES) at Universidad de Caldas (Colombia) and is part of the EGEO research group of the Universidad Nacional (Medellín). His main research area is the regional geology and tectono–stratigraphic evolution of convergent margins.



Carlos BORRERO attained a BS in geology from Universidad Nacional de Colombia (Bogotá, 1983). Stratigraphy, volcanology, field geology, and hazard and risk assessment and management have been the focus of his long career in academia at Universidad de Caldas (Manizales, 1985–2015) and as a consultant geologist (1991–present). Currently, he is semiretired.



Alejandro ARENAS is a geologist of the Departamento de Ciencias Geológicas at the Universidad de Caldas (Manizales, Colombia) and has an MS in earth sciences from the Universidad de Caldas (Manizales, Colombia). Alejandro has worked in REDCOM as a professional for Ecopetrol in the field of reservoir development. Alejandro is currently a researcher at the Instituto de Investigaciones en Estratigrafía (IIES) and belongs to the Grupo de Investigación en Estratigrafía y Vulcanología (GIEV) Cumanday. He has strong capabilities in 3D modeling and seismic interpretation.



Felipe VALLEJO is a geologist from the Universidad de Caldas (Colombia), MS and PhD student in geology at Universidad de Salamanca (Spain). Felipe works as a researcher and consultant at the Instituto de Investigaciones en Estratigrafía (IIES) of the Universidad de Caldas (Colombia). Felipe is also part of the Grupo de Investigación en Estratigrafía y Vulcanología (GIEV)

Cumanday. His work has been focused on building a biostratigraphic and biochronologic framework based on calcareous nannofossils for the Caribbean and Pacific Basins of Colombia.



Raúl TREJOS is a geologist from the Universidad de Caldas (Colombia) and has an MS in earth sciences from the Universidad de Salamanca (Spain). He is currently a PhD student in geology at the Universidad de Salamanca. Since 2013, Raúl has worked as a researcher at the Instituto de Investigaciones en Estratigrafía (IIES) – Universidad de Caldas and belongs to the Grupo de Investigación en Estratigrafía y Vulcanología (GIEV) Cumanday. He is recognized as a junior researcher by the Ministerio de Ciencias, Tecnología e Innovación in Colombia. His main experience is in micropaleontology (foraminifera).

investigación en Estratigrafía y Vulcanología (GIEV) Cumanday. He is recognized as a junior researcher by the Ministerio de Ciencias, Tecnología e Innovación in Colombia. His main experience is in micropaleontology (foraminifera).



Ángelo PLATA obtained his bachelor's degree in biology from the Universidad Industrial de Santander, Colombia, in 2007. He worked at the Colombian oil company Ecopetrol for 5 years as a junior biostratigrapher before going to Spain in 2012 to obtain his Master of Earth Science degree from the Department of Geology, Universidad de Salamanca. After returning from Universidad

de Salamanca, he began his current role as palynologist in chief of the Palynology Lab for Instituto de Investigaciones en Estratigrafía, Universidad de Caldas, where he studies terrestrial palynomorphs and marine diatoms. Currently, Angelo is a candidate for his PhD at Universidad de Salamanca.



José-Abel FLORES is a geologist in the Department of Geology of the Universidad de Salamanca (Spain) and obtained his PhD in sciences at the Universidad de Salamanca in 1997. A specialist in calcareous nannofossils, he has been a full professor of micropaleontology and oceanography since 2006 and an invited professor in several institutions in Europe, the Americas, and

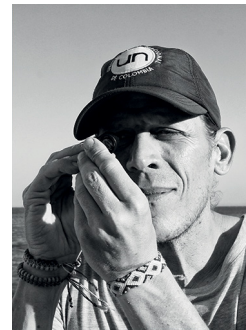
Japan. He centered his research in biostratigraphy and paleoceanography, participating in five ODP/IOPD expeditions and working with different hydrocarbon companies (Repsol, Gas Natural, Petrobras, Ecopetrol, Exxon). His interest and expertise cover the Cretaceous to present-day environments, combining microfossil and biogeochemistry information. In recent years, he has participated in several Colombian projects with the Universidad de Caldas, particularly the paleoceanographic evolution of tertiary basins, the consequences of the communication between the Atlantic and the Pacific, and the definition of a high-resolution astronomically calibrated scale based on micro and calcareous nannofossils.



Agustín CARDONA is graduated with a degree in geology from Universidad EAFIT in 1999. He obtained MS and PhD degrees in geochemistry and geotectonics, respectively, from the Universidade de São Paulo, Brasil. Subsequently, he was a postdoctoral fellow at the Smithsonian Tropical Research Institute (2006–2011), working in several paleogeographic-oriented projects in northern Colombia and Panamá.

Since 2012, he has served as full-time professor at the Universidad Nacional de Colombia in Medellín. His main interest is related to

regional tectonics of convergent margins, especially the Andean and Caribbean Orogens.



Sergio RESTREPO is a geologist from Universidad Nacional de Colombia. He holds a PhD in geology and geography from the Department of Geological Sciences at the University of Florida (UF, 2009) and is currently an associate professor in the Departamento de Geociencias y Medio Ambiente at Universidad Nacional de Colombia and adjunct postdoctoral researcher at University of

Florida. Sergio completed two postdoctoral studies under the auspices of the Smithsonian Institution (2009–2010) and the National Science Foundation (2011). During his doctoral and postdoctoral work, Sergio received research support from GSA, AGI, NSF, and the COMPTON Foundation, among others. Since 2010, Sergio has collaborated in several interdisciplinary projects carried out by the Instituto de Investigaciones en Estratigrafía (Universidad de Caldas, Colombia) while also developing some investigations supported by Colciencias and the National Geographic Society. Sergio's work in geosciences concentrates on the use of geochronology, thermochronology, and isotopic tools to understanding morphotectonic process over various spatio-temporal scales, as well as on the development of educational tools to advance earth and environmental literacy among rural communities. Geographically, Sergio's work focuses on the Andes, the Caribbean, and Central America.



Ángel BARBOSA is a Colombian geologist who obtained his bachelor's degree from the Universidad de Caldas in 2009 and an MS in geological sciences in 2012. His master's thesis focused on low-temperature thermochronology applied to understand the thermotectonic coevolution of the south part of the Colombian Western Cordillera and the Tumaco Basin. He has worked on several

projects in Colombia involving geological mapping, sampling, and the use of analytic techniques such as mass spectrometry to obtain thermo and geochronologic data. Angel is currently a PhD candidate at the University of Florida, where he has served as a TA, teaching several courses, including physical geology, engineering and environmental geology, and introduction to earth science. His research interests include understanding the Cenozoic tectonic evolution of the NW Andes using the magmatic and sedimentary record within sedimentary basins and cordilleran massifs and investigating the role of sediments in the origin and evolution of continental crust.



Hugo MURCIA is a geologist from the Universidad de Caldas, Colombia, who received his MS in earth sciences from the Universidad Nacional Autónoma de México, México, and his PhD in geology from the University of Auckland, New Zealand. Hugo works as a professor at the Departamento de Ciencias Geológicas as a researcher at the Instituto de Investigaciones en Estratigrafía

(IIES), both at Universidad de Caldas, Colombia. Hugo also belongs to the Grupo de Investigación en Estratigrafía y Vulcanología (GIEV) Cumanday and is recognized as an associate researcher by the Ministerio de Ciencias, Tecnología e Innovación in Colombia. He specializes in volcanology and petrology.



Carlos GIRALDO is a geologist of the Departamento de Ciencias Geológicas de la Universidad de Caldas (Manizales, Colombia, 2014) and a student of the Master of Earth Sciences program at the Universidad de Caldas. During 2014–2015, he worked at the Instituto de Investigaciones Marinas y Costeras José Benito Vives de Andréis (INVE-MAR) in areas related to marine geology.

Since 2015, he has been linked to the Instituto de Investigaciones en Estratigrafía (IIES) and the Grupo de Investigación en Estratigrafía y Vulcanología (GIEV) Cumanday. His research field is related to ichnology, sedimentology, and stratigraphy, and its integration into sedimentary basin analysis to reconstruct ancient depositional environments and interpret their possible sequence stratigraphic framework.



Sergio CELIS is a geologist from the Universidad de Caldas (Colombia), has an MS in earth sciences from the same university, and received his PhD in earth sciences from the University of Granada (Spain). Sergio is a researcher at the Instituto de Investigaciones en Estratigrafía (IIES) and has experience as a professor in the Departamento de Ciencias Geológicas at the Universidad

de Caldas. Sergio also belongs to the Grupo de Investigación en Estratigrafía y Vulcanología (GIEV) Cumanday and is recognized as a junior researcher by the Ministerio de Ciencias, Tecnología e Innovación in Colombia. His main experience is in ichnology and basin analysis.



Sergio A. LÓPEZ is graduated with a bachelor's degree in geology from the Universidad de Caldas, Colombia, and received a master's degree in earth and environmental sciences from the Universidad EAFIT, Medellín, Colombia, with an emphasis on morphodynamics of tropical deltaic systems. He currently holds a doctoral candidate position in the Department of Geological Sciences

from the Universidad de Buenos Aires, Argentina. He has worked as a researcher in interdisciplinary projects on modern deltas (Universidad EAFIT, 2004–2008), active tectonics and geodynamics (Servicio Geológico Colombiano, 2008–2010), and as advisor of the new ventures technical team from the Agencia Nacional de Hidrocarburos (2011–2017).


Chapter 9



Cenozoic Marine Carbonate Systems of Colombia

<https://doi.org/10.32685/pub.esp.37.2019.09>

Published online 26 November 2020

Juan Carlos SILVA-TAMAYO^{1*} , Daniel RINCÓN-MARTÍNEZ² ,
Lina M. BARRIOS³ , Juan C. TORRES-LASSO⁴ ,
and Chixel OSORIO-ARANGO⁵ 

Abstract In this chapter, we report existing and new lithostratigraphic information and Sr-isotope chemostratigraphic ages of several Cenozoic marine carbonate successions deposited within numerous Colombian basins. This information is used to link main changes in the shallow marine carbonate factory to regional environmental/tectonic events in the tropical SE Circum-Caribbean. Our results and the available literature show that during the Eocene – early Oligocene transition, carbonate successions developed along the Alta Guajira (Macarao Formation) and the San Jacinto (Toluviejo and Arroyo de Piedra Formations) Basins, northern Colombia. These successions, which deposited along rimmed carbonate banks, mostly display heterozoan biotic associations, dominated by red algae and large benthic foraminifera. The development of this carbonate factory occurred during an interval of hot-house conditions through which mesotrophic and oligophotic marine conditions predominated. During the late Oligocene, carbonate sedimentation occurred along the Alta Guajira Basin (Siamana Formation), Lower Magdalena Valley Basin (Cicuco Limestones of the Ciénaga de Oro Formation), and Western Cordillera of Colombia (Vijes Formation). Predominant mesotrophic conditions resulted in the coexistence of mixed photozoan–heterozoan biotic associations and the development of patchy coral reefs along the predominantly siliciclastic continental shelves. During the early Miocene, carbonate deposition was absent in most of the Colombian sedimentary basins and was restricted to the Alta Guajira Basin, where photozoan biotic associations dominated the emerging rimmed coral–dominated carbonate platforms attached to the continental shelves. The change in coral reef architecture along the Alta Guajira Basin coincides with the onset of a global climate optimum and of local marine oligotrophic and euphotic conditions. The replacement of photozoan by heterozoan biotic associations in the Alta Guajira Basin during the middle Miocene likely resulted from the return to mesotrophic/oligophotic conditions due to the enhancement of the sediment supply to the Caribbean as the docking of the Panamá Block to northern South America reached its acme. The enhanced sediment supply to the Caribbean decreased the occurrence of well-developed reefs along the Caribbean region of Colombia (continental) during the late Miocene and Pliocene. This decrease, which parallels global trends, is only interrupted by the deposition of the late Miocene San Andrés and Pleistocene San Luis Formations (Los Cayos Basin), where photozoan

- 1 director.testlabgeoambiental@gmail.com
CEO at Testlab Geoambiental
Testlab Laboratorio Alimentos y Aguas S.A.S.
Research Group One–Health
Calle 45D n.º 60–16
Medellín, Colombia
- 2 daniel.rincon@ecopetrol.com.co
Ecopetrol S.A
Instituto Colombiano del Petróleo
Centro de Innovación y Tecnología
Bucaramanga, Santander, Colombia
- 3 lina.barrios@mmu.ac.uk
Manchester Metropolitan University
School of Science and the Environment
Environment and Ecology Research Centre–
EERC
Chester St, Manchester, M1 5GD, United Kingdom
- 4 juan.lasso.col@furg.br
Universidade Federal do Rio Grande
Instituto de Geociências
Rio Grande, Rio Grande do Sul, Brasil
Universidade de Caldas
Departamento de Geología
Manizales, Colombia
- 5 cyosorio@unal.edu.co
Smithsonian Tropical Research Institute
Panamá, Panamá
Universidad Nacional de Colombia
Sede Medellín
Departamento de Ingeniería Geológica
Medellín, Colombia

* Corresponding author

Citation: Silva-Tamayo, J.C., Rincón-Martínez, D., Barrios, L.M., Torres-Lasso, J.C. & Osorio-Aran-go, C. 2020. Cenozoic marine carbonate systems of Colombia. In: Gómez, J. & Mateus-Zabala, D. (editors), *The Geology of Colombia, Volume 3 Paleogene – Neogene*. Servicio Geológico Colombiano, *Publicaciones Geológicas Especiales* 37, p. 249–282. Bogotá. <https://doi.org/10.32685/pub.esp.37.2019.09>

biotic associations prevailed, and the Pleistocene La Popa Formation (San Jacinto Basin), which displays mixed photozoan–heterozoan biotic associations.

Keywords: Colombia, Cenozoic, stratigraphy, carbonate sedimentology, photozoan carbonate, heterozoan carbonate, environmental archives.

Resumen En este capítulo reportamos información litoestratigráfica existente y nueva y edades quimioestratigráficas de isótopos de Sr de varias sucesiones carbonáticas marinas del Cenozoico que se depositaron en diferentes cuencas colombianas. Esta información se usa para relacionar los principales cambios en las fábricas de carbonatos marinos poco profundos con eventos ambientales/tectónicos regionales en el Caribe suroriental. Nuestros resultados y la literatura disponible muestran que durante la transición Eoceno–Oligoceno temprano se desarrollaron sucesiones de carbonatos en las cuencas Alta Guajira (Formación Macarao) y San Jacinto (formaciones Toluviejo y Arroyo de Piedra), al norte de Colombia. Estas sucesiones, que se depositaron en bancos bordeados por carbonatos, presentan en su mayoría asociaciones biológicas heterozoarias, dominadas por algas rojas y foraminíferos bentónicos grandes. El desarrollo de esta fábrica carbonática tuvo lugar durante un intervalo de invernadero a través del cual predominaron condiciones marinas mesotróficas y oligofóticas. Durante el Oligoceno tardío, la sedimentación de carbonatos ocurrió en la Cuenca Alta Guajira (Formación Siamana), Cuenca del Valle Inferior del Magdalena (Calizas del Cicuco de la Formación Ciénaga de Oro) y cordillera Occidental colombiana (Formación Vijos). Las condiciones mesotróficas predominantes dieron como resultado la coexistencia de asociaciones biológicas mixtas fotozoarias–heterozoarias y el desarrollo de arrecifes de coral irregulares a lo largo de las plataformas continentales predominantemente siliciclásticas. En el Mioceno temprano, el depósito de carbonatos estuvo ausente en la mayoría de cuencas sedimentarias colombianas y se restringió a la Cuenca Alta Guajira, donde las asociaciones biológicas fotozoarias dominaron las plataformas carbonáticas emergentes bordeadas por corales unidas a las plataformas continentales. El cambio en la arquitectura de los arrecifes de coral a lo largo de la Cuenca Alta Guajira coincide con el inicio de un clima global óptimo y de condiciones marinas locales oligotróficas y eufóticas. El reemplazo de asociaciones biológicas fotozoarias por asociaciones heterozoarias en la Cuenca Alta Guajira durante el Mioceno medio probablemente se debió al regreso a las condiciones mesotróficas/oligofóticas debido al aumento en el aporte de sedimentos al Caribe a medida que la acreción del Bloque de Panamá al norte de Suramérica alcanzó su auge. Este aumento en la sedimentación redujo la aparición de arrecifes bien desarrollados a lo largo de la región Caribe de Colombia (continental) durante el Mioceno tardío y Plioceno. Esta disminución, que es paralela a las tendencias globales, solo es interrumpida por el depósito de las formaciones San Andrés del Mioceno tardío y San Luis del Pleistoceno (Cuenca Los Cayos), donde asociaciones biológicas fotozoarias prevalecieron, y de la Formación La Popa del Pleistoceno (Cuenca San Jacinto), que muestra predominio de asociaciones mixtas fotozoarias–heterozoarias.

Palabras clave: Colombia, Cenozoico, estratigrafía, sedimentología de carbonatos, carbonato de fotozoarios, carbonato de heterozoarios, archivos ambientales.

1. Introduction

The marine carbonate sedimentary factory comprises the production, deposition, and early modification of carbonate sediments (James & Jones, 2016). There are two main marine carbonate factories: The benthic carbonate factory that develops on the seafloor, and the pelagic carbonate factory that develops

in the water column (Figure 1). Such carbonate factories continuously produce carbonate sediments, which exhibit wide range of grain sizes and can be produced inorganically or biologically or by a combination of both (James & Jones, 2016).

Tropical marine carbonate factories are restricted to the latitudinal range between 15° N and 15° S, an area characterized by a warm sea surface temperature, low nutrient level, high at-

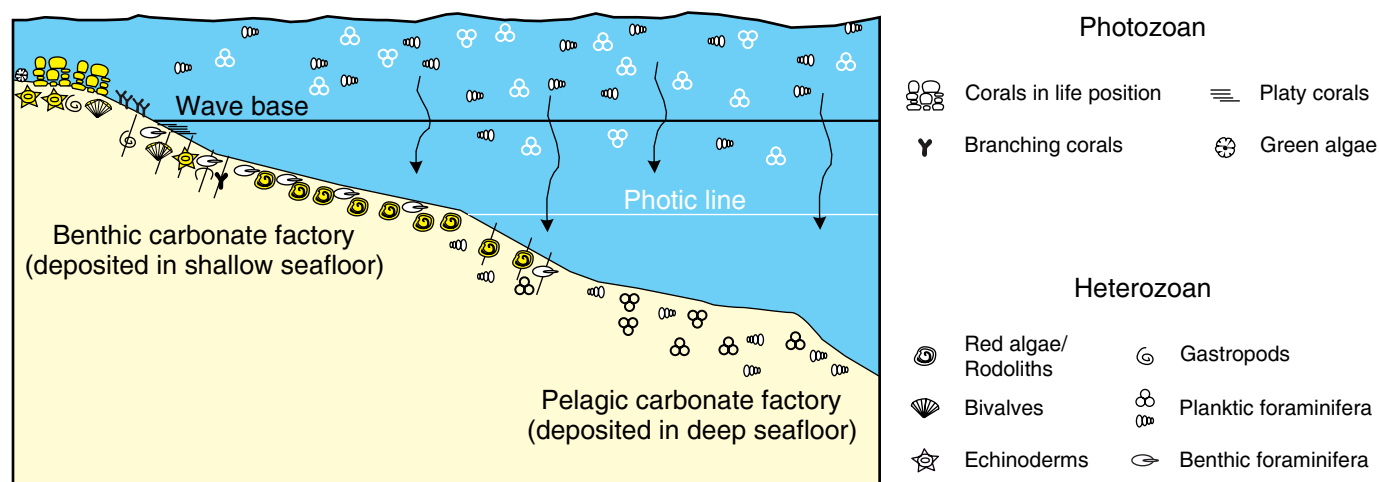


Figure 1. Main tropical marine biogenic carbonate producers and carbonate factories with respect to water depth.

mospheric humidity, and heavy rainfall. Seasonal fluctuations in both temperature and precipitation also influence the marine currents, clastic nutrient input, and freshwater discharges into the marine basins (Lockwood, 1974). Although the warm ocean temperature in tropical areas is the main mechanism promoting carbonate production, additional factors such as chemical saturation, salinity, turbidity, nutrient availability, and tectonic activity not only control such production on short time scales but also influence the type of carbonate factories (Budd, 2000; Frost, 1977; Johnson et al., 2008, 2009; Klaus et al., 2011; Mutti et al., 2005; Renema et al., 2016; Wilson, 2002, 2008, 2012, 2015).

Carbonate-secreting organisms account for most of the carbonate production of tropical marine carbonate factories. The occurrence of different types of carbonate producers and, thus, the type of carbonate factory depends on diverse environmental factors, i.e., light penetration, water salinity, nutrient availability, oxygen levels, and temperature (James & Jones, 2016; Wilson, 2012). Photozoans such as green calcareous algae, symbiotic larger benthic foraminifera (LBF), scleractinian corals, and siliceous sponges, which are organisms that depend on light to produce their own food by photosynthesis, constitute the main tropical carbonate factory (James & Jones, 2016; Wilson, 2012). The photozoan carbonate factory occurs in tropical marine areas characterized by oligotrophic (low nutrients), euphotic (highly illuminated), and warm ocean waters. The heterozoan carbonate factory consists of heterotrophic organisms, such as bryozoans, brachiopods, echinoderms, mollusks, azooxanthellate corals, and calcareous red algae. While calcareous red algae are not heterotrophs, they are common components in these carbonates. Although the heterozoan carbonate factory typically occurs in temperate regions, it may occur in tropical marine areas, where dimmed (euphotic-aphotic), moderate-to-high nutrient (mesotrophic, eutrophic), and cold ocean waters prevail (Figures 2, 3). Unlike the photozoan biotic associations, the heterozoan biotic associations are highly resistant to low

oxygen conditions and may survive and adapt to variable salinity conditions (Figure 4; James & Jones, 2016; Wilson, 2012).

While much has been learned from living systems, many questions remain unanswered concerning how prehistoric events shaped ancient shallow marine carbonate factories in the tropical oceans (Wilson, 2012). Although on longer time-scales, global environmental/climatic events, biological evolution, geodynamics, and paleogeographic changes seem to have played important roles in the evolution of Cenozoic tropical carbonate factories, it has been observed that local parameters may play an overriding role that can mask the global signals. Therefore, it is necessary to understand regional variability before determining global implications (Wilson, 2012).

In this chapter, we compile published and report new lithostratigraphic and biostratigraphic information, as well as Sr-isotope chemostratigraphic data from several shallow marine Cenozoic carbonates successions from western and northern Colombia, including the Arroyo de Piedra, Toluviejo, Vijes, Macarao, Siamana, Ciénaga de Oro (Cicuco Limestones), San Andrés, and La Popa Formations (Figures 5, 6). This information is used to better constrain their carbonate factories, depositional age, and depositional settings. It is also used to investigate spatial and temporal changes in the shallow marine carbonate systems and ultimately relate such changes to climatic, environmental, and tectonic events.

2. Materials and Methods

The lithostratigraphic information for carbonates from the Arroyo de Piedra, Toluviejo, Siamana, Ciénaga de Oro, San Andrés, and La Popa Formations have been reported elsewhere (Ortiz & Niño, 1999; Ortiz et al., 1998; Reyes et al., 2009; Rosero et al., 2014; Salazar-Franco et al., 2016; Silva-Tamayo et al., 2017). In this chapter, we present new lithostratigraphic information from the Macarao and Vijes Formations. The car-

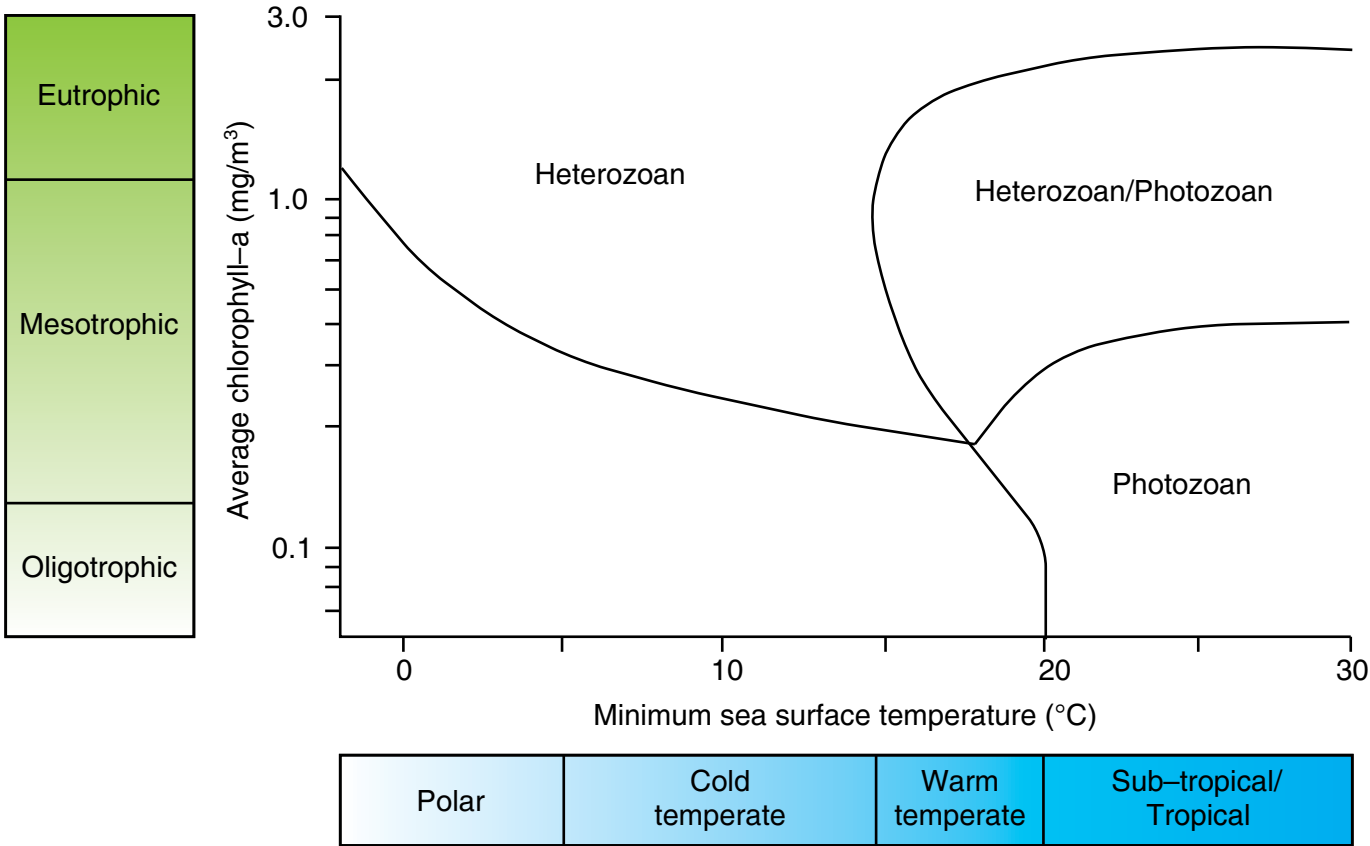


Figure 2. Variations in marine biogenic carbonate producers and carbonate factories with respect to nutrient levels and seawater temperature (James & Jones, 2016).

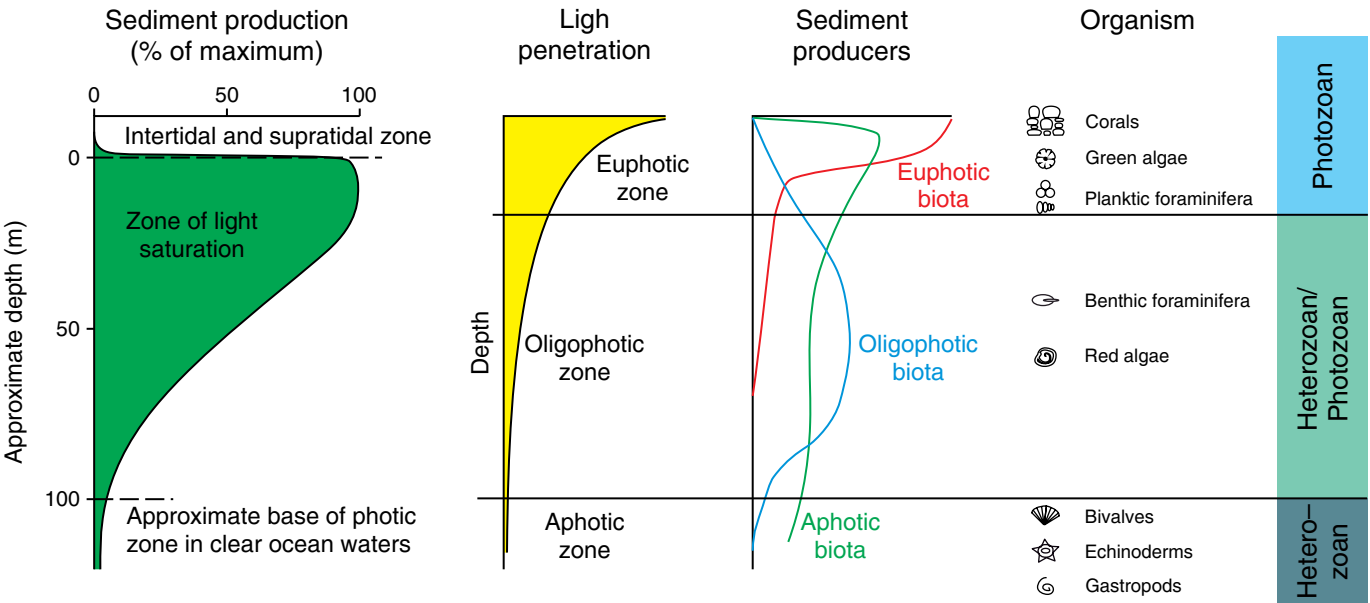


Figure 3. Variations in marine biogenic carbonate producers and carbonate factories with respect to light penetration and light saturation (James & Jones, 2016).

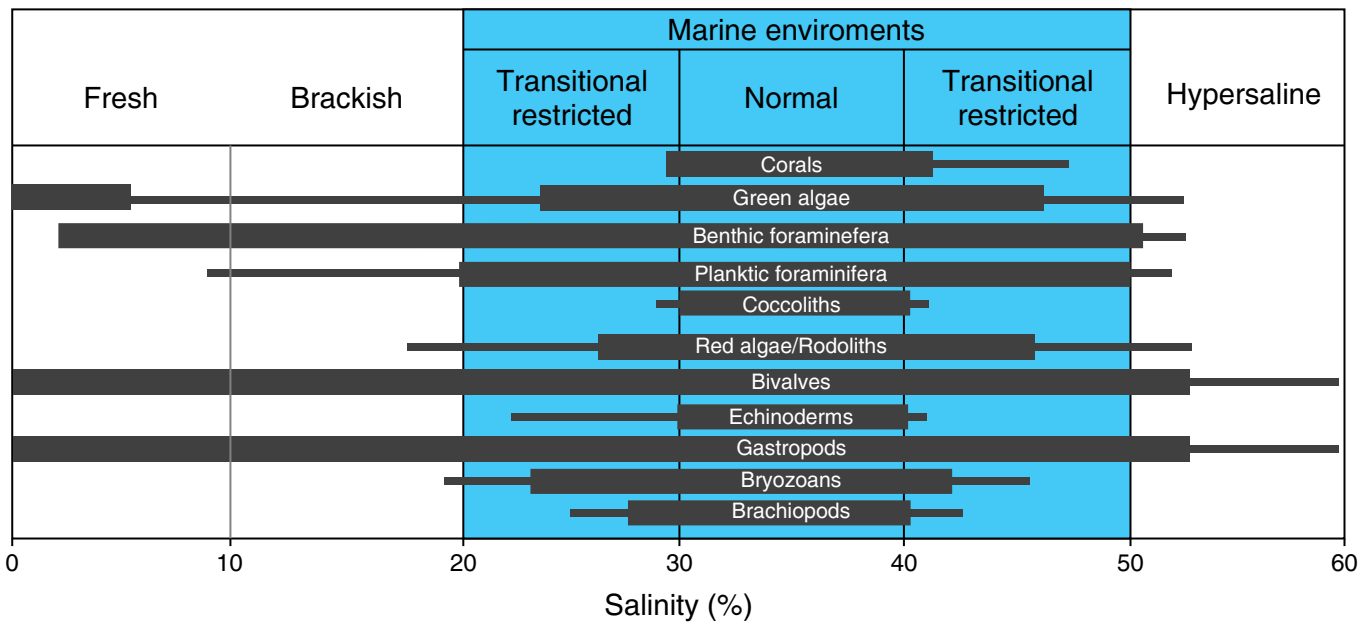


Figure 4. Variations in the occurrence of different marine carbonate producers with respect to salinity (James & Jones, 2016).

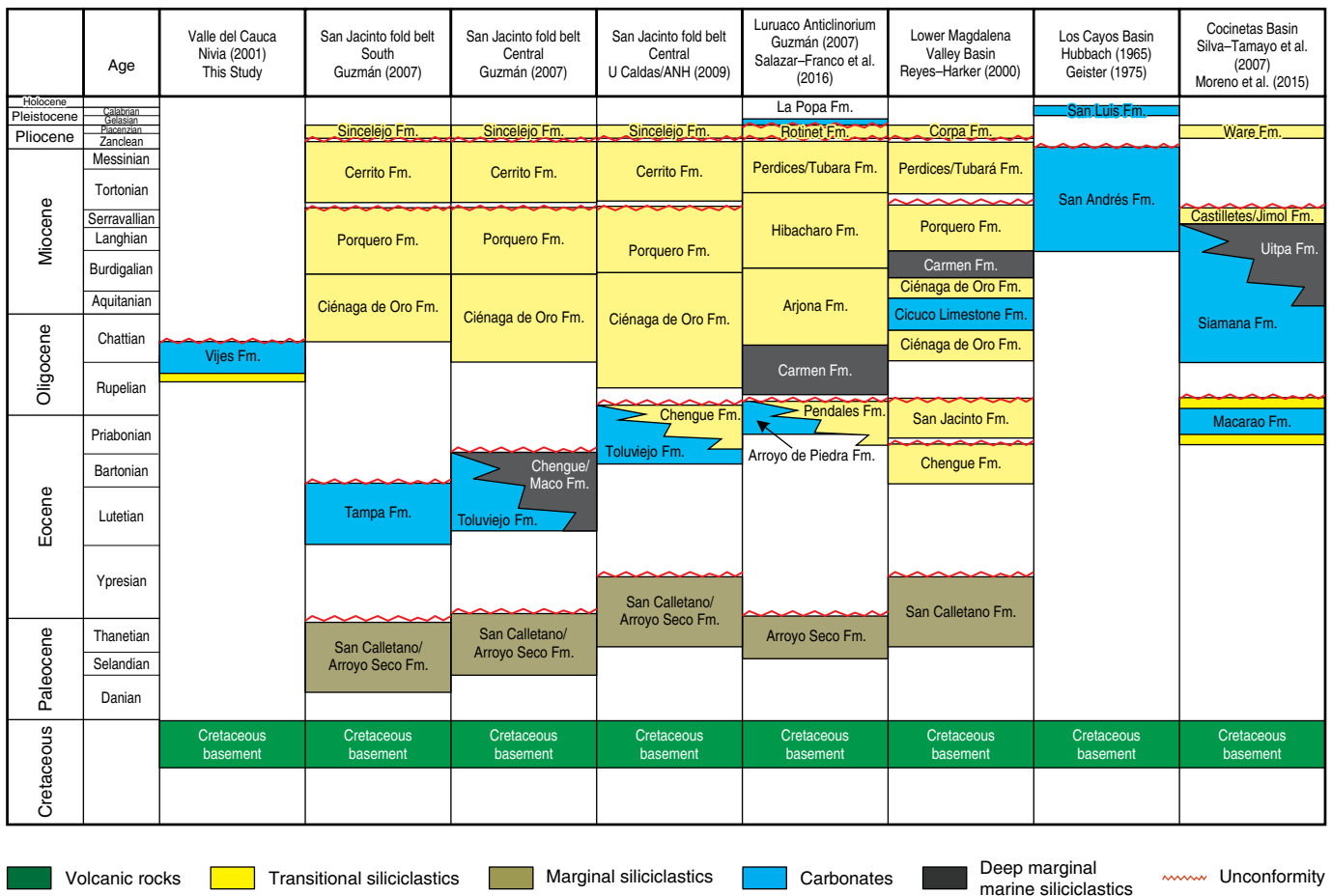


Figure 5. Litho and chronostratigraphic chart of the studied basins.

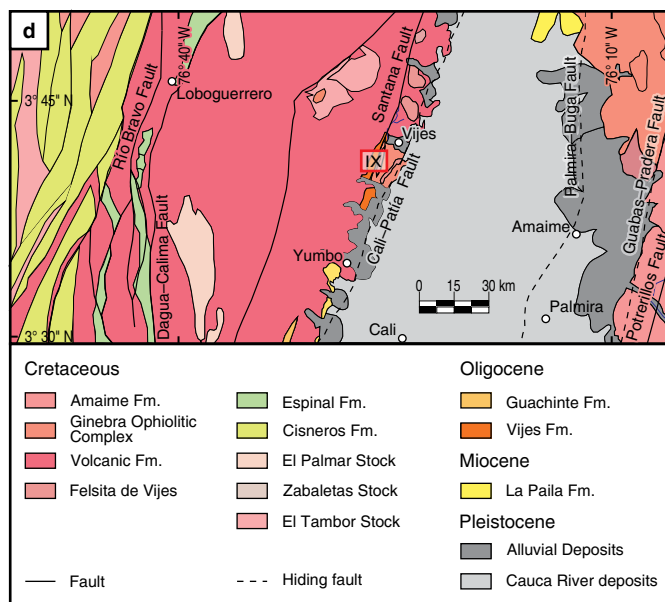
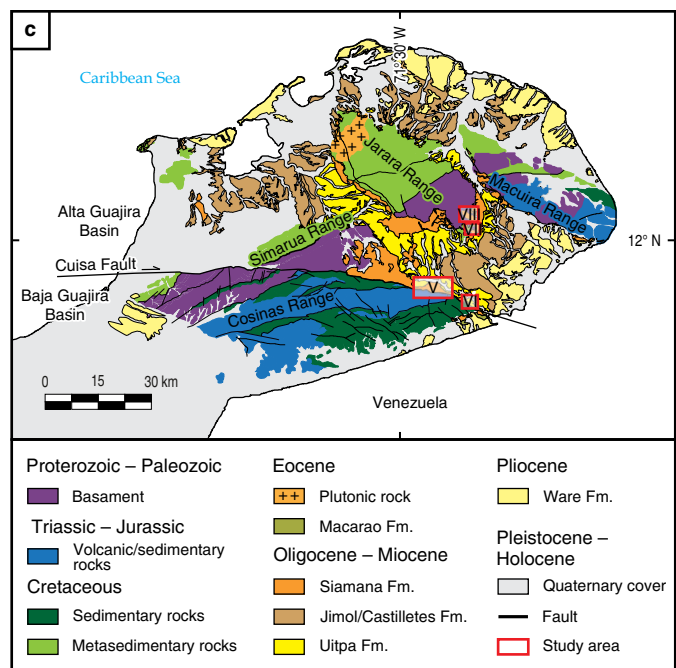
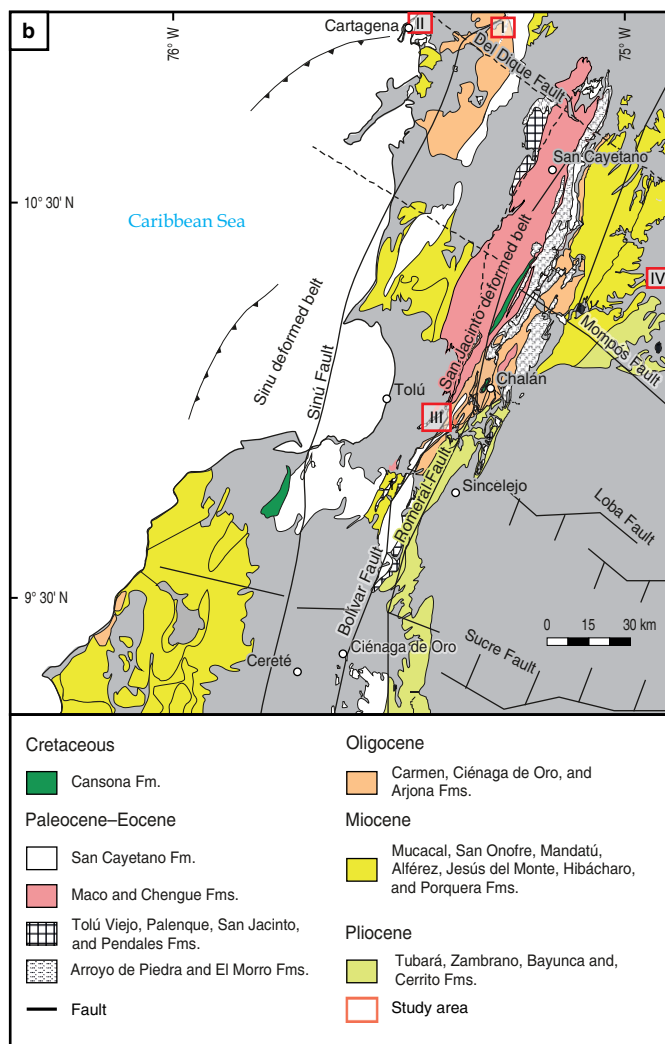
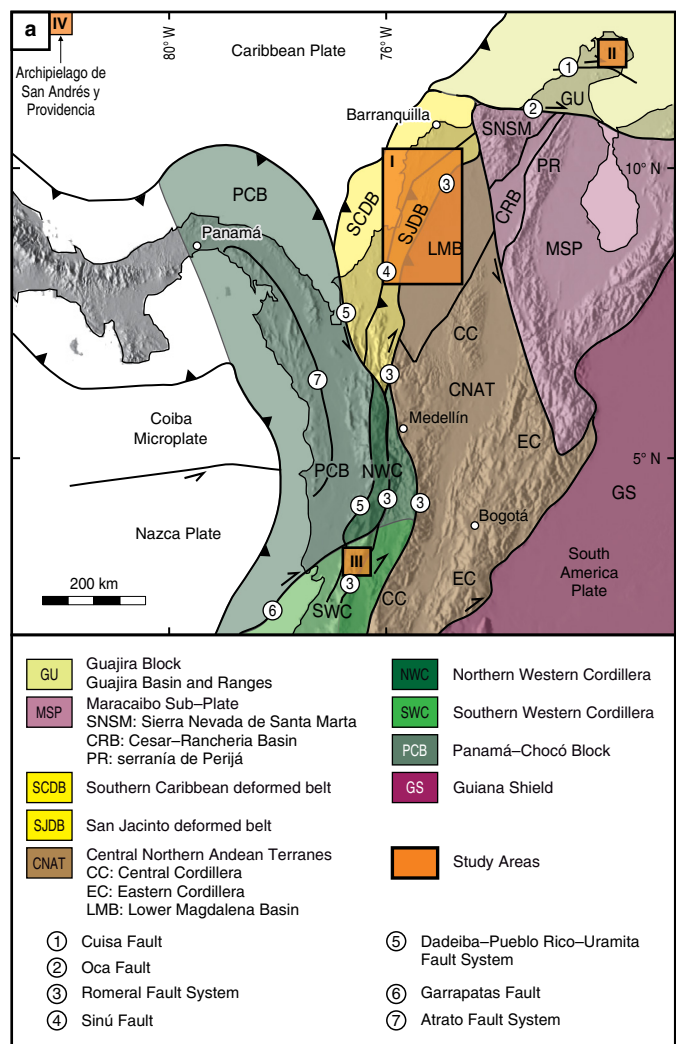




Figure 6. (a) Tectonic map of Colombia (after Cediel et al., 2003). Orange squares represent the areas where Cenozoic marine carbonates occur: (I) SJDB; (II) Alta Guajira Basin; (III) Western Cordillera of Colombia; (IV) Los Cayos Basin. **(b)** Geologic map of the San Jacinto Basin (after Bermúdez et al., 2009). Roman numbers represent the locations of the stratigraphic sections reported in this study: (I) Luruaco Anticlinorium (Arroyo de Piedra Formation); (II) Luruaco Anticlinorium (La Popa Formation); (III) SJDB (Toluviejo Formation); (IV) Cicuco Height (Cicuco Limestones). **(c)** Geologic map of the Alta Guajira (after Zuluaga et al., 2009). Roman numbers represent the locations of the stratigraphic sections reported by Silva–Tamayo et al. (2017) for the Siamana Formation: (V) Sillamahana section; (VI) Flor de La Guajira section; (VII) Uitpa Creek section; (VIII) Ekyeps Creek section. **(d)** Geologic map of part of the Western Cordillera of Colombia (after Nivia, 2001) and location of the stratigraphic section (IX) where the Vije Formation crops out.

bonate textural classification was performed following Dunham (1962) and Embry & Klovan (1971). Facies analyses and environmental interpretations were carried out following Tucker & Wright (2009) and Wilson (2012).

Strontium isotope stratigraphy is an alternative tool to date marine carbonate successions and has been commonly used to complement biostratigraphic analyses (McArthur & Howarth, 2004; McArthur et al., 2012). In this work, we compiled available biostratigraphic information and contrasted it against available and new Sr–isotope chemostratigraphic data to constrain the depositional ages of the reported carbonate successions. The Sr–isotope chemostratigraphic depositional ages were determined by contrasting the $^{87}\text{Sr}/^{86}\text{Sr}$ values (Table 1) from the studied carbonates against the $^{87}\text{Sr}/^{86}\text{Sr}$ values of the Cenozoic global seawater reported by McArthur & Howarth (2004) and McArthur et al. (2012) (Figure 7). The chemostratigraphic method relies on the fact that carbonates preserve the isotopic signature of the seawater during their deposition. It also relies on the premise that the Sr isotope composition of the world's oceans is homogeneous in terms of time scales similar to the ocean mixing time, given its residence time of ca. 3 Ma. Because the isotopic signature of the ocean varies through geological time as a result of the imbalances between continental weathering and hydrothermal alteration of the mid–ocean ridges, the evolution of $^{87}\text{Sr}/^{86}\text{Sr}$ values of marine carbonates has been used to investigate changes in global tectonics (Jacobsen & Kaufman, 1999; Spooner, 1976; Wickman, 1948).

The $^{87}\text{Sr}/^{86}\text{Sr}$ compositions of carbonates from the Siamana, Arroyo de Piedra, and Toluviejo Formations have been reported elsewhere (Rosero et al., 2014; Salazar–Franco et al., 2016; Silva–Tamayo et al., 2017). Here, we report the $^{87}\text{Sr}/^{86}\text{Sr}$ compositions of carbonates from the Vije Formation and La Popa Formation. In all cases, the $^{87}\text{Sr}/^{86}\text{Sr}$ composition of carbonates was obtained following the methods reported by Rosero et al. (2014) and Silva–Tamayo et al. (2017). Briefly, microdrilled carbonate powders were obtained from polished slabs of carbonate hand samples. Microdrilling was performed to avoid secondary carbonate facies such as telodiagenetic diagenetic cements, carbonate veins, and carbonates derived from weathering. Following Rosero et al. (2014), Salazar–Franco et al. (2016), and Silva–Tamayo et al. (2017), the microdrilled powders were preferentially obtained from the red algal carbonate

fraction, excluding those of La Popa Formation, which were obtained from corals.

The microdrilled powders were placed in 15–ml Savillex vials and dissolved in 0.5 M HNO_3 . The Sr fraction was separated in Eichron Sr spec columns using 3.5 to 0.05 M HNO_3 . The Sr fraction was loaded onto single Re filaments with Ta_2O_5 activator. Mass spectrometric analyses were carried out on an automated VG Sector multi–collector instrument fitted with adjustable 10^{11} ohms faraday collectors and a Daly photomultiplier (Ducea & Saleeby, 1998) at the University of Arizona, Tucson. Typical runs consisted of the acquisition of 100 isotopic ratios. Fifteen analyses of National Institute of Standards and Technology (NIST) standard NBS987 yielded mean ratios of $^{87}\text{Sr}/^{86}\text{Sr} = 0.710265 \pm 7$ and $^{84}\text{Sr}/^{86}\text{Sr} = 0.056316 \pm 12$. The Sr isotopic ratios of standards and samples were normalized to the commonly accepted $^{86}\text{Sr}/^{88}\text{Sr}$ ratio of 0.1194. The estimated analytical ($2\sigma_{\text{d}}$) uncertainties for samples analyzed in this study were $^{87}\text{Sr}/^{86}\text{Sr} < 0.0012\%$. Procedural blanks averaged from five determinations were Sr–120 pg.

3. Lithostratigraphy

3.1. Middle to Upper Eocene Carbonates

3.1.1. Arroyo de Piedra Formation

The Arroyo de Piedra Formation occurs along the Luruaco Anticlinorium, the northernmost sector of the San Jacinto deformed belt (SJDB) (Figure 6b; Guzmán, 2007; Guzmán et al., 2004). It was originally described in a stratigraphic section near the municipality of Arroyo de Piedra by Bueno (1970). In this section, the Arroyo de Piedra Formation discordantly overlies the San Cayetano/Arroyo Seco Formation and is discordantly overlain by the Carmen Formation (Figure 5). According to Bueno (1970), the Arroyo de Piedra Formation is ca. 500 m thick, with the thickest sections lying towards the east of the SJDB. It consists of a basal series of thin–bedded siliceous mudstones and gray calcareous mudstones, overlain by a series of lenticular coarse bedded, red algal, biosparitic limestones. Guzmán et al. (2004) suggested that the Arroyo de Piedra Formation is correlative to the Pendales Formation, which also crops out along the Luruaco Anticlinorium (Figure 5). Regionally, the Arroyo de

Table 1. $^{87}\text{Sr}/^{86}\text{Sr}$ composition of some of the reported carbonate successions (Rosero *et al.*, 2014; Salazar-Franco *et al.*, 2016; Silva-Tamayo *et al.*, 2017; Torres-Lasso, 2014).

Stratigraphic unit	Sample ID	Locality	Carbonate type	$^{87}\text{Sr}/^{86}\text{Sr}$
La Popa	Boca1(1.35–1.40)	Z–well	Coralline	0.709097
La Popa	Boca1(6.55–6.61)	Z–well	Coralline	0.709106
La Popa	Boca1(9.08–9.02)	Z–well	Coralline	0.709106
La Popa	Boca1(14.33–14.4)	Z–well	Coralline	0.709122
La Popa	LMR–AP–09B	Y–well	Coralline	0.70910
La Popa	LMR–AP–14	Y–well	Coralline	0.70906
La Popa	LMR–MZ–09B	Y–well	Coralline	0.70904
La Popa	LMR–MZ–13	Y–well	Coralline	0.70910
Vijes	VCT–05	Vijes	Rodalgal/Coralline	0.70808
Vijes	VCT–12	Vijes	Rodalgal/Coralline	0.70811
Vijes	VCT–26	Vijes	Rodalgal/Coralline	0.70810
Vijes	VCT–30	Vijes	Rodalgal/Coralline	0.70804
Siamana	540029–5	Parajimaru	Coralline	0.708825
Siamana	540027–5	Parajimaru	Coralline	0.708708
Siamana	540027–1	Parajimaru	Coralline	0.708483
Siamana	540024–1a	Ekyeps Hill	Coralline	0.708502
Siamana	540026–2	Ekyeps Hill	Coralline	0.708368
Siamana	540026–1	Ekyeps Hill	Coralline	0.708324
Siamana	540025–1	Ekyeps Hill	Coralline	0.708348
Siamana	450051	Ekyeps Creek	Rodalgal	0.7086740
Siamana	540050–18	Ekyeps Creek	Rodalgal	0.7086631
Siamana	540050–14	Ekyeps Creek	Rodalgal	0.7086032
Siamana	540050–8	Ekyeps Creek	Rodalgal	0.7086556
Siamana	540050–1	Ekyeps Creek	Rodalgal	0.7086304
Siamana	540051–20	Ekyeps Creek	Rodalgal	0.7086032
Siamana	540051–4	Ekyeps Creek	Rodalgal	0.7085094
Siamana	540052–16	Ekyeps Creek	Coralline	0.7084935
Siamana	540052–13	Ekyeps Creek	Coralline	0.7084850
Siamana	540052–7	Ekyeps Creek	Coralline	0.7084530
Siamana	540052–1	Ekyeps Creek	Coralline	0.7084024
Siamana	540053–11	Ekyeps Creek	Coralline	0.7084000
Siamana	540053–6	Ekyeps Creek	Coralline	0.7083972
Siamana	540053–1	Ekyeps Creek	Coralline	0.7083643
Siamana	540023–4	Uitpa	Rodalgal/Coralline	0.7083850
Siamana	540023–5	Uitpa	Rodalgal/Coralline	0.7083367
Siamana	540023–22	Uitpa	Rodalgal/Coralline	0.7083339
Siamana	540023–23	Uitpa	Rodalgal/Coralline	0.7083119
Siamana	540023–26	Uitpa	Rodalgal/Coralline	0.7081399
Siamana	540023–13d	Uitpa	Rodalgal/Coralline	0.7081267
Siamana	540023–18a	Uitpa	Rodalgal/Coralline	0.7081284
Siamana	540023–19	Uitpa	Rodalgal/Coralline	0.708142
Siamana	540025–1	Uitpa	Rodalgal/Coralline	0.7081475
Siamana	540023–2	Uitpa	Rodalgal/Coralline	0.708131

Table 1. $^{87}\text{Sr}/^{86}\text{Sr}$ composition of some of the reported carbonate successions (Rosero et al., 2014; Salazar-Franco et al., 2016; Silva-Tamayo et al., 2017; Torres-Lasso, 2014) (*continued*).

Stratigraphic unit	Sample ID	Locality	Carbonate type	$^{87}\text{Sr}/^{86}\text{Sr}$
Siamana	540023-1	Uitpa	Rodalgal/Coraline	0.7081855
Siamana	540054-21	Sillamahana	Rodalgal/Coraline	0.70354
Siamana	540054-19	Sillamahana	Rodalgal/Coraline	0.7082140
Siamana	540054-14	Sillamahana	Rodalgal/Coraline	0.7081452
Siamana	540054-10	Sillamahana	Rodalgal/Coraline	0.7081245
Siamana	540054-6	Sillamahana	Rodalgal/Coraline	0.7080420
Siamana	540054-3	Sillamahana	Rodalgal/Coraline	0.7080300
Siamana	540054-1	Sillamahana	Rodalgal/Coraline	0.7080300
Siamana	540030-1	Flor Guajira	Rodalgal/Coraline	0.708854
Siamana	540030-2	Flor de La Guajira	Rodalgal/Coraline	0.708385
Siamana	540030-3	Flor de La Guajira	Rodalgal/Coraline	0.708158
Siamana	540030-4	Flor de La Guajira	Rodalgal/Coraline	0.7080635
Siamana	540030-5	Flor de La Guajira	Rodalgal/Coraline	0.7080317
Macarao	360150-1	Flor de La Guajira	Rodalgal	0.707911
Macarao	360150-5	Flor de La Guajira	Rodalgal	0.707843
Macarao	360150-13	Flor de La Guajira	Rodalgal	0.707867
Macarao	360153-26	Flor de La Guajira	Rodalgal	0.7078023
Toluviejo	P8 279.57	P8-well	Rodalgal	0.70762
Toluviejo	P8 274.99	P8-well	Rodalgal	0.70760
Toluviejo	P8 264.19	P8-well	Rodalgal	0.70757
Toluviejo	P8 220.13	P8-well	Rodalgal	0.70742
Toluviejo	P8 204.59	P8-well	Rodalgal	0.70744
Toluviejo	P8 203.85	P8-well	Rodalgal	0.70750
Toluviejo	P8 198.49	P8-well	Rodalgal	0.70746
Toluviejo	P8 193.06	P8-well	Rodalgal	0.70735
Toluviejo	P8 192.49	P8-well	Rodalgal	0.70744
Arroyo de Piedra	PP-01	Arroyo de Piedra	Rodalgal	0.707729
Arroyo de Piedra	PP-04	Arroyo de Piedra	Rodalgal	0.707638
Arroyo de Piedra	PP-08	Arroyo de Piedra	Rodalgal	0.707776
Arroyo de Piedra	PP-11	Arroyo de Piedra	Rodalgal	0.707762
Arroyo de Piedra	PP-13	Arroyo de Piedra	Rodalgal	0.707729
Arroyo de Piedra	PP-16	Arroyo de Piedra	Rodalgal	0.707751
Arroyo de Piedra	AP-01	Arroyo de Piedra	Rodalgal	0.707743
Arroyo de Piedra	AP-02	Arroyo de Piedra	Rodalgal	0.707739
Arroyo de Piedra	AP-04	Arroyo de Piedra	Rodalgal	0.707734
Arroyo de Piedra	AP-05	Arroyo de Piedra	Rodalgal	0.707734
Arroyo de Piedra	AP-09	Arroyo de Piedra	Rodalgal	0.707763
Arroyo de Piedra	AP-10	Arroyo de Piedra	Rodalgal	0.707676
Arroyo de Piedra	AP-15	Arroyo de Piedra	Rodalgal	0.707286
Arroyo de Piedra	AP-19	Arroyo de Piedra	Rodalgal	0.707717
Arroyo de Piedra	AP-22	Arroyo de Piedra	Rodalgal	0.707718
Arroyo de Piedra	7701'6''	X-well	Rodalgal	0.707707
Arroyo de Piedra	7697'4''	X-well	Rodalgal	0.707772

Table 1. $^{87}\text{Sr}/^{86}\text{Sr}$ composition of some of the reported carbonate successions (Rosero et al., 2014; Salazar–Franco et al., 2016; Silva–Tamayo et al., 2017; Torres–Lasso, 2014) (*continued*).

Stratigraphic unit	Sample ID	Locality	Carbonate type	$^{87}\text{Sr}/^{86}\text{Sr}$
Arroyo de Piedra	7695'	X–well	Rodalgal	0.707764
Arroyo de Piedra	7693'3"	X–well	Rodalgal	0.707834
Arroyo de Piedra	7688'5"	X–well	Rodalgal	0.707717
Arroyo de Piedra	7682'3"	X–well	Rodalgal	0.707990
Arroyo de Piedra	7680'6"	X–well	Rodalgal	0.707768
Arroyo de Piedra	7678'10"	X–well	Rodalgal	0.707749
Arroyo de Piedra	7675'3"	X–well	Rodalgal	0.707699

Piedra Formation is correlated with the Toluviéjo, San Jacinto, Maco, Chengue, and Tampa Formations (Figure 5). Although no paleontological data have been published, DUQUE–CARO in Guzmán et al. (2004) suggests that the Arroyo de Piedra Formation was deposited during the middle Eocene (Lutetian) to early Oligocene (earliest Rupelian).

Recently, Salazar–Franco et al. (2016) studied the carbonates of the Arroyo de Piedra Formation near the type locality and in cores from one stratigraphic well (Well–X). The lower part of the Arroyo de Piedra Formation displays thin–to–medium bedded aggradational gray siltstones, with parallel lamination and abundant wood fragments (Figure 8a). Occasionally, thin–to–medium lenticular beds of packstones and grainstones with fragments of red algae and clay intraclasts are present. LBF as well as traces of bryozoans, corals, and echinoderm fragments can also be found. Bioclastic limestones, mixed carbonate–siliciclastic (grainstones, packstones, and rudstones with intraclasts) and, to a lesser proportion, fine–grain siliciclastic sedimentites overlay the abovementioned strata (Figure 8a). The bioclastic calcareous segments are composed of massive rhodolith rudstones, distributed in thick layers, with tabular and irregular geometries. These strata are overlaid with packstones, rudstones, and grainstones with abundant intraclasts with a clay to silt composition, arranged in middle layers with cross–stratification and lenticular and channel–shaped geometries. Calcareous red algae, LBF (*Orbitoides*, *Discocyclus*, *Nummulites*), other benthic foraminifera (Miliolids and Fusulinids), and planktonic foraminifera constitute the main allochemical components of these uppermost carbonate packages (Figure 8b–d).

Salazar–Franco et al. (2016) reported $^{87}\text{Sr}/^{86}\text{Sr}$ values between 0.707714–0.707771 for carbonates from the lower part of the Arroyo de Piedra Formation (Figure 7). According to these authors, such values correspond to 41–35 Ma, suggesting a middle to late Eocene (Lutetian – Priabonian) depositional age. For the middle part of the Arroyo de Piedra Formation, the same authors reported $^{87}\text{Sr}/^{86}\text{Sr}$ values between 0.707638–0.707776, which corresponds to 39–33.9 Ma, and suggested a middle to late Eocene (Bartonian – Priabonian) depositional age. The $^{87}\text{Sr}/^{86}\text{Sr}$ values between 0.707699–0.707834 (35–33 Ma) dis-

played by the upper carbonates were used by Salazar–Franco et al. (2016) to suggest a late Eocene (Priabonian) – early Oligocene (Rupelian) depositional age for the uppermost carbonates of the Arroyo de Piedra Formation. The Sr–isotope chemostratigraphic ages reported by Salazar–Franco et al. (2016) not only overlap the foraminifera biostratigraphic ages (Lutetian – Rupelian) ages reported by DUQUE–CARO in Guzmán et al. (2004) but also provide clues regarding the temporal evolution of the Arroyo de Piedra carbonates.

3.1.2. Macarao Formation

The Macarao Formation crops out along the Cocinetas Sub–basin, Alta Guajira Basin, and La Guajira Department, Colombia (Figure 6). It was initially defined by Renz (1960) and redefined by Rollins (1960) and Thomas (1972). The type section of the Macarao Formation is located near the “Flor de La Guajira” locality in the northeastern most part of La Guajira Department (Figure 6c; Rollins, 1960; Thomas, 1972). At this locality, the Macarao Formation is ca. 250 m thick and unconformably overlies the deformed Upper Cretaceous marine sedimentary successions of the Cocinas Range (Figure 5). Oligocene – Miocene marine carbonates from the Siamana Formation unconformably overlay the Macarao Formation (Rollins, 1960; Thomas, 1972). In its type section, the Macarao Formation consists of a series of glauconitic micaceous sandstones interbedded with thick massive fossiliferous mudstones and limestones (Rollins, 1960). It has been correlated with the Nazareth Formation of the Alta Guajira Basin and La Sierra Formation from the serranía de Perijá (Renz, 1960).

For this chapter, we studied the Macarao Formation near to its type section along the Cocinetas Sub–basin, Alta Guajira Basin, Colombia (Figure 6a, 6c). Although Rollins (1960) suggested that the Macarao Formation is ca. 250 m thick in its type section, in the new studied stratigraphic section, the Macarao Formation is only ca. 150 m thick (Figure 9a). The difference in thickness is due to the highly deformed nature of this stratigraphic unit in its type locality. In the new locality, the Macarao Formation consists of a series of tabular–aggradational rhodolithic grainstones, interbedded with a series of

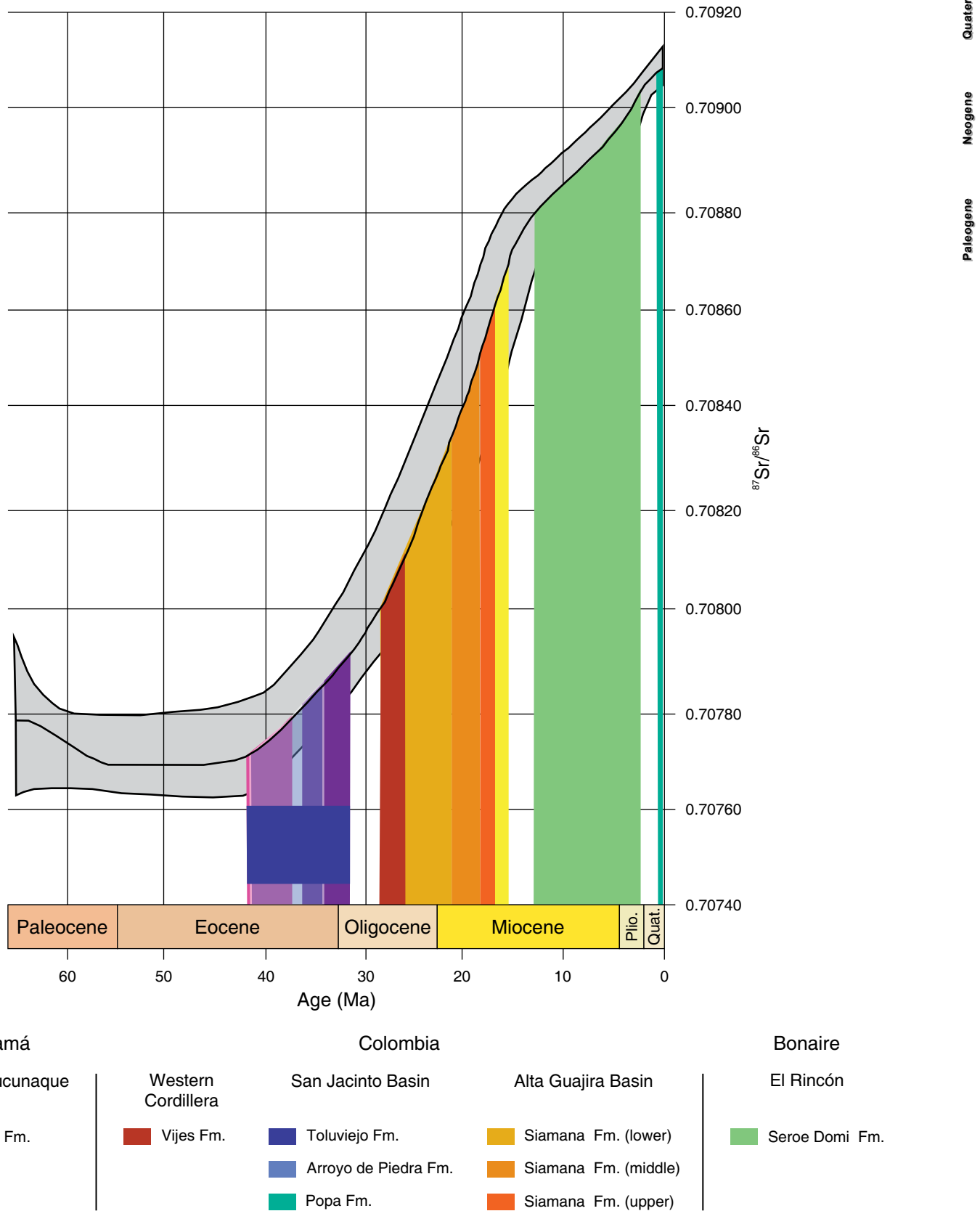


Figure 7. Evolution of the $^{87}\text{Sr}/^{86}\text{Sr}$ composition of the seawater and range of compositions of some of the reported carbonate successions. The Sr chemostratigraphic ages of carbonates were determined based on the correspondence of their $^{87}\text{Sr}/^{86}\text{Sr}$ compositions (see Table 1) and that of the seawater.

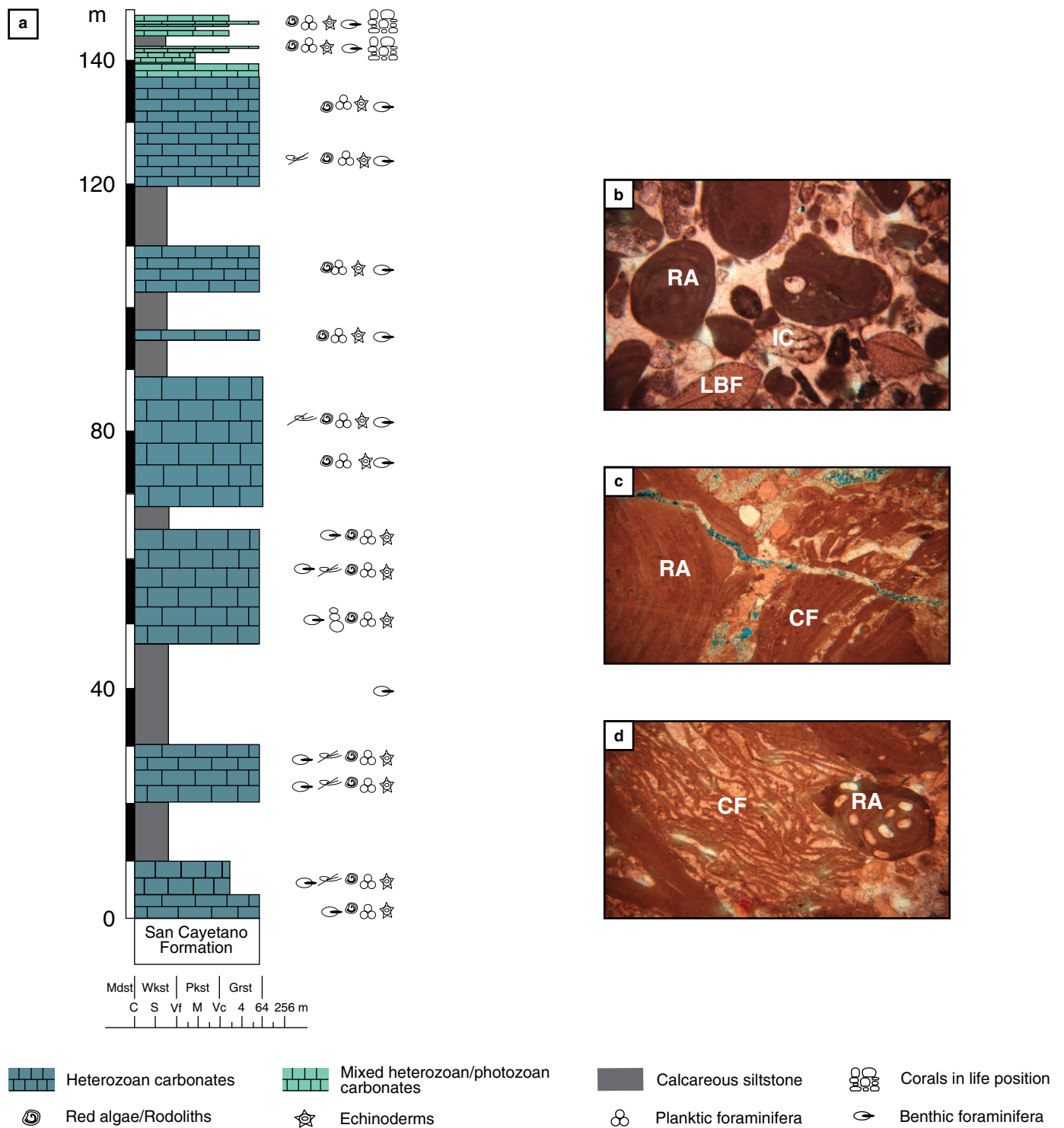


Figure 8. (a) Generalized lithostratigraphic column of the Arroyo de Piedra Formation along the Luruaco Anticlinorium. **(b)** Packstones with reworked red algal fragments (RA), intraclasts (IC), and larger benthic foraminifera (LBF). **(c)** Grainstone with fragments of corals (CF) and red algae (RA). **(d)** Grainstone with fragments of corals (CF) and red algae (RA).

quartz rich glauconitic sandstones (Figure 9a). In addition to coralline algae, the most common allochemicals of the grainstones are LBF (mainly *Nummulites* and lepidocyclinids), mollusks, bryozoans, and echinoderms. Mollusk and foramin-

ifera are found unfragmented, while bryozoans, echinoderms, and rhodoliths are often fragmented (Figure 9b–d).

Carbonates from the Macarao Formation display $^{87}\text{Sr}/^{86}\text{Sr}$ values between 0.7078023 and 0.707911 (Table 1). These

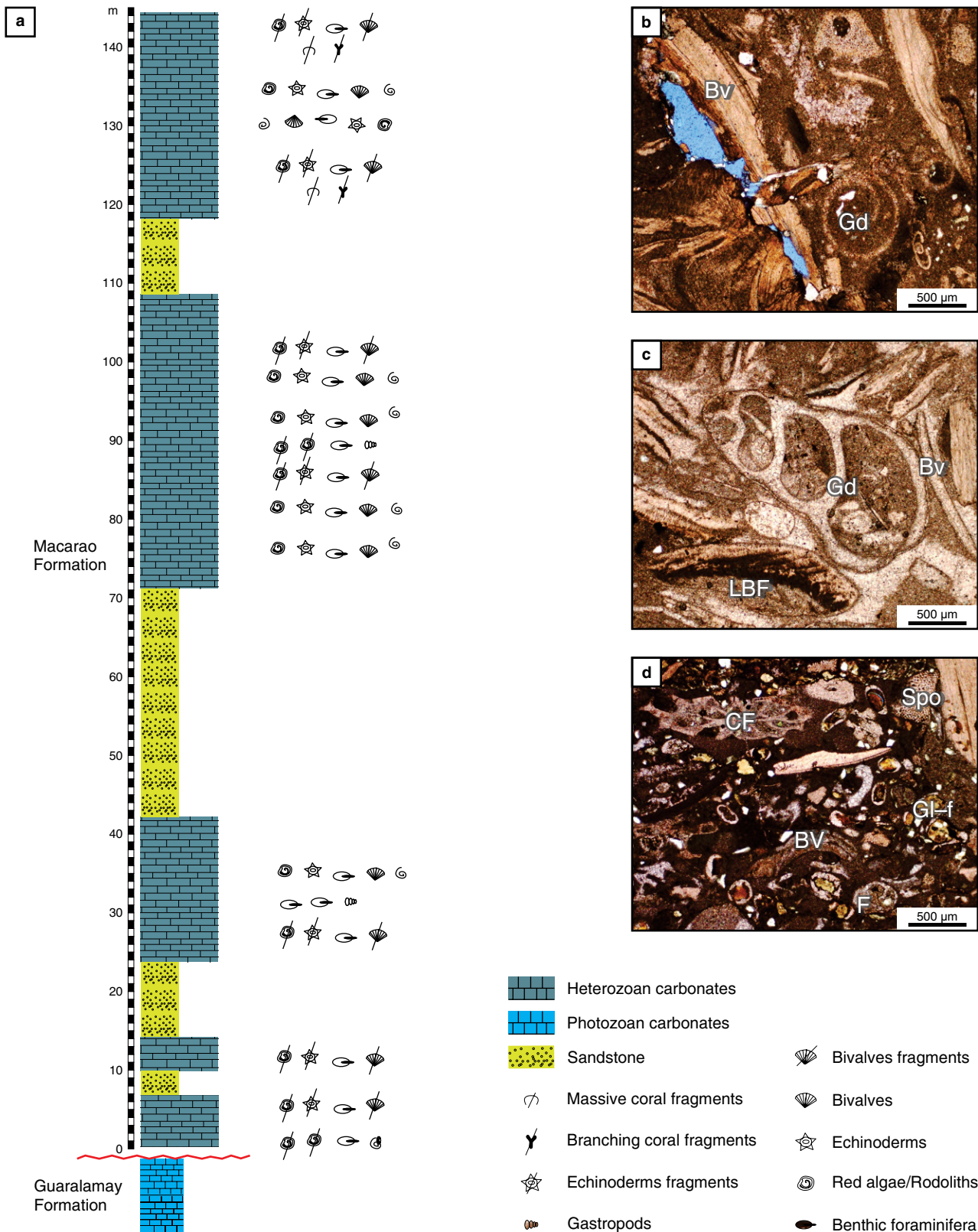


Figure 9. (a) Generalized lithostratigraphic column of the Macarao Formation. **(b)** Photomicrograph of grainstone with gastropods (Gd) and bivalves (Bv). **(c)** Photomicrograph of a grainstone with gastropods (Gd), bivalves (Bv), and larger benthic foraminifera (LBF). **(d)** Photomicrograph of a packstone with coral fragments (CF), sponge fragments (Spo), bivalves (BV), planktic foraminifera (F), and glauconite cement replacing foraminifera (GL-f).

values correspond to 36–32 Ma and suggest a late Eocene (Priabonian) depositional age. These ages partially overlap the foraminifera biostratigraphic ages suggested by (Rollins, 1960; Thomas 1972).

3.1.3. Toluvié Formation

The Toluvié Formation crops out along the central part of the SJDB. It was originally named “Series de Toluvié” (Guzmán et al., 2004). Kassem et al. (1967) and Duque-Caro (1968) proposed the formal name of the Toluvié Formation for this stratigraphic unit. Although no official type section has been proposed for the Toluvié Formation, the most accepted type locality is near the Toluvié municipality, Sucre Department, Colombia. According to Guzmán et al. (2004), the Toluvié Formation unconformably overlies the late Paleocene – early Eocene San Cayetano Formation and is unconformably overlain by the Oligocene Carmen Formation. According to Guzmán et al. (2004), in its type section, the Toluvié Formation mainly consists of a series of brown limestones with abundant lepidocycline macroforaminifers, *Nummulites*, red algal rhodoliths, oncoliths, and fragments of echinoderms and mollusks. It also displays fine-to-medium-grained lithic sandstones and coarse-grained carbonate-rich sandstones with abundant glauconite, marls, gray mudstones, and fine-to-medium-grained sandstones. Previous analyses of planktonic foraminifera (Bermúdez et al., 2009; Duque-Caro, 1975; Guzmán et al., 2004), palynology (Alfonso et al., 2009; Bermúdez et al., 2009), LBF (Alfonso et al., 2009), and calcareous nannofossils (Bermúdez et al., 2009) suggested a middle to late Eocene age (Lutetian – Priabonian) for the Toluvié Formation. Additionally, DUQUE-CARO in Guzmán et al. (2004) correlates it with the Arroyo de Piedra and Pendales Formations of the Luruaco Anticlinorium and the Chengue, Maco, San Jacinto, and Tampa Formations from the central and southern part of the SJDB.

Near the type locality, at Porvenir Hill (Figures 6b, 10b), the Empresa Colombiana de Petróleos S.A. (Ecopetrol) obtained a detailed description of the sedimentological characteristics from the Toluvié Formation (Ortiz et al., 1998). In this section, the lowermost part of the Toluvié Formation displays a series of calcareous sandy siltstones, composed of very fine sand-sized quartz grains, within a calcareous matrix. Locally, concentrations of LBF (Orbitoidacea, *Discocyclina*, and *Nummulites*) are observed, as well as *Thalassinoides* burrows and undifferentiated bioturbation (Figure 10). Higher in the stratigraphy, red algae rhodolith packstones, displaying sponges, LBF (Orbitoidacea and *Discocyclina*), and benthic foraminifera (Nodosariacea, Buliminacea) occur, as well as fragments of corals, pelecypods, and ostracods. A thin-bedded boundstone layer of sponges and *Acropora* coral fragments has been found

interbedded with a rhodolithic packstone. The upper part of the Toluvié Formation displays fine-grained, mud-supported, lithic arkose, with the presence of pelecypods shells, echinoderm spicules, and LBF (*Nummulites*).

In a northern stratigraphic section, Bermúdez et al. (2009) and Rosero et al. (2014) studied the Toluvié Formation in the core ANH P-8 well (Figures 6b, 10a). In this core, the Toluvié Formation discordantly overlies the San Cayetano/Arroyo Seco Formation (Figure 10a). It consists of thick layers of interbedded sandstones and aggradational fossiliferous wackestones and packstones. Rhodoliths and millimetric-to-centimetric benthic foraminifera (mainly *Nummulites* and lepidocyclinids) constitute the main allochems of these carbonates. The wackestones also display decimeter oncoids, mollusks, and echinoderms as subordinate allochems (Figure 10c–e).

Rosero et al. (2014) used $^{87}\text{Sr}/^{86}\text{Sr}$ chemostratigraphy in to determine the depositional age of the Toluvié Formation. They reported $^{87}\text{Sr}/^{86}\text{Sr}$ values between 0.707444–0.707598 for carbonates from the ANH P-8 well. These values fall below those displayed by global Cenozoic carbonates and therefore below the accepted values for the Cenozoic seawater (Figure 7). According to Rosero et al. (2014), the low $^{87}\text{Sr}/^{86}\text{Sr}$ values displayed by carbonates from the Toluvié Formation do not reflect the seawater values and therefore cannot be used to infer the depositional age of the Toluvié Formation in the P-8 well. Foraminifera and calcareous nannofossil assemblages reported for the P-8 well suggest a late Eocene (Priabonian) to early Oligocene (Rupelian) depositional age (Bermúdez et al., 2009). Salazar-Franco et al. (2016) used these depositional ages, as well as lithology and carbon and oxygen isotopes, to correlate the upper Arroyo de Piedra Formation and the Toluvié Formation (P-8 well).

3.2. Late Oligocene to Early Miocene Carbonates

3.2.1. Ciénaga de Oro Formation

The Ciénaga de Oro Formation was first referred to in internal reports of the company Intercol (Guzmán et al., 2004). It crops out along the central and southern part of the SJDB of the San Jacinto Basin, and it is also found in the subsurface along the Lower Magdalena Valley Basin along the San Jorge and Plato Sub-basins. The Ciénaga de Oro Formation mainly consists of deltaic siliciclastic successions, which display fining-upward packages of fine to coarse-grained sandstones interbedded with fossiliferous siltstones. Based on both palynology (Bermúdez et al., 2009; Dueñas, 1977, 1986) and planktonic foraminiferal data (Bermúdez et al., 2009), an Oligocene – middle Miocene depositional age has been proposed for the Ciénaga de Oro Formation. This formation has been correlated with siltstone–

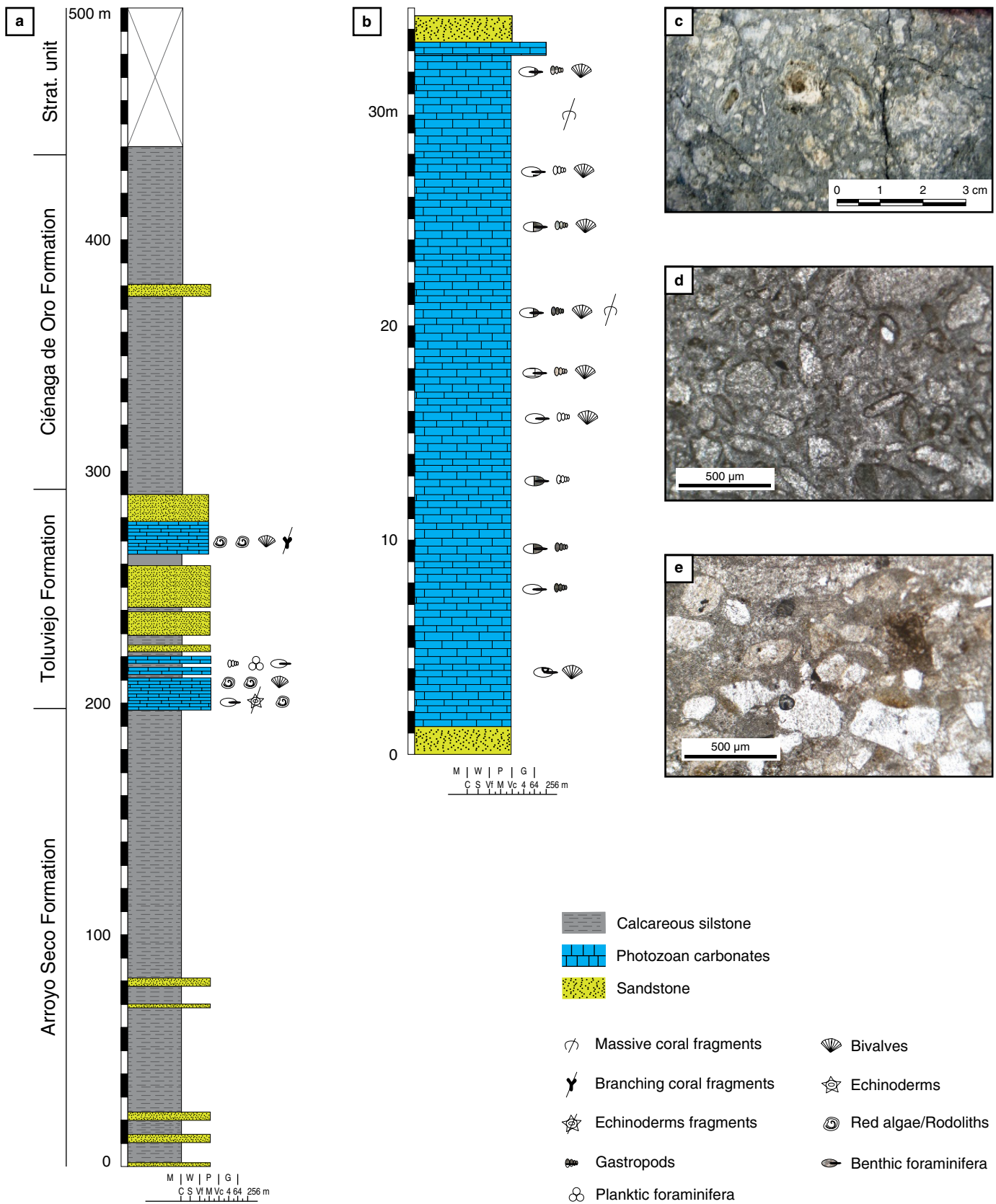


Figure 10. Generalized lithostratigraphic column of the Tuluviejo Formation. **(a)** Slim-hole P-8 from the Agencia Nacional de Hidrocarburos (After Bermúdez et al., 2009). **(b)** Porvenir Hill section stratigraphic column (After Ortiz et al., 1998). **(c)** Hand sample of rhodolitic limestone. **(d)** Photomicrograph of coral fragment. **(e)** Photomicrograph of wackestone displaying echinoderm fragments and quartz sand.

dominated successions from the Carmen and Floral Formations from the central and northern parts of the Lower Magdalena Valley Basin (Bermúdez et al., 2009).

In the Plato Sub-basin, the Ciénaga de Oro Formation also displays subordinate carbonate packages, which occur in the subsurface (Figure 5; Reyes-Harker et al., 2000). Some of those packages have been reported in El Dificil and Cicuco gas oil fields (Ortiz & Niño, 1999). Swolf (1946) originally reported the sedimentological characteristics of the Ciénaga de Oro Formation limestones (Cicuco Limestones). Ortiz & Niño (1999) analyzed cores from thirteen wells in the Cicuco and Boquete fields, drilled between the Brazo de Mompós and Brazo de Loba in the Lower Magdalena Valley (Figure 6b). The authors found that in all wells, the Cicuco Limestones conformably overlays a series of basal conglomeratic sandstones, which display fragments of pelecypods and gastropods, as well as abundant uniserial benthic foraminifera (Figure 11). The basal conglomeratic sandstones are overlain by sandy limestones, which grade to pure limestones towards the top. These limestones mainly display LBF (*Sorites*) and mollusk shell fragments. Higher in the stratigraphy, calcareous sandstones are present, which are rich in shell fragments from gastropods and pelecypods. Such calcareous sandstones grade to sandy limestones and wackestones, the main allochemical components of which are benthic foraminifera, echinoderms, corals, and red algae (*Lithophyllum*). A series of coral and red algal packstones/wackestones, characterized by abundant skeletal fragments consisting mainly of coral heads and branching corals (*Porites*), with variable amounts of large echinoderm spines, pelecypod shell fragments, benthic foraminifera, and rhodoliths, occur higher in the stratigraphic section. Boundstones, rudstones, and floatstones, characterized by abundant coral debris (*Porites*, *Diploastrea*, *Montastrea*, *Siderastrea*), LBF (*Operculinoides*, *Heterostegina*, *Lepidocyclina*), mollusk shell fragments, and red algae (*Mesophyllum*, *Lithophyllum*, and rhodoliths), also occur in the uppermost part of the Cicuco Limestones (Figure 11). Overlying the limestone in some wells are found terrigenous and bioclast rich grainstones and calcareous sandstone (Ortiz & Niño, 1999).

3.2.2. Siamana Formation

The Siamana Formation was originally defined by Renz (1960). It crops out around the Macuira and Jarara Ranges and to the north of the Cosinas Range, along the Cocinetas Sub-basin of the Alta Guajira Basin, La Guajira Department, Colombia (Figure 6c). The type section of the Siamana Formation is located near the Sillamahana locality. According to Renz (1960), the Siamana Formation consists of a basal series of marly polymictic conglomerates followed by a series of fossiliferous sandy limestones interspersed with mudstones and shales, with abundant

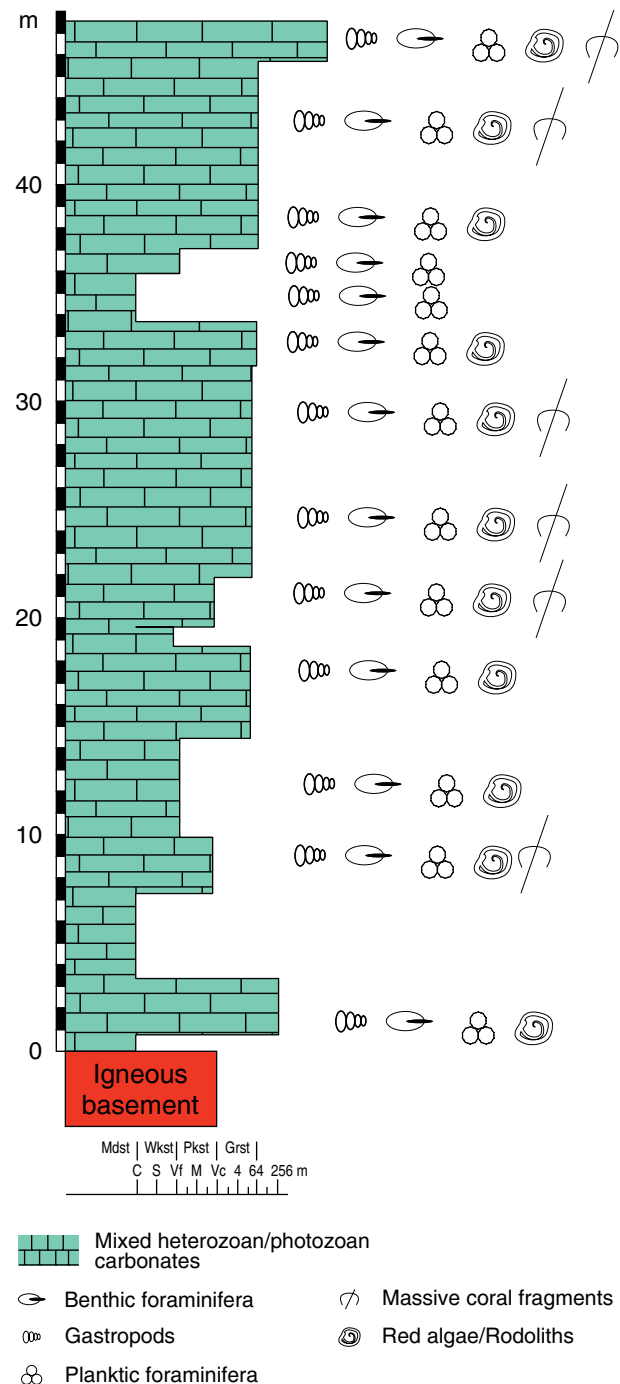


Figure 11. Generalized lithostratigraphic column of the Cicuco Limestones (Ciénaga de Oro Formation) (Ortiz & Niño, 1999).

bivalves and gastropods (Rollins, 1960). Locally, thin layers of calcareous and fine-grained clayey sandstones are present. Higher in the section, the development of coral reef limestones is common (Rollins, 1960).

Silva-Tamayo et al. (2017) studied the Siamana Formation using surface stratigraphic sections along the Cocinetas Sub-basin, Alta Guajira Basin, northern Colombia (Figure

6a). According to these authors, the undeformed Siamana Formation discordantly overlies the deformed Macarao Formation, as well as the pre-Cenozoic crystalline basement of the Cosinetas Sub-basin. The basal part of the Siamana Formation (Sillamahana and Flor de La Guajira sections; Figure 12a–c) consists of mixed carbonate siliciclastic successions, in which polymictic conglomerates are interbedded with restricted framestones, rudstones, grainstones, and wackestones. The framestones, which are mostly composed of massive corals, are also found unconformably capping the deformed Macarao Formation (Figure 12b, 12d). Massive corals, echinoderms, and calcareous algae constitute the main allochemical components of rudstones, grainstones, and wackestones. The basal mixed carbonate siliciclastic succession is overlain by a series of packstone, grainstones, rudstones, and framestones. The framestones mainly consist of massive and ramified corals (Figure 12d). Ramified corals constitute the predominant component of the rudstones. Instead, coral fragments, brachiopods, echinoderms, and bivalves are the main allochemical components of packstones and grainstones, which also contain LBF (*Nummulites*) and benthic foraminifera (Miliolids, Fusulinids) (Figure 12e, 12f). While the packstones and grainstones are the most predominant, they are not laterally continuous and vary laterally to restricted framestones and rudstones. The middle part of the Siamana Formation (Uitpa stratigraphic section, Figure 13) displays a basal series of boundstones, bafflestones, and framestones, characterized by a highly diverse coral assemblage; i.e., ramose, platy, and massive corals (Figure 13b–e). These facies extend laterally for several kilometers and display predominantly aggradational stacking patterns that change laterally (locally) to fining-upward grainstones and packstones, consisting of fragments of corals, mollusks, echinoderms, bivalves, and foraminifera. The uppermost part of the Siamana Formation displays a series of laterally continuous (kilometrical) aggradational strata, mainly composed of centimeter-to-decimeter rhodalgal biostromes (Ekyeps Creek stratigraphic section, Figure 14a). Echinoderms and foraminifera constitute subordinate allochemicals of these biostromes. These coralline algae successions are finally overlain by a series of fining upward cycles of grainstones to packstones constituted predominantly by coralline algae fragments and foraminifera (Figure 14b–e).

Carbonates from the lower part of Siamana Formation display $^{87}\text{Sr}/^{86}\text{Sr}$ values between 0.708030 and 0.708385 (Figure 7), suggesting a late Oligocene (Chattian) – early Miocene (Aquitania) depositional age (28–22 Ma). $^{87}\text{Sr}/^{86}\text{Sr}$ values between 0.708348 and 0.708485 are displayed by carbonates from the middle part of the Siamana Formation (Figure 7), suggesting a depositional age of early Miocene (Aquitania – Burdigalian), between 21 and 18 Ma (Silva–Tamayo et al., 2017). Carbonates from the upper part of the Siamana Formation display $^{87}\text{Sr}/^{86}\text{Sr}$ values between 0.708502 and 0.708674, suggesting a deposi-

tional age of early to middle Miocene (Burdigalian – Langhian), between 18 and 15 Ma (Figure 7).

3.2.3. Vijes Formation

The Vijes Formation crops out along the eastern flank of the Western Cordillera of Colombia and west of the Cauca–Patía Basin (Dueñas et al., 2000). Its type section is located near the town of Vijes, Valle del Cauca Department, southwestern Colombia (Figure 6d). Dueñas et al. (2000) reported the first lithostratigraphic information on the Vijes Formation from stratigraphic cores. According to these authors, the Vijes Formation unconformably overlies the volcanic basement of the Western Cordillera of Colombia. The lower part of the Vijes Formation displays polymictic conglomerates overlain by a series of coral and red algae-rich limestones. The middle part of the Vijes Formation displays, in turn, alternating mudstones and fine-grained sandstones. The upper part of the formation mostly displays quartz sandstones. Dueñas et al. (2000) used the occurrence of the foraminiferal biozones P18–P21 to suggest an Oligocene (Rupelian – Chattian) depositional age for the Vijes Formation.

In this chapter, we further study the Vijes Formation in a surface stratigraphic section (Figure 6d). In this section, the Vijes Formation is approximately 130 m thick and displays a basal polymictic conglomerate overlain by a series of alternating coarsening-upward, and fining-upward packages of wackestones, packstones, and grainstones (Figure 15a). These sedimentary packages display abundant LBF, fragments of bivalves, echinoderms, gastropods, and occasionally bryozoans, calcareous red algae fragments, and oncoliths. These carbonate packages also display variable amounts of fine-grained quartz sand. Higher in the stratigraphy, the sedimentary succession displays a coarsening-upward character, and the sedimentary packages become thicker and more aggradational. The wackestones display abundant coarse conglomeratic sand and angular quartz fragments, as well as foraminifera, algae, mollusks, and oncoliths. The grainstones display fragments of algae, gastropods, and bivalves. A new fining-upward set of strata displaying grainstones, packstones, and wackestones is observed higher in the stratigraphy. Carbonates from this new set display fragments of algae, foraminifera, and mollusk, as well as abundant quartz. The upper part of the sedimentary succession displays aggradational packages of packstones and wackestones. Algae, gastropods, bivalves, and echinoderms are the main allochemical components. These aggradational carbonate packages are overlain by a series of massive sandstones with low fossil content. The uppermost part of the sedimentary succession displays a set of coarsening upward sandstones, which display fragments of algae, mollusks, and foraminifera. Some grainstones with abundant quartz sand and fragments of algae, foraminifera, and mollusks also occur in this part of the sedimentary succession (Figure 15b–e).

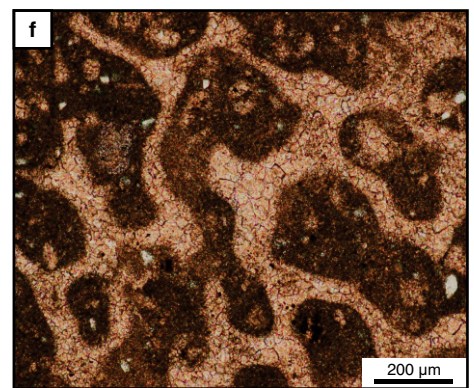
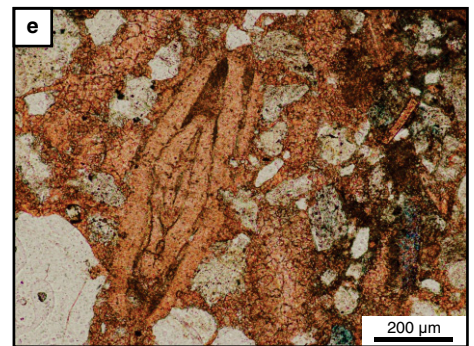
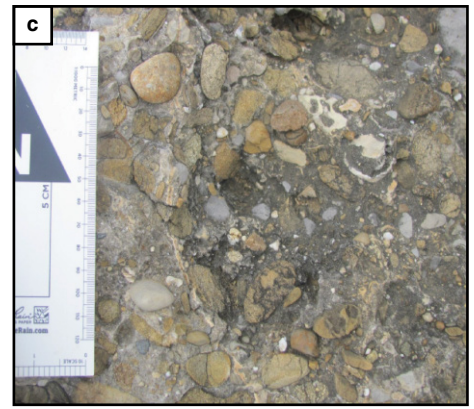
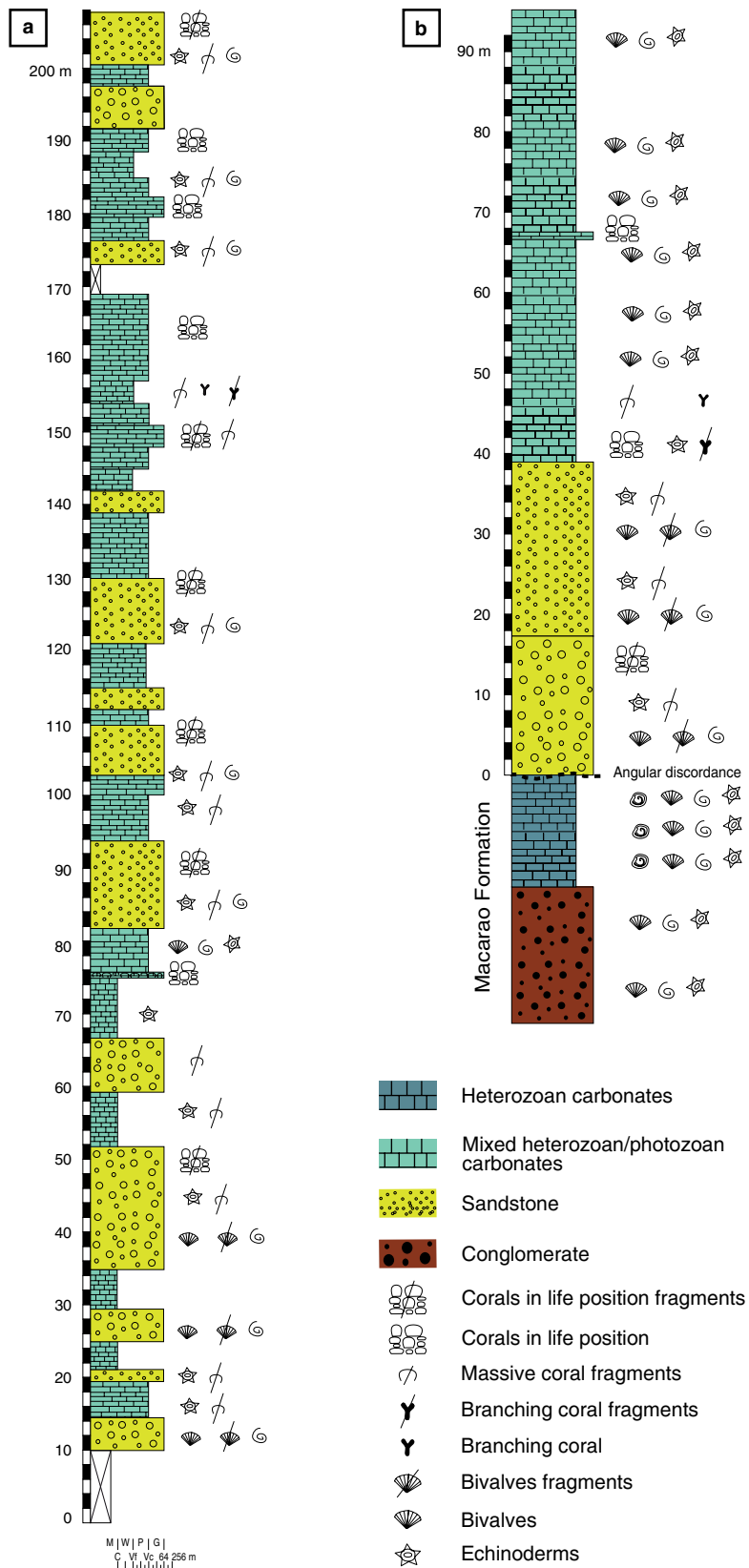


Figure 12. Generalized lithostratigraphic column of the lowermost Siamana Formation (Silva-Tamayo et al., 2017). **(a)** Sillamahana stratigraphic section. **(b)** Flor de La Guajira stratigraphic section. **(c)** Basal conglomerate in the Sillamahana section. **(d)** Framestone from the lowermost part of the Flor de La Guajira stratigraphic section. **(e)** Photomicrograph of a packstone displaying larger benthic foraminifera (LBF) and quartz sand (Q). **(f)** Photomicrograph of a coral fragment.

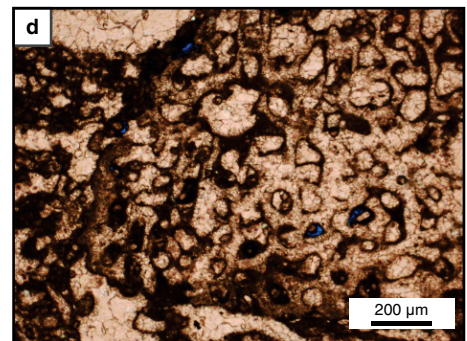
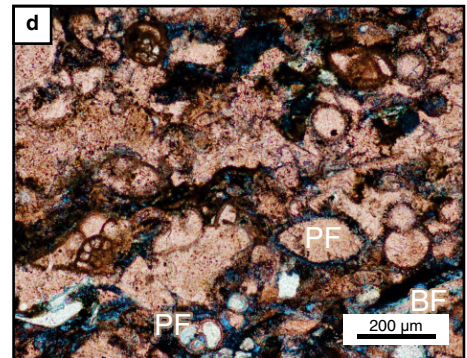
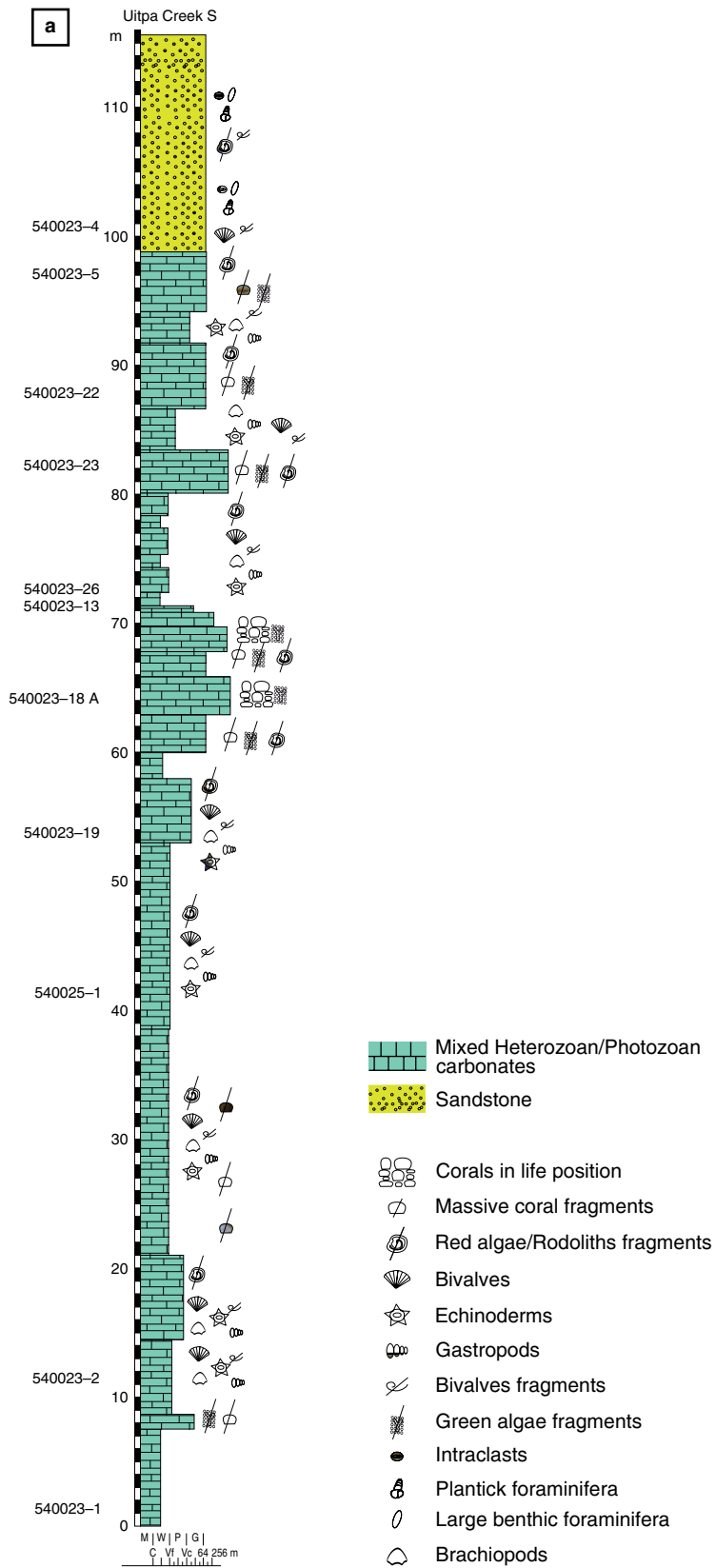


Figure 13. (a) Generalized lithostratigraphic column of the middle part of the Siamana Formation in the Uitpa Creek stratigraphic section (Silva-Tamayo et al., 2017). **(b)** Framestones from the upper part of the stratigraphic section. **(c)** Rudstone from the lowermost part of the stratigraphic section. **(d)** Photomicrograph of a packstone from the middle part of the stratigraphic section displaying planktic foraminifera (PF) and bivalve fragments (BF). **(e)** Photomicrograph of a coral fragment of framestone from the uppermost part of the stratigraphic section.

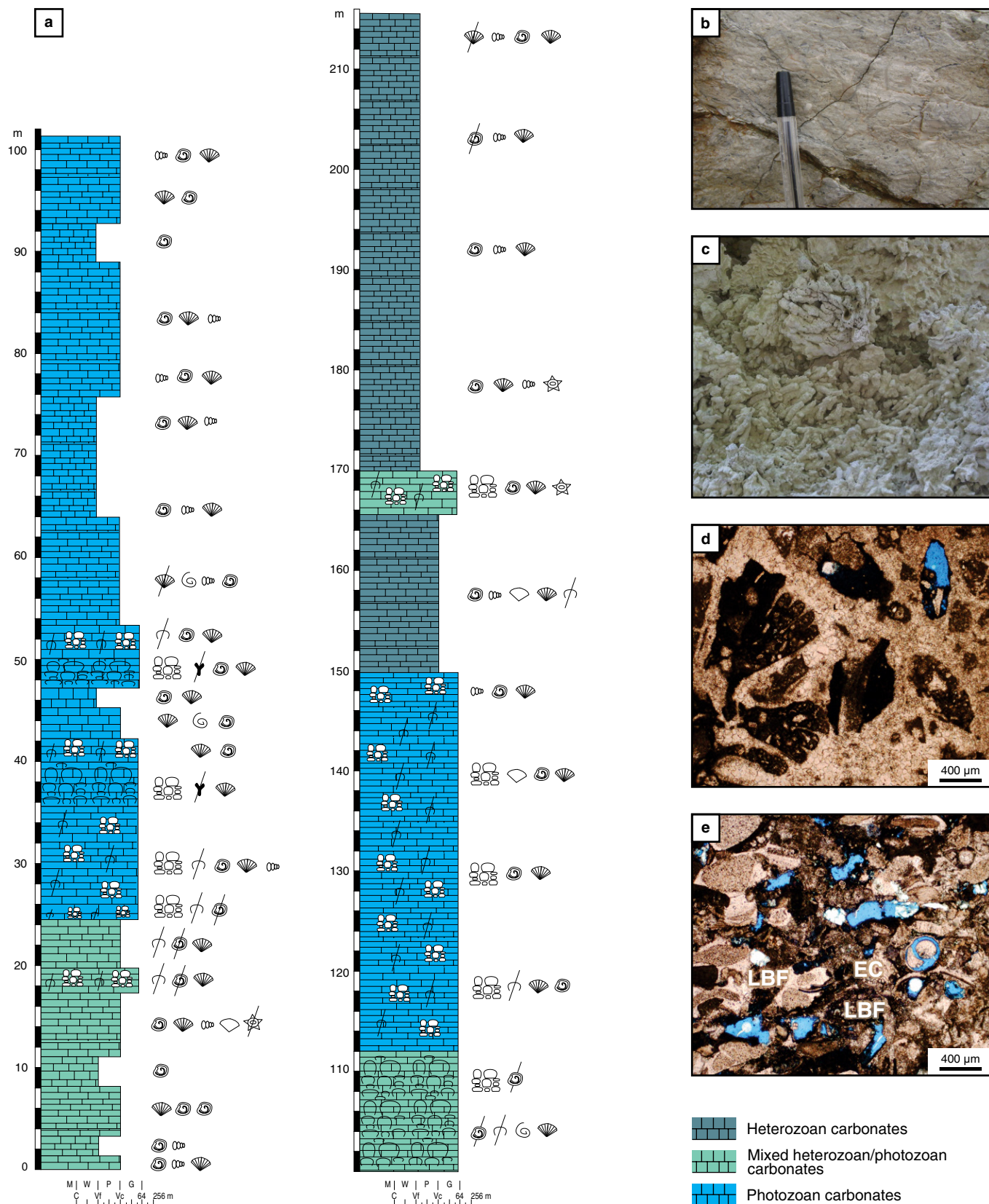


Figure 14. (a) Generalized lithostratigraphic column from the upper part of the Siamana Formation of the Ekyeps Creek stratigraphic sections (Silva-Tamayo *et al.*, 2017). (b) Large benthic foraminifera grainstone from the uppermost part of the Siamana Formation. (c) Framestone from the lower part of the Ekyeps Creek stratigraphic section. (d) Photomicrograph of coral fragment from the lower part of the stratigraphic section. (e) Photomicrograph of grainstone from the middle part of the stratigraphic section. (EC) Echinoderm; (LBF) larger benthic foraminifera.

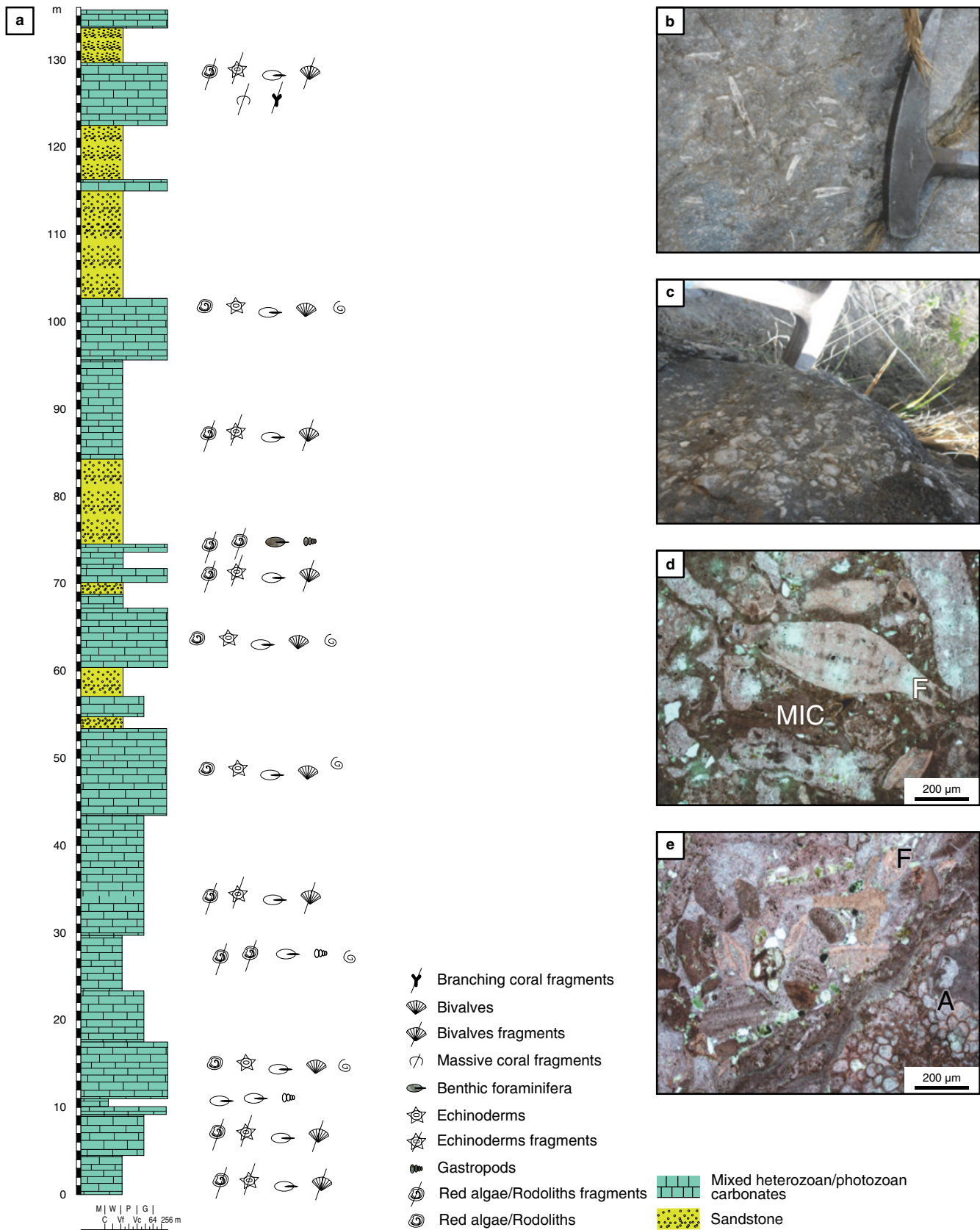


Figure 15. (a) Generalized lithostratigraphic column of the Vijes Formation (Torres–Lasso, 2014). **(b)** Grainstone displaying rhodolith and gastropods. **(c)** Rhodolith from the lower part of the Vijes Formation. **(d)** Photomicrography of a grainstone from the upper part of the Vijes formation displaying benthic foraminifera (F) and micritic cement (MIC). **(e)** Photomicrograph of grainstone from the lowermost part of the Vijes Formation displaying green algal fragments (A) and benthic foraminifera (F).

Carbonates from the Vjies Formation display $^{87}\text{Sr}/^{86}\text{Sr}$ values between 0.708035 and 0.708111 (Figure 7). These values suggest a late Oligocene (Chatian) depositional age, between 26–28 Ma. The Chatian age partially overlaps those proposed for the Vjies Formation based on palynomorphs and foraminifera biostratigraphy (Dueñas *et al.*, 2000).

3.3. Middle to Late Miocene Carbonates

3.3.1. San Andrés Formation

The middle – late Miocene San Andrés Formation was first described by Hubach (1956). It crops out in the center of the San Andrés Island, Colombia, along the Los Cayos Basin of the Lower Nicaragua Rise (Figure 6a). No type section has been proposed for the San Andres Formation. The available lithostratigraphic information comes from well cores from the Servicio Geológico Colombiano (well PP–III–003; Vargas–Cuervo, 2004). In this core, the San Andrés Formation reaches 113 m in thickness, although seismic information suggests that this carbonate unit is ca. 250 m thick. According to Bürgl (1959), the San Andrés Formation corresponds to lagoon and reefal deposits characterized by mudstones, wackestones, and packstones. Red algae and mollusks constitute the main allochems (Bürgl, 1959; Hubach, 1956). The San Andrés Formation has been correlated to the Providencia Formation (Providencia Island), the Martinez Reef Formation from the Nicaragua Rise, and the White Limestone from Jamaica (Geister, 1992).

3.4. Pleistocene and Recent Carbonates

3.4.1. La Popa Formation

According to Barrera (2001), the first reference of the name La Popa is found as La Popa Group in Anderson (1926 in Barrera, 2001), but the origin of this name as La Popa Formation was first used in a description by Bürgl (1957 in Barrera, 2001) of the strata constituting La Popa Hill in Cartagena. La Popa Formation emerges on a series of less abrupt and elongated hills between Cartagena and Barranquilla. The lithology is composed of solid clays that gradually pass upwards to reefal limestones. The age of this unit has been very controversial. However, Barrera (2001) postulates, based on the stratigraphic position and the microfauna recently collected by Servicio Geológico Colombiano, a Pleistocene age for this unit.

La Popa Formation was recently studied in one slim-hole stratigraphic well (Z well) along the Luruaco Anticlinorium of the SJDB (Figure 6b; Reyes *et al.*, 2009). In this well, La Popa Formation consists of a basal siliciclastic unit and an upper carbonate unit (ca. 25 m thick). Carbonates from La Popa Formation consist of interbedded aggradational packstones of framestones, grainstones, packstones, wackestones,

and mudstones (Figure 16a). The framestones usually consist of different associations of massive corals in life position. The grainstones usually display fragments of massive corals as well as fragments of brachiopods, bivalves, gastropods, and green algae. Fragments of corals, gastropods, and echinoderms constitute the main allochemical components of the wackestones (Figure 16b–d). The interbedded siltstones are fossiliferous (fragments of bivalves, gastropods, green algae) and display parallel planar laminations, as well as moderate bioturbation.

Carbonates from La Popa Formation display $^{87}\text{Sr}/^{86}\text{Sr}$ values of 0.709097 and 0.709122 (Figure 7). These values suggest a Pleistocene depositional age for La Popa Formation. These ages partially overlap the ages proposed by Barrera (2001).

3.4.2. San Luis Formation

The Pleistocene San Luis Formation crops out in the San Andres Island, Colombia, along the Los Cayos Basin of the Lower Nicaragua Rise (Figure 6a). It was first described by Hubach (1956) and later on defined by Geister (1973, 1975). According to Geister (1973), the San Luis Formation is 15 m thick and mainly consists of biogenic packstones and grainstones. Corals constitute the main allochems of the San Luis Formation limestones. The Pleistocene depositional age of the San Luis Formation was obtained by Geister (1973), who used radiocarbon dating of carbonate remains.

3.5. Modern Marine Carbonate Areas of Colombia

Modern Colombian marine carbonate areas occur along the Colombian Caribbean continental shelf and as part of oceanic (Caribbean and Pacific) coral reef areas (Figure 17). These marine carbonate areas include several types of coral reef ecosystems and their interactions with other strategic ecosystems such as sea grass meadows and mangroves (Díaz *et al.*, 2000, 2003), because all of them contain several coral species and other calcifying organisms. These areas cover approximately 2860 km². Most of these areas (76.5%) correspond to the San Andrés and Providencia Archipelago, where isolated carbonate platforms occur, characterized by the presence of fringing and barrier reefs, pinnacles, and atolls dominated by photozoans (corals) (Díaz *et al.*, 2000; Instituto de Hidrología, Meteorología y Estudios Ambientales (IDEAM), 2017). Although the archipelago is located near the Central American continental shelf, it is affected by the Western Caribbean Current, the cyclonic Panamá–Colombia Gyre and its countercurrent, and the Magdalena River discharges (Criales *et al.*, 2002), which prevent the Central American siliciclastic input from reaching the carbonate systems. The combination of these particular features allows the occurrence of euphotic and oligotrophic marine conditions,

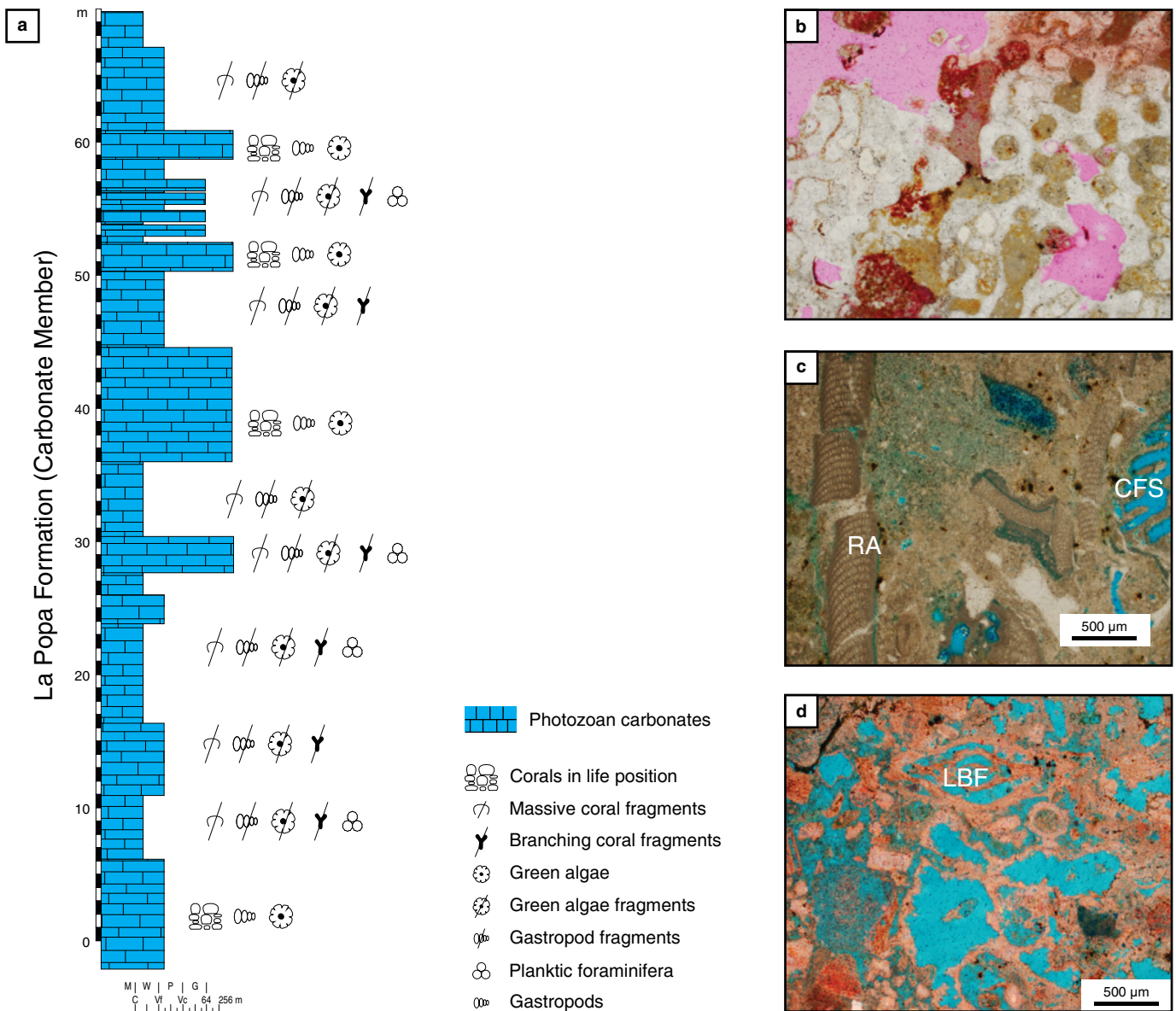


Figure 16. (a) Generalized lithostratigraphic column of La Popa Formation at well Y. **(b)** Photomicrograph of a coral fragment from the upper part of La Popa Formation. **(c)** Photomicrograph of wackestone from the lower part of La Popa Formation displaying red algal fragments (RA) and shadows of coral fragments (CFS). **(d)** Photomicrograph of limestone from the lower-most part of La Popa Formation displaying vuggy porosity and shadows of larger benthic foraminifera (LBF).

which in turn promote the preservation of a predominantly photozoan carbonate factory.

The second largest concentration of marine carbonate sedimentary areas occurs in the central sector of the Colombian Caribbean coast and its continental shelf (Figure 17). The San Bernardo and Rosario Archipelagos, the Tortuguilla and Fuerte Islands, and the Salmedina, Tortugas, and Bushnell lows, among others, are carbonate sedimentary successions that deposit on top of a series of topographic highs at the bottom of the continental shelf (Barrios, 2000; Díaz et al., 2000; Garzón-Ferreira et al., 2001). Modern carbonate sedimentary areas occur along portions of the coast with alternating coves or bays with

rocky cliffs. This is the case for Urabá, near the border with Panamá, Santa Marta, and Parque Nacional Natural Tayrona. In these areas, algal rugs, coral reefs, beach rocks, meadows of seagrass, and sand plains occur. At the northern end of Colombia, on the shores of La Guajira Peninsula, similar areas also occur, which are mostly dominated by coral formations of limited extent (Díaz et al., 2000).

The Pacific continental and Oceanic marine areas display the least extensive carbonate sedimentation areas. While the continental areas are dominated by fringing and patchy coral reefs, those of the oceanic areas are dominated by fringing coral reefs and coralline biostromes. The development of coral reefs

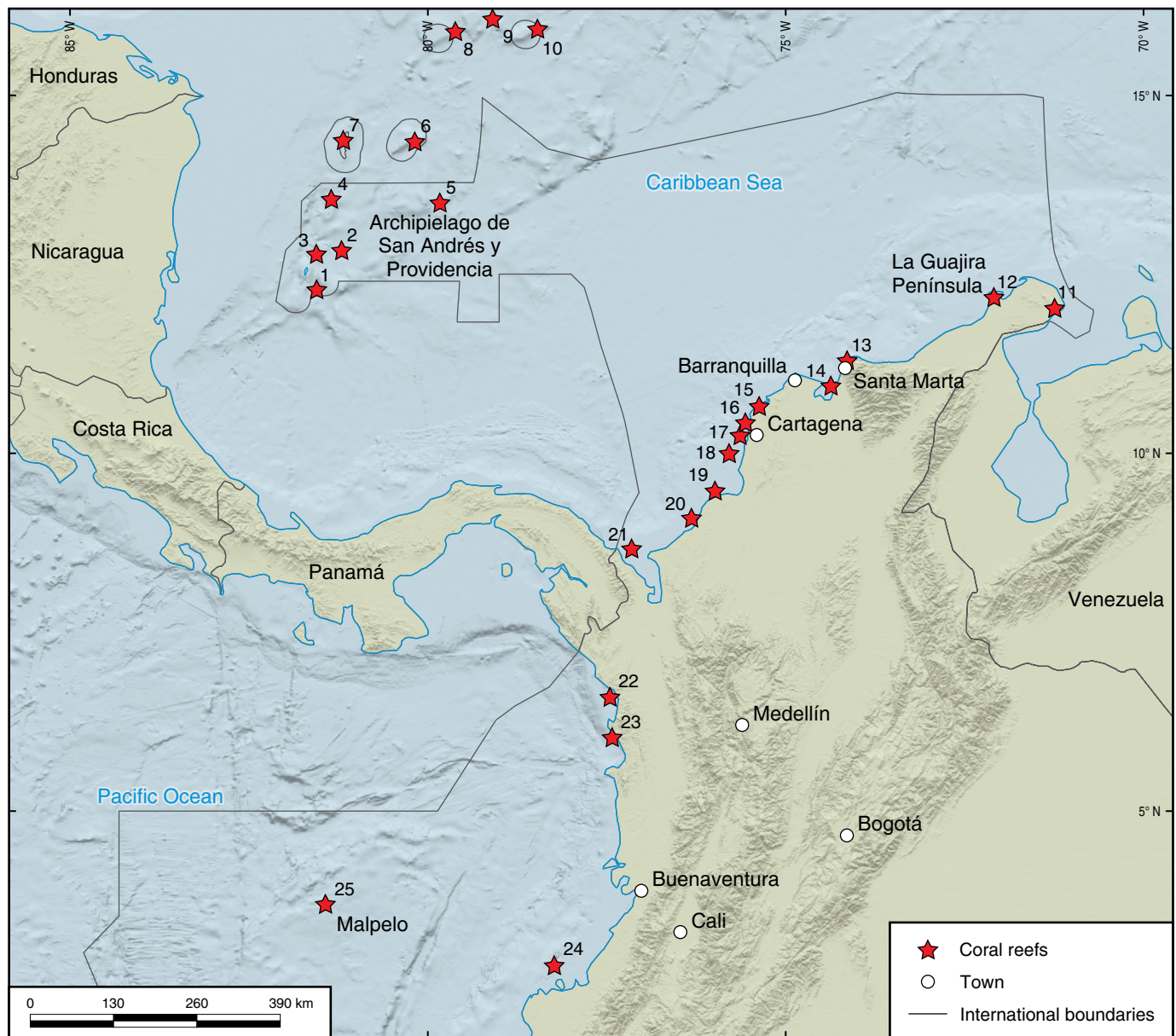


Figure 17. Locations of modern marine carbonate areas (coral reefs) in Colombia. Colombian coral reef areas: (1) Albuquerque Cay; (2) Courtown Cay; (3) San Andres Island; (4) Providence Island; (5) Roncador Bank; (6) Serrana Bank; (7) Quitasueño Bank; (8) Serrana Bank; (9) Alicia Bank; (10) Nuevo Cay; (11) Puerto López; (12) La Vela Bank; (13) Parque Nacional Natural Tayrona; (14) Banco de las Ánimas; (15) Santa Marta; (16) Salmedina Bank; (17) Rosario Island; (18) Tortuga Bank; (19) San Bernardo Island; (20) Tortuguilla Island; (21) Capurgana; (22) Cupica; (23) Utría; (24) Gorgona; (25) Malpelo. Modified from Barrios (2000) and Díaz *et al.* (2000).

in the Colombian Pacific follows the observed pattern for other tropical eastern Pacific coral reef formations (Barrios, 2007).

4. Evolution of the Carbonate Factories

Figure 18 presents a proposed model of the evolution of the Cenozoic carbonate factories from Colombia. The oldest Cenozoic shallow-water carbonate records correspond to the middle Eocene Arroyo de Piedra Formation (northern portion of the SJDB). It mainly consists of rhodolith packstones

and rudstones. These carbonate facies display red algae and LBF as the main allochemical components (Salazar-Franco *et al.*, 2016). The allochemical composition, together with the presence of claystone-siltstone intraclasts and interbedded calcareous mudstones and siltstones suggest that the Arroyo de Piedra Formation was deposited in three coeval environments: (1) Middle-proximal ramp rhodolith beds; (2) outer ramp/slope channels and lobes, mainly fed from the middle-ramp carbonate factory; and (3) outer ramp/slope open marine areas developed during a regional transgression (Figure

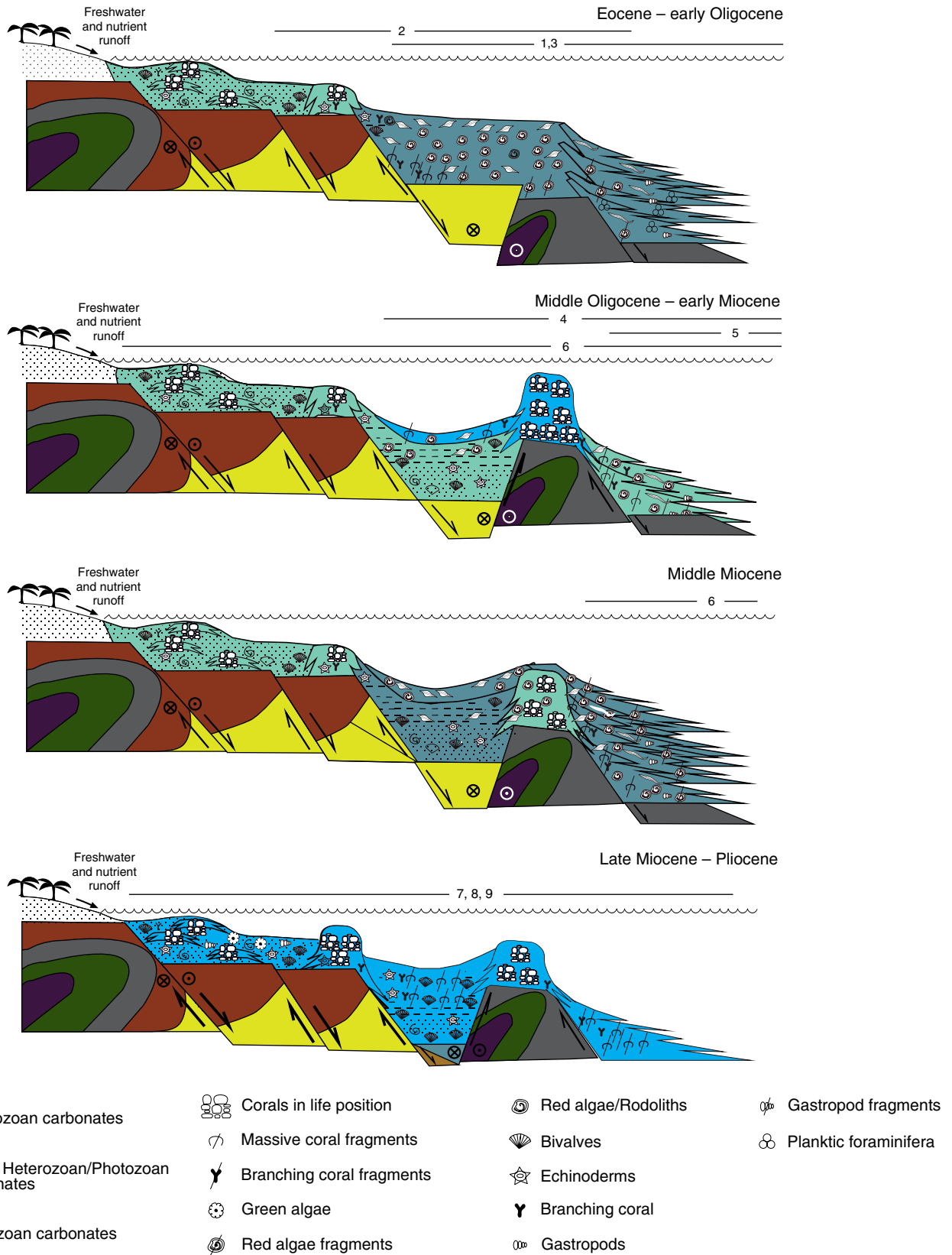


Figure 18. Schematic evolution of the Cenozoic shallow marine carbonate factories in Colombia. Numbers designate the range of variation in depositional style for each of the studied carbonate units. (1) Arroyo de Piedra Formation; (2) Toluviejo Formation; (3) Macarao Formation; (4) Cicuco Limestones; (5) Vijes Formation; (6) Siamana Formation; (7–9) San Andrés, San Luis, and La Popa Formations.

18). Transgressive–highstand systems are represented by the middle–proximal carbonate factory, while lowstand systems are characterized by the presence of reworked calcareous sedimentites. Transgressive events are characterized by the presence of open–sea facies (Figure 8; Salazar–Franco et al., 2016). The heterozoan biotic associations that characterize the carbonate factory of the Arroyo de Piedra Formation suggest a deposition under nutrient–rich (mesotrophic) oligophotic–to–mesophotic marine conditions.

Heterozoan biotic associations are also recorded in the central part of the SJDB, at the base of the Toluvié Formation in the P8 well (Bermúdez et al., 2009). There, the carbonates of the Toluvié Formation consist of wackestones and packstones, rich in red algal rhodoliths, which represents an initial carbonate deposition, which occurred during a period of relative sea level rise (Figure 10). A second transgressive cycle begins with the deposition of LBF grainstones and packstones, rich in red algal rhodoliths and LBF, as well as boundstones, rich in sponges and coral fragments, and it is also observed in the Porvenir Hill (Figure 10b; Ortiz et al., 1998). Such a biotic composition significantly differs from that observed in the Arroyo de Piedra Formation, where calcareous red algae are the dominant components. The significant abundance of LBF followed by red algae and the subordinate presence of coral fragments suggest the coexistence of both photozoan and heterozoan carbonates. The biotic association indicates clear, warm, oligotrophic waters, with a very low contribution of siliciclastic material (Tucker & Wright, 1990). These sedimentologic features of the Toluvié carbonate factory, together with the presence of carbonate rich siltstones and claystones, suggest deposition along a shallow restricted platform, on which lagoon, patch reef, and tidal bar depositional environments coexisted (Figure 18; Ortiz et al., 1998).

The transgressive deepening tendency of the calcareous system in the Toluvié Formation is followed by a regressive shallowing cycle, characterized by the presence of wackestones displaying a heterozoan biotic association that normally develops under nutrient–rich (mesotrophic), oligophotic–to–mesophotic marine conditions (oncolites, mollusks, and echinoderms; Figure 10). The switch in the biotic community might be the effect of the shallowing cycle, which includes the progressive inclusion of detrital material, increased nutrient availability, and increased turbidity of the water. The presence of river systems adding sediment to the continental shelf is supported by the lateral occurrence of calcareous mudstones from the Chengue Formation, which have been interpreted as deposition along a deep inner mixed siliciclastic–carbonate shelf (Bermúdez et al., 2009; Guzmán, 2007).

During the late Eocene, the heterozoan biotic associations constituted the dominant carbonate factory along the Alta Guajira Basin (Macarao Formation). The presence of coralline algae and LBF (mainly *Nummulites* and lepidocyclinids) suggests deposition under oligophotic–to–mesophotic and nutrient–rich

(mesotrophic) marine conditions. The aggradational stacking pattern of the studied carbonates together with the presence of thick aggradational massive quartz sandstones suggests that the carbonate successions of the Macarao Formation were also deposited as rhodalgial biostromes along a mixed siliciclastic–carbonate shelf (Figure 18; Tucker & Wright, 1990).

The middle Oligocene to lower Miocene carbonates from the Cicuco Limestones (Ciénaga de Oro Formation) at the Lower Magdalena Valley exhibit a facies association typical of rimmed carbonate shelves (Figures 11, 18). The presence of red alga–rich packstones and grainstones with low terrigenous content is interpreted as isolated carbonate banks (patch–reefs of coralline algae) deposited on top of basement heights. The presence of red algal bioclastic grainstones, wackestones, and packstones, rich in siliciclastic debris suggests a deposition along a back–reef sandy belt of coralline algae (Ortiz & Niño, 1999). This proposal is supported by the occurrence of mixed heterozoan–photozoan biotic associations consisting of crustose coralline algae (*Melobesieae*), LBF (Camerinidae, Orbitoididae), sponges (Calcispongiae), corals, and mollusks (Pelecypoda). The predominance of heterozoan biotic associations over photozoan biotic associations suggests that the deposition of carbonates occurred under mesotrophic marine conditions. The basal coarsening upward carbonates (Figure 11), deposited at the base of these paleo–highs, evidence a transgressive system that gradually evolves towards a high–stand, which occurs when the rate of sea level rise decreases, allowing the establishment of reef facies and shelf edge deposits that prograde seaward. Finally, the siliciclastic contributions observed at the top of the limestones suggest a lowstand event that, in some, cases led to the burial of the carbonates and in others to subaerial exposure.

To the southwest, in the eastern flank of the Western Cordillera, and during the Oligocene, the carbonate factory of the Vije Formation consists of heterozoan biotic associations. The presence of LBF, bivalves, echinoderms, gastropods, bryozoans, calcareous red algae, and oncolites suggests a deposition under dimmed (oligophotic/aphotic) and highly mesotrophic marine conditions. The fining–upward stacking patterns of the studied carbonates along with the presence of interbedded massive sandstones suggest a deposition along rimmed carbonate banks developed along the shelves of the Western Cordillera of the Colombia volcano–sedimentary basement (Figure 18).

The lowermost part of the Siamana Formation, deposited during the late Oligocene, displays facies associations typical of mixed siliciclastic/carbonate shelves. The mixed heterozoan–photozoan carbonate factory consists of bivalves, gastropods, echinoderms, corals, and LBF. The mixed carbonate factory occurs as isolated carbonate banks (i.e., patchy coral reefs) deposited on top of basement heights, which laterally change towards siliciclastic fan deltas (Figure 18). The decrease in siliciclastic material with section height along with the decrease

in the occurrence of heterozoan biotic associations marks a shift in depositional style from a mixed siliciclastic–carbonate shelf into a predominant carbonate shelf, in which unrimmed carbonate banks are detached from the siliciclastic continental shelf (Figure 18). The middle part of the Siamana Formation, deposited during the early Miocene, mostly displays tabular aggradational packages of floatstones, rudstones, framestones, packstones, and grainstones. The dominance of coral fragments, benthic foraminifera, and red algae, along with the decrease in siliciclastic material, also suggest deposition along a detached/unrimmed carbonate bank dominated by coral reefs (Figure 18). The absence of siliciclastic material and predominance of massive corals in the hundreds-of-meters-wide framestones, floatstones, and rudstones, suggest that the predominant photozoan carbonate factory developed under oligotrophic/euphotic marine conditions. The predominance of photozoan biotic associations over heterozoan biotic associations suggest that the deposition of carbonates from the middle part of the Siamana Formation occurred under low mesotrophic marine conditions.

The upper part of the Siamana Formation (early – middle Miocene) exhibits two main intervals of highly diverse coral-dominated tabular and aggradational framestones, rudstones, and floatstones. These characteristics suggest important changes in the carbonate factory from mixed photozoan–heterozoan-dominated to mostly photozoan-dominated biotic assemblages (Figure 18). The presence of diverse coral reefs in the kilometer-wide framestone/rudstone/floatstone intervals suggests that deposition along fringing reef systems in isolated rimmed carbonate platforms developed along the continental shelf. The development of these coral reefs was favored by the absence of sediment supply from the continental shelf and occurrence of oligotrophic and euphotic marine conditions. The uppermost part of the Siamana Formation displays a series of tabular thick-bedded packstones and grainstones, as well as biostromes, which consist of red algae, rhodoliths, and benthic and planktic foraminifera. The change in the carbonate factory from a photozoan-dominated to a heterozoan-dominated biotic association suggests an important change in the environmental conditions from oligotrophic to mesotrophic conditions. This change was likely associated with an increase in the siliciclastic sediment supply to the continental shelf along the Cocinetas Sub-basin.

The Pleistocene carbonates of La Popa Formation display sedimentary facies that have been interpreted as fringing reefs (Reyes et al., 2009). The mixed carbonate factory is composed of photozoan and heterozoan biotic associations. These biotic associations, along with the presence of aggradational packages of framestones, grainstones, packstones, and wackestones interbedded with calcareous mudstones, suggest deposition along carbonate banks attached to the continental shelf (Figure 18). The presence of corals, brachiopods, bivalves, gastropods, and green algae suggest a wide range of photic conditions (from eu-

photic to aphotic), as well as deposition under oligotrophic and low mesotrophic marine conditions. Modern coral reefs in the area grow on carbonates from La Popa Formation (Díaz et al., 2000), and the variety of associated flora and fauna resemble the conditions of the ancient coral reef formations.

5. Processes Controlling Temporal Changes in the Colombian Eocene – Miocene Shallow Marine Carbonate Factories

The evolution of several Cenozoic sedimentary basins in northern South America has been influenced by the interaction of different tectonic blocks (i.e., the Central and South American Blocks and the Caribbean and Nazca Plates) (Cediel et al., 2003). An important tectonic event that influenced the evolution of the Cenozoic sedimentary basins in northern South America is the middle Eocene initial interaction between Central America and South America (Farris et al., 2011; Montes et al., 2012). This event, which caused the opening of several middle Eocene marginal basins, was followed by the onset of low-angle flat subduction of the Caribbean Plate under the South American Plate during the late Eocene – Oligocene interval (Mora et al., 2017). This tectonic reorganization resulted in fore-arc extension and enhanced subsidence, and siliciclastic sedimentation along several of the middle Eocene incipient marginal basins in northern South America. In the San Jacinto and Alta Guajira Basins, these conditions favored the coeval occurrence of late Eocene coarse-grained clastic and shallow marine carbonate sedimentation (Mora et al., 2017). The increase in sediment and nutrient supply from the emerged orogens into these basins, amplified by the Eocene hothouse conditions (Zachos et al., 2001, 2008), could be a mechanism to explain the predominance of heterozoan biotic associations over photozoan biotic associations as the main carbonate factory along the studied Colombian Cenozoic basins (i.e., Arroyo de Piedra Formation of the San Jacinto Basin and Macarao Formation of the Alta Guajira Basin; Figure 19). An alternative mechanism triggering the predominance of middle – late Eocene heterozoan carbonate factories could be the occurrence of local coastal upwelling currents, which cause local drops in sea surface temperatures while increasing the delivery of high nutrient loads to shallow waters (Figure 19). The occurrence of upwelling currents would have been enhanced by the early closure of the Panamá Isthmus, which also invigorated the west boundary current along the Caribbean (Schmidt, 2007).

During the middle Oligocene – early Miocene interval, several intramountain sedimentary basins experienced increased subsidence in the northern Andes (Montes et al., 2015; Mora et al., 2010; Silva-Tamayo et al., 2008). These basins acted as main catchment of sediments derived from the Eocene-uplifted

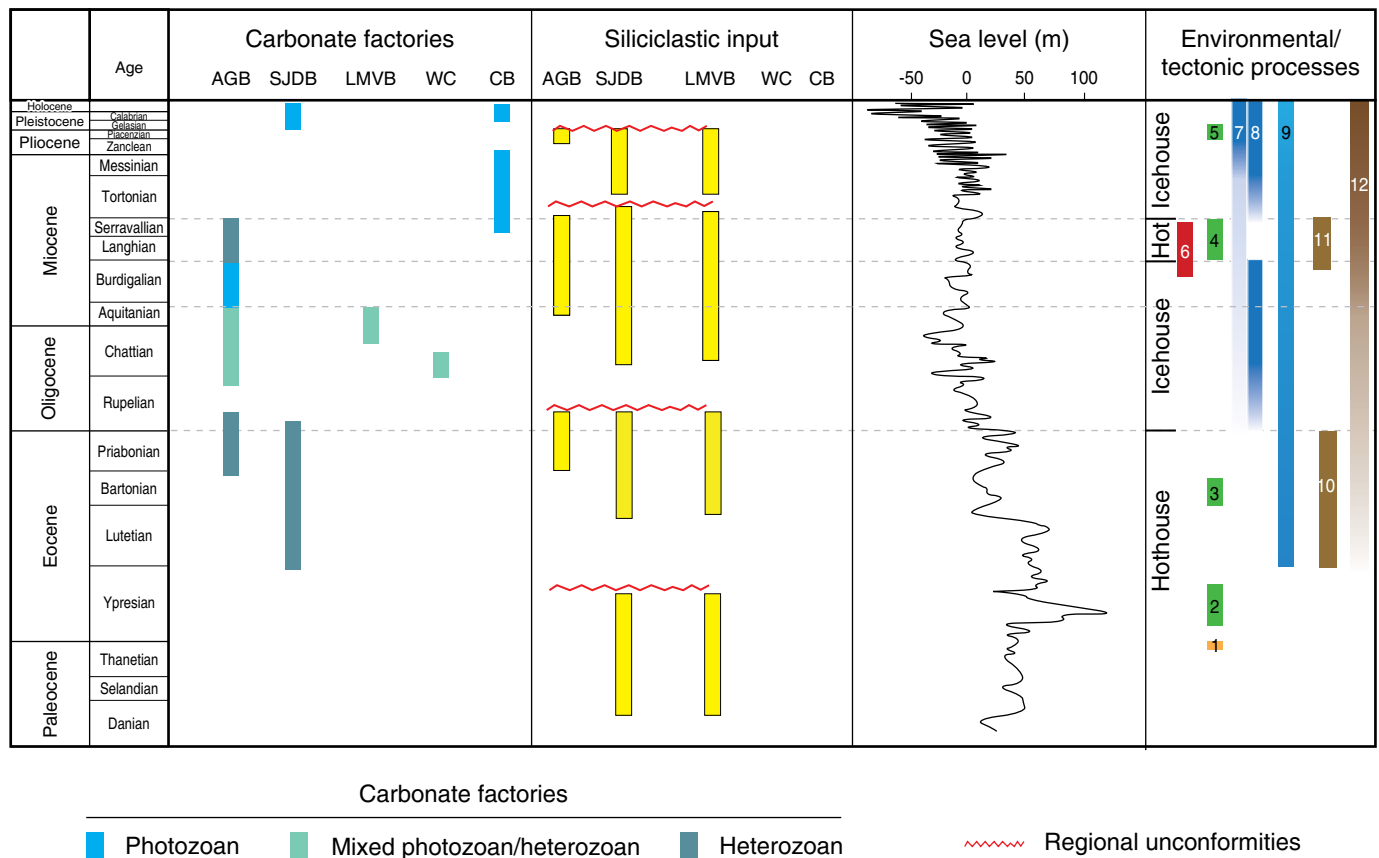


Figure 19. Evolution of the Cenozoic carbonate factories along the: (AGB) Alta Guajira Basin; (SJDB) San Jacinto deformed belt of the San Jacinto Basin; (LMVB) Lower Magdalena Valley Basin; (WC) Western Cordillera of Colombia; (CB) Los Cayos Basin. The occurrence of siliciclastic input into the different basins is subsequently constrained (Bermúdez et al., 2009; Dueñas et al., 2000; Moreno et al., 2015; Reyes–Harker et al., 2000; Silva–Tamayo et al., 2017; Vargas–Cuervo, 2004). Cenozoic sea level curve after Miller et al. (2005) and Zachos et al. (2001, 2008). The major Cenozoic environmental processes are as follows: (1) Paleocene – Eocene Thermal Maximum; (2) middle Eocene Climate Optimum; (3) late Eocene Climate Optimum; (4) middle Miocene Climate Optimum; (5) late Pliocene Climate Optimum; (6) Monterrey event; (7) Northern Hemisphere glacier formation; (8) Southern Hemisphere glacier formation; (9) strength of the west boundary current. The major tectonic events along northern South America are as follows: (10) Initial interaction between Central and South America; (11) final docking of Central America to South America; (12) Andean orogeny.

orogens (Montes et al., 2015; Mora et al., 2010), resulting in a decrease in the sediment supply to the continental shelves and, thus, in either a lack of deposition or reduced siliciclastic sedimentation in the marginal basins (Figure 19). The decreased sediment supply to the continental shelves, along with the decrease in global temperatures and sea level (Miller et al., 2005; Zachos et al., 2001, 2008), explains the occurrence of mixed photozoan–heterozoan biotic associations in the Alta Guajira (Siamana Formation), Lower Magdalena Valley (Ciénaga de Oro Formation), and Western Cordillera of Colombia (Vijes Formation) (Figure 19). These environmental conditions would have continued during the early Miocene, accounting for the development of highly diverse coral reefs in the Alta Guajira Basin and in general along the Circum–Caribbean (Budd, 2000).

Montes et al. (2015) proposed that final exhumation of the Panamá Isthmus occurred by the middle Miocene (Figure 18). The Langhian–Serravallian tectonic interaction between

Panamá and northern South America would have, conversely, enhanced the uplift of the Northern Andes (Mora et al., 2010; Restrepo–Moreno et al., 2009; Villagómez et al., 2011), resulting in a high sediment supply to both the Caribbean and the Pacific. The enhanced sediment supply to the Caribbean would have increased ocean water turbidity. The increase in nutrient availability along the Caribbean together with the combined action of the increased sediment supply from the emerged Andes and Panamá Isthmus would have further favored the proliferation of calcareous alga–rich carbonates during this time and the decrease in coral diversity (Figure 19), as calcareous algae are more resistant to turbidity and high influxes of nutrients than corals (Halfar & Mutti, 2005). The occurrence of widespread middle Miocene calcareous alga successions along the Caribbean and the concomitant disappearance of coral reef successions ultimately suggest that enhanced sediment influxes during the middle Miocene (Budd, 2000) would have been another causal

effect of the changes in the carbonate factories, due to deteriorating ocean water conditions.

The late Miocene – early Pliocene interval witnessed a decrease in the occurrence of marine carbonates along with an increase in coral biodiversity in the Circum-Caribbean (Johnson et al., 2008). The San Andrés Formation in Los Cayos Basin, however, displays high coral diversity. This could have been associated with the onset of free-living solitary and flabelo-meandroid corals (Klaus et al., 2011), and the appearance of *Acropora*-dominated coral reefs during the Miocene – Pliocene transition (McNeill et al., 1997), which marks an important change in coral adaptation to the adverse oceanographic conditions along the Circum-Caribbean modulated by rapid fluctuations in sea level (Renema et al., 2016). The onset of *Acropora*-dominated coral reefs during the early Pliocene would explain the successful occurrence of highly diverse coral reefs in La Popa and San Luis Formations during a period of deteriorated regional environmental conditions, i.e., enhanced sediment supply (Figure 19).

The prolonged period of reef coral species origination that took place between the late Miocene and early Pliocene (Budd & Johnson, 1999) was followed by sequential extinctions of shallow-water species throughout the Pliocene and deeper water corals in the middle Pleistocene (Getty et al., 2001; Maier et al., 2007). Currently, algae are the most abundant biotic component in nearly all coral reefs of Colombia, ranging from 30% in Rosario Islands to 53% in the San Andrés Archipelago (Rodríguez-Ramírez et al., 2010). Temporal analyses suggest a loss of coral covering *Acropora palmata*, as well as an increased algal cover, particularly in Rosario Islands (Rodríguez-Ramírez et al., 2010). In addition to modern natural disturbances, such as hurricanes, bleaching events, and epidemic diseases, which can also be the indirect result of human activities, factors directly linked to anthropogenic disturbances (high sea surface temperatures, sedimentation, and turbidity) have been defined as the main causes of this environmental change (Restrepo & Alvarado, 2001). Similar to other Caribbean localities, it is highly likely that most near-shore coral reef environments are doomed to further decline under the increasing human population and predicted future climate change scenarios, which may result in prolonged sea surface warming, massive coral bleaching, and extreme weather events accompanied by increased runoff impacts to the coastal areas (Restrepo et al., 2016).

6. Conclusions

Detailed stratigraphy and Sr-isotope dating of several shallow marine carbonate successions from different Colombian basins allowed the linking of major variation in the SE Circum-Caribbean Cenozoic carbonate factories to major regional environmental changes. Predominantly heterozoan biotic associations constituted the main carbonate factory along the San Jacinto and

Alta Guajira Basins during the middle – late Eocene and middle Miocene intervals. The occurrence of calcareous alga-dominated factories resulted from increased marine upwelling and enhanced sediment delivery to the SE Circum-Caribbean as the Panamá Isthmus emerged above sea level and the Northern Andes experienced enhanced uplift. Photozoan biotic associations, dominated by corals, constituted the main shallow carbonate factory during the middle Oligocene – early Miocene interval. The occurrence of these carbonate factories was restricted to the Alta Guajira Basin, Lower Magdalena Valley Basin, and Western Cordillera of Colombia. The occurrence of coral reef-dominated factories during the middle Oligocene – early Miocene interval paralleled the onset of the Antarctic glaciations and a decrease in sediment supply to the Caribbean Basin. The continental margin of northern South America registered a lack of marine carbonate deposition during the late Miocene – late Pliocene interval, which was related to the increase in siliciclastic sedimentation into the SE Circum-Caribbean. This decrease in occurrence of carbonate successions was interrupted by a single episode of carbonate sedimentation (La Popa Formation) along the San Jacinto Basin during the Pleistocene. This episode of carbonate deposition was related to the onset of *Acropora*-dominated coral reefs along the Caribbean, which successfully flourished during a period of rapid fluctuations in sea level. The adverse local environmental conditions that affected the late Miocene – Pleistocene carbonate sedimentation along the continental margin did not affect Los Cayos Basin, where highly diverse coral-dominated carbonate successions occur.

Acknowledgments

This work was supported by the financial aid of the Empresa Colombiana de Petróleo and the research office from the Universidad de Caldas, Manizales, Colombia (Grants VIP0025311 and VIP0027411 to Juan Carlos SILVA-TAMAYO and Andrés PARDO-TRUJILLO). The work favored access to slims-hole cores from the Agencia Nacional de Hidrocarburos. Juan Carlos SILVA-TAMAYO is thankful to the Smithsonian Tropical Research Institute for providing financial support through a post-doctoral scholarship sponsored by the Empresa Colombiana de Petróleo. Juan Carlos SILVA-TAMAYO is also thankful with Testlab Laboratorio Analisis Alimentos y Aguas S.A.S. for providing additional funding. The authors are thankful to James S. KLAUS and an anonymous reviewer for their comments, which greatly improved the quality of the manuscript.

References

- Alfonso, M., Herrera, J.M., Navarrete, R.E., Bermúdez, H.D., Calderón, J.E., Parra, F.E., Sarmiento, G., Vega, F. & Perrilliat, M. 2009. Cartografía geológica, levantamiento de columnas estratigráficas, toma de muestras y análisis bioestratigráficos.

- Sector de Chalán, Cuenca Sinú–San Jacinto. ANH–ATG, unpublished report, 120 p. Bogotá.
- Barrera, R. 2001. Memoria explicativa: Geología de las planchas 16 Galerazamba y 17 Barranquilla. Scale 1:100 000. Ingeominas, 54 p. Bogotá.
- Barrios, L.M. 2000. Evaluación de las principales condiciones de deterioro de los corales pétreos en el Caribe colombiano. Master thesis, Universidad Nacional de Colombia. 144 p. Santa Marta, Colombia.
- Barrios, L.M. 2007. Taxonomy and general ecology of marine invertebrates from Las Perlas Archipelago, Panamanian tropical eastern Pacific. Doctoral thesis, Heriot–Watt University, 218 p. Edinburgh, UK.
- Bermúdez, H.D., Grajales, J.A., Restrepo, L.C. & Rosero, J.S. 2009. Estudio Integrado de los núcleos y registros obtenidos de los pozos someros tipo “slim holes” en la Cuenca Sinú. Informe final, Tomo 1. ANH–Universidad de Caldas, 73 p. Bogotá.
- Budd, A.F. 2000. Diversity and extinction in the Cenozoic history of Caribbean reefs. *Coral Reefs*, 19(1): 25–35. <https://doi.org/10.1007/s003380050222>
- Budd, A.F. & Johnson, K.G. 1999. Origination preceding extinction during late Cenozoic turnover of Caribbean reefs. *Paleobiology* 25, 188–200. <https://doi.org/10.1017/S009483730002649X>
- Bueno, R. 1970. Eleventh Field Conference: The geology of the Tubará region, Lower Magdalena Basin. In: Colombian Society of Petroleum Geologists and Geophysicists, Geological Field Trips Colombia 1959–1978. Ediciones Geotec Ltda, p. 299–324. Bogotá.
- Bürgl, H. 1959. Resumen de la estratigrafía de Colombia. Servicio Geológico Nacional, Internal report 1248, 18 p. Bogotá.
- Cediel, F., Shaw, R.P. & Cáceres, C. 2003. Tectonic assembly of the northern Andean Block. In: Bartolini, C., Buffler, R.T. & Blickwede, J. (editors), The circum–Gulf of Mexico and the Caribbean: Hydrocarbon habitats, basin formation, and plate tectonics. American Association of Petroleum Geologists, Memoir 79, p. 815–848. Tulsa, USA.
- Crales, M.M., Yeung, C., Amaya, F., López, A., Jones, D.L. & Richards, W.J. 2002. Larval supply of fishes, shrimps, and crabs into the nursery ground of the Ciénaga Grande de Santa Marta, Colombian Caribbean. *Caribbean Journal of Science*, 38(1–2): 52–65.
- Díaz, J.M., Barrios, L.M., Cendales, M.H., Garzón–Ferreira, J., Geister, J., López–Victoria, M., Ospina, G.H., Parra–Velandia, F., Pinzón, J., Vargas–Ángel, B., Zapata, F.A. & Zea, S. 2000. Áreas coralinas de Colombia. Invemar, Publicaciones Especiales (5), 176 p. Santa Marta, Colombia.
- Díaz, J.M., Barrios, L.M. & Gomez, D.I., editors. 2003. Las praderas de pastos marinos en Colombia: Estructura y distribución de un ecosistema estratégico. Invemar, Publicaciones Especiales (10), 163 p. Santa Marta, Colombia.
- Ducea, M. & Saleeby, J. 1998. A case for delamination of the deep batholithic crust beneath the Sierra Nevada, California. *International Geology Review*, 40(1): 78–93. <https://doi.org/10.1080/00206819809465199>
- Dueñas, H. 1977. Estudio palinológico del pozo Q–E–22 Oligoceno Superior a Mioceno Inferior, Planeta Rica, Norte de Colombia. *Boletín Geológico*, 22(3): 96–115.
- Dueñas, H. 1986. Geología y palinología de la Formación Ciénaga de Oro, región Caribe colombiana. Publicaciones Geológicas Especiales del Ingeominas (18): p. 1–64. Bogotá.
- Dueñas, H., Navarrete, R.E., Mojica, J., Pardo, M. & Camargo, R. 2000. Edad de la Formación Vije en el pozo V3A, Oligoceno del piedemonte oriental de la cordillera Occidental, departamento del Valle del Cauca, Colombia. *Geología Colombiana*, (25): 25–43.
- Dunham, R.J. 1962. Classification of carbonate rocks according to depositional texture. In: Ham, W.E. (editor), Classification of carbonate rocks, American Association of Petroleum Geologists, Memoir 1, p. 108–121. Tulsa, USA.
- Duque–Caro, H. 1968. Observaciones generales a la bioestratigrafía y geología regional en los departamentos de Bolívar y Córdoba. *Boletín de Geología* (24): 71–87.
- Duque–Caro, H. 1975. Los foraminíferos planctónicos y el terciario de Colombia. *Revista Española de Micropaleontología*, 7(3): 403–427
- Embry, A.F. & Klovan, E.J. 1971. A late Devonian reef tract of north-eastern Banks Island, N.W.T. *Bulletin of the Canadian Petroleum Geology*, 19(4): 730–781.
- Farris, D.W., Jaramillo, C., Bayona, G., Restrepo–Moreno, S.A., Montes, C., Cardona, A. & Mora, A., Speakman, R.J., Glascock, M.D. & Valencia, V. 2011. Fracturing of the Panamanian Isthmus during initial collision with South America. *Geology*, 39(11): 1007–1010. <https://doi.org/10.1130/G32237.1>
- Frost, S.H. 1977. Cenozoic reef systems of the Caribbean: Prospects for paleoecologic synthesis. In: Frost, S.H., Weiss, M.P. & Saunders, J.B. (editors), Reefs and related carbonates: Ecology and sedimentology. American Association of Petroleum Geologists, 4: p. 93–110. Tulsa, USA. <https://doi.org/10.1306/St4393C8>
- Garzón–Ferreira, J., Gil–Agudelo, D.L., Barrios, L.M. & Zea, S. 2001. Stony coral diseases observed in southwestern Caribbean reefs. *Hydrobiologia*, 460(1–3): 65–69.
- Geister, J. 1973. Los arrecifes de la isla de San Andrés. *Mitteilungen aus dem Instituto Colombo–Aleman de Investigaciones Científicas*, 7: p. 211–228. Santa Marta, Colombia.
- Geister, J. 1975. Riffbau und geologische entwicklungsgeschichte der insel San Andrés, westliches Karibisches Meer, Kolumbien. *Stuttgarter Beiträge zur Naturkunde, Geologie und Paläontologie*, (15): p. 1–203. Stuttgart, Germany.
- Geister, J. 1992. Modern reef development and Cenozoic evolution of an oceanic island/reef complex: Isla de Providencia, western Caribbean Sea, Colombia. *Facies*, 27(1): 1–70.
- Getty, S.R., Asmerom, Y., Quinn, T.M. & Budd, A.F. 2001. Accelerated Pleistocene coral extinctions in the Caribbean Basin shown by uranium–lead (U–Pb) dating. *Geology*, 29(7):

- 639–642. [https://doi.org/10.1130/0091-7613\(2001\)029<0639:APCEIT>2.0.CO;2](https://doi.org/10.1130/0091-7613(2001)029<0639:APCEIT>2.0.CO;2)
- Guzmán, G. 2007. Stratigraphy and sedimentary environment and implications in the Plato Basin and the San Jacinto belt north-western Colombia. Doctoral thesis, Université de Liège, 275 p. Liège, Belgium.
- Guzmán, G., Gómez, E. & Serrano, B.E. 2004. Geología de los cinturones del Sinú, San Jacinto y borde Occidental del Valle Inferior del Magdalena, Caribe Colombiano. Scale 1:300 000. Ingeominas, internal report, 134 p. Bogotá.
- Halfar, J. & Mutti, M. 2005. Global dominance of coralline red–algal facies: A response to Miocene oceanographic events. *Geology* 33(6): 481–484. <https://doi.org/10.1130/G21462.1>
- Hubach, E. 1956. Aspectos geográficos y geológicos y recursos de las islas de San Andrés y Providencia. Cuadernos de Geografía de Colombia, (12): p. 1–37.
- Instituto de Hidrología, Meteorología y Estudios Ambientales (IDEAM). 2017. Mapa de ecosistemas continentales, costeros y marinos de Colombia, versión 2.1. Scale 1:1 200 000. Bogotá. http://www.ideam.gov.co/documents/11769/222663/E_EC-CMC_Ver21_100K.pdf/addc175f-3ac6-415b-9b9e-a1c4368b-5b3e (consulted in December 2017).
- Jacobsen, S.B. & Kaufman, A.J. 1999. The Sr, C and O isotopic evolution of Neoproterozoic seawater. *Chemical Geology*, 161(1–3): 37–57. [https://doi.org/10.1016/S0009-2541\(99\)00080-7](https://doi.org/10.1016/S0009-2541(99)00080-7)
- James, N.P. & Jones, B. 2016. Origin of carbonate sedimentary rocks. John Wiley & Sons, 464 p. Chichester, UK.
- Johnson, K.G., Jackson, J.B. & Budd, A.F. 2008. Caribbean reef development was independent of coral diversity over 28 million years. *Science*, 319(5869): 1521–1523. <https://doi.org/10.1126/science.1152197>
- Johnson, K.G., Sánchez–Villagra, M.R. & Aguilera, O.A. 2009. The Oligocene – Miocene transition on coral reefs in the Falcón Basin, NW Venezuela. *Palaos*, 24(1–2): 59–69.
- Kassem, T., Cáceres, C. & Cucalón, I. 1967. Memoria explicativa: Geología del Cuadrángulo E–8 Sincelejo. Servicio Geológico Nacional, unpublished report, 150 p. Bogotá.
- Klaus, J.S., Lutz, B.P., McNeill, D.F., Budd, A.F., Johnson, K.G. & Ishman, S.E. 2011. Rise and fall of Pliocene free–living corals in the Caribbean. *Geology*, 39(4): 375–378. <https://doi.org/10.1130/G31704.1>
- Lockwood, J.G. 1974. World climatology: An environmental approach. St. Marti's Press, 330 p. London, UK.
- Maier, K.L., Klaus, J.S., McNeill, D.F. & Budd, A.F. 2007. A late Miocene low–nutrient window for Caribbean reef formation? *Coral reefs*, 26(3): 635–639. <https://doi.org/10.1007/s00338-007-0254-6>
- McArthur, J.M. & Howarth, R.J. 2004. Sr–isotope stratigraphy: The Phanerozoic $^{87}\text{Sr}/^{86}\text{Sr}$ –curve and explanatory notes. In: Gradstein, F., Ogg, J. & Smith, A.G. (editors), *A Geological Time Scale 2004*. Cambridge University Press, p. 96–105. Cambridge, UK. <https://doi.org/10.1017/CBO9780511536045.008>
- McArthur, J.M., Howarth, R.J. & Shields–Zhou, G.A. 2012. Strontium isotope stratigraphy. In: Gradstein, F., Ogg, J., Schmitz, M. & Ogg, G. (editors), *The Geologic Time Scale 2012*. Elsevier, p. 127–144. Oxford, UK. <https://doi.org/10.1016/B978-0-444-59425-9.00007-X>
- McNeill, D.F., Budd, A.F. & Borne, P.F. 1997. Earlier (late Pliocene) first appearance of the Caribbean reef–building coral *Acropora palmata*: Stratigraphic and evolutionary implications. *Geology*, 25(10): 891–894. [https://doi.org/10.1130/0091-7613\(1997\)025<0891:ELPFAO>2.3.CO;2](https://doi.org/10.1130/0091-7613(1997)025<0891:ELPFAO>2.3.CO;2)
- Miller, K.G., Kominz, M.A., Browning, J.V., Wright, J.D., Mountain, G.S., Katz, M.E., Sugarman, P.J., Cramer, B.S., Christie–Blick, N. & Pekar, S.F. 2005. The Phanerozoic record of global sea–level change. *Science*, 310(5752): 1293–1298. <https://doi.org/10.1126/science.1116412>
- Montes, C., Cardona, A., McFadden, R., Morón, S.E., Silva, C.A., Restrepo–Moreno, S., Ramírez, D.A., Hoyos, N., Wilson, J., Farris, D., Bayona, G.A., Jaramillo, C.A., Valencia, V., Bryan, J. & Flores, J.A. 2012. Evidence for middle Eocene and younger emergence in central Panamá: Implications for isthmus closure. *Geological Society of America Bulletin*, 124(5–6): 780–799. <https://doi.org/10.1130/B30528.1>
- Montes, C., Cardona, A., Jaramillo, C., Pardo, A., Silva, J.C., Valencia, V., Ayala, C., Pérez–Ángel, L.C., Rodríguez–Parra, L.A., Ramírez, V. & Niño, H. 2015. Middle Miocene closure of the Central American Seaway. *Science*, 348(6231): 226–229. <https://doi.org/10.1126/science.aaa2815>
- Mora, A., Horton, B.K., Mesa, A., Rubiano, J., Ketcham, R.A., Parra, M., Blanco, V., García, D. & Stockli, D.F. 2010. Migration of Cenozoic deformation in the Eastern Cordillera of Colombia interpreted from fission track results and structural relationships: Implications for petroleum systems. *American Association of Petroleum Geologists Bulletin*, 94(10): 1543–1580. <https://doi.org/10.1306/01051009111>
- Mora, J.A., Oncken, O., Le Breton, E., Ibañez–Mejía, M., Faccenna, C., Veloza, G., Vélez, V., de Freitas, M. & Mesa, A. 2017. Linking Late Cretaceous to Eocene tectonostratigraphy of the San Jacinto fold belt of NW Colombia with Caribbean Plateau collision and flat subduction. *Tectonics* 36(11): 2599–2629. <https://doi.org/10.1002/2017TC004612>
- Moreno, J.F., Hendy, A.J.W., Quiroz, L., Hoyos, N., Jones, D.S., Zapata, V., Zapata, S., Ballen, G.A., Cadena, E., Cárdenas, A.L., Carrillo–Briceño, J.D., Carrillo, J.D., Delgado–Sierra, D., Escobar, J., Martínez, J.I., Martínez, C., Montes, C., Moreno, J., Pérez, N., Sánchez, R., Suárez, C., Vallejo–Pareja, M.C. & Jaramillo, C. 2015. Revised stratigraphy of Neogene strata in the Cocinetas Basin, La Guajira, Colombia. *Swiss Journal of Palaeontology*, 134(1): 5–43. <https://doi.org/10.1007/s13358-015-0071-4>
- Mutti, M., Droxler, A.W. & Cunningham, A.D. 2005. Evolution of the northern Nicaragua Rise during the Oligocene – Miocene: Drowning by environmental factors. *Sedimentary*

- Geology 175(1–4): 237–258. <https://doi.org/10.1016/j.sed-geo.2004.12.028>
- Nivia, Á. 2001. Memoria explicativa: Mapa geológico departamento del Valle del Cauca. Scale 1:250 000. Ingeominas, 148 p. Bogotá.
- Ortiz, A. & Niño, H. 1999. Estudio sedimentológico y estratigráfico de las calizas de Cicuco y Boquete en un sector de la isla de Mompós, Valle Inferior del Magdalena. Ecopetrol & Instituto Colombiano del Petróleo, unpublished report, 32 p. Bogotá.
- Ortiz, A., Blanco, A. & Corredor, G. 1998. Calidad de reservorio de las calizas de las formaciones Toluviejo y Ciénaga de Oro, Subcuenca Sinú–San Jacinto, Cuenca Caribe Colombiana. Instituto Colombiano del Petróleo & Ecopetrol, unpublished report, 88 p. Bogotá.
- Renema, W., Pandolfi, J.M., Kiessling, W., Bosellini, F.R., Klaus, J.S., Korpany, C., Rosen, B.R., Santodomingo, N., Wallace, C.C., Webster, J.M. & Johnson, K.G. 2016. Are coral reefs victims of their own past success? *Science Advances*, 2(4), e1500850. <https://doi.org/10.1126/sciadv.1500850>
- Renz, O. 1960. Geología de la parte sureste de la península de La Guajira (República de Colombia). III Congreso Geológico Venezolano. *Memoirs*, III, p. 317–346.
- Restrepo, J.D. & Alvarado, E.M. 2011. Assessing major environmental issues in the Caribbean and Pacific coast of Colombia, South America: An overview of fluvial fluxes, coral reef degradation, and mangrove ecosystems impacted by river diversion. In: Wolanski, E., & McLusky, D.S. (editors), *Treatise on estuarine and coastal Science*. Academic Press, p. 289–314. Waltham, USA. <https://doi.org/10.1016/B978-0-12-374711-2.01117-7>
- Restrepo, J.D., Park, E., Aquino, S. & Latrubesse, E.M. 2016. Coral reefs chronically exposed to river sediment plumes in the southwestern Caribbean: Rosario Islands, Colombia. *Science of the Total Environment* 553: 316–329. <https://doi.org/10.1016/j.scitotenv.2016.02.140>
- Restrepo–Moreno, S.A., Foster, D.A., Stockli, D.F. & Parra–Sánchez, L.N. 2009. Long–term erosion and exhumation of the “Altiplano Antioqueño”, northern Andes (Colombia) from apatite (U–Th)/He thermochronology. *Earth and Planetary Science Letters*, 278(1–2): 1–12. <https://doi.org/10.1016/j.epsl.2008.09.037>
- Reyes–Harker, A., Montenegro–Buitrago, G. & Gomez, P.D. 2000. Evolucion Tectonoestratigráfica del Valle Inferior del Magdalena, Colombia. VII Simposio Bolivariano de Exploración Petrolera en las Cuencas Subandinas. *Memoirs*, p. 293–309. Caracas, Venezuela.
- Reyes, L., Ortiz, A. & Guzmán, G. 2009. Facial Changes and stratigraphy in the Popa Formation: An example from northern Cartagena, Colombia. X Simposio Bolivariano de Exploración Petrolera en las Cuencas Subandinas. Abstract. Cartagena, Colombia.
- Rodríguez–Ramírez, A., Reyes–Nivia, M.C., Zea, S., Navas–Camacho, R., Garzón–Ferreira, J., Bejarano, S., Herrón, P. & Orozco, C. 2010. Recent dynamics and condition of coral reefs in the Colombian Caribbean. *Revista de Biología Tropical*, 58(suplemento 1): 107–131. <https://doi.org/10.15517/RBT.V58I1.20027>
- Rollins, J.F. 1960. Stratigraphy and structure of the Goajira Peninsula, northwestern Venezuela and northeastern Colombia. Doctoral thesis, University of Nebraska, 151 p. Lincoln, USA.
- Rosero, S., Silva, J.C., Sial, A.N., Borrero, C., & Pardo, A. 2014. Quimioestratigrafía de isótopos de estroncio de algunas sucesiones del Eoceno – Mioceno del cinturón de San Jacinto y el Valle Inferior del Magdalena. *Boletín de Geología* 36(1): p. 15–27.
- Salazar–Franco, A.M., Silva–Tamayo, J.C., Bayona, G., Méndez–Duque, J. & Lara, M. 2016. Chemostratigraphy of upper Eocene – lower Oligocene carbonate successions in the Southern Caribbean Margin (San Jacinto deformed belt of Colombia). XII Simposio de Exploración Petrolera en Cuencas Subandinas. Abstract, p. 55–56. Bogotá.
- Schmidt, D.N. 2007. The closure history of the Central American seaway: Evidence from isotopes and fossils to models and molecules. In: Williams, M., Haywood, A.M., Gregory, F.J. & Schmidt, D.N. (editors), *Deep–time perspectives on climate change: Marrying the signal from computer models and biological proxies*. The Geological Society of London, p. 427–442. <https://doi.org/10.1144/TMS002.19>
- Silva–Tamayo, J.C., Sierra, G.M. & Correa, L.G. 2008. Tectonic and climate driven fluctuations in the stratigraphic base level of a Cenozoic continental coal basin, northwestern Andes. *Journal of South American Earth Sciences*, 26(4): 369–382. <https://doi.org/10.1016/j.jsames.2008.02.001>
- Silva–Tamayo, J.C., Lara, M.E., Nana–Yobo, L., Erdal, Y.D. Sanchez, J. & Zapata–Ramírez, P.A. 2017. Tectonic and environmental factors controlling on the evolution of Oligo – Miocene shallow marine carbonate factories along a tropical SE Circum–Caribbean. *Journal of South American Earth Sciences*, 78: 213–237. <https://doi.org/10.1016/j.jsames.2017.06.008>
- Spooner, E.T.C. 1976. The strontium isotopic composition of seawater, and seawater–oceanic crust interaction. *Earth and Planetary Science Letters*, 31(1), 167–174. [https://doi.org/10.1016/0012-821X\(76\)90108-4](https://doi.org/10.1016/0012-821X(76)90108-4)
- Swolf, H. 1946. El Difícil Limestone. Ecopetrol, Internal report 007, 90 p. Bogotá.
- Thomas, D.J. 1972. The tertiary geology and systematic paleontology (Phylum Mollusca) of the Guajira Peninsula, Colombia, South America. Doctoral thesis. State University of New York at Binghamton, 147 p. New York, USA.
- Torres–Lasso, J.C. 2014. Estratigrafía, quimioestratigrafía y petrografía de la Formación Vije, Valle Del Cauca: Implicaciones para la datación y caracterización de potenciales reservorios carbonáticos en el occidente y Caribe colombiano. Bachelor thesis, Universidad de Caldas, 66 p. Manizales, Colombia.
- Tucker, M.E. & Wright, V.P. 1990. *Carbonate Sedimentology*. Blackwell Scientific Publications, 482 p. London, UK. <https://doi.org/10.1002/9781444314175>
- Tucker, M.E. & Wright, V.P. 2009. *Carbonate sedimentology*. John Wiley & Sons, 468 p. Chichester, UK.

- Vargas–Cuervo, G. 2004. Geología y aspectos geográficos de la isla de San Andrés, Colombia. *Geología Colombiana*, (29): 73–89.
- Villagómez, D., Spikings, R., Magna, T., Kammer, A., Winkler, W. & Beltrán, A. 2011. Geochronology, geochemistry and tectonic evolution of the Western and Central Cordilleras of Colombia. *Lithos*, 125(3–4): 875–896. <https://doi.org/10.1016/j.lithos.2011.05.003>
- Wickman, F.E. 1948. Isotope ratios: A clue to the age of certain marine sediments. *The Journal of Geology*, 56(1): 61–66. <https://doi.org/10.1086/625478>
- Wilson, M.E.J. 2002. Cenozoic carbonates in southeast Asia: Implications for equatorial carbonate development. *Sedimentary Geology* 147(3–4): 295–428. [https://doi.org/10.1016/S0037-0738\(01\)00228-7](https://doi.org/10.1016/S0037-0738(01)00228-7)
- Wilson, M.E.J. 2008. Global and regional influences on equatorial shallow–marine carbonates during the Cenozoic. *Palaeogeography, Palaeoclimatology, Palaeoecology*, 265 (3–4): 262–274. <https://doi.org/10.1016/j.palaeo.2008.05.012>
- Wilson, M.E.J. 2012. Equatorial carbonates: An earth systems approach. *Sedimentology*, 59(1): 1–31. <https://doi.org/10.1111/j.1365-3091.2011.01293.x>
- Wilson, M.E.J. 2015. Oligo – Miocene variability in carbonate producers and platforms of the Coral Triangle biodiversity hotspot: Habitat mosaics and marine biodiversity. *Palaaios* 30(1): 150–168. <https://doi.org/10.2110/palo.2013.135>
- Zachos, J.C., Pagani, M., Sloan, L., Thomas, E. & Billups, K. 2001. Trends, rhythms, and aberrations in global climate 65 Ma to present. *Science*, 292(5517): 686–693. <https://doi.org/10.1126/science.1059412>
- Zachos, J.C., Dickens, G.R. & Zeebe, R.E. 2008. An early Cenozoic perspective on greenhouse warming and carbon–cycle dynamics. *Nature* 451(7176): 279–283. <https://doi.org/10.1038/nature06588>
- Zuluaga, C.A., Ochoa–Yarza, A., Muñoz, C.A., Guerrero, N.M., Martínez, A.M., Medina, P.A., Pinilla, A., Ríos, P.A., Rodríguez, B.P., Salazar, E.A. & Zapata, V.L. 2009. Memoria de las planchas 2, 3, 5 y 6 (con parte de las planchas 4, 10 y 10Bis). Proyecto de investigación: Cartografía e historia geológica de la Alta Guajira. Ingeominas, internal report, 504 p. Bogotá.

Explanation of Acronyms, Abbreviations, and Symbols:

Ecopetrol Empresa Colombiana de Petróleos S.A.
LBF Larger benthic foraminifera

NIST National Institute of Standards and Technology
SJDB San Jacinto deformed belt

Authors' Biographical Notes



Juan Carlos SILVA-TAMAYO is CEO at Testlab Geambiental–Testlab Laboratorio Análisis Alimentos y Aguas S.A.S. He holds a BS in geology from the EAFIT University Medellín, Colombia, a Master of Science in environmental and sedimentary sciences from the Universidade Federal de Pernambuco, Recife, Brasil, and a PhD in geochemistry from the Universitat Bern, Bern, Switzerland.

He was also a Marie Curie Postdoctoral Fellow at the Department of Earth and Environment at Stanford University, USA, and the Department of Earth and Environment at the University of Leeds, UK. His research primarily focuses on sedimentary geology, stratigraphy, and low–temperature isotope geochemistry.



Daniel RINCÓN-MARTÍNEZ, PhD, is a researcher at the Instituto Colombiano del Petróleo of Ecopetrol S.A., Piedecuesta, Colombia. His primary field of research is micropaleontology, particularly benthonic and planktonic foraminifera and its application to paleoceanography, sequence stratigraphy, and paleoecology. His research projects encompass rocks formed in a wide

variety of depositional environments (marginal, shallow, and deep marine) and ages (Mesozoic to Neogene). In recent years, RINCÓN-MARTÍNEZ has focused attention on Paleogene shallow–marine carbonate systems and compared them to basinal pelagic records for regional analysis of southern Caribbean geology.



Lina M. BARRIOS is a marine biologist with PhD in marine ecology (two main thesis topics: connectivity and proxy indicators of climate change). Her main area of work is the population and community ecology (ecological genetics) of tropical marine organisms, including conservation biology and biodiversity. Most of her work involves international and multithematic groups

around the world (e.g., tropical eastern Pacific, Caribbean, North Sea, Mediterranean Sea, and China Sea). Since 2003, she has worked on comparative ecology (tropical vs. temperate environments) as a lecturer and researcher. Her research has taken her into fascinating questions regarding coral connectivity and gene expression under climate change—ocean acidification scenarios (<https://www.ecologicalgenetics.org/lina-barrios-gardelis>).



Juan C. TORRES-LASSO holds a master's degree in physical, chemical, and geological oceanography from the Federal University of Rio Grande in Brazil. The main research interests of TORRES-LASSO focus on physical and chemical oceanography as well as on the investigation of the evolution of reefal calcareous organisms through geological time, on the quantification of

the dependency of reef formation on climatic variations, and on the constraints of ocean physicochemical characteristics that affect calcareous organisms, making them adapt to these changes. Currently, he is working at the Instituto de Investigaciones Marinas y Costeras (Invemar) in Colombia.







Chixel OSORIO-ARANGO is a geologic engineer from the Universidad Nacional de Colombia. She has worked on several projects related to sedimentary geology and stratigraphy, and on the exploration of clay minerals that can be used as biocide agents. She currently works as an independent consultant.

Chapter 10



From Facies Analysis, Stratigraphic Surfaces, and Depositional Sequences to Stratigraphic Traps in the Eocene – Oligocene Record of the Southern Llanos Basin and Northern Magdalena Basin

<https://doi.org/10.32685/pub.esp.37.2019.10>
Published online 19 June 2020

Víctor M. CABALLERO^{1*} , Guillermo RODRÍGUEZ², Julián F. NARANJO³ ,
Andrés MORA⁴ , and Felipe DE LA PARRA⁵ 

Abstract Available outcrop sections, rock cores, and well logs, as well as previous sedimentary geology and palynology studies, provide the opportunity to study shallow marine and continental rock records within the context of unconformity-bounded depositional sequences. This approach provides insight into the sedimentary evolution of reservoirs and their properties in the Middle Magdalena Basin and the southern Llanos Basin in Colombia.

This work illustrates and analyzes facies and facies successions of the Eocene – Oligocene stratigraphic units in the Nuevo Mundo Syncline in the northern Middle Magdalena Basin and the southern Llanos Basin. The facies analysis results support the identification of subaerial unconformities, transgressive ravinement surfaces, flooding surfaces, depositional environments, and depositional sequences. Stratigraphic correlation allows the identification of spatial and temporal distributions of the facies, the stratigraphic architecture of reservoirs and potential of several types of plays in these basins, in addition to the common stratigraphic histories.

Thirteen facies were combined into ten facies successions, which led to the identification of three depositional sequences in the southern Llanos Basin and two in the Nuevo Mundo Syncline. A strongly developed paleosol and an unconformity at the base of the Eocene units allowed a buried, preserved landscape from the end of the Paleocene to be identified in the southern Llanos Basin, and the same relief features were identified in the Middle Magdalena Basin and Eastern Cordillera. The first depositional sequence comprises the Lower Mirador, Upper Mirador, and lower part of the C8 Member of the Carbonera Formation in the southern Llanos Basin and the La Paz and Esmeraldas Formations in the Nuevo Mundo Syncline. The second depositional sequence is composed of Oligocene basal sandstones and the upper part of the C8 Member of the Carbonera Formation in the southern Llanos Basin and the Oligocene Mugrosa Formation in the Middle Magdalena Basin. The third sequence is composed of both the C7 and C6 Members of the Carbonera Formation in the southern Llanos Basin.

- 1 victor.caballero@ecopetrol.com.co
Ecopetrol S.A.
Instituto Colombiano del Petróleo
Centro de Innovación y Tecnología
Km 7 vía Bucaramanga–Piedecuesta
Piedecuesta, Santander, Colombia
- 2 guillermo.rodriguez@ecopetrol.com.co
Ecopetrol S.A.
Instituto Colombiano del Petróleo
Centro de Innovación y Tecnología
Km 7 vía Bucaramanga–Piedecuesta
Piedecuesta, Santander, Colombia
- 3 julian.naranjo@ecopetrol.com.co
Ecopetrol S.A.
Instituto Colombiano del Petróleo
Centro de Innovación y Tecnología
Km 7 vía Bucaramanga–Piedecuesta
Piedecuesta, Santander, Colombia
- 4 andres.mora@ecopetrol.com.co
Ecopetrol S.A.
Vicepresidencia de Exploración
Bogotá, Colombia
- 5 felipe.delaparra@ecopetrol.com.co
Ecopetrol S.A.
Instituto Colombiano del Petróleo
Centro de Innovación y Tecnología
Km 7 vía Bucaramanga–Piedecuesta
Piedecuesta, Santander, Colombia

* Corresponding author

Citation: Caballero, V.M., Rodríguez, G., Naranjo, J.F., Mora, A. & De La Parra, F. 2020. From facies analysis, stratigraphic surfaces, and depositional sequences to stratigraphic traps in the Eocene – Oligocene record of the southern Llanos Basin and northern Magdalena Basin. In: Gómez, J. & Mateus-Zabala, D. (editors), The Geology of Colombia, Volume 3 Paleogene – Neogene. Servicio Geológico Colombiano, Publicaciones Geológicas Especiales 37, p. 283–330. Bogotá. <https://doi.org/10.32685/pub.esp.37.2019.10>

The porosities and permeabilities allowed the identification of the favorable reservoir units in these basins and the geometries and lithologies below and above the buried landscape explain several types of traps/plays that must be searched for in these basins, including paleogeomorphic traps, such as buried hills, fluvial and incised valleys, and erosional pinchouts, and previously identified stratigraphic traps, such as depositional pinchouts, onlap pinchouts, and facies changes.

Keywords: *origin and depositional history of sedimentary basins, facies analysis, facies successions, sequence stratigraphy correlation, Llanos Basin, Middle Magdalena Basin, reservoir architecture, stratigraphic trap, reservoir properties.*

Resumen Las secciones de afloramiento, núcleos y registros de pozo disponibles, así como estudios previos de sedimentología y palinología, son una oportunidad para estudiar los registros sedimentarios marinos someros y continentales en el contexto de la estratigrafía de secuencias. En la Cuenca del Valle Medio del Magdalena y sur de la Cuenca de los Llanos, este enfoque proporciona información sobre la evolución de los reservorios y sus propiedades.

En este trabajo se ilustran y analizan las facies y sucesiones de facies en las unidades estratigráficas del Eoceno–Oligoceno en el Sinclinal de Nuevo Mundo localizado en la parte norte de la Cuenca del Valle Medio del Magdalena y en el sector sur de la Cuenca de los Llanos. El análisis de facies contribuye en la identificación de discordancias subaéreas, superficies de ravinamiento transgresivo, superficies de inundación, ambientes de depósito y secuencias de depósito. La correlación estratigráfica permite identificar la distribución temporal y espacial de facies, la arquitectura estratigráfica de los reservorios y el potencial de varios tipos de trampas en estas cuencas, además de las historias estratigráficas comunes.

Trece facies fueron combinadas en diez sucesiones de facies, lo que ayudó a identificar tres secuencias de depósito en el sur de la Cuenca de los Llanos y dos en el Sinclinal de Nuevo Mundo. Un paleosuelo fuertemente desarrollado y una discordancia en la base de las unidades del Eoceno permitieron identificar un paisaje enterrado y fosilizado desde el final del Paleoceno en el sur de la Cuenca de los Llanos, este mismo paisaje ya había sido identificado en la Cuenca del Valle Medio del Magdalena y en la cordillera Oriental. La primera secuencia de depósito incluye las formaciones Mirador Inferior y Mirador Superior y la parte baja del Miembro C8 de la Formación Carbonera en el sur de la Cuenca de los Llanos y las formaciones La Paz y Esmeraldas en el Sinclinal de Nuevo Mundo. La segunda secuencia de depósito está compuesta por las areniscas basales del Oligoceno y la parte superior del Miembro C8 de la Formación Carbonera en el sur de la Cuenca de los Llanos y la Formación Mugrosa del Oligoceno en la Cuenca del Valle Medio del Magdalena. La tercera secuencia está compuesta por los miembros C7 y C6 de la Formación Carbonera en el sur de la Cuenca de los Llanos.

Los valores de porosidad y permeabilidad permitieron identificar las mejores unidades reservorio en estas cuencas y las geometrías y litologías debajo y encima del paisaje fosilizado explican varios tipos de trampas que deberían buscarse en estas cuencas, incluyendo trampas paleogeomorfológicas, tales como colinas enterradas, valles fluviales y valles incisos y pinchamientos por erosión, y también trampas estratigráficas identificadas previamente, tales como pinchamientos por depósito, pinchamientos por *onlap* y cambios de facies.

Palabras clave: *origen e historia de depósito de cuencas sedimentarias, análisis de facies, sucesiones de facies, correlación de secuencias estratigráficas, Cuenca de los Llanos, Cuenca del Valle Medio del Magdalena, trampa estratigráfica, propiedades de reservorio.*

1. Introduction

The deposition of the sedimentary rocks in the Middle Magdalena Basin (MMB), Eastern Cordillera (EC), and Llanos Basin in Colombia has been controlled by tectonics, eustasy, and climate (Cooper et al., 1995; Gómez et al., 2005a; Mora et al., 2008, 2010, 2015; Bayona et al., 2008, 2012, 2013; Parra et al., 2010, 2012; Ramírez–Arias et al., 2012). Extensional tectonics and eustasy controlled the deposition of the Mesozoic rocks in rift basins across the entire Magdalena Basin, Eastern Cordillera, and Llanos Basin (LLB) (Etayo–Serna et al., 1969, 1983; Fabre 1985, 1987), whereas compressive tectonics and climate mainly controlled the uplift of the Central and Eastern Cordilleras during the Late Cretaceous – Cenozoic (Gómez et al., 2003, 2005a, 2005b; Mora et al., 2006, 2009, 2010, 2013; Bayona et al., 2008, 2013; Horton et al., 2010a, 2010b; Caballero et al., 2010; Saylor et al., 2011, 2012a; Nie et al., 2010, 2012; Moreno et al., 2011; Villagómez et al., 2011).

Late Cretaceous – Cenozoic flexural subsidence in front of uplifting terrains created the accommodation space for sediment to be deposited as it was generated in the new source areas. The sedimentary response (e.g., facies, facies successions, geometry, stacking pattern, distribution, depositional trends) can be linked to changes in base level controlled by tectonics, climate, sources of sediment, and sedimentary basin geomorphology.

The areas of the Middle Magdalena Basin, axial Eastern Cordillera Basin, and Llanos Basin were once part of a unique foreland basin that was coupled to the Central Cordillera during the early Paleocene (Gómez et al., 2003, 2005a, 2005b; Saylor et al., 2011; Horton, 2010b; Moreno et al., 2011; Nie et al., 2010, 2012). By the Late Paleocene – Oligocene, the foreland basin was increasingly fragmented due to the reactivation of faults in the former Mesozoic rift system (Dengo & Covey, 1993; Colletta et al., 1990; Cooper et al., 1995; Mora et al., 2006), and a bivergent fold–thrust belt developed (Cooper et al., 1995; Sarmiento–Rojas et al., 2006; Bayona et al., 2008, 2013; Tesón et al., 2013).

This process resulted in three main separate sedimentary systems as the fold–thrust belt deformation migrated to the east in the Eastern Cordillera (Mora et al., 2010; Saylor et al., 2011; Bayona et al., 2013): the intermontane Middle Magdalena Basin on the western flank of the Eastern Cordillera, the axial intermontane Eastern Cordillera (Floresta and synorogenic basins within the Eastern Cordillera), and the Llanos Basin near the eastern flank of the Eastern Cordillera. The current foreland basin system consists of a hinterland composed of the Magdalena Basin and the Eastern Cordillera and a foreland basin that corresponds to the Llanos Basin.

The synorogenic sedimentary deposits in the Magdalena Basin, axial Eastern Cordillera, and Llanos Basin contain the sedimentary record of orogenesis as well as the sedimentary and stratigraphic histories of the Magdalena Valley, Eastern

Cordillera, and Llanos Basin. This record has been previously analyzed, but no attempt to correlate the events, depositional trends, and common stratigraphic histories has been attempted. Analysis of the sedimentary record and stratigraphic correlations will enable us to identify the common or distinct stratigraphic histories during the latest Paleocene to Oligocene.

In this study we illustrate, with unpublished images, the facies and facies successions in the southern Llanos Basin (SLLB), which is subdivided into the foothills of the Eastern Cordillera, the western sector of the Llanos Basin (WSLLB), and the eastern sector of the Llanos Basin (ESLLB) (Figure 1). We build upon our previous work by complementing the descriptions and illustrations of the facies and facies successions in the Nuevo Mundo Syncline (NMS) with published studies in the Middle Magdalena Basin and the axial Eastern Cordillera sedimentary basin.

The facies analysis supports the identification and characterization of bounding surfaces and depositional sequences. These units were traced throughout the basins using the sequence stratigraphic surfaces to study the distribution, lateral continuity, and stratigraphic architecture of the reservoirs rocks as well as to compare their potential as stratigraphic plays.

1.1. Previous Work in the Middle Magdalena Basin

The along–strike lower Eocene rock record of the Middle Magdalena Basin is dominated by a sandy fluvial system with proximal facies to the south in the area of the Guaduas Syncline and distal facies to the NE in the region north of the basin near the NMS. In the southern part of the MMB, the early Eocene proximal facies of an alluvial to fluvial system is represented by the Middle–Upper Hoyón Formation. This unit consists of an alluvial matrix–supported conglomerate, reddish siltstones, and sandstone intervals with horizontal bedding, cross–bedding, and E–NE paleocurrent directions (Gómez et al., 2003; Bayona et al., 2013). The distal facies of the system to the north is represented by the La Paz Formation. The La Paz Formation is not continuous across strike in the MMB due to the presence of an intrabasin high, the La Cira–Infantas–Sogamoso Paleohigh (LCISP). The paleohigh is more than 130 km long by 25 km wide, is located in the center of the basin and extends N–NE from southern Puerto Parra to the area of the Sogamoso Field (Suárez, 1997; Gómez et al., 2005a; Caballero, 2010). This unit consists of amalgamated, cross–bedded sandstones and fluvial floodplain mudstones and rippled sandstones (Suárez, 1997; Gomez et al., 2005a). The fluvial valleys of this landscape were fed by competing sources in the Central Cordillera, uplifts inside the Middle Magdalena Basin and areas of the western flank of the Eastern Cordillera (Gomez et al., 2005a; Caballero et al., 2013b; Moreno et al., 2011; Lamus et al., 2013).

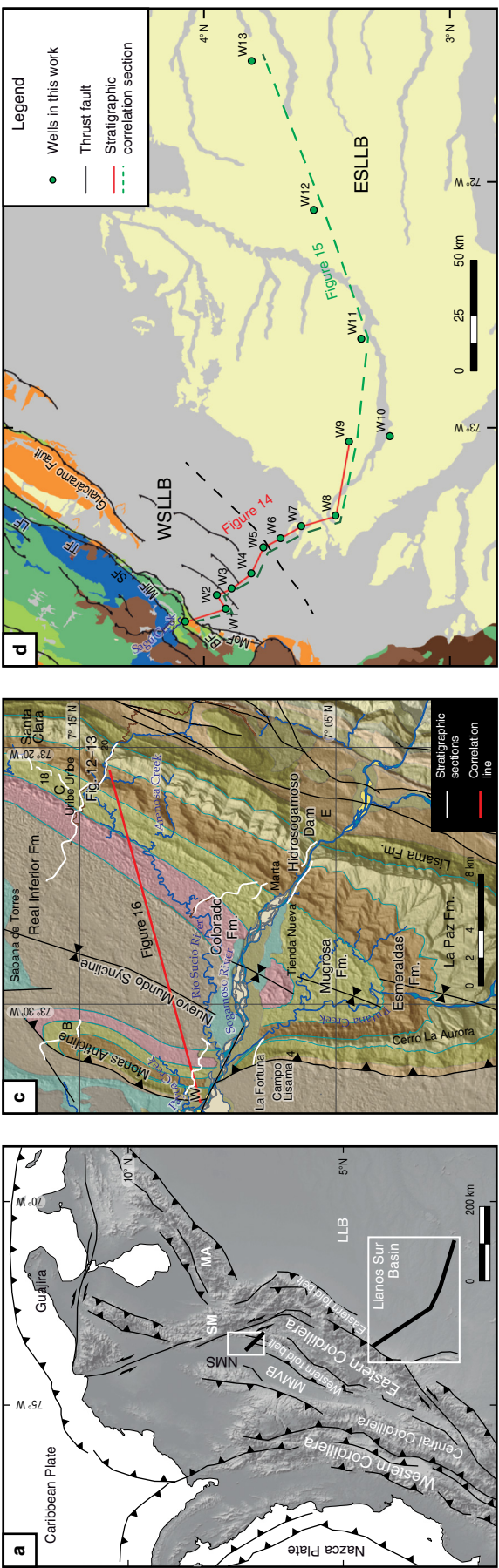
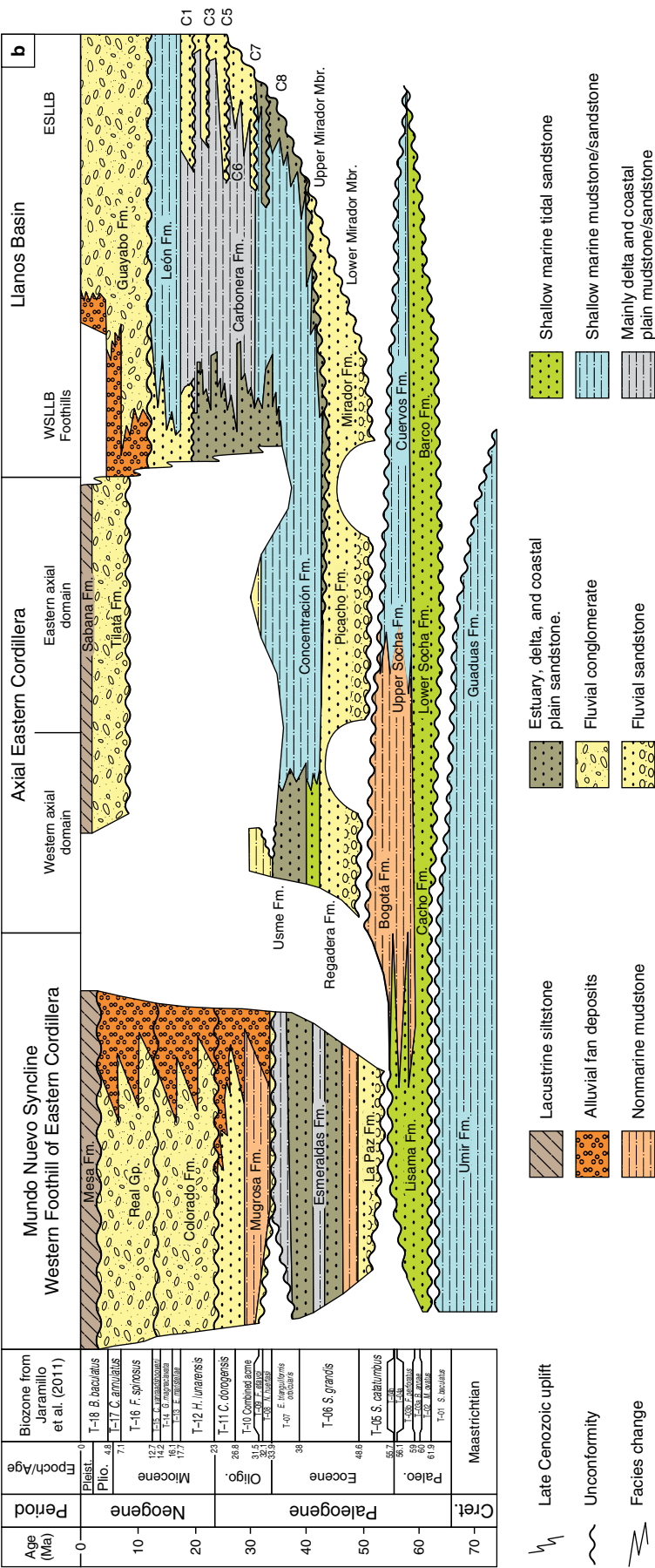


Figure 1. (a) Locations of the main three cordilleras; the insets indicate the locations of both study areas. (NMS) Nuevo Mundo Syncline; (SM) Santander Massif; (MA) Mérida Andes; (MMVB) Middle Magdalena Valley Basin; (LLB) Llanos Basin. **(b)** Wheeler diagram showing the time stratigraphic units in the Middle Magdalena and Llanos Basins (after Mora et al., 2010). Data from MMV and NMS: This study and Caballero et al. (2010, 2013a). Data from western and eastern axial EC: Bayona et al. (2013). Data from southern Llanos Basin: This study. (WSLLB) western sector of the Llanos Basin; (ESLLB) eastern sector of the Llanos Basin; (Fm.) Formation. **(c)** Locations of stratigraphic columns (white lines) and stratigraphic correlation and section in the NMS. **(d)** Location of a stratigraphic correlation section and well cores in the Llanos Basin used in this study. (LF) Lengupá Fault; (TF) Tesalia Fault; (SF) Servitá Fault; (MiF) Mirador Fault; (BF) Boa Fault; (MoF) Monserrate Fault.

In the eastern part of the MMB, the La Paz Formation is 1090 m thick in the NMS and pinches out 38 km to the west above the axial LCISP (Suárez, 1997; Gómez et al., 2005a; Caballero, 2010). The Cantagallo sandstones in the western part of the Middle Magdalena Basin (Yariguí–Cantagallo Oil Field) are the fluvial equivalent to the La Paz Formation in the eastern region; it is 580 m thick in the Yariguí–1 well and pinches out above the LCISP approximately 18 km to the east (Suárez, 1997).

The middle – upper Eocene rock record is composed of fluvial sandstones and mudstones of the Armadillo Member of the San Juan de Rio Seco Formation in the Guaduas Syncline, where paleocurrent measurements indicate paleoflow to the north (Gómez et al., 2003), and the fine-grained fluvial meandering Esmeraldas Formation in the northern region of the MMB, which shows variable paleocurrents with SE paleoflow in the lower section, W–NW paleocurrents in the middle section, and SE paleocurrents in the upper section (Suárez, 1997; Gómez et al., 2005a, Caballero, 2010; Caballero et al., 2010). Across strike, the middle – upper Eocene deposits extend across most of the Middle Magdalena Basin. The Esmeraldas Formation has an equivalent unit in the northwestern part of the MMB, the upper part of the Cantagallo sandstones (Suárez, 1997; Gómez et al., 2005a). Los Corros fossil horizon at the top of the Esmeraldas Formation is not continuous and is restricted to the central and northern parts of the Middle Magdalena Basin (Morales, 1958; Gómez et al., 2005a).

A recent palynological study of the Esmeraldas Formation in the Middle Magdalena Basin found that this unit is late – early Eocene to late Eocene in age and is time-equivalent with the upper part of the Picacho Formation and the lower part of the Concentración Formation in the Eastern Cordillera and with the middle–upper part of the Mirador Formation and the lower part of the C8 Member of the Carbonera Formation in the LLB (Rodríguez–Forero et al., 2012). By integrating the data from Pardo–Trujillo (2004) with their results, Rodríguez–Forero et al. (2012) suggested an early Eocene age for the La Paz Formation based on its stratigraphic position (T–05 of Jaramillo et al., 2011).

The Oligocene rock record comprises variegated and mainly reddish brown pedogenized mudstone and claystone with interbedded discontinuous muddy granule coarse sand-

stones of the alluvial Oligocene Mugrosa Formation in the NMS (Caballero et al., 2013a). In the southern Middle Magdalena Basin, the equivalent Almacigos Member of the San Juan de Rio Seco Formation is composed of nearly the same facies with thick mudstone intervals containing decimeter–to meter–scale cross-bedded sandstones that grade upward into thick layers of variegated mudstones with caliche and paleosols (Gómez et al., 2003). Floodplain cumulative paleosols and channelized sands were deposited in the northern part of the basin (Suárez, 1997).

1.2. Previous Work in the Axial Eastern Cordillera

Correlations between the axial Eastern Cordillera, Llanos Foothills, Llanos Basin, and the Magdalena Basin have been performed in several previous studies. According to these studies, the Maastrichtian – Paleocene activity formed two depocenters in Colombia, one in the Magdalena Valley and the other to the east of the western flank of the Eastern Cordillera, the axial Eastern Cordillera – Llanos Basins (Bayona et al., 2013). Deformation and intraplate magmatism shifted to the eastern flank of the Eastern Cordillera during the late Paleocene – early Eocene and separated the second depocenter in the axial Eastern Cordillera and the Llanos Basin during early Eocene. In the early Eocene, three depocenters (the Magdalena Valley, axial Eastern Cordillera, and Llanos Basins) were separated by low-amplitude uplifts that exposed the Cretaceous sedimentary cover and were filled by sediments from the Central Cordillera to the west, the craton to the east, and local uplifts (Bayona et al., 2010, 2013).

Farther to the north in the axial Eastern Cordillera Basin, the Floresta Basin records depositional environments ranging from shallow marine to low-gradient fluvial and estuarine deposits from the Maastrichtian to the Oligocene. The sediment provenance for this basin was from the Guiana Craton during the Cretaceous – early Paleocene and from the Central Cordillera from the mid–Paleocene until the middle Eocene. During the late Eocene to Oligocene, the source was the fold–thrust belt of the Eastern Cordillera (Saylor et al., 2011, 2012a).

Previous studies suggest that the southernmost part of the axial Eastern Cordillera was connected to the Upper Magdalena Basin, the axial Eastern Cordillera, the foothills of the Eastern

Cordillera, and the southern Llanos Basin from the Paleocene to early Eocene, forming a N–NE–oriented fluvial to coastal plain sedimentary system that was linked to the Maracaibo Sea (Caserio *et al.*, 1997, Reyes–Harker *et al.*, 2015). The Middle Magdalena Basin was a N–NE–oriented fluvial to estuarine system that was confined by the Central Cordillera and the low uplifts of the Los Cobardes–Peñon Anticlines and was connected to the Maracaibo Basin to the north. By the Oligocene, the Magdalena Valley Basin, the axial Eastern Cordillera Basin, and the Llanos Basin had separated.

1.3. Previous Work in the Llanos Basin

In the foothills of the Eastern Cordillera, previous studies (Ramon & Fajardo, 2006) interpreted the Lower Mirador Formation as coastal plain facies that were deposited in channels, crevasse splays, swamps, and flood–plain environments and the Upper Mirador Formation as being composed of bay fill, bay–head delta, and channel facies. Jaramillo *et al.* (2009) found that this unit is diachronous in the Llanos Basin; they dated this unit as early to middle Eocene in outcrops exposed along the Llanos Foothills and as Oligocene in the stable foreland basin to the east. Pulham (1994), Cooper *et al.* (1995), and Cazier *et al.* (1995) interpreted the Mirador Formation in the Cusiana Field as incised valley fill after a period of falling base level at the end of the Paleocene.

The Mirador Formation is thicker to the north and thinner to the south; it is approximately 100 m thick in the Medina area (Parra *et al.*, 2009a) and 131–144 m thick in the Cusiana area (Cazier *et al.*, 1995). These thicknesses reported to the north include both the Lower and Upper Mirador Formation. To the south in the area of the Ariari River, the Lower Mirador Formation is 30 m thick, and in the Macarena Formation is only 15 m thick (Sandoval, 2016).

Paleogeographic reconstruction of the Cenozoic strata in Colombia shows that the lower Eocene strata of the Mirador Formation are dominated by sandy fluvial facies and that the middle – upper Eocene is dominated by mudstones and sandstones that accumulated along a NNE–elongated fluvial system with periods of marine ingression (Reyes–Harker *et al.*, 2015; Santos *et al.*, 2008). This late Eocene depositional configuration continued in the Oligocene with the accumulation of mudstones of the C8 Member of the Carbonera Formation to the west and coeval sandstone deposits to the east; these sandstones predominate along the eastern border of the southern Llanos Basin and are called Oligocene basal sandstones or basal sandstones of the Carbonera Formation (Malagón, 1997; Bayona *et al.*, 2006).

The Carbonera Formation was deposited in a basin that extended to the west far beyond the present–day Llanos Basin (Villamil, 1999). The sandy units are interpreted as nearshore, coastal plain and deltaic deposits, whereas the muddy units are transgressive shales (Ramon & Fajardo, 2006). Mondragón *et*

al. (2016) named the basal sandstones of the early Eocene in the central part of the Llanos Basin the C9 Member of the Carbonera Formation; however, these sandstones are part of the C8 Member of the Carbonera Formation, especially in the ESLLB.

Several profiles of the Carbonera Formation were measured in the Medina Basin in the foothills of the Eastern Cordillera. The C8 Member of the Carbonera Formation is approximately 200 m thick and is characterized by thick intervals of dark gray mudstone with cross–laminated sandstones and coal of a marine–influenced deltaic plain. The C7 Member of the Carbonera Formation is composed of a set of thickening and coarsening–upward tide–influenced delta facies successions. In the Medina Basin, the C6 Member of the Carbonera Formation consists of fluvial channel conglomerates and sandstones with interbedded scarce alluvial plain variegated mudstones covered by thick intervals of variegated mudstones on the western flank and thick intervals of dark gray mudstone with cross–laminated sandstones and coal of a marine–influenced deltaic plain on the eastern flank. Both the C7 and C6 Members of the Carbonera Formation vary in thickness from 1150 m on the western flank to 450 m on the eastern flank of the Medina Basin (Parra *et al.*, 2009a, 2010).

2. Materials and Methods

The descriptions of the facies and facies successions are based on several measured stratigraphic sections in outcrops in the Llanos Foothills and well cores throughout the Llanos Basin (Figure 1a, 1d). The data in this study from the Middle Magdalena Basin are mostly based on measured outcrop stratigraphic sections from the eastern and western limbs of the Nuevo Mundo Syncline (Caballero, 2010; Caballero *et al.*, 2010, 2013a, 2013b) (Figure 1c).

We described the facies using the methodology proposed by Farrell *et al.* (2012), which is a texture–based classification of clastic sedimentary facies that conveys information about the sedimentary processes responsible for their deposition. Postdepositional features that require very short to extensive periods of time after physical deposition of the sediments, such as bioturbation and paleosol development, were also considered as criteria for facies identification. The ichnofossils and bioturbation were described following the guides and criteria of Gerard & Bromley (2008). The paleosol identification and nomenclature were based on Kraus (1999) as well as the useful paleosol classification nomenclature of Catuneanu (2006).

We describe the textures, compositions, sedimentary structures, thicknesses, and contact relationships between the facies and facies successions. Sedimentary structures are among the most valuable data for interpreting the depositional environments of rocks. The structures are especially useful in determining the energy level and direction of flow of the transporting medium and the biological activity, and they are often the only

way to define the sedimentary processes by which sediment is deposited (Weimer, 1975).

The biozones identified in the correlated sections were classified at the Biostratigraphy Laboratory at Instituto Colombiano del Petróleo (ICP) following the palynology zonation proposed by Jaramillo et al. (2011). The correlations were used to determine the distribution of facies throughout the basins, and the stratigraphic distribution and abundance of ecological important palynomorphs were also used to support the depositional environment interpretations. In addition, palynology provides information about the depositional environments. For example, it is possible to distinguish nonmarine and marine organic matter. The former is dominated by continental particles and freshwater algae, whereas marine organic matter contains marine algae, such as dinoflagellates and acritarchs.

Gamma ray logs aided in the identification of sharp versus gradational trends and changes in stacking patterns, and they allowed the identification of candidate surfaces for unconformities, maximum flooding surfaces, truncations, and context. Pattern-matching analysis aided in the correlations. All of the information was integrated using the sequence stratigraphy methodology proposed by van Wagoner et al. (1990), van Wagoner & Bertram (1995), Posamentier & Allen (1999), and Catuneanu (2006), which was calibrated with palynology analysis using proprietary information at the ICP.

Facies analysis is fundamental for interpreting stratigraphic surfaces, such as marine erosion surfaces, unconformities, maximum flooding surfaces, fluvial incision, and subaerial exposure. The regional correlations integrated information from well logs, facies from outcrops/cores, biozones, and stratigraphic markers such as paleosols and coal beds. This information and analysis aided in the identification of time lacunas, facies changes, transposition of facies and environments, and changes in the depositional trends and unconformities (Walker, 1984; Walker & James, 1992; van Wagoner & Bertram, 1995; van Wagoner et al., 1990; Shanley & McCabe, 1994; Posamentier & Allen, 1999; Kraus, 1999; Catuneanu, 2006). These analyses resulted in a synthetic sequence stratigraphic framework that was calibrated with biostratigraphy data.

3. Results

3.1. Facies Description

“A facies is a body of rock characterized by a particular combination of lithology, physical, and biological structures that bestow an aspect (“facies”) different from the bodies of rock above, below, and laterally adjacent” (Walker & James, 1992).

In the following sections, we describe, illustrate, and interpret the processes that generated each facies or association of facies in the Eocene to Oligocene Mirador Formation and the C8, C7, and C6 Members of the Carbonera Formation in the SLLB and the La

Paz, Esmeraldas, and Mugrosa Formations in the NMS (Figures 2 to 6). We then describe, illustrate with stratigraphic columns, and interpret the facies successions in these lithostratigraphic units in terms of the environmental context of their occurrence (Figures 7 to 13). Using correlations, we depict the spatial and temporal distributions of the facies and facies successions and interpret the depositional environments of these units (Figures 14 to 17). Finally, we depict the distribution of the depositional systems in maps (Figures 18 to 20).

3.1.1. Facies and Facies Associations, Descriptions, and Interpretations

3.1.1.1. Facies 1 (F1): sG x, sG h, sG m, sG imb

Facies: Clast-supported pebble conglomerate with sandy matrix. Clasts are pebbles and cobbles with very rounded shapes that are mainly composed of quartz with chert (possible second sedimentary cycle) (Figures 2b, 4a).

Sedimentary structures: Planar to trough cross-bedding, planar beds, imbricated clasts, graded to aggradational sets, no organic structures. x = cross-bedded; h = horizontally bedded; m = massive; imb = imbricated.

Thickness and contacts: Erosive base, sharp to gradational transition from gS x to S x. Sets 1 to 4 m thick in the Mirador Formation in the WSLB (Figure 2a, 2b) and 0.5 to 24 m thick in the southern part of the La Paz Formation in the NMS. Composed of pebble to cobble conglomerates with clasts 2 to 15 cm in diameter.

Interpretation: Bedload sediment deposited in an upper flow regime (dilute stream flows) by traction (sG x), rolling (sG imb), or fluidized flow (sG m). The sandy matrix infiltrated during the waning of the event (sG m) (Rust, 1977). Massive aspect = hyperconcentrated flows.

3.1.1.2. Facies 2 (F2): S x, gmS x, mS x, mS m, S x rh

Facies: Medium- to coarse-grained sandstone (S x), gravelly sandstone (gS x), and muddy sandstone (mS x) (Figures 2c, 2e, 4b, 5a). Rhythmic cross-bedded sandstone (S x rh) with mud draped over each sandy foreset in the upper part of the Lower Mirador and Esmeraldas Formations (Figure 2d, 2e left photo). Muddy or gravelly muddy sandstones (mS x, gmS m, gmS x) are also present, especially in the Mugrosa Formation (Figure 6c, 6d, 6g). And massive sandstone (S m) as in La Paz Formation (Figure 4c).

Sedimentary structures: Planar to trough cross-bedding, massive bedding. No organic structures observed.

Thickness and contacts: From 40 cm to 1.5 m thick in the lower Eocene Mirador Formation and basal Oligocene sandstones of the C8, C7, and C6 Members of the Carbonera Formation in the ESLLB. Sets are 60 cm to 2 m thick in the La Paz

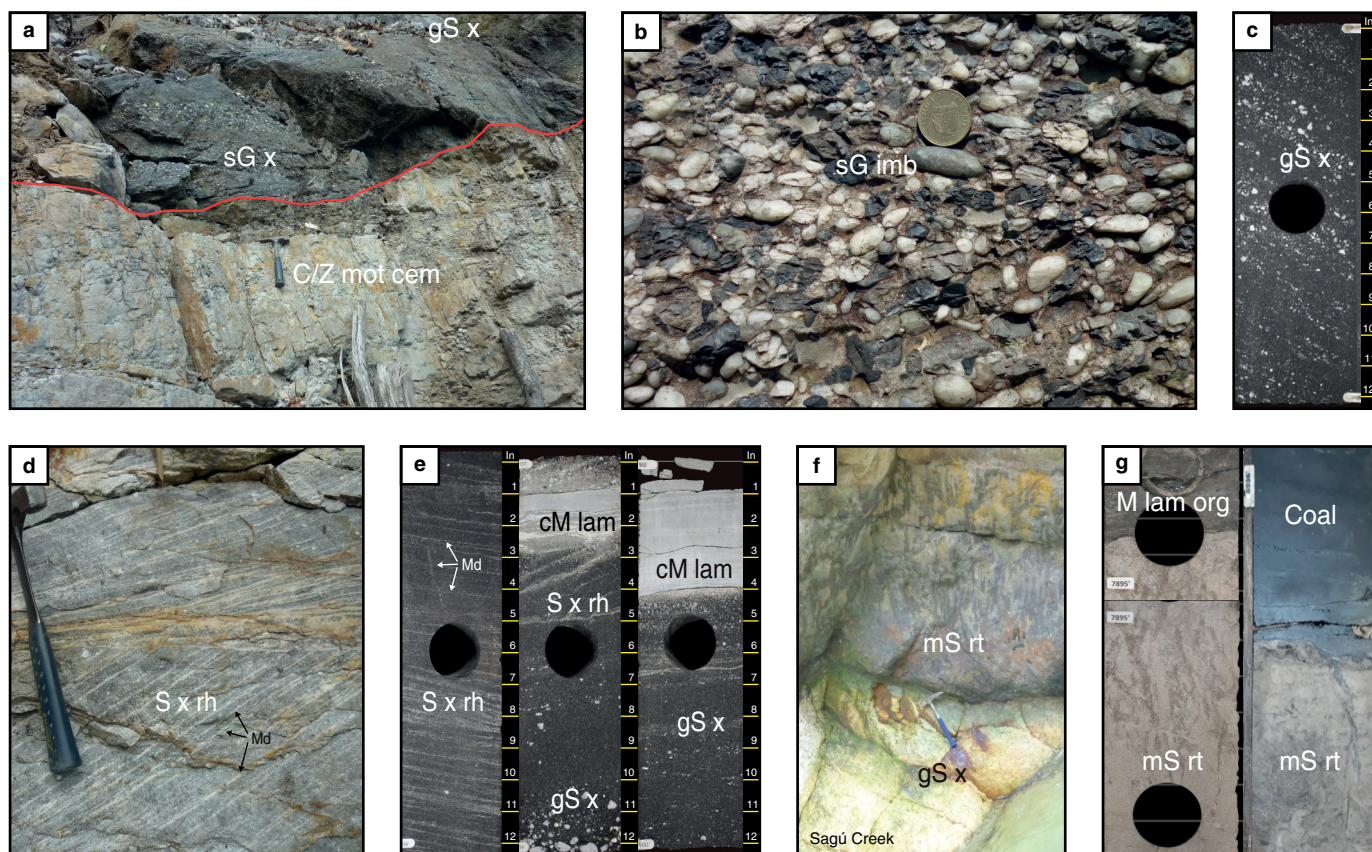


Figure 2. Images of the lower Eocene Lower Mirador Formation facies in the LLB. **(a)** Conglomerate facies (sG x) over well-developed paleosol (C/Z mot cem). This paleosol defines the Paleocene/Eocene unconformity (red line). **(b)** Detail of the conglomeratic facies with imbricated clasts (sG imb). **(c)** Conglomeratic sandstones with planar cross-bedding (gS x). **(d, e)** Cross-bedded rhythmic sandstone (S x rh) with mud drapes (Md) and clayey mudstone laminated (cM lam) between sets of cross-beds. **(f)** Rooted and mottled muddy sandstone (mS rt) above conglomeratic sandstone (gS x). **(g)** Same facies (mS rt) in cores with carbonaceous mudstone (M lam carb) or coal above the rooted sandstone. (a, b, d, and f): Outcrops in the foothills, (c, e): well 1 to well 4, (g): wells 1 and 7.

and Esmeraldas Formations and from 0.5 to 2 m thick in the Mugrosa Formation.

Interpretation: High-energy deposits transported in dilute stream flows by traction and rolling particles in a subaquatic migrating dune field with abundant bedload (Collinson et al., 2006). Interpretation depends on the associated facies and the stratigraphic context. Rhythmic structures and surfaces mean rapid and cyclic changes from high to low energy and are probably of tidal origin (Nio & Yang, 1991).

3.1.1.3. Facies 3 (F3): S h, mS h, gmS h

Facies: Fine- to coarse-grained sandstone, horizontally bedded (S h), planar-bedded muddy sandstone (mS h), or planar-bedded gravelly muddy sandstone (gmS h). This facies is present in the Mugrosa Formation in the NMS (Figure 6i, 6j). In the ESLLB, this facies is present in the Oligocene basal sandstones and C7 Member of the Carbonera Formation (Figures 10a, 11a3, 11b4).

Sedimentary structures: Planar bedding.

Thickness and contacts: Up to 2 m thick in the Mugrosa Formation. In the La Paz Formation, it is medium- to coarse-grained and is 0.5 to 1.5 m thick; in the southern Llanos Basin, it is 0.5 to 1 m thick.

Interpretation: Planar or flat bedding is indicative of an upper flow regime in which the energy of the current is strong and destroys the bedforms to form planar beds. It is a confined (high-sediment concentration in stream flows) or unconfined laminar or sheet flow (hyperconcentrated flows and upper flow regime). Its depositional environment can be distinguished by other attributes (Blair & McPherson, 2009; Lunt et al., 2004).

3.1.1.4. Facies 4 (F4): mS rt, mS rt mot

Facies: Fine- to coarse-grained rooted muddy sandstone (mS rt), rooted and mottled reddish to yellowish muddy sandstone (mS rt mot). In the southern LLB, it is composed of white mud-

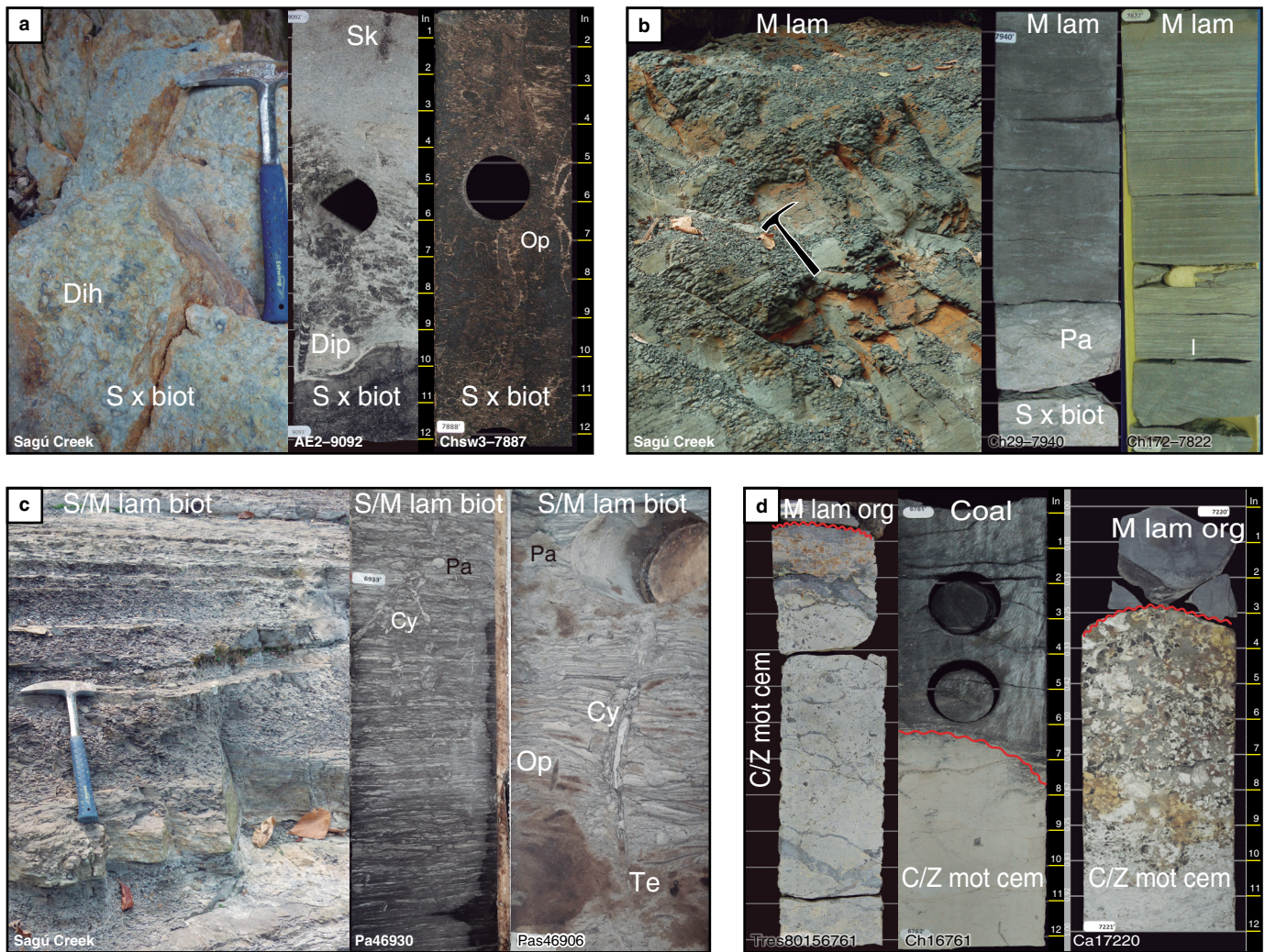


Figure 3. Images of the outcrop (left) and core (right) of the middle – upper Eocene facies of the Upper Mirador Formation and the C8 Member of the Carbonera Formation in the southern LLB. **(a)** Bioturbated fine- to medium-grained cross-bedded sandstones (S x biot). **(b)** Gray to olive gray laminated mudstone (M lam) with thin lenses of silt or very fine sandstone. **(c)** Laminated and bioturbated fine heterolithic sandstone/mudstone (S/M lam biot). **(d)** Paleocene mottled and cemented, well-developed paleosol (C/Z mot cem) below dark gray carbonaceous, coaly mudstone (M lam org) and coal. The red line marks the Paleocene/middle Eocene unconformity. Outcrop images in (a), (b), and (c) are from the Sagú area in the foothills. Cores (a) and (b) are from wells 6, 7, and 8. (Sk) *Skolithos*; (Dih and Dip) *Diplocraterium*; (Op) *Ophiomorpha*; (Pa) *Paleophycus*; (Cy) *Cylindrichnus*; (Te) *Teichichnus*; (l) lenses.

dy sandstone (kaolinite) covered by a thin layer of coal or carbonaceous mud 5 to 15 cm thick (Figure 2g). In the NMS, it is generally associated with variegated mudstone and is present in the lower section of the La Paz Formation (Figure 4f), the lower part of the Esmeraldas Formation (Figure 5c, 5d), and the Mugrosa Formation (Figure 6f).

Sedimentary structures: No physical structures preserved (or structures destroyed by postdepositional processes). Vertical bioturbation structures, root traces.

Thickness and contacts: 1 to 4 m thick in the lower Eocene rocks of the Mirador Formation in the WSLLB (Figure 2g, left core) but less than 1 m thick in the ESLLB (Figure 2g, right core).

Interpretation: After deposition, the sandstones were sub-aerially exposed and colonized by vegetation for a period of time; weathering and bioturbation masked and destroyed the primary sedimentary structures and mixed the sand with mud. Eventually, the vegetation was preserved as a thin layer of coal or carbonaceous mudstones conforming the paleo-organic soil horizon over the rooted sandstone.

3.1.1.5. Facies 5 (F5): S r, S r biot

Facies: Very fine- to fine-grained, well-sorted sandstones with current or wave ripple laminations (S r), sometimes bioturbated (S r biot). Present in the NMS at the top of the lower section of

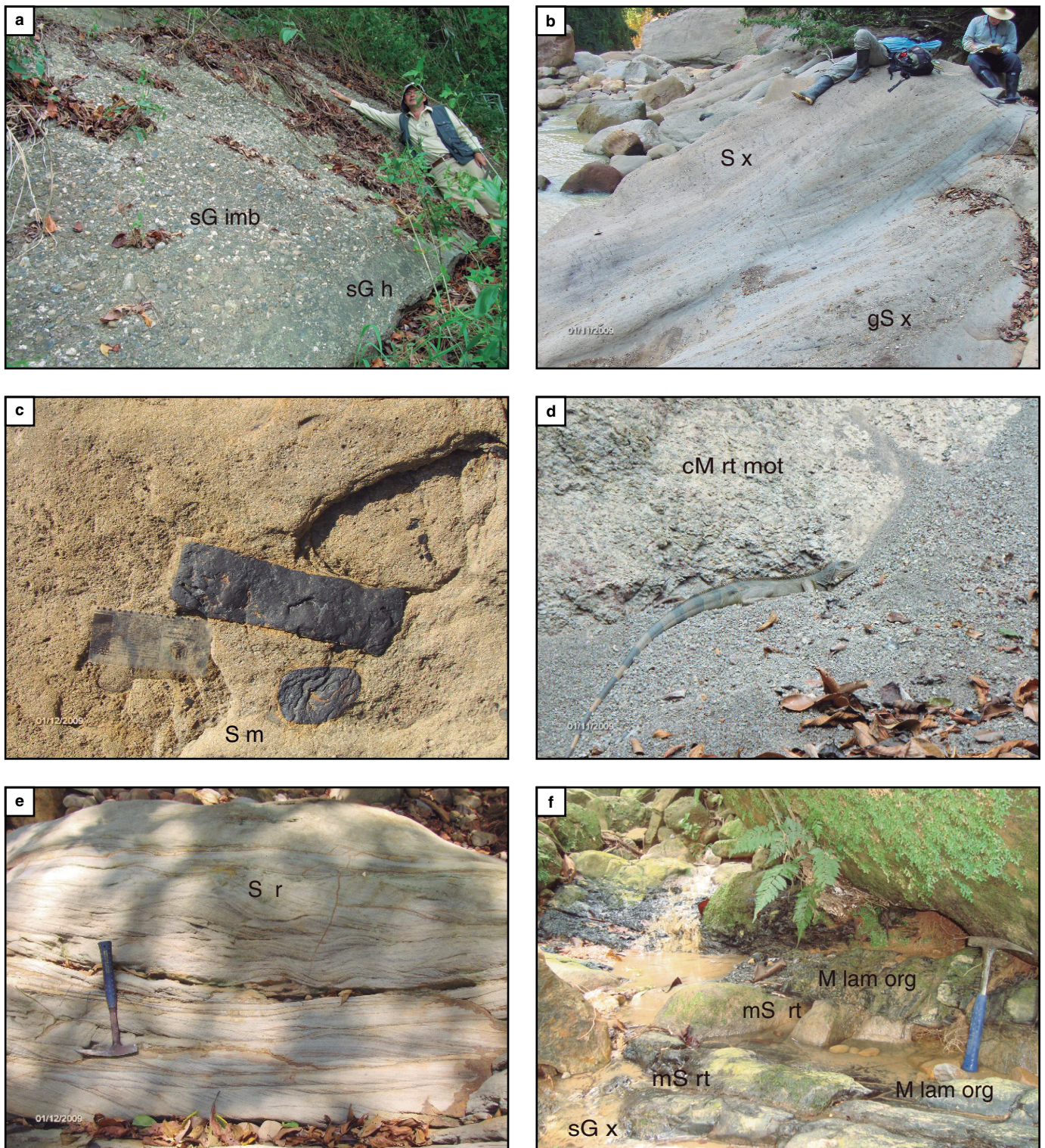


Figure 4. Illustration of the facies identified in the lower Eocene La Paz Formation on the eastern limb of the Nuevo Mundo Syncline (NMS). **(a)** Basal conglomerates (sG imb, sG h). **(b)** Very thick amalgamated trough cross-bedded sandstones (S x, gS x). **(c)** Massive sandstones (S m) containing decimeter-scale intraclasts of coal hydraulically equivalent to sand. **(d)** Variegated mudstones (cM rt mot) (the iguana is 50 cm long) of the Upper La Paz Formation. **(e)** Current and sinusoidal rippled sandstone (S r). **(f)** A rooted sandstone (mS rt) overlain by a thin layer of carbonaceous mudstone (M lam org) at the top of a conglomerate/sandstone (sG x) cycle in the southern basal section of the La Paz Formation.

the La Paz Formation (Figure 4e, unidirectional ripples) and in the Esmeraldas Formation (Figure 5e, bidirectional ripples). In the Oligocene basal sands of the C8 Member of the Carbonera Formation in the ESSLB, this facies contains irregular wavy discontinuous laminations (Figures 10b, 11a2, 11a3).

Sedimentary structures: Wave ripple laminations, sometimes bioturbated by ichnogenes such as *Ophiomorpha* and *Teichichnus*.

Thickness and contacts: Beds 20 to 50 cm thick.

Interpretation: Migration of ripples in a lower flow regime, which were partly or locally colonized and bioturbated. The environmental interpretation depends on the context: it can be fluvial, estuarine, tidal flat, shallow marine, or lacustrine and may also be present at the tops of turbiditic flows (Reineck & Singh, 1973). Bioturbation indicates a lower shoreface to inner shelf (Clifton, 2006). This kind of bioturbation is only found in the Upper Mirador Formation and the C8 Member of the Carbonera Formation in the LLB.

3.1.1.6. Facies 6 (F6): S x biot

Facies: Fine- to medium-grained well-sorted sandstone with planar cross-bedding burrowed by *Ophiomorpha*, *Teichichnus*, *Skolithos*, and *Diplocraterion* (Figure 3a). Present in the Upper Mirador Formation in the WSSLB (Figure 3a).

Sedimentary structures: Planar cross-bedding and bioturbation by marine ichnofacies; found in sandy marginal marine or lacustrine systems.

Thickness and contacts: Beds 10 cm to 1 m thick; stacked bedsets 3 to 4 m thick.

Interpretation: This facies results from the migration of straight crested dunes in a lower flow regime that were colonized and bioturbated by organisms. The environment is interpreted as a shallow marine, likely upper shoreface subenvironment (Reineck & Singh, 1973; Clifton, 2006; Collinson et al., 2006), although this type of association can also be found in sandy marginal estuarine systems.

3.1.1.7. Facies 7 (F7): S/M w, l, f

Facies: Fine to very fine, well-sorted sand interlayered with medium gray mud with wavy (S/M w), lenticular (S/M l), and flaser bedding (S/M f). These facies are present in the upper part of the Esmeraldas Formation (Figure 5b, 5f) and in the lower Oligocene deposits in the ESSLB (Figure 10i).

Sedimentary structures: Wavy, lenticular, and flaser bedding.

Thickness and contacts: Heterolithic layers 1 to 3 m thick.

Interpretation: Two alternating and repeating stages of deposition: a lower flow regime (sand) followed by a stage of still water (mud). These conditions occur in tidal flats or below the wave base in the lower shoreface (Reineck & Singh,

1973; Nio & Yang, 1991); the sedimentary structures indicate the former.

3.1.1.8. Facies 8 (F8): M lam

Facies: Dark gray laminated mudstone (M lam), locally thin isolated lenses of silt or very fine sandstone, locally bioturbated with *Teichichnus*, *Planolites*, *Thalassinoides*, and *Phycodes*? (Figure 3b). This facies contains lower – middle Eocene palynological assemblages (biozones T-05 – T-06). De La Parra et al. (2014) also recorded the presence of marine palynomorphs (dinoflagellates and foram linings) as well as mangrove pollen (*Lanagiolopolis crassa*). The Oligocene interval (zone T-08) contains high abundances of freshwater-brackish algae (*Botryococcus*-spp.).

Sedimentary structures: Horizontal laminations in wells and outcrops and subtle wavy to lenticular laminations.

Thickness and contacts: From a few centimeters to several meters thick. Very thick in the Upper Mirador Formation and the C8 Member of the Carbonera Formation in the LLB (Figure 3b).

Interpretation: This facies is interpreted as a subaqueous vertical settling deposit below the fair-weather wave base. When it contains thin silt laminae, the very fine sand or silt was deposited during interruptions between more energetic waves. This facies could be a marine shelf mudstone (Reineck & Singh, 1973; Clifton, 2006).

3.1.1.9. Facies 9 (F9): S/M lam biot

Facies: Fine- to very fine-grained, well-sorted sandstones and medium-gray colored mudstones interbedded with thin to thick laminae. Common evidence of bioturbation by *Ophiomorpha*, *Teichichnus*, *Diplocraterion*, *Cylindrichnus*, and *Thalassinoides*. Present in the middle – upper Eocene to lower Oligocene C8 Member of the Carbonera Formation in the LLB (Figure 3c) and in the LLB.

Sedimentary structures: Wavy and lenticular laminations to wavy ripple laminations in sands, bioturbated by *Teichichnus*, *Paleophycus*, *Diplocraterion*, and *Cylindrichnus*.

Thickness and contacts: Centimeters to meters thick.

Interpretation: Vertical settling of mud and low-energy storms that shed sand in a subaqueous environment near the fair-weather wave base due to seasonal variations. This facies could indicate a lower shoreface environment (Reineck & Singh, 1973), although heterolithic laminations may also be found in coastal plains (seasonal variations) and tidal flats (daily variations).

3.1.1.10. Facies 10 (F10): M org, M lam org

Facies: Dark gray to black carbonaceous mudstone with local pyrite nodules. Massive (M org) to horizontally laminated (M

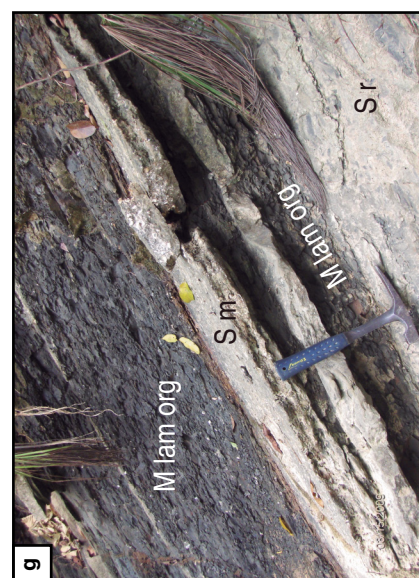
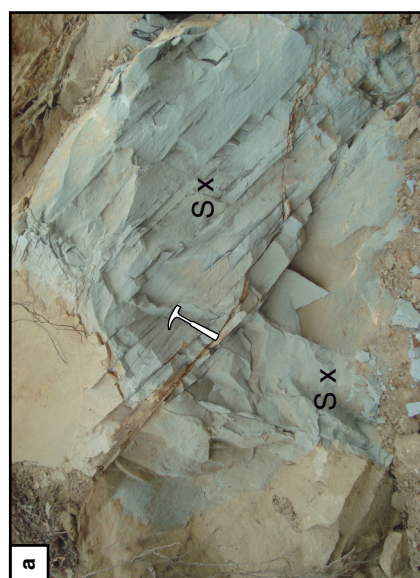
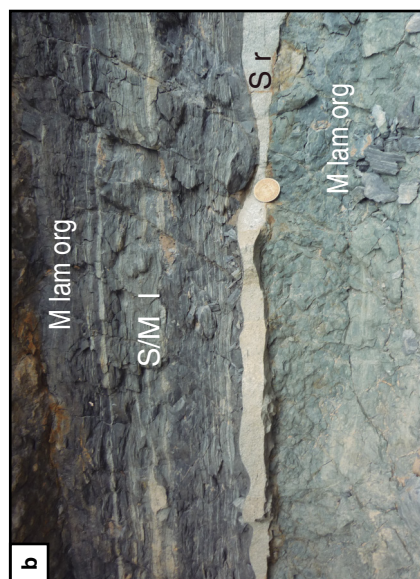
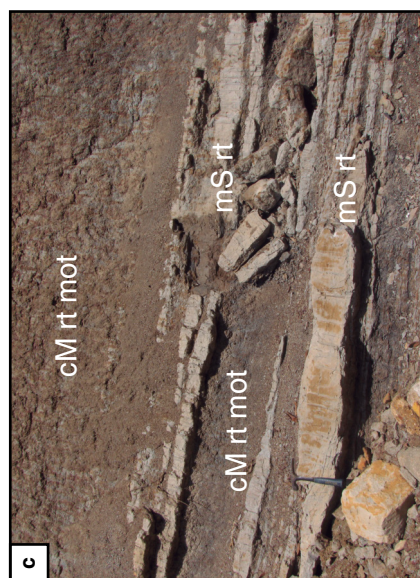


Figure 5. Middle – upper Eocene facies of the Esmeraldas Formation on the eastern flank of the NMS. **(a)** Thick bedset of planar cross-bedded, medium- to coarse-grained sandstone (S x) (hammer is 45 cm long). **(b, f)** Inter laminations of dark gray mudstone (M lam org) with ripple-laminated, fine- to very fine-grained sandstone (S/M l, f) producing ripple (S r), lenticular, or flaser laminations. **(c)** Variegated mudstone (cM rt mot) with rooted sandstone (mS rt). **(d)** Detail of rooted sandstone (mS rt). **(e)** Ripple-laminated, fine- to very fine-grained sandstone (S r), some of which is bidirectional. **(g, h)** Gray carbonaceous mudstones with shells of gastropods (M lam org) intercalated with massive fossiliferous sandstone (S m) in the Upper Esmeraldas Formation (Los Corros horizon) which are over sandstones with ripple laminations (S r). **(i)** Concentric laminated stromatolite (Strom) structure over sandstones (S m) in the Esmeraldas Formation.

lam org), horizontal burrows, plant debris can be present (Figure 9c, 9d). This facies is found in the middle Eocene rocks of the southern Llanos Basin (Figure 2g left and Figure 3d right). In the NMS, this facies was observed in the lower to middle part of the La Paz Formation (Figure 4f) and in the upper part of the Los Corros fossil marker in the Esmeraldas Formation (Figure 5g, 5h).

Sedimentary structures: Massive to horizontal laminations, horizontal burrows, and plant remains; thin coal interbeds.

Thickness and contacts: Up to 6 m thick in the middle Eocene of the ESLLB; a few cm to meters thick in the La Paz and Esmeraldas Formations in the NMS.

Interpretation: Deposited by vertical accretion in ponded water with a large contribution of vegetal carbonaceous material. It is a marginal paralic deposit that formed in coastal plain swamps and marshes or lacustrine environments (Cecil, 1990) as well as on the coastal plain or a floodplain, where poorly drained conditions could lead to reducing conditions that preserved the organic matter (Shanley & McCabe, 1994).

3.1.1.11. Facies 11 (F11): cM rt mot, cM lam

Facies: White or light gray, violet to reddish brown clayey massive mudstone (cM m), laminated mudstone (cM lam), rooted and mottled (cM rt mot). It is present in the Toro Shale Member of the La Paz Formation (Figure 4d) on the western limb of the NMS. It is a well-developed variegated clayey mudstone that is strongly pedogenized. This facies is also present in the lower section of the Esmeraldas Formation (Figure 5c) and in the entire Oligocene Mugrosa Formation (Figure 6e, 6f). Also in the ESLLB clayey mottled mudstone (cM mot).

Sedimentary structures: Highly bioturbated by roots and other vertical burrows. Highly pedogenized with variegated colors.

Thickness and contacts: Up to 10 m thick on the eastern limb of the NMS in the middle section of the La Paz Formation. It is the most abundant facies in the Mugrosa Formation, with intervals more than 30 m thick.

Interpretation: This facies corresponds to a floodplain deposit exposed subaerially and affected by pedogenic processes.

3.1.1.12. Facies 12 (F12): C/Z mot cem

Facies: White to greenish cream pedogenized silty claystone. This paleosol was observed in outcrops in the WSLLB (Figure 2a) and

in cores in the ESLLB (Figure 3d). This facies is a more cemented duricrust than facies cM mot and cM lam. Z = silt, C = clay.

Sedimentary structures: Strongly mottled with ferricretes or silcretes, root traces, ferruginous nodules, and duricrusts.

Thickness and contacts: 1 to 6 m thick observed in cores of the LLB and outcrops in the NMS. This facies is located below the base of the Eocene unconformity, and it may correspond to the paleosol profile in the Paleocene strata.

Interpretation: Weathering of this material over a long period of time and development of a paleosol (higher than mS rt, mS rt mot, and cM rt mot).

3.1.1.13. Facies 13: (F13): Coal

Facies: Coal appears shiny or dull in cores as seams (Figure 3d). It is located at the top of the channel facies, and it decreases in thickness due to erosion of the overlying coarse-grained facies and/or ravinement surfaces between nonmarine and marine facies (Figures 8 and 9). It is thicker at the base or within the organic laminated mudstones (Figure 9, FS3 at base).

Sedimentary structures: Contains local pyrite nodules; it is located over rooted muddy sandstone or between laminated organic mudstone.

Thickness and contacts: 10 to 80 cm thick coal seams.

Interpretation: Coal forms in swamps or mires in plains. The accumulation of peat (primary material of coal) indicates drowning of a coastal or alluvial plain due to base level rise and a corresponding high water table. These swamps develop vegetation ecosystems that supply large quantities of organic matter. These organic materials deplete the dissolved oxygen in the water, promoting reducing conditions that preserve the organic matter to produce coal during burial.

3.2. Facies Successions (FS) in the Southern Llanos and Nuevo Mundo Syncline

A facies succession is defined as a vertical stack of facies characterized by a progressive change in one or more parameters of the facies, such as thickness, grain size, abundance of sand versus mud, or sedimentary structures (Walker & James, 1992). In the stratigraphic sections presented in this study, the facies successions are the building blocks of the stratigraphic units and are normally repeated several times vertically (i.e., in time). After interpreting the sedimentary processes that deposited each

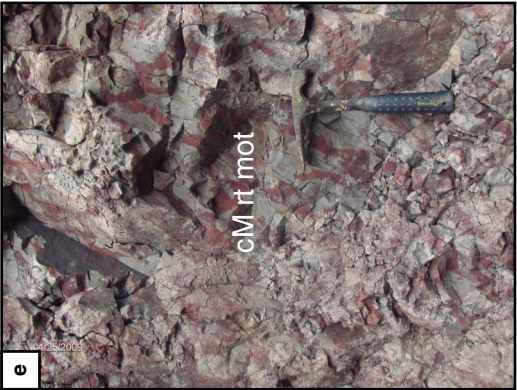
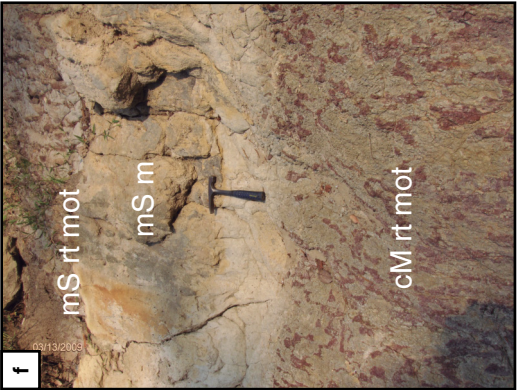
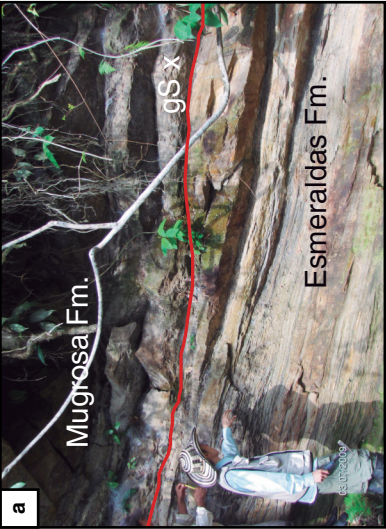
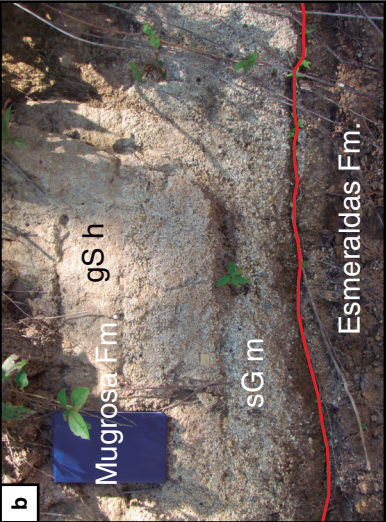
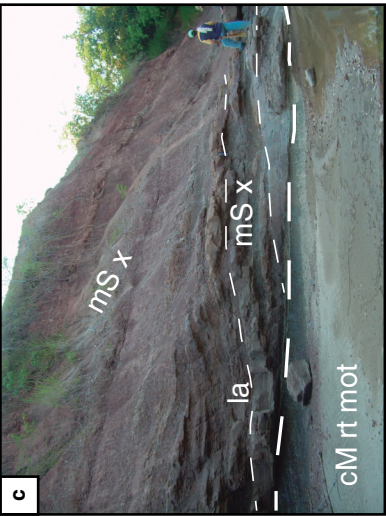


Figure 6. Facies in the Oligocene Mugrosa Formation on the eastern limb of the NMS. **(a, b)** Gravelly cross-bedded sandstones (gS x) in 6a; massive sandy conglomerate (sG m) to plane-bedded gravelly sandstone (gS h) in 6b, both overlie lacustrine–estuarine facies of the Esmeraldas Formation (red line is the Eocene/Oligocene unconformity). **(c)** Point bar deposit showing lateral accretion (la) and erosive base over variegated mudstone (cM rt mot); the muddy cross-bedded sandstone (mS x) forms the point bar. **(d, g)** Variegated mudstone (cM rt mot) containing cross-bedded muddy sandstone (mS x) with an erosive contact at the base of the sandstone. **(e)** Rooted mottled mudstone (cM rt mot). **(f)** Massive muddy sandstone (mS m) and rooted and mottled reddish muddy sandstone (mS rt mot) in gradational contact with the underlying variegated mudstone (cM rt mot). **(h)** Muddy trough cross-bedded sandstone (mS x). **(i, j)** Planar-bedded gravelly–muddy sandstone (gmS h) encased in variegated mudstone. (Fm.) Formation.

FS and correlating them with the nearest wells or outcrops, is possible to determine the sedimentary system. The vertical trend of sets of facies successions generally provides important clues about the changes in the depositional system.

The depositional trends are called progradational, retrogradational, or aggradational. Progradational means nonmarine, continental, or proximal facies that shift toward primarily marine, lacustrine, or distal facies; retrogradational means marine, lacustrine, or distal facies that shift toward primarily nonmarine, continental, or proximal facies; and aggradational means that there is no change in depositional trend (Coe, 2003; Catuneanu, 2006). A sedimentary trend can also be erosion and incision or bypass and development of paleosol.

3.2.1. Facies Succession 1 (FS1): Fluvial Braided Deposits

This succession is composed of facies F1 and F2 and consists of an amalgamated fining-upward pebble conglomerate to sandstone that begins with a cross-bedded, imbricated or planar-bedded pebble sandy conglomerate (sG x, sG imb, sG h) followed by a sharp or gradational contact with planar-bedded granule to coarse-grained sandstone or cross-bedded medium- to coarse-grained sandstone (gS h, gS x, S x). Its lower contact is a subaerial unconformity above a strongly developed paleosol (Figures 7, 8).

This facies succession is interpreted as the basic fluvial braided channel bar system with scarce to absent interbedded mudstones. These successions have a fining-upward trend with single story to multistory stacks of coarse sandstones in the Lower Mirador and La Paz Formations. In cores from wells in the foothills and the WSLLB, from base to top, the last cycle of FS1 is overlain by fine- to coarse-grained, yellowish white rooted muddy sandstone (mS rt). The FS1 fluvial facies are inferred to be lower Eocene in the WSLLB, and at Sagú Creek (Figure 7), the overlying shales are early to middle Eocene (De La Parra et al., 2014). In the Nuevo Mundo Syncline, these facies in the La Paz Formation are early Eocene in age (Rodríguez-Forero et al., 2012).

FS1 indicates a low accommodation, high-energy environment with high-gradient rivers that winnow the mud out of the sand and deposit only sand. In the Nuevo Mundo Syn-

cline, however, the La Paz Formation contains some intervals of floodplain mudstones in the middle part of the unit. These floodplain mudstones could be interpreted as high-order fluvial cycles with increased accommodation space (Suárez, 1997) (Figure 12).

3.2.2. Facies Succession 2 (FS2): Shallow Marine Low-Energy Shoreface

This succession is composed of facies F6, F8, F5, and F9. In general, FS2 coarsens upward from a laminated mudstone facies (M lam) that gradually increases in sand to become a laminated to bioturbated sandstone/mudstone (S/M lam biot), which is overlain by fine to very fine-grained, well-sorted sandstone with wavy ripples that is sometimes bioturbated (S r biot). These facies are capped by a bioturbated cross-bedded medium-grained sandstone (S x biot) (Figures 7, 8). The contacts between the facies in the succession are transitional to sharp. In some cases, the contacts consist of laminated mudstone over which there is an increase of sandy interbeds with a wavy lower contact, and the change in grain size from mud to fine sandstone is not gradual but sharp. The change sometimes appears to be from coarse-grained to fine-grained, such as in Figure 9 at the contact with the ravinement surface between 10 and 12 m depth. In the WSLLB, FS2 ranges in thickness from 1 m to 20 m (Figures 7, 8), whereas in the ESLLB, the thicknesses range from less than 1 m to 12 m.

The succession sometimes shows a simple intercalation of laminated mudstone bioturbated by *Planolites* or *Thalassinoides* (M lam) in sharp contact with bioturbated wave ripple-laminated fine-grained sandstone (S r biot). These interbeds are repeated several times upward, such as in well 7 (Figure 9), and they were probably generated during high-frequency cycles of regression/transgression along a low-energy shoreline (Clifton, 2006).

FS2 contains marine palynomorphs such as dinoflagellates and foraminifer linings as well as mangrove pollen (*Lanag-iopollis crassa*). According to biostratigraphic studies, the facies in this succession are early – middle Eocene at Sagú Creek (De La Parra et al., 2014), whereas in well 7, the same facies are late Eocene to Oligocene, indicating that FS2 becomes younger to the east of the Llanos Basin.

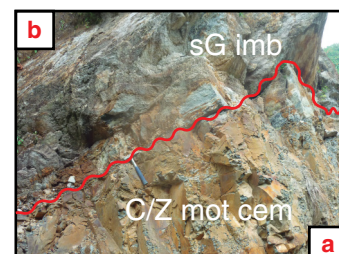
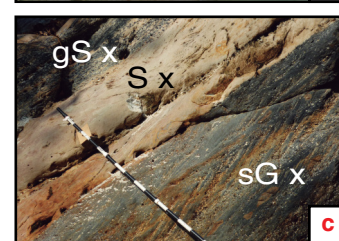
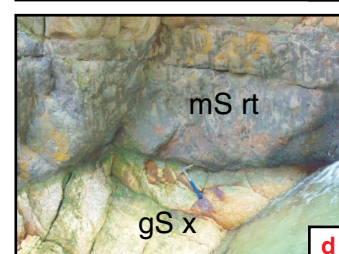
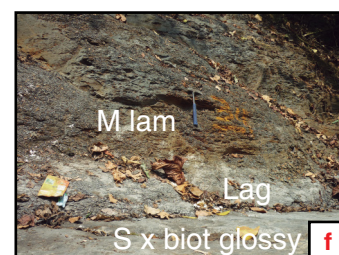
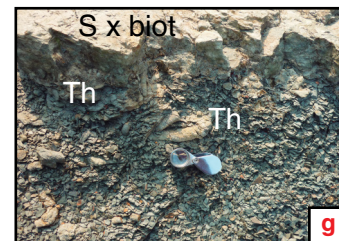
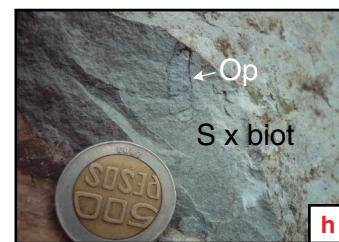
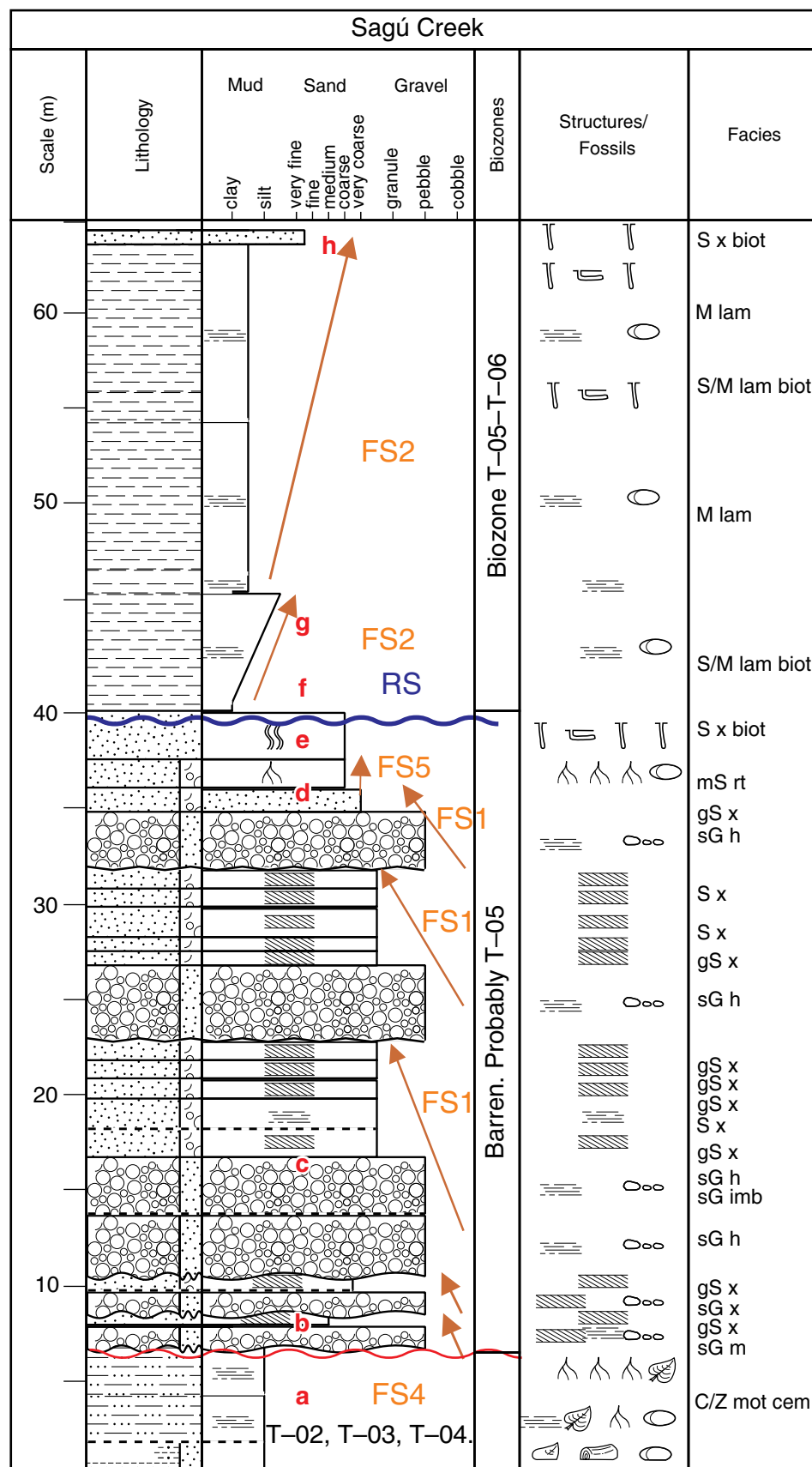




Figure 7. Lower – middle Eocene marginal and marine facies successions of the Mirador and C8 units at Sagú Creek in the foothills. From the base to the top, five cycles of fluvial braided channels and sand bars (FS1) of the Mirador Formation disconformably overlie the Cuervos Formation paleosol (FS4) (the red line indicates the disconformity). The last (FS1) is capped by a coastal plain compound paleosol horizon (FS5). The transgressive erosion surface (RS) eroded a sand bed, in which *Diplocraterion hibachi* (Dih) marks the beginning of the marine transgression. After the ravinement surface, we interpreted two cycles of shallow marine, low-energy shoreline to offshore deposits (FS2) that correspond to the C8 unit. See images of the facies in front of the column. The facies indicated by letters a to h are shown in the right column. (Lag) gravel lag; (Th) *Thalassinoides*; (Op) *Ophiomorpha*.

The vertical trend of FS2 is interpreted as deposition in a shallow marine low-energy foreshore to shoreface system (Clifton, 2006). This facies succession has not been documented in the Eocene – Oligocene rocks of the NMS or in the Middle Magdalena Basin.

3.2.3. Facies Succession 3 (FS3): Backshore Swamp–Lacustrine Fill Deposit

This succession is composed of facies F10, F4, and coal. FS3 is a coarsening-upward succession and begins with dark gray to black carbonaceous mudstone with pyrite that is bioturbated by *Planolites* and sometimes *Thalassinoides* (M org, M lam org), which are in gradational contact with overlying fine-grained sandstone (mS rt), which in turn is overlain by a thin layer of coal that is 5 to 15 cm thick (Figure 9c–f).

In the ESLLB, FS3 overlies a strong greenish white strongly developed paleosol (C/Z mot cem) that represents an unconformity (Figure 3d). In the ESLLB, FS3 is the continental equivalent of the shallow marine FS2 succession in the WSLLB.

FS3 is also present in Oligocene basal sands (Figure 10g) and the C7 and C6 Members of the Carbonera Formation. (Figure 11a5, 11b1, 11c7). In the Lower Oligocene strata in the Llanos Basin, this facies contains high abundances of *Botryococcus* spp. as well as few marine palynomorphs (foraminifer lining tests), suggesting lacustrine to brackish environments.

In the NMS, this succession is scarcely present in the lower-middle section of the La Paz Formation (Figure 4f), the middle section of the Esmeraldas Formation (Figure 12b1), and at the top of this unit in the Los Corros fossil horizon. The palynological record of the Los Corros fossil horizon in the MMB (Figure 12b4) shows a relative abundance of freshwater algae (*Pediastrum* spp., *Botryococcus* spp.), suggesting a lacustrine environment (Rodríguez–Forero et al., 2012).

The carbonaceous mudstone was deposited by vertical accretion in ponded water with a large contribution of vegetal carbonaceous material. This mudstone is a marginal paralic deposit that formed in coastal plain swamps and marshes or along the margins of lacustrine environments (Cecil, 1990). The poorly drained conditions in coastal and fluvial plains can lead to reducing conditions that preserve organic matter (Shanley & McCabe, 1994).

3.2.4. Facies Succession 4 (FS4): Strongly Developed Paleosol

This succession is composed of facies F12. FS4 is composed of white to greenish cream silty claystone that is strongly pedogenized (C/Z mot cem) and kaolinitic in composition. This succession is a very mature and well-developed paleosol composed of ferricrete or silcrete. Root traces, nodules, and crusts are common (Figures 2a, 3d, 9a, 9b). This paleosol is 1 to 6 m thick in some wells in the Llanos Basin, but its thickness is variable across the basin. This paleosol is located at the top of the Paleocene, Cretaceous, or Paleozoic units in cores from the southern Llanos Basin. In the Middle Magdalena Basin, below the La Paz Formation, the equivalent paleosol is varicolored, including whitish gray and violet, sometimes with white vertical pedogenic features and nodules of calcium carbonate.

We interpret this unit to be the result of subaerial exposure of the preexisting substrate and weathering over a long period of time. This type of paleosol forms during periods of landscape degradation and/or episodes of landscape stability that may last more than one million years (Kraus, 1999). This kind of paleosol can form during a period of base level fall; thus, it is called an interfluvial paleosol and marks a sequence boundary (Kraus, 1999). The genesis of this kind of paleosol is related to allogenic controls, such as base level changes, global or regional climate changes, and/or regional tectonics.

3.2.5. Facies Succession 5 (FS5): Coastal Plain–Backshore Compound Paleosol

This succession is composed of facies F4, F10, and/or F13. This facies succession includes rooted, muddy, fine- to coarse-grained sandstone (mS rt) covered by a layer of carbonaceous mudstone (M lam org) and/or coal layers. This facies succession is 0.5 m to 4.30 m thick in the lower Eocene rocks of the Mirador Formation in the WSLLB (Figure 8b, 8c), but it is less than 1.5 m thick in the ESLLB (Figure 9e, 9f). The carbonaceous mudstone is bioturbated with *Planolites* and *Glossifungites* below the sandstones of the next depositional cycle in the ESLLB.

Tandon & Gibling (1994) identified this type of profile with studding cyclothems and called them seat earths, which

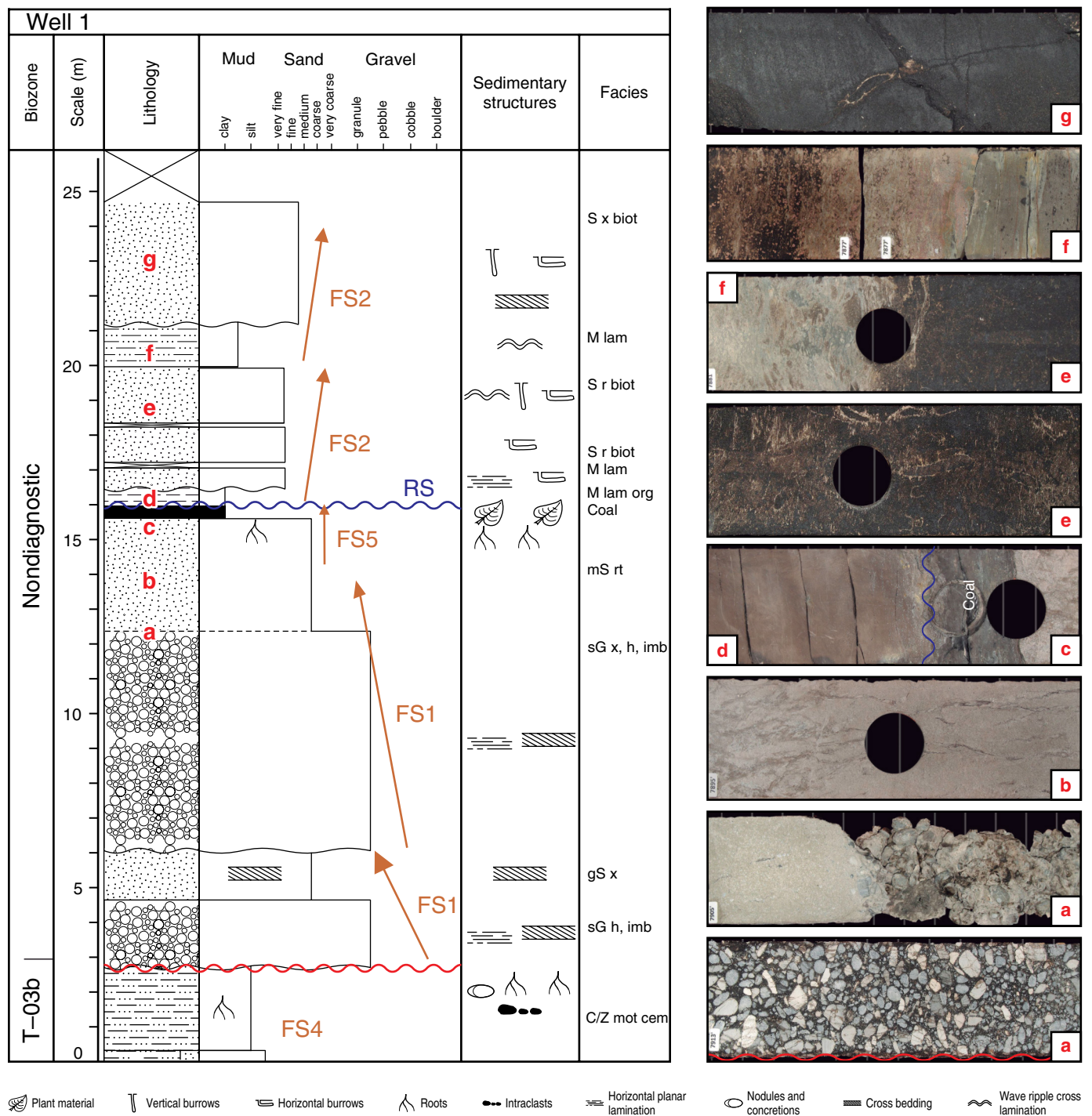


Figure 8. Lower – middle Eocene fluvial marginal and marine facies successions of the Mirador Formation in the WSLLB (well 1). Stacked braided channel and bar sands of the facies succession (FS1) disconformably overlie a strongly developed paleosol (FS4) of the Cuervos Formation. FS1 is capped by a coastal plain compound paleosol horizon (FS5) that is capped by coal. Here, the ravinement surface (RS) erodes the coal bed. After the ravinement surface are two cycles of a shallow marine, low-energy shoreface facies succession (FS2). There is a significant change in thickness of the fluvial facies successions with respect to Sagú Creek (Figure 7). The facies indicated by letters a to g are shown in the right column.

correspond to soils underlying coal seams, but most of them are weakly developed, vertically stacked profiles in aggradational systems (Kraus, 1999). This situation appears to be the case in the southern Llanos Basin and NMS, in which the

paleosols developed as sedimentation proceeded. The sedimentation was sporadic and rapid, erosion was insignificant, and pedogenic processes had short periods of time to act on the substrate.

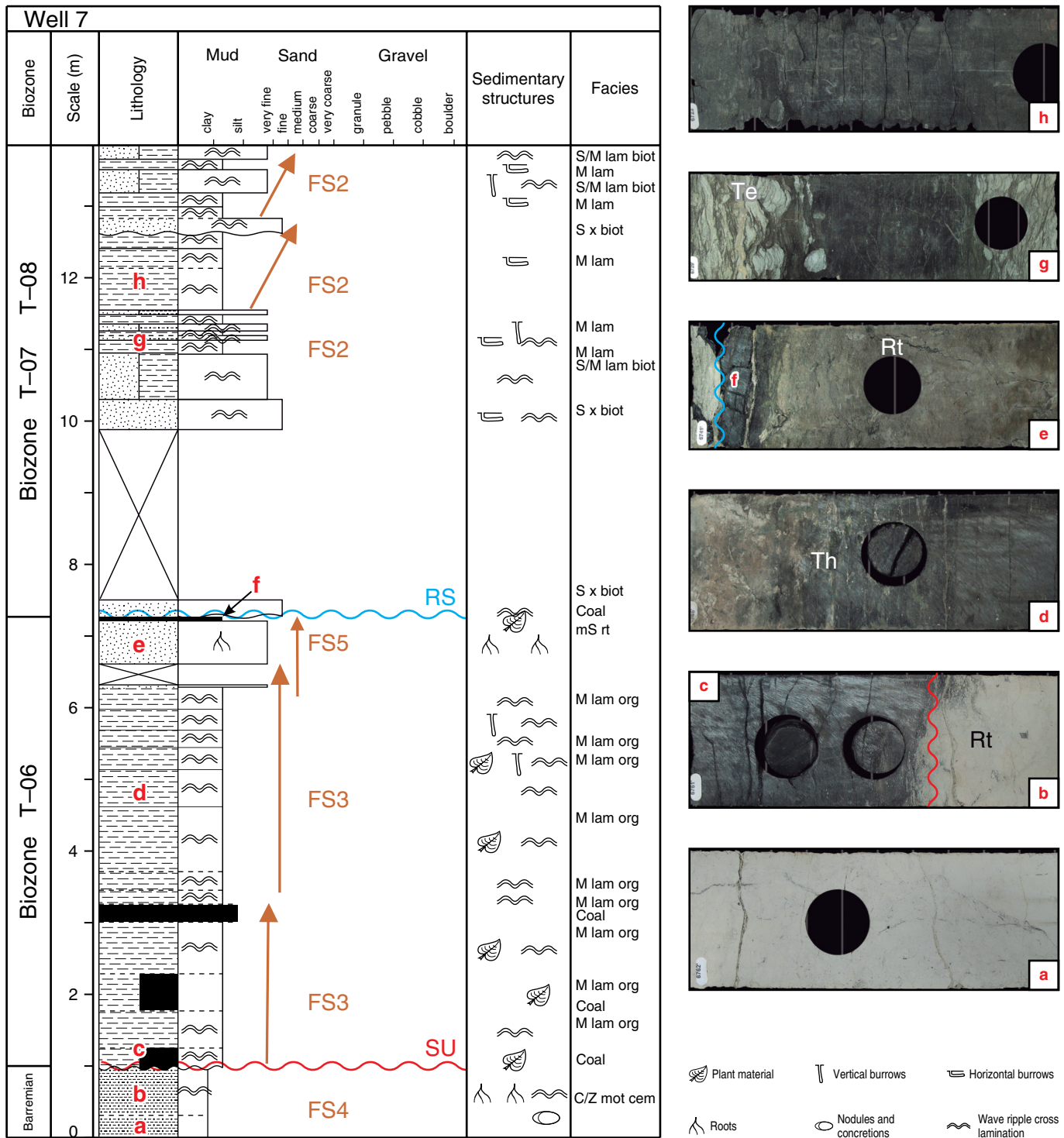
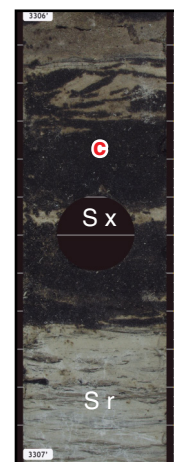
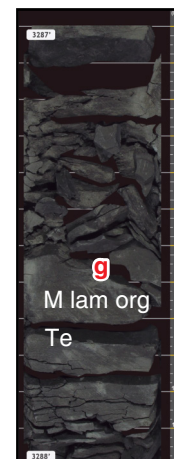
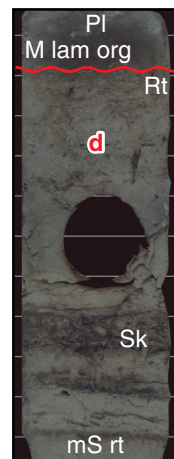
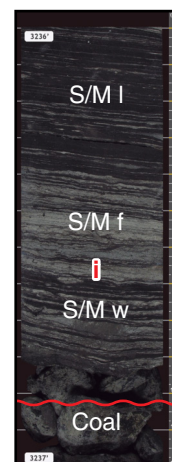
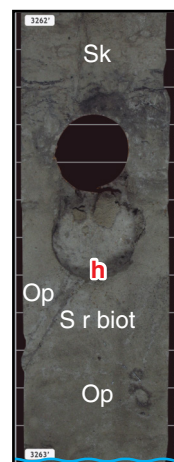
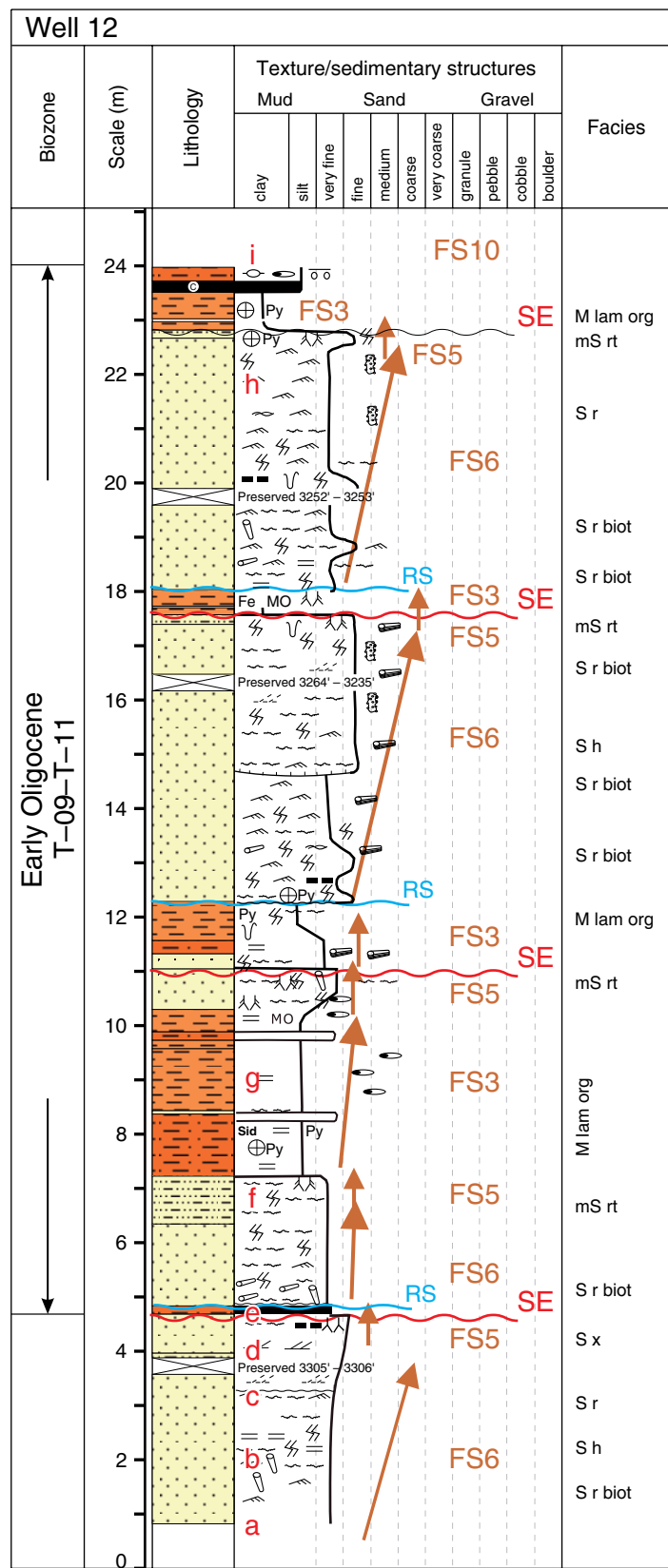


Figure 9. Middle – upper Eocene continental and marginal marine facies in well 7 in the ESSLB. From the base to the top: strongly developed paleosol (FS4) on rocks of the Cuervos Formation (the red line shows the unconformity). Above the unconformity, we interpreted two cycles of backshore swamp–lacustrine deposits (FS3) capped by a coastal plain compound paleosol (FS5). The ravinement surface (blue line) erodes a thin coal layer and marks the beginning of several marine facies successions (FS2). The facies indicated by letters a to h are shown in the right column. (Te) *Teichichnus*; (Th) *Thalassinoides*; (Rt) root traces.

In the studied areas, this facies corresponds to a paleosol profile that developed over a sandstone substrate (abandoned



- Lenticular lamination
- Planolites
- Contemporary penile deformation
- MO Organic material
- ✂ Ghosts of roots
- ✂ Ripples
- Py Pyrite
- ✂ Undifferentiated bioturbation
- ✂ Wave ripple
- ✂ Wavy bedding
- ✂ Skolithos
- ✂ Paleophycus
- ✂ Flat parallel lamination
- ✂ Relict of cross bedding
- ✂ Fragments of carbonaceous material
- ✂ Undifferentiated burrows
- ✂ Teichichnus
- ✂ Ophiomorpha
- ✂ Cross stratification
- Sid Siderite nodules
- ⊕ Nodules
- Fe Iron oxides



Figure 10. Lower Oligocene basal sandstones of the Carbonera Formation from well 12 in the ELLB; these strata are coeval with the shales of the C8 Member in the WLLB. Four facies successions that consist of shoreline successions (FS6) are overlain by a backshore compound paleosol (FS5) separated by subaerial exposure surfaces (SE). The backshore swamp–lacustrine deposit (FS3) oscillates around the compound paleosol (FS5) between the first and second (FS6–FS5) successions. At the top of the core, we interpreted mudstone/sandstone (FS10) as estuarine intertidal flat deposits above an exposure surface. The facies indicated by letters a to i are shown in the right column. (Sk) *Skolithos*; (Op) *Ophiomorpha*; (Pl) *Planolites*; (Rt) root traces; (Pa) *Paleophycus*; (Gl) *Glossifungites*; (Te) *Teichichnus*.

paleosol was preserved as a thin layer of coal or became part of the carbonaceous mudstone once poorly drained conditions occurred because of the rise in the water table.

This paleosol developed on the fluvial braided facies (FS1) (Figure 8b, 8c), but in some wells, the carbonaceous mud or coal is absent because it was eroded by the transgressive erosion surface, such as at Sagú Creek (Figure 7d). In well 7 in the ELLB, this paleosol profile covers the middle Eocene backshore swamp or lacustrine deposit (FS3) (Figure 9e, 9f). In the easternmost wells of the ELLB, FS5 is at the top of the prograding shoreline sandstones of the Oligocene basal sandstone member of the Carbonera Formation (Figures 10d, 11a4, 11b6). Finally, this facies succession covers fluvial channel sandstones of the C7 Member of the Carbonera Formation (Figure 11c4, 11c5).

3.2.6. Facies Succession 6 (FS6): Prograding Open Shoreline Succession

This succession is composed of facies F5, F3, and F2. The typical succession is composed of very fine- to fine-grained sandstones with wavy ripples (S r, S r biot) and very fine- to fine-grained sandstones with horizontal laminations (S h, S h biot), which are sometimes bioturbated by *Skolithos*, *Ophiomorpha*, and *Teichichnus*. These fine-grained sandstones are overlain by cross-bedded medium sandstone (S x) (Figure 10a–c). The thickness of the unit succession is between 5 and 8 m, but it repeats several times to reach nearly 40 m of sands. This facies succession is common in the Oligocene basal sandstones of the C8 Member of the Carbonera Formation toward the ELLB. In some cycles, the shallowing-upward open shoreline succession (FS6) is capped by a coastal plain–backshore compound paleosol (FS5) and then by backshore swamp facies (FS3) (Figures 10a–e, 11a1–a6, 11b3–b6). This facies succession is not present in the NMS.

FS6 is interpreted as a progradational cycle unit, but it contains sets that have a retrogradational pattern as the transgression continues to the east. This succession was deposited during high-frequency cycles of base level rise/fall that generated repeated progradational deposits (Clifton, 2006). FS6 is interpreted as a stacking of high-frequency cycles that occurred during the transgression, probably forming an estuary. This facies could be the marginal or transitional equivalent to the FS2 facies succession, which is composed of subaqueous shoreface deposits.

Its development responds to a balance between sedimentation and base level rise, when sedimentation is greater than base level rise, prograding distributary mouth bars (deltaic settings) or prograding shoreface deposits (open shoreline settings) are present. If sedimentation is less than base level rise, retrogradation of the shoreline occurs, and an estuary forms. If sedimentation is much less than base level rise, the transgression advances toward the continent, putting foreshore–shoreface sandstone over marsh to swamp or backshore deposits through a ravinement surface (Clifton, 2006).

3.2.7. Facies Succession 7 (FS7): Fluvial Floodplain–Cumulative Paleosol

This succession is composed of facies F11 and F4. FS7 consists of variegated clayey mudstone (facies cM rt mot) that is one to 30 meters thick. FS7 is identified by the presence of root traces, bioturbation that masks the primary sedimentary structures, a mottled aspect, and very thick intervals. FS7 commonly includes rooted mottled muddy fine to coarse sandstone (mS rt) interlayered within variegated mudstones (Figures 5c, 6f).

In the NMS, the floodplain deposits begin to appear in the lower Eocene lower-middle section of the La Paz Formation (Figure 12a2) and continue in the lower part of the Esmeraldas Formation (Figure 12b1). FS7 resumes in the Oligocene rocks of the Mugrosa Formation and continues in the units above (Figure 13).

FS7 was deposited in a fluvial floodplain. The interlayering with rooted muddy sandstones (mS rt mot) is typical of crevasse splay and flooding events that were deposited on the floodplain. Simultaneously with the steady sedimentation, pedogenesis occurred by subaerial exposure and development of vegetation with low rates of erosion. Because floodplains are regularly flooded over geologic time, this process decreases the rate of pedogenesis (Krauss, 1999).

The varicolored or variegated color was produced by oscillation of the water table on the floodplain and concomitant oxidation or reduction of the soil, producing ferric or ferrous iron, respectively. Gray colors (reducing conditions) formed when the water table was high and the substrate was drowned, whereas red, orange, or yellow colors (oxidizing conditions) occurred when the water table was low and air entered the well-drained soil.

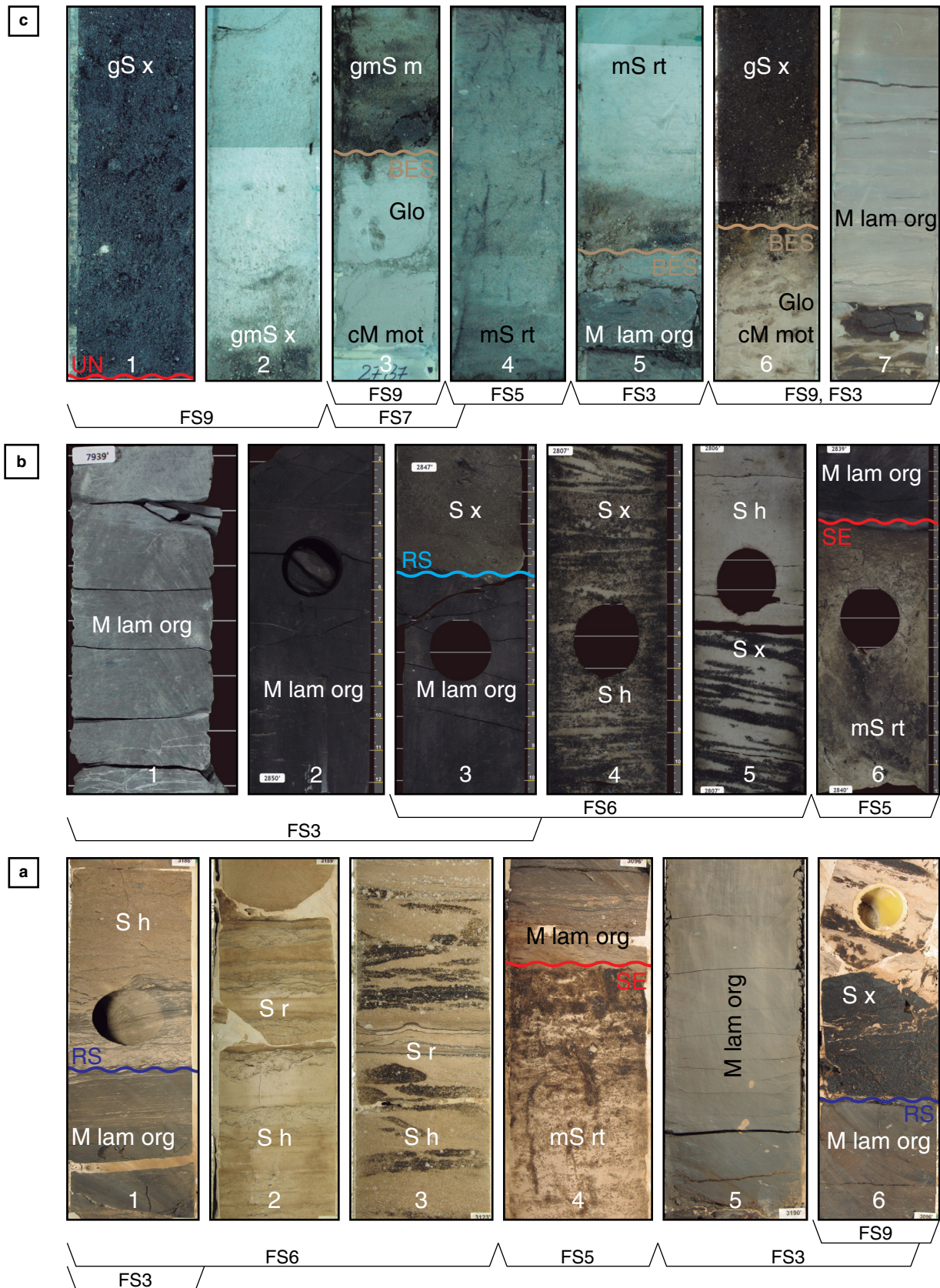




Figure 11. (a, b) Oligocene basal sandstones of the Carbonera Formation in the ESLLB (see location in Figures 1 and 15). **(c)** Is from the C7 Member of the Carbonera Formation. **(a)** Well 10 showing, from left to right, backshore swamp–lacustrine deposits (FS3) eroded by a ravinement surface (RS). Above the RS is a prograding shoreline succession (FS6) capped by a coastal plain–backshore compound paleosol (FS5), which indicates subaerial exposure (SE). After the SE, backshore swamp–lacustrine deposits (FS3) complete a prograding cycle. Another cycle begins at the ravinement surface below a mouth bar sandstone (FS9). These cycles are 5–8 m thick. **(b)** Well 11 showing, from left to right, the same cycle as that described previously: backshore swamp–lacustrine deposits (FS3) eroded by a ravinement surface and overlain by a prograding shoreline succession (FS6) capped by a coastal plain–backshore compound paleosol (FS5), indicating subaerial exposure, and then, backshore swamp or lacustrine mudstone (FS3). **(c)** Well 13 showing the C7 Member of the Carbonera Formation. The base of C7 is an unconformity (UN), and the unit consists of fluvial cycles that begin on a basal erosion surface (BES). From left to right, fluvial channel and bar sandstones (FS9) are capped by a coastal plain–backshore compound paleosol (FS5) and then backshore swamp or lacustrine mudstone (FS3) or floodplain cumulative paleosol (FS7). (Glo) *Glossifungites*.

3.2.8. Facies Succession 8 (FS8): Crevasse Splay to Sheetflood Deposits

This succession consists of facies F2, F3, and F4. FS8 is composed of planar–bedded, massive or small–scale cross–stratified sandstone (mS h, mS m, S x, mS rt) and sometimes rooted sandstone in gradational contact with the variegated mudstones (cM m, cM rt mot, cM lam) of the cumulative paleosol (FS7). These sandstone beds have limited lateral extents of tens of meters. Crevasse splay successions are less than 1 m thick and up to 6 m thick when stacked (Figure 13b, 13c). These deposits do not have evidence of erosion, and because they are unconfined, there is no evidence of sand bar development. The sedimentary structures change upsection from planar/massive bedding to ripple lamination.

In the lower and middle section of the Esmeraldas Formation (Figure 12b1) and Oligocene Mugrosa Formation (Figure 6f, 6i, 6j), FS8 includes beds of muddy sandstone or gravelly muddy sandstone with planar or massive bedding (mS h, mS m) over floodplain mudstones (FS7).

The association with floodplain mudstones and the limited thickness and lateral extent are interpreted as evidence of crevasse splays in a fluvial system or sheetflood deposits in alluvial fan and fluvial plain systems. Some channels form sandstone bodies in erosive contact with floodplain mudstones, and the scour and fill structures can be interpreted as distributary channels in an alluvial fan (Figure 13d). Planar bed deposits or massive muddy sand sheets between the floodplain mudstones are interpreted as sediment gravity flows, such as sheetflow deposits associated with hyperconcentrated flows (Figure 13c) (Blair & McPherson, 1994).

3.2.9. Facies Succession 9 (FS9): Fluvial Meandering Channel and Bar Deposits

This succession consists of facies F1, F2, and F5. FS9 consists of facies (gmS x or mS m) with erosive bases (in most cycles, only a conglomeratic lag) followed by trough cross–bedded, very coarse–grained sandstone to planar cross–bedded medi-

um–grained sandstone (S x), and finally current ripple sandstone (S r) or a compound paleosol (FS5).

The progression from large–scale trough cross–bed sets to smaller–scale planar cross–bed sets in sandstone and to finer–grained ripple sandstone is attributed to waning flow on a point bar of a meandering channel. These point bars form along the concave part of a meander by helicoidal flow in the channel that erodes the outer concave bank toward the inner convex bank. This helical flow component transports sediment up the sloping bank and adjacent point bars. Only gravel is deposited in the base of the channel; the remaining sediment is transported laterally to construct a point bar (Boggs, 1987).

This facies succession was interpreted in the C7 Member of the Carbonera Formation in the ESLLB (Figure 11c), which contains a typical fining–upward succession from erosional lag, channel, floodplain, and/or crevasse deposits.

FS9 was observed in the NMS at the top of the lower section of the La Paz Formation, where it is 5 to 14 m thick (Figure 12a2). In the Esmeraldas Formation, it is 3 to 30 m thick and is tidally influenced (Figure 12b2, 12b3), and in the Oligocene Mugrosa Formation, it is 1 to 3 m thick (Figure 13f).

3.2.10. Facies Succession 10 (FS10): Estuarine Intertidal Deposits

This succession consists of facies F5, F7, and F10. FS10 is composed of current ripple–laminated fine sandstone (S r) in beds less than 1 m thick, sometimes with bidirectional cross–laminations (Figure 5e). FS10 contains layers of heterolithic sandstone/mudstone (S/M), which consists of fine– to very fine–grained well–sorted sandstones interlayered with medium gray mud and rhythmic with wavy (S/M w), lenticular (S/M l), and flaser laminations (S/M f) approximately 1 to 10 m thick. This facies also includes thick layers of carbonaceous mudstone (M lam org) (Figure 5f).

This facies was deposited in an estuarine intertidal flat environment, where sand layers accumulated during periods of current activity, and mud accumulated during slack water periods



Figure 12. Fluvial facies successions of the La Paz and Esmeraldas Formations in the Sucio River, eastern flank of the NMS. **(a)** La Paz Formation fluvial facies successions, including from the base to the top: (1) stacked cycles of single-story to multistory braided channels and bars (FS1); (2) single channel fill and floodplain cumulative paleosol (FS9, FS7); (3) crevasse splay floodplain swamp facies succession (FS8, FS7); and (4) stacked braided channel and bar facies successions (FS1). **(b)** Esmeraldas Formation coastal plain to lacustrine successions. From base to top: (1) fluvial meandering point bar crevasse and floodplain swamp facies (FS9, FS7); (2, 3) 4–8 m thick meandering tidal unit bar; and (4) backshore swamp–lacustrine fill deposit (FS3) in a lacustrine to fluvial tidal environment (FS10). (Mdst.) mudstone; (Ss.) sandstone; (Cgl.) conglomerate; (Fm.) Formation.

(Reineck & Singh, 1973, Nio & Yang, 1991). In the NMS, FS10 is described in the Esmeraldas Formation. The interpretation of an estuarine environment is strengthened by the discovery of stromatolitic structures in the sandstones of the Esmeraldas Formation (Figure 5i). In the Llanos Basin, this facies succession is present in the C8 Member of the Carbonera Formation (Figure 10i).

The deposition of mud and sand in these strata requires that both sand and mud were available in the environment and that periods of current activity alternated with periods of still water (Reineck & Singh, 1973). These environments occur when base level rises near a river mouth, the mouth is flooded, and the deposits are tidally influenced (Boyd et al., 2006).

The difference with the laminated and bioturbated sandstone/mudstone (S/M lam biot) described previously is the preservation and type of sedimentary structures. In the S/M lam biot facies, organic structures predominate over the physical structures, which are wavy to horizontal laminations, whereas in the S/M w, l, f facies, physical structures predominate over organic structures, and the physical structures are flaser, lenticular, and wavy bedding. Another difference is the ichnogenera present in the S/M lam biot, which is not present in the S/M w, l, f facies.

3.3. Distribution of Facies, Stratigraphic Surfaces, and Facies Trends

We first identify and describe the correlation surfaces that have stratigraphic significance because these surfaces mark changes in facies and define the architecture of the bodies of the rocks in the Llanos Basin and MMB. Facies trends refer to how facies change over time, and the changes are recorded in the bounding surfaces; these changes could be from erosion, aggradation, progradation, or retrogradation. All of these changes are responses of the sedimentary system to the controls of tectonics, eustasy, and climate as reflected in base level change or relative sea level change (Catuneanu, 2006).

The distributions of the facies in the two study areas were determined by sequence stratigraphic correlations supported by available biostratigraphy data (biozones) and the facies analysis and successions described previously to develop a sequence stratigraphic framework.

3.4. Stratigraphic Surfaces and Markers

3.4.1. Interfluvial Paleosol below the Subaerial Unconformity

The strongly developed paleosol (FS4) is a stratigraphic marker in the studied basins. The strongly developed paleosol is located below the subaerial unconformity at the base of the Lower Mirador and La Paz Formations. The paleosol drapes an interfluvial ancient landscape in the southern Llanos Basin and NMS and was identified on the Paleocene, Cretaceous, Paleozoic, and older rocks in the southern Llanos Basin (Figure 15) and over Jurassic and Cretaceous rocks on the La Cira–Infantas–Sogamoso Paleohigh in the MMB (Figure 18). This paleosol may have been eroded in the main trunk valleys in the ancient fluvial landscape.

3.4.2. Subaerial Unconformity at the Base of the Mirador and La Paz Formations

The subaerial unconformity (SU) at the base of the Mirador Formation is present in all of the wells studied in the southern Llanos Basin and foothills of the Eastern Cordillera. This surface is located above the mature, well-developed FS4 paleosol. The subaerial unconformity is diachronous because it puts upper Paleocene rocks in contact with lower Eocene rocks in the foothills and WSLB, but in the ESLB, it puts upper Paleocene rocks in contact with middle Eocene or younger rocks to the east (Figures 14, 15).

The subaerial unconformity at the base of the La Paz Formation is identified by its lacuna with the units below, especially in the western part of the MMB (Rodríguez–Forero et al., 2012). In the NMS, the basal conglomerates of FS1 from the La Paz Formation are in erosive contact with the Lisama Formation (Figures 16, 17). In the MMB, the unconformity is an erosive and diachronous surface that truncates Paleocene, Jurassic, and Cretaceous rocks on the axial La Cira–Infantas–Sogamoso Paleohigh (LCISP) in the Magdalena Valley and the basement rocks in the Central Cordillera (Figure 18) (Suárez, 1997; Gómez et al., 2003, 2005a).

3.4.3. Transgressive Ravinement Surface

The transgressive erosion surface or transgressive ravinement surface (Catuneanu, 2006) puts the fining-upward facies suc-

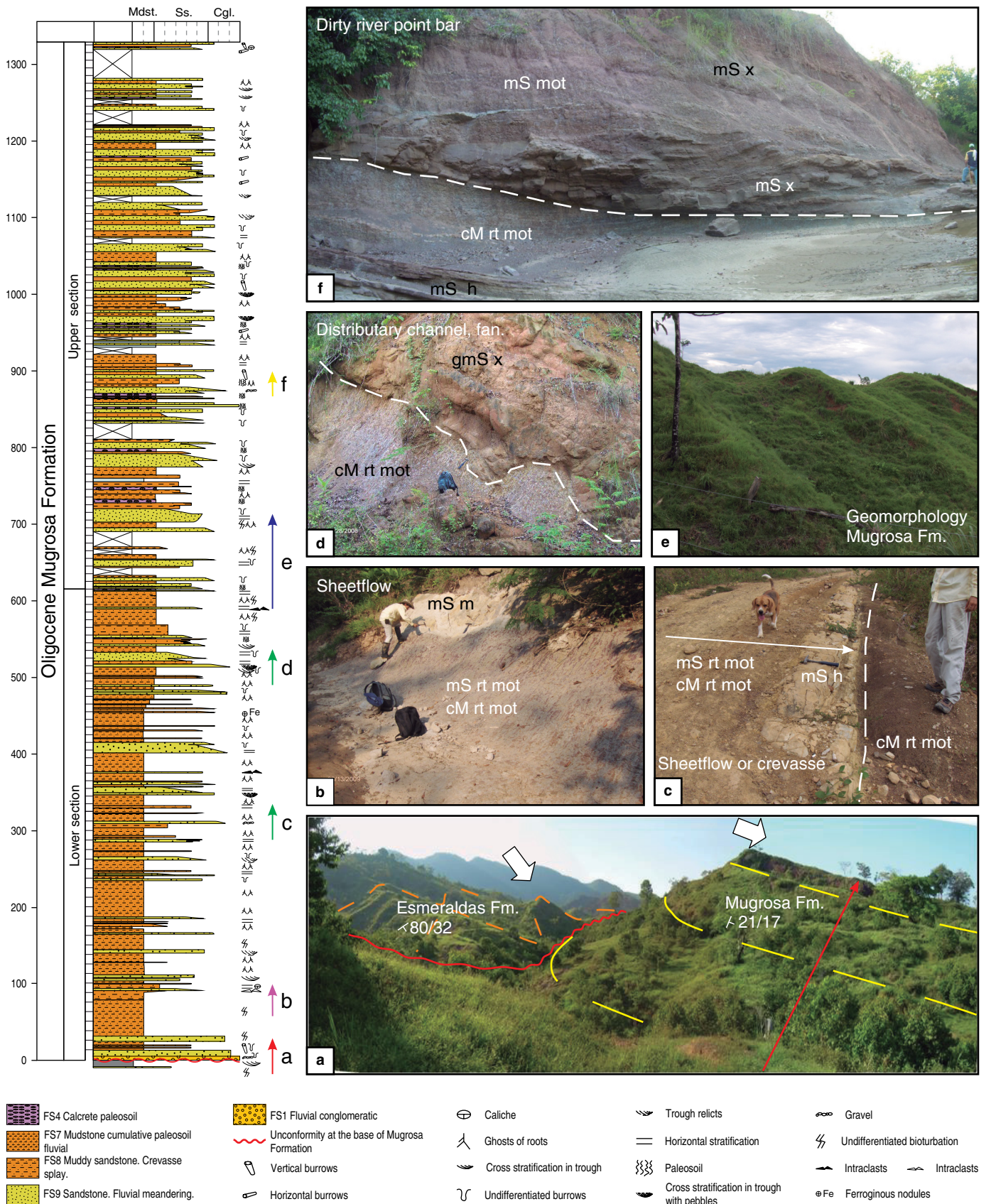


Figure 13. Oligocene fluvial to alluvial facies successions in the NMS. The lower section of the Mugrosa Formation is mainly composed of variegated to reddish brown floodplain deposits (FS7) with embedded thin fluvial channel sandstones (FS9) and a crevasse splay or sheetflood succession (FS8). In general, the Mugrosa Formation is a coarsening-upward alluvial plain succession. **(a)** Field view of the unconformity between the Mugrosa Formation and the overlying Esmeraldas Formation (red line) on the western limb of the NMS. **(b, c)** Solitary sheetflow deposit (FS8) interbedded with floodplain deposits (FS7). **(d)** Fluvial channel facies FS9 scouring and filling fluvial flood plain cumulative paleosol FS7. **(e)** Present geomorphology after subaerial exposure of the Mugrosa Formation. **(f)** Meander point bar deposit FS9 eroding fluvial floodplain cumulative paleosols of FS7 which overlay crevasse splay deposits FS8. (Mdst.) mudstone; (Ss.) sandstone; (Cgl.) conglomerate; (Fm.) Formation.

cession of the Lower Mirador below (Figures 7, 8) in contact with coarsening-upward, shallow marine facies successions of the Upper Mirador Formation and the lower C8 Member of the Carbonera Formation above. The transgressive ravinement surface is a diachronous surface. In the WSLLB, this event occurs in the middle Eocene and erodes lower Eocene fluvial deposits, whereas in the ESLLB, it occurs during the late Eocene and reworks the previous subaerial unconformity in wells 5, 6, and 8 (Figures 14, 15).

In the Middle Magdalena Valley, the facies contact between the La Paz and Esmeraldas Formations corresponds stratigraphically to the ravinement surface in the southern Llanos Basin. However, in the NMS, the contact is conformable and marks a change in facies and stacking pattern from multistory braided fluvial sandstones to floodplain cumulative paleosols. This change is from facies successions deposited under low accommodation conditions in the La Paz Formation to a facies succession deposited under high accommodation conditions in the Esmeraldas Formation.

3.4.4. Flooding Surfaces

Three maximum flooding events formed maximum flooding surfaces (MFSs) in the southern Llanos Basin. The MFSs can be identified in wells and delineated by identifying the maximum peaks in the gamma ray logs and by changes in the log patterns. These maximum flooding surfaces occur in the lower and upper parts of the C8 Member and the upper part of the C6 Member of the Carbonera Formation. At least two of them are truncated by the overlying unconformities.

The MFS in the lower C8 Member of the Carbonera Formation coincides roughly with the Eocene – Oligocene boundary. This MFS is truncated by the unconformity at the base of the Oligocene basal sandstones (Figure 15). The MFS in the upper C8 Member of the Carbonera Formation is truncated by the unconformity at the base of the C7 Member (Figure 15). The latest Oligocene MFS within the C6 Member of the Carbonera Formation is at the top of the sandstones of the C6 Member of the Carbonera Formation. Its continuity eastward was not determined in this work, but it may be truncated to the east.

In the Nuevo Mundo Syncline, the maximum flooding surface was interpreted to occur during a period of high accommodation space within the lacustrine coastal plain facies

(FS3) and estuarine intertidal facies (FS10) of the Esmeraldas Formation, roughly corresponding with the Los Corros fossil horizon (Figures 12b4, 16). The fossil markers of Los Corros, Mugrosa, and Cira have been reported as flooding events in the MMB (Morales, 1958; Gómez et al., 2005a).

3.4.5. Oligocene Unconformities in the Carbonera and Mugrosa Formations

The lower lower Oligocene unconformity at the base of the basal sandstones of the C8 Member of the Carbonera Formation in the ESLLB is an erosive contact between the Oligocene basal sandstones above the shales of the lower segment of the C8 Member of the Carbonera Formation (Figure 14). This surface marks a change in the stacking patterns and a transposition of facies from coarsening-upward marine facies to fining-upward open shoreline to fluvial and estuarine facies in the basal sandstones. This unconformity was previously identified in the foothills and in the WSLLB at the base of the T1, an operational name for the basal sandstones of the Carbonera Formation (Malagón, 1997) (Figure 15).

The upper lower Oligocene unconformity is at the base of the C7 Member of the Carbonera Formation and corresponds to an erosive contact, a transposition of facies, and a change in the stacking pattern from coarsening-upward shelf mudstones and sandstones (FS2) of the upper C8 Member to fining-upward fluvial facies (FS1–FS5) of the C7 Member. This unconformity is observed in the GR pattern, especially in the eastern part of the Llanos Basin (Figure 15). This surface is not well constrained in the central part of the basin and the ESLLB.

The Mugrosa–Esmeraldas contact is an unconformity that occurs at the Eocene – Oligocene boundary. On the eastern limb of the NMS, this unconformity is erosive with the Esmeraldas Formation truncated by fluvial facies (FS1) of the overlying Mugrosa Formation (Figure 6a). There is a facies transposition from lacustrine and tidal flat estuarine facies (FS3–FS9) of the Esmeraldas Formation to alluvial facies (FS1, FS7, FS8) of the Mugrosa Formation. On the western limb, the Mugrosa Formation overlaps the Esmeraldas Formation on what has been reported as a growth unconformity (Gómez et al., 2005a) (Figure 13a). In the MMB, this unconformity was previously identified as a regional unconformity at the base of tectonosequence 2 of Suárez (1997) (Figure 17a, 17b, 17c).

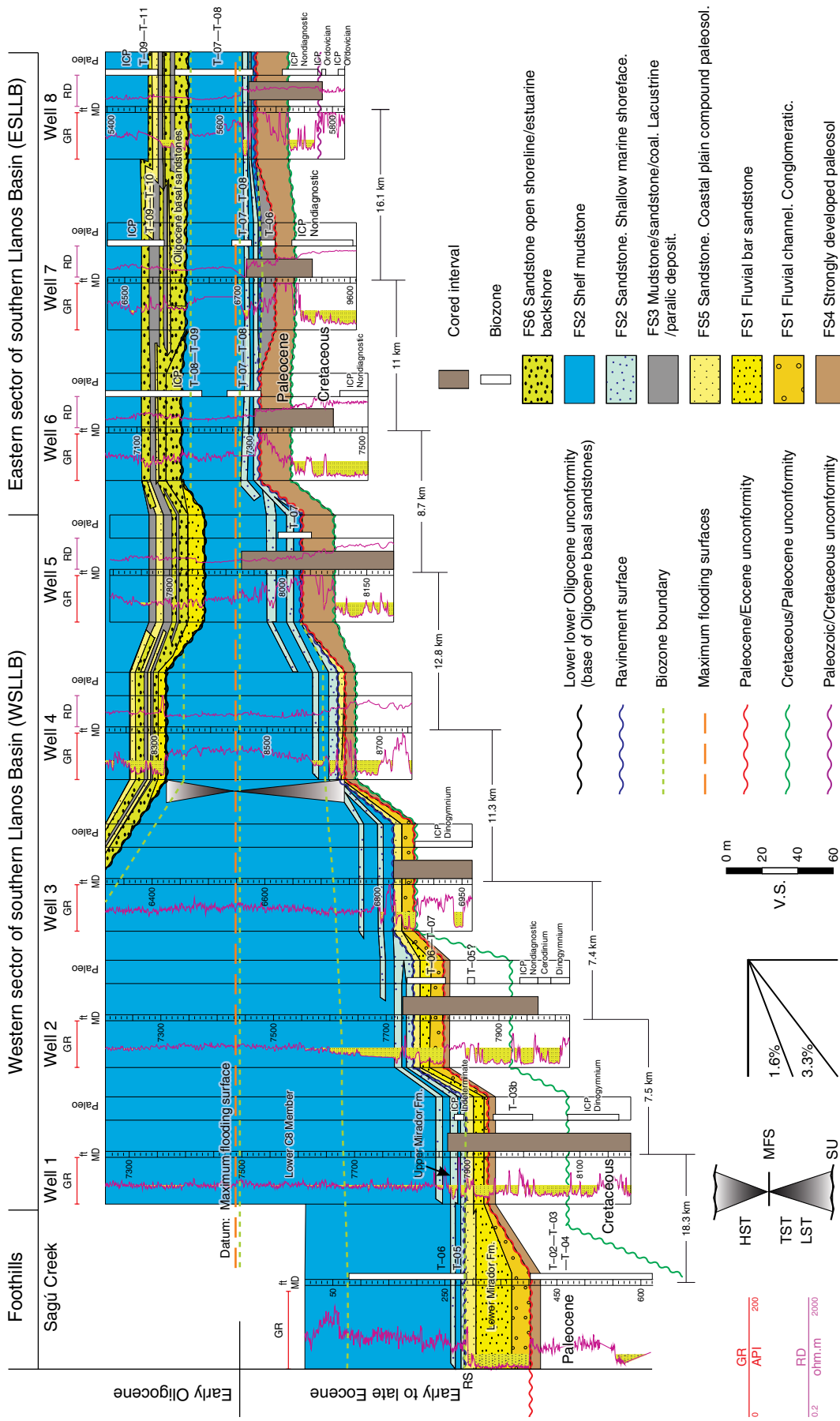


Figure 14. Distribution of facies in the southern Llanos Basin. The strongly developed paleosol (FS₄) is diachronous and puts upper Paleocene rocks in contact with lower Eocene rocks in the WSLB and upper Paleocene rocks in the ESLLB. The Lower Mirador Formation becomes younger to the east and includes fluvial to marginal sediments (FS₁, FS₅) of early – middle Eocene age. The middle Eocene backshore swamp and lacustrine facies cover the relief of the unconformity in well 7. The ravinement surface erodes the Lower Mirador Formation and records the onset of a marine transgression across the basin. The marine facies include facies successions (FS₂) that preserved a pre-Eocene landscape. In the earliest Oligocene, several foreshore-backshore facies successions (FS₆, FS₃), called the Oligocene basal sandstones here, advanced westward. These are part of the C8 Member of the Carbonera Formation in the WSLB. The correlation datum is the maximum flooding surface at the Eocene – Oligocene boundary. (GR) gamma ray; (MD) measured depth; (RD) deep resistivity; (ICP) Instituto Colombiano del Petróleo; (Fm.) Formation; (HST) highstand systems tract; (MFS) maximum flooding surface; (TST) transgressive systems tract; (LST) lowstand systems tract; (SU) subaerial unconformity.

3.5. Facies Trends in the Eocene – Oligocene

3.5.1. Early Eocene: Lower Mirador and La Paz Formations

The Lower Mirador and La Paz Formations consist of amalgamated braided channel–fill sandstones (FS1) above a subaerial unconformity. FS1 fines upward and forms an aggradational multistory sandstone complex with scarce floodplain deposits (Figures 7, 8, 12a1). The Lower Mirador and La Paz Formations lap onto (fluvial onlap; Catuneanu, 2006) the subaerial unconformity (Figures 14, 18). The Lower Mirador Formation is capped by an erosion surface, which is the ravinement surface. In the southern Llanos Basin, these braided facies are covered by a sandy coastal plain backshore compound paleosol (FS5), and in the NMS, the fluvial facies of the La Paz Formation are covered by a muddy floodplain cumulative paleosol (FS7) (Figures 14, 16).

The Lower Mirador wedge is 35 m thick at Sagú Creek and pinches out in well 4, 38 km to the east (Figure 14). In the MMB, the La Paz Formation was deposited on both margins of the basin and pinches out above the axial La Cira–Infantas–Sogamoso Paleohigh. The western wedge is 580 m thick near the Cantagallo Fault and pinches out above the LCISP, approximately 18 km to the east. The eastern wedge is 1090 m thick on the eastern limb of the NMS and pinches out 38 km to the west above the axial LCISP (Figure 18) (Suárez, 1997; Gómez et al., 2005a; Caballero, 2010).

The porosity and permeability were measured in several conglomerates of the Lower Mirador Formation in the southern Llanos Basin. The porosity of the basal muddy conglomerates of the Mirador Formation varies from 6.4 to 9.1%, and the permeability is very low (0.8–0.81 mD). These properties are very different in the fluvial multistory sandstones of the Lower Mirador Formation; the porosity is 10–20 %, and the permeability is 100–10 000 mD.

The porosity and permeability in the La Paz Formation in the eastern part of the MMB vary from 10 to 20% and from 100 to 1500 mD, respectively. In the Provincia Field, these properties vary from 8 to 16.7% and from 13.6 to 409.2 mD, respectively (Suarez, 1997). The Cantagallo sandstones, which are the equivalent of the La Paz Formation in the western part of the MMB, have porosities of 15–25 % and permeabilities of 100–1000 mD.

The porosity of the fluvial facies of the Mirador Formation in the Cusiana Field varies from 7.7 to 11.7%, and the permeability varies between 33.4 and 402 mD, although these values differ in different high–frequency cycles (Fajardo, 1995).

3.5.2. Middle to Late Eocene and Earliest Oligocene: Upper Mirador Formation, Lower C8 Member of the Carbonera Formation

During the middle Eocene, coarsening–upward, shallow marine low–energy shoreface facies (FS2) were deposited in the foothills

and the WSLLB, whereas backshore swamp to lacustrine facies (FS3) were deposited in the topographic lows of the interfluvial area of the ESLLB (see well 7 in Figure 14). The marine facies lap onto the ravinement surface above the Lower Mirador Formation in the WSLLB, and the backshore swamp to lacustrine facies lap onto the subaerial unconformity above the strongly developed paleosol (FS4) in the eastern part of the ESLLB. By the late Eocene and earliest Oligocene, FS2 reached the El Melón High to the east, onlapping the previous backshore facies and the paleosol (FS4) on the topographic highs. The maximum flooding surface formed at the end of the Eocene. After the maximum flooding surface, deposition of progradational facies (FS2) of the C8 Member of the Carbonera Formation resumed, but they were truncated by the lower lower Oligocene unconformity at the base of the Oligocene basal sands in the El Melón High (Figures 14, 15).

This landward shift of the facies forms a transgression with a retrogradational stacking pattern, in which high–order coarsening–upward facies (FS2) lap onto the ravinement surface and advance toward the margins of the basin. These lithologies preserve part of a previous landscape that was created in the late Paleocene in the ESLLB (Figures 14, 15). This wedge–shaped transgressive unit is 213 m thick in well 1 and pinches out on the El Melón High (Well 9) approximately 110 km to the east (Figure 15).

The porosity varies from 5 to 7%, and the permeability varies from 1 to 60 mD in the medium– to fine–grained, cross–bedded, bioturbated sandstones facies of the Upper Mirador Formation in the Cupiagua Oil Field (Ramon & Fajardo, 2006). In the southern Llanos Basin, the Upper Mirador sandstones have porosities between 5 and 15% and permeabilities of 0.1–100 mD. Adjacent to the El Melón High in the ESLLB, the porosity of FS2 in the upper Eocene sandstones is 20–25 %, and the permeability is 100–10 000 mD.

3.5.3. Middle – Upper Eocene: Esmeraldas Formation

In the Middle Magdalena Valley, the Esmeraldas Formation consists of fluvial meandering channel and bar sandstones (FS1) and fluvial floodplain–cumulative paleosols (FS7), which transition to very thick fluvial tidally influenced meandering channels and bar sandstones (FS9) intercalated with fluvial tidally influenced floodplain or intertidal deposits (FS7, FS10) with a retrogradational trend. These facies then transition to intertidal sandstones/mudstones (FS10) and lacustrine mudstones (FS3) with channelized tidal meandering sandstones (FS9). These tidally influenced fluvial deposits are temporally equivalent to marine maximum flooding surfaces. Near the top, meandering sandstones (FS9) intercalated with lacustrine and intertidal mudstones (FS3, FS10) are observed in a progradational trend until the contact with the Mugrosa Formation (Figures 12b2, 16).

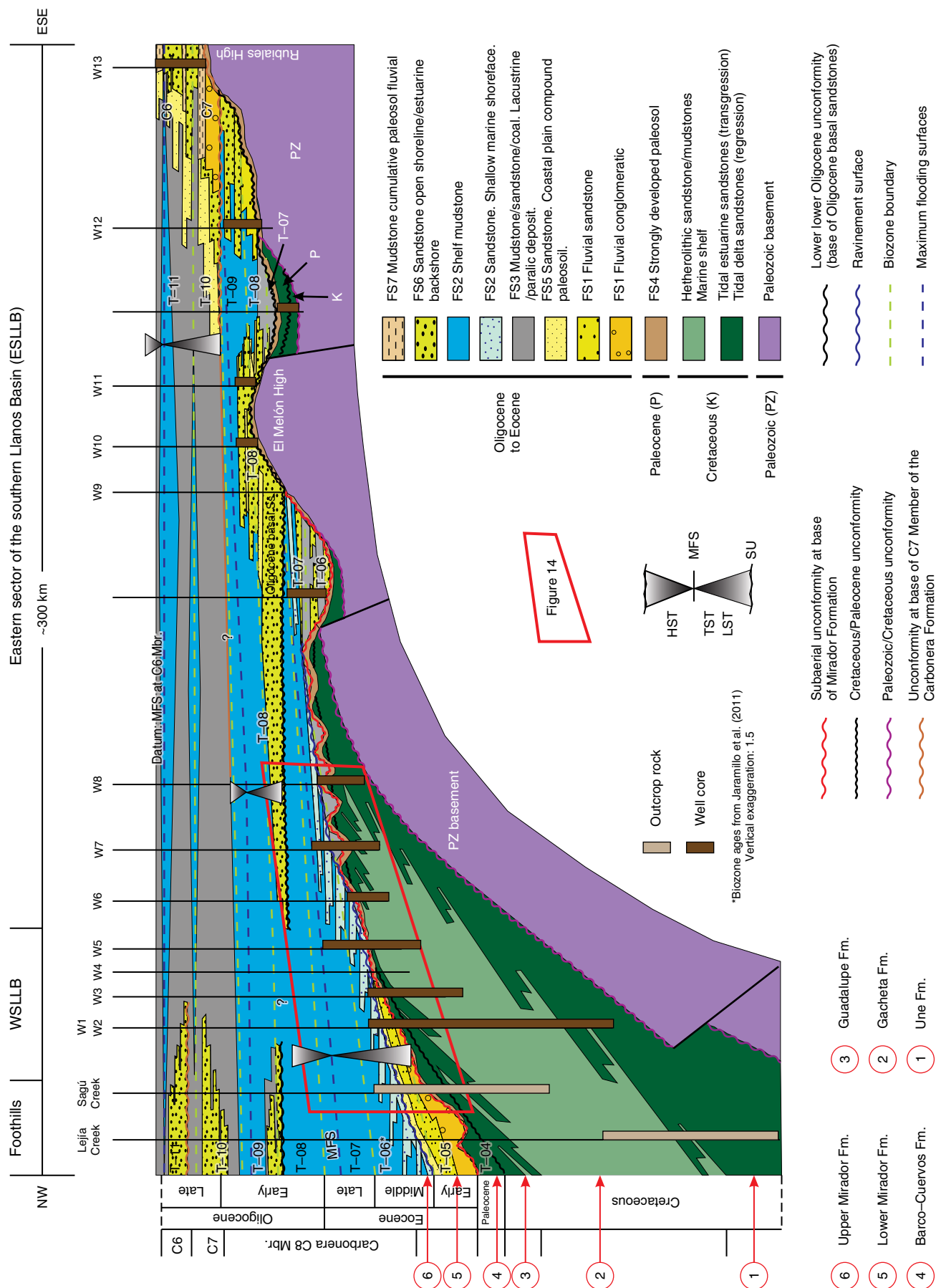


Figure 15. Regional schematic stratigraphic correlation showing the facies trends and depositional sequences in the southern Llanos Basin (see well location in Figure 1d). Three depositional sequences are shown in the correlation: (i) Between the unconformity above the strongly developed paleosol and the lower lower Oligocene unconformity; the LST is the Lower Mirador Formation, the TST is the Upper Mirador Formation and lower C8 Member, the MFS is in the shales of the C8, and the HST is the shales of the lower C8 Member eroded in the ESLLB. (ii) Between the lower lower Oligocene unconformity and the base of the C7 unconformity; the LST is the Oligocene basal sandstones, the TST is the shales of the upper C8 Member, and the HST is the progradational shales of the C8 Member. The MFS is between these shales. (iii) Only the LST–TST that comprises the C7 and C6 Members of the Carbonera Formation is shown. The MFS is on the shales of the upper part of the C6 Member. The Eocene – Oligocene wedge is 1044 thick in the foothills and 93 m thick on the Rubiales High. Graphic is not to scale. (WSLLB) western sector of the Llanos Basin; (MFS) maximum flooding surface; (Mbr.) Member; (Fm.) Formation; (Ss.) sandstone; (HST) highstand systems tract; (TST) transgressive systems tract; (LST) lowstand systems tract; (SU) subaerial unconformity.

During the middle to late Eocene, the Esmeraldas Formation drapes and pinches out toward the Central Cordillera, and it was deposited in most of the MMB. This wedge reaches a thickness of 1255 m in the NMS and thins to 50 m in well Yariguí-1 in the western of the MMB (Suárez, 1997). This wedge fossilized the landscape throughout which the fluvial system of the La Paz Formation established in early Eocene (Figure 18) (Suárez, 1997; Gómez et al., 2005a; Caballero et al., 2013b; Reyes–Harker et al., 2015). The reservoir sandstones of the Esmeraldas Formation have porosity between 10–20 % and 100–200 mD of permeability.

3.5.4. Oligocene

3.5.4.1. Early Oligocene: Oligocene Basal Sandstones and Upper C8 Member of the Carbonera Formation

Above the lower lower Oligocene unconformity, several fining-upward high-order cycles and facies successions (FS6–FS5–FS3) were deposited in the ESLLB, whereas in the WSLLB, these shallowing-upward facies successions are separated by subaerial exposure surfaces and minor ravine surfaces, as described in the cores from wells 10 and 11 (Figures 10, 11a, 11b). This basal high-frequency cycle was deposited in erosional contact as a progradational wedge above the unconformity, whereas the upper sets have a retrogradational pattern until the MFS. These facies are sandier over the El Melón and Rubiales High.

At the end of the early Oligocene and the beginning of the late Oligocene, FS2 of the upper part of the C8 Member of the Carbonera Formation retrograded over the basal sandstones. The thickness of this unit between the lower lower Oligocene unconformity and the base of the C7 Member of the Carbonera Formation unconformity is 277 m in the WSLLB, 120 m on the El Melón High, and it pinches out on the Rubiales High 210 km to the east (Figure 15). The average porosity of the Oligocene basal sandstones around the El Melón High varies between 20 and 30%, and the permeability varies between 1000 and 10 000 mD.

3.5.4.2. Late Oligocene: C7 and C6 Members of the Carbonera Formation

Several fining-upward fluvial cycles were deposited above the upper lower Oligocene unconformity; these cycles form the C7 Member of the Carbonera Formation. The fluvial cycles consist of granule sandstones (FS9) capped by a coastal plain compound paleosol (FS5), backshore swamp–lacustrine fill (FS3), and/or fluvial floodplain deposits (FS7). The fining-upward fluvial to coastal plain cycles of the C7 Member of the Carbonera Formation were deposited in a progradational pattern, but the upper C6 cycles are coarsening-upward in a retrogradational pattern until the MFS at top of the C6 Member of the Carbonera Formation (Figures 11c, 15).

The C7 and C6 Members of the Carbonera Formation are fluvial and sandier toward the easternmost part of the southern Llanos Basin and muddier and paralic toward the center of the basin. In the southern part of the LLB, the thickness varies from 554 m in well 1 to 150 m on the El Melón High and 93 m in well 13 on the Rubiales High (Figure 15).

In the fluvial sandstones of the C7 Member of the Carbonera Formation on the Rubiales High, the porosity varies from 25 to 30%, and the permeability varies between 100 and 10 000 mD.

3.5.4.3. Oligocene: Mugrosa Formation

The Mugrosa Formation begins with fluvial sandstones that unconformably overlie the Esmeraldas Formation on the eastern and western flanks of the NMS (Figures 13, 17). The Mugrosa Formation consists mainly of a fluvial floodplain cumulative paleosol (FS7) with embedded fluvial channel sandstones (FS1). The cumulative paleosol includes levels of calcareous calcrete paleosol and sheetflood deposits (FS8) in a coarsening-upward, progradational stacking pattern (Figures 13, 16).

In the southern MMB, the Mugrosa Formation consists of decimeter- to meter-scale cross-bedded sandstone beds that grade upward into thick layers of variegated mudstones with caliche and paleosols (Gómez et al., 2003). In the northern part of the basin, floodplain variegated mudstones (cumulative pa-

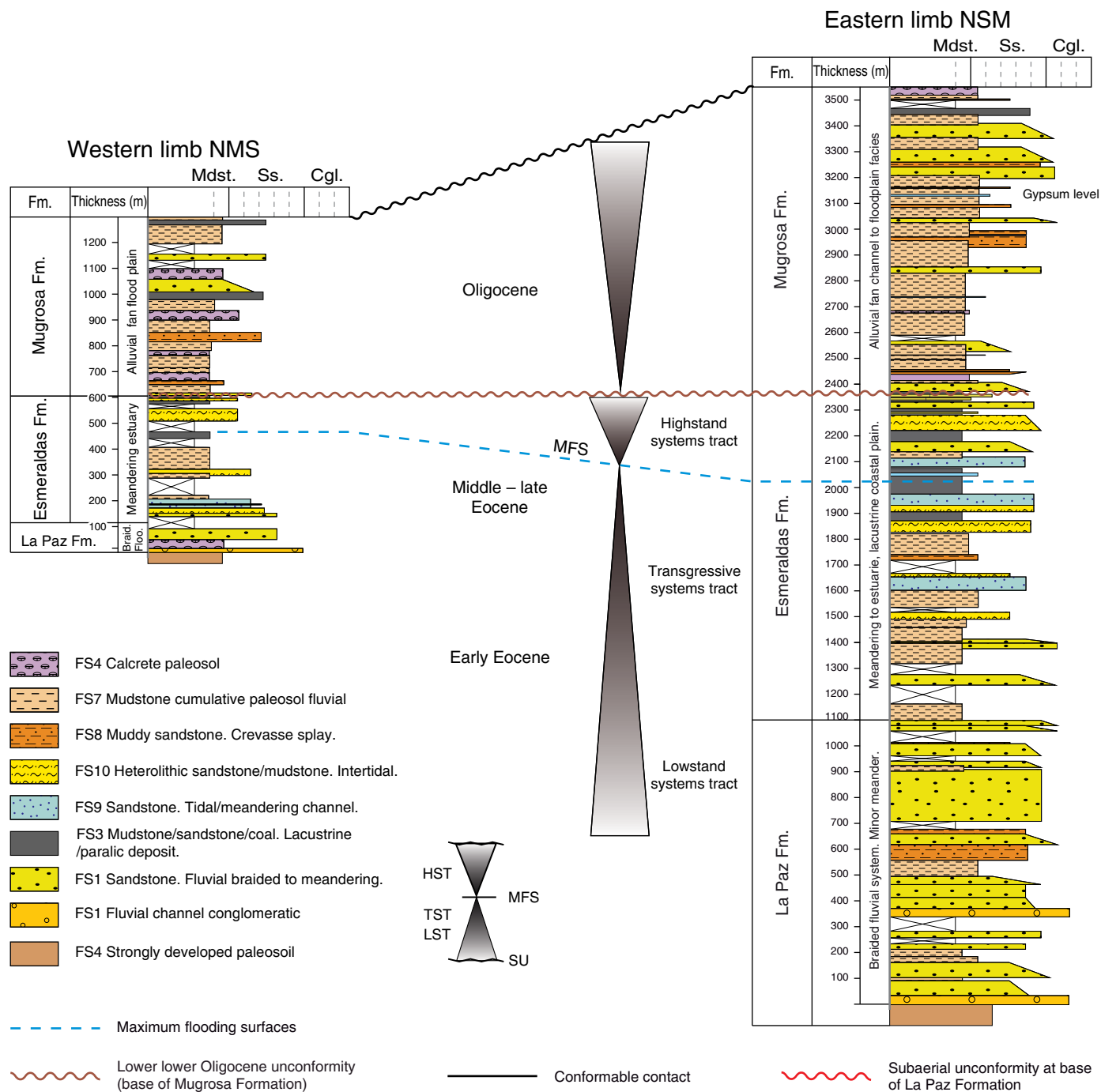


Figure 16. Correlation of Eocene to Oligocene units in the NMS. One depositional sequence and a nonmarine HAST are shown. (i) Braided to meandering facies successions (FS1, FS7, and FS8) in the lower Eocene La Paz Formation form the LST; these fluvial facies transition to floodplain, fluvial to estuarine and lacustrine facies (FS1/FS9, FS7, FS10, FS3) of the Lower–Middle Esmeraldas Formation and compose the TST. The MFS is on estuarine–lacustrine facies in the upper part of the Esmeraldas Formation; the HST is composed of the progradational upper part of the Esmeraldas Formation. (ii) The HAST is composed of the Oligocene Mugrosa Formation, which is composed of sheet sandstones, a cumulative paleosol, distributary channels in alluvial bajadas, calcrete paleosols in the fluvial plain, and a few meandering channel and crevasse splay facies successions (FS7, FS4, FS9). The wedge–shape geometry of the units indicates tectonic control on deposition with more accommodation space on the eastern limb. The location of the correlation is shown in Figure 1c. (HAST) high–accommodation systems tract (Catuneanu, 2006); (Mdst.) mudstone; (Ss.) sandstone; (Cgl.) conglomerate; (Fm.) Formation; (MFS) maximum flooding surface; (HST) highstand systems tract; (TST) transgressive systems tract; (LST) lowstand systems tract; (SU) subaerial unconformity.

leisol) with channelized sands were deposited in the Mugrosa Formation (Suárez, 1997). The thickness of the Mugrosa Formation varies from 1330 m on the eastern limb of the NMS to 700 m on the eastern limb of the NMS and 580 m in the Yariguí Field, and it pinches out to the northwest (Suárez, 1997) (Figure 17a).

The porosity in the Mugrosa Formation in the Cantagallo area varies between 15 and 25%, and the permeability varies from 10 to 1000 mD; in the provincial area, the Mugrosa Formation has porosities of 8–15 % and permeabilities of 70–150 mD.

4. Discussion

4.1. Latest Paleocene – Earliest Eocene Fluvial Landscape

The subaerial unconformity identified at the base of the Lower Mirador Formation in the southern Llanos Basin records a time interval of subaerial exposure, nondeposition, or erosion (lacuna) as well as intense weathering. The unconformity at the base of the La Paz Formation in the MMB records the same conditions that were previously identified (Gómez et al., 2003, 2005a) and is equivalent in age and stratigraphic position to the unconformity in the southern Llanos Basin.

The strongly developed paleosol identified in this study records subaerial exposure with intense weathering in the interfluvial areas of a fluvial landscape at the end of the Paleocene. The paleosol is well preserved in the interfluvial sectors and is ubiquitous in the southern Llanos Basin, although it varies in thickness based on its topographic position in the landscape in the latest Paleocene. Erosion or deposition halted its development along trunk valleys and incised valleys where it was truncated, but it was preserved in the interfluvies, where pedogenic processes were dominant and erosion was not significant. The strongly developed paleosol at the base of the La Paz Formation on the western limb of the NMS is called the Toro shale (Caballero, 2010; Caballero et al., 2010); this soil corresponds to that described by Morales (1958) in the MMB. Several similar cases have been studied in other basins and different geological periods, in which interfluvial paleosols are correlated with incised valley fills along strike (Aitken & Flint, 1996; O'byrne, & Flint, 1996) and form a sequence boundary.

The unconformity was initially identified in the central foothills of the Eastern Cordillera. In the Cusiana area, this unconformity is present at the base of the Lower Mirador Formation (Fajardo, 1995; Ramon & Fajardo, 2006) and above a deep paleosol (Pulham et al., 1997). Recently, a paleosol in the same stratigraphic position was reported in a well core in the northern foothills (Bayona et al., 2015). The paleosol was reported to be late Paleocene – early Eocene in age and developed on volcanoclastic deposits.

Previous studies have identified tectonic deformation and uplift during the late Paleocene and earliest Eocene in the Central Cordillera, MMB, and western flank of the Eastern Cordillera (Gómez et al., 2003, 2005a; Parra et al., 2012; Bayona et al., 2013; Caballero et al., 2013b). Other studies have identified the reactivation of older structures on the eastern flank of the Eastern Cordillera (Bayona et al., 2013; Mora et al., 2013) and within the southern Llanos Basin and Llanos Foothills, where the Mirador Formation unconformably overlies Cretaceous rocks (Mora et al., 2013).

We interpret that the tectonic activity during the latest Paleocene – earliest Eocene resulted in the development of a subaerial fluvial landscape over the MMB, EC, and Llanos Basin. The landscape consisted of paleohighs in the MMB (La Cira–Infantas–Sogamoso Paleohigh) and low–relief highs on the western and eastern flanks of the Eastern Cordillera, the axial Eastern Cordillera, and the southern Llanos Basin and Llanos Foothills. This tectonic activity caused a fall in base level, and by the early Eocene, at least three trunk fluvial incised valleys (main trunk valleys) flowed north to northeast. These fluvial valleys were located in the Middle Magdalena Valley, the axial Eastern Cordillera, and the WSLB (Figure 18). This fluvial system configuration was proposed previously (Bayona et al., 2013).

4.2. Early Eocene Lowstand Systems Tract

The Paleocene tectonic activity continued into the early Eocene (Parra et al., 2012; Mora et al., 2013; Bayona et al., 2013). Accommodation space was available along the main trunk valleys and localized incised valleys on the flanks of the growing tectonic structures. The La Paz, Upper Socha–Picacho, and Lower Mirador Formations were deposited in these incised fluvial valleys. The incised valley model was previously interpreted for the Cusiana area to the north (Pulham et al., 1997). This model is supported by the fluvial onlap of the Lower Mirador and La Paz Formations onto a truncated, strongly developed paleosol, the geometry and stacking pattern of the sandstones, and the low rate of accommodation space generation, as indicated by the fluvial braided facies.

Compound and cumulative paleosols were deposited at the top of the Lower Mirador and La Paz Formations; these paleosols suggest that the accommodation space was slowly increasing and that the sedimentation was almost constant. This slow increase in accommodation space was likely due to the large volumes of sediment from the increasing influence of the exhumed La Cira–Infantas Paleohighs in the axial Magdalena Basin, the low–amplitude uplifts in the axial Eastern Cordillera and the uplifts in the southern Llanos Basin. These conditions promoted progradation of facies onlap onto the paleotopography. The configuration of the lowstand systems tract (LST) and the compound and cumulative paleosols

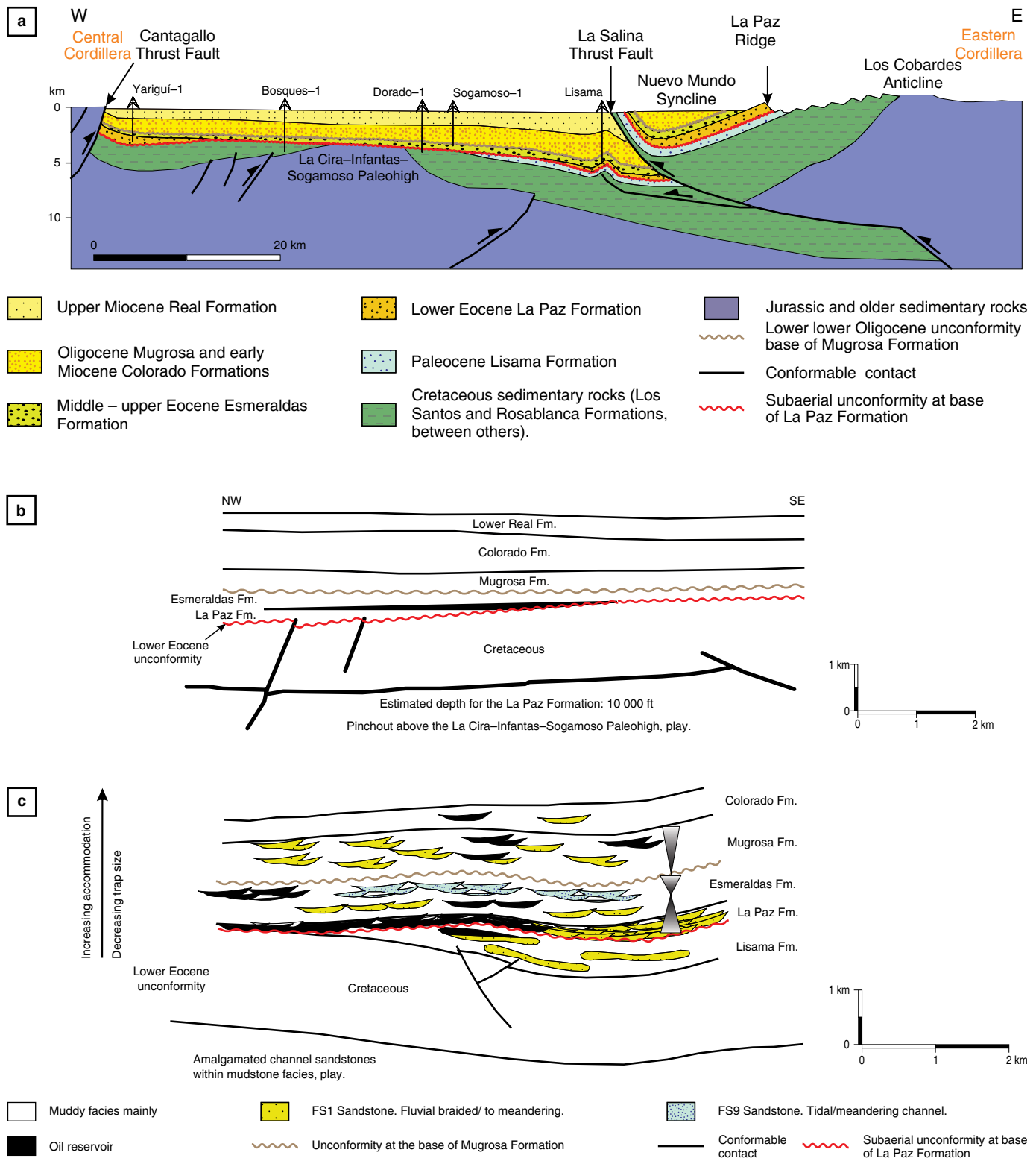


Figure 17. Regional schematic stratigraphic sections showing the facies trends and depositional sequences in the MMB. **(a)** Stratigraphic section between the eastern and western areas of the MMB. **(a)** The La Paz Formation was deposited above a subaerial unconformity on the two margins of the MMB and by a topographic high, the La Cira-Infantas-Sogamoso Paleohigh (LCISP). The Esmeraldas Formation covers and preserves the pre-existing topography. The Mugrosa was deposited after a period of erosion represented by the lower lower Oligocene unconformity (after Gómez et al., 2005a). **(b, c)** Types of stratigraphic plays in the Eocene – Oligocene units. **(b)** Pinchout of amalgamated sandstones FS1 of the La Paz Formation above the LCISP. Modified from Suárez (1997). **(c)** Amalgamated channel belts (FS1 or FS9), embedded within mudstones of: cumulative paleosol in Mugrosa and Colorado Formations and swamp to lacustrine or estuarine intertidal in Lisama and Esmeraldas Formations. Location in Figure 19. Modified from Suárez (1997). (Fm.) Formation.

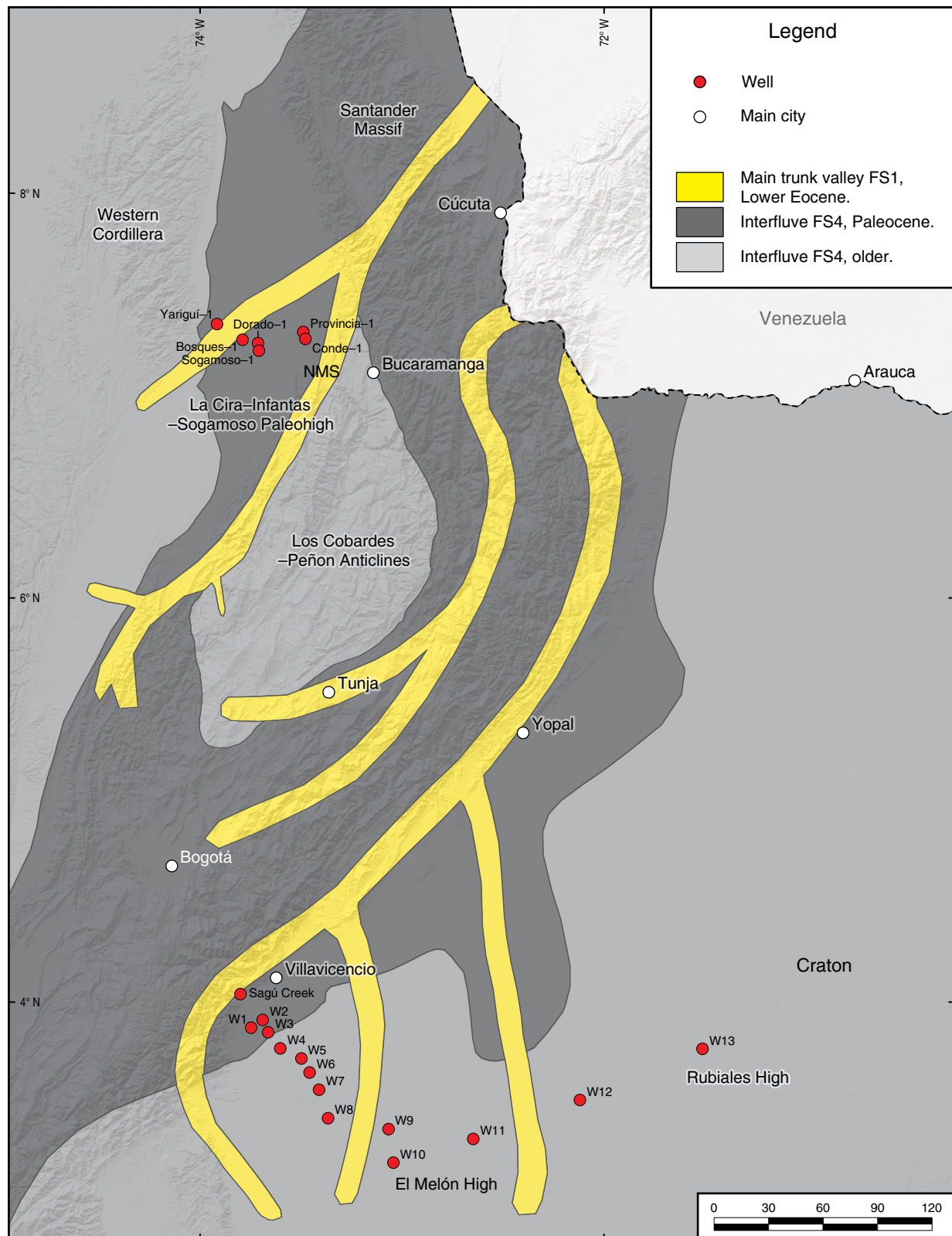


Figure 18. Interpreted paleogeographic configuration at the end of the Paleocene. As the result of tectonic uplift and the resulting base level fall, three incised trunk valleys developed in a fluvial continental landscape; these valleys were located in the MMB, the axial Eastern Cordillera, and the Llanos Basin. Between the fluvial valleys, the subaerially exposed interfluvial area allowed the development of the strongly developed paleosol (FS4) over Paleocene and older rocks. Modified from Bayona et al. (2013). (NMS) Nuevo Mundo Syncline.

indicate subaerial exposure at the end of the early Eocene, likely due to the progradation of fluvial facies over the pre-existing topography.

The LST was completely deposited by the end of the early Eocene and occupied two depocenters, one in the Eastern Cordillera and the western Llanos Basin and the other in the Magdalena Basin. The morphology at the end of the early Eocene was a wider coastal – fluvial plain in the southern Llanos Basin and NMS (Figure 19).

4.3. Middle – Late Eocene Transgressive Systems Tract

According to previous studies, during the middle – late Eocene, tectonic deformation and loading advanced to the Eastern Cordillera (Bayona *et al.*, 2008, 2013; Parra *et al.*, 2009b; Mora *et al.*, 2010; Saylor *et al.*, 2012b), and the Santander Massif began to be uplifted, initially from the northwestern area toward the southeastern area of the massif (Caballero *et al.*, 2013a; 2013b; Mora *et al.*, 2015). The tectonic loading prompted flexural subsidence on both flanks of the Eastern Cordillera and established the conditions for the base level to rise and allow the marine waters to transgress into the southern Llanos Basin. On the western margin of the EC, the base level rose, and marine tidal waters eventually drowned the fluvial system to form an estuarine and then lacustrine system during the late Eocene in the NMS and Middle Magdalena Valley Basin (Caballero *et al.*, 2013a, 2013b; Mora *et al.*, 2013; Reyes–Harker *et al.*, 2015). This lacustrine system is recorded in the Los Corros fossil horizon (Morales *et al.*, 1958; Gómez *et al.*, 2005a). The change in facies succession between the La Paz and Esmeraldas Formations indicates a base level rise from a fluvial plain to a coastal plain with a meandering tidally influenced estuarine system and finally intertidal flats with lacustrine deposition systems in the NMS (Figure 20).

In the southern Llanos Basin, the Upper Mirador Formation and the lower part of the C8 Member of the Carbonera Formation recorded the marine transgression. These units form the transgressive systems tract (TST) in the MMB and Llanos Basins. The TST is limited by the ravinement surface and the MFS in the lower C8 Member of the Carbonera Formation. The highstand systems tract (HST) of this first sequence is the least well preserved by the erosion of the earliest Oligocene unconformity, but it consisted of prograding marine facies of the lower section of the C8 Member (Figure 20).

The integration of facies analysis and depositional trends and the sedimentary environments support previous interpretations of the configuration of the middle – late Eocene paleogeography (Bayona *et al.*, 2013; Caballero *et al.*, 2013b; Silva *et al.*, 2013; Reyes–Harker *et al.*, 2015) and its extent toward the Maracaibo Basin and to the Maracaibo shoreline (Figure 21). The middle – late Eocene marine ingressions were also previous-

ly identified in the central Llanos Foothills and the axial Eastern Cordillera (Cooper *et al.*, 1995; Villamil, 1999; Bayona *et al.*, 2008; Santos *et al.*, 2008). The connection of this marine–lacustrine embayment system with the sea was discussed previously (Santos *et al.*, 2008; Jaramillo *et al.*, 2011; Rodríguez–Forero *et al.*, 2012).

4.4. Oligocene Divergent Stratigraphic Histories

Accelerated exhumation of the Floresta and Santander Massifs (Bayona *et al.*, 2008; Parra *et al.*, 2009b; Mora *et al.*, 2015) and the entire Mesozoic ancestral graben in the Eastern Cordillera (Parra *et al.*, 2009a, 2009b; Mora *et al.*, 2010; Saylor *et al.*, 2011, 2012a) occurred during the Oligocene. At this time, the MMB became a closed basin between the Santander Massif, the western flank of the Eastern Cordillera, and the Central Cordillera. The Oligocene facies record in the MMB indicates tectonic and climate controls on deposition of the alluvial Murgosa Formation and no control of the regional base level by the Maracaibo Sea (Caballero *et al.*, 2013a, 2013b) (Figure 21).

In the foothills and the Llanos Basin, the tectonic loads of the Eastern Cordillera resulted in accelerated flexural subsidence and increased accommodation space. The previous shallow marine conditions of the late Eocene continued through the Oligocene. The subsidence in the foothills and WSLB drove the deposition of the upper part of the C8 Member of the Carbonera Formation under shallow marine shelf conditions, whereas in the ESLLB, the basal Oligocene sandstones were deposited above an unconformity. These deposits likely indicate that increased flexural subsidence occurred in the western part of the southern Llanos Basin (foredeep), whereas to the east, flexural uplift (forebulge) is recorded in the unconformity at the base of the Oligocene basal sandstones (Figure 21).

The second depositional sequence is composed of Oligocene basal sandstones and shales of the upper C8 Member of the Carbonera Formation between the lower lower Oligocene unconformity and the unconformity at the base of the C7 Member of the Carbonera Formation. The LST–TST corresponds to the Oligocene basal sandstones of the Carbonera Formation between the lower lower Oligocene unconformity and the maximum flooding surface; the HST corresponds to the shales (FS2) of the upper part of the C8 Member of the Carbonera Formation between the MFS and the upper lower Oligocene unconformity at the base of the C7 Member of the Carbonera Formation.

The rapid subsidence and prevailing marine conditions during the early Oligocene were also interpreted in previous studies in the northern Llanos Basin and Medina Basin (Bayona *et al.*, 2008; Parra *et al.*, 2009a).

The fluvial – coastal plain and lacustrine conditions reached the southern Llanos Basin by the late Oligocene with the deposition of the C7 and C6 Members of the Carbonera Formation

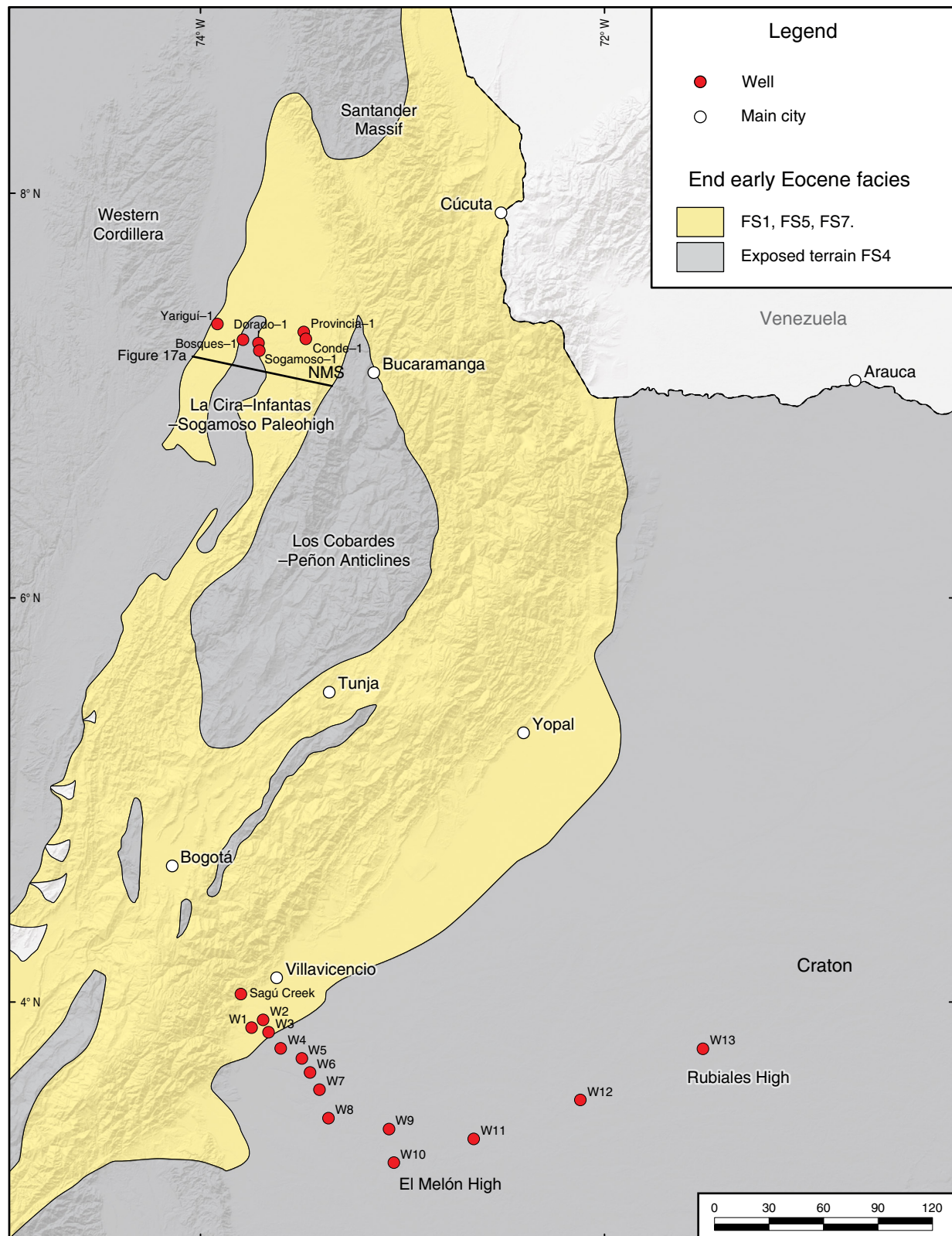


Figure 19. Early Eocene facies distribution. Through the early Eocene, as the tectonic activity gradually decreased, the base level transitioned from falling to rising, and the accommodation space slowly increased, likely because of the high sediment supply from the uplifted terrains. The previous landscape began to fill with a fluvial coastal plain wedge that onlapped onto the previous paleotopography. At the end of the early Eocene, these fluvial coastal plain facies (FS1, FS7, FS5) prograded and extended to form two depocenters, one in the MMB and the other covering the axial Eastern Cordillera and the western part of the Llanos Basin. These rocks correspond to the lowstand systems tract of the first depositional sequence. Modified from Reyes-Harker et al. (2015). (NMS) Nuevo Mundo Syncline.

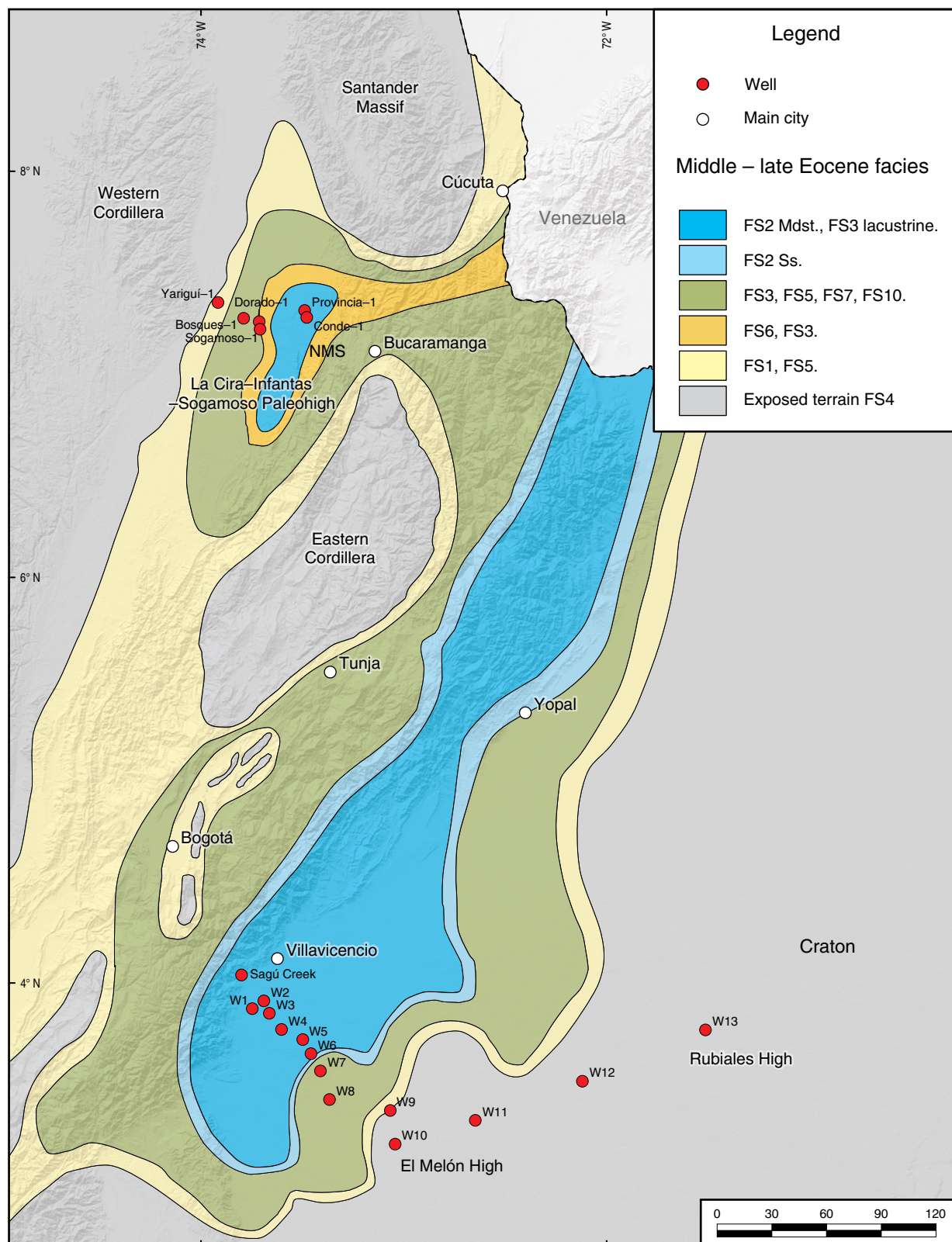


Figure 20. Middle to late Eocene facies distribution. Tectonic deformation translated to the Eastern Cordillera and Santander Massif during the middle Eocene. This deformation generated tectonic loads and flexural subsidence along both margins of the EC and the Santander Massif. The subsidence allowed marine waters to mainly enter the Llanos Basin; in the MMB, the tidal influence likely occurred as a result of overall base level rise and formed a tidally influenced fluvial to lacustrine system before the end of the Eocene. The distribution of facies shown in this map forms the TST and HST of the first depositional sequence. Modified from Reyes–Harker et al. (2015). (Mdst.) mudstone; (Ss.) sandstone; (NMS) Nuevo Mundo Syncline.

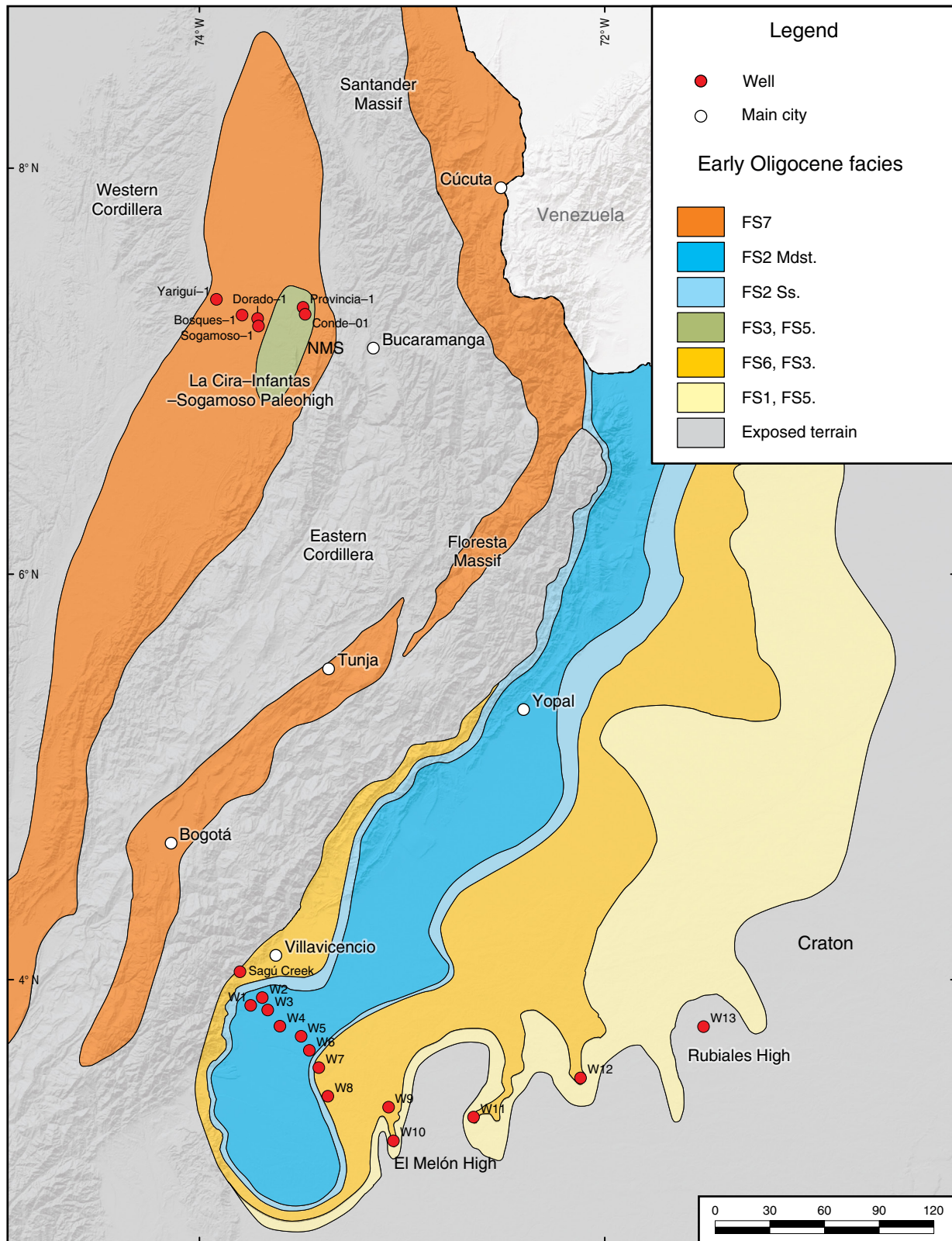


Figure 21. Early Oligocene facies distribution. By the early Oligocene, accelerated exhumation of the Floresta and Santander Massifs and the entire EC took place. The MMB became a closed basin, and an alluvial-fluvial system was established. In the Llanos, flexural subsidence continued in the foothills and WSLLB, where marine mudstones were mainly deposited, whereas in the ESLLB, low accommodation space, likely caused by forebulge migration, set the conditions for deposition of the Oligocene basal sandstones. The transgression continued into the early Oligocene. In the southern LLB, these deposits compose the second depositional sequence. Modified from Reyes-Harker et al. (2015). (Mdst.) mudstone; (Ss.) sandstone; (NMS) Nuevo Mundo Syncline.

(Figure 22). The third depositional sequence is composed of the C7–C6 Members of the Carbonera Formation between the upper lower Oligocene unconformity at the base of the C7 Member and an unconformity at the base of the C5 Member of the Carbonera Formation (Caycedo & Catuneanu, 2018).

The fluvial sandstones and organic lacustrine mudstones of the C7 and C6 Members of the Carbonera Formation between the upper lower Oligocene unconformity and the MFS make up the lowstand–transgressive systems tract. The HST is composed of the upper part of the C6 Member through the unconformity at the base of C5 Member of the Carbonera Formation.

4.5. Tectonic Controls on Deposition in the Llanos and Middle Magdalena Basins

Thickness differences of an order of magnitude were identified between the Eocene to Oligocene units in the southern Llanos Basin and those in the MMB. From the Chichimene area to the Rubiales area, the Lower Mirador Formation varies in thickness from 35 m to 0 m over a distance of 38 km. In the Middle Magdalena Basin, the thickness of the La Paz Formation varies from 1090 m in the NMS to 0 above the axial La Cira–Infantas–Sogamoso Paleohigh 38 km to the west. The western wedge of the La Paz Formation varies from 580 m thick in the Yariguí Field to 0 m above the axial LCISP (Figure 18).

The total thickness of the middle Eocene – Late Oligocene deposits in the southern Llanos Basin varies from 1044 m in the WSLLB to 93 m above the Rubiales High, 250 km to the east (Figure 15). In the MMB, the thickness varies from 2585 m on the eastern border (NMS) to approximately 630 m in the Yariguí Oil Field, and it laps onto the Cachira High 68 km to the northwest (Suárez, 1997; Gómez *et al.*, 2005a).

The wedge-shaped geometry of these deposits is evidence of differential subsidence of the basin, which is indicative of tectonic control on the deposition (Figures 15, 18). The large difference in thickness of the units between the basins indicates a significant difference in the mechanism that generated the accommodation space during the early Eocene to Oligocene in both basins. Based on the tectonic setting at that time, it can be inferred that the orogenic loads were located near the MMB, which generated more accommodation space than in the LLB, as has been suggested in previous studies (e.g., Gómez *et al.*, 2005a; Horton *et al.*, 2010a, 2010b; Mora *et al.*, 2013; Reyes–Harker *et al.*, 2015).

These tectonic factors controlled the lateral extent and thickness of the reservoir rocks in the MMB and southern Llanos Basin. The reservoir rocks in the LLB have greater lateral extents than those in the MMB (hundreds of km versus tens of km), but the reservoirs in the LLB are thinner than those in the MMB (several m to hundreds of m). This study documents that the reservoir facies in both areas are different. They are more

fluvial (i.e., more muddy sandstones and continental mudstones and less lateral continuity) in the NMS, versus more marginal to marine facies in the LLB (i.e. sandstones are more laterally continuous, they have less muddy matrix and shale horizons are, in general regional flooding events, instead of subaerial flood plain deposits).

The tectonic events that controlled the rate of subsidence, the amount and type of sediment and, indirectly, the rate of sedimentation influenced the porosity and permeability of the sandy units in both basins (e.g., Ramon & Fajardo, 2006; Cooper *et al.*, 1995).

Based on the porosity and permeability, the best reservoirs in the MMB and southern Llanos Basin are as follows:

1. The Lower Mirador amalgamated sandstones (FS1) in the foothills and WSLLB, the lower Oligocene basal sandstones (FS6) toward the ESLLB and the fluvial channel sandstones (FS9) of the C7 Member of the Carbonera Formation have the best reservoir properties, with porosities of 10–30 % and permeabilities of 100–10 000 mD.
2. The transgressive marine shoreface sandstones of the Upper Mirador Formation in the WSLLB have porosities of 5–15 % and permeabilities of 0.1–100 mD; these sandstones are sandier and thicker in the ESLLB, with porosities of 20–25 % and permeabilities of 100–10 000 mD.
3. In the western MMB, the lower Eocene amalgamated sandstones (FS1) of the La Paz Formation (Cantagallo sandstones) have porosities of 15–25 % and permeabilities of 100–1000 mD, the Mugrosa Formation has porosities of 15–25 % and permeabilities of 10–1000 mD, and the La Paz Formation in the eastern part of the MMB has porosities of 10–20 % and permeabilities of 100–1500 mD.
4. The Esmeraldas Formation in the eastern MMB has porosities of 10–20 % and permeabilities of 100–200 mD.
5. The Mugrosa Formation in the eastern MMB has porosities of 8–15 % and permeabilities of 70–150 mD.

The Oligocene Mugrosa Formation was deposited in a closed intermountain basin. We interpret that the conditions of high accommodation space and large sediment supply from the uplifting terrains around the basin led to an increase in the mud and silt available to form the matrix of the sandstones, which decreased the porosity and permeability.

4.6. Potential for Stratigraphic Plays

There is enormous potential for stratigraphic traps in the MMB and Llanos Basin. As we illustrated in this study, we identified lateral facies changes, pinchouts, unconformities with resulting truncated beds, and buried landscapes that include buried erosional hills and incised valleys on older reservoir rocks covered by thick strongly developed paleosols, which were then flooded and draped by marine shale facies. Several types of stratigraphic traps have been postulated in the southern Llanos

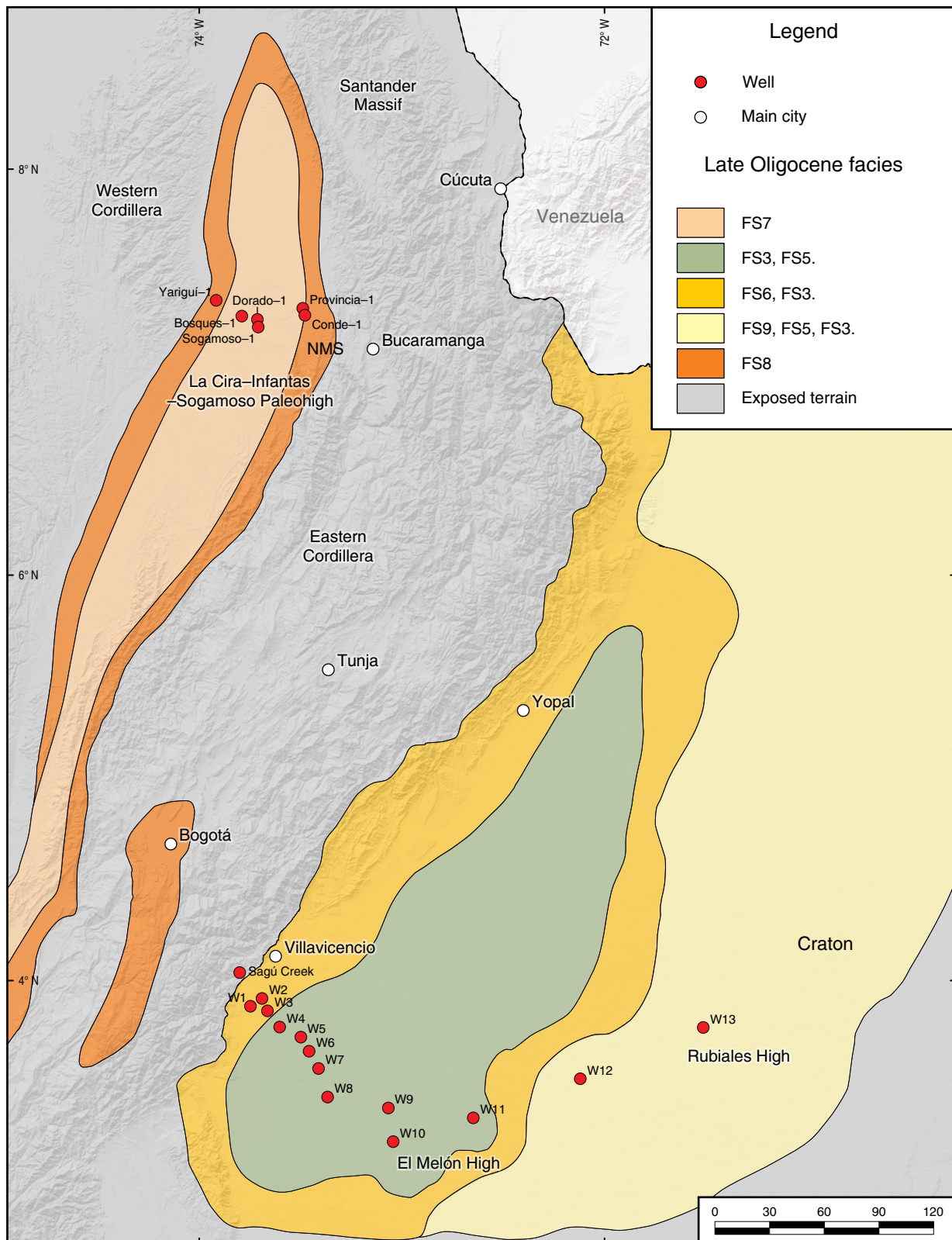


Figure 22. Late Oligocene facies distribution. The fluvial and coastal plain facies of the C7 and C6 Members of the Carbonera Formation were deposited in the Llanos Basin, and the MMB continued to be filled by alluvial-fluvial facies. The depositional limit migrated eastward. These deposits form the third depositional sequence. Modified from Reyes-Harker et al. (2015). (NMS) Nuevo Mundo Syncline.

Basin (Mora *et al.*, 2018). In Figures 15 and 17, we identify several of these plays for detailed study:

1. **Geomorphic features:** The preserved landscape that formed at the end of the Paleocene on Cretaceous and Paleocene reservoir rocks, such as the Guadalupe and Barco–Cuervos Formations (Figures 14, 15) and the sandstones of the Jurassic Girón Formation and basal Los Santos, Rosablanca, and Lisama Formations on both flanks of the La Cira–Infantas–Sogamoso intrabasinal paleohigh (Figure 17a), have potential for underlying geomorphic features, such as buried hills, unconformity traps, and fluvial incised valleys.
2. **The impermeable strongly developed paleosol (FS4)** below the unconformity that is in direct contact with the reservoirs and the lacustrine (FS3) or marine (FS2) shales above the unconformity provides an effective seal for the underlying reservoir sandstones, forming buried hills or unconformity traps in the southern Llanos Basin and MMB. The Camoa Field in Colombia is an example of a buried hill play (Mora *et al.*, 2018). Detailed work must be performed to search for these plays in other areas of the Llanos Basin and MMB. These traps are common and have been discovered around the world (Zhai & Zha, 1982).
3. **Erosional pinchouts or erosional truncations of reservoir units of the Lower Mirador Formation and Barco and Guadalupe sandstones by the transgressive ravinement surface,** which were later overlain by transgressive shales, form stratigraphic traps (see wells 1 to 5 in Figure 15), such as the stratigraphic trap of the T2 operational unit in the southern Llanos Basin.
4. **Depositional pinchouts, such as the Oligocene basal sandstones against the preserved landscape in the southern Llanos Basin** (see wells 6–12 in Figure 15), which were sealed during the later marine transgression and deposition of the Upper Mirador and C8 shales of the Carbonera Formation; an example is the pinchout of the La Paz Formation against the LCIS Paleohigh in the MMB and sealing by mudstones of the Esmeraldas Formation (Figure 17b).
5. **Stratigraphic traps, such as amalgamated channel belt sandstones or shoreline strips of sandstones sealed by floodplain, lacustrine, tidal, or marine mudstones.** The Oligocene basal sandstones in the southern Llanos Basin (Figure 15) and the Esmeraldas and Mugrosa Formations in the MMB (Figure 17c) have this potential.
6. **Incised valleys.** We believe that there is potential for incised valley sandstones reservoirs to be discovered in the Llanos Basin and in the MMB. In addition to the main trunk valleys that formed at the beginning of the Eocene, there should be incised valleys on Paleocene rocks in the basins, which are tributaries of these main trunk fluvial valleys. This play concept was exploited previously in the

Cusiana and Cupiagua Oil Fields (Pulham *et al.*, 1997; Ramon & Fajardo, 2006).

5. Conclusions

This study presents a comprehensive illustration and analysis of facies and facies successions of Eocene to Oligocene rocks in the NMS and southern LLB. The facies analysis allowed the identification of unconformity–bounded depositional sequences and systems tracts. The geometries and depositional trends allowed the common stratigraphic processes that occurred in these basins to be identified.

The LLB and the MMB likely shared the same stratigraphic base level and stratigraphic history during the Eocene, as indicated by the synchronicity in facies, facies successions, and stacking patterns from fluvial braided incised valley fills to meandering, estuarine, and lacustrine sediments in the MMB and low–energy shallow marine sediments in the LLB. From the Oligocene onwards, the MMB was isolated from the LLB as an intermontane closed and internally drained basin.

This fundamental change from a foreland to intermontane setting was associated with a stronger influence of the orogenic loads and close proximity to the source areas in the Middle Magdalena Basin and weaker influence of the orogenic loads and increased distance to the source areas in the Llanos Basin. We document that these factors controlled the facies and their properties, such as the porosity and permeability. Therefore, starting in the Oligocene, the sandy units were less laterally continuous and muddier in the MMB and interbedded with thick floodplain sandy mudstones, in contrast to the continuous, sandier, and marine–influenced units in the LLB, while the total thickness of the sedimentary record was greater in the MMB.

The lower Eocene sandstones in both basins are subtly fining–upward, single–story to multistory, aggradational to progradational, braided amalgamated sandstone wedges. These sandstones form excellent reservoirs and have very high porosities and permeabilities (10–25 % and 100–10 000 mD, respectively). This facies is thicker in the La Paz Formation in the MMB than it is in the Mirador Formation in the southern Llanos Basin.

The middle – late Eocene transgressive sandstones in the WSLLB are coarsening–upward mudstones and sandstones that were deposited in shoreface strips parallel to the shoreline in a retrogradational pattern. At least two important strips were identified; in the WSLLB, they are up to 20 m thick but are muddier (5–15 % porosity and 0.1–100 mD permeability) than in the ESLLB, where these strips are up to 12 m thick but are sandier around the El Melón and Rubiales Highs with excellent reservoir properties (20–25 % porosity and 100–10 000 mD).

The Eocene Esmeraldas Formation facies are fluvial tidally influenced meandering point bar and channel facies belts, which

are wide laterally and continuous in the axial direction of the river system. These sandstones have fair to good continuity and thickness, as is observed in outcrops, and they are embedded between cumulative clayey mudstone paleosols or intertidal muddy flats. These sandstones are good reservoirs (10–20 % porosity and 100–200 mD permeability) in the eastern part of the MMB.

The lower Oligocene basal sandstones (Carbonera basal sandstones) are shallowing-upward, progradational open shoreline to backshore estuarine cycles that are 5–8 m thick. Several cycles of these facies successions are up to 40 m thick and are in a retrogradational stacking pattern forming sandstone strips parallel to the shoreline. These sandstones have excellent porosities and permeabilities (20–30 % and 1000–10 000 mD, respectively).

The Oligocene Mugrosa Formation sandstone facies are fluvial meandering point bar and channel facies belts embedded between cumulative clayey mudstone paleosols. These sandstones are good reservoirs (8–15 % porosity and 70–150 mD permeability) in the eastern part of the MMB and amalgamated sandstones (15–25 % porosity and 10–1000 mD permeability) in the western part of the MMB.

The upper Oligocene C7 and C6 Members of the Carbonera Formation are meandering fluvial systems with channel and bar sandstone belts between cumulative paleosol and paralic mudstones and coals. These sandstones are excellent reservoirs (10–30 % porosity and 100–10 000 mD permeability).

Acknowledgments

The authors acknowledge Ecopetrol S.A. for its support to develop and publish this contribution. The authors are grateful to Andrés MANTILLA, Andrés REYES-HARKER, Freddy NIÑO, and Ricardo GÓMEZ from the Instituto Colombiano del Petróleo for their support and encouragement. This manuscript was improved by the important reviews and comments of Germán BAYONA and Octaviano CATUNEANU, to whom we are very grateful. We thank Daniela MATEUS ZABALA and the editorial board of the SGC for helpful comments that improved the chapter presentation.

References

- Aitken, J.F. & Flint, S.S. 1996. Variable expressions of interfluvial sequence boundaries in the Breathitt Group (Pennsylvanian), eastern Kentucky, USA. In: Howell, J.A. & Aitken, J.F. (editors), High resolution sequence stratigraphy: Innovations and applications. Geological Society of London, Special Publication 104, p. 193–206. London. <https://doi.org/10.1144/GSL.SP.1996.104.01.12>
- Bayona, G., Reyes-Harker, A., Jaramillo, C., Rueda, M., Aristizabal, J., Cortés, M. & Gamba, N. 2006. Distinguishing tectonic versus eustatic flooding surfaces in the Llanos Basin of Colombia, and implications for stratigraphic correlations. IX Simposio Bolivariano de Exploración Petrolera en las Cuencas Subandinas. 13 p. Cartagena, Colombia.
- Bayona, G., Cortés, M., Jaramillo, C., Ojeda, G., Aristizabal, J. J. & Reyes-Harker, A. 2008. An integrated analysis of an orogen-sedimentary basin pair: Latest Cretaceous – Cenozoic evolution of the linked Eastern Cordillera orogen and the Llanos Foreland Basin of Colombia. *Geological Society of America Bulletin*, 120(9–10): 1171–1197. <https://doi.org/10.1130/B26187.1>
- Bayona, G., Montenegro, O.C., Cardona, A., Jaramillo, C. & Lamus, F. 2010. Estratigrafía, procedencia, subsidencia y exhumación de las unidades paleógenas en el Sinclinal de Usme, sur de la zona axial de la cordillera Oriental. *Geología Colombiana*, 35(1): 5–35.
- Bayona, G., Cardona, A., Jaramillo, C., Mora, A., Montes, C., Valencia, V., Ayala, C., Montenegro, O. & Ibañez-Mejía, M. 2012. Early Paleogene magmatism in the northern Andes: Insights on the effects of oceanic plateau-continent convergence. *Earth and Planetary Science Letters*, 331–332: 97–111. <https://doi.org/10.1016/j.epsl.2012.03.015>
- Bayona, G., Cardona, A., Jaramillo, C., Mora, A., Montes, C., Caballero, V., Mahecha, H., Lamus, F., Montenegro, O., Jimenez, G., Mesa, A. & Valencia, V. 2013. Onset of fault reactivation in the Eastern Cordillera of Colombia and proximal Llanos Basin; response to Caribbean–South American convergence in early Palaeogene time. In: Nemčok, M., Mora, A. & Cosgrove, J.W. (editors), Thick-skin-dominated orogens: From initial inversion to full accretion, Geological Society of London, Special Publication 377, p. 285–314. London. <https://doi.org/10.1144/SP377.5>
- Bayona, G., Cardona, A., Tellez, G., Garzon, A., Pinzon, D., Mendez, J., Ramirez, C. & Rueda, M. 2015. Magmatismo Paleoceno–Eoceno temprano? en la cuenca proximal de los Llanos. XV Congreso Colombiano de Geología. *Memoirs*, p. 560–564. Bucaramanga.
- Blair, T.C. & McPherson, J.G. 2009. Processes and forms of alluvial fans. In: Parsons, A.D. & Abrahams, A.D. (editors), *Geomorphology of desert environments*, 2nd edition. Springer, p. 413–467. Dordrecht, the Netherlands. https://doi.org/10.1007/978-1-4020-5719-9_14
- Boggs, S.Jr. 1987. Principles of sedimentology and stratigraphy. Merriall Publishing Company. 784 p.
- Boyd, R., Dalrymple, R.W. & Zaitlin, B.A. 2006. Estuarine and incised-valley facies models. *SEPM Society for Sedimentary Geology*, 84: 171–236. <https://doi.org/10.2110/pec.06.84.0171>
- Caballero, V. 2010. Evolución tectono-sedimentaria del Sinclinal de Nuevo Mundo, cuenca sedimentaria Valle Medio del Magdalena Colombia, durante el Oligoceno–Mioceno. Master Thesis, Universidad Industrial de Santander, 149 p. Bucaramanga.

- Caballero, V., Parra, M. & Mora, A. 2010. Levantamiento de la cordillera Oriental de Colombia durante el Eoceno tardío–Oligoceno temprano: Proveniencia sedimentaria en el Sinclinal de Nuevo Mundo, cuenca Valle Medio del Magdalena. *Boletín de Geología*, 32(1): 45–77.
- Caballero, V., Mora, A., Quintero, I., Blanco, V., Parra, M., Rojas, L.E., Lopez, C., Sánchez, N., Horton, B.K., Stockli, D. & Duddy, I. 2013a. Tectonic controls on sedimentation in an intermontane hinterland basin adjacent to inversion structures: The Nuevo Mundo Syncline, Middle Magdalena Valley, Colombia. In: Nemčok, M., Mora, A. & Cosgrove, J.W. (editors), *Thick-skin-dominated orogens: From initial inversion to full accretion*. Geological Society of London, Special Publication 377, p. 315–342. London. <https://doi.org/10.1144/SP377.12>
- Caballero, V., Parra, M., Mora, A., Lopez, C., Rojas, L.E. & Quintero, I. 2013b. Factors controlling selective abandonment and reactivation in thick-skin orogens: A case study in the Magdalena Valley, Colombia. In: Nemčok, M., Mora, A. & Cosgrove, J.W. (editors), *Thick skin-dominated orogens: From initial inversion to full accretion*. Geological Society of London, Special Publications 377, p. 343–367. London. <https://doi.org/10.1144/SP377.4>
- Caballero, V.M., Rodríguez, G., Naranjo, J.F., Mora, A. & De La Parra, F. 2020. From facies analysis, stratigraphic surfaces, and depositional sequences to stratigraphic traps in the Eocene – Oligocene record of the southern Llanos Basin and northern Magdalena Basin. In: Gómez, J. & Mateus-Zabala, D. (editors), *The Geology of Colombia, Volume 3 Paleogene – Neogene*. Servicio Geológico Colombiano, Publicaciones Geológicas Especiales 37, p. 283–330. Bogotá. <https://doi.org/10.32685/pub.esp.37.2019.10>
- Casero, P., Salel, J. F. & Rossato, A. 1997. Multidisciplinary correlative evidence for polyphase geological evolution of the foot-hills of the cordillera Oriental (Colombia). VI Simposio Bolivariano de Exploración Petrolera en la Cuenca Subandinas. Proceedings 1, 19 p. Cartagena.
- Catuneanu, O. 2006. Principles of sequence stratigraphy. *Developments in Sedimentology*. Elsevier, 375 p. Amsterdam, Netherlands.
- Caycedo, H.R. & Catuneanu, O. 2018. Stratigraphic architecture of incised valleys and unincised channel systems in the Carbonera Formation (C6–C1 Members: Upper Oligocene – Lower Miocene), Llanos Basin, Colombia. *Journal of Geodynamics*, 129: 202–218. <https://doi.org/10.1016/j.jog.2018.01.011>
- Cazier, E. C., Hayward, A.B., Espinosa, G., Velandia, J., Mugniot, J-F. & Leel Jr., W.G. 1995. Petroleum geology of the Cusiana Field, Llanos Basin Foothills, Colombia. *American Association of Petroleum Geologists Bulletin*, 79(10): 1444–1462.
- Cecil, C.B. 1990. Paleoclimate controls on stratigraphic repetition of chemical and siliciclastic rocks. *Geology*, 18(6): 533–536. [https://doi.org/10.1130/0091-7613\(1990\)018<0533:PCOS-RO>2.3.CO;2](https://doi.org/10.1130/0091-7613(1990)018<0533:PCOS-RO>2.3.CO;2)
- Clifton, H.E. 2006. A Reexamination of facies models for clastic shorelines. In: Posamentier, H.W. & Walker, R.G. (editors), *Facies models revisited*. SEPM Society for Sedimentary Geology, Special Publication 84, p. 293–337. <https://doi.org/10.2110/pec.06.84.0293>
- Coe, A. L., editor. 2003. *The sedimentary record of sea-level change*. Cambridge University Press, 288 p.
- Colletta, B., Hebrard, F., Letouzey, J., Werner, P., & Rudkiweicz, J.L. 1990. Tectonic style and crustal structure of the Eastern Cordillera, Colombia from a balanced cross section. In: Letouzey, J. (editor), *Petroleum and tectonics in mobile belts*. Editions Technip, p. 81–100. Paris.
- Collinson, J., Mountney, N. & Thompson, D. 2006. *Sedimentary structures*, 3rd Edition. Terra Publishing, 302 p.
- Cooper, M. A., Addison, F.T., Alvarez, R., Coral, M., Graham, R.H., Hayward, A.B., Howe, S., Martinez, J., Naar, J., Peñas, R., Pulham, A.J. & Taborda, A. 1995. Basin development and tectonic history of the Llanos Basin, Eastern Cordillera, and Middle Magdalena Valley, Colombia. *American Association of Petroleum Geologists Bulletin*, 79(10): 1421–1443.
- De La Parra, F., Paez, M., Cárdenas, O., Bedoya, O. & Pinzon, D. 2014. Informe palinológico de las secciones caño Sagú, caño Las Blancas y pozos Castilla–18 y Cristal–1. *Ecopetrol–ICP, Informe interno 20–14*. 31 p.
- Dengo, C.A. & Covey, M.C. 1993. Structure of the Eastern Cordillera of Colombia: Implications for trap styles and regional tectonics. *American Association of Petroleum Geologists Bulletin*, 77(8): 1315–1337.
- Etayo–Serna, F., Renzoni, G. & Barrero, F. 1969. Contornos sucesivos del mar cretáceo en Colombia. I Congreso Colombiano de Geología. *Memoirs*, p. 217–252. Bogotá.
- Etayo–Serna, F., Barrero, D., Lozano, H., Espinosa, A., González, H., Orrego, A., Ballesteros, I., Forero, H., Ramírez, C., Zambraño–Ortiz, F., Duque–Caro, H., Vargas, R., Núñez, A., Álvarez, J., Ropaín, C., Cardozo, E., Galvis, N., Sarmiento, L., Alberts, J.P., Case, J.E., Singer, D.A., Bowen, R.W., Berger, B.R., Cox, D.P. & Hodges, C.A. 1983. Mapa de terrenos geológicos de Colombia. *Publicaciones Geológicas Especiales del Ingeominas 14(1)*, p. 1–235. Bogotá.
- Fabre, A. 1985. Dinámica de la sedimentación cretácica en la región de la Sierra Nevada del Cocuy (cordillera Oriental de Colombia). In: Etayo–Serna, F. & Laverde–Montaño, F. (editors), *Proyecto cretácico: Contribuciones*. Publicaciones Geológicas Especiales del Ingeominas 16, p. XIX–1–XIX–20. Bogotá.
- Fabre, A. 1987. Tectonique et génération d’hydrocarbures: un modèle de l’évolution de la Cordillère Orientale de Colombie et du bassin des Llanos pendant le Crétacé et le Tertiaire. *Archives des Sciences Genève*, 40: 145–190.
- Fajardo, A. 1995. 4–D stratigraphic architecture and 3–D reservoir fluid–flow model of the Mirador Formation, Cusiana Field, foothills area of the cordillera Oriental, Colombia. Master thesis, Colorado School of Mines, 186 p. Golden.

- Farrell, K. M., Harris, W.B., Mallinson, D.J., Culvert, S.J., Riggs, S.R., Pierson, J., Self-Trail, J.M. & Lautier, J.C. 2012. Standardizing texture and facies codes for a process-based classification of clastic sediment and rock. *Journal of Sedimentary Research*, 82(6): 364–378. <https://doi.org/10.2110/jsr.2012.30>
- Gerard, J. & Bromley, R.G. 2008. *Ichnofabrics in clastic sediments: Applications to sedimentological core studies: A practical guide*. Total Compagnie Française des Pétroles, Association des Sédimentologues Français, Repsol. 100 p.
- Gómez, E., Jordan, T.E., Allmendinger, R.W., Hegarty, K., Kelley, S. & Heizler, M. 2003. Controls on architecture of the Late Cretaceous to Cenozoic southern Middle Magdalena Valley Basin, Colombia. *Geological Society of America Bulletin*, 115(2): 131–147. [https://doi.org/10.1130/0016-7606\(2003\)115<0131:COAOTL>2.0.CO;2](https://doi.org/10.1130/0016-7606(2003)115<0131:COAOTL>2.0.CO;2)
- Gómez, E., Jordan, T.E., Allmendinger, R.W., Hegarty, K. & Kelley, S. 2005a. Syntectonic Cenozoic sedimentation in the northern Middle Magdalena Valley Basin of Colombia and implications for exhumation of the northern Andes. *Geological Society of America Bulletin*, 117(5–6): 547–569. <https://doi.org/10.1130/B25454.1>
- Gómez, E., Jordan, T.E., Allmendinger, R.W. & Cardozo, N. 2005b. Development of the Colombian foreland–basin system as a consequence of diachronous exhumation of the northern Andes. *Geological Society of America Bulletin*, 117(9–10): 1272–1292. <https://doi.org/10.1130/B25456.1>
- Horton, B.K., Parra, M., Saylor, J.E., Nie, J., Mora, A., Torres, V., Stockli, D.F. & Strecker, M.R. 2010a. Resolving uplift of the northern Andes using detrital zircon age signatures. *Geological Society of America Today*, 20(7): 4–9. <https://doi.org/10.1130/GSATG76A.1>
- Horton, B.K., Saylor, J.E., Nie, J., Mora, A., Parra, M., Reyes–Harker, A. & Stockli, D.F. 2010b. Linking sedimentation in the northern Andes to basement configuration, Mesozoic extension, and Cenozoic shortening: Evidence from detrital zircon U–Pb ages, Eastern Cordillera, Colombia. *Geological Society of America Bulletin*, 122(9–10): 1423–1442. <https://doi.org/10.1130/B30118.1>
- Jaramillo, C., Rueda, M., Bayona, G., Santos, C., Florez, P. & Parra, F. 2009. Biostratigraphy breaking paradigms: Dating the Mirador Formation in the Llanos Basin of Colombia. In: Demchuk, T.D. & Gary, C.A. (editors), *Geologic problem solving with microfossils: A volume in honor of Garry D. Jones*. SEPM, Society for Sedimentary Geology, Special Publication 93, p. 29–40. Tulsa. <https://doi.org/10.2110/sepmsp.093.029>
- Jaramillo, C.A., Rueda, M. & Torres, V. 2011. A palynological zonation of the Cenozoic of the Llanos and Llanos Foothills of Colombia. *Palynology*, 35(1): 46–84. <https://doi.org/10.1080/01916122.2010.515069>
- Kraus, M. J. 1999. Paleosols in clastic sedimentary rocks: Their geological applications. *Earth–Science Reviews*, 47(1–2): 41–70. [https://doi.org/10.1016/S0012-8252\(99\)00026-4](https://doi.org/10.1016/S0012-8252(99)00026-4)
- Lamus, F., Bayona, G., Cardona, A. & Mora, A. 2013. Procedencia de las unidades cenozoicas del Sinclinal de Guaduas: Implicación en la evolución tectónica del sur del Valle Medio del Magdalena y orógenos adyacentes. *Boletín de Geología*, 35(1): 17–42.
- Lunt, I.A., Bridge, J.S. & Tye, R.S. 2004. A quantitative, three-dimensional depositional model of gravelly braided rivers. *Sedimentology*, 51(3): 377–414. <https://doi.org/10.1111/j.1365-3091.2004.00627.x>
- Malagón, C. 1997. Análisis facial, arquitectura estratigráfica y caracterización de las areniscas T1, Formación Carbonera, Campo Apiay, Colombia. VI Simposio Bolivariano de Exploración Petrolera en las Cuencas Subandinas. American Association of Petroleum Geologists/Datapages Combined Publications Database. 4 p. Bogotá.
- Mondragón, J.C., Carrillo, G., Rueda, M., Medina, A., Becerra, I., Morales, M. & Rodríguez, G. 2016. House keeping time? The basal Tertiary sequence in the Llanos Foreland Basin. Simposio Bolivariano de Exploración Petrolera en Cuencas Subandinas. Bogotá.
- Mora, A., Parra, M., Strecker, M.R., Kammer, A., Dimaté, C. & Rodríguez, F. 2006. Cenozoic contractional reactivation of Mesozoic extensional structures in the Eastern Cordillera of Colombia. *Tectonics*, 25(2): 19 p. <https://doi.org/10.1029/2005TC001854>
- Mora, A., Parra, M., Strecker, M.R., Sobel, E.R., Hooghiemstra, H., Torres, V. & Vallejo–Jaramillo, J. 2008. Climatic forcing of asymmetric orogenic evolution in the Eastern Cordillera of Colombia. *Geological Society of America Bulletin*, 120(7–8): 930–949. <https://doi.org/10.1130/B26186.1>
- Mora, A., Gaona, T., Kley, J., Montoya, D., Parra, M., Quiroz, L.I., Reyes, G. & Strecker, M.R. 2009. The role of inherited extensional fault segmentation and linkage in contractional orogenesis: A reconstruction of Lower Cretaceous inverted rift basins in the Eastern Cordillera of Colombia. *Basin Research*, 21(1): 111–137. <https://doi.org/10.1111/j.1365-2117.2008.00367.x>
- Mora, A., Horton, B.K., Mesa, A., Rubiano, J., Ketcham, R.A., Parra, M., Blanco, V., Garcia, D. & Stockli, D.F. 2010. Migration of Cenozoic deformation in the Eastern Cordillera of Colombia interpreted from fission track results and structural relationships: Implications for petroleum systems. *American Association of Petroleum Geologists Bulletin*, 94(10): 1543–1580. <https://doi.org/10.1306/01051009111>
- Mora, A., Reyes–Harker, S., Rodríguez, G., Tesón, E., Ramírez–Arias, J.C., Parra, M., Caballero, V., Mora, J.P., Quintero, I., Valencia, V., Ibañez–Mejía, M., Horton, B.K. & Stockli, D.F. 2013. Inversion tectonics under increasing rates of shortening and sedimentation: Cenozoic example from the Eastern Cordillera of Colombia. In: Nemčok, M., Mora, A. & Cosgrove, J.W. (editors), *Thick–skin–dominated orogens: From initial inversion to full accretion*. Geological Society of London, Special Publication 377, p. 411–442. London. <https://doi.org/10.1144/SP377.6>
- Mora, A., Parra, M., Rodríguez–Forero, G., Blanco, V., Moreno, N., Caballero, V., Stockli, D., Duddy, I. & Ghorbal, B. 2015. What

- drives orogenic asymmetry in the northern Andes?: A case study from the apex of the northern Andean oroclinal. In: Bartolini, C. & Mann, P. (editors), *Petroleum geology and potential of the Colombian Caribbean margin*. American Association of Petroleum Geologists, Memoir 108, p. 547–586. <https://doi.org/10.1306/13531949M1083652>
- Mora, A., Villamizar, C., Cardozo, E., Caballero, V., Gelvez, J., Gomez, R., Lozada, S., Valencia, A., Beltrán R., Franco, M. & Tejada, M. L. 2018. Geological processes controlling stratigraphic traps in the southern Llanos Basin. Conference: Cumbre del Petróleo y Gas 2018. 6 p. Bogotá.
- Morales, L. 1958. General geology and oil occurrences of Middle Magdalena Valley, Colombia. In: Weeks, L.G. (editor), *Habitat of oil*. American Association of Petroleum Geologists, Special Publication SP18, p. 641–695. Tulsa, USA.
- Moreno, C.J., Horton, B.K., Caballero, V., Mora, A., Parra, M. & Sierra, J. 2011. Depositional and provenance record of the Paleogene transition from foreland to hinterland basin evolution during Andean orogenesis, northern Middle Magdalena Valley Basin, Colombia. *Journal of South American Earth Sciences*, 32(3): 246–263. <https://doi.org/10.1016/j.jsames.2011.03.018>
- Nie, J., Horton, B.K., Mora, A., Saylor, J.E., Housh, T.B., Rubiano, J. & Naranjo, J. 2010. Tracking exhumation of Andean ranges bounding the Middle Magdalena Valley Basin, Colombia. *Geology*, 38(5): 451–454. <https://doi.org/10.1130/G30775.1>
- Nie, J., Horton, B.K., Saylor, J.E., Mora, A., Mange, M., Garziona, C.N., Basu, A., Moreno, C.J., Caballero, V. & Parra, M. 2012. Integrated provenance analysis of a convergent retroarc foreland system: U–Pb ages, heavy minerals, Nd isotopes, and sandstone compositions of the Magdalena Valley Basin, northern Andes, Colombia. *Earth–Science Reviews*, 110(1–4): 111–126. <https://doi.org/10.1016/j.earscirev.2011.11.002>
- Nio, S.D. & Yang, C.S. 1991. Diagnostic attributes of clastic tidal deposits: A review. In: Smith, D.G., Reinson G.E., Zaitlin, B.A. & Rahmani, R.A. (editors), *Clastic tidal sedimentology*. Canadian Society of Petroleum Geologists, Memoir 16, p. 3–27. Calgary.
- O’Byrne, C.J. & Flint, S. 1996. Interfluvial sequence boundaries in the Grassy Member, Book Cliffs, Utah: Criteria for recognition and implications for subsurface correlation. In: Howell, J.A. & Aitken, J.F. (editors), *High resolution sequence stratigraphy: Innovations and applications*. Geological Society of London, Special Publication 104, p. 207–220. London. <https://doi.org/10.1144/GSL.SP.1996.104.01.13>
- Pardo-Trujillo, A. 2004. Paleocene – Eocene palynology and palynofacies from northeastern Colombia and western Venezuela. Doctoral thesis, Université de Liège, 103 p. Liège.
- Parra, M., Mora, A., Jaramillo, C., Strecker, M.R., Sobel, E.R., Quiroz, L.I., Rueda, M. & Torres, V. 2009a. Orogenic wedge advance in the northern Andes: Evidence from the Oligocene – Miocene sedimentary record of the Medina Basin, Eastern Cordillera, Colombia. *Geological Society of America Bulletin*, 121(5–6): 780–800. <https://doi.org/10.1130/B26257.1>
- Parra, M., Mora, A., Sobel, E.R., Strecker, M.R. & González, R. 2009b. Episodic orogenic front migration in the northern Andes: Constraints from low–temperature thermochronology in the Eastern Cordillera, Colombia. *Tectonics*, 28(4): p. 1–27. <https://doi.org/10.1029/2008TC002423>
- Parra, M., Mora, A., Jaramillo, C., Torres, V., Zeilinger, G. & Strecker, M.R. 2010. Tectonic controls on Cenozoic foreland basin development in the north–eastern Andes, Colombia. *Basin Research*, 22(6): 874–903. <https://doi.org/10.1111/j.1365-2117.2009.00459.x>
- Parra, M., Mora, A., López, C., Rojas, L.E. & Horton, B.K. 2012. Detecting earliest shortening and deformation advance in thrust–belt hinterlands: Example from the Colombian Andes. *Geology*, 40(2): 175–178. <https://doi.org/10.1130/G32519.1>
- Posamentier, H.W. & Allen, G.P. 1999. Siliciclastic sequence stratigraphy–Concepts and applications. *SEPM Concepts in Sedimentology and Paleontology*. Society for Sedimentary Geology, 7, 210 p. <https://doi.org/10.2110/csp.99.07>
- Pulham, A.J. 1994. The Cusiana Field, Llanos Basin, Eastern Colombia: High resolution sequence stratigraphy applied to late Palaeocene – early Oligocene estuarine, coastal plain and alluvial clastic reservoirs. In: Johnson, S.D. (editor), *High resolution sequence stratigraphy: Innovation and applications*. University of Liverpool, Abstract Volume, p. 63–68.
- Pulham, A.J., Mitchell, A., MacDonald, D. & Daly, C. 1997. Reservoir modeling in the Cusiana Field, Llanos Foothills, Eastern Cordillera: Characterization of a deeply–buried, low–porosity reservoir. VI Simposio Bolivariano de Exploración Petrolera en las Cuencas Subandinas. Proceedings I, p 198–216.
- Ramírez–Arias, J.C., Mora, A., Rubiano, J., Duddy, I., Parra, M., Moreno, N., Stockli, D. & Casallas, W. 2012. The asymmetric evolution of the Colombian Eastern Cordillera. Tectonic inheritance or climatic forcing? New evidence from thermochronology and sedimentology. *Journal of South American Earth Sciences*, 39: 112–137. <https://doi.org/10.1016/j.jsames.2012.04.008>
- Ramon, J.C. & Fajardo, A. 2006. Sedimentology, sequence stratigraphy, and reservoir architecture of the Eocene Mirador Formation, Cupiagua Field, Llanos Foothills, Colombia. In: Harris, P.M. & Weber, L.J. (editors), *Giant hydrocarbon reservoirs of the world: From rocks to reservoir characterization and modeling*. American Association of Petroleum Geologists, Memoir 88/SEPM Special Publication, p. 433–469. <https://doi.org/10.1306/1215884M883276>
- Reineck, H. E. & Singh, I.B. 1973. *Depositional sedimentary environments with reference to terrigenous clastics*. Springer–Verlag, 551 p. Berlin.
- Reyes–Harker, A., Ruiz–Valdivieso, C.F., Mora, A., Ramírez–Arias, J.C., Rodríguez, G., De La Parra, F., Caballero, V., Parra, M., Moreno, N., Horton, B.K., Saylor, J.E., Silva, A., Valencia, V., Stockli, D. & Blanco, V. 2015. Cenozoic paleogeography of the Andean foreland and retroarc hinterland of Colombia. *American Association of Petroleum Geologists Bulletin*, 99(8): 1407–1453. <https://doi.org/10.1306/06181411110>

- Rodríguez–Forero, G., Oboh–Ikuenobe, F.E., Jaramillo–Munoz, Rueda–Serrano, M.J. & Cadena–Rueda, E. 2012. Palynology of the Eocene Esmeraldas Formation, Middle Magdalena Valley Basin, Colombia. *Palynology*, 36(Supplement 1): 96–111. <https://doi.org/10.1080/01916122.2012.650548>
- Rust, B.R. 1977. Depositional models for braided alluvium. *Fluvial Sedimentology*, Memoir 5, p. 605–625.
- Sandoval, J. R. 2016. Correlaciones y paleogeografía del Cretácico Superior a Oligoceno entre la subcuenca Yarí–Caguán y las cuencas Llanos y Putumayo, Colombia. Master Thesis, Universidad Industrial de Santander, 97 p. Bucaramanga.
- Santos, C., Jaramillo, C., Bayona, G., Rueda, M. & Torres, V. 2008. Late Eocene marine incursion in north–western South America. *Palaeogeography, Palaeoclimatology, Palaeoecology*, 264(1–2): 140–146. <https://doi.org/10.1016/j.palaeo.2008.04.010>
- Sarmiento–Rojas, L.F., van Wess, J.D. & Cloetingh, S. 2006. Mesozoic transtensional basin history of the Eastern Cordillera, Colombian Andes: Inferences from tectonic models. *Journal of South American Earth Sciences*, 21(4): 383–411. <https://doi.org/10.1016/j.jsames.2006.07.003>
- Saylor, J.E., Horton, B.K., Nie, J., Corredor–Herrera, J.A. & Mora, A. 2011. Evaluating foreland basin partitioning in the northern Andes using Cenozoic fill of the Floresta Basin, Eastern Cordillera, Colombia. *Basin Research*, 23(4): 377–402. <https://doi.org/10.1111/j.1365-2117.2010.00493.x>
- Saylor, J.E., Horton, B.K., Stockli, D.F., Mora, A. & Corredor, J. 2012a. Structural and thermochronological evidence for Paleogene basement–involved shortening in the axial Eastern Cordillera, Colombia. *Journal of South American Earth Sciences*, 39: 202–215. <https://doi.org/10.1016/j.jsames.2012.04.009>
- Saylor, J.E., Stockli, D.F., Horton, B. H., Nie, J. & Mora, A. 2012b. Discriminating rapid exhumation from syndepositional volcanism using detrital zircon double dating: Implications for the tectonic history of the Eastern Cordillera, Colombia. *Geological Society of America Bulletin*, 124(5–6): 762–779. <https://doi.org/10.1130/B30534.1>
- Shanley, K.W. & McCabe, P.J. 1994. Perspectives on the sequence stratigraphy of continental strata. *American Association of Petroleum Geologists Bulletin*, 78(4): 544–568. <https://doi.org/10.1306/BDF9258-1718-11D7-8645000102C1865D>
- Silva, A., Mora, A., Caballero, V., Rodríguez, G., Ruiz, C., Moreno, N., Parra, M., Ramírez–Arias, J.C., Ibañez, M. & Quintero, I. 2013. Basin compartmentalization and drainage evolution during rift inversion: Evidence from the Eastern Cordillera of Colombia. In: Nemčok, M., Mora, A. & Cosgrove, J.W. (editors), *Thick–skin–dominated orogens: From initial inversion to full accretion*. Geological Society of London, Special Publication 377: p. 369–409. London. <https://doi.org/10.1144/SP377.15>
- Suárez, M.A. 1997. Facies analysis of the upper Eocene La Paz Formation, and regional evaluation of the post–middle Eocene stratigraphy, northern Middle Magdalena Valley Basin. Master thesis, University of Colorado, 88 p. Boulder.
- Tandon, S.K. & Gibling, M.R. 1994. Calcrete and coal in late Carboniferous cyclothems of Nova Scotia, Canada: Climate and sea–level changes linked. *Geology*, 22(8): 755–758. [https://doi.org/10.1130/0091-7613\(1994\)022<0755:CACILC>2.3.CO;2](https://doi.org/10.1130/0091-7613(1994)022<0755:CACILC>2.3.CO;2)
- Tesón, E., Mora, A., Silva, A., Namsom, J., Teixell, A., Castellanos, J., Cassallas, W., Julivert, M., Taylor, M., Ibañez–Mejía, M. & Valencia, V.A. 2013. Relationship of Mesozoic graben development, stress, shortening magnitude, and structural style in the Eastern Cordillera of the Colombian Andes. In: Nemčok, M., Mora, A. & Cosgrove, J. W. (editors), *Thick–skin–dominated orogens: From initial inversion to full accretion*. Geological Society of London, Special Publication 377: 257–283. London. <http://dx.doi.org/10.1144/SP377.10>
- van Wagoner, J.C., Mitchum, R.M., Campion, K.M. & Rahmanian, V.D. 1990. Siliciclastic sequence stratigraphy in well logs, cores, and outcrops: Concepts for high–resolution correlation of time and facies. *American Association of Petroleum Geologists, Methods in Exploration Series 7*, 55 p. Tulsa, USA. <https://doi.org/10.1306/Mth7510>
- van Wagoner, J.C. & Bertram, G. T., editors. 1995. Sequence stratigraphy of foreland basin deposits: Outcrop and surface examples from the Cretaceous of North America. *American Association of Petroleum Geologists, Memoir 64*, 487 p.
- Villagómez, D.R., Spikings, R., Magna, T., Kammer, A., Winkler, W. & Beltrán, A. 2011. Geochronology, geochemistry and tectonic evolution of the Western and Central Cordilleras of Colombia. *Lithos*, 125 (3–4): 875–896. <https://doi.org/10.1016/j.lithos.2011.05.003>
- Villamil, T. 1999. Campanian – Miocene tectonostratigraphy, depocenter evolution and basin development of Colombia and western Venezuela. *Palaeogeography, Palaeoclimatology, Palaeoecology*, 153(1–4): 239–275. [https://doi.org/10.1016/S0031-0182\(99\)00075-9](https://doi.org/10.1016/S0031-0182(99)00075-9)
- Walker, R.G. 1984. Facies models, 2nd edition. *Geoscience Canada Reprint Series 1*. Geological Association of Canada 211, 317p. Waterloo, Ontario, Canada.
- Walker, R. G. & James, N. P., editors. 1992. Facies models: Response to sea level change. *Geological Association of Canada, Geo-Text 1*, 454 p.
- Weimer, R.J. 1975. Deltaic and shallow marine sandstones: Sedimentation, tectonics and petroleum occurrences. *Education Course Note Series #2*. Colorado School of Mines. American Association of Petroleum Geologists, 2, 164 p.
- Zhai, G. & Zha, Q. 1982. Buried–hill oil and gas pools in the North China Basin. *The American Association of Petroleum Geologists, Memoir 32*, p. 317–335.

Explanation of Acronyms, Abbreviations, and Symbols:

EC	Eastern Cordillera	MMB	Middle Magdalena Basin
ESLLB	Eastern sector of the Southern Llanos Basin	NMS	Nuevo Mundo Syncline
FS	Facies successions	SLLB	Southern Llanos Basin
HAST	High–accommodation systems tract	SU	Subaerial unconformity
HST	Highstand systems tract	T2	Amalgamated reservoirs sandstones of the Mirador, Barco, and Guadalupe Formations
ICP	Instituto Colombiano del Petróleo	TST	Transgressive systems tract
LCISP	La Cira–Infantas–Sogamoso Paleohigh	WSLLB	Western sector of the Southern Llanos Basin
LLB	Llanos Basin		
LST	Lowstand systems tract		
MFS	Maximum flooding surface		

Authors' Biographical Notes



Víctor M. CABALLERO is a senior geologist and researcher of stratigraphy, sedimentology, and depositional systems at Ecopetrol–ICP. He received his BS and Master of Science degrees in geology from the Universidad Industrial de Santander at Bucaramanga Colombia. His research interests include sedimentology, sequence stratigraphy, thermochronology, geochronology, and basin analysis.



Andrés MORA is the technical leader of onshore Colombia and foothills exploration at Ecopetrol. He received his BS in geology from the Universidad Nacional de Colombia and PhD from the Institut für Geowissenschaften, Universität Potsdam. His research interests include structural geology, petroleum exploration, and petroleum geology.



Guillermo RODRÍGUEZ is a palynologist at Ecopetrol–ICP. He received his BS in geology degree from the Universidad Nacional de Colombia and his Master of Science degree from the Missouri University of Science and Technology. His research interests include Cenozoic palynology, biostratigraphy, and general stratigraphy.



Felipe DE LA PARRA is a biostratigrapher and chief of the biostratigraphy team at Ecopetrol–ICP. He received his BS in geology degree from the Universidad Nacional de Colombia, a Master of Science degree from the University of Florida and a PhD from the University of Oxford.



Julián F. NARANJO is a geologist with expertise in sedimentary petrology and sedimentology at Ecopetrol–ICP. He received his BS in geology degree from the Universidad Industrial de Santander at Bucaramanga Colombia and his Master of Science degree from the National University of Ireland. His research interests include sedimentary petrology, sedimentology, and sequence stratigraphy.

Chapter 11



Oligocene – Miocene Coal-Bearing Successions of the Amagá Formation, Antioquia, Colombia: Sedimentary Environments, Stratigraphy, and Tectonic Implications

Juan Carlos SILVA-TAMAYO^{1*} , Mario LARA² , and Ana Milena SALAZAR-FRANCO³ 

Abstract The Amagá Formation is a late Oligocene – middle Miocene tropical siliciclastic succession that was deposited along several semi-isolated intramontane (pull-apart) sedimentary basins in the northernmost part of the Colombian Andes. Despite the fact that these coal-bearing sedimentary records constitute one of the most complete late Oligocene – middle Miocene continental successions deposited along the hinterland of the northern Andes convergent margin, limited geologic information is available in the literature about their sedimentology and stratigraphy. In this contribution, we report new detailed stratigraphic information from the Amagá Formation in the Santa Fe de Antioquia–San Jerónimo Sub-basin and integrate it with previously published sedimentologic, sequence stratigraphic, biostratigraphic, geochronologic, and thermochronologic information about the sedimentary successions in this formation, which crop out along the Amagá–Venecia, Fredonia–La Pintada–Valparaíso, and Santa Fe de Antioquia–San Jerónimo Sub-basins. This integrative approach allows us to assess the mechanisms controlling the sedimentologic evolution of tropical hinterland/intramontane successions along Andean-type convergent margins.

Our approach allows us to subdivide the Amagá Formation into two members, i.e., the Lower and Upper Members. Regionally, the Lower Member records a change in sedimentary environments from a braided river system to a meandering river system. This change occurred during a period of increasing sediment accommodation space, which coincides with the late Oligocene (28–25 Ma) break-up of the Farallon Plate into the Nazca and Cocos Plates. The Upper Member of the Amagá Formation displays a facies association typical of braided river systems, and it was deposited during a period of decreasing sediment accommodation space. This decrease in sediment accommodation space likely resulted from a major regional uplift event associated with the early Miocene change from oblique to orthogonal convergence between the Nazca and South American Plates and the early Miocene (23–21 Ma) docking of the Panamá–Chocó Block to northern South America.

Keywords: Amagá Formation, sequence stratigraphy, northwestern Andes, Oligocene – Miocene tectonics, Panamá–Chocó Block.

Citation: Silva-Tamayo, J.C., Lara, M. & Salazar-Franco, A.M. 2020. Oligocene – Miocene coal-bearing successions of the Amagá Formation, Antioquia, Colombia: Sedimentary environments, stratigraphy, and tectonic implications. In: Gómez, J. & Mateus-Zabala, D. (editors), *The Geology of Colombia, Volume 3 Paleogene – Neogene. Servicio Geológico Colombiano, Publicaciones Geológicas Especiales 37*, p. 331–353. Bogotá. <https://doi.org/10.32685/pub.esp.37.2019.11>

<https://doi.org/10.32685/pub.esp.37.2019.11>
Published online 24 June 2020

- 1 director.testlabgeoambiental@gmail.com
CEO at Testlab Geoambiental
Testlab Laboratorio Alimentos
y Aguas S.A.S.
Research Group One-Health
Calle 45D n.º 60–16
Medellín, Colombia
 - 2 Universidad Nacional de Colombia
Sede Medellín
Facultad de Minas
Departamentos de Materiales y Minerales
Carrera 80 n.º 65–223
Medellín, Colombia
 - 3 Corporación Geológica ARES
Calle 44a n.º 53–96
Bogotá, Colombia
Universidad de Caldas
Departamento de Ciencias Geológicas
Instituto de Investigaciones en
Estratigrafía (IIES)
Calle 65 n.º 26–10
Manizales, Colombia
- * Corresponding author

Supplementary Information:

S: <https://www2.sgc.gov.co/LibroGeologiaColombia/tgc/sgcpubesp37201911s.pdf>

Resumen La Formación Amagá es una sucesión siliciclástica tropical del Oligoceno tardío–Mioceno medio depositada a lo largo de varias cuencas sedimentarias semiaisladas intramontañosas (tracción) en la parte más septentrional de los Andes colombianos. A pesar de que estos registros sedimentarios con capas de carbón constituyen una de las sucesiones continentales del Oligoceno tardío–Mioceno medio más completas depositadas a lo largo del interior del margen convergente de los Andes del norte, la información geológica disponible sobre su sedimentología y estratigrafía es limitada. En esta contribución reportamos información estratigráfica nueva y detallada de la Formación Amagá en la Subcuenca de Santa Fe de Antioquia–San Jerónimo. Integramos esta información con datos publicados de sedimentología, estratigrafía de secuencias, bioestratigrafía, geocronología y termocronología de las sucesiones sedimentarias en esta formación, que aflora a lo largo de las subcuencas de Amagá–Venecia, Fredonia–La Pintada–Valparaíso y Santa Fe de Antioquia–San Jerónimo. Este enfoque integrador nos da la posibilidad de evaluar los mecanismos que controlan la evolución sedimentológica de sucesiones intramontañosas tropicales a lo largo de márgenes convergentes de tipo andino.

Este estudio nos permitió subdividir la Formación Amagá en dos miembros, el Miembro Inferior y el Miembro Superior. A nivel regional, el Miembro Inferior registra un cambio en los ambientes sedimentarios de un sistema de río trenzado a uno de río meándrico. Este cambio se produjo durante un período de aumento del espacio de alojamiento o acumulación de sedimentos en la cuenca, que coincide con la división de la Placa Farallon en las placas de Nazca y de Cocos en el Oligoceno tardío (28–25 Ma). El Miembro Superior de la Formación Amagá muestra asociaciones típicas de facies de sistemas de ríos trenzados, depositadas durante un período de disminución del espacio de acomodación de los sedimentos. Esta disminución de espacio probablemente se debió a un importante evento regional de levantamiento asociado al cambio mioceno temprano de convergencia oblicua a ortogonal entre la Placa de Nazca y la Placa de Suramérica y al avance y colisión del Bloque Panamá–Chocó al norte de Suramérica en el Mioceno temprano (23–21 Ma).

Palabras clave: *Formación Amagá, estratigrafía de secuencias, noroccidente de los Andes, tectónica oligocena–miocena, Bloque Panamá–Chocó.*

1. Introduction

The Cenozoic Amagá Formation is a hinterland/intramontane fluvial siliciclastic succession that crops out in the northernmost part of the Colombian Andes between what is currently known as the Central and Western Cordilleras of Colombia (Figure 1). These late Oligocene – middle Miocene tropical continental sedimentary successions, some of which display important occurrences of economically exploitable coalbeds (Grosse, 1926; Guzmán, 1991), were deposited in several semi-isolated pull-apart basins (Figures 1, 2; Guzmán & Sierra, 1984). These coal-bearing siliciclastic continental sedimentary records have been studied by several authors since the early 20th century (i.e., Grosse, 1926; Guzmán & Sierra, 1984; Delsant & Tejada, 1987; Guzmán, 1991, 2003, 2007a; Murillo, 1998; Correa & Silva-Tamayo, 1999; Hernández, 1999; González, 2001; Sierra et al., 2003; Silva-Tamayo et al., 2008; Henao, 2012; Sierra &

Marín-Cerón, 2012; Páez-Acuña, 2013; Rojas-Galvis & Salazar-Franco, 2013; etc.). Although most of these works focused on investigating the evolution of the Amagá Formation, some of them have also focused on quantifying the economic exploitability of the coal reserves of the Amagá Formation.

To date, few studies have integrated sedimentologic and sequence stratigraphic analyses of the Amagá Formation (i.e., Silva-Tamayo et al., 2008), and very few published studies have focused on investigating how the Cenozoic tectonic evolution of the northern Andes controlled the evolution of these tropical intramontane siliciclastic successions, which temporally coincides with periods of major plate tectonic reconfiguration along this margin (Montes et al., 2015; Piedrahita et al., 2017; Lara et al., 2018; León, et al., 2018).

To further contribute to the knowledge of the evolution of the coal-bearing Amagá Formation, here, we report new detailed stratigraphic information from the Amagá Formation

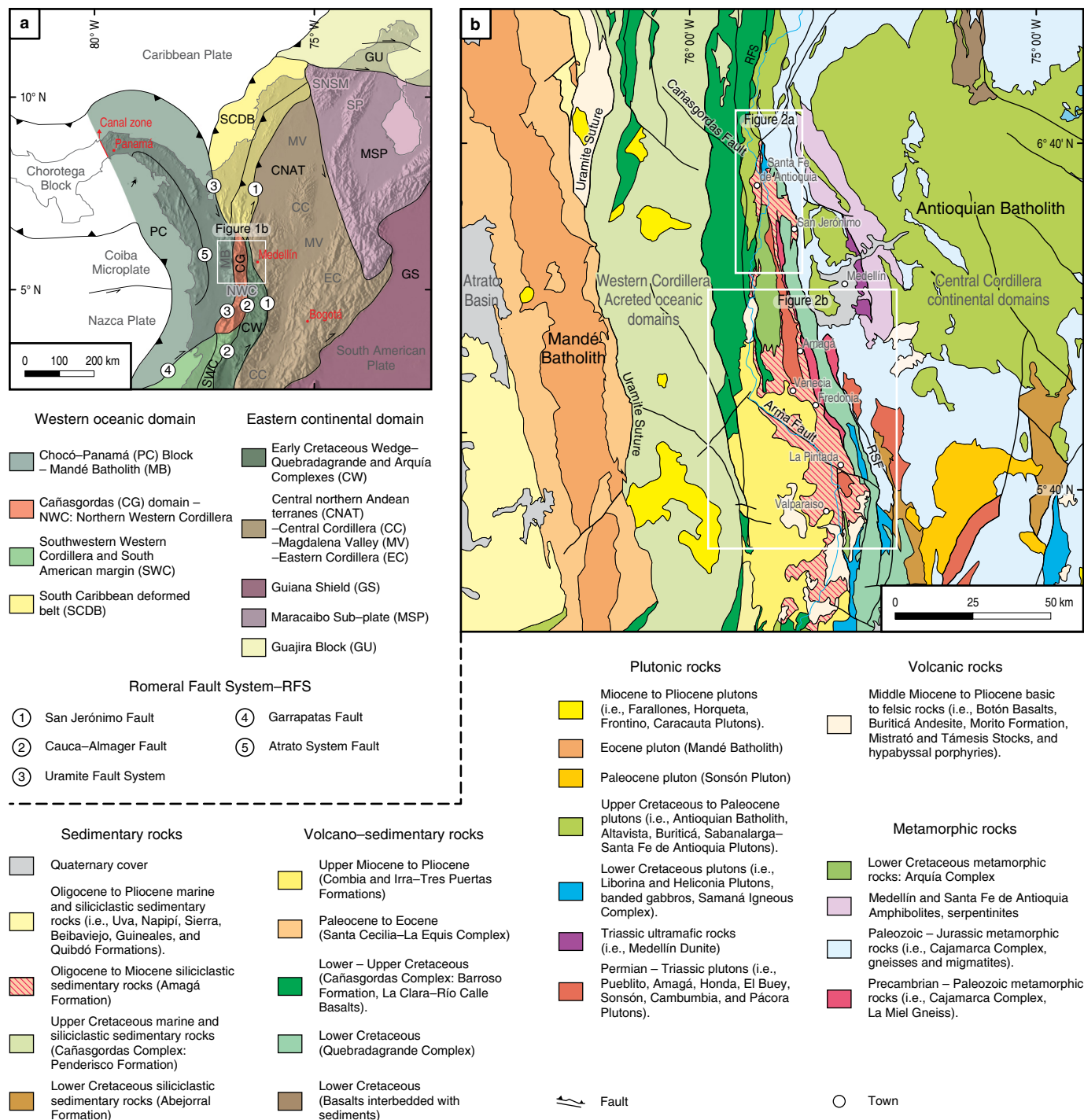


Figure 1. Geological setting and location of the study area. **(a)** Lithotectonic domains of the northwestern South America and Panamanian area (modified from Cedié et al., 2003). **(b)** Geological setting of the northwestern Andes (modified from Gómez et al., 2015). (SNSM) Sierra Nevada de Santa Marta; (SP) serranía de Perijá; (RFS) Romeral Fault System.

along the Santa Fe de Antioquia–San Jerónimo (SS) Sub-basin. We present a review of previously published studies focusing on the stratigraphy of the Amagá Formation along the Amagá–Venecia (AV) and Fredonia–La Pintada–Valparaíso (FPV) Sub-basins, which are located further south of the SS Sub-basin. Sequence stratigraphic analyses are used to propose

a genetic stratigraphic correlation of those sedimentary records and to assess the stratigraphic division of the Amagá Formation. These sequence stratigraphic data, complemented with previously published biostratigraphic, geochronologic (U–Pb detrital zircon ages), and thermochronologic (zircon fission-track cooling ages) data, are used to investigate how changes in the

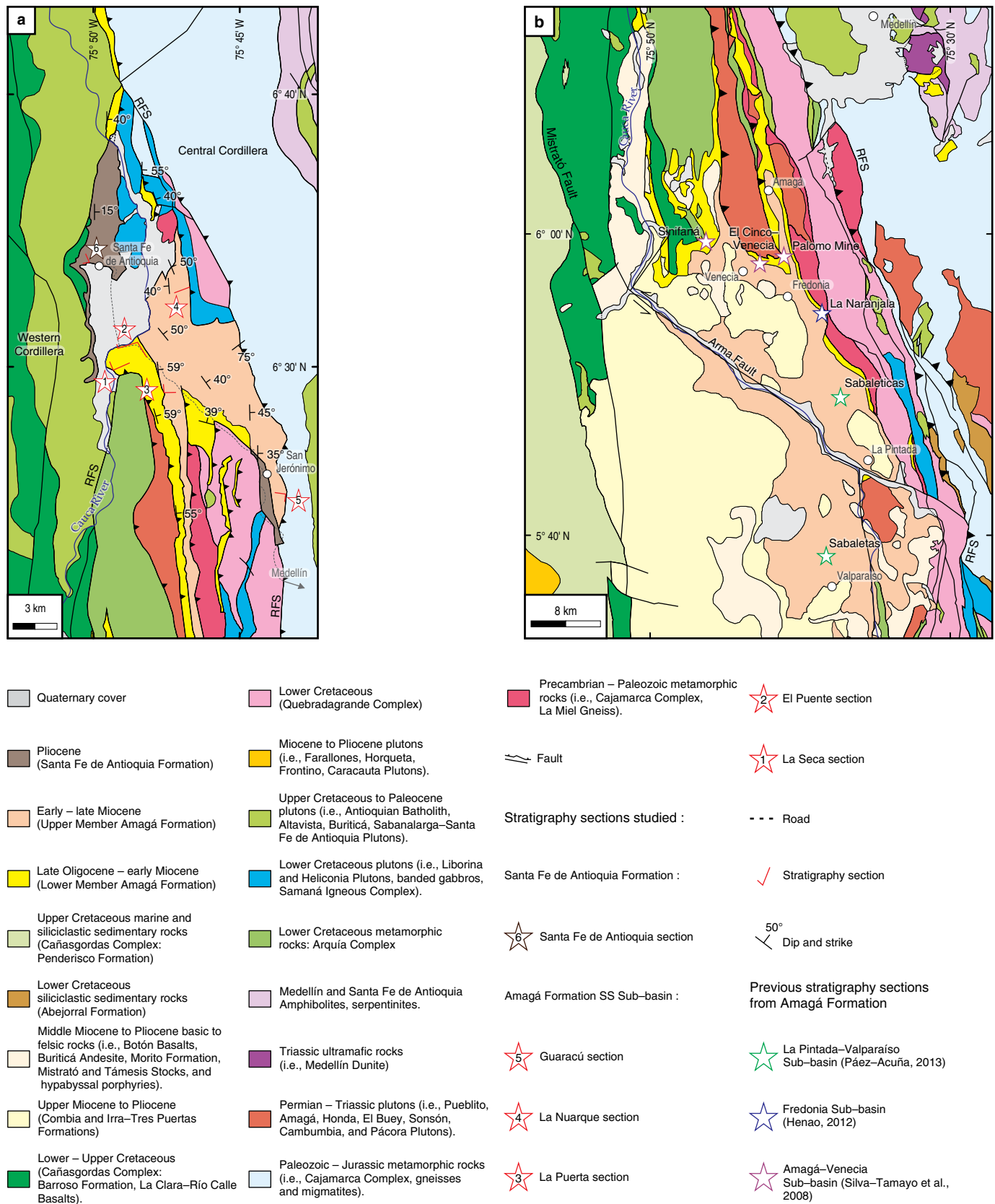


Figure 2. (a) Geological setting and location of Santa Fe de Antioquia and San Jerónimo Sub-basins of the Amagá Formation, study area (modified from González, 2001; Gómez et al., 2015; Montes et al., 2015). (b) Geological setting and location of Amagá-Venecia, Fredonia-La Pintada-Valparaíso Sub-basins of the Amagá Formation (modified from González, 2001; Gómez et al., 2015). (RFS) Romeral Fault System.

stratigraphic and sedimentologic characteristics of the Amagá Formation paralleled changes in Andean tectonics during the Oligocene – Miocene. The results of this work are ultimately used to further contribute to the investigation of the influence of changes in Andean tectonics on the deposition of intramontane siliciclastic successions along the northern Andes.

2. Geologic Setting

The Cenozoic evolution of the northern Andes has been influenced by important changes in tectonic setting, such as the late Oligocene break-up of the Farallon Plate into the Nazca and Cocos Plates (25–23 Ma; Pilger, 1984; Lonsdale, 2005; Pindell & Kennan, 2009; Escalona & Mann, 2011) and the early Miocene initial docking and collision of the Panamá–Chocó (PC) Block to northern South America (23–21 Ma; Montes et al., 2015; Lara et al., 2018). These changes in tectonic regime resulted in the formation of several pull-apart basins between the Central Cordillera and Western Cordillera of Colombia along what is today known as the Romeral Suture. The opening of these basins allowed for the deposition of several hinterland/intramontane siliciclastic successions, such as the Amagá Formation, which is the stratigraphic unit that is the focus of this work. The continued interaction between the PC and South American Blocks considerably increased during the middle Miocene and marked the end of the deposition of the Amagá Formation (ca. 15–13 Ma; Montes et al., 2015; Lara et al., 2018). This interaction also resulted in the emergence of the Panamá Isthmus and the subsequent closure of the Central America Seaway during the late Miocene – Pliocene (Duque-Caro, 1990; O’Dea et al., 2016; Lara et al., 2018). This event coincided with the onset of late Miocene – Pliocene arc magmatism along the different pull-apart basins where the Amagá Formation was deposited (MacDonald, 1980; Restrepo et al., 1981; Leal-Mejía, 2011; Rodríguez & Zapata, 2014). It also resulted in the deposition of several intramontane fluvial sedimentary successions, such as the Pliocene siliciclastic Santa Fe de Antioquia Formation, which unconformably overlies the Amagá Formation in the SS Sub-basin (Figures 1b, 2a; Lara et al., 2018; this work).

The Amagá Formation is an intramontane fluvial siliciclastic succession that contains important occurrences of economically exploitable coalbeds (Grosse, 1926; González, 1980). It crops out along the northwesternmost part of the northern Andes, between the Western and Central Cordilleras of Colombia, within a series of south–north–trending pull-apart basins that follow the trace of the strike of the Romeral Fault System (RFS) (Figures 1, 2; Guzmán, 1991; Sierra et al., 2003; Silva-Tamayo et al., 2008; Sierra & Marín-Cerón, 2012). The RFS is the tectonic suture that separates the allochthonous oceanic domains of western Colombia from the autochthonous continental domains located to the east (Figure 1a; Cedié et al.,

2003; Moreno-Sánchez & Pardo-Trujillo, 2003; Chicangana, 2005; Cochran et al., 2014; Spikings et al., 2015).

Ospina (1911) was the first to produce a preliminary map of the lithologic units of the Amagá Formation near Amagá town. Posada (1913) was the first to propose a formal stratigraphic hierarchical name for this siliciclastic record, i.e., “Formación Carbonífera de Amagá”. Grosse (1926) renamed this sedimentary record “Terciario Carbonífero de Antioquia” and subdivided it into two units based on the presence or absence of coal-bearing layers. van der Hammen (1958), following the work of Grosse (1926), formally named it the “Antioquia Formation”. González (1980) finally proposed the name “Amagá Formation”, which is still in use. González (1980) and Delsant & Tejada (1987) also subdivided the Amagá Formation into three members based on the presence or absence of coal. Sierra et al. (2003) finally subdivided the Amagá Formation based on its facies associations, variations in depositional environments, and changes in the compositional modes of its major petrofacies. Silva-Tamayo et al. (2008) used high-resolution lithostratigraphic analyses to investigate the depositional style of the Amagá Formation in the AV Sub-basin and proposed a sequence stratigraphic framework for the Amagá Formation. Based on their findings, these authors also redefined the Amagá Formation and divided it into two members, i.e., the Lower and Upper Members.

The Amagá Formation unconformably overlies and/or is often found in fault contact with the metamorphic and igneous basement of the Central Cordillera and Western Cordillera of Colombia, i.e., the Cretaceous Quebradagrande and Arquía Complexes, Cretaceous Sabanalarga Batholith, and Triassic Pueblito and Amagá Stocks, among others (Figures 1b, 2; Grosse, 1926; González, 2001). The Amagá Formation is overlain, discordantly to para-conformably, by a series of upper Miocene – Pliocene volcano-sedimentary successions from the Combia, Morito, Irra-Tres Puertas, and Santa Fe de Antioquia Formations (Leal-Mejía, 2011; Rodríguez & Zapata, 2014; Lara et al., 2018; this work). It is also intruded by late Miocene (11–6 Ma) hypabyssal porphyries (Figures 1b, 2b) and volcanic rocks (with adakitic affinity) from the Combia Formation in the AV and FPV Sub-basins (MacDonald 1980; Restrepo et al., 1981; Leal-Mejía, 2011; Rodríguez & Zapata, 2014; Borrero & Toro-Toro, 2016). The Amagá Formation has mainly been studied along the AV and FPV Sub-basins, where important coalbeds occur (Figures 1b, 2b; Grosse, 1926; González, 1980; Correa & Silva-Tamayo, 1999; Sierra et al., 2003; Silva-Tamayo et al., 2008; Henao, 2012; Páez-Acuña, 2013; and references therein). The Amagá Formation also crops out to the north of the AV Sub-basin, along the SS Sub-basin, which is the focus of the present study (Figures 1b, 2a; Lara et al., 2018; this work).

The depositional age of the Amagá Formation is controversial. Scheibe (1919) was the first to propose a depositional

age for the Amagá Formation. This author proposed a Tertiary age based on the presence of undifferentiated Tertiary paly-nomorphs in the Lower Member in the AV Sub-basin. Later, Grosse (1926) reported the presence of Eocene – Oligocene palynomorphs in the Lower Member of the Amagá Formation in the AV Sub-basin and interpreted those ages as the maximum depositional age of the Amagá Formation. Eocene palynomorphs have also been reported for the Lower Member of the Amagá Formation in both the SS (Ramírez *et al.*, 2015 and references therein) and AV Sub-basins (Londoño *et al.*, 2013 and references therein). However, the presence of Eocene paly-nomorphs in the Amagá Formation is controversial and has recently been attributed to the reworking of pre-existing Eocene sedimentary units that crop out along the track of the RFS (Lara *et al.*, 2018). Although Pons (1984) reported Oligocene – Miocene palynomorphs in the Lower Member of the AV Sub-basin, the lack of stratigraphic control in that work makes it difficult to assess the reliability of this age of the Lower Member.

The upper depositional age of the Amagá Formation is less controversial. A late Miocene upper depositional age can be proposed based on the 10–7 Ma age of the overlying volcanic (adakitic affinity) deposits of the Combia and Monitos Formations (Borrero & Toro-Toro, 2016) and the occurrence of the 6 to 11 Ma hypabyssal porphyritic intrusions cross-cutting the Upper Member in the AV Sub-basin (MacDonald, 1980; Restrepo *et al.*, 1981; Leal-Mejía, 2011; Rodríguez & Zapata, 2014). The middle Miocene upper depositional age of the Amagá Formation is further supported by the presence of 13 Ma detrital zircons in the Upper Member of the Amagá Formation in the SS Sub-basin (Montes *et al.*, 2015). In this sub-basin, the Amagá Formation is unconformably overlain by the Santa Fe de Antioquia Formation, which contains 4.8 Ma detrital zircons (Lara *et al.*, 2018).

Detrital zircon fission-track (ZFT) and magnetic susceptibility anisotropy (ASM) data suggest that several deformational and exhumation events affected both the Lower and Upper Members of the Amagá Formation in the AV Sub-basin. These events have been related to the Oligocene break-up of the Farallon Plate into the Nazca and Cocos Plates as well as to the Miocene collision of the PC Block to northern South America (Ramírez-Arias *et al.*, 2012; Sierra & Marín-Cerón, 2012; Piedrahita *et al.*, 2017; Lara *et al.*, 2018). Lara *et al.* (2018) used the detrital zircon fission-track data and U–Pb detrital zircon ages from the Upper Member to propose a short lag time between the erosion of its sediment source areas and the sedimentation of the Upper Member.

Finally, the Amagá Formation has been regionally correlated with marginal continental and transitional siliciclastic deposits from the Cauca–Patía and San Jacinto Basins (Figure 3; references therein). However, these correlations must be regarded with caution given the lack of consensus on the ages of these formations.

3. Methods

In this contribution, we report both previously published and unpublished sedimentologic and stratigraphic information about the Amagá Formation. Four previously published composite stratigraphic columns of the Amagá Formation from the AV and FPV Sub-basins are presented in Figures 4–6 (Silva-Tamayo *et al.*, 2008; Henao, 2012; Páez-Acuña, 2013). In addition, one new composite stratigraphic column of the Amagá Formation from the SS Sub-basin is herein reported for the first time (Figure 7). One new stratigraphic column of consolidated but uncemented sediments unconformably overlying the Amagá Formation in the SS Sub-basin (named the Santa Fe de Antioquia Formation; Lara *et al.*, 2018) is also presented in detail here for the first time (Figure 7).

The sedimentary facies analyses of the Amagá and Santa Fe de Antioquia Formations in the SS Sub-basin were performed following Miall (1985, 1996). The sequence stratigraphic analyses were performed following Cross (1988) and Ramón & Cross (1997). These same methods were previously used by Silva-Tamayo *et al.* (2008) to subdivide the Amagá Formation into two members and later used by Henao (2012) and Páez-Acuña (2013) to study the sedimentary records in the AV and FPV Sub-basins. Briefly, variations in facies associations and variations in stratigraphic stacking patterns were used to define stratigraphic cycles. Variations in the preservation of geomorphic elements, such as channels, flood plains, point bars, and paleosols, were also considered when defining stratigraphic cycles. Long-term variations in stratigraphic cycles were subsequently used to define changes in the base level position along the basin, i.e., changes in the accommodation space (A)/sediment supply (S) ratio (A/S) (Cross, 1988; Ramón & Cross, 1997), and to correlate the different reported stratigraphic sections. Briefly, continental sedimentary successions displaying coarse-grained material and coarsening-upward and/or aggradational stacking patterns are considered to have been deposited during periods of low A/S. The low diversity of sedimentary facies and low preservation of fine-grained facies and geomorphic elements such as flood plains, lakes, point bars, and paleosols are also expected under low A/S conditions. Sediments deposited under low A/S conditions are also characterized by high degrees of channel amalgamation and the presence of erosional surfaces. During periods of high A/S, in turn, continental sedimentary successions display high facies diversity and especially the high preservation of fine-grained sediments and geomorphic features. The presence of coarse-grained material, i.e., conglomerates and coarse-grained sandstone, tends to decrease as the A/S increases. Enhanced accommodation space allows for the migration of rivers; therefore, the amalgamation of channels is low. This results in fining-upward stratigraphic cycles and a higher degree of symmetry between fining-upward and coarsening-upward cycles.

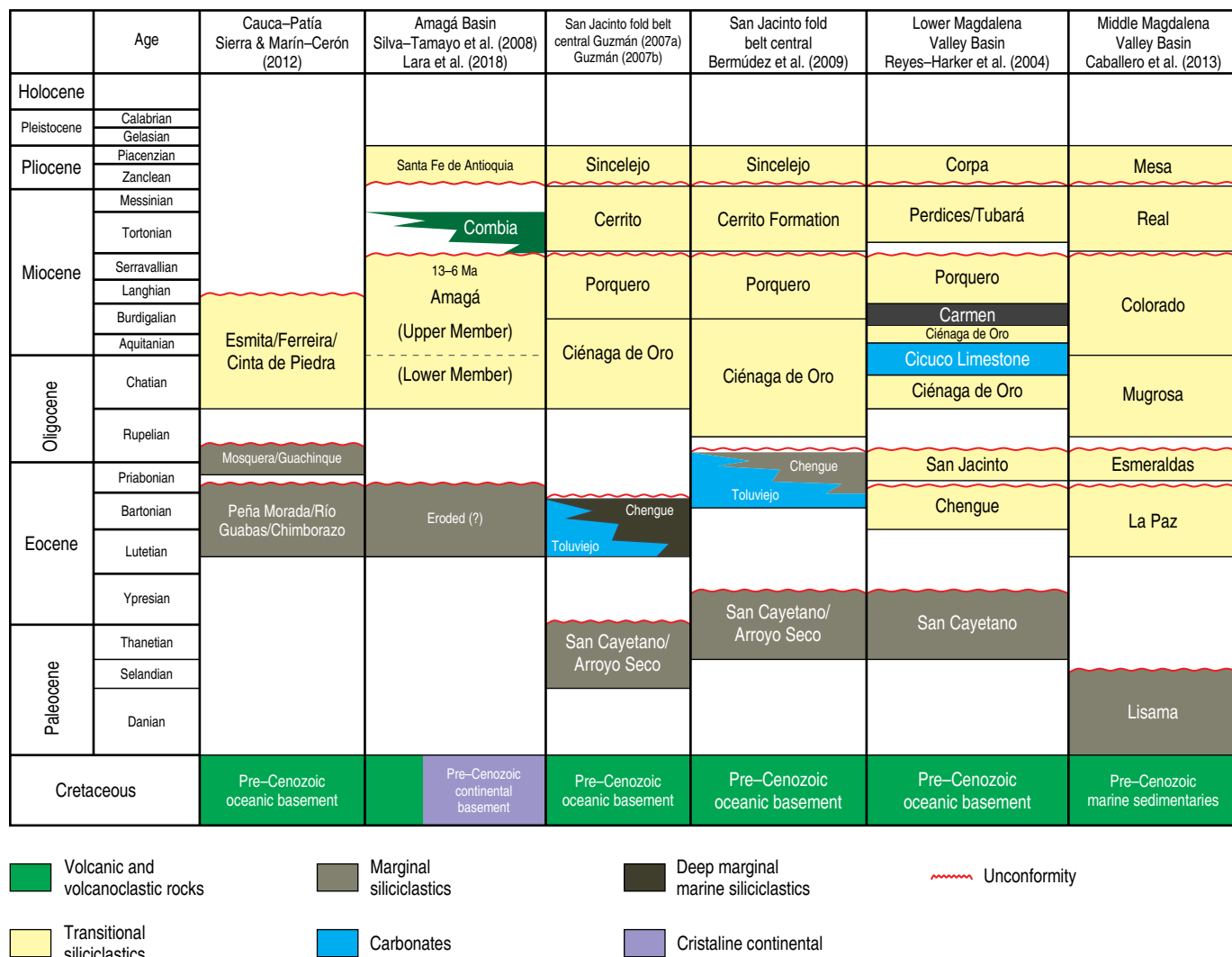


Figure 3. General Cenozoic litho-chronostratigraphic chart of western Colombia (references therein).

4. Results

4.1. Available and Published Lithostratigraphic Information

Sierra et al. (2003) and Silva-Tamayo et al. (2008) reported sedimentologic information for the Amagá Formation in the AV Sub-basin (Figures 1b, 2b, 4). The thickness of the Amagá Formation in this sub-basin is ca. 570 m. The Lower Member of the Amagá Formation unconformably overlies pre-Cenozoic rocks from the basement of the Central Cordillera of Colombia. The lowermost part of the Lower Member displays a series of aggradational conglomerates and conglomeratic sandstones overlain by fining-upward coarse- to medium-grained sandstones interbedded with slightly bioturbated (plant roots) siltstones and coals. Higher in the stratigraphy, the sandstones become medium to fine-grained and display both fining- and coarsening-upward characteristics. These sandstones, which

also display a fining-upward trend, are interbedded with bioturbated siltstones and organic carbon-rich siltstones (coalbeds). The uppermost part of the Lower Member displays a decrease in the ratio of siltstone to sandstone, with the latter being coarser-grained and displaying mixed fining-upward and coarsening-upward trends. The lowermost part of the Upper Member of the Amagá Formation in the AV Sub-basin displays a basal series of thick, aggradational and coarsening-upward medium- to coarse-grained sandstones (Figure 4). Higher in the stratigraphy, the sandstone become thinner and interbedded with bioturbated (plant roots) siltstones. Unlike those in the Lower Member, the siltstones in the Upper Member are organic carbon-poor, which is reflected by the absence of coalbeds. The uppermost part of the Upper Member of the Amagá Formation in the AV Sub-basin displays a new increase in the proportion of sandstone to siltstone, with the former becoming more aggradational and thicker than those from the lowermost portion of the Upper Member.

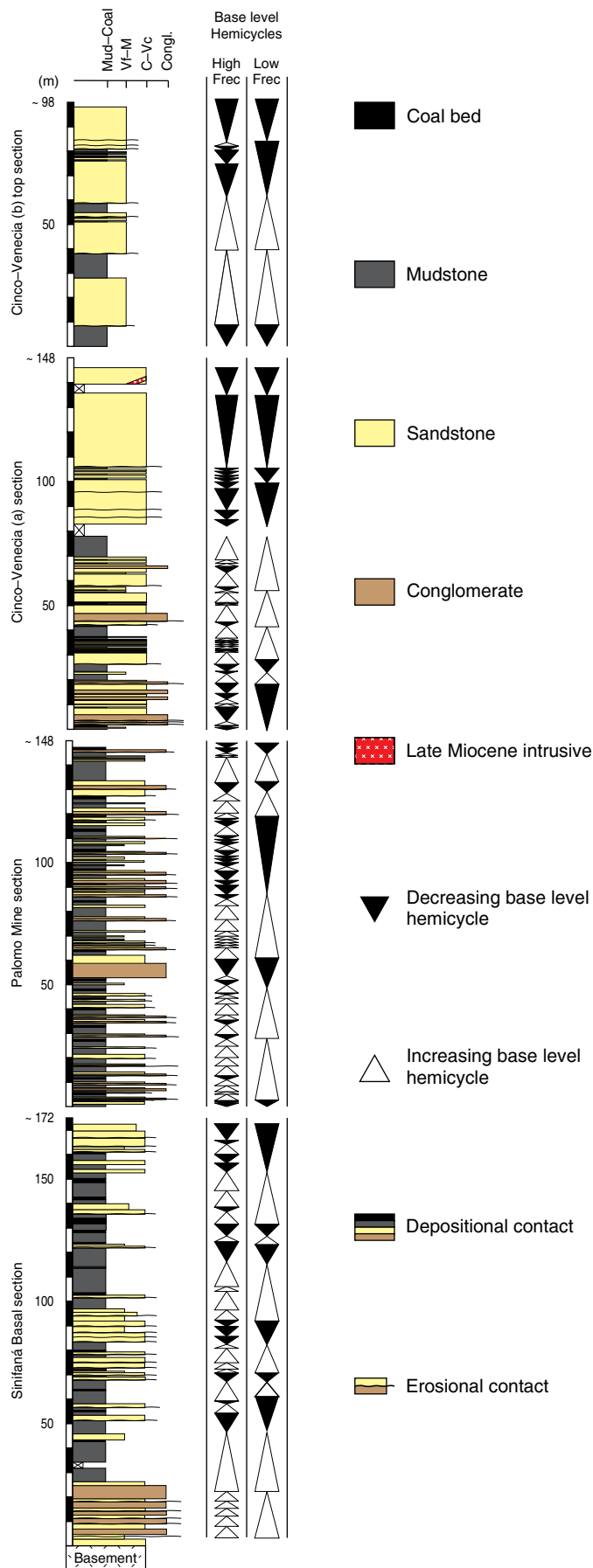


Figure 4. Lithostratigraphy of the Amagá Formation in the Amagá-Venecia Sub-basin (Silva-Tamayo *et al.*, 2008).

Henao (2012) reported the sedimentologic and stratigraphic characteristics of the Amagá Formation along the FPV Sub-basin (Figures 1b, 2b, 5). In this sub-basin, the Amagá Formation is 345 m thick, but only the Lower Member of the Amagá Formation crops out. According to this author, the Amagá Formation unconformably overlies the pre-Cenozoic basement of the Central Cordillera of Colombia (Figures 1b, 2b, 5). The stratigraphic section reported by Henao (2012) displays a series of basal interbedded aggradational conglomeratic and coarse-grained sandstones. Higher in the stratigraphy, the conglomeratic sandstones become less frequent, and a series of fining-upward sandstones interbedded with bioturbated and organic carbon-rich siltstones (now coalbeds) occur. Even higher in the stratigraphy, these siltstones become more frequent and are interbedded with fining-upward medium to fine-grained sandstones. The uppermost part of the stratigraphic section reported by Henao (2012) is dominated by bioturbated and organic carbon-rich siltstones interbedded with limited fining-upward medium to coarse-grained sandstones (Figure 5).

Páez-Acuña (2013) reported sedimentologic and stratigraphic information for the two stratigraphic sections (Sabale-tas and Sabaleticas sections) of the Amagá Formation from the FPV Sub-basin (Figures 1b, 2b, 6). The approximate composite thickness of the Amagá Formation is 257 m, but the base of the Amagá Formation does not crop out in either section. In the Sabaleticas stratigraphic section, the lowermost part of the Amagá Formation mostly displays aggradational, coarsening-upward medium-grained sandstones interbedded with bioturbated siltstones. These siltstones become more frequent higher in the stratigraphy, while the sandstones become thinner and fine upwards (Figures 2b, 6b). The lowermost part of the Sabaletas stratigraphic section displays a series of aggradation-al coarsening-upward medium- to coarse-grained sandstones with sporadic conglomeratic sandstones. Higher in the stratigraphy, the conglomeratic sandstones become less frequent, and the medium-grained sandstones become less aggradational and are interbedded with organic carbon-poor bioturbated siltstones (Figures 2b, 6a).

4.2. New Lithostratigraphic Information

The following paragraphs describe the six studied stratigraphic sections from the SS Sub-basin, which is the focus of this study. Figures 1b, 2a, and 7 show the generalized stratigraphic location and log of the Amagá Formation in the SS Sub-basin. The thickness of the Amagá Formation in this sub-basin is approximately 754 m. Figure 1 of the Supplementary Information shows the stratigraphic logs of the studied stratigraphic sec-

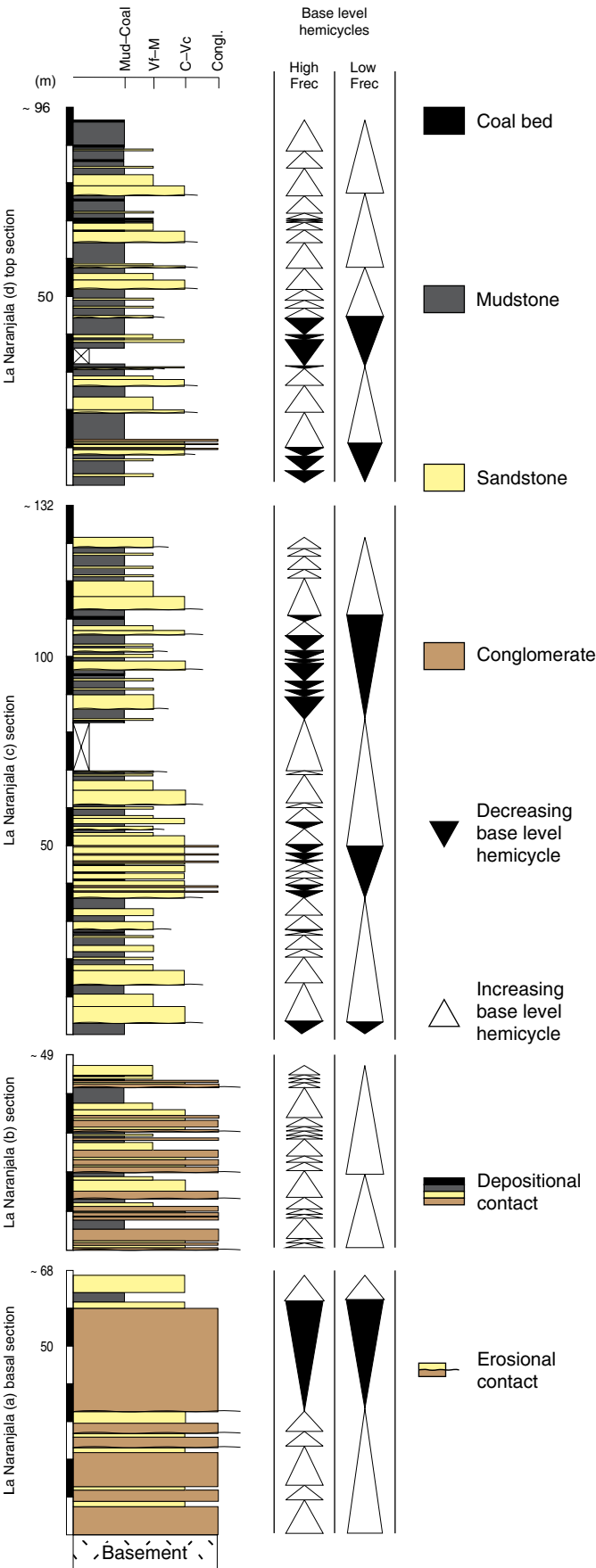


Figure 5. Lithostratigraphy of the Amagá Formation in the Fredonia area of the Fredonia-La Pintada-Valparaíso Sub-basin (Henao, 2012).

tions in detail. Figure 7 and the Figure 1 of the Supplementary Information also show the stratigraphic log of a consolidated uncemented sedimentary succession (54 m thick) that unconformably overlies the Amagá Formation. Table 1 presents the nomenclature of the principal sedimentary environments and related facies associations observed in the Amagá Formation (modified from Miall, 1985).

4.2.1. La Seca Stratigraphic Section

La Seca stratigraphic section corresponds to the lowermost part of the Amagá Formation (Figures 2a, 7). In this section, the Amagá Formation is 74 m thick and discordantly overlies the metamorphic basement of the Central Cordillera of Colombia, i.e., the Arquía Complex. The lower part of the stratigraphic section consists of sub-horizontal strata of coarse (St) to medium-grained (Sp) massive sandstones interbedded with polymictic conglomerates (Gt) and massive (Gms) and laminated (Gm) conglomeratic sandstones (Figure 8a). The stratigraphic succession displays a predominantly fining-upward character. The fining-upward Gt, Gm, and Gms facies are separated by erosional contacts and are often found amalgamated (Figure 7). The basal sandstones and conglomeratic facies are overlain by a 22 m thick interval of intercalated massive mudstones (Fsc) and laminated mudstones (Fl). This fine-grained interval is, in turn, overlain by a coarsening-upward package (14 m thick) of laminated fine to medium-grained massive (Sh) and laminated sandstones (Shl) and medium to coarse-grained massive sandstones (St, Sp). The uppermost part of this section is characterized by intercalations of mudstone (Fsc) with centimeter-scale layers of carbonaceous material (C) and laminated fine-grained sandstones (Shl).

4.2.2. El Puente Stratigraphic Section

El Puente stratigraphic section is ca. 331 m thick (Figures 2a, 7). The lowermost part (0–70 m thick) of this succession consists of fine-grained sandstones displaying planar and trough cross laminations (facies Sr and Srl) interbedded with strata of fine to medium-grained (Sh) and coarse to medium-grained sandstones (Sp, St), massive mottled mudstones (Fs), and organic matter-rich gray mudstones (Fsc) (Figure 8b). Some centimeter-scale coal layers (C) can also be found interbedded with the gray mudstones. An important increase in the grain size of the sandstones is observed between the heights of 34 and 70 m, where medium to coarse-grained sandstones with large scale high angle parallel laminations (Stl) and bimodal cross

Neogene
Paleogene

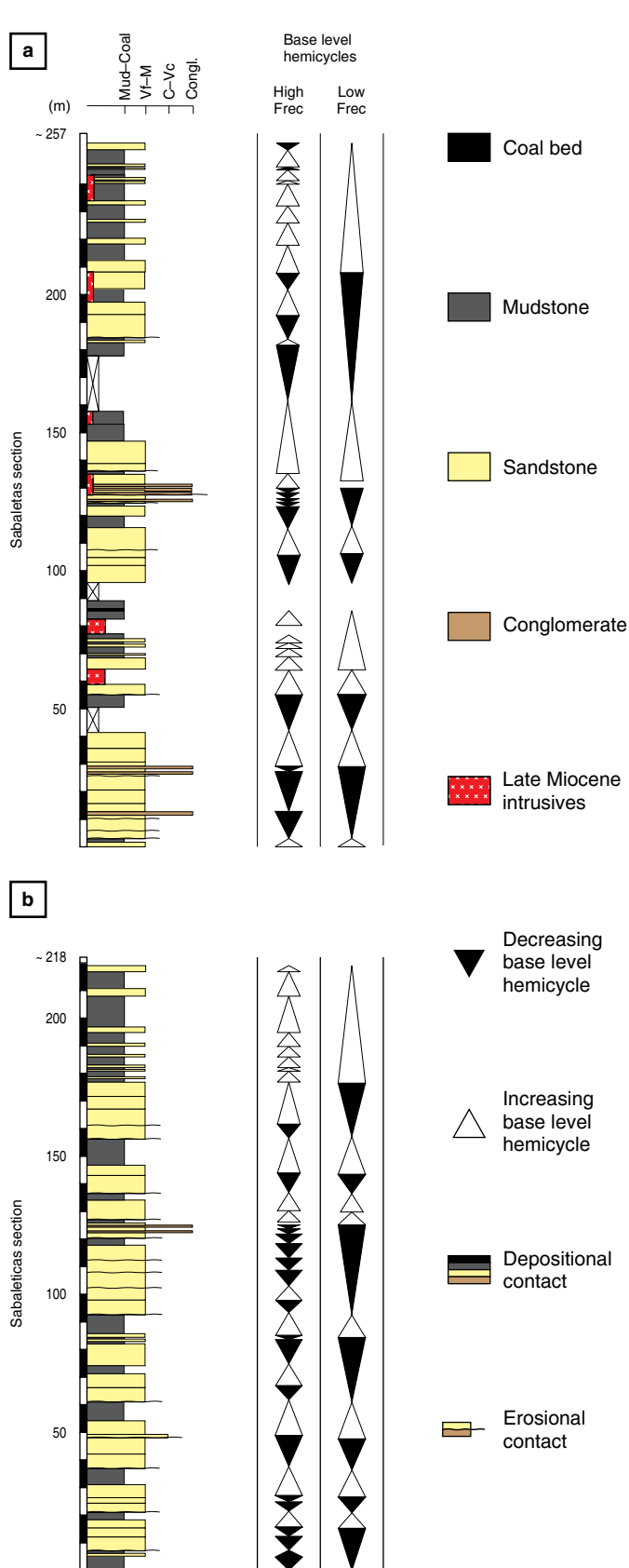


Figure 6. Lithostratigraphy of the Amagá Formation in the Valparaíso area of the Fredonia-La Pintada-Valparaíso Sub-basin (Páez-Acuña, 2013).

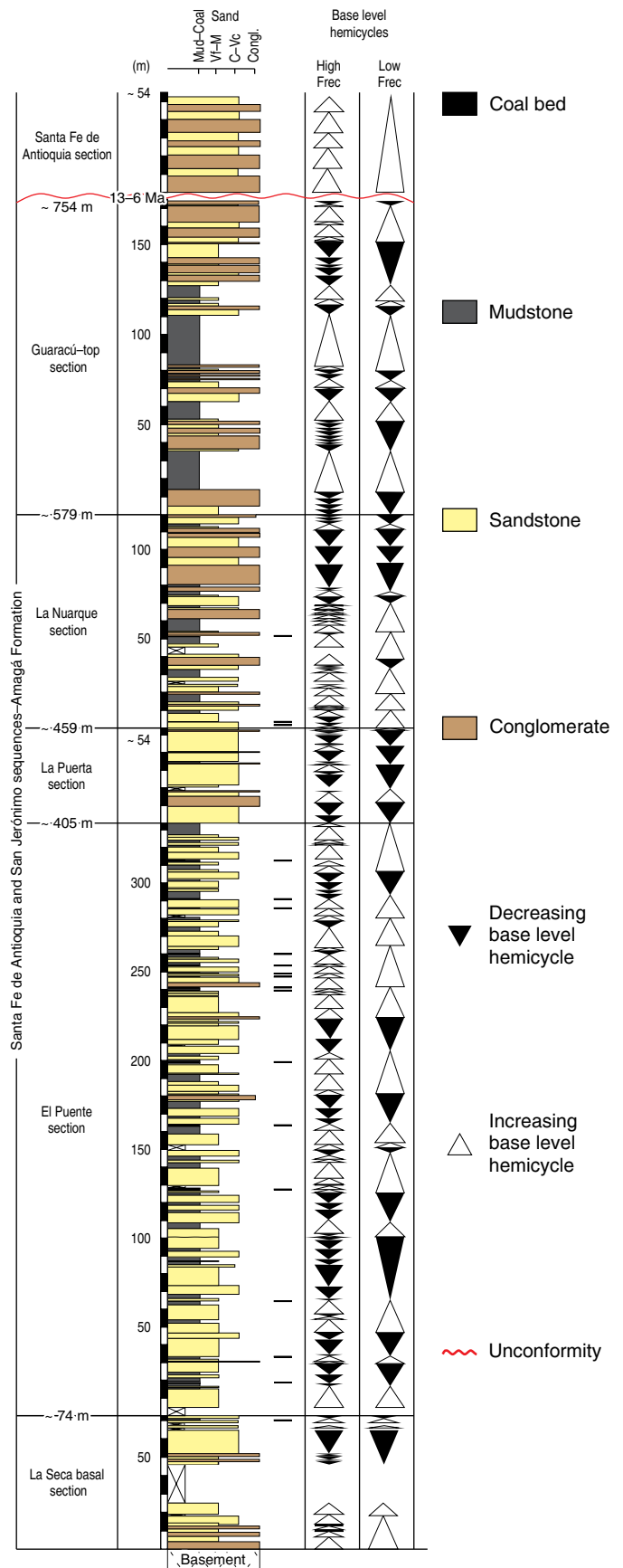


Figure 7. Lithostratigraphy of the Amagá and Santa Fe de Antioquia Formations in the Santa Fe de Antioquia-San Jerónimo Sub-basin.

Table 1. Principal sedimentary environments and related facies associations observed in the Amagá Formation.

Facies association	Facies	Facies code	Characteristics
Meandering channels	• Fine-grained sandstones with planar laminations.	Srl	• Fine-grained sandstone. It usually displays laminations. It is up to 1 m thick.
	• Fine-grained sandstone with trough laminations.	Sr	• Fine-grained sandstone. It can be found amalgamated and can be up to 2 m thick.
	• Fine- to medium-grained massive sandstone.	Sh	• Fine- to medium-grained sandstone up to 2 m thick.
	• Fine- to medium-grained laminated sandstone.	Shl	• Medium-grained sandstone up to 2 m thick.
	• Fine- to medium-grained sandstone with ripples.	Shcr	• Fine- to medium-grained sandstone. It can be amalgamated and is up to 2 m thick.
	• Fine- to medium-grained sandstone with high-angle parallel cross laminations.	Shlh	• Fine- to medium-grained sandstone up to 2 m thick.
	• Fine- to medium-grained sandstone with cross lamination.	Shc	• Fine- to medium-grained sandstone. It can be amalgamated and is up to 2 m thick.
	• Fine- to medium-grained sandstone with bimodal and trough cross stratification and laminations.	Shcb	• Amalgamated sandstone up to 3 m thick.
	• Fine- to medium-grained sandstone with large-scale cross stratification.	Shlc	• Amalgamated sandstone up to 5 m thick.
	• Fine- to medium-grained sandstone with climbing ripples.	Shcri	• Fine- to medium-grained sandstone with climbing ripples. Usually up to 2 m thick.
	• Fine- to medium-grained sandstone with undulated laminations.	Shu	• Fine- to medium-grained sandstone. It can be up to 2 m thick.
	• Coarse-grained sandstone with high-angle parallel cross laminations.	Stlh	• Coarse-grained sandstone up to 2 m thick.
	• Coarse-grained sandstone with bimodal cross stratification and laminations.	Stc	• Coarse-grained sandstone. It can be amalgamated and up to 3 m thick.
	• Coarse-grained sandstone with bimodal and trough cross stratification and laminations.	Stcb	• Coarse-grained sandstone. It can be amalgamated and up to 5 m thick.
	• Coarse-grained massive sandstone.	St	• Coarse-grained sandstone that is 0.5 to 5.0 m thick.
	• Medium-grained massive sandstone.	Sp	• Medium-grained massive sandstone that is 0.5 to 5.0 m thick.
Braided channels	• Massive mudstones.	Fsc	• Black, gray to green massive mudstones, up to 5 m thick.
	• Laminated mudstones.	Fl	• Black, gray to green laminated mudstones, up to 5 m thick.
	• Fine- to medium-grained massive sandstone.	Sh	• Fine- to medium-grained sandstone up to 2 m thick.
	• Fine- to medium-grained laminated sandstone.	Shl	• Fine- to medium-grained sandstone up to 2 m thick.
	• Coarse-grained massive sandstone.	St	• Coarse-grained sandstone that is 0.5 to 5.0 m thick.
	• Coarse-grained laminated sandstone.	Stl	• Coarse-grained laminated sandstone. Up to 5 m thick.
	• Coarse-grained sandstone with trough cross stratification.	Stt	• Coarse-grained sandstone. Up to 5 m thick and can be amalgamated.
	• Coarse-grained sandstone with planar cross stratification and laminations.	Stc	• Coarse-grained sandstone. Up to 5 m thick and can be amalgamated.
	• Medium-grained massive sandstone.	Sp	• Medium-grained massive sandstone 0.5 to 5.0 m thick.
	• Polymictic conglomerates.	Gt	• Clasts displaying several compositions. Generally very massive.
	• Conglomeratic sandstone with continuous parallel lamination.	Gm	• Coarse-grained sandstone 1 to 5 m thick.
	• Massive conglomeratic sandstone.	Gms	• Coarse-grained sandstone 1 to 5 m thick.
Crevasse	• Fine- to medium-grained sandstone with cross lamination.	Shc	• Sandstone up to 1 m thick.
	• Fine- to medium-grained sandstone with large-scale cross stratification.	Shlc	• Sandstone up to 1 m thick.
	• Fine- to medium-grained sandstone with climbing ripples.	Shcr	• Sandstone up to 1 m thick.
	• Fine- to medium-grained sandstone with undulating laminations.	Shu	• Sandstone up to 1 m thick.
Humid flood plain	• Laminated mudstones.	Fl	• Black, gray to green laminated mudstones, up to 5 m thick.
	• Massive mudstones.	Fs	• Black, gray to green massive mudstones, up to 5 m thick.
	• Coal/organic-rich mudstones.	C	• Coalbed organic matter.

Source: Data modified from Miall (1985).

Neogene

Paleogene

laminations (Stc) occur. Coarse-grained and medium-grained sandstones displaying trough cross stratification (Stcb, Shcb), as well as coarse-grained and medium-grained sandstones displaying parallel high angle cross laminations (Shlh, Stlh), are also common. These sandstones are strongly amalgamated, display several erosional surfaces, and contain some levels of polymictic conglomerates. Sandstones with calcareous concretions are also common.

A slight decrease in the amount of amalgamated sandstones and an increase in the amount of mudstones (facies Fsc, Fl) occurs between 70 and 85 m in height (Figures 2a, 7). The sandstones become thinner, and some display undulating laminations and small-scale ripples (facies Shu and Shcr). An important increase in fine-grained facies, i.e., organic-rich muds, occurs between the heights of 85 and 109 m. The sandstones are thicker and display unidirectional cross stratification, parallel laminations, and undulating laminations (facies Shc, Shl, Shu). Between the heights of 109 and 204 m, the proportions of sandstones and mudstones are similar. The coarse-grained sandstones with trough and parallel cross stratification (facies Stcb, Stlh) become abundant. The fine to medium-grained sandstones display undulating laminations, small and large-scale cross stratification, and climbing ripples (facies Shl, Shlc, Shcr). Between 204 and 238 m in height, there is an increase in the facies of St and Sp. Erosional surfaces separating amalgamated channels are also present. From 240 to 330 m in height, there is an increase in fine-grained facies, such as Fm, Fsc, and C. These sandstones usually belong to the Sp, Sr, and Sh facies.

4.2.3. La Puerta Stratigraphic Section

La Puerta stratigraphic section (ca. 54 m thick; Figures 2a, 7) consists of coarse-grained sandstones displaying parallel lamination and trough and planar cross stratification (facies Stl, Stt, Stc) (Figure 8c). The sandstone packages display erosional surfaces separating amalgamated channels. Some conglomerate levels with trough and planar cross stratification (facies Gt, Gm) are also present. The sandstones display calcareous concretions. A few interbedded green-gray mudstones, which are both massive and laminated and contain plant remains (facies Fsc and Fm), are also present.

4.2.4. La Nuarque Stratigraphic Section

This stratigraphic section crops out along the La Nuarque Creek in the northeastern part of the SS Sub-basin and is ca. 120 m thick (Figures 2a, 7, 8d). The lowermost part of the section (0 to 40 m in height) displays basal fine to coarse-grained sandstones displaying planar laminations and trough cross stratification (facies Stl, Stt). The sandstone packages display erosional surfaces and are interbedded with green mudstones, which contain poorly preserved organic matter (facies

Fsc, Fl). Some conglomeratic horizons that are a few centimeters in thickness (facies Gms and Gt) are also present. The coarse-grained facies become less abundant between 40 and 62 m in height. In this interval, facies Fsc, Fl, and C become more abundant. A few medium to coarse-grained sandstones are interbedded between the fine-grained facies. Between 62 and 82 m in height, the conglomeratic facies become more common (Gt and Gms). The proportions of the fine-grained facies (Fsc, Fl, and C) are similar to those in the lowermost part of the section. Between the heights of 82 and 120 m, the amounts of fine-grained facies substantially decrease, and the coarse-grained sandstone and conglomeratic facies become abundant (facies Gt, Gm, St, Sp) (Figure 7).

4.2.5. Guaracú Stratigraphic Section

The Guaracú stratigraphic section is ca. 175 m thick (Figures 2a, 7). It consists of amalgamated coarse-grained sandstones, massive and polymictic conglomerates, and conglomeratic sandstone (facies Gm, Gms, St, Sp) (Figure 8e). The sandstones display mudstone intraclasts and calcareous concretions, as well as common erosional surfaces between amalgamated sandstones and conglomerates (Figure 7). This section also displays massive mudstones interbedded with the main sandstone packages.

4.2.6. Santa Fe de Antioquia Stratigraphic Section

The Santa Fe de Antioquia stratigraphic section is ca. 54 m thick (Figures 2a, 7, 8f). It consists of consolidated but uncemented sandstones and conglomerates. This stratigraphic section starts with para-conglomerates displaying fining-upward gradations and clast imbrications (facies Gm). These para-conglomerates unconformably overlie the Santa Fe de Antioquia Batholith and overlie the Amagá Formation along an angular unconformity. Higher in the stratigraphic section, both ortho- and para-conglomerates (facies Gm and Gms), as well as coarse-grained sandstones displaying both trough cross stratification and planar cross stratification (Stt, Stc), occur. Based on its unconformable position on top of the Amagá Formation and the U-Pb detrital zircon ages reported by Lara *et al.* (2018), we consider this sedimentary succession to be part of an additional stratigraphic unit, which is herein named the Santa Fe de Antioquia Formation.

5. Discussion

5.1. Sedimentary Environments

The lowermost part of the Amagá Formation in the SS Sub-basin crops out along La Seca stratigraphic section. In this section, it displays aggradational and fining-upward thick-bedded coarse-grained sandstones and conglomerates with

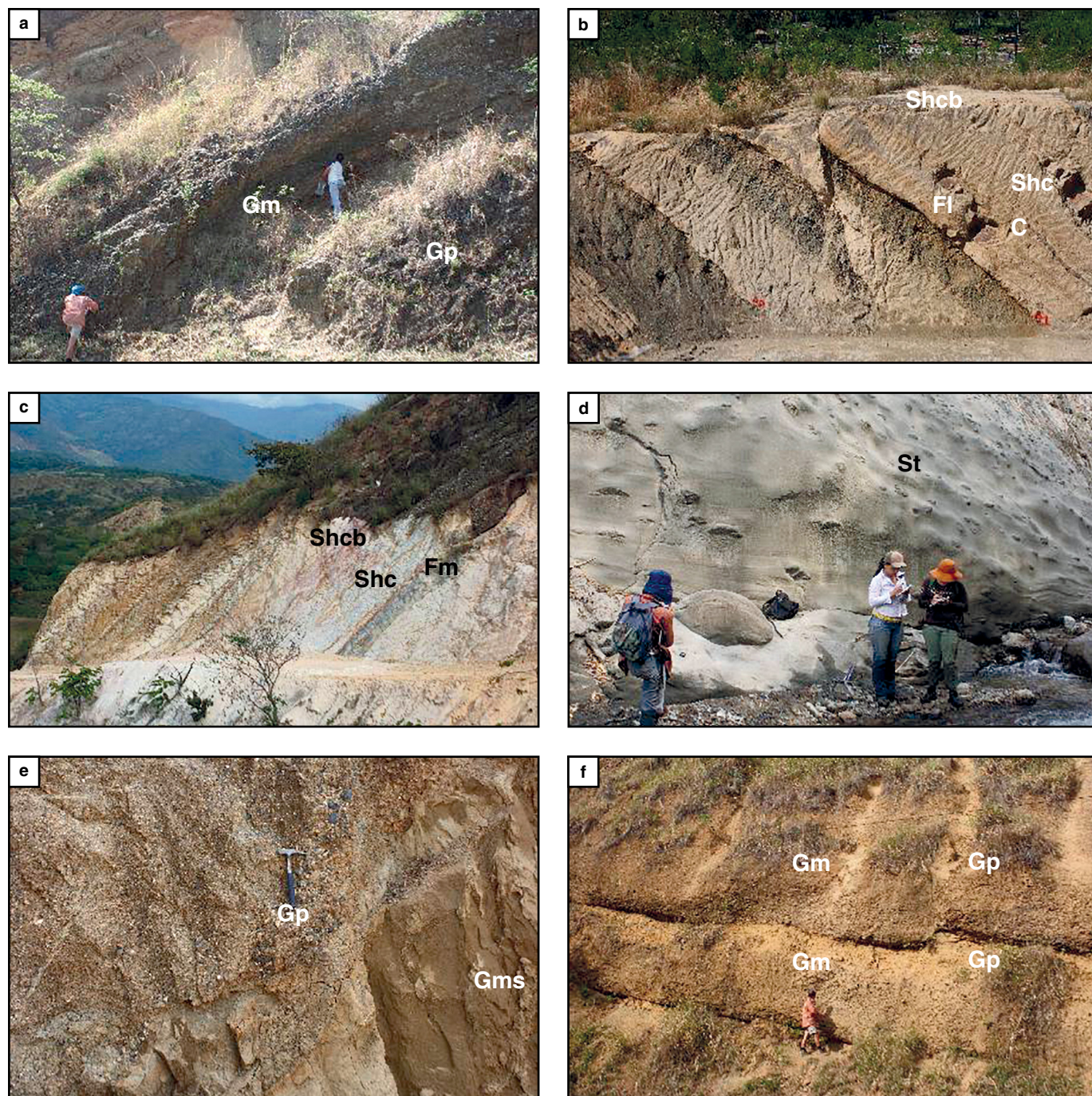


Figure 8. Images of outcrops of the Santa Fe de Antioquia and San Jerónimo sequences from the Amagá Formation. **(a)** Conglomerates and conglomeratic sandstones from the La Seca stratigraphic section. **(b)** Interbedded fining-upward sandstones and organic-rich mudstones from El Puente stratigraphic section. **(c)** Aggradational sandstones from La Puerta stratigraphic section. **(d)** Aggradational sandstones from La Nuarque stratigraphic section. **(e)** Conglomerates and conglomeratic sandstones from the Guaracú stratigraphic section. **(f)** Conglomerates and conglomeratic sandstones from the Santa Fe de Antioquia Formation. See Table 1 for facies descriptions.

poorly preserved fine-grained sedimentary facies. These facies, along with the poor preservation of fine-grained facies and geomorphic elements (i.e., flood plains), suggest that their deposition was associated with a braided river system (Figure 7; Table 1; Figure 1 of the Supplementary Information). The presence of highly amalgamated channels and the asymmetry

of the stratigraphic cycles are consistent with this interpretation and suggest that they were deposited under the condition of low accommodation space. Following Silva-Tamayo et al. (2008), we suggest that the sedimentary record from La Seca stratigraphic section corresponds to the Lower Member of the Amagá Formation.

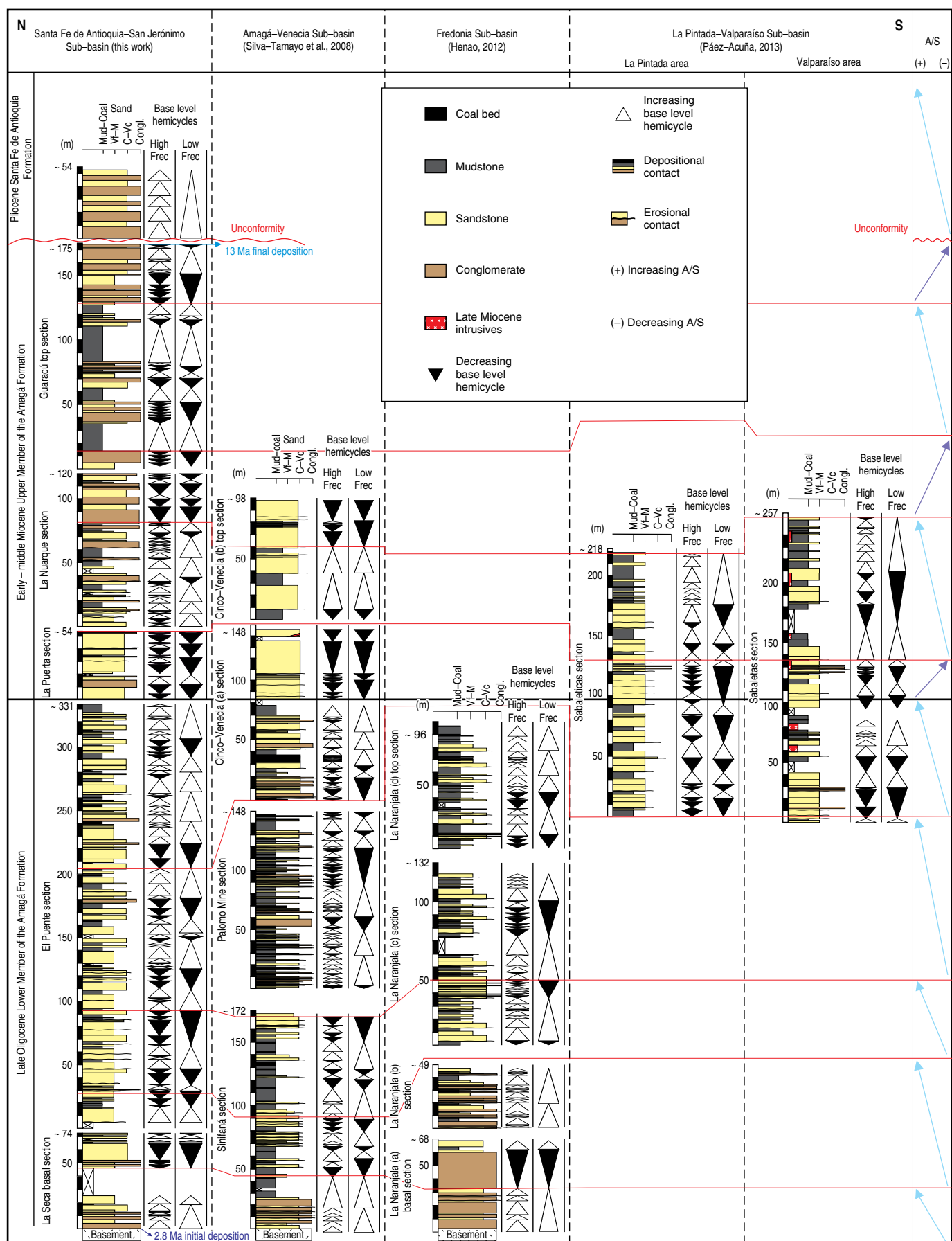


Figure 9. Sequence stratigraphic correlation of the sedimentary records of the Amagá Formation in the Santa Fe de Antioquia–San Jerónimo, Amagá–Venecia, and Fredonia–La Pintada–Valparaíso Sub-basins. A/S = accommodation space/sediment supply ratio.

The middle and upper parts of the Lower Member of the Amagá Formation crop out along El Puente stratigraphic section (Figures 7, 9; Table 1; Figure 1 of the Supplementary Information). This section displays predominantly symmetric and fining-upward stratigraphic cycles, as well as a significant increase in the diversity of low-energy sedimentary facies (i.e., Fm, Fl, Fsc, and C) compared to La Seca stratigraphic section. It also displays the high preservation of geomorphic elements such as flood plains, point bars, and crevasse splay deposits. These characteristics suggest that their deposition was associated with a meandering river system under the condition of high accommodation space along the basin (Figure 7; Table 1; Figure 1 of the Supplementary Information).

The Upper Member of the Amagá Formation crops out in La Puerta, La Nuarque, and Guaracú stratigraphic sections. The lowermost part of the Upper Member (in the La Puerta section) mostly consists of aggradational and coarsening-upward amalgamated sandstones and conglomerates and displays poorly preserved fine-grained geomorphologic features such as flood plains. These characteristics suggest that it was deposited along a braided river system under the condition of low sediment accommodation (Figures 7, 9; Table 1; Figure 1 of the Supplementary Information). The change from a braided river to a meandering river environment is not the only main feature that allows us to divide the Amagá Formation into two members. As highlighted by Lara et al. (2018), the change in the composition of the sandstone from chemically mature to chemically immature is another characteristic that differentiates the Lower Member of the Amagá Formation from the Upper Member.

Higher in the stratigraphy, in La Nuarque stratigraphic section, the Upper Member of the Amagá Formation displays a subtle increase in the diversity of fine-grained sedimentary facies. Here, the sandstones become finer and the sandstone packages become thinner. They also display a lower degree of amalgamation compared to the sandstones from La Puerta section. These sedimentary packages from La Nuarque stratigraphic section also display predominantly fining-upward stacking patterns. These characteristics indicate that their deposition involved a different energy level than the sedimentary units from La Puerta stratigraphic section. These characteristics, along with the increase in the presence of greenish fine-grained sediments (mudstones and siltstones) and the presence of organic-rich mudstones, also suggest that they were deposited along a meandering river system during a period of humid climate. The uppermost part of La Nuarque stratigraphic section displays a significant increase in medium- to coarse-grained sandstones and conglomerates. It is almost devoid of fine-grained facies.

These characteristics suggest a return to a braided river system (Figure 7; Table 1; Figure 1 of the Supplementary Information).

The uppermost part of the Upper Member of the Amagá Formation crops out in the Guaracú stratigraphic section. This section mainly consists of coarsening-upward conglomerates and medium to coarse-grained sandstones interbedded with thick massive mudstones separating the sandstone packages. These facies suggest that they were deposited along a braided river system. The uppermost part of this stratigraphic succession displays conglomerates and sandstones with predominantly aggradational stacking patterns. These patterns suggest a significant decrease in accommodation space and an increase in the sediment supply. The coarse-grained nature of this succession, together with the presence of aggradational packages, suggests that it was deposited along a braided river system (Figure 7; Table 1; Supplementary Figure 1).

Finally, the Santa Fe de Antioquia Formation displays thick tabular aggradational conglomerates and fining-upward sandstones interbedded with limited and thin siltstones. The amalgamated nature of these coarse-grained sedimentary facies, as well as the presence of several erosional surfaces, suggest that they were deposited along a braided river system (Figure 7; Table 1; Figure 1 of the Supplementary Information).

5.2. Sequence Stratigraphic Framework

To date, several sedimentologic studies have focused on the Amagá Formation (i.e., Grosse, 1926; Guzmán & Sierra, 1984; Delsant & Tejada, 1987; Guzmán, 1991, 2003, 2007a; Muriillo, 1998; Hernández, 1999; Correa & Silva-Tamayo, 1999; González, 2001; Sierra et al., 2003; Silva-Tamayo et al., 2008; Henao, 2012; Sierra & Marín-Cerón, 2012; Páez-Acuña, 2013; etc.). However, few studies have integrated the sedimentologic and sequence stratigraphic analyses of this unit (Guzmán, 2007b; Silva-Tamayo et al., 2008).

Silva-Tamayo et al. (2008) used high-resolution lithostratigraphic analyses to investigate the depositional style of the Amagá Formation and proposed a sequence stratigraphic framework for it (Figure 9). These authors used changes in sedimentary stacking patterns, facies diversity, and the preservation of geomorphic elements to constrain changes in the accommodation space (A) – sediment supply (S) ratio (A/S) during the deposition of the Amagá Formation along the AV Sub-basin. According to these authors, the lower part of the Lower Member of the Amagá Formation displays facies associations and stratigraphic stacking patterns implying that its deposition was associated with a braided river system and low A/S conditions. Silva-Tamayo et al. (2008) also suggested

that the upper part of the Lower Member of the Amagá Formation displays facies associations typical of a meandering river system, thus implying an increase in A/S conditions. Silva-Tamayo *et al.* (2008) also proposed that the Upper Member of the Amagá Formation in the AV Sub-basin displays a change towards a braided river depositional system, thus indicating a decrease in A/S conditions.

In this contribution, we use the changes in sedimentary stacking patterns, facies diversity, and the preservation of geomorphic elements reported for the Amagá Formation in the SS Sub-basin and those identified in other sub-basins (i.e., the AV and FPV Sub-basins, Silva-Tamayo *et al.* 2008; Henao, 2012; Páez-Acuña, 2013) to propose a sequence stratigraphic framework for the Amagá Formation (Figure 9).

Important sedimentologic and stratigraphic changes are observed in the Amagá Formation in the SS Sub-basin (Figures 7, 9). The lowermost part of the Amagá Formation in the SS Sub-basin (La Seca stratigraphic section) displays thick conglomerates and sandstones with the poor preservation of sedimentary structures and geomorphic elements. It also displays very asymmetrical stratigraphic cycles, which preferentially fine upwards at the base and coarsen upwards at the top. The facies associations and stratigraphic stacking patterns are typical of braided rivers and suggest deposition under low A/S conditions. Similar facies associations and stratigraphic cycles have been reported by Silva-Tamayo *et al.* (2008) for the Lower Member of the Amagá Formation in the AV Sub-basin (Sinifaná section) and by Henao (2012) and Páez-Acuña (2013) in the FPV Sub-basin (Fredonia area, sections a and b of La Naranjala stratigraphic section) (Figures 4, 5, 6, 9).

Higher in the stratigraphy, the Amagá Formation displays facies associations typical of meandering rivers (El Puente stratigraphic section). The lower and middle parts of this stratigraphic section display a high diversity of sedimentary facies, as well as the high preservation of fine-grained facies (Figures 7, 9). It also displays the high preservation of geomorphic elements such as channels, flood plains, and crevasse splays. The high diversity of facies results in predominantly symmetrical fining-upward – coarsening-upward cycles. These characteristics suggest an important increase in A/S conditions compared to the record from La Seca stratigraphic section (Figure 9). The upper part of the sedimentary succession from El Puente stratigraphic section displays an increase in coarse-grained sediments. The presence of thicker channel sandstones, together with the moderate preservation of geomorphic elements such as flood plains and point bars, suggest a moderate decrease in A/S conditions (Figure 9). Silva-Tamayo *et al.* (2008) also reported high and moderate A/S conditions in the middle and upper parts of the Lower Member of the Amagá Formation in the AV Sub-basin (Unit II and lower part of Unit III, Palomos Mine, and lower El Cinco-Venecia stratigraphic sections). Henao (2012) reported similar facies associations and stratigraphic cycles for

the La Naranjala stratigraphic sections c and d in the Fredonia areas of the FPV Sub-basin (Figure 9).

The sedimentary record from the La Puerta stratigraphic section, which constitutes the lowermost part of the Amagá Formation, consists of very aggradational and amalgamated, medium- to coarse-grained sandstones and conglomerates (Figures 7, 9; Figure 1 of the Supplementary Information). These units also display poorly preserved fine-grained sedimentary facies and geomorphic elements. These characteristics reflect a significant decrease in A/S conditions. These decreased A/S conditions would have occurred regionally and resulted in the deposition of sedimentary successions along braided river systems, as suggested by the occurrence of similar sedimentologic and stratigraphic features in the lowermost part of the Upper Member of the Amagá Formation in the AV (Silva-Tamayo *et al.*, 2008) and FPV (middle part of the Sabaletas and Sabaleticas sections – Henao, 2012; Páez-Acuña, 2013) Sub-basins (Figure 9). As discussed by Silva-Tamayo *et al.* (2008), the strong decrease in A/S conditions regionally marks the limit between the Lower and Upper Members of the Amagá Formation. As discussed below, this decrease occurred between 23 and 15 Ma and resulted from major changes in the tectonic regime occurring along the northern Andes.

La Nuarque stratigraphic section in the SS Sub-basin displays a basal increase in fine-grained facies and a subsequent increase in the predominance of amalgamated conglomerate-sandstone packages with a low diversity of sedimentary structures (Figure 9). The presence of asymmetrical stratigraphic cycles and facies associated with braided river systems suggests their deposition under very low A/S conditions. Similar stratigraphic and sedimentological characteristics have been reported in the upper part of the Upper Member of the Amagá Formation along the AV and FPV Sub-basins (Figure 9; Silva-Tamayo *et al.*, 2008; Páez-Acuña, 2013).

The uppermost part of the Upper Member of the Amagá Formation in the SS Sub-basin crops out at the Guaracú Creek. It displays facies associations typical of braided river systems. The presence of abundant fine-grained sedimentary facies and geomorphic elements (i.e., flood plains) suggests an increase in A/S conditions compared to the middle part of the Upper Member (La Nuarque stratigraphic section). These moderate A/S conditions are supported by the presence of several erosional surfaces within the thick amalgamated conglomerate packages and the very low diversity of fine-grained sedimentary facies and geomorphic elements. This increase in A/S conditions cannot be inferred for the AV and FPV Sub-basins due to the lack of sedimentary records cropping out along those sub-basins (Figure 9; Silva-Tamayo *et al.*, 2008; Páez-Acuña, 2013).

The sequence stratigraphic characteristics of the Amagá Formation in the SS Sub-basin are very similar to those reported by Silva-Tamayo *et al.* (2008) for this formation in the AV Sub-basin and those reported by Henao (2012) and Páez-

Acuña (2013) for the Amagá Formation in the FPV and SS Sub-basins. Although important variations in sedimentary environments can be observed, the temporal variations in stratigraphic cycles are very similar within sub-basins and can be used to differentiate the Lower and Upper Members (following Silva–Tamayo et al., 2008). These differences in sedimentary environments, which result in lateral variations in sedimentary facies, can be attributed to autogenetic processes typical of continental environments (Cross, 1988).

Finally, in the SS Sub-basin, the sedimentary record from the Amagá Formation is discordantly overlain by a series of thick massive sandstones and ortho-conglomerates (Figure 9). The absence of fine-grained sedimentary facies and the presence of very asymmetrical stratigraphic cycles suggest very low A/S conditions. These low A/S conditions are consistent with the presence of facies associations reflecting braided river systems. This unit has not been reported in the AV and FPV Sub-basins, where the Amagá Formation is discordantly overlain by Serravallian – Tortonian (late Miocene) volcanoclastic successions from the Combia Formation.

5.3. Regional Implications

This work presents new sedimentologic and stratigraphic information for the Amagá Formation along the SS Sub-basin. It also presents the first systematic sequence stratigraphic correlation of the sedimentary records of the Amagá Formation cropping out along three different interconnected sub-basins, i.e., the SS, AV, and FPV Sub-basins (Figure 9; Figure 1 of the Supplementary Information). These sedimentological and sequence stratigraphic data allow us to identify major changes in the accommodation space/sediment supply ratio (A/S) of the Amagá Formation, which can in turn be correlated to major geologic events affecting the northern Andes.

Recent provenance studies in the SS Sub-basin of the Amagá Formation (Montes et al., 2015; Lara et al., 2018) have shown important variations in the source areas of the sediments from the Amagá Formation. Montes et al. (2015) and Lara et al. (2018) reported U–Pb detrital zircon ages for the Lower Member of the Amagá Formation that suggest that the Western and Central Cordilleras of Colombia were already exhumed during its deposition and constituted the main sediment source areas of the Lower Member of the Amagá Formation. This interpretation is in line with that of Silva–Tamayo et al. (2008), who suggested a north-trending paleocurrent direction for the river system of the Amagá Formation. Montes et al. (2015) and Lara et al. (2018) also suggested that the Upper Member of the Amagá Formation had two very distinctive sediment source areas, i.e., the South America Block and the PC Block. While Montes et al. (2015) suggested that the input of sediments from the PC Block to the Romeral paleo-suture started in the middle Miocene (15 Ma), Lara et al. (2018) suggested that such sediment

input started as early as the early Miocene (23 Ma). The differences in sediment provenance between the Lower and Upper Members of the Amagá Formation parallel our proposed major regional changes in A/S conditions, which controlled the deposition of this formation. This implies that the sedimentologic evolution of the Amagá Formation was mainly controlled by a major change in tectonic setting along northern South America, specifically, the Oligocene – Miocene interaction between the PC and South American Blocks.

The initial interaction of the PC Block with northwestern South America has been proposed to have begun as early as the late Eocene (Müller et al., 1999; Farris et al., 2011; Montes et al., 2012a, 2012b, 2015). The interactions between these two blocks seem to have increased during the late Eocene – early Oligocene, coinciding with the break-up of the Farallon Plate into the Nazca and Cocos Plates (Pilger, 1984; Lonsdale, 2005), as well as during the late Oligocene, coinciding with the change from oblique convergence to orthogonal convergence between the Nazca and South American Plates between 28 and 25 Ma (Pilger, 1984; Müller et al., 1999; Lonsdale, 2005). The late Eocene – early Oligocene interaction between these tectonic blocks caused pervasive erosion along both the PC Block and the Central Cordillera of Colombia (Restrepo–Moreno et al., 2009; Farris et al., 2011; Barbosa–Espitia et al., 2013); this erosion resulted in a regional late Eocene – early Oligocene sedimentary hiatus along the westernmost part of the Middle Magdalena Valley Basin (Reyes–Harker et al., 2015), the Cauca–Patía Basin, and the southern part of the San Jacinto Basin (Alfaro & Holz, 2014; Rosero et al., 2014). This sedimentary hiatus cannot be identified along the different sub-basins where the Amagá Formation was deposited, as no pre-late Oligocene sedimentary records occur along these sub-basins.

Several marginal continental and transitional Eocene sedimentary records have been identified along diverse basins located along the trace of the Romeral paleo-suture, e.g., the Cauca–Patía and San Jacinto Basins. The presence of those Eocene sedimentary records may suggest the potential occurrence of already eroded marginal continental–transitional Eocene sediment along the sub-basins where the Amagá Formation was deposited. The existence of those pre-existing Eocene sediments, which would have potentially served as a source area for the Amagá Formation, is supported by the presence of reworked Eocene palynomorphs in the Lower Member of the Amagá Formation (Lara et al., 2018). The erosion and lack of preservation of those Eocene sediments along the sub-basins where the Amagá Formation crops out imply that a major tectonic event differentially affected the Cenozoic sedimentary basins located along the Romeral paleo-suture between the late Eocene – early Oligocene. This potential major tectonic event could have been related to uplift resulting from the change from a fore-arc to a hinterland/intramontane tectonic setting along the northern Andes. A similar change has been already proposed

for the Tumaco Basin, which is located to the south of the study area (Echeverri *et al.*, 2015).

This late Eocene – early Oligocene change in tectonic setting would have led to the opening of the different pull-apart basins where the Amagá Formation was deposited. Piedrahita *et al.* (2017) interpreted the occurrence of late Eocene and late Oligocene zircon fission-track cooling ages to propose an Oligocene depositional age for the Lower Member of the Amagá Formation. These ages are in line with the presence of Oligocene palynomorphs in the Lower Member (Pons, 1984). Lara *et al.* (2018) used these chronologic constraints to suggest that the lag time between sediment erosion and the deposition of the Lower Member was short and occurred soon after the opening of the different pull-apart basins where the Amagá Formation was deposited in the early Oligocene.

Piedrahita *et al.* (2017) also reported an early Miocene (22 Ma) zircon fission-track cooling age for the Upper Member of the Amagá Formation. This age can be interpreted as the maximum depositional age of the Upper Member of the Amagá Formation. The six-million-year gap between the late Oligocene – early Miocene cooling events reported by Piedrahita *et al.* (2017) suggests that the Lower Member of the Amagá Formation was deposited during a period of increasing accommodation space and rapid landscape development. These conditions explain the sedimentologic/stratigraphic characteristics of the Lower Member of the Amagá Formation, which records an evolution from braided river to meandering river sedimentary deposits during a period of increasing A/S conditions (Figure 9).

Piedrahita *et al.* (2017) related the occurrence of early Miocene zircon fission-track cooling ages in the Upper Member of the Amagá Formation to a major uplift event and the related basement exhumation of the Central Cordillera of Colombia during the accretion of the PC Block to northern South America. The early Miocene zircon fission-track cooling ages reported by Piedrahita *et al.* (2017), along with the early Miocene palynological ages reported by Ramírez *et al.* (2015), suggest that the lag time between the early Miocene exhumation and erosion of the Central Cordillera and the deposition of the Upper Member of the Amagá Formation was short. The implied rapid early Miocene exhumation of the Central Cordillera of Colombia coincides with the proposed major change in the depositional style from a meandering river system to a braided river system, which indicates that a decrease in A/S conditions occurred along the track of the Romeral Fault System. It also coincides with the major change in the compositional modes of the sandstones of the Amagá Formation (Silva-Tamayo *et al.*, 2008; Lara *et al.*, 2018).

Farris *et al.* (2011) and Lara *et al.* (2018) suggested that the major peak of the interaction and collision between the PC Block and the South American margin occurred between 25–23 Ma, when the break-up of the Farallon Plate also occurred (Pilger, 1984; Pardo-Casas & Molnar, 1987; Lonsdale, 2005; Barckhausen *et al.*, 2008). During this time, more precisely, at

the Oligocene – Miocene boundary, faster and accelerated tectonic convergence between the Americas also occurred (Müller *et al.*, 1999). According to Müller *et al.* (1999), an increase in the rate of motion of the Caribbean Plate from 3.6 mm/y (early Eocene) to 9.9 mm/y (late Oligocene – early Miocene) at 85° W dramatically changed the tectonic regime of the Caribbean Plate and increased the deformation occurring along the circum Caribbean. The enhanced convergence between the Caribbean Plate and northern South America explains the faster deformation and exhumation that occurred in the northern Andes during the Oligocene – Miocene interval (Reyes-Harker *et al.*, 2015 and references therein). These data are in line with our interpretation and provide a further explanation of the regional processes that would have controlled the changes in depositional style displayed by the Amagá Formation.

Montes *et al.* (2015) used detrital zircon ages to suggest that the final docking of the PC Block to northern South America occurred by 13 Ma. However, such docking could have occurred as early as the early Miocene, with more convergence occurring between the PC Block and northern South America in the middle Miocene (Lara *et al.*, 2018). The increased interaction between the PC and South American Blocks, as well as the resulting higher degree of exhumation along the Romeral paleo-suture, explain the predominance of sedimentary facies typical of braided river systems in the uppermost part of the Amagá Formation. Regionally, this middle Miocene increase in tectonic exhumation corresponds to the change in the deformation front towards the Eastern Cordillera (Alfaro & Holz, 2014; Reyes-Harker *et al.*, 2015 and references therein).

The 13 Ma detrital zircons reported by Montes *et al.* (2015) from the Upper Member of the Amagá Formation and the late Miocene (11–6 Ma) magmatic arc rocks that intruded the Amagá Formation (Restrepo *et al.* 1981; Aspden *et al.*, 1987; Silva-Tamayo *et al.*, 2008; Leal-Mejía, 2011; Rodríguez & Zapata, 2014) allow us to suggest a middle Miocene age (13–11 Ma) as the maximum depositional age for this unit. During the late Miocene, the rate of motion of the Caribbean Plate decreased to 5.2 mm/y, and the exhumation of the northern Andes was not as significant (Müller *et al.*, 1999; Mora *et al.*, 2013; Reyes-Harker *et al.*, 2015). However, this apparent tectonic quiescence conflicts with the occurrence of volcanism of adakitic affinity along the track of the Romeral paleo-suture, which affected the Amagá Formation. This adakitic-affinity volcanism resulted in the deposition of volcano-sedimentary successions from the Combia Formation above the Amagá Formation. This change in sedimentation implies that a new change in tectonic setting from a hinterland/intramontane to an intra-arc tectonic setting occurred along the Romeral Fault System.

The change in tectonic setting would have promoted the strong deformation of the Amagá Formation along some of the studied sub-basins, which would have occurred between 13 and 4.8 Ma, as suggested by the 4.8 Ma detrital zircon ages obtained

from the Santa Fe de Antioquia Formation, which overlies the Amagá Formation in the SS Sub-basin. These 4.8 Ma detrital zircon ages could be associated with source areas such as the volcanic products of the Pliocene Combia Formation or some currently undiscovered hypabyssal bodies cropping out along the northern Andes (Lara et al., 2018). These detrital zircon ages, which suggest a minimum hiatus of ca. 8 Ma between the depositions of the Amagá and Santa Fe de Antioquia Formations, coincide with the shift of the deformation front eastward towards its current position along the Guaicáramo Fault System (Reyes–Harker et al., 2015 and references therein). This shift, as well as the deposition of the Santa Fe de Antioquia Formation, would have finally coincided with the final and complete closure of the Central America Seaway, as proposed by Lara et al. (2018).

5.4. Implications for Coal Exploration in the Amagá Formation

The Amagá Formation displays commercially exploitable coal deposits. Most of them have been found in the middle and upper parts of the Lower Member along the AV and FPV Sub-basins (Figure 9). These coal deposits are associated with the flood plains of meandering river system deposits (Silva–Tamayo et al., 2008). However, no coalbeds have been reported in the SS Sub-basin. Our records suggest that the middle and upper parts of the Lower Member of the Amagá Formation in the SS Sub-basin display predominantly coarser facies associations than their correlatives in the AV and FPV Sub-basins. Based on the sedimentologic and stratigraphic characteristics of the Amagá Formation along the AV and FPV Sub-basins, we suggest that these sub-basins were affected by higher subsidence rates than the SS Sub-basin. Although these differences in subsidence, which likely resulted from autogenic processes within different sub-basins, can explain the higher occurrence of organic-rich siltstones and thus coalbeds in the AV and FPV Sub-basins, they do not explain their differences in organic carbon maturity and thus the absence of coalbeds in the SS Sub-basin. The sandstones from the Amagá Formation in the SS Sub-basin (Rojas–Galvis & Salazar–Franco, 2013) display similar diagenetic features as those in the AV and FPV Sub-basins (Correa & Silva–Tamayo, 1999; Guzmán, 2007b; Henao, 2012; Páez–Acuña, 2013). However, the presence of silica cements and diagenetic sericite in the sedimentary records from the AV and FPV Sub-basins suggests that these units were submitted to higher temperatures under a high diagenetic fluid to rock ratio. Miocene intrusive rocks affecting the sedimentary records from the AV and FPV Sub-basins have been reported and are associated with the volcanism of the Combia Formation. We suggest that the low thermal maturity of organic matter-rich deposits, and therefore the absence of coalbeds, in the SS Sub-basin is probably best explained by the absence of intrusive beds affecting the sedimentary record of the Amagá Formation in that sub-basin.

6. Conclusions

We performed sedimentologic and sequence stratigraphic analyses of the Amagá Formation in three pull-apart basins occurring along the trace of the Romeral paleo-suture in the northernmost part of the Andes. Important variations in the depositional style and sequence stratigraphic patterns of the Amagá Formation have been identified. These changes allowed us to divide the Amagá Formation into two members (i.e., the Lower and Upper Members). These changes also paralleled the major changes in regional tectonics occurring along the Northern Andean Orogenic Belt. The deposition of the Amagá Formation occurred along a series of intramontane/hinterland basins that formed after the break-up of the Farallon Plate into the Nazca and Cocos Plates and the change from oblique convergence to orthogonal convergence between the Nazca and South American Plates. The Lower Member, which documents the change from a regional fore-arc to a hinterland tectonic setting, records a change from braided to meandering river systems during a period of increasing sediment accommodation space. The Upper Member of the Amagá Formation, which displays facies associations typical of braided river systems, was deposited during a period of decreasing sediment accommodation space. The decrease in sediment accommodation space that was dominant during the deposition of the Upper Member of the Amagá Formation likely resulted from a major regional uplift event associated with the early Miocene docking of the PC Block to northern South America. The cessation of the deposition of the Amagá Formation occurred during the late Miocene and paralleled the change from a hinterland/intramontane to an intra-arc tectonic setting along the Romeral Fault System. This work finally allowed us to identify the occurrence of Pliocene consolidated but uncemented fluvial sedimentary units deposited by braided rivers along one of the studied sub-basins. These sediments constitute a new stratigraphic unit (the Santa Fe de Antioquia Formation) along the SS Sub-basin, which discordantly overlies the Amagá Formation. The Pliocene age of the Santa Fe de Antioquia Formation suggests the occurrence of a sedimentary hiatus in the SS Sub-basin. This hiatus paralleled the occurrence of adakitic volcanism along the other two studied sub-basins, which in turn promoted the thermal maturation of the sedimentary record and thus the occurrence of economically exploitable coalbeds.

Acknowledgments

This investigation was supported by the Asociación Colombiana de Geólogos y Geofísicos del Petróleo (ACGGP) and the Corporación Geológica ARES, Bogotá, through the ARES–Corrigan grant to Ana Milena SALAZAR–FRANCO, as well as by the Colciencias Young Researchers and Innovators grant

(n.º 645, 2014) to Mario LARA and Ana Milena SALAZAR-FRANCO. Juan Carlos SILVA-TAMAYO is thankful to the University of Houston for its support through the tenure-track startup seed money grant. The authors are thankful to Andrés PARDO and Carlos GUZMÁN for their assistance in the field and their enriching scientific discussions. The authors are thankful to the Instituto de Investigaciones Estratigráficas (IIES) of the Universidad de Caldas, Manizales, for allowing the use of its facilities during the course of this research. We are also thankful to Maria Isabel MARÍN-CERÓN, editor, and one anonymous reviewer for their constructive suggestions, which helped improve this manuscript.

References

- Alfaro, E. & Holz, M. 2014. Review of the chronostratigraphic charts in the Sinú–San Jacinto Basin based on new seismic stratigraphic interpretations. *Journal of South American Earth Sciences*, 56: 139–169. <https://doi.org/10.1016/j.jsames.2014.09.004>
- Aspden, J.A., McCourt, W.J. & Brook, M. 1987. Geometrical control of subduction-related magmatism: The Mesozoic and Cenozoic plutonic history of western Colombia. *Journal of the Geological Society*, 144(6): 893–905. <https://doi.org/10.1144/gsjgs.144.6.0893>
- Barbosa-Espitia, A.A., Restrepo-Moreno, S., Pardo-Trujillo, A., Ochoa, D. & Osorio, J.A. 2013. Uplift and exhumation of the southernmost segment of the Western Cordillera and development of the Tumaco Basin. XIV Congreso Colombiano de Geología. *Memoirs*, p. 387. Bogotá.
- Barckhausen, U., Ranero, C.R., Cande, S.C., Engels, M. & Weinrebe, W. 2008. Birth of an intraoceanic spreading center. *Geology*, 36(10): 767–770. <https://doi.org/10.1130/G25056A.1>
- Bermúdez, H.D., Alvarán, M., Grajales, J.A., Restrepo, L.C., Rosero, J.S., Guzmán, C., Ruiz, E.C., Navarrete, R.E., Jaramillo, C. & Osorno, J.F. 2009. Estratigrafía y evolución geológica de la secuencia sedimentaria del cinturón plegado de San Jacinto. XII Congreso Colombiano de Geología. 27 p. Paipa, Boyacá.
- Borrero, C. & Toro-Toro, L.M. 2016. Vulcanismo de afinidad adaquítica en el Miembro Inferior de la Formación Combia (Mioceno tardío) Al sur de la subcuenca de Amagá, noroccidente de Colombia. *Boletín de Geología*, 38(1): 87–100. <https://doi.org/10.18273/revbol.v38n1-2016005>
- Caballero, V., Mora, A., Quintero, I., Blanco, V., Parra, M., Rojas, L.E., López, C., Sánchez, N., Horton, B.K., Stockli, D. & Duddy, I. 2013. Tectonic controls on sedimentation in an intermontane hinterland basin adjacent to inversion structures: The Nuevo Mundo Syncline, Middle Magdalena Valley, Colombia. In: Nemčok, M., Mora, A. & Cosgrove, J.W. (editors), *Thick-skin-dominated orogens: From initial inversion to full accretion*. Geological Society of London, Special Publication 377, p. 315–342. <https://doi.org/10.1144/SP377.12>
- Cediel, F., Shaw, R.P. & Cáceres, C. 2003. Tectonic assembly of the northern Andean block. In: Bartolini, C., Buffler, R.T. & Blickwede, J. (editors), *The circum-Gulf of Mexico and the Caribbean: Hydrocarbon habitats, basin formation, and plate tectonics*. American Association of Petroleum Geologists, Memoir, 79, p. 815–848. Tulsa, USA.
- Chicangana, G. 2005. The Romeral Fault System: A shear and deformed extinct subduction zone between oceanic and continental lithospheres in northwestern South America. *Earth Sciences Research Journal*, 9(1): 50–64.
- Cochrane, R., Spikings, R., Gerdes, A., Winkler, W., Ulianov, A., Mora, A. & Chiaradia, M. 2014. Distinguishing between in-situ and accretionary growth of continents along active margins. *Lithos*, 202–203: 382–394. <https://doi.org/10.1016/j.lithos.2014.05.031>
- Correa, L.G. & Silva-Tamayo, J.C. 1999. Estratigrafía y petrografía del Miembro Superior de la Formación Amagá en la sección El Cinco–Venecia–quebrada la Sucia. Bachelor thesis, Universidad EAFIT, 47 p. Medellín.
- Cross, T. 1988. Controls on coal distribution in transgressive–regressive cycles, Upper Cretaceous, Western Interior, USA. In: Wilgus, C.K., Hastings, B.S., Posamentier, H., van Wagoner, J., Ross, C.A.S. & Kendal, C.G.St.C. (editors), *Sea-level changes: An integrated approach*. Society for Sedimentary Geology, Special Publication 42, p. 371–389. <https://doi.org/10.2110/pec.88.01.0371>
- Delsant, B. & Tejada, E. 1987. Utilización de análisis litoestratigráficos detallados para correlación de mantos de carbón en la Formación Amagá, Antioquia. *Boletín de Geología*, 17(31): 3–13.
- Duque-Caro, H. 1990. The Choco Block in the northwestern corner of South America: Structural, tectonostratigraphic, and paleogeographic implications. *Journal of South American Earth Sciences*, 3(1): 71–84. [https://doi.org/10.1016/0895-9811\(90\)90019-W](https://doi.org/10.1016/0895-9811(90)90019-W)
- Echeverri, S., Cardona, A., Pardo, A., Monsalve, G., Valencia, V.A., Borrero, C., Rosero, S. & López, S. 2015. Regional provenance from southwestern Colombia fore-arc and intra-arc basins: Implications for middle to late Miocene orogeny in the northern Andes. *Terra Nova*, 27(5): 356–363. <https://doi.org/10.1111/ter.12167>
- Escalona, A. & Mann, P. 2011. Tectonics, basin subsidence mechanisms, and paleogeography of the Caribbean–South American Plate boundary zone. *Marine and Petroleum Geology*, 28(1): 8–39. <https://doi.org/10.1016/j.marpetgeo.2010.01.016>
- Farris, D.W., Jaramillo, C., Bayona, G., Restrepo-Moreno, S.A., Montes, C., Cardona, A., Mora, A., Speakman, R.J., Glascock, M.D. & Valencia, V. 2011. Fracturing of the Panamanian Isthmus during initial collision with South America. *Geology*, 39(11): 1007–1010. <https://doi.org/10.1130/G32237.1>
- Gómez, J., Montes, N.E., Nivia, Á. & Diederix, H., compilers. 2015. Geological Map of Colombia 2015. Scale 1:1 000 000. Ser-

- vicio Geológico Colombiano, 2 sheets. Bogotá. <https://doi.org/10.32685/10.143.2015.936>
- González, H. 1980. Geología de las planchas 167 Sonsón y 187 Salamina. Scale 1:100 000. Boletín Geológico, 23 (1): 174 p.
- González, H. 2001. Memoria explicativa: Mapa geológico del departamento de Antioquia. Scale 1:400 000. Ingeominas, 240 p. Bogotá.
- Grosse, E. 1926. Estudio geológico del terciario carbonífero de Antioquia en la parte occidental de la cordillera Central de Colombia, entre el río Arma y Sacaoljal, ejecutado en los años de 1920–1923. Dietrich Reimer, 361 p. Berlin.
- Guzmán, C.A. 1991. Condiciones de depositación de la Formación Amagá entre Amagá y Angelópolis. Master thesis, Universidad Nacional de Colombia, 197 p. Medellín.
- Guzmán, C.A. 2003. Clasificación, origen y evolución de las cuencas sedimentarias asociadas con la Formación Amagá. VI Congreso Nacional de Ciencia y Tecnología del Carbón. Memoirs CD ROM, 1 p. Medellín.
- Guzmán, C.A. 2007a. Estudio diagenético preliminar de la Formación Amagá. Boletín de Geología, 29(1): 13–20.
- Guzmán, C.A. & Sierra, G.M. 1984. Ambientes sedimentarios de la Formación Amagá. Bachelor thesis, Universidad Nacional de Colombia, 213 p. Medellín.
- Guzmán, G. 2007b. Stratigraphy and sedimentary environment and implications in the Plato Basin and the San Jacinto belt north-western Colombia. Doctoral thesis, Université de Liège, 275 p. Liège, Belgium.
- Henao, J.E. 2012. Estratigrafía y petrografía de las areniscas de la secuencia quebrada La Naranjala, municipio de Fredonia, Miembro Inferior de la Formación Amagá. Bachelor thesis, Universidad EAFIT, 53 p. Medellín.
- Hernández, I. 1999. Petrografía de las areniscas de la sección Peñitas–Mina Excarbón, Miembro Inferior de la Formación Amagá, Titiribí, Antioquia. Bachelor thesis, Universidad EAFIT, 90 p. Medellín.
- Lara, M., Salazar–Franco, A.M. & Silva–Tamayo, J.C. 2018. Provenance of the Cenozoic siliciclastic intramontane Amagá Formation: Implications for the early Miocene collision between Central and South America. Sedimentary Geology, 373: 147–162. <https://doi.org/10.1016/j.sedgeo.2018.06.003>
- Leal–Mejía, H. 2011. Phanerozoic gold metallogeny in the Colombian Andes: A tectono–magmatic approach. Doctoral thesis, Universitat de Barcelona, 989 p. Barcelona.
- León, S., Cardona, A., Parra, M., Sobel, E.R., Jaramillo, J.S., Glodny, J., Valencia, V.A., Chew, D., Montes, C., Posada, G., Monsalve, G. & Pardo–Trujillo, A. 2018. Transition from collisional to subduction–related regimes: An example from Neogene Panama–Nazca–South America interactions. Tectonics, 37(1): 119–139. <https://doi.org/10.1002/2017TC004785>
- Londoño, C.I., Sierra, G.M. & Marín–Cerón, M.I. 2013. Por qué la Formación Amagá no puede ser oligocena? XIV Congreso Colombiano de Geología y Primer Simposio de Exploradores. Memoirs, p. 525. Bogotá.
- Lonsdale, P. 2005. Creation of the Cocos and Nazca Plates by fission of the Farallon Plate. Tectonophysics, 404(3–4): 237–264. <https://doi.org/10.1016/j.tecto.2005.05.011>
- MacDonald, W.D. 1980. Anomalous paleomagnetic directions in late tertiary andesitic intrusions of the Cauca depression, Colombian Andes. Tectonophysics, 68(3–4): 339–348. [https://doi.org/10.1016/0040-1951\(80\)90183-3](https://doi.org/10.1016/0040-1951(80)90183-3)
- Miall, A.D. 1985. Architectural–element analysis: A new method of facies analysis applied to fluvial deposits. Earth–Science Reviews, 22(4): 261–308. [https://doi.org/10.1016/0012-8252\(85\)90001-7](https://doi.org/10.1016/0012-8252(85)90001-7)
- Miall, A.D. 1996. The geology of fluvial deposits: Sedimentary facies, basin analysis, and petroleum geology. Springer–Verlag, 582 p. Berlin. <https://doi.org/10.1007/978-3-662-03237-4>
- Montes, C., Cardona, A., McFadden, R., Moron, S.E., Silva, C.A., Restrepo–Moreno, S., Ramírez, D.A., Hoyos, N., Wilson, J., Farris, D., Bayona, G.A., Jaramillo, C.A., Valencia, V., Bryan, J. & Flores, J.A. 2012a. Evidence for middle Eocene and younger land emergence in central Panama: Implications for isthmus closure. Geological Society of America Bulletin, 124(5–6): 780–799. <https://doi.org/10.1130/B30528.1>
- Montes, C., Bayona, G., Cardona, A., Buchs, D.M., Silva, C.A., Morón, S., Hoyos, N., Ramírez, D.A., Jaramillo, C.A. & Valencia, V. 2012b. Arc–continent collision and orocline formation: Closing of the Central American Seaway. Journal of Geophysical Research: Solid Earth, 117(B4): 25 p. <https://doi.org/10.1029/2011JB008959>
- Montes, C., Cardona, A., Jaramillo, C., Pardo, A., Silva, J.C., Valencia, V., Ayala, L.C., Pérez–Ángel, L.C., Rodríguez–Parra, L.A., Ramírez, V. & Niño, H. 2015. Middle Miocene closure of the Central American Seaway. Science, 348(6231): 226–229. <https://doi.org/10.1126/science.aaa2815>
- Mora, A., Reyes–Harker, A., Rodríguez, G., Tesón, E., Ramírez–Arias, J.C., Parra, M., Caballero, V., Mora, J.P., Quintero, I., Valencia, V., Ibañez–Mejía, M., Horton, B.K. & Stockli, D.F. 2013. Inversion tectonics under increasing rates of shortening and sedimentation: Cenozoic example from the Eastern Cordillera of Colombia. In: Nemčok, M., Mora, A. & Cosgrove, J.W. (editors), Thick–skin–dominated orogens: From initial inversion to full accretion. Geological Society of London, Special Publication 377, p. 411–442. London. <https://doi.org/10.1144/SP377.6>
- Moreno–Sánchez, M. & Pardo–Trujillo, A. 2003. Stratigraphical and sedimentological constraints on Western Colombia: Implications on the evolution of the Caribbean Plate. In: Bartolini, C., Buffler, R.T. & Blickwede, J. (editors), The circum–Gulf of Mexico and the Caribbean: Hydrocarbon habitats, basin formation, and plate tectonics. American Association of Petroleum Geologists, Memoirs 79, p. 891–924.
- Müller, R.D., Royer, J.Y., Cande, S.C., Roest, W.R. & Maschenkov, S. 1999. New constraints on the Late Cretaceous/Tertiary plate

- tectonic evolution of the Caribbean. In: Mann, P. (editor), *Sedimentary basins of the world*, 4 (Caribbean Basins): 33–59. Elsevier Science, Amsterdam. [https://doi.org/10.1016/S1874-5997\(99\)80036-7](https://doi.org/10.1016/S1874-5997(99)80036-7)
- Murillo, S. 1998. Petrografía de las areniscas de la secuencia quebrada la Sucia–Mina Palomos. Miembro Inferior de la Formación Amagá. Bachelor thesis, Universidad EAFIT, 150 p. Medellín.
- O’Dea, A., Lessios, H.A., Coates, A.G., Eytan, R.I., Restrepo–Moreno, S.A., Cione, A.L., Collins, L.S., de Queiroz, A., Farris, D.W., Norris, R.D., Stallard, R.F., Woodburne, M.O., Aguilera, O., Aubry, M.P., Berggren, W.A., Budd, A.F., Cozzuol, M.A., Coppard, S.E., Duque–Caro, H., Finnegan, S., Gasparini, G.M., Grossman, E.L., Johnson, K.G., Keigwin, L.D., Knowlton, N., Leigh, E.G., Leonard–Pingel, J.S., Marko, P.B., Pyenson, N.D., Rachello–Dolmen, P.G., Soibelzon, E., Soibelzon, L., Todd, J.A., Vermeij, G.J. & Jackson, J.B.C. 2016. Formation of the Isthmus of Panama. *Science Advances*, 2(8): 11 p. <https://doi.org/10.1126/sciadv.1600883>
- Ospina, T. 1911. *Reseña geológica de Antioquia*. Imprenta La Organización, 128 p. Medellín.
- Páez–Acuña, L.A. 2013. Análisis estratigráfico y de proveniencia del Miembro Superior de la Formación Amagá en los sectores de la Pintada y Valparaíso (Cuenca Amagá, Andes noroccidentales). Bachelor thesis, Universidad EAFIT, 150 p. Medellín.
- Pardo–Casas, F. & Molnar, P. 1987. Relative motion of the Nazca (Farallon) and South American Plates since Late Cretaceous time. *Tectonics*, 6(3): 233–248. <https://doi.org/10.1029/TC006i003p00233>
- Piedrahita, V.A., Bernet, M., Chadima, M., Sierra, G.M., Marín–Cerón, M.I. & Toro, G.E. 2017. Detrital zircon fission–track thermochronology and magnetic fabric of the Amagá Formation (Colombia): Intracontinental deformation and exhumation events in the northwestern Andes. *Sedimentary Geology*, 356: 26–42. <https://doi.org/10.1016/j.sedgeo.2017.05.003>
- Pilger, R.H. 1984. Cenozoic plate kinematics, subduction and magmatism: South American Andes. *Journal of the Geological Society*, 141(5): 793–802. <https://doi.org/10.1144/gsjgs.141.5.0793>
- Pindell, J.L. & Kennan, L. 2009. Tectonic evolution of the Gulf of Mexico, Caribbean and northern South America in the mantle reference frame: An update. In: James, K.H., Lorente, M.A. & Pindell, J.L. (editors), *The origin and evolution of the Caribbean Plate*. Geological Society of London, Special Publications 328, p. 1–55. <https://doi.org/10.1144/SP328.1>
- Pons, D. 1984. La flore du bassin houiller d’Antioquia (Tertiaire de Colombie). 109^e Congrès National des Sociétés Savantes, II, p. 37–56. Dijon, France.
- Posada, J. de la C. 1913. Notas sobre la Formación Carbonífera de Amagá. *Anales de la Escuela Nacional de Minas*, 1(5): 286–288. Medellín.
- Ramírez–Arias, J.C., Mora, A., Rubiano, J., Duddy, I., Parra, M., Moreno, N., Stockli, D. & Casallas, W. 2012. The asymmetric evolution of the Colombian Eastern Cordillera: Tectonic inheritance or climatic forcing? New evidence from thermochronology and sedimentology. *Journal of South American Earth Sciences*, 39: 112–137. <https://doi.org/10.1016/j.jsames.2012.04.008>
- Ramírez, E., Pardo–Trujillo, A., Plata, A., Vallejo, F. & Trejos, R. 2015. Edad y ambiente de la Formación Amagá (sector de Santa Fé de Antioquia–Sopetrán) con base en evidencias palinológicas. XV Congreso Colombiano de Geología. *Memoirs*, p. 277–281. Bucaramanga.
- Ramón, J.C. & Cross, T. 1997. Characterization and prediction of reservoir architecture and petrophysical properties in fluvial channel sandstones, Middle Magdalena Basin, Colombia. *Ciencia, Tecnología & Futuro*, 1(3): 19–46.
- Restrepo, J.J., Toussaint, J.F. & González, H. 1981. Edades miopliocenas del magmatismo asociado a la Formación Combia, departamentos de Antioquia y Caldas, Colombia. *Geología Norandina*, (3): 21–26.
- Restrepo–Moreno, S.A., Foster, D.A., Stockli, D.F. & Parra–Sánchez, L.N. 2009. Long–term erosion and exhumation of the “Altiplano Antioqueño,” northern Andes (Colombia) from apatite (U–Th)/He thermochronology. *Earth and Planetary Science Letters*, 278(1–2): 1–12. <https://doi.org/10.1016/j.epsl.2008.09.037>
- Reyes–Harker, A., Montenegro, B.M. & Gómez, P.D. 2004. Tectonoestratigrafía y evolución geológica del Valle Inferior del Magdalena. *Boletín de Geología*, 26(42): 19–38.
- Reyes–Harker, A., Ruiz–Valdivieso, C.F., Mora, A., Ramírez–Arias, J.C., Rodríguez, G., De la Parra, F., Caballero, V., Parra, M., Moreno, N., Horton, B.K., Saylor, J.E., Silva, A., Valencia, V., Stockli, D. & Blanco, V. 2015. Cenozoic paleogeography of the Andean foreland and retroarc hinterland of Colombia. *American Association of Petroleum Geologists Bulletin*, 99(8): 1407–1453. <https://doi.org/10.1306/06181411110>
- Rodríguez, G. & Zapata, G. 2014. Descripción de una nueva unidad de lavas denominada andesitas basálticas de El Morito–correlación regional con eventos magmáticos de arco. *Boletín de Geología*, 36(1): 85–102.
- Rojas–Galvis, L.J. & Salazar–Franco, A.M. 2013. Estratigrafía secuencial y análisis integrado de procedencia de las sedimentitas de la Formación Amagá en la Subcuenca Santa Fe de Antioquia. Bachelor thesis, Universidad de Caldas, 92 p. Manizales.
- Rosero, S., Silva–Tamayo, J.C., Sial, A.N., Borrero, C. & Pardo, A. 2014. Quimioestratigrafía de isótopos de estroncio de algunas sucesiones del Eoceno–Mioceno del cinturón de San Jacinto y el Valle Inferior del Magdalena. *Boletín de Geología*, 36(1): 15–27.
- Scheibe, R. 1919. *Geología del sur de Antioquia*. Compilación de Estudios Geológicos Oficiales en Colombia, I: 97–167. Bogotá.

- Sierra, G. & Marín–Cerón, M.I. 2012. Amagá, Cauca and Patía Basins. In: Cediell, F. (editor), *Petroleum Geology of Colombia*, 2, Agencia Nacional de Hidrocarburos and Universidad EAFIT, 104 p. Medellín.
- Sierra, G.M., Silva, J.C. & Correa, L.G. 2003. Estratigrafía secuencial de la Formación Amagá. *Boletín de Ciencias de la Tierra*, (15): 9–22.
- Silva–Tamayo, J.C., Sierra, G.M. & Correa, L.G. 2008. Tectonic and climate driven fluctuations in the stratigraphic base level of a Cenozoic continental coal basin, northwestern Andes. *Journal of South American Earth Sciences*, 26(4): 369–382. <https://doi.org/10.1016/j.jsames.2008.02.001>
- Spikings, R., Cochrane, R., Villagómez, D., van der Lelij, R., Vallejo, C., Winkler, W. & Beate, B. 2015. The geological history of northwestern South America: From Pangaea to the early collision of the Caribbean Large Igneous Province (290–75 Ma). *Gondwana Research*, 27(1): 95–139. <https://doi.org/10.1016/j.gr.2014.06.004>
- van der Hammen, T. 1958. Estratigrafía del terciario y Maastrichtiano continentales y tectogénesis de los Andes colombianos. *Boletín Geológico*, 6(1–3): 67–128.

Explanation of Acronyms, Abbreviations, and Symbols:

ASM	Anisotropy of magnetic susceptibility	RFS	Romeral Fault System
AV	Amagá–Venecia	SS	Santa Fe de Antioquia–San Jerónimo
FPV	Fredonia–La Pintada–Valparaíso	ZFT	Zircon fission–track
PC	Panamá–Chocó		

Authors' Biographical Notes



Juan Carlos SILVA–TAMAYO is CEO at Testlab Geambiental–Testlab Laboratorio Análisis Alimentos y Aguas S.A.S. He holds a BS in geology from the EAFIT University Medellín, Colombia, a Master of Science in environmental and sedimentary sciences from the Universidade Federal de Pernambuco, Recife, Brasil, and a PhD in geochemistry from the Universitat Bern,

Bern, Switzerland. He was also a Marie Curie Postdoctoral Fellow at the Department of Earth and Environment at Stanford University, USA, and the Department of Earth and Environment at the University of Leeds, UK. His research primarily focuses on sedimentary geology, stratigraphy, and low–temperature isotope geochemistry.



Mario LARA is currently a Master's degree student and an assistant teacher at the Universidad Nacional de Colombia, Medellín, Colombia. He holds a BS in geological engineering from the Universidad Nacional de Colombia, Medellín, Colombia. He has been a young researcher sponsored by the Colombian Research Council, Colciencias (www.colciencias.gov.co) at Corporación






Geológica ARES (<http://www.cgares.org>). Mario's primary research interest is the petrology, provenance, tectonic, and basin analysis, and geology around the circum–Caribbean in the northwestern South American.



Ana Milena SALAZAR–FRANCO is a young research scientist at Corporación Geológica ARES (<http://www.cgares.org>). She holds a BS in geology from the Universidad de Caldas, Manizales, Colombia. She has been a young researcher sponsored by the Colombian Research Council, Colciencias (www.colciencias.gov.co) at Corporación Geológica ARES. Ana's primary

research interest is the sedimentary geology and stratigraphy in northwestern South America.

The Combia Volcanic Province: Miocene Post-Collisional Magmatism in the Northern Andes

Marion WEBER^{1*} , José Fernando DUQUE² , Susana HOYOS³ ,
Andrés L. CÁRDENAS-ROZO⁴ , Jorge GÓMEZ TAPIAS⁵ , and Rob WILSON⁶

Abstract A transtensional basin setting originated the Combia Volcanic Province in the northern Andes of Colombia. Volcanism is heterogeneous encompasses tholeiitic, calc-alkaline, and shoshonitic magmatic series. A review of existing geochemical and geochronological data suggests that all magma series coexisted between 12 and 6 Ma but originated from different processes. Tholeiites formed via the melting of a modified primitive mantle source, with limited sedimentary or continental-contaminant input. Calc-alkaline magmas are mainly adakitic and formed from fractionation of garnet and amphibole at high pressures from a hydrous melt from an enriched source. Petrographic and mineral chemistry of garnet-bearing rocks indicate that magmas underwent at least three ascent phases that include: (1) crystallization of high-pressure phenocryst phases at 900 °C and 1200 GPa in a mantle-derived melt, (2) stalling of differentiated magma at lower-pressure conditions, and (3) stalling at shallower conditions, where decompression occurred. Shoshonitic magmas formed via from a mantle with sedimentary or continental-contaminant input source in the plagioclase stability field. Finally, Combia Volcanic Province's formation was enhanced by the Caldas Tear, a slab window developed by the subduction of the Sandra Ridge beneath the South American Plate.

Keywords: *Combia Formation, shallow-volcanic intrusions, tholeiitic magmatism, calc-alkaline magmas, adakites, shoshonitic magmatism, igneous garnet.*

Resumen La Provincia Volcánica de Combia en el norte de los Andes de Colombia se formó en un ambiente de cuenca transtensional. El vulcanismo es heterogéneo y comprende series magmáticas toleíticas, calcoalcalinas y shoshoníticas. Una revisión de los datos geoquímicos y geocronológicos existentes sugiere que las tres composiciones de magma coexistieron entre 12 y 6 Ma, pero se originaron por diferentes procesos. Las toleitas se formaron a partir de una fuente de manto primitivo modificada, con limitado suministro de contaminante sedimentario o continental. Los magmas calcoalcalinos son principalmente adakíticos y se formaron del fraccionamiento de granate y anfíbol a altas presiones a partir de un fundido hidratado proveniente de una fuente enriquecida. Los datos petrográficos y de química mineral de rocas con granate indican que estos magmas experimentaron por lo menos tres fases de ascenso que incluyen: (1) cristalización de las fases de fenocristales de alta presión a 900 °C y 1200 GPa en un fundido derivado del manto, (2) estancamiento del magma diferenciado a más bajas

Citation: Weber, M., Duque, J.F., Hoyos, S., Cárdenas-Rozo, A.L., Gómez, J. & Wilson, R. 2020. The Combia Volcanic Province: Miocene post-collisional magmatism in the northern Andes. In: Gómez, J. & Mateus-Zabala, D. (editors), The Geology of Colombia, Volume 3 Paleogene – Neogene. Servicio Geológico Colombiano, Publicaciones Geológicas Especiales 37, p. 355–394. Bogotá. <https://doi.org/10.32685/pub.esp.37.2019.12>

<https://doi.org/10.32685/pub.esp.37.2019.12>
Published online 26 November 2020

- 1 mweber@una.edu.co
Universidad Nacional de Colombia
Sede Medellín
Departamento de Geociencias y Medio Ambiente
Carrera 80 n.º 65-223
Medellín, Colombia
 - 2 jduquet@eafit.edu.co
Universidad EAFIT
Departamento de Ciencias de la Tierra
Carrera 49 n.º 7 sur-50
Medellín, Colombia
 - 3 shoyosm1@eafit.edu.co
shoyos@mit.edu
Universidad EAFIT
Departamento de Ciencias de la Tierra
Carrera 49 n.º 7 sur-50
Medellín, Colombia
Massachusetts Institute of Technology
Department of Earth, Atmospheric, and Planetary Sciences
77 Massachusetts Avenue, 54-918, Cambridge, MA 02139
USA
 - 4 acarde17@eafit.edu.co
Universidad EAFIT
Departamento de Ciencias de la Tierra
Carrera 49 n.º 7 sur-50
Medellín, Colombia
 - 5 mapageo@sgc.gov.co
Servicio Geológico Colombiano
Dirección de Geociencias Básicas
Grupo Mapa Geológica de Colombia
Diagonal 53 n.º 34-53
Bogotá, Colombia
 - 6 robnewwilson@gmail.com
University of Leicester
School of Geography, Geology & the Environment
Leicester LE1 7RH
United Kingdom
- * Corresponding author

Supplementary Information:

- S1: <https://www2.sgc.gov.co/LibroGeologiaColombia/tgc/sgcpubesp37201912s1.pdf>
- S2: <https://www2.sgc.gov.co/LibroGeologiaColombia/tgc/sgcpubesp37201912s2.pdf>
- S3: <https://www2.sgc.gov.co/LibroGeologiaColombia/tgc/sgcpubesp37201912s3.pdf>
- S4: <https://www2.sgc.gov.co/LibroGeologiaColombia/tgc/sgcpubesp37201912s4.pdf>

condiciones de presión y (3) estancamiento en condiciones superficiales, donde ocurrió la descompresión. Los magmas shoshoníticos se formaron a partir de una fuente mantélica con aporte sedimentario o continental, en el campo de estabilidad de la plagioclasa. La formación de la Provincia Volcánica de Combia fue acentuada por el *Caldas Tear*, una ventana en la placa desarrollada por la subducción del *Sandra Ridge* bajo la Placa de Suramérica.

Palabras clave: *Formación Combia, intrusivos volcánicos someros, magmatismo toleítico, magmas calcoalcalinos, adakitas, magmatismo shoshonítico, granate ígneo.*

1. Introduction

The Andes are among the most extensive active volcanic chains in the world (Figure 1). They represent an essential record of continental–crust construction and modification processes. Volcanic activity is caused by the eastward subduction of the Nazca Plate beneath the South American Plate (Harmon et al., 1984). It is divided into four distinct zones (from south to north): The Austral Volcanic Zone, the Southern Volcanic Zone, the Central Volcanic Zone, and the Northern Volcanic Zone (Figure 1; Stern & Kilian, 1996; Thorpe et al., 1984). Each of these zones is characterized by differences in the magmatic activity related to variances in the subduction configuration (e.g., subduction angle, velocity) and intrinsic, differential properties in both subducting and overriding plates (e.g., age and thickness). Of these segments, the Northern Volcanic Zone remains the least studied and well known due to a long history of political unrest in the region.

In Colombia, the Andean belt comprises three cordilleras separated by deep, fluvial valleys (i.e., Western, Central, and Eastern Cordilleras) (Figure 1). The geographic limit between the Western and Central Cordilleras is marked by the Cauca River valley, which is the superficial expression of the Cauca–Romeral Fault System. Today, this paleosubduction zone constitutes a suture zone between a Permian – Triassic, continental–basement domain to the east and a Cretaceous, oceanic–basement domain to the west (e.g., Aspden & Litherland, 1992) (Figure 2), which resulted from the complex history of subduction–accretion that occurred throughout the Late Cretaceous until today (Horton et al. 2010; Kennan & Pindell, 2009; Pindell et al., 2005).

The establishment of the current subduction configuration and Neogene magmatism along the Western Cordillera started in the mid–Miocene, with the accretion of the Panamá–Chocó Block onto the South American margin (Duque–Caro, 1990; Montes et al., 2012, 2015). Recent studies suggest that normal subduction of the Nazca Plate initiated around 14 to 9 Ma, and accretion of the Panamá–Chocó Block occurred before 12 Ma (Montes et al., 2012, 2015; Wagner et al., 2017). Magmatism ceased between 6 and 4 Ma due to the flat–slab subduction of the Nazca Plate underneath South America. Magmatism resumed at 3 Ma along the length of the arc, south of the *Caldas Tear* (Wagner et al., 2017).

Among the Neogene magmatic events in the Cauca River valley, the Combia Formation (CF) comprises a middle to upper Miocene (ca. 12 to 6 Ma) volcanoclastic–sedimentary sequence located in the middle and northern parts of the valley, and represents a distinctive magmatic occurrence (Figure 2). The CF was deposited within the intramontane, semi–isolated Amagá Basin, which formed between the basement rocks from the Western and Central Cordilleras in the northernmost Colombian Andes (Figure 2; Lara et al., 2018). The CF mainly comprises basic tholeiitic magmas, linked to crustal thinning and basin extension (Bernet et al., 2020; Dunia, 2005; Jaramillo, 1976; Jaramillo et al., 2019). Furthermore, calc–alkaline, andesitic to dacitic, shallow, volcanic porphyries of the Cauca Shallow Volcanic Intrusions (CSVI) are spatially associated with the CF, even though some authors define them as a single, separate unit (e.g., Borrero & Toro–Toro, 2016; Calle & González, 1980; Tassinari et al., 2008). Moreover, the cartographic resolution of the volcanic products recorded in the CF does not record individual event levels. Only a few studies have discussed their genesis and tectonic setting (e.g., Bernet et al., 2020; Jaramillo et al., 2019; Marriner & Millward, 1984; Rodríguez & Zapata, 2014). Several authors (Bissig et al., 2017; Jaramillo, 1976; Ramírez et al., 2006) suggest that the CSVI and the CF were generated by a subduction zone related to the magmatic arc. In addition, they argue that the magmatic setting started as a protoarc (tholeiitic series) and then moved towards a more mature arc (calc–alkaline series). Additionally, these studies also suggest differentiation and contamination from the input of a mature crustal end–member (Dunia, 2005; Marriner & Millward, 1984).

The CF has been traditionally considered to be late Miocene in age (ca. 6 to ca. 10 Ma; Ramírez et al., 2006), mostly based on cross–cutting relationships with the CSVI. Recent studies on basaltic andesites (formerly considered part of the CF) have suggested the presence of an older, magmatic arc, located to the west of the Amagá Basin (Rodríguez & Zapata, 2014; Zapata & Rodríguez, 2011). Consequently, these authors propose to splitting the middle Miocene magmatism into two different magmatic arcs with different ages and geographical locations: The earlier shoshonitic arc and a later tholeiitic and calc–alkaline arc represented by the CF and CSVI magmas. The shoshonitic arc comprises El Botón basalts and El Morito basaltic andesites (Figure 2; Rodríguez & Zapata, 2014; Zapata & Rodríguez, 2011).

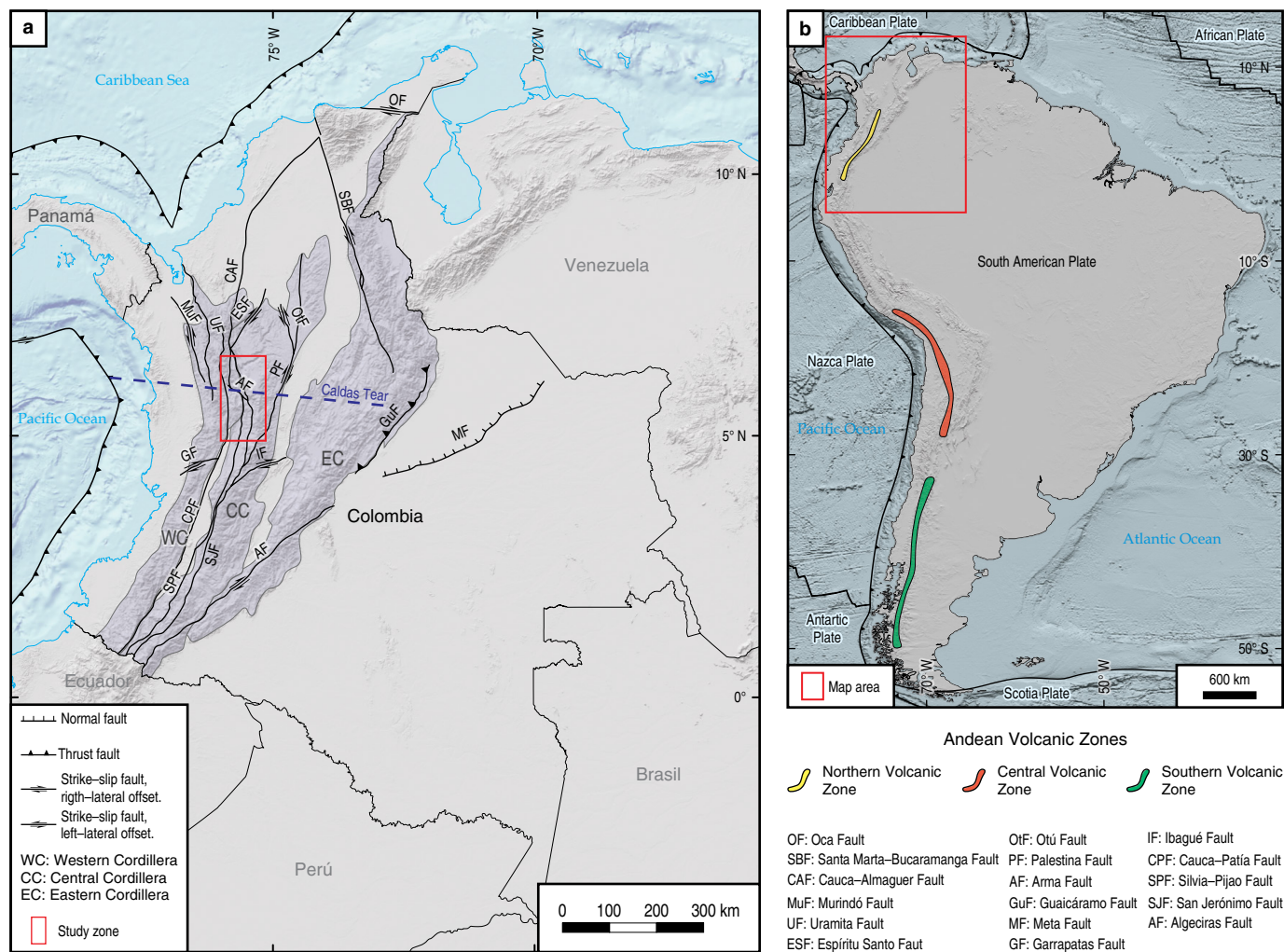


Figure 1. (a) Tectonic setting of the Andes in Colombia. The CVP is located within the rectangle. **(b)** Geographic distribution of the volcanic zones in the Andes (after Harmon et al., 1984).

The present work represents an effort to synthesize an essential amount of petrography, field relationships, mineral chemistry, geochronological, and geochemical data previously reported associated with volcanic, volcanoclastic, hypabyssal, porphyritic magmatism and sedimentary rocks of the Combia Formation found along the Cauca River valley. The authors here combine unpublished petrography, mineral chemistry, geochronological, and geochemical data with previous data available from Jaramillo (1976), Álvarez (1983), Marriner & Millward (1984), Ordóñez-Carmona (2001), Dunia (2005), Tejada et al. (2007), Tassinari et al., (2008), Leal-Mejia (2011), Borrero & Toro-Toro (2016), Bissig et al. (2017), Jaramillo et al. (2019), and Bernet et al. (2020) to better understand this unique geological occurrence in Colombia.

2. The Combia Formation

In this chapter, we present the previous studies published on the Combia Formation.

The CF was first defined by Grosse (1926) as the “Neo-Tertiary volcanics” and “Neo-Tertiary sediments” in the Alto Combia locality (Fredonia, Colombia; Figure 3). In this work, he also divided the CF into a Lower Member (Volcanic Neo-Tertiary) and an Upper Member (Sedimentary Neo-Tertiary). In general, Grosse (1926) described the CF as a mixture of sedimentary and volcanoclastic packages: “Conglomerates, sandstones, schistose clay, tuffitic conglomerates, tuffitic sandstones, tuffs, crystal tuffs, ash and agglomerate tuffs, and basaltic and andesitic lava flows”. Later, the unit was renamed the Combia Formation by Calle et al. (1980), who, based on lithology, divided it into two members (i.e., Sedimentary and Volcanic).

Jaramillo (1976) conducted a detailed petrographic and geochemical study of the volcanic rocks and determined the tholeiitic character of the basaltic to andesitic flows of the CF, which are interbedded with pyroclastic material, as well as the calc-alkaline nature of magmas from the Cauca porphyritic intrusions (cf. CSMV). Petrographically, based on phenocryst content, he divided the basalts into three types: plagioclase, hypersthene, and augite

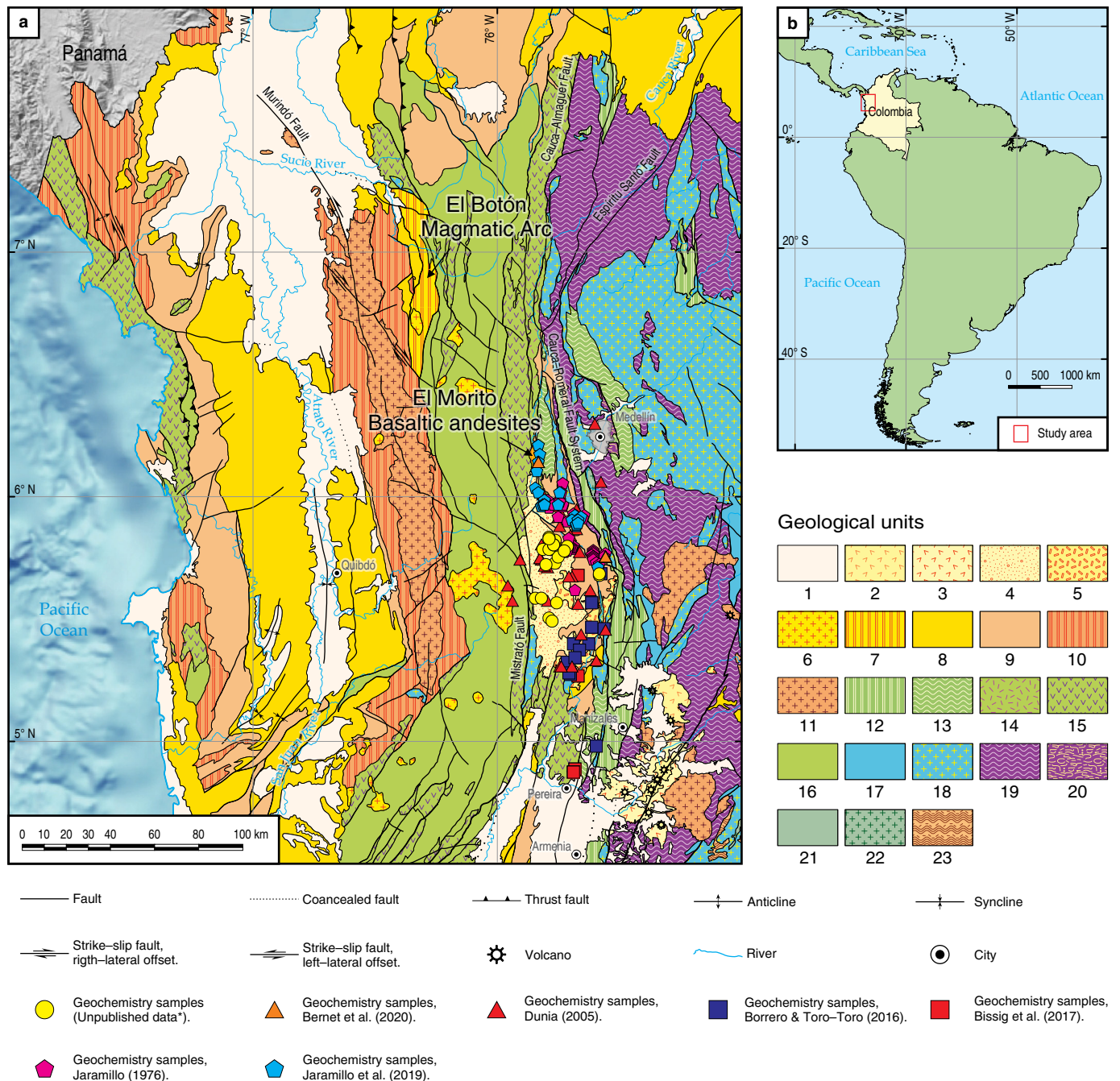


Figure 2. (a) Geological map of the Western of Colombia simplified from Alcárcel & Gómez (2017), and location of the geochemistry samples used in this study. Geological units: (1) Quaternary deposits and volcanoclastic deposits; (2) Quaternary volcanites; (3) Pliocene volcanites; (4) Combia Formation; (5) Miocene sub-volcanic bodies; (6) Miocene plutons; (7) El Botón Magmatic Arc; (8) Neogene sedimentites; (9) Eocene – Miocene sedimentites; (10) Paleogene volcanites and volcanosedimentites; (11) Paleogene plutons; (12) Cretaceous sedimentites, volcanites, gabbros, and ultramafic rocks; (13) Lower Cretaceous metamorphic rocks; (14) Upper Cretaceous gabbros and ultramafic rocks; (15) Upper Cretaceous basalts; (16) Upper Cretaceous sedimentites; (17) Mesozoic sedimentary and volcanoclastic rocks; (18) Mesozoic plutons; (19) Triassic metamorphic rocks and plutons; (20) Triassic ultramafic rocks; (21) Paleozoic sedimentites; (22) Paleozoic plutons; and (23) Stenian – Tonian metamorphic rocks. **(b)** Location of the geological map area. Unpublished data* from Tejada et al. (2007) and Project “Caracterización Estratigráfica, Petrogenética y Geocronológica de la Formación Combia, Acuerdo Específico No 009–2004 con la Universidad Nacional de Colombia”.

basalts. Furthermore, Jaramillo (1976) determined that some basic dikes that intruded the Amagá Formation (AF) are part of the CF (i.e., in the areas of the Quebrada Popala and Río Poblano).

The AF is a terrestrial, siliciclastic succession dominated by meandering (Lower Member) to braided (Upper Member) rivers in a pull-apart, tectonic regime during the late Oligocene to middle

Miocene (Lara et al., 2018). Jaramillo (1976) also reported two dikes that cut the CF at the Alto Combia location and described them as an alkaline–rock unit similar to absarokites. Finally, he suggested that both the CF and CSVI are the outcome of the presence of a ‘permeable zone’, which allowed the migration of different magma batches, generated under different conditions and/or depths, through the continental crust.

Later, Marriner & Millward (1984), in an integrated geochemical study of Colombian volcanism, and based on the tholeiitic, chemical character of the CF, suggested an island–arc tectonic setting for its formation. Based mainly on geographic location and age, they proposed a single province in northern Colombia, which includes both the CF and the recent axial, calc–alkaline volcanism of the Central Cordillera (Figure 1).

Extensive geological mapping has been performed over time by various projects of the Servicio Geológico Colombiano (Figure 2; e.g., Álvarez, 1983; Calle & González, 1980, 1982; Dunia, 2005; Mahecha et al., 2006; Tejada & Betancourt, 2006; Tejada et al., 2007). Among these studies, Dunia’s (2005) report integrates petrographic, geochemical, and geophysical analyses of the Amagá Basin, including the CF and CSVI. Mafic rocks of the volcanic member are described as agglomerates, andesites, and feldspathic basalts. Moreover, the latter are divided (based on textural features) into porphyritic basalts, augite basalts, amygdalar basalts, and glomeroporphyritic basalts. Furthermore, Dunia (2005) also included andesitic and basaltic dikes and sills that cut through both the AF and CF and suggested that they are genetically linked to basaltic rocks. Finally, the Farallones Batholith and Támesis Stock are coetaneous with Combia–magmatic activity (González, 2010; Zapata & Rodríguez, 2013). According to Dunia (2005), the two compositional–magma series formed during juvenile–arc activity, which later evolved into a mature calc–alkaline, volcanic arc via differentiation, and the accretion of the Chocó Block, as proposed by Duque–Caro (1990), which may be responsible for the magmatism.

Detailed mapping of the area near the municipalities of Pueblorrico and Jericó (Tejada & Betancourt, 2006) enabled Tejada et al. (2007) to locally divide the CF into eight units based on lithological differences and age, from oldest to youngest: (i) tuffs 1 (N1ct1); (ii) basalts 1 (N1cb1); (iii) hornblende, basaltic andesites (N1cab); (iv) basalts 2 (N1cb2); (v) agglomerates (N1ca); (vi) interspersed basalts, tuffs and agglomerates (N1cbta); (vii) tuffs 2 (N1ct2); and (viii) hypabyssal rocks that comprise basalt dikes and sills, hornblende, andesitic porphyries and one garnet–bearing, hornblende, andesitic porphyry (N1cds, N1cp, and N1cpg, respectively). Moreover, they suggested that the presence of garnet indicates wet conditions during calc–alkaline magma formation at 9 Kbar and 1000 °C. Subsequently, the CF originated from various explosive and extrusive stages, and the basaltic rocks may have formed in a back–arc or immature arc. In contrast, the porphyries represent

typical magmas of a subduction zone with an added continental component (Tejada et al., 2007).

Additional geochemical research on the CSVI on the lower volcanic rocks from the Cauca and Amagá regions (Borrero & Toro–Toro, 2016) shows that adakitic signature magmas could be related to melts originated in a previously metasomatized mantle located in a subduction zone.

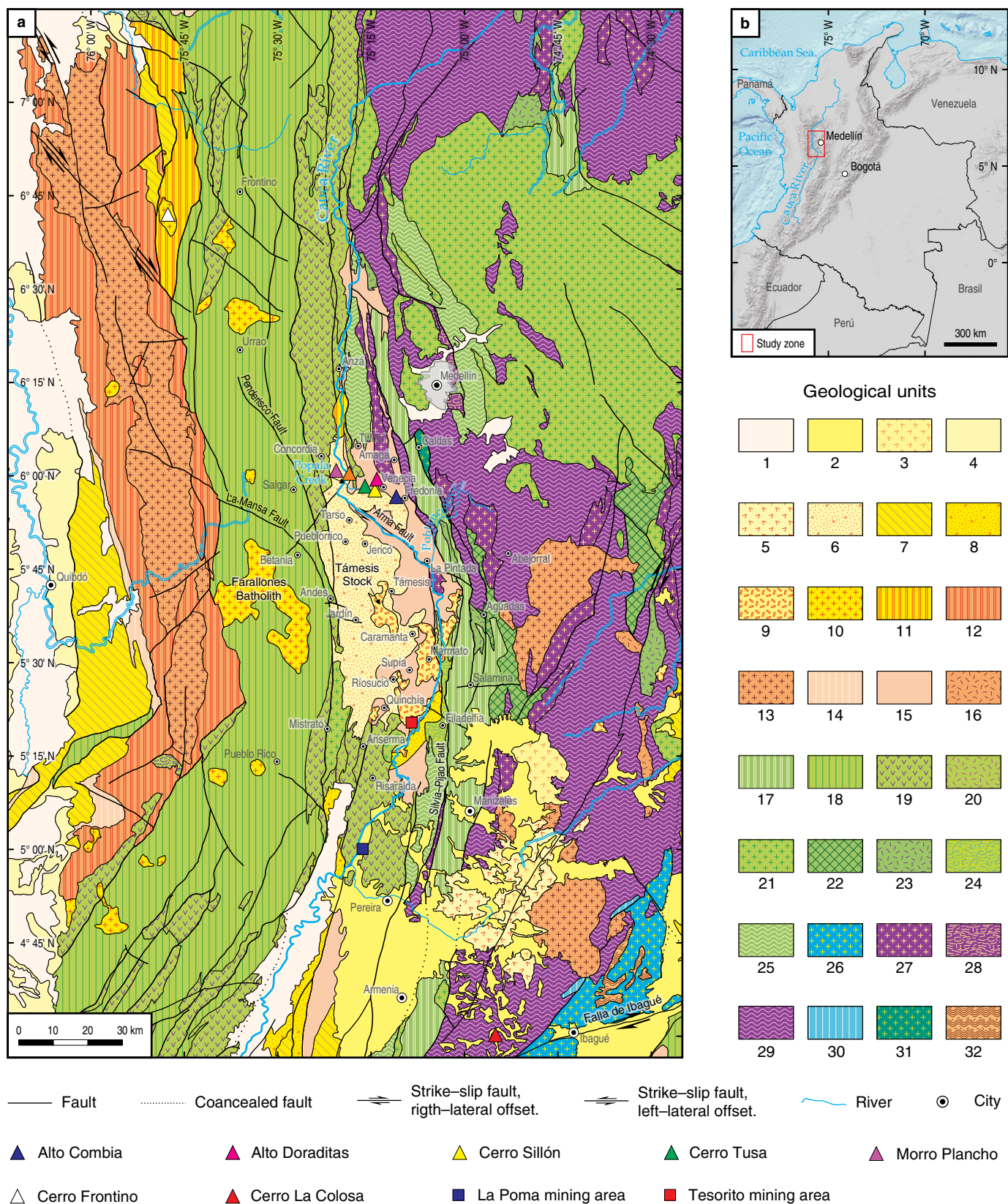
Additional interest in the CF has arisen because of copper, gold, and molybdenum deposits associated with the CSVI. Tassinari et al. (2008) studied the origin of Marmato gold deposits. Leal–Mejía (2011), Leal–Mejía et al. (2019), and Shaw et al. (2019) focused their studies on Phanerozoic gold metallogeny in the northern Andes, including gold–bearing associated porphyries in the CF. Most recently, Bissig et al. (2017) studied the origin of garnet–bearing magmas in the Colombian Middle Cauca Metallogenic Belt.

Tassinari et al. (2008) suggested a juvenile, mantle–derived magma as the primary source of calc–alkaline to tholeiitic magmatism, based on isotopic data. However, they did not exclude a minor magmatic contribution resulting from the partial melting of the lower continental crust. In the Marmato Stock, hydrothermal activity occurred at 5.6 Ma, which is later than the reactivation of the Cauca–Romeral Fault System at approximately 6.3 Ma.

Bissig et al. (2017) described the garnet–bearing porphyry systems of Tesorito and El Poma located in the Colombian Middle Cauca Metallogenic Belt. They interpreted their formation as occurring from a rapidly ascending magma that melted in the lower crust, at pressures above 1 GPa. Furthermore, they suggested that a change in the geodynamic environment may have removed garnet from the melt. This enabled the generation of middle– to upper–crustal magma chambers, which accounts for the later, garnet–free, porphyritic rocks.

Finally, new interest has arisen in the CF that is associated with the magmatic evolution of the northern Andes after the fragmentation of the Farallón Plate ca. 23 Ma (Lonsdale, 2005; Marriner & Millward, 1984), and the development of diverse magmatic activity. Two recent contributions, which include geochemical, geochronological, and isotopic data, focus on the petrogenesis and tectonic setting of the CF (Bernet et al., 2020; Jaramillo et al., 2019).

Jaramillo et al. (2019) suggested that 9 to 5.2 Ma magmatism in the area comprising the Combia Volcanic Complex, formed mainly from the mantle, interacted with older crustal material and underwent magmatic differentiation. They suggested that the basalts represent the oldest, erupting phase at ca. 9 Ma and are overlain by more differentiated, calc–alkaline rocks. They related the different magmatic compositions (i.e., tholeiitic, calc–alkaline, and adakitic) to differences in dry– and wet–melting conditions in the continental crust associated with crustal thickness. Their proposed formation model suggests that Combia magmatism is related to oblique subduction and substantial structural inheritance.



Bernet et al. (2020) presented three stratigraphic sections in the eastern Amagá Basin and proposed that the origin of magmas of the CF resulted from a metasomatized mixture of a

mantle source with the lower crust. Chemical signatures were created by differences in the depth of melting and other possible processes, such as AFC and MASH. These authors determined

Figure 3. (a) Geological map of the area, simplified from Gómez et al. (2015). Geological units: (1) Quaternary deposits; (2) Quaternary volcanoclastic deposits; (3) Quaternary volcanites; (4) Pliocene sedimentites; (5) Pliocene volcanites; (6) Combia Formation; (7) Neogene marine sedimentites; (8) Miocene volcanoclastic deposit; (9) Miocene sub-volcanic bodies; (10) Miocene plutons; (11) El Botón Magmatic Arc; (12) Santa Cecilia La Equis Complex; (13) Paleogene plutons; (14) Oligocene–Miocene marine sedimentites; (15) Oligocene continental sedimentites; (16) Paleocene mafic plutons; (17) Cretaceous sedimentites, volcanites, gabbros, and ultramafic rocks; (18) Upper Cretaceous sedimentites; (19) Upper Cretaceous basalts; (20) Upper Cretaceous gabbros and ultramafic rocks; (21) Upper Cretaceous plutons; (22) Lower Cretaceous sedimentites; (23) Lower Cretaceous mafic rocks; (24) Lower Cretaceous ultramafic rocks; (25) Lower Cretaceous metamorphic rocks; (26) Jurassic plutons; (27) Triassic plutons; (28) Triassic ultramafic rocks; (29) Triassic metamorphic rocks; (30) Permian–Triassic sedimentites; (31) Ordovician plutonic rocks; (32) Stenian–Tonian metamorphic rocks. **(b)** Location of the geological map area.

that Miocene – Pliocene magmatism is associated with an extension–compression regime and that an extensional pull–apart event (12–9 Ma) was followed by convergence (9–6 Ma) that formed calc–alkaline magmas.

3. Petrography and Outcrop Evidence

The CF unconformably overlies the AF. Both units were emplaced and restricted to the Amagá Basin, which, as well as similar basins aligned along the Cauca–Patía River depression, formed as a pull–apart basin due to Oligocene – Miocene Cauca–Romeral Fault System activity (Sierra, 1994).

The CF has generally been divided into a Lower Member, mainly recording volcanic activity, both explosive (pyroclastic–density current and fall–out deposits) and extrusive (lava flows), and an Upper Member, dominated by reworked primary volcanoclastic rocks and secondary volcanoclastics (such as lahars and debris avalanches; Murcia et al., 2013), as described by Grosse (1926), Calle & González (1980; 1982), Ríos & Sierra (2004), and Marín–Cerón et al. (2019). In this review, to obtain a synthesized, petrological understanding of the variety of rocks found in the CF, we have classified them into volcanic, sedimentary, and intrusive lithofacies.

3.1. Volcanic Lithofacies

The magmatic rocks that constitute the CF can be separated into two major groups: (1) Volcanic effusive deposits, which here include La Popala and Río Poblano Dikes, as well as El Sillón Stock, given their geochemical similarity with basaltic, lava flows (Álvarez, 1983; Dunia, 2005; Jaramillo, 1976; Tejada et al., 2007), and (2) pyroclastic density current deposits.

3.1.1. Volcanic Effusive Deposits

Within this group, there are both intrusive and extrusive rock bodies with basaltic and intermediate compositions.

3.1.2. Basaltic Lava Flows

These rocks can be divided according to textural variation into porphyritic, glomeroporphyritic, and vesicular basalts. The for-

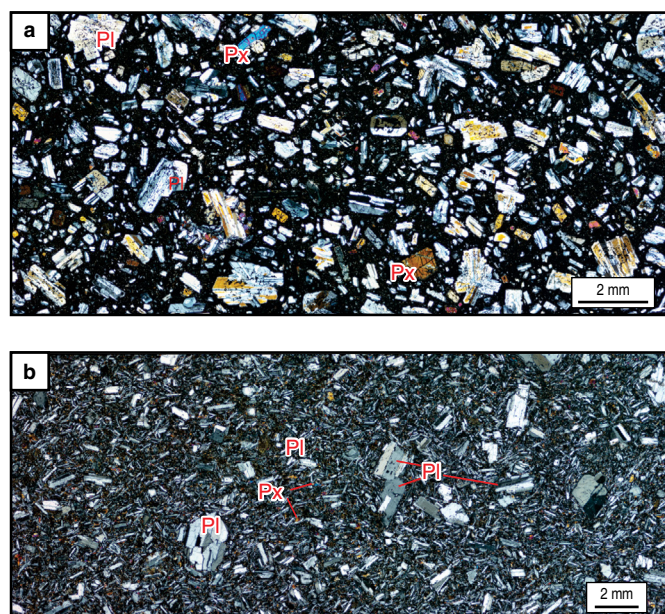


Figure 4. Panoramic microphotographs of porphyritic basalts, under crossed polarized light. **(a)** Large plagioclase (Pl) and pyroxene (Px) phenocrysts in a matrix of plagioclase, pyroxene (orthopyroxene and clinopyroxene), and opaque microliths in glass. Sieve texture is conspicuous in the plagioclase crystals. Sample MJG-011 from Betancourt & Tejada (2006). **(b)** The trachytic texture is shown by basalt with plagioclase phenocrysts in a groundmass of plagioclase and pyroxene microliths. Sample HJ-11 from Mahecha & Ortíz (2006).

mer is also subdivided into three types based on the significant phenocryst phase (i.e., plagioclase, augite, and hypersthene).

Porphyritic basalts: These rocks are characterized by plagioclase and pyroxene phenocrysts in an aphanitic matrix, varying from holocrystalline to hypocrySTALLINE. The matrix is mostly composed of tabular–shaped plagioclase and pyroxene microliths and glass, which are commonly locally altered to palagonite and other clay materials (Figure 4a). In general, a chaotic texture dominates, although a well–defined trachytic–flow texture can be seen (Figure 4b).

Plagioclase is the most common phenocryst in these samples. Crystals are subhedral to euhedral and range in size from approximately 0.5 to 3 mm. Albite and albite–carlsbad twinning are present in the majority of crystals and are normal to oscillato-

ry zonation. In some samples, plagioclase–overgrowth textures, skeletal crystals, and spongy rims are evident (Figure 4a). The microliths vary in size from 0.5 to >0.1 mm and show albite twinning. Augite phenocrysts and microlith crystals are anhedral to subhedral and are commonly associated with abundant disseminated opaque minerals (magnetite), and glass. Normal zonation and twinning are conspicuous, and exsolution and embayment textures are also common. In general, crystals are fractured. Hypersthene crystals are less abundant and are euhedral to subhedral, in some cases with exsolution lamellae and carlsbad twinning. In some examples, coronas composed of augite or other clinopyroxenes surround orthopyroxene. Mineral embayments are evidence of the dissolution of pyroxene–phenocryst phases.

Glomeroporphyritic basalts: These rocks are characterized by plagioclase, augite, and olivine, phenocrystal clusters of 1 to 3 mm, and microphenocrysts that also show this cumulative texture. The matrix comprises plagioclase, pyroxene, olivine microliths, opaques, and glass (Figure 5). The olivine phenocrysts and microliths are subhedral, commonly fractured and altered to iddingsite. In all major minerals, zonation is less common than in the other two classifications.

Vesicular basalts: These rocks are the least common of the basaltic lava flows. They contain abundant vesicles and amygdules of up to 4 mm in diameter. These basalts comprise scarce, plagioclase phenocrysts in a vitreous matrix with microliths of plagioclase and pyroxene (Figure 6). Fractures and vesicles are filled with slightly oxidized zeolites, mainly heulandite, chabazite, mordenite, and philipsite, but celadonite, quartz, and calcite are also present (Gelves et al., 2016).

3.1.2.1. Andesitic Volcanics

Intermediate (andesitic) dikes and flows described by Dunia (2005) and Jaramillo et al. (2019) are intercalated within pyroclastic rocks in the CF. These are characterized by a fine-grained matrix with pyroxene and amphibole phenocrysts with intersertal, glomeroporphyritic, and subophitic textures. They show evidence of silicification and contain amygdules filled with zeolites.

Due to their composition, age, stratigraphic position, and field relationships, these rocks could be genetically related to the CSVI.

3.1.3. Pyroclastic Density Current Deposits

Different pyroclastic deposits, which are products of explosive eruptions, have been reported by various authors in several sections within the CF (Calle & González, 1980; Hoyos & Duque–Trujillo, 2017; Ramírez et al., 2006;). The most commonly reported explosive products are fall tuffs, followed by pyroclastic density current deposits. The latter are scarce but, when found, constitute an unambiguous indication of for-

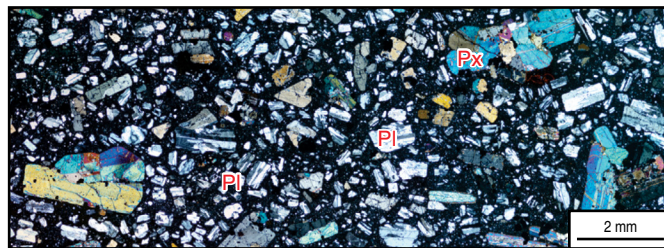


Figure 5. Panoramic microphotograph of a glomeroporphyritic basalt, under crossed polarized light. Sample exhibits seriate porphyritic texture, with phenocrystal clusters of plagioclase (Pl) and augite in a matrix of plagioclase, pyroxene (Px; orthopyroxene and clinopyroxene), opaques, and glass. Sample HJ–180 from Mahecha & Ortíz (2006).

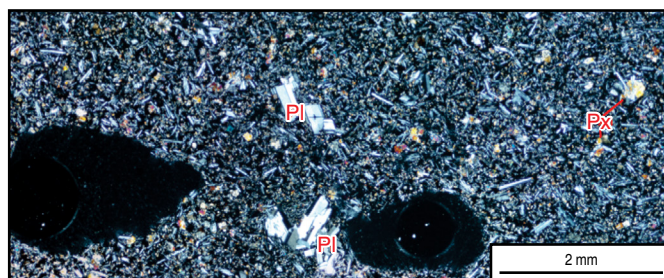


Figure 6. Microphotograph of vesicular basalt, under crossed polarized light. The sample exhibits porphyritic texture, with plagioclase (Pl) phenocrysts in a vitreous matrix with plagioclase and pyroxene (Px; orthopyroxene and clinopyroxene) microliths. Vesicles are two large dark areas, both with air bubbles in the resin. Sample from the Igneous Rocks Collection of Universidad EAFIT, Medellín.

mation by pyroclastic density currents because of its high-welding grade, the vitrophyric texture of the matrix, fiamme texture, vitreous, and pumiceous cognate clasts, columnar jointing, etc.

On the other hand, unequivocally identifying tuffaceous deposits is challenging, particularly where the reworking processes of primary volcanic sequences have been intense. Nevertheless, Hoyos & Duque–Trujillo (2017) reported extended, pyroclastic density current deposits only in the western margin of the Cauca River valley, specifically along the Bolombolo–Concordia section, and small sequences of the same pyroclastic density current deposits in the eastern margin of the Cauca River valley, where the Amagá River discharges into the Cauca River.

These pyroclastic density current deposits are mainly composed of broken plagioclase, pyroxene, and amphibole crystals. Moreover, lithic fragments are also common (mainly basaltic andesites and glass shards). Pumice fragments exhibit eutaxitic and fiamme textures, indicating that these deposits were formed by pyroclastic–flow density currents and were emplaced hot enough to be welded. The matrix of these rocks

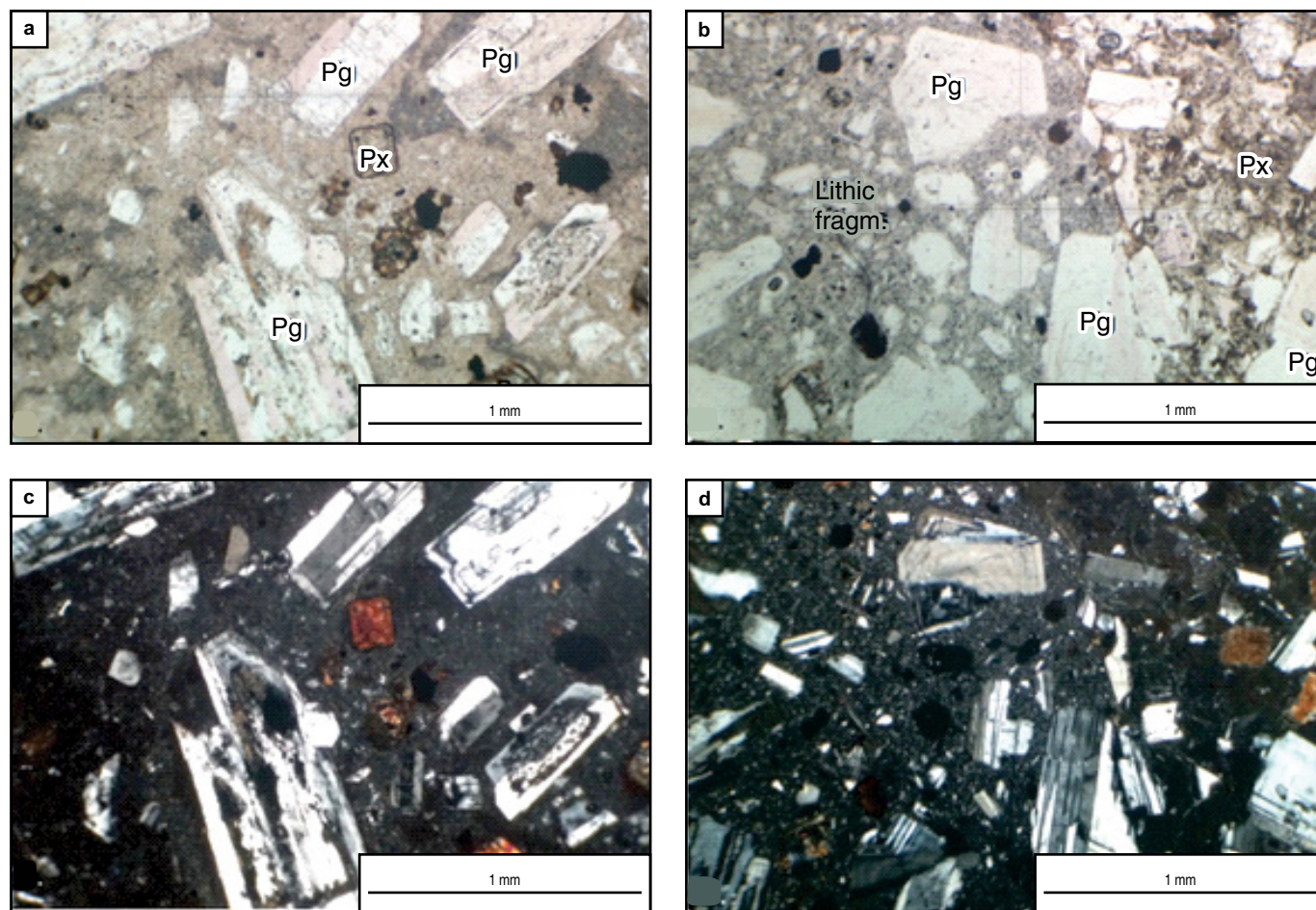


Figure 7. Microphotograph of a welded pyroclastic density current deposit (Sample Conc 03) from the Bolombolo–Concordia section. Note the boundary between lithic fragment and matrix in (b). (a) and (c) parallel polarized light and, (b) and (d) cross-polarized light. (Pg) Plagioclase, (Px) Pyroxene.

is coherent and presents eutaxitic and trachytic textures with microlites of the main-forming minerals and rock fragments. Minerals and rock fragments show the same textures as already described for the lavas and CSVI. Finally, the composition of the welded pyroclastic density current deposits in the CF, combined with the fluidal textures observed in most of the lithic clasts in the samples, is characterized by eruptive pulses, which include parts of the volcanic edifice, possibly domes, and lava flows. Juvenile materials (pumice and glass shards) were also involved during those eruptions and were then flattened (more or less bed oriented), forming a fiamme texture in these deposits (Figure 7).

Several authors (e.g., Calle & González, 1980, 1982; Grosse, 1926; Jaramillo, 1976; Jaramillo et al., 2019; Tejada et al., 2007) have described “agglomerates” as a common constituent of the CF. These have been described as thick layers of block or breccia tuffs with massive structures, including rounded and subspherical fragments, with sizes varying between 1 and 50 cm, with occasional larger blocks (up to 1 m). The included blocks are composed of massive porphyritic basalts,

vesiculated basalts, andesites, garnet-bearing andesites, and other pyroclastic rocks. Most of these fragments show thermal alteration in their boundaries. The matrix is mainly composed of glass, which varies from relatively fresh to palagonite, with plagioclase microlites, pyroxene, hornblende, and olivine. Because the term agglomerate is used for fluidal-shaped, volcanic bombs deposited near a volcanic vent (Németh & Martin, 2007), we suggest using the term lithic-breccia, as suggested by McPhie et al. (1993).

These volcanic, lithic-breccia deposits are interpreted as proximal facies formed from explosion-derived, highly concentrated, pyroclastic density currents (Németh & Martin, 2007), which were involved in the eruptive process of some of the volcanic rocks, volcanoclastic rocks, and porphyritic intrusions related to this volcanism. These lithic-breccia deposits are associated with basaltic lava flows along the Jericó–Puente Iglesias (Tejada & Betancourt, 2006), Jericó–Tarso, and Jericó–Tamesis roads. Jaramillo et al. (2019) reported that these rocks are intercalated with other pyroclastic rocks (primary and secondary) and cut by andesitic dikes in the Fredonia region.

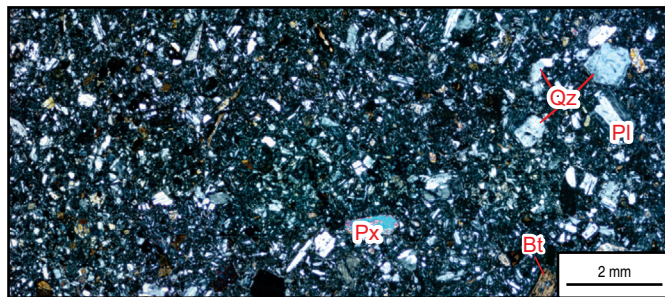


Figure 8. Microphotography of a medium-coarse sandstone, under cross-polarized light. The sample exhibits subangular clasts of plagioclase (Pl), quartz (Qz), pyroxene (Px; orthopyroxene and clinopyroxene), and biotite (Bt). Sample CPG-392 from Ríos & Sierra (2004).

3.2. Sedimentary Lithofacies

These lithofacies contain the non-volcanic, clastic sedimentites of the CF. These sedimentary sequences are composed (in clast-size order) of conglomerates and breccias, fine- to medium-coarse-grained sandstones (Figure 8), and siltstones. The sediment supply of these rocks is derived from the Amagá and Combia (volcanic lithofacies) Formations. Specifically, conglomerates and breccias contain clasts composed of basalt, andesite, and tuff (CF), as well as sandstones (AF; Calle & González, 1980; Grosse, 1926; Ríos & Sierra, 2004).

Ríos & Sierra (2004) synthesized sedimentary sequences into four facies assemblages: (i) fluvial channels, (ii) debris and hyperconcentrated flows, (iii) debris flows intercalated with fluvial channels and alluvial plains, and (iv) pyroclastic flows intercalated with alluvial plains and reworked pyroclastic material. These facies assemblages were obtained from the study of Bolombolo–Peñalisa (140 m thickness) and Guineales–Peñalisa (167 m thickness) surface sections. The Bolombolo–Peñalisa section documents an alluvial-plain deposit interbedded with pyroclastic and debris flows. On the other hand, the Guineales–Peñalisa section shows fluvial channels interbedded with debris and hyperconcentrated flows. Both alluvial plain and fluvial channels are adjacent environments in a fluvial-sedimentary complex. Therefore, based on Ríos & Sierra (2004) report, it is possible to establish that changes in sedimentary facies assemblages in the CF are limited to autocyclic processes. Moreover, the beds formed by pyroclastic and debris-hyperconcentrated flows show short-term interruptions in the fluvial system due to the CF's volcanic activity, thereby promoting the formation of local lacustrine deposits.

3.3. Intrusive Lithofacies (Cauca Shallow Volcanic Intrusions; CSVI)

In general, the middle to late Miocene (ca. 12 to 6 Ma) shallow volcanic intrusions located along the Cauca River valley (north

of ca. 4° N) (Figure 3) are considered a continuous magmatic belt in the northern part of the Western Cordillera with an extension of ca. 100 km (Álvarez, 1983; Borrero & Toro-Toro, 2016; Leal-Mejía, 2011). The CSVIs are commonly distinguishable in the field due to their positive relief from the sedimentary country rocks (AF and CF) and the Romeral mélange (Cediel et al., 2003).

According to Leal-Mejía (2011), the CSVI can be grouped into four segments according to their geographic location: (1) Quinchía–Dos Quebradas, (2) Marmato–Supia–Orofino, (3) La Quebradona–La Aurora, and (4) Titiribí. Nevertheless, these shallow volcanic bodies can be split into two different groups of shallow volcanic intrusives based on their geomorphological and compositional features: (1) Those that are restricted to the Amagá Basin (Amagá Basin), and (2) those emplaced outside the Amagá Basin along the Cauca River (Cauca River) (Figure 3).

Although some authors have considered that the volcanoclastic sequence of the CF and CSVI may correspond to the same magmatic event (Borrero & Toro-Toro, 2016; Calle & González, 1980; Grosse, 1926; Jaramillo et al., 2019; Leal-Mejía, 2011), there is no agreement as to whether both the Amagá Basin–CSVI and Cauca River–CSVI were formed from the same magmatism (Borrero & Toro-Toro, 2016; Leal-Mejía, 2011).

The CSVIs are mostly round-shaped bodies in map view (e.g., La Pintada and Marmato, intruding the Quebradagrande Complex and the Amagá, Irra, and Combia Formations) (Figure 9). These intrusives are mostly andesitic-dacitic in composition, characterized by a seriate, porphyritic texture, in a gray, microlithic-groundmass. Centimetric plagioclase constitutes a typical phenocryst phase in all CSVIs. Furthermore, they have phenocrysts of quartz, amphibole, biotite, and/or occasional garnet as accessory phases. Plagioclase crystals are subhedral, with a tabular habit and oscillatory zonation. Sieve and skeletal textures are also common in the plagioclase (Figure 10a). Hornblende phenocrysts are sometimes zoned and embayed and occasionally show dehydration-reaction rims to secondary amphibole and opaques (Figure 10b). Although uncommon, when present, most garnet crystals are either euhedral phenocrysts or show breakdown rims often surrounded by a plagioclase corona (Figure 10c). Garnet is also commonly present as inclusions in plagioclase and amphibole, indicating early crystallization. Phenocrysts float in an aphanitic to microlithic, pilotaxitic- or fine-granular matrix composed of microliths of plagioclase, amphibole, pyroxene, opaques, and devitrified glass. Textures are porphyritic, microporphidic, and trachytic. Some of these bodies contain xenoliths of the surrounding rocks (basalts and schists).

Characteristic of the the Amagá Basin–CSVI are intrusions of laccoliths and dikes of different sizes into the sedimentary AF (e.g., Cerro Tusa and Cerro Corcovado; Figure 11). These intrusives are mostly basaltic to andesitic in composition, contrasting with the slightly more differentiated composition of the Cauca River–CSVI. In general, these intrusives are porphyritic to glom-



Figure 9. Panoramic view of La Pintada Intrusives, part of the Cauca Shallow Volcanic Intrusions (CSV). The Combia Formation (CF) sediments and Amagá Formation (AF) can also be seen. Picture from Mauricio Montoya (<https://www.flickr.com/photos/mauriciomontoya/>). The picture was taken towards the east at 11 km from the CSVI (1200 masl).

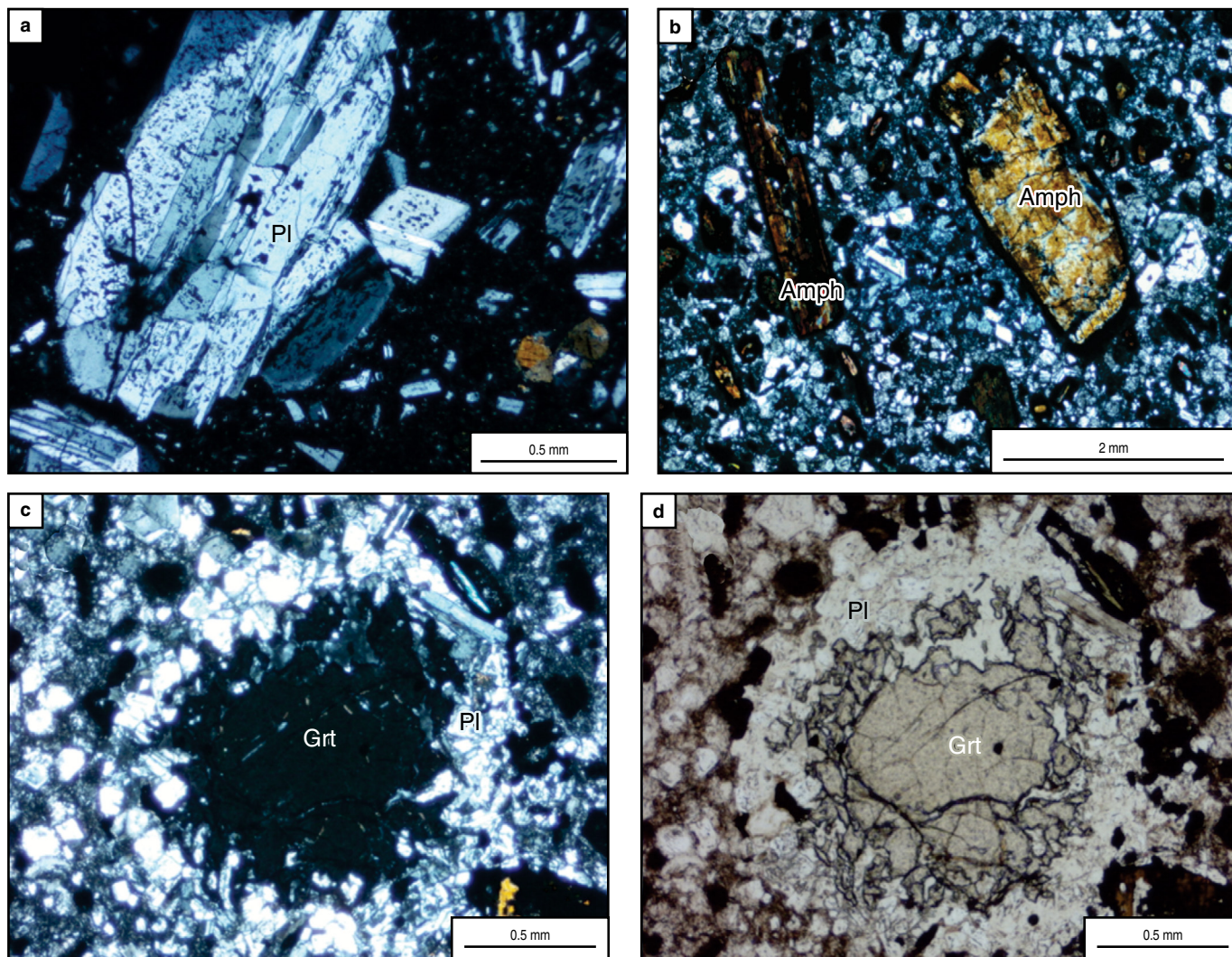


Figure 10. Common petrographic textures from volcanic rocks of the Combia Formation. **(a)** Sieve and skeletal textures in plagioclase (Pl) crystals. Note also the presence of oscillatory zoning on the edges of the crystal. Sample MJG-46-1 from Betancourt & Tejada (2006). **(b)** Dehydration rims around amphibole (Amph). Sample MJG-132 from Betancourt and Tejada (2006). **(c), (d)** Plagioclase (Pl) corona rims around garnet (Grt). Sample MJG-132 from Betancourt and Tejada (2006). Sample under cross polarized light is shown in (c) and under parallel polarized light in (d).

eroporphyritic in texture. Plagioclase is the most common phenocryst, although amphibole is also common. Glomeroporphyritic textures are formed by plagioclase, amphibole, biotite, and olivine. The groundmass consists mainly of plagioclase microliths and amphibole, pyroxene, biotite, and/or olivine in a trachytic texture.

Petrographic evidence, such as sieve and skeletal textures, oscillatory zonation in plagioclase, clinopyroxene coronas over orthopyroxene, and olivine breakdown, indicates that magma mixing, and disequilibrium were common processes in these magmas before being emplaced.

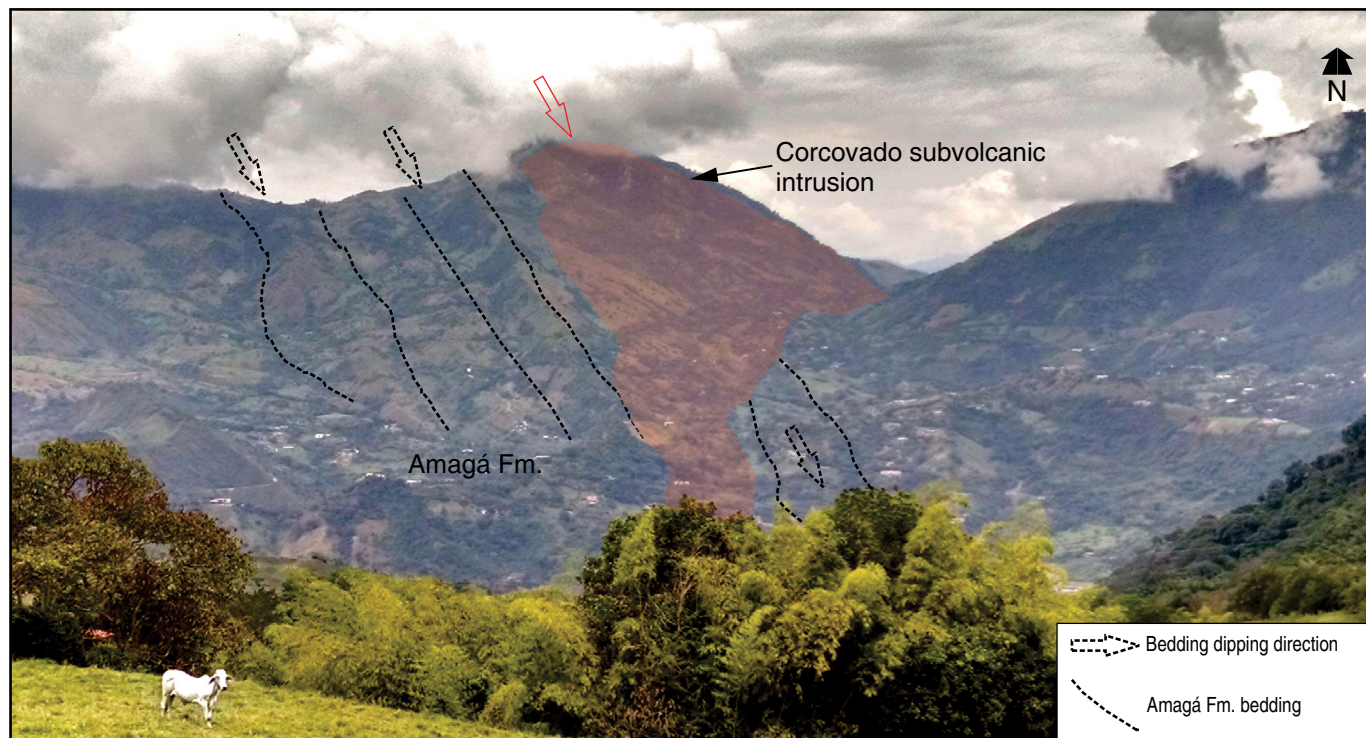


Figure 11. View of the Cerro Corcovado from the south. Notice that the intrusion has the same dipping as the Amagá Formation strata, indicating that it must have intruded as a sill and then was tilted together with the Amagá Formation.

4. Major and Trace Element Geochemistry

A complete dataset (see Table 1 of the Supplementary Information 1) of 202 analyses of the igneous rocks of the CVP has been analyzed (Bernet et al., 2020; Bissig et al., 2017; Borrero & Toro–Toro, 2016; Dunia, 2005; Jaramillo, 1976; Jaramillo et al., 2019; Marriner & Millward, 1984; Tejada et al., 2007). Data from the project “Caracterización Estratigráfica, Petrogenética y Geocronológica de la Formación Combia, Acuerdo Específico No 009–2004 con la Universidad Nacional de Colombia” are also included. For representation, volcanoclastic rocks were excluded, as well as samples with high LOI values (≥ 3 wt%), as these are possibly related to alteration and secondary processes associated with hydrothermal alteration and mineralization (e.g., Leal–Mejía, 2011; Tassinari et al., 2008). Most of the excluded samples are basalts (alteration in these rocks is also evident by abundant zeolite and secondary calcite). Samples from the shoshonitic El Botón and El Morito (Rodríguez & Zapata, 2014; Zapata & Rodríguez, 2011) may represent the first magmatism of modern subduction and are also included in the dataset. In this case, only samples with LOIs higher than 5 wt% were excluded, as determined by Müller et al. (1992) for these rocks. Finally, the geochemistry of the CF and CSVI, as initially determined by Jaramillo (1976), reflects a tholeiitic and calc–alkaline series (Figure 12). Both series are separated by a compositional gap at ca. 58 wt% SiO_2 . It is important to

note that dikes and sills of both series intrude the AF and CF (Bernet et al., 2020; Dunia, 2005; Jaramillo, 1976; Jaramillo et al., 2019; Tejada et al., 2007).

4.1. Tholeiitic Series

This series comprises the lava flows of the CF and some mafic intrusives (e.g., La Popala, Río Poblano, Alto Doraditas, and Cerro Sillón), as well as one sample from Quebrada La Popala described as a layered diabase. The tholeiitic series is mainly basalts to andesites that conform to a tight compositional cluster, according to the total alkali vs. silica plot of LeMaitre et al. (2002) (Figure 13). SiO_2 ranges from 50.30 to 61.53 wt%, and Al_2O_3 ranges from 12.89 to 19.49 wt%. MgO and FeO_T vary from 1.43 to 6.98 wt% and 6.06 to 10.93 wt%, respectively. CaO varies between 4.48 and 12.24 wt%; Na_2O is low, between 1.74 and 4.11 wt%; and K_2O is relatively high, between 0.66 and 2.99 wt% (Figures 12, 14). Most samples cluster in the tholeiitic field of the AFM triangular plot of Miyashiro (1974) and the medium–K to high–K area of the K_2O vs. SiO_2 diagram (Gill, 1981) (Figure 12).

The N–MORB normalized (Sun & McDonough, 1989), multielement diagrams of the tholeiitic series have similar patterns and relative abundances of incompatible elements (Figure 15). Three different groups within the tholeiitic series can be identified under slightly different La/Yb and La/Sm ratios (Figure 14) and the different sizes of element anomalies: Group

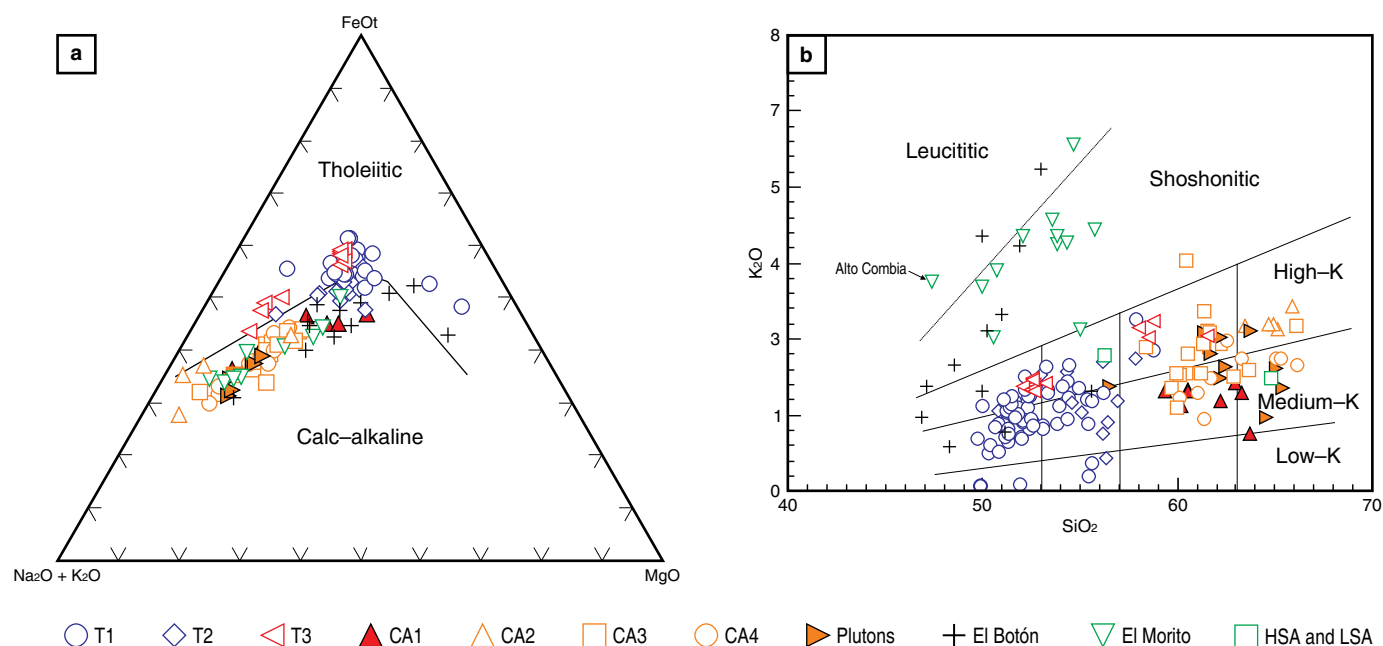


Figure 12. (a) AFM diagram for differentiation of tholeiitic vs. calc-alkaline magma series, after Miyashiro (1974). (b) K_2O vs. SiO_2 diagram distinguishing low-K, medium-K, and high-K series, after Gill (1981). High Silica Adakites (HSA), Low Silica Adakites (LSA) after Martin et al. (2005).

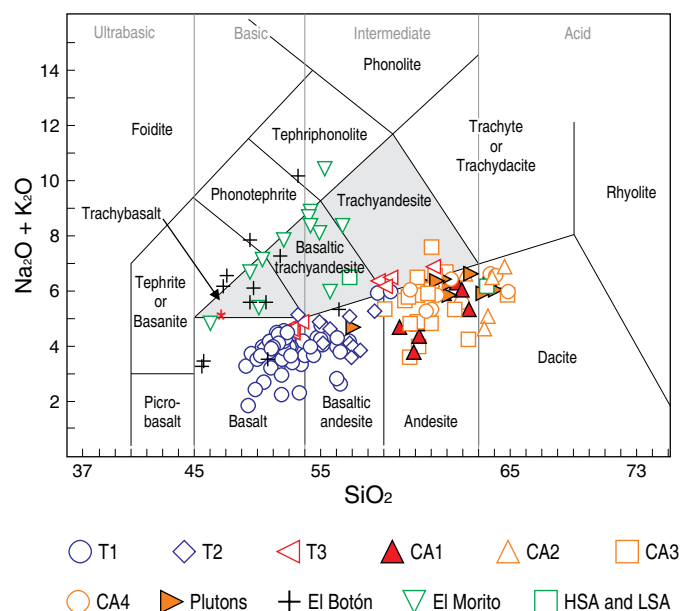


Figure 13. Rock classification diagram after Le Maitre et al. (2002). The Alto Combia sample (Jaramillo, 1976) is highlighted with a red star. Green squares denote High Silica Adakites (HSA), Low Silica Adakites (LSA) after Martin et al. (2005).

T1, Group T2, and Group T3. Overall, the patterns show a negative anomaly for Nb and a slightly less marked anomaly for Ti (Figure 14), all of which have been considered indicative of subduction-related origin for these rocks (Bernet et al., 2020; Dunia, 2005; Jaramillo et al., 2019; Marriner & Millward, 1984;

Tejada et al., 2007). Furthermore, positive Ba and Sr anomalies are also evident (Figure 14). La Popala sample is the most differentiated of the Group T1 rocks, with a parallel REE pattern, indicating crystal fractionation. Nevertheless, variation diagrams define two separate trends for Group T2 and T3 (Figures 14, 16), which suggests that differentiation through crystal fractionation is not the only process involved forming of these rocks. Group T2 overbridges the compositional gap toward the calc-alkaline series. Group T3 includes trachy-andesitic magmas and can be differentiated from other groups based on low Sr/Y and the highest absolute concentrations of Y, Zr, and high FeOt (Figures 14, 15).

REE patterns for the tholeiitic series are relatively flat and somewhat LREE enriched compared to HREEs (Figure 17). Group T1 has a lower La/Yb ratio than the other groups. Some samples show a slight positive Eu anomaly, possibly due to plagioclase as a phenocryst phase.

4.2. Calc-Alkaline Series

The calc-alkaline series comprises mainly andesites and dacites of the CSVI. Nevertheless, samples from El Poma and Tesorito localities are also integrated into the dataset (Bisig et al., 2017; Dunia, 2005). The two associated coetaneous plutonic units, the Farallones Batholith and the Tamesis Stock, are also shown (Dunia, 2005). The calc-alkaline series shows a better-defined trend in the variation diagrams than the tholeiitic series. SiO_2 contents varies from 54.97 wt% (basaltic andesites) to 66.13 wt% (dacites) (Figure 14). The MgO

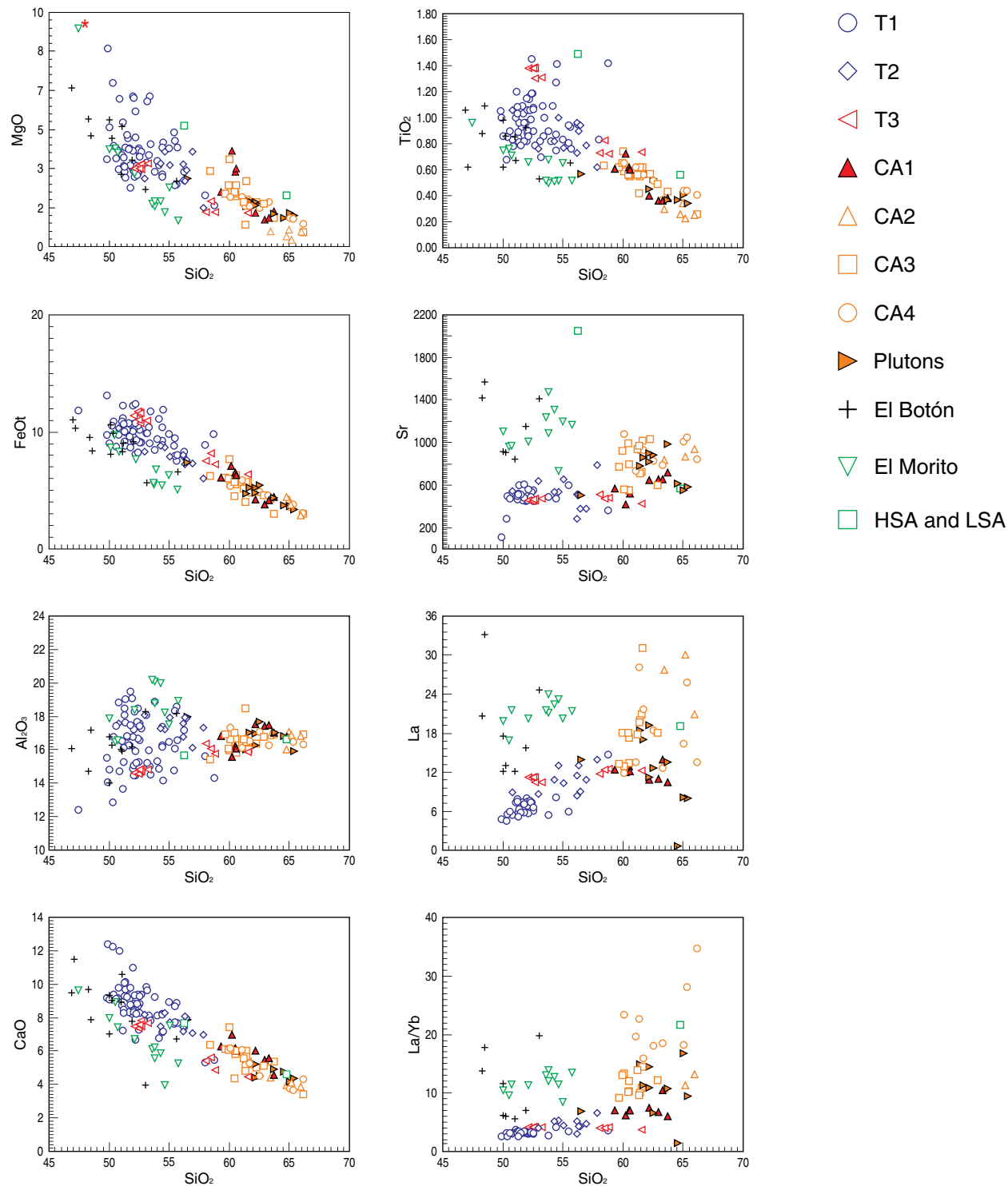


Figure 14. Harker variation diagrams of selected major and trace elements for the Combia Volcanic Province lavas. The Alto Combia sample (Jaramillo, 1976) is highlighted with a red star. High Silica Adakites (HSA), Low Silica Adakites (LSA) after Martin et al. (2005).

content ranges from 0.31 to 4.09 wt%; Al_2O_3 content ranges from 15.56 to 18.50 wt%; and K_2O contents ranges from 0.62 to 4.04 wt% (Figure 12). Samples follow the calc-alkaline field trend (Figure 12) and the medium-K to high-K area of

the K_2O vs. SiO_2 diagram, and therefore, some are high-K calc-alkaline rocks. Garnet-bearing samples of Tejada et al. (2007) and Bissig et al. (2017) are included here, as these samples plot in the calc-alkaline field.

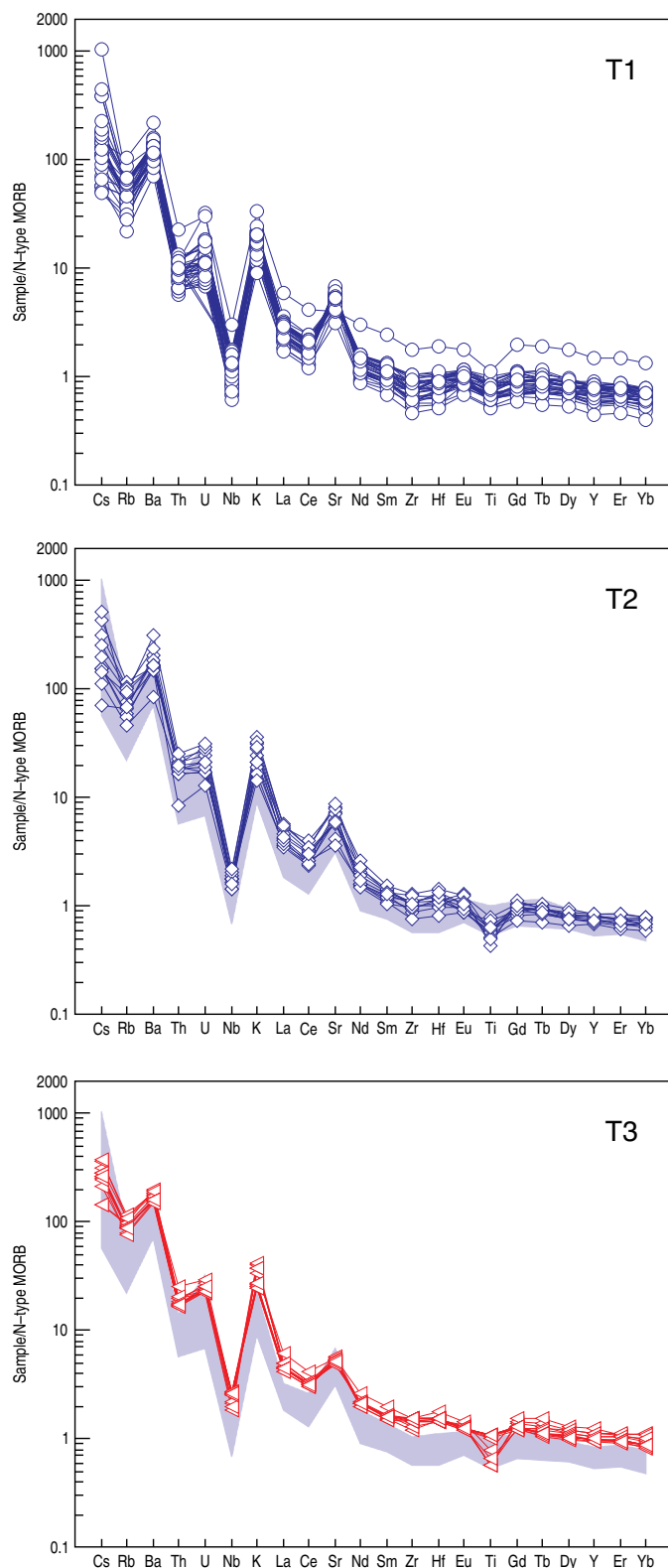


Figure 15. N-MORB-normalized trace-element patterns for the tholeiitic series of the Combia Volcanic Province. Normalization values from Taylor & McLennan (1985). Symbols as in Figure 12.

The N-MORB (Sun & McDonough, 1989) multielement diagrams are more differentiated (Figure 18), and the La/Yb

ratios are higher than those of the tholeiitic samples. Sr and Y content ranges from 374 to 1200 ppm and 5.6 to 27.3 ppm, respectively (Figure 14). Additionally, the negative Nb and Ti and positive K and Sr anomalies are more evident, and there is a positive Hf anomaly in some samples.

REE patterns are more variable than those of the tholeiitic series (Figure 19). Samples were divided into several calc-alkaline groups: Group CA1 (includes garnet-bearing samples) has the lowest La/Yb of the calc-alkaline suite, Group CA2, and CA3 have an intermediate La/Yb, and Group CA4 has the highest La/Yb values of the series. Overall, these samples show a spoon-shaped pattern (Figure 19), indicating that amphibole was significant in magma formation and evolution processes. This is particularly evident in Group CA2.

In general, the Farallones Batholith and Tamesis Stock (Dunja, 2005) have similar compositions when compared to the calc-alkaline series, and variations within these rocks overlap the variations shown by the CSVI. Therefore, a similar petrogenetic origin is likely. Unfortunately, due to the nature of these rocks, nocross-cutting or field relationship has been reported to support this observation.

Some characteristics of the calc-alkaline series are typical of adakites (Figures 12, 20). These characteristics include: $\text{SiO}_2 > 56 \text{ wt\%}$, $\text{Al}_2\text{O}_3 > 15 \text{ wt\%}$, MgO generally $< 3 \text{ wt\%}$, low Y ($< 15 \text{ ppm}$), and HREE relative to the island arc ADR, high Sr $> 400 \text{ ppm}$, $\text{Na}_2\text{O} > 3.5 \text{ wt\%}$, $\text{K}_2\text{O}/\text{Na}_2\text{O}$ approximately 0.4, and low $^{87}\text{Sr}/^{86}\text{Sr}$ ratios (ca. 0.7040) (Castillo, 2012; Defant & Drummond, 1990; Martin et al., 2005). Therefore, these rocks can be classified as adakites (e.g., Borrero & Toro-Toro, 2016). They also plot within the compositional field of High Silica Adakites, as proposed by Martin et al. (2005) (Figure 20b). Nevertheless, La/Yb is relatively low for most of the Group CA1 (garnet-bearing) compared to the typical adakite signatures. Possible differences may be due to the presence of garnet, which would lower this ratio, as will be discussed further in the text.

4.3. Shoshonite Series

Eleven samples, mainly trachybasalts and trachyandesite, define this series (Figure 12). They comprise El Morito basaltic andesites and the Alto Combia absarokite, mirroring El Botón basalts of Zapata & Rodríguez (2011). SiO_2 for these rocks ranges between 55.78 and 50 wt%, MgO between 1.12 and 4.18 wt%, and Al_2O_3 between 16.48 and 20.02 wt%. These rocks have high alkalis, with K_2O ranging from 2.7 for the more mafic rocks to 6.08 wt% for the more felsic rocks (Figure 12). The N-MORB (Sun & McDonough, 1989) multielement diagrams are more differentiated (Figure 21), and the La/Yb ratios are higher. The Sr and Y contents range from 374 to 1200 ppm, and 5.6 to 27.3, respectively (Figure 14). Additionally, they show negative Nb and Ti and positive K and Sr anomalies.

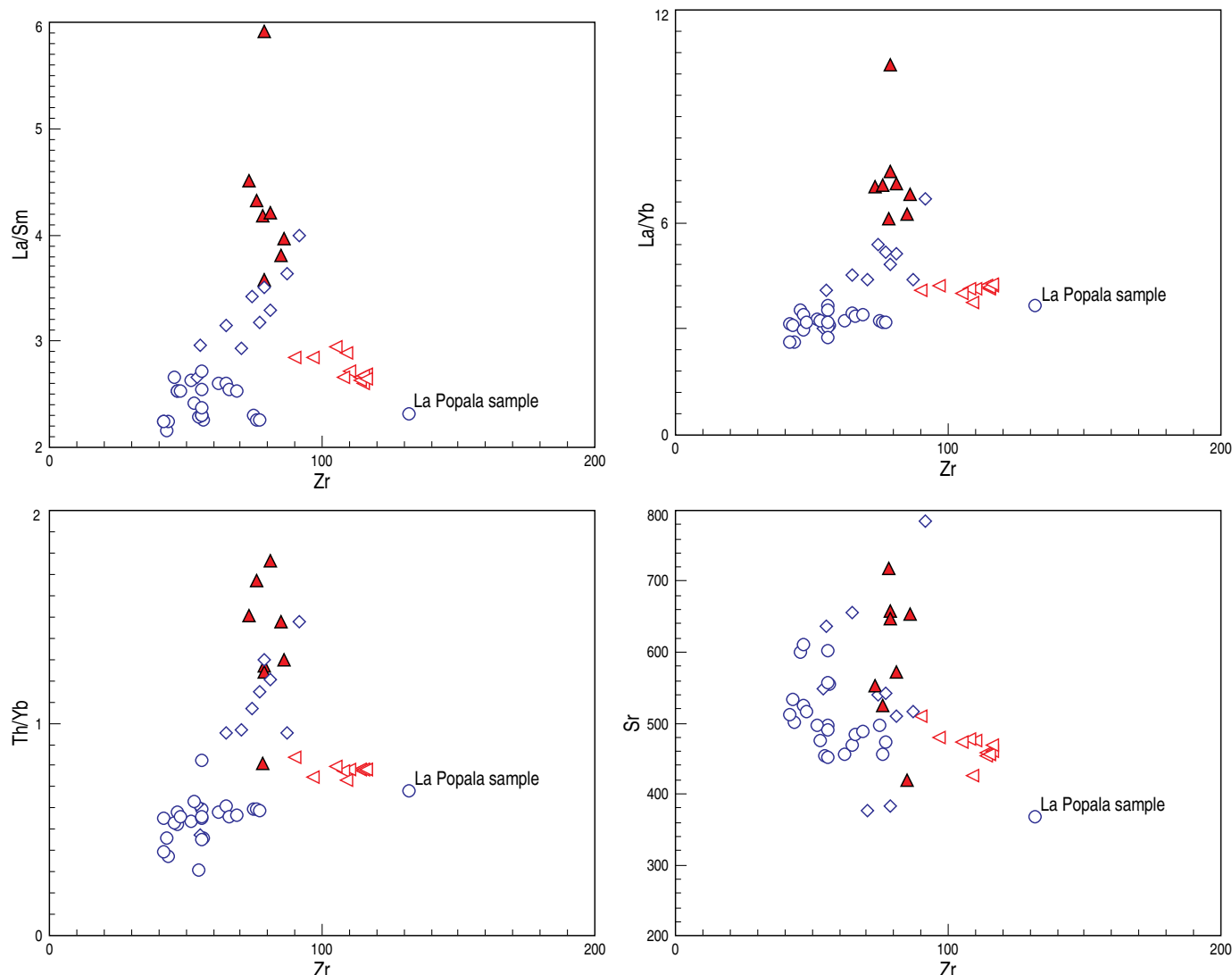


Figure 16. Harker variation diagrams of selected trace elements and ratios vs. Zr for the tholeiitic series of the Combia Volcanic Province. Samples of Group CA1, which includes garnet-bearing samples, of the calc-alkaline series also shown. Symbols as in Figure 12.

4.4. Isotope Data

Present-day $^{87}\text{Sr}/^{86}\text{Sr}$ ratios versus $^{143}\text{Nd}/^{144}\text{Nd}$ isotope values of published (Bernet et al., 2020; Jaramillo et al., 2019; Leal-Mejía, 2011; Ordóñez-Carmona, 2001; Tassinari et al., 2008) and unpublished samples are presented in Figure 22 (see Table 2 of the Supplementary Information 1). The CF and CSVI define a tight sub-linear array, which generally extends from 0.70378 to 0.70533 and 0.512906 to 0.512612, although some outliers are present. Most of the data fall within the mantle array. In general, the data spread towards the lower crust or sediment fields. Most Group T1 and T3 samples cluster at ca. $^{87}\text{Sr}/^{86}\text{Sr}$ 0.79390 and $^{143}\text{Nd}/^{144}\text{Nd}$ at 0.52195, and calc-alkaline samples are slightly more enriched. Some samples, including the garnet-bearing rocks, tend toward lower Sm–Nd and higher Rb–Sr

isotope ratios, indicating either variable sedimentary input or assimilation of older basement rocks.

Pb–isotope analysis from the CVP, Farallones Batholith, and Támesis Stock (data from Bernet et al., 2020; Leal-Mejía, 2011; Tassinari et al., 2008) shows isotopic ratios of $^{206}\text{Pb}/^{204}\text{Pb}$, $^{208}\text{Pb}/^{204}\text{Pb}$, and $^{207}\text{Pb}/^{204}\text{Pb}$ ranging from 18.91 to 19.22, 38.59 to 38.93, and 15.56 to 15.68, respectively (Figure 23). In general, samples show a linear trend that falls within the Northern Volcanic Zone (Compilation by Marín-Cerón et al., 2019). Although the lead-isotope signatures of two CF samples and the Farallones Batholith and the Támesis Stock (Leal-Mejía, 2011) are in the same linear trend as the CF samples, they are more radiogenic. The data generally plot between the altered oceanic crust, Pacific sediments, and the Cretaceous basement, suggesting crust mantle contamination and assimilation.

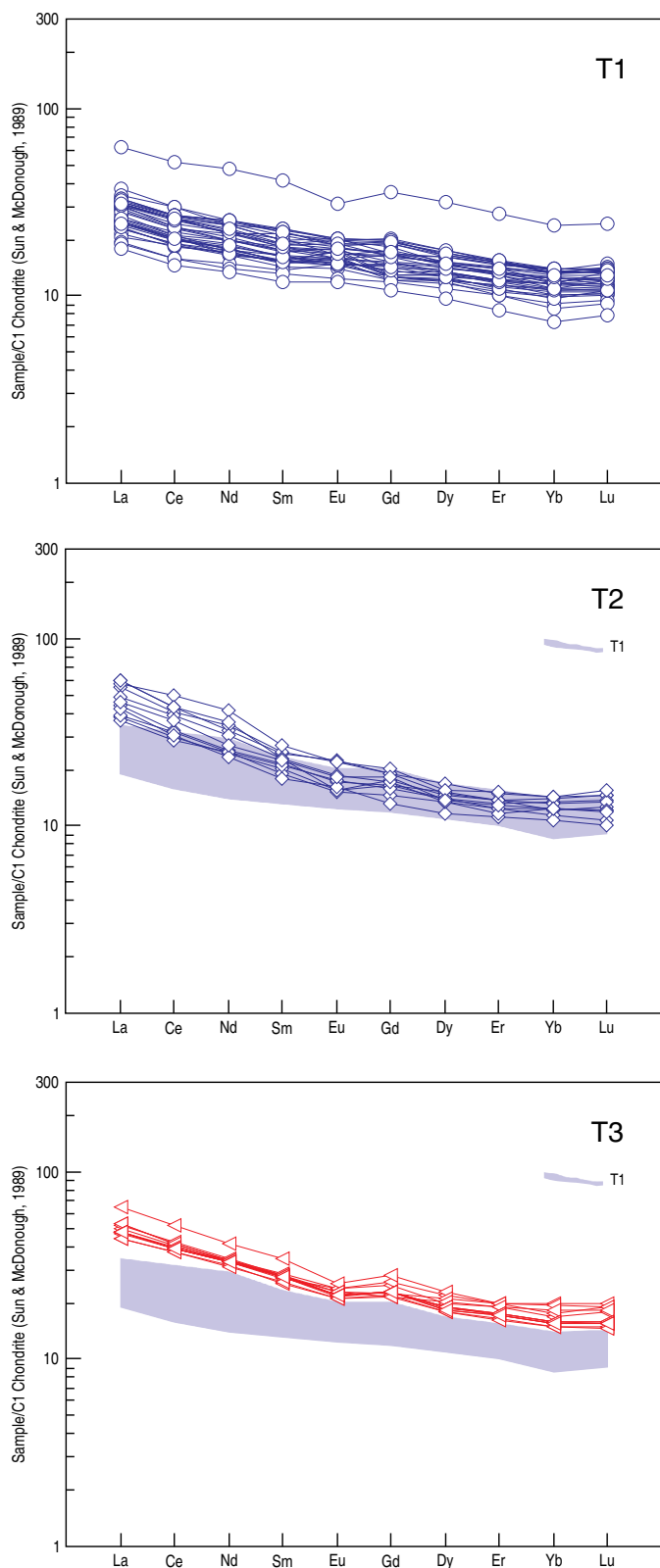


Figure 17. Figure REE patterns normalized to chondrite for the tholeiitic series of the Combia Volcanic Province. Normalization values from Sun & MacDonough (1974). Group T1 tholeiitic lavas are shown for comparison. Symbols as in Figure 12.

5. Geochronology

Recently, Rodríguez & Zapata (2014) proposed to split the middle Miocene magmatism into two different magmatic arcs with different ages and geographical locations: An earlier shoshonitic El Botón arc and a later tholeiitic and calc-alkaline arc of the CF, including CSVI magmas.

El Botón magmatic arc constitutes a series of magmatic products, all of them emplaced on accreted rocks with oceanic affinity from the Western Cordillera and Cauca River basin, including rocks from the Amagá Basin, the Cañasgordas Block, and Romeral suture zone. These magmas have geochemical characteristics of shoshonitic affinity and ages ranging between 12.5 and 9 Ma (Rodríguez & Zapata, 2014). Moreover, Zapata & Rodríguez (2013) define El Botón magmatic arc based on magmatic units such as: El Morito basaltic andesites and El Cangrejo latibasalt (9.1 ± 0.7 Ma in Restrepo et al., 1981a), Cerro Frontino gabbro (10.17 ± 0.41 Ma in Zapata & Rodríguez, 2013), and El Botón basalts (10.55 ± 0.28 Ma, in Zapata & Rodríguez, 2011).

The CF, constituted by volcanic and subvolcanic products, has a tholeiitic to calc-alkaline affinity and is younger than the shoshonitic El Botón Magmatic Arc (Figure 2), as shown by their radiometric ages with an age span between 9 and 6 Ma (Jaramillo et al., 2019; Rodríguez & Zapata, 2014). Nevertheless, it is common to find inherited zircons between 12 and 11 Ma in CF magmatic rocks (cf. Bernet et al., 2020; Hoyos et al., submitted; Jaramillo et al., 2019). These rocks probably originally crystallized in magmas coeval with El Botón and El Morito units.

Analyzing the distribution of different ages obtained over middle Miocene volcanic products in Colombia, a general pattern of younging to the east is evident (Figure 24; see Table 1 of the Supplementary Information 2). Middle Miocene magmatism in Colombia began in the northernmost part of the Western Cordillera with the intrusion of several mostly basic magmas between 17 and 10 Ma. After 10 Ma, this magmatism migrated to the Cauca valley, and no more magmatism is registered in the Western Cordillera after that (Figure 24; see Table 1 of the Supplementary Information 2). Gabbroic intrusions represent early magmatism as Cerro Frontino and basaltic flows as the Santa Cecilia, La Equis, and El Botón. After ca. 10 Ma, the magmatism migrated and was established on the northern segment of the Cauca valley, specifically in the Amagá Basin, represented by several shallow volcanic intrusions and some lava flows (e.g., El Cangrejo basalt). South of the Amagá Basin, in the middle Cauca valley, there is another critical intrusion cluster, La Colosa (Leal-Mejía, 2011), constituted by a series of dioritic porphyries and granodioritic intrusions.

Along with the basic magmatism in western Colombia, volumetrically important magmatism with ages ranging between ca.

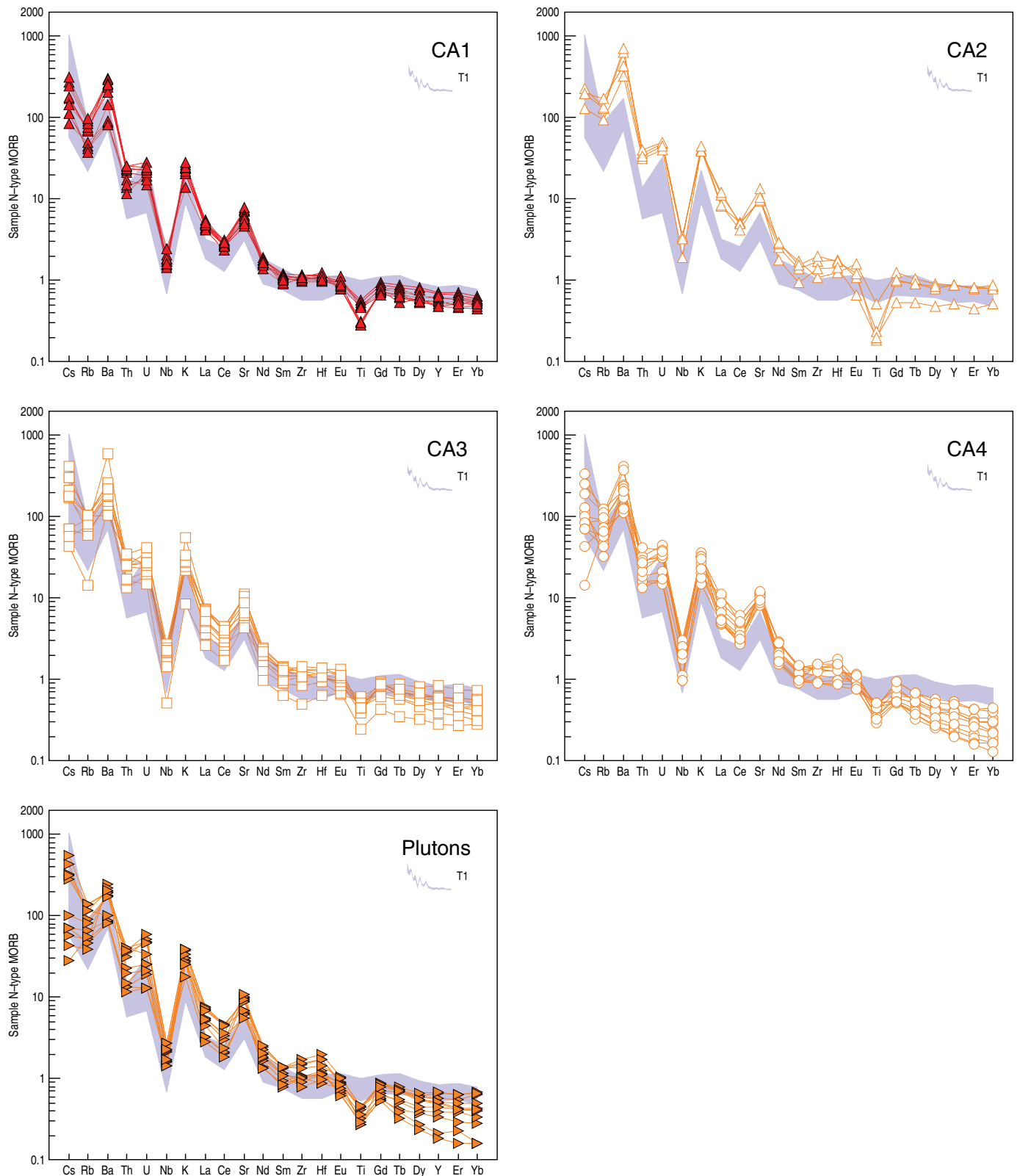


Figure 18. N-MORB-normalized trace-element patterns for the calc-alkaline series of the Combia Volcanic Province. Normalization values from Taylor & McLennan (1985). Symbols as in Figure 12. Group T1 tholeiitic lavas are shown for comparison. Plutonic rocks are plotted separately.

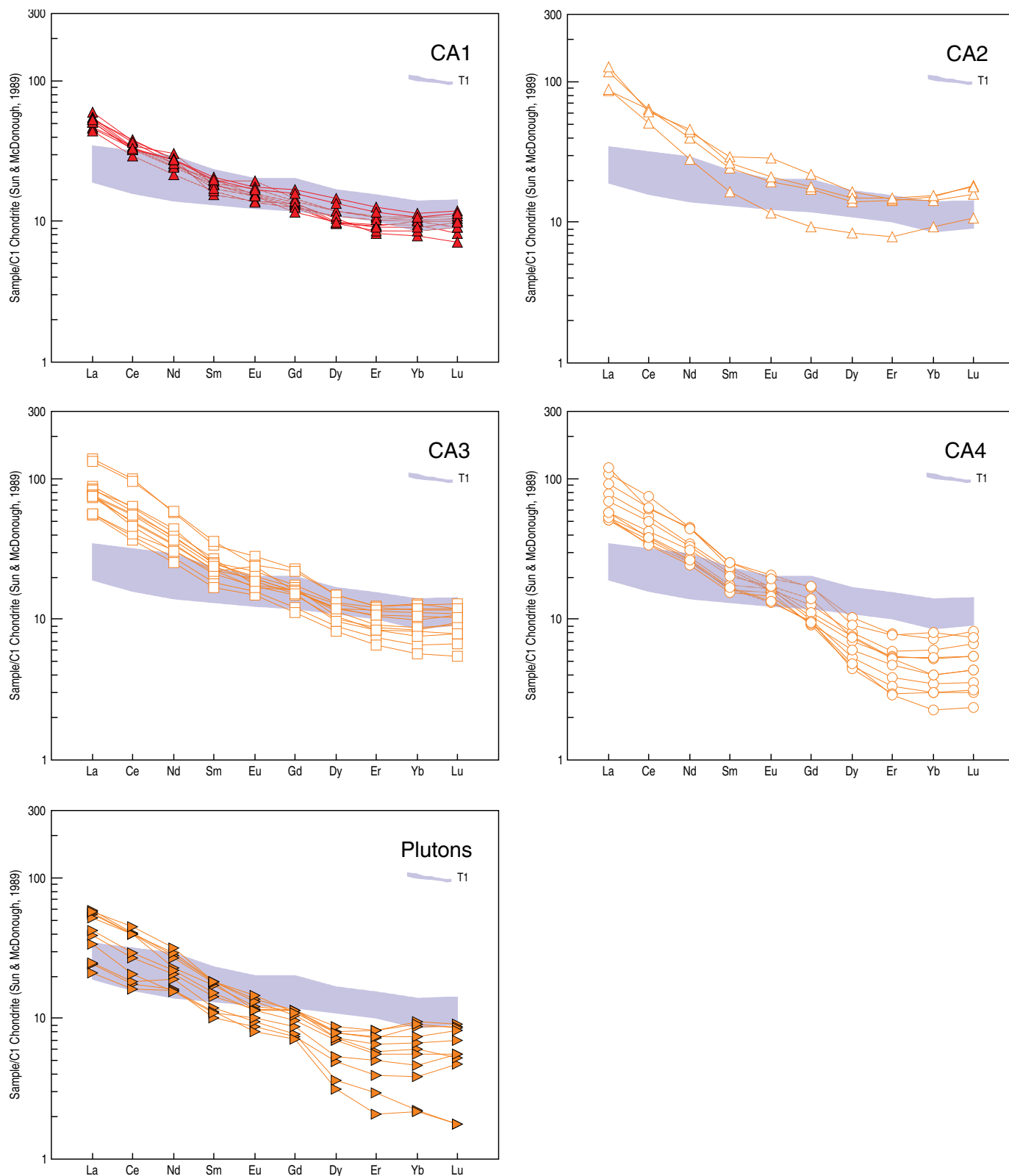


Figure 19. Figure REE patterns normalized to chondrite for the calc-alkaline series of the Combia Volcanic Province. Normalization values from Sun & MacDonough (1974). Symbols as in Figure 12. Group T1 tholeiitic lavas are shown for comparison. Plutonic rocks are plotted separately.

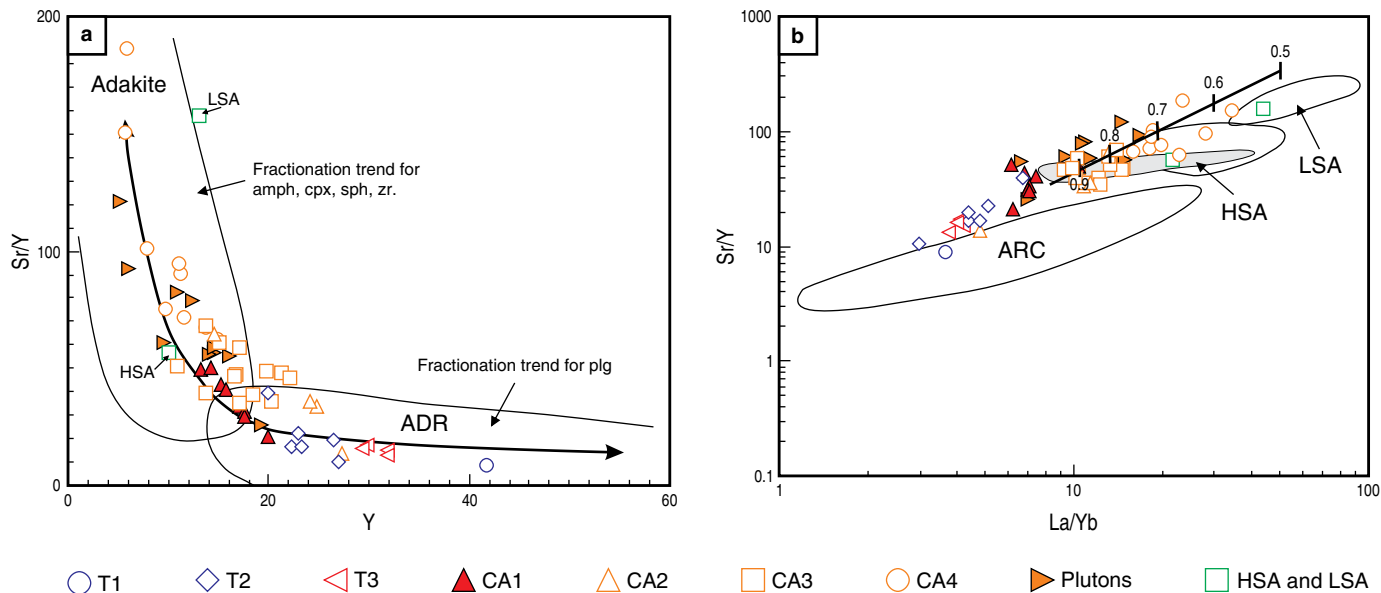


Figure 20. Diagrams showing adakite definitions. Only lavas with $\text{SiO}_2 > 56$ are plotted. **(a)** Diagram showing Sr/Y vs. Y distribution between adakites and “normal” arc andesite, dacite, and rhyolite (ADR) lavas (modified after Drummond & Defand, 1990; Richards & Kerrich, 2007). The fractionation trend for various minerals is also shown (after Richards & Kerrich, 2007). **(b)** Sr/Y vs. La/Yb diagram with fields for High Silica Adakites (HSA), Low Silica Adakites (LSA), and “ordinary” arc magmas (ARC) after Martin et al. (2005). Also shown the calculated fractional crystallization trend of garnet and amphibole as the main fractionating phases (see text for details).

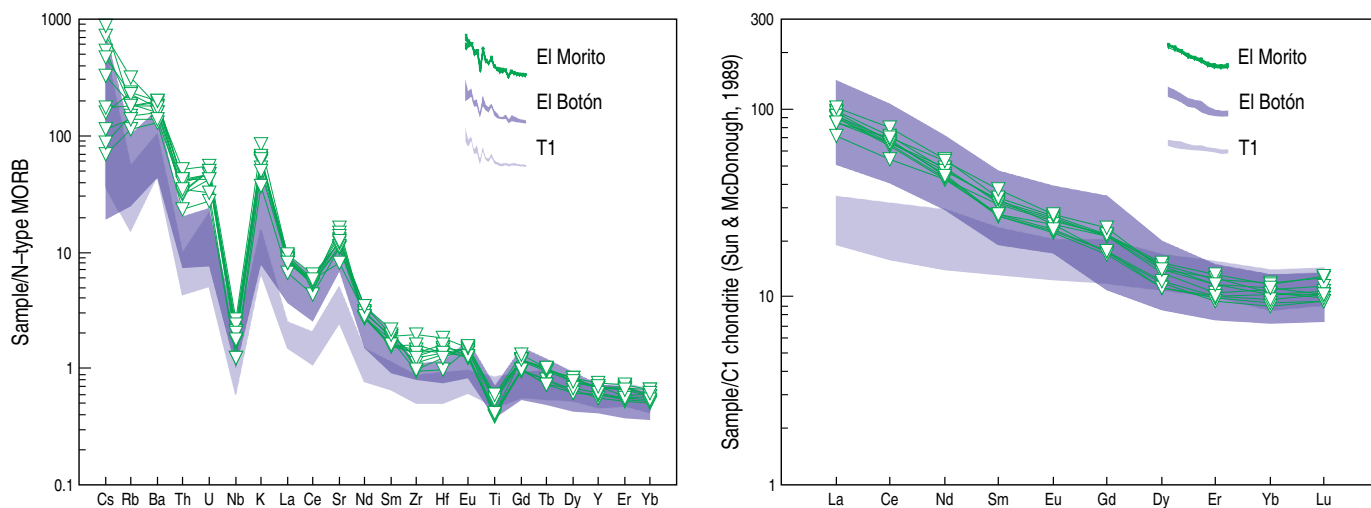


Figure 21. N-MORB-normalized trace-element patterns and REE patterns normalized to chondrite for the shoshonitic series of the Combia Volcanic Province (El Morito lavas). Normalization values from Taylor & McLennan (1985) and Sun & MacDonough (1974). Symbols as in Figure 12. Shown for comparison are El Botón lavas (Zapata & Rodríguez, 2011) and T1 tholeiitic lavas.

12 and 6 Ma (Figure 24) had occurred. Younger ages between 6 and 4 Ma (Figure 24; see Table 1 of the Supplementary Information 2) would represent cooling ages of ca. 6 Ma intrusions and associated hydrothermal activity, not intrusion or formation ages. Middle Miocene intermediate magmatism in western Colombia began between ca. 14 and 12 Ma with a widespread magmatism affecting both the Western Cordillera and the Cauca valley (on both southern and northern segments). Nevertheless, this magmatism was especially intense in the northern part of

the Cauca valley and mainly concentrated along the Cauca Fault, which possibly served as a magma emplacement conduit (Figure 24). $^{40}\text{Ar}/^{39}\text{Ar}$ determined ages for these shallow volcanic intrusives lie within this range (Figure 24). Cerro Tusa, one of the most outstanding vestiges of this magmatism, and considered a volcanic plug (Calle & Gonzalez, 1980; Grosse, 1926), yields a reliable $^{40}\text{Ar}/^{39}\text{Ar}$ in hornblende age of 7.93 ± 0.14 Ma (Figure 25a). Garnet-bearing shallow volcanic intrusive porphyries, north of Jericó, yield two $^{40}\text{Ar}/^{39}\text{Ar}$ ages in hornblende of ca. 8.8

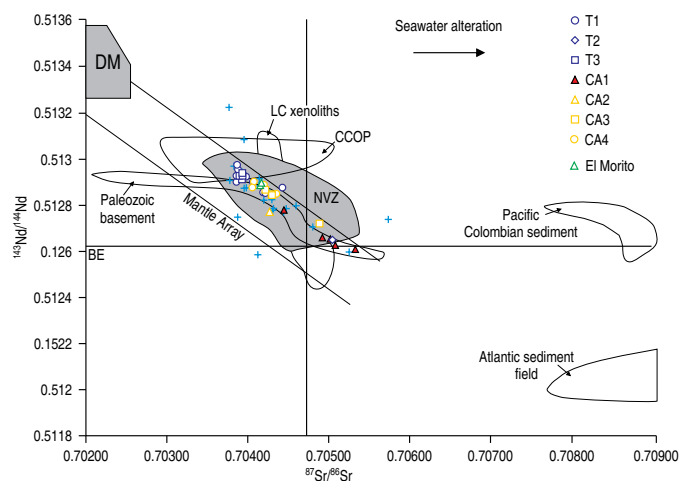


Figure 22. $^{143}\text{Nd}/^{144}\text{Nd}$ vs. $^{87}\text{Sr}/^{86}\text{Sr}$ diagram. Comparison of the CF and CSVI rock data with the Northern Volcanic Zone. Northern Volcanic Zone (NVZ) data from James & Murcia (1984), Francis et al. (1977), Hawkesworth et al. (1979), Barragan et al. (1998), Bourdon et al. (2002), Errázuriz-Henao et al. (2019); Caribbean-Colombian oceanic plateau (CCOP) data from Kerr et al. (1996, 1997); Pacific Colombian Sediment from Errázuriz-Henao et al. (2019), Atlantic Sediment Field taken from data compilation plot from Errázuriz-Henao et al. (2019), Lower Crustal (LC) xenoliths from Weber et al. (2002). Main oceanic mantle reservoirs after Zindler and Hart (1986): Depleted Mantle (DM), and Bulk Silicate Earth (BE).

Ma (Figure 25b, 25c). These ages overlap the explosive volcanic deposits associated with the CF.

Different pyroclastic density current units, exposed near the Amagá River (Figure 25d) and along the Morro Plancho, Concordia (Figure 25e, 25f), were dated and presented here, all yielding the same age, ca. 8.5 Ma. Samples were obtained from outcrops with altitudinal differences of ca. 1000 m. The Morro Plancho sequence is located at ca. 1500 masl, whereas the Amagá River sequence is located at ca. 500 masl. Because these two sequences yield the same age and have identical petrographic characteristics, we interpret them as part of the same deposit or at least formed by subsequent eruptions. Transtensional displacements could explain the outcrop positions along NW–SE to N–S faults. The ages obtained for the explosive deposits are concordant with previously published ages for the CSVI surrounding the Amagá Basin area (Figure 24). Jaramillo et al. (2019) report an age of ca. 8.3 Ma for the overlying pyroclastic sequence, including lithic breccia deposits, the same as that reported on the other side of the Amagá Basin between Jericó, Támesis, and Jardín. Based on the ages reported here for the pyroclastic density current units, we suggest that these ages could be genetically linked with lithic breccia deposits.

The Irra Formation correlates by lithology, time, and space with the CF. This formation, deposited to the south of the CF, within the Cauca River valley, is a succession of interbedded polymictic conglomerates and reworked pyroclastic material

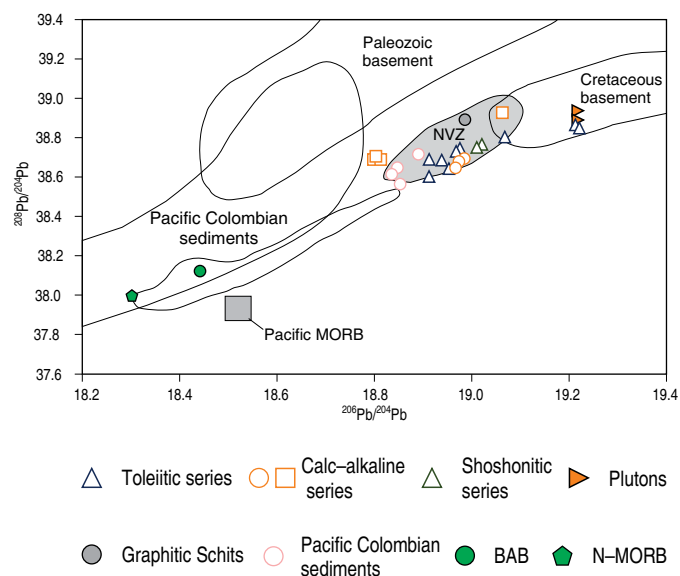


Figure 23. $^{208}\text{Pb}/^{204}\text{Pb}$ vs. $^{206}\text{Pb}/^{204}\text{Pb}$ diagram showing the Pb isotopic composition for samples of the Combia Volcanic Province. Data from Tassinari et al. (2008), Leal-Mejía (2011), and Bernet et al. (2020), in comparison with potential inputs (plot modified from data compilation plot from Marín-Cerón et al., 2010, 2019). NVZ: Northern Volcanic Zone. Colombian Pacific sediments data from Errázuriz-Henao et al. (2019), mean N-MORB and BAB from Gale et al. (2013).

packages (Sierra, 1994). The age of the pyroclastic deposits, late Miocene (6.3 ± 0.2 Ma fission tracks in zircon; Toro et al., 1999), overlaps with those obtained for some subvolcanic intrusives emplaced along the Cauca River depression (e.g., Irra porphyry; Támesis Stock, Marmato porphyry, La Felisa Stock). Considering that (i) the mentioned pyroclastic deposits are coeval with corresponding magmatic intrusives in each area, and (ii) the Cauca River depression and the Amagá Basin intrusives correspond to the same continuous magmatism, which affected the Western Cordillera, we propose that the volcano-sedimentary member of the CF and at least the upper members (A and B) of the Irra Formation represent a coeval singular geological event that is recorded in adjacent extensional basins.

6. Garnet-Bearing Samples

Garnet-bearing porphyritic rocks in the Neogene middle Cauca valley were first reported from the Chinchiná and Palestina areas (García, 1983). Later, garnets were described from two localities in the Jericó area (Dunia, 2005; Tejada & Betancourt, 2006; Tejada et al., 2007) and Tesorito and El Poma in the Colombian Middle Cauca Metallogenic Belt (Bissig et al., 2017). The composition is variable and will be described elsewhere (Hoyos et al., submitted). Zircon U–Pb and new $^{40}\text{Ar}/^{39}\text{Ar}$ ages (Figure 25a–c) for garnet-bearing porphyritic

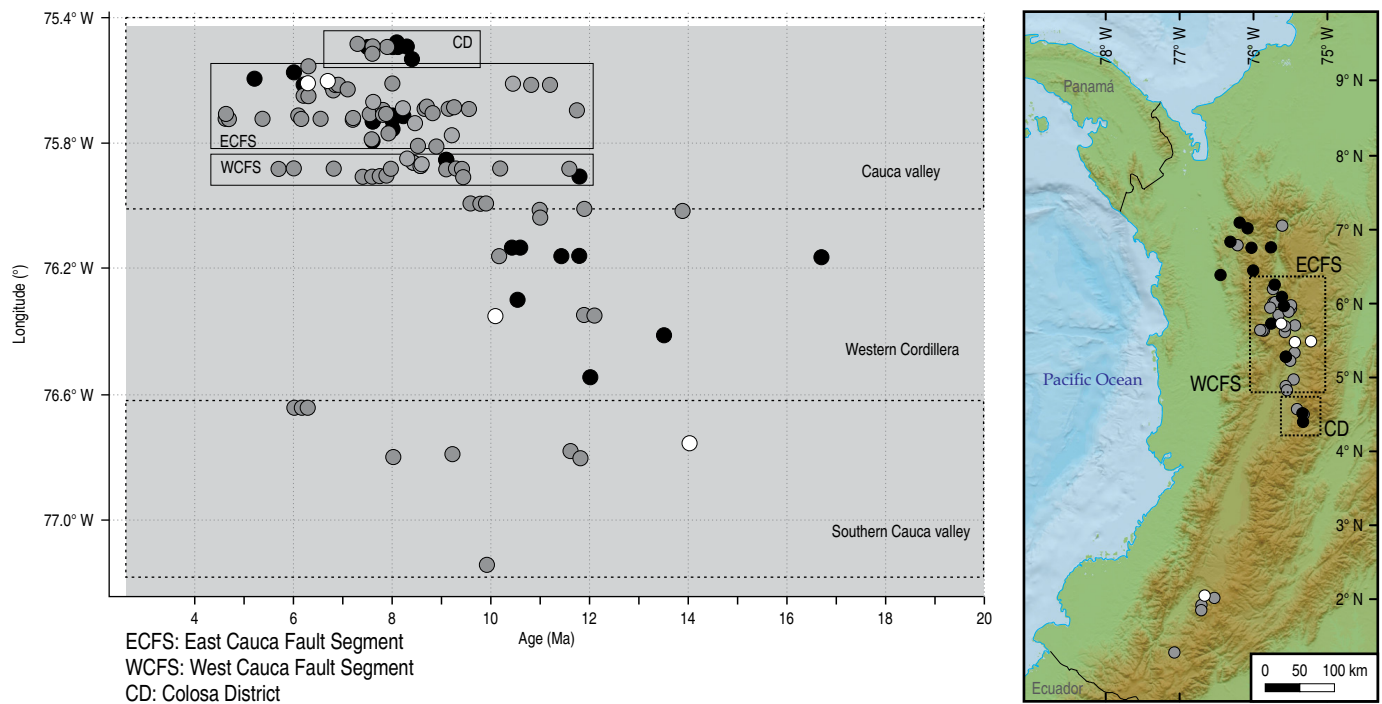


Figure 24. Age distribution of the Miocene intrusive, subvolcanic, and volcanic rocks from western Colombia, including the Combia Formation magmatic rocks. **(a)** Age (Ma) versus Longitude (°). **(b)** Geographic distribution of compiled analyses. Colour in symbols varies with rock composition: Basic rocks (black), intermediate rocks (gray), differentiated rocks (white). Plotted samples correspond to Table 1 of the Supplementary Information 2.

ic rocks indicate that these rocks formed at ca. 12 Ma in El Poma location and at ca. 9 Ma in El Tesorito and Jericó locations during the early stages of magmatic activity in the Cauca valley. The Jericó $^{40}\text{Ar}/^{39}\text{Ar}$ ages possibly represent cooling ages, and therefore magmatic crystallization ages are likely to be slightly older. Nevertheless, these magmas crystallize at shallow crustal levels, and thus cooling was fast, and the differences in both ages are small.

To constrain the significance of these rocks within the CF, we present the mineral chemistry of two garnet-bearing samples (MJG-132 and MJG-134) from the Jericó area and one andesite sample from Cerro Tusa (MW-1) (Figure 26). The analyzed minerals were garnet, plagioclase, amphibole phenocrysts, and microlith matrix phases (see Tables 1, 2, 3 of the Supplementary Information 3).

6.1. Garnet

Garnet is mainly almandine, characterized by XFe compositions ranging from 0.54 to 0.61, XMg compositions ranging from 0.14 to 0.20, and XCa from 0.16 to 0.23 (Figure 26a–c). Generally, garnet crystals show a darker pink core and a colorless rim. Furthermore, there is a compositional break in larger garnets, with garnet compositions being more Ca-rich in the centers (e.g., garnet in sample MJG-134 varies in terms of XCa content, from approximately 0.66 to 0.58, and

XMg from approximately 0.44 to 0.45), and more Mn and Mg enriched at the rims. Consequently, at least two garnet generations are preserved (core Grt 1 and rim Grt 2) (Figure 26). The presence of Mn–Mg-enriched and Ca-depleted overgrowth garnets indicates an abrupt change in crystallization conditions during their formation within the magma. High grossular garnets would represent the second generation (Grt 2), which in turn shows a slight Ca increase towards the outermost rim (Figure 26c).

Three scenarios could explain these zonation profiles: (1) Post-formation diffusion at garnet rims under the growth of a new crystallization phase within the magma (e.g., plagioclase coronas around garnet are common, and zonation could therefore suggest Ca depletion due to Ca–plagioclase formation). Nevertheless, the slight increase in Ca from the inner Grt 2 to the outermost rim precludes this possibility. Furthermore, plagioclase coronas are common in similar porphyritic garnet-bearing rocks, where zonation profiles are flat (e.g., Bissig *et al.*, 2017). (2) Changes in physicochemical conditions of the magma after the crystallization of Grt 1. This could happen because of the introduction of a different liquid component (magma mixing or fluid introduction), assimilation of wall rock material, or transition to shallower crustal levels, where a different composition of garnet would crystallize. Any of these processes would better explain the coupled Ca, Mn, and Mg profiles shown. (3) The second garnet formation reflects the

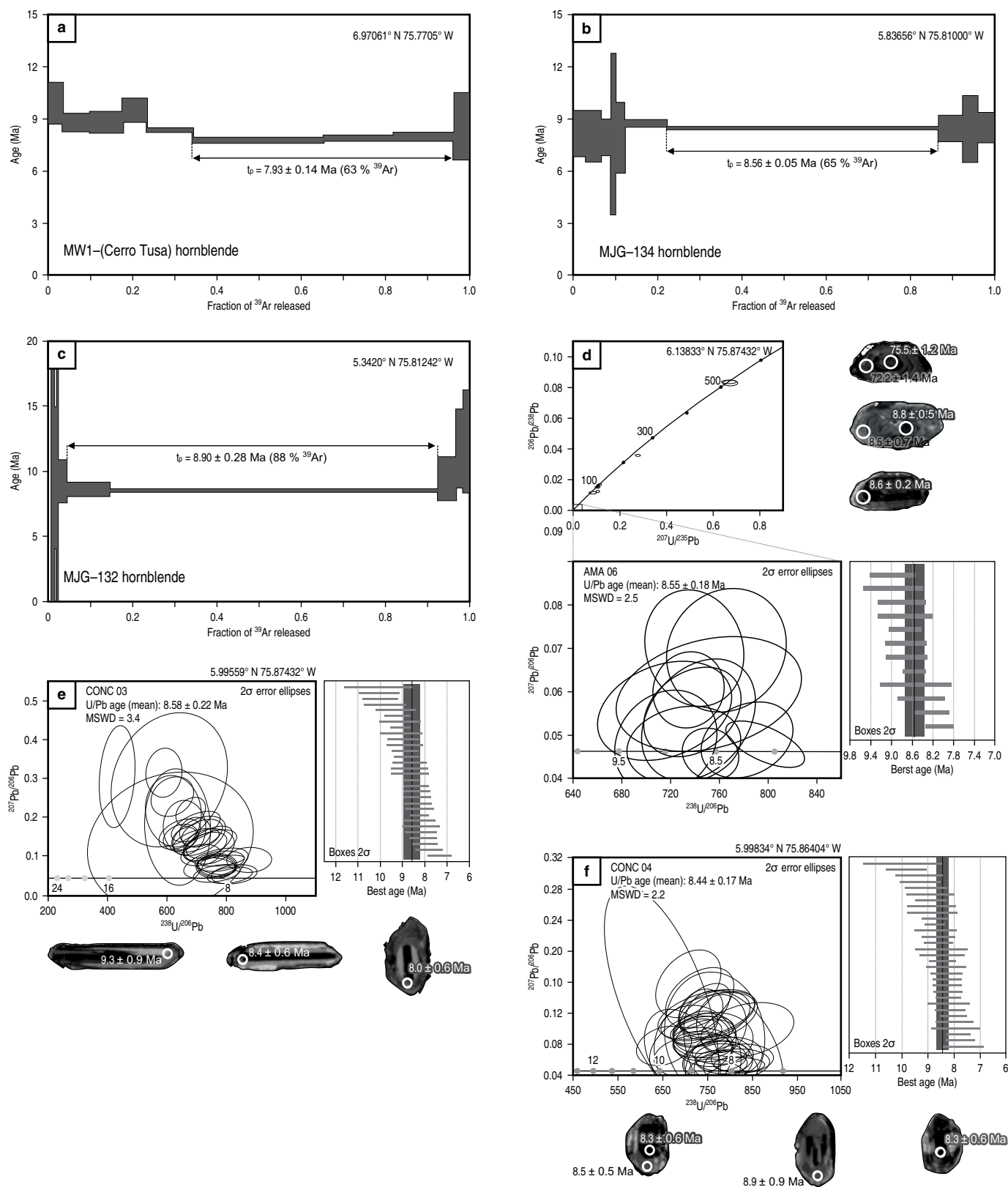


Figure 25. New $^{40}\text{Ar}/^{39}\text{Ar}$ ages from **(a)** Cerro Tusa and **(b–c)** Jericó garnet-bearing intrusive. **(d–f)** U–Pb ages from pyroclastic density current deposits from Concorcía–Cauca river section.

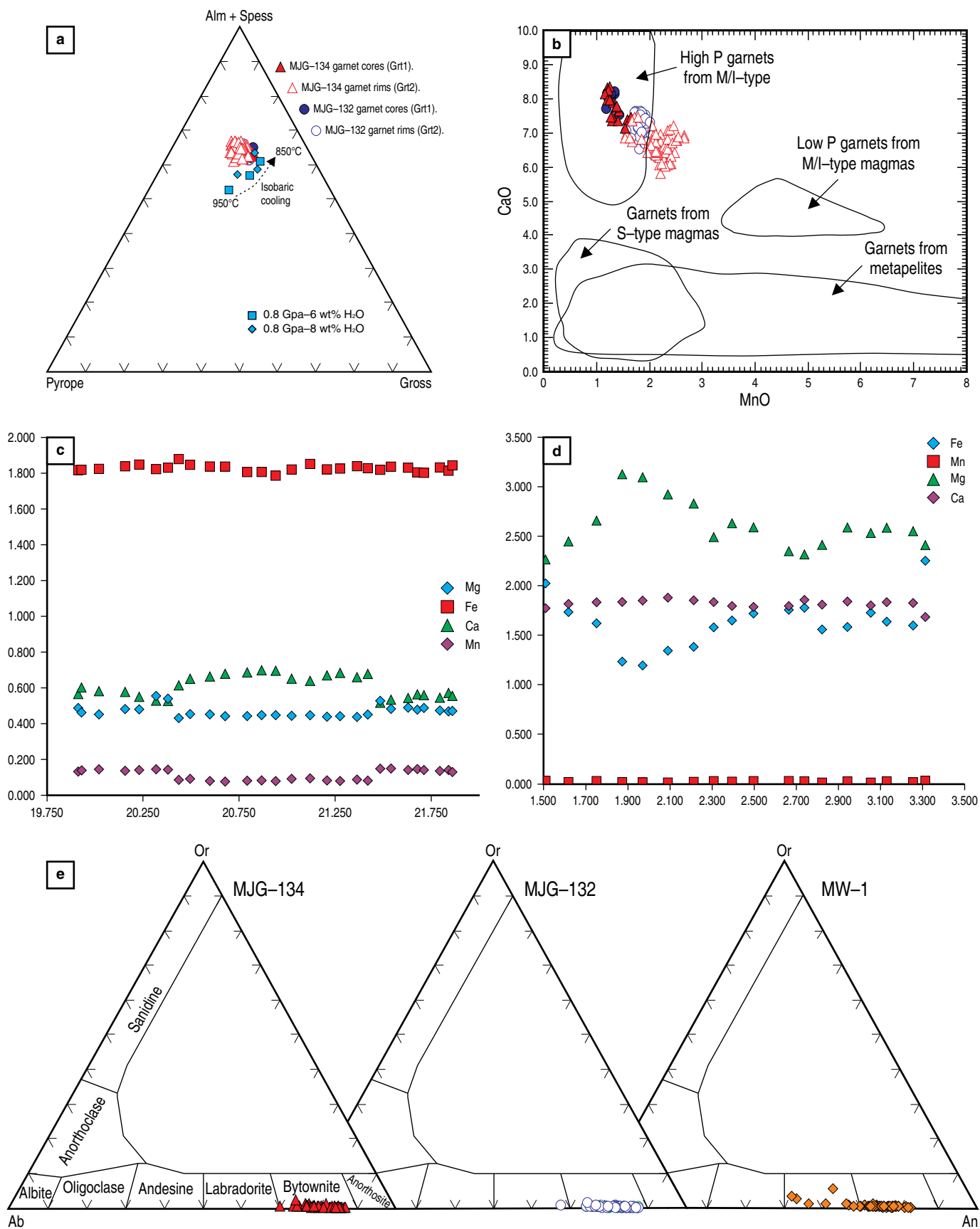


Figure 26. Mineral chemistry of garnet, amphibole, and plagioclase in the Combia Formation porphyritic rocks. **(a)** Garnet phenocryst composition on the Grss–Alm–Py diagram. Experimental garnet compositions and isobaric cooling trend from Alonso–Perez et al. (2009) are also shown. **(b)** CaO and MnO binary diagram. Fields are from Harangi et al. (2001) and references therein. **(c)** Representative garnet zonation profile. **(d)** Representative amphibole zonation profile. **(e)** Plagioclase composition in the Ab–An–Or ternary diagram.

introduction of a new crystallization phase in the magma (e.g., plagioclase), which changed the fractionated liquid's overall Ca composition.

The CF garnet compositions are similar to those reported from El Tesorito and El Poma (Bissig et al., 2017). They also resemble the experimental garnets obtained by Alonso–Perez et al. (2009) from andesitic compositions with 6 to 8 wt% H₂O at 0.8 GPa and 850 to 900 °C. Furthermore, according to the experimental data under these conditions, the modal amount of garnet at 0.8 GPa decreases with a decrease in H₂O at the expense of plagioclase and amphibole formation ($\text{grt} + \text{liq1} = \text{amph} + \text{plg} + \text{liq2}$), which would agree with the petrographic evidence (i.e., plagioclase rims and amphibole rims) shown by CSVI garnet phenocrysts (Figure 10c).

6.2. Plagioclase

Plagioclase phenocrysts in all samples are oscillatory zoned (Figure 10a). Most of them are classified as bytownite. Overall, cores are more calcium-enriched than rims composition, although some variability is present, and are less well developed in the Cerro Tusa andesite sample (Figure 26e). Plagioclase inclusions in garnets are highly calcic (labradorite), similar in composition to cores in zoned phenocrysts and some matrix microliths (e.g., Cerro Tusa).

6.3. Amphibole

Amphibole in garnet-bearing samples is mainly pargasitic hornblende, and Mg# ranges from 0.439 to 0.693. Most phenocrysts show a compositional break, with more Mg-rich and Al- and Fe-poor cores than rim compositions (Figure 26d). Nevertheless, some amphiboles show composite zoning profiles. There is also evidence of some reverse zoning at the crystal rims, possibly due to magma–crystal interactions during matrix cooling. Amphibole inclusions in garnet are more pargasitic than matrix crystals. Some amphiboles enclose smaller garnet crystals, indicating crystal growth after Grt 1 was already formed.

Amphiboles in the andesitic magma of Cerro Tusa have an overall darker rim than their centers, but zonation is nevertheless patchy. Even though cores are slightly more Mg-rich, chemical variation is present to a much lesser extent than garnet-bearing samples. The compositions are mainly ferro-pargasitic, and Mg# ranges from 0.223 to 0.337.

To obtain further constraints on magma crystallization depths, thermobarometric calculations were performed on amphibole crystals (Figure 27). Estimations of pressure and temperature were calculated using an empirical calibration based on the composition of amphibole from calc-alkaline magmas, proposed by Ridolfi & Renzulli (2012) and Ridolfi et al. (2010). The results obtained are plotted in Figure 27 and listed in Table 1 of the Supplementary Information 4.

Pressures obtained using the calibration range between 309 and 502 MPa, which correspond to ca. 18 km depth calculated for cores and ca. 11 km depth for rims, considering an upper crustal density of 2.7 g/cm³. The temperature calculations for these samples range between 950 °C in the cores and 880 °C in the rims (Figure 27a). These temperatures agree with the PT constraints for the garnet determined above.

Although all analyzed crystals are close to the boundary of compositionally consistent amphiboles (dashed lines in Figure 27a), some of them exceed the H₂O melt stability limit. However, the estimated water contents account for uncertainties of 15% (Figure 27b). Pressure and temperature characterization of these crystals indicate that the analyzed amphiboles crystallized close to the instability boundary, making these crystals prone to destabilization with small P–T changes.

Further constraints on pressure and temperature conditions can be obtained via a comparison with compositions of experimentally obtained amphiboles. Crystallization and melting experiments have shown that the contents of Al₂SiO₅, Mg#, and Na+K in amphibole are pressure- and temperature-dependent (Alonso–Perez et al., 2009; Ribeiro et al., 2016; Samaniego et al., 2010;). Amphibole from the garnet-bearing samples overlaps the high-pressure (HP) compositional fields (>400 MPa) in Al₂SiO₅, Mg#, and Na+K for amphibole plots (after Ribeiro et al., 2016) and is somewhat higher than the calculated pressures and temperatures from geothermobarometric calculations shown above.

Physical conditions during the last magma evolution stages are difficult to evaluate via mineral chemistry. However, the amphibole reaction rims found in the CSVI intrusives, especially in the Amagá Basin–CSV (Figure 10b), suggest that these rocks respond to water loss throughout the melt adiabatic ascent from the reservoir to upper-level magmatic chambers (Rutherford & Hill, 1993). Therefore, magmas resided in shallow chambers prior to intrusion into the AF sedimentary beds or eruption to the surface.

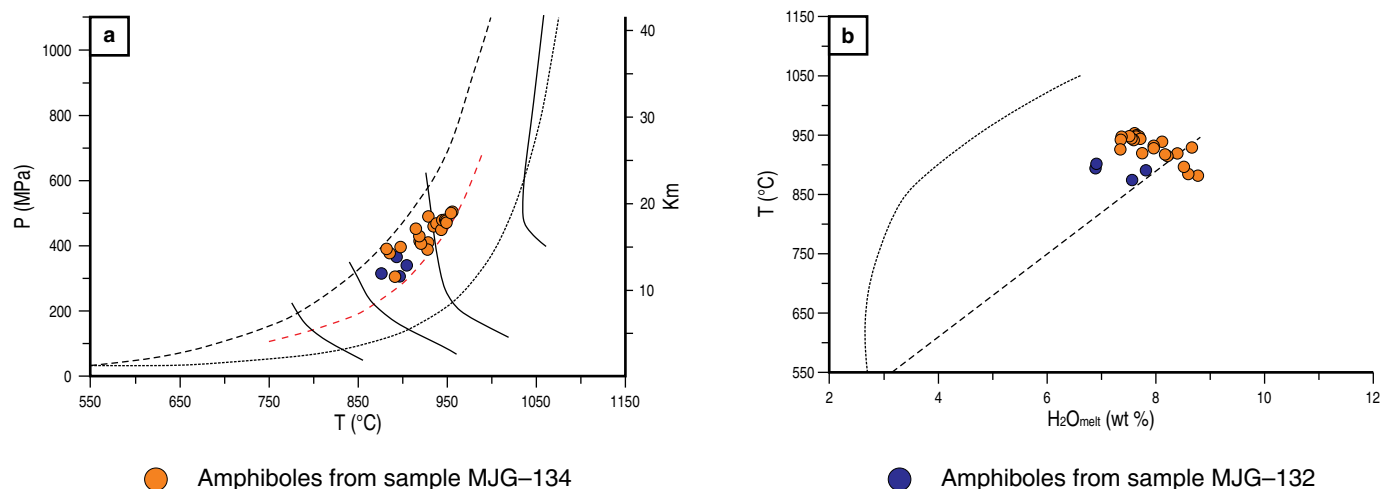


Figure 27. Estimated pressures and temperatures for the Jericó garnet-bearing intrusives (MJG-132 and MJG-134). **(a)** Pressure (MPa) vs. Temperature (°C) and **(b)** Temperature (°C) vs. H₂O melt (wt%). Pressures and temperatures were calculated after Ridolfi & Renzulli's (2012) formulation based on amphibole composition. Mineral data and calculations are presented in Table 1 of the Supplementary Information 4.

7. Discussion

7.1. Garnet-Bearing Rocks

Few worldwide localities report primary garnet in volcanic rocks. As a primary phenocryst, garnet is more common in peraluminous magmas, such as the Pyrenean dacite–rhyolite suits (e.g., Gilbert & Rogers, 1989; Muñoz, 1992), the Trinity Peninsula in Antarctica (e.g., Hamer & Moyes, 1982), and NW England (e.g., Fitton, 1972; Thirlwall & Fitton, 1983). On the other hand, primary garnets in metaluminous rocks (e.g., andesites) occur in volcanism-related settings in NE Japan (Miyashiro, 1955; Kano & Yashima, 1976; Kawabata & Takafuji, 2005; Shuto *et al.*, 2013), Central Anatolia (e.g., Aydar & Gourgaud, 2002), the Northland Arc in New Zealand (Bach *et al.*, 2012; Day *et al.*, 1992; Green, 1992; Smith *et al.*, 1989), and evolved magmas in the Pannonian Basin (e.g., Embey–Iszstán *et al.*, 1985; Harangi *et al.*, 2001). Furthermore, Green (1992) adopted the terms S-type, M-type, or I-type originally proposed by Chappell & White (1974) for silicic igneous rocks and applied them to garnet-bearing volcanic rocks.

Green (1977, 1992) determined that the CaO content in garnet is dependent on the magma type and the pressure and temperature of crystallization. Garnets formed under high-pressure conditions are characterized by high CaO (>5 wt%) and, as pressure decreases, MnO contents tend to increase (> 3wt%) without a coupled decrease in CaO.

Garnets occurring in CSVI rocks are similar to garnets crystallized in M-type and I-type intermediate and mafic magmas at high pressures (Figure 26a). In addition, they have a CaO-rich core, which is surrounded by CaO-poor secondary garnet. Consequently, this evidence suggests at least two growth stages,

which is also reflected by amphibole phenocryst zonation. Interestingly, these rocks have shown to have abundant xenoliths, and interestingly, some garnet-bearing samples have more radiogenic Sr–Nd isotope values within the whole suite, which could indicate the addition of a crustal component (Figure 22)

Ca-rich almandine garnet is not stable in high-pressure magmas, and it is likely to be completely reabsorbed in long-residence magma chambers under shallow crustal conditions. Thus, garnet survival in volcanic rocks is expected to be a function of rapid magma ascent through the crust (e.g., Fitton, 1972; Gilbert & Rogers, 1989; Harangi *et al.*, 2001). Nevertheless, the addition of a Mn component increases garnet stability (Green, 1972), which could account for preserving some of the garnet in the CSVI. Secondary overgrowth (Grt 2) would increase the possibility of garnet preservation. An additional factor in garnet stability determined in recent studies is the presence of H₂O-content in the magmatic liquid (Alonso-Perez *et al.*, 2009). For some of the CSVI Group CA1 magmas it is possible that garnet was reabsorbed, and therefore is not present as a phenocrystal phase.

Amphibole in these samples also indicates at least two formation stages evidenced by the differences in calculated pressures and temperatures in cores and rims (17–19 km–950 °C and 11 km–900 °C, respectively). Furthermore, the outermost amphibole rims and sieve textures in plagioclase indicate degasification and chemical/physical disequilibrium (respectively) during the last stages of magma ascent to the surface (Figure 28).

Therefore, we conclude that the garnet-bearing magmas in the CSVI suite show at least three formation stages through phenocrystal evolution: (i) Magma formation and crystallization of Grt1 and Amph1, (ii) changes in physicochemical conditions either due to pressure decrease or magma contamination,

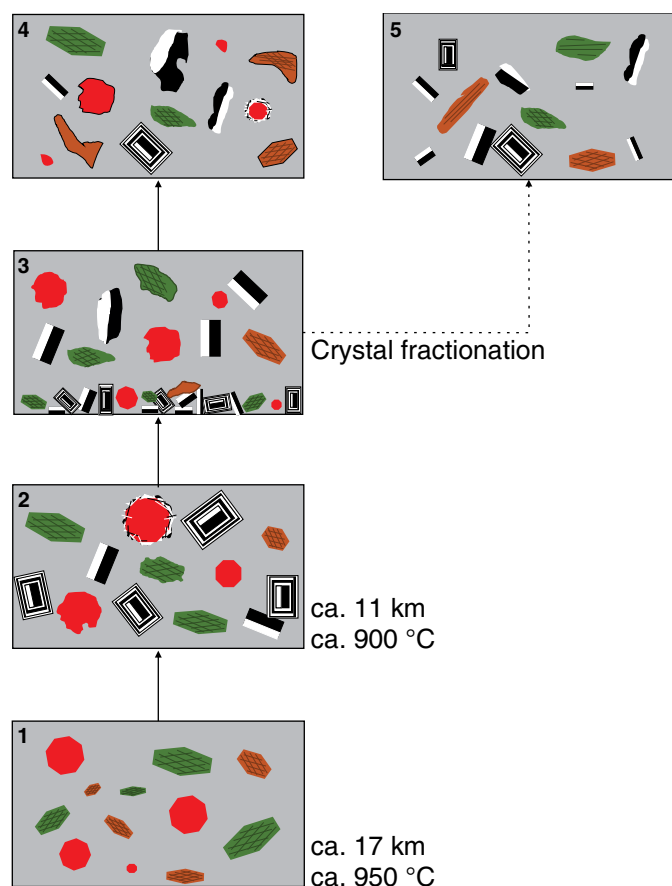


Figure 28. Magma crystallization model proposed for CSVI calc-alkaline rocks. Stages: (1) Early phenocrysts formation phases at ca. 17 to 19 km deep and ca. 950 °C; (2) reabsorption of early formed phenocrysts and crystallization of the second generation of phenocrysts at ca. 11 km and ca. 900 °C; (3) removal of some phenocrysts to evolve into stages 4 and 5; (4) early formed phenocrysts disequilibrium and degasification/dehydration textures in amphibole and plagioclase due to chemical (magma mixing) and physical (P–T changes) variation in shallow magma chambers; and (5) adakitic magmas formed via crystal fractionation.

whereby Grt2 and Amph2 are formed, and possibly the onset of extensive Plg crystallization, and (iii) degasification and rapid ascent to the surface (Figure 28).

7.2. The Adakite Connection

The CSVI has been linked to adakite formation (Bissig et al., 2017; Borrero & Toro-Toro, 2016; Jaramillo et al., 2019). As shown previously, most of the calc-alkaline series have all the characteristics of adakitic magmas. Adakites are rocks that have received considerable attention due to their significance in understanding crustal recycling at convergent margins, and their similarities with the Archean Tonalite–Trondhjemite–Granodiorite series are essential to understand Earth’s initial differentiation and the onset of plate tectonic movement (see Castillo,

2012 for a review). The general REE patterns of adakite are considered to indicate that garnet is involved in the formation process of these magmas, as garnet controls REE fractionation, most likely by being formed during melting, and therefore retaining HREEs in favor of LREEs.

Various adakite formation models have been hypothesized, generally involving the melting of young ocean crust in subduction zone settings (cf. Castillo, 2012; e.g., Defant & Drummond, 1990). Nevertheless, some adakites are thought to form via high-pressure (HP) fractionation of water-rich mantle melts (Hidalgo & Rooney, 2010, 2014; Macpherson et al., 2006; Ribeiro et al., 2016; Richard & Kerrich, 2007) or by AFC processes (i.e., mantle melts are reinjected into a shallow crustal magma chamber; e.g., Castillo et al., 1999; Ribeiro et al., 2016). Under the HP conditions, model fractionating phases that determine the adakite character would be garnet and HP amphibole, as the magma would be within the stability field of these minerals (Castillo, 2006; Macpherson et al., 2006; Ribeiro et al., 2016; Richards & Kerrich, 2007). Plagioclase fractionation, which controls the magma’s Sr content, would be delayed due to the presence of water in the hydrous melt (Müntener et al., 2001). The adakites formed via fractionation are very similar to High Silica Adakites compositions (Martin et al., 2005).

Under the HP fractionation scenario garnet-bearing samples from the CSVI could represent possible “primitive” magmas, where garnet and amphibole have not been separated from the melt. This would account for the less differentiated REE profiles of Group CA1 samples (Figure 19). If, garnet and amphibole, and plagioclase to a lesser extent, are separated from the melt through time, the result should correspond to at least some of the calc-alkaline rocks. To test this hypothesis, we applied the Rayleigh equilibrium fractionation formula and considered the garnet-bearing samples as a starting composition for magma differentiation. We used the partition coefficients proposed by Hidalgo et al. (2007) for amphibole, clinopyroxene, magnetite, and plagioclase, and the partition coefficients of Irving & Frey (1978) for garnet. Our results show that the magma composition of group CA3 can be obtained by fractionation of 18:8:2:2 amphibole–garnet–magnetite–pyroxene (Figure 29), with 80% remaining melt. The listric patterns of Group CA4 magmas can also be obtained by approximately fractionating 20:6 amph:grt in Group CA2 magmas and 80 to 85% remaining melt. Consequently, our assumptions adjust to the model of adakite formation via crystal fractionation of an arc magma (Alonso-Perez et al., 2009; Macpherson et al., 2006; Richards & Kerrich, 2007).

We also used the Dy/Dy* versus Dy/Yb diagram of Davidson et al. (2013) to determine amphibole and clinopyroxene vs. garnet fractionation (Figure 30). The Dy/Dy* versus Dy/Yb quantifies the curvature seen in many chondrite-normalized REE patterns due to mineral fractionation. Amphibole and clinopyroxene can significantly decrease Dy/Dy*, but amphibole

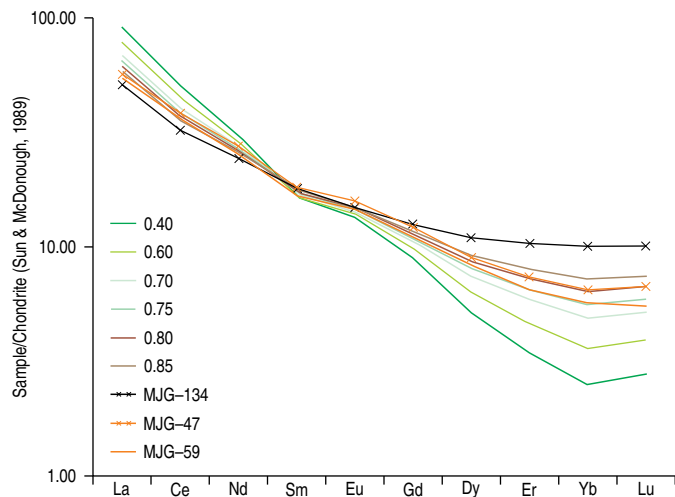


Figure 29. C1 Chondrite normalized REE patterns for Rayleigh fractionation modelling of Group CA1 garnet-bearing sample MJG-134. Patterns for 40%, 60%, 70%, 75%, 80%, and 85% remaining melt are shown. Samples MJG-47 and MJG-59 of Group CA2 are shown for comparison.

has greater effect on reducing Dy/Yb. The figure shows the CVP data. The calc-alkaline data show less well-defined trends than the tholeiitic series, except for Group CA1. This group offers a broad linear array parallel to the tholeiitic series and the calculated primitive composition plots towards a more LREE-enriched MORB. The other rocks of the series tend towards the middle and upper crust composition, which suggests that either the primitive arc magmas differentiated towards toward continental crust-like compositions or mixed with them during differentiation (Davidson et al., 2013). Nevertheless, a considerably higher Dy/Yb trend is evident in samples from groups CA3 and CA4, consistent with garnet involvement during differentiation.

7.3. Crustal Input and Magma Origin

Evidence of interaction between a mantle source and a crustal contaminant is given by the trace element characteristics that magmas attain when these processes occur. Various ratios have been used as proxies to determine the nature of this interaction (e.g., Pearce, 2008; Plank, 2005).

On the Th/Yb vs. Nb/Yb plot of Pearce (2008) (Figure 31), magmatic rocks containing a large recycled crustal component (e.g., continental margins and subduction zones) have Th/Yb ratios that lie above the MORB–OIB array and are the product of selective Th addition (Pearce, 2008). In this diagram, the tholeiitic series plots in a tight compositional cluster above the N–MORB to E–MORB composition transition, which can be interpreted as either (i) a modified depleted mantle source or (ii) representing crust–magma interaction processes. There is only a slight vertical increase in Th/Yb from the more primitive basalts

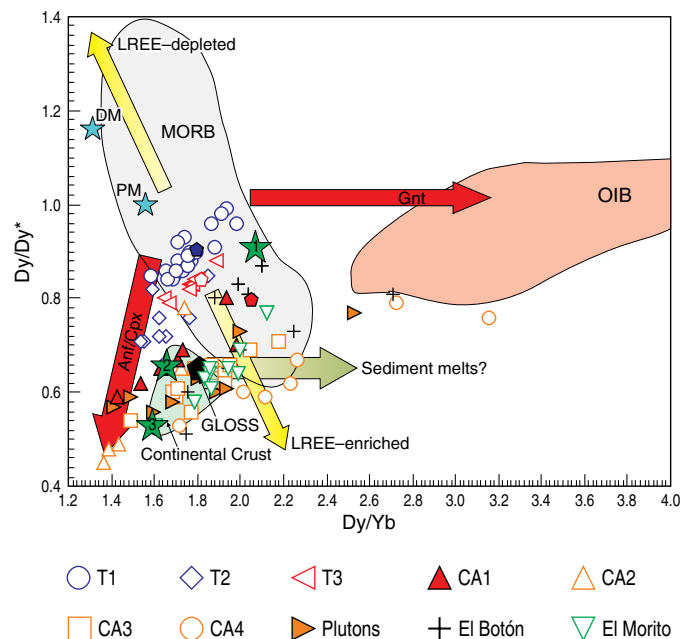


Figure 30. Dy/Dy* vs. Dy/Yb diagram after Davidson et al. (2013). $Dy/Dy^* = Dy_N / (La_N 4/13 \times Yb_N 9/13)$. Arrows indicate mineral control and melting. (PM) primitive mantle; (DM) depleted mantle; (GLOSS) average global subducting sediment; numbers in green stars: 1 = Upper Continental Crust, 2 = Middle Continental Crust, and 3 = Lower Continental Crust. Pentagons denote recalculated primitive magmas at 48% SiO₂.

(Group T1) towards the Group T2 samples. The calc-alkaline series shows an overall parallel trend above the mantle array and commences above the E–MORB, with the garnet-bearing samples. This trend suggests either fractional crystallization of a magma formed from a more enriched mantle source than the tholeiitic series or crustal assimilation. Nevertheless, the more ⁸⁷Sr/⁸⁶Sr-enriched samples do not show the highest Th/Yb values, suggesting that fractional crystallization is an important process of the calc-alkaline series. The shoshonite series defines a well-developed curved trend together with the less differentiated El Botón arc data (Rodríguez & Zapata, 2014), suggesting assimilation and fractional crystallization.

TiO₂/Yb vs. Nb/Yb relations of basaltic rocks indicate original mantle source compositions of magmatic rocks, as they are independent of alteration and subduction enrichment processes (Pearce, 2008) (Figure 31). Most samples plot on the MORB array. Group T1 of the tholeiitic series spreads from the N–MORB towards the E–MORB transition, whereas Group T2 clusters around the transition line. The calc-alkaline series is also shown and is less homogeneous but plots towards E–MORB and spreads towards higher TiO₂/Yb values.

The Th/La ratio has been used as an indicator of sediment input into arc systems, as the excess of Th is considered to derive from subducted sediments (Plank, 2005). The Th/La and Sm/La ratios for the tholeiitic and calc-alkaline series show

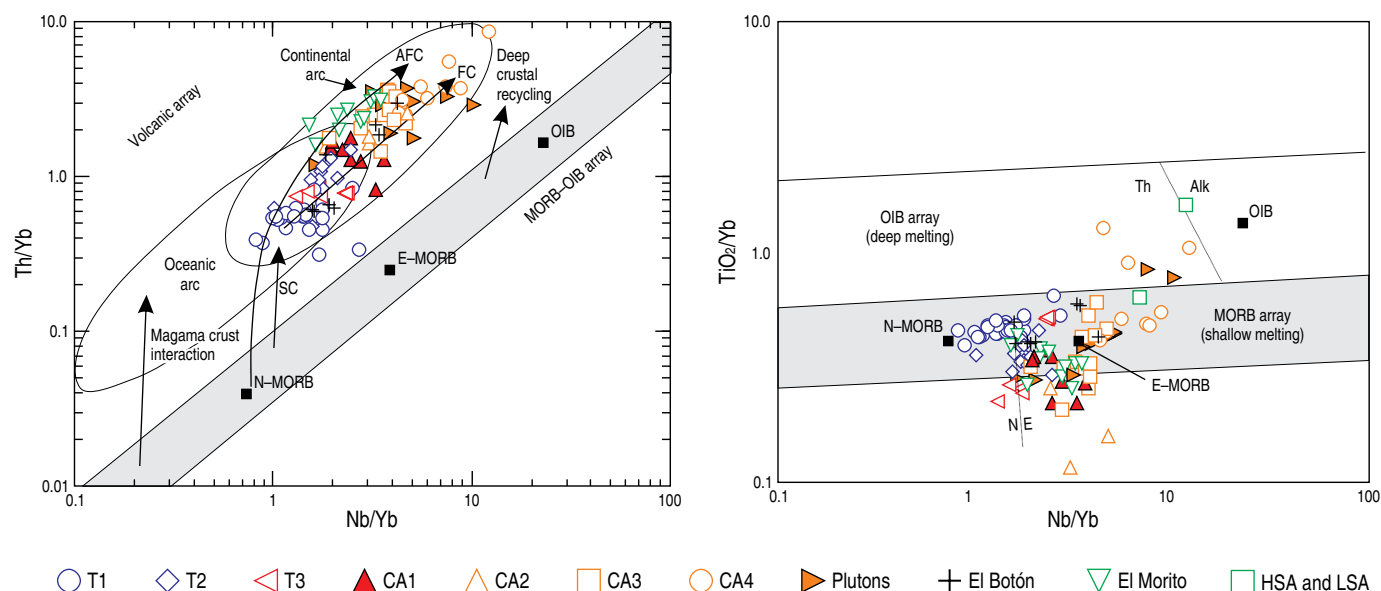


Figure 31. Th/Yb vs. Nb/Yb and TiO₂ vs. Nb/Yb plots of Pearce (2008) for the Combia Volcanic Province rocks. SC: Sediment Component, AFC: Assimilation and Crustal Contamination, FC: Fractional Crystallization.

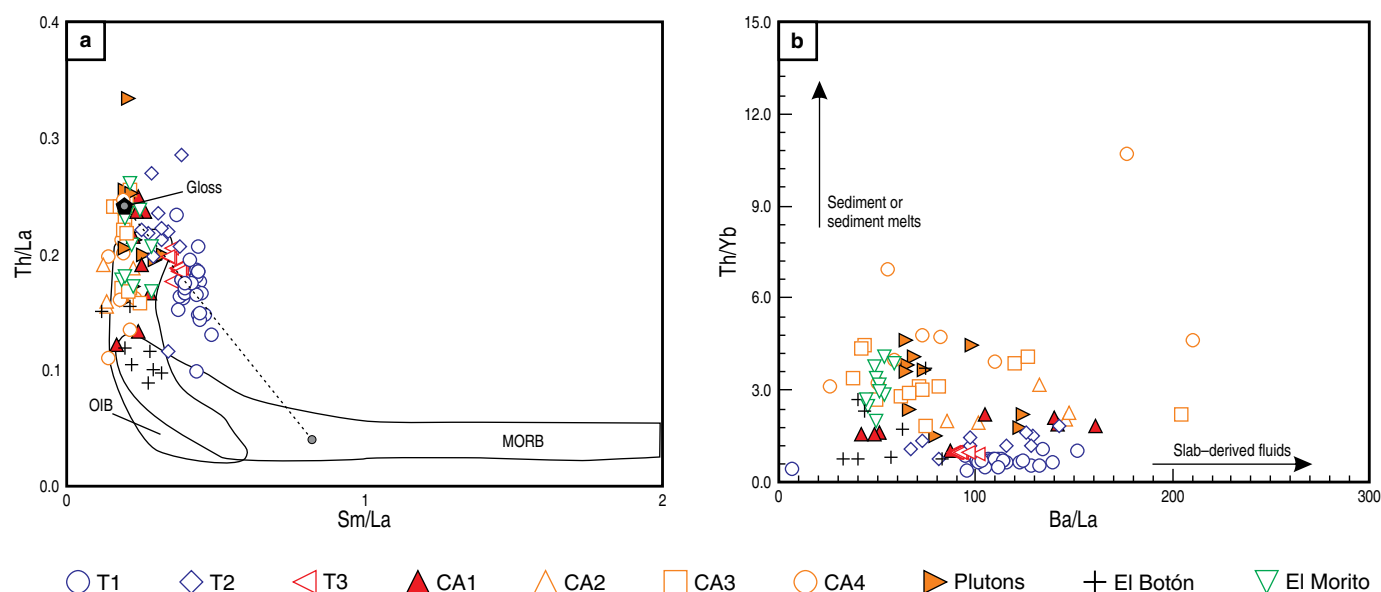


Figure 32. (a) Th/La vs. Sm/La (after Plank 2005) for the Combia Volcanic Province rocks. GLOSS from Plank & Langmuir (1998). (b) Th/Yb vs. Ba/La (after Woodhead et al., 2001).

two distinct trends and define the variable influence of subducted sediment (Figure 32). The regression line calculated for the tholeiitic series indicates a somewhat enriched MORB endmember mixed with possible sediment. Interestingly, the calculated endmember is similar to the Global Subducting Sediment composition GLOSS from Plank & Langmuir (1998). The calc-alkaline and shoshonite series denote a vertical trend that suggests a more enriched mantle endmember mixing with a sedimentary component. Additional constraints are given by the

Ba/La ratio, which indicates slab dehydration fluids, as Ba is a mobile element, whereas La is immobile in fluids (Staudigel et al., 1996; Woodhead et al., 2001). The CF tholeiitic series plots towards a high Ba/La ratio (up to 150) and defines a linear trend that suggests the influence of slab-derived fluids. In both diagrams Group T2 plots above the T1 and T3 Groups, towards the garnet-bearing samples, suggesting contamination. The CF and CSVI calc-alkaline and shoshonitic series plot toward higher Th/Yb, indicating a sediment component for these rocks.

In the Dy/Dy* versus Dy/Yb diagram of Davidson *et al.* (2013) (Figure 30), the samples plot towards an LREE-enriched mantle array, and the more differentiated groups gradually spread towards lower Dy/Dy. Davidson *et al.* (2013) suggest that this may be due to the variable incorporation of sediment. The tholeiitic series plots on the MORB field and individual trends for the defined groups tend to show positive slopes, suggesting clinopyroxene differentiation. The tholeiitic Groups T1 and T3 plot parallel to one another, “stepping down” towards higher Dy/Yb and lower Dy/Dy*. Group T2 does not follow the same parallel trend, plotting towards Group CA1, suggesting contamination. The calculated primitive melts (SiO₂ at 48%) plot towards the center of the field defined by MORB data.

The Sr–Nd radiogenic isotope data for the CF and CSMV rocks are low and generally fall into the mantle array. There is a spread towards more enriched Sr, which indicates some variable contribution of a sediment/crustal component. Most of the tholeiitic rocks are less radiogenic than the shoshonitic and calc-alkaline rocks. The calc-alkaline series partially overlaps, which suggests that a similar source formed them. Nevertheless, some CSMV samples plot towards more enriched sediment or crustal Sr values and include some of the garnet-bearing samples. Therefore, garnet-bearing samples probably show evidence of crustal or sediment contamination. As shown previously, these rocks carry xenoliths, and there is evidence that the magmas that formed these rocks ascended in three distinct phases and thus were exposed to changes in magma composition, be it by the addition of another magma, continental crust, or sediment components. Jaramillo *et al.* (2019) determined that the more evolved magmas of the CSMV formed at deeper crustal levels (ca. 50 km for dacites, ca. 17 km for basalts), which would enable more assimilation and homogenization for these rocks. Lead isotope systematics also confirm the interaction of various components, including the mantle wedge, oceanic sediment, and a crustal endmember, the Cretaceous basement, that comprises accreted rocks.

7.4. The Shoshonitic Series

One crucial aspect is the evidence of shoshonitic magmatism (12.5 and 9 Ma; Zapata & Rodríguez, 2011) in the Amagá Basin (Jaramillo, 1976; Rodríguez & Zapata, 2014; this study), which is associated with a more widespread event that includes El Botón basalts to the west (Figure 2). The known age for this magmatism in the Amagá Basin (9.1 ± 0.7 Ma in Restrepo *et al.*, 1981a), and the absarokite intrusion in the CF, described by Jaramillo (1976), suggest that volcanism was coeval with other volcanic activity.

Reverse Petrogen calculations on the more primitive samples of El Botón basalts indicate that these rocks melted in the lower crust, at ca. 10 kbar and ca. 1250 °C (Krein *et al.* in review). In the Dy/Dy* versus Dy/Yb diagram of Davidson *et al.* (2013) (Figure 30), the shoshonitic samples define a different,

steeper trend than the other series, plotting from high Dy/Yb MORB compositions, towards upper continental crust compositions. The trend suggests mainly amphibole or clinopyroxene fractionation in the formation of the more evolved rocks.

Shoshonitic magmas form in various tectonic settings, including within plates, continental rifts, ocean islands, oceanic arcs, back-arc extensional zones, and continental arcs (Müller *et al.*, 1992). The Colombian shoshonitic rocks are related to the continental arc after the collision of the Chocó–Panamá Block (Lara *et al.*, 2018). Basic to intermediate shoshonitic magmas are generally considered to have formed by low degrees of melting of previously modified mantle rocks, where LILEs and LREEs have been transferred from a subducting slab (e.g., Aldanmanz *et al.*, 2000; Morrison, 1980). Th–Ba–Nb systematics indicate addition of subducted sediment melts and crystal fractionation processes in the formation of these rocks in the CVP.

7.5. Tectonic Scenario

In this review, we consider the following important aspects for the interpretation of line series:

1. Field relationships in the Amagá Basin indicate a volcanic province that formed due to the presence of a short-lived magmatic event resulting from transtensional tectonics in a sedimentary basin. The underlying extensional event of the Amagá Basin would have begun during the early Miocene (23–21 Ma), indicated by the sedimentation of the AF (Lara *et al.*, 2018; Ramírez *et al.*, 2015), and it seems to be associated with Panamá–Chocó Block docking against the South American Plate approximately 25–23 Ma (Farris *et al.*, 2011) via a fast-oblique convergence phase along a sinistral strike-slip fault (Müller *et al.*, 2008).
2. The magmatism along the Cauca River valley and the Amagá Basin can be divided into tholeiitic, calc-alkaline, and shoshonitic series. The calc-alkaline includes garnet-bearing andesites and adakites. Nb–Ta and Zr negative anomalies in all series are evidence of a subduction zone setting. The tholeiitic magma series originated from fractionation of a heterogeneous mantle source modified by variable degrees of slab-derived fluids. Adakites are the result of garnet and amphibole fractionation and crustal contamination. Shoshonites possibly formed by fractionation of magmas created by low degrees of melting of mantle source modified through addition of a sediment/crustal component.
3. Tholeiitic magmatism is a unique feature of the Amagá Basin, and therefore we propose the term Combia Volcanic Province (CVP). However, records of shoshonitic, calc-alkaline (garnet-bearing and adakitic) magmatism are present in other areas. Specifically, shoshonitic magmatism is present in the northwest (Figure 2; Rodríguez & Zapata, 2014). There are records, from 12.5 to 9 Ma, of

garnet-bearing and adakite magmatism in the south (Figure 2; Bissig et al., 2017). Adakites are also present to the south of the Amagá Basin and are part of the more recent volcanic activity (e.g., Toro-Toro et al., 2008). Furthermore, after magmatism was established at 9 Ma along the Cauca River valley and the Amagá Basin, the tholeiitic, calc-alkaline, and shoshonitic series coexisted at the same time in the CVP.

4. The mineral chemistry of garnets and amphiboles in garnet-bearing rocks indicates at least three formation–emplacement stages for the calc-alkaline series: (i) Magma formation and crystallization of initial garnet and amphibole, (ii) changes in physicochemical conditions triggering Plg crystallization, and (iii) degasification and rapid ascent to the surface (Figure 28).
5. The occurrence of shoshonitic, calc-alkaline (incl. garnet-bearing and adakitic), and tholeiitic rocks in the Amagá Basin suggests that magma production occurred at different depths, as was proposed by Jaramillo et al. (2019) for tholeiitic and calc-alkaline magmatism, and through variations in the different involved processes. The shoshonitic rocks formed through fractionation at levels where plagioclase is still stable, whereas adakites developed within the garnet stability field, and therefore at deeper levels. Tholeiitic magmas would have formed from a mantle beneath shallow crustal levels.

As a result, the considerations above allow us to propose two different but coeval sources for the CF and CSVI magmatism in the Cauca extensional basin: A primitive source, modified by dehydration fluids of the previously subducted slab (i.e., tholeiitic magmas) and a more contaminated magma source (i.e., calc-alkaline magmas, most of which are adakitic and shoshonitic).

Vargas & Mann (2013) proposed an east–west–striking slab tear, named Caldas Tear within the subducted Nazca Plate (Figures 1, 33). It separates two distinct subducted slab segments. The Caldas Tear is an extension of the Sandra Ridge, and both constitute a major weakness along the southern flank of the Panamá Arc indenter (Vargas & Mann, 2013). The Sandra Ridge is a volcanic high with a band of seismicity, interpreted as residual or reactivated tectonism along an imperfect late Miocene plate suture (Lonsdale, 1991, 2005).

The ridge subduction setting is a possible scenario for the formation of CVP rocks. Vargas & Mann (2013) argued that the east–west aligned volcanic activity, the formation of adakites (Borrero et al., 2009), and the presence of outlier volcanic centers (e.g., Paipa-Iza and San Diego (Pardo et al., 2005)) are all indicators that the Caldas Tear may penetrate the upper crust as a fault zone and consequently provides a conduit for the upward rise of magmas formed at different levels and hydrothermal fluids produced by slab melting on either side of the Caldas Tear. It would also enable the mixing of melts from these various

sources. An additional aspect is that a slab window would allow the heat supply to melt multiple components of the mantle and overlying crust extensively. The orthogonal configuration of the Sandra Ridge subduction would explain differences in magmatic products on either side of the subducting plates (Thorkelson & Breitsprecher, 2005).

A recently proposed model determines that a flat slab system developed from a typical arc at ca. 14 Ma when magmatic activity was present along Colombia's Pacific margin. Then, at 9 to 6 Ma gradual flattening of the slab occurred, and magmatic activity ceased and was finally renewed after ca. 4 Ma south of the Caldas Tear (Wagner et al., 2017). Under this scenario, the boundary between the northern segment of the modern flat subducting Nazca Plate and the steeper southern segment is determined by the Caldas Tear (Chiarabba et al., 2016; Yarce et al., 2014) controlled the formation of the Amagá Basin. They represent a surface expression of this complex tectonic system during the Miocene, perhaps indicating that magmatic activity occurred during the gradual flattening of the slab. Therefore, the Caldas Tear was already established at ca. 12 Ma.

Jaramillo et al. (2019) suggests that the presence of tholeiitic rocks in the Amagá Basin is linked to the oblique subduction of the Nazca Plate and to the existence of remobilized structural discontinuities. Thus, the presence of tholeiitic rocks is a result of a more significant structural component due to the change in the convergence angle. Although we do not preclude that oblique subduction plays an important role in the formation of the Amagá Basin and therefore is linked to the formation of the CVP, we also consider that other controls such as the Caldas Tear must have played an important role in the generation of this unique Neogene rock association in the northern Andes.

The melting of a homogeneous, previously modified mantle source formed the tholeiitic magma series. Element variability and Nb–Ta–Zr anomalies, typical of subduction, indicate initial modification by enriched fluids (Group T1), mineral fractionation (Group T3), and possible contamination of crustal and/or sedimentary input (T2). Therefore, they are likely to melt from the modified mantle wedge above the subducting plate (Figure 33f). The majority of these melts are primitive arc basalts, and some andesitic differentiates, with an overall homogeneous composition, which suggests that most magmas ascended directly to the surface, with few or no modifications. Nevertheless, some of these primitive magmas could have been emplaced into lower crustal magma chambers being subjected to open system processes (assimilation, magma mixing, melt extraction, and fractional crystallization) as proposed by Bryan et al. (2010). This phenomenon has also promoted magma diversification observed in the Cauca River valley (Figure 33).

The calc-alkaline adakite magma series is the product of HP fractionation of enriched mantle melts, which we believe are likely to have formed above the downgoing subduction of the Nazca Plate (Figure 33). Our findings support the model

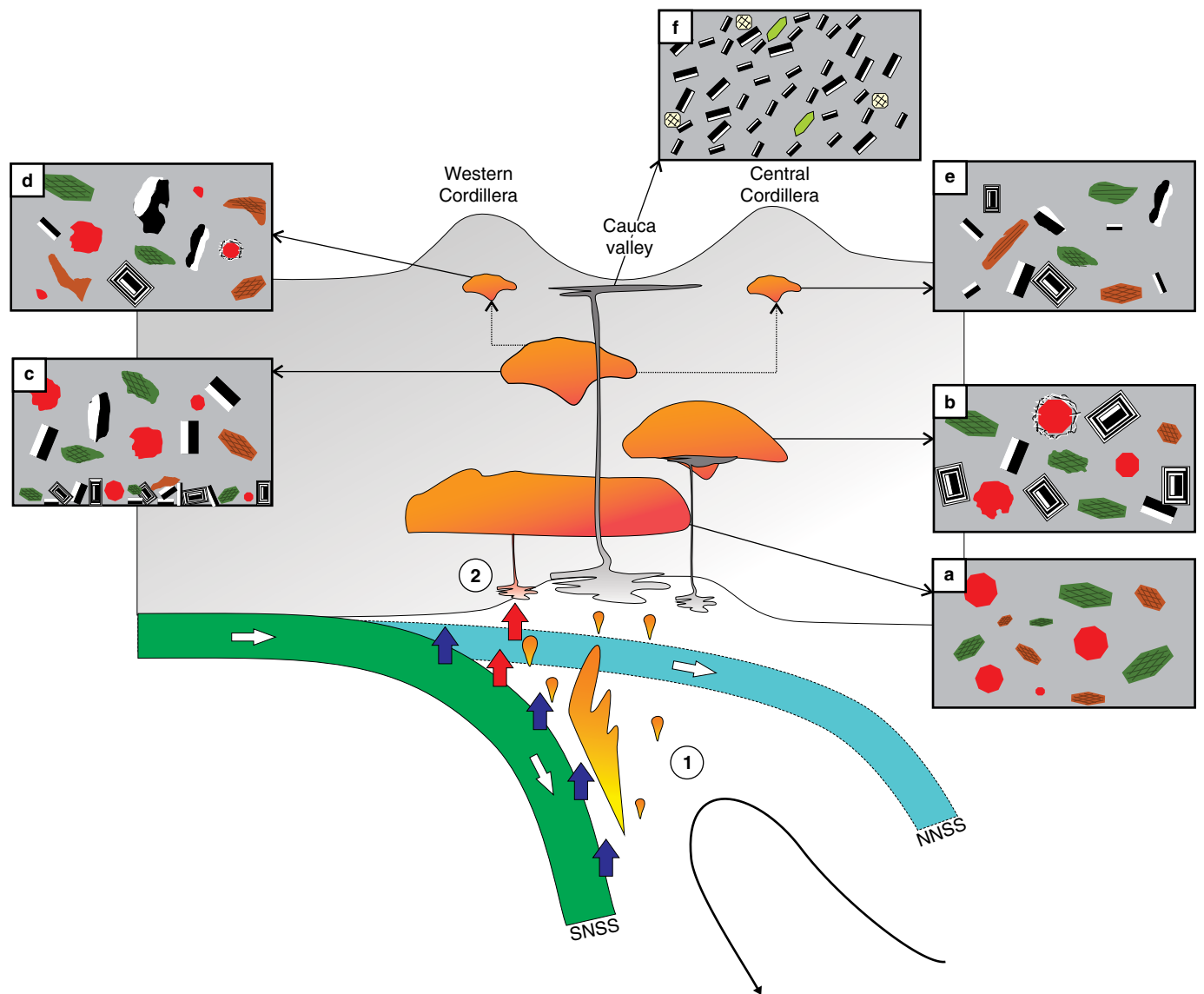


Figure 33. Petro-tectonic model of generation of the Combia Volcanic Province calc-alkaline and tholeiitic magmas (modified from Ribeiro et al., 2016). (1) Dehydration and partial melting occur on the downgoing oceanic crust slab (Nazca Plate), including associated marine sediments that provide incompatible elements to the diverse magmas. The Nazca Plate is split into two segments by the Caldas Tear (Vargas & Mann, 2013): Northern (NNSS) and Southern (SNSS) Subduction Segments. Slab tear provides heat to partial melting (red arrows) of the mantle and overlying crust. (2) High-pressure melts are formed and stall at ca. 18 km, crystallizing garnet and HP amphibole. (a) Plagioclase begins to crystallize and (b) crystal fractionation of garnet, amphibole, and plagioclase operates to generate a wide diversity of magmas (c–e). Tholeiitic magmas from modified mantle sources are emplaced in the upper crust (f). Shoshonitic magmas would fractionate at (a), after magmas separated from the modified mantle.

of Bissig et al. (2017), where the initial hydrous melts in the middle Cauca valley form high-pressure magmatic storage reservoirs, where garnet and high-Mg amphiboles crystallize (Figure 33a). Separation of these minerals from the melt is an essential factor in the adakite-like nature of the resulting fractionated magmas. In the Amagá Basin, new mineral growth (secondary garnet and amphibole) records change magma composition, possibly injecting new mantle melts or crustal contamination. The presence of disequilibrium textures such as sieve textures and reabsorbed phenocrysts and more

radiogenic isotopic signatures supports magma mixing and/or crustal contamination. This scenario is likely to occur at shallower depths, where plagioclase begins to crystallize from the melt (Figure 33b). Fractionation of garnet, amphibole, and to a lesser extent, plagioclase would have occurred at some point in the middle to the upper crust. They formed a wide diversity of magmas (few of them garnet-bearing and most of them garnet-free magmas) beginning from a garnet-bearing magma (Figure 33c–e). We propose that the opening of the Caldas Tear in the downgoing subducting plate is an essential

control for some garnet-bearing magmas. Before the complete fractionation, they reached the surface at the beginning of volcanism in the middle Cauca valley from approximately 12 Ma to 9 Ma (e.g., Hoyos et al., submitted).

Disequilibrium coronas around the amphibole showed that most of these magmas underwent dehydration at low pressures via volcano degassing from a shallow magma chamber (Figure 33d) for a considerable time. Some amphibole crystals present more than one disequilibrium corona, indicating that after a degassing period, the magma chamber was refilled with magma input with a similar composition, allowing the amphibole to regrow around the breakdown corona. This continuous magma replenishment occurred from one magma chamber to another, sometimes with contrasting magmas creating identifiable mingling and mixing textures. Nevertheless, sometimes it would have happened with similar magmas, making it challenging to identify the mixing process.

8. Conclusions

The CF stratigraphy currently divides it between the Lower Member and the Upper Member (Calle & González 1980, 1982; Grosse 1926). However, the CF records highly active volcanism operating in a varying pull-apart basin that frequently changed its topographic relief. Therefore, fluvial environments (and their accommodation spaces) were also adjusted continuously to the new physical features. As a result, the CF documents the utmost heterogeneity of the lithofacies that cannot be constrained to specific isochronous intervals. Accordingly, we propose to stratigraphically group the CF into only one unit.

The magmatic event responsible for the formation of the CF was active between 9 and 6 Ma. During this time, intense magmatic activity dominated the Cauca valley with the intrusion of an essential volume of subvolcanic andesites (including Cerro Tusa and La Pintada Intrusives). Moreover, basaltic intrusions fed composite volcanoes, which formed lava flows, pyroclastic density currents, and lahars, which remobilized the primary volcanic deposits. On the other hand, the so-called 'El Botón Magmatic Arc' (characterized by a shoshonitic affinity and exclusively related Western Cordillera rocks with oceanic affinity) was active prior to the Colombian magmatism between 12.5 and 9 Ma. Nevertheless, it was part of the same tectonic event.

The CVP is characterized by the presence of variable magmatic series. They are tholeiitic, calc-alkaline, and shoshonitic. The calc-alkaline series includes adakites and garnet-bearing rocks, whereby the adakites resulted from garnet fractionation within the garnet stability field of andesitic magmas. The geochemical variability shown within the CVP results from the variable contribution of a modified mantle, sediment and crustal components, coupled with differentiation processes. The formation of the CVP is controlled by the Panamá-Chocó docking

against the South American Plate through oblique convergence and the Caldas Tear.

Acknowledgments

The Servicio Geológico Colombiano funded the unpublished data presented here through the project "Caracterización Estratigráfica, Petrogenética y Geocronológica de la Formación Combia, Acuerdo Específico No 009–2004 con la Universidad Nacional de Colombia". Within this project we would like to especially thank Jennifer Andrea BETANCOURT-DEVIA and María Lucía TEJADA-AVELLA for their valuable participation during the fieldwork and sample descriptions. Jhon ORTÍZ-TRUJILLO and Hernando MAHECHA-CARREÑO are also acknowledged. Fabián PANIAGUA-AGUIRRE is thanked for extensive petrography analyses and Jennifer Andrea BETANCOURT-DEVIA for sample processing. The authors wish to acknowledge the Geochronological Research Centre (CP-Geo) and geochemical laboratories of the Universidade de São Paulo. We would also like to thank Eliana MARÍN RINCÓN for her help with graphics and figures. We are very grateful to David BUCHS and Karoly NEMETH, whose thorough and insightful reviews significantly improved the manuscript.

References

- Agencia Nacional de Hidrocarburos & Universidad de Caldas. 2011. Estudio integrado de los núcleos y registros obtenidos de los pozos someros (slim holes) perforados por la ANH. Agencia Nacional de Hidrocarburos, unpublished report, 304 p. Manizales.
- Alcárcel-Gutiérrez, F.A. & Gómez, J., compilers, 2017. Mapa Geológico de Colombia 2017. Scale 1:2000000. Servicio Geológico Colombiano. Bogotá.
- Aldanmaz, E., Pearce, J.A., Thirlwall, M.F. & Mitchell, J.G. 2000. Petrogenetic evolution of late Cenozoic, post-collision volcanism in western Anatolia, Turkey. *Journal of Volcanology and Geothermal Research*, 102(1–2): 67–95. [https://doi.org/10.1016/S0377-0273\(00\)00182-7](https://doi.org/10.1016/S0377-0273(00)00182-7)
- Alonso-Perez, R., Müntener, O. & Ulmer, P. 2009. Igneous garnet and amphibole fractionation in the roots of island arcs: Experimental constraints on andesitic liquids. *Contributions to Mineralogy and Petrology*, 157(4): 541–558. <https://doi.org/10.1007/s00410-008-0351-8>
- Álvarez, A.J. 1983. Geología de la cordillera Central y el occidente colombiano y petroquímica de los intrusivos granitoides meso-cenozoicos. *Boletín Geológico*, 26(2): 1–175.
- Aspden, J.A. & Litherland, M. 1992. The geology and Mesozoic collisional history of the Cordillera Real, Ecuador. *Tectonophysics*, 205(1–3): 187–204. [https://doi.org/10.1016/0040-1951\(92\)90426-7](https://doi.org/10.1016/0040-1951(92)90426-7)
- Aydar, E. & Gourgaud, A. 2002. Garnet-bearing basalts: An example from Mt. Hasan, Central Anatolia, Turkey. *Mineralogy*

- and Petrology, 75(3–4): 185–201. <https://doi.org/10.1007/s007100200023>
- Bach, P., Smith, I.E.M. & Malpas, J.G. 2012. The origin of garnets in andesitic rocks from the Northland Arc, New Zealand, and their implication for sub-arc processes. *J Petrology*, 53(6): 1169–1195. <https://doi.org/10.1093/petrology/egs012>
- Barragan, R., Geist, D., Hall, M., Larson, P. & Kurz, M. 1998. Subduction controls on the compositions of lavas from the Ecuadorian Andes. *Earth and Planetary Science Letters*, 154(1–4): 153–166. [https://doi.org/10.1016/S0012-821X\(97\)00141-6](https://doi.org/10.1016/S0012-821X(97)00141-6)
- Bernet, M., Mesa-García, J., Chauvel, C., Ramírez Londoño, M.J. & Marín-Cerón, M.I. 2020. Thermochronological, petrographic and geochemical characteristics of the Combia Formation, Amagá Basin, Colombia. *Journal of South American Earth Sciences*, 104: 1–21. <https://doi.org/10.1016/j.jsames.2020.102897>
- Bissig, T., Leal-Mejía, H., Stevens, R.B. & Hart, C.J. 2017. High Sr/Y magma petrogenesis and the link to porphyry mineralization as revealed by garnet-bearing I-type granodiorite porphyries of the Middle Cauca Au–Cu Belt, Colombia. *Economic Geology*, 112(3): 551–568. <https://doi.org/10.2113/econgeo.112.3.551>
- Borrero, C. & Toro-Toro, L.M. 2016. Vulcanismo de afinidad adakítica en el Miembro Inferior de la Formación Combia (Mioceno Tardío) al sur de la Subcuenca de Amagá, noroccidente de Colombia. *Boletín de Geología*, 38(1): 87–100. <http://dx.doi.org/10.18273/revbol.v38n1-2016005>
- Borrero, C., Toro, L.M., Alvarán, M. & Castillo, H. 2009. Geochemistry and tectonic controls of the effusive activity related with the ancestral Nevado del Ruiz Volcano, Colombia. *Geofísica Internacional*, 48(1): 149–169.
- Bourdon, E., Eissen, J.-P., Monzier, M., Robin, C., Martin, H., Cotten, J. & Hall, M.L. 2002. Adakite-like lavas from Antisana Volcano (Ecuador): Evidence for slab melt metasomatism beneath the Andean Northern Volcanic Zone. *Journal of Petrology*, 43(2): 199–217. <https://doi.org/10.1093/petrology/43.2.199>
- Bryan, S.E., Peate, I.U., Peate, D.W., Self, S., Jerram, D.A., Mawby, M.R., Marsh, J.S. & Miller, J.A. 2010. The largest volcanic eruptions on Earth. *Earth–Science Reviews*, 102(3–4): 207–229. <https://doi.org/10.1016/j.earscirev.2010.07.001>
- Calle, B. & González, H. 1980. Memoria explicativa: Geología y geoquímica de la plancha 166 Jericó. Scale 1:100 000. Ingeominas, Internal report 1822, 250 p. Bogotá.
- Calle, B. & González, H. 1982. Memoria explicativa: Geología y geoquímica de la plancha 186 Riosucio. Scale 1:100 000. Ingeominas, Internal report 1878, 120 p. Medellín.
- Calle, B., González, H., de la Peña, R., Escorche, E., Durango, J., Ramírez, O., Alvarez, E., Calderón, M., Álvarez, J., Guarín, G., Rodríguez, C., Muñoz, J. & Durán, J. 1980. Geología de la plancha 166 Jericó. Scale 1:100 000. Ingeominas. Bogotá.
- Castillo, P.R. 2006. An overview of adakite petrogenesis. *Chinese Science Bulletin*, 51(3): 257–268. <https://doi.org/10.1007/s11434-006-0257-7>
- Castillo, P.R. 2012. Adakite petrogenesis. *Lithos*, 134–135: 304–316. <https://doi.org/10.1016/j.lithos.2011.09.013>
- Castillo, P.R., Janney, P.E. & Solidum, R.U. 1999. Petrology and geochemistry of Camiguin Island, southern Philippines: Insights to the source of adakites and other lavas in a complex arc setting. *Contributions to Mineralogy and Petrology*, 134(1): 33–51. <https://doi.org/10.1007/s004100050467>
- Cediel, F., Shaw, R.P. & Cáceres, C. 2003. Tectonic assembly of the northern Andean Block. In: Bartolini, C., Buffler, R.T. & Blickwede, J. (editors), *The circum-Gulf of Mexico and the Caribbean: Hydrocarbon habitats, basin formation, and plate tectonics*. American Association of Petroleum Geologists, Memoir 79, p. 815–848. Tulsa, USA.
- Chappell, B.W. & White, A.J.R. 1974. Two contrasting granite types. *Pacific Geology*, 8: 173–174.
- Chiarabba, C., De Gori, P., Faccenna, C., Speranza, F., Seccia, D., Dionicio, V. & Prieto, G.A. 2016. Subduction system and flat slab beneath the Eastern Cordillera of Colombia. *Geochemistry, Geophysics, Geosystems*, 17(1): 16–27. <https://doi.org/10.1002/2015GC006048>
- Davidson, J., Turner, S. & Plank, T. 2013. Dy/Dy*: Variations arising from mantle sources and petrogenetic processes. *Journal of Petrology*, 54(3): 525–537. <https://doi.org/10.1093/petrology/egs076>
- Day, R.A., Green, T.H. & Smith, I.E.M. 1992. The origin and significance of garnet phenocrysts and garnet-bearing xenoliths in miocene calc-alkaline volcanics from Northland, New Zealand. *Journal of Petrology*, 33(1):125–161. <https://doi.org/10.1093/petrology/33.1.125>
- Defant, M.J. & Drummond, M.S. 1990. Derivation of some modern arc magmas by melting of young subducted lithosphere. *Nature*, 347(6294): 662–665. <https://doi.org/10.1038/347662a0>
- Drummond, M.S. & Defant, M.J. 1990. A model for trondhjemite-tonalite-dacite genesis and crustal growth via slab melting: Archean o modern comparisons. *Journal of Geophysical Research: Solid Earth*, 95(B13): 21503–21521. <https://doi.org/10.1029/JB095iB13p21503>
- Dunia. 2005. Complementación geológica, geoquímica y geofísica (magnetométrica) de las planchas 166, 167, 186 y 187. Ingeominas, unpublished report, 576 p. Bogotá.
- Duque-Caro, H. 1990. The Choco Block in the northwestern corner of South America: Structural, tectonostratigraphic, and paleogeographic implications. *Journal of South American Earth Sciences*, 3(1): 71–84. [https://doi.org/10.1016/0895-9811\(90\)90019-W](https://doi.org/10.1016/0895-9811(90)90019-W)
- Embey-Isztin, A., Noske-Fazekas, G., Kurat, G. & Brandstätter, F. 1985. Genesis of garnets in some magmatic rocks from Hungary. *Tschermaks mineralogische und petrographische Mitteilungen*, 34: 49–66. <https://doi.org/10.1007/BF01082457>
- Farris, D.W., Jaramillo, C., Bayona, G., Restrepo-Moreno, S.A., Montes, C., Cardona, A., Mora, A., Speakman, R.J., Glascock, M.D. & Valencia, V. 2011. Fracturing of the Panamanian Isthmus

- during initial collision with South America. *Geology*, 39(11): 1007–1010. <https://doi.org/10.1130/G32237.1>
- Fitton, J.G. 1972. The genetic significance of almandine–pyrope phenocrysts in calc–alkaline Borrowdale Volcanic Group, northern England. *Contributions to mineralogy and petrology*, 36(3): 231–248. <https://doi.org/10.1007/BF00371434>
- Francis, P.W., Moorbath, S. & Thorpe, R.S. 1977. Strontium isotope data for recent andesites in Ecuador and north Chile. *Earth and Planetary Sciences Letters*, 37(2): 197–202. [https://doi.org/10.1016/0012-821X\(77\)90164-9](https://doi.org/10.1016/0012-821X(77)90164-9)
- Gale, A., Dalton, C.A., Langmuir, C.H., Su, Y. & Schilling, J.G. 2013. The mean composition of ocean ridge basalts. *Geochemistry, Geophysics, Geosystems*, 14(3): 489–518. <https://doi.org/10.1029/2012GC004334>
- García, M. 1983. Petrografía detallada de los pórfidos granatíferos de Chinchiná, Caldas. Bachelor thesis, Universidad Nacional de Colombia, 142 p. Bogotá.
- Gelves, J.F., Sierra-Gallego, G. & Márquez, M.A. 2016. Mineralogical characterization of zeolites present on basaltic rocks from Combia geological formation, La Pintada, Colombia. *Microporous and Mesoporous Materials*, 235: 9–19. <https://doi.org/10.1016/j.micromeso.2016.07.035>
- Gilbert, J.S. & Rogers, N.W. 1989. The significance of garnet in the Permo–Carboniferous volcanic rocks of the Pyrenees. *Journal of the Geological Society*, 146(3): 477–490. <https://doi.org/10.1144/gsjgs.146.3.0477>
- Gill, J.B. 1981. *Orogenic andesites and plate tectonics*. Springer-Verlag. 392 p. Berlin. <https://doi.org/10.1007/978-3-642-68012-0>
- Gómez, J., Montes, N.E., Nivia, Á. & Diederix, H., compilers. 2015. Geological Map of Colombia 2015. Scale 1:1 000 000. Servicio Geológico Colombiano, 2 sheets. Bogotá. <https://doi.org/10.32685/10.143.2015.936>
- González, H. 1980. Geología de las planchas 167 Sonsón y 187 Salamina. Scale 1:100 000. *Boletín Geológico*, 23(1): 1–174.
- González, H. 2010. Geoquímica, geocronología de las unidades litológicas asociadas al sistema de fallas Cauca–Romeral, sector centro-sur. Tomo I. Ingeominas, unpublished report, 412 p. Medellín.
- Green, T.H. 1972. Crystallization of calc–alkaline andesite under controlled high–pressure hydrous conditions. *Contributions to Mineralogy and Petrology*, 34(2): 150–166. <https://doi.org/10.1007/BF00373770>
- Green, T.H. 1977. Garnet in silicic liquids and its possible use as a P–T indicator. *Contributions to Mineralogy and Petrology*, 65(1): 59–67. <https://doi.org/10.1007/BF00373571>
- Green, T.H. 1992. Experimental phase equilibrium studies of garnet-bearing I-type volcanics and high-level intrusives from Northland, New Zealand. *Earth and Environmental Science Transactions of The Royal Society of Edinburgh*, 83(1–2): 429–438. <https://doi.org/10.1017/S0263593300008105>
- Grosse, E. 1926. Estudio geológico del terciario carbonífero de Antioquia en la parte occidental de la cordillera Central de Colombia, entre el río Arma y Sacaolal, ejecutado en los años de 1920–1923. Dietrich Reimer, 361 p. Berlin.
- Hamer, R.D. & Moyes, A.B. 1982. Composition and origin of garnet from the Antarctic Peninsula volcanic group of Trinity Peninsula. *Journal of the Geological Society London*, 139(6): 713–720. <https://doi.org/10.1144/gsjgs.139.6.0713>
- Harangi, S., Downes, H., Kósa, L., Szabó, C., Thirlwall, M.F., Mason, P.R.D. & Matthey, D. 2001. Almandine garnet in calc–alkaline volcanic rocks of the northern Pannonian Basin (eastern–central Europe): Geochemistry, petrogenesis and geodynamic implications. *Journal of Petrology*, 42(10): 1813–1844. <https://doi.org/10.1093/petrology/42.10.1813>
- Harmon, R.S., Barreiro, B.A., Moorbath, S., Hoefs, J., Francis, P.W., Thorpe, R.S., Déruelle, B., McHugh, J. & Viglino, J.A. 1984. Regional O–, Sr–, and Pb–isotope relationships in late Cenozoic calc–alkaline lavas of the Andean Cordillera. *Journal of the Geological Society*, 141(5): 803–822. <https://doi.org/10.1144/gsjgs.141.5.0803>
- Hawkesworth, C.J., Norry, M.J., Roddick, J.C., Baker, P.E., Francis, P.W. & Thorpe, R.S. 1979. $^{143}\text{Nd}/^{144}\text{Nd}$, $^{87}\text{Sr}/^{86}\text{Sr}$, and incompatible element variations in calc–alkaline andesites and plateau lavas from South America. *Earth and Planetary Science Letters*, 42(1): 45–57. [https://doi.org/10.1016/0012-821X\(79\)90189-4](https://doi.org/10.1016/0012-821X(79)90189-4)
- Henrichs, I.A. 2013. Caracterização e idade das intrusivas do sistema Pórfiro Yarumalito, magmatismo Combia, Colombia. Doctoral thesis, Universidade Federal do Rio Grande do Sul, 68 p. Porto Alegre, Brasil.
- Hidalgo, P.J. & Rooney, T.O. 2010. Crystal fractionation processes at Baru volcano from the deep to shallow crust. *Geochemistry, Geophysics, Geosystems*, 11(12): 1–29. <https://doi.org/10.1029/2010GC003262>
- Hidalgo, P.J. & Rooney, T.O. 2014. Petrogenesis of a voluminous Quaternary adakitic volcano: The case of Baru volcano. *Contributions to Mineralogy and Petrology*, 168(3): 1–19. <https://doi.org/10.1007/s00410-014-1011-9>
- Hidalgo, S., Monzier, M., Martin, H., Chazot, G., Eissen, J.P. & Cotten, J. 2007. Adakitic magmas in the Ecuadorian volcanic front: Petrogenesis of the Iliniza volcanic complex, Ecuador. *Journal of Volcanology and Geothermal Research*, 159(4): 366–392. <https://doi.org/10.1016/j.jvolgeores.2006.07.007>
- Horton, B.K., Parra, M., Saylor, J.E., Nie, J., Mora, A., Torres, V., Stockli, D.F. & Strecker, M.R. 2010. Resolving uplift of the northern Andes using detrital zircon age signatures. *GSA Today*, 20(7): 4–10. <https://doi.org/10.1130/GSATG76A.1>
- Hoyos, S. & Duque-Trujillo, J.F. 2017. Determinación de focos de emisión en ignimbritas de la Formación Combia a partir de análisis de fábrica magnética. XVI Congreso Colombiano de Geología. *Memoirs*, p. 1301–1302. Santa Marta.
- Hoyos, S., Weber, M., Cárdenas-Rozo, A.L., Cottrell, E., Duque, J.F., Beltrán-Triviño, A., von Quadt, A. & Gómez Tapias, J. 2020. Late Miocene garnet-bearing andesites in the Northern An-

- des and their tectonic implications. Manuscript submitted for publication.
- Irving, A.J. & Frey, F.A. 1978. Distribution of trace elements between garnet megacrysts and host volcanic liquids of kimberlitic rhyolitic composition. *Geochimica et Cosmochimica Acta*, 42(6): 771–787. [https://doi.org/10.1016/0016-7037\(78\)90092-3](https://doi.org/10.1016/0016-7037(78)90092-3)
- James, D.E. & Murcia, L.A. 1984. Crustal contamination in northern Andean volcanics. *Journal of the Geological Society*, 141(5): 823–830. <https://doi.org/10.1144/gsjgs.141.5.0823>
- Jaramillo, J.M. 1976. Volcanic rocks of the rio Cauca Valley, Colombia. Master thesis, Rice University, 46 p. Houston, USA.
- Jaramillo, J.S., Cardona, A., Monsalve, G., Valencia, V. & León, S. 2019. Petrogenesis of the late Miocene Combia volcanic complex, northwestern Colombian Andes: Tectonic implication of short term and compositionally heterogeneous arc magmatism. *Lithos* 330–331: 194–220. <https://doi.org/10.1016/j.lithos.2019.02.017>
- Kano, H. & Yashima, R. 1976. Almandine–garnets of acid magmatic origin from Yamanogawa. *Journal of the Japanese Association of Mineralogists, Petrologists and Economic Geology*, 71(4): 106–119. <https://doi.org/10.2465/ganko1941.71.106>
- Kawabata, H. & Takafuji, N. 2005. Origin of garnet crystals in calc–alkaline volcanic rocks from the Setouchi volcanic belt, Japan. *Mineralogical Magazine*, 69(6): :951–971. <https://doi.org/10.1180/0026461056960301>
- Kennan, L. & Pindell, J.L. 2009. Dextral shear, terrane accretion and basin formation in the northern Andes: Best explained by interaction with a Pacific–derived Caribbean Plate? In: James, K.H., Lorente, M.A. & Pindell, J.L. (editors), *The origin and evolution of the Caribbean Plate*. Geological Society of London, Special Publication 328, p. 487–531. <https://doi.org/10.1144/SP328.20>
- Kerr, A.C., Tarney, J., Marriner, G.F., Nivia, Á., Klaver, G.T. & Saunders, A.D. 1996. The geochemistry and tectonic setting of late Cretaceous Caribbean and Colombian volcanism. *Journal of South American Earth Sciences*, 9(1–2): 111–120. [https://doi.org/10.1016/0895-9811\(96\)00031-4](https://doi.org/10.1016/0895-9811(96)00031-4)
- Kerr, A.C., Marriner, G.F., Tarney, J., Nivia, Á., Saunders, A.D., Thirlwall, M.F. & Sinton, C.W. 1997. Cretaceous basaltic terranes in western Colombia: Elemental, chronological and Sr–Nd isotopic constraints on petrogenesis. *Journal of Petrology*, 38(6): 677–702. <https://doi.org/10.1093/petrology/38.6.677>
- Krein, S.B., Molitor, Z.J. & Grove, T.L. In Review at JGR: Solid Earth. ReversePetrogen: A Multiphase Dry Reverse Fractional Crystallization–Mantle Melting Thermobarometer applied to 13,589 Mid–Ocean Ridge Basalt Glasses.
- Lara, M., Salazar–Franco, A.M. & Silva–Tamayo, J.C. 2018. Provenance of the Cenozoic siliciclastic intramontane Amagá Formation: Implications for the early Miocene collision between Central and South America. *Sedimentary Geology*, 373: 147–162. <https://doi.org/10.1016/j.sedgeo.2018.06.003>
- Leake B.E., Woolley A.R., Arps C.E.S., Birch W.D., Gilbert M.C., Grice J.D., Hawthorne F.C., Kato A., Kisch H.J., Krivovichev V.G., Linthout K., Laird J., Mandarino J., Maresch W.V., Nickel E.H., Schumaker J.C., Smith D.C., Stephenson N.C.N., Ungaretti L., Whittaker E.J.W. & Youzhi G. 1997. Nomenclature of amphiboles: Report of the subcommittee on amphiboles of the International Mineralogical Association Commission on New Minerals and Mineral Names. *Mineralogical magazine*, 61(405): 295–321
- Leal–Mejía, H. 2011. Phanerozoic gold metallogeny in the Colombian Andes: A tectono–magmatic approach. Doctoral thesis, Universitat de Barcelona, 989 p. Barcelona.
- Leal–Mejía, H., Shaw, R.P. & Melgarejo I Draper, J.C. 2019. Spatial–temporal migration of granitoid magmatism and the Phanerozoic tectono–magmatic evolution of the Colombian Andes. In: Cedié, F. & Shaw, R.P. (editors), *Geology and tectonics of northwestern South America: The Pacific–Caribbean–Andean junction*. Frontiers in Earth Sciences. Springer, p. 253–410. Cham, Germany. https://doi.org/10.1007/978-3-319-76132-9_5
- Le Maitre, R.W., Streckeisen, A., Zanettin, B., Le Bas, M.J., Bonin, B., Bateman, P., Bellieni, G., Dudek, A., Efremova, S., Keller, J., Lameyre, J., Sabine, P.A., Schmid, R., Sørensen, H. & Woolley, A.R., editors. 2002. *Igneous rocks: A classification and glossary of terms. Recommendations of the International Union of Geological Sciences Subcommittee on the systematics of igneous rocks*. Cambridge University Press, 236 p. Cambridge, UK. <https://doi.org/10.1017/CBO9780511535581>
- Lesage, G., Richards, J.P., Muehlenbachs, K. & Spell, T.L. 2013. Geochronology, geochemistry, and fluid characterization of the late Miocene Buriticá gold deposit, Antioquia Department, Colombia. *Economic Geology*, 108(5): 1067–1097. <https://doi.org/10.2113/econgeo.108.5.1067>
- Lonsdale, P. 1991. Structural patterns of the Pacific floor offshore of peninsular California. In: Dauphin, J.P. & Simoneit, B.R.T. (editors), *The gulf and peninsular province of the Californias*. American Association of Petroleum Geologists, Memoir 47, p. 87–125. Tulsa, USA.
- Lonsdale, P. 2005. Creation of the Cocos and Nazca Plates by fission of the Farallon Plate. *Tectonophysics*, 404(3–4): 237–264. <https://doi.org/10.1016/j.tecto.2005.05.011>
- MacDonald, W.D. 1980. Anomalous paleomagnetic directions in late tertiary andesitic intrusions of the Cauca depression, Colombian Andes. *Tectonophysics*, 68(3–4): 339–348. [https://doi.org/10.1016/0040-1951\(80\)90183-3](https://doi.org/10.1016/0040-1951(80)90183-3)
- Macpherson, C.G., Dreher, S.T. & Thirlwall, M.F. 2006. Adakites without slab melting: High pressure differentiation of island arc magma, Mindanao, the Philippines. *Earth and Planetary Science Letters*, 243(3–4): 581–593. <https://doi.org/10.1016/j.epsl.2005.12.034>
- Mahecha, H., Ortiz, J., Tejada, M.L., Paniagua, F. & Weber, M. 2006. Cartografía geológica de las vulcanitas de la Formación Combia, en un área de 200 km² en los alrededores del municipio de Jardín, departamento de Antioquia, Colombia. Ingeominas, unpublished report, 27 p. Bogotá.

- Marín-Cerón, M.I., Moriguti, T., Makishima, A. & Nakamura, E. 2010. Slab decarbonation and CO₂ recycling in the southwestern Colombian volcanic arc. *Geochimica et Cosmochimica Acta*, 74(3): 1104–1121. <https://doi.org/10.1016/j.gca.2009.10.031>
- Marín-Cerón, M.I., Leal-Mejía, H., Bernet, M. & Mesa-García, J. 2019. Late Cenozoic to modern-day volcanism in the northern Andes: A geochronological, petrographical, and geochemical review. In: Cedié, F. & Shaw R.P. (editors), *Geology and tectonics of northwestern South America: The Pacific–Caribbean–Andean junction*. *Frontiers in Earth Sciences*. Springer, p. 603–648. Cham, Germany. https://doi.org/10.1007/978-3-319-76132-9_8
- Marriner, G.F. & Millward, D. 1984. The petrology and geochemistry of Cretaceous to recent volcanism in Colombia: The magmatic history of an accretionary plate margin. *Journal of the Geological Society*, 141(3): 473–486. <https://doi.org/10.1144/gsjgs.141.3.0473>
- Martin, H., Smithies, R.H., Rapp, R., Moyen, J.-F. & Champion, D. 2005. An overview of adakite, tonalite–trondhjemite–granodiorite (TTG), and sanukitoid: Relationships and some implications for crustal evolution. *Lithos*, 79(1–2): 1–24. <https://doi.org/10.1016/j.lithos.2004.04.048>
- McPhie, J., Doyle, M. & Allen, R.L. 1993. *Volcanic textures: A guide to the interpretation of textures in volcanic rocks*. Centre for Ore Deposits and Exploration Studies, University of Tasmania, 196 p. Hobart, Australia.
- Miyashiro, A. 1955. Pyroxene garnets in volcanic rocks. *Journal of Geological Society of Japan*, 61(721): 463–470. <https://doi.org/10.5575/geosoc.61.463>
- Miyashiro, A. 1974. Volcanic rock series in island arcs and active continental margins. *American Journal of Science*, 274(4): 321–355. <https://doi.org/10.2475/ajs.274.4.321>
- Montes, C., Bayona, G., Cardona, A., Buchs, D.M., Silva, C.A., Morón, S., Hoyos, N., Ramírez, D.A., Jaramillo, C. & Valencia, V. 2012. Arc–continent collision and orocline formation: Closing of the Central American Seaway. *Journal of Geophysical Research: Solid Earth*, 117(B4), 1–25. <https://doi.org/10.1029/2011JB008959>
- Montes, C., Cardona, A., Jaramillo, C., Pardo, A., Silva, J.C., Valencia, V., Ayala, C., Pérez-Ángel, L.C., Rodríguez-Parra, L.A., Ramírez, V. & Niño, H. 2015. Middle Miocene closure of the Central American Seaway. *Science*, 348(6231): 226–229. <https://doi.org/10.1126/science.aaa2815>
- Morrison, G.W. 1980. Characteristics and tectonic setting of the shoshonite rock association. *Lithos* 13(1): 79–108. [https://doi.org/10.1016/0024-4937\(80\)90067-5](https://doi.org/10.1016/0024-4937(80)90067-5)
- Müller, D., Rock, N.M.S. & Groves, D.I. 1992. Geochemical discrimination between shoshonitic and potassic volcanic rocks in different tectonic settings: A pilot study. *Mineralogy and Petrology*, 46(4): 259–289. <https://doi.org/10.1007/BF01173568>
- Müller, R.D., Sdrolias, M., Gaina, C. & Roest, W.R. 2008. Age, spreading rates, and spreading asymmetry of the world's ocean crust. *Geochemistry, Geophysics, Geosystems*, 9(4): 1–19. <https://doi.org/10.1029/2007GC001743>
- Müntener, O., Kelemen, P.B. & Grove, T.L. 2001. The role of H₂O during crystallization of primitive arc magmas under uppermost mantle conditions and genesis of igneous pyroxenites: An experimental study. *Contributions to Mineralogy and Petrology*, 141(6): 643–658. <https://doi.org/10.1007/s004100100266>
- Muñoz, J.A. 1992. Evolution of a continental collision belt: ECORS–Pyrenees crustal balanced cross-section. In: McClay, K.R., (editor), *Thrust Tectonics*. Springer Science, p. 235–246. London, UK.
- Murcia, H.F., Borrero, C.A., Pardo, N., Alvarado, G.E., Arnosio, M. & Scolamacchia, T. 2013. Depósitos volcánico-clásticos: Términos y conceptos para una clasificación en español. *Revista Geológica de América Central*, 48:15–39.
- Németh, K. & Martin, U. 2007. *Practical volcanology: Lecture notes for understanding volcanic rocks from field based studies*. Geological Institute of Hungary, 221 p. Budapest, Hungary.
- Ordóñez-Carmona, O. 2001. *Caracterização isotópica Rb–Sr e Sm–Nd dos principais eventos magmáticos nos Andes colombianos*. Doctoral thesis, Universidad de Brasília, 176 p. Brasília.
- Pardo, N., Cepeda, H. & Jaramillo, J. 2005. The Paipa volcano, Eastern Cordillera of Colombia, South America: Volcanic stratigraphy. *Earth Sciences Research Journal*, 9(1): 3–18.
- Pearce, J.A. 2008. Geochemical fingerprinting of oceanic basalts with applications to ophiolite classification and the search for Archean oceanic crust. *Lithos*, 100(1–4): 14–48. <https://doi.org/10.1016/j.lithos.2007.06.016>
- Pindell, J., Kennan, L., Maresch, W.V., Stanek, K.P., Draper, G. & Higgs, R. 2005. Plate–kinematics and crustal dynamics of circum-Caribbean arc–continent interactions: Tectonic controls on basin development in proto-Caribbean margins. In: Avé-Lallemant, H.G. & Sisson, V.B. (editors), *Caribbean–South American Plate interactions, Venezuela*. Geological Society of America, Special Paper 394, p. 7–52. <https://doi.org/10.1130/0-8137-2394-9.7>
- Plank, T. 2005. Constraints from thorium/lanthanum on sediment recycling at subduction zones and the evolution of the continents. *Journal of Petrology*, 46(5): 921–944. <https://doi.org/10.1093/petrology/egi005>
- Plank, T. & Langmuir, C.H. 1998. The chemical composition of subducting sediment and its consequences for the crust and mantle. *Chemical Geology*, 145(3–4): 325–394. [https://doi.org/10.1016/S0009-2541\(97\)00150-2](https://doi.org/10.1016/S0009-2541(97)00150-2)
- Ramírez, D.A., López, A., Sierra, G.M. & Toro, G.E. 2006. Edad y proveniencia de las rocas volcánico-sedimentarias de la Formación Combia en el suroccidente antioqueño, Colombia. *Boletín de Ciencias de la Tierra*, (19): 9–26.
- Ramírez, E., Pardo-Trujillo, A., Plata, A., Vallejo, F. & Trejos, R. 2015. Edad y ambiente de la Formación Amagá, sector de

- Santa Fé de Antioquia–Sopetrán, con base en evidencias palinológicas. XV Congreso Colombiano de Geología. Memoirs, p. 277–281. Bucaramanga, Colombia.
- Restrepo, J.J. 1991. Datación de algunos plutones de Antioquia por el método de trazas de fisión. *Boletín de Ciencias de la Tierra*, (10): 95–107.
- Restrepo, J.J., Toussaint, J.F. & González, H. 1981a. Edades miopliocenas del magmatismo asociado a la Formación Combia, departamentos de Antioquia y Caldas, Colombia. *Geología Norandina*, (3): 21–26.
- Restrepo, J.J., Toussaint, J.F., Zuluaga, J. & Hoyos, P. 1981b. Algunas consideraciones sobre la geología de la parte septentrional de la cordillera Occidental. *Boletín de Ciencias de la Tierra*, (5–6): 85–107.
- Ribeiro, J.M., Maury, R.C. & Grégoire, M. 2016. Are adakites slab melts or high–pressure fractionated mantle melts? *Journal of Petrology*, 57(5): 839–862. <https://doi.org/10.1093/petrology/egw023>
- Richards, J.P. & Kerrich, R. 2007. Special Paper: Adakite–like rocks: Their diverse origins and questionable role in metallogenesis. *Economic Geology*, 102(4): 537–576. <https://doi.org/10.2113/gsecongeo.102.4.537>
- Ridolfi, F. & Renzulli, A. 2012. Calcic amphiboles in calc–alkaline and alkaline magmas: Thermobarometric and chemometric empirical equations valid up to 1130 °C and 2.2 GPa. *Contributions to Mineralogy and Petrology*, 163(5): 877–895. <https://doi.org/10.1007/s00410-011-0704-6>
- Ridolfi, F., Renzulli, A. & Puerini, M. 2010. Stability and chemical equilibrium of amphibole in calc–alkaline magmas: An overview, new thermobarometric formulations and application to subduction–related volcanoes. *Contributions to Mineralogy and Petrology*, 160(1): 45–66. <https://doi.org/10.1007/s00410-009-0465-7>
- Ríos, A.M. & Sierra, M.I. 2004. La Formación Combia: Registro de la relación entre el volcanismo neógeno y la sedimentación fluvial, sección Guineales–Bolombolo, suroeste antioqueño. Bachelor thesis, Universidad EAFIT, 106 p. Medellín.
- Rodríguez, G. & Zapata, G. 2014. Descripción de una nueva unidad de lavas denominada andesitas basálticas de El Morito–correlación regional con eventos magmáticos de arco. *Boletín de Geología*, 36(1): 85–102.
- Rutherford, M.J. & Hill, P.M. 1993. Magma ascent rates from amphibole breakdown: An experimental study applied to the 1980–1986 Mount St. Helens eruptions. *Journal of Geophysical Research: Solid Earth*, 98(B11): 19667–19685. <https://doi.org/10.1029/93JB01613>
- Samaniego, P., Robin, C., Chazot, G., Bourdon, E. & Cotten, J. 2010. Evolving metasomatic agent in the northern Andean subduction zone, deduced from magma composition of the long–lived Pichincha volcanic complex, Ecuador. *Contributions to Mineralogy and Petrology*, 160(2): 239–260. <https://doi.org/10.1007/s00410-009-0475-5>
- Shaw, R.P., Leal–Mejía, H., & Melgarejo I Draper, J.C. 2019. Phanerozoic metallogeny in the Colombian Andes: A tectono–magmatic analysis in space and time. In: Cediél, F. & Shaw R.P. (editors), *Geology and tectonics of northwestern South America: The Pacific–Caribbean–Andean junction*. *Frontiers in Earth Sciences*. Springer, p. 411–549. Cham, Germany. https://doi.org/10.1007/978-3-319-76132-9_6
- Shuto, K., Sato, M., Kawabata, H., Osanai, Y., Nakano, N. & Yashima, R. 2013. Petrogenesis of middle Miocene primitive basalt, andesite and garnet–bearing adakitic rhyodacite from the Ryozen Formation: Implications for the tectono–magmatic evolution of the NE Japan arc. *Journal of Petrology*, 54(12), 2413–2454. <https://doi.org/10.1093/petrology/egt052>
- Sierra, G.M. 1994. Structural and sedimentary evolution of the Irra Basin, northern Colombian Andes. Master thesis, State University of New York, 102 p. Binghamton, USA.
- Smith, I.E.M., Ruddock, R.S. & Day, R.A. 1989. Miocene arc–type volcanic/plutonic complexes of the Northland Peninsula, New Zealand. *Royal Society of New Zealand Bulletin*, 26: 205–213.
- Staudigel, H., Plank, T., White, B. & Schmincke, H.U. 1996. Geochemical fluxes during seafloor alteration of the basaltic upper oceanic crust: DSDP Sites 417 and 418. In: Bebout, G.E., Scholl, D.W., Kirby, S.H. & Platt, J.P. (editors), *Subduction: Top to bottom*. *Geophysical Monograph Series*, 96, p. 19–38. <https://doi.org/10.1029/GM096p0019>
- Stern, C.R. & Kilian, R. 1996. Role of the subducted slab, mantle wedge and continental crust in the generation of adakites from the Andean Austral Volcanic Zone. *Contributions to Mineralogy and Petrology*, 123(3): 263–281. <https://doi.org/10.1007/s004100050155>
- Sun, S.S. & McDonough, W.F. 1989. Chemical and isotopic systematics of oceanic basalts: Implications for mantle composition and processes. In: Saunders, A.D. & Norry, M.J. (editors), *Magmatism in the ocean basins*. *Geological Society of London, Special Publication* 42, p. 313–345. <https://doi.org/10.1144/GSL.SP.1989.042.01.19>
- Tassinari, C.C.G., Díaz–Pinzon, F. & Buenaventura, J. 2008. Age and sources of gold mineralization in the Marmato mining district, NW Colombia: A Miocene – Pliocene epizonal gold deposit. *Ore Geology Reviews*, 33(3–4): 505–518. <https://doi.org/10.1016/j.oregeorev.2007.03.002>
- Taylor, S.R. & McLennan, S.M. 1985. *The Continental Crust: Its composition and evolution; an examination of the geochemical record preserved in sedimentary rocks*. Blackwell Scientific Publications, 312 p. Oxford.
- Tejada, M.L. & Betancourt, J.A. 2006. Cartografía geológica de las vulcanitas de la Formación Combia en un área de 200 km² en los alrededores de los municipios de Jericó y Pueblorrico, departamento de Antioquia, Colombia. Ingeominas, unpublished report, 54 p. Bogotá.
- Tejada, M., Betancourt, J., Nivia, Á., Weber, M. & Gómez, J. 2007. Cartografía geológica y caracterización geoquímica de la For-

- mación Combia en los alrededores de Jericó y Pueblorrico, departamento de Antioquia, Colombia. XI Congreso Colombiano de Geología. Memoirs, CD ROM, 24 p. Bucaramanga.
- Thirlwall, M.F. & Fitton, J.G. 1983. Sm–Nd garnet age for the Ordovician Borrowdale Volcanic Group, English Lake District. *Journal of the Geological Society London*, 140(3): 511–518. <https://doi.org/10.1144/gsjgs.140.3.0511>
- Thorkelson, D.J. & Breitsprecher, K. 2005. Partial melting of slab window margins: Genesis of adakitic and non-adakitic magmas. *Lithos* 79(1–2): 25–41. <https://doi.org/10.1016/j.lithos.2004.04.049>
- Thorpe, R.S., Francis, W.W. & O’Callaghan, L. 1984. Relative roles of source composition, fractional crystallization and crustal contamination in the petrogenesis of Andean volcanic rocks. *Philosophical Transactions of the Royal Society of London, A, Mathematical, Physical and Engineering Sciences*, 310(1514): 675–692. <https://doi.org/10.1098/rsta.1984.0014>
- Toro, G., Restrepo, J.J., Poupeau, G., Sáenz, E. & Azdimousa, A. 1999. Datación por trazas de fisión de circones rosados asociados a la secuencia volcano-sedimentaria de Irra, Caldas. *Boletín de Ciencias de la Tierra*, (13): 28–34.
- Toro–Toro, L.M., Alvarán–Echeverri, M. & Borrero–Peña, C.A. 2008. Rocas con afinidad adakítica al sureste de Manizales: Rasgos petrogenéticos y geoquímicos. *Boletín de Geología*, 30(2): 49–60.
- Touissaint, J.F. 1999. Evolución geológica de Colombia: Precámbrico, Paleozoico, Mesozoico, Cenozoico. Universidad Nacional de Colombia, CD ROM, 243p. Bogotá.
- Vargas, C.A. & Mann, P. 2013. Tearing and breaking off of subducted slabs as the result of collision of the Panama arc–indenter with northwestern South America. *Bulletin of the Geological Society of America*, 103(3): 2025–2046. <https://doi.org/10.1785/0120120328>
- Wagner, L.S., Jaramillo, J.S., Ramírez–Hoyos, L.F., Monsalve, G., Cardona, A. & Becker, T.W. 2017. Transient slab flattening beneath Colombia. *Geophysical Research Letters*, 44(13): 6616–6623. <https://doi.org/10.1002/2017GL073981>
- Weber, M.B.I., Tarney, J., Kempton, P.D. & Kent, R.W. 2002. Crustal make-up of the northern Andes: Evidence based on deep crustal xenolith suites, Mercaderes, SW Colombia. *Tectonophysics*, 345(1–4): 49–82. [https://doi.org/10.1016/S0040-1951\(01\)00206-2](https://doi.org/10.1016/S0040-1951(01)00206-2)
- Woodhead, J.D., Hergt, J.M., Davidson, J.P. & Eggins, S.M. 2001. Hafnium isotope evidence for ‘conservative’ element mobility during subduction zone processes. *Earth and Planetary Science Letters*, 192(3): 331–346. [https://doi.org/10.1016/S0012-821X\(01\)00453-8](https://doi.org/10.1016/S0012-821X(01)00453-8)
- Yarce, J., Monsalve, G., Becker, T.W., Cardona, A., Poveda, E., Alvira, D. & Ordoñez–Carmona, O. 2014. Seismological observations in northwestern South America: Evidence for two subduction segments, contrasting crustal thicknesses and upper mantle flow. *Tectonophysics*, 637: 57–67. <https://doi.org/10.1016/j.tecto.2014.09.006>
- Zapata, G. & Rodríguez, G. 2011. Basalto de El Botón, arco volcánico mioceno de afinidad shoshonítica al norte de la cordillera Occidental de Colombia. *Boletín Ciencias de la Tierra*, (30): 77–91.
- Zapata, G. & Rodríguez, G. 2013. Petrografía, geoquímica y edad de la Granodiorita de Farallones y las rocas volcánicas asociadas. *Boletín de Geología*, 35(1): 81–96.
- Zindler, A. & Hart, S. 1986. Chemical geodynamics. *Annual Review of Earth and Planetary Sciences*, 14(1): 493–571. <https://doi.org/10.1146/annurev.ea.14.050186.002425>

Explanation of Acronyms, Abbreviations, and Symbols:

ADR	Andesite dacite rhyolite	HREE	Heavy rare earth element
AF	Amagá Formation	LILE	Large-ion lithophile element
AFC	Assimilation and fractional crystallization	LOI	Loss on ignition
CF	Combia Formation	LREE	Light rare earth element
CSVl	Cauca Shallow Volcanic Intrusions	MASH	Melting, assimilation, storage, homogenization.
CVP	Combia Volcanic Province	MORB	Mid ocean ridge basalt
E–MORB	Enriched–mid ocean ridge basalt	N–MORB	Normal–mid ocean ridge basalt
GLOSS	Global subducting sediment	OIB	Oceanic island basalt
HP	High–pressure	REE	Rare earth element

Authors' Biographical Notes



Marion WEBER has a PhD in geochemistry from Leicester University and is a full professor at the Departamento de Geociencias y Medio Ambiente from the Universidad Nacional de Colombia Sede Medellín. Research interests comprise metamorphic petrology and geochemistry applied to understand the evolution of the Caribbean region. Dr. WEBER currently holds the position of the museum director of the University Geosciences Museum.



Jose Fernando DUQUE is a PhD geologist from Universidad Nacional Autónoma de México (UNAM) and is an associate professor at Departamento de Ciencias de la Tierra from Universidad EAFIT, Colombia. Dr. DUQUE is interested in regional tectonic processes, using relations between magmatism, deformation, and geodynamic processes to understand evolution of the continental margins overtime.



Susana HOYOS is a PhD student at the Massachusetts Institute of Technology (MIT) in the Department of Earth, Planetary, and Atmospheric Sciences (EAPS).



Andrés L. CÁRDENAS-ROZO has a PhD in geology (paleontology major) from the University of South Florida (USF), and is an associate professor at Departamento de Ciencias de la Tierra from Universidad EAFIT, Colombia. His research interests are related to stratigraphic architecture and obtaining biological and geological signatures from the sedimentary record.



Jorge GÓMEZ TAPIAS is a geologist and has worked as a cartographer at the Servicio Geológico Colombiano for 20 years, during which time, he has authored approximately 70 geological maps. He is the coordinator of the Grupo Mapa Geológico Colombiano of the Dirección de Geociencias Básicas, which was recognized by Colciencias as a research group in 2017. GÓMEZ

is the first author of the Geological Map of Colombia at a scale of 1:1 M —editions 2007 and 2015— and of the 26 map sheets of the Geological Atlas of Colombia at a scale of 1:500 K and is the co-editor of the book *Compilando la geología de Colombia: Una visión a 2015*. Since February 2018, he has served as vice president for South America on the Commission for the Geological Map of the World. He was a co-coordinator and the first author of the Geological Map of South America at a scale of 1:5 M 2019. Since October 2020, he was elected as a member of the International Union of Geological Sciences (IUGS) Nominating Committee for the term 2020–2024. Currently, he is the editor-in-chief of *The Geology of Colombia*. GÓMEZ is in charge of coordinating all the activities related to the project and the editorial process.

Rob WILSON was principal experimental officer and electron probe microanalysis specialist in the Department of Geology at the University of Leicester (UK) before retirement in 2015. He is now an honorary visiting fellow of the School of Geography, Geology & the Environment at the University of Leicester.



Chapter 13



The Morales Formation (New Unit): Record of Fluvial–Lacustrine Environments and the Beginning of the Miocene Explosive Volcanism in the Patía Sub–basin (SW Colombia)

<https://doi.org/10.32685/pub.esp.37.2019.13>

Published online 26 November 2020

Andrés F. GALLEGO–RÍOS¹, Andrés PARDO–TRUJILLO^{2*} ,
Guillermo A. LÓPEZ–PLAZAS³, and Sebastián ECHEVERRI⁴ 

Abstract The sedimentary rocks of the Patía Sub–basin (SW Colombia) record the Cenozoic geologic evolution of western Colombia from the Paleogene to the Holocene. In this research, we report a new Miocene stratigraphic unit near Mercaderes town (Cauca Department). A 563 m–thick sequence is described in detail and divided from bottom to top into three lithological assemblages. (I) The upper segment of the conglomeratic member of the Esmita Formation is formed by 33 m–thick beds of clast–supported lithic conglomerates interbedded with lenticular litharenites, with trough and planar cross–bedding. They are interpreted as braided river deposits. (II) The Morales Formation, which is defined in this work, presents 470 m thick composed mainly of parallel laminated gray–black mudstones interbedded with thin sandstone beds, with parallel and ripple laminations, graded bedding, and soft–sediment deformation structures. Plant fragments, pollen, and spores are common. Towards the top, sandstone and poly–mictic conglomerate beds increase. They are interpreted as lake, marsh, and crevasse splay deposits adjacent to fluvial channels. (III) The bottom of the Galeón Formation is composed by 7 m thick of sandstones and conglomerates rich in volcanic fragments accumulated in a fluvial environment with simultaneous volcanic activity.

The petrographic study (conventional and heavy minerals) identifies mainly litharenites and feldspathic litharenites, whose fragments suggest igneous (volcanic and plutonic), sedimentary (mudstones and sandstones), and metamorphic (high–pressure metamorphic rocks and graphitic schists) sources, which are correlated with the basement exposed at the present in the Central and Western Cordilleras.

We review a volcanoclastic sandstone obtained from the bottom of the Galeón Formation that provides the youngest population of U/Pb ages in detrital zircons of ca. 15.4 Ma, interpreted as the depositional age. The sudden increase in volcanic components allows us to interpret this time as the onset of strong volcanism in the basin, which continues currently in the Central Cordillera. This age and new palynological studies suggest a Burdigalian – early Langhian (ca. 19–15.4 Ma) age for the Morales Formation, which improves the chronostratigraphy of the region. Lower Miocene mud–dominated successions have been described in different basins of Colombia (the Cauca–Patía,

- 1 geoand22@hotmail.com
Universidad de Caldas
Departamento de Ciencias Geológicas
Calle 65 n.º 26–10
Manizales, Colombia
- 2 andres.pardo@ucaldas.edu.co
Universidad de Caldas
Instituto de Investigaciones en Estratigrafía (IIES)
Grupo de Investigación en Estratigrafía y Vulcanología (GIEV)
Manizales, Colombia
- 3 guillermolopez.geo@gmail.com
Universidad de Caldas
Departamento de Ciencias Geológicas
Calle 65 n.º 26–10
Manizales, Colombia
- 4 juanesebasecheverri@gmail.com
Universidad de Caldas
Instituto de Investigaciones en Estratigrafía (IIES)
Grupo de Investigación en Estratigrafía y Vulcanología (GIEV)
Manizales, Colombia
Universidad Nacional de Colombia
Grupo de Investigación en Geología y Geofísica (EGEO)
Medellín, Colombia

* Corresponding author

Supplementary Information:

S: <https://www2.sgc.gov.co/LibroGeologiaColombia/tgc/sgcpubesp37201913s.pdf>

Citation: Gallego–Ríos, A.F., Pardo–Trujillo, A., López–Plazas, G.A. & Echeverri, S. 2020. The Morales Formation (new unit): Record of fluvial–lacustrine environments and the beginning of the Miocene explosive volcanism in the Patía Sub–basin (SW Colombia). In: Gómez, J. & Mateus–Zabala, D. (editors), The Geology of Colombia, Volume 3 Paleogene – Neogene. Servicio Geológico Colombiano, Publicaciones Geológicas Especiales 37, p. 395–415. Bogotá. <https://doi.org/10.32685/pub.esp.37.2019.13>

Middle and Upper Magdalena, Llanos, and Caribbean Basins) and can be related to a regional period of tectonically induced accommodation.

Keywords: *Patía Sub-basin, Morales Formation, middle Miocene, stratigraphy, petrography, provenance, vulcanism.*

Resumen Las rocas sedimentarias de la Subcuenca Patía (SW de Colombia) registran la evolución geológica cenozoica del oeste de Colombia desde el Paleógeno hasta el Holoceno. En este trabajo se reporta una nueva unidad estratigráfica del Mioceno cerca de la población de Mercaderes (departamento del Cauca). Se describe en detalle una secuencia de 563 m de espesor y se divide de base a techo en tres conjuntos litológicos. (I) La parte superior del miembro conglomerático de la Formación Esmita está formada por 33 m de estratos gruesos de conglomerados líticos clastosoportados intercalados con estratos lenticulares de litoarenitas, con estratificación inclinada planar y en artesa. Estos estratos se interpretan como depósitos de un río trenzado. (II) La Formación Morales, que se define en esta investigación, tiene 470 m de espesor y se compone principalmente de lodolitas de color gris-negro con laminación plana paralela intercaladas con estratos delgados de areniscas, con laminación *ripple* y plana paralela, gradación normal y estructuras de deformación sinsedimentaria. Son frecuentes los restos de plantas, polen y esporas. Hacia su parte superior se presenta un incremento en estratos de areniscas y conglomerados polimícticos. Esta unidad se interpreta como depósitos de lagos, pantanos y de desbordamiento adyacentes a canales fluviales. (III) La base de la Formación Galeón está compuesta por 7 m de areniscas y conglomerados ricos en fragmentos volcánicos acumulados en un ambiente fluvial con actividad volcánica simultánea.

En el estudio petrográfico (minerales convencionales y pesados) se identificaron principalmente litoarenitas y litoarenitas feldespáticas, cuyos fragmentos sugieren fuentes ígneas (volcánicas y plutónicas), sedimentarias (lodolitas y areniscas) y metamórficas (rocas de alta presión y esquistos grafitosos) que se correlacionan con los basamentos expuestos en las cordilleras Central y Occidental.

Se revaluó una arenisca volcanoclástica obtenida en la base de la Formación Galeón que proporcionó la población más joven de circones detríticos con edades U–Pb de ca. 15,4 Ma, interpretadas como la edad de depósito. El repentino aumento de los componentes volcánicos permite interpretar esta edad como el inicio de un fuerte vulcanismo en la cuenca, el cual continúa hoy en día en la cordillera Central. Esta edad y los nuevos estudios palinológicos sugieren una edad Burdigaliano–Langhiano temprano (ca. 19–15,4 Ma) para la Formación Morales, lo que mejora la cronoestratigrafía de la región. Se han descrito sucesiones lodosas del Mioceno inferior en diferentes cuencas de Colombia (Cauca–Patía, Valle Medio y Valle Superior del Magdalena, Llanos y el Caribe). Estas pueden estar relacionadas con un periodo de acomodación originado por la tectónica.

Palabras clave: *Subcuenca Patía, Formación Morales, Mioceno medio, estratigrafía, petrografía, procedencia, vulcanismo.*

1. Introduction

The Patía Sub-basin (SW Colombia, Figure 1) is filled by Cenozoic (Eocene – Holocene) siliciclastic sedimentites thicker than ca. 3000–4700 m (Barrero et al., 2006; Ruiz, 2002), which overlie a basic igneous and volcanic–sedimentary Cretaceous basement (Barrero et al., 2006; Borrero et al., 2012; Ruiz, 2002). Hydrocarbon seeps have been found in Cenozoic de-

posits (Grosse, 1935), revealing an active petroleum system. However, there are few studies about the paleoenvironment, age, and origin of these deposits, which makes it difficult to determine the paleogeography and the distribution of rocks of economic interest, and to correlate events of regional significance (e.g., tectonic events). The Universidad de Caldas, in agreement with the Agencia Nacional de Hidrocarburos (ANH), performed geological mapping around the town of

Mercaderes (Cauca Department) in 2010 in order to identify potential hydrocarbon source, reservoir, and seal rocks. New stratigraphic, petrographic, and geochemical data obtained along Morales Creek (south of Mercaderes town) on the eastern flank of the Mercaderes Syncline were obtained to investigate the paleoenvironment, provenance, and age of the stratigraphic units (Figure 1). In this chapter, we describe a new siliciclastic unit with a thickness of 470 m, named the Morales Formation. It overlies the conglomeratic member of the Esmita Formation and is overlain by the volcanoclastic Galeón Formation (Figure 2; León et al., 1973). Its facies and paleontological content suggest that fluvial–lacustrine deposits accumulated during the Miocene.

2. Geological Framework

The Patía Sub–basin is a N–NE–oriented elongated depression ca. 140 km in length separating the Central and Western Cordilleras of SW Colombia (Figure 1a). It is limited to the east and west by the Romeral and Cali–Patía Fault Systems, respectively (Barrero et al., 2006). To the north, the Tambo–Popayán paleo-high separates it from the Cauca Sub–basin (Ruiz, 2002). The sedimentary fill comprises ca. 3000–4700 m–thick, clastic sedimentary successions (Barrero et al., 2006; Ruiz, 2002), which were discordantly deposited over a Mesozoic basement (Barrero et al., 2006). The basement comprises Jurassic? – Cretaceous mafic and ultramafic plutonic and volcanic rocks (Figure 1a; e.g., Quebradagrande, Los Azules, and Barroso–Amaime Complexes; Orrego et al., 1996). In some cases, these igneous rocks are associated with marine sedimentary rocks (e.g., pelagic, hemipelagic, and turbiditic deposits; e.g., Pardo–Trujillo et al., 2002). The volcanic rocks of the Barroso–Amaime Complex include massive and pillow basalts with plateau and arc-related geochemical affinities (Kerr et al., 1998; Nivia, 2001; Rodríguez & Arango, 2013). According to Barrero et al. (2006), the basement originated from the oblique collision of oceanic rocks against the NW margin of South America, which generated thrusting, folding, and clastic marine sedimentation. The collision migrated from Ecuador to the N of Antioquia (Colombia) during the Late Cretaceous – Paleocene (Barrero et al., 2006; Kerr et al., 1997; Moreno–Sánchez & Pardo–Trujillo, 2003; Pindell & Kennan, 2009; Villagómez et al., 2011). Currently, the Western Cordillera is composed of plateau basalts and Upper Cretaceous sedimentary deposits (Pardo–Trujillo et al., 2002, 2020), with mylonitic deformation in some cases (Nivia, 2001). The plateau sequences are intruded by Paleogene – Neogene tonalitic plutons (Gómez et al., 2015b). To the east of the basin, in the western border of the Central Cordillera, four different structural complexes crop out, limited by faults with a N40°E trend (Maya & González, 1995); from west to east, they are (Figure 1a; Orrego et al., 1996) as follows: (1) Cretaceous basalts, tuffs, gabbro, and ultramafic igneous rocks (Los Azules

Complex); (2) Cretaceous metamorphic rocks (amphibolite and black schists, quartzites, and local blueschists; Arquía Complex); (3) Lower Cretaceous volcanic and marine sedimentary rocks (Quebradagrande Complex); and (4) Permian, Triassic, and Jurassic igneous and metamorphic rocks (Cajamarca Complex) (Blanco et al., 2014).

During the Eocene – Oligocene, the sedimentation in the Patía Sub–basin was related to transcurrent tectonics along the continental margin, linked to the oblique subduction of oceanic terranes beneath the irregular continental margin of South America (Barrero et al., 2006). During the Neogene, volcanic activity increased and significantly impacted the sedimentation in SW Colombian basins (e.g., Tumaco and Cauca–Patía; Echeverri et al., 2015). According to geochronological data, the Miocene volcanism and magmatism migrated from the W (Western Cordillera) to the axis of the Central Cordillera, where it is currently located, probably due to changes in the angle of the subduction zone (Echeverri et al., 2015). Neogene hypabyssal rocks that cut the sedimentary sequences are very common in the Patía Sub–basin (González, 2010; Ruiz, 2002). The Eocene – Miocene sedimentary units were affected by thrust and fold systems with western vergence involving the oceanic basement associated with the late Miocene – Pliocene Andean orogenic pulse (Barrero & Laverde, 1998). In contrast, the Pliocene? – Quaternary units are horizontal and form terraces at different topographic levels.

No consensus regarding the age and nomenclature of these units exists (Figure 2). Grosse (1935) was one of the pioneers who studied the Cenozoic deposits of the basin. He named these rocks from bottom to top as follows: (1) “Eoterciario”, composed of quartz–rich conglomerates, sandstones, and mudstones with some characteristic coal beds in this interval; (2) “Medioterciario inferior”, composed of sandstones, conglomeratic sandstones, and conglomerates interbedded with mudstones, some of them with gastropods and lamellibranches; (3) “Medioterciario superior”, composed of tuffaceous sandstones, claystones, tuffs (agglomerates), and conglomerates; (4) “Neoterciario” (Pliocene?), composed of clays, tuffs, agglomerates, and tuffaceous sandstones, although Grosse (1935) pointed out the difficulty of recognizing the last two units due to their lithological similarities; and (5) Quaternary, represented by the “Capas Táficas de Mercaderes”. The author indicated that this unit can be differentiated because it is not folded and partially covers the former units with an angular unconformity. Grosse (1935) did not indicate a precise age for the “Eoterciario” and “Medioterciario” units.

León et al. (1973) formally defined the Esmita Formation (Figure 2) along the Esmita River, located ca. 51 km to the NE of Mercaderes town; this unit overlies the Mosquera Formation in transitional contact. The authors divided the unit, from bottom to top, into three informal members: (1) fossiliferous silty, (2) sandy, and (3) conglomeratic. They indicated

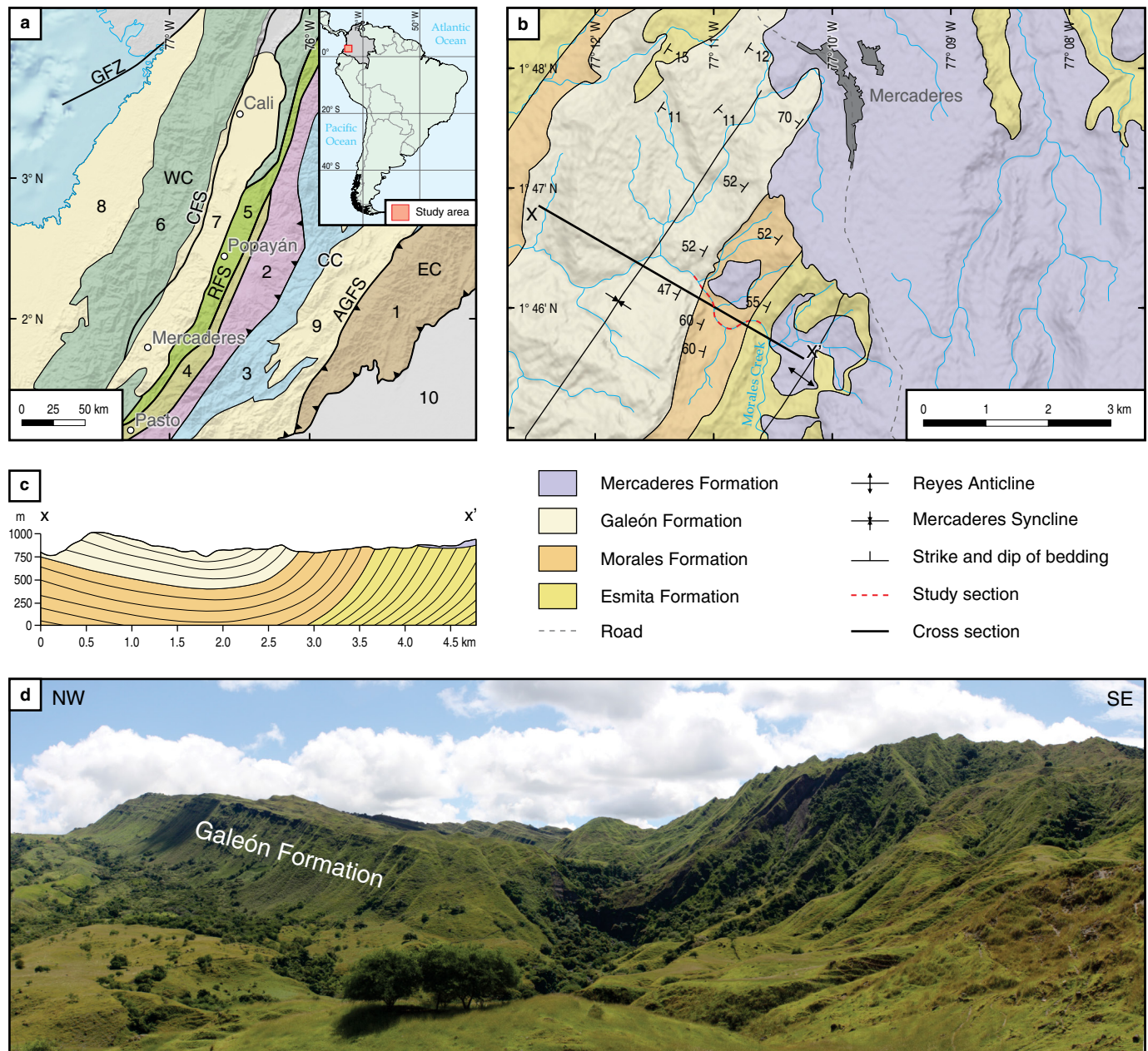


Figure 1. (a) Location of SW Colombia in South America, and simplified geological map showing the main geological units without the Pliocene – Quaternary volcanic cover (modified from Gómez et al., 2015a): (1) Precambrian metamorphic rocks (Garzon Massif); (2) Cajamarca Complex; (3) Jurassic plutonic and volcanic rocks; (4) Quebradagrande Complex; (5) Arquía Complex; (6) Cretaceous mafic and ultramafic volcanic and plutonic rocks, including the Barroso–Amaime and Los Azules Complexes (Orrego et al., 1996), and marine sedimentary rocks (mainly in the Western Cordillera); (7) Patía Sub-basin; (8) Tumaco Basin; (9) Upper Magdalena Valley Basin; (10) Caguán–Putumayo Basin. (WC) Western Cordillera; (CC) Central Cordillera; (EC) Eastern Cordillera; (AGFS) Algeciras–Garzón Fault System; (RFS) Romeral Fault System; (CFS) Cali–Patía Fault System; (GFZ) Garrapatas Fault Zone. (b) Geological map of the study area (Universidad de Caldas fieldwork map performed in 2010). (c) Geologic cross-section that shows the stratigraphic relations of the various units. (d) Morphology of the Galeón Formation on the axial axis of the Mercaderes Syncline.

a Miocene age based on fossil marine mollusks (*Mytilus* sp., *Balcis* sp., *Bittium* sp., *Rissoina sagraiana*, and *Neverita neveridis*) found in the lower and middle members. Duque–Caro (1973, written communication, in León et al., 1973) suggested a late Miocene age based on the presence of *Ammonia*

beccarii (Figure 2). The authors indicated shallow brackish water marshes as the depositional environment. The Esmite Formation is overlain by the Galeón Formation. It was initially named Galeón's Formation by Keizer et al. (1955, unpublished, in van der Hammen, 1958). Van der Hammen et

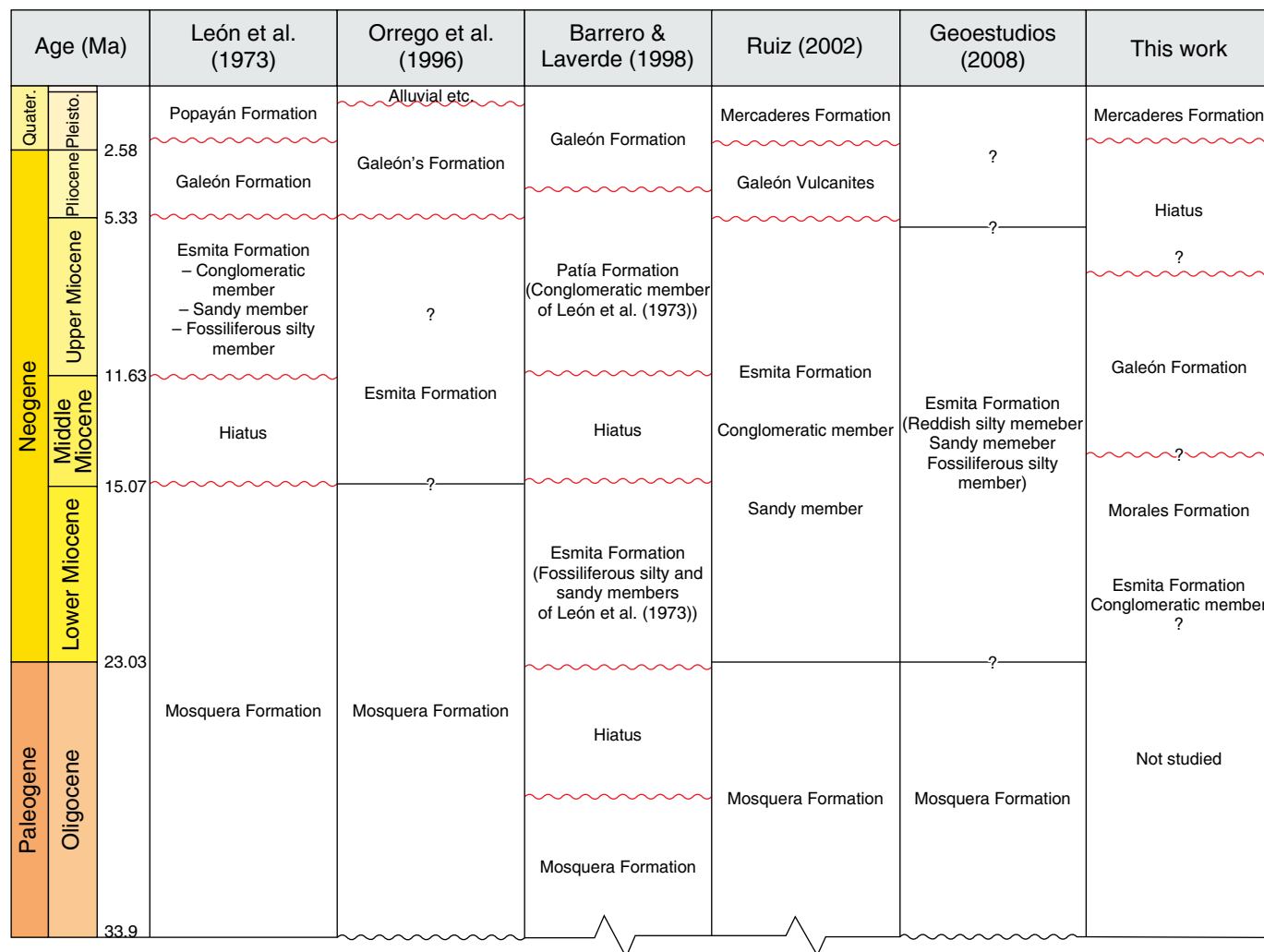


Figure 2. Different stratigraphic nomenclatures and ages proposed for the Cenozoic deposits of the Patía Sub–basin.

al. (1955, in León et al., 1973) suggested an early Pliocene age for this unit.

Orrego et al. (1996) described the Mosquera and Esmita Formations (Figure 2) in the 387–Bolívar geologic map to the west of the study area. They pointed out that the Esmita Formation stratigraphy is different from that described by León et al. (1973) in the 386–Mercaderes geologic map. Among the differences, they mentioned the presence of a sequence of purple siltstones and claystones interbedded with sandstones located in the upper part of the Esmita Formation. Orrego et al. (1996) indicated that this discrepancy is probably related to mistakes in stratigraphic interpretation due to structural problems. They proposed a detailed revision of the stratigraphy and structural geology of the area. An Oligocene – Miocene age was proposed for the Mosquera Formation, and a middle – late Miocene age was indicated for the Esmita Formation based on stratigraphic relationships and regional correlations.

Barrero & Laverde (1998) performed an analysis of seismic lines and regional geological information from the Cauca–Patía

Basin. They restricted the name Esmita Formation to the fossiliferous silty and sandy members of León et al. (1973), and indicated an Oligocene – early Miocene age (Figure 2). The conglomeratic member was called the Patía Formation, following Murcia et al. (1981), and a late Miocene – early Pliocene age was suggested. Finally, they mentioned the upper Pliocene – Holocene Galeón Formation (Figure 2).

In the Mercaderes area, the Servicio Geológico Colombiano (Ruiz, 2002) employed the following stratigraphic terms from base to top: Mosquera Formation, Esmita Formation, Galeón Vulcanites, and Mercaderes Formation (Figure 2). He identified two members of the Esmita Formation, which from base to top are the (1) sandy member and (2) conglomeratic member (Figure 2). The lithological and paleontological data of the sandy member suggest a transitional–continental environment, where sandstones and conglomerates accumulated in fluvial channels. Ruiz (2002) suggested an early Miocene (Aquitian) age based on the presence of *Lymnaea* found in Matacea Creek. He indicated that the conglomeratic member of

the Esmita Formation is disconformably overlain by the Galeón Vulcanites (equivalent to the Galeón Formation) of Pliocene – early Pleistocene age (León *et al.*, 1973). The Pleistocene Mercaderes Formation (Ruiz, 2002) is composed of volcanic and volcanoclastic deposits and covers the previous units above an angular unconformity.

Geoestudios (2008; Figure 2) described the Esmita Formation in three sections: El Boquerón, Guanabanal, and La Despensa Creeks. They identified the fossiliferous silty and sandy members of León *et al.* (1973) in the lower and middle parts of the unit. At the top, they defined a reddish siltstone member that could be correlated with the sequence of purple siltstones and claystones interbedded with sandstones mentioned by Orrego *et al.* (1996). The authors suggested muddy tidal plains, tidal channels, and fluvial environments for the unit. Palynologic studies performed at La Despensa Creek indicated a late Oligocene to middle Miocene age for the Mosquera and Esmita Formations (Geoestudios, 2008).

3. Methods

The studied rocks were described in well-exposed outcrops along Morales Creek using Jacob's staff (Patacci, 2016). This method allowed the identification of sedimentary facies and the interpretation of the depositional physical processes (Figure 3; Table 1). The Morales Formation was defined following the procedures for establishing stratigraphic units in the International Stratigraphic Guide (Murphy & Salvador, 1999). The facies identified were classified with a code based on their granulometry and sedimentary structures, according to Miall (2006). Subsequently, facies associations and architectural elements were identified in order to interpret the depositional environments (Table 2) and their variations over time.

From the 65 collected samples, 15 were used for petrographic analysis: 4 from the Esmita Formation, 10 from the Morales Formation, and one from the base of the Galeón Formation. The analyses were conducted in the Sedimentary Petrography Laboratory of the Instituto de Investigaciones en Estratigrafía (IIES) of the Universidad de Caldas and followed the Gazzi–Dickinson method (Ingersoll *et al.*, 1984). The composition and texture of the clasts, such as grain size, roundness, and calibration, were measured. The Folk (1974) nomenclature was used to classify the sandstones. To improve the interpretation of the provenance of sediments, the heavy mineral fractions (densities $> 2.82 \text{ g/cm}^3$) of four samples were analyzed. The heavy fractions were concentrated with sodium polytungstate (density of 2.9 g/cm^3); subsequently, thin sections were assembled using a resin with a refractive index similar to that of Canadian balsam ($n = 1.539$). More than 300 grains per slide were counted using the ribbon counting method. The mineralogical identification was realized according to Mange & Maurer (1992). The data were represented on bar charts to visualize and group the pop-

ulations and interpret their origin. Finally, the petrographic data were integrated into the regional geology in order to interpret source rocks.

We reviewed the U/Pb Laser Ablation Inductively Coupled Plasma Mass Spectrometry (LA–ICP–MS) detrital zircon ages of the Galeón Formation reported by Echeverri *et al.* (2015), and decomposed the ages on the relative probability diagrams employed by Density Plotter (Vermeesch, 2013). The morphology of zircon grains was revealed by cathodoluminescence imaging and described in terms of the growth rates of the crystal faces relative to each other. To assess zircon morphology, we implemented the characterization described by Corfu *et al.* (2003).

To determine the amount and type of organic matter contained in the deposits of the Morales Formation, total organic carbon (TOC) and pyrolysis analyses were performed on 5 samples using the LECO and Rock–Eval techniques, respectively, in the laboratories of Schlumberger (Colombia).

4. Results

4.1. Definition of the Morales Formation in SW Colombia

The term Morales Formation is proposed to include the fine-grained unit that overlies the conglomeratic member of the Esmita Formation and underlies the Galeón Formation (Galeón Vulcanites of Ruiz, 2002) in the Mercaderes area (Figure 3). This unit differs in lithology and geomorphology from the adjacent units (Esmita and Galeón Formations; Figure 3) and therefore, can be mapped separately on a 1:25 000 map. The most important features of the unit are described below.

4.2. Stratotype and Type Locality

The proposed stratotype crops out four kilometers to the southwest of Mercaderes town, along Morales Creek on the eastern flank of the Mercaderes Syncline (Figure 1b, 1c, 1d). Its geomorphological expression as a valley allows the unit to extend up to 9.2 km towards the SW, along the eastern and western flanks of the Mercaderes Syncline and to the west of Arboledas town (Cauca Department). To the north, it is covered by the volcanoclastic deposits of the Mercaderes Formation (Figure 1). The origin of the name comes from Morales Creek, a Patía River tributary. The map base 386–IV of the Instituto Geográfico Agustín Codazzi (2005) was used.

Figure 3. Stratigraphic log of the studied section with locations of samples analyzed. (Q) quartz; (F) feldspar; (L) lithic fragments, the main components for classification of sandstones in percentages. The pink arrows and the numbers indicate the facies associations. See Tables 1, 2 for the descriptions and interpretations of lithofacies.

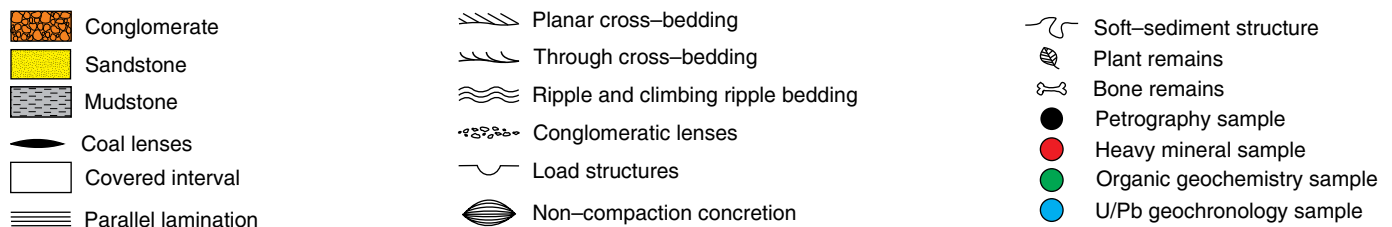
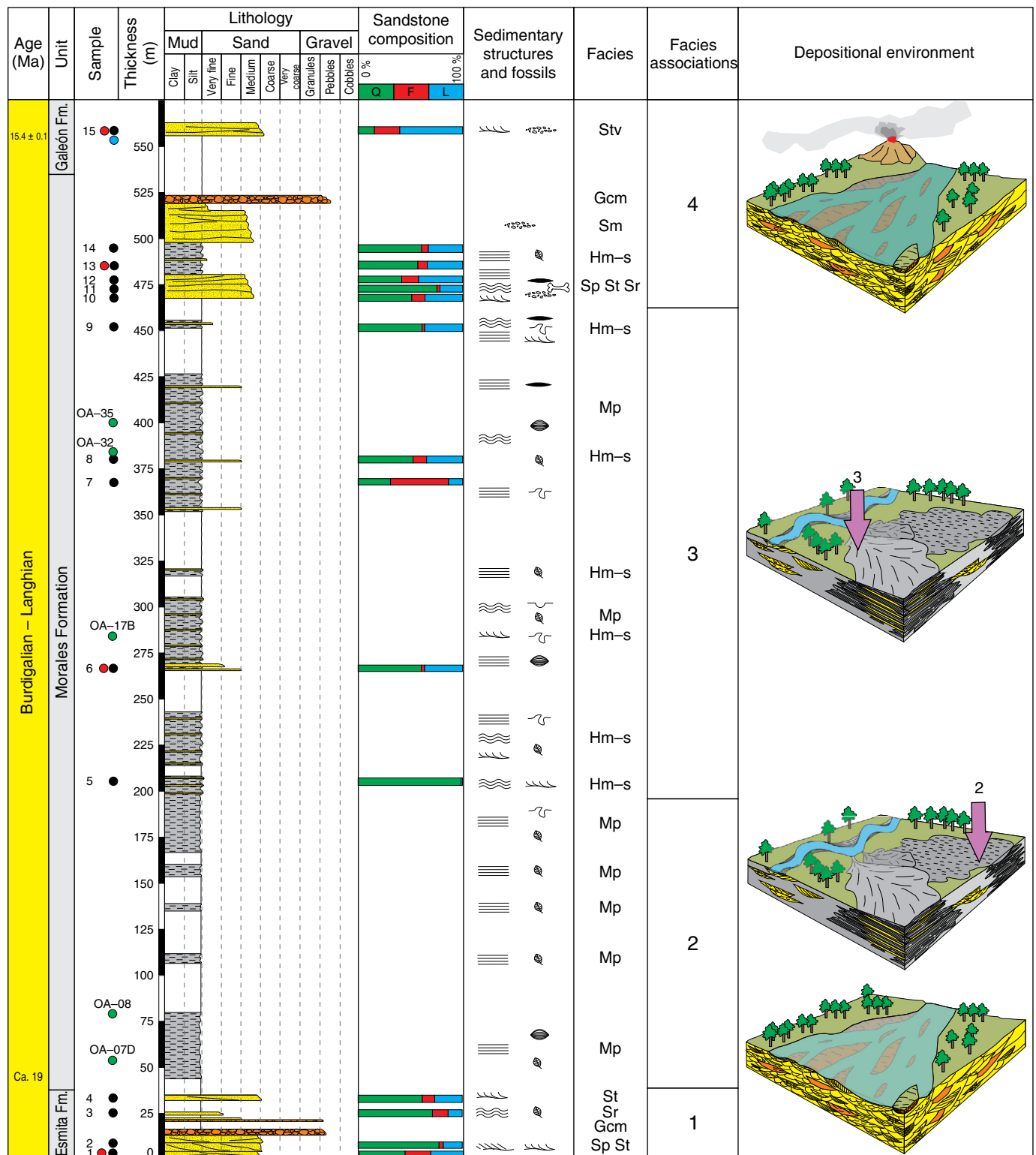


Table 1. Lithofacies codes used in this research (modified from Miall, 2006).

Code	Description	Interpretation
Gcm	Tabular and lenticular strata of structureless clast-supported polymictic conglomerates; subangular to subrounded, poorly sorted clasts. Locally, they have incipient clast orientation.	Pseudoplastic debris flow, longitudinal bedforms, lag deposits, sieve deposits (Miall, 2006).
Sp	Tabular and lenticular strata of medium-grained feldspathic lithic sandstones and conglomerates with planar cross stratification.	Migration of transverse bedforms associated with unidirectional Newtonian flows under low-flow conditions (Miall, 2006).
St	Tabular and lens-shaped strata of medium-grained feldspathic lithic sandstones, poorly to moderately sorted, with trough cross stratification. The top of the sequence features volcanic fragments and conglomeratic lenses (Stv).	Migration of sinuously crested and linguoid dunes under lower flow regime (Miall, 2006).
Sr	Tabular and lenticular beds of medium-grained lithic sandstones, with ripple and climbing ripple laminations.	Migration of ripples, in some cases with constant sand inflow, under lower flow regime (Miall, 2006).
Sm	Tabular and lenticular beds of structureless, medium-grained lithic sandstones, with local conglomeratic lenses.	Hyper-concentrated sediment flow deposits near the bottom of the channel (Miall, 2006).
Hm-s	Heterolithic facies. Thin beds of mudstones and fine- to very fine-grained sandstones. The mudstones have parallel lamination. The sandstones have ripple and climbing ripple laminations, normal grading and soft-sediment deformation structures (e.g., slumped, convoluted).	Particle settlement from suspension that alternated with low-energy currents; the deformation structures may be related to high sediment load and/or seismic activity (Potter et al., 2005).
Mp	Dark gray-black mudstones with parallel laminations, soft-sediment deformation structures and calcareous concretions.	Low-energy settings, settlement of particles from suspension in anoxic environments (Miall, 2006).

Table 2. Architectural elements in fluvial deposits (modified from Miall, 2006 and Potter et al., 2005).

Number in the log of Figure 3	Lithofacies associations	Interpretation
1, 4	Gcm, Sp, St, Sr, Sm, and a low proportion of Hm-s	Gravel and sand bars. Common in fluvial channels with high energy and load capacity (Miall, 2006).
3	Hm-s, Mp	Overflow and settlement of particles from suspension in low-energy environments. Typical of floodplains, swamps, lakes, and peat bogs (Potter et al., 2005).
2	Mp	Swamp and shallow lake deposits with low oxygen content at the bottom. Associated with alluvial plains (Miall, 2006).

4.2.1. Coordinates

Initial point (base of the unit): E: 989 005; N: 686 417 (origin Bogotá) (1° 45' 49" N; 77° 10' 46" W). Final point (top of the unit): E: 988 477; N: 686 898 (origin Bogotá) (1° 46' 04" N; 77° 11' 02" W).

4.2.2. Stratigraphic Limits and Thickness

The lower contact is conformable with the conglomerates and sandstones of the Esmita Formation. The upper limit with the sandstones and conglomerates of the Galeón Formation is covered by recent alluvial deposits (Figure 3). The Galeón Formation shows a sudden increase in the percentage of volcanic clasts. The measured thickness in Morales Creek reaches 470 m.

4.2.3. General Description

From bottom to top, the Morales Formation consists mainly of thin beds of gray to black laminated mudstones with some inter-

calated thin layers of lithic sandstones (heterolithic beds). The mudstones have parallel lamination, and the sandstones have ripple and climbing ripple laminations and normal grading. The heterolithic facies have soft-sediment deformation structures (e.g., slumps and clastic injection dikes). In the upper part of the unit (last 55 m), there is an increase in tabular and lenticular, medium to thick beds of lithic sandstones and polymictic conglomerates (Figure 3; Table 1).

4.2.4. Age

The Morales Formation has relatively abundant pollen, spores, and plant remains (Martínez et al., 2013). A sample analyzed from the basal volcanoclastic beds of the Galeón Formation (Figure 4; Echeverri et al., 2015) that overlies the top of the Morales Formation shows ages between 12 and 15 Ma (Table 1 of the Supplementary Information). This sample shows three U/Pb detrital zircon peaks with a wide domain of middle Miocene ages (Langhian; 83%, 15.4 ± 0.1 Ma), which is considered the depositional age, while the Oligocene (Chattian; 6%, 25.8

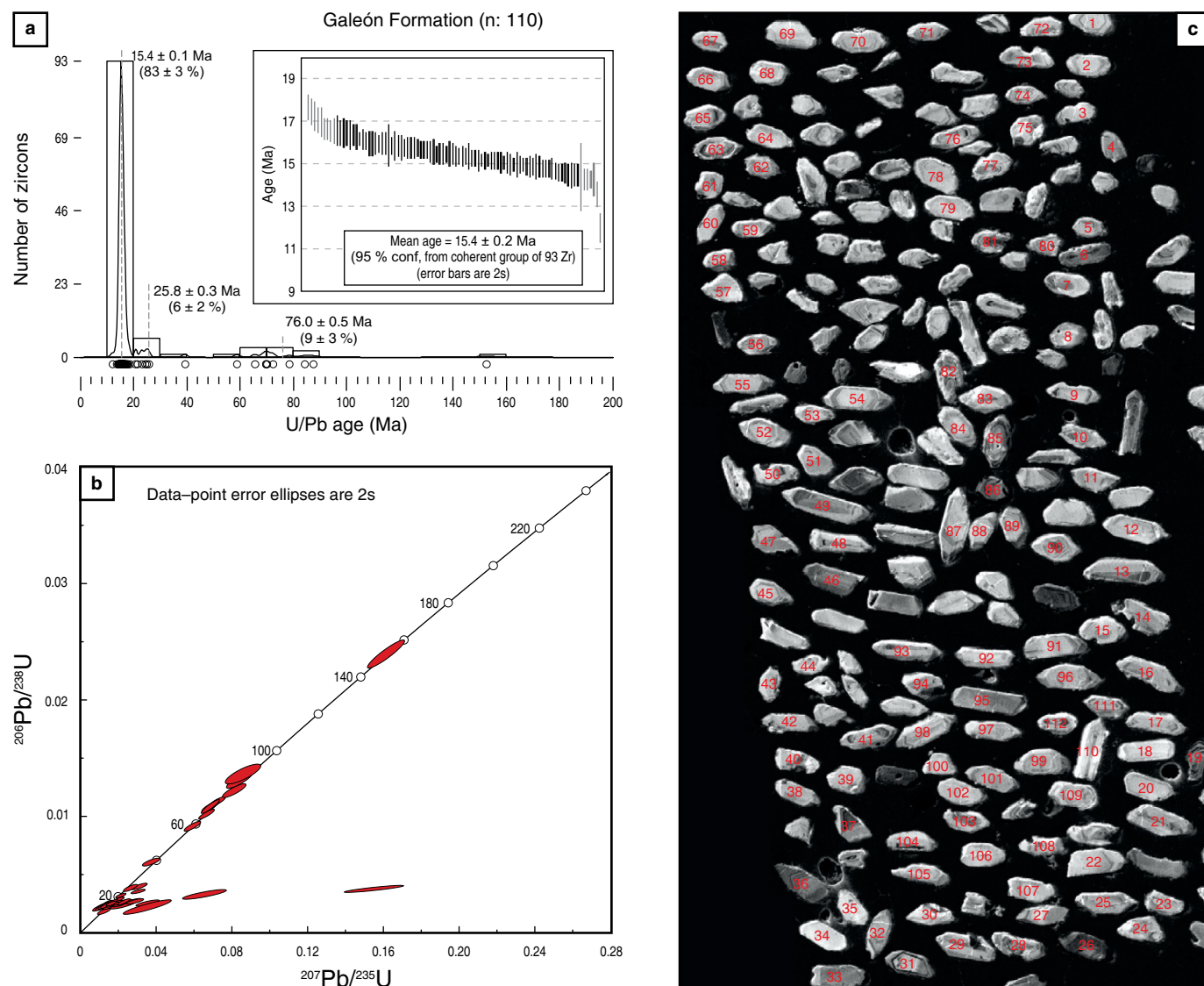


Figure 4. U/Pb LA-ICP-MS detrital zircon geochronology from the Galeón Formation (after Echeverri et al., 2015). **(a)** Probability density plot that shows the U/Pb detrital zircon peaks obtained with Density Plotter (Vermeesch, 2013). The inset shows the weighted mean age plot of the most common population of zircons. **(b)** Tera–Wasserburg concordia diagram. **(c)** Cathodoluminescence images of the detrital zircons analyzed. Red numbers indicate the dated zircons.

± 0.3 Ma) and Late Cretaceous (Campanian; 9%, 76.0 ± 0.5 Ma) ages occur less frequently (Figure 4a, 4b). In the middle Miocene population, exclusively igneous zircons, which are euhedral, subhedral, and prismatic with oscillatory zonation, are observed (Figure 4c). Additionally, Oligocene and Cretaceous populations contain zircons of igneous origin. Zircons with overgrowths associated with metamorphic events are absent. In summary, the age of the basal strata of the Galeón Formation is estimated at ca. 15.4 Ma. Additionally, the presence of *Clavatricolpites densiclavatus*, *Nijssenosporites fossulatus*, and *Echitricolporites maristellae* in the lower part of the Morales Formation indicates an age not older than Burdigalian (ca. 19 Ma, early Miocene), according to the zonation of Jaramillo et al. (2011) for the Llanos area (Martínez et al., 2013). Thus, the

age of the Morales Formation is not older than ca. 19 Ma, and not younger than ca. 15.4 Ma.

4.2.5. Organic Geochemistry

The TOC of the Morales Formation samples fluctuates between 0.26 and 1.08 (poor quality of source rock). The hydrogen index (HI) fluctuates between 121 and 229 (mainly gas-prone organic matter), the oxygen index fluctuates between 14 and 31, and the Tmax between 428 and 436 °C. Kerogen is mainly types II–III and has a very low remaining hydrocarbon potential (Figure 5; Table 2 of the Supplementary Information). The organic matter is mainly continental, as indicated by the contents of plant organic matter, pollen spores, and freshwater algae (Martínez

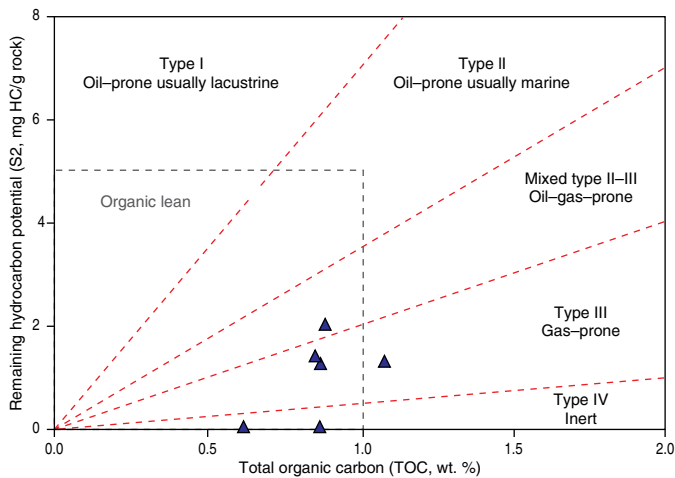


Figure 5. Remaining hydrocarbon potential vs. TOC and kerogen types of the studied samples from the Morales Formation.

et al., 2013). According to the color of the palynomorphs, the thermal alteration index (TAI) is -2 to 2 (thermally immature rocks according to Traverse, 2007).

4.3. Facies Analysis

Figure 6a shows the geomorphological expression of the units studied. Seven lithofacies are identified in this area (Table 1).

4.3.1. Gcm (Conglomerate, Clast-supported, Massive)

Tabular and lenticular thick beds of structureless (massive), poorly sorted clast-supported pebbly conglomerates, with subangular to subrounded clasts. They are composed of quartz, chert, and volcanic rock fragments (Figures 3, 6b; Table 1).

4.3.2. Sp (Sandstone, Planar Cross-stratification)

Tabular and lenticular thick beds of well to poorly sorted lithic and feldspathic medium-grained sandstones, with subrounded to subangular grains. They have planar cross-stratification marked by oriented pebbly levels. Locally, conglomerates and conglomeratic sandstones are present (Figures 3, 6c, 6h; Table 1).

4.3.3. St (Sandstone, Trough Cross-bedding)

Lenticular and tabular beds of gray poorly to moderately sorted lithic and feldspathic medium-grained sandstones, with subangular to subrounded grains and trough cross-bedding. The top of the sequence features volcanic fragments (Stv facies; Figures 3, 6d, 6e, 6f, 6h; Table 1).

4.3.4. Sr (Sandstone, Ripple Laminations)

Tabular and lens-shaped strata of gray poorly sorted lithic medium-grained sandstones, with subrounded to subangular grains. They have ripple laminations (in some cases climbing ripples) as internal structures (Figures 3, 6g, 6h; Table 1).

4.3.5. Sm (Sandstone, Massive)

Tabular beds of greenish-gray medium-grained lithic sandstones, moderately sorted, structureless (massive), with local conglomeratic lenses containing subrounded to subangular clasts (Figures 3, 6i; Table 1).

4.3.6. Hm-s (Heterolithic, Mudstone-Sandstone)

Succession of thin beds of mudstones interlayered with sandstones. The mudstones have parallel lamination. The sandstones are very fine in grain size, with parallel, trough, and climbing ripple laminations and graded beds. Load casts and soft-sediment deformation structures are also common (Figures 3, 6j, 6n, 6o; Table 1). Plant remains are frequent.

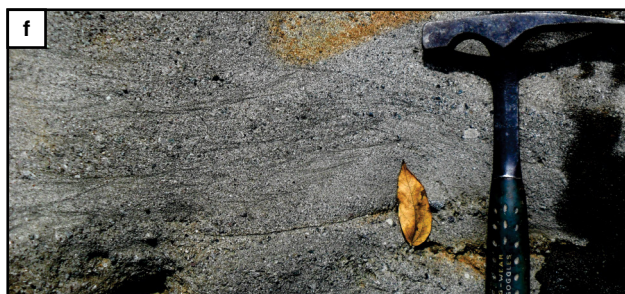
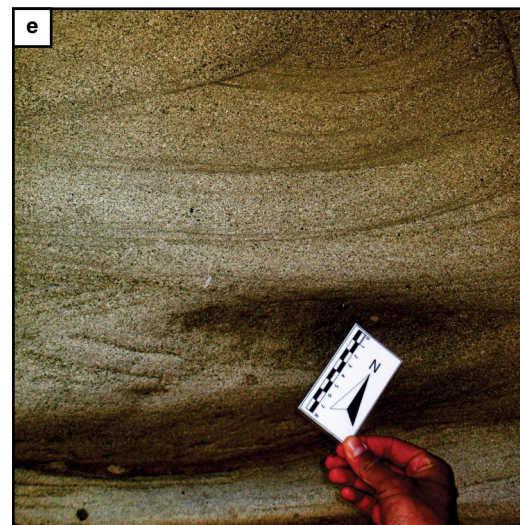
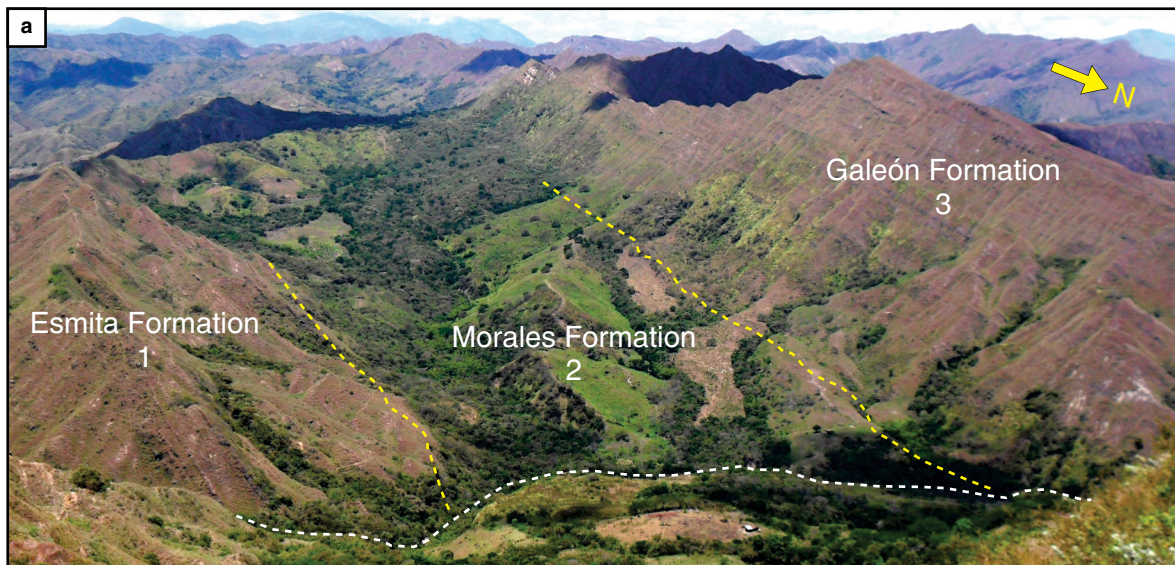
4.3.7. Mp (Mudstone, Parallel Lamination)

Dark gray mudstones with parallel lamination and local deformation structures and locally uncompacted calcareous concretions. It is commonly associated with the Hm-s facies (Figures 3, 6k, 6l, 6m; Table 1). Plant remains, pollen, and spores are relatively common in this facies.

4.4. Facies Associations

Four facies associations are identified (Figure 3; Table 2).

Figure 6. Morphology and facies of the studied section. **(a)** Geomorphology of the studied stratigraphic units. The dotted line corresponds to the studied section (Morales Creek). **(b)** Structureless conglomerate with clast-supported pebbles (Gcm; Esmita Formation). **(c)** Sandstones and conglomeratic sandstones with planar cross stratification (Sp; Esmita Formation). **(d), (e)** Sandstones with trough cross-bedding (St; Esmita Formation). **(f)** Sandstones and conglomeratic sandstones rich in volcanic clasts with trough cross-bedding (Stv; Galeón Formation). **(g)** Sandstones with climbing lamination (Sr; Esmita Formation).



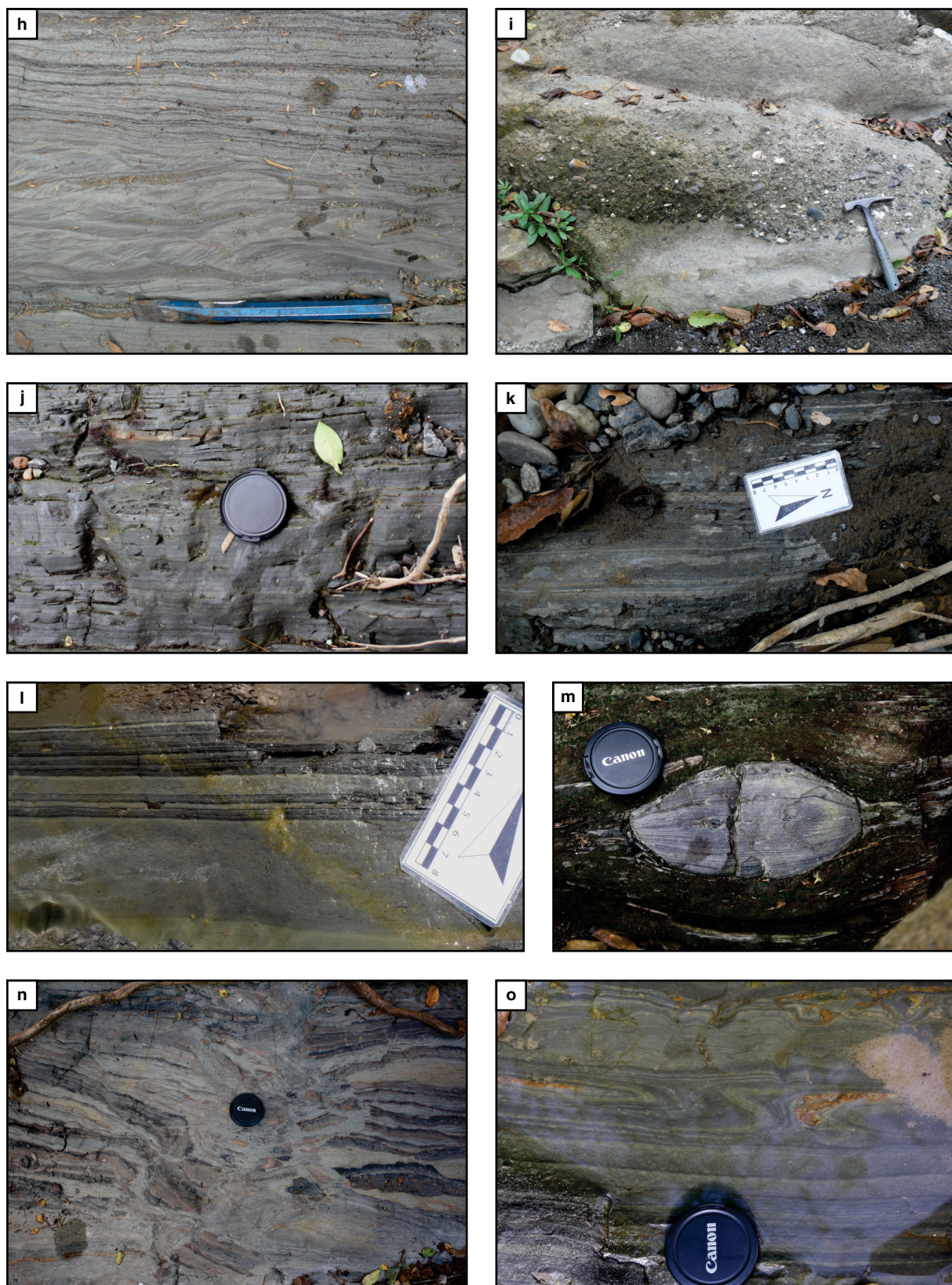


Figure 6. Morphology and facies of the studied section. **(h)** Sandstones with parallel laminations (Sp), trough cross-bedding (St), and climbing ripple lamination (Sr) (Morales Formation). **(i)** Massive sandstones (Sm) with conglomeratic lenses (Morales Formation). **(j)** Mudstones (claystones and siltstones) with parallel lamination (Morales Formation). **(k), (l)** Heterolithic facies with parallel lamination (Mp) and plant debris (Morales Formation). **(m)** Early diagenetic muddy concretion (Morales Formation). **(n), (o)** Soft-sediment deformation structures in heterolithic facies (convolute and slumped beds, respectively; Morales Formation) (*continued*).

4.4.1. Facies Association 1 (0–33 m; Conglomeratic Member of the Esmita Formation)

It consists mainly of amalgamated lenticular beds with the Sp, St, Sr, and Gcm lithofacies (Figure 6; Table 1), some of them with fining–upward patterns a few meters in thickness. The Gcm facies can be related to debris flow deposits associated with longitudinal fluvial bars (Miall, 2006) (Table 1). Its relations with Sp, St, and Sr facies can be associated with the deposition of dunes in abandoned channels or sand wedges at the edges of bars (Einsele, 2000). The fining–upward pattern can be related to lateral migration and sudden abandonment of channels by avulsion (Einsele, 2000). The absence of fine–grained overbank and alluvial plain deposits, as well as the random arrangement between coarse–grained lithofacies, suggests braided fluvial deposits (cf. Miall, 2006; Figure 3; Table 2).

4.4.2. Facies Association 2 (33–179 m; Morales Formation)

It is dominated by the Mp lithofacies with a low percentage of thin sandstone beds (Figure 3; Table 2). These deposits can be related to low–energy environments associated with swamps and shallow (?) lakes developed in alluvial plains, relatively far from the main channel (Figure 3; Table 2). This interpretation is also supported by the exclusive presence of continental microfossils (e.g., pollen and spores; Martínez et al., 2013). The dark gray color of this facies can be associated with anoxic–dysoxic environments (Potter et al., 2005). Continental lakes occur in areas of crustal subsidence, such as rift zones, continental sag basins, and foreland and back–arc basins (Einsele, 2000).

4.4.3. Facies Association 3 (179–455 m; Morales Formation)

In this part of the section, the Mp and Hm–s facies are the most common, but there is an important increase in the frequency of thin sandstone beds. They are interpreted as swamp and distal overbank deposits in a fluvial plain (cf. Miall, 2006). Muds and silts were deposited during floods as suspension deposits in temporary floodplain lakes and ponds marginal to the main channel (Potter et al., 2005). Plant remains, pollen, spores, and coal lenses linked to the type III kerogen confirm the association with continental deposits.

4.4.4. Facies Association 4 (470–563 m; Morales and Galeón Formations)

In this part, the mudstones are in contact with sandstones and conglomerates (Sp, St, Sr, Sm, and Gcm; Figures 3, 6; Table

1). They can be interpreted as fluvial channel and crevasse splay deposits. After a covered interval of 30 m, in the 525–555 m interval, there is an increase in thick beds of volcanoclastic amalgamated sandstones, including mainly lenticular Stv lithofacies (Figure 6, Table 1). This lithofacies, together with Gcm, characterizes the base of the Galeón Formation (Figure 3; Table 2). Stv and Gcm are the most common facies association in the unit, which has a thickness of more than 400 m in the core of the Mercaderes Syncline. Thus, a braided fluvial environment is proposed with a strong supply of volcanic materials.

4.5. Petrography

The studied sandstones are mainly moderately to poorly sorted litharenites, feldspathic litharenites, and sublitharenites (Figure 7a), with medium to very fine grain sizes, subangular to subrounded grains and clay matrix contents between 0 and 18% (Table 3 of the Supplementary Information). They plot mainly in the recycled orogen fields (quartzose and transitional) in the tectonic provenance diagrams (Figure 7b, 7c; Dickinson et al., 1983).

The sandstones are composed mainly of monocrystalline quartz (Qm; 28–12 %) (Figure 8a–8c), and most grains have wavy extinction. The three uppermost samples of the Esmita Formation show an increase in polycrystalline (Qp) mosaic quartz (11–21 %; e.g., Figure 8d). Plagioclase grains are present in most of the slides (0–35 %), some of which are twinned or zoned (Figure 8e). Bone fragments are locally present (Figure 8f, 8g). The lithic fragments are as follows, in order of abundance: sedimentary rocks (mudstones and sandstones; 1–17 %); metamorphic rocks (graphitic schists; 1–10 %) (Figure 8h), which increase in percentage towards the top of the section; intermediate volcanic rocks (1–15 %), which abruptly increase towards the base of the Galeón Formation (40%) (Figure 8h, 8i); and plutonic rocks (0–1 %). Other minerals present in the samples are hornblende (1–8 %), biotite (1–5 %), muscovite (1–5 %), epidote (1–5 %), and chlorite (1–3 %) (Figure 8b). The cement may be calcite, quartz, or chlorite (Figure 8a–8c).

4.6. Heavy Minerals

Figure 9 shows the types and percentages of heavy minerals reported in each stratigraphic unit (see also Table 4 of the Supplementary Information). The minerals identified, in order of abundance, are epidote, zircon, apatite, garnet, hornblende, olivine, and hypersthene with lower proportions of muscovite, biotite, clinozoisite, enstatite, and glaucophane (Figure 9a, 9b). Chlorite and spinel are found only in sample 15 from the Galeón Formation, and glaucophane is found in samples 6 and 13 from the Morales Formation.

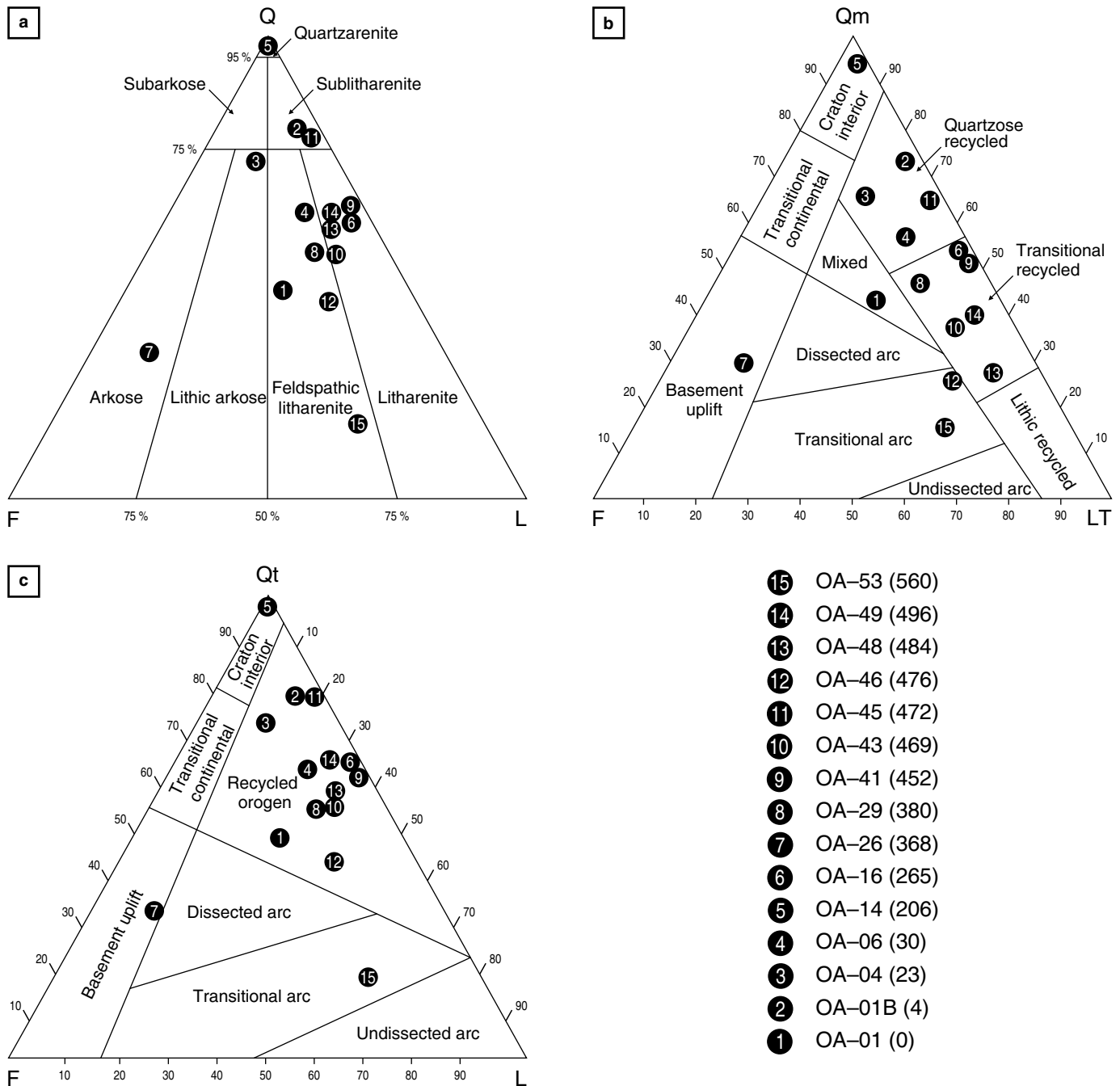


Figure 7. (a) QFL modal classification diagram of the studied sandstones (Folk, 1974); (b), (c) Tectonic provenance diagrams (Dickinson et al., 1983): (Q) total quartz (no chert); (F) potassium feldspar + plagioclase; (L) lithic fragments (no chert); (Qm) monocrystalline quartz; (LT) total lithics (including chert); (Qt) total quartz (including chert). The values to the left in circles correspond to the numbers of the samples represented in the stratigraphic log (Figure 3), and the OA codes show the numbers of field samples. The numbers in parentheses show the thickness in meters above the section.

A dominance of anhedral and subhedral subrounded to sub-angular grains is observed (Figure 9). Hornblende (46%), apatite (25%), and epidote (18%) are abundant in the Esmita Formation (Figure 9a). In the Morales Formation, the most abundant minerals are zircon (11 to 30 %), epidote (22 to 27 %), apatite (9 to 24 %), and garnet (2 to 22 %),

followed by hornblende (1 to 13 %), tourmaline (5%), rutile (2%), hypersthene (0.3 to 6 %), olivine (3%), muscovite (3%), glaucophane (1%), clinozoisite (3%), biotite (2%), and enstatite (1%). The Galeón Formation contains garnet (39%), zircon (20%), epidote (14%), and apatite (12%) as the most abundant minerals, followed by olivine (7%), tour-

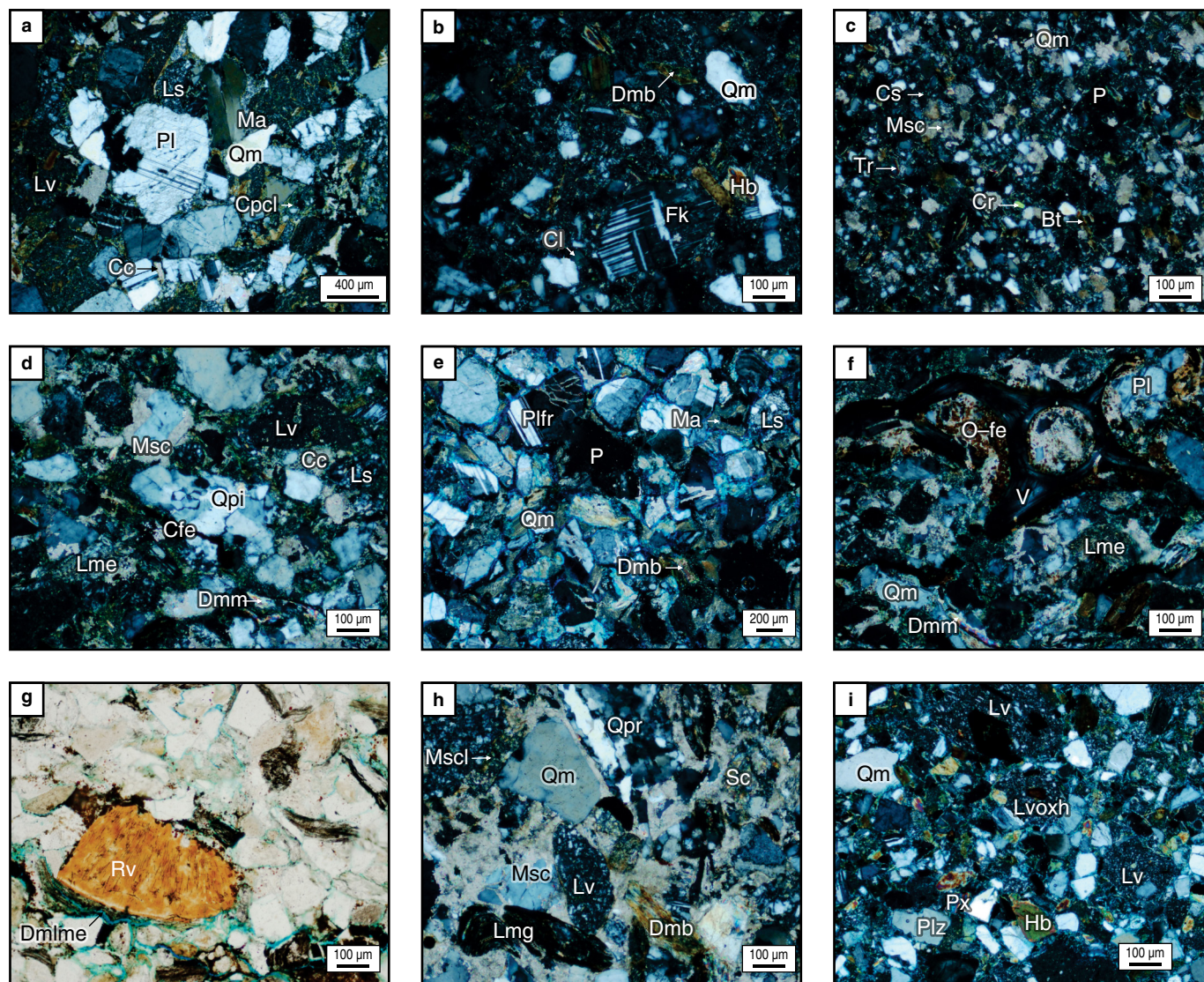


Figure 8. Photomicrographs of the studied sandstones. **(a)** Feldspathic litharenite (sample 1; Esmita Formation) with monocrystalline quartz (Qm), plagioclase (Pl), intermediate volcanic rocks (Lv), siliceous siltstone (Ls), chlorite cement (Cpcl), clay matrix (Ma), and calcareous cement (Cc); crossed nicols. **(b)** Lithic arkose (sample 3; Esmita Formation) with monocrystalline quartz (Qm), potassium feldspar (Fk), hornblende (Hb), chlorite (Cl), and deformed biotite (Dmb); crossed nicols. **(c)** Quartz arenite (sample 5; Morales Formation) composed of monocrystalline quartz (Qm), biotite (Bt), zircon (Cr), tourmaline (Tr), siliceous metasomatism by carbonates (Msc), siliceous cement (Cs), and pores (P); crossed nicols. **(d)** Litharenite (sample 6; Morales Formation) with polycrystalline quartz of igneous origin (Qpi), metamorphic schist (Lme), volcanic rocks (Lv), sedimentary rocks (Ls), mechanical deformation of muscovite (Dmm), siliceous metasomatism by carbonates (Msc), carbonate cement (Cc), and ferruginous cement (Cfe); crossed nicols. **(e)** Arkose (sample 7; Morales Formation) with monocrystalline quartz (Qm), fractured plagioclase (Plfr), sedimentary lithic fragments (Ls), deformed biotite (Dmb), clay matrix (Ma), and pores (P); crossed nicols. **(f)** Sublitharenite (sample 11; Morales Formation) with monocrystalline quartz (Qm), plagioclase (Pl), schist (Lme), mechanical deformation of muscovite (Dmm), cross sections of vertebrae (V), and iron oxides (O–fe); crossed nicols. **(g)** Immature sublitharenite (sample 11; Morales Formation) with phosphatic remains (Rv) and schists (Dmlme); parallel nicols. **(h)** Feldspathic litharenite (sample 12; Morales Formation) with monocrystalline quartz (Qm), recrystallized polycrystalline quartz (Qpr), intermediate volcanic (Lv), graphitic schists (Lmg), sericite (Sc), deformed biotite (Dmb), metasomatic silica and carbonate (Msc), and metasomatic chlorite and silica (Msc); crossed nicols. **(i)** Feldspathic litharenite (sample 15; Galeón Formation) with monocrystalline quartz (Qm), zoned plagioclase (Plz), hornblende (Hb), volcanic lithic fragments (Lv) with oxyhornblende (Lvoxh) and pyroxene (Px); crossed nicols.

maline (4%), rutile (2%), spinel (1%), muscovite (1%), and chlorite (1%) with lower proportions of hypersthene (0.3%), enstatite (0.3%), biotite (0.30%), and hornblende (0.3%) (Figure 9a).

5. Discussion

The Morales Formation accumulated in swamps, lakes, and overbank fluvial environments, under anoxic–dysoxic condi-

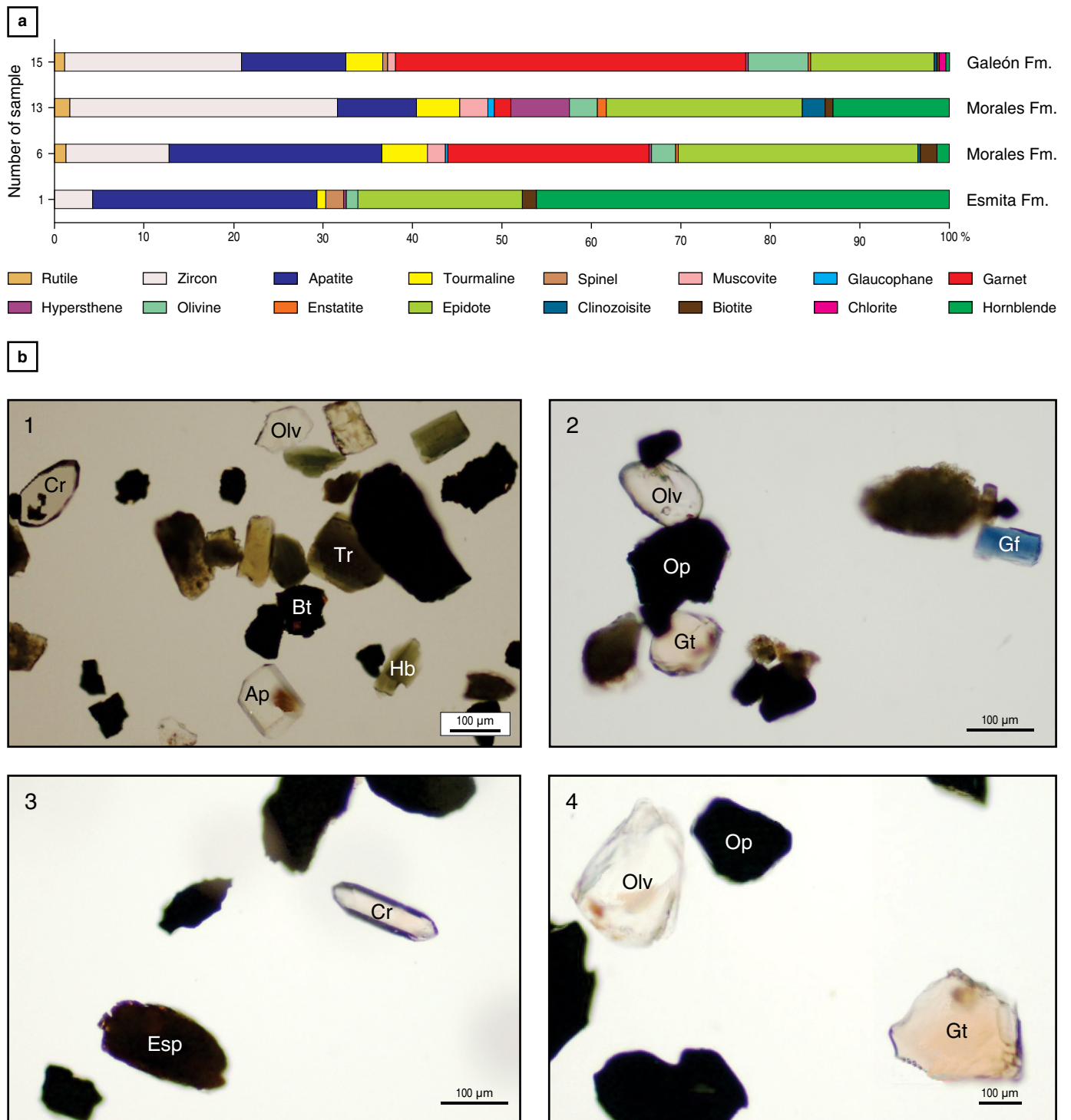


Figure 9. (a) Heavy mineral bar diagrams for the analyzed sandstones from the Morales Creek stratigraphic section. The numbers in the ordinate represent the sample codes in Figure 3. (b) Photomicrographs of the heavy mineral assemblage. (1) Sample 1 (Esmita Formation); (2) Sample 6 (Morales Formation); (3) Sample 15 (Galeón Formation); (4) Sample 15 (Galeón Formation). Abbreviations: hornblende (Hb), olivine (Olv), biotite (Bt), garnet (Gt), spinel (Esp), tourmaline (Tr), apatite (Ap), zircon (Cr), glaucofane (Gf), and opaque minerals (Op).

tions. The exclusive presence of plant debris, pollen, and spores suggests continental environments. This interpretation is further supported by the type III kerogen obtained from the pyrolysis analysis (Figure 5). The sandstones and conglomerates of the

Galeón Formation can be interpreted as fluvial braided deposits dominated by gravel and sand bars. Although the Esmita and Morales Formations have low percentages of volcanic porphyritic fragments, the Galeón Formation shows an abrupt

increase in volcanic rock fragments, glass, and crystals (Figure 3). Based on the occurrence of mainly ca. 15 Ma subhedral to euhedral zircons identified, we favor an increase in magmatic arc activity during the middle Miocene. This detrital magmatic record can be associated with the exhumation of the Neogene porphyritic subvolcanic bodies exposed along the Patía valley, which originated from the subduction of the Nazca Plate in the Colombian Pacific (Echeverri et al., 2015). Neogene magmatic rocks extend from the Western Cordillera to the Central Cordillera (Barbosa, 2003). In the lower Miocene deposits of the Upper Magdalena Valley (Honda Formation), the volcanic deposits are thinner and finer-grained than those identified in the Patía Sub–basin. This difference is probably explained by the proximity of the volcanic centers to our study area.

The sandstone petrography (conventional and heavy minerals) reveals that the sedimentites of the Esmita and Morales Formations came from multiple sources and can be related to a recycled orogen (Figure 7). The presence of glaucophane in the Morales Formation suggests a high–pressure metamorphic source, such as the Arquía Complex (Jambaló, western border of the Central Cordillera), where a $^{40}\text{Ar}/^{39}\text{Ar}$ Late Cretaceous metamorphic age was obtained for blueschists (Bustamante et al., 2011). Other minerals that can be related to metamorphic sources are epidote, clinozoisite, chlorite, muscovite, tourmaline, and eventually rutile (Figure 9). Additionally, deformed metamorphic and recrystallized metamorphic quartz grains associated with foliated rock fragments (e.g., graphitic schist) are identified (Figure 8). It is important to mention that towards the top of the studied section, the percentage of garnets increases significantly (Galeón Formation; Figure 9, sample 15). Weber et al. (2002) reported, within the Pliocene – Pleistocene volcanic deposits of the area (Mayo River), tuffs with mafic and felsic fragments (granulites, amphibolites, gneisses, hornblendites, pyriboleites, and pyroxenites) rich in garnets associated with a mantle wedge. Our data show that garnet-rich tuffs are present in this area at least from the middle Miocene.

The sedimentary and volcanic fragments can be related to the Diabásico and Dagua Groups, or alternatively to the Quebradagrande Complex (Maya & González, 1995), which crop out in the Western and Central Cordilleras, respectively (Figure 1; Gómez et al., 2015a). Pardo–Trujillo et al. (2020) mentioned that some parts of the Western Cordillera emerged during the early – middle Miocene based on petrographic and detrital zircon evidence in the neighboring Tumaco Basin (Figure 1). This result is consistent with a sedimentary and volcanic source located to the west of the basin. Nevertheless, the petrography of the volcanic and sedimentary lithic fragments of the Quebradagrande rocks are similar to these units. The potassium feldspar, biotite, zircon, tourmaline, and hornblende probably came from the Paleogene – Neogene granitoids that crop out in the Western Cordillera (Figure 9); however, the Central Cordillera basement has Triassic, Juras-

sic, and Cretaceous plutonic rocks, which makes interpretation difficult. It is also possible that some rounded grains of the ultrastable heavy mineral phases, such as apatite and zircon, were reworked from Paleogene or Cretaceous sedimentary units. A geochemical study of detrital zircons in sandstones (e.g., Hf isotopes) can help to discriminate some igneous and metamorphic sources.

Lower – middle Miocene fluvial and marine fine-grained units in NW South America have been described in several regions of Colombia (e.g., de la Parra et al., 2019; Hoorn et al., 2010; Jaramillo et al., 2017). In the Upper Magdalena Valley sector, van der Wiel & van den Bergh (1992) mentioned a fine-grained unit of 700 m–thick lacustrine–fluvial deposits in the lower part of the Honda Formation (Neiva Sub–basin). The radiometric dating of thin volcanic layers in this unit reveals K/Ar ages of 15.8 ± 0.6 Ma and 14.3 ± 0.5 Ma, which can be partially correlated with the top of the Morales Formation and the base of the Galeón Formation. Similarly, de la Parra et al. (2019), based on palynological evidence, suggested the occurrence of extensive lacustrine systems in the Middle and Upper Magdalena Valley Basins (e.g., Colorado and Barzalosa Formations). The age of these lakes can be associated with the “Pebas phase” of the Pebas system (ca. 16–11.3 Ma) in the Amazonian Basin, in which a mega wetland expanded, reaching its maximum extent (Hoorn et al., 2010).

As mentioned, the Galeón Formation concordantly overlies the Morales Formation on the axial axis of the Mercaderes Syncline. Nevertheless, the sudden change in composition of the Galeón Formation could also be related to a disconformity (Figure 2). The ca. 15.4 Ma U/Pb age obtained for the base of the Galeón Formation, which is not Pliocene as proposed by León et al. (1973) and Ruiz (2002), constrains the age of the angular unconformity that exists between the volcanoclastic Galeón and Pleistocene Mercaderes Formations (Figure 1). We suggest that this unconformity was produced during the late Miocene? – Pliocene interval (Figure 2). This unconformity can thus be compared to the angular unconformity reported between the volcanoclastic La Paila and Zarzal Formations in the northern segment of the Cauca Sub–basin, where a late Miocene – Pliocene age has been estimated (Alfonso et al., 1994; Barrero et al., 2006; López et al., 2009). However, more geochronological information is needed to solve this problem.

There is no detailed structural research in the study area. Surface geologic mapping and seismic information show that the Cauca–Patía sedimentary rocks compose part of a thick-skinned thrust and related fold system with a west vergence (Alfonso et al., 1994; Barrero & Laverde, 1998; Barrero et al., 2006). According to regional information, during the Cenozoic, the western region of Colombia experienced compression and wrench tectonics due to the ENE oblique subduction of the Farallón and Nazca Plates below the South American margin (Pardo–Casas & Molnar, 1987; Somoza & Ghidella, 2012). In

this scenario, we speculate that the subsidence that allowed the accumulation of hundreds of meters of mud-dominated sediments in the Morales Formation could have been formed in pull-apart basins associated with wrench faults.

6. Conclusions

In the Neogene deposits of the Patía Sub-basin (SW Colombia), a new unit, named the Morales Formation, is defined. It consists of a sedimentary succession with a thickness of 470 m, composed mainly of gray-black mudstones with some intercalations of thin sandstone beds, interpreted as lake, swamp, and overbank deposits accumulated in fluvial systems. The data presented in this work linked to the regional geology of the Llanos and the Middle and Upper Magdalena Valley Basins suggest the occurrence of extensive lacustrine systems in the Colombian intramontane basins during the early Miocene.

The ca. 15 Ma (zircon U/Pb) age obtained for the basal strata of the Galeón Formation is interpreted as the onset of intense volcanic activity in the Patía Sub-basin. Thus, the Galeón Formation is older than had been considered in the geological literature. These data and the new palynologic information indicate a Burdigalian – early Langhian (ca. 19–15 Ma) age for the Morales Formation.

The studied sandstones are litharenites, feldspathic litharenites, sublitharenites, arkoses, and lithic arkoses. Their components were derived from sedimentary, metamorphic, plutonic, and volcanic rocks associated with the Western and Central Cordilleras. With the current state of knowledge, it is difficult to discriminate the provenances of the sediments. Some of them (e.g., glaucofane and probably garnet) can be associated with the basement of the Central Cordillera.

Acknowledgments

We thank the Universidad de Caldas and the Agencia Nacional de Hidrocarburos for their financial support (contract 092 of 2009). Thanks to geologists Juan Sebastián ROSE-RO and Diana OCHOA for their advice. Professor Agustín CARDONA (Universidad Nacional de Colombia Sede Medellín) helped us in the preparation and identification of heavy minerals. Special thanks to the staff of the Instituto de Investigaciones en Estratigrafía (Universidad de Caldas) for their technical and logistical support, especially to Edward OSORIO and Juan Pablo BETANCUR. We give special thanks to Jorge GÓMEZ TAPIAS (Servicio Geológico Colombiano) for his help during the translation and editing of this chapter. We thank the reviewers and editor for the comments that improved this manuscript. The Fundación Carolina supported Andrés PARDO-TRUJILLO with a postdoctoral stay in Salamanca (Spain, 2018) for the finalization of this

document. Andrés PARDO-TRUJILLO especially thanks the scientific and technical staff of the Universidad de Salamanca for their hospitality and support, especially professor and friend José Abel FLORES.

References

- Alfonso, C.A., Sacks, P.E., Secor, D.T., Rine, J. & Perez, V. 1994. A Tertiary fold and thrust belt in the Valle del Cauca Basin, Colombian Andes. *Journal of South American Earth Sciences*, 7(3–4): 387–402. [https://doi.org/10.1016/0895-9811\(94\)90023-X](https://doi.org/10.1016/0895-9811(94)90023-X)
- Barbosa, G. 2003. Memoria explicativa: Mapa geológico del departamento del Cauca. Scale 1:250 000. Ingeominas, 221 p. Santiago de Cali, Colombia.
- Barrero, D. & Laverde, F. 1998. Estudio integral de evaluación de la geología y potencial de hidrocarburos de la cuenca “intramontana” Cauca–Patía. Ecopetrol, Internal report 4977, 83 p. Bogotá.
- Barrero, D., Laverde, F., Ruiz, C.C. & Alfonso, C.A. 2006. Oblique collision and basin formation in western Colombia: The origin, evolution and petroleum potential of Cauca–Patía Basin. IX Simposio Bolivariano de Exploración Petrolera en las Cuencas Subandinas. Proceedings in CD room, p. 1–13 p. Cartagena, Colombia.
- Blanco-Quintero, I.F., García-Casco, A., Toro, L.M., Moreno-Sánchez, M., Ruiz, E.C., Vinasco, C.J., Cardona, A., Lázaro, C. & Morata, D. 2014. Late Jurassic terrane collision in the northwestern margin of Gondwana (Cajamarca Complex, eastern flank of the Central Cordillera, Colombia). *International Geology Review*, 56(15): 1852–1872. <https://doi.org/10.1080/00206814.2014.963710>
- Borrero, C., Pardo, A., Jaramillo, C.M., Osorio, J.A., Cardona, A., Flores, A., Echeverri, S., Rosero, S., García, J. & Castillo, H. 2012. Tectonostratigraphy of the Cenozoic Tumaco Forearc Basin (Colombian Pacific) and its relationship with the northern Andes orogenic build up. *Journal of South American Earth Sciences*, 39: 75–92. <https://doi.org/10.1016/j.jsames.2012.04.004>
- Bustamante, A., Juliani, C., Hall, C.M. & Essene, E.J. 2011. $^{40}\text{Ar}/^{39}\text{Ar}$ ages from blueschists of the Jambaló region, Central Cordillera of Colombia: Implications on the styles of accretion in the northern Andes. *Geologica Acta*, 9(3–4): 351–362. <https://doi.org/10.1344/105.000001697>
- Corfu, F., Hanchar, J.M., Hoskin, P.W.O. & Kinny, P. 2003. Atlas of zircon textures. *Reviews in Mineralogy and Geochemistry*, 53(1): 469–500. <https://doi.org/10.2113/0530469>
- de la Parra, F., Pinzón, D., Rodríguez, G., Bedoya, O. & Benson, R. 2019. Lacustrine systems in the early Miocene of northern South America: Evidence from the Upper Magdalena Valley, Colombia. *Palaaios*, 34(10): 490–505. <https://doi.org/10.2110/palo.2019.025>

- Dickinson, W.R., Beard, L.S., Brackenridge, G.R., Erjavec, J.L., Ferguson, R.C., Inman, K.F., Knepp, R.A., Lindberg, F.A. & Ryberg, P.T. 1983. Provenance of North American Phanerozoic sandstones in relation to tectonic setting. *Geological Society of America Bulletin*, 94(2): 222–235. [https://doi.org/10.1130/0016-7606\(1983\)94<222:PONAPS>2.0.CO;2](https://doi.org/10.1130/0016-7606(1983)94<222:PONAPS>2.0.CO;2)
- Echeverri, S., Cardona, A., Pardo, A., Monsalve, G., Valencia, V.A., Borrero, C., Rosero, S. & López, S. 2015. Regional provenance from southwestern Colombia fore–arc and intra–arc basins: Implications for middle to late Miocene orogeny in the northern Andes. *Terra Nova*, 27(5): 356–363. <https://doi.org/10.1111/ter.12167>
- Einsele, G. 2000. Sedimentary basins. Evolution, facies, and sediment budget, 2nd edition. Springer–Verlag, 792 p. Berlin, Germany. <https://doi.org/10.1007/978-3-662-04029-4>
- Folk, R.L. 1974. Petrology of sedimentary rocks. Hemphill Publishing Company, 182 p. Austin, USA.
- Geostudios. 2008. Levantamiento de columnas estratigráficas y realización de análisis petrográficos, petrofísicos, bioestratigráficos y geoquímicos en las áreas de Pasto–El Bordo, Cali–Buga y Buga–Cartago (Cuenca Cauca–Patía). ANH, unpublished report, 382 p. Bogotá.
- Gómez, J., Montes, N.E., Nivia, Á. & Diederix, H., compilers. 2015. Geological Map of Colombia 2015. Scale 1:1 000 000. Servicio Geológico Colombiano, 2 sheets. Bogotá. <https://doi.org/10.32685/10.143.2015.936>
- Gómez, J., Nivia, Á., Montes, N.E., Diederix, H., Almanza, M.F., Alcárcel, F.A. & Madrid, C.A. 2015b. Explanatory notes: Geological Map of Colombia. In: Gómez, J. & Almanza, M.F. (editors), *Compilando la geología de Colombia: Una visión a 2015*. Servicio Geológico Colombiano, Publicaciones Geológicas Especiales 33, p. 35–60. Bogotá.
- González, H. 2010. Geoquímica, geocronología de las unidades litológicas asociadas al Sistema de Fallas Cauca–Romerol, sector centro–sur. Tomo I. Ingeominas, unpublished report, 412 p. Medellín.
- Grosse, E. 1935. Acerca de la geología del sur de Colombia II: Informe rendido al Ministerio de Industrias sobre un viaje por la cuenca del Patía y el departamento de Nariño. *Compilación de los Estudios Geológicos Oficiales en Colombia, III*: 139–231. Bogotá.
- Hoorn, C., Wesselingh, F.P., ter Steege, H., Bermúdez, M.A., Mora, A., Sevink, J., Sanmartín, I., Sánchez–Meseguer, A., Anderson, C.L., Figueiredo, J.P., Jaramillo, C., Riff, D., Negri, F.R., Hooghiemstra, H., Lundberg, J., Stadler, T., Särkinen, T. & Antonelli, A. 2010. Amazonia through time: Andean uplift, climate change, landscape evolution, and biodiversity. *Science*, 330(6006): 927–931. <https://doi.org/10.1126/science.1194585>
- Ingersoll, R.V., Bullard, T.F., Ford, R.L., Grimm, J.P., Pickle, J.D. & Sares, S.W. 1984. The effect of grain size on detrital modes: A test of the Gazzi–Dickinson point–counting method. *Journal of Sedimentary Research*, 54(1): 103–116. <https://doi.org/10.1306/212F83B9-2B24-11D7-8648000102C1865D>
- Instituto Geográfico Agustín Codazzi. 2005. Carta general, plancha 386 Mercaderes. Scale 1:100 000. Bogotá.
- Jaramillo, C., Rueda, M. & Torres, V. 2011. A palynological zonation for the Cenozoic of the Llanos and Llanos Foothills of Colombia. *Palynology*, 35(1): 46–84. <https://doi.org/10.1080/01916122.2010.515069>
- Jaramillo, C., Romero, I., D’Apolito, C., Bayona, G., Duarte, E., Louwye, S., Escobar, J., Luque, J., Carrillo–Briceno, J., Zapata, V., Mora, A., Schouten, S., Zavada, M., Harrington, G., Ortiz, J. & Wesselingh, F. 2017. Miocene flooding events of western Amazonia. *Science Advances*, 3(5): 1–11. <https://doi.org/10.1126/sciadv.1601693>
- Kerr, A.C., Marriner, G.F., Tarney, J., Nivia, Á., Saunders, A.D., Thirlwall, M.F. & Sinton, C.W. 1997. Cretaceous basaltic terranes in western Colombia: Elemental, chronological and Sr–Nd isotopic constraints on petrogenesis. *Journal of Petrology*, 38(6): 677–702. <https://doi.org/10.1093/petrology/38.6.677>
- Kerr, A.C., Tarney, J., Nivia, Á., Marriner, G.F. & Saunders, A.D. 1998. The internal structure of oceanic plateaus: Inferences from obducted cretaceous terranes in western Colombia and the Caribbean. *Tectonophysics*, 292(3–4): 173–188. [https://doi.org/10.1016/S0040-1951\(98\)00067-5](https://doi.org/10.1016/S0040-1951(98)00067-5)
- León, L.A., Padilla, L.E. & Marulanda, N. 1973. Geología, recursos minerales y geoquímica de la parte NE del cuadrángulo 0–5 El Bordo, departamento del Cauca. Ingeominas, Internal report 1652, 235 p. Popayán.
- López, M.C., Moreno–Sánchez, M., Toro, L.M., Bedoya, E., Castaño, L., Cifuentes, P., Giraldo, D., Gómez, A., Gómez, N., Betancur, Y. & Ruiz, E. 2009. Estratigrafía de la Formación La Paila, un potencial reservorio de hidrocarburos en la Cuenca Cauca–Patía. Agencia Nacional de Hidrocarburos & Universidad de Caldas, unpublished report, 319 p. Bogotá.
- Mange, M.A. & Maurer, H.F.W. 1992. Heavy minerals in colour. Chapman & Hall, 147 p. London, UK. <https://doi.org/10.1007/978-94-011-2308-2>
- Martínez, J., Pardo–Trujillo, A. & Plata, A. 2013. Palinología del Mioceno inferior en depósitos fluvio–lacustres de la Subcuenca Patía (Formación Morales, SW Colombia). Universidad de Caldas, unpublished report, 14 p. Manizales, Colombia.
- Maya, M. & González, H. 1995. Unidades litodémicas en la cordillera Central de Colombia. *Boletín Geológico*, 35(2–3): 43–57.
- Miall, A.D. 2006. The geology of fluvial deposits. Sedimentary facies, basin analysis, and petroleum geology. 4th corrected printing. Springer, 582 p. Berlin, Germany. <https://doi.org/10.1007/978-3-662-03237-4>
- Moreno–Sánchez, M. & Pardo–Trujillo, A. 2003. Stratigraphical and sedimentological constraints on western Colombia: Implications on the evolution of the Caribbean Plate. In: Bartolini, C., Buffler, R.T. & Blickwede, J. (editors), *The circum–Gulf of Mexico and the Caribbean: Hydrocarbon habitats, basin formation, and plate tectonics*. American Association of Petroleum Geologists, Memoir 79, p. 891–924. Tulsa, USA.

- Murcia, A., Orrego, A. & Pérez, G. 1981. Geologic reconnaissance of the southernmost Cauca–Patía depression. 20th Field Conference, guide book. Colombian Society of Petroleum Geologists and Geophysicists, 62 p. Bogotá.
- Murphy, M.A. & Salvador, A. 1999. International Stratigraphic Guide: An abridged version. *Episodes*, 22(4): 255–271.
- Nivia, Á. 2001. Memoria explicativa: Mapa geológico del departamento del Valle del Cauca. Scale 1:250 000. Ingeominas, 148 p. Bogotá.
- Orrego, A., París, G., Ibáñez, D. & Vásquez, E. 1996. Memoria explicativa: Geología y geoquímica de la plancha 387 Bolívar. Scale 1:100 000. Ingeominas, Internal report 2196, 170 p. Popayán.
- Pardo–Casas, F. & Molnar, P. 1987. Relative motion of the Nazca (Farallón) and South American Plates since Late Cretaceous time. *Tectonics*, 6(3): 233–248. <https://doi.org/10.1029/TC006i003p00233>
- Pardo–Trujillo, A., Moreno–Sánchez, M. & Gómez, A.d.J. 2002. Estratigrafía de algunos depósitos del Cretáceo Superior en las cordilleras Central y Occidental de Colombia: implicaciones regionales. *Geo–Eco–Trop*, 26 (2): 1–113.
- Pardo–Trujillo, A., Echeverri, S., Borrero, C., Arenas, A., Vallejo, F., Trejos, R., Plata, Á., Flores, J.A., Cardona, A., Restrepo, S., Barbosa, Á., Murcia, H., Giraldo, C., Celis, S. & López, S.A. 2020. Cenozoic geologic evolution of the southern Tumaco Forearc Basin (SW Colombian Pacific). In: Gómez, J. & Mateus–Zabala, D. (editors), *The Geology of Colombia*, Volume 3 Paleogene – Neogene. Servicio Geológico Colombiano, Publicaciones Geológicas Especiales 37, p. 215–247 Bogotá. <https://doi.org/10.32685/pub.esp.37.2019.08>
- Patacci, M. 2016. A high–precision Jacob’s staff with improved spatial accuracy and laser sighting capability. *Sedimentary Geology*, 335: 66–69. <https://doi.org/10.1016/j.sed-geo.2016.02.001>
- Pindell, J.L. & Kennan, L. 2009. Tectonic evolution of the Gulf of Mexico, Caribbean and northern South America in the mantle reference frame: An update. In: James, K.H., Lorente, M.A. & Pindell, J.L. (editors), *The origin and evolution of the Caribbean Plate*. Geological Society of London, Special Publications 328, p. 1–55. <https://doi.org/10.1144/SP328.1>
- Potter, P.E., Maynard, J.B. & Depetris, P.J. 2005. *Mud and mudstones: Introduction and overview*. Springer, 297 p. Berlin, Germany. <https://doi.org/10.1007/b138571>
- Rodríguez, G. & Arango, M.I. 2013. Formación Barroso: Arco volcánico toleítico y diabasas de San José de Urama: Un prisma acrecionario T–MORB en el segmento norte de la cordillera Occidental de Colombia. *Boletín de Ciencias de la Tierra*, (33): 17–38.
- Ruiz, S. 2002. Memoria explicativa: Geología de la plancha 386 Mercaderes. Scale 1:100 000. Ingeominas, 62 p. Bogotá.
- Somoza, R. & Ghidella, M.E. 2012. Late Cretaceous to recent plate motions in western South America revisited. *Earth and Planetary Science Letters*, 331–332: 152–163. <https://doi.org/10.1016/j.epsl.2012.03.003>
- Traverse, A. 2007. *Paleopalynology*. 2nd edition. Springer, 813 p. Dordrecht, The Netherlands. <https://doi.org/10.1007/978-1-4020-5610-9>
- van der Hammen, T. 1958. Estratigrafía del terciario y Maestrichtiano continentales y tectogénesis de los Andes Colombianos. *Boletín Geológico*, 6(1–3): 67–128.
- van der Wiel, A.M. & van den Bergh, G.D. 1992. Uplift, subsidence, and volcanism in the southern Neiva Basin, Colombia, Part 1: Influence on fluvial deposition in the Miocene Honda Formation. *Journal of South American Earth Sciences*, 5(2): 153–173. [https://doi.org/10.1016/0895-9811\(92\)90036-X](https://doi.org/10.1016/0895-9811(92)90036-X)
- Vermeesch, P. 2013. Multi–sample comparison of detrital age distributions. *Chemical Geology*, 341: 140–146. <https://doi.org/10.1016/j.chemgeo.2013.01.010>
- Villagómez, D., Spikings, R., Magna, T., Kammer, A., Winkler, W. & Beltrán, A. 2011. Geochronology, geochemistry and tectonic evolution of the Western and Central Cordilleras of Colombia. *Lithos*, 125(3–4): 875–896. <https://doi.org/10.1016/j.lithos.2011.05.003>
- Weber, M.B.I., Tarney, J., Kempton, P.D. & Kent, R.W. 2002. Crustal make–up of the northern Andes: Evidence based on deep crustal xenolith suites, Mercaderes, SW Colombia. *Tectonophysics*, 345(1–4): 49–82. [https://doi.org/10.1016/S0040-1951\(01\)00206-2](https://doi.org/10.1016/S0040-1951(01)00206-2)

Explanation of Acronyms, Abbreviations, and Symbols:

ANH	Agencia Nacional de Hidrocarburos	LA–ICP–MS	Laser ablation inductively coupled plasma
HI	Hydrogen index		mass spectrometry
IIES	Instituto de Investigaciones en Estratigrafía	TAI	Thermal alteration index
		TOC	Total organic carbon

Authors' Biographical Notes



Andrés F. GALLEGO-RÍOS is geologist of the Departamento de Ciencias Geológicas at Universidad de Caldas (Manizales, 2012). He has worked as geologist in different geological consulting companies, executing local and regional stratigraphic and tectonic projects. He has also worked as a geologist describing well cores from several basins in Colombia.



Andrés PARDO-TRUJILLO is a geologist in the Departamento de Ciencias Geológicas at the Universidad de Caldas (Manizales, 1998). Andrés obtained his MS in vegetal micropaleontology in 1997 and his PhD in Science from Liège University (Belgium, 2004). He has worked since 1989 as a professor in the Departamento de Ciencias Geológicas at Universidad de Caldas, Colombia, in sedimentology, regional geology, palynology, and field geology. From 2006–2009, he worked as an advisor at the Agencia Nacional de Hidrocarburos (ANH), where he participated in the geological study of several Colombian sedimentary basins. Andrés is currently the director of the Instituto de Investigaciones en Estratigrafía (IIES) and of the Grupo de Investigación en Estratigrafía y Vulcanología (GIEV) at the Universidad de Caldas. His main interest is the study of the geological

and biological evolution of the NW corner of South America during the Cretaceous – Cenozoic.



Guillermo A. LÓPEZ-PLAZAS is geologist of the Departamento de Ciencias Geológicas at Universidad de Caldas (Manizales, 2012). He has worked as a geologist for different geological consulting companies. He has also worked as a well logger and geologist in several basins of Colombia.



Sebastián ECHEVERRI is a geologist from the Universidad de Caldas, with an MS in Earth sciences from the same university and PhD in science and geotectonics from the Universidade de São Paulo, Brasil. Sebastián works as a researcher in the Grupo de Investigación en Estratigrafía y Vulcanología (GIEV) Cumanday–Instituto de Investigaciones en Estratigrafía (IIES) at the Universidad de Caldas and is part of the EGEO research group at the Universidad Nacional Sede Medellín. His main research area is the regional geology and tectonostratigraphic evolution of convergent margins.

Chapter 14



New Contributions to Knowledge about the Chocó–Panamá Arc in Colombia, Including a New Segment South of Colombia

<https://doi.org/10.32685/pub.esp.37.2019.14>

Published online 5 June 2020

Gilberto ZAPATA–GARCÍA^{1*} and Gabriel RODRÍGUEZ–GARCÍA²

Abstract Geological mapping and petrographic, lithogeochemical, and geochronologic analyses show that the volcanic rocks and plutons that constitute the Chocó–Panamá Arc are segmented into three sectors: North (Santa Cecilia–La Equis Complex and Acandí Batholith); Central (Santa Cecilia–La Equis Complex and Mandé Batholith); and South (Timbiquí Formation and Napi Tonalite). In this study we include the South segment, which was not considered part of the Chocó–Panamá Arc in previous studies. This magmatism occurred during the Eocene (Ypresian Stage). The rocks of the Santa Cecilia–La Equis Complex and the Timbiquí Formation are constituted of basalts and andesites interbedded with pyroclastic facies of tuffs and agglomerates. These are subalkaline and plot in the tholeiitic–normal calc–alkaline series. The Acandí Batholith presents two granitic facies: the main facies is a tonalite–granodiorite–quartz diorite, and the secondary is a gabbro–diorite, located towards the edges of the intrusive. Both are metaluminous subalkaline, low potassium tholeiitic, and medium potassium calc–alkaline. The Mandé Batholith is constituted by tonalites and quartz diorites, with porphyritic facies near the Santa Cecilia–La Equis Complex. These rocks are subalkaline within the tholeiitic series. The Chocó–Panamá Arc in the Central segment is limited by the recent sediments of the Atrato River, on the west, and by tectonic boundaries such as the Dabeiba–Pueblo Rico and the Amurrapá Faults, on the east, which separate this block from the accreted oceanic sequences with oceanic plateau geochemical affinities. The South segment is a tectonic block in contact with the Dagua Structural Complex, bounded by Piedramadura Fault. According to the ages obtained in this study, and by other authors using K–Ar, Ar–Ar, and U–Pb dating, the Chocó–Panamá Arc magmatism in Colombia occurred between 56.5 and 37 Ma.

Keywords: northwest South America, Western Cordillera, lithogeochemistry, geochronology.

Resumen La cartografía geológica y los análisis petrográficos, litogeoquímicos y geocronológicos muestran que las vulcanitas y plutones que conforman el Arco Chocó–Panamá comprenden tres segmentos: Norte (Complejo Santa Cecilia–La Equis y Batolito de Acandí), Central (Complejo Santa Cecilia–La Equis y Batolito de Mandé) y Sur (Formación Timbiquí y Tonalita de Napi). En este trabajo incluimos el segmento Sur, que en estudios anteriores no se consideró como parte del Arco Chocó–Panamá. Este magmatismo ocurrió durante el Eoceno (Ypresiano). Las rocas del Complejo Santa Cecilia–La Equis y de la Formación Timbiquí son basaltos y andesitas intercaladas con

- 1 gilbertozapatag@yahoo.com
Servicio Geológico Colombiano
Dirección de Geociencias Básicas
Grupo de Estudios Geológicos Especiales
Calle 24A n.º 50A–31
Bello, Antioquia, Colombia
- 2 grodriguez@sgc.gov.co
Servicio Geológico Colombiano
Dirección de Geociencias Básicas
Grupo de Estudios Geológicos Especiales
Calle 75 n.º 79A–51
Medellín, Colombia

* Corresponding author

Supplementary Information:

S: <https://www2.sgc.gov.co/LibroGeologiaColombia/tgc/sgcpubesp37201914s.pdf>

Citation: Zapata–García, G. & Rodríguez–García, G. 2020. New contributions to the knowledge about the Chocó–Panamá Arc in Colombia, including a new segment south of Colombia. In: Gómez, J. & Mateus–Zabala, D. (editors), *The Geology of Colombia, Volume 3 Paleogene – Neogene*. Servicio Geológico Colombiano, *Publicaciones Geológicas Especiales* 37, p. 417–450. Bogotá. <https://doi.org/10.32685/pub.esp.37.2019.14>

facies piroclásticas de tobas y aglomerados. Estas rocas son subalcalinas y se grafican en los campos de las series toleítica y calcoalcalina normales. El Batolito de Acandí presenta dos facies graníticas: una principal tonalita–granodiorita–cuarzodiorita y la segunda gabro–diorita, que se encuentra hacia los bordes del cuerpo intrusivo. Ambas facies son subalcalinas metaluminosas de la serie toleítica baja en potasio y calcoalcalina con contenido medio de potasio. El Batolito de Mandé está constituido por tonalitas y cuarzodioritas, con facies porfídicas hacia los contactos con el Complejo Santa Cecilia–La Equis. Estas rocas son subalcalinas de la serie toleítica. En el segmento Central, el Arco Chocó–Panamá está limitado, al occidente, por sedimentos recientes del río Atrato y, al oriente, por límites tectónicos como las fallas de Dabeiba–Pueblo Rico y Amurrapá, que separan este bloque de las secuencias oceánicas acrecionadas con afinidades geoquímicas de meseta oceánica (*plateau*). El segmento Sur es un bloque tectónico en contacto con el Complejo Estructural Dagua, limitado por la Falla de Piedramadura. De acuerdo con las edades obtenidas en este estudio, y por otros autores que usaron los métodos K–Ar, Ar–Ar y U–Pb, el magmatismo del Arco Chocó–Panamá en Colombia ocurrió entre 56,5 y 37 Ma.

Palabras clave: noroccidente de Suramérica, cordillera Occidental, litogeoquímica, geocronología.

1. Introduction

We present new petrographic, lithogeochemical, and geochronological data for the Chocó–Panamá Arc in Colombia. A new block is included, named the South segment (Figure 1), which had not been mentioned in previous studies.

The Chocó–Panamá Arc is exposed west of the Colombian Western Cordillera and is a Late Cretaceous – Eocene plutonic–volcanic arc of tholeiitic to calc–alkaline affinity, consisting of basaltic and andesitic lavas that are associated with plutons of dominantly tonalitic composition (Duque–Caro, 1990; Pindell, 1993).

Previous geological studies have used different names to describe the blocks that compose the Colombian northwestern Andes, including units from different geotectonic environments that lack clear spatiotemporal relationships. Etayo–Serna et al. (1983) grouped the Santa Cecilia–La Equis Complex and the Mandé Batholith in the Cañasgordas Terrane and the Timbiquí Formation and the Napi Tonalite in the Dagua Terrane. Restrepo & Toussaint (1989) defined the Cuna Terrane and included the Mandé Batholith. Duque–Caro (1990) grouped the Dabeiba and Baudó Arcs, the Istmina deformed zone, and the Atrato–Chucunaque Basins in the Chocó Block. Salazar et al. (1991) suggested grouping the Santa Cecilia and La Equis Formations (Calle & Salinas, 1986) and the Mandé Batholith into the Santa Cecilia–La Equis Complex. González (2001) proposed that the Santa Cecilia–La Equis Complex should include only the basic volcanic rocks, excluding the intrusive bodies (e.g., the Mandé Batholith). In this study, the Chocó–Panamá Arc is considered a block outside the Cuna Terrane.

This research reviews the current knowledge about the Chocó–Panamá Arc, describes its different segments, and shows

the petrographic, lithogeochemical, and geochronological characteristics of the three segments of the arc: (1) North: Santa Cecilia–La Equis Complex and Acandí Batholith; (2) Central: Santa Cecilia–La Equis Complex and Mandé Batholith; and (3) South: Timbiquí Formation and Napi Tonalite (Figure 1). Data from Panamá to the border with Ecuador are compared and integrated, and new petrographic, lithogeochemical, and Ar–Ar radiometric data are presented in order to define the characteristics of the Chocó–Panamá Arc.

2. Geological Framework

The interaction of the Nazca, Cocos, Caribbean, and South American Plates has shaped the geological configuration of western Colombia. Buchs et al. (2010), Barat et al. (2014), Molnar & Sykes (1969), Montes et al. (2012), Pindell (1993), and Pindell & Kennan (2009) consider that the triple junction among the plates began in the Campanian and lasted until the early Oligocene, marked by the termination of magmatism in the Chocó–Panamá Block.

The Western Cordillera constitutes accreted allochthonous terranes composed of Upper Cretaceous – Eocene volcanic and plutonic rocks, which originally formed in oceanic plateau and oceanic arc environments and collided with the South American continental margin (Echeverri et al., 2015; Kerr et al., 1997; Montes et al., 2012; Pindell et al., 1988, 2005; Pindell & Kennan, 2009; Rodríguez & Zapata, 2013; Toussaint, 1996; Vilagómez et al., 2011).

The Chocó–Panamá Arc is exposed along the western foothills of the Western Cordillera and is bounded by recent sediments to the west and regional fault systems to the east, including the Dabeiba–Pueblo Rico Fault System. The latter

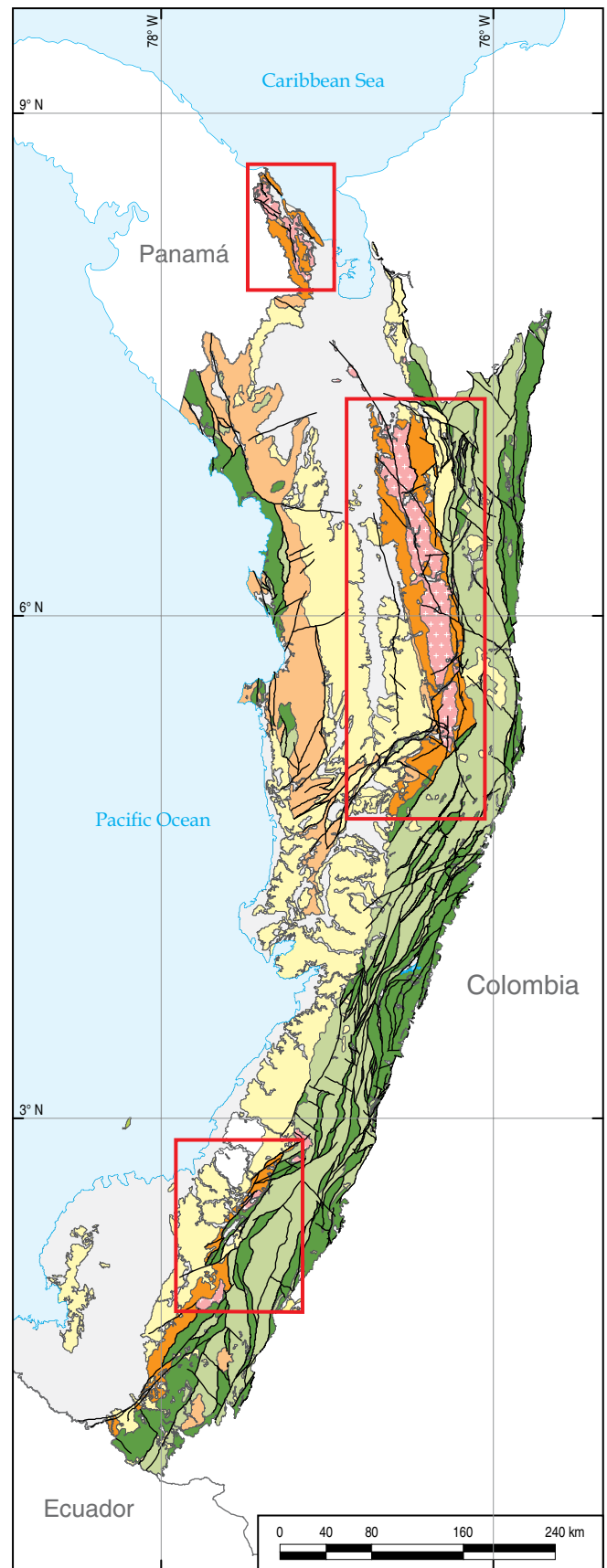
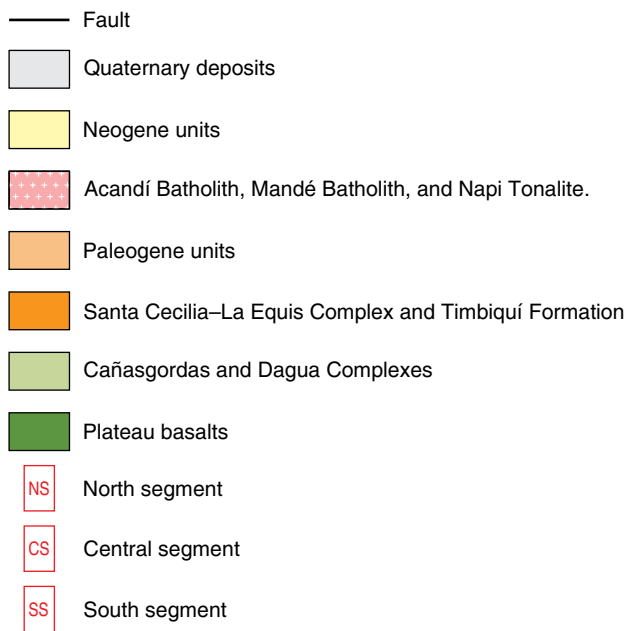


Figure 1. Chocó–Panamá Arc segments in Colombia. Modified from Gómez et al. (2015a).

fault serves as the regional fundamental boundary with the Cretaceous volcanic rocks of the Cañasgordas Group.

In Colombia, the Chocó–Panamá Arc basement is composed of rocks with plateau geochemical affinities (this study), similar to the basement rocks in Panamá (Buchs et al., 2010; Montes et al., 2012). The basaltic rocks with oceanic affinity have been named the Diabasic Group (Barrero, 1979; Nelson, 1962) and/or Volcanic Formation (Aspden, 1984) to the south of the cordillera, La Trinidad Basalts in the central zone (Parra, 1983), and the Barroso Formation to the north (Álvarez & González, 1978). In this work, the nomenclature proposed by Rodríguez & Arango (2013), in which the San José de Urama Diabase (oceanic crust) is separated from the Barroso Formation (arc volcanic rocks), is used.

Oceanic plateau sequences of the Western Cordillera are generally considered Late Cretaceous (ca. 90 Ma) in age (e.g., Kerr et al., 1997; Nivia, 2001; Rodríguez & Arango, 2013; Villagómez et al., 2011; Weber et al., 2015), but recent regional studies suggest a much broader, still poorly defined age range (Kerr et al., 1997; Nivia, 1996, 1998, 2001; Villagómez et al., 2011; Rodríguez & Arango, 2013; Weber et al., 2015). Additionally, El Palmar Gabbro (with oceanic plateau geochemical affinity) was dated at 100 Ma (Villagómez, 2010), and Whattam & Stern (2015) compiled the Ar–Ar and U–Pb ages published by Kerr et al. (1997), Villagómez (2010), and Serrano et al. (2011), which range from 100 to 81 Ma, suggesting the presence of older rocks in the Western Cordillera.

On top of the basalts with oceanic affinity (plateau), a tholeiitic to calc–alkaline arc was emplaced (the Barroso–Sabanalarga Arc) (Rodríguez & Arango, 2013), constituting basalts, andesites, tuffs, and volcanic breccias, which are intruded by gabbroic to tonalitic plutons with ages between 103 and 83 Ma (Correa et al., 2017; Rodríguez et al., 2012; Rodríguez & Arango, 2013). According to Zapata–Villada et al. (2017), the accretion of the oceanic units to the South American continent occurred after 86 Ma.

Upper Cretaceous turbiditic sedimentary sequences composed of discontinuous fault–bounded belts of stretched rhomboid-shaped assemblages of mudstones, wackes, sandstones, cherts, conglomerates, limestones, tuffs, and volcanic breccias with superimposed dynamic deformation were deposited atop this basement. These rocks are the Dagua Complex in the south (Nivia, 2001) and the Penderisco Formation in the north (Álvarez & González, 1978).

The Chocó–Panamá Arc in Colombia is composed of basaltic to andesitic volcanic rocks and intermediate plutonic rocks, which are divided into three segments.

The Northern segment includes La Iguana, Tripogadí, and Darién highlands in Colombia, extending into Panamá and forming the oroclinal curvature in the San Blas Range. The areas present volcanic rocks of basic to intermediate composition (the Santa Cecilia–La Equis Complex) exposed in two elongated belts parallel to the cordillera, including the Acandí Batholith (Figure 2).

The Central segment extends from the Aguasal–Amurrapá Fault in the south (Arboleda et al., 2009) to the alluvial sediments of the Atrato River in the north and west, bordering the plateau basalts (Cañasgordas Block) along the Dabeiba–Pueblo Rico Fault (Rodríguez et al., 2010a) in the east. This segment is composed of the Santa Cecilia–La Equis Complex, which is exposed as strips on both sides of the Mandé Batholith (Figure 3). These units were intruded in the Miocene by arc plutons with ages between 12 and 9 Ma (Nudillales Monzonite, Carauta Monzodiorite, and Valle de Pérdidas Quartz diorite) and volcanic rocks of alkaline affinity related to El Botón Arc (Rodríguez & Zapata, 2012; Zapata & Rodríguez, 2011).

The southern segment is a tectonic block exposed in Guapi (Cauca Department) that buttresses the Dagua Structural Complex along the Piedramadura Fault on the southwestern slope of the cordillera (Geología Regional y Prospección Ltd., 2014a, 2014b, 2014c). This segment includes the middle Eocene – Oligocene volcano–sedimentary rocks from the Timbiquí Formation (Annells et al., 1988), exposed in a belt that trends northeast, which is intruded by the Napi Tonalite and the Munchica Gabbro (Figure 4). The volcanic rocks of the Timbiquí Formation have been considered an andesitic sequence of subaerial volcanism possibly formed in an area near a continental margin in the emerging part of an arc (Geología Regional y Prospección Ltd., 2014b, 2014c).

3. Materials and Methods

Data from several regional mapping projects associated with contracts signed by the Servicio Geológico Colombiano (SGC) and the Agencia Nacional de Hidrocarburos (ANH) and from published articles were compiled to characterize the origins of the three segments that constitute the Chocó–Panamá Arc. Thin sections from the Central segment were revised, databases were organized by lithological units, and samples were georeferenced, including petrographic, geochemical, and geochronological descriptions. The analysis and interpretation of the results were conducted for each unit and segment, excluding the alkaline samples from El Botón Arc. Finally, the data supporting this chapter are presented in Tables 1 to 12 of the Supplementary Information.

3.1. Petrography

New petrographic analyses, data from previous SGC projects and maps from plates 319, 341, and 363 of the ANH (Geología Regional y Prospección Ltd., 2014a, 2014b, 2014c) were considered.

The petrographic description of the Santa Cecilia–La Equis Complex in the North and Central segments was based on 302 petrographic analyses: 24 from the North segment by Rodríguez et al. (2010b) and 279 from the Central segment, including 55 from Buchely et al. (2009). To describe the Acandí Batholith, 51 thin sections from Rodríguez et al. (2010b) were reanalyzed.

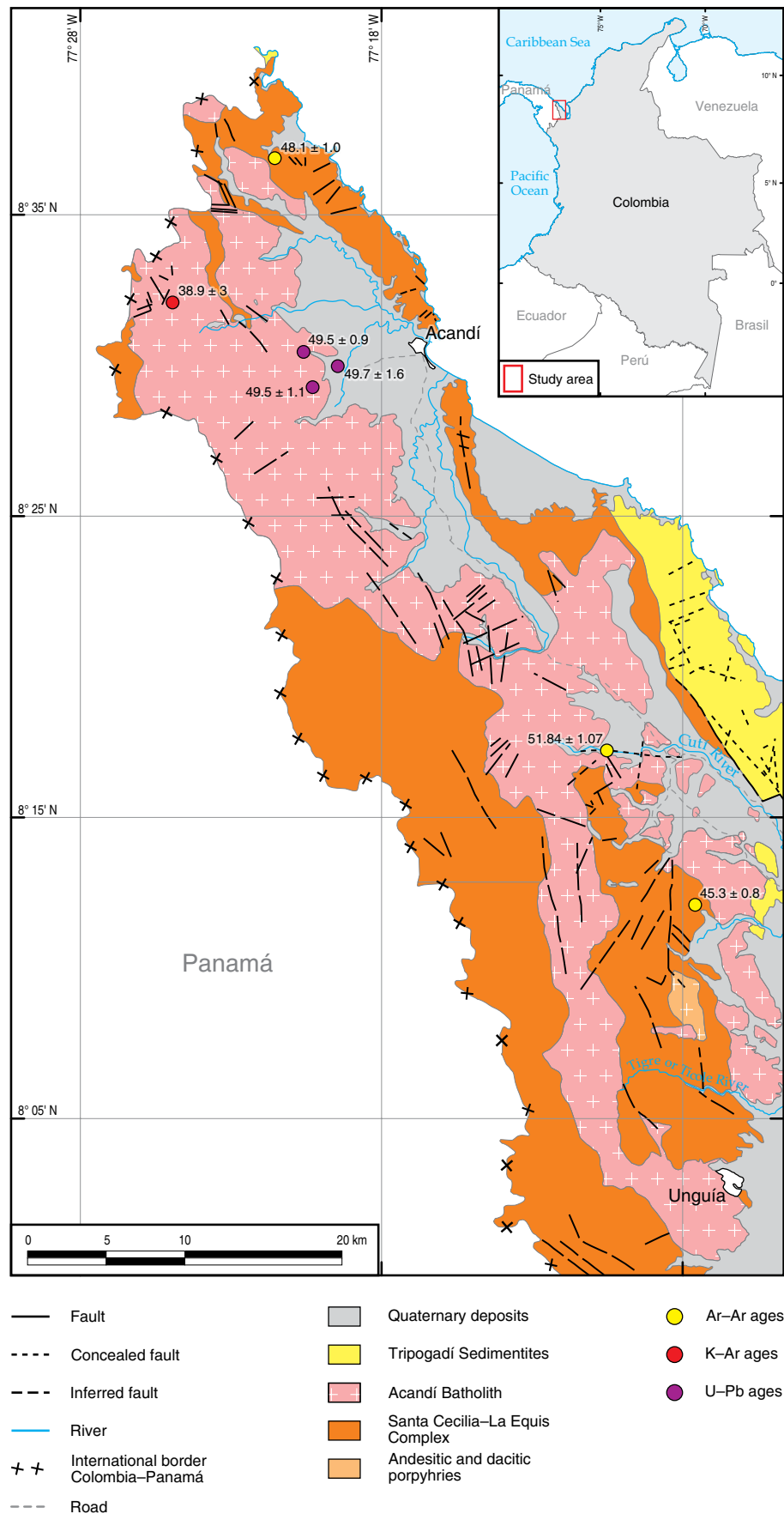


Figure 2. Geology and dates of the Chocó–Panamá Arc, North segment. Modified from Rodríguez et al. (2010b).

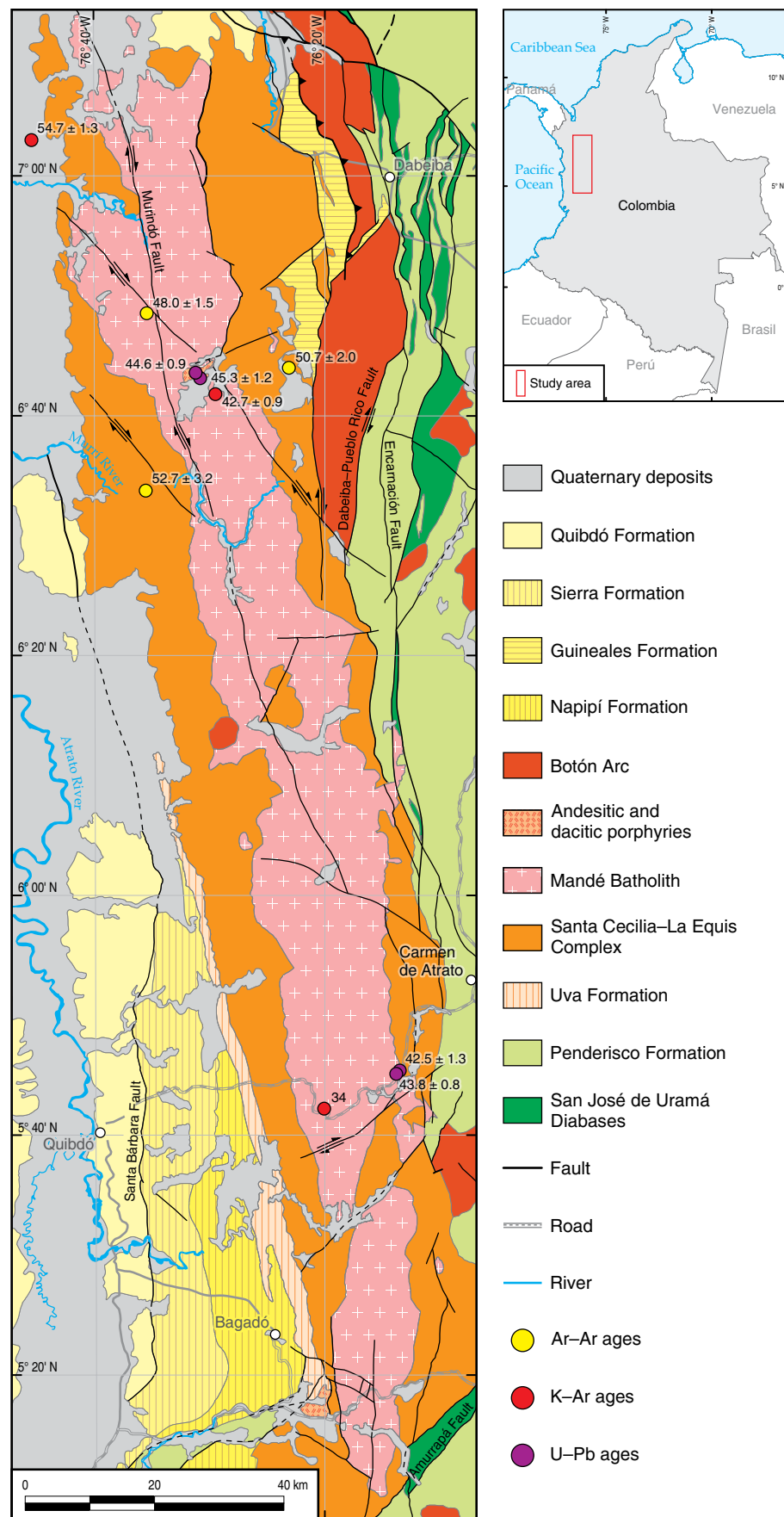
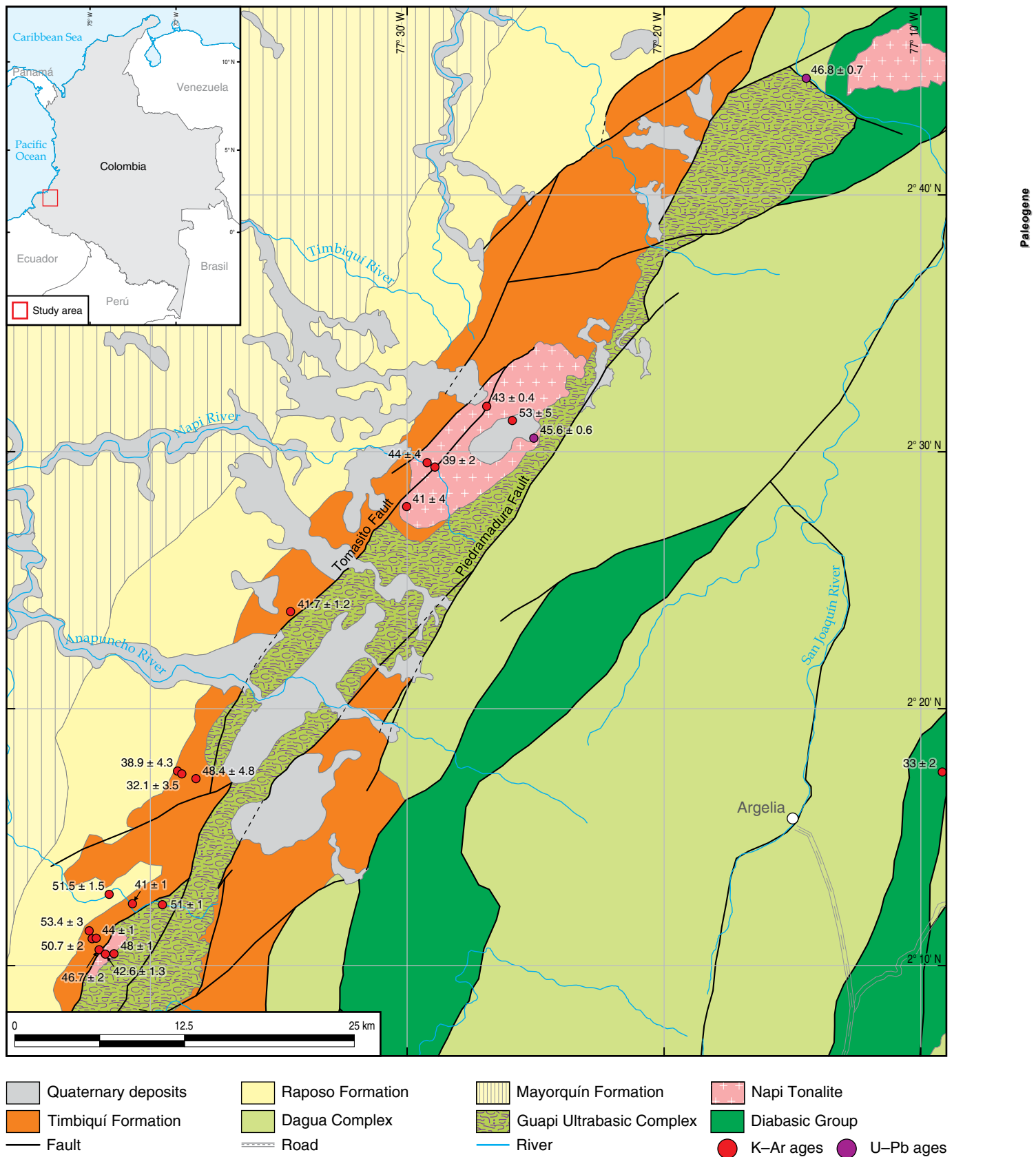


Figure 3. Geology and dates of the Chocó-Panamá Arc, Central segment. Modified from Gómez et al. (2015a).



To describe the Mandé Batholith in the Central segment, 266 thin sections from different SGC projects were studied, most of which were reanalyzed in this research to complete the mineralogical descriptions and perform modal counts. To describe the Timbiquí Formation and Napi Tonalite (South segment), data from Geología Regional y Prospección Ltd. (2014a, 2014b, 2014c) were considered. The data include descriptions of 21 thin sections of volcanic rocks and 16 analyses of the Napi Tonalite and other associated intrusive bodies.

3.2. Whole-Rock Geochemistry

Major and minor oxides, trace elements, and rare earth elements were analyzed by ActLabs, Canadá, using 100 g of sample and ICP-MS (inductively coupled plasma mass spectrometry) methodology with lithium metaborate-tetraborate complete fusion. The samples were pulverized to -200 mesh in a non-contaminating mill. Some samples from Salazar et al. (2005) were reanalyzed by ICP-MS for 62 major and trace elements.

To interpret the major oxides and classify the rocks, values were recalculated on an anhydrous basis and were graphed in the TAS diagrams (total alkali-silica diagram) of Le Bas et al. (1986) and Middlemost (1985) for volcanic and intrusive rocks, respectively, as recommended by Le Maitre et al. (2002).

3.3. Geochronology

Four samples were analyzed by ActLabs, Canadá with the Ar-Ar step heating dating method. The rocks were prepared in a noncontaminating mill at -200 mesh. The samples were wrapped in aluminum foil and loaded into a vacuum-sealed quartz vessel with K and Ca salts and LP-6 biotite packs, used as a flux monitor, interspersed with the samples. Samples were irradiated in the nuclear reactor for 48 hours. The flux monitors were placed every two samples, allowing the exact determination of the flow gradients inside the tube. After the flow monitors were run, J values were calculated for each sample using the gradient of the flow tested. The LP-6 biotite featured an estimated age of 128.1 Ma. The neutron gradient reading did not exceed 0.5% of the sample size. The isotope composition of Ar was calculated on a Micromass 5400 static mass spectrometer. The 1200 °C target reading of ^{40}Ar did not exceed $n \cdot 10^{-10}$ cc STP. The plateau ages from the age ranges integrated by several gas fractions released by the gradual heating of samples represented more than 50% of the ^{39}Ar released by the sample, and the released fractions were within a confidence level of 1σ .

4. Results

This section presents the petrography, lithogeochemistry, and radiometric dating results for the Santa Cecilia-La Equis Com-

plex, Acandí Batholith, Mandé Batholith, Timbiquí Formation, and Napi Tonalite.

4.1. Petrography of Volcanic Rocks

4.1.1. Santa Cecilia-La Equis Complex

This complex includes lavas petrographically classified as porphyritic augite basalts, two-pyroxene basalts, and andesitic basalts with porphyritic, glomeroporphyritic, and amygdaloidal textures. The rock matrix (30–75 %) is holocrystalline to hyalocrystalline, microlitic, and sometimes fluidal and trachitic. The phenocrysts and microcrysts are augite, plagioclase (labradorite), and occasionally olivine. Amygdules are filled with quartz, chalcedony, zeolites, calcite, epidote, and chlorite in both aggregates and crystals. The two-pyroxene basalts contain orthopyroxene and clinopyroxene. The accessory minerals are opaque minerals and sphene.

The pyroclastic rocks are basaltic breccias and tuffs. The matrix presents poor selection with sizes ranging from fine ash to lapilli. The lithic fragments are porphyritic, amygdaloidal, and augite basalts and tuffs. Crystals include augite, calcium plagioclase, and volcanic glass.

Within the northern Santa Cecilia-La Equis Complex, some thin sections are classified as basalts with inequigranular-hypidiomorphic textures. The crystals show intergranular, intersertal and subophitic adjustments and include plagioclase, pyroxene, and accessory minerals such as opaques, sphene, and epidote. These crystals possibly correspond to xenoliths from older basement (plateau). Most rocks of the Santa Cecilia-La Equis Complex in the Central segment (>75%) are basalts and andesites (Figure 5).

4.1.2. Timbiquí Formation

This unit is exposed in the South segment, forming two NW-oriented belts adjacent to the Napi Tonalite and the Guapi ultramafic rocks. The Timbiquí Formation is composed of pyroclastic rocks (lithic, crystalline, and vitric tuffs with basalt and andesite fragments), basaltic andesites, and andesites, interbedded with siltstones and black cherts intervals. The flows show porphyritic and glomeroporphyritic textures with plagioclase, augite, olivine, and hornblende phenocrysts. The matrix is hyalocrystalline to vitreous with fluidal texture, with plagioclase microliths, hornblende, and pyroxene. Amygdules are filled with chlorite, epidote, and quartz.

In the Timbiquí Formation, all of the samples are basalts and andesites (Figure 5). In the QAFP diagram, the Timbiquí Formation rocks are restricted to a single point because of the total lack of quartz and feldspar in the petrographic analysis.

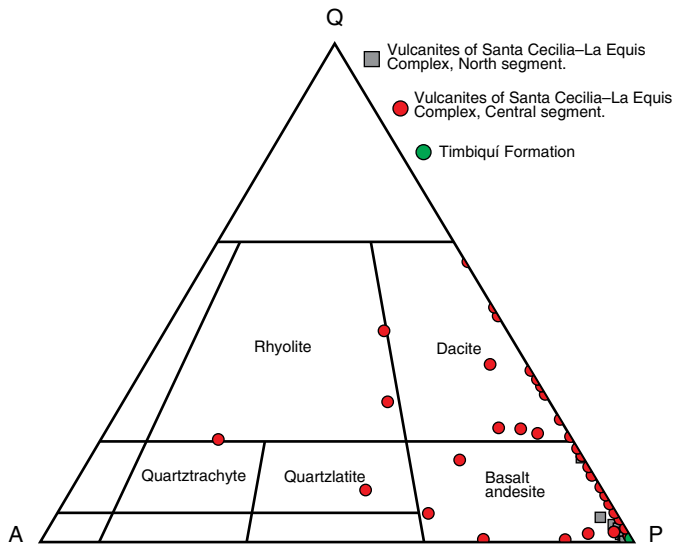


Figure 5. Modal compositions of volcanic rocks from the Chocó–Panamá Arc (Streckeisen, 1979). Vulcanites of the Santa Cecilia–La Equis Complex North segment (gray), Central segment (red), and Timbiquí Formation (green).

4.2. Petrography of Plutonic Rocks

The plutonic rocks are black and gray and white speckled, composed of plagioclase, quartz, biotite, hornblende, and K–feldspar, equigranular to inequigranular, and fine to medium grained. These rocks are cut by dikes and minor porphyry units. Plutonic rocks intrude the volcanic rocks and produce thermal metamorphism in the interaction zone.

4.2.1. Acandí Batholith

The batholith shows wide lithological variation with tonalite–granodiorite–monzogranite–quartz diorite facies (Figure 6), as well as gabbro–diorite and dikes. Tonalite is the most common rock type, with allotriomorphic, subidiomorphic, hypidiomorphic, granular, and inequigranular textures. Tonalites present quartz, plagioclase (oligoclase and andesine), orthoclase, hornblende, and biotite. The accessory minerals are opaque minerals, apatite, sphene, and occasionally zircon and rutile. The gabbro–diorite facies includes diorite, microdiorite, gabbro, hornblende gabbro, microgabbro, gabbro-norite, and monzogabbro. These rocks are intruded by stocks and andesite and porphyritic dacite dikes (Rodríguez et al., 2010a).

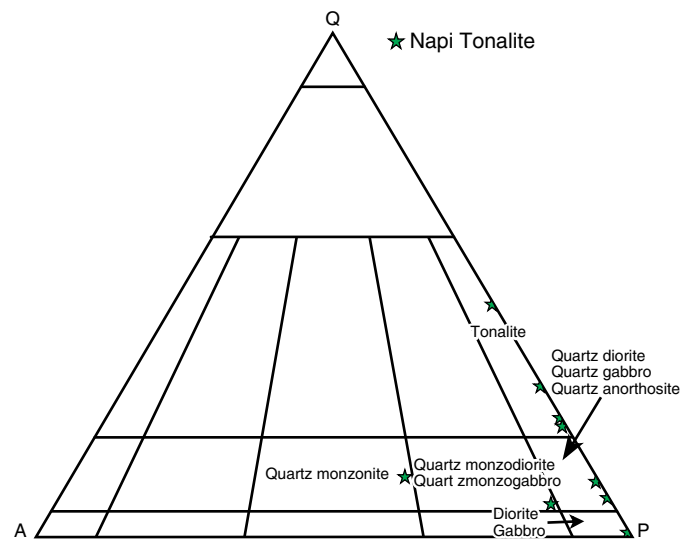
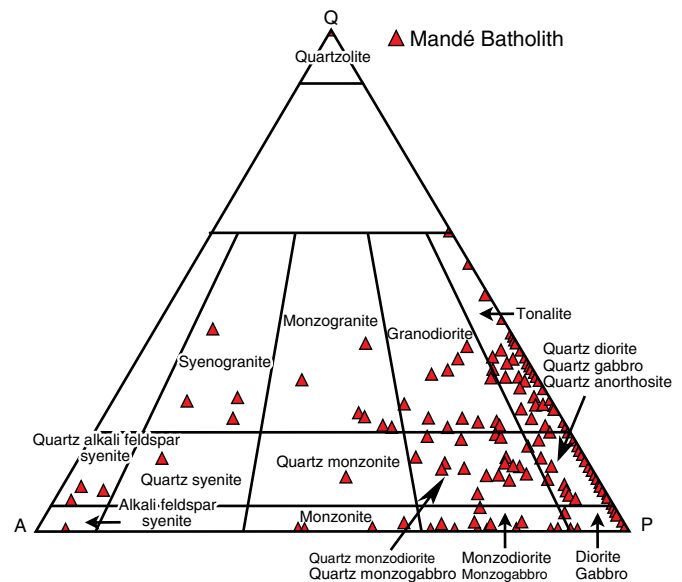
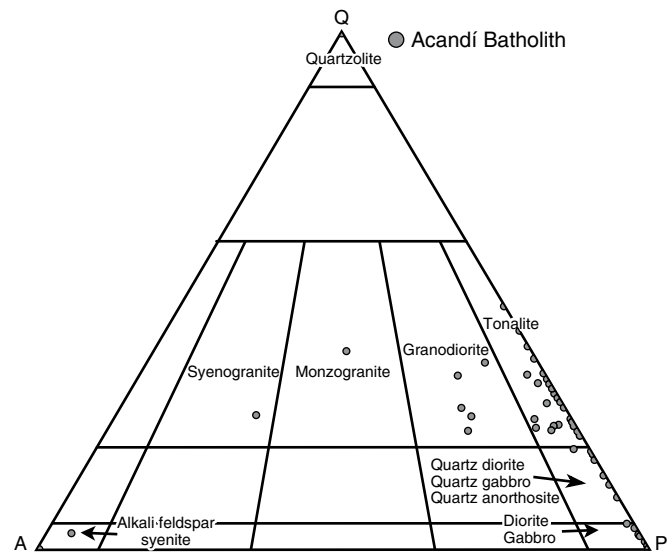


Figure 6. Modal compositions of plutonic rocks from the Chocó–Panamá Arc (Streckeisen, 1976). Acandí Batholith (gray), Mandé Batholith (red), and Napi Tonalite (green).

4.2.2. Mandé Batholith

This intrusive unit is of diverse lithological composition, including tonalite and quartz diorite with subordinate granodiorite (Figure 6). The gabbro–diorite facies is most common near the eastern boundary, in contact with the Santa Cecilia–La Equis Complex. Porphyry units intrude the plutonic rocks and include disseminated Cu–Au and Cu–Mo mineralization zones (Pantanos–Pegadorcito, Ramírez et al., 1979; Murindó, Guarín & Álvarez, 1975; and Acandí, Álvarez & Parra, 1979; Sillitoe et al., 1982). The contact between the granitoid unit and the volcanic rocks of the Barroso Formation (basalts and andesites) is intrusive and develops hornfels and intrusive breccia zones (González & Londoño, 2002).

The Mandé Batholith presents subidiomorphic and hypidiomorphic, inequigranular to granular, poikilitic and graphic textures. Plagioclase (andesine) is the prevailing mineral, followed by quartz, hornblende, alkali feldspar, and biotite. The accessory minerals include apatite, zircon, sphene, and opaque minerals. The alteration minerals include chlorite, epidote, sericite, saussurite, and kaolinite.

The porphyries that intrude the Mandé Batholith vary from andesitic to dacitic. The andesitic porphyries feature hornblende and plagioclase phenocrysts in a crystalline matrix of feldspar and fine quartz. As an accessory mineral, bipyramidal quartz with apatite inclusions is present, featuring thin reaction crowns at the contacts with the matrix. The porphyritic dacites are composed of bipyramidal quartz phenocrysts with corroded edges, plus plagioclase and chlorite produced by hydrothermal alteration. The matrix is holocrystalline, aphanitic, and composed of feldspar and quartz.

4.2.3. Napi Tonalite

This unit is composed of quartz diorite, tonalite, diorite, and gabbro (Figure 6). It includes plagioclase (oligoclase and andesine), quartz, potassium feldspar, hornblende, and biotite, as well as opaque minerals, sphene, zircon, and apatite as accessory minerals. The alteration minerals are chlorite, epidote, sericite, clay minerals, and calcite.

The gabbroic facies rocks are classified as pyroxene–hornblende melanogabbro, leucogabbro, quartz gabbro, and pyroxene–hornblende gabbro.

4.3. Geochemistry of Volcanic Rocks

The Santa Cecilia–La Equis Complex, in the North segment, presents LOI values between 2 and 5.06%, suggesting moderate alteration of the rocks. In the Central segment, most of the rocks have LOI <3%, which is indicative of low alteration, except for samples 80588 (LOI = 4.04%), 119082 (LOI = 6.24%), 701803 (LOI = 5.09%), and 702760 (LOI =

4.48%), which indicate alteration. The rocks of the Timbiquí Formation have LOI <3%, except for samples APO–0036–P (LOI = 6.2%), APO–0065–LT (LOI = 4%), CDG–0262P (LOI = 5.3%), and CDG–0267P (LOI = 3.8%), which are indicative of moderate to high alteration. Additionally, in the Hughes diagram (Hughes, 1972), some samples from the Santa Cecilia–La Equis Complex (North segment) and the Timbiquí Formation (South segment) plot in the spilite field, indicating albitization probably due to contact with seawater during the crystallization of the rocks; three samples from the Santa Cecilia–La Equis Complex plot within the field of potassic alteration (706413, 703017, 702633) (Figure 7a).

The Santa Cecilia–La Equis Complex in the North and Central segments presents SiO₂ values between 46 and 60%, low K₂O contents between 0.07 and 3.1% (with most samples between 0.5 and 1.5%), TiO₂ <1%, and MgO between 2.65 and 10.99%. MgO, CaO, and Fe₂O₃ decrease, and Na₂O increases as SiO₂ increases. The remaining oxides show wide dispersions without defined tendencies. The Timbiquí Formation in the South segment presents SiO₂ contents between 49.17 and 65.75% and low values of TiO₂ <1%, K₂O <1.4, and MgO <9.64, and other oxide values are similar to those of the Santa Cecilia–La Equis Complex (Table 1). The chemical classification of the rocks matches the petrographic classification in the three segments, varying between basalts and dacites, but mostly andesites and basaltic andesites (Figure 7a, 7b).

The Santa Cecilia–La Equis Complex and the Timbiquí Formation are subalkaline and plot in the tholeiitic and normal calc–alkaline series (Figures 7c, 7f). These rocks are mostly basic to intermediate and metaluminous, with A/CNK ratios between 0.5 and 1.2 and A/NK values between 1.1 and 4.5. Some are peraluminous (Figure 7d), as suggested by the high values of loss on ignition (LOI) and the alteration diagram (Figure 7a; Table 1); however, not all are altered, and some could have been formed due to sediment contamination, hydrous melting of mafic rocks or melting of pelitic or semipelitic rocks.

In the Y vs. Sr/Y diagram, most of the volcanic samples of the Santa Cecilia–La Equis Complex and the Timbiquí Formation plot in the field of normal arc rocks, with only very few data in the adakitic series (Figure 7e).

The Santa Cecilia–La Equis Complex and the Timbiquí Formation present trace element patterns with negative Nb and Zr anomalies and positive Cs, Th, Sr, Ba, and Pb anomalies, characteristic of magma generated in arc environments (Pearce, 1996; Pearce et al., 1984). These results show a progressive decrease in LILE toward HFSE (Figure 8). The Nb anomalies are greater in the Santa Cecilia–La Equis Complex rocks than in the Timbiquí Formation. The rare earth element (REE) patterns normalized to the Nakamura chondrite (Nakamura, 1974) are subparallel in the rocks of the three segments, with negative slopes and patterns that are comparable to those of rocks derived from subduction environments above the associated sub-

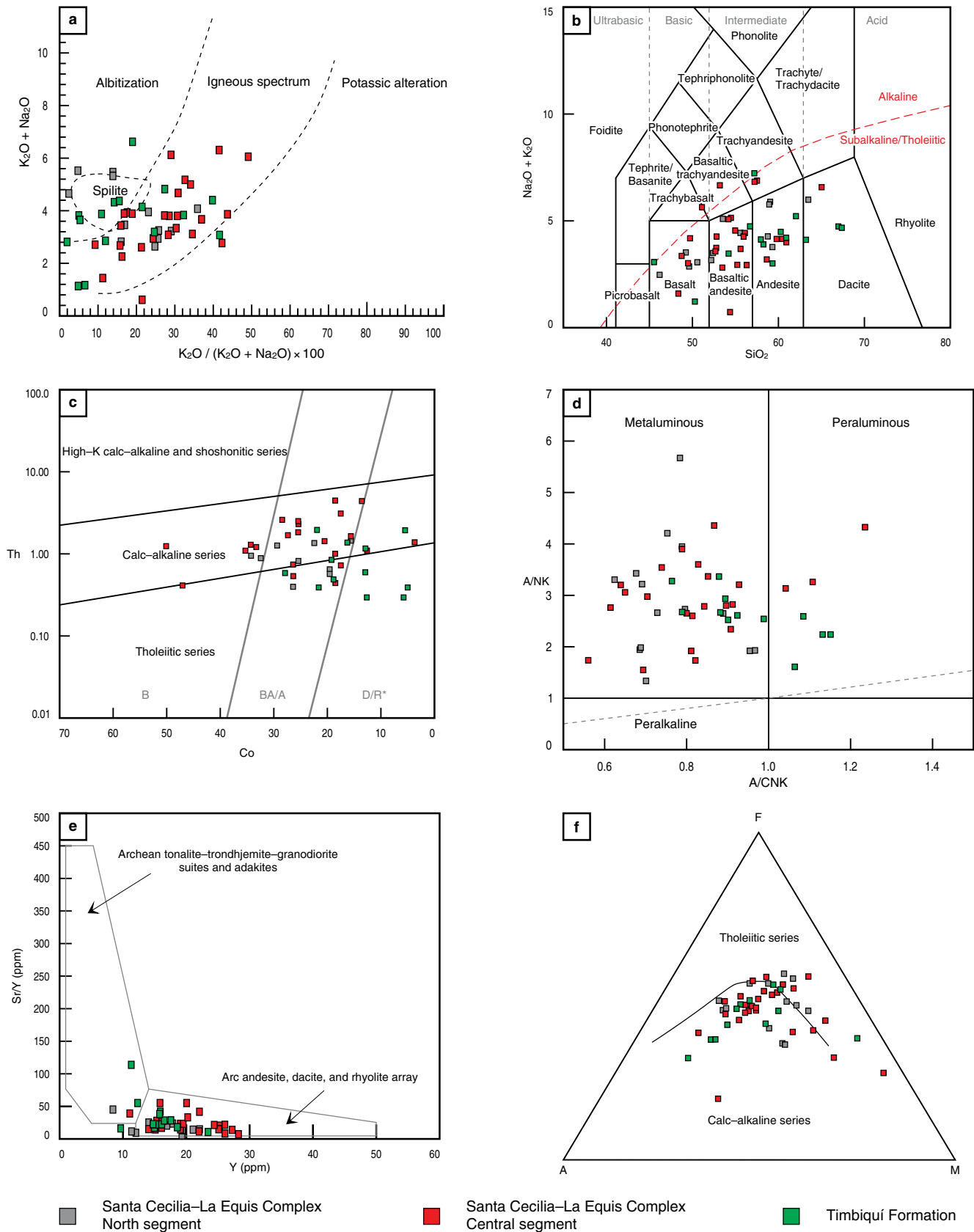


Figure 7. Classification and discrimination diagrams for the Santa Cecilia–La Equis Complex and the Timbiquí Formation volcanites. **(a)** Hughes diagram (Hughes, 1972). **(b)** TAS diagram (Le Bas et al., 1986). **(c)** Co vs. Th diagram (Hastie et al., 2007). **(d)** Shand (1943) alumina saturation index diagram. **(e)** Y vs. Sr/Y diagram (Hansen et al., 2002). **(f)** AFM diagram (Irvine & Baragar, 1971). Santa Cecilia–La Equis Complex North segment (gray), Central segment (red), and Timbiquí Formation (green).

Table 1. Major oxides in rocks of the Santa Cecilia-La Equis Complex and Timbiquí Formation.

Sample	Latitude N	Longitude W	SiO ₂	Al ₂ O ₃	Fe ₂ O ₃ (T)	MnO	MgO	CaO	Na ₂ O	K ₂ O	TiO ₂	P ₂ O ₅	LOI	Total
Santa Cecilia-La Equis Complex (North segment)														
900009	8° 39' 51.42"	77° 21' 37.91"	55.34	14.87	8.34	0.14	2.94	7.23	2.95	0.56	0.68	0.13	5.06	98.24
900010	8° 39' 05.45"	77° 21' 52.11"	50.77	15.6	7.44	0.15	7.17	8.14	4.75	0.07	0.53	0.06	3.72	98.39
900081	8° 31' 45.04"	77° 17' 02.89"	62.93	12.91	9.05	0.14	2.64	4.78	5.72	0.25	0.71	0.08	0.61	99.83
900084	8° 34' 42.62"	77° 18' 28.11"	58.06	17.38	8.18	0.1	2.94	4.84	5.02	0.76	0.79	0.1	2.45	100.6
900087	8° 34' 34.97"	77° 20' 50.91"	47.63	19.86	9.59	0.15	4.13	11	2.44	0.96	0.74	0.17	2.75	99.44
900093	8° 31' 42.72"	77° 22' 23.07"	45.1	21.07	10.51	0.14	5.28	12.7	2.02	0.37	0.63	0.03	1.75	99.57
900296	8° 07' 31.37"	77° 07' 01.51"	50.37	16.18	9.37	0.17	5.73	10.1	2.52	0.83	0.62	0.14	3.57	99.6
900308	8° 06' 18.85"	77° 09' 39.201"	49.75	16.06	12.32	0.22	5.44	10.5	2.55	0.46	0.9	0.16	2.08	100.4
900315	8° 12' 17.71"	77° 07' 18.24"	57.45	16.83	7.67	0.12	3.54	6.87	3.26	0.93	0.61	0.28	3.06	100.6
900316	8° 12' 27.55"	77° 07' 15.13"	48	17.57	9.43	0.19	7.37	10.5	2.11	0.66	0.71	0.18	4.04	100.8
900317	8° 11' 57.56"	77° 07' 31.21"	54.39	16.72	7.15	0.12	5.15	9.15	2.83	1.51	0.48	0.16	3.01	100.7
Santa Cecilia-La Equis Complex (Central segment)														
7103	6° 39' 47.33"	76° 17' 24.50"	51.49	15.88	9.97	0.15	5.12	10.6	2.49	1.03	0.67	0.25	2.16	99.75
7106	6° 50' 31.77"	76° 21' 23.74"	55.63	18.16	7.29	0.1	2.8	6.71	3.56	1.75	0.65	0.25	3.17	100.1
95494	6° 05' 44.59"	76° 13' 37.71"	55.03	17.86	6.26	0.18	2.22	6.94	3.94	2.66	0.5	0.36	4.17	100.1
95498	6° 04' 57.70"	76° 14' 30.042"	50.3	17	7.59	0.26	3.65	7.7	2.91	1.23		0.8		99.85
95499	6° 05' 44.59"	76° 13' 37.71"	55.03	17.86	6.26	0.18	2.22	6.94	3.94	2.66		0.496	4.17	100.1
700567	6° 05' 47.68"	76° 29' 29.59"	51.74	18.18	9.3	0.1	4.61	9.19	2.18	0.56	0.68	0.11	2.97	99.62
119082	5° 29' 53.13"	76° 13' 55.029"	46.32	16.34	10.35	0.21	5.23	9.69	2.25	1.66	0.79	0.28	6.24	99.35
700717	6° 26' 13.47"	76° 34' 26.40"	55.02	18.2	8.9	0.16	3.41	10.1	2.68	0.25	0.64	0.17	1.08	100.6
700796	6° 12' 39.02"	76° 25' 55.40"	58.57	16.85	6.56	0.2	3.17	6.82	2.95	1.07	0.44	0.13	2.02	98.77
700812	6° 13' 32.43"	76° 28' 39.27"	54.96	14.24	7.52	0.15	7.43	9.77	2.43	0.43	0.47	0.13	1.16	98.7
700821	6° 21' 48.52"	76° 27' 44.11"	58.38	16.92	6.95	0.2	3.34	7.04	2.94	1.11	0.49	0.12	1.39	98.89
700830	6° 14' 46.76"	76° 29' 50.53"	57.77	17.1	8.06	0.11	2.79	8.7	2.41	0.73	0.46	0.12	1.11	99.36
700990	6° 05' 15.07"	76° 26' 40.26"	47.24	17.3	9.97	0.18	5.52	15.1	1.36	0.16	0.61	0.09	1.47	98.96
701803	5° 11' 15.55"	76° 16' 42.47"	50.47	20.1	7.41	0.13	3.78	8.41	3.39	0.66	0.74	0.28	5.09	100.5
702376	5° 04' 44.77"	76° 23' 48.88"	51.76	14.88	11.34	0.24	4.86	6.46	4.68	1.82	0.78	0.46	2.05	99.33
702476	5° 40' 38.55"	76° 25' 44.77"	47.47	11.24	11.54	0.19	11	10.7	1.71	1.19	0.61	0.28	2.77	98.69
702633	5° 14' 39.12"	76° 14' 12.20"	42.38	18.39	6.77	0.13	10.2	5.8	1.95	0.98	0.37			86.98

Table 1. Major oxides in rocks of the Santa Cecilia–La Equis Complex and Timbiquí Formation (*continued*).

Sample	Latitude N	Longitude W	SiO ₂	Al ₂ O ₃	Fe ₂ O ₃ (T)	MnO	MgO	CaO	Na ₂ O	K ₂ O	TiO ₂	P ₂ O ₅	LOI	Total
Santa Cecilia–La Equis Complex (Central segment)														
702760	5° 10' 53.08"	76° 12' 28.28"	59.89	15	7.42	0.14	3.8	7.16	2.52	1.41	0.52	0.19	2.36	100.4
702769	5° 10' 29.61"	76° 04' 46.64"	63.59	15.3	2.72	0.1	3.84	5.32	3.37	3.07	0.28			97.59
702999	6° 09' 12.56"	76° 15' 03.31"	47	15	3.52	0.28	7.96	11.19	0.5	0.13		0.85		99.47
703017	6° 05' 18.37"	76° 14' 05.75"	50.48	18.25	7.47	0.23	2.4	8.43	3.34	1.42		0.513	6.52	99.54
703084	6° 14' 30.17"	76° 20' 26.37"	54.52	20.21	7.84	0.15	2.9	7.07	3.47	0.7	0.52	0.11	2.64	100.1
706407	7° 00' 52.75"	76° 17' 53.74"	50.01	14.01	11.73	0.17	5.42	9.31	3.79	1.74	0.98	0.57	2.47	100.2
706413	6° 45' 40.43"	76° 17' 19.93"	46.85	16.11	12.2	0.18	6.76	9.46	1.91	1.3	1.06	0.22	3.82	99.88
Timbiquí Formation (South segment)														
APO-0036-P	2° 41' 07.47"	77° 09' 21.27"	58.14	18.73	3.33	0.11	1.54	6.34	3.62	1.3	0.35	0.19	6.2	99.81
APO-0054-LG	2° 44' 06.76"	77° 13' 58.16"	61.65	16.87	6.57	0.15	2.7	4.91	3.86	0.18	0.52	0.13	2.3	99.85
APO-0065-LT	2° 46' 52.80"	77° 14' 22.43"	54.39	17.44	7.91	0.19	3.22	7.25	2.81	1.77	0.55	0.25	4	99.79
APO-0069-LT	2° 47' 37.17"	77° 14' 57.76"	58.44	16.85	6.93	0.21	2.8	6.58	3.48	0.9	0.48	0.16	3	99.85
CDG-0254P	2° 03' 59.93"	77° 35' 39.85"	58.45	15.94	6.82	0.17	4.26	8.78	2.95	0.04	0.91	0.12	1.4	99.84
CDG-0256BP	2° 03' 59.93"	77° 35' 39.85"	49.17	16.56	7.18	0.13	9.64	13.45	1.13	0.05	0.45	0.04	1.9	99.77
CDG-0260P	2° 03' 55.80"	77° 33' 56.72"	57.59	16.91	6.75	0.12	4.4	8.3	3.73	0.18	0.77	0.13	0.9	99.84
CDG-0262P	2° 04' 17.98"	77° 33' 37.67"	54.76	16.95	7.64	0.12	3.22	7.2	2.71	1.23	0.43	0.19	5.3	99.71
CDG-0267P	2° 04' 44.40"	77° 32' 11.37"	54.88	17.33	8.7	0.15	3.97	3.02	5.7	1.26	0.62	0.27	3.8	99.7
CDG-0272P	2° 05' 32.02"	77° 31' 02.13"	52.31	17.11	10.2	0.2	4.6	7.88	2.56	0.8	0.67	0.2	3.2	99.76
CLM-0436	2° 25' 43.76"	77° 32' 11.34"	65.18	16.21	4.52	0.19	2.22	3.75	3.94	0.68	0.34	0.14	2.7	99.88
CLM-0454	2° 24' 35.22"	77° 29' 25.09"	59.64	17.08	6.9	0.2	2.83	6.54	3.71	0.42	0.45	0.14	1.9	99.85
CLM-0436-L	2° 25' 43.76"	77° 32' 11.34"	65.75	16.19	4.4	0.19	2.05	3.87	3.98	0.62	0.34	0.12	2.4	99.89

Source: Data from Buchely et al. (2009), Geología Regional y Prospección Ltda. (2014a, 2014b, 2014c), Rodríguez et al. (2010a, 2010b), and this research.

ducted plate, with light rare earth elements (LREE) enriched by 10–100 times and depletion ≤ 10 in heavy rare earth elements (HREE) (Figure 8).

The Eu/Eu* ratios are close to 1 for the Santa Cecilia–La Equis Complex and the Timbiquí Formation. $(\text{La/Yb})_n$ ratios range between 1 and 5, with slightly higher values in the Central segment of the Santa Cecilia–La Equis Complex and slightly lower values for the Timbiquí Formation. The $(\text{La/Sm})_n > 1$ ratio shows that LREE are increased relative to HREE in all samples.

4.4. Geochemistry of Intrusive Rocks

The Acandí Batholith presents SiO_2 values that range between 47.68% and 62.86% (sample 900328 shows a high value of 72.68%), low K_2O contents between 0.06 and 0.83%, $\text{TiO}_2 < 1\%$, MgO between 2.27 and 5.04% (sample 900008 shows a value of 10.16%), and CaO between 1.35 and 5.58%. The Mandé Batholith includes rocks with SiO_2 values between 44.30 and 70.91%, low K_2O contents between 0.06 and 1.69%, $\text{TiO}_2 < 1\%$, MgO between 1.20 and 8.05% (except samples RM–3508, 700784 with values of 11.1 and 14.2%), and CaO between 2.14 and 15.10%. The Napi Tonalite presents SiO_2 between 41.08 and 64.43%, low K_2O contents between 0.08 and 2.31%, $\text{TiO}_2 < 1\%$, MgO between 1.05 and 7.38%, and CaO between 4.55 and 14.07%. For the three plutons, the Al_2O_3 , CaO , MgO , and TiO_2 contents decrease as SiO_2 increases. Na_2O increases with SiO_2 , albeit with greater dispersion than other major elements (Table 2).

The chemical classification of the samples is very consistent with the petrographic classification of the Acandí and Mandé Batholiths and Napi Tonalite. These rocks vary in composition among gabbro, granodiorite, diorite, tonalite, peridotite–gabbro (Munchica Intrusive, samples MZD–0014 and CAQ–0416), and granite with high SiO_2 values (Acandí and Mandé Batholiths, samples 900328 and 174670, respectively) (Figure 9a, 9b).

Rocks are mostly basic to intermediate and metaluminous with A/CNK ratios between 0.6 and 1.1 and A/NK values between 1.5 and 5. A few samples are peraluminous (Figure 9c), probably due to sediment contamination, based on the low values for LOI (Table 2).

The rocks of the Acandí, Mandé, and Napi Intrusives are low–K tholeiitic to calc–alkaline. Several that are rich in MgO are grouped separately (RM–3508, 7111, 700784, and 900008). In these samples, the SiO_2 content is not a factor to separate the two series (Figure 9e).

In the alkali–lime index (MALI) and Fe–index diagrams (Frost et al., 2001; Frost & Frost, 2008), the rocks of the Acandí, Mandé, and Napi Intrusives are dominantly calcic granites with alkali–lime index values between –13.83 and 3.52. Additionally, these rocks plot in the field of magnesian granitoids, which are probably related to island arc magmas that followed

relatively oxidizing differentiation trends (Figure 9d, 9f; Frost et al., 2001). The magnesian series show a close affinity to relatively hydrous, oxidizing magmas, and source regions (Frost & Lindsley, 1991), which is broadly consistent with subduction–related origins.

The Acandí and Mandé Batholiths and Napi Tonalite show similar patterns of trace elements vs. N–MORB, with negative Nb, Ti, and Zr anomalies and positive anomalies and high values of Cs, Ba, Th, Sr, and Rb. These are common features of magmas generated in an arc environment (Pearce, 1996; Pearce et al., 1984) in which a progressive decrease in LILE toward HFSE occurs (Figure 10). The Nb anomalies are similar for the three plutons (samples 700967, 700784, and 7135 of the Mandé Batholith show a positive Y anomaly).

The REE patterns normalized to the Nakamura chondrite (Nakamura, 1974) in the Acandí Batholith rocks show a negative slope. Two samples show a slightly flat pattern (900059 and 900304), and samples 900008 and 900311 are more depleted and primitive, with values that are 10 times less than the chondrite values in LREE and HREE (sample 900311 has a positive Eu anomaly). The REE patterns for all samples are similar to those of rocks generated in subduction environments above the subducted plate (Figure 10).

The Mandé Batholith rocks show parallel REE patterns, with few samples with flatter patterns that segment the main pattern (174670, 700967, and 700618). The most primitive rocks of the Mandé Batholith show REE values < 10 times those of chondrites with positive Eu anomalies, and those with LREE values > 10 show slight negative Eu anomalies. The REE patterns for all Mandé Batholith samples are similar to those of rocks generated in arcs, with a negative slope from LREE to HREE (Figure 10).

The Napi Tonalite presents several patterns. Some samples show patterns similar to oceanic crust rocks (CLM–0449P, CLM–0377P, CLM–388P, and APO0056LG), with decreasing LREE and flat HREE. The remaining samples show negative slopes from LREE to HREE, similar to patterns of rocks generated in arc environments. At least three different patterns are identified in these two plutons (Figure 10).

The Eu/Eu* ratios for the samples from the Acandí and Mandé Batholiths and the Napi Tonalite are between 0.71 and 1.45, many of which are near 1. Values of $(\text{La/Yb})_n$ are between 1 and 5.5 (except for samples RM–3501, RM–3509, and 7105 of the Mandé Batholith with values of 14.5, 8.1, and 6.4, respectively) and $(\text{La/Yb})_n < 1$ in some Napi Tonalite rocks (CLM–0447P, APO–0107–D, CAQ–0416–P, CLM–0377–P, and CLM–0388–P), with overall values of $(\text{La/Yb})_n$ that are lower than those of the Acandí and Mandé Batholiths. The Mandé and Acandí Batholith ratios are $(\text{La/Sm})_n > 1$ in all rocks, showing LREE enrichment relative to HREE. Napi Tonalite samples CLM–0447P, APO–0107D, CAQ–0416P, CLM–0388P, and MZD–0010–L have values of $(\text{La/Sm})_n$

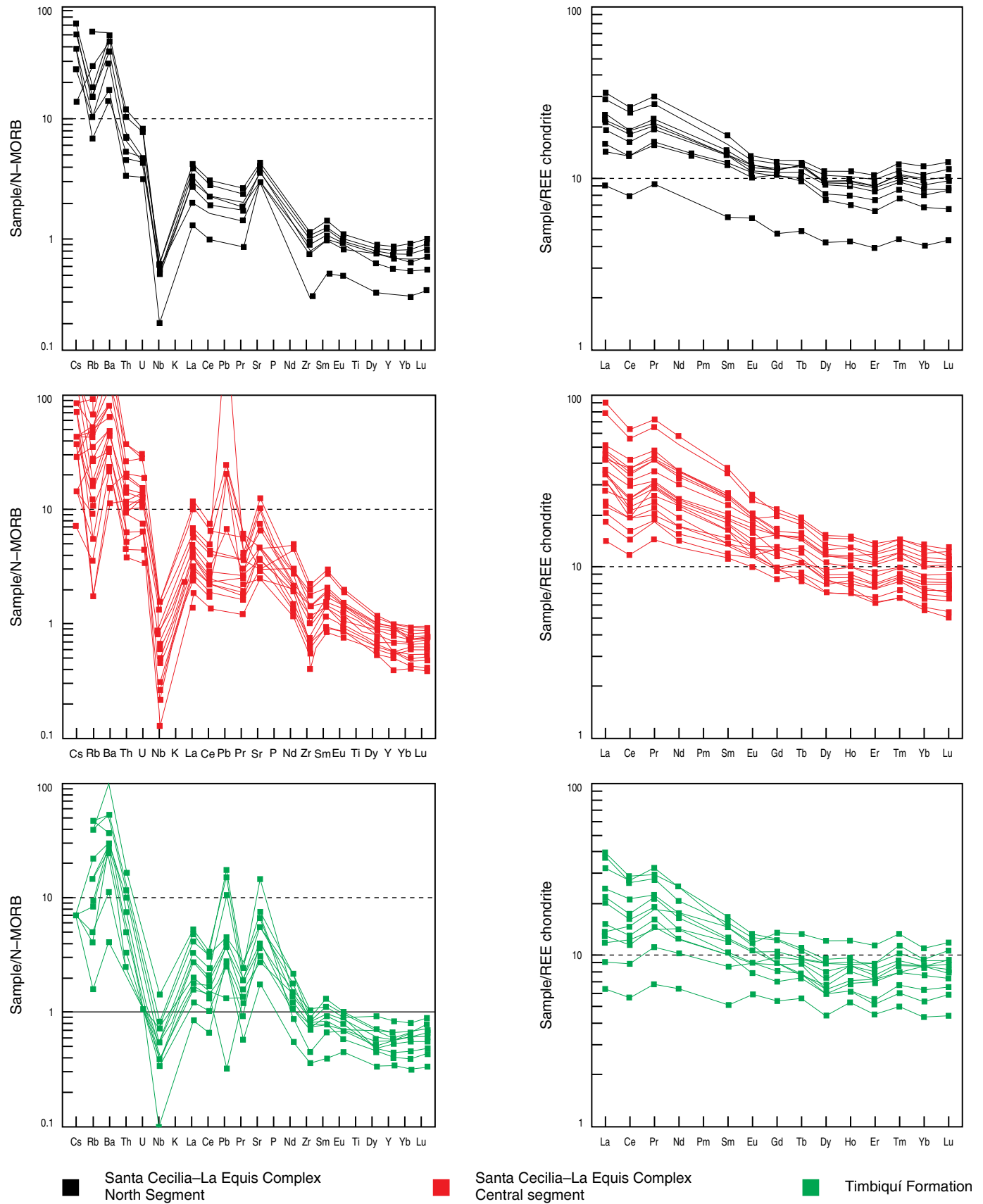


Figure 8. Multi-element diagrams normalized to N-MORB (Sun & McDonough, 1989) and rare earth element diagrams normalized to Nakamura chondrite (Nakamura, 1974) for volcanic rocks of the Chocó–Panamá Arc. Santa Cecilia–La Equis Complex North segment (black), Central segment (red), and Timbiquí Formation (green).

Table 2. Major oxides in rocks of the Acandí Batholith, Mandé Batholith, and Napi Tonalite.

Sample	Latitude N	Longitude W	SiO ₂	Al ₂ O ₃	Fe ₂ O ₃ (T)	MgO	CaO	Na ₂ O	K ₂ O	TiO ₂	P ₂ O ₅	MnO	LOI
Acandí Batholith													
900008	8° 35' 45.81"	77° 21' 25.99"	50.99	15.97	6.79	10.1	13.3	1.35	0.11	0.19	0.05	0.13	2.1
900059	8° 38' 15.66"	77° 23' 46.28"	56.64	14.88	9.98	4.86	6.02	4.98	0.06	0.83	0.12	0.16	2.42
900064	8° 35' 09.51"	77° 22' 57.50"	61.71	16.77	5.69	2.55	6.06	3.5	0.19	0.37	0.17	0.16	3.63
900072	8° 30' 30.33"	77° 20' 00.68"	61.14	16.42	6.67	2.69	6.76	3.02	0.96	0.46	0.14	0.16	0.6
900090	8° 31' 23.07"	77° 20' 40.94"	62.86	16.89	5.76	2.24	6.42	3.25	0.73	0.41	0.12	0.17	1.72
900304	8° 03' 20.04"	77° 07' 46.85"	49.41	20.27	9.9	4.84	11.2	2.17	0.54	0.75	0.27	0.19	1.33
900307	8° 06' 28.33"	77° 09' 08.31"	50.09	18.96	9.71	4.87	10.2	2.96	0.93	0.75	0.18	0.18	1.89
900311	8° 02' 23.15"	77° 06' 27.52"	47.68	21.12	9.97	5.04	13.2	1.59	0.35	0.7	0.04	0.16	0.96
900328	8° 02' 49.75"	77° 09' 49.48"	72.14	13.96	3.75	0.72	2.27	5.58	0.19	0.55	0.09	0.06	1.09
900369	8° 17' 10.70"	77° 10' 24.99"	62.39	16.22	6.27	2.96	6.26	2.98	0.77	0.48	0.09	0.14	1.19
900378	8° 07' 12.33"	77° 05' 59.81"	60.58	16.88	6.58	2.95	7.83	3.44	0.13	0.46	0.14	0.13	0.68
900059	8° 38' 15.66"	77° 23' 46.28"	56.64	14.88	9.98	4.86	6.02	4.98	0.06	0.83	0.12	0.16	2.42
900448	8° 12' 09.58"	77° 05' 57.73"	59.81	17.1	6.86	3.27	7.29	2.9	0.75	0.48	0.14	0.19	1.29
Mandé Batholith													
7072	6° 29' 06.85"	76° 28' 32.33"	58.38	18.3	7.03	3.07	8.12	3.16	0.56	0.47	0.16	0.17	1.08
7074	6° 25' 42.301"	76° 28' 41.52"	52.45	19.41	9.22	4.12	9.3	3.15	0.56	0.66	0.21	0.23	1.33
7075	6° 25' 27.51"	76° 28' 21.98"	64.81	16.25	5.19	2.26	5.42	3.59	1.12	0.43	0.13	0.12	0.72
7076	6° 25' 14.43"	76° 22' 53.54"	50.57	16.83	11.04	6.53	11.4	2.42	0.3	0.59	0.17	0.21	0.7
7110	6° 32' 11.04"	76° 27' 00.14"	63.26	14.43	7.67	3.04	6.08	2.97	1.4	0.72	0.23	0.12	0.74
7111	7° 06' 10.27"	76° 40' 28.23"	48.2	17.65	8.03	9.3	13.8	1	0.24	0.3	0.04	0.19	1.44
7134	6° 06' 04.45"	76° 16' 05.12"	61.82	16.02	6.6	2.39	5.19	4	1.93	0.59	0.22	0.14	0.67
7135	6° 07' 16.04"	76° 15' 56.88"	49.43	17.16	11.12	5.76	10.39	2.7	0.46	0.66	0.12	0.18	0.86
7146	6° 59' 17.26"	76° 35' 58.84"	68.6	15.72	3.66	1.58	4.71	3.2	1.15	0.31	0.12	0.11	1.22
7149	6° 57' 33.91"	76° 38' 48.34"	63.4	16.8	5.31	2.21	6.05	3.36	0.81	0.4	0.15	0.16	0.8
7195	5° 38' 45.78"	76° 19' 22.44"	54.09	17.37	9.13	4.08	8.04	3.11	1.2	0.78	0.25	0.16	1.48
80912	5° 10' 55.37"	76° 39' 19.06"	49.11	23.41	5.57	5.05	15.1	1.16	0.14	0.16	0.02	0.09	1.18
95177	7° 01' 17.51"	76° 38' 09.69"	48.76	17.9	11.91	6.17	12.2	1.25	0.23	0.72	0.01	0.19	0.87
95181	4° 36' 30.25"	76° 38' 36.56"	64.21	16.49	6.19	2.3	5.35	3.28	0.18	0.46	0.13	0.21	1.92
95765	7° 04' 47.96"	76° 35' 38.95"	63.69	16.64	5.4	2.3	5.68	3.47	1.36	0.41	0.13	0.14	1.1
95768	7° 02' 03.22"	76° 35' 03.28"	63.52	17.12	5.32	2.19	5.89	3.61	1.23	0.4	0.14	0.16	0.91

Table 2. Major oxides in rocks of the Acandí Batholith, Mandé Batholith, and Napi Tonalite (continued).

Sample	Latitude N	Longitude W	SiO ₂	Al ₂ O ₃	Fe ₂ O ₃ (T)	MgO	CaO	Na ₂ O	K ₂ O	TiO ₂	P ₂ O ₅	MnO	LOI
Mandé Batholith													
95774	5° 37' 43.35"	76° 35' 48.69"	62.53	16.93	5.88	2.21	6.07	3.4	1.19	0.44	0.15	0.16	0.78
95829	6° 51' 07.30"	76° 34' 56.14"	67.02	16.69	4.03	1.64	4.9	3.85	1.29	0.32	0.13	0.15	0.87
95830	7° 00' 43.88"	76° 34' 55.22"	65.16	16.38	4.97	2.02	5.65	3.44	1.22	0.37	0.14	0.15	1.35
95836	6° 41' 26.32"	76° 36' 03.16	63.39	16.98	5.66	2.39	6.25	3.42	1.13	0.42	0.15	0.17	0.66
174670	6° 43' 33.17"	76° 34' 22.09"	70.91	16.73	2.16	1.2	2.14	4.27	1.69	0.14	0.09	0.02	1.65
700130	5° 39' 08.28"	76° 19' 48.08"	54.11	18.03	8.17	3.78	8.09	3.43	1.12	0.63	0.21	0.18	2.52
700612	6° 12' 10.08"	76° 29' 44.23"	50.12	17.97	9.26	6.64	11.66	2.41	0.4	0.59	0.06	0.16	0.92
700615	6° 11' 14.65"	76° 28' 21.35"	53.77	17.77	8.67	4.98	9.51	2.84	0.31	0.67	0.13	0.15	1.01
700618	6° 12' 45.85"	76° 29' 08.41"	53.36	14.53	9.08	8.05	10.82	1.37	0.73	0.52	0.08	0.14	1.29
700784	6° 13' 55.21"	76° 20' 50.65"	47.76	10.39	11.17	14.2	10.47	1.27	0.32	0.39	0.06	0.23	2.58
700817	6° 20' 40.86"	76° 25' 44.52"	16.5	7.98	7.98	3.17	6.16	3.83	0.39	0.45	0.21	0.2	2.37
700852	6° 23' 03.83"	76° 22' 30.13"	50	15.78	11.73	7.58	8.57	3.07	0.37	0.58	0.19	0.18	1.98
700853	6° 20' 17.90"	76° 23' 26.08"	55.29	15.63	9.3	5.74	9.49	2.41	0.39	0.5	0.14	0.14	1.16
700854	6° 23' 56.04"	76° 24' 01.78"	54.39	15.52	9.71	5.25	8.93	2.81	0.87	0.87	0.31	0.16	1.19
700875	6° 33' 58.32"	76° 25' 12.59"	50.22	17.82	8.84	7.15	10.7	2.55	1.22	0.53	0.1	0.15	1.58
700905	6° 16' 46.15"	76° 21' 22.94"	44.3	20.5	12.09	6.35	13.48	1.03	0.06	0.56	0.02	0.17	0.51
700952	5° 10' 48.67"	75° 09' 33.70"	54.56	20.19	5.94	3.4	10.5	3.01	0.28	0.36	0.13	0.06	1.33
700967	6° 24' 15.02"	76° 19' 44.70"	47.77	19.06	11.02	5.77	10.07	2.9	0.5	0.72	0.15	0.27	1.31
700972	6° 09' 36.36"	76° 19' 55.71"	47.83	18.96	10.5	4.83	10.32	3.06	0.38	0.75	0.27	0.21	1.51
700977	6° 07' 52.42"	76° 22' 43.35"	49.64	18.12	10.97	6.17	11.23	2.21	0.15	0.59	0.1	0.18	0.71
701005	6° 07' 09.47"	76° 15' 16.24"	52.43	17.58	8.87	5.14	7.97	2.87	1.21	0.53	0.15	8.87	2.89
701012	6° 06' 40.26"	76° 16' 13.20"	65.78	15.6	4.83	2.22	5.01	3.63	1.58	0.39	0.16	−0.5	0.89
701153	6° 11' 08.03"	76° 26' 42.15"	62.53	16.71	4.8	3.12	6.9	3.49	0.57	0.46	0.11	0.18	1.1
701155	6° 11' 44.047"	76° 29' 47.51"	48.2	18.32	9.04	8	12.92	1.39	0.11	0.38	0.02	0.16	1.13
701728	6° 42' 05.88"	76° 18' 54.27"	55.98	17.77	8.53	4.08	7.18	3.28	1.14	0.58	0.16	0.12	1.53
GZ-1818	7° 00' 10.79"	76° 28' 35.70"	58.33	16.09	7.87	4.37	8.79	2.74	0.52	0.5	0.11	0.14	1.11
GZ-1867	5° 39' 05.97"	76° 28' 41.31"	58.79	14.6	8.17	4.6	5.99	4.28	0.7	0.88	0.08	0.14	1.65
HCA-1208	6° 46' 48.58"	76° 30' 55.11"	54.2	14.17	10.57	6.62	9.28	2.12	1.19	0.63	0.14	0.2	0.86
HCA-1215	6° 39' 50.28"	76° 30' 45.82"	50.57	16.17	9.72	7.88	11.3	2.51	0.38	0.51	0.12	0.18	1.24
HCA-1221	6° 41' 14.89"	76° 30' 19.68"	54.11	17.25	8.8	5.19	9.88	2.81	0.69	0.51	0.13	0.17	1.13

Table 2. Major oxides in rocks of the Acandí Batholith, Mandé Batholith, and Napi Tonalite (*continued*).

Sample	Latitude N	Longitude W	SiO ₂	Al ₂ O ₃	Fe ₂ O ₃ (T)	MgO	CaO	Na ₂ O	K ₂ O	TiO ₂	P ₂ O ₅	MnO	LOI
Mandé Batholith													
HCA-1278	6° 41' 22.42"	76° 26' 30.14"	56.93	18.22	6.97	2.75	8.44	3.31	1.12	0.45	0.28	0.14	2.38
HCP-1437	6° 42' 11.33"	76° 29' 51.94"	61.04	15.16	7.61	2.86	6.54	3.52	1.28	0.62	0.17	0.15	0.75
RM-3501	6° 49' 02.03"	76° 30' 48.44"	51.65	17.62	10.04	4.49	8.21	3.41	0.52	0.66	0.18	0.16	1.54
RM-3508	6° 48' 34.40"	76° 31' 19.41"	50.96	10.85	8.11	11.1	12.9	1.25	1.45	0.47	0.26	0.16	2.1
RM-3509	6° 52' 49.91"	76° 31' 07.71"	59.48	15.42	7.9	3.27	7.35	2.85	1.66	0.66	0.21	0.15	0.82
RM-3518	6° 53' 43.63"	76° 31' 10.91"	56.46	16.07	8.09	4.61	8.37	2.86	1.4	0.59	0.26	0.13	1.34
RM-3520	5° 12' 15.75"	76° 31' 33.38"	49.78	18.43	9.7	5.96	10	3.45	0.41	0.49	0.07	0.17	1.75
RM-3529	6° 50' 05.41"	76° 29' 30.20"	49	18.34	10.11	5.77	12.3	2.31	0.27	0.58	0.11	0.14	0.87
RM-3539	5° 11' 36.02"	76° 31' 17.17"	55.62	17.74	7.91	4.56	8.44	3.01	0.52	0.51	0.11	0.13	1.9
RM-3548	5° 10' 02.24"	76° 30' 52.90"	67.57	14.7	4.96	1.82	4.86	4.65	0.29	0.54	0.16	0.07	0.88
Napi Tonalite													
APO-0049	2° 43' 17.35"	77° 12' 37.93"	60.64	17.55	5.95	2.93	5.77	3.52	0.92	0.47	0.15	0.15	1.8
APO-0056	2° 44' 32.22"	77° 14' 26.14"	55.47	17.67	7.81	4.26	8.72	3.04	0.11	0.6	0.09	0.15	1.9
APO-0107-D	2° 38' 47.74"	77° 20' 33.98"	56.93	17.65	7.79	3.39	8.07	2.96	0.23	0.52	0.13	0.17	2
CAQ-0190P	2° 52' 12.96"	77° 08' 36.50"	58.51	16.35	5.57	3.33	4.55	4.08	0.66	0.4	0.08	0.14	6.2
CAQ-0346-P	2° 23' 40.15"	77° 35' 07.08"	46.34	15.69	8.28	7.38	7.28	1.03	1.28	0.56	0.05	0.06	11.8
CAQ-0416-P	2° 09' 43.59"	77° 28' 05.96"	42.9	18.69	13.04	5.96	12.99	1.97	0.78	0.84	0.56	0.21	1.7
CAQ-0420R	2° 10' 36.14"	77° 27' 58.89"	56.75	16.65	6.45	3.96	7.33	4.14	1.02	0.59	0.25	0.13	2.5
CLM-0377-P	2° 30' 22.56"	77° 25' 17.53"	53.19	17.7	9.03	5.14	7.61	2.28	0.08	0.66	0.09	0.27	3.8
CLM-0388-P	2° 30' 33.65"	77° 27' 48.38"	52.94	19.96	4.68	5.15	8.32	4.8	0.45	0.66	0.12	0.1	2.6
CLM-0447-L	2° 24' 48.80"	77° 30' 38.43"	52.78	18.09	8.72	4.98	9.13	2.98	0.36	0.7	0.12	0.16	1.8
CLM-0447P	2° 24' 48.80"	77° 30' 38.43"	52.83	18.13	8.37	4.81	9.06	3	0.37	0.66	0.11	0.16	2.3
CLM-0449P	2° 24' 50.76"	77° 30' 18.24"	44.2	19.34	10.6	5.56	10.7	2.1	0.65	0.96	0.05	0.18	5.4
MZD-0010-L	2° 28' 21.36"	77° 20' 12.84"	53.09	18.95	7.93	2.94	8.48	3.46	2.31	0.58	0.43	0.21	1.3
MZD-0014-R	2° 28' 46.81"	77° 21' 08.27"	41.08	18.79	14.08	6.13	14.07	1.38	0.73	0.98	0.89	0.24	1.3
MZD-0022-R	2° 28' 28.85"	77° 22' 50.19"	64.43	16.79	3.64	1.05	4.99	4.12	1.43	0.28	0.13	0.08	2.9

Source: Data from Buchely et al. (2009), Geología Regional y Prospección Ltda. (2014a, 2014b, 2014c), Rodríguez et al. (2010a, 2010b), and this research.

< 1 with LREE decreasing relative to HREE, matching the REE pattern of the Nakamura chondrite (Nakamura, 1974) (Figure 10).

4.5. Geotectonic Environment of the Chocó–Panamá Arc

The geochemical discrimination and tectonic environment diagram of Condie & Kröner (2013) shows similar distributions between the Santa Cecilia–La Equis Complex, Timbiquí Formation, the Acañí and Mandé Batholiths, and Napi Tonalite (Figure 11a, 11b). The volcanic and plutonic units of the Chocó–Panamá Arc plot in the field of continental arcs at the interface with oceanic arcs. In Pearce (2008) and Wood (1980) the samples are distributed within the active continental margin arc field with a few samples in the island arc field.

4.6. Geochronology

This study reports four new Ar–Ar ages: One from the Santa Cecilia–La Equis Complex, one from the Acañí Batholith, one from the Mandé Batholith and one from the porphyritic units that intrude the Acañí Batholith (Table 3).

Sample IGM–900317 is a porphyritic basalt of the Santa Cecilia–La Equis Complex collected in the Cutí River Basin, composed of plagioclase, clinopyroxene, and orthopyroxene phenocrysts in a microlitic matrix. The sample yields a three-stage plateau age of 45.3 ± 1.6 Ma, featuring 75.9% ^{39}Ar . The integrated age of sample IGM–900317 is 45.6 ± 1.6 Ma (Figure 12). The inverse isochron shows a linear trend, suggesting an age of 45.3 ± 2.6 Ma with MSWD = 0.64. The age was extracted from a whole-rock analysis and corresponds to the Lutetian Stage of the Eocene.

Few dates are available for the Santa Cecilia–La Equis Complex. Buchely et al. (2009) obtained an Ar–Ar age of 50.7 ± 2.0 Ma from a volcanic basalt glass, revealing a plateau age of 55 Ma, interpreted as the total fusion age.

The tonalite sample IGM–900369 was collected from the Acañí Batholith along the Tanela River. It is an inequigranular, hypidiomorphic, fine- to medium-grained rock with plagioclase (51%), quartz, hornblende, and biotite. It presents a four-stage plateau with 62.5% ^{39}Ar , suggesting an age of 51.84 ± 2.14 Ma, and an integrated age of 51.54 ± 2.04 Ma. The inverse isochron diagram reveals a linear trend in all points except at 900 °C, yielding an age of 48.13 ± 5.76 Ma with MSWD = 0.34 (Figure 13). The ages are from whole-rock analysis and correspond to the Ypresian Stage of the Eocene.

The Ar–Ar dating of tonalite from the Acañí Batholith agrees with the results of Buchely et al. (2009), yielding an age of 51.84 ± 2.14 Ma for this unit. Montes et al. (2015) published three U–Pb crystallization ages in zircon between 49.5 ± 0.9

and 49.7 ± 1.6 Ma. This range matches the age of the Mandé Batholith (Table 4).

The tonalite sample (IGM–706477) from the Mandé Batholith, collected along the Medellín–Quibdó road between Carmen de Atrato and El Doce, yields an age range with three high-temperature stages. A plateau featuring 92.9% ^{39}Ar reveals an age of 53.07 ± 1.92 Ma, with an integrated age of 54.47 ± 2.1 Ma. The inverse isochron reveals a linear trend with an age of 49.49 ± 3.66 Ma, with MSWD = 0.29 (Figure 14). Ages were extracted from hornblende and correspond to the Ypresian Stage of the Eocene.

The andesite porphyry sample IGM–900005 from the unit of andesitic porphyry bodies consists of plagioclase, hornblende, and biotite phenocrysts embedded in a felsite microcrystalline matrix. The sample yields a six-stage plateau with an age of 48.1 ± 2.0 Ma and an integrated age of 47.1 ± 2.0 Ma (86.3% ^{39}Ar). The inverse isochron shows a linear trend yielding an age of 46.2 ± 5.4 Ma, with MSWD = 1.6 (Figure 15). The age obtained from the whole-rock analysis corresponds to the Ypresian Stage of the Eocene.

5. Discussion and Conclusions

5.1. Arc Composition

The Chocó–Panamá Arc in Colombia is exposed against the western margin of the Colombia Plateau and is fragmented in segments extending from Panamá to Ecuador. At least three segments or blocks are similar in lithology, geochemical composition, and age. Previous research has associated the Timbiquí Formation and the Napi Tonalite with the Santa Cecilia–La Equis Complex and the Mandé Batholith (Echeverri et al., 2015; Geología Regional y Prospección Ltd., 2014a, 2014b, 2014c; Rodríguez et al., 2010a), although this correlation remained unsupported. Additionally, the San Blas Complex and the Azuero Marginal Complex in Panamá have been associated with the Chocó–Panamá Arc (Barat et al., 2014; Montes et al., 2012; Ramírez et al., 2016).

The Chocó–Panamá Arc is formed of volcanic units (Santa Cecilia–La Equis Complex, Timbiquí Formation) composed of basalt, andesite, and dacite lava flows, pillow lavas, and pyroclastic rocks such as breccias, agglomerates, and tuffs (Buchely et al., 2009; Calle & Salinas, 1986; Cossio, 1994; Geología Regional y Prospección Ltd., 2014a, 2014b, 2014c; González, 2001; Rodríguez et al., 2010b, 2013) and plutonic units (Mandé, Acañí Batholiths and Napi Tonalite), of gabbroic to granitic composition, with prevailing quartz diorite and tonalite.

The petrographic and geochemical data suggest that the initial composition of the arc was metaluminous subalkaline tholeiitic basaltic lavas and gabbros that later evolved to calc-alkaline continental margin arc rocks, characterized by metalu-

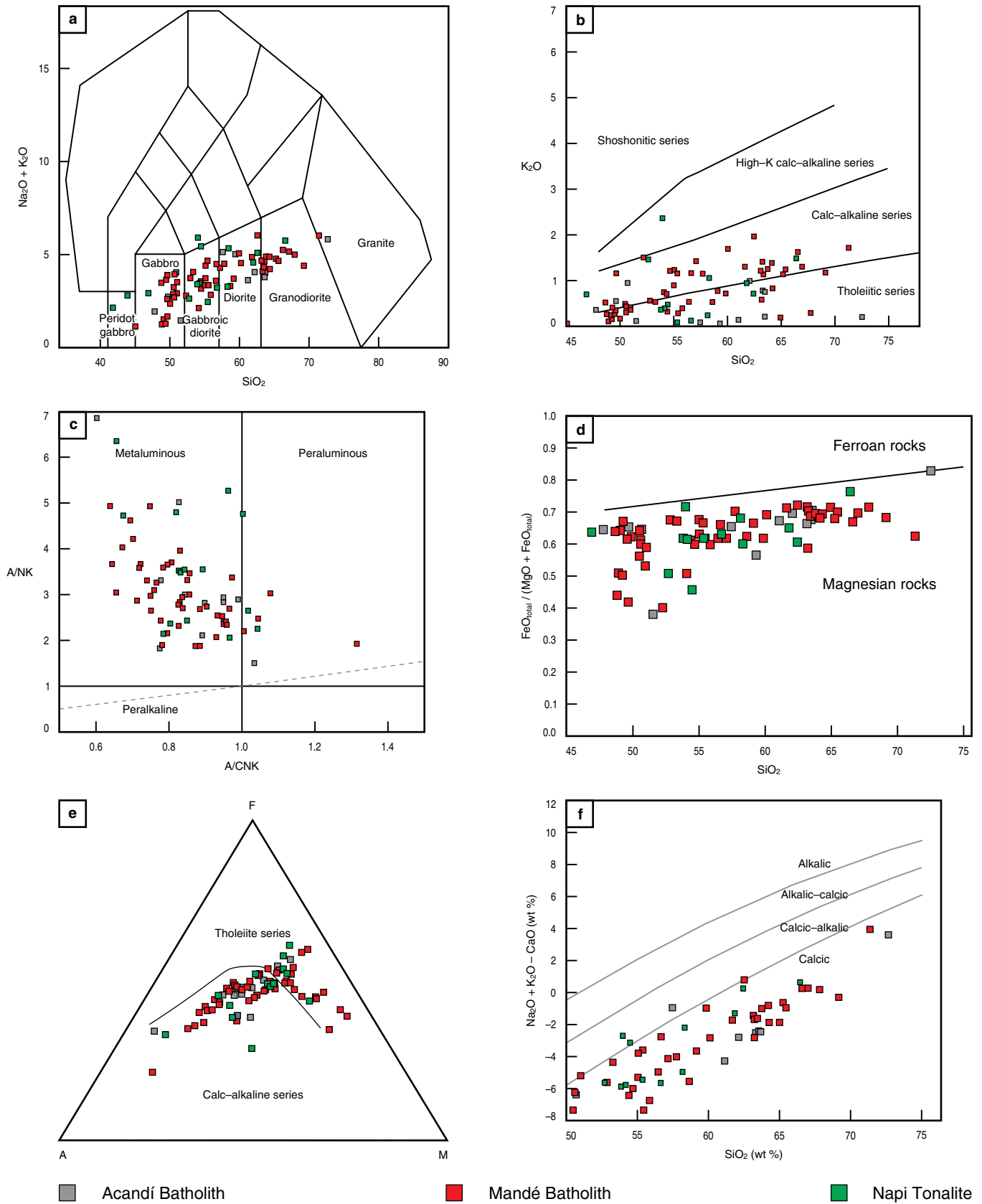


Figure 9. Classification diagrams for the Acandí Batholith (gray), Mandé Batholith (red), and Napi Tonalite (green). **(a)** TAS diagram (Middlemost, 1994). **(b)** K_2O vs. SiO_2 diagram (Peccerillo & Taylor, 1976). **(c)** Aluminosity-alkalinity diagram (Shand, 1943). **(d)** Diagram to discriminate between ferroan and magnesian rocks (Frost & Frost, 2008). **(e)** AFM diagram (Irvine & Baragar, 1971). **(f)** Alkali-lime vs. SiO_2 diagram after Frost et al. (2001).

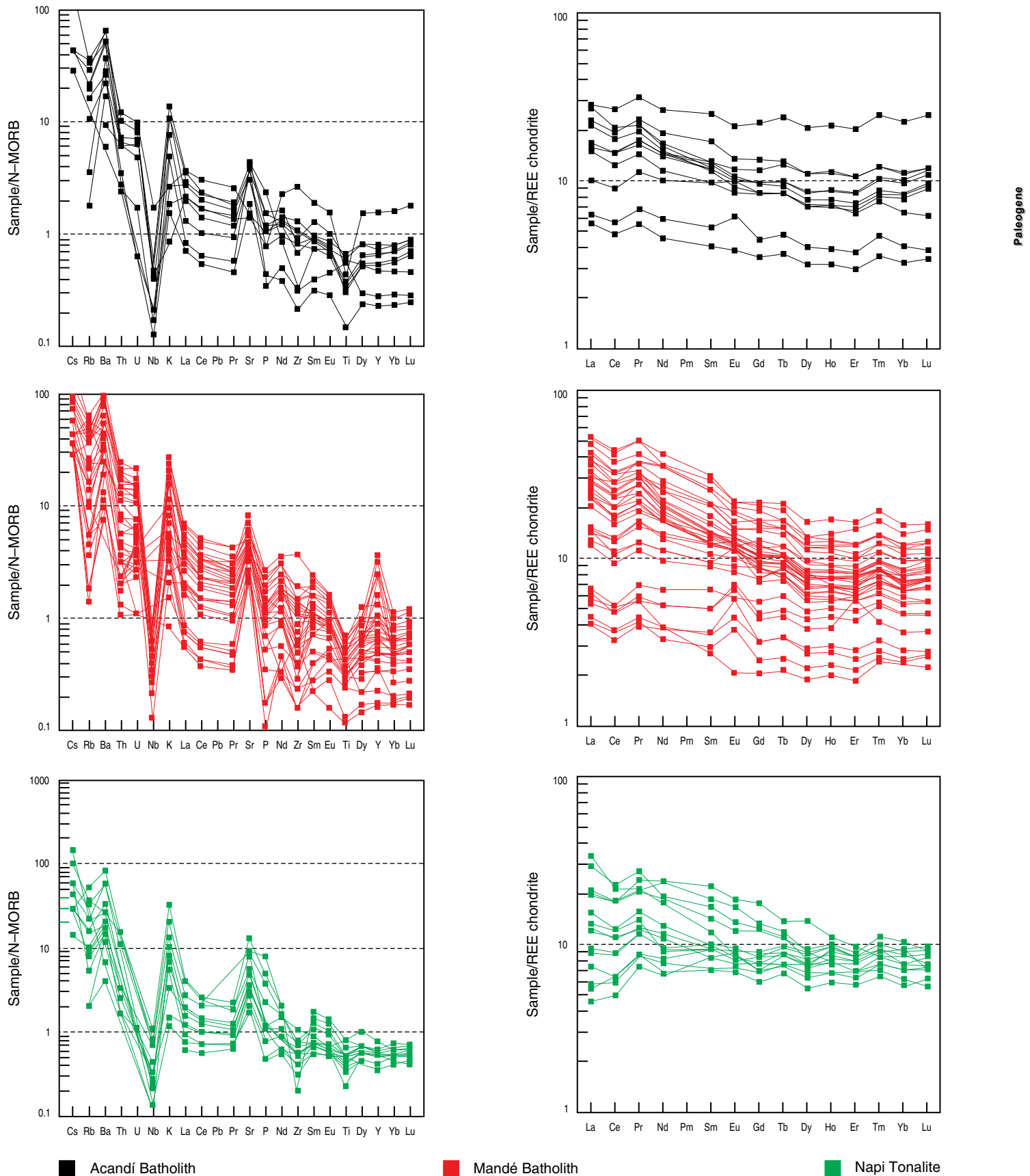


Figure 10. Trace elements vs. N-MORB diagram (Sun & McDonough, 1989) and rare earth elements vs. chondrite (Nakamura, 1974). Acandí Batholith (black), Mandé Batholith (red), and Napi Tonalite (green).

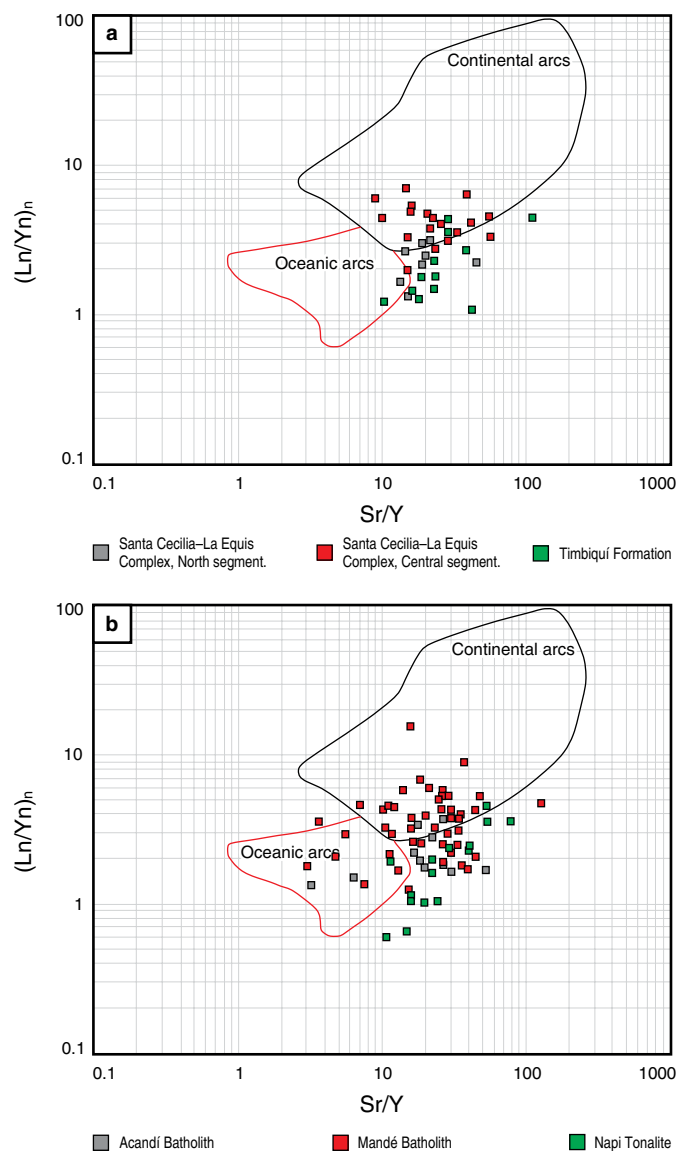


Figure 11. Tectonic environment discrimination diagrams for the Chocó-Panamá Arc (Condie & Kröner, 2013). **(a)** Santa Cecilia-La Equis Complex North segment (gray), Central segment (red), and Timbiquí Formation South segment (green). **(b)** Acandí Batholith (gray), Mandé Batholith (red), and Napi Tonalite (green).

minous subalkaline intermediate andesite and plutonic quartz diorites and tonalities, as sediments and water entered the mantle along the subducted slab (Álvarez & Parra, 1979; Guarín & Álvarez, 1975; Ingeominas & Organización de las Naciones Unidas, 1982; Ramírez et al., 1979; Sillitoe et al., 1982).

The multielement diagrams show that the igneous rocks studied have typical arc geochemical affinities. Trace element patterns are characterized by negative Nb, Ti, and Zr anomalies and positive Cs, Ba, Th, Sr, and Rb anomalies and depletions in LREE relative to HREE. Different REE patterns vs. chondrites are recognized in this research for both volcanic and plutonic

Table 3. Ar-Ar ages of rocks from the Chocó-Panamá Arc.

IGM	Latitude N	Longitude W	IIA (Ma) \pm 2s	TFA (Ma) \pm 2s	WMPA (Ma) \pm 2s	Ca/K	Comments	Petrographic Observations
900317	8° 11' 57.5644"	77° 07' 31.2052"	45.3 \pm 2.6	45.6 \pm 1.6	45.3 \pm 1.6	2.7–78.9	Three steps plateau	Porphyritic basalt Santa Cecilia-La Equis Complex
900369	8° 17' 10.7021"	77° 10' 24.9930"	48.13 \pm 5.76	51.54 \pm 2.04	51.84 \pm 2.14	7.25–13.92	Four steps plateau	Acandí Batholith tonalite
706477	5° 44' 43.6155"	76° 16' 30.8074"	49.49 \pm 3.66	54.47 \pm 2.1	53.07 \pm 1.92	2.31–24.98	Three steps high temperature plateau	Mandé Batholith tonalite
900005	8° 36' 53.0117"	77° 21' 44.3220"	46.2 \pm 5.4	47.1 \pm 2.0	48.1 \pm 2.0	2.61–17.45	Six steps plateau	Porphyritic andesite-andesite and dacite

Note: (TFA) Total fusion age; (IIA) Inverse isochrone age; (WMPA) Weighted mean plateau age; (Ca/K) Apparent Ca/K ratios; (WMPA) Weighted mean intermediate plateau age. 2s \pm 1 = Estimated uncertainty (2s)

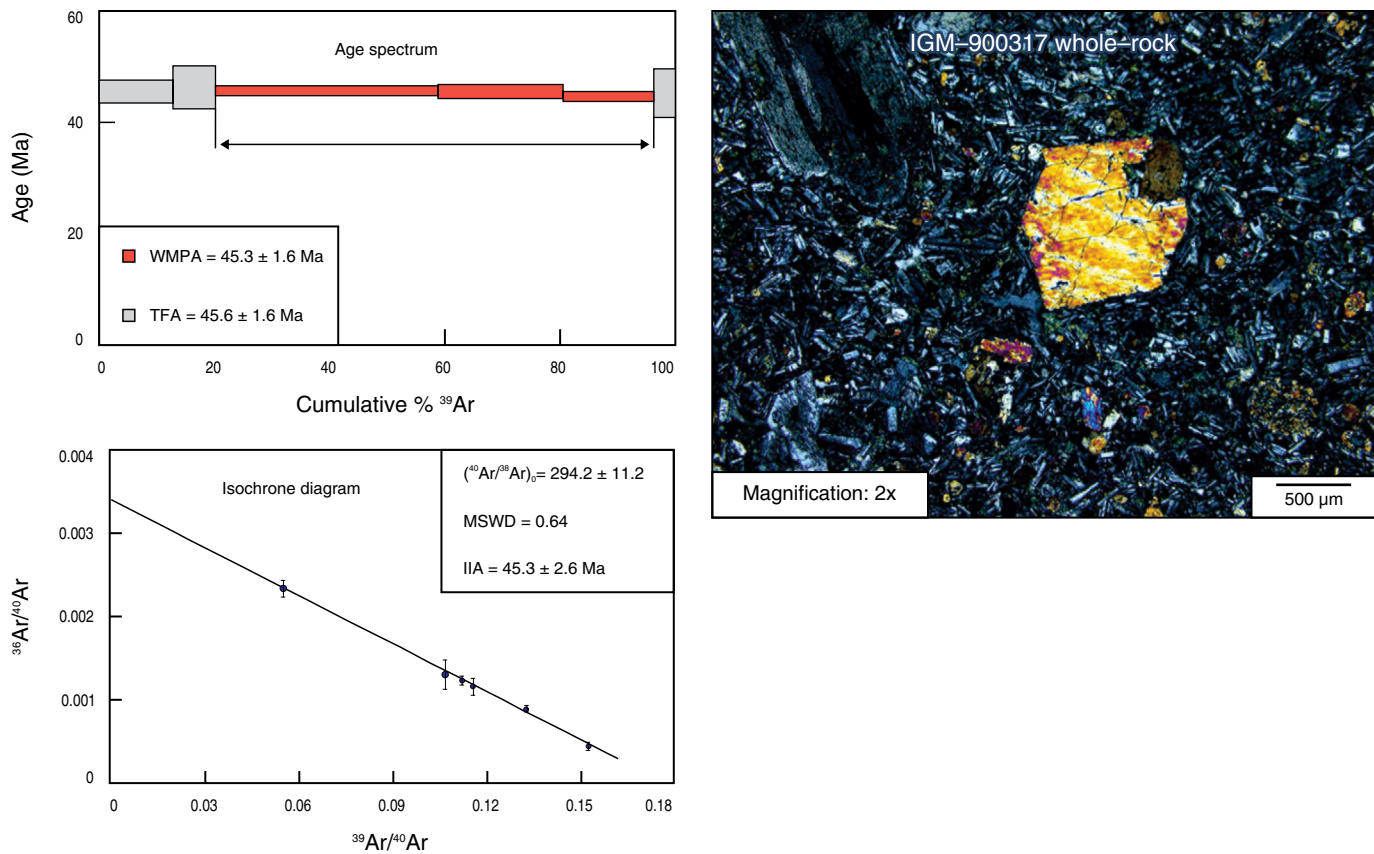


Figure 12. Sample IGM-900317 age range, Santa Cecilia–La Equis Complex basalt.

rocks, suggesting more than one magmatic pulse in the evolution of the Chocó–Panamá Arc.

5.2. Age

The ages of the different Chocó–Panamá Arc components (volcanic and plutonic rocks) are compiled in Gómez et al. (2015b) as a part of the Geological Map of Colombia (Table 4). The arc volcanic rocks from the Santa Cecilia–La Equis Complex (Central segment) yield Ar–Ar ages in volcanic glass of 50.7 ± 2.0 Ma, 55.1 ± 1.5 Ma, and 36.7 ± 11.5 Ma (Buchely et al., 2009). The latter age, with high error, suggests Ar loss and low reliability for the date. Such ages are considered close to the rock crystallization age because they were obtained in volcanic glass that cooled rapidly. In the Acandí zone (North segment), the Santa Cecilia–La Equis Complex yields a whole-rock Ar–Ar age of 45.3 ± 1.6 Ma (this study). For the Timbiquí Formation (South segment), McCourt et al. (1990) reported K–Ar ages of 53.4 ± 3 Ma and 41 ± 1 Ma (Ypresian – Bartonian) in andesites and 46.7 ± 2 Ma (Lutetian) for andesitic dikes that cut the unit, describing a pyroclastic event at 32.1 ± 3.5 Ma (Rupelian Stage of the Oligocene). These data suggest that volcanism in the Chocó–Panamá Arc occurred at least between 56.5 and 45 Ma (Ypresian – Lutetian).

The Acandí Batholith (North segment) yields a whole-rock Ar–Ar cooling age (tonalite) of 51.84 ± 2.14 Ma (this study). The Mandé Batholith (Central segment) presents a K–Ar date of 54.7 ± 1.3 (Sillitoe et al., 1982) to 34 Ma (Botero, 1975); Ar–Ar ages in basic facies (gabbro-norite) between 53.6 ± 2.9 and 52.7 ± 3.2 Ma (Buchely et al., 2009), interpreted as closure ages of the pluton basic facies; and Ar–Ar ages in hornblende and biotite from the intermediate facies (tonalite) between 52.7 ± 3.2 and 48.0 ± 1.5 Ma (Buchely et al., 2009; this study), which correspond to cooling ages. Most of the Ar–Ar ages in tonalites are slightly younger than those of the basic facies, matching the macroscopic observations of the lithological relationships in the pluton (Table 4).

The Ar–Ar ages reported in this study are older than the zircon U–Pb ages obtained by Montes et al. (2015) 43.8 ± 0.8 Ma and 42.5 ± 1.3 Ma for the Mandé Batholith and ages between 49.7 ± 1.6 and 49.5 ± 0.9 Ma for the Acandí Batholith (Table 4). This discrepancy may be caused by excess argon or by analyses conducted in different facies of the pluton.

McCourt et al. (1990) determined K–Ar ages between 53 ± 5 and 39 ± 2 Ma (Ypresian – Bartonian) for the Napi Tonalite (South segment). Additionally, the authors suggest that the Balsitas Leucotonalite, with a K–Ar age of 48 ± 1 Ma (Ypresian), and an andesite dike that segments the leucotonalite, with an

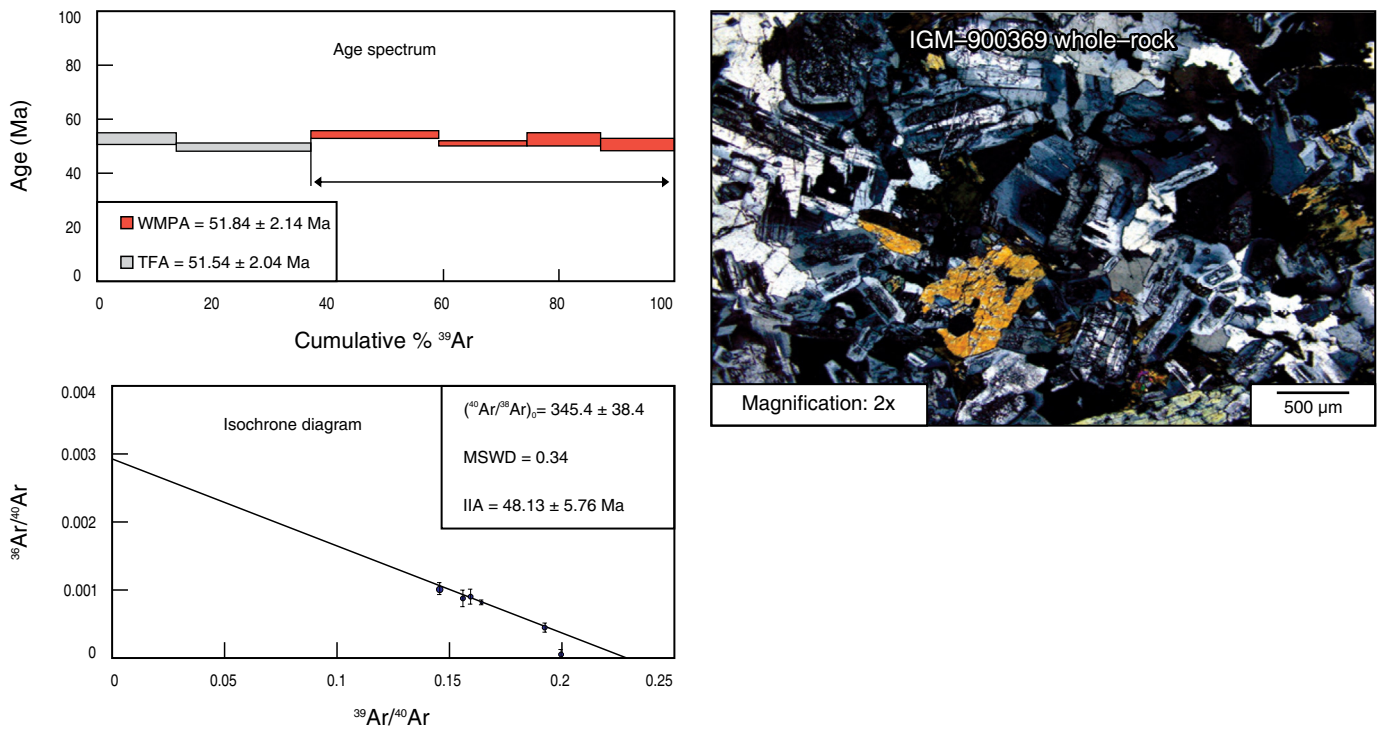


Figure 13. Sample IGM-900369 age range, Acandí Batholith tonalite.

age of 42.6 ± 1.3 Ma (Lutetian), are of similar lithological composition. El Salto Tonalite yields a K–Ar age of 51 ± 1 Ma (Ypresian) and is also correlated with the Napi Tonalite according to the authors (Table 4).

Geología Regional y Prospección Ltd. (2014a, 2014b, 2014c) report two U–Pb zircon LA–ICP–MS ages of 46.8 ± 0.7 Ma and 45.6 ± 0.6 Ma (Lutetian) for dioritic and granodioritic rocks associated with the Guapi Ultramafite.

Mineralized porphyry units intruding the volcanic rocks of the Santa Cecilia–La Equis Complex and the Acandí and Mandé Batholiths yield K–Ar and Ar–Ar cooling ages (Table 4) between 54.7 ± 1.3 (Murindó project) and 42.7 ± 0.9 Ma (Pantanos project) (Sillitoe et al., 1982). Leal–Mejía (2011) report two U–Pb zircon ages from mineralized porphyry units from the central sector, yielding crystallization ages of 45.3 ± 1.2 Ma and 44.6 ± 0.9 Ma. The K–Ar and Ar–Ar ages are considered minimum ages of the emplacement of the copper porphyry system and match those of Río Pito, an extension of the Acandí Batholith in Panamá (Sillitoe et al., 1982).

The K–Ar, Ar–Ar, and U–Pb ages of the plutonic rocks from the Acandí and Mandé Batholiths, Napi Tonalite, Balsitas Leucotonalite, El Salto Tonalite, dioritic and granodioritic facies associated with the Guapi Ultramafite, and units of mineralized andesitic and dacitic porphyries from the North and Central segments of the arc suggest that plutonism associated with the Chocó–Panamá Arc began ca. 56 Ma (Ypresian) and ended ca. 37 Ma (Bartonian). These ages are similar to the zircon U–Pb and Ar–Ar ages obtained in the San Blas and Azuero margin-

al complexes in Panamá (Montes et al., 2012; Ramírez et al., 2016; Wegner et al., 2011).

Wegner et al. (2011) report Ar–Ar ages in hornblende of 49.4 ± 1.0 Ma in the Cerro Azul Gabbro and 47.2 ± 1.3 Ma in the Mamoni Quartz diorite. Additionally, Montes et al. (2012), Ramírez et al. (2016), and Villagómez (2010) report that the cooling ages of the Mandé Batholith are similar to those of the San Blas Complex in Panamá and suggest that these plutonic bodies cooled and were exhumed during different episodes between 47 and 9 Ma by tectonic, volcanic, and erosional events.

The geochronological, stratigraphic, and lithogeochemical relationships of the Timbiquí Formation and Napi Tonalite present characteristics similar to those of the Acandí and Mandé Batholiths and the Santa Cecilia–La Equis Complex, suggesting that they are part of the Chocó–Panamá Arc and represent a dispersed segment of the arc.

5.3. Arc Basement

Buchs et al. (2010) and Montes et al. (2012) provide clear evidence of the occurrence of an oceanic plateau at the base of the Eocene volcanic arc in Panamá; however, little is known about the basement of the Chocó–Panamá Arc in Colombia. At the western edge of the North segment, the discordant marine sedimentites and breccia sequences of the Tripogadí Sedimentites and the Triganá Breccias (Rodríguez & Sierra, 2010; Rodríguez et al., 2010b) rest on an unknown basement. In the Central segment, the western boundary with the San José de

Table 4. Radiometric ages of different Chocó–Panamá Arc units (updated from Gómez et al., 2015b and Geología Regional y Prospección Ltd., 2014a, 2014b, 2014c).

Sample	Lithology	Latitude N	Longitude W	Age (Ma)	Dating method	Material analyzed	Reference
Santa Cecilia–La Equis Complex (North segment)							
IGM–900317	Porphyritic basalt	8° 11' 57.5644"	77° 07' 31.2052"	45.3 ± 1.6	Ar–Ar	Volcanic glass	Present study
Santa Cecilia–La Equis Complex (Central segment)							
IGM–706917	Porphyritic basalt	6° 44' 37.27"	76° 23' 20.65"	50.7 ± 2.0	Ar–Ar	Volcanic glass	Buchely et al. (2009)
Timbiquí Formation							
AM2589	Andesitic tuff	2° 17' 28.05"	77° 38' 45.82"	32.1 ± 3.5	K–Ar		McCourt et al. (1990)
HV309		2° 17' 31.77"	77° 09' 04.59"	33 ± 2	K–Ar		McCourt et al. (1990)
AM2588	Andesite	2° 17' 31.97"	77° 38' 54.48"	38.9 ± 4.3	K–Ar		McCourt et al. (1990)
BX12	Andesite	2° 23' 42.98"	77° 34' 29.58"	41.7 ± 1.2	K–Ar		McCourt et al. (1990)
BX70	Andesite	2° 12' 16.60"	77° 40' 39.02"	41 ± 1	K–Ar		McCourt et al. (1990)
BX72A	Andesite	2° 11' 01.67"	77° 42' 03.70"	44 ± 1	K–Ar		McCourt et al. (1990)
BX76	Timbiquí Formation dike	2° 10' 34.91"	77° 41' 56.95"	46.7 ± 2	K–Ar		McCourt et al. (1990)
BX72	Andesite	2° 11' 00.63"	77° 42' 13.12"	50.7 ± 2	K–Ar		McCourt et al. (1990)
BX71	Andesite	2° 11' 15.25"	77° 42' 20.19"	53.4 ± 3	K–Ar		McCourt et al. (1990)
Acandí Batholith							
IGM–900369	Tonalite	8° 17' 10.7021"	77° 10' 24.9930"	51.84 ± 2.14	Ar–Ar	Total rock	Present study
GA–001	Granitoide	8° 30' 33.84"	77° 20' 13.56"	49.5 ± 0.9	U–Pb	Zircon	Montes et al. (2015)
VM–001	Granitoide	8° 26' 21.48"	77° 19' 19.56"	49.7 ± 1.6	U–Pb	Zircon	Montes et al. (2015)
VM–003	Granitoide	8° 50' 54.492"	77° 20' 24.719"	49.5 ± 1.1	U–Pb LA–ICP–MS	Zircon	Montes et al. (2015)
Mandé Batholith							
Ch–51	Granodiorite	5° 43' 08.99"	76° 20' 56.17"	34	K–Ar	Biotite	Botero (1975)
IGM–304958	Quartzdiorite	8° 32' 03.45"	77° 25' 01.08"	38.9 ± 3	K–Ar	Sericite	Álvarez & Parra (1979)
IGM–706956	Tonalite	6° 48' 31.90"	76° 35' 26.53"	48.0 ± 1.5	Ar–Ar	Hornblende and biotite	Buchely et al. (2009)
UAKA 80–22	Tonalite	8° 27' 51.45"	77° 49' 01.18"	48.1 ± 1	K–Ar	Hydrothermal sericite	Sillitoe et al. (1982)
IGM–706477	Tonalite	5° 44' 43.6155"	76° 16' 30.8074"	53.07 ± 1.92	Ar–Ar	Total rock	Present study
IGM–706957	Tonalite	6° 48' 31.90"	76° 35' 26.53"	48 ± 1.5	Ar–Ar	Hornblende and biotite	Buchely et al. (2009)
IGM–707151	Gabbroiorite	6° 34' 0.50"	76° 35' 29.06"	52.7 ± 3.2	Ar–Ar	Total rock	Buchely et al. (2009)
DV–165	Granitoide	5° 46' 04.80"	76° 14' 56.40"	43.8 ± 0.8	U–Pb	Zircon	Montes et al. (2015)
DV–167	Granitoide	5° 46' 15.24"	76° 14' 51.00"	42.5 ± 1.3	U–Pb	Zircon	Montes et al. (2015)

Table 4. Radiometric ages of different Chocó–Panamá Arc units (updated from Gómez et al., 2015b and Geología Regional y Prospección Ltd., 2014a, 2014b, 2014c) (*continued*).

Sample	Lithology	Latitude N	Longitude W	Age (Ma)	Dating method	Material analyzed	Reference
Napi Tonalite							
BX61	Hornblende diorite	2° 29' 24.04"	77° 28' 52.79"	39 ± 2	K–Ar		McCourt et al. (1990)
HCPI0	Hornblende quartz tonalite	2° 27' 49.62"	77° 30' 00.51"	41 ± 4	K–Ar		McCourt et al. (1990)
JCM3504	Hornblende gabbro	2° 31' 44.11"	77° 26' 47.97"	43 ± 0.4	K–Ar		McCourt et al. (1990)
BX60	Hornblende tonalite	2° 29' 31.95"	77° 29' 07.54"	44 ± 4	K–Ar		McCourt et al. (1990)
AM2602	Hornblende tonalite	2° 31' 10.78"	77° 25' 53.86"	53 ± 5	K–Ar		McCourt et al. (1990)
Guapi Ultramafite							
APO0056	Diorite/granodiorite	2° 44' 32.22"	77° 14' 26.14"	46.8 ± 0.7	U–Pb LA–ICP–MS	Zircon	Geología Regional y Prospección Ltd. (2014a, 2014b, 2014c)
CLM–0376 R	Granodiorite	2° 30' 33.05"	77° 25' 02.48"	45.6 ± 0.6	U–Pb LA–ICP–MS	Zircon	Geología Regional y Prospección Ltd. (2014a, 2014b, 2014c)
El Salto Pluton							
BX68	Moscovitic pegmatite	2° 12' 23.81"	77° 39' 30.20"	51 ± 1	K–Ar		McCourt et al. (1990)
Balsitas Pluton							
BX73	Andesite dike	2° 10' 24.66"	77° 41' 42.43"	42.6 ± 1.3	K–Ar		McCourt et al. (1990)
BX74	Tonalite	2° 10' 24.07"	77° 41' 24.67"	48 ± 1	K–Ar		McCourt et al. (1990)
Mandé Porphyry Units							
UAKA 80–23	Porphyritic dacite	6° 41' 50.10"	76° 29' 47.93"	42.7 ± 0.9	K–Ar	Hydrothermal sericite	Sillitoe et al. (1982)
WR–238	Porphyritic tonalite	6° 43' 35.7"	76° 31' 16.9"	44.6 ± 0.9	U–Pb LA–MC–ICP–MS	Zircon	Leal–Mejía (2011)
WR–237	Porphyritic tonalite	6° 43' 24.40"	76° 31' 07.40"	45.3 ± 1.2	U–Pb LA–MC–ICP–MS	Zircon	Leal–Mejía (2011)
IGM–900005	Porphyritic andesite	8° 36' 53.01"	77° 21' 44.32"	48.1 ± 2.0	Ar–Ar	Total rock	Present study
UAKA 79–42	Porphyritic tonalite	7° 02' 50.12"	76° 44' 47.95"	54.7 ± 1.3	K–Ar	Hornblende	Sillitoe et al. (1982)
Porphyry units (South segment)							
BX20R	Andesitic porphyry	2° 12' 44.36"	77° 41' 35.96"	51.5 ± 1.5	K–Ar		McCourt et al. (1990)
AM2586	Andesitic porphyry	2° 17' 14.44"	77° 38' 10.96"	48.4 ± 4.8	K–Ar		McCourt et al. (1990)

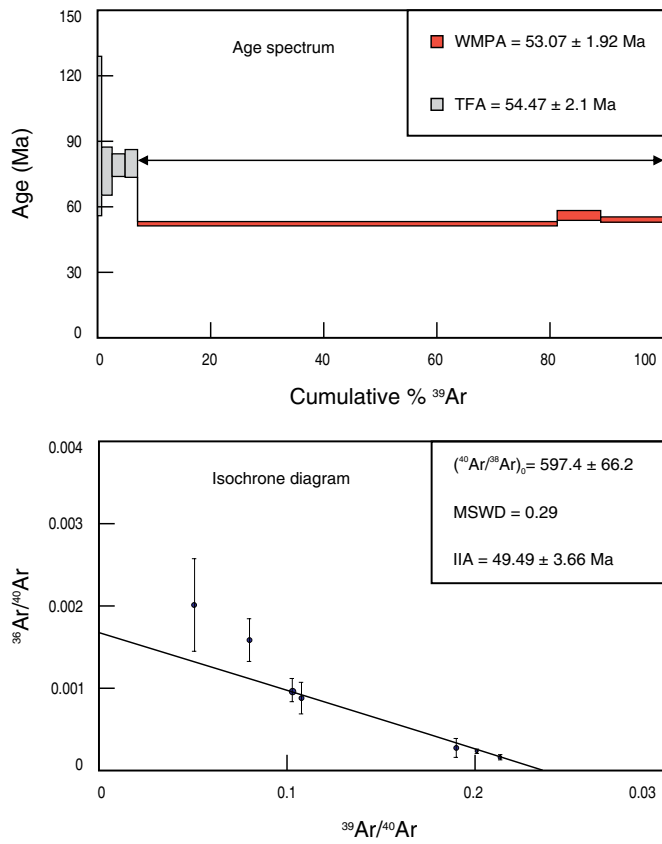


Figure 14. Sample IGM-706477 age range, Mandé Batholith tonalite.

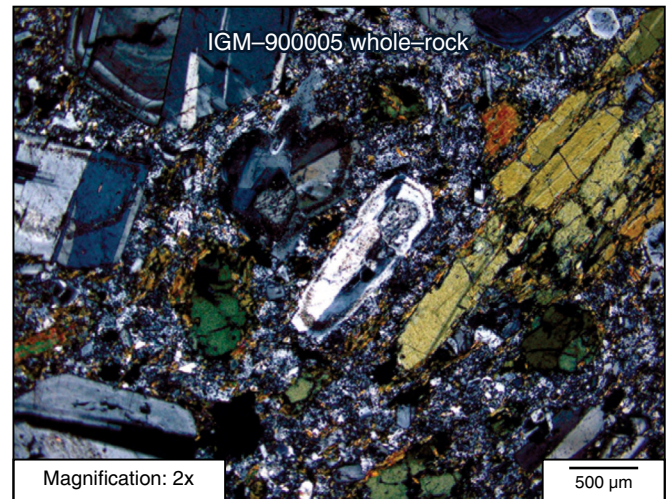
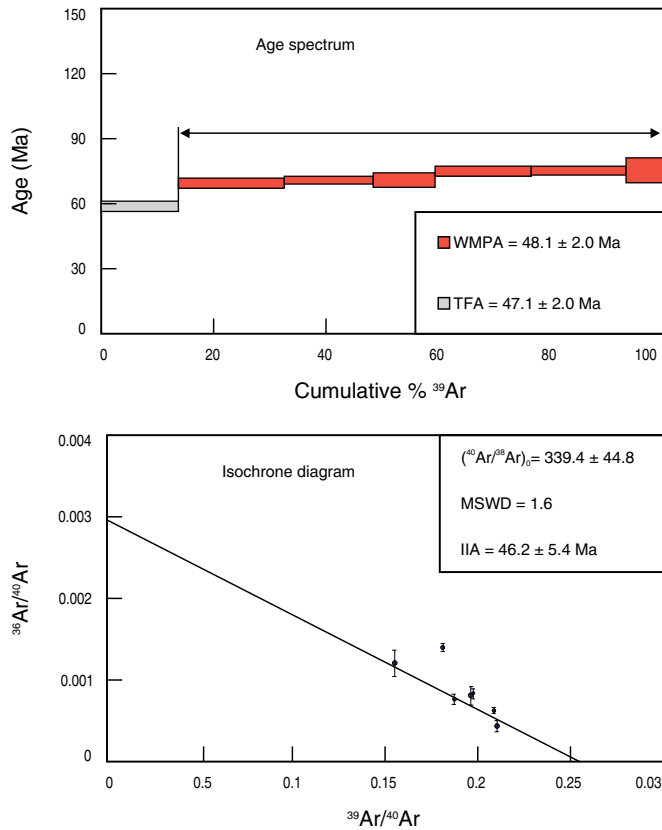


Figure 15. Sample IGM-900005 age range, porphyritic andesite of andesite units and porphyritic dacite.

Urama Diabase (Rodríguez & Arango, 2013) or the Cañasgordas Block (González, 2001) is limited by the Uramita, Dabeiba–Pueblo Rico, and Avirama Faults (Rodríguez & Zapata, 2012), and the basement on which the arc formed is unknown. In the South segment, the eastern boundary with the Dagua Structural Complex is Piedramadura Fault (Geología Regional y Prospección Ltd., 2014a, 2014b, 2014c), under which the arc basement is unknown.

Four samples of basalt and subalkaline tholeiitic diabase (corresponding to basalts with ophitic and subophitic textures composed of crisscrossed plagioclase crystals, clinopyroxene and intersertal glass) distributed along the western edge of the Santa Cecilia–La Equis Complex in the Central segment of the arc present SiO_2 contents between 45.5 and 50.8%, flat REE patterns (similar to those of the San Jose de Urama Diabase), and $(\text{La}/\text{Yb})_n$ ratios between 1 and 2. Samples plot within the oceanic basalt field (MORB–OIB), grouped in an intermediate position and outside the Gorgona Basalt and the Colombia Plateau (San José de Urama Diabase) fields. These data may suggest that the arc is built on rocks of oceanic affinity, with different geochemical compositions from the Colombia Plateau and Gorgona Basalt (Table 5, Figure 16).

Echeverri et al. (2015) considered that the Timbiquí Formation and granitoids of arc affinity may be related to the southeastern segment of the Caribbean Plate, including the Panamá Isthmus and the northwest sector of the Colombian continental margin. This area includes a basaltic substrate with plateau affinity and a superimposed magmatic arc <70 Ma. Therefore, the interaction with South America may have lasted from late Eocene to Miocene and may not be related to the rocks of the Colombian Western Cordillera, which would already have been accreted.

This geological context is similar to that of western and central Panamá, where the pre–Oligocene volcanic fronts are emplaced within and on top of the oceanic plateau sequences interpreted to belong to the Caribbean Large Igneous Province (Buchs et al., 2010; Montes et al., 2012). This similarity is consistent with our hypothesis that the pre–Oligocene volcanic front in Panamá and the studied sequences in western Colombia originally belonged to a single intraoceanic volcanic arc.

These four representative data from the oceanic basement where the Chocó–Panamá Arc formed suggest a T–MORB oceanic crust different from the Colombia Plateau of the Western Cordillera. The Chocó–Panamá Arc originally formed as an island arc that later evolved into a continental margin arc (Figure 17) and collided with the western margin of the Colombia Plateau between 37 and 12 Ma. This age range corresponds to the ending of the magmatic activity associated with the Chocó–Panamá Arc and the origin of El Botón Arc, between 12 and 8.5 Ma (Rodríguez & Zapata, 2012; Zapata & Rodríguez, 2011). This latter event intruded the rocks of the Chocó–Panamá Arc and Colombia Plateau. The collision is recorded by the deposi-

Table 5. Trace element values for four diabase and basalt samples with affinity to oceanic crust from the Santa Cecilia–La Equis Complex.

IGM	Lati- tude N	Lon- gitude W	Sc	Be	V	Cr	Co	Ni	Cu	Zn	Ga	Ge	Rb	Sr	Y	Zr	Nb	In	Sn	Sb	Cs	Ba	La	Ce	Pr	Nd	Sm	Eu	Gd	Tb	Dy	Ho	Er	Tm	Yb	Lu	Hf	Ta	W	Ti	Bi	Th	U					
			95885	5° 56'	76° 15'	46	0.5	287	278	42	119	193	118	13	1.6	2	108	18	42	2.7	0.1	1	0.4	0.1	44	3.1	7.5	1.2	6.2	2.1	0.8	2.5	0.5	3.3	0.7	2.1	0.3	2	0.3	1.4	0.2	0.3	0	0.1	0.2	0.1		
		40.00"																																														
95888	5° 58'	76° 14'	46	0.5	271	111	38	83	253	95	17	1.4	5	487	18	55	3	0.1	0.5	0.1	0.1	123	3.3	8.2	1.3	7.3	2.4	1	2.8	0.5	3.4	0.7	2.1	0.3	1.9	0.2	1.7	0.2	0.3	0.1	0	0.2	0.1					
	15.76"	41.22"																																														
700337	5° 49'	76° 14'	49	0.5	293	369	45	107	121	76	13	1.4	1	103	17	47	2.7	0.1	0.5	0.1	0.1	24	6	12	1.5	6.9	2	0.7	2.5	0.5	3.2		1.9	0.3	1.9	0.3	1.9	0.2	0.5	0.1	1	0.3	0.1					
	41.25"	09.55"																																														
703317	6° 26'	76° 20'	36	0	175	570	37	240	40	60	10	1	4	132	14	45	1.5	0	0	0.9	0	94	2.7	6.8	1.2	5.9	1.7	0.6	2.3	0.4	2.5	0.5	1.5	0.2	1.4	0.2	1.2	0.1	0	0	0	0.2	0.1					
	17.87"	10.56"																																														

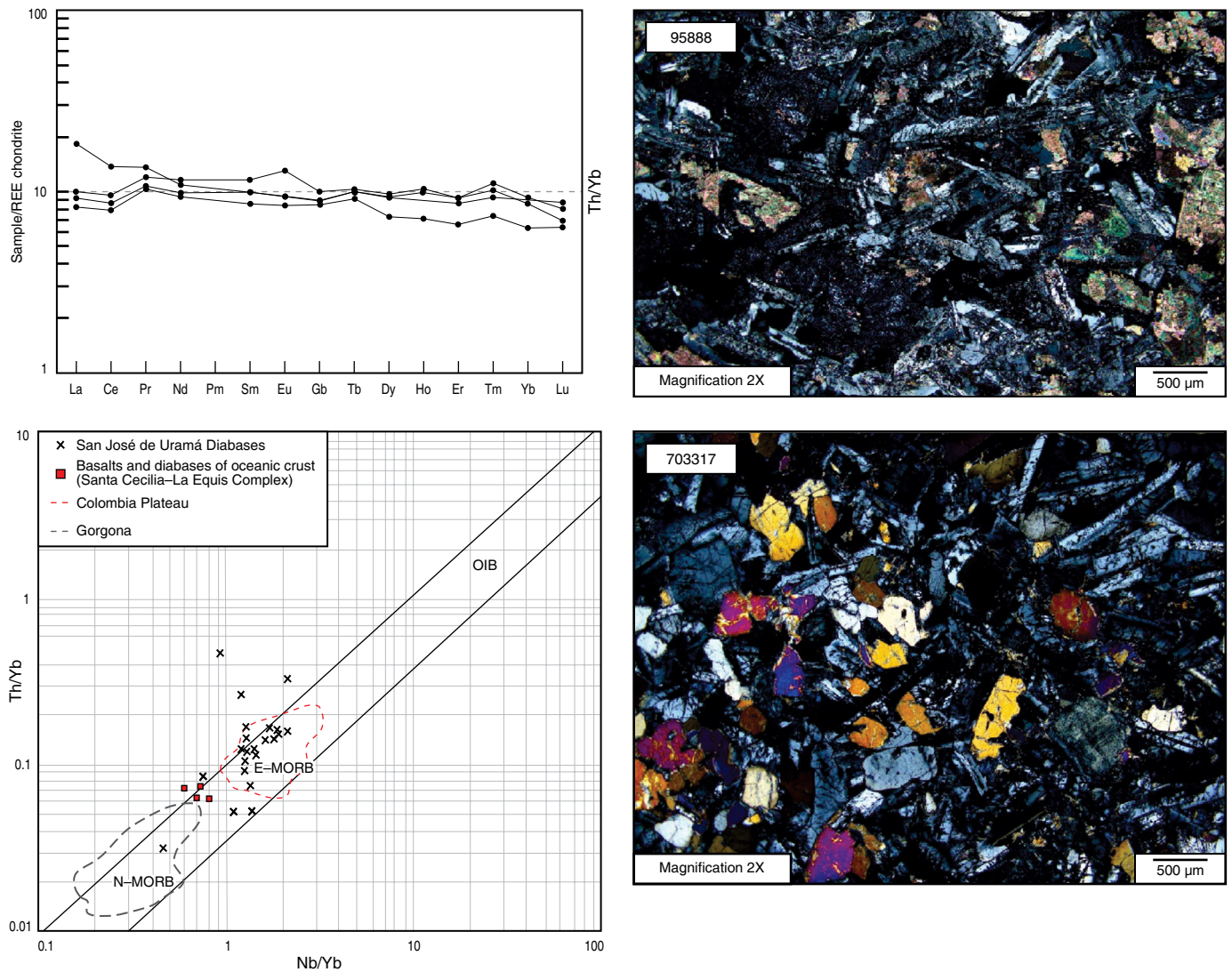


Figure 16. Spider chart of rare earth elements vs. Nakamura chondrite (Nakamura, 1974) and Pearce (2008) oceanic crust rock discrimination diagram for rocks with oceanic affinity in the Santa Cecilia–La Equis Complex, Central segment, and microscopic appearance of samples IGM-95888 and IGM-703317.

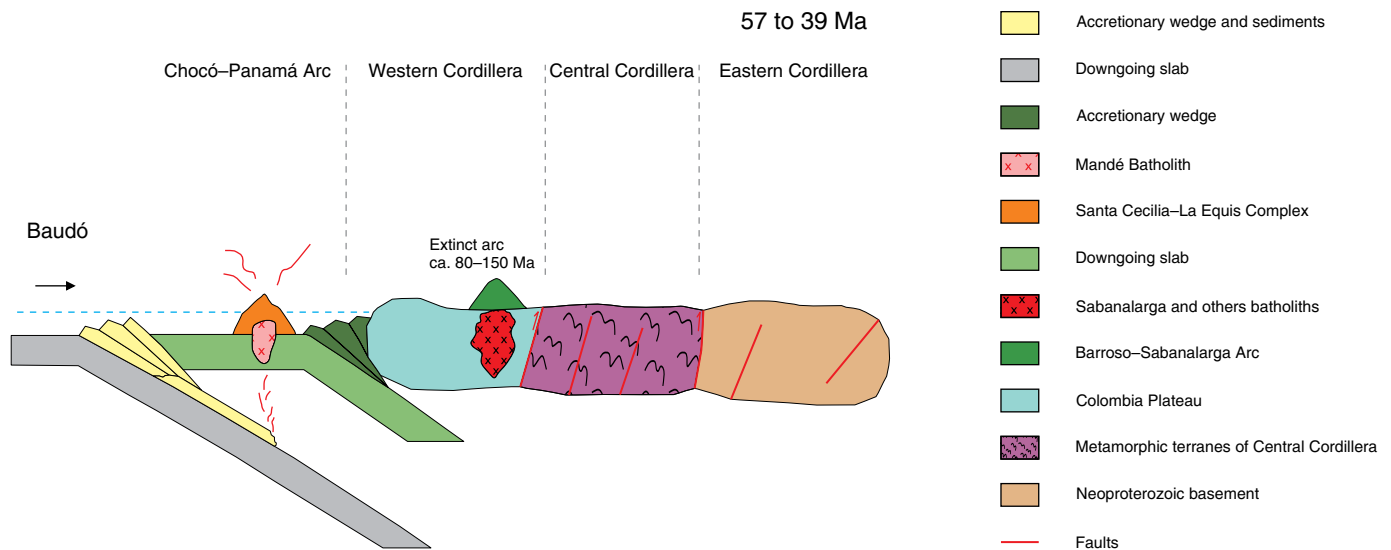


Figure 17. Evolutionary model of the Chocó–Panamá Arc.

tion of units such as the Triganá Breccias (Rodríguez & Sierra, 2010) in the North segment and the Guineales Formation (Rodríguez et al., 2016) in the Central segment.

Acknowledgments

We thank the Servicio Geológico Colombiano, for supplying data used in this study for petrographic analysis, lithochemistry, and radiometric dating. Such data were collected by several generations of geologists during projects in the Western Cordillera. We also thank the geologists Francy Helena ORTIZ for generating several figures for this manuscript and Diego RAMÍREZ for helping edit the text in English. We further thank David BUCHS and Diego VILLAGÓMEZ for the comments and corrections made to the manuscript.

References

- Álvarez, E. & González, H. 1978. Memoria explicativa: Geología y geoquímica del cuadrángulo I-7 Urrao. Ingeominas, Internal report 347 p. Medellín.
- Álvarez, E. & Parra, E. 1979. Evaluación del prospecto de cobre y molibdeno en las cabeceras del río Muerto, municipio de Acaandí, departamento del Chocó. Proyecto Col-76/030. Ingeominas-Naciones Unidas, Internal report 1799, 203 p. Medellín.
- Annells, R.N., Forero, H.F. & Rodríguez, C.A. 1988. Geology and gold potencial of the Timbiqui and Napi River Basins, Cauca Department, Colombia. Ingeominas-British Geological Survey, Technical Report WC/88/45, 99 p. Nottingham.
- Arboleda, G., Celada, C., Forero, S., Montealegre, V., Padilla, J.C., Carmona, J. & Medina, E. 2009. Cartografía geológica y muestreo geoquímico en la parte norte de la cordillera Occidental, planchas 165 y 185 (396 km²). Contrato n.º 392 de 2007. Ingeominas-UTAGS-GE, unpublished report, 178 p. Bogotá.
- Aspden, J.A. 1984. The geology of the Western Cordillera and Pacific coastal plain in the Department of Valle del Cauca (sheets 261, 278, 279, 280 and 299). Ingeominas-Misión Británica (British Geological Survey), Internal report 1959, 61 p. Cali.
- Barat, F., Mercier de Lépinay, B., Sosson M., Müller C., Baumgartner P.O. & Baumgartner-Mora, C. 2014. Transition from the Farallon Plate subduction to the collision between South and Central America: Geological evolution of the Panamá Isthmus. *Tectonophysics*, 622:145–167. <https://doi.org/10.1016/j.tecto.2014.03.008>
- Barrero, D. 1979. Geology of the central Western Cordillera, west of Buga and Roldanillo, Colombia. *Publicaciones Geológicas Especiales del Ingeominas*, 4:1–75 p. Bogotá.
- Botero, G. 1975. Edades radiométricas de algunos plutones colombianos. *Revista Minería*, 27(169–178): 8336–8342. Medellín.
- Buchely, F., Parra, E., Castillo, H., González, F., Dávila, C. & Romero, O. 2009. Realización de la cartografía geológica y muestreo geoquímico en las planchas 144, 145, 128, 129, 113 y 114 (1580 km²). Contrato n.º 390 de 2007. Ingeominas-GRP, unpublished report, 172 p. Bogotá.
- Buchs, D.M., Arculus, R.J., Baumgartner, P.O., Baumgartner-Mora, C. & Ulianov, A. 2010. Late Cretaceous arc development on the SW margin of the Caribbean Plate: Insights from the Golfito, Costa Rica, and Azuero, Panamá, complexes. *Geochemistry, Geophysics, Geosystems*, 11(7): 35 p. <https://doi.org/10.1029/2009GC002901>
- Calle, B. & Salinas, R. 1986. Memoria explicativa: Geología y geoquímica de la plancha 165 Carmen de Atrato. Scale 1:100 000. Ingeominas, 140 p. Medellín.
- Condie, K.C. & Kröner, A. 2013. The building blocks of continental crust: Evidence for a major change in the tectonic setting of continental growth at the end of the Archean. *Gondwana Research*, 23(2): 394–402. <https://doi.org/10.1016/j.gr.2011.09.011>
- Correa, T., Zapata J.P., Rincón, A.V., Obando, M.G., Ortiz, F.H. & Rodríguez, G. 2017. Edades U-Pb y Ar-Ar obtenidas durante la cartografía 1:50 000 del borde occidental de la plancha 130 Medellín Occidental. XVI Congreso Colombiano de Geología. *Memoirs*, p. 1223–1228. Santa Marta.
- Cossio, U. 1994. Memoria explicativa: Mapa geológico generalizado del departamento del Chocó; geología, recursos minerales y amenazas geológicas. Ingeominas, Internal report 2176, 44 p. Medellín.
- Duque-Caro, H. 1990. El Bloque del Chocó en el noroccidente suramericano: Implicaciones estructurales, tectonoestratigráficas y paleogeográficas. *Boletín Geológico*, 31(1): 47–71. Bogotá.
- Echeverri, S., Cardona, A., Pardo-Trujillo, A., Borrero, C., Rosero, S. & López, S. 2015. Correlación y geocronología Ar-Ar del basamento cretácico y el relleno sedimentario Eoceno superior-Mioceno (Aquitano inferior) de la cuenca de antearco de Tumaco, SW de Colombia. *Revista Mexicana de Ciencias Geológicas*, 32(2): 179–189.
- Etayo-Serna, F., Barrero, D., Lozano, H., Espinosa, A., González, H., Orrego, A., Ballesteros, I., Forero, H., Ramírez, C., Zambraño-Ortiz, F., Duque-Caro, H., Vargas, R., Núñez, A., Álvarez, J., Ropaín, C., Cardozo, E., Galvis, N., Sarmiento, L., Alberts, J.P., Case, J.E., Singer, D.A., Bowen, R.W., Berger, B.R., Cox, D.P. & Hodges, C.A. 1983. Mapa de terrenos geológicos de Colombia. *Publicaciones Geológicas Especiales del Ingeominas*, 14(1): 1–135. Bogotá.
- Frost, B.R. & Frost, C.D. 2008. A geochemical classification for feldspathic igneous rocks. *Journal of Petrology*, 49(11): 1955–1969. <https://doi.org/10.1093/petrology/egn054>
- Frost, B.R. & Lindsley, D.H. 1991. The occurrence of iron-titanium oxides in igneous rocks. In: Lindsley, D.H. (editor), *Oxide Minerals: Petrologic and Magnetic Significance*. Mineralogical Society of America, *Reviews in Mineralogy* 25: 433–468.
- Frost, B.R., Barnes C.G., Collins, W.J., Arculus, R.J., Ellis, D.J. & Frost, C.D. 2001. A geochemical classification for granitic rocks. *Journal of Petrology*, 42(11): 2033–2048. <https://doi.org/10.1093/petrology/42.11.2033>

- Geología Regional y Prospección Ltd. 2014a. Memoria explicativa: Plancha 318 Bubuey–319 Micay. 395 p. Bogotá.
- Geología Regional y Prospección Ltd. 2014b. Memoria explicativa: Plancha 341 El Plateado. 436 p. Bogotá.
- Geología Regional y Prospección Ltd. 2014c. Memoria explicativa: Plancha 363 Argelia. 434 p. Bogotá.
- Gómez, J., Montes, N.E., Nivia, Á. & Diederix, H., compilers. 2015. Geological Map of Colombia 2015. Scale 1:1 000 000. Servicio Geológico Colombiano, 2 sheets. Bogotá. <https://doi.org/10.32685/10.143.2015.936>
- Gómez, J., Montes, N.E., Alcárcel, F.A. & Ceballos, J.A. 2015b. Catálogo de dataciones radiométricas de Colombia en ArcGIS y Google Earth. In: Gómez, J. & Almanza, M.F. (Editores), *Compilando la geología de Colombia: Una visión a 2015*. Servicio Geológico Colombiano, Publicaciones Geológicas Especiales 33: 63–419. Bogotá.
- González, H. 2001. Memoria explicativa: Mapa Geológico del departamento de Antioquia. Scale 1:400 000. Ingeominas, 240 p. Medellín.
- González, H. & Londoño, A.C. 2002. Catálogo de unidades litoestratigráficas de Colombia: Batolito de Mandé, cordillera Occidental. Ingeominas, 19 p. Bogotá.
- Guarín, G. & Álvarez, E. 1975. Geología y geoquímica de los prospectos de pórfido cuprífero en el área de Murindó (sectores La Rica, Jarapetó y Táparos), municipio de Riosucio, departamento del Chocó. Ingeominas, Internal report 1738, 105 p. Medellín.
- Hansen, J., Skjerlie, K.P., Pedersen, R.B. & De La Rosa, J. 2002. Crustal melting in the lower parts of island arcs: An example from the Bremanger Granitoid Complex, west Norwegian Caledonides. *Contributions to Mineralogy and Petrology*, 143(3): 316–335. <https://doi.org/10.1007/s00410-001-0342-5>
- Hastie, A.R., Kerr, A.C., Pearce, J.A. & Mitchell, S.F. 2007. Classification of altered volcanic island arc rocks using immobile trace elements: Development of the Th–Co discrimination diagram. *Journal of Petrology*, 48(12): 2341–2357. <https://doi.org/10.1093/petrology/egm062>
- Hughes, C.J. 1972. Spilites, keratophyres, and the igneous spectrum. *Geological Magazine*, 109(6): 513–527. <https://doi.org/10.1017/S0016756800042795>
- Ingeominas & Organización de las Naciones Unidas. 1982. Mineralización de cobre y molibdeno en el municipio de Acandí, departamento del Chocó. Unpublished report, DP/UN/COL–76–030/1, 65 p. Bogotá.
- Irvine, T.N. & Baragar, W. 1971. A guide to the chemical classification of the common volcanic rock. *Canadian Journal of Earth Sciences*, 8(5): 523–548. <https://doi.org/10.1139/e71-055>
- Kerr, A.C., Marriner, G.F., Tarney, J., Nivia, A., Saunders, A.D., Thirlwall, M.F. & Sinton, C.W. 1997. Cretaceous basaltic terranes in western Colombia: Elemental, chronological and Sr–Nd isotopic constraints on petrogenesis. *Journal of Petrology*, 38(6): 677–702. <https://doi.org/10.1093/petrology/38.6.677>
- Leal–Mejía, H. 2011. Phanerozoic gold metallogeny in the Colombian Andes: A tectono–magmatic approach. Doctoral thesis, Universitat de Barcelona, 989 p. Barcelona.
- Le Bas, M.J., Le Maitre, R.W., Streckeisen, A. & Zanettin, B. 1986. A chemical classification of volcanic rocks based on the total alkali–silica diagram. *Journal of Petrology*, 27(3): 745–750. <https://doi.org/10.1093/petrology/27.3.745>
- Le Maitre, R.W., Streckeisen, A., Zanettin, B., Le Bas, M.J., Bonin, B., Bateman, P., Bellieni, G., Dudek, A., Efremova, S., Keller, J., Lameyre, J., Sabine, P.A., Schmid, R., Sørensen, H. & Woolley, A.R., editors. 2002. *Igneous rocks: A classification and glossary of terms. Recommendations of the International Union of Geological Sciences Subcommission on the systematics of igneous rocks*. Cambridge University Press, 236 p. Cambridge, UK. <https://doi.org/10.1017/CBO9780511535581>
- McCourt, W.J., Muñoz, C.A. & Villegas, H. 1990. Regional geology and gold potential of the Guapi–Napi drainage basin and upper Timbiquí River, Cauca Department, SW Colombia. British Geological Survey & Ingeominas, unpublished report, WC/90/34, 241 p. Cali.
- Middlemost, E.A.K. 1985. *Magmas and magmatic rocks. An Introduction to igneous petrology*. Longman Ltd, 266 p. London, New York.
- Middlemost, E. A. K. 1994. Naming materials in magma/igneous rock system. *Earth–Science Reviews*, 37(3–4): 215–224. [https://doi.org/10.1016/0012-8252\(94\)90029-9](https://doi.org/10.1016/0012-8252(94)90029-9)
- Molnar, P. & Sykes, L.R. 1969. Tectonics of the Caribbean and Middle America regions from focal mechanisms and seismicity. *Geological Society of America Bulletin*, 80(9): 1639–1684. [http://dx.doi.org/10.1130/0016-7606\(1969\)80\[1639:TOTCAM\]2.0.CO;2](http://dx.doi.org/10.1130/0016-7606(1969)80[1639:TOTCAM]2.0.CO;2)
- Montes, C., Bayona, G., Cardona, A., Buchs, D.M., Silva, C.A., Morón, S., Hoyos, N., Ramirez, D.A., Jaramillo, C.A. & Valencia, V. 2012. Arc–continent collision and orocline formation: Closing of the Central American seaway. *Journal of Geophysical Research: Solid Earth*, 117(B4): 25 p. <https://doi.org/10.1029/2011JB008959>
- Montes, C., Cardona, A., Jaramillo, C., Pardo, A., Silva, J.C., Valencia, V., Ayala, C., Pérez–Ángel, L.C., Rodríguez–Parra, L.A., Ramírez, V. & Niño, H. 2015. Middle Miocene closure of the Central American Seaway. *Science*, 348(6231): 226–229 p. <https://doi.org/10.1126/science.aaa2815>
- Nakamura, N. 1974. Determination of REE, Ba, Fe, Mg, Na and K in carbonaceous and ordinary chondrites. *Geochimica et Cosmochimica Acta*, 38(5): 757–775. [https://doi.org/10.1016/0012-8252\(94\)90029-9](https://doi.org/10.1016/0012-8252(94)90029-9)
- Nelson, W.H. 1962. Contribución al conocimiento de la cordillera Occidental, sección carretera Cali–Buenaventura. *Boletín Geológico*, 10(1–3): 81–108.
- Nivia, A. 1996. El Complejo Estructural Dagua, registro de deformación de la provincia litosférica oceánica cretácica occidental en un prisma acrecionario. VII Congreso Colombiano de Geología. *Memoirs*, 3, p. 54–67. Bogotá.

- Nivia, A. 1998. Memoria explicativa: Mapa geológico del departamento del Valle. Scale 1:250 000. Ingeominas, Internal report 2320, 111 p. Cali.
- Nivia, A. 2001. Memoria explicativa: Mapa geológico del departamento del Valle del Cauca. Scale 1:250 000. Ingeominas. 148p. Bogotá.
- Parra, E. 1983. Geología y geoquímica de la plancha 223 El Cairo, Valle. Ingeominas, Internal report 1914, 138 p. Medellín.
- Pearce, J.A. 1996. User's guide to basalt discrimination diagrams. In: Wyman D.A. (editor), Trace element geochemistry of volcanic rocks: Applications for massive sulphide exploration. Geological Association of Canada, short course notes, 12: p. 79–113. Winnipeg, Canada.
- Pearce, J.A. 2008. Geochemical fingerprinting of oceanic basalts with applications to ophiolite classification and the search for Archean oceanic crust. *Lithos*, 100(1–4): 14–48. <https://doi.org/10.1016/j.lithos.2007.06.016>
- Pearce, J.A., Harris, N.B.W. & Tindle, A.G. 1984. Trace element discrimination diagrams for the tectonic interpretation of granitic rocks. *Journal of Petrology*, 25(4): 956–983. <https://doi.org/10.1093/petrology/25.4.956>
- Peccerillo, A. & Taylor, S.R. 1976. Geochemistry of Eocene calc-alkaline volcanic rocks from Kastamonu area, northern Turkey. *Contributions to Mineralogy and Petrology*, 58(1): 63–81. <https://doi.org/10.1007/BF00384745>
- Pindell, J.L. 1993. Regional synopsis of Gulf of Mexico and Caribbean evolution. In: Pindell, J.L. & Perkins, B.F. (editors), *Mesozoic and Early Cenozoic Development of the Gulf of Mexico and Caribbean Region: A Context for Hydrocarbon Exploration*. Gulf Coast Section SEPM Foundation, 13th Annual Research Conference, p. 251–274. Houston, Texas. <https://doi.org/10.5724/gcs.92.13.0251>
- Pindell, J.L. & Kennan, L. 2009. Tectonic evolution of the Gulf of Mexico, Caribbean and Northern South America in the mantle reference frame: An update. In: James, K.H., Lorente, M.A. & Pindell, J.L. (editors), *The origin and evolution of the Caribbean Plate*. Geological Society of London, Special Publication 328, p. 1–55. <https://doi.org/10.1144/SP328.1>
- Pindell, J.L., Cande, S.C., Pittman III, W.C., Rowley, D.B., Dewey, J.F., Labrecque, J. & Haxby, W. 1988. A plate–kinematic framework for models of Caribbean evolution. *Tectonophysics*, 155(1–4): 121–138. [https://doi.org/10.1016/0040-1951\(88\)90262-4](https://doi.org/10.1016/0040-1951(88)90262-4)
- Pindell, J.L., Kennan, L., Maresch, W.V., Stanek, K.P., Draper, G. & Higgs, R. 2005. Plate kinematics and crustal dynamics of circum-Caribbean arc–continent interactions: Tectonic controls on basin development in proto-Caribbean margins. In: Avé-Lallemand, H.G. & Sisson, V.B. (editors), *Caribbean–South American Plate interactions: Constraints from the Cordillera de La Costa Belt, Venezuela*. Geological Society of America, Special Paper 394, p. 7–52. <https://doi.org/10.1130/0-8137-2394-9.7>
- Ramírez, O., Arias, A., Alminas, H.V. & Mosier, E.L. 1979. Estudio geoquímico en el área Pantanos–Pegadorcito, municipios de Frontino y Dabeiba, Antioquia. *Boletín Geológico*, 22(2): 53–98. Bogotá.
- Ramírez, D.A., Foster, D.A., Min, K., Montes, C., Cardona, A. & Sadowe, G. 2016. Exhumation of the Panamá basement complex and basins: Implications for the closure of the Central American seaway. *Geochemistry, Geophysics, Geosystems*, 17(5): 1758–1777. <https://doi.org/10.1002/2016GC006289>
- Restrepo, J.J. & Toussaint, J.F. 1989. Terrenos alóctonos en los Andes colombianos: Explicación de algunas paradojas geológicas. V Congreso Colombiano de Geología. *Memoirs* 1: 92–107. Bucaramanga.
- Rodríguez, G. & Arango, M.I. 2013. Formación Barroso: Arco volcánico toleítico y diabasas de San José de Urama: Un prisma acrecionario T–MORB en el segmento norte de la cordillera Occidental de Colombia. *Boletín Ciencias de la Tierra*, (33): 17–38.
- Rodríguez, G. & Sierra, M.I. 2010. Las Sedimentitas de Tripogadí y las Brechas de Triganá: Un registro de volcanismo de arco, corrientes de turbidez y levantamiento rápido Eoceno en el noroccidente de Sur América. *Geología Colombiana*, (35): 74–86.
- Rodríguez, G. & Zapata, G. 2012. Características del plutonismo Mioceno superior en el segmento norte de la cordillera Occidental e implicaciones tectónicas en el modelo geológico del noroccidente colombiano. *Boletín Ciencias de la Tierra*, (31): 5–22.
- Rodríguez, G. & Zapata, G. 2013. Análisis comparativo entre la Formación Barroso y el Complejo Quebradagrande: Un arco volcánico toleítico–calcoalcalino, segmentado por el Sistema de Fallas de Romeral en los Andes del norte? *Boletín Ciencias de la Tierra*, (33): 39–58.
- Rodríguez, G., Zapata, G. & Gómez, J.F. 2010a. Geología de la parte oriental de la plancha 114 Dabeiba. Scale 1:100 000. Ingeominas, 175 p. Medellín.
- Rodríguez, G., Sierra, M.I., Zapata, G., Correa, T. & Peláez J.R. 2010b. Memoria explicativa: Geología de las planchas 58 Sapzurro (Capurganá), 68 Acandí y 79 bis Unguía (cerro Tagarí). Scale 1:100 000. Ingeominas, 245 p. Medellín.
- Rodríguez, G., Arango, M.I. & Bermúdez, J.G. 2012. The Sabanalarga Batholith, arc plutonism in the suture zone between continental and oceanic crust in the northern Andes. *Boletín Ciencias de la Tierra*, (32): 81–98.
- Rodríguez, G., Zapata, G. & Gómez, J.F. 2013. Memoria explicativa: Geología de la plancha 114 Dabeiba. Scale 1:100 000. Ingeominas, 211 p. Medellín.
- Rodríguez, G., Arango, M.I., Zapata, G. & Bermúdez, J.G. 2016. Estratigrafía, petrografía y análisis multi–método de procedencia de la Formación Guineales, norte de la cordillera Occidental de Colombia. *Boletín de Geología*, 38(1): 101–124. <https://doi.org/10.18273/revbol.v38n1-2016006>
- Salazar, G., James, M. & Tisl, M. 1991. El Complejo Santa Cecilia–La Equis: Evolución y acreción de un arco magmático en el norte de la cordillera Occidental, Colombia. *Simpósio de magmatismo andino y su marco tectónico*. *Memoirs*, (2): 142–160. Manizales.
- Salazar, G., González, L.M., Muñoz, R., Güiza, S. & Moreno, G. 2005. Caracterización de unidades litogeoquímicas de la cordillera

- Occidental: Fase I, plancha 165. Ingeominas, unpublished report, 58 p. Bogotá.
- Serrano, L., Ferrari, L., López Martínez, M., Maria Petrone, C., Jaramillo, C. 2011. An integrative geologic, geochronologic and geochemical study of Gorgona Island, Colombia: implications for the formation of the Caribbean Large Igneous Province. *Earth and Planetary Science Letters*, 309(3–4): 324–336. <https://doi.org/10.1016/j.epsl.2011.07.011>
- Shand, S.J. 1943. Eruptive rocks. Their genesis, composition, classification, and their relation to ore deposits, with a chapter on meteorites. John Wiley & Sons, 444 p. New York.
- Sillitoe, R.H., Jaramillo, L., Damon, P.E., Shafiqullah, M. & Escobar, R. 1982. Setting, characteristics, and age of the Andean porphyritic copper belt in Colombia. *Economic Geology*, 77(8): 1837–1850. <https://doi.org/10.2113/gsecongeo.77.8.1837>
- Streckeisen, A. 1976. To each plutonic rock its proper name. *Earth–Science Reviews*, 12(1):1–33. [https://doi.org/10.1016/0012-8252\(76\)90052-0](https://doi.org/10.1016/0012-8252(76)90052-0)
- Streckeisen, A. 1979. Classification and nomenclature of volcanic rocks, lamprophyres, carbonatites, and melilitic rocks: Recommendations and suggestions of the IUGS Subcommittee on the Systematics of Igneous Rocks. *Geology*, 7(7): 331–335. [https://doi.org/10.1130/0091-7613\(1979\)7<331:-CANOVR>2.0.CO;2](https://doi.org/10.1130/0091-7613(1979)7<331:-CANOVR>2.0.CO;2)
- Sun, S.S. & McDonough, W.F. 1989. Chemical and isotopic systematics of oceanic basalts: Implications for mantle composition and processes. In: Saunders, A.D. & Norry, M.J. (editors), *Magma-tism in the ocean basins*. Geological Society of London, Special Publication 42, p. 313–345. <https://doi.org/10.1144/GSL.SP.1989.042.01.19>
- Toussaint, J.F. 1996. Evolución geológica de Colombia: 3 Cretácico. Universidad Nacional de Colombia, 277 p. Medellín.
- Villagómez, D.R. 2010. Thermochronology, geochronology and geochemistry of the Western and Central Cordilleras and Sierra Nevada de Santa Marta, Colombia: The tectonic evolution of NW South America. Doctoral thesis, University of Geneva, 126 p. Geneva, Switzerland.
- Villagómez, D., Spikings, R., Magna, T., Kammer, A., Winkler, W. & Beltrán, A. 2011. Geochronology, geochemistry and tectonic evolution of the Western and Central Cordilleras of Colombia. *Lithos*, 125(3–4): 875–896. <https://doi.org/10.1016/j.lithos.2011.05.003>
- Weber, M., Gómez, J., Cardona, A., Duarte, E., Pardo–Trujillo, A. & Valencia, V.A. 2015. Geochemistry of the Santa Fé Batholith and Buriticá Tonalite in NW Colombia—Evidence of subduction initiation beneath the Colombian Caribbean Plateau. *Journal of South American Earth Sciences*, 62: 257–274. <https://doi.org/10.1016/j.jsames.2015.04.002>
- Wegner, W., Wörner, G., Harmon, R.S. & Jicha, B.R. 2011. Magmatic history and evolution of the Central American Land Bridge in Panamá since Cretaceous times. *Geological Society of America Bulletin*, 123(3–4): 703–724. <https://doi.org/10.1130/B30109.1>
- Whattam, S.A. & Stern, R.J. 2015. Late Cretaceous plume–induced subduction initiation along the southern margin of the Caribbean and NW South America: The first documented example with implications for the onset of plate tectonics. *Gondwana Research*, 27(1): 38–63. <https://doi.org/10.1016/j.gr.2014.07.011>
- Wood, D.A. 1980. The application of a Th–Hf–Ta diagram to problems of tectonomagmatic classification and to establishing the nature of crustal contamination of basaltic lavas of the British Tertiary Volcanic Province. *Earth and Planetary Science Letters*, 50(1): 11–30. [https://doi.org/10.1016/0012-821X\(80\)90116-8](https://doi.org/10.1016/0012-821X(80)90116-8)
- Zapata, G. & Rodríguez, G. 2011. Basalto de El Botón, arco volcánico mioceno de afinidad shoshonítica al norte de la cordillera Occidental de Colombia. *Boletín Ciencias de la Tierra*, (30): 77–91.
- Zapata–Villada, J.P., Restrepo, J.J., Cardona–Molina, A. & Martens, U. 2017. Geoquímica y geocronología de las rocas volcánicas básicas y el Gabro de Altamira, cordillera Occidental (Colombia): Registro de ambientes de plateau y arco oceánico superpuestos durante el Cretácico. *Boletín de Geología*, 39(2): 13–30. <https://doi.org/10.18273/revbol.v39n2-2017001>

Explanation of Acronyms, Abbreviations, and Symbols:

ANH	Agencia Nacional de Hidrocarburos	MSWD	Mean square weighted deviation
Ap	Apatite	N–MORB	Normal mid–ocean ridge basalts
Bt	Biotite	OIB	Oceanic island basalts
Cal	Calcite	OI	Olivine
Chl	Chlorite	Op	Opaque
Cpx	Clinopyroxene	Opx	Orthopyroxene
Ep	Epidote	Phnocr	Phenocrystals
Hbl	Hornblende	Pl	Plagioclase
HFSE	High field strength element	QAFP	Quartz, Alkali feldspar, Plagioclase
HREE	Heavy rare earth element	Qtz	Quartz
ICP–MS	Inductively coupled plasma mass spectrometry	REE	Rare earth element
Kfs	Potassium feldspar	RF	Rock fragments
LA–ICP–MS	Laser ablation inductively coupled plasma mass spectrometry	SGC	Servicio Geológico Colombiano
LILE	Large ion lithophile element	STP	Standard temperature and pressure
LOI	Loss on ignition	TAS	Total alkali silica
LREE	Light rare earth element	T–MORB	Transitional mid–ocean ridge basalts
MALI	Alkali–lime index	Tr	Trace elements
Ms	Muscovite	Tr–Act	Tremolite–Actinolite
		Ttn	Titanite
		Zrn	Zircon

Authors' Biographical Notes



Gilberto ZAPATA–GARCÍA graduated with a degree in mining and geological engineering from the Russian State Geological Prospecting University (Российский государственный геологоразведочный университет) (MGRI–RSGPU) in 1977 and specialized in urban–regional planning at the Universidad Nacional de Colombia, Sede Medellín in 2000. He worked in

geological mapping at a scale of 1:100,000, exploration, and petrography at Servicio Geológico Colombiano, from 1978 to 2017. Since 2014, he has been a member of the Proyecto Estudios Geológicos Especiales, participating in studies on Jurassic magmatism in Colombia.



Gabriel RODRÍGUEZ–GARCÍA graduated in 1987 with a degree in geological engineering from the Universidad Nacional de Colombia, Sede Medellín. Subsequently, he completed specialization studies at the École Nationale Supérieure des Mines de Paris in 1995, specializing in technical evaluation–economics of mining projects. He has worked for 30 years at the Servicio

Geológico Colombiano. He was the head of cartography of the regional headquarters of Ibagué, and acts as coordinator of projects and regional cartography and of work groups for the exploration and evaluation of deposits. He currently coordinates the Medellín headquarters and the Grupo de Estudios Geológicos Especiales of the Servicio Geológico Colombiano. He has previously been a professor of Colombian Geology, Field Geology I, and Physical Geology at Universidad EAFIT and the director of geology of Grupo Argos. He has authored over 100 publications, including geological maps, memoirs, and scientific articles in geology.

Chapter 15



Isthmian Bedrock Geology: Tilted, Bent, and Broken

<https://doi.org/10.32685/pub.esp.37.2019.15>

Published online 30 April 2020

Camilo MONTES^{1*}  and Natalia HOYOS² 

Abstract A review of the bedrock geology of the Isthmus of Panama highlights tectonic deformation—tilting, bending, and breaking—, as the major controlling factor in the sites and modes of Cenozoic sedimentation. Deformation in Paleocene – early Eocene times folded and faulted a basement complex composed of plateau basalts, pelagic and hemipelagic sequences, and an overprinted magmatic arc. This deformation episode brought parts of the isthmus from lower bathyal depths to subaerial exposure, bringing about basement cooling and eroding the plutonic bodies that make up the roots of a Campanian to Eocene arc. A clastic–carbonate, less deformed, upper Eocene and younger sedimentary sequence onlaps nonconformably the basement complex. Southward tilting of the isthmus controlled the accumulation of the clastic wedge, recording first shallow marine depositional environments, followed by deepening, and then by shoaling. This sequence resulted from basin tilting that simultaneously raised the San Blas Range, eroding it, while deepening the axis of the Chucunaque Basin. Bending and breaking of the isthmus took place as it was being detached from the trailing edge of the Caribbean Plate, and marked the start of left–lateral offset of the isthmus in late Eocene times.

Keywords: *Panama, isthmus, deformation.*

Resumen Una revisión de la geología del basamento del Istmo de Panamá muestra que la deformación tectónica —el basculamiento, la flexión y la ruptura— es el factor principal que controla los sitios y modos de sedimentación cenozoica. La deformación durante el Paleoceno–Eoceno temprano plegó y falló el complejo de basamento compuesto por basaltos de *plateau*, secuencias pelágicas y hemipelágicas, y un arco magmático sobreimpuesto. Este episodio de deformación trajo partes del istmo desde las profundidades batiales inferiores a exposición subaérea, provocando el enfriamiento de rocas del basamento y la erosión de los cuerpos plutónicos que forman las raíces del arco Campaniano–Eoceno. Una secuencia sedimentaria clástica–calcárea, menos deformada, del Eoceno superior y más joven cubre discordantemente el complejo de basamento. El basculamiento del istmo hacia el sur controló la acumulación de la cuña clástica, registrando primero ambientes deposicionales marinos poco profundos, seguidos por profundización y luego somerización. Esta secuencia resultó del basculamiento de la cuenca que levantó simultáneamente la cordillera de San Blas, erosionándola, mientras se profundizaba el eje de la Cuenca de Chucunaque. La flexión y la ruptura del istmo ocurrieron cuando este se despegó de la parte trasera de la Placa del Caribe, marcando el inicio del desplazamiento sinistral del istmo a finales del Eoceno.

Palabras clave: *Panamá, istmo, deformación.*

1 camilomontes@uninorte.edu.co
Universidad del Norte
Km 5 vía al mar
Barranquilla, Colombia

2 nbotero@uninorte.edu.co
Universidad del Norte
Km 5 vía al mar
Barranquilla, Colombia

* Corresponding author

Citation: Montes, C. & Hoyos, N. 2020. Isthmian bedrock geology: Tilted, bent, and broken. In: Gómez, J. & Mateus-Zabala, D. (editors), *The Geology of Colombia, Volume 3 Paleogene – Neogene. Servicio Geológico Colombiano, Publicaciones Geológicas Especiales 37*, p. 451–467. Bogotá. <https://doi.org/10.32685/pub.esp.37.2019.15>

1. Introduction

The Isthmus of Panama is part of an intraoceanic volcanic arc that is actively colliding with northwestern South America (Kellogg & Vega, 1995), the last of several collisions (Cardona et al., 2011, 2012) recorded along this accretional margin (Cediel et al., 2003; Kennan & Pindell, 2009). Because the isthmian segment of the arc has enjoyed a longer history of geological exploration, better access, and logistical conditions than the segment already attached to South America, a review of its bedrock geology is justified in a volume about the Geology of Colombia. Better knowledge of our neighbor's geology may shed light on some of the many shared geological processes that are recorded in the westernmost Andes and the Choco Block. The geology of the isthmus—across national boundaries—is key to understanding the patterns of tropical biodiversity and faunal exchanges, the start of northern hemisphere glaciations, and the birth of the modern Caribbean Sea.

In very general terms, the Isthmus of Panama is an oceanic plateau onto which a young volcanic arc was built, and then subsequently broken, bent, and tilted. Deformation on the isthmus controlled the location and sedimentation mode of depocenters, where clastics and carbonates accumulated after middle/late Eocene times. Arc volcanism in the isthmus started in Late Cretaceous times (Buchs et al., 2010; Wegner et al., 2011), onto a thickened oceanic plateau (Kerr et al., 2003) that had been interacting during most of the Cenozoic with subducting plate asperities born in the Galapagos hotspot (Hoernle et al., 2004), including ridges and large intraoceanic volcanoes (Buchs et al., 2011a). The evolution of this originally near-linear (Rodríguez-Parra et al., 2017) intraoceanic arc was interrupted in late Eocene times by whole arc deformation, fracturing, oroclinal bending (Montes et al., 2012a; Recchi & Metti, 1975), affecting magmatism and causing widespread subaerial exposure. Later, in Oligocene times, land connections to North America (Bloch et al., 2016; Kirby & MacFadden, 2005; Rincón et al., 2015), and in middle Miocene times to South America, completed the land bridge between the Americas (León et al., 2018; Montes et al., 2015). It is the Neogene history of the Isthmus of Panama that remains the most controversial (Coates & Stallard, 2013; Jaramillo et al., 2017; Leigh et al., 2013; Molnar, 2017; O'Dea et al., 2016), in particular, the time of sill rise from lower bathyal to become a continuous land path between southernmost Central America and South America.

In this contribution we provide a general review of the bedrock geology of the Isthmus of Panama based on published literature and several years of field expeditions in the Canal Basin, eastern Panama, and the Azuero Peninsula. Since comprehensive reviews already exist examining the marine biota (Lessios, 2008), paleoceanographic (Molnar, 2008), biogeographic (Jaramillo, 2018; Leigh et al., 2013), and molecular data (Bacon et al., 2015) on isthmus closure, it is perhaps a good opportunity

to provide a review of the bedrock geology and deformation of the isthmus, a subject often overlooked in the controversy over time of closure. The emphasis of this review is to show that deformation (bending, tilting, breaking) is a major ingredient in the geological evolution of the isthmus, we therefore focus our discussion around this point. We first discuss the geometry, composition, and evolution of the basement complex, we then discuss the cover sequences, while highlighting observations on isthmian deformation. We finish this review by evaluating possible avenues of future research on isthmian geology, which despite a long history of geological investigations, and much improved logistical access conditions, still features large tracts of virtually unexplored land.

2. Isthmus Geology

Geologic research in the isthmus had an early start in the late XIX century resulting from multiple commissions evaluating some eight possible interoceanic canal routes, most of them in today's Panama and Darien (e.g., Reclus & De Vaisseau, 1880; Verbrugghe, 1879). While these early exploration efforts were concerned with the engineering details and financial prospects of canal construction, they also gathered basic topographic and geologic information about the proposed interoceanic canal routes. Choosing the best route for the interoceanic canal was however, an exercise of political maneuvering, little concerned with geologic/geotechnical considerations. The French *Compagnie Universelle*, charged with the digging of the canal under the direction of Ferdinand DE LESSEPS, obtained a concession from the Colombian government in 1879, and started excavations with only vague geological insights in 1881 (Douville, 1898; Hill et al., 1898). Digging progressed for more than 20 years at great human and financial cost, completing a large percentage of the excavation needed (see photographic material in Hill et al., 1898) before bankruptcies, Panama independence in 1903, and an operational take over by the United States in 1904 (de Banville, 2004).

It was not until 1910, with the bulk of the excavation nearly finished and reservoir flooding on the way, that the opportunities afforded by the unprecedented man-made digs were first realized (see Vaughan, 1946). Paleontological and biostratigraphic studies of the Canal Basin quickly followed (e.g., Berry, 1914; MacDonald, 1919) from a fruitful cooperation between the Canal Commission, the U.S. Geological Survey, and the Smithsonian Institution. Then, massive landslides of the fossiliferous clays of the Culebra and Cucaracha Formations in 1915–1916 blocked the recently opened Canal (see Brown, 1920), prompting in-depth geological and geotechnical studies of the Canal to begin in earnest (Becker, 1917; Lutton & Banks, 1970; MacDonald, 1947). This cooperation yielded beautiful geologic maps of the Canal Basin, as well as a solid stratigraphic and structural framework of the central part of the isthmus,

all with a paleontological emphasis (see for instance Woodring & Thompson, 1949; Woodring, 1973; Stewart et al., 1980).

Away from the Canal Basin, studies motivated by Alexander Agassiz's early observations (Hill et al., 1898), and by mineral prospecting, recognized most of the basic geological elements of the isthmus (Hershey, 1901). These studies were much later complemented by the UNDP (United Nations Development Program) geologic and resource maps in the Azuero Peninsula (Giudice & Recchi, 1969), and in other regions of Panama including Darien and Bocas del Toro (United Nations Development Program, 1972). Petroleum exploration efforts also motivated early expeditions to Darien and the Chucunaque–Tuira basins setting up the basic stratigraphic framework (Shelton, 1952; Terry, 1956) in use today. During the last years of World War II, and the beginning of the Cold War, expansion of the canal became a military strategic priority, prompting the review of alternative routes to the east, including the Darien region (binational by then, Tavelli, 1947), evaluating the use of nuclear cratering as the main excavation technique (Sheffey et al., 1969).

2.1. Isthmus Basement and Cover

A distinction between basement and cover is used throughout this contribution. We call cover sequences those sequences, mostly sedimentary in origin, but also volcanic and volcanoclastic, that are separated by a nonconformity from a mostly volcanic, volcanoclastic and plutonic basement that is typically more intensely deformed than the cover above. This nonconformity records a period of deformation, cooling, exhumation, and erosion of the basement sequences before the accumulation of sequences above, which typically start in middle to late Eocene times. The distinction between basement and cover is concealed and blurred by a younger magmatic arc that is present west of the Canal Basin and north of the Azuero Peninsula (Figure 1), and also by the presence of accreted terranes along the southwestern edge of the isthmus. We therefore restrict our discussion to the older arc (see Rooney et al., 2015 for a review of the younger arc).

2.2. Isthmus Basement

The basement of the Isthmus of Panama consists of a Campanian to Eocene magmatic arc (Hoernle et al., 2008; Montes et al., 2012a; Wegner et al., 2011) built onto the southwestern, trailing edge of the Caribbean Plate (Pindell & Kennan, 2009). The Caribbean Plate that served as basement for the construction of the arcs is a complex, thickened oceanic plateau, buoyant and shallower than normal oceanic crust, with no magnetic anomalies (Case et al., 1990). This basement complex—plateau plus overlapping arc—seems fairly uniform throughout the isthmus, except for a magmatic hiatus in the San Blas Range. The transition from plateau to arc volcanism may have been

marked by a period of pelagic/hemipelagic sedimentation that thus may serve as a regional key marker. Regional Bouguer anomalies over the San Blas Range (Figure 1, >120 milligal; Case, 1974; Westbrook, 1990) confirm that basement ranges consist of raised blocks of oceanic crust that host granitic intrusions. Geophysical anomalies are remarkably parallel and continuous along the axis of the San Blas Range, the Chucunaque Basin, and the North Panama Deformed Belt (Westbrook, 1990), suggesting continuity of lithologic units and structure, as also shown by geologic maps (Coates et al., 2004; Ministerio de Comercio e Industrias, 1991; Shelton, 1952).

2.2.1. The Plateau

The proto-Caribbean province came to be a Large Igneous Province (LIP) as Galapagos hotspot plume activity thickened it through ~70 Ma of hotspot volcanism (from 139 Ma to 69 Ma; Hoernle et al., 2002, 2004) to form one or several plateaus (~89 to 75 Ma pulses; Lissina, 2005; Baumgartner et al., 2008; Buchs et al., 2011b) collectively grouped—perhaps loosely—within the Caribbean Large Igneous Plateau (CLIP). This plateau may contain a much more diverse collection of fragments incorporated by subduction or collisions. Once the thickened Caribbean Plate was on a collision course with the westward-drifting American plates, its higher buoyancy favored accretion and preservation of its frontal fragments on the American margins. Fragments detached from the colliding leading edge of this plate are found today as accreted blocks along the northwestern margin of South America and the Antilles (e.g., Nivia, 1996; see review in Kerr et al., 2003). The processes involved in the formation of this plateau consolidated a complex igneous basement that seemingly left little or no trace of the original proto-Caribbean oceanic plate onto which the plume volcanism took place. The exception to this in the isthmus may be distorted beds of red cherts and radiolarites intermingled with lava flows found only in the Azuero Peninsula near Torio (Hershey, 1901), south of Malena (Coniacian; Kolarsky et al., 1995), and fringing the Chortis Block in Nicaragua (Upper Triassic – Cretaceous; Baumgartner et al., 2008), among others. These strata may represent remnants of the pre-Campanian ocean floor onto which long-lived plateau volcanism took place.

Once the plateau was established, and while the Caribbean Plate was ploughing through the Americas with west-dipping subduction at its leading edge (Kennan & Pindell, 2009), subduction also started along its trailing edge, giving birth to the Central American arc in Cretaceous times (~70 Ma, Lissina, 2005; ~75–73 Ma, migrating east, Buchs et al., 2011b; ~71 Ma, and migrating east, Wegner et al., 2011). The location of this early Central American arc should outline an edge where the Caribbean Plate was thick, buoyant, perhaps still hot, at the time of subduction initiation. It is however, difficult to discriminate

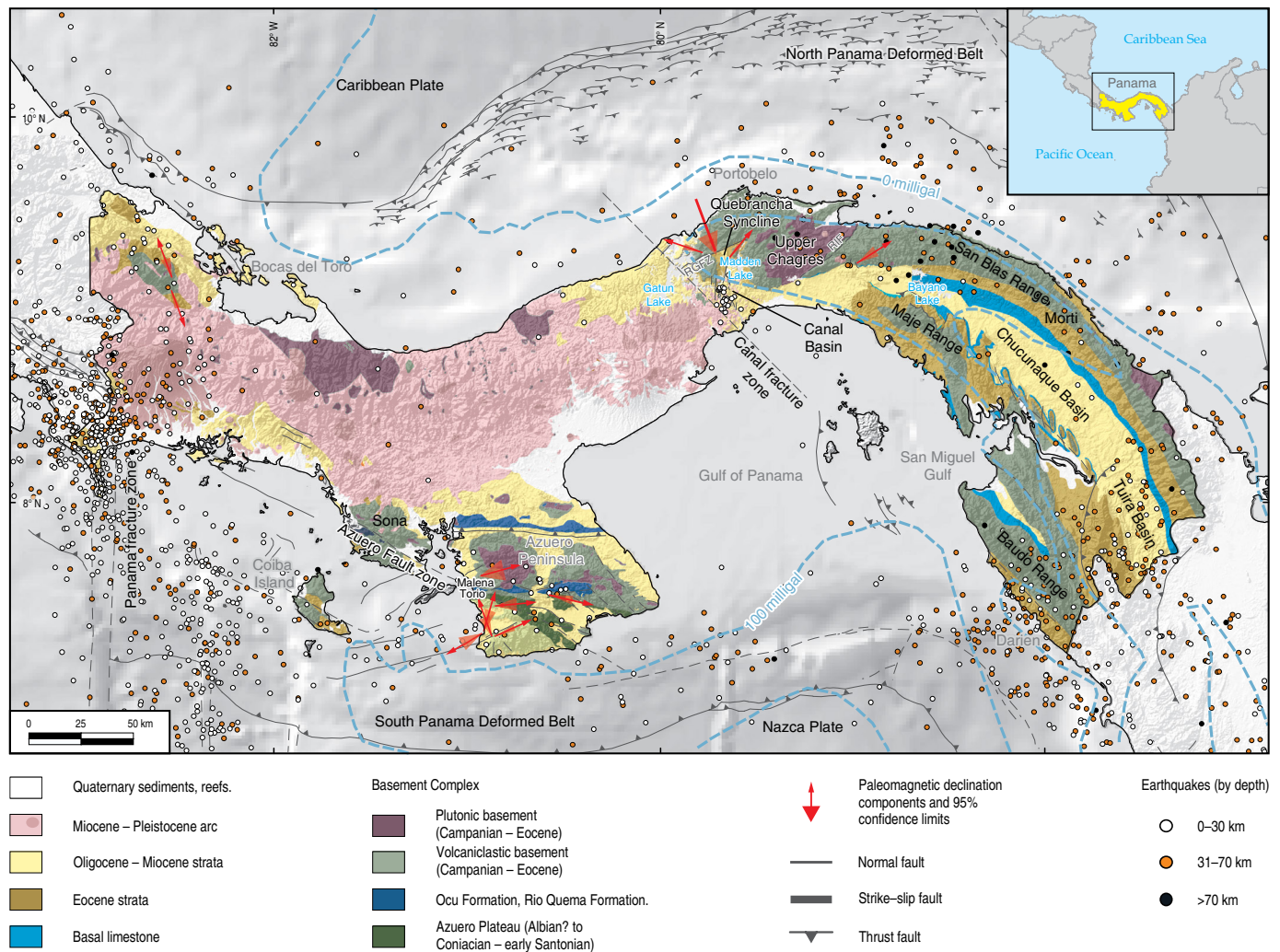


Figure 1. Geologic map of the Isthmus of Panama (modified from Buchs et al., 2010; Cowan et al., 1998; Di Marco et al., 1995; Giudice & Recchi, 1969; Kesler et al., 1977; Kirby et al., 2008; Ministerio de Comercio e Industrias, 1991; Montes et al., 2012b, 2015; Silver et al., 1990; Stewart et al., 1980; Rodríguez-Parra et al., 2017; Woodring, 1957). Topography and earthquakes from Amante & Eakins (2009), U.S. Geological Survey (2010, 2017). (RGFZ) Rio Gatun Fault zone; (RIF) Rio Indio Fault.

the magmatic products of the Galapagos hotspot from the first subduction-related magmatism, especially where Galapagos-modified crust is being subducted. Temporal and geochemical continuity between the last Galapagos-derived magmatism in the Caribbean Plate and the first subduction-related arc magmatism, open the possibility that subduction may have instead started as a result of the interaction between the hot plume and the cold lithosphere around it, thus hypothetically pushing the date of subduction initiation as far back as ~100 Ma (Whattam & Stern, 2015).

While the Caribbean Plate drifted away from the Galapagos hotspot, and became isolated by inward-dipping subduction zones along its leading and trailing edges, the hotspot continued its activity giving rise to plate asperities (Buchs et al., 2011a, 2016; Hoernle et al., 2002; Lissina, 2005) onto the Farallon Plate (Lonsdale, 2005; Lonsdale & Klitgord, 1978). These asperities—seamounts and ridges—were sequentially transported

to the Central American trench where they eventually docked to a margin that thus contains the compressed history of the Galapagos hotspot. Docking of the more buoyant fragments, and subduction of the Galapagos-modified plate, left isotopic tracers that have been used to track margin-parallel asthenospheric flow as far west as Nicaragua (Gazel et al., 2011; Hoernle et al., 2008). The basement of the isthmus, has therefore always been interacting either directly or indirectly with the Galapagos hotspot. Directly, through the formation of large igneous provinces over nearly 70 Ma; indirectly, as plate asperities born in the hotspot have been brought to the trench, and have been either accreted, or assimilated in the asthenospheric flow.

2.2.2. Basement Composition

The basement of the isthmus is therefore made of thickened, long-lived Galapagos-derived oceanic plateau magmatic prod-

ucts (mostly submarine basalts) intercalated with two main sequences, also part of the basement complex: a Campanian – Maastrichtian pelagic and hemipelagic strata interbedded with submarine basalt flows and volcanoclastic materials, and a Campanian to Eocene subduction–related magmatic arc, volcanic and plutonic, and only partially subaerial. This of course, becomes a major source of ambiguity when mapping isthmus basement in the field, where distinct tectono–stratigraphic sequences are virtually identical basaltic successions. Geochemically also, most plateau and early arc and arc volcanism are mafic with geochemical and isotopic signatures derived from, or contaminated by, Galapagos hotspot materials. Unambiguous geochemical discrimination of plateau versus arc volcanism (e.g., Li et al., 2015), also remains a challenge in the isthmus.

2.3. Volcanic–Granitic Basement

The volcanic basement in most of the isthmus is composed of basalt flows, pillow basalt, diabase, interbedded chert and other siliceous sedimentary rocks intruded by granitoids and mafic dykes. Such sequences, with some variation, have been reported in the Morti River headwaters (Maury et al., 1995; Tavelli, 1947), near San Miguel Gulf (Bandy & Casey, 1973; Barat et al., 2014; Case, 1974), in the upper Chagres River (Wörner et al., 2005), and in a nearly 4 km thick sequence east of the Canal Basin (Montes et al., 2012b). Geologic explorations along the coastal transect of the northern flank of the San Blas Range confirm that its composition remains mostly basaltic and granitic, with granitoids between 59 and 39 Ma (Montes et al., 2015), but lacking the interbedded pelagic sediments ubiquitous in the southern flank of this range. This basement continues uniformly east to the Cuchillo Hills in the Darien region, perhaps with a greater thickness of the volcanic–volcanoclastic component with mafic tuffs, volcanic breccias, and cherts as young as middle Eocene (Barat et al., 2014), and magmatic activity as young as ~19 Ma (Whattam et al., 2012) correlative to the younger arc. Further east this sequence may continue into the Western Cordillera of Colombia (Case et al., 1971) with the Mande Batholith (Villagómez et al., 2011; Montes et al., 2015; see review in León et al., 2018).

A similar basement composition has been reported, and more thoroughly studied in the Azuero Peninsula, both in its eastern and western sides. In the eastern side of the peninsula, Corral et al. (2016) describe and map the ~1600 m thick Rio Quema Formation, a folded unit that sits on top of a basement that is composed of basalts, pillow basalts, and interbedded chert. The Rio Quema Formation contains a lower, crystal-rich sandy unit, a middle hemipelagic limestone unit, and siltstone upper unit, all intruded by dikes and a mineralized dacite. The Rio Quema Formation is covered by younger volcanic and volcanoclastic material with arc affinities. In the western side of the Azuero Peninsula, Buchs et al. (2011b) describe a basement

sequence consisting of massive, columnar, and pillow basalts interbedded with small volumes red siliceous pelagic sediment with Coniacian – early Santonian radiolarians. This sequence is covered by hemipelagic limestones of the Ocu Formation and interbedded basalts, and then volcanic and plutonic rocks with arc affinities.

2.4. Hemipelagic and Pelagic Sequences

A key marker horizon that may help discriminate the different tectono–stratigraphic packages within the basement complex is defined by hemipelagic light-colored carbonates, and pelagic siliceous sequences. These pelagic/hemipelagic sequences may correspond to the B'' horizon mapped, nearly reached in the ODP 999 in the Kogi Rise in the Caribbean Plate interior (Abrams & Hu, 2000; Bowland, 1993; Röhl & Abrams, 2000). Geologic maps of the eastern Azuero Peninsula by Corral et al. (2011, 2013), and by Montes et al. (2012b) in the southern flank of the San Blas Range, have delineated the outcrop pattern, and cross-cutting relationships of hemipelagic carbonates and pelagic mudstone and chert with the tectono–stratigraphic units above and below. Both studies use these sequences to separate plateau products from arc products, thought to represent the transition from plume volcanism to subduction–related volcanism.

Despite being a conspicuous unit (or units), the tectono–stratigraphic position of the hemipelagic sequences in the Azuero Peninsula remains unclear. Buchs et al. (2011b) report them resting on the CLIP, interbedded with the early arc system, and also within the accreted intraoceanic islands (Buchs et al., 2011a). These unusually thick hemipelagic limestones are characteristically light-colored, bioturbated, and contain planktonic foraminifera dated as late Campanian to Maastrichtian (Buchs et al., 2010; Corral et al., 2013; Fisher & Pessagno, 1965; Giudice & Recchi, 1969). Hemipelagic carbonates include the Torio Limestone and Ocu Formation, no more than 200 m thick in the Azuero Peninsula (Giudice & Recchi, 1969; Hershey, 1901), 350 m thick in Coiba Island (Kolarsky et al., 1995), ~1 km thick in eastern Azuero (Rio Quema Formation; Corral et al., 2016), and ~1 km thick in Bocas del Toro (Changuinola Formation; Fisher & Pessagno, 1965). Reports of hemipelagic limestones with similar ages also come from the San Miguel Gulf, the Portobelo Peninsula (Barat et al., 2014), extending the range of these limestones to the central and easternmost isthmus.

Still very poorly studied, the undifferentiated basalt sequences (Stewart et al., 1980) in the upper Chagres River catchment area are interbedded with thin pelagic beds of black siliceous siltstones, shales with thin sandstone stringers, and cherts. The siliceous pelagic sequence could be correlative to the hemipelagic limestone units above described, perhaps recording deeper accumulation environments. The age of this

pelagic–hemipelagic sequence must be younger than the mafic volcanics on which it rests (pre–Campanian?), and older than the oldest granitoids that intrude them in the San Blas Range (~59 Ma; Montes et al., 2012b, 2015).

2.4.1. Basement Age

Several magmatic arcs are superimposed in the isthmus, with magmatic activity being nearly continuous west of the Canal Basin, and with magmatic gaps east of it. As stated above, only those arc–related rocks of Campanian to Eocene age are included within the basement complex. Those include intrusives in the eastern and western edges of the San Blas Range yielding hornblende and feldspar K/Ar ages between ~61 and 48 Ma (Kesler et al., 1977). Similarly, Ar/Ar dates in amphibole and plagioclase of unreported rock type, in its western half, range between ~66 and 41 Ma (Wegner et al., 2011). U/Pb zircon geochronological studies in granitoids of the basement complex exposed in the San Blas Range confirmed this age distribution with dates between ~59 and 39 Ma (Montes et al., 2012b, 2015; Ramírez et al., 2016), further constrained by zircon U/Pb detrital analyses in modern river sands, and in Eocene – Miocene strata (Montes et al., 2012b; Ramírez et al., 2016). Geochronological K/Ar, Ar/Ar, and U/Pb dates in the Azuero Peninsula range from ~71 to 41 Ma in basalts and granitoids (Corral et al., 2016; Giudice & Recchi, 1969; Kesler et al., 1977; Lissina, 2005; Montes et al., 2012a; Wegner et al., 2011). Two Ar/Ar step–heating plateau ages from the volcanoclastic sediments of the Rio Quema Formation are reported but discarded (143 ± 11 Ma and 105 ± 3 Ma; Corral et al., 2016), solely on the basis of being too old, therefore requiring further scrutiny as they still are within the age range of radiolarian determinations.

Lack of detailed geologic maps in the western side of the Azuero Peninsula hinders efforts to construct a reliable geochronological framework. Coastal transects along southwestern Azuero and Sona peninsulas report a large spread of ages with Ar/Ar step–heating plateaus between ~71 and 20 Ma (Hoernle et al., 2002). It has been noted though, that these ages are in conflict with the ages of overlying cover strata (Eocene Tonosi Formation; Kolarsky et al., 1995), so step–heating plateau ages may have suffered from Ar loss, and therefore may be unreliable (Buchs et al., 2011a). Since detailed geologic maps are yet to be produced in southwestern Azuero, the relationships of Eocene strata to sampled basalt sequences are still open to debate, as it is the tectono–stratigraphic affinity (plateau basement versus exotic accreted seamounts) of dated samples along coastal transects. Although geologic maps of southeastern Azuero show a nonconformable relationship of Eocene strata to isthmus basement (Mann & Kolarsky, 1995), such relationship may not be extrapolated to southwestern Azuero across the Azuero–Sona

Fault zone, as this fault may represent the basement versus exotic boundary.

2.4.2. Basement Cooling Ages

The cooling history of the isthmus is recorded by numerous intermediate and felsic intrusive bodies exposed in the Azuero Peninsula and the San Blas Range all along the isthmus. Middle Eocene cooling events recorded by thermochronometers have been tied to exhumation and erosion by mapping the nonconformable relationship between the basement complex and upper Eocene and younger sedimentary sequences (Figure 2). Basement sequences below this nonconformity are pervasively deformed, tightly folded and faulted, while sequences above are simply tilted and folded (see for instance Figure 3c in Montes et al., 2012b). Cooling of the basement rocks in the San Blas Range is consistent with those nonconformities: apatite fission track and apatite and zircon U–Th/He analyses from 58–54 Ma granitoid bodies east of the Canal Basin record cooling from ~200 °C to ~70 °C (47–42 Ma), and cooling below ~40 °C between 12 and 9 Ma (Montes et al., 2012b). Apatite–zircon U–Th/He and fission–track thermochronology from the central part of the isthmus mark a cooling event between 22–28 Ma, with a peak at ~25 Ma, simultaneous with the onset of magmatism in the Canal Basin (Farris et al., 2011). Ramírez et al. (2016), using apatite–zircon U–Th/He, and fission tracks, show that most of the plutonic bodies of the isthmus were intruded and rapidly cooled to below ~200–110 °C by 30–40 Ma. The same authors, using modern sands from the Mamoni and Portogandi Rivers (draining the southern and northern flanks of the San Blas Range respectively) reveal a large spread of apatite–He ages (41–9 Ma) that together with the stratigraphic sequences onlapping the basement complex, suggest southward tilting of a crustal block (Figure 2, see below). In general, thermochronology of basement sequences shows a coherent history of early cooling of the roots of the magmatic arc (perhaps at shallow crustal levels), erosion, and development of a corresponding, regional nonconformity throughout the San Blas Range and the Azuero Peninsula.

2.4.3. Basement Deformation

The basement of the isthmus is intensely folded and faulted (Corral et al., 2016; Fisher & Pessagno, 1965; Montes et al., 2012b). Only locally this basement complex develops dynamic metamorphic lithologic types as foliated basalts and mylonites along the Azuero–Sona Fault zone (Buchs et al., 2011b; Hershey, 1901; Mann & Corrigan, 1990; Tournon et al., 1989), and along the Rio Gatun Fault zone (Wörner et al., 2005). The hemipelagic carbonate–basalt sequences described above serve as strain markers,

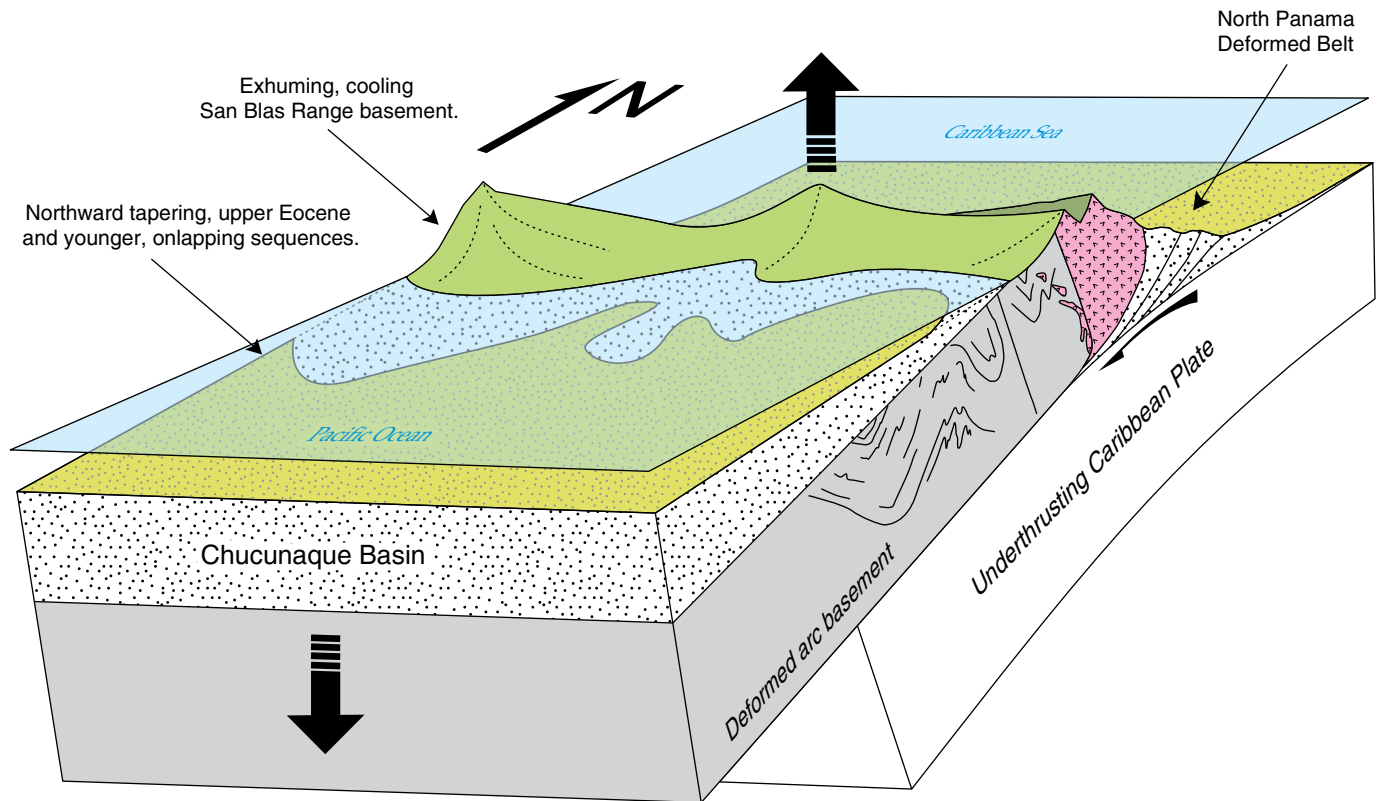


Figure 2. Conceptual diagram showing tilting of the Isthmus of Panama, exhumation and erosion of the basement complex and development of a northward-tapering, upper Eocene and younger sequence. See text for explanation.

revealing intense folding and faulting within the basement complex, marking a period of significant deformation after accumulation of these hemipelagic sequences, and before the accumulation of the first Eocene clastic/carbonate strata (Montes et al., 2012b).

Fault-related rocks in the Azuero Peninsula have been grouped as a melange (Buchs et al., 2010, 2011b) along the Azuero–Sona Fault zone. Vannucchi et al. (2006, 2007, 2013) in Costa Rica classify the Osa Melange as coherent, mappable blocks of fault-related rocks recording fragile to ductile conditions. Whether the sequences Vannucchi and co-workers refer to, are continuous into the Azuero Peninsula as coherent units, or they are a chaotic mixture of fault rocks and olistostromes formed in a subduction channel is still matter of debate. Detailed mapping should help locate the boundary, and the nature of the sequences involved, between the autochthonous plateau-related basalts, and the exotic, seamount-related basalt sequences.

In summary, the basement of the Isthmus of Panama consists of a fairly homogeneous deformed belt of submarine basalts and andesites, interlayered with pelagic and hemipelagic sequences of Campanian – Maastrichtian ages, and rare occurrences of red, older radiolarites, probably pre-Campanian in age. This complex is intruded by intermediate granitoids (68 to 39 Ma) that cooled quickly after intrusion, and were intense-

ly deformed, exposed, and eroded before late Eocene times. A younger set of Galapagos-born oceanic asperities was accreted in early Paleogene times to the southwestern border of the isthmus and is therefore not considered part of the basement of the isthmus.

2.5. Isthmus Cover Sequences

We consider cover sequences those packages of rock accumulated after middle to late Eocene times, and discriminated from the basement by the absence of pervasive deformation. The absence of Paleocene – lower Eocene strata (Kolarksky & Mann, 1995; Woodring, 1957), marks a prominent, isthmus-wide hiatus, probably related to the accretion of plate asperities born in the Galapagos hotspot (Buchs et al., 2011a; Lissina, 2005), collisions with other plateaus (Kerr & Tarney, 2005), or very early interactions with South America (Barat et al., 2014).

Cover sequences are mostly clastic and carbonates in two main, and strikingly different onshore sedimentary basins: the Canal and the Chucunaque basins. Middle Eocene and younger sedimentary packages are also preserved in the Azuero Peninsula, in the Quebro, Mariato, and Tonosi valleys. Offshore, the North Panama Deformed Belt (Silver et al., 1990), and the Gulf of Panama to the south (Kolarksky et al., 1995), are sites of

active sedimentation and contain mostly Neogene sedimentary packages (Barat et al., 2014). Cover sequences are influenced by volcanism where interbedded tuffs and volcano–sedimentary packages are abundant.

2.5.1. Canal Basin

The Canal Basin is defined by a complex collection of fault-bound compartments containing a very heterogeneous, but generally thin (~500 m), mostly clastic infill, intruded by large subvolcanic, mafic bodies and spotted by volcanic edifices. In a broader sense, the Canal Basin—centered around the Culebra Cut—also includes the Quebrancha Syncline, and the Alajuela (Madden) Basin to the north, as well as the Gatun Basin to the northwest. The Canal Basin sits at the westernmost tip of the San Blas Range, where not only the San Blas Range basement complex has its last outcrops (Stewart et al., 1980), but also where nearly continuous gravity anomalies following the axis of the range have their first break, and are found displaced to the southern Azuero Peninsula (Case, 1974; Westbrook, 1990). A fault, sometimes called the Canal fracture zone (Wolters, 1986), needed to explain the ~100 km left–lateral offset of the Campanian to Eocene magmatic arc from Azuero to the San Blas Range, must be located—but concealed—by younger volcanics west of the Canal (Montes et al., 2012a; Recchi & Metti, 1975). This fault may be continuous north of the North Panama Deformed Belt, as inferred by changes in seismic facies (Figure 16b of Bowland, 1993), and the texture in regional gravity anomaly maps (Figure 4 of Carvajal–Arenas & Mann, 2018). This northwest–trending fault, roughly parallel to the East Panama Deformed Belt (Mann & Kolarsky, 1995), was active at ~28 Ma (Montes et al., 2012a) and could be the master fault along which the isthmus reached its present northward–convex shape. As the isthmus was being offset along this fault, northeast–trending, strike–slip, right–stepping faults became active (Rio Gatun and Rio Indio faults) that, if both have a dextral character, must have defined an extensional step–over, with conjugate N–S trending, and NNE–trending faults (Azota and Pedro Miguel faults). Extension, subsidence, vertical–axis rotation, and a change in the character of volcanism from a hydrous subduction magmatism to extensional arc magmatism took place between 21–25 Ma as a result of this kinematic arrangement, and tectonic thinning of the crust of the isthmus (Farris et al., 2011, 2017; Montes et al., 2012a).

Sedimentation in the Canal compartment (see comprehensive description in Woodring, 1957) was nearly always punctuated by some volcanic activity (Farris et al., 2017). It starts with very coarse–grained, volcanic and volcanoclastic interfingering deposits of the middle Oligocene (~25 Ma; Rooney et al., 2011), Bohio and Bas Obispo Formations. These units are overlain by the volcanoclastic, tuffaceous, fossil–rich, lower Miocene (~21 Ma; Bloch et al., 2016) Las Cascadas Formation, grading to

the east and northeast into a tuffaceous shallow–marine Caimito Formation. Shallow marine conditions were established by ~19 Ma (Montes et al., 2012b) in the Canal compartment with the accumulation of the Culebra Formation. This sequence is followed by the subaerial Cucaracha Formation, and then by the volcanic Pedro Miguel Formation (~18 Ma; Wegner et al., 2011). Younger deposits are present to the south of the Culebra Cut, but in general are poorly exposed.

Sedimentation in the Canal compartment is coeval with sedimentation in the other compartments, except for the presence of Eocene strata in the Quebrancha and Alajuela compartments (Coryell & Embich, 1937; Tripathi & Zachos, 2002), predating the opening of the Canal compartment. Upper Eocene strata in the westernmost San Blas Range is probably related to the beginning of the Paleocene–Eocene tilting of the isthmus (see below). Rediscovered upper Miocene fossiliferous strata in the Alajuela compartment (MacFadden et al., 2017), suggests continuity of Gatun, Chucunaque, and Alajuela Formations across the isthmus at that time. The Gatun compartment, on the other hand, acted as the up–thrown block of the Rio Gatun Fault, with no record of sedimentation before the accumulation of the clastic and volcanoclastic wedges of the Gatun (Hidalgo et al., 2011; Rooney et al., 2015) and Chagres Formations (upper Miocene; Collins et al., 1996).

2.5.2. Chucunaque Basin

The Chucunaque Basin is an elongated, east–plunging, oroclinally curved (Montes et al., 2012a) trough whose north–northeastern flank is defined by a simple, south and southwest–dipping onlap onto the basement complex above described. The south–southwestern limb of this trough is more complex, where en–echelon left–stepping, left–lateral, north–south trending folds start near the Baudo Range, and culminate in the Maje Range (Mann & Corrigan, 1990; Mann & Kolarsky, 1995; Stephan et al., 1986). Cross–sections showing normal faults (Barat et al., 2014) are not supported by any geologic mapping, so they may not represent the structure of the basin. Onlapping strata are older (middle – upper Eocene), near the northern compartments of the Canal Basin, getting younger to the east, so that middle Miocene strata directly onlap volcanic and volcanoclastic rocks that may be considered basement in the Darien region (Coates et al., 2004; Shelton, 1952). This basin could be continuous southward into the Atrato Basin (Coates et al., 2004; Duque–Caro, 1990).

The sedimentary sequence in the Chucunaque–Tuira Basin starts with the middle – upper Eocene Gatuncillo Formation, which is better known in the Canal Basin, but has outcrops as far east as the Mamoni–Terabla River, and other affluents of the Bayano River in the westernmost area of the Chucunaque Basin (Terry, 1956; Tripathi & Zachos, 2002). The Gatuncillo Formation is a fining–upward mudstone, conglomerate–sand–

stone, and carbonate unit, of very variable thickness and facies, that nonconformably rests on the volcanic–plutonic basement complex (Woodring, 1957), deposited in fluvial to shallow–marine environments. To the east in the Darien region, the sedimentary sequence starts with ~400 m shale, limestone, and arkosic sandstone with large foraminifera (Shelton, 1952; lower bathyal, middle upper Oligocene Pocorna Formation, Coates et al., 2004; shallow marine, upper Oligocene, Barat et al., 2014), sitting nonconformably onto volcanic basement. This unit is conformably followed by hard, gray, tuffaceous limestone, locally nearly lithographic, more massive to the base (Shelton, 1952; lower bathyal, middle Miocene Clarita Formation, Coates et al., 2004), directly onlapping the basement to the east (Shelton, 1952). This unit grades transitionally to a massive, uniform dark brown, calcareous foraminiferal shale with leaf remains and tuffs and thin sandstone beds (Arusa Formation of Shelton, 1952; or middle bathyal, middle to upper Miocene Tapaliza Formation of Coates et al., 2004; near–shore depths, Barat et al., 2014). This unit transitionally changes to a more conglomeratic and arkosic unit, with shales and dark brown/black carbonaceous material and lignite beds (Aquaqua Formation of Shelton, 1952; or neritic, upper Miocene Tuirá Formation of Coates et al., 2004). This is in turn followed by the more regionally extensive, and lithologically more uniform Chucunaque Formation, correlative to the Gatun (Collins et al., 1996), and Alajuela (MacFadden et al., 2017) Formations.

Ages reported by Coates et al. (2004), for Cenozoic strata in the Chucunaque Formation have been confirmed using nannofossils and other microfossils (Barat et al., 2014). A major difference between these two studies, however, resides in paleobathymetric interpretations (see above), highlighting the need of a multi–proxy approach that includes—and prioritizes—sedimentological observations over microfossil inferences. Microfossils can be transported and reworked, severely limiting their usefulness as paleobathymetric indicators (see discussion in Jorissen et al., 2007). Multi–proxy approaches that include sedimentological, or ichnological analyses are conspicuously absent in paleobathymetric estimations in isthmian strata (Coates et al., 2004; Collins et al., 1996).

2.5.3. Offshore Deformed Belts, North, and South

Large negative gravity anomalies over the north and south Panama deformed belts outline the position of thick prisms of deformed, low–density strata (Case et al., 1990; Westbrook, 1990), thickened by Neogene convergence (Breen et al., 1988; Camacho et al., 2010; Reed & Silver, 1995; Reed et al., 1990; Silver et al., 1990, 1995). To the north, this deformed belt may contain a thick, Eocene and younger sedimentary sequence involved in an accretional belt with northward vergence (Reed & Silver, 1995; Rodríguez & Sierra, 2010; see seismic sections in

Barat et al., 2014). To the south, surface sections, seismic sections, and boreholes have shown the presence of thick, middle Eocene and younger clastic sequences resting nonconformably on basement complex rocks (Kolarksky & Mann, 1995; Kolarksky et al., 1995; Mann & Kolarksky, 1995). These clastic sedimentary sequences may have resulted from erosion of the axis of the San Blas Range, and the Azuero Peninsula (Herrera et al., 2012; Krawinkel et al., 1999; Pérez–Consuegra et al., 2018) as they shed clastic materials to the north and south, including high–quartz clastics product of the erosion of intermediate and felsic intrusives, which were at the surface from latest Eocene times (Montes et al., 2012b; Ramírez et al., 2016). Deformation along the North Panama Deformed Belt may have started in middle Miocene times resulting from incipient south–dipping underthrusting/subduction of the Caribbean Plate under the Panama Block defining a Wadati–Benioff zone (Camacho et al., 2010; Wolters, 1986). A younging–eastward sequence directly overlapping the basement (see above) may record the direction of subduction/underthrusting initiation. Since penetration of the Caribbean Plate is ~150 km (Camacho et al., 2010), and assuming the current convergence rate of 11 mm/yr (Kellogg & Vega, 1995), a minimum age of underthrusting/subduction initiation would be middle Miocene. A slower convergence rate, likely during the initial stages of underthrusting of the Caribbean Plate, would push the age of initiation to Oligocene, and perhaps latest Eocene times (Figure 2).

2.6. The Isthmus Is Tilted, Bent, and Broken

An overall isthmus–wide southward tilting was recognized since the very first geological explorations of the isthmus (Hershey, 1901). This overall tendency can also be read in geological maps of the San Blas Range (Coates et al., 2004; Montes et al., 2012b; Shelton, 1952) that show a simple northward onlap of Eocene – Oligocene strata onto the deformed basaltic/granitic basement complex below, and a corresponding southward thickening of the same strata. The first post–hiatus strata (upper Eocene) record shallow marine, or even fluvial accumulation environments that later become deeper, punctuated by small hiatuses, that get progressively shallower towards the top. Although unencumbered by sedimentological data, paleobathymetric analyses (Coates et al., 2004) show first fluvial/coastal environments, followed by relative deepening, and then shoaling accumulation environments. Such sequence is better explained by an isthmus–wide tilting, erosion, and progressive filling of sedimentary basins, all while highlands to the north provided clastic materials to fill up the basin (Montes et al., 2012b). Southward tilting predicts that as the San Blas Range gained elevation, so the Chucunaque Basin gained accommodation space. It is therefore the interplay between subsidence rate and sediment availability—not a passive sill shoaling from ocean depths—that dictates changes in bathymetry. Detrital

thermochronology in modern river sands on both flanks of the San Blas Range independently suggest that the wide distribution of cooling ages found (Ramírez et al., 2016), is better explained by tilting and exposure of the upper crustal section of the San Blas Range.

The isthmus is also bent. Paleomagnetic data in the isthmus show that the northward-convex shape of the isthmus may be the result of oroclinal bending (Montes et al., 2012a) that would have taken place after magmatic arc shut-down (~39 Ma), and was nearly completed around the time arc reinitiation, and Canal Basin opening in late Oligocene times. The incipient subduction/overthrusting mapped by Camacho et al. (2010), suggest that the isthmus detached from the trailing edge of the Caribbean Plate east of the Canal Basin. Approximately 150 km of subduction/overthrusting resulted from tightening the orocline that started forming following initial collision with western South America, starting at ~25 Ma (Farris et al., 2011). An under-thrusted, buoyant Caribbean plate provides geodynamic support for the tilted San Blas Range. The western half of the isthmus was affected by the collision of intraoceanic plate asperities born in the Galapagos hotspot (Buchs et al., 2011a), causing vertical-axis rotations in the Azuero Peninsula (Rodríguez-Parra et al., 2017), and shifting magmatic focus to the north during Paleocene – Eocene times.

The Canal Basin is broken at the point where the isthmus reaches its lowest topographic elevation, originally reaching ~90 m above sea-level, thus making it the best location for the construction of the interoceanic canal. The Canal Basin is also the point where the Campanian to Eocene magmatic arc is displaced nearly 100 km to the northwest (Lissina, 2005; Montes et al., 2012a; Recchi & Metti, 1975; Wolters, 1986), and where geophysical anomalies indicate changing basement types (Case, 1974; Westbrook, 1990). Tightening of the orocline, and left-lateral displacement of the arc may have contributed to thin the crust of the isthmus, changing magma sources, and open the Canal Basin (Farris et al., 2011, 2017).

3. A Way Forward for Isthmian Geology

This attempt to provide a review of current understanding of isthmian geology highlights just a few of the many issues in this topic. For instance, the stratigraphic location of the pelagic/hemipelagic strata within the basement sequences. Also, the bathymetry recorded by Neogene strata in the Chucunaque Basin, or the nature, or even the existence, of the Canal Basin Fault zone, and the cause of the Paleocene – Eocene deformation in the isthmus. Finally, the age of accretion and location of the boundary between the plateau and accreted sequences. A recurrent underlying problem that is common to most of these issues is rooted in the lack of consistent, standardized, detailed geologic maps at scales larger than 1:250 000. This problem is particularly acute in the eastern part of the isthmus,

and even more pronounced east of the border in the Choco–Darién region. Another related problem is the reliance of single proxies to interpret paleobathymetric data, when a multi-proxy approach that includes sedimentological, ichnological, or other primary features, that cannot be transported, would provide more reliable results.

In general, except for the Canal Basin, most of the isthmus has only been through one generation of geologic mapping, and most of it has only been reconnaissance mapping at very general scales (1:250 000 or smaller). As noted by Woodring in 1957, even in the thickest jungle conditions, the availability of closely-spaced drainages and steep topography offer a very rich network of fresh outcrops where accurate geologic maps can be made. The geology of the isthmus is far too complex to attempt understanding it without basic geologic mapping to support analytical efforts.

Acknowledgments

We thank Smithsonian Tropical Research Institute (STRI), Ricardo Perez S.A., Ministerio de Industria y Comercio, the Panama Canal Authority, The University of Florida, and Universidad de los Andes for logistical and scientific support. Natalia HOYOS was partially funded by The Canadian Queen Elizabeth II Diamond Jubilee Scholarships (QES), a partnership among Universities in Canada, the Rideau Hall Foundation (RHF), Community Foundations of Canada (CFC). The QES–AS is made possible with financial support from IDRC and SSHRC. Natalia HOYOS was also partially supported by the Fulbright Visiting Scholar Program. This review benefited from the enthusiastic help and sharp observations of more than 100 undergraduate and graduate students, professional geologists, paleontologists, biologists that took part in field expeditions, Canal paleontological rescue, and university field camps. Thanks to Dr. Agustín CARDONA and David BUCHS for comments and suggestions.

References

- Abrams, L.J. & Hu, M. 2000. Data report: Depth to volcanic basement at Site 999, Kogi Rise, Colombian Basin. In: Leckie, R.M., Sigurdsson, H., Acton, G.D. & Draper, G. (editors), *Proceedings of the Ocean Drilling Program, Scientific Results* 165, p. 219–224. College Station, USA. <https://doi.org/10.2973/odp.proc.sr.165.028.2000>
- Amante, C. & Eakins, B.W. 2009. ETOPO1 1 Arc-minute global relief model: Procedures, data sources and analysis. NOAA Technical Memorandum NESDIS NGDC–24. National Oceanic and Atmospheric Administration, 25 p.
- Bacon, C.D., Silvestro, D., Jaramillo, C., Smith, B.T., Chakrabarty, P. & Antonelli, A. 2015. Biological evidence supports an early and complex emergence of the Isthmus of Panama. *Proceed-*

- ings of the National Academy of Sciences of the United States of America, 112(19): 6110–6115. <https://doi.org/10.1073/pnas.1423853112>
- Bandy, O.L. & Casey, R.E. 1973. Reflector horizons and paleobathymetric history, eastern Panama. *Geological Society of America Bulletin*, 84(9): 3081–3086. [https://doi.org/10.1130/0016-7606\(1973\)84<3081:RHAPHE>2.0.CO;2](https://doi.org/10.1130/0016-7606(1973)84<3081:RHAPHE>2.0.CO;2)
- Barat, F., De Lépinay, B.M., Sosson, M., Müller, C., Baumgartner, P.O. & Baumgartner-Mora, C. 2014. Transition from the Farallon Plate subduction to the collision between South and Central America: Geological evolution of the Panama Isthmus. *Tectonophysics*, 622: 145–167. <https://doi.org/10.1016/j.tecto.2014.03.008>
- Baumgartner, P.O., Flores, K., Bandini, A.N., Girault, F. & Cruz, D. 2008. Upper Triassic to Cretaceous radiolaria from Nicaragua and northern Costa Rica—The Mesquito composite oceanic terrane. *Ophioliti*, 33(1): 1–19.
- Becker, G.F. 1917. Mechanics of the Panama Canal slides. In: White, D. (editor), *Shorter contributions to general geology*, 1916. Professional paper 98–N. U.S. Geological Survey, p. 253–261. Washington D.C. <https://doi.org/10.3133/pp98N>
- Berry, E.W. 1914. Fossil plants in the Panama Canal zone. *Science*, 39(1001): p. 357. <https://doi.org/10.1126/science.39.1001.357>
- Bloch, J.I., Woodruff, E.D., Wood, A.R., Rincón, A.F., Harrington, A.R., Morgan, G.S., Foster, D.A., Montes, C., Jaramillo, C., Jud, N.A., Jones, D.S. & MacFadden, B.J. 2016. First North American fossil monkey and early Miocene tropical biotic interchange. *Nature*, 533(7602): 243–246. <https://doi.org/10.1038/nature17415>
- Bowland, C.L. 1993. Depositional history of the western Colombian Basin, Caribbean Sea, revealed by seismic stratigraphy. *Geological Society of America Bulletin*, 105(10): 1321–1345. [https://doi.org/10.1130/0016-7606\(1993\)105<1321:DHOTWC>2.3.CO;2](https://doi.org/10.1130/0016-7606(1993)105<1321:DHOTWC>2.3.CO;2)
- Breen, N.A., Tagudin, J.E., Reed, D.L. & Silver, E.A. 1988. Mud-cored parallel folds and possible melange development in the north Panama thrust belt. *Geology*, 16(3): 207–210. [https://doi.org/10.1130/0091-7613\(1988\)16\[207:MPFAPM\]2.0.CO;2](https://doi.org/10.1130/0091-7613(1988)16[207:MPFAPM]2.0.CO;2)
- Brown, R.M. 1920. Five years of the Panama Canal: An evaluation. *Geographical Review*, 9(3): 191–198. <https://doi.org/10.2307/207257>
- Buchs, D.M., Arculus, R.J., Baumgartner, P.O., Baumgartner-Mora, C. & Ulianov, A. 2010. Late Cretaceous arc development on the SW margin of the Caribbean Plate: Insights from the Golfito, Costa Rica, and Azuero, Panama, complexes. *Geochemistry, Geophysics, Geosystems*, 11(7): 1–35. <https://doi.org/10.1029/2009GC002901>
- Buchs, D.M., Arculus, R.J., Baumgartner, P.O. & Ulianov, A. 2011a. Oceanic intraplate volcanoes exposed: Example from seamounts accreted in Panama. *Geology*, 39(4): 335–338. <https://doi.org/10.1130/G31703.1>
- Buchs, D.M., Baumgartner, P.O., Baumgartner-Mora, C., Flores, K. & Bandini, A.N. 2011b. Upper Cretaceous to Miocene tectonostratigraphy of the Azuero area (Panama) and the discontinuous accretion and subduction erosion along the middle American margin. *Tectonophysics*, 512(1–4): 31–46. <https://doi.org/10.1016/j.tecto.2011.09.010>
- Buchs, D.M., Hoernle, K., Hauff, F. & Baumgartner, P.O. 2016. Evidence from accreted seamounts for a depleted component in the early Galapagos plume. *Geology*, 44(5): 383–386. <https://doi.org/10.1130/G37618.1>
- Camacho, E., Hutton, W. & Pacheco, J.F. 2010. A new look at evidence for a Wadati–Benioff zone and active convergence at the North Panama Deformed Belt. *Bulletin of the Seismological Society of America*, 100(1): 343–348. <https://doi.org/10.1785/0120090204>
- Cardona, A., Valencia, V., Bayona, G., Duque, J., Ducea, M., Gehrels, G., Jaramillo, C., Montes, C., Ojeda, G. & Ruiz, J. 2011. Early-subduction-related orogeny in the northern Andes: Turonian to Eocene magmatic and provenance record in the Santa Marta Massif and Rancheria Basin, northern Colombia. *Terra Nova*, 23(1): 26–34. <https://doi.org/10.1111/j.1365-3121.2010.00979.x>
- Cardona, A., Montes, C., Ayala, C., Bustamante, C., Hoyos, N., Montenegro, O., Ojeda, C., Niño, H., Ramírez, V., Valencia, V., Rincón, D., Vervoort, J.D. & Zapata, S. 2012. From arc-continent collision to continuous convergence, clues from Paleogene conglomerates along the southern Caribbean–South America Plate boundary. *Tectonophysics*, 580: 58–87. <https://doi.org/10.1016/j.tecto.2012.08.039>
- Carvajal–Arenas, L.C. & Mann, P. 2018. Western Caribbean intraplate deformation: Defining a continuous and active microplate boundary along the San Andres Rift and Hess Escarpment fault zone, Colombian, Caribbean Sea. *American Association of Petroleum Geologists Bulletin*, 102(8): 1523–1563. <https://doi.org/10.1306/12081717221>
- Case, J.E. 1974. Oceanic crust forms basement of eastern Panamá. *Geological Society of America Bulletin*, 85(4): 645–652. [https://doi.org/10.1130/0016-7606\(1974\)85<645:OCFBOE>2.0.CO;2](https://doi.org/10.1130/0016-7606(1974)85<645:OCFBOE>2.0.CO;2)
- Case, J.E., Durán, L.G., López, A. & Moore, W.R. 1971. Tectonic investigations in western Colombia and eastern Panama. *Geological Society of America Bulletin*, 82(10): 2685–2711. [https://doi.org/10.1130/0016-7606\(1971\)82\[2685:TIIWCA\]2.0.CO;2](https://doi.org/10.1130/0016-7606(1971)82[2685:TIIWCA]2.0.CO;2)
- Case, J.E., Shagam, R. & Giegengack, R.F. 1990. Geology of the northern Andes: An overview. In: Dengo, G. & Case, J.E. (editors), *The Caribbean region*. Geological Society of America, p. 177–200. Boulder, USA. <https://doi.org/10.1130/DNAG-GNA-H.177>
- Cediel, F., Shaw, R.P. & Cáceres, C. 2003. Tectonic assembly of the northern Andean Block. In: Bartolini, C., Buffler, R.T. & Blickwede, J. (editors), *The circum-Gulf of Mexico and the*

- Caribbean: Hydrocarbon habitats, basin formation, and plate tectonics. American Association of Petroleum Geologists, Memoir 79, p. 815–848. Tulsa, USA.
- Coates, A.G. & Stallard, R.F. 2013. How old is the Isthmus of Panama? *Bulletin of Marine Science*, 89(4): 801–813. <https://doi.org/10.5343/bms.2012.1076>
- Coates, A.G., Collins, L.S., Aubry, M.P. & Berggren, W.A. 2004. The geology of the Darien, Panama, and the late Miocene – Pliocene collision of the Panama arc with northwestern South America. *Geological Society of America Bulletin*, 116(11–12): 1327–1344. <https://doi.org/10.1130/B25275.1>
- Collins, L.S., Coates, A.G., Berggren, W.A., Aubry, M.P. & Zhang, J. 1996. The late Miocene Panama isthmian strait. *Geology*, 24(8): 687–690. [https://doi.org/10.1130/0091-7613\(1996\)024<0687:TLMPIS>2.3.CO;2](https://doi.org/10.1130/0091-7613(1996)024<0687:TLMPIS>2.3.CO;2)
- Corral, I., Grier, A., Gómez-Gras, D., Corbella, M., Canals, Á., Pineda-Falconett, M. & Cardellach, E. 2011. Geology of the Cerro Quema Au–Cu deposit (Azuerio Peninsula, Panama). *Geologica Acta*, 9(3–4): 481–498. <https://doi.org/10.1344/105.000001742>
- Corral, I., Gómez-Gras, D., Grier, A., Corbella, M. & Cardellach, E. 2013. Sedimentation and volcanism in the Panamanian Cretaceous intra-oceanic arc and fore-arc: New insights from the Azuerio Peninsula (SW Panama). *Bulletin de la Société Géologique de France*, 184(1–2): 35–45. <https://doi.org/10.2113/gssgfbull.184.1-2.35>
- Corral, I., Cardellach, E., Corbella, M., Canals, Á., Gómez-Gras, D., Grier, A. & Cosca, M.A. 2016. Cerro Quema (Azuerio Peninsula, Panama): Geology, alteration, mineralization, and geochronology of a volcanic dome-hosted high-sulfidation Au–Cu deposit. *Economic Geology*, 111(2): 287–310. <https://doi.org/10.2113/econgeo.111.2.287>
- Coryell, H.N. & Embich, J.R. 1937. The Tranquilla Shale (upper Eocene) of Panama and its foraminiferal fauna. *Journal of Paleontology*, 11(4): 289–305.
- Cowan, H.A., Dart, R.L. & Machette, M.N. 1998. Map of Quaternary faults and folds of Panama and its offshore regions. Scale 1:750 000. U.S. Geological Survey, 1 sheet. <https://doi.org/10.3133/ofr98779>
- de Banville, M. 2004. Canal Français: L’aventure illustrée des français au Panama. 1880–1904. Éditeur Canal Valley, 194 p.
- Di Marco, G., Baumgartner, P.O. & Channell, J.E.T. 1995. Late Cretaceous – early Tertiary paleomagnetic data and a revised tectonostratigraphic subdivision of Costa Rica and western Panama. In: Mann, P. (editor), *Geologic and tectonic development of the Caribbean Plate boundary in southern Central America*. Geological Society of America, Special Paper 295, p. 1–27. Boulder, USA. <https://doi.org/10.1130/SPE295-p1>
- Douville, H. 1898. Sur l’âge des couches traversées par le canal de Panama. *Bulletin de la Société Géologique de France*, 3(26): 587–600.
- Duque-Caro, H. 1990. Neogene stratigraphy, paleoceanography and paleobiogeography in northwest South America and the evolution of the Panama Seaway. *Palaeogeography, Palaeoclimatology, Palaeoecology*, 77(3–4): 203–234. [https://doi.org/10.1016/0031-0182\(90\)90178-A](https://doi.org/10.1016/0031-0182(90)90178-A)
- Farris, D.W., Jaramillo, C., Bayona, G., Restrepo-Moreno, S.A., Montes, C., Cardona, A., Mora, A., Speakman, R.J., Glascock, M.D. & Valencia, V. 2011. Fracturing of the Panamanian Isthmus during initial collision with South America. *Geology*, 39(11): 1007–1010. <https://doi.org/10.1130/G32237.1>
- Farris, D.W., Cardona, A., Montes, C., Foster, D. & Jaramillo, C. 2017. Magmatic evolution of Panama Canal volcanic rocks: A record of arc processes and tectonic change. *PLOS ONE*, 12(5): 1–44. <https://doi.org/10.1371/journal.pone.0176010>
- Fisher, S.P. & Pessagno, E.A. 1965. Upper Cretaceous strata of northwestern Panama. *American Association of Petroleum Geologists Bulletin*, 49(4): 433–444. <https://doi.org/10.1306/A6633630-16C0-11D7-8645000102C1865D>
- Gazel, E., Hoernle, K., Carr, M.J., Herzberg, C., Saginor, I., van den Bogaard, P., Hauff, F., Feigenson, M.D. & Swisher III, C. 2011. Plume–subduction interaction in southern Central America: Mantle upwelling and slab melting. *Lithos*, 121(1–4): 117–134. <https://doi.org/10.1016/j.lithos.2010.10.008>
- Giudice, D. & Recchi, G. 1969. Geología del área del proyecto minero de Azuerio. Programa para el desarrollo de las Naciones Unidas, 53 p.
- Herrera, F., Manchester, S.R. & Jaramillo, C. 2012. Permineralized fruits from the late Eocene of Panama give clues of the composition of forests established early in the uplift of Central America. *Review of Paleobotany and Palynology*, 175: 10–24. <https://doi.org/10.1016/j.revpalbo.2012.02.007>
- Hershey, O.H. 1901. The geology of the central portion of the Isthmus of Panama. University of California, Bulletin of the Department of Geology, 2(8): 231–267.
- Hidalgo, P.J., Vogel, T.A., Rooney, T.O., Currier, R.M. & Layer, P.W. 2011. Origin of silicic volcanism in the Panamanian Arc: Evidence for a two-stage fractionation process at El Valle Volcano. *Contributions to Mineralogy and Petrology*, 162(6): 1115–1138. <https://doi.org/10.1007/s00410-011-0643-2>
- Hill, R.T., Dall, W.H., Bagg, M., Vaughan, T.W., Wolff, J.E., Turner, H.W. & Sjögren, A. 1898. The geological history of the Isthmus of Panama and portions of Costa Rica: Based upon a reconnaissance made for Alexander Agassiz. *Bulletin of the Museum of Comparative Zoology at Harvard College*, 28(5): 149–285.
- Hoernle, K., van den Bogaard, P., Werner, R., Lissinna, B., Hauff, F., Alvarado, G. & Garbe-Schönberg, D. 2002. Missing history (16–71 Ma) of the Galapagos hotspot: Implications for the tectonic and biological evolution of the Americas. *Geology*, 30(9): 795–798. [https://doi.org/10.1130/0091-7613\(2002\)030<0795:MHMOTG>2.0.CO;2](https://doi.org/10.1130/0091-7613(2002)030<0795:MHMOTG>2.0.CO;2)

- Hoernle, K., Hauff, F. & van den Bogaard, P. 2004. 70 m.y. history (139–69 Ma) for the Caribbean Large Igneous Province. *Geology*, 32(8): 697–700. <https://doi.org/10.1130/G20574.1>
- Hoernle, K., Abt, D.L., Fischer, K.M., Nichols, H., Hauff, F., Abers, G.A., van den Bogaard, P., Heydolph, K., Alvarado, G., Protti, M. & Strauch, W. 2008. Arc-parallel flow in the mantle wedge beneath Costa Rica and Nicaragua. *Nature*, 451(7182): 1094–1097. <https://doi.org/10.1038/nature06550>
- Jaramillo, C. 2018. Evolution of the Isthmus of Panama: Biological, paleoceanographic, and paleoclimatological implications. In: Hoorn, C., Perrigo, A. & Antonelli, A. (editors), *Mountains, climate and biodiversity*. Wiley–Blackwell, p. 323–338. Chichester, UK.
- Jaramillo, C., Montes, C., Cardona, A., Silvestro, D., Antonelli, A. & Bacon, C.D. 2017. Comment (1) on “Formation of the Isthmus of Panama” by O’Dea et al. *Science Advances*, 3(6): 1–8. <https://doi.org/10.1126/sciadv.1602321>
- Jorissen, F.J., Fontanier, C. & Thomas, E. 2007. Paleooceanographical proxies based on deep-sea benthic foraminiferal assemblage characteristics. In: Hillaire-Marcel, C. & de Vernal, A. (editors), *Proxies in late Cenozoic paleoceanography*. Elsevier Science, p. 263–325. [https://doi.org/10.1016/S1572-5480\(07\)01012-3](https://doi.org/10.1016/S1572-5480(07)01012-3)
- Kellogg, J.N., & Vega, V., 1995. Tectonic development of Panama, Costa Rica, and the Colombian Andes: Constraints from Global Positioning System geodetic studies and gravity. In: Mann, P. (editor), *Geologic and tectonic development of the Caribbean Plate boundary in southern Central America*. Geological Society of America, Special Paper 295, p. 75–90. Boulder, USA. <https://doi.org/10.1130/SPE295-p75>
- Kennan, L. & Pindell, J.L. 2009. Dextral shear, terrane accretion and basin formation in the northern Andes: Best explained by interaction with a Pacific-derived Caribbean Plate? In: James, K.H., Lorente, M.A. & Pindell, J.L. (editors), *The origin and evolution of the Caribbean Plate*. Geological Society of London, Special Publication 328, p. 487–531. <https://doi.org/10.1144/SP328.20>
- Kerr, A.C. & Tarney, J. 2005. Tectonic evolution of the Caribbean and northwestern South America: The case for accretion of two Late Cretaceous oceanic plateaus. *Geology*, 33(4): 269–272. <https://doi.org/10.1130/G21109.1>
- Kerr, A.C., White, R.V., Thompson, P.M.E., Tarney, J. & Saunders, A.D. 2003. No oceanic plateau–no Caribbean Plate? The seminal role of an oceanic plateau in Caribbean Plate evolution. In: Bartolini, C., Buffler, R.T. & Blickwede, J. (editors), *The circum-Gulf of Mexico and the Caribbean: Hydrocarbon habitats, basin formation, and plate tectonics*. American Association of Petroleum Geologists, Memoir 79, p. 126–168. Tulsa, USA.
- Kesler, S.E., Sutter, J.F., Issigonis, M.J., Jones, L.M. & Walker, R.L. 1977. Evolution of porphyry copper mineralization in an oceanic island arc: Panama. *Economic Geology*, 72(6): 1142–1153. <https://doi.org/10.2113/gsecongeo.72.6.1142>
- Kirby, M.X. & MacFadden, B. 2005. Was southern Central America an archipelago or a peninsula in the middle Miocene? A test using land-mammal body size. *Palaeogeography, Palaeoclimatology, Palaeoecology*, 228(3–4): 193–202. <https://doi.org/10.1016/j.palaeo.2005.06.002>
- Kirby, M.X., Jones, D.S. & MacFadden, B.J. 2008. Lower Miocene stratigraphy along the Panama Canal and its bearing on the Central American Peninsula, PLOS ONE, 3(7): 1–14. <https://doi.org/10.1371/journal.pone.0002791>
- Kolarsky, R.A. & Mann, P. 1995. Structure and neotectonics of an oblique-subduction margin, southwestern Panama. In Mann, P. (editor), *Geologic and tectonic development of the Caribbean Plate boundary in southern Central America*. Geological Society of America, Special Paper 295, p. 131–157. Boulder, USA. <https://doi.org/10.1130/SPE295-p131>
- Kolarsky, R.A., Mann, P. & Monechi, S. 1995. Stratigraphic development of southwestern Panama as determined from integration of marine seismic data and onshore geology. In Mann, P. (editor), *Geologic and tectonic development of the Caribbean Plate boundary in southern Central America*. Geological Society of America, Special Paper 295, p. 159–200. Boulder, USA. <https://doi.org/10.1130/SPE295-p159>
- Krawinkel, H., Wozazek, S., Krawinkel, J. & Hellmann, W. 1999. Heavy-mineral analysis and clinopyroxene geochemistry applied to provenance analysis of lithic sandstones from the Azuero–Soná Complex (NW Panama). *Sedimentary Geology*, 124(1–4): 149–168. [https://doi.org/10.1016/S0037-0738\(98\)00125-0](https://doi.org/10.1016/S0037-0738(98)00125-0)
- Leigh, E.G., O’Dea, A. & Vermeij, G.J. 2013. Historical biogeography of the Isthmus of Panama. *Biological Reviews*, 89(1): 148–172. <https://doi.org/10.1111/brv.12048>
- León, S., Cardona, A., Parra, M., Sobel, E.R., Jaramillo, J.S., Glodny, J., Valencia, V.A., Chew, D., Montes, C., Posada, G., Monsalve, G. & Pardo-Trujillo, A. 2018. Transition from collisional to subduction-related regimes: An example from Neogene Panama–Nazca–South America interactions. *Tectonics*, 37(1): 119–139. <https://doi.org/10.1002/2017TC004785>
- Lessios, H.A. 2008. The great American schism: Divergence of marine organisms after the rise of the Central American Isthmus. *Annual Review of Ecology Evolution, and Systematics*, 39: 63–91. <https://doi.org/10.1146/annurev.ecolsys.38.091206.095815>
- Li, C., Arndt, N.T., Tang, Q. & Ripley, E.M. 2015. Trace element indiscrimination diagrams. *Lithos*, 232: 76–83. <https://doi.org/10.1016/j.lithos.2015.06.022>
- Lissina, B. 2005. A profile through the Central American landbridge in western Panama: 115 Ma interplay between the Galápagos hotspot and the Central American subduction zone. Doctoral thesis, Christian-Albrechts-Universität zu Kiel, 102 p. Kiel, Germany.

- Lonsdale, P. 2005. Creation of the Cocos and Nazca Plates by fission of the Farallon Plate. *Tectonophysics*, 404(3–4): 237–264. <https://doi.org/10.1016/j.tecto.2005.05.011>
- Lonsdale, P. & Klitgord, K.D. 1978. Structure and tectonic history of the eastern Panama Basin. *Geological Society of America Bulletin*, 89(7): 981–999. [https://doi.org/10.1130/0016-7606\(1978\)89<981:SATHOT>2.0.CO;2](https://doi.org/10.1130/0016-7606(1978)89<981:SATHOT>2.0.CO;2)
- Lutton, R.J. & Banks, D.C. 1970. Study of clay shale slopes along the Panama Canal. Report 1: East Culebra and west Culebra slides and the model slope. U.S. Army Engineer Waterways Experiment Station. Technical report, 385 p. Vicksburg, USA.
- MacDonald, D.F. 1919. The sedimentary formations of the Panama Canal zone, with special reference to the stratigraphic relations of the fossiliferous beds. In: Vaughan, T.W. (editor), *Contributions to the geology and paleontology of the Canal zone, Panama, and geologically related areas in Central America and the West Indies*. Smithsonian Institution, United States National Museum, Press Bulletin 103, p. 525–545. Washington D.C.
- MacDonald, D.F. 1947. Panama Canal slides. Department of operation and maintenance, Special Engineering Division, Balboa Heights Canal Zone, 73 p.
- MacFadden, B.J., Jones, D.S., Jud, N.A., Moreno–Bernal, J.W., Morgan, G.S., Portell, R.W., Pérez, V.J., Moran, S.M. & Wood, A.R. 2017. Integrated chronology, flora and faunas, and paleoecology of the Alajuela Formation, late Miocene of Panama. *PLOS ONE*: 12(1): 1–27. <https://doi.org/10.1371/journal.pone.0170300>
- Mann, P. & Corrigan, J. 1990. Model for late Neogene deformation in Panama. *Geology*, 18(6): 558–562. [https://doi.org/10.1130/0091-7613\(1990\)018<0558:MFLNDI>2.3.CO;2](https://doi.org/10.1130/0091-7613(1990)018<0558:MFLNDI>2.3.CO;2)
- Mann, P. & Kolarsky, R.A. 1995. East Panama Deformed Belt: Structure, age, and neotectonic significance. In: Mann, P. (editor), *Geologic and tectonic development of the Caribbean Plate boundary in southern Central America*. Geological Society of America, Special Paper 295, p. 111–130. Boulder, USA. <https://doi.org/10.1130/SPE295-p111>
- Maury, R.C., Defant, M.J., Bellon, H., de Boer, J.Z., Stewart, R.H. & Cotten, J. 1995. Early tertiary arc volcanics from eastern Panama. In: Mann, P. (editor), *Geologic and tectonic development of the Caribbean Plate boundary in southern Central America*. Geological Society of America, Special Paper 295, p. 29–34. Boulder, USA. <https://doi.org/10.1130/SPE295-p29>
- Ministerio de Comercio e Industrias. 1991. Mapa Geológico de Panamá. Scale 1:500 000. Ministerio de Comercio e Industrias–División General de Recursos Minerales, 1sheet.
- Molnar, P. 2008. Closing of the Central American Seaway and the ice age: A critical review. *Paleoceanography and Paleoclimatology*, 23(2): 1–15. <https://doi.org/10.1029/2007PA001574>
- Molnar, P. 2017. Comment (2) on “Formation of the Isthmus of Panama” by O’Dea et al. *Science Advances*, 3(6): 1–4. <https://doi.org/10.1126/sciadv.1602320>
- Montes, C., Bayona, G., Cardona, A., Buchs, D.M., Silva, C.A., Morón, S., Hoyos, N., Ramírez, D.A., Jaramillo, C. & Valencia, V. 2012a. Arc–continent collision and orocline formation: Closing of the Central American Seaway. *Journal of Geophysical Research: Solid Earth*, 117(B4): 1–25. <https://doi.org/10.1029/2011JB008959>
- Montes, C., Cardona, A., McFadden, R., Moron, S.E., Silva, C.A., Restrepo–Moreno, S., Ramírez, D.A., Hoyos, N., Wilson, J., Farris, D.W., Bayona, G., Jaramillo, C., Valencia, V., Bryan, J. & Flores, J.A. 2012b. Evidence for middle Eocene and younger land emergence in Central Panama: Implications for isthmus closure. *Geological Society of America Bulletin*, 124(5–6): 780–799. <https://doi.org/10.1130/B30528.1>
- Montes, C., Cardona, A., Jaramillo, C., Pardo, A., Silva, J.C., Valencia, V., Ayala, C., Pérez–Ángel, L.C., Rodríguez–Parra, L.A., Ramírez, V. & Niño, H. 2015. Middle Miocene closure of the Central American Seaway. *Science*, 348(6231): 226–229. <https://doi.org/10.1126/science.aaa2815>
- Nivia, Á. 1996. The Bolivar mafic–ultramafic complex, SW Colombia: The base of an obducted oceanic plateau. *Journal of South American Earth Sciences*, 9(1–2): 59–68. [https://doi.org/10.1016/0895-9811\(96\)00027-2](https://doi.org/10.1016/0895-9811(96)00027-2)
- O’Dea, A., Lessios, H.A., Coates, A.G., Eytan, R.I., Restrepo–Moreno, S.A., Cione, A.L., Collins, L.S., de Queiroz, A., Farris, D.W., Norris, R.D., Stallard, R.F., Woodburne, M.O., Aguilera, O., Aubry, M. –P., Berggren, W.A., Budd, A.F., Cozzuol, M.A., Coppard, S.E., Duque–Caro, H., Finnegan, S., Gasparini, G.M., Grossman, E.L., Johnson, K.G., Keigwin, L.D., Knowlton, N., Leigh, E.G., Leonard–Pingel, J.S., Marko, P.B., Pyenson, N.D., Rachello–Dolmen, P.G., Soibelzon, E., Soibelzon, L., Todd, J.A., Vermeij, G.J. & Jackson, J.B.C. 2016. Formation of Isthmus of Panama. *Science Advances*, 2(8): 1–11. <https://doi.org/10.1126/sciadv.1600883>
- Pérez–Consuegra, N., Góngora, D.E., Herrera, F., Jaramillo, C., Montes, C., Cuervo–Gómez, A.M., Hendy, A., Machado, A., Cárdenas, D. & Bayona, G. 2018. New records of Humiriaceae fossil fruits from the Oligocene and early Miocene of the western Azuero Peninsula, Panamá. *Boletín de la Sociedad Geológica Mexicana*, 70(1): 223–239. <http://dx.doi.org/10.18268/BSGM-2018v70n1a13>
- Pindell, J.L. & Kennan, L. 2009. Tectonic evolution of the Gulf of Mexico, Caribbean and northern South America in the mantle reference frame: An update. In: James, K.H., Lorente, M.A. & Pindell, J.L. (editors), *The origin and evolution of the Caribbean Plate*. Geological Society of London, Special Publication 328, p. 1–55. <https://doi.org/10.1144/SP328.1>
- Ramírez, D.A., Foster, D.A., Min, K., Montes, C., Cardona, A. & Sadowe, G. 2016. Exhumation of the Panama basement complex and basins: Implications for the closure of the Central American Seaway. *Geochemistry, Geophysics, Geosystems*, 17(5): 1758–1777. <https://doi.org/10.1002/2016GC006289>

- Recchi, G. & Metti, A. 1975. Lámina 17. In: Molo, J.C. (editor), Atlas Nacional de Panamá. Instituto Geográfico Nacional Tommy Guardia, p. 71. Panamá.
- Reclus, A. & De Vaisseau, L. 1880. Explorations aux Isthmes de Panama et de Darien. *Le Tour du Monde*, 21(1): 321–400.
- Reed, D.L. & Silver, E.A. 1995. Sediment dispersal and accretionary growth of the North Panama Deformed Belt. In: Mann, P. (editor), *Geologic and tectonic development of the Caribbean Plate boundary in southern Central America*. Geological Society of America, Special Paper 295, p. 213–223. Boulder, USA. <https://doi.org/10.1130/SPE295-p213>
- Reed, D.L., Silver, E.A., Tagudin, J.E., Shipley, T.H. & Vrolijk, P. 1990. Relations between mud volcanoes, thrust deformation, slope sedimentation, and gas hydrate, offshore north Panama. *Marine and Petroleum Geology*, 7(1): 44–54. [https://doi.org/10.1016/0264-8172\(90\)90055-L](https://doi.org/10.1016/0264-8172(90)90055-L)
- Rincón, A.F., Bloch, J.I., Macfadden, B.J. & Jaramillo, C. 2015. New early Miocene protoceratids (Mammalia, Artiodactyla) from Panama. *Journal of Vertebrate Paleontology*, 35(5): 1–22. <https://doi.org/10.1080/02724634.2015.970688>
- Rodríguez, G. & Sierra, M.I. 2010. Las Sedimentitas de Tripogadí y las Brechas de Triganá: Un registro de volcanismo de arco, corrientes de turbidez y levantamiento rápido Eoceno en el noroccidente de Sur América. *Geología Colombiana*, 35: 74–86.
- Rodríguez-Parra, L.A., Gaitán, C., Montes, C., Bayona, G. & Rapalini, A. 2017. Arc–seamount collision: Driver for vertical–axis rotations in Azuero, Panama. *Studia Geophysica et Geodaetica*, 61(2): 199–218. <https://doi.org/10.1007/s11200-016-1173-1>
- Röhl, U. & Abrams, L.J. 2000. High–resolution, downhole, and non-destructive core measurements from Sites 999 and 1001 in the Caribbean Sea: Application to the late Paleocene Thermal Maximum. In: Leckie, R.M., Sigurdsson, H., Acton, G.D. & Draper, G. (editors), *Proceedings of the Ocean Drilling Program, Scientific Results 165*, p. 191–203. College Station, USA. <https://doi.org/10.2973/odp.proc.sr.165.009.2000>
- Rooney, T.O., Franceschi, P. & Hall, C.M. 2011. Water–saturated magmas in the Panama Canal region: A precursor to adakite–like magma generation? *Contributions to Mineralogy and Petrology*, 161(3): 373–388. <https://doi.org/10.1007/s00410-010-0537-8>
- Rooney, T.O., Morell, K.D., Hidalgo, P. & Franceschi, P. 2015. Magmatic consequences of the transition from orthogonal to oblique subduction in Panama. *Geochemistry, Geophysics, Geosystems* 16(12): 4178–4208. <https://doi.org/10.1002/2015GC006150>
- Sheffey, J.P., Woodbury, H.G., Noble, C.C., Groves, R.H. & McGregor, E.W. 1969. Summary of geology and rock physical properties. U.S. Army Engineer Nuclear Cratering Group & Lawrence Radiation Laboratory, University of California, 1027 p. California.
- Shelton, B.J. 1952. Geology and petroleum prospects of Darien, south-eastern Panama. Master thesis, Oregon State College, 62 p. Corvallis, USA.
- Silver, E.A., Reed, D.L., Tagudin, J.E. & Heil, D.J. 1990. Implications of the north and south Panama thrust belts for the origin of the Panama orocline. *Tectonics*, 9(2): 261–281. <https://doi.org/10.1029/TC009i002p00261>
- Silver, E.A., Galewsky, J. & McIntosh, K.D. 1995. Variation in structure, style, and driving mechanism of adjoining segments of the North Panama Deformed Belt. In: Mann, P. (editor), *Geologic and tectonic development of the Caribbean Plate boundary in southern Central America*. Geological Society of America, Special Paper 295, p. 225–233. Boulder, USA. <https://doi.org/10.1130/SPE295-p225>
- Stephan, J.F., Blanchet, R. & Mercier de Lepinay, B. 1986. Northern and southern Caribbean festoons (Panama, Colombia–Venezuela and Hispaniola–Puerto Rico), interpreted as pseudosubductions induced by the east–west shortening of the pericaribbean continental frame. In: Wezel, F.C. (editor), *The origin of arcs*. Elsevier, *Developments in Geotectonics* 21, p. 401–422. Amsterdam, the Netherlands. <https://doi.org/10.1016/B978-0-444-42688-8.50022-9>
- Stewart, R.H., Stewart, J.L. (compilers) & Woodring, W.P. (collaborator). 1980. Geologic map of the Panama Canal and vicinity, Republic of Panama. Scale 1:100 000. U.S. Geological Survey, *Miscellaneous Investigations Series*, Map I-1232, 1 sheet. <https://doi.org/10.3133/i1232>
- Tavelli, J.A. 1947. Geologic Explorations, Caledonia Bay, Route 17, Geology and Topography. Panama Canal Company, 21 p.
- Terry, R.A. 1956. A geological reconnaissance of Panama. *California Academy of Science, Occasional Papers* 23–25, 91 p. San Francisco, USA.
- Tournon, J., Triboulet, C. & Azema, J. 1989. Amphibolites from Panama: Anticlockwise P–T paths from a pre–Upper Cretaceous metamorphic basement in Isthmian Central America. *Journal of Metamorphic Geology*, 7(5): 539–546. <https://doi.org/10.1111/j.1525-1314.1989.tb00616.x>
- Tripathi, A. & Zachos, J.C. 2002. Late Eocene tropical sea surface temperatures: A perspective from Panama. *Paleoceanography and Paleoclimatology*, 17(3): 4–14–14. <https://doi.org/10.1029/2000PA000605>
- United Nations Development Program. 1972. Reconnaissance geochemical survey of Bocas del Toro, Maje, Pirre and San Blas–Darien. United Nations, Technical report 2, 79 p. Panamá.
- U.S. Geological Survey. 2010. Global multi–resolution terrain elevation data 2010 (GMTED2010). https://topotools.cr.usgs.gov/gmted_viewer/viewer.htm (consulted in July 2018).
- U.S. Geological Survey. 2017. Search earthquake catalog. <https://earthquake.usgs.gov/earthquakes/search/> (consulted in November 2018).
- Vannucchi, P., Fisher, D.M., Bier, S. & Gardner, T.W. 2006. From seamount accretion to tectonic erosion: Formation of Osa Mélangé and the effects of Cocos Ridge subduction in southern Costa Rica. *Tectonics*, 25(2): 1–19. <https://doi.org/10.1029/2005TC001855>

- Vannucchi, P., Fisher, D.M. & Gardner, T.W. 2007. Reply to comment by David M. Buchs & Peter O. Baumgartner on “From seamount accretion to tectonic erosion: Formation of Osa Mélangé and the effects of the Cocos Ridge subduction in southern Costa Rica”. *Tectonics*, 26(3): 1–2. <https://doi.org/10.1029/2007TC002129>
- Vannucchi, P., Sak, P.B., Morgan, J.P., Ohkushi, K. & Ujiie, K. 2013. Rapid pulses of uplift, subsidence, and subduction erosion offshore Central America: Implications for building the rock record of convergent margins. *Geology*, 41(9): 995–998. <https://doi.org/10.1130/G34355.1>
- Vaughan, T.W. 1946. Initiation of geological investigations in the Panama Canal zone. *Science*, 104(2696): 209. <https://doi.org/10.1126/science.104.2696.209>
- Verbrugghe, L. 1879. A travers l’isthme de Panama. Tracé interocéanique de L.N.B. Wyse et A. Reclus, Imprimerie de A. Quantin, 476 p. Paris.
- Villagómez, D., Spikings, R., Magna, T., Kammer, A., Winkler, W. & Beltrán, A. 2011. Geochronology, geochemistry and tectonic evolution of the Western and Central Cordilleras of Colombia. *Lithos*, 125(3–4): 875–896. <https://doi.org/10.1016/j.lithos.2011.05.003>
- Wegner, W., Wörner, G., Harmon, R.S. & Jicha, B.R. 2011. Magmatic history and evolution of the Central American land bridge in Panama since the Cretaceous times. *Geological Society of America Bulletin*, 123(3–4): 703–724. <https://doi.org/10.1130/B30109.1>
- Westbrook, G.K., compiler. 1990. Gravity anomaly map of the Caribbean region. Scale 1:5 000 000. In: Dengo, G. & Case, J.E. (editors), *The Caribbean region*. Geological Society of America, plate 7, p. 537. Boulder, USA. <https://doi.org/10.1130/DNAG-GNA-H>
- Whattam, S.A. & Stern, R.J. 2015. Late Cretaceous plume–induced subduction initiation along the southern margin of the Caribbean and NW South America: The first documented example with implications for the onset of plate tectonics. *Gondwana Research*, 27(1): 38–63. <https://doi.org/10.1016/j.gr.2014.07.011>
- Whattam, S.A., Montes, C., McFadden, R.R., Cardona, A., Ramírez, D. & Valencia, V. 2012. Age and origin of earliest adakitic–like magmatism in Panama: Implications for the tectonic evolution of the Panamanian magmatic arc system. *Lithos*, 142–143: 226–244. <https://doi.org/10.1016/j.lithos.2012.02.017>
- Wolters, B. 1986. Seismicity and tectonics of southern Central America and adjacent regions with special attention to the surroundings of Panama. *Tectonophysics*, 128(1–2): 21–46. [https://doi.org/10.1016/0040-1951\(86\)90306-9](https://doi.org/10.1016/0040-1951(86)90306-9)
- Woodring, W.P. 1957. Geology and description of tertiary mollusks (gastropods: Trochidae to Turritellidae). Geology and paleontology of Canal zone and adjoining parts of Panama. U.S. Geological Survey, Professional Paper 306–A, 135 p.
- Woodring, W.P. 1973. Description of tertiary mollusks (additions to gastropods, scaphopods, pelecypods: Nuculidae to Malleidae). Geology and paleontology of Canal zone and adjoining parts of Panama. U.S. Geological Survey, Professional Paper 306–E: 453–531.
- Woodring, W.P. & Thompson, T.F. 1949. Tertiary formations of Panama Canal zone and adjoining parts of Panama. *American Association of Petroleum Geologists Bulletin*, 33(2): 223–247.
- Wörner, G., Harmon, R.S., Hartmann, G. & Simon, K. 2005. Igneous geology and geochemistry of the upper río Chagres Basin. In: Harmon, R.S. (editor), *The río Chagres, Panama: A multidisciplinary profile of a tropical Watershed*. Springer, p. 65–82. Dordrecht, the Netherlands.

Explanation of Acronyms, Abbreviations, and Symbols:

CLIP	Caribbean Large Igneous Plateau	STRI	Smithsonian Tropical Research Institute
LIP	Large Igneous Province	UNDP	United Nations Development Program
ODP	Ocean Drilling Program		

Authors' Biographical Notes



Camilo MONTES is currently professor of geology at the Universidad del Norte in Barranquilla. He obtained his undergraduate degree in geology from Universidad Nacional de Colombia, and his MS and PhD at the University of Tennessee. Camilo's main research interests are the late Mesozoic – Cenozoic tectonic evolution of the Caribbean and the north-western corner of South America, and its

implications in climate and biotas. Basic geologic mapping is at the basis of all of his research and educational efforts.



Natalia HOYOS obtained her undergraduate degree in geology from Universidad EAFIT, Colombia (1996) and completed her master's degree in environmental science at the University of New Haven, U.S. (2000), and PhD in geography at the University of Florida, U.S. (2004). She moved to Panama in 2010 to work as a postdoc at the Smithsonian Tropical Research Institute, and

returned to Colombia in 2011 to work with Corporación Geológica ARES. Since 2014, Natalia HOYOS is affiliated with Universidad del Norte (Colombia). Her research interests include the use of remote sensing data and geographic analyses for geologic mapping and the study of human–environment interactions.

Photography Natalia HOYOS: Lina Pérez–Angel

Chapter 16



Zircon U–Pb and Fission–Track Dating Applied to Resolving Sediment Provenance in Modern Rivers Draining the Eastern and Central Cordilleras, Colombia

Cindy Lizeth URUEÑA–SUÁREZ^{1*} , Mary Luz PEÑA–URUEÑA^{2*} , Jimmy Alejandro MUÑOZ–ROCHA³ , Lorena del Pilar RAYO–ROCHA⁴ , Nicolas VILLAMIZAR–ESCALANTE⁵ , Sergio AMAYA–FERREIRA⁶ , Mauricio IBAÑEZ–MEJIA⁷ , and Matthias BERNET⁸

Abstract Determining the crystallization and cooling ages of detrital zircons from ancient sedimentary rocks or modern river sediments is a powerful method for tracing the sediment provenance and exhumation of orogenic mountain belts. Here, we present a study of the U–Pb and fission–track dating of detrital zircons from: (1) the sedimentary cover units of the Eastern Cordillera between Bogotá and Villavicencio and (2) the modern river sediments of the Guatiquía and Guayuriba Rivers, which drain the eastern flank of the Eastern Cordillera, and those of the Magdalena River at Girardot, which drains the western flank of the Eastern Cordillera and the eastern part of the Central Cordillera. We use our data to highlight the advantages and limitations of using zircon U–Pb and fission–track dating in provenance studies, including the identification of original source areas, sediment recycling and the difficulty of detecting amagmatic orogens in the detrital zircon record. The data obtained in this study allow us to better understand the association between the exhumation of sources and their detrital zircon signatures in the modern rivers that drain part of the Eastern Cordillera.

Keywords: Detrital zircon, Eastern Cordillera of Colombia, Exhumation, Provenance.

Resumen La determinación de edades de cristalización y de enfriamiento de circones detríticos en rocas sedimentarias antiguas o sedimentos de ríos actuales es un poderoso método para trazar la proveniencia del sedimento y la exhumación de cinturones orogénicos. Aquí presentamos un estudio de dataciones U–Pb y trazas de fisión en circones de (1) las unidades sedimentarias de la cordillera Oriental entre Bogotá y Villavicencio y (2) sedimentos fluviales actuales de los ríos Guatiquía y Guayuriba, los cuales drenan el flanco oriental de la cordillera Oriental, y sedimentos del río Magdalena en Girardot, que drena el flanco occidental de la cordillera Oriental y la parte oriental de la cordillera Central. Usamos nuestros datos para resaltar las ventajas y limitaciones de usar dataciones U–Pb y trazas de fisión para estudios de proveniencia, incluyendo la identificación de áreas fuente originales, el reciclaje de sedimentos y la dificultad de detectar orógenos

Citation: Urueña–Suárez, C.L., Peña–Urueña, M.L., Muñoz–Rocha, J.A., Rayo–Rocha, L.P., Villamizar–Escalante, N., Amaya–Ferreira, S., Ibañez–Mejía, M. & Bernet, M. 2020. Zircon U–Pb and fission–track dating applied to resolving sediment provenance in modern rivers draining the Eastern and Central Cordilleras, Colombia. In: Gómez, J. & Mateus–Zabala, D. (editors), *The Geology of Colombia, Volume 3 Paleogene – Neogene*. Servicio Geológico Colombiano, Publicaciones Geológicas Especiales 37, p. 469–490. Bogotá. <https://doi.org/10.32685/pub.esp.37.2019.16>

<https://doi.org/10.32685/pub.esp.37.2019.16>
Published online 3 June 2020

- 1 cindy.urueña@geol.lu.se
Lund University
Department of Geology
Sölvegatan 12. Lund, Sweden
 - 2 mlpena@sgc.gov.co
Servicio Geológico Colombiano
Dirección de Asuntos Nucleares
Carrera 50 n.º 26–20
Bogotá, Colombia
 - 3 jamunoz@sgc.gov.co
Servicio Geológico Colombiano
Dirección de Asuntos Nucleares
Carrera 50 n.º 26–20
Bogotá, Colombia
 - 4 lrayo@sgc.gov.co
Servicio Geológico Colombiano
Dirección de Geociencias Básicas
Diagonal 53 n.º 34–53
Bogotá, Colombia
 - 5 nvillamizar@sgc.gov.co
Servicio Geológico Colombiano
Dirección de Asuntos Nucleares
Carrera 50 n.º 26–20
Bogotá, Colombia
 - 6 samaya@sgc.gov.co
Servicio Geológico Colombiano
Dirección de Recursos Minerales
Diagonal 53 n.º 34–53
Bogotá, Colombia
 - 7 ibanezm@arizona.edu
Department of Geosciences
University of Arizona
Tucson, Arizona, 85721, USA
 - 8 matthias.bernet@univ-grenoble-alpes.fr
Université Grenoble Alpes
Institut des Sciences de la Terre
1381 rue de la piscine, CS 40700, 38058
Grenoble cedex 9, France
- * Corresponding authors

Supplementary Information:
S: <https://www2.sgc.gov.co/LibroGeologiaColombia/tgc/sgcpubesp37201916s.pdf>

no magmáticos en el registro de circones detríticos. Los datos obtenidos en este estudio nos permitieron entender mejor la asociación entre la exhumación de fuentes y sus firmas detríticas en ríos actuales que drenan parte de la cordillera Oriental.

Palabras clave: *circón detrítico, cordillera Oriental de Colombia, exhumación, proveniencia.*

1. Introduction

Provenance studies that utilize the crystallization or cooling ages of detrital zircons have been proven to be useful in making paleogeographic reconstructions (e.g., Gehrels & Pecha, 2014), identifying tectonically induced changes in drainage patterns (e.g., Davis *et al.*, 2010), placing time constraints on surface uplift (e.g., Horton *et al.*, 2010), and fingerprinting pulses of magmatism (Caricchi *et al.*, 2014). In recent decades, much progress has been made in the use of different geo- and thermochronological methods to gain information about sediment provenance and the exhumation of sediment source areas. Each individual dating technique offers unique information about provenance and exhumation. The strength of these analyses lies in combining different dating techniques on the same samples or even within the same grains to obtain crystallization and cooling ages that represent the geological history and processes that control a given source-to-sink system. Although apatite fission-track and U–Pb double-dating have been developed and used in provenance studies (Mark *et al.*, 2016), the most suitable mineral for this type of analysis is zircon (e.g., Bernet *et al.*, 2006; Rahl *et al.*, 2003; Reiners *et al.*, 2005), as zircons are present in many upper crustal magmatic, metamorphic, and sedimentary rocks and are resistant to weathering. In this work, we use new examples of modern river samples from the Colombian Andes to explain how zircon fission-track (ZFT) and U–Pb dating can be used in provenance studies to better understand the temporal association between sources and depositional sites (Carter & Moss, 1999) and how the evolution of orogenic mountain belts in settings where large amounts of sediment are recycled from sedimentary source rocks and volcanic input may complicate the exhumational signal in such data (e.g., Carter & Moss, 1999; Jourdan *et al.*, 2013). ZFT data, which provide information about the most recent thermal history and exhumation of source rocks, can complement U–Pb data, which reflect the original zircon crystallization age and its ultimate provenance.

Zircon U–Pb geochronology is the most common technique applied to provenance studies of detrital materials, including the sedimentary basins of the Colombian Andes (Horton *et al.*, 2010; Nie *et al.*, 2010). The strength of this method lies in the ability of detrital zircons to retain the spectra of ages that characterize the timing of the igneous and/or metamorphic (re-)crystallization of their source terranes. This type of information is useful for establishing stratigraphic correlations and identifying sediment source areas and/or their transport and depositional histories (Kosler & Sylvester, 2003). In the same sense, ZFT

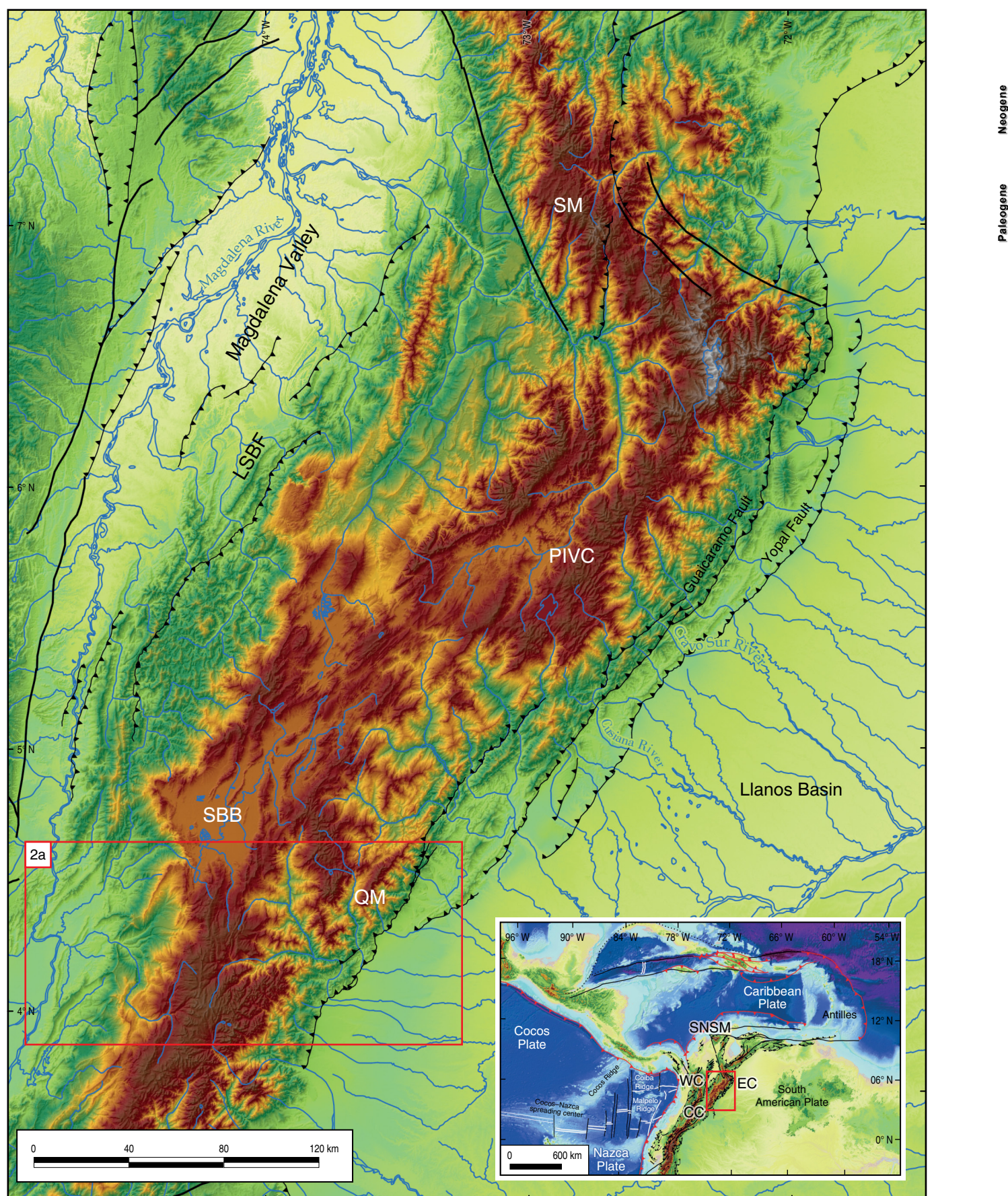
data provide robust information about the most recent thermal history of a sediment source area after it cools below the ZFT closure temperature of approximately 250–200 °C, depending on the cooling rate, which is invaluable for elucidating the tectonic and exhumation processes in a range of geodynamic settings, especially during the evolution of convergent orogenic belts (Bernet & Garver, 2005; Brandon *et al.*, 1998; Reiners & Brandon, 2006). Nonetheless, in cases of very slow cooling and/or reheating in the source area, detrital zircons may also reflect partial annealing in the source area, with apparent cooling ages that cannot be directly associated with a tectonic event or a particular orogenic phase (Bernet *et al.*, 2001, 2006, 2009).

The purpose of this chapter is to present the U–Pb and fission-track data from the first source-to-sink study of the Servicio Geológico Colombiano (SGC) Geochronology Laboratory, using the tested analytical procedures and their application to resolve specific geological problems. The goal of this preliminary study is to determine the provenance signal in the modern river sediments of rivers draining the eastern and western foothills of the Eastern Cordillera in Colombia using the combined ZFT and zircon U–Pb dating of the same samples. The detrital sediments studied here were taken from the Magdalena River at Girardot on the western flank of the Eastern Cordillera and from the Guatiquía and Guayuriba Rivers in the eastern foothills of the Eastern Cordillera (Figure 1).

2. Geological Framework

The geology of Colombia is tectonically and morphologically characterized by the stable Precambrian basement of the Amazon Craton in the eastern part of the country (Ibañez-Mejía & Cordani, 2020), as well as by the highlands of the Andean Belt, in which three cordilleras are separated from each other by intermountain valleys (Figure 1). Rivers such as the Bogotá River drain the Eastern Cordillera to the west into the Magdalena River (Figure 2). The Magdalena River is one of the most important drainage systems of the Northern Andes, as it

Figure 1. Shaded relief image of the Eastern Cordillera showing the main geomorphological and tectonic structures: Magdalena Valley; (SM) Santander Massif; (LSBF) La Salina–Bituima Fault System; (PIVC) Paipa–Iza Volcanic Complex; (QM) Quetame Massif; (SBB) Sabana de Bogotá Basin; Llanos Basin. Note the NE–SW trend of the cordillera, as well as the location of the study area (red box). The box in the smaller map shows the tectonic setting: (EC) Eastern Cordillera; (CC) Central Cordillera; (WC) Western Cordillera; (SNSM) Sierra Nevada de Santa Marta.



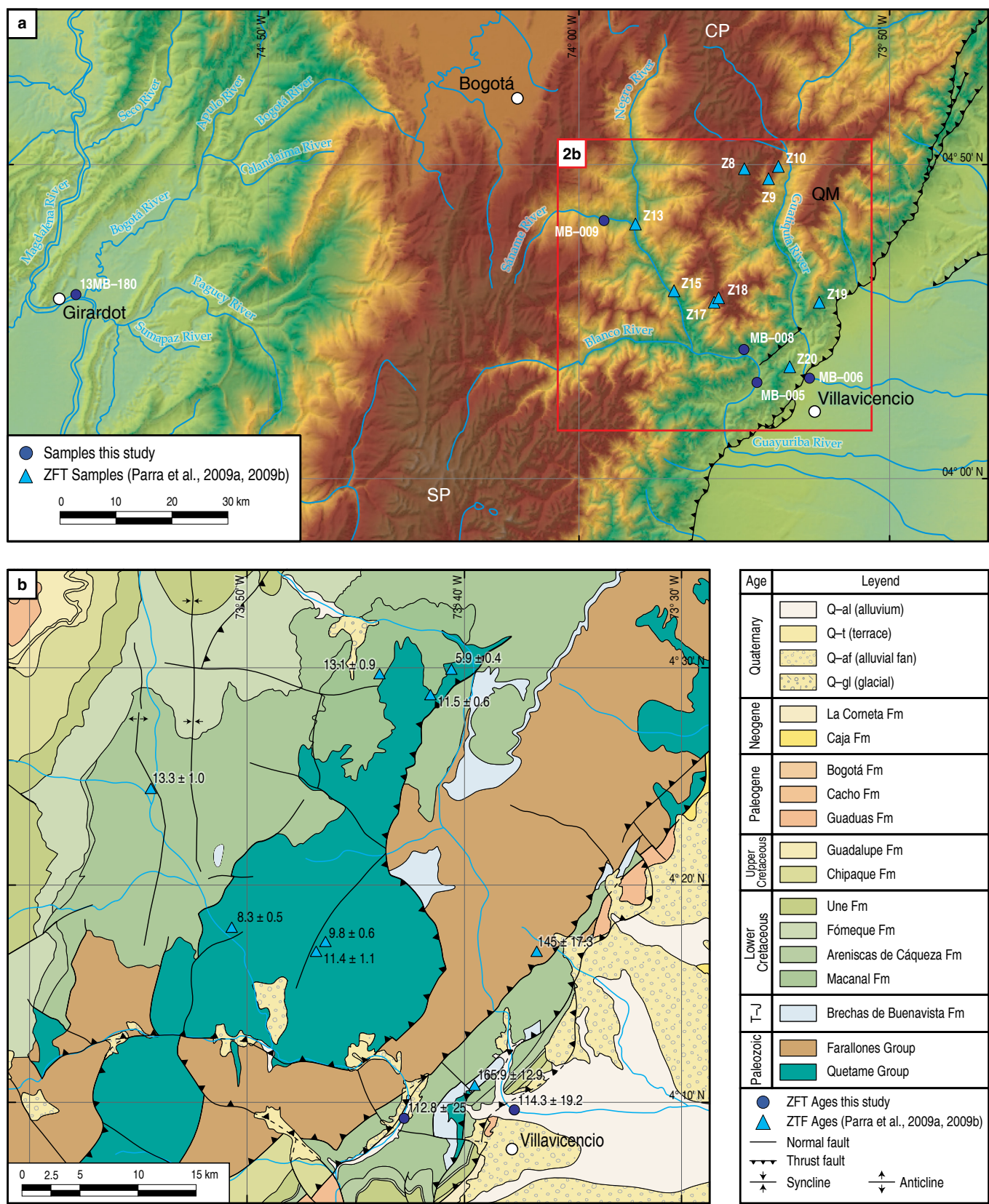


Figure 2. (a) Shaded relief image of the study area showing the main river discharge in the Eastern and Western Cordilleras (Bogotá River, Guayuriba River, Guatiquía River). Locations of samples collected in this study are shown as blue circles, and those of Parra et al. (2009a, 2009b) are shown as blue triangles. (QM) Quetame Massif; (SP) Sumapaz Paramo; (CP) Chingaza Paramo. **(b)** Simplified and modified geological map from Gómez et al. (2015) with the locations of samples analyzed for zircon fission-track ages in this study shown as blue circles and those of Parra et al. (2009a, 2009b) shown as blue triangles.

crosses Colombia from south to north over a distance of 1000 km, collecting all of the tributaries coming from the western flank of the Eastern Cordillera, the eastern flank of the Central Cordillera, and, further downstream, the western Cordillera at the confluence with the Cauca River near Magangué. On the east side of the Eastern Cordillera, the drainage configuration is different. The rivers run from the foothills across the Llanos Basin from west to east to ultimately join either the Orinoco or Amazon Rivers. The Guatiquía and Guayuriba Rivers are two of the most important tributaries of the Meta River, which is part of the Orinoco Basin. With their springs in the Chingaza and Sumapaz Paramo regions in the Eastern Cordillera (Figure 2a), they drain Precambrian (Garzón Massif), Paleozoic (Quetame Massif), and Cretaceous sedimentary cover rocks (Figure 2b).

Different authors have used thermochronology and U–Pb geochronology to describe how the surface uplift, exhumation and deformation history of the Eastern Cordillera is related to the drainage and sedimentary basin evolution of the Llanos Foreland, which is limited by the Guaicáramo Fault System (i.e., Bande et al., 2012; Horton et al., 2010; Mora et al., 2008; Nie et al., 2010; Parra et al., 2009a, 2009b; Saylor et al., 2013). The evolution of the Eastern Cordillera as a highland started during the middle Eocene to Oligocene, and it intensified during the Miocene – Pliocene, after the tectonic inversion of pre-existing Jurassic and Early Cretaceous graben structures and mid-crustal low-angle detachment faults (Colleta et al., 1990; Cooper et al., 1995; Dengo & Covey, 1993; Mora et al., 2006, 2009; Sarmiento-Rojas et al., 2006).

Since the Eocene, compressional deformation has migrated to the east (Mora et al., 2010; Parra et al., 2009a, 2009b, 2012), and a late Paleogene to Neogene foreland basin sequence began recording the erosional exhumation history of the adjacent basement highs in the Eastern Cordillera. According to Mora et al. (2008), the eastern flank has the highest mean elevations, and its topography exhibits deeply incised river canyons with dissected basement rocks. Based on thermochronological analyses, this topography has been interpreted as a cause and consequence of rapid exhumation rates, which have been attributed to climatic and tectonic forcing (Parra et al., 2009a, 2009b). The asymmetry in orogenic processes is believed to be caused by two main factors: (1) structural inheritance during inversion, and (2) initial topographic growth between 6 and 3 Ma, which built an orographic barrier that subsequently intercepted easterly moisture-bearing winds, thus leading to focused precipitation and enhanced erosion (Mora et al., 2008).

Although the initial surface uplift was probably moderate, after the Oligocene, the rise of the Eastern Cordillera blocked the arrival of zircons derived from the Guiana Shield to the hinterland interior. This dramatic change in local topography caused a shift in the sediment provenance of the sedimentary units deposited in the intermontane Magdalena River Basin

(Horton et al., 2010; Nie et al., 2010), which has developed between the Central and Eastern Cordilleras since the Eocene.

3. Materials and Methods

3.1. Sampling

In this study, two samples were collected along a Bogotá–Villavicencio transect in a stratigraphic section of Paleozoic to Upper Cretaceous rocks (Figures 2, 3; Table 1); additionally, two river sediment samples of the main tributaries of the eastern flank of the Eastern Cordillera were collected close to Villavicencio, and one was collected from a sandbar in the Magdalena River at Girardot. The U–Pb dating of detrital zircons was conducted on river sediment samples, and ZFT dating was performed on both sedimentary rock and river samples. The oldest units in the area correspond to the metamorphic and metasedimentary rocks of the Quetame Group, which are stratigraphically overlain by the Devonian sedimentary rocks of the Farallones Group (Areniscas de Gutiérrez Formation), the Jurassic sedimentary rocks of the Brechas de Buenavista Formation, and a Cretaceous sedimentary section represented by the rocks of the Cáqueza and Une Formations, as well as the Upper Cretaceous Chipaque Formation. Active sediment samples from the Guatiquía and Guayuriba Rivers were collected in proximity to the drainage slope inflection that represents the transition from the orogenic hinterland to the foreland basin system. These two rivers extend from approximately the central axis of the mountain range and flow towards the east, mainly eroding Cretaceous and tertiary units. On the western flank of the Eastern Cordillera, one sample was taken from the Magdalena River on a sandbar close to the Girardot bridge, downstream of its confluence with the Bogotá River (Table 1). The Upper Magdalena River Basin drains not only the western flank of the Eastern Cordillera but also a large part of the Central Cordillera volcanic arc and crystalline basement.

3.2. U–Pb Dating by LA–ICP–MS

Sedimentary provenance studies commonly use the U–Pb dating of detrital zircon grains as a tool with which to characterize the provenance of sediments, provided that the age spectra of their potential source areas are known. This approach allows researchers to establish potential correlations between different sedimentary units and permits the quantification of the maximum depositional ages of strata in the absence of datable volcanic material (Dickinson & Gehrels, 2009; Gehrels, 2011). Laser ablation–inductively coupled plasma–mass spectrometry (LA–ICP–MS) is particularly well suited for provenance studies, which are usually based on a large number of measurements (typically approximately 100–120 grains per sample) in order to identify all major sedimentary source components (Vermeesch, 2004; Bernet & Garver,

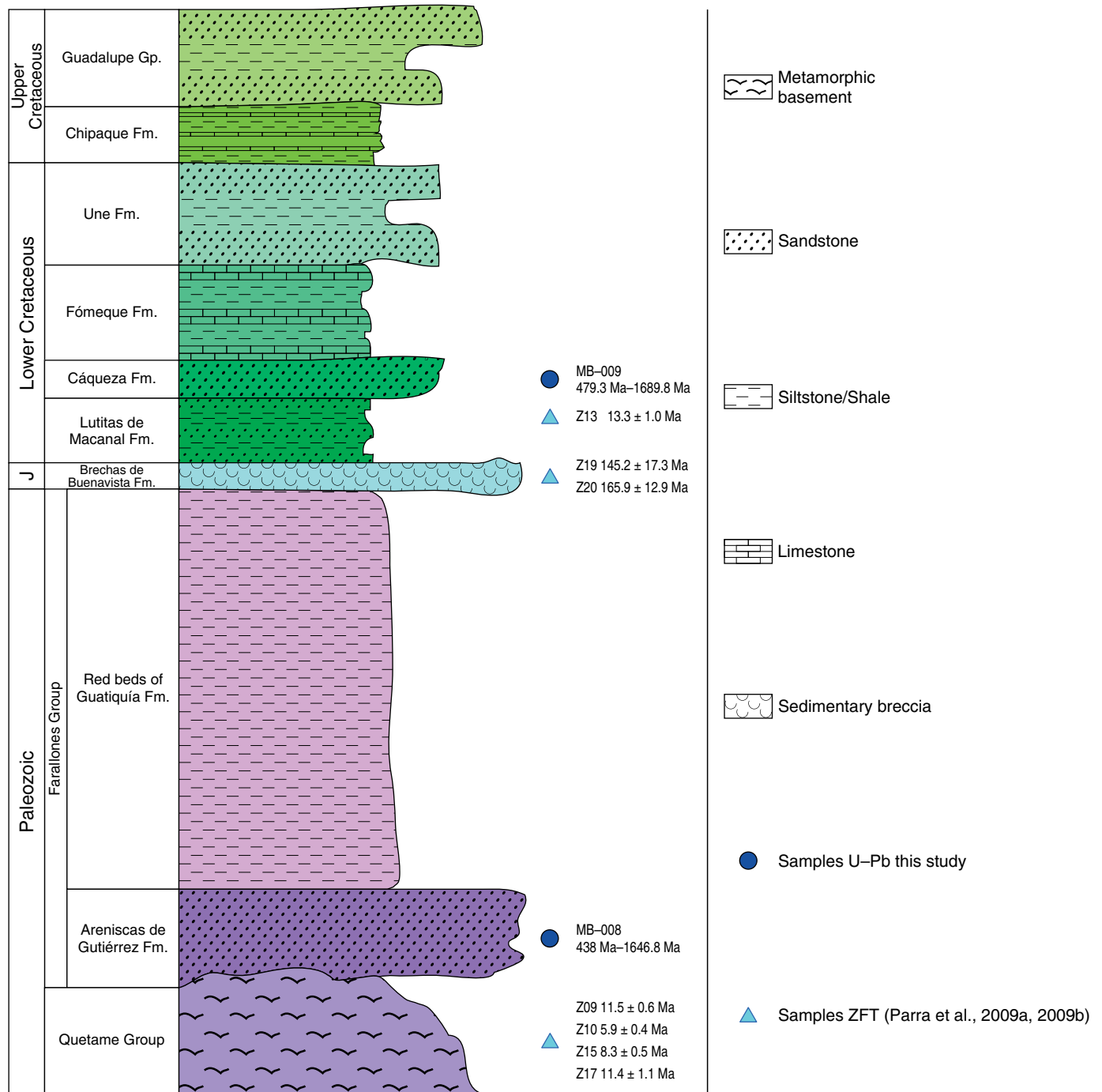


Figure 3. Schematic Paleozoic – Upper Cretaceous stratigraphic section with the locations of bedrock samples presented in this study (blue circles) and by Parra et al. (2009a, 2009b) (blue triangles).

Table 1. Sample information.

Sample	Latitude N	Longitude W	Altitude (masl)	Lithology	Stratigraphic unit	Depositional age
MB005	4° 9' 12.312"	73° 42' 49.284"	714	Sand	Recent	0 Ma
MB006	4° 9' 36.468"	73° 37' 44.76"	450	Sand	Recent	0 Ma
MB008	4° 12' 21.204"	73° 44' 4.776"	880	Metasandstone	Areniscas de Gutiérrez Fm.	Devonian
MB009	4° 24' 40.608"	73° 57' 35.496"	1713	Quartz arenite	Cáqueza Fm.	ca. 127 Ma
13MB180	4° 17' 35.16"	74° 48' 36.036"	261	Sand	Recent	0 Ma

2005). Nevertheless, Pullen et al. (2014) recently demonstrated that large- n datasets ($n = 300$ to 1000) yield better precision in the distribution of U–Pb detrital zircon data and better approximate the true relative abundances of the major components in samples with multi-modal age spectra. In this study, we analyzed approximately 220 detrital zircon grains from each sample.

Detrital zircons from the Guayuriba, Guatiquía, and Magdalena River samples were mounted in epoxy resin together with age standards and polished to expose their internal grain surfaces. Cathodoluminescence (CL) images were taken using a Gatan MiniCL detector, attached to a JEOL JSM IT-300–LV scanning electron microscope (SEM) at the SGC in order to guide where analytical spots were placed on cores and/or rims; the operating conditions for SEM–CL images included an accelerating voltage of 15 kV and a probe current of 60 nA.

Following imaging, zircons were analyzed at the Geochronology laboratory of the SGC using LA–ICP–MS. The instruments used were a Thermo Scientific® Element2 magnetic-sector ICP–MS coupled to a Photon Machine® ‘Excite’ excimer laser system (193 nm). The mosaic images used for the selection of ablation spots were constructed using the Chromium2 software at 75% magnification. The following laser settings were used: a spot size of 20 or 35 μm ; a laser fluence of 6.91 J/cm²; and an output energy of 94%. The number of pulses per burst was 126; they were fired at a frequency of 8 Hz for a total ablation duration of 28 seconds per analysis. The mass spectrometer was tuned with Sri Lanka zircons to maximize the signals of the isotopes of interest, i.e., ²³⁸U, ²³⁵U, ²⁰⁷Pb, ²⁰⁶Pb, ²⁰⁸Pb, ²³²Th, ²⁰²Hg, and ²⁰⁴(Pb + Hg), and to minimize the oxide (²⁵⁴(UO)⁺/²³⁸U⁺) production at the sample interface.

Instrumental fractionation was corrected using a standard-sample bracketing approach, i.e., by analyzing reference zircon materials after every five unknowns and normalizing the data relative to the known (\pm CA)–ID–TIMS ages of the reference zircons. For further discussion of the data acquisition and reduction routines followed in this study, see Ibañez–Mejía et al. (2015) and Pullen et al. (2014). To validate the accuracy of our method, Plešovice crystals were analyzed alongside each sample and treated as unknowns during data reduction. These crystals have a known ID–TIMS age of 337.13 ± 0.37 Ma (Slama et al., 2008); thus, the results obtained here (see Supplementary Information) demonstrate that our analytical approach is accurate and precise within $\pm 2\%$, which is typical for U–Pb zircon analyses using LA–SC–ICP–MS methods (e.g., Chang et al., 2006; Frei & Gerdes, 2009; Ibañez–Mejía et al., 2015; Schaltegger et al., 2015; Pullen et al., 2014).

Probability distribution diagrams were constructed using only ²⁰⁶Pb/²³⁸U ages that were concordant to determine the frequency and distribution of the values represented (i.e., the individual apparent ages) in each sample. The results were represented in concordia diagrams (Wetherill, 1956), where the obtained ²⁰⁶Pb/²³⁸U and ²⁰⁷Pb/²³⁵U isotopic ratios were plot-

ted to assess age concordance. Diagrams were constructed by discarding data that were more than 10% discordant based on the difference between the calculated ²⁰⁶Pb/²³⁸U and ²⁰⁷Pb/²⁰⁶Pb apparent ages for each spot. These diagrams were constructed in ISOPLOT V3.75® (Ludwig, 2012). The individual spot uncertainties in the data presented here include internal analytical uncertainties only and are reported at the 2 σ level. Determining the total uncertainties for each spot or mean age in this method requires the propagation of external reproducibility and other systematic sources of uncertainty, which, in our sessions, yielded average values of ca. 0.9% for the determination of ²⁰⁶Pb/²³⁸U and ca. 0.7% for that of ²⁰⁷Pb/²⁰⁶Pb. Consequently, the total uncertainties in the mean ages of the samples and reference zircons are reported in the form of $\pm A/B$, where the first level of uncertainty A considers only the internal analytical uncertainties, and the second level B reflects the propagation of the external reproducibility of the standards and other sources of systematic error (see Ibañez–Mejía et al., 2015 for more details).

3.3. Zircon Fission–Track Dating

The sample preparation used for fission–track analysis at the Thermochronology Laboratory of the SGC consisted of mounting zircon aliquots (with grain sizes of approximately 75 to 250 μm) in Teflon® sheets, polishing the mounts to expose their internal grain surfaces, and etching the grains in a NaOH–KOH melt at 228 °C. Two to three grain mounts were prepared per sample and were etched for different lengths of time in order to obtain countable fission–tracks in the full grain age spectrum (e.g., Bernet et al., 2004). After etching, the grain mounts of all samples were cleaned and covered with mica sheets as external detectors. All samples were irradiated with thermal neutrons together with age standards and IRMM541 dosimeter glasses at well-thermalized reactor in Garching, Germany, using a nominal fluence of 0.5×10^{15} n.cm^{−2}. After irradiation, mica detectors were etched for 18 minutes at 21 °C with 48% HF to reveal induced tracks. All samples were analyzed using an Olympus BH2 optical microscope and the FTStage 4.04 system at the Thermochronology Laboratory of the Institut des Sciences de la Terre, University Grenoble Alpes. Tracks were counted dry at a magnification of 1250X; 100 grains were analyzed per sample, and fission–track grain ages were calculated using the Binomfit software of Brandon (see Ehlers et al., 2005). The Fish Canyon Tuff and Buluk Tuff age standards were used for zeta calibration.

4. Results

4.1. Zircon U–Pb Dating

Devonian sedimentary rocks (sample MB–008) show relevant age peaks at 468.3 ± 0.7 Ma, representing 24% of the data, as well as main peaks at 905, 991, 1158, 1304, and 1500.1 ± 1.7

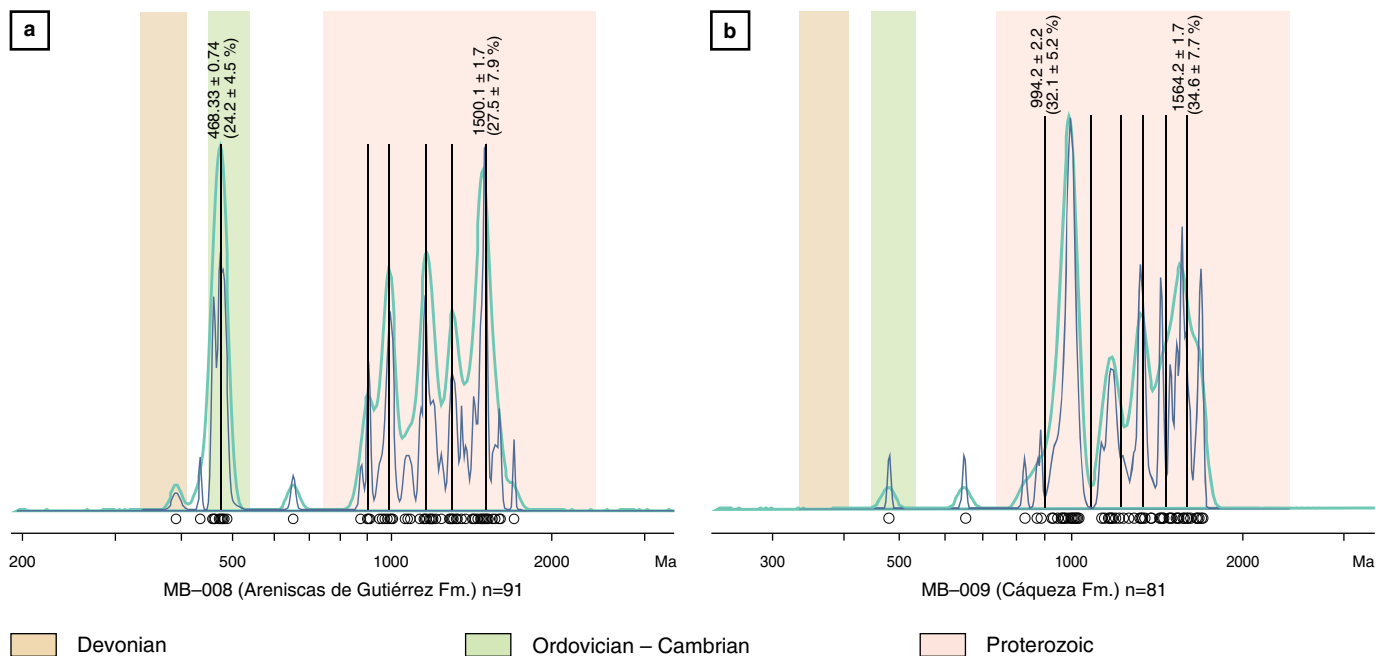


Figure 4. Zircon U–Pb ages with peak ages from probability density plots (dark blue line) and kernel density estimates (light blue line) (using RadialPlotter by Vermeesch, 2009). **(a)** Sample MB008, Devonian bedrock. **(b)** Sample MB009, Cretaceous bedrock.

Ma, representing 27.5% of the data; the oldest age is 1702.3 Ma (Figure 4a). In contrast, Cretaceous sedimentary rocks (sample MB–009) have only two grains with apparent ages of 479.3 ± 3.1 Ma and 650 ± 4.2 Ma; the remaining 94% of the data comprise peaks at 994.2 ± 2.2 Ma, 1177 Ma, 1320 Ma, 1438 Ma, 1564.2 ± 1.7 Ma and 1685 Ma (Figure 4b).

The detrital zircon U–Pb ages of the modern river sands from the eastern flank of the Eastern Cordillera are distributed between 830 and 1830 Ma, with a discrete peak at ca. 443 Ma (Figure 5). The Guayuriba River (MB–005) data define several (concordant) apparent age populations at 443.6 ± 3.6 Ma (which contains only a small proportion of the dated grains), 1027.8 ± 3.1 Ma, 1198.3 ± 2.9 Ma, 1336.4 Ma, 1407.2 Ma, 1527.7 Ma, and 1665.8 Ma (Figure 5a). Similarly, the zircons from the Guatiquía River (MB–006) define five populations at 451.4 ± 2.2 Ma, 1022.8 ± 3.3 Ma, 1189.5 Ma, 1322 Ma, 1518.3 Ma, and 1756.6 Ma (Figure 5b). On the other hand, the detrital zircon age spectra from our Magdalena River sample (13MB–180) are markedly different, as they are represented by four populations separated in two broad age ranges: the first range is represented by peaks falling between 156.76 ± 0.45 Ma and 268.56 ± 0.9 Ma, and the second range is represented by peaks distributed between 1068.9 ± 4.8 Ma and 1483.6 ± 6.5 Ma (Figure 5c). All of these data are included in the Supplementary Information.

The SEM–CL images of the detrital zircons from the river samples show the internal structures and zoning patterns of the different age populations found with U–Pb dating. The Guayuriba River sample (Figure 6, MB–005) shows at least seven age populations, and all of its imaged grains mainly exhibit oscillatory zoning.

Some of these grains are often perturbed by convoluted local textures and characterized by complex crystal zoning patterns with local magmatic resorption (e.g., early Mesoproterozoic crystals), and the oldest grains show thin overgrowth rims. In the Guatiquía River sample (Figure 7, MB–006), oscillatory zoning patterns are also predominant, but some of the middle to late Mesoproterozoic grains display convoluted to chaotic zoning; as with the Guayuriba zircons, the oldest grains show thin overgrowth rims. The Magdalena River detrital zircons (Figure 8, 13MB–180) mainly show oscillatory zoning patterns, which often exhibit areas of local recrystallization and homogenization. Although it is not possible to determine the mechanisms and number of cycles that many of these re-worked zircons have experienced, their inheritance patterns suggest a magmatic origin for most of them. The grains that show overgrowth rims may suggest the presence of overprinting metamorphic events, but most of the observed rims are too thin to be dated.

4.2. Detrital Zircon Fission–Track Analysis

The fission–track data obtained from the three river samples are presented in Table 2 and Table 3. The fission–track ages obtained for the Guayuriba River sample (MB005) show a spectrum of ages ranging from 8.8 to 530.1 Ma (Figure 9). The dispersion is very high (99.4%); accordingly, the $P(\chi^2)$ value is zero. Using the peak–fitting algorithm (Galbraith & Green, 1990), three statistically representative peaks can be detected at 15.6 ± 2 Ma, 110 ± 10 Ma, and 229 ± 18 Ma (Figure 9a). The Guatiquía River sample (MB006) shows a similar grain

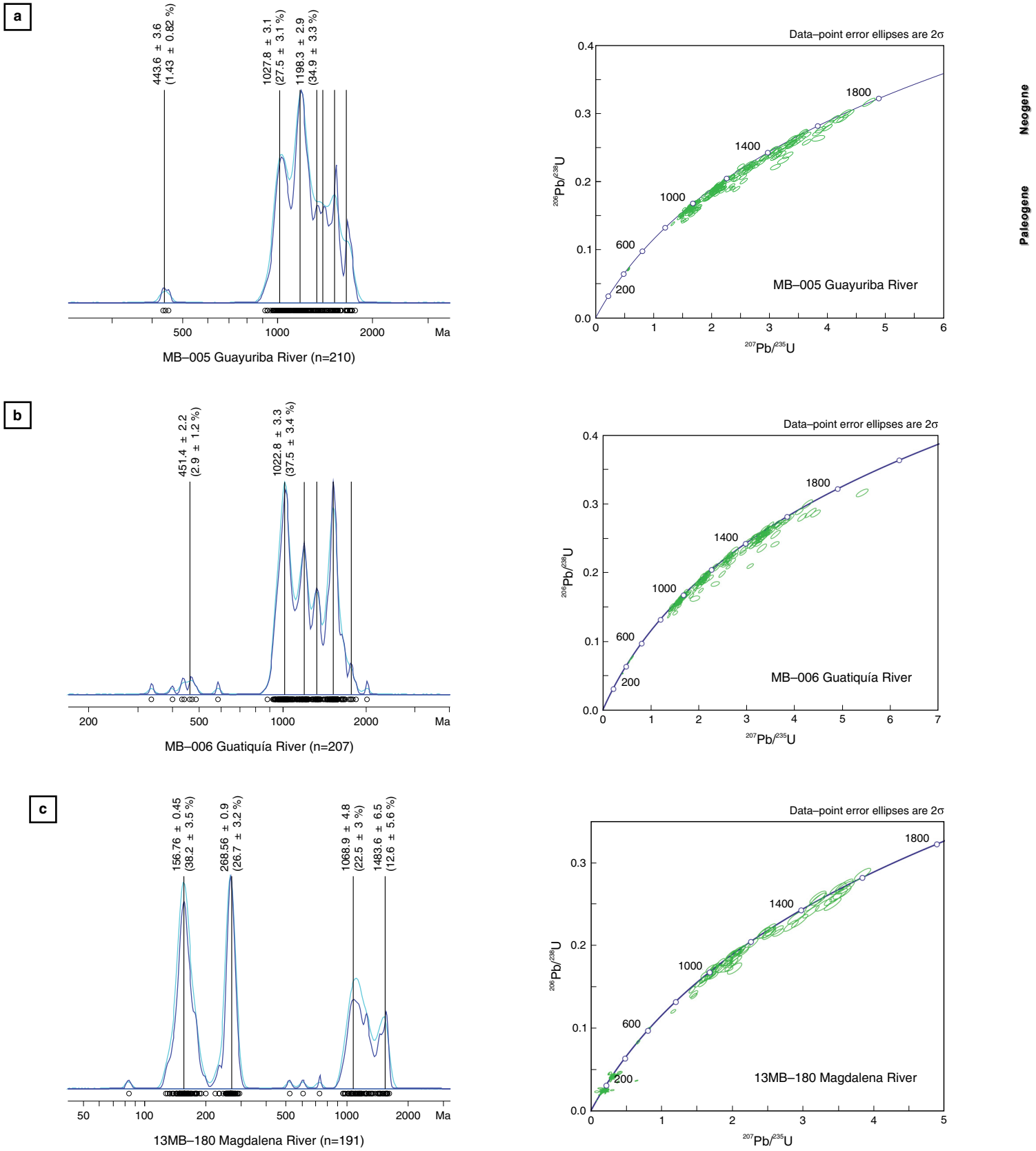


Figure 5. Zircon U–Pb age spectra with peak ages from probability density plots (dark blue line), kernel density estimates (light blue line) and concordia diagrams depicting $^{206}\text{Pb}/^{238}\text{U}$ and $^{207}\text{Pb}/^{235}\text{U}$ data for zircon grains from: **(a)** Guayuriba River sample MBoo5, **(b)** Guatiquía River sample MBoo6, and **(c)** Magdalena River sample 13MB180.

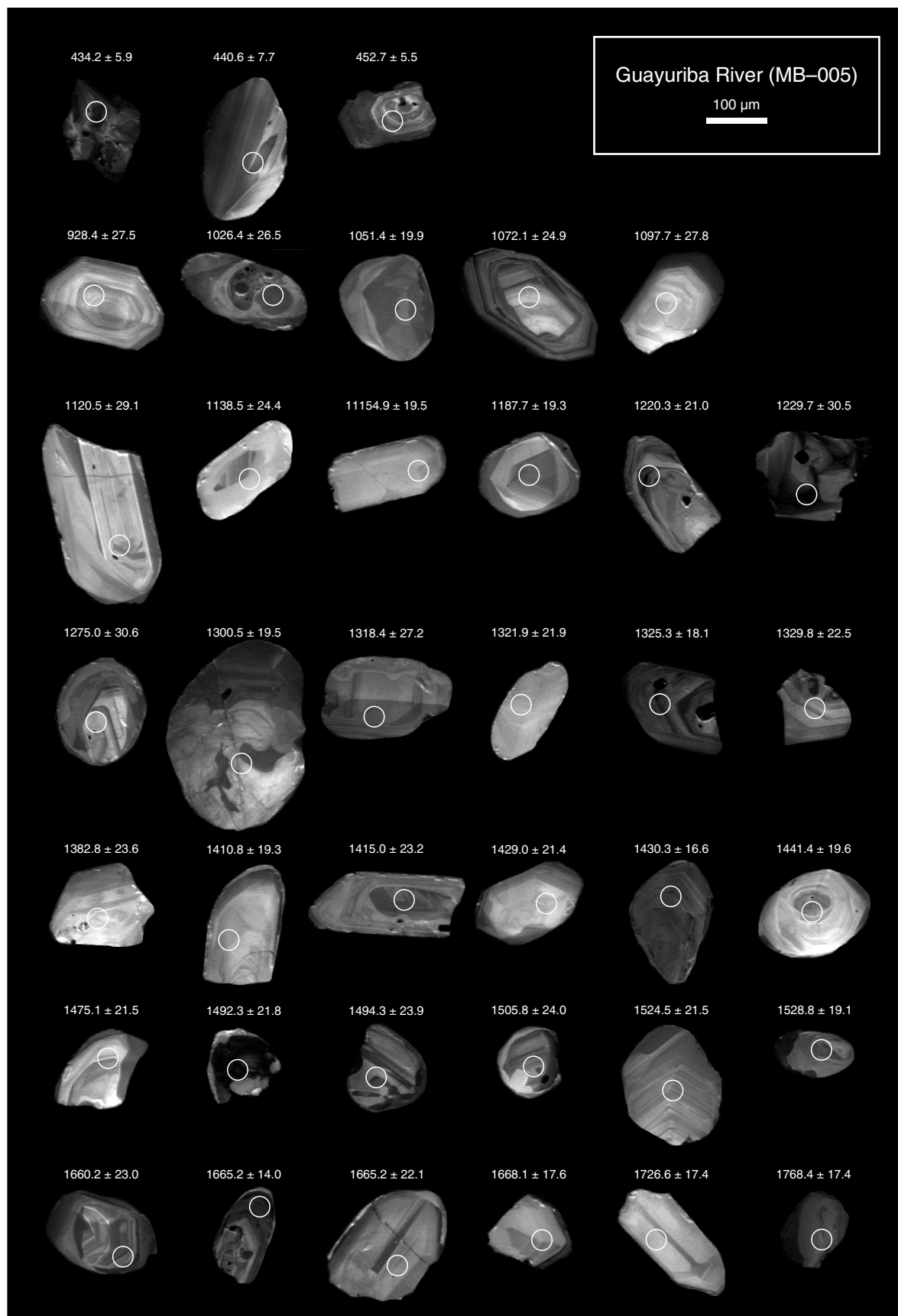


Figure 6. Cathodoluminescence images (SEM-CL) of representative detrital zircon populations of Guayuriba River sample (MB-005); U/Pb ages in Ma with 2-sigma uncertainty. Circles represent the areas used for analyses.

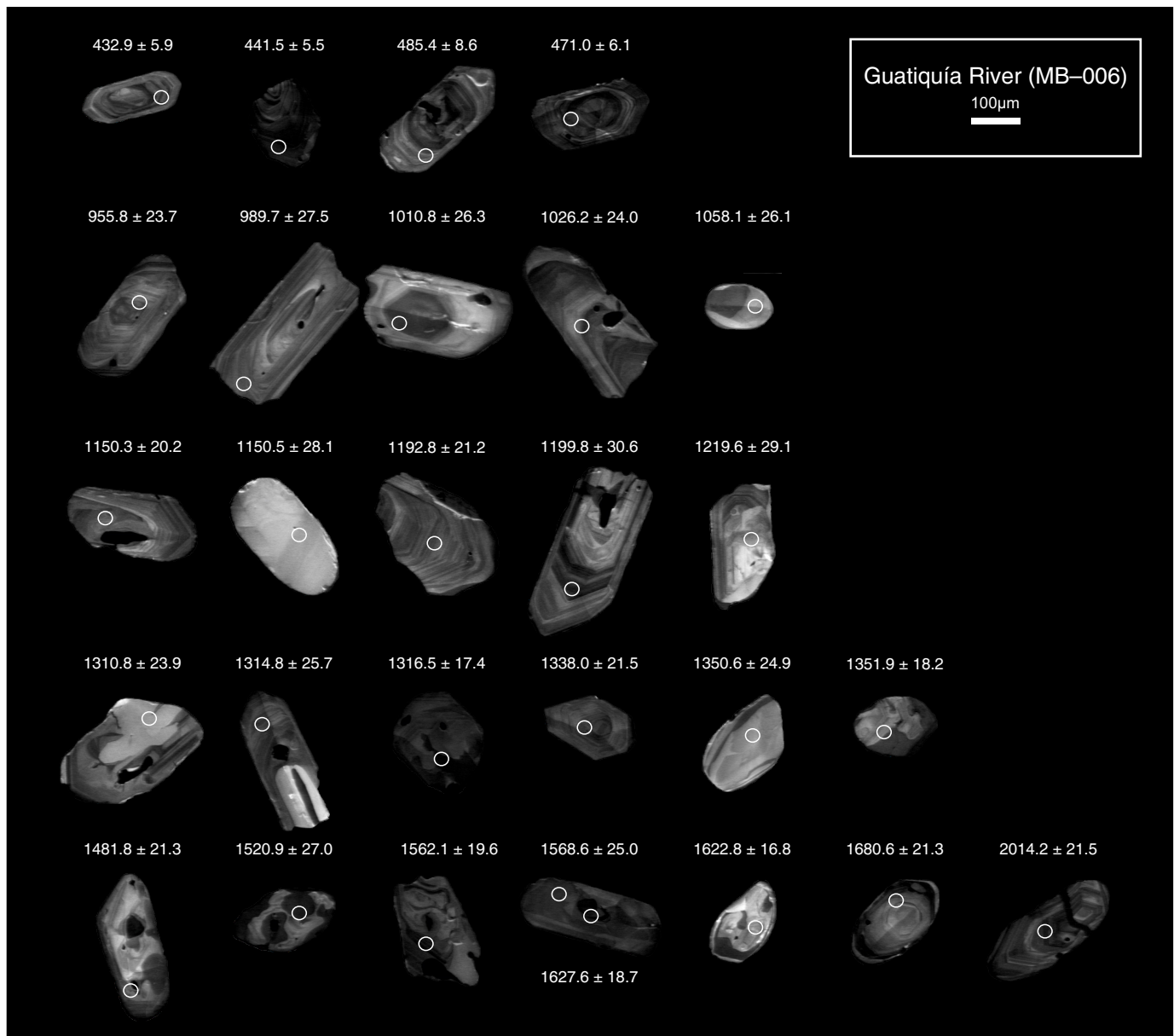


Figure 7. Cathodoluminescence images (SEM–CL) of representative detrital zircon populations of Guatiquía River sample (MB-006); U/Pb ages in Ma with 2-sigma uncertainty. Circles represent the areas used for analyses.

age distribution between 19.4 and 476.0 Ma, although it shows a smaller dispersion of 66.6%. Nevertheless, four statistically robust age peaks can be detected at 22.5 ± 3.5 Ma, 49.3 ± 4.6 Ma, 98.2 ± 9.2 Ma, and 194 ± 13 Ma, although the first one only corresponds to 3.8% of the data (Figure 9b).

The Magdalena River sample (13MB180) shows ages ranging from 28.1 to 327.9 Ma, with a dispersion of 36.3%. The main peak ages are 46.4 ± 4.6 Ma, 91.5 ± 5.6 Ma, and 233 ± 42 Ma (Figure 9c). Using Kolmogorov–Smirnov (KS) statistics, we compared the grain age distributions between rivers. The ZFT grain age distributions from the Guayuriba and Guatiquía Rivers are similar, whereas the ZFT grain age distribution of the Magdalena River sample is statistically significantly different (Figure 10a).

5. Discussion

5.1. Provenance Information from Detrital Zircon U–Pb Ages

The U–Pb dating of detrital zircons is a well-established provenance tool that has been widely used in many different tectonic settings. This method provides information about the distribution of crystallization ages from the original source region, which can be combined with careful analyses of igneous and/or metamorphic overgrowth rims (if present) to track intermediate source areas and sediment recycling. The data obtained here provide an opportunity to discuss the strengths and short-

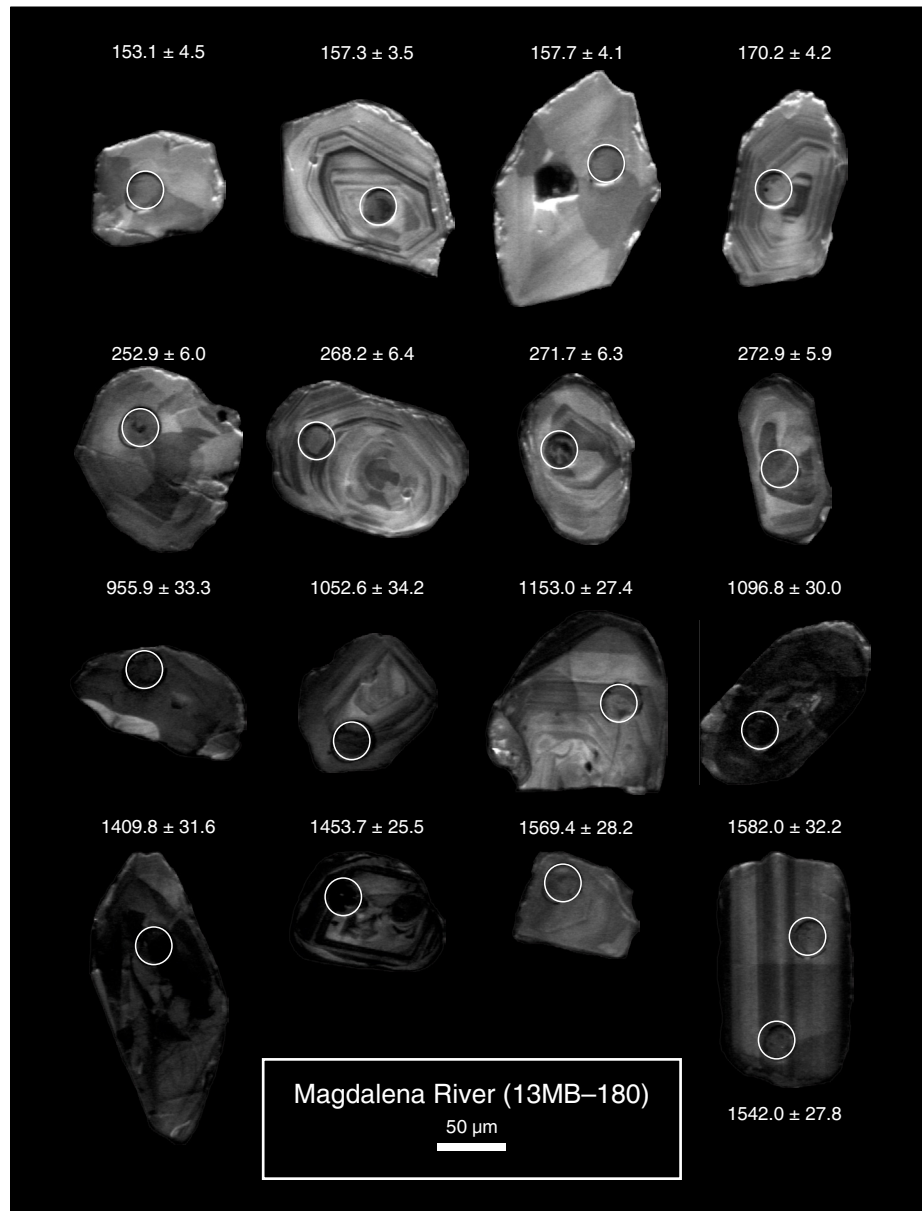


Figure 8. Cathodoluminescence images (SEM-CL) of representative detrital zircon populations of Magdalena River sample (13MB-180); U/Pb ages in Ma with 2-sigma uncertainty. Circles represent the areas used for analyses.

comings of these methods by combining our new bedrock and modern river data. There is currently no consensus on the best way to interpret detrital zircon U-Pb age spectra in terms of the significance of peak heights when plotted on probability density function plots, differences in the relative abundances of peaks between different samples in stratigraphic successions, or which statistics should be applied to decompose the observed grain age spectra (Gehrels, 2011). Nonetheless, the different age peaks determined here using the RadialPlotter program (Vermeesch, 2009, 2012) are consistent with the zircon U-Pb data obtained from other studies in the Eastern Cordillera (Horton et al., 2010; Nie et al., 2010). The comparison of bedrock detrital zircon U-Pb data from Devonian and Cretaceous sedimentary

rocks in the Eastern Cordillera along the Bogotá–Villavicencio stratigraphic section hints at possible changes in the sediment provenance of these units. For the Devonian sedimentary rocks, a significant Ordovician zircon U-Pb age peak represents a source in the Cambrian – Ordovician crystalline basement of the Eastern Cordillera. The new zircon U-Pb data presented in this study are compatible with the zircon U-Pb data of Horton et al. (2010), who also proposed an igneous source for Ordovician zircons corresponding to the local lower Paleozoic Andean basement rocks, which are related to magmatic activity in the Floresta and Santander Massifs (e.g., García-Ramírez et al., 2017; Jiménez-Triana, 2016; Restrepo-Pace, 1995; van der Lelij et al., 2016). On the other hand, zircons with Meso-

Table 2. Zircon fission–track central age data.

Sample	n	q_s (10^{-6} cm^{-2})	N_s	q_i (10^{-6} cm^{-2})	N_i	q_t (10^{-5} cm^{-2})	$P(\chi^2)$	Dispersion (%)	Age (Ma)*	$\pm 2 \sigma$	U (ppm)	$\pm 1 \sigma$
MB005	100	6.72	9231	1.30	1792	3.84	0.0	99.4	112.8	25	170	9
MB006	100	7.40	8140	1.71	1880	3.83	0.0	66.6	114.3	19.2	223	12
13MB180	100	7.33	8131	2.32	2575	3.82	0.0	36.3	84.1	10.5	304	14

*Fission–track age is given as Central Age (Galbraith & Laslett, 1993).

Note: Samples were counted dry with a BX51 Olympus microscope at 1250X magnification. Central ages and age ranges were determined with the BINOMFIT program of Brandon (see in Ehlers et al., 2005), using a zeta factor of 142.39 ± 6.48 .

Table 3. Zircon fission–track peak age data.

Sample	n	Age range (Ma)	P1	$\pm 2 \sigma$	%	P2	$\pm 2 \sigma$	%	P3	$\pm 2 \sigma$	%	P4	$\pm 2 \sigma$	%	P5	$\pm 2 \sigma$	%
MB005	100	8.8–530.1	15.6	4.0	11.4	110	20	33.9	229	36.0	54.7	–	–	–	–	–	–
MB006	100	19.4–476.0	22.5	7.0	3.8	49.3	9.2	12.4	98.2	18.4	26.0	194	26.0	57.8	–	–	–
13MB180	100	28.1–327.9	33.6	8.4	5.0	58.5	17	15	85.0	11.0	50.0	113	34.0	24.0	245	82	5.0

Note: Peak ages were determined with the RadialPlotter program of Vermeesch (2009).

proterozoic and Neoproterozoic U–Pb ages were most likely derived from basement sources such as the Garzón Massif or the Putumayo Basin, which are related to orogenic events associated with the assembly of Rodinia (Ibañez–Mejía et al., 2011). Therefore, we conclude that two principal sediment source areas existed for the Devonian sedimentary rocks. In the detrital zircon age spectra obtained from the modern river samples analyzed here, the Upper Ordovician signal is relatively minor but likely corresponds to the recycling of inherited zircons from the Farallones Group.

In contrast, the zircon ages of the Lower Cretaceous sedimentary rocks are restricted to Proterozoic ages. The disappearance of Phanerozoic zircons in the detrital age spectra is most likely related to the evolution of the basin from late–stage extension to thermal subsidence during the mid–Cretaceous and a lack of proximal basement erosion due to sedimentary infilling and burial (Horton et al., 2010). This suggests that the Ordovician arc terranes that were exposed in the Devonian were buried during the Cretaceous.

The modern river detrital zircon U–Pb spectra of the Guayuriba and Guatiquía Rivers samples indicate that the formation of the Eastern Cordillera, which has been forming since the Eocene, is not detectable in the zircon U–Pb record. Even the data reported by Saylor et al. (2013) for the Cusiana and Cravo Sur Rivers, which are located further to the north of our study area, show similar signals as those obtained here, in addition to the appearance of some younger grains with ages of approximately 100 Ma in Cravo Sur derived from Cenozoic units that crop out in the foothills of the Eastern Cordillera. These zircons are simply recycled from the sedimentary cover units or sourced from the Precambrian basement; however, no zircons with U–Pb ages reflecting the Eastern Cordilleran orogenesis exist. This interpretation is complemented by CL

images showing zircons with internal oscillatory zoning related to primary magmatic sources and recrystallized edges due to ancient metamorphic events. Furthermore, the oldest grains are broken, with sub–rounded edges. All of these data are indicative of sedimentary recycling. This is not a surprising result, as the Eastern Cordillera is, for the most part, an amagmatic mountain belt, and the level of regional metamorphic overprinting that it experienced was insufficient to leave a trace in the detrital zircon U–Pb age record. The magmatic activity related to the evolution of the Eastern Cordillera and that close to the study area is restricted to only two known events, namely: (1) the intrusion of gabbros and doleritic dikes during peak extension in the Late Cretaceous (Fabre & Delaloye, 1983; Moreno–Murillo et al., 2007; Vásquez et al., 2010); and (2) acidic volcanism occurring in the Paipa–Iza Volcanic Complex (Figure 1), which was active throughout the Pliocene – Pleistocene surface uplift of the Eastern Cordillera (Bernet et al., 2016). Nevertheless, evidence of these two sources is difficult to detect in the detrital zircon record because: (1) gabbros have low fertility for zircon crystallization and thus will be poorly represented in the detrital record (Moecher & Samson, 2006), and (2) Paipa–Iza Volcanic Complex zircons have dominantly Proterozoic and Paleozoic core and rim ages, and only a few rims and overgrowths reflecting Pliocene – Pleistocene volcanic activity have been detected (Bernet et al., 2016).

The Magdalena River sample detrital zircon U–Pb data reflect the zircon U–Pb ages of the Upper Magdalena River Basin, which covers the western flank of the Eastern Cordillera and the eastern flank of the Central Cordillera. Figure 10b shows the differences between the detrital zircon age distributions found in the rivers on the east flank of the Eastern Cordillera and those the west flank, as represented by the Magdalena River, thus denoting the influence of the sedi-

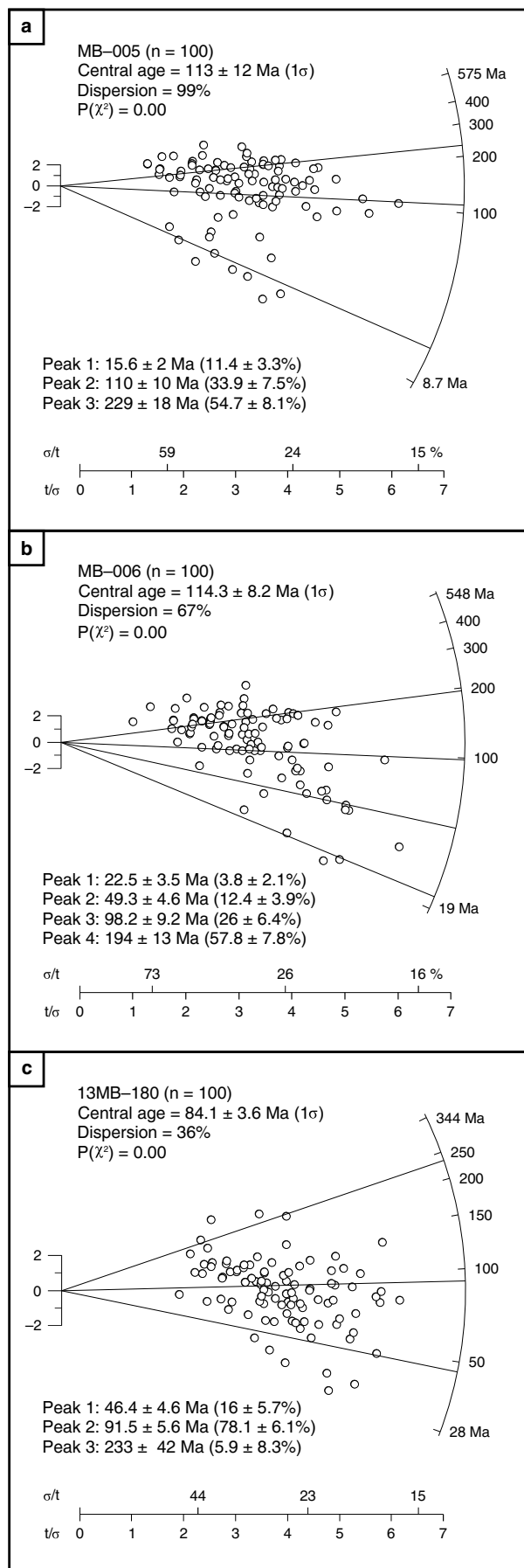


Figure 9. Radial plots of zircon fission-track data with main peak age populations of three river samples: **(a)** Guayuriba River (MB005), **(b)** Guatiquía River (MB006), and **(c)** Magdalena River (13MB180). The plots were made and peak ages were determined with the RadialPlotter program of Vermeesch (2009).

ments of the Central Cordillera. Although this drainage basin includes the active Nevado del Huila Volcano of the Central Cordillera, the youngest zircon U–Pb age peak determined in the Magdalena River sample reflects Jurassic plutonism (Bustamante *et al.*, 2010, 2016; Zapata *et al.*, 2016) but not recent volcanic input. The volcanic signal is too weak to be detected, as the quantity of young volcanic zircons is negligible compared to the zircons derived from the erosion of the crystalline basement and sedimentary cover rocks. Considering that 191 detrital zircons from sample 13MB–180 were analyzed, we conclude that the abundance of modern volcanic crystals in this sample must be $<0.5\%$ (at least 1 data point) for them to have avoided detection. Because of this detection limit problem, it is useful in many provenance and exhumation studies to analyze a much larger number of zircons (e.g., Pullen *et al.*, 2014) and/or to combine detrital zircon U–Pb dating with fission-track dating on the same samples or within the same individual grains (e.g., Bernet *et al.*, 2006; Carter & Bristow, 2000, 2003; Carter & Moss, 1999; Jourdan *et al.*, 2013).

Other peaks in this sample, such as those with Permian ages, could be related to magmatic activity in the Upper Magdalena Valley (Leal–Mejía, 2011; Rodríguez *et al.*, 2017). The old peaks at 1068.9 Ma and 1483.6 Ma are related to either the erosion of basement units in the Eastern Cordillera and serranía de Las Minas (e.g., Ibañez–Mejía *et al.*, 2011) or the reworking of Paleozoic and Mesozoic sedimentary rocks in the area containing material from Amazon Craton sources.

5.2. Provenance Information from Detrital Zircon Fission-Track Ages

It is very common for cooling ages derived from detrital samples to cluster in certain age groups instead of representing a continuum of ages across the drainage area (Bernet & Spiegel, 2004; Bernet *et al.*, 2001, 2004; Cervený *et al.*, 1988; Spiegel *et al.*, 2000), which has been shown in a range of studies performed in orogens around the world (e.g., Bernet *et al.*, 2009; Garver & Kamp, 2002; Stewart & Brandon, 2004). The number of age clusters or peaks that can be determined depends on the exhumation rates and relief in the drainage area, but the representation or significance of each peak depends on the number of grains dated per sample (Bernet, 2013; Naylor *et al.*, 2015). The more grains that are analyzed, the more peaks can be fitted with peak-fitting routines if the age range is sufficiently large and the peaks are well separated (Brandon, 1996;

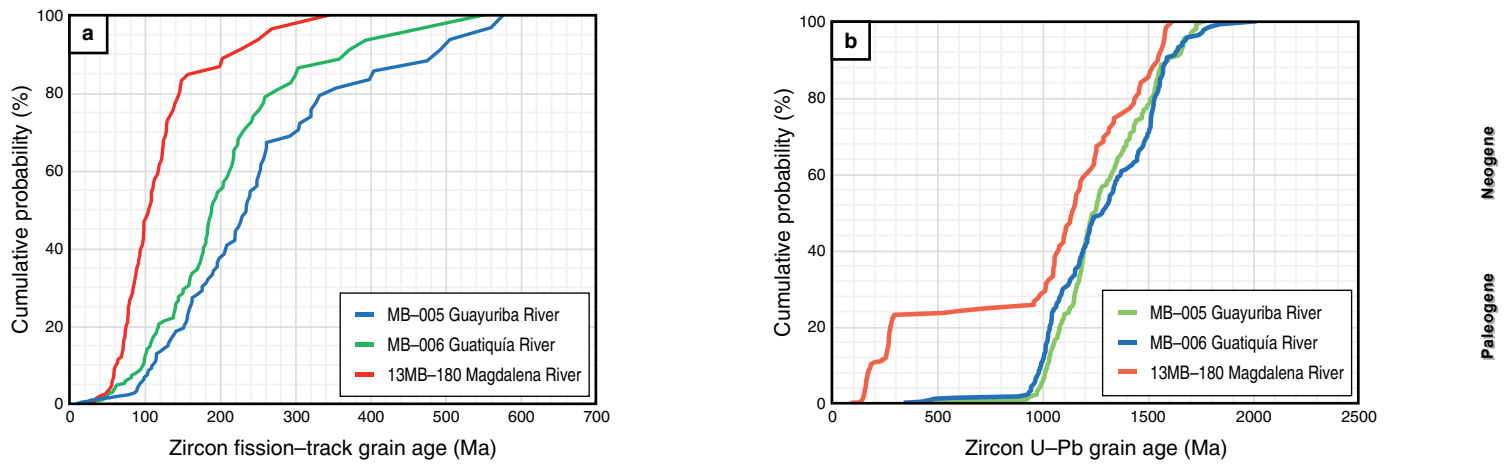


Figure 10. Cumulative probability density plots for Kolmogorov–Smirnov (KS–statistics) comparison of samples from three rivers: **(a)** Zircon fission–track grain age distributions and **(b)** U–Pb grain age distributions.

Galbraith & Green, 1990; Naylor et al., 2015). If bedrock zircon fission–track data are available, then modern river detrital zircon fission–track data can be compared to bedrock data to determine the sediment provenance (e.g., Bernet et al., 2001, 2004, 2009). This provides a baseline for provenance studies of ancient sandstones in associated sedimentary basins when studying long–term records of exhumation. In the absence of post–depositional thermal resetting, detrital zircon fission–track grain ages in ancient sedimentary rocks can only be the same or older than their actual sedimentation age.

In this study, we can compare the detrital zircon fission–track data of the Guayuriba and Guatiquía Rivers samples with the bedrock zircon fission–track data of Parra et al. (2009a, 2009b) from the Bogotá–Villavicencio section (Figure 2b). The documented bedrock zircon fission–track ages range from 5.9 ± 0.4 Ma (sample Z10, Quetame Group) to 165.9 ± 12.9 Ma (sample Z20, Brechas de Buenavista Formation) in the frontal fold–and–thrust belt of the Eastern Cordillera. This bedrock age range contrasts with the single grain age spectra of 8.8 to 530.1 Ma and 19.4 to 476.0 Ma obtained in the Guayuriba River and the Guatiquía River, respectively, in this study.

Parra et al. (2009a, 2009b) defined an exhumed zircon fission–track partial annealing zone along the Bogotá–Villavicencio profile. This means that the rocks containing partially annealed zircons remained at elevated temperatures of 180–220 °C for 50 my or more during their burial in the basin (Reiners & Brandon, 2006). Partially annealed zircons provide “apparent” cooling ages that neither precisely reflect orogenic cooling nor maintain a pre–depositional provenance signal but rather represent a partially reset age signal. However, fully annealed zircons reflect orogenic exhumation. The central ages of fully reset zircons range from 5.9 to 24 Ma from the Quetame Group to the middle of the Lower Cretaceous Macanal Formation, where the base of the exhumed ZFT partial annealing zone is located. The central ages of the partially reset zircons from within the partial

annealing zone range from 61 to 166 Ma. The exhumation of the ZFT partial annealing zone started around 24 Ma; it was contemporaneous with major exhumation in the Santander Massif and the Antioquia Batholith in the Central Cordillera, which was linked to the collision of the Panamá–Chocó Block with the northwestern South American Plate (Amaya et al., 2017; Restrepo–Moreno et al., 2009). The exhumation of the ZFT partial annealing zone continued until the Pliocene – Pleistocene, and it was deformed and segmented during the formation and surface uplift of the Eastern Cordillera. This landscape is currently being eroded by surface processes, such as river incision, and its cooling and exhumation history is reflected in the detrital grain ages of the Guayuriba and Guatiquía River samples. The youngest detrital zircon fission–track age peaks of both rivers fall between 15 and 22 Ma. The zircons corresponding to these age peaks, which represent approximately 4–11 % of the analyzed grains, were derived from the fully reset zone (the Quetame Group to the middle Macanal Formation). The partially reset zircons with age peaks of approximately 50 to 110 Ma, which represent approximately 33–38 % of the analyzed grains, were derived from within the exhumed partial annealing zone (the upper Macanal to Chipaque Formations). Finally, 55–60 % of the Guayuriba and Guatiquía Rivers sample detrital zircons fall within the approximately 190–230 Ma age peaks, which were derived from Upper Cretaceous to Paleocene sedimentary rocks that were not affected by post–depositional partial annealing. Therefore, the two well–mixed modern river samples provide a complete representation of the bedrock cooling history in the drainage basins, including ages not observed in the 22 bedrock samples analyzed by Parra et al. (2009a, 2009b). Nonetheless, the Parra et al. (2009a, 2009b) data are critical for determining where the partial annealing zone is exposed in the drainage area, therefore making both datasets complementary. This demonstrates the usefulness of combining bedrock and modern river studies to understand orogenic evolution processes.

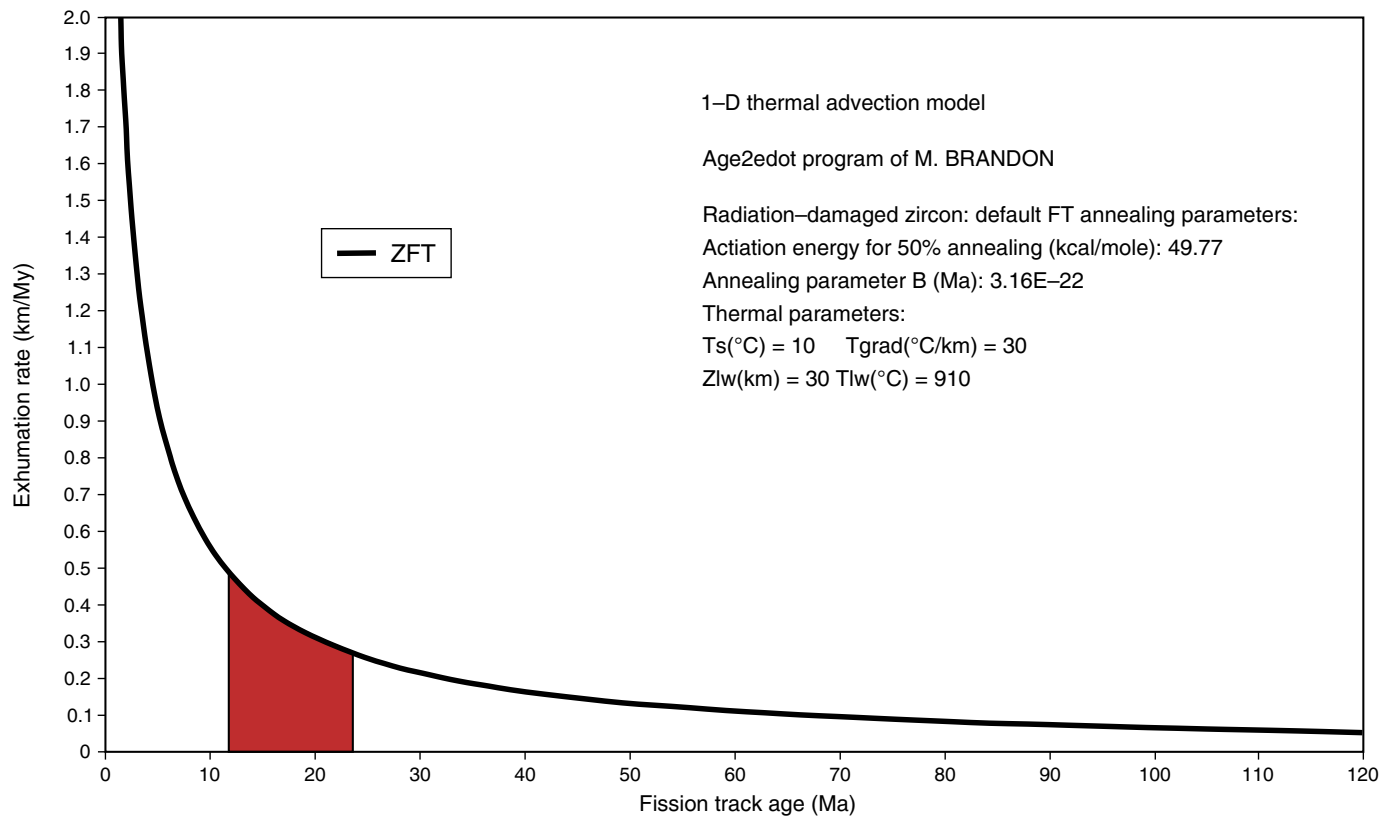


Figure 11. Model showing the estimated exhumation rates in relation to the zircon fission-track cooling ages of the younger age peaks of the Guayuriba and Guatiquía Rivers samples using the age2edot program of M. BRANDON (see Ehlers *et al.*, 2005).

The detrital ZFT peak ages can be used to estimate the long-term average exhumation rates within the drainage basins, assuming a monotonous cooling history, using the age2edot software of Brandon (see Ehlers *et al.*, 2005). Zircons with apparent Miocene cooling ages from the fastest exhuming areas in the Eastern Cordillera indicate exhumation rates on the order of approximately 0.3–0.4 km/My (Figure 11). These exhumation rates are moderately fast compared to those in other orogenic systems (see Montgomery & Brandon, 2002).

The Magdalena River sample, which yields a ZFT age spectrum of 28–328 Ma and age peaks at approximately 46, 92, and 230 Ma, does not show the same exhumation signal as the Guayuriba and Guatiquía Rivers samples (Figure 9). The youngest age peak of the Magdalena River sample is approximately 20–30 my older than the youngest age peak of the Guayuriba and Guatiquía Rivers. This means that the exhumation occurring in the Upper Magdalena River Basin is slower than that on the eastern flank of the Eastern Cordillera, thus reflecting the asymmetric evolution of the Eastern Cordillera (Mora *et al.*, 2008) and highlighting that volcanic zircons with young cooling ages are too low in abundance and therefore could not be detected. Similar to the zircon U–Pb data, the ZFT ages of the Magdalena River indicate that many of these zircons were recycled from older sedimentary units.

6. Conclusions

The U–Pb and ZFT data of the bedrock and modern river sediments of the Eastern Cordillera between Bogotá and Villavicencio, as well as the Magdalena River at Girardot, highlight the applications and complexities associated with interpreting detrital zircon age data. The main challenge of this technique is to use the observed grain age distributions to assign statistical significance to the observed age groups or peaks, and then to use these to identify the sediment provenance, detect sediment recycling and determine the cooling and exhumation histories of sediment source areas.

The new U–Pb and ZFT data presented here allow us to make first-order observations about the provenance signals in modern rivers on the east and west flanks of the Eastern Cordillera, close to the Villavicencio and Girardot areas. On the east flank of the Eastern Cordillera, our data clearly show that the zircon U–Pb age spectra of the Paleozoic through Mesozoic sedimentary section being eroded are related to sources in the Amazon Craton, the magmatic Paleozoic basement of the same Eastern Cordillera, and the exhumation of proximal Precambrian basement blocks. On the other hand, the Magdalena River sample indicates the presence of these same Eastern Cordillera sources plus the addition of younger Permian – Triassic and Jurassic zircons derived

from the reworking of Upper Magdalena Valley sedimentary units and/or the crystalline basement of the Central Cordillera.

The ZFT data presented here complement the existing record of recent exhumation for the Eastern Cordillera determined based on the dating of bedrock samples, thus indicating that moderate exhumation rates occurred over the last 20 my and verifying the asymmetric nature of the surface uplift occurring across the length of the Eastern Cordillera fold-and-thrust belt.

Acknowledgments

We acknowledge Agencia Nacional de Hidrocarburos for setting up the fission–track laboratory at the SGC at Bogotá. We are thankful to Yolanda CAÑÓN and the group of geologists for their help during fieldwork. Zircon irradiations were supported by the fission–track laboratory of the Institut des Sciences de la Terre, Université Grenoble Alpes. Matthias BERNET acknowledges the support of the Université Grenoble Alpes for a sabbatical leave in 2013, during which the fieldwork for this study was done, and the CNRS of study leave to Colombia in 2017–2018. We gratefully acknowledge the constructive reviews by Massimiliano ZATTIN and Andrew CARTER, as well as the editors, which helped improve this manuscript.

References

- Amaya, S., Zuluaga, C.A. & Bernet, M. 2017. New fission–track age constraints on the exhumation of the central Santander Massif: Implications for the tectonic evolution of the northern Andes, Colombia. *Lithos*, 282–283: 388–402. <https://doi.org/10.1016/j.lithos.2017.03.019>
- Bande, A., Horton, B.K., Ramírez, J.C., Mora, A., Parra, M. & Stockli, D.F. 2012. Clastic deposition, provenance, and sequence of Andean thrusting in the frontal Eastern Cordillera and Llanos foreland Basin of Colombia. *Geological Society of America Bulletin*, 124(1–2): 59–76. <https://doi.org/10.1130/B30412.1>
- Bernet, M. 2013. Detrital zircon fission–track thermochronology of the present-day Isère River drainage system in the western Alps: No evidence for increasing erosion rates at 5 Ma. *Geosciences*, 3(3): 528–542. <https://doi.org/10.3390/geosciences3030528>
- Bernet, M. & Garver, J.I. 2005. Fission–track analysis of detrital zircon. *Reviews in Mineralogy & Geochemistry*, 58(1): 205–237. <https://doi.org/10.2138/rmg.2005.58.8>
- Bernet, M. & Spiegel, C. 2004. Introduction: Detrital thermochronology. In Bernet, M. & Spiegel, C. (editors), *Detrital thermochronology—Provenance analysis, exhumation, and landscape evolution of mountain belts*. Geological Society of America, Special Paper 378, p. 1–6. Boulder, Colorado. <https://doi.org/10.1130/0-8137-2378-7.1>
- Bernet, M., Zattin, M., Garver, J.I., Brandon, M.T. & Vance, J.A. 2001. Steady-state exhumation of the European Alps. *Geology*, 29(1): 35–38. [https://doi.org/10.1130/0091-7613\(2001\)029<0035:S-SEOTE>2.0.CO;2](https://doi.org/10.1130/0091-7613(2001)029<0035:S-SEOTE>2.0.CO;2)
- Bernet, M., Brandon, M.T., Garver, J.I. & Molitor, B.R. 2004. Fundamentals of detrital zircon fission–track analysis for provenance and exhumation studies with examples from the European Alps. In: Bernet, M. & Spiegel, C. (editors), *Detrital thermochronology—Provenance analysis, exhumation, and landscape evolution of mountain belts*. Geological Society of America, Special Paper 378, p. 25–36. Boulder, Colorado. <https://doi.org/10.1130/0-8137-2378-7.25>
- Bernet, M., van der Beek, P., Pik, R., Huyghe, P., Mugnier, J.L., Labrin, E. & Szulc, A. 2006. Miocene to recent exhumation of the central Himalaya determined from combined detrital zircon fission–track and U/Pb analysis of Siwalik sediments, western Nepal. *Basins Research*, 18(4): 393–412. <https://doi.org/10.1111/j.1365-2117.2006.00303.x>
- Bernet, M., Brandon, M., Garver, J., Balestrieri, M.L., Ventura, B. & Zattin, M. 2009. Exhuming the Alps through time: Clues from detrital zircon fission–track thermochronology. *Basin Research*, 21(6): 781–798. <https://doi.org/10.1111/j.1365-2117.2009.00400.x>
- Bernet, M., Urueña, C., Amaya, S. & Peña, M.L. 2016. New thermo and geochronological constraints on the Pliocene–Pleistocene eruption history of the Paipa–Iza Volcanic Complex, Eastern Cordillera, Colombia. *Journal of Volcanology and Geothermal Research*, 327: 299–309. <https://doi.org/10.1016/j.jvolgeores.2016.08.013>
- Brandon, M.T. 1996. Probability density plot for fission–track grain–age samples. *Radiation Measurements*, 26(5): 663–676. [https://doi.org/10.1016/S1350-4487\(97\)82880-6](https://doi.org/10.1016/S1350-4487(97)82880-6)
- Brandon, M.T., Roden–Tice, M.K. & Garver, J.I. 1998. Late Cenozoic exhumation of the Cascadia accretionary wedge in the Olympic Mountains, northwest Washington State. *Geological Society of America Bulletin*, 110(8): 985–1009. [https://doi.org/10.1130/0016-7606\(1998\)110<0985:LCEOTC>2.3.CO;2](https://doi.org/10.1130/0016-7606(1998)110<0985:LCEOTC>2.3.CO;2)
- Bustamante, C., Cardona, A., Bayona, G., Mora, A., Valencia, V., Gehrels, G. & Vervoort, J. 2010. U–Pb LA–ICP–MS geochronology and regional correlation of Middle Jurassic intrusive rocks from the Garzón Massif, Upper Magdalena Valley and Central Cordillera, southern Colombia. *Boletín de Geología*, 32(2): 93–109.
- Bustamante, C., Archanjo, C.J., Cardona, A. & Vervoort, J.D. 2016. Late Jurassic to Early Cretaceous plutonism in the Colombian Andes: A record of long–term arc maturity. *Geological Society of America Bulletin*, 128(11–12): 1762–1779. <https://doi.org/10.1130/B31307.1>
- Caricchi, L., Simpson, G. & Schaltegger, U. 2014. Zircons reveal magma fluxes in the Earth’s crust. *Nature*, 511(7510): 457–461. <https://doi.org/10.1038/nature13532>
- Carter, A. & Bristow, C.S. 2000. Detrital zircon geochronology: Enhancing the quality of sedimentary source information through improved methodology and combined U–Pb and fission–

- track techniques. *Basin Research*, 12(1): 47–57. <https://doi.org/10.1046/j.1365-2117.2000.00112.x>
- Carter, A. & Bristow, C.S. 2003. Linking hinterland evolution and continental basin sedimentation by using detrital zircon thermochronology: A study of the Khorat Plateau Basin, eastern Thailand. *Basin Research*, 15(2): 271–285. <https://doi.org/10.1046/j.1365-2117.2003.00201.x>
- Carter, A. & Moss, S.J. 1999. Combined detrital–zircon fission–track and U–Pb dating: A new approach to understanding hinterland evolution. *Geology*, 27(3): 235–238. [https://doi.org/10.1130/0091-7613\(1999\)027<0235:CDZFTA>2.3.CO;2](https://doi.org/10.1130/0091-7613(1999)027<0235:CDZFTA>2.3.CO;2)
- Cerveny, P.F., Naeser, N.D., Zeitler, P.K., Naeser, C.W. & Johnson, N.M. 1988. History of uplift and relief of the Himalaya during the past 18 million years: Evidence from fission–track ages of detrital zircons from sandstones of the Siwalik Group. In: Kleinspehn, K.L. & Paola, C. (editors), *New perspectives in basin analysis: Frontiers in sedimentary geology*. Springer–Verlag, p. 43–61. New York. https://doi.org/10.1007/978-1-4612-3788-4_3
- Chang, Z., Vervoort, J.D., McClelland, W.C. & Knaack, C. 2006. U–Pb dating of zircon by LA–ICP–MS. *Geochemistry, Geophysics, Geosystems*, 7(5): 1–14. <https://doi.org/10.1029/2005GC001100>
- Colleta, B., Hebrard, F., Letouzey, J., Werner, P. & Rudkiewicz, J.L. 1990. Tectonic style and crustal structure of the Eastern Cordillera (Colombia) from a balanced cross section. In: Letouzey, J. (editor), *Petroleum and tectonics in mobile belts*. Editions Technip, p. 81–100. Paris.
- Cooper, M.A., Addison, F.T., Álvarez, R., Coral, M., Graham, R.H., Hayward, A.B., Howe, S., Martínez, J., Naar, J., Penas, R., Pulham, A.J. & Taborda, A. 1995. Basin development and tectonic history of the Llanos Basin, Eastern Cordillera, and Middle Magdalena Valley, Colombia. *American Association of Petroleum Geologists Bulletin*, 79(10): 1421–1442. <https://doi.org/10.1306/7834D9F4-1721-11D7-8645000102C1865D>
- Davis, S.J., Dickinson, W.R., Gehrels, G.E., Spencer, J.E., Lawton, T.F. & Carroll, A.R. 2010. The Paleogene California River: Evidence of Mojave–Uinta paleodrainage from U–Pb ages of detrital zircons. *Geology*, 38(10): 931–934. <https://doi.org/10.1130/G31250.1>
- Dengo, C. & Covey, M.C. 1993. Structure of the Eastern Cordillera of Colombia: Implications for trap styles and regional tectonics. *American Association of Petroleum Geologists Bulletin*, 77(8): 1315–1337. <https://doi.org/10.1306/BDF8E7A-1718-11D7-8645000102C1865D>
- Dickinson, W.R. & Gehrels, G.E. 2009. Use of U–Pb ages of detrital zircons to infer maximum depositional ages of strata: A test against a Colorado Plateau Mesozoic database. *Earth and Planetary Science Letters*, 288(1–2): 115–125. <https://doi.org/10.1016/j.epsl.2009.09.013>
- Ehlers, T.A., Chaudhri, T., Kumar, S., Fuller, C.W., Willett, S.D., Ketcham, R.A., Brandon, M.T., Belton, D.X., Kohn, B.P., Gleadow, A.J.W., Dunai, T.J. & Fu, F.Q. 2005. Computational tools for low–temperature thermochronometer interpretation. *Reviews in Mineralogy and Geochemistry*, 58(1): 589–622. <https://doi.org/10.2138/rmg.2005.58.22>
- Fabre, A. & Delaloye, M. 1983. Intrusiones básicas cretácicas en las sedimentitas de la parte central de la cordillera Oriental. *Geología Norandina*, (6): 19–28.
- Frei, D. & Gerdes, A. 2009. Precise and accurate in situ U–Pb dating of zircon with high sample throughput by automated LA–SF–ICP–MS. *Chemical Geology*, 261(3–4): 261–270. <https://doi.org/10.1016/j.chemgeo.2008.07.025>
- Galbraith, R.F. & Green, P.F. 1990. Estimating the component ages in a finite mixture. *International Journal of Radiation Applications and Instrumentations. Part D. Nuclear Tracks and Radiation Measurements*, 17(3): 197–206. [https://doi.org/10.1016/1359-0189\(90\)90035-V](https://doi.org/10.1016/1359-0189(90)90035-V)
- Galbraith, R.F. & Laslett, G.M. 1993. Statistical models for mixed fission track ages. *Nuclear tracks and radiation measurements*, 21(4): 459–470. [https://doi.org/10.1016/1359-0189\(93\)90185-C](https://doi.org/10.1016/1359-0189(93)90185-C)
- García–Ramírez, C.A., Rey–León, V. & Valencia, V.A. 2017. Orthogneisses from the Silos–Babega strip, Santander Massif, Colombia: Evidences of Famatinian Orogeny in the north Andes. *Andean Geology*, 44(3): 307–327. <https://doi.org/10.5027/andgeoV44n3-a04>
- Garver, J.I. & Kamp, P.J.J. 2002. Integration of zircon color and zircon fission–track zonation patterns in orogenic belts: Application to the southern Alps, New Zealand. *Tectonophysics*, 349(1–4): 203–219. [https://doi.org/10.1016/S0040-1951\(02\)00054-9](https://doi.org/10.1016/S0040-1951(02)00054-9)
- Gehrels, G.E. 2011. Detrital zircon U–Pb geochronology: Current methods and new opportunities. In: Busby, C. & Azor, A. (editors), *Tectonics of sedimentary basins: Recent advances*. Blackwell Publishing Ltd, p. 47–62. <https://doi.org/10.1002/9781444347166.ch2>
- Gehrels, G.E. & Pecha, M. 2014. Detrital zircon U–Pb geochronology and Hf isotope geochemistry of Paleozoic and Triassic passive margin strata of western North America. *Geosphere*, 10(1): 49–65. <https://doi.org/10.1130/GES00889.1>
- Gómez, J., Montes, N.E., Nivia, Á. & Diederix, H., compilers. 2015. Geological Map of Colombia 2015. Scale 1:1 000 000. Servicio Geológico Colombiano, 2 sheets. Bogotá. <https://doi.org/10.32685/10.143.2015.936>
- Horton, B.K., Saylor, J.E., Nie, J., Mora, A., Parra, M., Reyes–Harker, A. & Stockli, D.F. 2010. Linking sedimentation in the northern Andes to basement configuration, Mesozoic extension, and Cenozoic shortening: Evidence from detrital zircon U–Pb ages, Eastern Cordillera, Colombia. *Geological Society of America Bulletin*, 122(9–10): 1423–1442. <https://doi.org/10.1130/B30118.1>
- Ibañez–Mejía, M. & Cordani, U.G. 2020. Zircon U–Pb geochronology and Hf–Nd–O isotope geochemistry of the Paleoproterozoic to Mesoproterozoic basement in the westernmost Guiana Shield.

- In: Gómez, J. & Mateus–Zabala, D. (editors), *The Geology of Colombia, Volume 1 Proterozoic – Paleozoic*. Servicio Geológico Colombiano, Publicaciones Geológicas Especiales 35, p. 65–90. Bogotá. <https://doi.org/10.32685/pub.esp.35.2019.04>
- Ibañez–Mejía, M., Ruiz, J., Valencia, V.A., Cardona, A., Gehrels, G.E. & Mora, A.R. 2011. The Putumayo Orogen of Amazonia and its implications for Rodinia reconstructions: New U–Pb geochronological insights into the Proterozoic tectonic evolution of northwestern South America. *Precambrian Research*, 191(1–2): 58–77. <https://doi.org/10.1016/j.precamres.2011.09.005>
- Ibañez–Mejía, M., Pullen, A., Arenstein, J., Gehrels, G.E., Valley, J., Ducea, M.N., Mora, A.R., Pecha, M. & Ruiz, J. 2015. Unraveling crustal growth and reworking processes in complex zircons from orogenic lower–crust: The Proterozoic Putumayo Orogen of Amazonia. *Precambrian Research*, 267: 285–310. <https://doi.org/10.1016/j.precamres.2015.06.014>
- Jiménez–Triana, C. 2016. Caracterización petrológica y geoquímica de la unidad Ortogneis, Macizo de Santander, Colombia. Master thesis, Universidad Nacional de Colombia, 106 p. Bogotá.
- Jourdan, S., Bernet, M., Tricart, P., Hardwick, E., Paquette, J.L., Guillot, S., Dumont, T. & Schwartz, S. 2013. Short–lived, fast erosional exhumation of the internal western Alps during the late early Oligocene: Constraints from geothermochronology of pro– and retro–side foreland basin sediments. *Lithosphere*, 5(2): 211–225. <https://doi.org/10.1130/L243.1>
- Kosler, J. & Sylvester, P.J. 2003. Present trends and the future of zircon in geochronology: Laser ablation ICPMS. *Reviews in Mineralogy and Geochemistry*, 53(1): 243–275. <https://doi.org/10.2113/0530243>
- Leal–Mejía, H. 2011. Phanerozoic gold metallogeny in the Colombian Andes: A tectono–magmatic approach. Doctoral thesis, Universitat de Barcelona, 989 p. Barcelona.
- Ludwig, K.R. 2012. User’s manual for Isoplot 3.75. A geochronological toolkit for Microsoft Excel. Berkeley Geochronology Center, Special Publication 5, 75 p. Berkeley, USA.
- Mark, C., Cogné, N. & Chew, D. 2016. Tracking exhumation and drainage divide migration of the western Alps: A test of the apatite U–Pb thermochronometer as a detrital provenance tool. *Geological Society of America Bulletin*, 128(9–10): 1439–1460. <https://doi.org/10.1130/B31351.1>
- Moecher, D.P. & Samson, S.D. 2006. Differential zircon fertility of source terranes and natural bias in the detrital zircon record: Implications for sedimentary provenance analysis. *Earth and Planetary Science Letters*, 247(3–4): 252–266. <https://doi.org/10.1016/j.epsl.2006.04.035>
- Montgomery, D.R. & Brandon, M.T. 2002. Topographic controls on erosion rates in tectonically active mountain ranges. *Earth and Planetary Science Letters*, 201(3–4): 481–489. [https://doi.org/10.1016/S0012-821X\(02\)00725-2](https://doi.org/10.1016/S0012-821X(02)00725-2)
- Mora, A., Parra, M., Strecker, M.R., Kammer, A., Dimaté, C. & Rodríguez, F. 2006. Cenozoic contractional reactivation of Mesozoic extensional structures in the Eastern Cordillera of Colombia. *Tectonics*, 25(2): 1–19. <https://doi.org/10.1029/2005TC001854>
- Mora, A., Parra, M., Strecker, M.R., Sobel, E.R., Hooghiemstra, H., Torres, V. & Vallejo–Jaramillo, J. 2008. Climatic forcing of asymmetric orogenic evolution in the Eastern Cordillera of Colombia. *Geological Society of America Bulletin*, 120(7–8): 930–949. <https://doi.org/10.1130/B26186.1>
- Mora, A., Gaona, T., Kley, J., Montoya, D., Parra, M., Quiroz, L.I., Reyes, G. & Strecker, M.R. 2009. The role of inherited extensional fault segmentation and linkage in contractional orogenesis: A reconstruction of Lower Cretaceous inverted rift basins in the Eastern Cordillera of Colombia. *Basin Research*, 21(1): 111–137. <https://doi.org/10.1111/j.1365-2117.2008.00367.x>
- Mora, A., Horton, B.K., Mesa, A., Rubiano, J., Ketcham, R.A., Parra, M., Blanco, V., García, D. & Stockli, D.F. 2010. Migration of Cenozoic deformation in the Eastern Cordillera of Colombia interpreted from fission track results and structural relationships: Implications for petroleum systems. *American Association of Petroleum Geologists Bulletin*, 94(10): 1543–1580. <https://doi.org/10.1306/01051009111>
- Moreno–Murillo, J.M., Concha–Perdomo, A.E. & Lozano, E.L. 2007. Petrogénesis y geoquímica del cuerpo ígneo de Pajarito, Boyacá, Colombia. *Geología Colombiana*, 32: 111–126.
- Naylor, M., Sinclair, H.D., Bernet, M., van der Beek, P. & Kirstein, L.A. 2015. Bias in detrital fission track grain–age populations: Implications for reconstructing changing erosion rates. *Earth and Planetary Science Letters*, 422: 94–104. <https://doi.org/10.1016/j.epsl.2015.04.020>
- Nie, J., Horton, B.K., Mora, A., Saylor, J.E., Housh, T.B., Rubiano, J. & Naranjo, J. 2010. Tracking exhumation of Andean ranges bounding the Middle Magdalena Valley Basin, Colombia. *Geology*, 38(5): 451–454. <https://doi.org/10.1130/G30775.1>
- Parra, M., Mora, A., Sobel, E.R., Strecker, M.R. & González, R. 2009a. Episodic orogenic–front migration in the northern Andes: Constraints from low–temperature thermochronology in the Eastern Cordillera, Colombia. *Tectonics*, 28(4): 1–27. <https://doi.org/10.1029/2008TC002423>
- Parra, M., Mora, A., Jaramillo, C., Strecker, M.R., Sobel, E.R., Quiroz, L., Rueda, M. & Torres, V. 2009b. Orogenic wedge advance in the northern Andes: Evidence from the Oligocene – Miocene sedimentary record of the Medina Basin, Eastern Cordillera, Colombia. *Geological Society of America Bulletin*, 121(5–6): 780–800. <https://doi.org/10.1130/B26257.1>
- Parra, M., Mora, A., López, C., Rojas, L.E. & Horton, B.K. 2012. Detecting earliest shortening and deformation advance in thrust belt hinterlands: Example from the Colombian Andes. *Geology*, 40(2): 175–178. <https://doi.org/10.1130/G32519.1>
- Pullen, A., Ibañez–Mejía, M., Gehrels, G.E., Ibañez–Mejía, J.C. & Pecha, M. 2014. What happens when n=1000? Creating large–n geochronological datasets with LA–ICP–MS for geologic investigations. *Journal of Analytical Atomic Spectrometry*, 29(6): 971–980. <https://doi.org/10.1039/C4JA00024B>

- Rahl, J.M., Reiners, P.W., Campbell, I.H., Nicolescu, S. & Allen, C.M. 2003. Combined single-grain (U–Th)/He and U/Pb dating of detrital zircons from the Navajo Sandstone, Utah. *Geology*, 31(9): 761–764. <https://doi.org/10.1130/G19653.1>
- Reiners, P.W. & Brandon, M.T. 2006. Using thermochronology to understand orogenic erosion. *Annual Review Earth Planetary Sciences*, 34: 419–466. <https://doi.org/10.1146/annurev.earth.34.031405.125202>
- Reiners, P.W., Campbell, I.H., Nicolescu, S., Allen, C.M., Hourigan, J.K., Garver, J.I., Mattinson, J.M. & Cowan, D.S. 2005. (U–Th)/(He–Pb) double-dating of detrital zircons. *American Journal of Science*, 305(4): 259–311. <https://doi.org/10.2475/ajs.305.4.259>
- Restrepo–Moreno, S.A., Foster, D.A., Stockli, D.F. & Parra–Sánchez, L.N. 2009. Long-term erosion and exhumation of the “Altiplano Antioqueño”, northern Andes (Colombia) from apatite (U–Th)/He thermochronology. *Earth and Planetary Science Letters*, 278(1–2): 1–12. <https://doi.org/10.1016/j.epsl.2008.09.037>
- Restrepo–Pace, P. 1995. Late Precambrian to early Mesozoic tectonic evolution of the Colombian Andes, based on new geochronological, geochemical and isotopic data. Doctoral thesis, University of Arizona, 194 p.
- Rodríguez, G., Zapata, G., Arango, M.I. & Bermúdez, J.G. 2017. Caracterización petrográfica, geoquímica y geocronología de rocas granitoides pérmicas al occidente de La Plata y Pacarní, Huila, Valle Superior del Magdalena, Colombia. *Boletín de Geología*, 39(1): 41–68. <https://doi.org/10.18273/revbol.v39n1-2017002>
- Sarmiento–Rojas, L.F., van Wess, J.D. & Cloetingh, S. 2006. Mesozoic transtensional basin history of the Eastern Cordillera, Colombian Andes: Inferences from tectonic models. *Journal of South American Earth Sciences*, 21(4): 383–411. <https://doi.org/10.1016/j.jsames.2006.07.003>
- Saylor, J.E., Knowles, J.N., Horton, B.K., Nie, J. & Mora, A. 2013. Mixing of source populations recorded in detrital zircon U–Pb age spectra of modern river sands. *The Journal of Geology*, 121(1): 17–33. <https://doi.org/10.1086/668683>
- Schaltegger, U., Schmitt, A.K. & Horstwood, M.S.A. 2015. U–Th–Pb zircon geochronology by ID–TIMS, SIMS, and laser ablation ICP–MS: Recipes, interpretations, and opportunities. *Chemical Geology*, 402: 89–110. <https://doi.org/10.1016/j.chemgeo.2015.02.028>
- Slama, J., Kosler, J., Condon, D., Crowley, J.L., Gerdes, A., Hancher, J.M., Horstwood, M.S.A., Morris, G.A., Nasdala, L., Norberg, N., Schaltegger, U., Schoene, B., Tubrett, M.N. & Whitehouse, M.J. 2008. Plešovice zircon—A new natural reference material for U–Pb and Hf isotopic microanalysis. *Chemical Geology*, 249(1–2): 1–35. <https://doi.org/10.1016/j.chemgeo.2007.11.005>
- Spiegel, C., Kuhlemann, J., Dunkl, I., Frisch, W., von Eynatten, H. & Balogh, K. 2000. The erosion history of the central Alps: Evidence from zircon fission-track data of the foreland basin sediments. *Terra Nova*, 12(4): 163–170. <https://doi.org/10.1046/j.1365-3121.2000.00289.x>
- Stewart, R.J. & Brandon, M.T. 2004. Detrital–zircon fission-track ages for the “Hoh Formation”: Implications for late Cenozoic evolution of the Cascadia subduction wedge. *GSA Bulletin*, 116(1–2): 60–75. <https://doi.org/10.1130/B22101.1>
- van der Lelij, R., Spikings, R., Ulianov, A., Chiaradia, M. & Mora, A. 2016. Paleozoic to Early Jurassic history of the northwestern corner of Gondwana, and implications for the evolution of the Iapetus, Rheic and Pacific oceans. *Gondwana Research*, 31: 271–294. <https://doi.org/10.1016/j.gr.2015.01.011>
- Vásquez, M., Altenberger, U., Romer, R.L., Sudo, M. & Moreno–Murrillo, J.M. 2010. Magmatic evolution of the Andean Eastern Cordillera of Colombia during the Cretaceous: Influence of previous tectonic processes. *Journal of South American Earth Sciences*, 29(2): 171–186. <https://doi.org/10.1016/j.jsames.2009.02.003>
- Vermeesch, P. 2004. How many grains are needed for a provenance study? *Earth and Planetary Science Letters*, 224(3–4): 441–451. <https://doi.org/10.1016/j.epsl.2004.05.037>
- Vermeesch, P. 2009. RadialPlotter: A Java application for fission-track, luminescence and other radial plots. *Radiation measurements*, 44(4): 409–410. <https://doi.org/10.1016/j.radmeas.2009.05.003>
- Vermeesch, P. 2012. On the visualization of detrital age distributions. *Chemical Geology*, 312–313: 190–194. <https://doi.org/10.1016/j.chemgeo.2012.04.021>
- Wetherill, G.W. 1956. Discordant uranium–lead ages, I. *Eos, Transactions American Geophysical Union*, 37(3): 320–326. <https://doi.org/10.1029/TR037i003p00320>
- Zapata, S., Cardona, A., Jaramillo, C., Valencia, V. & Vervoort, J. 2016. U–Pb LA–ICP–MS geochronology and geochemistry of Jurassic volcanic and plutonic rocks from the Putumayo region (southern Colombia): Tectonic setting and regional correlations. *Boletín de Geología*, 38(2): 21–38. <https://doi.org/10.18273/revbol.v38n2-2016001>

Explanation of Acronyms, Abbreviations, and Symbols:

CA–ID–TIMS	Chemical abrasion thermal ionization mass spectrometry isotopic dilution	LA–SC–ICP–MS	Laser ablation single–cell inductively coupled plasma mass spectrometry
CL	Cathodoluminescence	SEM	Scanning electron microscope
ID–TIMS	Thermal ionization mass spectrometry isotopic dilution	SGC	Servicio Geológico Colombiano
LA–ICP–MS	Laser ablation inductively coupled plasma mass spectrometry	ZFT	Zircon fission–track

Authors’ Biographical Notes



Cindy Lizeth URUEÑA–SUÁREZ has a Master of Sciences in geology graduate from Universidad Nacional de Colombia. Her research focuses on the regional geology, metamorphic petrology, and geochemistry of crystalline rocks. She has a broad professional experience in low–temperature thermochronology and U–Pb geochronology. During 5 years, she was linked as a geologist at the Servicio Geológico Colombiano. Currently, she is a Doctoral student in Geology at Lund University, Sweden.



Mary Luz PEÑA–URUEÑA has a Master of Sciences in Chemistry from Universidad Nacional de Colombia and is a Doctoral student in Geosciences. She has studied coal chemistry and nuclear chemistry applications and led the implementation of the thermochronology and geochronology laboratories and stable isotope geochemistry techniques at the Servicio Geológico Colombiano. Currently, she works for the Servicio Geológico Colombiano as a coordinator of the “Investigaciones y Aplicaciones Nucleares y Geocronológicas” Group.



Jimmy Alejandro MUÑOZ–ROCHA has a BS in chemistry graduate from Universidad Nacional de Colombia; Master’s in Integrated Management System and the prevention of occupational hazards from Universidad Internacional de la Rioja, España. In his professional trajectory, he has performed as a chief of chemistry and environmental analytical laboratories in the quality certification,

implementation and validation of analytical methodologies. Currently, he is working as a chemist in the U–Pb geochronology laboratory of the Servicio Geológico Colombiano.



Lorena del Pilar RAYO–ROCHA is a geologist and has a Master of Science in geology, graduated from Universidad Nacional de Colombia. Her professional experience is related to geothermal exploration, the geochemistry of igneous rocks, and thermochronology. She was working as a geologist in the Scanning Electron Microscope Laboratory of the Servicio Geológico Colombiano. Currently, she belongs to the Dirección de Geociencias Básicas in the Geología de Volcanes group.



Nicolas VILLAMIZAR–ESCALANTE is a geologist graduate from Universidad Industrial de Santander. He obtained his Master of Science degree in geology from the Universidad Nacional de Colombia Sede Bogotá. His research focuses on structural geology, microtectonics, and thermochronology. Currently, he is working as a geologist at the Servicio Geológico Colombiano in the low–temperature thermochronology and U–Pb geochronology laboratories.



Sergio AMAYA-FERREIRA is a geologist at the Universidad Nacional de Colombia, Bogotá, and is also a specialist in environmental engineering at the Universidad Industrial de Santander. He received his Master of Science degree in geology from the Universidad Nacional de Colombia Sede Bogotá, and a Doctoral degree in geosciences from the same university. Dr. AMAYA's main research

interest is the evolution of mountain ranges and sedimentary basins using low-temperature thermochronology (AFT and ZFT) and provenance analysis. He has worked as an associate professor at the School of Geology at the Universidad Industrial de Santander and as a specialized geologist in the fission-track laboratory at the Servicio Geológico Colombiano. He has also guided the following research projects in thermochronology and geochronology: "Structure and geological evolution of the crystalline basement of the Santander Massif, Eastern Cordillera, Colombia", "Petrological characterization of the Berlin Orthogneiss Unit, Santander Massif, Colombia", and "Evaluation of thermal maturity of gas associated with coals of the Umir Formation in the Middle Magdalena Valley and of the Guaduas Formation in the Umbita Syncline, Eastern Cordillera, Colombia". The first two projects have contributed to broadening our understanding of the evolution of the northern Andes in the South American northwestern fringe, which remains under discussion. The thermal maturity assessment projects have contributed to determining the potential of unconventional coal bed methane hydrocarbons in Colombia's coal basins. Currently, Dr. AMAYA is a member of the Grupo de Exploración de Minerales Metálicos in the Dirección de Recursos Minerales of the Servicio Geológico Colombiano and is currently working on a research project concerning the "application of multidisciplinary approaches, petrological, geochronological, and thermochronological, to the exploration of deposits".



Mauricio IBÁÑEZ-MEJÍA graduated as a geologist from the Universidad Nacional de Colombia, Bogotá, in 2007. He obtained MS (2010) and PhD (2014) degrees in petrology and geochemistry from the University of Arizona, USA, followed by two years as a W.O. Crosby postdoctoral fellow in the Massachusetts Institute of Technology in Cambridge, USA, and four years as an assistant

professor in the Department of Earth and Environmental Sciences at University of Rochester, USA. He is currently an assistant professor in the Department of Geosciences at the University of Arizona, USA. His main research interests are in the fields of isotope geochemistry, geochronology, petrology, and crustal evolution.



Matthias BERNET has a PhD in geology from Yale University, USA. Since 2010, he has been the advisor of the thermochronology laboratory at the Servicio Geológico Colombiano, collaborated on several research projects of the Servicio Geológico Colombiano and helped with the implementation of the research facilities of the "Investigaciones y Aplicaciones Nucleares y Geocronológicas"

Group. He is an expert in using detrital thermochronology, clastic sedimentology, and multi-disciplinary provenance analyses to study the exhumation histories of mountain belts in the northern Andes of Colombia and Venezuela, the European Alps, the Himalaya, and the Tibetan Plateau. Currently, he is the director of the ISTerre Thermochronology Laboratory at the Université Grenoble Alpes in France.

Different Levels of Exhumation across the Bucaramanga Fault in the Cepitá Area of the Southwestern Santander Massif, Colombia: Implications for the Tectonic Evolution of the Northern Andes in Northwestern South America

Sergio AMAYA-FERREIRA^{1*} , Carlos Augusto ZULUAGA² ,
and Matthias BERNET³ 

Abstract Apatite and zircon fission-track data from crystalline rocks collected along an east-to-west elevational profile across the Bucaramanga strike-slip fault in the Cepitá area and thermal history modeling show the four-stage thermal history of the southwestern Santander Massif of the northern Andes in Colombia. A 60 my phase of burial heating from the Late Jurassic to the Late Cretaceous was followed by three cooling phases beginning in approximately 65–60 Ma, which were related to regional tectonic events. The Late Cretaceous – early Paleocene accretion of an island arc and interactions of the Caribbean Plate with the northwestern South America plate first triggered the surface uplift and erosional exhumation of the Santander Massif. During the late Oligocene – early Miocene, the collision of the Panamá–Chocó Block with northwestern South America caused an acceleration in the cooling and exhumation of the Santander Massif and differential surface uplift to the east and west of the Bucaramanga Fault in the Cepitá area. The present-day topography of the Santander Massif probably formed at that time. Locally recorded late Miocene cooling may be related to movement on the secondary fault pattern in the study area or minor magmatic activity.

Keywords: *exhumation, fission-track analysis, Santander Massif, Bucaramanga Fault, thermal modeling.*

Resumen Datos de huellas de fisión en apatito y zircón de rocas cristalinas colectadas a lo largo de un perfil de elevación este-oeste a través de la Falla de Bucaramanga, falla de rumbo, en el área de Cepitá y el modelamiento de la historia termal muestran una historia termal en cuatro etapas para el suroeste del Macizo de Santander de los Andes del norte en Colombia. A los 60 millones de años, una fase de calentamiento por enterramiento desde el Jurásico Tardío al Cretácico Tardío fue seguida por tres fases de enfriamiento que comenzaron aproximadamente a los 65–60 Ma, y están relacionadas con eventos tectónicos regionales. En el Cretácico Tardío–Paleoceno temprano, la acreción de un arco de islas y las interacciones de la Placa del Caribe con el noroccidente de la Placa de Suramérica desencadenaron el primer levantamiento de superficie y la

Citation: Amaya-Ferreira, S., Zuluaga, C.A. & Bernet, M. 2020. Different levels of exhumation across the Bucaramanga Fault in the Cepitá area of the southwestern Santander Massif, Colombia: Implications for the tectonic evolution of the northern Andes in northwestern South America. In: Gómez, J. & Mateus-Zabala, D. (editors), *The Geology of Colombia, Volume 3 Paleogene – Neogene*. Servicio Geológico Colombiano, *Publicaciones Geológicas Especiales* 37, p. 491–507. Bogotá. <https://doi.org/10.32685/pub.esp.37.2019.17>

<https://doi.org/10.32685/pub.esp.37.2019.17>
Published online 22 May 2020

- 1 samaya@sgc.gov.co, samayaf@unal.edu.co
Servicio Geológico Colombiano
Dirección de Recursos Minerales
Diagonal 53 n.º 34–53
Bogotá, Colombia
 - 2 cazuluagacas@unal.edu.co
Universidad Nacional de Colombia
Sede Bogotá
Departamento de Geociencias
Carrera 30 n.º 45–03
Bogotá, Colombia
 - 3 matthias.bernet@univ-grenoble-alpes.fr
Université Grenoble Alpes
Institut des Sciences de la Terre
1381 rue de la piscine, CS 40700, 38058
Grenoble cedex 9, France
- * Corresponding author

exhumación erosiva del Macizo de Santander. Durante el final del Oligoceno y el Mioceno temprano, la colisión del Bloque Panamá–Chocó con el noroeste de Suramérica provocó la aceleración del enfriamiento y de la exhumación del Macizo de Santander y la elevación diferencial de la superficie al este y al oeste de la Falla de Bucaramanga en el área de Cepitá. Probablemente, la topografía actual del Macizo de Santander se formó en ese momento. El enfriamiento del Mioceno tardío registrado localmente puede estar relacionado con el movimiento en el patrón de falla secundaria en el área de estudio o con la actividad magmática menor.

Palabras clave: *exhumación, análisis de huellas de fisión, Macizo de Santander, Falla de Bucaramanga, modelamiento termal.*

1. Introduction

The rise of orogenic mountain belts, particularly in the northern Andes, has a significant influence on regional climate and atmospheric circulation and precipitation patterns, and forms barriers to species migration and the creation of new habitats and ecological niches (e.g., Hoorn et al., 2010; Mapes et al., 2003). For paleogeographic reconstructions, it is important to link the exhumation of deep-seated crystalline rocks and the formation of high orogenic topography with the plate-tectonic evolution of the area of interest. Here, we present a study on the exhumation history of the southern Santander Massif in northeastern Colombia because this mountain belt holds a key position in the northern Andes, forming the northwest-striking continuation of the Eastern Cordillera at the junction between the Eastern Cordillera and the Mérida Andes in Venezuela to the east (Figure 1). The Santander Massif is part of the so-called Maracaibo Block, which is delineated by the Santa Marta–Bucaramanga and Oca strike-slip Fault Systems and the southwestern fold-and-thrust belt of the Mérida Andes (Figure 1; e.g., Colletta et al., 1997; Mann et al., 2006). The Maracaibo Block also includes the Sierra Nevada de Santa Marta and the serranía de Perijá (Figure 1). The cooling history of the crystalline rocks of the central and southern Santander Massif has been previously studied with low-temperature thermochronology, with apatite fission-track (AFT) ages ranging from 20 to 7 Ma and zircon fission-track (ZFT) ages ranging from 172 to 20 Ma (Amaya et al., 2017; Shagam et al., 1984; van der Lelij et al., 2016; Villagómez et al., 2011). In addition, from outcrops to the east of the city of Bucaramanga and the Bucaramanga Fault, Mora et al. (2015) first presented AHe ages between 8.2 and 16 Ma and ZHe ages between 22.6 and 24.2 Ma. Along the same profile, Amaya et al. (2017) demonstrated an exhumed ZFT partial annealing zone, which was rapidly exhumed between 25 and 20 Ma. All these data show the importance of late Oligocene regional tectonics driving the exhumation of the Santander Massif along the Bucaramanga Fault, which is related to the break-up of the Farallón Plate and the collision of the Panamá–Chocó Block with northwestern South America (Farris et al., 2011; Taboada et al., 2000; O’Dea et al., 2016). This regional tectonic influence has already been shown in the exhumation of the Antioquian

Batholith in the Central Cordillera (Restrepo–Moreno et al., 2009). Parra et al. (2012) argued, on the basis of AFT data from the Nuevo Mundo Syncline sedimentary basin fill and thermal modeling, for a Paleocene – early Eocene (60–50 Ma) phase of pronounced shortening and cooling of the western margin of the Eastern Cordillera associated with tectonic inversion and the first surface uplift and erosion of the Eastern Cordillera. However, the Parra et al. (2012) study lacked information from ZFT or zircon (U–Th)/He thermochronometers and therefore the pre-depositional thermal histories in their models were fully unconstrained. Regardless, the absence of Cretaceous sedimentary cover rocks in large areas of the Santander Massif, which are otherwise widespread in the Eastern Cordillera of Colombia, suggests erosion was an important process during the exhumation history of the Santander Massif. Evidence of Paleogene and Neogene erosional exhumation of the Santander Massif basement and sedimentary cover rocks is preserved in the stratigraphic sequences of the Lisama, La Paz, Esmeraldas, Mugrosa, Colorado, and Real Formations in the Nuevo Mundo, Armas, and Andes Synclines of the Middle Magdalena Valley (Figure 1; Caballero et al., 2013; Parra et al., 2012; Sánchez et al., 2012). Deformation of the Middle Magdalena Valley area probably began during the Paleocene, with structures such as the Lisama Anticline (Caballero et al., 2013).

The objective of this study was to more precisely constrain the exhumation history of the southwestern Santander Massif in the Cepitá area, to the east and west of the Chicamocha River (Figure 2). Thus far, very few and spatially dispersed thermochronological data have been published from this region (Caballero et al., 2013; Shagam et al., 1984; van der Lelij et al., 2016). Therefore, we present data of 10 AFT and 9 ZFT samples collected from igneous and metamorphic crystalline rocks along a profile across the Chicamocha Canyon and the Bucaramanga Fault System near Cepitá, referred to here as the western and eastern blocks of the Santander Massif (Figures 2, 3), respectively. The Chicamocha River does not exactly follow the trace of the Bucaramanga Fault System but does mark the present-day morphologic separation between the two blocks. While the western block reaches an elevation of only approximately 1600 m in the study area, the eastern block rises to more than 3200 m in this part of the Santander Massif (Figure 3). Expo-

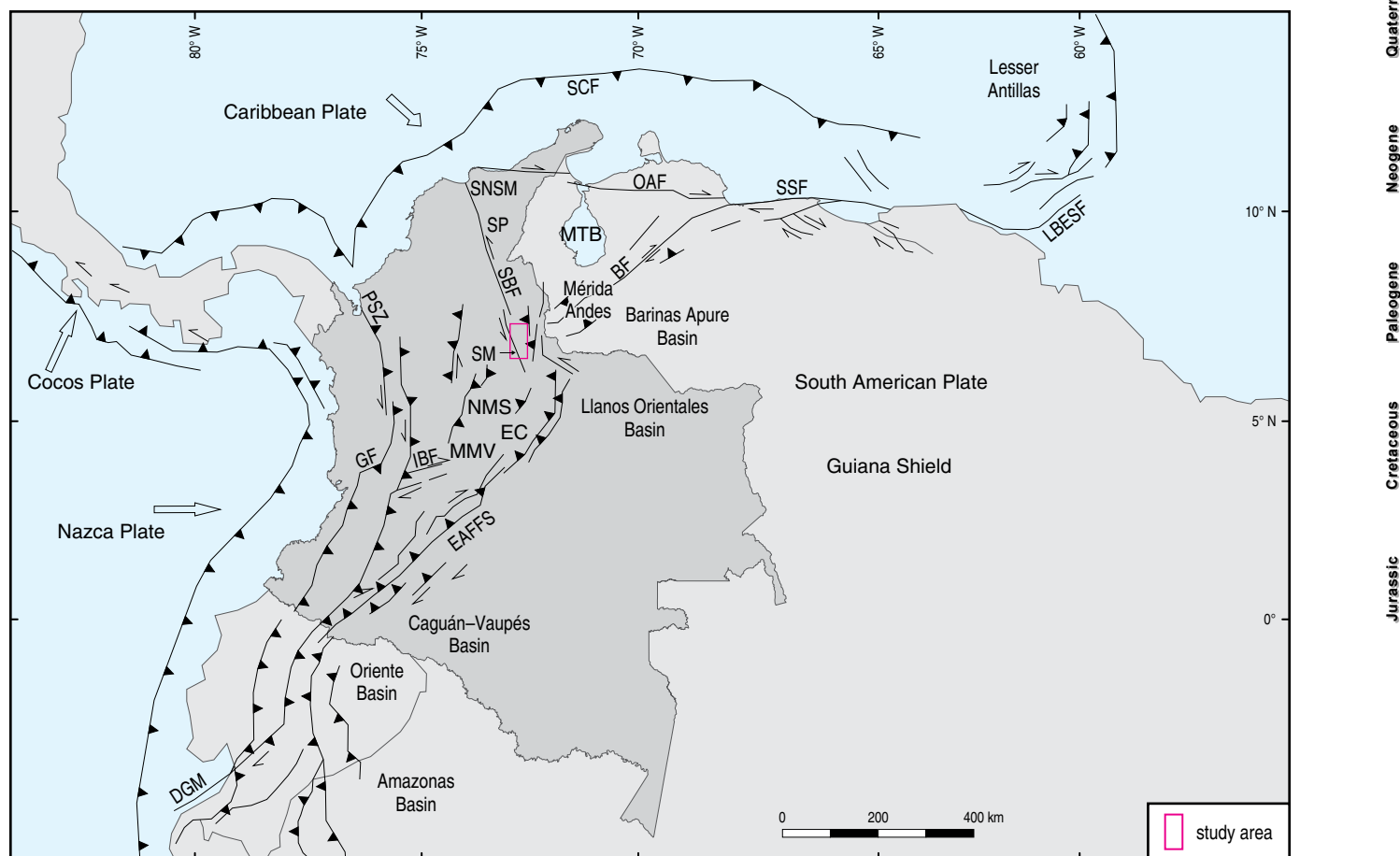


Figure 1. Overview map showing the major tectonic features of northern South America (modified from Colmenares & Zoback, 2003). (SCF) Southern Caribbean Marginal Fault; (SNSM) Sierra Nevada de Santa Marta; (OAF) Oca-Ancón Fault; (SSF) San Sebastián Fault System; (LBESF) Los Bajos-El Soldado Fault System; (SP) serranía de Perijá; (MTB) Maracaibo Triangular Block; (SBF) Santa Marta-Bucaramanga Fault; (BF) Boconó Fault; (PSZ) Panamá suture zone; (SM) Santander Massif; (GF) Garrapatas Fault; (IBF) Ibagué Fault; (NMS) Nuevo Mundo Syncline; (EC) Eastern Cordillera; (MMV) Middle Magdalena Valley; (EAFFS) Eastern Andean Front Fault System; (DGM) Dolores-Guayaquil Megashear.

sure of crystalline rocks at high surface elevations implies both exhumation and surface uplift. The thermochronological data of this study were used in *t*-*T* models to provide constraints on the timing of cooling. The cooling histories were then interpreted in terms of erosional and tectonic exhumation. To constrain the difference in relative surface uplift between the western and eastern blocks, ZFT cooling ages at similar elevations on both sides of the Bucaramanga Fault were compared. Furthermore, the apparent fission-track cooling ages were translated into exhumation rates (e.g., Willett & Brandon, 2013) for the crystalline rocks that were buried beneath sedimentary rocks at least since the Late Jurassic and throughout most of the Cretaceous.

2. Geological Setting

The fault-bounded triangular Maracaibo Block in the northern Andes is an interesting geological feature, as this block not only hosts the highest coastal mountain belt in the world including the 5700 m-high Pico Cristobal Colón of the Sierra Nevada de Santa Marta, but also features the Santander Massif, the serranía

de Perijá, and the Mérida Andes of Venezuela along two of its three sides (Figure 1). Even if two of the main bounding faults of the Maracaibo Block, the dextral Oca Fault to the north and the sinistral Santa Marta-Bucaramanga Fault on its western flank, are strike-slip fault systems with an unknown vertical offset, considerable topographic surface elevations have been attained in the Sierra Nevada de Santa Marta and the Santander Massif (up to 4530 m at Paramo del Almorzadero). The Santa Marta-Bucaramanga Fault extends for over 600 km from Santa Marta in the north to the Chicamocha Canyon, approximately 40–70 km south of Bucaramanga, where it ceases defining the western margin of the Santander Massif (Figure 1). The Boconó strike-slip fault dominates the late Miocene to Pliocene evolution and exhumation of the Mérida Andes of Venezuela (Bermúdez et al. 2010, 2011, 2013; Kohn et al. 1984), but the southeastern fold-and-thrust belt is thought to delimit the Maracaibo Block to the southeast against the South American continental plate (e.g., Figure 1; Colletta et al., 1997; Mann et al., 2006).

Late Proterozoic to Paleozoic metamorphic rocks intruded by Triassic and Jurassic plutonic rocks form the crystalline core

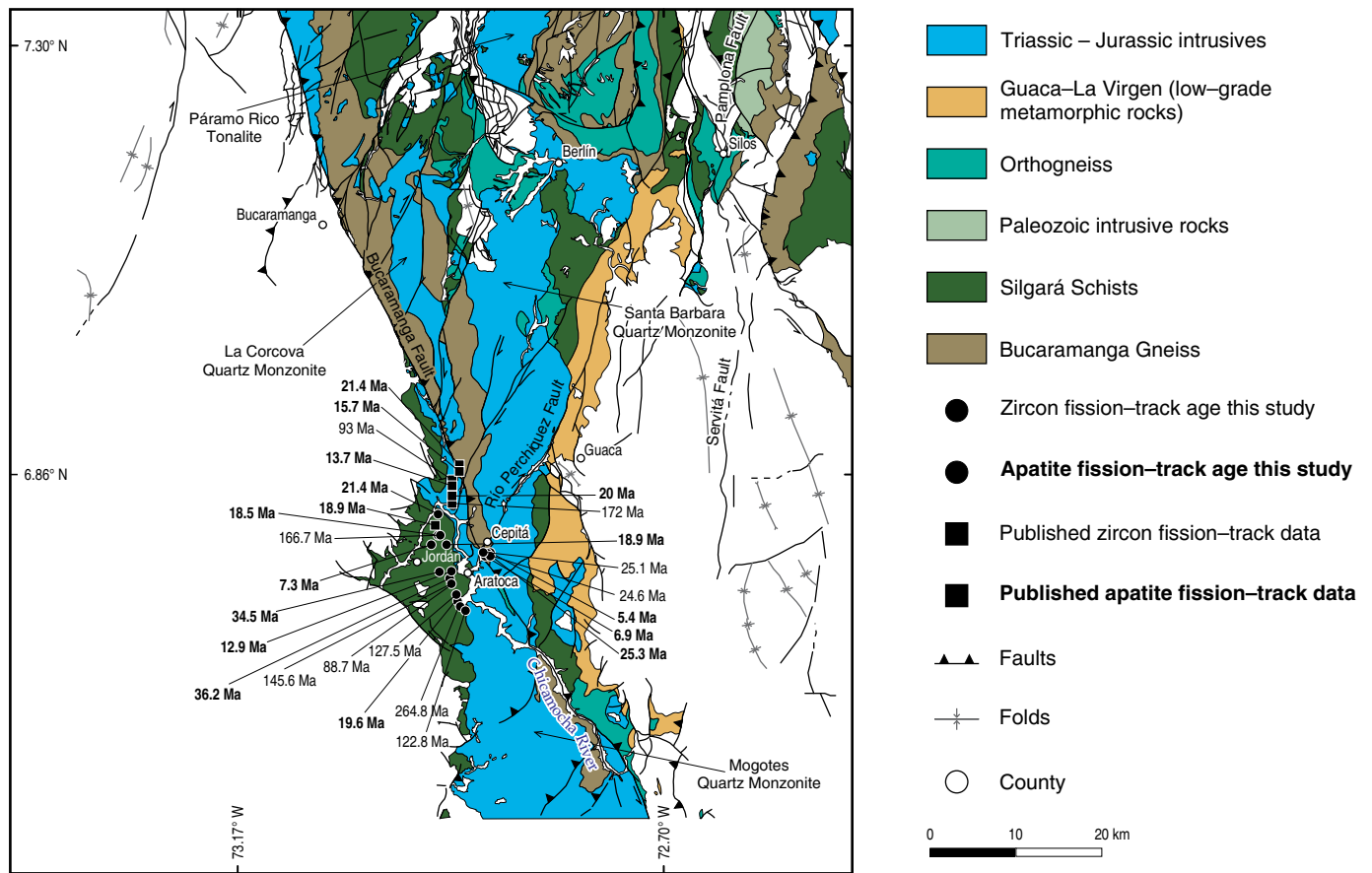


Figure 2. Geological map and sample locations. Taken and modified from Zuluaga & López (2018).

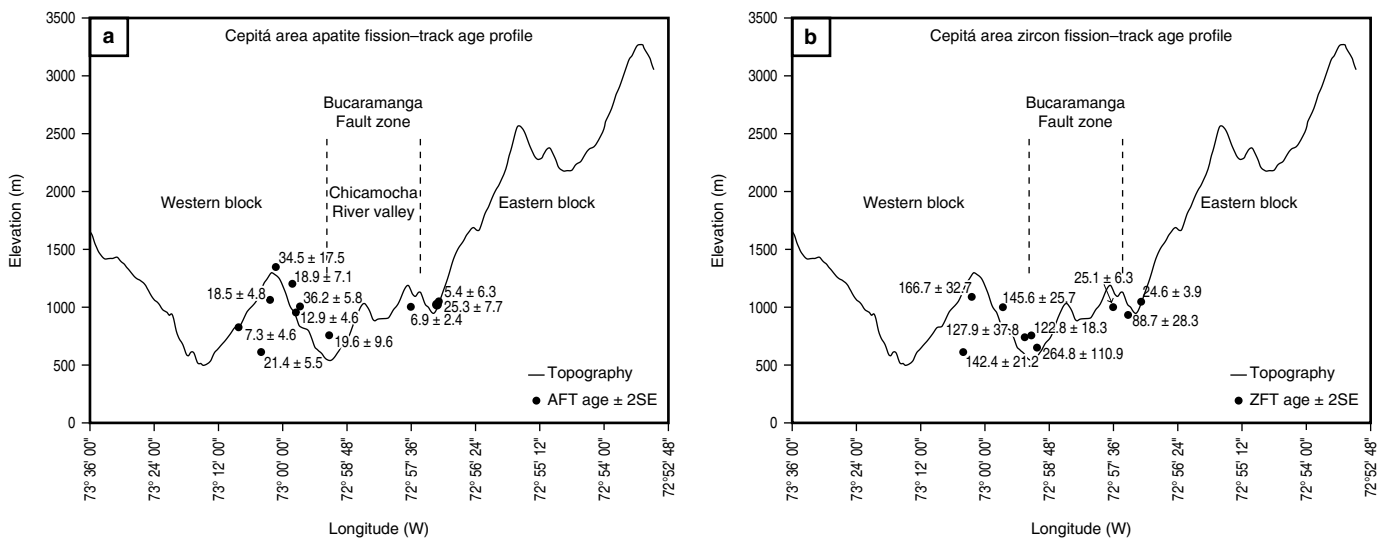


Figure 3. Topographic profile with sample locations.

of the Santander Massif (Goldsmith et al., 1971). In this study, only the late Proterozoic Bucaramanga Gneiss, Paleozoic Silgará Schists, Jurassic Mogotes Batholith and Pescadero Granite are of interest because samples were only collected from these lithological units to the east and west of the Chicamocha River

(Figures 2, 3). The Jurassic and Cretaceous sedimentary cover rocks, with a cumulative thickness of ca. 2500 to ca. 3500 m (Shagam et al., 1984), were used as a constraint for thermal history modeling for the phase and amplitude of the Jurassic and Cretaceous burial heating in the study area. A zircon fission

track age in the study area of 172.0 ± 16.4 Ma from the Pescadero Granite of van der Lelij et al. (2016) indicates that burial heating was insufficient to fully reset the zircon fission-track system to the west of the Bucaramanga Fault. Our samples of the western profile were collected between 612 and 1347 m elevation between Cepitá and Aratoca, whereas eastern profile samples were collected from elevations ranging between 900 and 1050 m to the east of Cepitá (Figure 2; Table 1).

The Chicamocha River is a tributary of the Magdalena River. In the Cepitá area, the Chicamocha River flows in a N–NW direction, before following the secondary NE–SW–oriented fault pattern of the Santander Massif and turning to the SW and flowing toward the village of Jordán (Figure 2). In the study area, the Chicamocha Canyon shows at least 1000 m of incision with respect to the highest elevations of the western block (Figure 3).

3. Methods

3.1. Fission-Track Analysis

Sample preparation for the fission-track analysis was completed at the Servicio Geológico Colombiano in Bogotá, following the methodology described by Amaya et al. (2017). All samples were irradiated at the FRM II research reactor in Garching, Germany. For track length measurements of horizontally confined tracks, apatite samples were irradiated with ^{252}Cf at the University of Melbourne. Samples were analyzed dry at 1250x with an Olympus BX51 optical microscope, using the FTStage 4.04 system of Trevor Dumitru in the fission-track laboratory of the Servicio Geológico Colombiano in Bogotá and in the fission-track laboratory at ISTerre, Université Grenoble Alpes.

3.2. Time-Temperature History Modeling

For t–T history modeling of the western profile samples, we used the QTQt program (v 4.6) of Gallagher (2012) to model age pairs of samples for which we have AFT and ZFT data and length measurements of horizontally confined tracks in apatite. The QTQt program determines cooling history scenarios using a Bayesian transdimensional Markov Chain Monte Carlo approach, which determines simple thermal history models to avoid over interpretation of the observed data (Gallagher, 2012). The output models were the maximum likelihood (best-fit) or expected (weighted mean from the posterior distribution) models. The program permits the insertion of constraint boxes to include other geological information on the timing of subsidence, burial, or exhumation in the model. AFT data are used to constrain a cooling history below 110 °C (Donelick et al., 2005). ZFT data can constrain the cooling history at temperatures below ca. 240 °C for radiation-damaged zircons and common orogenic cooling rates (e.g., Bernet, 2009; Brandon et al., 1998).

Our study also employed the most robust and revealing method plotting length against a kinetic parameter (Dpar), noting whether trends exist and, if possible, defining coherent kinetic populations (e.g., Burtner et al., 1994). This approach not only can result in more accurate age interpretation but also allows length data to be segregated to enable proper inverse modeling. Because fission-track lengths shorten as a function of the thermal history they have undergone, a set of length measurements constitutes an integrated record of the temperatures experienced by a sample.

3.3. Exhumation Rate Estimates

First-order exhumation rates based on AFT and ZFT ages can be estimated from the simple 1–D thermal advection model age2dot created by Mark BRANDON (see Ehlers et al., 2005). For these first-order estimates, we assumed a constant pre-exhumation thermal gradient of 30 °C/km, which we acknowledge is a very simplistic assumption but sufficient for the purpose of this study. The AFT model was selected for chlorine apatite, which is justifiable with regard to the measured Dpar values shown in Table 2. For the ZFT model, we selected annealing parameters for radiation-damaged zircon, given that the ZFT cooling ages are on average older than 100 Ma for the western block. For the eastern block samples 13SACZ03 and 07, we used a zero-damage model, considering that these zircons rapidly cooled below the zircon fission-track closure temperature and through the zircon partial annealing zone between 25 and 20 Ma (Table 3).

4. Results

4.1. Fission-Track Data

The samples from the western profile, to the west of the Chicamocha River and the Bucaramanga Fault zone, have AFT ages between 36 and 7 Ma depending on elevation (Figure 4a). The lowest sample, i.e., 12SACEP11 from the Silgará Schists, yields a central AFT age of 21.4 ± 5.5 Ma and was collected at 612 m along the secondary fault pattern of the Santander Massif (Figures 2, 3; Table 2). Sample 12SACEP16 from the Silgará Schists yields a central AFT age of 18.9 ± 7.1 Ma, with a mean Dpar value of 1.88 μm . Sample 12SACEP08 yields a central AFT age of 12.9 ± 4.6 Ma, with a mean Dpar value of 2.17 μm . The highest sample of the western block, i.e., 12SACEP17 from the Silgará Schists, was collected at 1347 m and has a central AFT age of 34.5 ± 17.5 Ma. The oldest AFT age in the western block, i.e., 36.2 ± 5.8 Ma, was recorded for sample 13SACZ01 at 945 m. Forty-nine horizontally confined track length measurements yielded an average c-axis projected track length of 13.84 ± 2.74 μm . The mean Dpar value of these samples is 1.92 μm .

Table 1. Fission-track samples, Cepitá area, Santander Massif.

Sample	Longitude (°W)	Latitude (°N)	Elevation (m)	Lithology	Stratigraphic unit
Western block					
12SACEP02	−72.9838216	6.7535936	651	mica schist	Silgará Schists
12SACEP05	−72.9876257	6.7615073	741	amphibolite	Silgará Schists
12SACEP06	−72.9855766	6.7638081	757	mica schist	Silgará Schists
12SACEP08	−72.9954973	6.7778402	952	mica schist	Silgará Schists
12SACEP11	−73.0067275	6.8158368	612	mica schist	Silgará Schists
12SACEP13	−73.0137446	6.7962065	826	mica schist	Silgará Schists
12SACEP14	−73.0039793	6.8029836	1063	mica schist	Silgará Schists
12SACEP16	−72.9970256	6.7981493	1202	garnet–mica schist	Silgará Schists
12SACEP17	−73.0021697	6.7789128	1347	mica schist	Silgará Schists
13SACZ01	−72.9954700	6.7778000	954	amphibolite	Silgará Schists
13SACZ02	−72.9942340	6.7715950	1006	granite	Pescadero Granite
13SACZ09	−72.9831889	6.7597976	652	granite	Pescadero Granite
Eastern block					
13SACZ03	−72.9514600	6.7744600	1050	quartz vein	Bucaramanga Gneiss
13SACZ04a	−72.9520300	6.7744000	1022	andesitic dike	Bucaramanga Gneiss
13SACZ04b	−72.9520300	6.7743618	1022	gneiss	Bucaramanga Gneiss
13SACZ05	−72.9555273	6.7735458	935	migmatite	Bucaramanga Gneiss
13SACZ07	−72.9601810	6.7795084	1003	gneiss	Bucaramanga Gneiss

Table 2. Santander Massif (Cepitá area) apatite fission-track data.

Sample	N	r_s (10^4 cm^{-2})	N_s	r_i (10^5 cm^{-2})	N_i	r_d (10^6 cm^{-2})	P(c ²)	U (ppm)	Central Age (Ma)	±2σ	MDpar (μm)	±2σ	Length** (μm)	±2σ	n° length
Western block															
12SACEP06	17	8.56	62	9.74	705	1.19	0.0	12	19.6	9.6	2.08	0.26	15.12	1.28	4
12SACEP08	20	5.53	38	7.08	486	1.19	19.4	9	12.9	4.6	2.17	0.19	15.11	1.19	11
12SACEP11	20	0.91	8	16.2	1420	1.19	0.9	20	21.4	5.5	1.94	0.18	15.64	0.76	55
12SACEP13	20	1.06	12	2.39	270	1.21	68.4	3	7.3	4.6	–	–	–	–	–
12SACEP14	20	6.13	74	5.46	659	1.20	55.9	7	18.5	4.8	–	–	–	–	–
12SACEP16	20	9.89	67	9.11	617	1.19	0.5	11	18.9	7.1	1.88	0.18	15.22	1.61	15
12SACEP17	20	3.07	20	1.46	95	1.20	80.5	2	34.5	17.5	1.98	0.26	14.00	1.51	11
13SACZ01*	20	4.26	49	1.96	225	1.10	80.4	3	36.2	5.8	1.92	0.20	13.84	2.74	49
Eastern block															
13SACZ04a	20	10.7	80	27.3	2051	1.23	0.1	33	6.9	2.4	1.98	0.31	15.52	1.36	53
13SACZ04b	15	50.6	54	34.8	371	1.27	94.0	41	25.3	7.7	2.38	0.46	15.88	1.09	12

Note: Fission-track age is given as central ages (Galbraith & Laslett, 1993). Samples were counted dry with BX51 Olympus microscopes at 1250x magnification at the Servicio Geológico Colombiano in Bogotá and at ISTerre, Grenoble. Ages were calculated with the BINOMFIT program of Brandon (2002), using a zeta value of 274.44 ± 11.56 (2SE) and the IRMM540R uranium glass standard (15 ppm U).

*Calculated with a zeta of 303.52 ± 9.90 (2SE).

**c-axis projected track lengths.

Table 3. Santander Massif (Cepitá area) zircon fission-track data.

Sample	N	r_s (10^{+6} cm^{-2})	N_s	r_i (10^{+5} cm^{-2})	N_i	r_d (10^{+5} cm^{-2})	$P(c^2)$	Dispersion (%)	Central Age (Ma)	$\pm 2\sigma$	U (ppm)	$\pm 2\sigma$
Western block												
12SACEP02	17	11.0	1640	7.19	107	3.45	0.0	73.7	264.8	110.9	233	83
12SACEP05	12	4.25	1390	6.27	205	3.40	0.0	42.7	127.5	37.8	512	73
12SACEP11	20	8.55	3329	12.3	480	3.45	1.9	19.3	142.4	21.2	142	14
12SACEP14	7	8.53	1395	10.4	170	3.46	17.4	11.7	166.7	32.7	120	19
13SACZ02	20	10.0	1917	13.5	259	3.38	2.6	22.5	145.6	25.7	159	20
13SACZ09	18	7.74	1874	12.6	305	3.40	15.9	10.3	122.8	18.3	148	17
Eastern block												
13SACZ03	10	12.7	696	101	557	3.38	6.0	14.2	24.6	3.9	1192	106
13SACZ05	20	16.8	2368	47.4	670	3.39	0.0	66.7	88.7	28.3	558	45
13SACZ07	20	3.60	1253	29.0	1010	3.39	0.0	49.9	25.1	6.3	340	23

Note: Fission-track age is given as central ages (Galbraith & Laslett, 1993). Samples were counted dry with BX51 Olympus microscopes at 1250x magnification at the Servicio Geológico Colombiano in Bogotá and at ISTERre, Grenoble. Ages were calculated with the BINOMFIT program of Brandon (2002), using a zeta value of 118.48 ± 3.85 (2SE) and the CN1 uranium glass standard (39.8 ppm U).

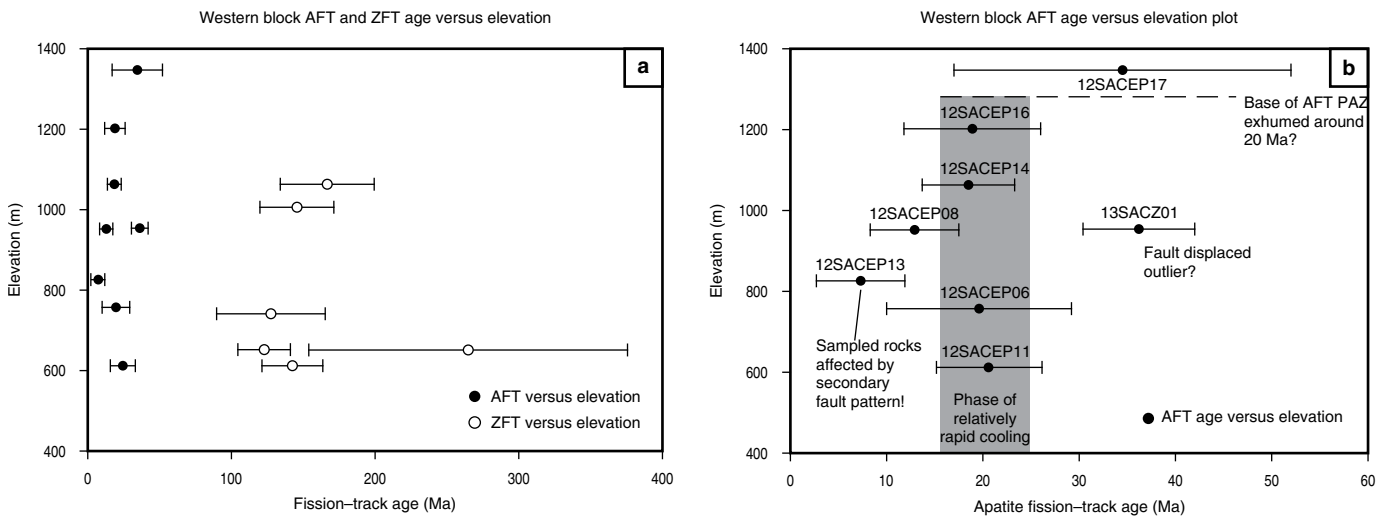


Figure 4. (a) Apatite and zircon fission-track age–elevation relationship of the western block profile in the Cepitá area of the southwestern Santander Massif. Ages are plotted with 2σ errors. (b) Apatite fission-track age–elevation relationship of the western block profile in the Cepitá area of the southwestern Santander Massif. Ages are plotted with 2σ errors. The base of the exhumed apatite fission-track partial annealing zones is shown with dashed line.

ZFT ages in the western block range between 123 and 265 Ma (Figure 4a; Table 3).

In the eastern profile, the AFT ages of two samples collected at the same elevation from an andesitic dike within the Bucaramanga Gneiss and the Bucaramanga Gneiss itself are 6.9 ± 2.4 Ma and 25 ± 7.7 Ma, with D_{par} values of $1.98 \mu\text{m}$ and $2.38 \mu\text{m}$ and mean track lengths of $15.52 \mu\text{m}$ and $15.88 \mu\text{m}$, respectively (Figure 2; Table 2). The ZFT ages of the three samples from the eastern block are approximately 25 Ma (samples 13SACZ03 and 07) and 89 Ma (sample 13SACZ05; Figure 2; Table 3).

Using a common pre–25 Ma thermal gradient of $30^\circ\text{C}/\text{km}$ and the age–offset of the ZFT ages of samples collected at similar elevations on both sides of the Bucaramanga Fault allows estimation of the relative uplift along the Bucaramanga Fault (Figure 5). Furthermore, the exhumed AFT and ZFT partial annealing zones can be constrained (Figures 4b, 5). The over-dispersion of single grain ages in individual samples, which is reflected by a $P(\chi^2)$ value $< 5\%$ (Tables 2, 3), indicate complex grain–age distributions. Over-dispersion may be due to the intrinsic variation in the uranium concentration and radioactive decay, given that spontaneous track formation follows a Poisson

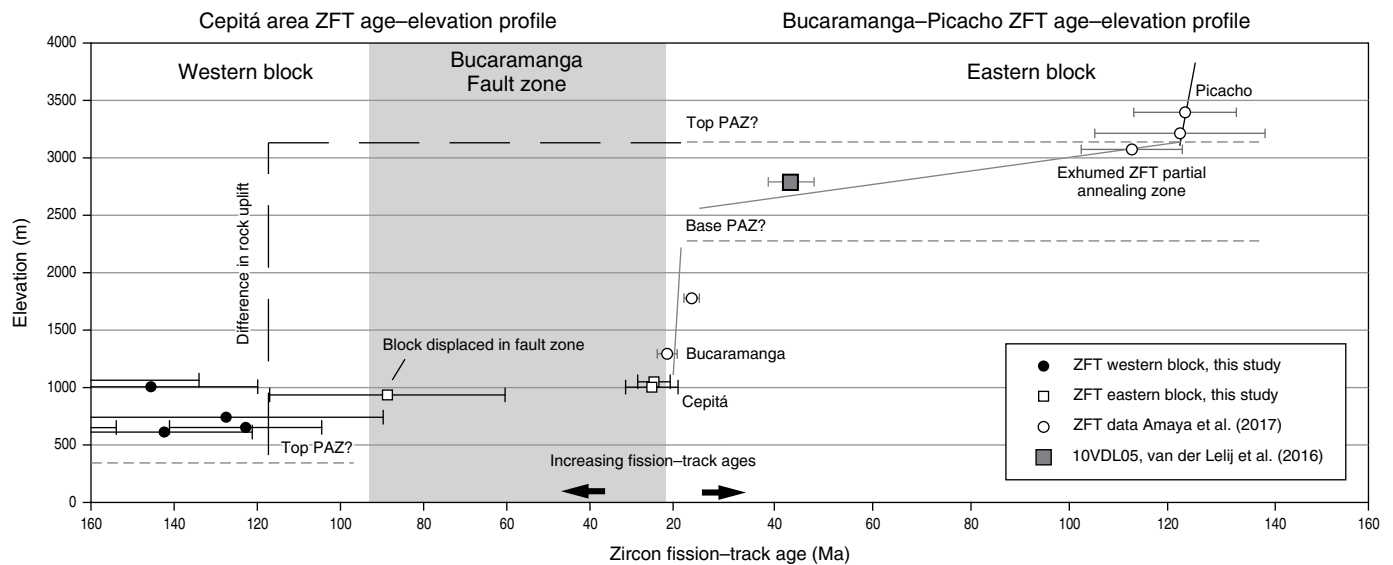


Figure 5. ZFT age–offset plot between the western and eastern blocks. This figure shows the relative uplift on both sides along the Bucaramanga Fault. Furthermore, exhumed ZFT partial annealing zones of each block can be seen.

distribution, equal to the formation of induced tracks. However, over–dispersion may also be indicative of a complex thermal history and partial annealing of fission tracks in apatite and zircon. The implication is that discordance in fission–track dating is more commonly the indication of a mixed distribution than of a poorly measured distribution. There are a number of possible reasons for this (see Galbraith & Laslett, 1993 or Galbraith, 2005 for details); however, in this study, we believe that the over–dispersion is a result of partial annealing and differences in annealing properties, as caused by variations in the chemical compositions of apatite (e.g., Donelick *et al.*, 2005, and references therein) or variations in the radiation damage of zircon (Brandon, 1992; Garver *et al.*, 2005).

4.2. Thermal History Modeling

We performed thermal history modeling for samples from the western profile, combining AFT age, Dpar, ZFT age, and AFT track length data. Although the track length data indicate relatively rapid cooling through the partial annealing zone (PAZ), the average Dpar values are in general $>1.75 \mu\text{m}$ (Figure 6), indicating that the analyzed apatites are relatively slow annealing (Donelick *et al.*, 2005). This condition is probably because annealing resistance increases with increasing chlorine content (Green *et al.*, 1985). We used our track length data to constrain our QTQt models. Furthermore, the models were based on apatite fission–track age, track length, Dpar value, zircon fission–track ages, and 100 000 attempted paths. The constraint boxes for inverse modeling were placed following the forward model to match the observed fission–track ages as closely as possible and the stratigraphic constraint box between 160 Ma to 130 Ma that constrains the Jurassic

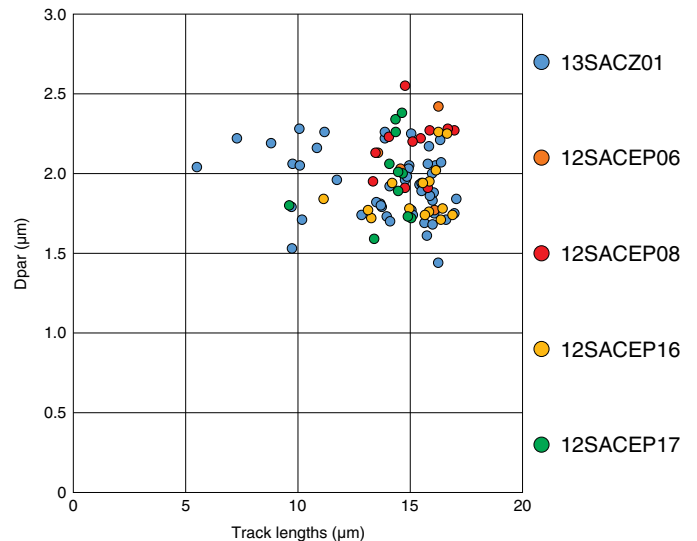


Figure 6. Plot of track length versus Dpar, showing trends defining coherent kinetic populations with values of track lengths of ca. 15 μm and Dpar >1.5 .

sedimentation (Sarmiento–Rojas *et al.*, 2006) and between 120 Ma to 60 Ma that constrains the burial of sedimentary rocks, at least since the Late Jurassic and throughout most of the Cretaceous (Sarmiento–Rojas *et al.*, 2006). Our track lengths data are similar to van der Lelij *et al.* (2016), who presented a mean AFT track length of $15.13 \pm 1.03 \mu\text{m}$ for sample 10VDL22 in the study area with an AFT age of 20 Ma (Figure 2; Table 4), which we used for constraining the t–T modeling of rapidly cooled AFT grains with apparent cooling ages $< \text{ca. } 25 \text{ Ma}$. This, in combination with AFT age, AFT Dpar, ZFT age, track length, and surface temperature data, al-

Table 4. Published fission-track data along the Bucaramanga Fault to the north of the Cepitá area.

Sample	Elevation (m)	Unit	AFT Age (Ma)	$\pm 2\sigma$	ZFT Age (Ma)	$\pm 2\sigma$	Reference
BC79-1	650	Pescadero Granite	13.7	1.7	93.0	10.0	Shagam et al. (1984)
BC79-6	625	Silgará Schists	18.9	2.2			Shagam et al. (1984)
10VDL22	640	Pescadero Granite	20.0	3.3	172.0	16.4	van der Lelij et al. (2016)
GC996-31	839	Silgará Schists	21.4	8.4			Caballero et al. (2013)
GC996-37	900	Silgará Schists	15.7	3.4			Caballero et al. (2013)

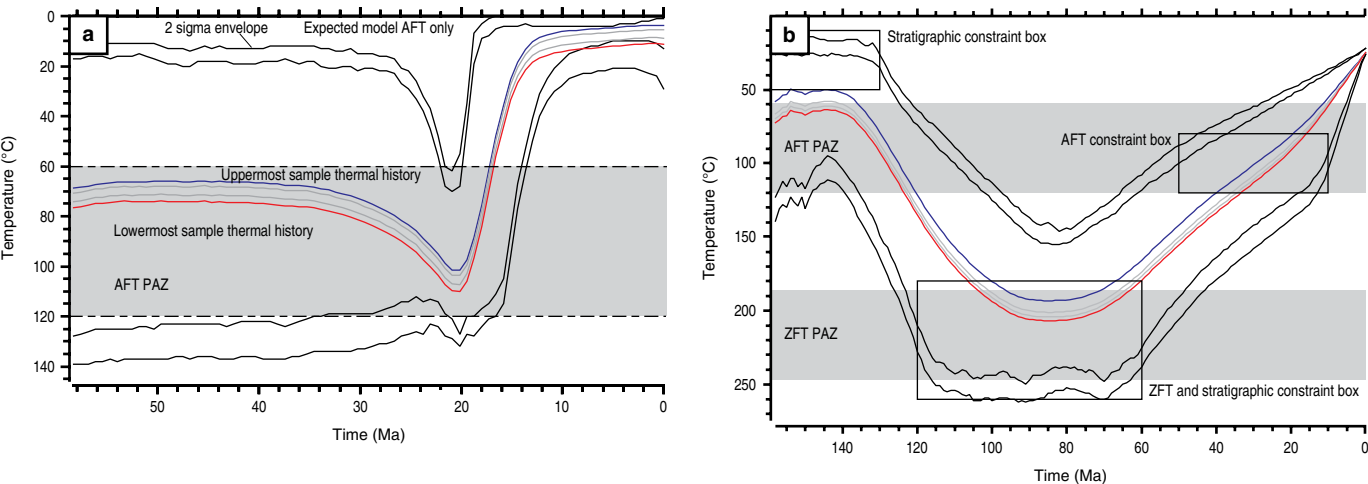


Figure 7. (a) AFT QTQt model of the western block. (b) ZFT QTQt model of the western block. In both plots the expected model for the thermal history solutions are shown. The profiles contain more than one sample. Any constraints are drawn as black boxes (Gallagher, 2012).

lows the presentation of a reasonable first-order expected t–T model (Figure 7). The AFT QTQt expected model shows that the western block was less affected by rapid late Oligocene – early Miocene cooling (Figure 7a) than the eastern block, despite the approximately 20 Ma cooling ages of samples 12SACEP06, 12SACEP11, 12SACEP14, and 12SACEP16. We believe this is because sample 12SACEP13, collected along the secondary fault on the western flank of the western block (Figure 2; Table 1), has a 7.3 ± 4.6 Ma cooling age. The QTQt model in Figure 7a shows an increase in cooling rates from ca. 0.5 °C/my between 50–10 Ma to ca. 5–8 °C over the past 5 to 10 my. We used the AFT data for constraining the ZFT QTQt model as shown in Figure 7b. Given that Upper Jurassic sedimentary rocks of the Girón Formation were deposited on the crystalline rocks of the western Santander Massif, we can constrain the thermal history with surface–temperature conditions between 155–140 Ma. Therefore, the western block underwent reheating between approximately 140 to 90 Ma at a rate of ca. 3 °C/my. From approximately 90 to approximately 65 Ma, the sampled rocks of the western block resided in the ZFT partial annealing zone and cooling started during the early Paleocene (Figure 7b).

4.3. Exhumation Rates

On the basis of the AFT ages, long-term exhumation rates during the Miocene – Pliocene were on the order of 0.2–0.3 km/my for the western block and 0.5–1.3 km/my for the eastern block (Figure 8). The partially reset ZFT ages of the western block indicate that the exhumation of the western block since the early Paleocene was not sufficient to exhume fully reset zircons. Because of partial annealing, no precise exhumation rates could be determined; however, these rates were on the order of 0.1–0.2 km/my. Samples 13SACZ04 and 13SACZ07 indicate that, on average, the eastern block has been exhumed at a rate of 0.3 km/my since approximately 25 Ma (Figure 8).

5. Discussion

5.1. Insights from Thermochronology

The t–T history modeling using our thermochronological data of the southwestern Santander Massif shows that the western and eastern blocks on both sides of the Bucaramanga Fault have different thermal histories. The inverse modeling of the ZFT data

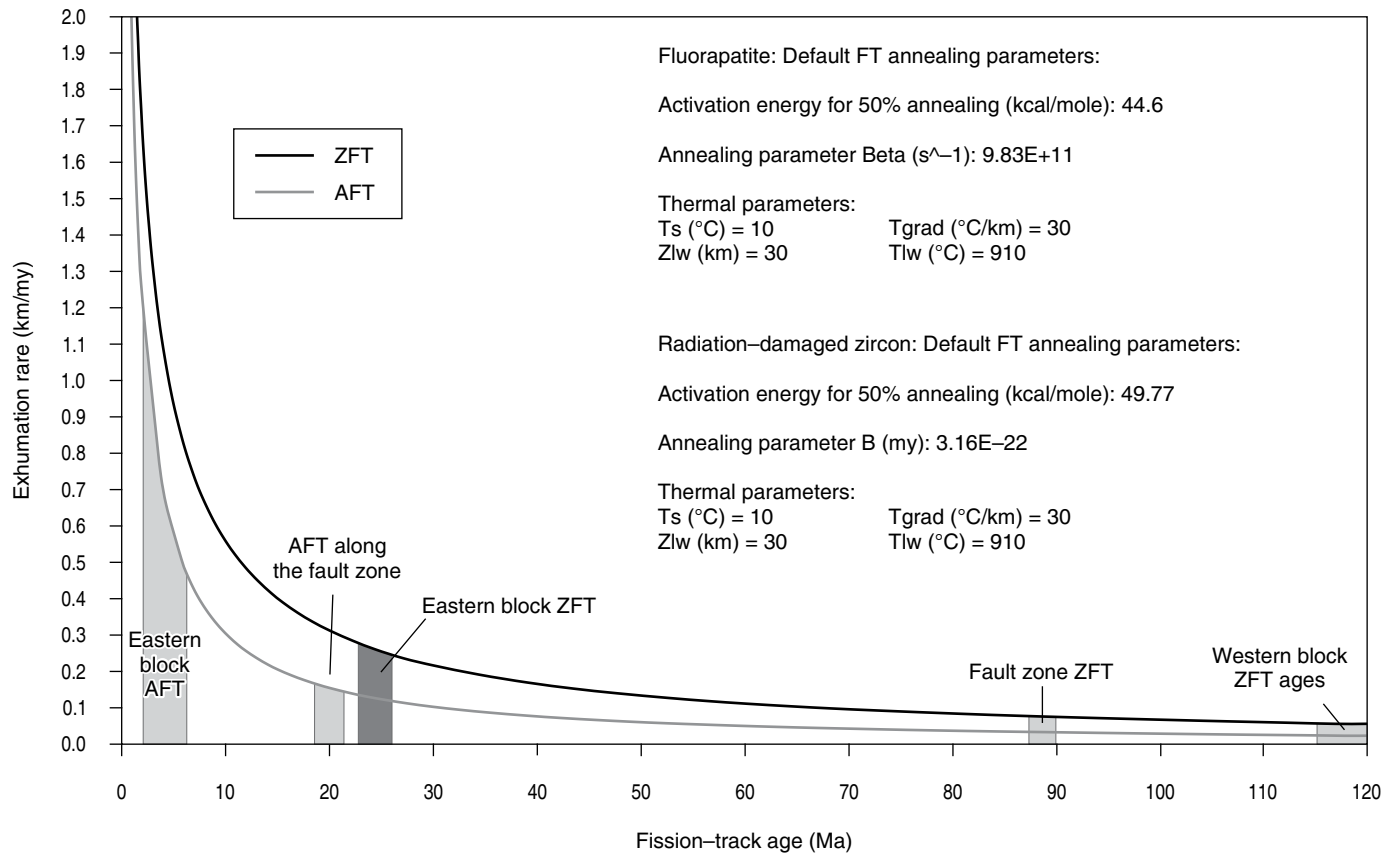


Figure 8. Relationship between fission-track age and exhumation rate determined for a 30 $^{\circ}C/km$ steady-state thermal gradient and an average surface temperature of 10 $^{\circ}C$ for the apatite and zircon fission-track system. The exhumation rates were estimated from the curves of the appropriate thermochronological system. Data obtained from the age2dot program of M. BRANDON (see Ehlers *et al.*, 2005).

of the western block shows burial heating since the Late Jurassic, followed by nearly isothermal conditions during the Late Cretaceous and monotonic cooling that started during the early Paleocene (Figure 7b). This monotonic cooling was most likely caused by erosional exhumation of the Santander Massif and removal of overlying sedimentary cover and crystalline basement rocks.

With the exception of sample 12SACEP13, the AFT ages of the western block show a typical age–elevation trend of an exhumed AFT partial annealing zone (Figure 4b), with exhumation and cooling below approximately 120 $^{\circ}C$ occurring at ca. 20 Ma. This is consistent with the published AFT ages at low elevations (625–900 m) of Caballero *et al.* (2013), Shagam *et al.* (1984), and van der Lelij *et al.* (2016) along the Bucaramanga Fault zone to the north of the Cepitá area (Figure 2; Table 4). Movement on the NE–SW–oriented secondary fault pattern seems to be more recent, given the late Miocene AFT cooling age of sample 12SACEP13 at 826 m. As the western block had already cooled below ca. 120 $^{\circ}C$ during the early Miocene, this younger cooling age may be related to cooling after frictional heating in the secondary fault zone; however, more research is needed to confirm this hypothesis.

The non-annealed to partially annealed ZFT ages of the western block may indicate residence of the rocks near the top

or just above of a fossil ZFT partial annealing zone, whose base is not yet exposed in the western block. The ZFT ages of 123 Ma to 167 Ma, found in the present study at 650–1350 m in the western block are similar to ZFT ages of 120–150 Ma found at 3200–3500 m in the eastern block of the Santander Massif to the east of Bucaramanga (Amaya *et al.*, 2017). This suggests a difference in uplift of approximately 2000 m between the western and eastern blocks. Based on the late Oligocene 25 Ma ZFT ages of samples 13SACZ03 and 13SACZ07 at similar elevations (1003 and 1050 m) of the eastern block in the Cepitá area (Table 3) and the approximately 25–20 Ma ZFT ages in the lower part of the Bucaramanga–Picacho profile of Amaya *et al.* (2017), the differential uplift started during the late Oligocene to early Miocene (Figure 5) but may have continued until the late Miocene – Pliocene, given the young AFT cooling ages of Amaya *et al.* (2017) to the east of the Bucaramanga fault.

The difference in the AFT ages of samples 13SACZ04a and 13SACZ04b and the ZFT age of sample 13SACZ03 from the eastern block at similar elevations of 1050 and 1022 m, respectively, is interesting sample 13SACZ04b was collected from the Bucaramanga Gneiss (Table 1) and shows an age of 25.3 ± 7.7 Ma during the rapid late Oligocene – early Miocene cooling also observed in the ZFT data. However, sample 13SACZ04a

was collected from an andesitic dike and has an apparent AFT cooling age of 6.9 ± 2.4 Ma (Tables 1, 2). Even if this age is not very well constrained, it suggests possibly short-lived magmatic activity, and hydrothermal fluid flow, in this part of the Santander Massif. The relation of this late Miocene magmatic activity to the formation of late Miocene hydrothermal gold mineralization in the California Vetas area of the Santander Massif (e.g., Mantilla–Figueroa et al., 2013; Urueña, 2014) or the volcanic activity at the same time in the Eastern Cordillera Paipa–Iza Complex (Bernet et al., 2016) is not clear at this stage and warrants further research. Nonetheless, we believe that based on field evidence this very minor magmatic activity in the study area did not affect the apatites of sample 13SACZ4b, and that the AFT age of that sample records exhumation cooling.

5.2. Regional Tectonic Control on Cooling and Exhumation

The thermal history model (Figure 7b), in combination with the AFT and ZFT age–elevation data of the western and eastern blocks discussed above, reveal a four-stage thermal history in connection with regional tectonic events for the southwestern Santander Massif. After the 60 my phase of subsidence and burial heating (stage 1) between the Late Jurassic and Late Cretaceous, cooling of the crystalline rocks of the Santander Massif started during the Late Cretaceous – early Paleocene. We believe this initiation of cooling was related to the Late Cretaceous accretion of an island–arc to the west of South America (e.g., Jaillard et al., 2000) and interaction of the Caribbean Plate with the western margin of South America (Bayona et al., 2013), which led to surface uplift and erosion in the area of the Santander Massif, as documented in the surrounding sedimentary basins, such as the Cesar Basin sedimentary record (e.g., lithic fragments in the Late Cretaceous to Paleocene Colón Formation) to the north of the Santander Massif (Figure 1; Ayala–Calvo et al., 2009; Bayona et al., 2013; Villamil, 1999) or the Nuevo Mundo Syncline to the west of the Santander Massif (Figure 1; Caballero et al., 2013).

The third stage of the thermal history is marked by rapid cooling and exhumation along the Bucaramanga Fault in the Santander Massif during the collision of the Panamá–Chocó Block with the northwestern South American plate at approximately 25 Ma (Farris et al., 2011; O’Dea et al., 2016), possibly as a result of the Farallón Plate break-up also at approximately 25 Ma (Taboada et al. 2000). This means the rocks were already being exhumed during the Oligocene, but exhumation particularly accelerated in the eastern block during the late Oligocene. This result is consistent with previously published thermochronological data reported by Amaya et al. (2017) from samples collected to the west of the Suratá Fault and near Bucaramanga, which indicate that cooling caused by exhumation of the PAZ occurred between 25 and 20 Ma, and from plutonic rocks that

intruded the Bucaramanga Gneiss and Silgará Schists, which also indicate that the exhumation of the Santander Massif was already underway during the Oligocene (Caballero et al., 2013). Furthermore, late Oligocene to early Miocene exhumation is a common phenomenon in the northern Andes and has already been described for the Antioquian Batholith of the Central Cordillera (Restrepo–Moreno et al., 2009), the Caparo Block of the southwestern Mérida Andes (Bermúdez et al., 2010; Kohn et al., 1984), and the Sierra Nevada de Santa Marta of the northern Santander Massif (Figure 9b).

Finally, late Miocene cooling ages, as observed along the secondary NE–SW–oriented fault pattern (sample 12SACEP13), and minor magmatic activity (sample 13SACZ04A) in the Santander Massif are approximately contemporaneous with the initiation of significant surface uplift of the Eastern Cordillera (Mora et al., 2009). Such young AFT cooling ages have also been found along the Boconó Fault in the Mérida Andes (Bermúdez et al., 2010, 2011; Kohn et al., 1984). Therefore, a regional tectonic driver was also likely responsible for this latest exhumation stage in the Santander Massif, which may have been related to the subduction of the Caribbean Plate and slab break-off (Vargas & Mann, 2013). However, we have not ruled out that the late Miocene cooling ages in the western Santander Massif indicate the initiation of exhumation in the eastern Santander Massif during the Pliocene – Pleistocene related to the buttress effect of the collision of the Chocó Block as described by Velandia (2017).

5.3. Topographic Evolution

The Bucaramanga Fault played a very important role in the exhumation of the crystalline basement and surface uplift of the Santander Massif to greater than 3600–4530 m in elevation, generating asymmetric topography as seen in the eastern and western blocks of the Bucaramanga Fault and other fault blocks within the Santander Massif (Amaya et al., 2017). The topography observed today in the Santander Massif is the result of all of the accumulated deformation of the massif since the beginning of its uplift by inversion of geological structures in the Late Cretaceous – early Paleocene until the Pliocene – Pleistocene when faulted structures in a NE direction accommodated the deformation, with displacement in course, possibly due to the collision and buttress effect of the Chocó Block (Velandia, 2017; Villamizar, 2017). Recently published studies have identified that the structure of the Santander Massif is composed of tectonic blocks (e.g., Amaya et al., 2017; van der Lelij et al., 2016), and in this study, we identified two tectonic blocks, namely, the western and eastern blocks of the Bucaramanga Fault, each with different thermal histories, as described above. Using our thermochronological data, a new model for the topographic evolution of the Santander Massif in the Cepitá area is proposed (Figures 9, 10). We believe that

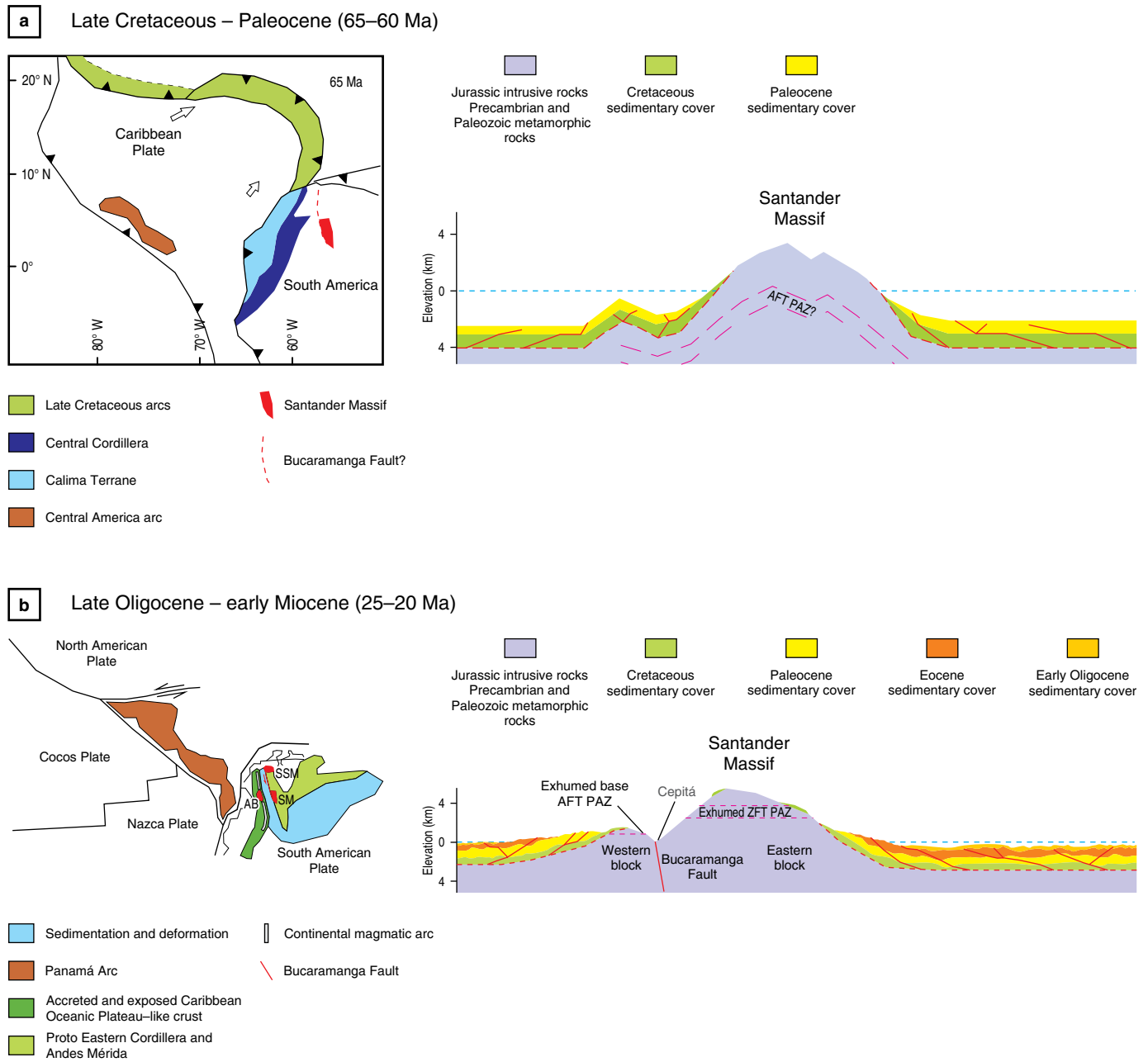


Figure 9. Model geodynamic topographic evolution of the Santander Massif. Crustal —scale cross— section from 65 Ma to 20 Ma, showing the relationship between exhumation and topographic evolution of Santander Massif and regional tectonics. **(a)** In Late Cretaceous and early Paleocene times, the collision of the Caribbean Plate with the northwestern South American continental margin produced reactivation of intraplate structures that contributed to the exhumation and surface uplift of the Santander Massif. **(b)** Regional tectonics setting, showing the collision of the Panamá Arc with the northwestern South American continental margin and its effects on the exhumation and topographic evolution of the Santander Massif. (SM) Santander Massif; (SNSM) Sierra Nevada de Santa Marta; (AB) Antioquian Batholith. (a) Position of the Caribbean Plate, Central America Arc, and direction of movement of the plates is taken and modified by Spikings et al. (2015). (b) Position of the Caribbean Plate, the Panamá Arc, and directions of movement of the plates, is taken and modified by Boschman et al. (2014).

the topographic development of the Santander Massif initiated during the Late Cretaceous – early Paleocene, although this development occurred along inversion structures and was not strong (Figure 9a). In contrast to the Mérida Andes, which reached their present-day elevation by the late Miocene (Ber-

múdez et al., 2017), the present-day topographic elevations of the Santander Massif were probably in place during the late Oligocene – early Miocene (Figure 9b), when the Panamá arc collided with northwestern South America. The surface uplift of the eastern block reached overall much higher surface



Figure 10. Photograph of the eastern block Bucaramanga Fault in the Cepitá area showing position of the paleozone of the partial annealing zone of the zircon fission track (PAZ-ZFT).

elevations than that of the western block (Figure 10), likely influenced by the isostatic response of the crystalline rocks of the eastern block, which was three times faster than that of the crystalline rocks of the western block, which are covered with sedimentary rocks (Braun et al., 2014).

6. Conclusion

Our main conclusions about the tectonic and thermal evolution of the Santander Massif from this thermochronological study are summarized as follows. (i) Cooling of the Santander Massif crystalline rocks, related to erosional exhumation, began during the Late Cretaceous – early Paleocene at approximately 65–60 Ma. (ii) A second cooling phase related to Bucaramanga Fault activity and erosion caused by the Panamá–Chocó Block collision with northwestern South America started during the late Oligocene to early Miocene. (iii) The latest phase of cooling occurred during the Pliocene – Pleistocene but can primarily be observed along the secondary fault pattern in the Santander Massif. All three phases of faster or slower cooling can be related to regional tectonic events in the northern Andes.

Our dataset furthermore illustrates that exhumation of the Santander Massif basement rocks on both sides of the Bucaramanga Fault was asymmetric because there is an approximately 2000 m difference in elevation between rocks with similar ZFT cooling ages in the eastern and western blocks, and the overall surface elevations of the eastern block are much higher than those of the western block.

Acknowledgments

We would like to thank the Thermochronology Laboratory of the Servicio Geológico Colombiano for allowing sample preparation, and we particularly acknowledge the help and support of

Mary Luz PEÑA, Yolanda CAÑÓN, Lorena RAYO, and Cindy URUEÑA. This research was supported by COLCIENCIAS grant 110156933549 and Universidad Nacional de Colombia grant 28170 awarded to Carlos ZULUAGA, and by LabEx International grant 2014 and a BQR Sud grant awarded to Matthias BERNET at ISTERre, Université Grenoble Alpes. The manuscript was improved through the constructive and detailed reviews of Roelant VAN DER LELIJ and Barry KOHN. We would also like to thank Barry KOHN for completing the ^{252}Cf irradiations of our AFT samples, which helped improve our thermal history models.

References

- Amaya, S., Zuluaga, C. & Bernet, M. 2017. New fission-track age constraints on the exhumation of the central Santander Massif: Implications for the tectonic evolution of the northern Andes, Colombia. *Lithos*, 282–283: 388–402. <https://doi.org/10.1016/j.lithos.2017.03.019>
- Ayala-Calvo, R.C., Bayona, G., Ojeda-Marulanda, C., Cardona, A., Valencia, V., Padrón, C.E., Yoris, F., Mesa-Salamanca, J. & García, A. 2009. Estratigrafía y procedencia de las unidades comprendidas entre el Campaniano y el Paleógeno en la Subcuenca de Cesar: Aportes a la evolución tectónica del área. *Geología Colombiana*, (34): 3–33.
- Bayona, G., Cardona, A., Jaramillo, C., Mora, A., Montes, C., Caballero, V., Mahecha, H., Lamus, F., Montenegro, O., Jiménez, G., Mesa, A. & Valencia, V. 2013. Onset of fault reactivation in the Eastern Cordillera of Colombia and proximal Llanos Basin; Response to Caribbean–South American convergence in early Palaeogene time. In: Nemčok, M., Mora, A. & Cosgrove, J.W. (editors), *Thick-skin-dominated orogens: From initial inversion to full accretion*. Geological Society of London, Special Publication 377, p. 285–314. <https://doi.org/10.1144/SP377.5>

- Bermúdez, M.A., Kohn, B.P., van der Beek, P.A., Bernet, M., O'Sullivan, P.B. & Shagam, R. 2010. Spatial and temporal patterns of exhumation across the Venezuelan Andes: Implications for Cenozoic Caribbean geodynamics. *Tectonics*, 29(5): 1–21. <https://doi.org/10.1029/2009TC002635>
- Bermúdez, M.A., van der Beek, P. & Bernet, M. 2011. Asynchronous Miocene – Pliocene exhumation of the central Venezuelan Andes. *Geology*, 39(2): 139–142. <https://doi.org/10.1130/G31582.1>
- Bermúdez, M.A., van der Beek, P. & Bernet, M. 2013. Strong tectonic and weak climatic control on exhumation rates in the Venezuelan Andes. *Lithosphere*, 5(1): 3–16. <https://doi.org/10.1130/L212.1>
- Bermúdez, M.A., Hoorn, C., Bernet, M., Carrillo, E., van der Beek, P.A., Garver, J.I., Mora, J.L. & Mehrkian, K. 2017. The detrital record of late-Miocene to Pliocene surface uplift and exhumation of the Venezuelan Andes in the Maracaibo and Barinas Foreland Basins. *Basin Research*, 29(S1): 370–395. <https://doi.org/10.1111/bre.12154>
- Bernet, M. 2009. A field-based estimate of the zircon fission-track closure temperature. *Chemical Geology*, 259(3–4): 181–189. <https://doi.org/10.1016/j.chemgeo.2008.10.043>
- Bernet, M., Urueña, C., Amaya, S. & Peña, M.L. 2016. New thermo and geochronological constraints on the Pliocene – Pleistocene eruption history of the Paipa-Iza Volcanic Complex, Eastern Cordillera, Colombia. *Journal of Volcanology and Geothermal Research*, 327(15): 299–309. <https://doi.org/10.1016/j.jvolgeores.2016.08.013>
- Boschman, L.M., van Hinsbergen, D.J.J., Torsvik, T.H., Spakman, W. & Pindell, J.L. 2014. Kinematic reconstruction of the Caribbean region since the Early Jurassic. *Earth–Science Reviews*, 138: 102–136. <https://doi.org/10.1016/j.earscirev.2014.08.007>
- Brandon, M.T. 1992. Decomposition of fission-track grain-age distributions. *American Journal of Science*, 292(8): 535–564. <https://doi.org/10.2475/ajs.292.8.535>
- Brandon, M.T. 2002. Decomposition of mixed grain age distributions using BINOMFIT. *On Track*, 24: 13–19.
- Brandon, M.T., Roden-Tice, M.K. & Garver, J.I. 1998. Late Cenozoic exhumation of the Cascadia accretionary wedge in the Olympic Mountains, Northwest Washington State. *Geological Society of America Bulletin*, 110(8): 985–1009. [https://doi.org/10.1130/0016-7606\(1998\)110<0985:LCEOTC>2.3.CO;2](https://doi.org/10.1130/0016-7606(1998)110<0985:LCEOTC>2.3.CO;2)
- Braun, J., Simon-Labric, T., Murray, K.E. & Reiners, P.W. 2014. Topographic relief driven by variations in surface rock density. *Nature Geoscience*, 7: 534–540. <https://doi.org/10.1038/ngeo2171>
- Burtner, R.L., Nigrini, A. & Donelick, R.A. 1994. Thermochronology of Lower Cretaceous source rocks in the Idaho–Wyoming Thrust Belt. *American Association of Petroleum Geologists Bulletin*, 78(10): 1613–1636.
- Caballero, V., Mora, A., Quintero, I., Blanco, V., Parra, M., Rojas, L.E., López, C., Sánchez, N., Horton, B.K., Stockli, D.F. & Duddy, I. 2013. Tectonic controls on sedimentation in an intermontane hinterland basin adjacent to inversion structures: The Nuevo Mundo Syncline, Middle Magdalena Valley, Colombia. In: Nemčok, M., Mora, A. & Cosgrove, J.W. (editors), *Thick-skin-dominated orogens: From initial inversion to full accretion*. Geological Society of London, Special Publication 377, p. 315–342. London. <https://doi.org/10.1144/SP377.12>
- Colletta, B., Roure, F., de Toni, B., Loureiro, D., Passalacqua, H. & Gou, Y. 1997. Tectonic inheritance, crustal architecture, and contrasting structural styles in the Venezuela Andes. *Tectonics*, 16(5): 777–794. <https://doi.org/10.1029/97TC01659>
- Colmenares, L. & Zoback, M.D. 2003. Stress field and seismotectonics of northern South America. *Geology*, 31(8): 721–724. <https://doi.org/10.1130/G19409.1>
- Donelick, R.A., O'Sullivan, P.B. & Ketcham, R.A. 2005. Apatite fission-track analysis. *Reviews in Mineralogy and Geochemistry*, 58(1): 49–94. <https://doi.org/10.2138/rmg.2005.58.3>
- Ehlers, T.A., Chaudhri, T., Kumar, S., Fuller, C.W., Willett, S.D., Ketcham, R.A., Brandon, M.T., Belton, D.X., Kohn, B.P., Gleadow, A.J.W., Dunai, T.J. & Fu, F.Q. 2005. Computational tools for low-temperature thermochronometer interpretation. *Reviews in Mineralogy and Geochemistry*, 58(1): 589–622. <https://doi.org/10.2138/rmg.2005.58.22>
- Farris, D.W., Jaramillo, C., Bayona, G., Restrepo-Moreno, S.A., Montes, C., Cardona, A., Mora, A., Speakman, R.J., Glascock, M.D. & Valencia, V. 2011. Fracturing of the Panamanian Isthmus during initial collision with South America. *Geology*, 39(11): 1007–1010. <https://doi.org/10.1130/G32237.1>
- Galbraith, R.F. 2005. *Statistics for fission tracks analysis*. Chapman & Hall/CRC, 240 p. Boca Ratón, Costa Rica.
- Galbraith, R.F. & Laslett, G.M. 1993. Statistical models for mixed fission track ages. *Nuclear tracks and radiation measurements*, 21(4): 459–470. [https://doi.org/10.1016/1359-0189\(93\)90185-C](https://doi.org/10.1016/1359-0189(93)90185-C)
- Gallagher, K., 2012. Transdimensional inverse thermal history modeling for quantitative thermochronology. *Journal of Geophysical Research: Solid Earth*, 117(B2): 1–16. <https://doi.org/10.1029/2011JB008825>
- Garver, J.I., Reiners, P.W., Walker, L.J., Ramage, J.M. & Perry, S.E. 2005. Implications for timing of Andean uplift from thermal resetting of radiation-damaged zircon in the Cordillera Huayhuash, northern Peru. *The Journal of Geology*, 113(2): 117–138.
- Goldsmith, R., Marvin, R.F. & Mehnert, H.H. 1971. Radiometric ages in the Santander Massif, Eastern Cordillera, Colombian Andes. U. S. Geological Survey, Professional Paper, 750–D: D44–D49.
- Green, P.F., Duddy, I.R., Gleadow, A.J.W., Tingate, P.R. & Laslett, G.M. 1985. Fission-track annealing in apatite: Track length measurements and the form of the Arrhenius plot. *Nuclear Tracks and Radiation Measurements*, 10(3): 323–328. [https://doi.org/10.1016/0735-245X\(85\)90121-8](https://doi.org/10.1016/0735-245X(85)90121-8)

- Hoorn, C., Wesselingh, F.P., ter Steege, H., Bermúdez, M.A., Mora, A., Sevink, J., Sanmartín, I., Sánchez-Meseguer, A., Anderson, C.L., Figueiredo, J.P., Jaramillo, C., Riff, D., Negri, F.R., Hooghiemstra, H., Lundberg, J., Stadler, T., Särkinen, T. & Antonelli, A. 2010. Amazonia through time: Andean uplift, climate change, landscape evolution, and biodiversity. *Science*, 330(6006): 927–931. <https://doi.org/10.1126/science.1194585>
- Jaillard, E., Hérail, G., Monfret, T., Díaz-Martínez, E., Baby, P., Lavenue, A. & Dumont, J.F. 2000. Tectonic evolution of the Andes of Ecuador, Peru, Bolivia and northernmost Chile. In: Cordani, U.G., Milani, E.J., Thomaz-Filho, A. & Campos, D.A. (editors), *Tectonic evolution of South America*, p. 481–559. Rio de Janeiro.
- Kohn, B.P., Shagam, R., Banks, P.O. & Burkley, L.A. 1984. Mesozoic–Pleistocene fission-track ages on rocks of the Venezuelan Andes and their tectonic implications. In: Bonini, W.E., Hargraves, R.B. & Shagam, R. (editors), *The Caribbean–South American Plate boundary and regional tectonics*, Geological Society of America, Memoir 162, p. 365–384. <https://doi.org/10.1130/MEM162-p365>
- Mann, P., Escalona, A. & Castillo, M.V. 2006. Regional geologic and tectonic setting of the Maracaibo supergiant Basin, western Venezuela. *American Association of Petroleum Geologists Bulletin*, 90(4): 445–477. <https://doi.org/10.1306/10110505031>
- Mantilla-Figueroa, L.C., Bissig, T., Valencia, V. & Hart, C.J.R. 2013. The magmatic history of the Vetás–California mining district, Santander Massif, Eastern Cordillera, Colombia. *Journal of South American Earth Sciences*, 45: 235–249. <https://doi.org/10.1016/j.jsames.2013.03.006>
- Mapes, B.E., Warner, T.T., Xu, M. & Negri, A.J. 2003. Diurnal patterns of rainfall in northwestern South America. Part I: Observations and context. *Monthly Weather Review*, 131(5): 799–812. [https://doi.org/10.1175/1520-0493\(2003\)131<0799:DPORIN>2.0.CO;2](https://doi.org/10.1175/1520-0493(2003)131<0799:DPORIN>2.0.CO;2)
- Mora, A., Gaona, T., Kley, J., Montoya, D., Parra, M., Quiroz, L.I., Reyes, G. & Strecker, M.R. 2009. The role of inherited extensional fault segmentation and linkage in contractional orogenesis: A reconstruction of Lower Cretaceous inverted rift basins in the Eastern Cordillera of Colombia. *Basin Research*, 21(1): 111–137. <https://doi.org/10.1111/j.1365-2117.2008.00367.x>
- Mora, A., Casallas, W., Ketcham, R.A., Gómez, D., Parra, M., Namson, J., Stockli, D.F., Almendral, A., Robles, W. & Ghorbal, B. 2015. Kinematic restoration of contractional basement structures using thermokinematic models: A key tool for petroleum system modeling. *American Association of Petroleum Geologists Bulletin*, 99(8): 1575–1598. <https://doi.org/10.1306/04281411108>
- O’Dea, A., Lessios, H.A., Coates, A.G., Eytan, R.I., Restrepo-Moreno, S., Cione, A.L., Collins, L.S., de Queiroz, A., Farris, D.W., Norris, R.D., Stallard, R.F., Woodburne, M.O., Aguilera, O., Aubry, M.P., Berggren, W.A., Budd, A.F., Cozzuol, M.A., Copard, S.E., Duque-Caro, H., Finnegan, S., Gasparini, G.M., Grossman, E.L., Johnson, K.G., Keigwin, L.D., Knowlton, N., Leigh, E.G., Leonard-Pingel, J.S., Marko, P.B., Pyenson, N.D., Rachello-Dolmen, P.G., Soibelzon, E., Soibelzon, L., Todd, J.A., Vermeij, G.J. & Jackson, J.B.C. 2016. Formation of Isthmus of Panama. *Science Advances*, 2(8): 1–11. <https://doi.org/10.1126/sciadv.1600883>
- Parra, M., Mora, A., López, C., Rojas, L.E. & Horton, B.K. 2012. Detecting earliest shortening and deformation advance in thrust belt hinterlands: Example from the Colombian Andes. *Geology*, 40(2): 175–178. <https://doi.org/10.1130/G32519.1>
- Restrepo-Moreno, S.A., Foster, D.A., Stockli, D.F. & Parra-Sánchez, L.N. 2009. Long-term erosion and exhumation of the “Altiplano Antioqueño”, northern Andes (Colombia) from apatite (U–Th)/He thermochronology. *Earth and Planetary Science Letters*, 278(1–2): 1–12. <https://doi.org/10.1016/j.epsl.2008.09.037>
- Sánchez, J., Horton, B.K., Tesón, E., Mora, A., Ketcham, R.A. & Stockli, D.F. 2012. Kinematic evolution of Andean fold-thrust structures along the boundary between the Eastern Cordillera and Middle Magdalena Valley Basin, Colombia. *Tectonics*, 31(3): 24 p. <https://doi.org/10.1029/2011TC003089>
- Sarmiento-Rojas, L.F., van Wess, J.D. & Cloetingh, S. 2006. Mesozoic transtensional basin history of the Eastern Cordillera, Colombian Andes: Inferences from tectonic models. *Journal of South American Earth Sciences*, 21(4): 383–411. <https://doi.org/10.1016/j.jsames.2006.07.003>
- Shagam, R., Khon, B.P., Banks, P.O., Dasch, L.E., Vargas, R., Rodríguez, G.I. & Pimentel, N. 1984. Tectonic implications of Cretaceous – Pliocene fission-track ages from rocks of the circum-Maracaibo Basin region of western Venezuela and eastern Colombia. In: Bonini, W.E., Hargraves, R.B. & Shagam, R. (editors), *The Caribbean–South American Plate boundary and regional tectonics*. Geological Society of America, Memoir 162, p. 385–412. <https://doi.org/10.1130/MEM162-p385>
- Spikings, R., Cochrane, R., Villagómez, D., van der Lelij, R., Vallejo, C., Winkler, W. & Beate, B. 2015. The geological history of northwestern South America: From Pangaea to the early collision of the Caribbean Large Igneous Province (290–75 Ma). *Gondwana Research*, 27(1): 95–139. <https://doi.org/10.1016/j.gr.2014.06.004>
- Taboada, A., Rivera, L.A., Fuenzalida, A., Cisternas, A., Philip, H., Bijwaard, H., Olaya, J. & Rivera, C. 2000. Geodynamics of the northern Andes: Subductions and intracontinental deformation (Colombia). *Tectonics*, 19(5): 787–813. <https://doi.org/10.1029/2000TC900004>
- Urueña, C.L. 2014. Metamorfismo, exhumación y termocronología del Neis de Bucaramanga. (Macizo de Santander, Colombia). Master thesis, Universidad Nacional de Colombia, 191 p. Bogotá.
- van der Lelij, R., Spikings, R.A. & Mora, A. 2016. Thermochronology and tectonics of the Mérida Andes and the Santander Massif, NW South America. *Lithos*, 248–251: 220–239. <https://doi.org/10.1016/j.lithos.2016.01.006>

- Vargas, C.A. & Mann, P. 2013. Tearing and breaking off of subducted slabs as the result of collision of the Panama Arc–indenter with northwestern South America. *Bulletin of the Seismological Society of America*, 103(3): 2025–2046. <https://doi.org/10.1785/0120120328>
- Velandia, F. 2017. Cinemática de las fallas mayores del Macizo de Santander—énfasis en el modelo estructural y temporalidad al sur de la Falla de Bucaramanga, Colombia. Doctoral thesis, Universidad Nacional de Colombia, 222 p. Bogotá.
- Villagómez, D., Spikings, R., Mora, A., Guzmán, G., Ojeda, G., Cortés, E. & van der Lelij, R. 2011. Vertical tectonics at a continental crust–oceanic plateau plate boundary zone: Fission track thermochronology of the Sierra Nevada de Santa Marta, Colombia. *Tectonics*, 30(4): 1–18. <https://doi.org/10.1029/2010TC002835>
- Villamil, T. 1999. Campanian – Miocene tectonostratigraphy, depocenter evolution and basin development of Colombia and western Venezuela. *Palaeogeography, Palaeoclimatology, Palaeoecology*, 153(1–4): 239–275. [https://doi.org/10.1016/S0031-0182\(99\)00075-9](https://doi.org/10.1016/S0031-0182(99)00075-9)
- Villamizar, N. 2017. Historia de exhumación del bloque este de la Falla de Bucaramanga usando termocronología de baja temperatura, Santander, Colombia. Master thesis, Universidad Nacional de Colombia, 112 p. Bogotá.
- Willett, S.D. & Brandon, M.T. 2013. Some analytical methods for converting thermochronometric age to erosion rate. *Geochemistry, Geophysics, Geosystems*, 14(1): 209–222. <https://doi.org/10.1029/2012GC004279>
- Zuluaga, C.A. & López, J.A. 2018. Ordovician orogeny and Jurassic low-lying orogen in the Santander Massif, northern Andes (Colombia). In: Cediel, F. & Shaw, R.P. (editors), *Geology and tectonics of northwestern South America: The Pacific–Caribbean–Andean junction*. Series: *Frontiers in Earth Sciences*. p. 195–250. Springer. https://doi.org/10.1007/978-3-319-76132-9_4

Explanation of Acronyms, Abbreviations, and Symbols:

AFT Apatite fission track
PAZ Partial annealing zone

ZFT Zircon fission track

Authors' Biographical Notes



Sergio AMAYA-FERREIRA is a geologist at the Universidad Nacional de Colombia, Bogotá, and is also a specialist in environmental engineering at the Universidad Industrial de Santander. He received his Master of Science degree in geology from the Universidad Nacional de Colombia Sede Bogotá, and a Doctoral degree in geosciences from the same university. Dr. AMAYA's main

research interest is the evolution of mountain ranges and sedimentary basins using low-temperature thermochronology (AFT and ZFT) and provenance analysis. He has worked as an associate professor at the School of Geology at the Universidad Industrial de Santander and as a specialized geologist in the fission-track laboratory at the Servicio Geológico Colombiano. He has also guided the following research projects in thermochronology and geochronology: “Structure and geological evolution of the crystalline basement of the Santander Massif, Eastern Cordillera, Colombia”, “Petrological characterization of the Berlin Orthogneiss Unit, Santander Massif, Colombia”, and “Evaluation of thermal maturity of gas associated with coals of the Umir Formation in the Middle Magdalena Valley and of the Guaduas Forma-

tion in the Umbita Syncline, Eastern Cordillera, Colombia”. The first two projects have contributed to broadening our understanding of the evolution of the northern Andes in the South American northwestern fringe, which remains under discussion. The thermal maturity assessment projects have contributed to determining the potential of unconventional coal bed methane hydrocarbons in Colombia's coal basins. Currently, Dr. AMAYA is a member of the Grupo de Exploración de Minerales Metálicos in the Dirección de Recursos Minerales of the Servicio Geológico Colombiano and is currently working on a research project concerning the “application of multidisciplinary approaches, petrological, geochronological, and thermochronological, to the exploration of deposits”.



Carlos Augusto ZULUAGA is an assistant professor and researcher in the Departamento de Geociencias of the Universidad Nacional de Colombia. He works on petrology applied to crustal evolution, thermodynamic modeling, and the tectonic evolution of the northern Andes.



Matthias BERNET has a PhD in geology from Yale University, USA. Since 2010, he has been the advisor of the thermochronology laboratory at the Servicio Geológico Colombiano, collaborated on several research projects of the Servicio Geológico Colombiano and helped with the implementation of the research facilities of the “Investigaciones y Aplicaciones Nucleares y Geocronológicas”

Group. He is an expert in using detrital thermochronology, clastic sedimentology, and multi-disciplinary provenance analyses to study the exhumation histories of mountain belts in the northern Andes of Colombia and Venezuela, the European Alps, the Himalaya, and the Tibetan Plateau. Currently, he is the director of the ISTerre Thermochronology Laboratory at the Université Grenoble Alpes in France.



Bogotá, Colombia
2020